SCHOLARLY PUBLICATIONS

A CURRENT AWARENESS BULLETIN
OF RESEARCH OUTPUT

@DTU

(32nd Edition)

AUGUST 2015

BY: CENTRAL LIBRARY

DELHI TECHNOLOGICAL UNIVERSITY
(FORMERLY *DELHI COLLEGE OF ENGINEERING)*
GOVT. OF N.C.T. OF DELHI
SHAHBAD DAULATPUR, MAIN BAWANA ROAD
DELHI 110042

PREFACE

This is the **Thirty Two** Issue of Current Awareness Bulletin started by Delhi Technological University, Central Library. The aim of the bulletin is to compile, preserve and disseminate information published by the faculty, students and alumni for mutual benefits. The bulletin also aims to propagate the intellectual contribution of Delhi Technological University (DTU) as a whole to the academia.

The bulletin contains information resources available in the internet in the form of articles, reports, presentations published in international journals, websites, etc. by the faculty and students of DTU. The publications of faculty and student which are not covered in this bulletin may be because of the reason that the full text either was not accessible or could not be searched by the search engine used by the library for this purpose.

The learned faculty and students are requested to provide their uncovered publications to the library either through email or in CD, etc to make the bulletin more comprehensive.

This issue contains the information published during **August 2015**. The arrangement of the contents is alphabetical. The full text of the article which is either subscribed by the university or available in the web is provided in this bulletin.

Central Library

CONTENTS

1. An Algorithmic approach to improve Network Performance for1G-EPON, ***7.1.Dr.Vibhakar Shrimali***, Dr. Sibaram Khara and Mr. Abhishek Gaur, ECE, DTU

2. Analysis of a Heat Pipe to Obtain Maximum Heat Transfer Rate, ***7.Anand Prakash Mall***, Thermal engineering, DTU

3. Optimization of Effective Parameters of Neem Oil Biodiesel using Taguchi Method and Anova, ***7.Anand Prakash Mall*** and ***3.Amit Pal***, Mechanical Engineering, DTU

4. BIO-HYDROGEN PRODUCTION: CURRENT TRENDS AND FUTURE PROSPECTS, Vinita Mishara and ***3.Isha Srivastava*** , Biotechnology, (page no. 56), DTU

5. Characterizing relatedness of web and requirements engineering, ***3.Akshi Kumar***, M.P.S. Bhatia and Rohit Beniwal, Computer Science & Engineering, DTU

6. Digital Watermarking of Video using DWT, PCA and Arnold Scrambling Technique applied on a Binary Watermark, ***3.Temshichang Jongko***, ***3.Jeebananda Panda*** and ***3.Asok Bhattacharyya***, E&C Engineering, DTU

7. Discussion on Principle of Super Position of Rate of Settlement in 2D and 3D Consolidations, Geotech Geol Eng. Doi 10.1007/s10706-015-9903-7, ***3.Anjeshnu Trivedi*** and ***3.Ashutosh Trivedi***, Civil Engineering, DTU

8. EFFECT OF WELDING VARIABLES ON TENSILE STRENGTH OF CU-STEEL WELDMENTS THROUGH DESIGN OF EXPERIMENTS AND REGRESSION MODEL, Surabhi Lata, Ramakant Rana, Alok Shankaran, Vinay Sharma, Amit Saraswat and ***3.Roop Lal***, Mechanical Engineering, DTU

9. Employment at High-end IT Enabled Services in India, ***3.Dr Seema Singh***, Economics, DTU

10. Enhanced ferroelectric photovoltaic response of BiFeO3/BaTiO3 multilayered structure, Savita Sharma, ***3.Monika Tomar***, Ashok Kumar, Nitin K. Puri and Vinay Gupta, Applied Physics, DTU

11. Evaluating Water Quality of River Yamuna in Delhi by Regression Analysis ***6.Shashank Shekhar Singh*** and ***3.Dr. S. K. Singh***, Environmental Engineering, DTU

12. EventBuilder: Real-time Multimedia Event Summarization by Visualizing Social Media, Rajiv Ratan shah, ***3.Anwar Dilawar Shaikh***, Yi yu, Wenjing Geng, Roger Zimmermann and Gangshan Wu, Computer Engineering, DTU

13. Fixed Bed Column Study and Adsorption Modelling on the Adsorption of Malachite Green dye from wastewater using Acid Activated Sawdust, ***3.S.K. Singh***, ***8.Dhruv Katoria***, ***8.Dhruv Mehta*** and ***8.Dhruv Sehgal***, Environmental Engineering, DTU

14. Flow Visualization around Perforated Circular Finned Tubes by CFD, ***8.Yogesh Pal1***, ***3. Naushad Ahmad Ansari*** and ***3.M. Zunaid***, Mechanical Engineering, DTU

15. Friedmann Cosmology with Matter Creation in Modified f (R,T) Gravity, ***3.Vijay Singh*** and ***3.C. P. Singh***, Applied Mathematics, DTU

16. Fuzzy Decision Approach for Selection of Sustainable and Green Materials for Green Buildings, Sunita Bansal, Srijit Biswas and ***3.S.K. Singh***, Environment Engineering, DTU

17. Holographic dark energy with statefinder diagnostic in modified f(R, T) gravity, ***3.C. P. Singh*** and ***3.Pankaj Kumar***, Applied Mathematics, DTU

18. Identification and Comparison of Flaws in Conventional Treatment Techniques of Fluoride, ***6.Shashank Shekhar Singh*** and ***3.Dr. S. K. Singh***, Environment Engineering, DTU

19. Improved Energy Efficient AODV Routing using K-means Algorithm for Cluster Head Selection, ***3.Arthur Ndlovu***, Computer Science and Engineering, DTU

20. Instability of Ion Beam Driven Electrostatic Ion-Cyclotron Waves in Collisional Magnetized Two-Ion Component Plasma, Jyotsna Sharma, ***3.Suresh C. Sharma*** and Daljeet Kaur, Applied Physics, DTU

21. Isolation of a Novel Laccase-producing Fungus from Litter in Upper Soil Horizon, Faria Fatima, Ira Chaudhary, ***3.Smita Rastogi*** and Neelam Pathak, Biotechnology, DTU

22. LEVERAGING INDIAN LABOUR FOR AUGMENTING FOREIGN DIRECT INVESTMENT, ***3.Dr. Archana Singh*** and ***6.Ms. Priya Gupta***, DSM, DTU

23. Mechanical properties and microstructure of spark plasma sintered nanostructured p-type SiGe thermoelectric alloys, ***3.Sivaiah Bathula***, M. Jayasimhadri and ***3.Ajay Dhar***, Applied Physics, DTU

24. Scope & Comparison Of Student Housing Industry In India, ***7.Sagar Agarwal*** , ***7.Kounal Gupta*** and ***7. Mayank Garg***, Mechanical Engineering, DTU

25. Sensor Node Deployment based on OTLBO in WSN, ***3.Anand prakash***, ***3.R.K.Yadav*** and ***3.Dr. Daya Gupta***, Computer Engineering, DTU

26. Single Feed Dual Band Circularly Polarized Patch Antenna with F and T Shaped Slots, Garima Rajput and ***8.1.Dr.P.K.Chopra***, Electronics Engineering, DTU

27. Skolem Graceful Signed Stars, ***3.Mukti Acharya*** and Tarkeshwar Singh, Applied mathematics, DTU

28. TCAD Analysis of Silicon-Germanium (SiGe) based Back-Contact Back-Junction (BC-BJ) solar cell as an alternative for silicon based cells, ***3.R. Pandey*** and ***3.R. Chaujar***, Engineering Physics, DTU

29. The Evaluation and Implementation of Various Techniques in Lean Manufacturing ***3.Ankit Agarwal***, ***3.Himanshu***, ***3.Anup Kumar*** and ***3.Dr.A.K.Madan***, Production and Industrial Engineering, DTU

30. Threshold voltage model of a Hetero Gate Dielectric Dual Material Gate GAA Tunnel FET ***3.J. Madan***, R.S. Gupta and ***3.R. Chaujar***, DTU

31. Traffic Noise Estimation using Genetic Algorithm (GA) Approach, ***3.Paras Kumar***, Mechanical Engineering, DTU

32. Two-phase anticipatory system design based on extended species 4 abundance model of biogeography for intelligent battlefield preparation, Lavika Goel, ***3.Daya Gupta*** and V.K. Panchal, Computer Science & Engineering, DTU

1. Vice Chancellor	***1.1. Ex Vice Chancellor***
2. Pro Vice Chancellor	***2.1. Ex Pro Vice Chancellor***
3. Faculty	***3.1. Ex Faculty***
4. Teaching-cum-Research Fellow	
5. Alumni	
6. Research Scholar	***6.1. Ex Research Scholar***
7. PG Scholar	***7.1. Ex PG Scholar***
8. Undergraduate Student	***8.1. Ex Undergraduate Student***

www.ijecs.in
International Journal Of Engineering And Computer Science ISSN: 2319-7242
Volume 4 Issue 8 Aug 2015, Page No. 13781-13785

An Algorithmic approach to improve Network Performance for 1G-EPON

Dr. Vibhakar Shrimali[1], Dr. Sibaram Khara[2], Mr. Abhishek Gaur[3]
[1](Associate Professor & Head, Ece Deptt. Gb Pant Govt. Engg. College, Delhi, India)
[2](Professor, School Of Electrical, Ece, Galgotias University, Greater Noida, India)
[2](Assistant Professor, Ece Deptt., Gb Pant Govt. Engg. College, Delhi, India)

Abstract – This paper proposes a novel 'TD-sense algorithm' for improve the network performance and compares it with a standard DBA_GATED algorithm. The algorithm is implemented by emulating an access network with the use of two 1G transceivers for 1G EPON. The algorithm is tested for Triple Play services that include simulated voice, video and data packets. The algorithm is found to maintain a better tradeoff between throughput and delay, than the existing DBA_GATED algorithm

Index Terms – OLT, ONU, Triple Play, Average Delay, Throughput, REGISTER, QOS, MTU

1. INTRODUCTION

Passive optical networks (PON) were developed to satisfy the demands of high bandwidth and larger coverage needs of future access networks [1]. A Passive Optical Network is a point-to-multipoint network that has no active elements in the path of the signals from source to destination [2]. The emergence of PON has reduced the cost to transmit data from Optical Line Terminal (OLT) which is located at the central office (CO) to Optical Network Unit (ONU) that provides broadband internet access to the subscribers. Ethernet PON (EPON), designated as IEEE 802.3ah, carries data traffic encapsulated in Ethernet frames over PON based network. 1G – EPON supports transmission and reception of data packets at the rate of 1 gigabits/second. The OLT uses Dynamic Bandwidth Allocation (DBA) to allocate bandwidth dynamically to the ONUs depending on the current traffic load at the ONU. We propose a novel algorithm for bandwidth allocation named 'TD (Throughput Delay)-Sense algorithm' wherein the OLT classifies the data traffic into two different types and allocate the bandwidth according to priority. This is implemented by using two 1G transceiver cards fixed to two computers connected by fiber optic cable, one acting as OLT and the other containing multiple ONUs. We have compared the performance of the novel algorithm with an existing algorithm.

2. DBA_GATED ALGORITHM

PON architecture comprises of an OLT located at a Central Office, connected to various ONUs through Optical Splitter. OLT acts as an interface between the core and the access network. The downstream channel from the OLT to the ONUs employs a single transmitter at the central office and the upstream channel is shared among the various ONUs[1]. The OLT broadcasts the traffic in the downstream channel

to all ONUs. DBA algorithm is used as medium access control mechanism which is employed to achieve the best possible usage of the bandwidth for the upstream channel usage from the ONU to the OLT. Each ONU calculates its bandwidth requirement as per its buffer contents. Then it sends a request frame to the OLT with the desired transmission window request. The OLT receives multiple requests from different ONUs at the same time. It then uses DBA algorithms to calculate the amount of bandwidth to be allotted to each ONU and sends the grants to each ONU, after which each ONU transmits in its own time window.

Multi point control protocol (MPCP) controls the upstream multiple access to allow efficient transmission of data. Five control messages namely GATE, REPORT, REGISTER_REQ, REGISTER and REGISTER_ACK are used for auto discovery and registration of the ONUs. [3]

In DBA_GATED algorithm, the OLT grants the preferred window size to each ONU. Further, if the same ONU has to send more data, it has to send another request to OLT. Though this algorithm provides a high level of QOS, the drawback is that an ONU with more data will block the other ONU with less data. This means ONU with fewer amounts of data has to wait for a long time until the ONU with more data completes its transmission. So in DBA_GATED algorithm, a single user is allowed to meet his demands and standard of service at the cost of other users, which is inequitable. [4]

3. TD-SENSE ALGORITHM

This is a novel algorithm proposed to gauge the performance of the network in terms of variation of both throughput and delay. This is implemented for Triple Play services where delay sensitive and delay non-sensitive applications exist. Video and voice over IP constitute the delay sensitive applications and other multimedia constitute the delay non-sensitive applications.

Delay sensitive application s typically range from 64 to 2500 bytes and are denoted as Type 0 traffic. Delay non-sensitive applications like huge video and data files extend from 5000 to 9000 bytes and are termed as Type 1 traffic. In this algorithm, the report message of all users is stored inside the buffers of the ONUs. The report message may be delay sensitive or non-sensitive.

DOI: 10.18535/ijecs/v4i8.28

Let T_1 = time when ONU sends a report to the OLT.
T_2 = time when the report is received at the OLT.
T (0) = Report length of the delay sensitive traffic in bytes or Type 0 traffic
T (1) = Report length of the non-delay sensitive traffic in bytes or Type 1 traffic
Channel free time = $T_2 - T_1$
Four possibilities exist in this approach. The following cases explain how scheduling will be done based on priority.

Case 1: When T (0) > $T_2 – T_1$, then T (0) will be scheduled and T (1) will not be scheduled. This condition indicates that delay sensitive traffic should be scheduled immediately and keeps the non-delay sensitive in buffer to be scheduled in the next cycle.

Case 2: When T (0) < $T_2 – T_1$, then T (0) will be scheduled and T (1) will be scheduled at the channel free time.

Case 3: When T (0) + T (1) < $T_2 – T_1$, then both T (0) and T (1) will be scheduled.

Case 4: When T (0) + T (1) > $T_2 – T_1$ and T (0) < $T_2 – T_1$, then both T (0) and T (1) will be scheduled but report length of T (1) will be cut down so that it can be accommodated in the channel free time.

The traffic generator module generates Type 0 traffic at the rate of $ß_1$ in Gbps and Type 1 traffic rate at the rate of $ß_2$ in Gbps. The offer load ß is given as

$$ß = b_1 ß_1 + b_2 ß_2 \quad (1)$$

Where b_1 = the mean packet size of Type 0 traffic varying from 64 to 1500 bytes.
b_2 = the mean packet size of Type 1 traffic varying from 5000-9000 bytes.

4. NETWOK DESIGN AND TOOLS

The set-up used two 1G Ethernet server adapters which are capable of handling data speeds up to 1.25 Gbps giving a real time functionality. The network uses optical fiber patch cords. In order to emulate a passive optical network two Linux loaded machines, one as OLT (Server Side) and the other as having network connection rather than a PON, the ONUs and the end multiple ONUs in it. Since this resembles a point-to-point nodes are to be simulated so as to follow the PON architecture as shown in the figure [1].

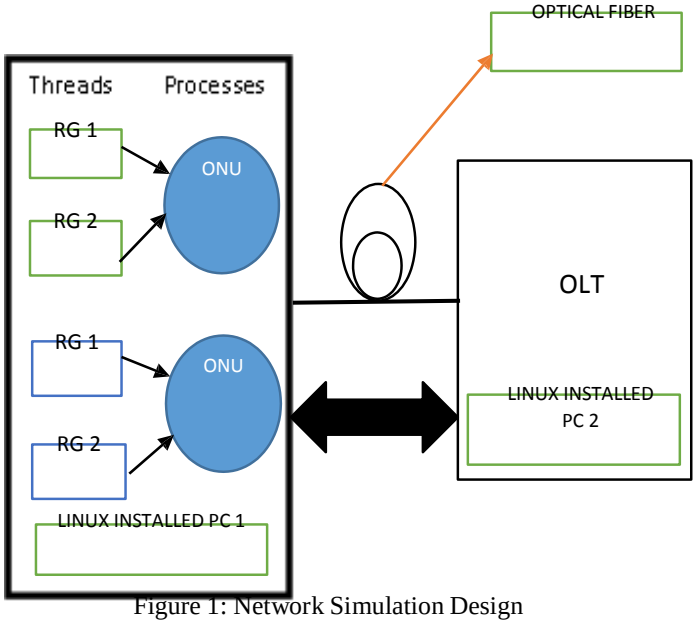

Figure 1: Network Simulation Design

The simulation was carried out by creating multiple processes which act as ONUs and each process has multiple threads running that act as end nodes. The multiple threads randomly generate the traffic. This is similar to the end nodes that generate real time traffic. Thus the entire setup of a passive splitter and the ONUs at different distances is simulated on a single system and the OLT on the other system.

A traffic generator module also known as random packet generator (RG) is used to generate packets and pump them into the network. The rate at which packets are generated is kept random so as to achieve the closest approximation to the real time scenarios. Two traffic generator modules are used in the simulation. The mathematical equation followed for generation of random packets is given as

$$X = - \log (1- \mu) \div \beta_1 \quad (2)$$

Where μ is the random number generated by the system and β_1 is the rate parameter varying from 0 to 1. This traffic generator module follows the exponential function.

The second traffic generation module implemented is based on Pareto Distribution that generates ON - OFF periods. The Pareto distribution is a heavy tailed distribution with a probability density function given by [6]

$$F(x) = \beta_2 * b^{\beta}_2 \div X^{\beta}$$

Where β2 is the shape parameter and b is the location parameter. The number of packets per second (ON period) follows the Pareto Distribution with the rate factor varying from 0.2 to 0.8. The OFF period also follows Pareto Distribution.

Using the above mathematical equations the packet size can be varied using the rate factors β_1 and β_2. Similarly packets of random lengths are generated in the range of 64 and 9000 bytes. Therefore each simulated thread, generates packets of

random length at random intervals of time. At the ONU, all the packets were collected and encapsulated into a packet size of 9000 bytes and sent to the OLT. We have used the MTU (Minimum Transfer Unit) to be 9000 bytes. This aids the transfer of packets at higher rates.

5. RESULTS AND DISCUSSION

The results of DBA_GATED and TD-sense algorithms were measured by considering various simulation parameters like delay, data throughput, offered load, traffic type and number of ONUs connected to OLT. Eight ONUs are simulated in one of the systems while the other system has OLT running in it. Exchanging of control messages between OLT and ONU plays an important role for synchronization. It is found that, when the transmission process is on, the low priority control messages get dropped at the socket level of OLT. This occurs because, the OLT, when ready to send data to an ONU1, receives a control message from ONU2. Since the transmission is in progress, the OLT drops this control message from its buffer. As a result, ONU2 starts waiting for the reply and at the same time OLT also waits for the control message from ONU2 which it had sent already. This gives rise to confusion, as OLT and ONU are waiting for each other's responses. To tackle this problem, we modified the communication between OLT and ONU at their socket level. OLT was made to use two sockets of different port numbers to communicate to a particular ONU wherein one socket deals with control message and the other port deals with data transfer. ONU uses the same socket for control message and data.

Packets are generated by various ONUs and transmitted to the OLT. A network bandwidth testing software, 'Netperf' was used to determine average throughput, bytes transmitted and the bytes received with a corresponding delay when the packets move from various ONUs to the OLT. The transceiver cards use 1490 nm as upstream wavelength and 1310 nm as downstream wavelength. The graphs given here (Fig. 1 & 2) show how the TD-sense algorithm is better in performance than the DBA_GATED algorithm. In DBA_GATED algorithm, OLT allocates the time window for the ONU's demands without considering whether the data is delay sensitive or not.

But in case of TD-Sense algorithm, the ONUs are allocated timing windows by OLT as per the report lengths stored in buffer. The data traffic present in the buffer are classified into delay sensitive (Type 0) and delay non sensitive (Type 1). If in a cycle, the buffer contains more number of report lengths of Type 0 traffic than Type 1, then Type 0 utilizes the channel free time. This would lead to Type 1 traffic waiting for subsequent cycles for accessing the channel free time, thus creating bandwidth starvation. TD-sense algorithm solves this by imposing the condition that if Type 0 traffic repeats many times for a given number of cycles, then in the next cycle, the TD-sense algorithm makes Type 1 traffic use the channel free time. Thus it is well suited for both delay sensitive applications like Voice over IP, Video on Demand and delay non-sensitive applications like huge data transfers between users.

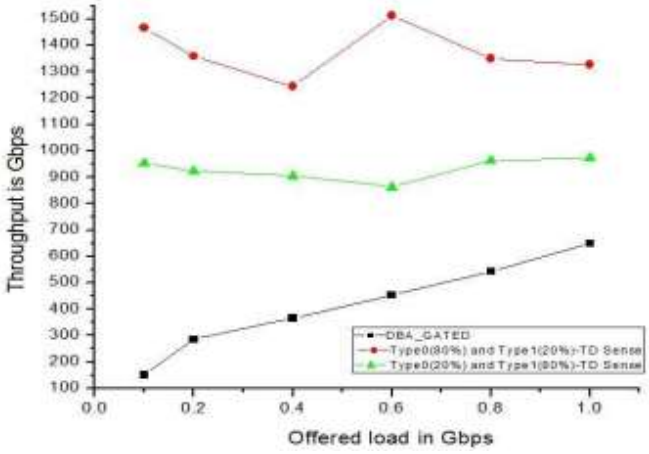

Figure 2: Throughput (Gbps) vs Offred Load (Gbps)

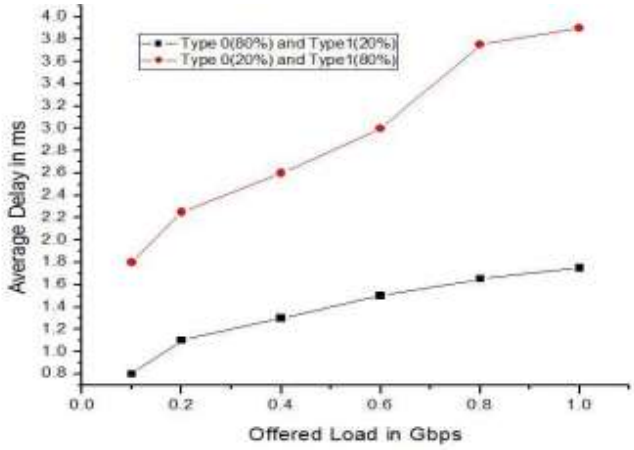

Figure 3: Average Delay (ms) vs Load (Gbps)

Given an offer load, TD-sense algorithm gives better throughput than DBA_GATED algorithm. It can be seen from Fig.1 that when delay sensitive traffic is more i.e., when Type 0 is 80% and Type 1 is 20%, the throughput is maximum in this case. There is a decrease in the throughput when the delay non-sensitive traffic is more i.e., Type 1 is 80% and Type 0 is 20%. In both the cases, TD-sense outperforms the DBA_GATED algorithm.

In DBA-GATED Algorithm the delay increases with increase in offer load. This happens because whatever window size an ONU requests, OLT grants it fully. In case of TD-Sense

Algorithm, the delay is the average delay which is the sum of ONU processing delay, OLT processing delay and Round Trip Delay. It can be seen in Fig.2, that the TD-sense algorithm minimizes the delay when the load is delay sensitive (i.e., Type 0 is 80%) and delay increases when the traffic is not delay sensitive (Type 1 is 80%).

Thus TD-sense algorithm maintains a tradeoff between throughput and delay by classifying the data traffic as delay sensitive and delay non-sensitive. However, we have found that, when the offer load is more than 1 Gbps, the throughput seems to be decreasing, the cause of which is to be explored. This may put a limitation on its applicability for higher offer loads.

6. CONCLUSION

This paper presents a novel 'TD-Sense algorithm' for Triple Play Services by simulating semi real access networks with the use of two 1G transceivers and simulating OLT and ONUs in two different systems. It is found that this algorithm maintains a tradeoff between throughput and delay. Bandwidth starvation is overcome in this algorithm. Also, it is more efficient than the DBA_GATED algorithm in terms of the throughput and delay. Real time video relaying through the network and measuring the network efficiency with the increasing number of ONUs can be further explored.

REFERENCES

[1] Neeharika Jana, Ganesh C. Sankaran, Krishna M.Sivalingam and Gerard Parr, "Performance analysis of dynamic bandwidth allocation algorithms for long reach PONs", IEEE 4th International Symposium on Advanced Networks and Telecommunication Systems,Mumbai,IEEE,3 pp., 2010

[2] A. S. Reaz, L. Shi, and B. Mukherjee, "Broadband access networks: Current and future directions," in Next-Generation Internet: Architectures and Protocols, B. Ramamurthy, G. Rouskas, and K. M. Sivalingam, Eds. Cambridge University Press, 2010.

[3] A. Mady and A. Tonini, "A vhdl implementation of onu auto-discovery process for epon," in Networking and Media Convergence, March 2009.

[4] GW Technologies Co., Ltd., www.gwtt.com, EPON Technology White Paper.

[5] Gutierrez and P. Garfias, "Next generation optical access networks: from tdm to wdm,"Trends in Telecommunications Technologie, 2010 under CC BY-NC-SA 3.0 license.

7. Biographies

Dr. Vibhakar Shrimali (vibhakar.shrimali@gmail.com)

Dr.Vibhakar Shrimali graduated in Electronics and Commicat ion Engineering from MBM Engineering College, Jodhpur, In dia, in 1987, and received his Masters' degree in Electronics a nd Communication Engineering from Delhi College of Engineering, Delhi India. He completed his PhD from IIT

Roorkee, and his research interest includes image processing, signalprocessing,microprocessors&wirelesscommunication. H e has been teaching electronics for the last around 22 years with emphasis to Medical Electronics. He is member of I nstitute of Electrical and Electronics Engineers (IEEE), USA, Society of Engineering in Medicine and Biology, Society (EM BS), USA, a fellow member of Institute of Electronics and Tele communication Engineers (IETE), India, Institute of Engineering (IE), India and Life member of Computer Society of India (CSI).He got selected from Union Public Service Commission(UPSC) in the year 2014 in G.B Pant Govt. Engg. College for the post of Associate Professor in ECE Deptt.

SibaramKhara (sibaram.khara@galgotiasuniversity.edu.in) obtained his M.tech degree in Electronics & Communication Engg. from NIT Allahabad & Doctorate Degree from Jadavpur University. He is currently a Professor in ECE Deptt. of Galgotias University, Greater Noida. He has given the additional charge of Dean(Academics) of University. He has teaching experience of more than 15 years & has presented more than 25 research papers in referred international journals. His research area includes wireless networking, converged networks, SDR(software defined radio) & Cognitive Radio.

ABHISHEK GAUR (a.abhishekgaur@rediffmail.com) *received his B.Tech degree in Electronics & Communication Engineering and M.Tech degree in Digital Communication from Guru Gobind Singh Indraprastha University, Delhi, India in 2010 & 2012 respectively. He is currently working as an Asst. Professor in G.B Pant Govt. Engg. College, Delhi, India in Deptt. of Electronics & Communication Engg. His research interests include Optical-Wireless converged Networks, Optical Access Networks, Consumer Electronics, Heterogeneous Networks (HETNET), LTE Networks, Electrical Machines, Digital Design, Control Systems, Microwaves, Antennas and Wireless Backhauling.*

International Journal of Research (IJR)
e-ISSN: 2348-6848, p- ISSN: 2348-795X Volume 2, Issue 08, August 2015
Available at http://internationaljournalofresearch.org

Analysis of a Heat Pipe to Obtain Maximum Heat Transfer Rate

Anand Prakash Mall
M.Tech (Thermal) Scholar, Delhi Technological University (D.T.U.), New Delhi, India
Mb No: +919415879658
Email Id: anandwrites@gmail.com

ABSTRACT
Maximum heat transfer rate is an important parameter in heat pipe performance. In the present study the maximum heat transfer rate has been calculated by using C++ program for the different operating temperature of a particular heat pipe dimension. For this purpose the selected fluids is water. Taking the dimension as constant and varying the temperature, the maximum heat transfer rate has been calculated.

Keywords: Heat Pipe; Max Heat Transfer Rate; Second Law of Thermodynamics; Entropy Generation; C++ Program; Algorithm

1. INTRODUCTION

A heat pipe is a simple device that can quickly transfer heat from one point to another. They are often referred to as the "superconductors" of heat as they possess an extraordinary heat transfer capacity & rate with almost no heat loss.

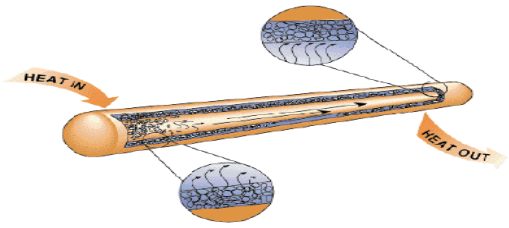

1.1. CONSTRUCTION

It consists of a sealed aluminium or copper container whose inner surfaces have a capillary wicking material. Heat pipe is divided in three regions along its length. These regions are: Evaporator region Adiabatic region Condenser region

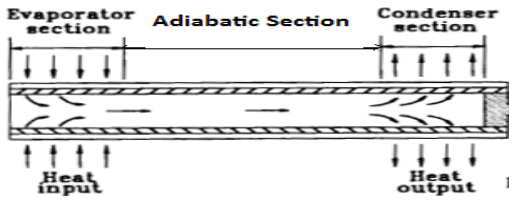

1.2. WORKING PRINCIPLE

Liquid (Inside the container) under its own pressure enters the pores of the capillary material, wetting all internal surfaces.

Applying heat along the surface of the heat pipe causes the liquid at that point to boil and enter a vapor state.

The gas, which then has a higher pressure, moves inside the sealed container to a colder location where it condenses thus giving up the latent heat of vaporization.

International Journal of Research (IJR)
e-ISSN: 2348-6848, p- ISSN: 2348-795X Volume 2, Issue 08, August 2015
Available at http://internationaljournalofresearch.org

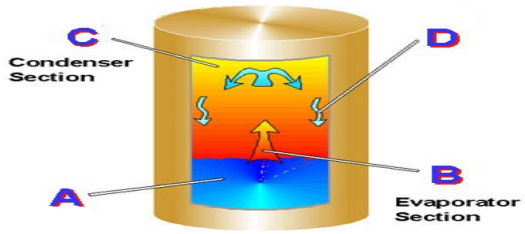

A. Heat is absorbed in the evaporating section.
B. Fluid boils to vapor phase.
C. Heat is released from the upper part of cylinder to the environment; vapor condenses to liquid phase.
D. Liquid returns by to the lower part of cylinder (evaporating section).

1.3. Pressure Variation along a Steady-State Heat Pipe

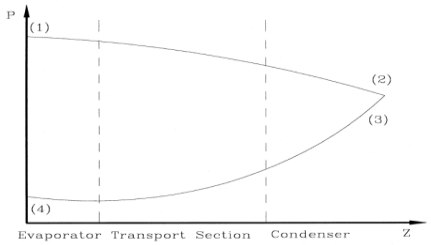

Pressure variation along a steady-state heat pipe.

1.4. Thermodynamic Cycle of a Heat Pipe Working Fluid

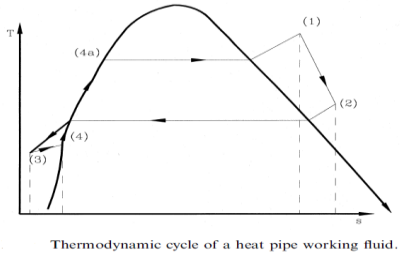

Thermodynamic cycle of a heat pipe working fluid.

1.5. DIFFERENCE BETWEEN HEAT PIPE AND THERMOSYPHON

Heat Pipe can transport heat against gravity by an evaporation-condensation cycle with the help of porous capillaries that form the wick. The wick provides the capillary driving force to return the condensate to the evaporator. This is not possible in Thermosyphon.

In Thermosyphon evaporator always must be below condenser region but in heat pipe there is no such type of condition.

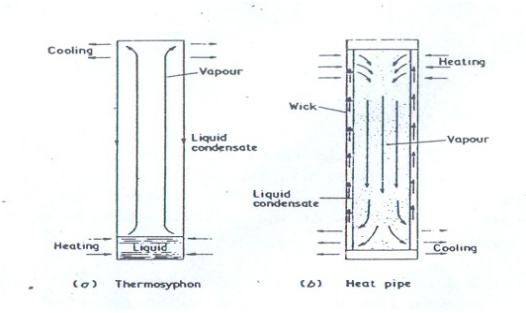

2. PRACTICAL DESIGN CONSIDERATIONS

The three basic components of a heat pipe are:

1. the container
2. the working fluid
3. the wick or capillary structure

In order to design and fabricate heat pipe , a suitable combination of these three components is very necessary .

2.1. The Container

The function of the container is to isolate the working fluid from the outside environment.

It must:

1. be leak-proof
2. maintain the pressure differential across its walls
3. enable transfer of heat to take place from and into the working fluid.

International Journal of Research (IJR)
e-ISSN: 2348-6848, p- ISSN: 2348-795X Volume 2, Issue 08, August 2015
Available at http://internationaljournalofresearch.org

2.1(i) Selection of the container material depends on many factors. These are as follows:

- Compatibility: The container should be compatible with working fluid and external environment. The two major results of incompatibility are corrosion and the generation of non condensable gas.
- Strength to weight ratio: A high strength to weight ratio is more important in spacecraft applications. The material should be non-porous to prevent the diffusion of vapor.
- Thermal conductivity: A high thermal conductivity ensures minimum temperature drop between the heat source and the wick.
- Ease of fabrication, including welding, mach inability and ductility
- Porosity
- Wet ability

2.2. The working fluid

A first consideration in the identification of a suitable working fluid is the operating vapour temperature range. Within the approximate temperature band, several possible working fluids may exist, and a variety of characteristics must be examined in order to determine the most acceptable of these fluids for the application considered.

2.2(i) The prime requirements of working fluid are:

- compatibility with wick and wall materials
- good thermal stability
- wet ability of wick and wall materials
- vapor pressure not too high or low over the operating temperature range
- high latent heat
- high thermal conductivity
- low liquid and vapor viscosities
- high surface tension
- acceptable freezing point

2.3. Wick or Capillary Structure

- The prime purpose of the wick is to generate capillary pressure to transport the working fluid from the condenser to the evaporator.
- It must be able to distribute the liquid around the evaporator section to any area where heat is likely to be received by the heat pipe.
- The selection of the wick for a heat pipe depends on many factors, several of which are closely linked to the properties of the working fluid.

3. THEORY OF HEAT PIPE

In order for the heat pipe to operate the maximum capillary pumping head (ΔPc) max must be greater than the total pressure drop in the pipe.

$(\Delta Pc)\ max >= \Delta Pl + \Delta Pv + \Delta Pg$

Where

ΔPl is the pressure difference in liquid phase.

ΔPv is the pressure difference in vapor phase.

ΔPg is gravitational head.

- The pressure drop ΔPl is required to return the liquid from the condenser to the evaporator.
- The pressure drop ΔPv is necessary to cause the vapor to flow from the evaporator to the condenser.
- The gravitational head ΔPg which may be zero, positive or negative.

International Journal of Research (IJR)
e-ISSN: 2348-6848, p- ISSN: 2348-795X Volume 2, Issue 08, August 2015
Available at http://internationaljournalofresearch.org

3.1. HEAT TRANSFER AND TEMPERATURE DIFFERENCE IN HEAT PIPES

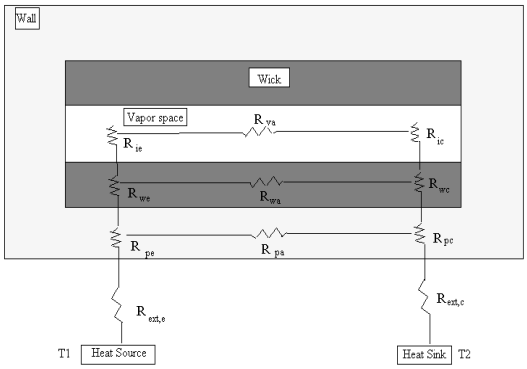

3.2. LIMITS TO HEAT TRANSPORT

- *Entrainment Limit-* at high vapor velocities, droplets of liquid in the wick are torn from the wick and sent into the vapor. Results in dry out.
- *Sonic limit-* occurs when the vapor velocity reaches sonic speed at the evaporator and any increase in pressure difference will not speed up the flow; it seems as if choking has occurred.
- *Viscous Limit-* at low temperatures the vapor pressure difference between the condenser and the evaporator may not be enough to overcome viscous forces. The vapor from the evaporator doesn't move to the condenser and the thermodynamic cycle doesn't occur.
- *Boiling Limit-* occurs when the radial heat flux into the heat pipe causes the liquid in the wick to boil and evaporate causing dry out.
- *Capillary limit-* occurs when the capillary pressure is too low to provide enough liquid to the evaporator from the condenser. Leads to dry out in the evaporator. Dry out prevents the thermodynamic cycle from continuing and the heat pipe no longer functions properly.

3.3.Heat Pipe Performance Map

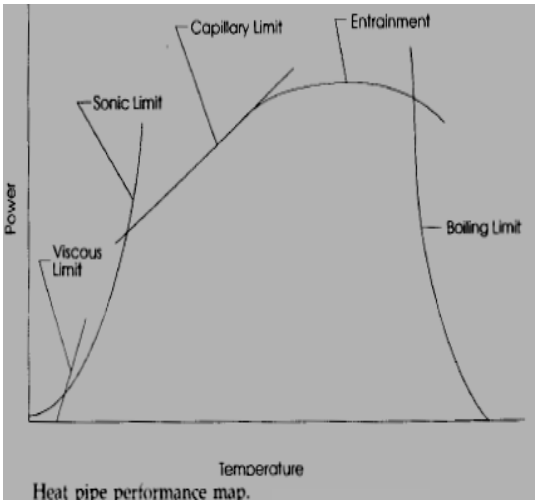

Heat pipe performance map.

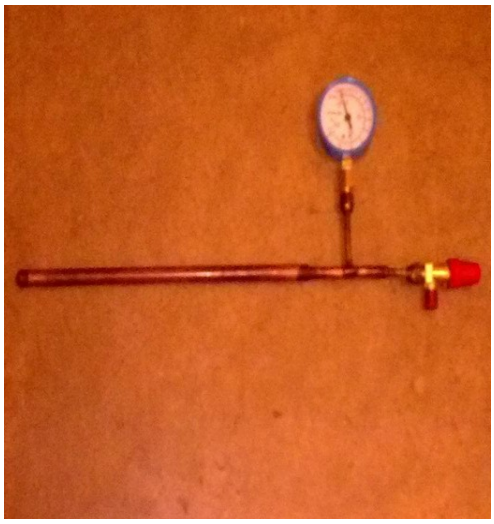

4. HEAT PIPE DESIGN

- **The container :** A copper tube
- **The working fluid :** Distilled Water
- **The wick or capillary structure:** Stainless Steel mesh.

International Journal of Research (IJR)
e-ISSN: 2348-6848, p- ISSN: 2348-795X Volume 2, Issue 08, August 2015
Available at http://internationaljournalofresearch.org

4.1. COMPATIBILITY DATA

WORKING FLUID	COMPATIBALE MATERIAL	INCOMPATIBALE MATERIAL
WATER	STAINLESS STEEL, COPPER, NICKEL, SILICA	ALUMINIUM, INCONEL
METHANOL	STAINLESS STEEL, COPPER, NICKEL, BRASS	ALUMINIUM
AMMONIA	ALUMINIUM, STAINLESS STEEL, COLD ROLLED STEEL, IRON	COPPER
ACETONE	ALUMINIUM, STAINLESS STEEL, COPPER, NICKEL	

REF. FAGHIRI, 1995

4.2.Design Parameters:

- Length of copper tube l= 300 mm
- ID of tube d = 10 mm
- Mesh No. = 250
- Thickness t = 0.18 mm
- Permeability of mesh K= 0.0000302 mm²
- Pore Radius rcap = 0.02 mm
- Critical Temperature of fluid(here water) T= 647.3 K
- Minimum Heat Transferred = 20W

4.3. FLOW CHART

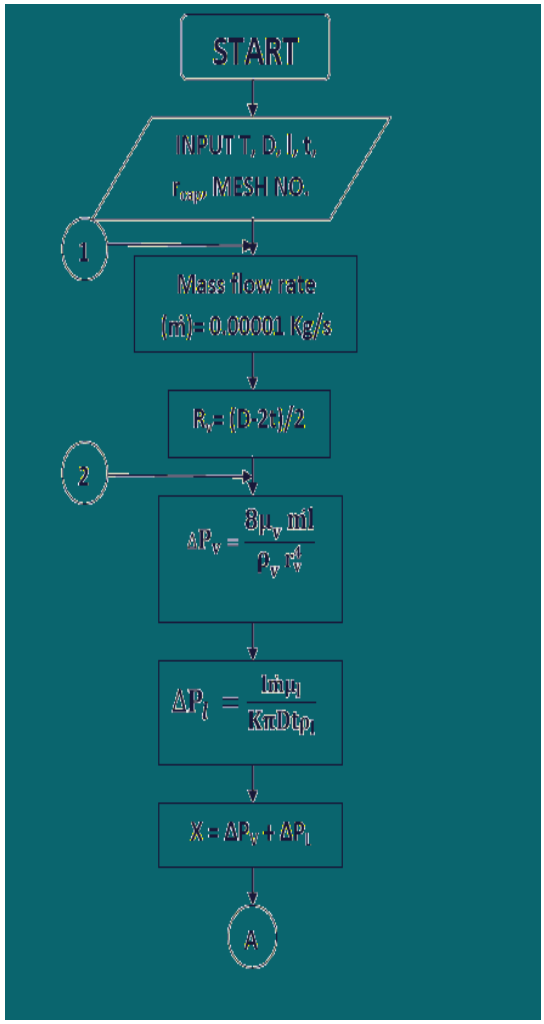

International Journal of Research (IJR)
e-ISSN: 2348-6848, p- ISSN: 2348-795X Volume 2, Issue 08, August 2015
Available at http://internationaljournalofresearch.org

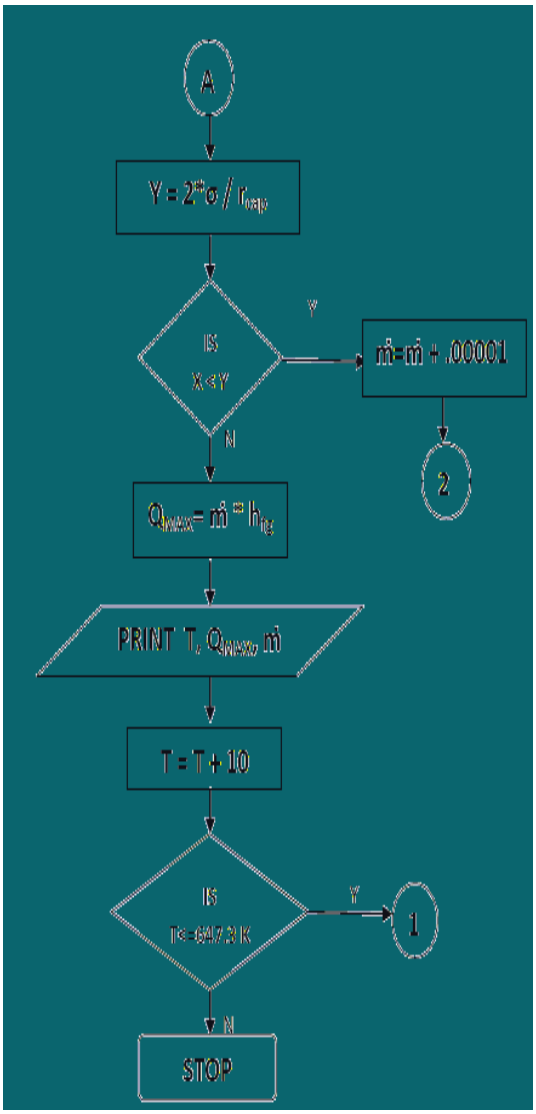

4.4. Program in C++:

```
#include<iostream.h>
#include<conio.h>
#include<math.h>
float vapvis(float);
float vapden(float);
float liqvis(float);
float liqden(float);
float latent(float);
float surften(float);
int main()
{
clrscr ();
int M;
char x;
float
l,D,T,t,r,K,X,Y,Pv,Pl,Pg,m,Re,VV,VD,LV,LD
,LH,ST,ang,an;
cout<<"Enter the length and diameter in mm
of heat pipe"<<endl; cin>>l>>D;
cout<<"enter the temperature in kelvin
"<<endl;
cin>>T;
cout<<"enter the mesh number, thickness of
wick section(mm), pore radius(mm), wick
permeability"<<endl;
cin>>M>>t>>r>>K;
cout<<"enter angle in degrees with
horizontal"<<endl;
cin>>an;
if (an! =0)
{
cout<<"Is condenser above evaporator? if yes
then press y(case sensitive)"<<endl;
cin>>x;
}
Float Rv= (D-2*t)/2; ang=an*3.141592/180;
if (x=='y')
{
```

International Journal of Research (IJR)
e-ISSN: 2348-6848, p- ISSN: 2348-795X Volume 2, Issue 08, August 2015
Available at http://internationaljournalofresearch.org

```
ang=ang*(-1);
}
while (T<=647.3)
{
VV=vapvis(T);
VD=vapden (T);
LD=liqden(T);
LV=liqvis(T);
LH=latent (T);
ST=surften(T);
m=.0000001;
do
{
Y=2*ST*1000/r;
Re=(4*VV*m*1000)/(pow(VD,2)*3.14*(D-2*t)); if(Re<2100.00) //flow is laminar
{
Pv=(8*VV*m*l*pow(10,9))/(VD*pow(Rv,4));
}
else
{
float f=.0791/pow(Re,.25);
Pv=(32*f*m*m*l*pow(10,12))/(3.14*3.14*VD*pow((D-2*t),5));
}
Pl=(LV*l*m*pow(10,9))/(LD*K*3.14*(D-2*t)*t);
Pg=LD*9.81*l*.001*sin(ang);
X=Pv+Pl+Pg;
m=m+.00000001; } while(X<Y);
float Qmax= (m-.00000001)*LH;
cout<<" Max. heat flow rate at temp "<<T<<" is "<<Qmax<<endl<<endl;
T=T+10.0;
}
getch();
}
float vapvis(float T)
{
float a=1.863533364888E-10*pow(T,2) - 1.093174408548E-07*T + 2.503537432010E-05; return a;
}
float vapden(float T)
{
float b=2.465052098940E+02*pow(T,-1.017763280122E+00); return b;
}
float liqvis(float T)
{
float c=1.794037761063E+06*pow (T,-3.756123222676E+00);
return c;
}
float liqden(float T)
{
float d=2.313127868709E-07*pow(T,4) - 2.847655191040E-04*pow(T,3) + 1.270517279667E-01*T*T - 2.458102900740E+01*T + 2.751294205932E+03;
return d;
}
```

International Journal of Research (IJR)
e-ISSN: 2348-6848, p- ISSN: 2348-795X Volume 2, Issue 08, August 2015
Available at http://internationaljournalofresearch.org

```
float latent(float T)
{
float e=-1.153092196908E-08*pow(T,6) +
2.957326884464E-05*pow(T,5)-
3.116886877126E-02*pow(T,4) +
1.724864190563E+01*pow(T,3) -
5.283238375547E+03*pow(T,2) +
8.468846719554E+05*T -
5.283675247708E+07;
return e;
}
float surften(float T)
{
float w=-9.195841005759*pow(10,-8)*T*T-
1.241539247906*pow(10,-
4)*T+1.171567879488*pow(10,-1);
return w;
}
```

4.5.GRAPH BETWEEN QMAX AND T

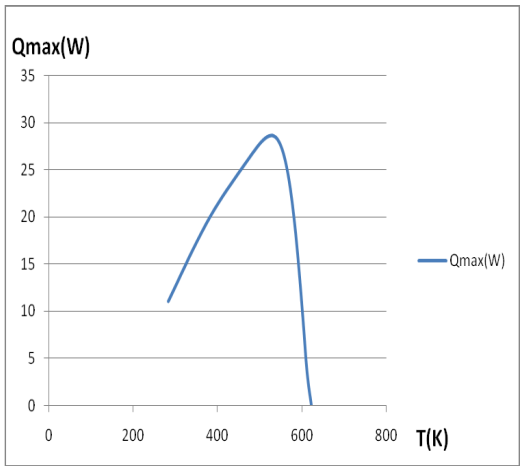

5. CALCULATIONS

In order for the heat pipe to operate the maximum capillary pumping head (Pc)max must be greater than the total pressure drop in the pipe. This pressure drop is made up of three components.

a) The pressure drop P_l required to return the liquid from the condenser to the evaporator.

b) The pressure drop P_v necessary to cause the vapor to flow from the evaporator to the condenser.

c) The gravitational head P_g which may be zero, positive or negative.

Thus

$(\Delta P_C)_{max} >= \Delta P_L + \Delta P_V + \Delta P_G$

If this condition is not met, the wick will dry out in the evaporator region and the pipe will not operate.

5.1.CAPILLARY PRESSURE ΔPc:

Pressure drop across a curved liquid interface is

$\Delta P = 2\sigma_l / R$

$R\cos\theta = r$

Where r is the effective radius of the wick pores and θ the contact angle. Hence the capillary head at the evaporator

$$\Delta P_e = 2\sigma_l\left(\frac{\cos\theta_e}{r_e}\right)$$

Similarly at the condenser

$$\Delta P_c = 2\sigma_l\left(\frac{\cos\theta_c}{r_c}\right)$$

The resultant capillary head will be

$$\Delta P_c = 2\sigma_l\left(\frac{\cos\theta_e}{r_e} - \frac{\cos\theta_c}{r_c}\right)$$

International Journal of Research (IJR)
e-ISSN: 2348-6848, p- ISSN: 2348-795X Volume 2, Issue 08, August 2015
Available at http://internationaljournalofresearch.org

This will have a maximum value when
$\cos\theta_e = 1$ and $\cos\theta_c = 0$.

Hence $(\Delta P_c)_{max} = \frac{2\sigma_1}{r_e}$

5.2.PRESSURE DIFFERENCE DUE TO FRICTION FORCES:

In this section we will consider the pressure differences in the liquid and vapor phases which are caused by frictional forces.

Laminar Flow - the Hagen Poiseuille equation: The steady state laminar flow of an incompressible fluid of constant viscosity μ, through a tube of circular cross section, radius a, is described by the Hagen-Poiseuille equation.This equation relates the velocity v_r of the fluid, at radius r, to the pressure difference P_2-P_1 across a tube length l.

$$v_r = \frac{a^2}{4\mu}\left[1 - \left(\frac{r}{a}\right)^2\right]\frac{P_2 - P_1}{l}$$

Turbulent Flow – the Fanning equation: The pressure drop for turbulent flow is usually related to the average velocity by the Fanning equation:

$$\frac{P_2 - P_1}{l} = \frac{4}{d} f \frac{1}{2}\rho v^2$$

Where f is the fanning factor.

f is related to Reynold's number and in the turbulent region is given by the Blasius equation:

$$f = \frac{0.0791}{Re^{0.25}} \quad , 2100 < R_e < 10^5$$

We see that if we write $f = \frac{16}{Re}$ for Re < 2100 the fanning equation reduces to the Hagen-Poiseuille form.

5.3.PRESSURE DIFFERENCE IN THE LIQUID PHASE ΔPl:

The flow regime in the liquid phase is almost always laminar. Since the liquid channels will not in general be straight nor of circular cross-section and will often be interconnected the Hagen-Poiseuille equation must be modified to take account of these differences.

It is usual for homogenous wick structure to use Darcy's Law for the calculation of ΔP_l.

Darcy's Law is written as

$$\Delta P_1 = \frac{\mu_1 l\dot{m}}{\rho_1 KA}$$

Where K is the wick permeability
A is the wick cross sectional area

5.4.PRESSURE DIFFERENCE IN VAPOR PHASE ΔPv:

The total vapour phase difference in pressure will be the sum of the pressure drops in the three regions, namely the evaporator drop ΔP_{ve} the adiabatic section drop ΔP_{va}, and the pressure drop in the condensing region ΔP_{vc}.

In the evaporator region the vapor pressure gradient will be necessary to carry out two functions.

1. To accelerate the vapour entering the evaporator section up to the axial velocity v. Since on entering the evaporator this vapour will have radial velocity but no axial velocity. The necessary pressure gradient will be termed as the inertial term ΔP_v'.

International Journal of Research (IJR)
e-ISSN: 2348-6848, p- ISSN: 2348-795X Volume 2, Issue 08, August 2015
Available at http://internationaljournalofresearch.org

2. To overcome frictional drag forces at the surface r=r_v at the wick. This is the viscous term $\Delta P_v''$.

$$\Delta P_v' = \rho v^2$$

$$\Delta Pv'' = \left(\frac{8\mu_v \dot{m}}{\pi r_v^4}\right)\frac{l_e}{2}$$

Hence

$$\Delta P_{ve} = \Delta P_v' + \Delta P_v''$$

$$= \rho v^2 + \left(\frac{8\mu_v \dot{m}}{\pi r_v^4}\right)\frac{l_e}{2}$$

The condenser region may be treated in a similar manner, but in this case axial momentum will be lost as the vapour stream is brought to rest so the inertial term will be negative, that is there will be pressure recovery. For the simple theory the two inertial terms will cancel and the total pressure drop in the vapour phase will be due entirely to the viscous terms.

In the adiabatic region the pressure difference will contain only the viscous term which will be given either by the Hagen-Poiseuille equation or the Fanning equation depending on whether the flow is laminar or turbulent.

For Laminar Flow:

$$\Delta P_{va} = \frac{8\mu_v m}{\pi r_v^4} l_a$$

for $R_e \leq 2100$

For Turbulent Flow:

$$\Delta P_{va} = \frac{2}{r_v} f \frac{1}{2} \rho_v v^2 l_a$$

for $R_e > 2100$

where $f = \frac{0.0791}{R_e^{0.25}}$

Hence the total vapour pressure drop is given by:

$$\Delta P_v = \Delta P_{ve} + \Delta P_{vc} + \Delta P_{va}$$

$$= \rho v^2 + \frac{8\mu_v \dot{m}}{\pi r_v^4}\left[\frac{l_e + l_c}{2} + l_a\right]$$

for laminar flow and no pressure recovery

$$\Delta P_v = \frac{8\mu_v \dot{m}}{\pi r_v^4}\left[\frac{l_e + l_c}{2} + l_a\right]$$

for laminar flow with full pressure recovery.

5.5.GRAVITATIONAL HEAD:

The pressure difference due to the hydrostatic head of the liquid may either be positive, negative or zero, depending on the relative positions of the evaporator and condenser. This pressure difference ΔP_g is given by the expression

$$\Delta P_g = \rho_l g \sin\Phi$$

Where ρ_l is the liquid density

g is the acceleration due to gravity

l is the heat pipe length

ϕ the angle made by the heat pipe with the horizontal.(ϕ is positive when the condenser is lower than the evaporator)

5.6.LIMITS TO HEAT TRANSPORT:

Upper limits to the heat transport capability of a heat pipe may be set by one or more factors.

Viscous Limit: At low temperature viscous forces are dominant in the vapour flow down the pipe. Busse has shown that the axial heat flux rapidly increases as the pressure in the condenser is reduced, the maximum heat flux occurring when the pressure is reduced to the zero. Busse carried out a two dimensional

International Journal of Research (IJR)
e-ISSN: 2348-6848, p- ISSN: 2348-795X Volume 2, Issue 08, August 2015
Available at http://internationaljournalofresearch.org

analysis, finding that the radial velocity component had a significant effect, he derived the following equation

$$q = \frac{rL\rho_v P_v}{16\mu_v^l}$$

Where P_v and ρ_v evaporator end of the pipe.

This equation agrees well with published data.
Sonic Limit: At a somewhat higher temperature choking at the evaporator exit may limit the total power handling capability of the heat pipe.

The sonic limit is given by:

$q=0.474\ L\ (\rho_v\ p_v)^{1/2}$

There is good agreement between this formula and experimental results.

Entrainment limit: Following equation gives the entrainment limiting flux

$$q= \sqrt{\frac{2\pi\rho_v L^2\sigma_l}{Z}}$$

Kemme's experiments suggest a rough correlation of this failure mode with the centre to centre wire spacing for z, and that a very fine screen will suppress entrainment.
Capillary Limits, (wicking Limits). In order for the heat pipe to operate, equation must be

satisfied, namely

$\Delta P_{c\ max} > \Delta P_l + \Delta P_v + \Delta P_g$

An expression for the maximum flow rate m_{max} may readily be obtained if we assume

1. The liquid properties do not vary along the pipe

2. The wick is uniform along the pipe

3. The pressure drop due to vapour flow can be neglected.

$$m_{max} = \left[\frac{\rho_l\sigma_l}{\mu_l}\right]\left[\frac{KA}{l}\right]\left[\frac{2}{r_e} - \frac{\rho_l g l}{\sigma_l}sin\Phi\right]$$

And the corresponding heat transport Q_{max}

$Q_{max} = m_{max}L$

$$= \left[\frac{\rho_l\sigma_l L}{\mu_l}\right]\left[\frac{KA}{l}\right]\left[\frac{2}{r_e} - \frac{\rho_l g l}{\sigma_l}sin\Phi\right]$$

The group $\frac{\rho_l\sigma_l L}{\mu_l}$ depends only on the properties of the working fluid and is known as the figure of merit M.
Burnout: Burnout will occur at the evaporator at high radial fluxes. A similar limit on peak radial flux will also occur at the condenser. For water and other non metallics vapour production in the wick become important a lower flux densities (130 KW/m^2) and there are no simple correlation. Because of phase equilibrium at interface, liquid at the evaporator **is** always superheated to some degree, but it is difficult to specify the degree of superheated needed to initiate bubbles in the wick. While boiling is often taken as a limiting feature in wicks, possibly upsetting the capillary action, Cornwell and Nair found that nucleation reduces the radial temperature difference and increases heat pipe conductance. One factor in support of this is the increased thermal conductivity of liquid saturated wicks in evaporator section, compared with that in the condenser.

Time believed that the time limit will become effective only when the bubbles generated within the wick become trapped there, forming a

International Journal of Research (IJR)
e-ISSN: 2348-6848, p- ISSN: 2348-795X Volume 2, Issue 08, August 2015
Available at http://internationaljournalofresearch.org

vapor blanket. Thus, some enhancement of radial heat transferring the evaporator section can be obtained by nucleate boiling effects.

6. CONCLUSION

- Heat pipe is tested in horizontal orientation.
- Rate of max heat transfer through the heat pipe has been calculated at different operating temperature.
- A graph has been plotted between max heat transfer rate and operating temperature.
- By seeing the graph ,we can select the operating temperature to minimize entropy generation in heat pipe.
- Heat transferred through Heat Pipe is approximately **15 times** the heat transferred through pure conduction in heat pipe.

6.1. ADVANTAGES

- Simple Structure
- Relatively Inexpensive
- Insensitive to gravitational field
- Silent and Reliable in its operation

6.2.APPLICATIONS

1. Space Technology

- Spacecraft temperature equalization
- Component cooling, temperature control and radiator design in satellites.
- Other applications include moderator cooling, removal of heat from the reactor at emitter temperature and elimination of troublesome thermal gradients along the emitter and collector in spacecrafts.

2. Heat pipes for Dehumidification and Air conditioning

3. Notebook and mobile PCs thermal control.

7. REFERENCES

[1] Cotter T.P., Principles and prospects for micro heat pipe, 5th International Heat Pipe Conference, Tsukuba, Japan, May 14-18, 1984.

[2]Gorla Rama Subba Reddy, Byrd Larry W., Pratt David M., Second law analysis for microscale flow and heat transfer, Applied Thermal Engineering 27 (2007) 1414–1423.

[3]Heat Pipe Design Handbook, National Aeronautics and Space Administration Goddard Space Flight Center Greenbelt, Maryland 2077, June 1979.

[4]Hung Y.M., Seng Q., Effects of geometric design on thermal performance of star-groove micro-heat pipes, International Journal of Heat and Mass Transfer 54 (2011) 1198–1209.

[5]Khalkhali H., Faghri A., Zuo Z.J., Entropy generation in a heat pipe system, Applied Thermal Engineering 19 (1999) 1027-1043.

[6]Kumar Vikas, Gangacharyulu D., Tathgirh Ram Gopal, Heat Transfer Studies of a Heat Pipe, Heat Transfer Engineering, 28(11):954–965, 2007.

[7]Lin Lanchao, Ponnappan Rengasamy, Leland John, High performance miniature heat pipe, International Journal of Heat and Mass Transfer 45 (2002) 3131–3142.

[8]P.Maheshkumar, C. Muraleedharan, Minimization of entropy generation in flat heat pipe, International Journal of Heat and Mass Transfer 54 (2011) 645–648.

[9]Reay D.A., Kew P.A., Heat Pipes, Fifth Edition 2006, Butterworth-Heinemann.

[10]Sugumar D., Tio Kek-Kiong, The Effects of Working Fluid on the Heat Transport Capacity of a Microheat pipe, ASME J. Heat Transfer January 2009, Vol. 131.

[11]Suh Jeong-Se, Greif Ralph, Grigoropoulos Costas P., Friction in micro-channel flow of a

liquid and vapour in trapezoidal and sinusoidal grooves, International Journal of Heat and Mass Transfer 44 (2001) 3103-3109.

[12]Tio Kek-Kiong, Liu Chang Yu, Toh Kok Chuan, Thermal analysis of micro heat pipes using a porous-medium model, Heat and Mass Transfer 36 (2000) 21-28.

[13]Vasiliev L.L., Micro and miniature heat pipes – Electronic component coolers, Applied Thermal Engineering 28 (2008) 266–273.

[14]Zuo Z.J, Faghri A., A network thermodynamic analysis of the heat Pipe, Int. J. Heat Mass Transfer. Vol. 41, No. 11 (1998) 1473-1484.

[15] P.D. Dunn and D.A.Reay, Heat Pipes, 4th Edition, Pergamon, New York[1994]

International Journal of Research (IJR)
e-ISSN: 2348-6848, p- ISSN: 2348-795X Volume 2, Issue 08, August 2015
Available at http://internationaljournalofresearch.org

Optimization of Effective Parameters of Neem Oil Biodiesel using Taguchi Method and Anova

Anand Prakash Mall[1] & Amit Pal[2]

[1]M.Tech (Thermal) Scholar, Delhi Technological University (DTU), New Delhi, India
Mb No: +919415879658: E-mail:anandwrites@gmail.com
[2]Dr. Amit Pal (Associate Professor), Dept. of Mechanical Engineering, Delhi Technological University (DTU), New Delhi, India
Mb No: Mb No: +919868543545: E-mail:amitpal@dce.ac.in

ABSTRACT

Currently, most of the biodiesel is produced from the edible/refined type oil using methanol and alkaline catalyst. However, large amount of non-edible type oils and fats are available in our country. In this study, crude neem oil is used as alternative fuel for biodiesel production. The difficulty with alkaline transesterification of these oils has contained large amounts of free fatty acids (FFA). These free fatty acids quickly react with the alkaline catalyst to produce soaps that inhibit the separation of the ester and glycerin.

A two-step transesterification process is developed to convert the high FFA oils to its mono-esters. Using 100 ml of oil, the optimum combination of parameters for pretreatment were found to be 0.45 v/v methanol-oil-ratio, 0.5% v/v H_2SO_4 acid catalyst, 50˚C and 45 min reaction time. After pretreatment of neem oil, transesterification reaction was carried out with 4.5:1 methanol-to-oil molar ratio, 1% KOH as alkaline catalyst, 75 min reaction time and 50˚C reaction temperature to produce the fatty acid methyl ester. This two step process gave maximum average yield of 70±2%.

Key Words: Optimization; Taguchi Method; Analysis of Variance (ANOVA) Method; Neem Oil Methyl Ester (Biodiesel)

International Journal of Research (IJR)
e-ISSN: 2348-6848, p- ISSN: 2348-795X Volume 2, Issue 08, August 2015
Available at http://internationaljournalofresearch.org

1. INTRODUCTION:

The use of alternative fuels instead of conventional fossil fuels is becoming increasingly significant due to decreasing petroleum reserves and increasing greenhouse gases, all of which lead to global warming, ozone depletion and political and health concerns (Fukuda et al., 2001). Plant oils have been used as alternative fuels for many years, since they are renewable and readily available. However, these oils cannot be used directly as fuel sources in diesel engines due to: (a) high viscosity which leads to poor fuel atomization during the injection process, (b) low volatility and (c) polymerization which results in deposit formation, incompletion combustion and poor emissions (Ma and Hanna, 1999; Meher et al., 2006). To overcome these disadvantages, oils can be converted into fatty acid methyl esters (FAME) which are also known as biodiesel. Biodiesel is an alternative fuel that is non-toxic, completely biodegradable and renewable and can be adapted easily without any modification to diesel engines.

Several processes have been developed for biodiesel production, such as pyrolysis, micro emulsification and transesterification. The chemical change of the products from the reactants caused by the thermal energy in the presence of air or nitrogen sparging is called a pyrolytic process. These products are similar to the petroleum-derived fuel. However, during the pyrolysis process, the removal of oxygen leads to reduce the environmental benefits (Ma and Hanna, 1999). The problem of the high viscosity of the substrates has been investigated using microemulsions with solvents (methanol, ethanol and 1-butanol) to meet the international standards of petroleum-derived fuels. However, an increase of lubricating oil viscosity, irregular injector needle sticking, incomplete combustion and heavy carbon deposits were reported in the laboratory screening endurance test. Therefore, transesterification process plays a vital role, in order to overcome these disadvantages.

The process of displacing alcohol from an ester to form another ester is called transesterification. Transesterification is the most simple and efficient method to produce biodiesel by using acids, alkalis, or enzymes as catalysts. Triglycerides with high free fatty acid and water contents are not essential for a biodiesel conversion process using an acid catalyst. However, the reaction rates are slower than those of the alkali catalytic process (Freedman et al., 1986). The alkali-catalysis transesterification process has been widely used in the biodiesel industry, because it gives a high yield of conversion of fatty acid methyl esters from triglycerides at low temperatures and pressures in a relatively short reaction time of 4-10 hours. However, it has several drawbacks including product separation, soap formation and negative environmental impacts such as greenhouse gas, CO, hydrocarbons, NOx and particles in exhaust emissions (Nielsen et al., 2008).

Neem is a tree in the family ‘maliaceae’ which grows various parts in Bangladesh. It’s scientific name ‘Azadirachtaindica’. The evergreen tree is large, reaching 12 to 18 meters in height with a girth of up to 1.8 to 2.4 meters. The seeds have 40% oil which has high potential for the production of biodiesel. It has a higher molecular weight, viscosity, density, and flash point than diesel fuel. Neem oil is generally light to dark brown, bitter and has a

International Journal of Research (IJR)
e-ISSN: 2348-6848, p- ISSN: 2348-795X Volume 2, Issue 08, August 2015
Available at http://internationaljournalofresearch.org

strong odor that is said to combine the odors of peanut and garlic [M.A. Fazal et al., 2011].

Neem comprises mainly of triglycerides and large amounts of triterpenoid compounds. It contains four significant saturated fatty acids, of which two are palmitic acid and two are stearic acid. It also contains polyunsaturated fatty acids such as oleic acid and linoleic acids [Muthu et al., 2010]

2. Taguchi Method to Optimize the Process Parameters:

Taguchi method is based on performing evaluation or experiments to test the sensitivity of a set of response variables to a set of control parameters (or independent variables) by considering experiments in "orthogonal array" with an aim to attain the optimum setting of the control parameters. Orthogonal arrays provide a best set of well balanced (minimum) experiments. Table2 (a) Shows eighteen standard orthogonal arrays along with the number of columns at different levels for these arrays. An array name indicates the number of rows and columns it has, and also the number of levels in each of the columns. For example array L4 (23) has four rows and three "2 level" columns. Similarly the array L18 (2137) has 18 rows; one "2 level" column; and seven "3 level" columns. Thus, there are eight columns in the array L18. The number of rows of an orthogonal array represents the requisite number of experiments. The number of rows must be at least equal to the degrees of the freedom associated with the factors i.e. the control variables. In general, the number of degrees of freedom associated with a factor (control variable) is equal to the number of levels for that factor minus one. For example, a case study has one factor (A) with "2 levels" (A), and five factors (B, C, D, E, F) each with "3 level". Table 2(b) depicts the degrees of freedom calculated for this case. The number of columns of an array represents the maximum number of factors that can be studied using that array.

Table 2(a) Standard orthogonal arrays

Orthogonal array	Number of rows	Maximum number of factors	Maximum number of columns at these levels			
			2	3	4	5
L_4	4	3	3	-	-	-
L_8	8	7	7	-	-	-
L_9	9	4	-	4	-	-
L_{12}	12	11	11	-	-	-
L_{16}	16	15	15	-	-	-
L_{16}'	16	5	-	-	5	-
L_{18}	18	8	1	7	-	-
L_{25}	25	6	-	-	-	6
L_{27}	27	13	-	13	-	-
L_{32}	32	31	31	-	-	-
L_{32}'	32	10	1	-	9	-
L_{36}	36	23	11	12	-	-
L_{36}'	36	16	3	13	-	-
L_{50}	50	12	1	-	-	11
L_{54}	54	26	1	25	-	-
L_{64}	64	63	63	-	-	-
L_{64}'	64	21	-	-	21	-
L_{81}	81	40	-	40	-	-

International Journal of Research (IJR)
e-ISSN: 2348-6848, p- ISSN: 2348-795X Volume 2, Issue 08, August 2015
Available at http://internationaljournalofresearch.org

The signal to noise ratios (S/N), which are log functions of desired output, serve as the objective functions for optimization, help in data analysis and the prediction of the optimum results. The Taguchi method treats the optimization problems in two categories: static problems and dynamic problems. For simplicity, the detailed explanation of only the static problems is given in the following text. Next, the complete procedure followed to optimize a typical process using Taguchi method is explained with an example.

Table 2(b) The degrees of freedom for one factor (A) in "2 levels" and five factors (B, C, D, E, F) in "3 levels"

Factors	Degrees of freedom
Overall mean	1
A	2-1 = 1
B, C, D, E, F	5 × (3-1) = 10
Total	12

Static problems

Generally, a process to be optimized has several control factors (process parameters) which directly decide the target or desired value of the output. The optimization then involves determining the best levels of the control factor so that the output is at the target value. Such a problem is called as a "STATIC PROBLEM". This can be best explained using a P-Diagram (Figure 2(a)) which is shown below ("P" stands for Process or Product). The noise is shown to be present in the process but should have no effect on the output. This is the primary aim of the Taguchi experiments - to minimize the variations in output even though noise is present in the process. The process is then said to have become ROBUST.

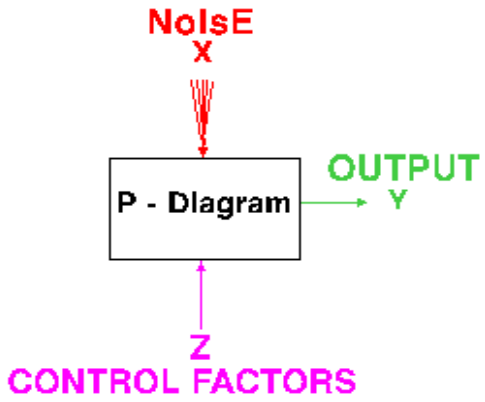

Figure 2(a) P-Diagram for static problems.

Signal to Noise (S/N) Ratio:

There are three forms of signal to noise (S/N) ratio that are of common interest for optimization of static problems.

[1] Smaller-the-better

This is expressed as

$n = -10 \log_{10}$ [mean of sum of squares of measured data]

This is usually the chosen S/N ratio for all the undesirable characteristics like "defects" for which the ideal value is zero. When an ideal value is finite and its maximum or minimum value is defined (like the maximum purity is 100% or the maximum temperature is 92 K or the minimum time for making a telephone connection is 1 sec) then the difference between the measured data and the ideal value is expected to be as small as possible. Thus, the generic form of S/N ratio becomes,

$n = -10 \log_{10}$ [mean of sum of squares of {measured – ideal}]

[2] Larger-the-better

This is expressed as

International Journal of Research (IJR)
e-ISSN: 2348-6848, p- ISSN: 2348-795X Volume 2, Issue 08, August 2015
Available at http://internationaljournalofresearch.org

n = −10 Log_{10} [mean of sum of squares of reciprocal of measured data]

This is often converted to smaller-the-better by taking the reciprocal of the measured data and next, taking the S/N ratio as in the smaller-the-better case.

[3] Nominal-the-best

This is expressed as

$$n = -10Log_{10}\left[\frac{square\ \ of\ mean}{variance}\right]$$

This case arises when a specified value is the most desired, meaning that neither a smaller nor a larger value is desired.

Application of Taguchi Method:

Determine the effect of four process parameters: Reaction temp (A), Catalyst Concentration (wt %) (B), Molar ratio (Methanol/Oil) (C) and Reaction time (D) on the yield of Neem Oil Methyl Ester (NOME). Also estimate the optimum setting of the above process parameters for maximum yield. Table 2(c) depicts the factors and their levels.

Table2(c) Factors and their levels

Factor		Levels		
		1	2	3
A	Reaction Temp (°C)	50	55	60
B	Catalyst Concentration (wt %)	1.0	1.25	1.50
C	Molar Ratio (Methanol/Oil)	4.5	6.0	7.5
D	Reaction Time(min)	55	65	75

2.1. Selection of the design matrix and performing the experiments

The present experiment is associated with four factors with each at three levels. Table 2(a) indicates that the best suitable orthogonal array is L9. Table 2(d) shows the design matrix for L9. Next conduct all the nine experiments and observe % yield of neem oil methyl ester (NOME). The summary statistic, ηi, for an experiment, i, is given by

$$n_i = -10Log_{10}\,C_i$$

where Ci refers to mean squared deviation for experiment i and the mean square refers to the average of the squares of the nine observations in the experiment i. Table 2(d) also depicts the observed value of ηi for all the nine experiments. This summary statistic ηi is called the signal to noise (S/N) ratio.

Table 2(d) L_9 array matrix experiment table.

Expt No	Column number and factor assigned				
	1 Reaction Temp (°C) (A)	2 Catalyst Concentration (wt %) (B)	3 Molar Ratio (Methanol/ Oil) (C)	4 Reaction Time (min) (D)	Observation, η (%)
1	1	1	1	1	37.14

International Journal of Research (IJR)
e-ISSN: 2348-6848, p- ISSN: 2348-795X Volume 2, Issue 08, August 2015
Available at http://internationaljournalofresearch.org

2	1	2	2	2	36.85
3	1	3	3	3	36.81
4	2	1	2	3	36.68
5	2	2	3	1	36.22
6	2	3	1	2	36.42
7	3	1	3	2	35.71
8	3	2	1	3	35.83
9	3	3	2	1	35.55

Table2 (e) Yield of Neem Oil Methyl Ester and S/N ratio (η)

Exp. No	**% Yield of Neem Oil Methyl Ester(NOME)**				**S/N ratio (η)**
	Sample 1	**Sample 2**	**Sample 3**	**Mean**	
1	70.8	73.9	71.3	72.0	37.14
2	65.2	70.4	74.1	69.9	36.85
3	68.9	70.2	68.8	69.3	36.81
4	66.6	69.2	69.1	68.3	36.68
5	61.8	68.5	64.4	64.9	36.22
6	65.8	67.9	65.2	66.3	36.42
7	58.2	63.5	61.9	61.2	35.71
8	57.3	66.6	63.0	62.3	35.83
9	58.2	61.4	60.4	60.0	35.55
			Mean	**66.0**	**36.35**

According to the analysis for the case of larger the better the mean squared deviations (MSD) of each experiment were evaluated using the following equation

$$MSD = \frac{1}{n} \sum_{i=1}^{n} (\frac{1}{y_i})^2$$

Where n is the number of repetitions of each experiment and yi the yield of Neem Oil methyl ester.

Then the S/N ratio was evaluated using the equation

S/N ratio = -10 Log (MSD)

The effect of parameter level is defined as the deviation it causes from the overall mean. Hence as a first step , calculating the overall mean value of S/N ratio for the experimental region defined by the factor levels in Table 2(f).

2.2. Calculation of factor effects

The effect of a factor level is defined as the deviation it causes from the overall mean. Hence as a first step, calculate the overall mean value of η for the experimental region defined by the factor levels in Table 2(d) as

$$m = \frac{1}{9}\sum_{i=1}^{9} n_i = \frac{1}{9}(n_1 + n_2 + n_3 + \cdots + n_9) = 36.35$$

The effect of the temperature at level A1 (at experiments 1, 2 and 3) is calculated as the difference of the average S/N ratio for these experiments (mA1) and the overall mean. The same is given as

The effect of temperature at level

$$A_1 = m_{A1} - m = \frac{1}{3}(n_1 + n_2 + n_3) - m$$

International Journal of Research (IJR)
e-ISSN: 2348-6848, p- ISSN: 2348-795X Volume 2, Issue 08, August 2015
Available at http://internationaljournalofresearch.org

Similarly,

The effect of temperature at level

$$A_2 = m_{A2} - m = \frac{1}{3}(n_4 + n_5 + n_6) - m$$

The effect of temperature at level

$$A_3 = m_{A3} - m = \frac{1}{3}(n_7 + n_8 + n_9) - m$$

Using the S/N ratio data available in Table 2(d). The average of each level of the four factors is calculated and listed in Table 2(f). These average values are shown in Figure 2(b) they are separate effect of each factor and are commonly called main effects.

Table 2(f) Average η for different factor levels

Factor		Levels		
		1	2	3
A	Reaction Temp (°C)	36.93*	36.44	35.69
B	Catalyst Concentration (wt %)	36.51*	36.30	36.26
C	Molar ratio(Methanol/ Oil)	36.46*	36.36	36.24
D	Reaction Time(min)	36.30	36.32	36.44*

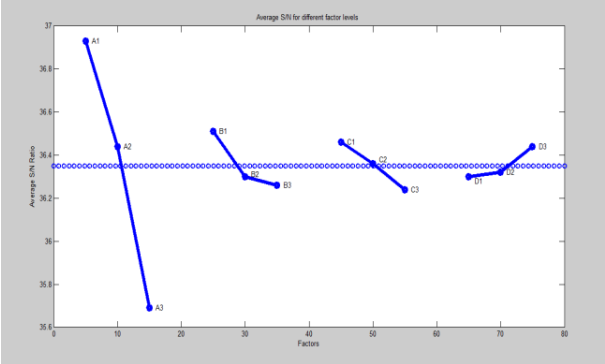

Figure 2(b) Plots of factor effects

2.3. Selecting optimum factor levels

Our goal in this experiment is to maximize the yield of Fatty Acid Methyl Ester (FAME). Since –log depicts a monotonic decreasing function, we have to maximize η. Hence the optimum level for a factor is the level that gives the highest value of η in the experimental region. From Figure 2(b) and the Table 2(f), it is observed that the optimum settings of reaction temp, catalyst concentration (wt %), molar ratio (methanol/oil) and reaction time are A1, B1, C1 and D3. Hence we can conclude that the setting A1B1C1D3 can give the highest η for Neem Oil Methyl Ester.

2.4. Developing the additive model for factor effects

The relation between η and the process parameters A, B, C and D can be approximated adequately by the following additive model:

$$n(A_i + B_j + C_k + D_l) = m + a_i + b_j + c_k + d_l + e$$

Where the term m refers to the overall mean (that is the mean of η for the experimental region). The terms ai, bj, ck and dl refer to the deviations from μ caused by the setting Ai, Bj, Ck, and Dl of factors A, B, C and D, respectively. The term e stands for the error. In additive model the cross- product terms

International Journal of Research (IJR)
e-ISSN: 2348-6848, p- ISSN: 2348-795X Volume 2, Issue 08, August 2015
Available at http://internationaljournalofresearch.org

involving two or more factors are not allowed. The above equation is utilized in predicting the S/N ratio at optimum factor levels.

2.5. Analysis of Variance (ANOVA)

Different factors affect the yield of NOME to a different degree. The relative magnitude of the factor effects are listed in Table 2(f). A better feel for the relative effect of the different factors is obtained by the decomposition of variance, which is commonly called as analysis of variance (ANOVA). This is obtained first by computing the sum of squares.

$Total\ Sum\ of\ Squares = \sum_{i=1}^{9} n_i^2 =$
$((37.14)^2 + (36.85)^2 + \cdots \ldots + (35.55)^2) =$
11898.80

$Sum\ of\ Squares\ Due\ to\ Mean$
$= (Number\ of\ Exp.)\ X\ m^2$
$= 9\ X\ (36.35)^2 = 11891.90$

$Total\ Sum\ of\ Squares(Sum\ of\ Squares\ of\ all\ 9\ Experiments) = \sum_{i=1}^{9} (n_i - m)^2 = 2.54$

$Sum\ of\ Squares\ due\ to\ factor\ A$
$= [(Number\ of\ Experiments\ at\ level\ A1) \times (m_{A1} - m)^2]$
$+ [(Number\ of\ Experiments\ at\ level\ A2) \times (m_{A2} - m)^2]$
$+ [(Number\ of\ Experiments\ at\ level\ A3) \times (m_{A3} - m)^2]$
$= [3 \times (36.93 - 36.35)^2]$
$+ [3 \times (36.44 - 36.35)^2]$
$+ [3 \times (35.69 - 36.35)^2] = 2.34$

$Sum\ of\ Squares\ due\ to\ factor\ B =$
$[(Number\ of\ Experiments\ at\ level\ B1) \times$ *mB1 –m2+ Number of Experiments at level B2× mB2 –m2+ Number of Experiments at level B3× mB3 –m2=3×36.51−36.352+ 3×36.30−36.352+* $[3 \times (36.26 - 36.35)^2] = 0.11$

$Sum\ of\ Squares\ due\ to\ factor\ C =$
$[(Number\ of\ Experiments\ at\ level\ C1) \times$ *mC1 –m2+ Number of Experiments at level C2× mC2 –m2+ Number of Experiments at level C3× mC3 –m2=3×36.46−36.352+ 3×36.36−36.352+* $[3 \times (36.24 - 36.35)^2] = 0.07$

$Sum\ of\ Squares\ due\ to\ factor\ D =$
$[(Number\ of\ Experiments\ at\ level\ D1) \times$ *mD1 –m2+ Number of Experiments at level D2× mD2 –m2+ Number of Experiments at level D3× mD3 –m2=3×36.30−36.352+ 3×36.32−36.352+* $[3 \times (36.44 - 36.35)^2] = 0.03$

So the sum of squares due to factor A, B, C and D computed as 2.34, 0.11, 0.07 and 0.03,

International Journal of Research (IJR)
e-ISSN: 2348-6848, p- ISSN: 2348-795X Volume 2, Issue 08, August 2015
Available at http://internationaljournalofresearch.org

respectively. Now all these sum of squares are tabulated in Table 2(g) this is called as the ANOVA table.

Table 2(g) ANOVA table for η (S/N Ratio)

Factor		Degree of freedom	Sum of squares	Mean Square =Sum of squares/Degree of freedom	F	Contribution (%)
A	Reaction Temp (°C)	2	2.34	1.170	46.8	92.12
B	Catalyst Concentration	2	0.11	0.055	2.2	4.33
C	Molar Ratio (Methanol/Oil)	2	0.07	0.035	1.4	2.76
D	Reaction Time (min)	2	0.03	0.015	0.6	0.79
Error		0	0			
Total		8	2.54			
(Error)		(4)	0.10	0.025		

In the present study, the degrees of freedom for the error will be zero. Hence an approximate estimate of the error sum of squares is obtained by pooling the sum of squares corresponding to the factors having the lowest mean square. The parameters C and D are used to estimate the error sum of squares. They account for four degrees of freedom and their sum of squares is 0.10. Referring to the sum of squares in table, the parameter A makes the largest contribution 92.12% to the total sum of squares. The factors B, C and D make 4.33 %, 2.76% and 0.79% each. The larger the contribution of a particular parameter to the total sum of squares, the larger the ability is of that factor to influence S/N ratio. Moreover, the larger F-value, the larger will be the factor effect in comparison to the error mean square.

Degrees of freedom

The degrees of freedom associated with the grand total sum of squares are equal to the number of rows in the design matrix.

The degree of freedom associated with the sum of squares due to mean is one.

The degrees of freedom associated with the total sum of squares will be equal to the number of rows in the design matrix minus one.

The degrees of freedom associated with the factor will be equal to the number of levels minus one.

International Journal of Research (IJR)
e-ISSN: 2348-6848, p- ISSN: 2348-795X Volume 2, Issue 08, August 2015
Available at http://internationaljournalofresearch.org

The degrees of freedom for the error will be equal to the degrees of freedom for the total sum of squares minus the sum of the degrees of freedom for the various factors.

In the present experiment, the degrees of freedom for the error will be zero. Hence an approximate estimate of the error sum of squares is obtained by pooling the sum of squares corresponding to the factors having the lowest mean square. As a rule of thumb, the sum of squares corresponding to the bottom half of the factors (as defined by lower mean square) are used to estimate the error sum of squares. In the present experiment, the factors C and D are used to estimate the error sum of squares. Together they account for four degrees of freedom and their sum of squares is 0.10.

2.6. Interpretation of ANOVA table

The major inferences from the ANOVA table are given in this section. Referring to the sum of squares in Table 2(g) the factor A makes the largest contribution to the total sum of squares [(2.34/2.54) x 100 = 92.12%]. The factor B makes the next largest contribution (4.33%) to the total sum of squares, whereas the factors C and D make only 2.76% and 0.79% contribution respectively. The larger the contribution of a particular factor to the total sum of squares, the larger the ability is of that factor to influence η. Moreover, the larger the F-value, the larger will be the factor effect in comparison to the error mean square or the error variance.

2.7. Prediction of η under optimum conditions

In the present experiment, the identified optimum condition or the optimum level of factors is A1B1C1D3. The value of η under the optimum condition is predicted using the additive model as

$$\begin{aligned} n_{opt} &= m + (m_{A1} - m) + (m_{B1} - m) \\ &\quad + (m_{C1} - m) + (m_{D3} - m) + e \\ &= 36.35 + (36.93 - 36.35) \\ &\quad + (36.51 - 36.35) \\ &\quad + (36.46 - 36.35) \\ &\quad + (36.44 - 36.35) + 0 = 37.29 \end{aligned}$$

International Journal of Research (IJR)
e-ISSN: 2348-6848, p- ISSN: 2348-795X Volume 2, Issue 08, August 2015
Available at http://internationaljournalofresearch.org

Table 2(h) Main effects plot of the control parameters

Reaction Temp (^{0}C)	50	55	60	**Catalyst Concentration (Wt %)**	1	1.25	1.50
S/N ratio (η)	36.93	36.44	35.69	**S/N ratio (η)**	36.51	36.30	36.26
Molar Ratio (Methanol/Oil)	4.5	6.0	7	**Reaction Time(min)**	55	65	75
S/N ratio (η)	36.46	36.36	36.24	**S/N ratio (η)**	36.30	36.32	36.44

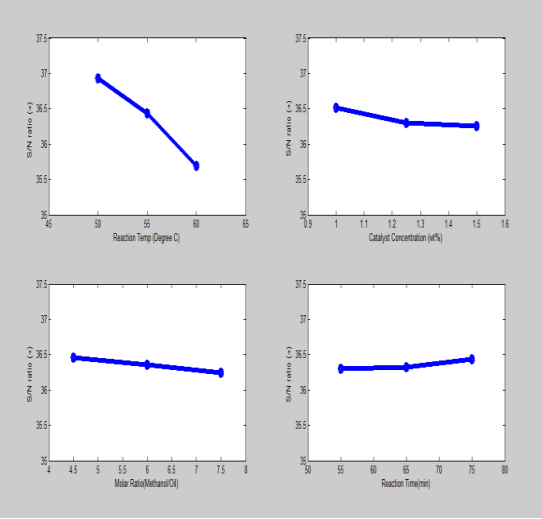

Fig. 2(c) Main effects plot of the control parameters

2.8 CONCLUSION:

Result of the Proposed Optimized Experimental Condition

The optimum conditions to achieve effective performance for the production of neem oil methyl ester and the contributions of each parameter to the S/N ratio under the optimal conditions are shown in Table 2(i)

Table 2(i) Optimum conditions for settling the control parameters and their contributions:

Parameters		**Level**	**Level description**	**Contribution**
A	Reaction Temperature	1	50°C	0.58
B	Catalyst Concentration	1	1.0 wt %	0.16
C	Methanol to Oil Molar Ratio	1	4.5:1	0.11
D	Reaction Time	3	75 min	0.09

International Journal of Research (IJR)
e-ISSN: 2348-6848, p- ISSN: 2348-795X Volume 2, Issue 08, August 2015
Available at http://internationaljournalofresearch.org

Total contribution from all parameters 0.94 Current grand average of performance 36.35 Expected result under optimum conditions 37.29

The calculated S/N ratio corresponding to nine set of experiments given in Table 2(d). The average S/N ratios of parameter at each level for neem oil methyl ester are shown in Table 2(f). Also the main effect plot for S/N ratio is shown in Fig 2(c). The average S/N ratio for maximum percentage yield of neem oil methyl ester is obtained at level 1 (Reaction Temperature 50°C), level 2 (Catalyst conc. 1.0%by wt), level 3 (Methanol to oil molar ratio 4.5:1) and level 4 (reaction time 75min). i.e., the optimum parameter setting for high percentage yield of neem oil methyl ester is A1B1C1D3. The results of ANOVA for S/N ratios are given in Table 2(g). The percentage of yield of neem oil methyl ester has been significantly improved using Taguchi Method.

The Taguchi method, which uses a set of orthogonal arrays for performing the fewest experiments, was employed to design experimental trials, with an ANOVA performed to more systematically analyze the relative importance of each experimental parameter on the production of neem oil methyl ester.

The reaction temperature, catalyst concentration and methanol to oil molar ratio were found to be significant parameters affecting the production of neem oil methyl ester. The contribution of the reaction temperature on the production process was larger than that of any other parameter. The yield of neem oil methyl ester obtained with the optimal experimental parameters was greater than that obtained from experiment no.1, which gave the highest yield from the experimental trials, and the theoretically expected value.

The experiments conducted under the optimized conditions showed a meaningful enhanced process performance. The Taguchi method provided a systematic and efficient mathematical approach to evaluate and optimize the process for the production of neem oil methyl ester, using only a few well-defined experimental sets for the optimization of the parameters.

Cost Analysis:

Sl.No.	Component	Cost (Rs.)
1	Sodium Hydroxide (Catalyst)	23/kg
2	Potassium hydroxide (Catalyst)	36/kg
3	Neem oil (Feedstock)	150/ litre
4	Methanol (Alcohol)	35/ litre
5	Glycerin (By product of Biodiesel)	75/ litre

Sl. No.	Component	Cost (Rs.)
1	Neem Oil – 100 ml	15
2	Two step transesterification Cost - 65 ml (45 ml + 20 ml) of Methanol	2.275

International Journal of Research (IJR)
e-ISSN: 2348-6848, p- ISSN: 2348-795X Volume 2, Issue 08, August 2015
Available at http://internationaljournalofresearch.org

	[4.5 Methanol/Oil Molar Ratio]	
3	Catalyst KOH 1.0 gm	0.036
4	Recovery (Glycerin 50 ml)	3.75
5	Total Cost (1 + 2 + 3 – 4)	17.311 – 3.75 = 13.561

Biodiesel production from 1 litre Neem Oil=0.70 Litre

So Cost of Biodiesel per litre = [(13.561 /100)*1000] / 0.70 = 193.73 Rs.

The cost of the biodiesel production can be minimized as possible to recover the used methanol. Recycling of methanol again and again in mass production and commercial use, the cost must be come to the lowest amount. Also the by-product such as glycerin and soap play an important role to minimize the cost.

3. INFERENCE

From all the experimentation performed above, it can be clearly observed that Neem Oil Methyl Ester (NOME) can be obtained by two step transesterification process only as the FFA content of neem oil is large. By using single step transesterification, the yield will be very less and in some case NOME cannot be obtained.

Taking together all these results, the optimized biodiesel yield of 74.30% was produced at reaction time of 75 min, catalyst amount of 0.50 g, temperature of 50°C, and methanol/oil molar ratio of 4.5.

ANOVA analysis showed that the temperature had the highest effect on the biodiesel yield followed by catalyst amount, methanol to oil molar ratio and reaction time

The result of this work showed that the maximum yields were obtained at lowest factor values. This will definitely have economic advantage on neem oil biodiesel production as low energy cost, low catalyst amount, low methanol/oil molar ratio, and low temperature are able to produce high biodiesel yield.

This was in agreement with the works of Awolu and Layokun, Meher et al., Jeong et al. and Marchetti and Errazu.

4. RECOMMENDATIONS.

In the optimization of parameters, KOH catalyst has been used with different concentration (1.0%, 1.25% and 1.5%) with the other parameters like methanol to oil molar ratio, reaction temperature and reaction time.

So, we can further do the optimization by using different catalyst types (NaOH, KOH and $NaOCH_3$), catalyst concentration, reaction temperature and methanol to oil ratio with three levels.

So Four Parameters and Three Level

No of experiment required = 3*3*3*3 =81.

But by using Taguchi Method of optimization

No of experiment required = 9 only.

5. KEY REFERENCES

[1.] Abebe K. Endalew, Yohannes Kiros, Rolando Zanzi. Heterogeneous catalysis for biodiesel production from Jatropha curcas oil (JCO). Energy 2011; Vol. 36: pp. 2693-2700.

[2.] Atul Dhar, Roblet Kevin, Avinash Kumar Agarwal. Production of biodiesel from high-FFA neem oil and its performance, emission and combustion characterization in a single cylinder DICI engine. Fuel Processing Technology 2012; Vol. 97: pp. 118–129.

[3.] Ayhan Demirbas. Progress and recent trends in biodiesel fuels. Energy Conversion and Management 2009; Vol. 50: pp. 14 - 34.

[4.] C. Martín , A. Moure , G. Martín ,E. Carrillo , H. Domínguez , J.C. Parajó. Fractional characterization of jatropha, neem, moringa, trisperma, castor and candlenut seeds as potential feedstocks for biodiesel production in Cuba. Biomass Bioenergy 2010; Vol. 34: pp. 533-538.

[5.] Deepak Tanwar, Ajayta, Dilip Sharma, Y. P. Mathur. Production and Characterization of Neem Oil Methyl Ester. International Journal of Engineering Research & Technology (IJERT) 2013; Vol. 2. : pp. 1896-1903.

[6.] Dennis Y.C. Leung, Xuan Wu, M.K.H. Leung. A review on biodiesel production using catalyzed transesterification. Applied Energy 2010; Vol. 87: pp. 1083-1095. .

[7.] E.F. Aransiola, E Betiku, DIO Ikhuomoregbe and TV Ojumu. Production of biodiesel from crude neem oil feedstock and its emissions from internal combustion engines. African Journal of Biotechnology 2012; Vol. 11: pp. 6178-6186

[8.] Freedman B, R. Butterfield and E. Pryde. Transesterification kinetics of soybean oil. Journal of the American oil Chemists Society 1986; Vol. 63: pp. 1375-80.

[9.] Fukuda H., A. Kondo and H. Noda. Biodiesel fuel production by transesterification of oils. Journal of Bioscience and Bioengineering 2001; Vol. 92: pp. 405-16.

[10.] GT Jeong, HS Yang, DH Park. Optimization of transesterification of animal fat ester using response surface methodology. Bioresour. Technol 2009; Vol. 100: pp. 25-30.

[11.] H.N.Pandey. Development of a New Catalyst for Bio-diesel Production. Ist International Conference on New Frontiers in Biofuels, DTU January 18-19, 2010, New Delhi.

[12.] H Ibrahim, A. S. Ahmed, I.M. Bugaje, Dabo Mohammed, C. D. Ugwumma. Synthesis of Bulk Calcium Oxide (Cao) Catalyst and its Efficacy for Biodiesel Production. Journal of Energy Technologies and Policy 2013; Vol. 3. : pp. 14-16.

[13.] Jon Von Gerpen. Biodiesel processing and production. Fuel Process Technol 2005; Vol. 86: pp. 1097–1107.

[14.] J.M. Marchetti, A.F Errazu. Esterification of free fatty acids using sulfuric acid as catalyst in the presence of triglycerides. Biomass. Bioenerg. 2008; Vol. 32: pp. 892–895.

[15.] Juan Calero, Gema Cumplido, Diego Luna , Enrique D. Sancho, Carlos Luna , Alejandro Posadillo, Felipa M. Bautista ,

Antonio A. Romero and Cristóbal Verdugo-Escamilla, Production of a Biofuel that Keeps the Glycerol as a Monoglyceride by Using Supported KF as Heterogeneous Catalyst . Energies 2014; Vol. 7: pp. 3764-3780.

[16.] L.C. Meher, D. Vidya Sagar, S.N. Naik. Technical aspects of biodiesel production by transesterification – a review. Renew. Sustain. Energy 2006; Vol. 10: pp. 248-268.

[17.] Madhu Agarwal, Kailash Singh, Ushant Upadhyaya and S P Chaurasia, Potential vegetable oils of Indian origin as biodiesel feedstock – An experimental study. Journal of Scientific & Industrial Research 2012; Vol. 71: pp. 285-289.

[18.] Maryam Hassani, Ghasem D Najafpour, Maedeh Mohammadi and Mahmood Rabiee. Preparation, Characterization and Application of Zeolite-based Catalyst for Production of Biodiesel from Waste Cooking Oil. Journal of Scientific & Industrial Research 2014; Vol. 73: pp. 129-133.

[19.] M A Hanna, Loren Isom and John Campbell, Biodiesel; Current perspectives and future. Journal of Scientific & Industrial Research 2005; Vol. 64: pp. 854-857.

[20.] Md. Hasan Alia, Mohammad Mashud, Md. Rowsonozzaman Rubel, Rakibul Hossain Ahmad, Biodiesel from Neem oil as an alternative fuel for Diesel engine. Procedia Engineering 2013; Vol. 56: pp. 625 – 630.

[21.] M.A. Fazal, A.S.M.A. Haseeb and H.H. Masjuki. Biodiesel feasibility study: An evaluation of material compatibility; performance; emission and engine durability. Renew. Sustain. Engy Reviews 2011; Vol.15: pp. 1314-1324.

[22.] Module 5, Lecture 4. Design for Reliability and Quality. IIT, Bombay.

[23.] Muthu, V. SathyaSelvabala, T. K. Varathachary, D. Kirupha Selvaraj, J. Nandagopal and S. Subramanian. Synthesis of biodiesel from neem oil using sulfated zirconia via tranesterification. Brazilian Journal of chemical Engineering 2010; Vol. 27: pp. 601-608.

[24.] N.Satya Sree, V.Madhusudhan Rao, P.Vijetha. Production of Bio-Diesel From Soap Stock of Cotton Seed Oil By Using Ferric Sulphate Catalyst Via A Two Step Heterogeneous Catalysis: Characteristics of Bio-Diesel Produced. International Journal of Scientific & Technology Research 2014; Vol. 3. : pp. 141-144.

[25.] Nielsen P. M., J. Brask and Fjerbaek. Enzymatic biodiesel production: Technical and economical considerations. European Journal of Lipid Science 2008; Vol. 110: pp. 692-700.

[26.] Olugbenga Olufemi Awolu and Stephen Kolawole Layokun. Optimization of two-step transesterification production of biodiesel from neem (Azadirachta indica) oil. International Journal of Energy and Environmental Engineering 2013; Vol. 4. : pp. 1-9.

[27.] Padmarag Deshpande, Kavita Kulkarni, A.D.Kulkarni. Supercritical Fluid Technology in Biodiesel Production: A Review. Chemistry and Materials Research 2011; Vol. 1. : pp. 27-32.

[28.] Poonam Gera, S.K.Puri and M.K. Jha. Use of Basic Heterogeneous Catalysts for Biodiesel Production: A Review. Ist International Conference on New Frontiers in Biofuels, DTU January 18-19, 2010, New Delhi.

[29.] Suman Singh, P.K.Omre, Kirtiraj Gaikwad. Standardization of Process Parameters for Neem Oil & Determination of Properties for Using as a Fuel. International Journal of Engineering Research and General Science 2014; Vol. 2. : pp. 1-7.

[30.] Talebian-Kiakalaieh, N. A. S. Amin, A. Zarei, H. Jaliliannosrati. Biodiesel Production from High Free Fatty Acid Waste Cooking Oil by Solid Acid Catalyst. Proceedings of the 6th International Conference on Process Systems Engineering (PSE ASIA) 25 - 27 June 2013, Kuala Lumpur.

[31.] Vivek and A. K. Gupta. Biodiesel production from karanja oil. Journal of Scientific & Industrial Research 2004; Vol. 63: pp. 39-47.

[32.] V. Manieniyan, R.Senthilkumar and Dr. S. Sivaprakasam. Experimental Investigation on Optimized Biodiesel (Based on Various Catalysts) used in a Twin Cylinder Diesel Engine. Ist International Conference on New Frontiers in Biofuels, DTU January 18-19, 2010, New Delhi.

ResearchGate

See discussions, stats, and author profiles for this publication at:
http://www.researchgate.net/publication/279757614

EFFECT OF FUNGAL BIOTIC STRESS ON PHYSIC NUT (JATROPHA CURCAS L.)

CHAPTER · JUNE 2015

DOWNLOADS
30

VIEWS
50

2 AUTHORS, INCLUDING:

Dr. Seweta Srivastava
U.P. Council of Agricultural Res…

56 PUBLICATIONS **12** CITATIONS

SEE PROFILE

Available from: Dr. Seweta Srivastava
Retrieved on: 18 August 2015

BIOENERGY

Opportunities and Challenges

BIOENERGY

Opportunities and Challenges

Edited by

R. Navanietha Krishnaraj

Jong-Sung Yu

APPLE ACADEMIC PRESS

Apple Academic Press Inc.
3333 Mistwell Crescent
Oakville, ON L6L 0A2
Canada

Apple Academic Press Inc.
9 Spinnaker Way
Waretown, NJ 08758
USA

©2016 by Apple Academic Press, Inc.

Exclusive worldwide distribution by CRC Press, a member of Taylor & Francis Group

No claim to original U.S. Government works

Printed in the United States of America on acid-free paper

International Standard Book Number-13: 978-1-77188-109-8 (Hardcover)

All rights reserved. No part of this work may be reprinted or reproduced or utilized in any form or by any electric, mechanical or other means, now known or hereafter invented, including photocopying and recording, or in any information storage or retrieval system, without permission in writing from the publisher or its distributor, except in the case of brief excerpts or quotations for use in reviews or critical articles.

This book contains information obtained from authentic and highly regarded sources. Reprinted material is quoted with permission and sources are indicated. Copyright for individual articles remains with the authors as indicated. A wide variety of references are listed. Reasonable efforts have been made to publish reliable data and information, but the authors, editors, and the publisher cannot assume responsibility for the validity of all materials or the consequences of their use. The authors, editors, and the publisher have attempted to trace the copyright holders of all material reproduced in this publication and apologize to copyright holders if permission to publish in this form has not been obtained. If any copyright material has not been acknowledged, please write and let us know so we may rectify in any future reprint.

Trademark Notice: Registered trademark of products or corporate names are used only for explanation and identification without intent to infringe.

Library of Congress Cataloging-in-Publication Data

Bioenergy : opportunities and challenges / [edited by] R. Navanietha Krishnaraj, and Jong-Sung Yu.

pages cm
Includes bibliographical references and index.
ISBN 978-1-77188-109-8 (alk. paper)
1. Biomass energy. 2. Microbial fuel cells. 3. Biodiesel fuels. 4. Lignocellulose.
I. Navanietha Krishnaraj, R. II. Yu, Jong-Sung.

TP339.B526 2015 662'.88--dc23 2015020359

Apple Academic Press also publishes its books in a variety of electronic formats. Some content that appears in print may not be available in electronic format. For information about Apple Academic Press products, visit our website at **www.appleacademicpress.com** and the CRC Press website at **www.crcpress.com**

ABOUT THE EDITORS

R. Navanietha Krishnaraj

R. Navanietha Krishnaraj, PhD, is currently working as the Technical Officer at the National Institute of Technology, Durgapur. Before joining NIT Durgapur, he was working at CSIR-Central Electrochemical Research Institute. He holds a BTech in biotechnology and PhD in the field of microbial fuel cells. His areas of interests include bioelectrocatalysis and nanobiotechnology. He has authored several research articles in reputed journals. He is a life member of several professional bodies.

Prof. Jong-Sung Yu

Prof. Jong-Sung Yu is one of the most renowned scientists in the field of electrochemical science. He is currently a Professor in the Department of Advanced Materials Chemistry at Korea University in Korea. He has a BS from Sogang University in Korea and a PhD in chemistry from the University of Houston in USA. He has several years of rich postdoctoral experience at Ohio State University, University of Houston, Pennsylvania State University, and Northwestern University. He is currently on the editorial boards of the *Journal of Experimental Nanoscience* (Taylor and Francis), *Frontiers in Fuel Cells*, and *Carbon Letter* (Korean Carbon Society). He was awarded an Excellent Research Award in the Inorganic Chemistry Division in 2011 and Material Chemistry Division in 2004 from the Korean Chemistry Society, and also was given a Korea Strategic Research Grant (2010–2015) in Energy Application. He has authored about 190 peer-reviewed articles and 60 patents. His research interests include nanostructured materials for storage, delivery, and conversion, with particular attention toward electrochemical applications such as fuel cell, battery, capacitor, solar cell, and sensors.

CONTENTS

List of Contributors ..... *ix*

List of Abbreviations ..... *xiii*

Preface ..... *xvii*

PART 1: BIOHYDROGEN PRODUCTION **1**

1. Thermophilic Biohydrogen Production: Challenges at the Industrial Scale **3**

Sudhir Kumar, Aditya Bhalla, Mohit Bibra, Jia Wang, Kayla Morisette, Subramanian M. Raj, David Salem, and Rajesh K. Sani

2. Bio-Hydrogen Production: Current Trends and Future Prospects **37**

Vinita Mishra and Isha Srivastava

PART 2: MICROBIAL FUEL CELLS **59**

3. Microbial Fuel Cells: A Promizing Alternative Energy Source **61**

M. J. Angelaa Lincy, B. Ashokkumar, V. S. Vasantha, and P. Varalakshmi

4. Challenges to and Opportunities in Microbial Fuel Cells **87**

J. Jayapriya and V. Ramamurthy

5. Systems Biology Approaches for Microbial Fuel Cell Applications **125**

R. Navanietha Krishnaraj, and Jong-Sung Yu

PART 3: BIOETHANOL PRODUCTION **141**

6. Potentials of *Oscillatoria annae* in Producing Bioethanol by Degradation of Selected Lignocellulosics **143**

P. Malliga, V. Viswajith, D. Malini, and R. Sabitha

7. Challenges in Harnessing the Potential of Lignocellulosic Biofuels and the Probable Combating Strategies **171**

Lakshmi Shri Roy, Vijay Kumar Garlapati, and Rintu Banerjee

PART 4: BIODESEL PRODUCTION 205

8. Biodiesel: Production, Opportunities and Challenges 207

Deeksha Sachdeva

9. An Overview of Reactor Designs for Biodesel Production 221

Vijay Kumar Garlapati, Lakshmi Shri Roy, and Rintu Banerjee

10. Studies on the Effect of Antioxidants on the Long-Term Storage Stability and Oxidation Stability of *Pongamia pinnata* and *Jatropha curcus* Biodiesel 241

A. Obadiah and S. Vasanth Kumar

11. Effect of Fungal Biotic Stress on Physic Nut (*Jatropha curcas* L.) 277

Seweta Srivastava and Asha Sinha

PART 5: CATALYSIS FOR BIOFUELS 297

12. A Chemist's Perspective on Bioenergy—Opportunities and Challenges 299

Sannapaneni Janardan, B. B. Pavankumar, Shivendu Ranjan, Nandita Dasgupta, Melvin Samuel, Chidambaram Ramalingam, Akella Sivaramakrishna, and Kari Vijayakrishna

Index 353

LIST OF CONTRIBUTORS

Rintu Banerjee
Microbial Biotechnology and DSP Laboratory, Agricultural and Food Engineering Department, IIT Kharagpur, Kharagpur, West Bengal – 721302

Aditya Bhalla
Department of Chemical and Biological Engineering, South Dakota School of Mines and Technology, 501 East St. Joseph Street, Rapid City, SD 57701–3995 USA

Mohit Bibra
Department of Chemical and Biological Engineering, South Dakota School of Mines and Technology, 501 East St. Joseph Street, Rapid City, SD 57701–3995 USA

Nandita Dasgupta
School of Bio Sciences and Technology, VIT University, Vellore, Tamil Nadu, India

Vijay Kumar Garlapati
Microbial Biotechnology and DSP Laboratory, Agricultural and Food Engineering Department, IIT Kharagpur, Kharagpur, West Bengal – 721302

Sannapaneni Janardan
Department of Chemistry, School of Advanced Sciences, VIT University, Vellore

J. Jayapriya
Department of Chemical Engineering, A.C. Tech, Anna University, Chennai – 600025, India

R. Navanietha Krishnaraj
Department of Biotechnology, National Institute of Technology Durgapur, Durgapur, West Bengal, India–713209

B. Ashok Kumar
Department of Genetic Engineering, School of Biotechnology, Madurai Kamaraj University, Madurai, Tamil Nadu

S. Vasanth Kumar
Department of Chemistry, Karunya University, Coimbatore – 641114, Tamilnadu, India

Sudhir Kumar
Department of Chemical and Biological Engineering, South Dakota School of Mines and Technology, 501 East St. Joseph Street, Rapid City, SD 57701–3995 USA

M. J. Angelaa Lincy
Department of Molecular Microbiology, School of Biotechnology, Madurai Kamaraj University, Madurai, Tamil Nadu

D. Malini
Professor, Department of Marine Biotechnology, Bharathidasan University, Tiruchirappalli–620024, Tamilnadu

P. Malliga
Professor, Department of Marine Biotechnology, Bharathidasan University, Tiruchirappalli–620024, Tamilnadu

Vinita Mishra
Cell Biology Lab, School of Biological Sciences and Biotechnology, Indian Institute of Advanced Research, Koba Institutional Area, Gandhinagar, 382 007, Gujarat, India; E-mail: vinita.mbif@gmail.com

Kayla Morisette
Department of Chemical and Biological Engineering, South Dakota School of Mines and Technology, 501 East St. Joseph Street, Rapid City, SD 57701–3995 USA

A. Obadiah
Department of Chemistry, Karunya University, Coimbatore – 641114, Tamilnadu, India

B. B. Pavankumar
Department of Chemistry, School of Advanced Sciences, VIT University, Vellore

Subramanian M. Raj
Department of Chemical and Biological Engineering, South Dakota School of Mines and Technology, 501 East St. Joseph Street, Rapid City, SD 57701–3995 USA

Chidambaram Ramalingam
School of Bio Sciences and Technology, VIT University, Vellore, Tamil Nadu, India

V. Ramamurthy
Department of Biotechnology, PSG College of Technology, Coimbatore – 641004, India

Shivendu Ranjan
School of Bio Sciences and Technology, VIT University, Vellore, Tamil Nadu, India

Lakshmi Shri Roy
Microbial Biotechnology and DSP Laboratory, Agricultural and Food Engineering Department, IIT Kharagpur, Kharagpur, West Bengal – 721302

R. Sabitha
Professor, Department of Marine Biotechnology, Bharathidasan University, Tiruchirappalli–620024, Tamilnadu

Deeksha Sachdeva
Department of Biochemistry, Punjab Agricultural University, Ludhiana, Punjab, India–141004; E-mail: sachdeeksha@gmail.com

David Salem
Department of Chemical and Biological Engineering, South Dakota School of Mines and Technology, 501 East St. Joseph Street, Rapid City, SD 57701–3995 USA

Melvin Samuel
School of Bio Sciences and Technology, VIT University, Vellore, Tamil Nadu, India

Rajesh K. Sani
Department of Chemical and Biological Engineering, South Dakota School of Mines and Technology, 501 East St. Joseph Street, Rapid City, SD 57701–3995 USA

Asha Sinhda
Department of Mycology and Plant Pathology, Institute of Agricultural Sciences, Banaras Hindu University, Varanasi – 221 005, U.P., India

Akella Sivaramakrishna
Department of Chemistry, School of Advanced Sciences, VIT University, Vellore

Isha Srivastava
Department of Biotechnology, Delhi Technological University (Formerly Delhi College of Engineering), Shahbad Daulatpur, Main Bawana Road, Delhi-110 042, India

Seweta Srivastava
Department of Mycology and Plant Pathology, Institute of Agricultural Sciences, Banaras Hindu University, Varanasi – 221 005, U.P., India; E-mail: shalu.bhu2008@gmail.com

P. Varalakshmi
Department of Molecular Microbiology, School of Biotechnology, Madurai Kamaraj University, Madurai, Tamil Nadu

V. S. Vasantha
Department of Natural Products, School of Chemistry, Madurai Kamaraj University, Madurai, Tamil Nadu

Kari Vijayakrishna
Department of Chemistry, School of Advanced Sciences, VIT University, Vellore

V. Viswajith
Professor, Department of Marine Biotechnology, Bharathidasan University, Tiruchirappalli–620024, Tamilnadu

Jia Wang
Department of Chemical and Biological Engineering, South Dakota School of Mines and Technology, 501 East St. Joseph Street, Rapid City, SD 57701–3995 USA

Jong-Sung Yu
Department of Advanced Materials Chemistry, Korea University, 2511 Sejong-ro, Sejong, 339-700, Korea

LIST OF ABBREVIATIONS

AC	activated charcoal
AEM	anion exchange membrane
AFC	alkaline fuel cell
AGCS	amber glass bottle with closed space
AGCSN	amber glass bottle with closed space containing nitrogen
AGOS	amber glass bottle with open space
ATP	adenosine triphosphate
ATSDR	Agency for Toxic Substances and Disease Registry
BEAMR	bioelectrochemically assisted microbial reactor
BES	bromoethanesulfonic
BioH2	biohydrogen
BPV	bio-photovoltaic cell
BRA	biotechnology risk assessment
BSES	biological simultaneous enzyme production and saccharification
BTL	biomass-to-liquid
CBH	contaminated barley hulls
CBP	consolidated bioprocess
CMCEs	chemically modified carbon electrodes
CN	cetane number
CNT	carbon nanotubes
COD	chemical oxygen demand
CoTMPP	cobalt tetramethylphenylporphyrin
CSTR	continuous stirred tank reactor
CV	cyclic voltammetry
CVD	chemical vapor deposition
CWP	cheese whey powder
DDG	dried distiller's grain
DG	diglycerides

DME	dimethyl ethanol
DMRB	dissimilatory metal reducing bacteria
DNSA	dinitrosalicylic acid
EAB	electrochemically active bacterial
FAME	fatty acid methyl ester
FFA	free fatty acids
FT	Fischer–Tropsch diesel
GC	gas chromatography
GECE	graphite/epoxy composite electrode
GHG	greenhouse gas
GM	genetic modification
GTZ	Gesellschaft für Technische Zusammenarbeit
GVL	g-valerolactone
HMF	hydroxymethylfurfural
HRT	hydraulic retention time
IP	induction point
JBD	Jatropha curcus biodiesel
KV	kinematic viscosity
ldh	lactate dehydrogenase gene
MB	methylene blue
MBR	membrane bioreactors
MCC	microcrystalline cellulose
MEC	microbial electrolysis cell
MFC	microbial fuel cell
MG	monoglycerides
MSW	municipal solid wastes
NAD	nicotinamide adenine dinucleotide
NR	neutral red
OGCS	ordinary glass bottle with closed space
OGCSN	ordinary glass bottle with closed space containing nitrogen
OGOS	ordinary glass bottle with open space
OSI	oil stability index
PBD	Pongamia (karanja) biodiesel
PEC	photoelectrochemical
PEM	proton exchange membrane

PFR	plug flow reactor
PNS	purple-nonsulfur
PSI	photosystem I
PSII	photosystem II
PY	pyrogallol
RTD	residence time distribution
RVC	reticulated vitreous carbon
RW	refinery wastewater
SDPF	sequential dark-photo fermentations
SEA	separator electrode assembly
SHF	separate hydrolysis and fermentation
SNG	synthetic natural gas
SPA	widely spaced electrodes
SSF	simultaneous saccharification and fermentation
SWG	switchgrass
TG	triglycerides
UF	ultra filtration
VSS	volatile suspended solids
WCO	waste cooking oil

PREFACE

Energy is one of the prime needs in the modern world. Energy demands are exponentially increasing in the recent years owing to rapid advancements in industrialization and population explosion. The conventional fossil fuels are depleting at rapid rates. The use of conventional sources such as coal or nuclear sources also causes several hazards to the environment.

Bioenergy sources such as bio-hydrogen, biodiesel, bioethanol, biofuel cells seem to be an ideal option for fulfilling the increasing energy demands. Several researchers all over the world are working in this sector, and it has led to drastic improvements in bioenergy research. However, the technology gap between research and commercialization still exist.

The objective of the book, *Bioenergy: Opportunities and Challenges*, is to offer engineers and technologists from different disciplines information to gain knowledge on the breadth and depth of this multifaceted field. The field of bioenergy is interdisciplinary. It requires the knowledge of biologists, chemists, physicists, and engineers. There is an urgent need to explore and investigate the current shortcomings and challenges of the current bioenergy technologies. The book, in short, will explore and convey the key concepts on factors hindering the real-time application of these bioenergy sources.

Bioenergy: Opportunities and Challenges provides valuable information for engineers and technologists working in this cutting-edge field. The book will also serve as a text for BTech and MSc courses in biotechnology and other allied disciplines. The book will also be useful to management students for bioenergy management and related courses.

PART 1

BIOHYDROGEN PRODUCTION

CHAPTER 1

THERMOPHILIC BIOHYDROGEN PRODUCTION: CHALLENGES AT THE INDUSTRIAL SCALE

SUDHIR KUMAR, ADITYA BHALLA, MOHIT BIBRA, JIA WANG, KAYLA MORISETTE, SUBRAMANIAN M. RAJ, DAVID SALEM, and RAJESH K. SANI

Department of Biotechnology and Bioinformatics, Jaypee University of Information Technology, Waknaghat, Solan, Himachal Pradesh, India

CONTENTS

1.1 Introduction 4
1.2 Feedstocks for H_2 Production 6
1.3 Routes of BioH_2 Production, Microorganisms, and H_2 Yields 10
1.3.1 BioH_2 Production from Readily Fermentable Substrates 10
1.3.2 BioH_2 Production from Complex Substrates 14
1.3.3 BioH_2 Production from Untreated Complex Substrates 18
1.4 Industrial Operation of H_2 Production 21
1.5 Decentralized Industrial Scale H_2 Production 24
1.6 Summary and Conclusioins 25
1.7 Acknowledgement 26
Keywords 27
References 27

ABSTRACT

Biohydrogen ($BioH_2$) production using lignocellulosic biomass has been extensively studied at laboratory scale. Localized availability of suitable feedstocks, their pretreatment costs, and lower rates of $BioH_2$ production make the industrial operation uneconomical. Several thermophilic and hyperthermophilic microorganisms can produce elevated levels of H_2 (~4 mol H_2/mol glucose) through the dark fermentation process. Decentralized thermophilic $BioH_2$ production in a single-step, consolidated process is desirable for successful industrial operation. In addition to lignocellulosic biomass, food wastes, and industrial effluents have been projected as economical substrates for H_2 production. Using these inexpensive and easily available substrates, the concept of 'waste to energy' can be achieved. There is, however, a lack of successful case studies of long-term industrial operations producing $BioH_2$. This chapter focuses on the need for $BioH_2$ production using thermophiles at realistic, commercial scales. Issues related to studying scale up requirements are discussed, together with goals for successful, industrial-scale production of $BioH_2$.

1.1 INTRODUCTION

Non-renewability and depletion of fossil fuels coupled with enhanced greenhouse gas emissions by their combustion warrants global search for alternative fuels. A variety of alternative fuels including biobutanol, biodiesel, bioethanol, biogas, biohydrogen ($BioH_2$) and other biomass-derived products are currently being examined. Among these, H_2 due to its high-energy efficiency (calorific value of 143 MJ/kg) and its ability to be converted into electrical energy in fuel cells, has gained much interest as a sustainable biofuel in the past few years. At present, most of the current H_2 supply (around 96%) comes from fossil fuels but with high production cost and negative environmental impact. To lower the production cost of H_2, microbe-mediated H_2 ($BioH_2$) can be an option, produced using readily available, carbon neutral, inexpensive, and renewable feedstocks such as lignocellulosic biomass. Though lignocellulosic biomass is inexpensive (US $2–4/GJ at a cost of US $39–60/dry ton biomass), its pretreatment

cost (US $15–25/GJ) exceeds that of fossil fuel (US$ 5–15/GJ), which makes the lignocellulosic BioH_2 production uneconomical [1]. In this context, a consolidated bioprocess (CBP) using lignocellulosics to biofuels in a single step could provide an efficient and economical process [2, 3]. Therefore, microorganisms that have the capability of enzymatic hydrolysis of lignocellulose and sugar fermentation to produce H_2 in a single reactor are desirable.

In the past few years, extensive research has been carried out on BioH_2 production under dark fermentation conditions using thermophilic and hyperthermophilic microorganisms due to their inherent advantage of improved reaction kinetics and stability at high temperatures [4–6]. Thermophilic microorganisms such as *Caldicellulosiruptor saccharolyticus*, *Thermococcus kodakaraensis*, and *Clostridium thermocellum* have been reported to produce cellulosic BioH_2 under dark fermentation processes [7–9]. BioH_2 production via dark fermentation is widely preferred over photo-fermentation and biophotolysis. The major advantages of dark fermentation are: (i) simplicity of reactor design; (ii) more efficient process operation; (iii) a wide variety of feedstocks utilization; and (iv) higher H_2 production rates compared to other biological methods of H_2 production [10–13].

Caldicellulosiruptor spp. are emerging as potential H_2-producers through CBP. Recently it has been reported that *C. saccharolyticus* DSM8903 produced H_2 (11.2 mmol/g switchgrass) directly from switchgrass without any physicochemical or biological treatment making it a promizing candidate for CBP of lignocellulosic biomass [4]. *C.bescii* produces a combination of lactate, acetate, H_2, and CO_2, and pyruvate acts as a major branch point with carbon routed to acetyl-CoA or lactate. Deletion of lactate dehydrogenase gene (ldh) from the chromosome of *C. bescii* has also been reported. This deletion resulted in production of acetate and H_2 through redirection of electron flow from lactate. These modified strains have been reported to grow on biomass without any conventional treatment and produced 3–4 mol H_2/mol glucose [14]. There are few reports on CBP of lignocellulosic feedstocks for H_2 production using thermophiles. It has been suggested that thermophilic CBP has advantages over mesophilic processes; for example, achieving theoretical maximum yield of 4 mol H_2/mol glucose, utilization of a wide range of biomasses as substrates,

increased substrate availability due to high temperatures, and reduced risk of microbial contamination [4, 7, 15–20].

BioH_2 is projected as a dominant biofuel, as a result of readily available lignocellulosic feedstocks, increasing knowledge of H_2-related metabolic pathways of H_2-producing native heterotrophs (dark fermentation) and phototrophs (photofermentation), and genetically engineered microbes. BioH_2 production using lignocellulosic biomass is well documented and has been proven at the laboratory scale [2, 4, 21, 23–26]. Globally available inexpensive raw materials in the form of food waste and industrial effluents have also been gaining interest for BioH_2 production [27–31]. Toyota and Hyundai have also been working to promote H_2 fuel vehicles in the USA and UK, and therefore investment opportunities are increasing in the H_2 sector. However, economical industrial production of this biofuel is a challenge for a number of reasons including high processing costs of raw materials, lower levels of substrate conversion efficiency, lack of appropriate microorganisms as well as bioreactor design, and low stoichiometric H_2 yield. This review briefly discusses issues related to scale up of BioH_2 production and demonstrates that this biofuel is a promising alternative fuel, especially when produced with thermophiles.

1.2 FEEDSTOCKS FOR H_2 PRODUCTION

Many different processes (e.g., electrolysis of H_2O, thermocatalytic reformation, solar thermochemical gasification, supercritical conversion, direct and indirect biophotolysis, photofermentation, and dark fermentation) have been demonstrated for H_2 production from a variety of feedstocks [9, 32–43]. However, local availability and cost of feedstocks and conversion technologies to produce H_2 are key factors determining the choice of feedstock and method of H_2 production. Since these factors vary from region to region, it is not necessary to develop a universal technology for H_2 production; one of several processes and feedstocks can be selected for H_2 production according to its cost-effectiveness in a given nation or region.

Production of H_2 from easily fermentable substrates such as glucose, xylose, sucrose, and starch has been achieved with high yields (in

some cases the maximum of 4 mol/mol glucose equivalents) as well as high rates, for example, 94 mmol/L/h [16, 32, 35–38]. The use of these easily fermentable substrates for the production of H_2 is not economically viable due to their high costs. For example, the cost of glucose is US $400–600/Metric Ton (MT). In theory, roughly 44 kg of H_2 can be obtained from one MT of glucose (assuming that 4 mol of H_2 can be produced from one mole of glucose under dark fermentative conditions), which can be sold for $31–$135 depending on the mode (on-site gas or off-site liquid) of H_2 production [44]. This means the cost of raw material is more than 3 folds higher than the price of product H_2, illustrating the need to select a cost-effective feedstock for the sustainable production of H_2. Table 1.1 summarizes various types of feedstocks (e.g., energy crops lignocellulosic residues, wastewater, complex solid wastes, and microalgae) for BioH_2 production with their comparative advantages and disadvantages.

TABLE 1.1 Feedstocks For BioH_2 Production

Feedstocks	Advantages	Disadvantages	References
Energy crops (e.g., sugarcane, sugar beet, sorghum, corn, wheat)	• Carbon neutral • High sugar and low lignin contents • Renewable • Short incubation time for H_2 production	• Environmental problems due to high dose of fertilizers and pesticides • Expensive • Increase in food price • Scarcity of arable land	[6, 22, 54]
Lignocellulosic residues (e.g., rice, wheat straw and bran, corn stover, sugarcane and sweet sorghum bagasse, wood waste, wood fibers, tree and shrub residues)	• Carbon neutral • Globally abundant, sustainable • Inexpensive • No competition for arable land, waste, land management • Renewable	• Depletion of soil organic content • High cost of pretreatment and saccharification • Inhibitory compounds • Long incubation time of H_2 production • Soil erosion hazard	[1, 3, 16, 111–113]

TABLE 1.1 (*Continued*)

Feedstocks	Advantages	Disadvantages	References
Wastewater (e.g., paper mill, distillery and molasses based, starch hydrolysate, cattle, cheese whey, olive mill, dairy, food industry waste water)	• Carbon neutral, renewable • High sugar/starch content • Inexpensive • Pollution control and wastewater treatment • Reduction of COD	• Complex chemical composition • Inhibition due to high organic load • Low reproducibility of the waste • Selection and separation of waste components	[35, 114–117]
Complex solid waste (e.g., kitchen food, municipal, mixed wastes)	• Carbon neutral • High sugar/starch content • Low conc. of inhibitors • Low cost and abundant • Reduction of BOD • Renewable	• Additional cost of separation of fermentable fraction of the waste • Low H_2 conversion efficiency due to high contents of proteins and fats	[6, 50, 118]
Microalgae	• Absence of lignin • Carbon neutral • CO_2 sequestration • Growth on wastewater • High carbohydrate and lipid contents • No need of arable land • Potency of genetic manipulation to increase productivity • Rapid growth rate • Short harvesting time	• Cross contamination of algal monocultures in open ponds • High cost of photobioreactors and dewatering process • Susceptibility of cross contamination of algae from bacteria, fungi and predators like protozoans, rotifers and crustaceans • Low H_2 production potential	[52, 53, 119, 120]

Lignocellulosic biomass may be the ideal feedstock for H_2 production because it is renewable, sustainable, and available abundantly. Crop residue is inexpensive ($39–60/MT) and produced worldwide at a level of about 2802×10^6 Mg/yr for cereal crops and 3758×10^6 Mg/year for 27 food crops [45]. Although, lignocellulosic biomass fits well in the overall concept of renewable fuel generation, the cost of pretreatment of lignocellulosic feedstocks makes the process industrially impractical as the pretreatment process alone adds the cost of US $15–25/GJ. Once pretreated, the efficiency of H_2 production largely depends upon the type of sugars and inhibitors released. The other globally available feedstocks such as municipal solid wastes (MSW), algal biomass, and industrial effluents also have good potential to produce H_2 [31, 35, 46–50]. Replacement of expensive carbon feedstocks with inexpensive wastes, for example, industrial effluents, could be one of the ways to overcome the economic barriers of BioH_2 production. Also, the use of inexpensive, abundantly available wastewaters as feedstock is environmentally advantageous [6]. However, due to the complex dynamic nature of wastewater (e.g., organic load, pH, salinity, sterility, and presence of biodegradable organics), extensive research is needed to understand the overall feasibility of this feedstock for BioH_2 production.

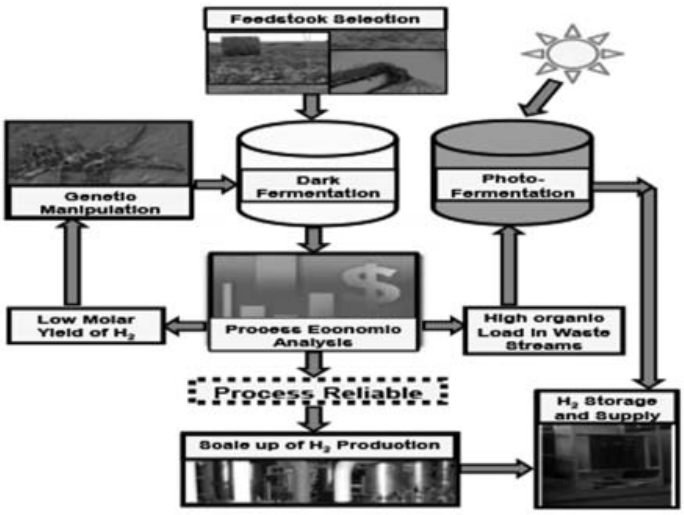

FIGURE 1.1 Global network for industrialization of H_2 production.

Recently, algal biomass has gained attention for production of various biofuels including H_2 [51–53], due to rich fermentable content. Rapid growth of algae in seawater, a short harvesting cycle, and the CO_2 sequestration property can make algae the best renewable source for biofuel production. Compared to lignocellulosics, microalgae require only a mild pretreatment (enzymatic saccharification) due to absence of lignin and hemicelluloses [22, 47, 54–56]. However, difficulties in propagating a monoculture of algae in open ponds need to be overcome for developing a cost-effective H_2 production system (Table 1.1).

1.3 ROUTES OF BIOH_2 PRODUCTION, MICROORGANISMS, AND H_2 YIELDS

1.3.1 BIOH_2 PRODUCTION FROM READILY FERMENTABLE SUBSTRATES

Biophotolysis of water using cyanobacteria and algae, photofermentation using photosynthetic bacteria, and dark fermentation using anaerobic fermentative bacteria are the routes of BioH_2 production. During the process of biophotolysis, microalgae or cyanobacteria use solar energy and splitting of water occurs in microbial photosynthesis. In photosystem I of microalgae, reduction of ferrodoxin takes place-producing H_2 by a hydrogenase enzyme (for details refer to Ref. [57]). While in photofermentation, ATP-requiring nitrogenase enzyme catalyzes H_2 production using various substrates in the absence of oxygen and nitrogen. Also in photofermentation, due to presence of reverse hydrogenase enzyme, H_2 oxidizes back to protons. So the net gain is the difference between the evolved H_2 by nitrogenase and H_2 consumed by reversed hydrogenase. H_2 uptake hydrogenase-free mutants are required to see the full potential of the photofermentation process. Hydrogenase encoding genes (hup) can be modified by insertion of resistance genes or by deletion of hup genes. Apart from this low efficiency of light conversion, high cost of photobioreactors and oxygen sensitivity of hydrogenase enzyme are the major limitations of photofermentation and biophotolysis.

During dark fermentation process, anaerobic bacteria use carbohydrates rich substrates under mesophilic (25–40 °C), thermophilic (40–65 °C) and

hyperthermophilic (>80 °C) conditions [58]. Oxygen sensitivity to hydrogenase enzyme is not an issue in dark fermentation and there is no need for solar energy. Thermophilic microbial dark fermentation, mainly due to high H_2 production rates compared to mesophilic dark fermentation, photofermentation, and biophotolysis, is a promising approach for $BioH_2$ production. Through metabolic engineering, the modified mesophilic strains of *Escherichia coli* are limited to produce 2 mol of H_2/mol of glucose [59, 60]. In contrast native or genetically modified thermophilic strains of *Clostridium* sp. can produce 4 mol H_2/mol glucose [61]. Elevated levels of H_2 production (i.e., ≥3.6 mol/mol of glucose) have been reported from various pure or mixed thermophilic and hyperthermophilic cultures (Table 1.2). Hyperthermophilic microorganisms such as *Thermotoga neapolitana* DSM 4359 and *Pyrococcus furiosus* DSM 3638 produced 3.8 mol H_2/mol of glucose consumed [62–64].

The thermophilic $BioH_2$ production process poses some inherent benefits at elevated temperature, such as lower risk of contamination from mesophiles, no need for reactor cooling, better mixing and lower viscosity, and removal of volatile products, which could minimize the chances of product inhibition [5, 65]. Another advantage of using thermophiles and hyperthermophiles (e.g., *Thermoanaerobacter tengcongensis* and *Pyrococcus furiosus*) is the presence of membrane bound NADPH-dependent hydrogenases, which can reduce transport energy input, and thus can make the process thermodynamically more favorable [66– 70]. Enhanced $BioH_2$ production has been observed with increase in reactor temperature. For example, Gadow et al. [71] showed higher H_2 yield (19.01 mmol H_2/g sugar consumed) by using a mixed culture in a continuous stirred tank reactor (CSTR) at 80 °C as compared to the temperatures 55 °C (15.2 mmol H_2/g sugar consumed) and 37 °C (0.6 mmol H_2/g sugar consumed). In another report, Kargi et al. [72] showed higher $BioH_2$ production from cheese whey powder at 55 °C (0.81 mol/mol glucose) as compared to the fermentation carried out at 35 °C (0.47 mol/mol glucose).

H_2 production by mixed cultures may be desirable when compared to pure culture fermentation due to the capability of producing greater yields [73]. Zeidan et al. [74] reported higher H_2 yield (3.7 mol/mol hexose sugar) by co-culture of *Caldicellulosiruptor* sp. as compared to monoculture (3.5 mol/mol hexose). Cell-free supernatant of *C. saccharolyticus* also enhanced the growth

of *C. kristjanssonii* in batch culture leading to increased biomass concentration, which proves a positive interspecies interaction. Table 1.2 summarizes H_2 production from readily fermentable sugars as first generation feedstock by pure cultures, co-cultures, and mixed cultures of thermophiles and hyperthermophiles.

TABLE 1.2 Overview of H_2-Producing Thermophiles and Hyperthermophiles Utilizing Readily Fermentable Substrates

Organism, Growth Temperature (°C), and Culturing Type	**Substrate**	**End Products**	**H_2 Yield (mol/mol)[a]**	**Reference**
Thermoanaerobacter mathranii A3N, 70 °C, and Batch	Glucose	Acetate, Butyrate, Lactate, Ethanol	2.64	[121]
Thermotoga neapolitana, 75 °C, and Batch	Xylose	Acetate, Lactate	2.22	[122]
Thermoanarobacterium thermosaccharolyticum, 60 °C, and Chemostat	Glucose	Acetate, Butyrate, Ethanol	2.07	[123]
Thermotoga neapolitana DSM 4359, 80 °C, and Batch	Glucose	Acetate, Lactate	3.8	[62]
Thermotoga neapolitana DSM 4359, 77 °C, and Batch	Glucose	Acetate, Butyrate	3.2	[76]
Thermoanaerobacterium sp., 50 °C, and Batch	Glucose	Acetate, Butyrate, Lactate, Ethanol	1.59	[18]
Thermoanaerobacterium saccharolyticum YS485, 55 °C, and Batch	Cellobiose	Acetate, Lactate, Ethanol	0.87	[124]
Thermotoga neapolitana DSM 4359, 85 °C, and Batch	Glucose	Acetate, Lactate	3.8	[63]
Pyrococcus furiosus DSM 3638, 90 °C, and Chemostat	Cellobiose	Acetate, Alanine, Ethanol	3.8	[67]
Cladicellulosiruptor saccharolyticus, 72 °C, and Batch	Glucose	Acetate, Lactate	3.3	[39]

TABLE 1.2 (*Continued*)

Organism, Growth Temperature (°C), and Culturing Type	**Substrate**	**End Products**	**H_2 Yield (mol/mol)[a]**	**Reference**
Thermococcus kodakaraensis TSF100, 85 °C, and Chemostat	Starch	Acetate, Alanine	3.3	[9]
Thermoanaerobacter tengcongensis JCM11007, 75 °C, and Batch	Starch	Acetate, Ethanol	2.8	[68]
Thermotoga elfii DSM 9442, 65 °C, and Batch	Glucose	Acetate	3.3	[43]
Caldicellulosiruptor saccharolyticus, 70 °C, and Controlled batch DSM 8903	Sucrose	Acetate, Lactate	3.3	[43]
Mixed Or Co-Cultures				
Thermoanaerobacterium thermosaccharolyticum, *Klebsiella* sp., *Bacillus coagulans* and *Sporolactobacillusnakayamae*, 70 °C, and Continuous	Arabinose or Glucose	Ethanol, Lactate, Acetate	1.10 or 0.75	[125]
Dominant species of *Thermoanarobacterium* and *Thermoanaerobacter*, 70 °C, and Batch	Glucose	Acetate, Butyrate, Ethanol, Propionate	2.38	[126]
Bacillus sp., *Anoxybacillus* sp., *Caloramator* sp., *Clostridium* sp., *Thermoanaerobacterium* sp. and *Caldicellulosiruptor* sp., 60 °C, and Batch	Xylose or Glucose	Acetate, Butyrate, Propionate, Ethanol, Lactate, Butanol	1.58 or 1.71	[127]
Bacillus coagulans and Thermoanaerobacterium, 60 °C, and Chemostat	Glucose	Lactate, Acetate, Formate, Butyrate, Ethanol	0.85	[128]
Co-culture (*Caldicellulosiruptor kristjanssonii* and *C. saccharolyticus*), 70 °C, and Batch	Glucose-xylose	Acetate	3.6	[37]

TABLE 1.2 (*Continued*)

Organism, Growth Temperature (°C), and Culturing Type	Substrate	End Products	H_2 Yield (mol/mol)[a]	Reference
Thermobrachiumcelere, Thermoanaerobacterium aotearoense, Clostridium thermopalmarium, 70 °C, and Batch	Xylose	Acetate, Ethanol	1.84	[129]
Mixed culture, 70 °C, and Batch	Xylose	Acetate, Ethanol, Lactate	1.62	[130]
Compost microflora and *Caldicellulosiruptor saccharolyticus*, 70 °C, and Batch	Glucose-Xylose	Acetate, Lactate	2.3	[88]

[a]mol of H_2 produced/mol of substrate consumed.

1.3.2 BIOH$_2$ PRODUCTION FROM COMPLEX SUBSTRATES

As discussed above, thermophilic and hyperthermophilic microbes can ferment mono- and disaccharides (e.g., glucose, xylose, arabinose, and cellobiose, Table 1.2) efficiently. However, the use of monosaccharides for biofuels competes with food use, and also the cost of monosaccharides (e.g., glucose) is more than 3-fold higher than the price of BioH_2 produced. Inexpensive feedstocks including lignocellulosic materials have been used as substrates for H_2 production by pure or mixed cultures of thermophiles and hyperthermophiles (Table 1.3). For example, rice straw [75, 76], cornstalk waste [77, 78], wheat straw [79, 80], corn stover [81], sweet sorghum [82], carrot pulp hydrolysate [83], vegetable kitchen waste [84], maize leaves and sugarcane baggase [7], shredded paper waste [31], and delignified wood fibers [20] have been reported for H_2 production by thermophiles.

Among reported thermophiles, *Caldicellulosiruptor saccharolyticus* has been identified as a suitable candidate for H_2 production. *C. saccharolyticus* produces thermostable cellulolytic and xylanolytic enzymes, and grows at ≥65 °C on a wide variety of lignocellulosic biomasses including switchgrass, sweet sorghum, sugarcane bagasse, wheat straw, maize

TABLE 1.3 Overview of H_2-Producing Thermophiles and Hyperthermophiles Utilizing Complex Substrates

Organism, Growth temperature (°C), and Culturing Type	**Substrate**	**End Products**	**H_2 Yield**	**Reference**
Clostridium pasteurianum, Clostridium stercorarium and *Thermoanaerobacterium saccharolyticum*, 55 °C, and Batch	Rice straw	Acetate, Butyrate	1.11 mmol H_2/g TS	[75]
Anaerobic mixed microflora, 55 °C, and CSTR	Cellulose	Acetate, Butyrate	15.16 mmol H_2/g Cellulose	[71]
Anaerobic mixed microflora, 60 °C, and CSTR	Cellulose	Acetate, Butyrate	19.01 mmol H_2/g Cellulose	[71]
Co-culture (*Clostridium thermocellum* and *Clostridium thermosaccharolyticum*), 55 °C, and Batch	Cornstalk waste	Ethanol, Acetate, Butyrate	3.04 mmol H_2/g Cornstalk	[77]
Thermoanaerobacterium saccharolyticum, T. *thermosulfurigenes*, *T.* sp., *Bacillus* sp., *Anoxybacillus* sp., *B. lentus*, and *Geobacillus* sp., 60 °*C*, and Batch	Sago starch	Acetate, Ethanol	19.72 mmol H_2/g Starch	[131]
Mixed anaerobic culture from rotted wood crumb, 50 °C, and Batch	Lime treated cornstalk waste	Not Reported	6.93 mmol H_2/g-TVS	[78]
Thermoanaerobacterium sp., *Thermoanaerobacter* sp., *Caloramater* sp. and *Anoxybacillus* sp., 60 °C, and Batch	Oil palm trunk hydrolysate	Acetate, Butyrate, Ethanol, Lactate, Butanol	13.42 mmol H_2/g sugar consumed	[127]
Thermoanaerobacterium saccharolyticum, Thermoanaerobacterium thermosaccharolyticum, *Anoxybacillus*sp., *Geobacillus* sp. and *Clostridium* sp., 60 °C, and Continuous	Cassava starch processing wastewater	Acetate, Ethanol	10.84 mmol H_2/g sugar consumed	[35]
Caldicellulosiruptor saccharolyticus, 60 °C, and Batch	Carrot pulp hydrolysate	Acetate, Lactate	2.8 mol H_2/mol Hexoses	[83]

TABLE 1.3 (*Continued*)

Organism, Growth temperature (°C), and Culturing Type	Substrate	End Products	H_2 Yield	Reference
Thermotoga neapolitana, 60 °C, and Batch	Carrot pulp hydrolysate	Acetate, Lactate	2.7 mol H_2/mol Hexoses	[83]
Thermoanaerobacterium thermosaccharolyticum, Clostridium sp., 55 °C, and CSTR	Vegetable kitchen waste	Butyrate, Lactate	1.7 mmol H_2/g COD	[84]
Thermotoga neapolitana, 75 °C and Batch	Potato stem peels	Acetate	2.6–3.8 mol H_2/ mol Glucose	[36]
Caldicellulosiruptor saccharolyticus, 72 °C and Batch	Potato stem peels	Acetate	2.4–3.4 mol H_2/ mol Glucose	[36]
Thermotoga neapolitana, 75 °C, and Batch	Rice straw	Not Reported	2.7 mmol H_2/g Rice Straw	[76]
Thermoanaerobacterium sp., 70 °C, and Batch	Sweet sorghum baggase	Acetate, Lactate	2.6 mol H_2/mol Hexoses	[82]
Thermoanaerobacterium thermosaccharolyticum W16, 60 °C, and Batch	Corn stover	Acetate, Butyrate, Ethanol	108.5 mmol H_2/L[#]	[81]
Caldicellulosiruptor saccharolyticus, 72 °C, and Batch	Miscanthus hydrolysate	Acetate, Lactate	3.4 mol H_2/mol Hexoses	[25]
Co-culture (*Clostridium thermocellum* and *Clostridium thermopalmarium*), 55 °C, and Batch	Cellulose	Acetate, Butyrate, Ethanol	1.36 mol H_2/mol Glucose Equivalent	[132]
Caldanaerobacter subteraneus, Thermoanaerobacter subteraneus, Thermoanarobacterium thermosaccharolyticum, 70 °C, and CSTR	Wheat straw hydrolysate	Acetate, Butyrate, Propionate, Ethanol, Lactate, Formate	9.46 mmolH_2/g Sugars	[79]
Thermotoga neapolitana, 80 °C, and Batch	Miscanthus hydrolysate	Acetate, Lactate	2.9 mol H_2/mol Hexoses	[25]

TABLE 1.3 (*Continued*)

Organism, Growth temperature (°C), and Culturing Type	Substrate	End Products	H_2 Yield	Reference
Caldicellulosiruptor saccharolyticus, 70 °C, and Batch	Maize leaves	Not Reported	1.87 mmol H_2/g of VS	[7]
Caldicellulosiruptor saccharolyticus, 70 °C, and Batch	Sugarcane baggase	Not Reported	0.87 mmol H_2/g of VS	[7]
Co-culture (*Clostridium thermocellum* JN4 and *Thermoanaerobacterium thermosaccharolyticum* GD17), 60 °C, and Batch	Cellulose	Acetate, Butyrate, Ethanol	1.8 mol H_2/mol Glucose	[8]
Clostridium thermocellum ATCC 27405, 60 °C, and Chemostat	Dried distiller's Grain (DDG)	Acetate, Lactate, Ethanol, Formate	1.7 mol H_2/mol Fermented Substrate	[133]
Thermoanaerobacterium sp., 60 °C, and Packed-bed reactor	Pulverized garbage and shredded paper waste	Not Reported	2.4 mol H_2/mol Hexoses	[31]
Clostridium thermocellum, 60 °C, and Batch	Delignified wood fibers	Acetate, Ethanol, Lactate, Formate	1.6 mol H_2/mol Fermented Substrate	[20]

[#]Concentrations.

leaves, and silphium [4, 7, 85]. *C. saccharolyticus* has a high number of ABC transporters for a wide variety of substrates, and can tolerate high partial pressures of H_2 [14, 86, 87]. Another thermophile, *C.owensensis* (ATCC 700167/DSM 13100) is capable of using a broad range of carbohydrates and producing H_2 as a metabolic by-product. Co-culturing of *C.owensensis* with the enriched compost microflora resulted in fast, simultaneous consumption of both glucose and xylose in the medium with a high specific H_2 production rate (3.6 mol H_2/mol sugar consumed, [88]). *C. Thermocellum* JN4 produces 0.8 mol H_2/mol glucose whereas, a two-fold increase (1.8 mol H_2/mol glucose) in H_2 production was observed

from microcrystalline cellulose when JN4 was co-cultured with *Thermoanaerobacterium thermosaccharolyticum* GD17 [8]. Overall, many thermophilic and hyperthermophilic microbes use complex substrates, and produce high H_2 yield near to 4 mol H_2/mol glucose, but with higher thermal energy consumption (at least 2.5 fold compared to mesophiles) for maintenance of their temperatures.

As we know, organic acids (acetate, butyrate, formate, lactate, and propionate) are by-products of dark fermentation. The highest theoretical yields of H_2 are associated with acetate as the only volatile fatty acid product. Even with 4 mol H_2/mol glucose ($C_6H_{12}O_6 + 2H_2O \rightarrow 2CH_3COOH + 2CO_2 + 4H_2$), we harness only 33% yield of H_2 because 12 mol of H_2 are theoretically available in one mole of glucose ($C_6H_{12}O_6 + 6H_2O \rightarrow 12H_2 + 6CO_2$). It is necessary to enhance BioH_2 production, and one such method is sequential dark-photo fermentations (SDPF). Organic acids produced during dark fermentation can be converted to H_2 and CO_2 by photofermentation [57, 89], and CO_2 produced can be used as a substrate during photofermentation. A microalgal-based SDPF system was shown to produce 6.5 mol H_2/mol hexose [90]. This SDPF system has advantages because it produces BioH_2 with low CO_2 emissions as well as high reduction in COD. The SDPF system has certain limitations, which poses a challenge for its successful implementation. The cost of photofermentation in the SDPF system is the main bottleneck in scaling up the process. Preliminary cost estimates in the literature indicate that photobiological H_2 could be produced in large-scale systems (100 ha and more) at a cost of 10–15 Euro/GJ (http://edepot.wur.nl/17056).

1.3.3 BIOH$_2$ PRODUCTION FROM UNTREATED COMPLEX SUBSTRATES

Thermophilic H_2 production is currently being carried out using pretreated (alkali and acid based, enzymatic hydrolysis-natural or synthetic mixture, hydrothermal, or ammonia) lignocellulosic substrates. For example, poplar leaves were first pretreated using acid and alkali

as well as enzymes, and then fermented using anaerobic mixed culture of bacteria for H_2 production [91]. This suggests that conversion of lignocellulose from specific energy crops, agricultural residues, or forest products to H_2 will require: (i) various physiochemical pretreatments; (ii) enzymatic pretreatment (enzymes cocktails to hydrolyze cellulose and hemicellulose into to fermentable sugars usually under conditions of high temperature and extreme pH); (iii) removal of inhibitors (e.g., 5-hydroxymethylfurfural, furfural, acetic acid, and phenolic compounds) released during pretreatment; and (iv) robust fermentative microbes. The inclusion of the pretreatment and inhibitors removal steps reduces the overall cost-efficiency of the conversion process.

A viable option to lower the costs of feedstock and lignocellulolytic commercial enzymes is to screen for and identify potent H_2-producing microorganisms (saccharolytic fermentative extremophiles) capable of using cellulose and hemicellulose directly from the biomass without pretreatment. This would eliminate the need for separate steps of pretreatment, lignocellulolytic thermostable enzymes production, enzymatic hydrolysis of biomass, and improve the process economics. However, information on such microorganisms, which produce H_2 from untreated lignocellulosic biomass, is relatively scarce. *Caldicellulosiruptor bescii* sp. nov. DSM 6725 used various types of untreated plant biomasses (poplar, low-lignin grasses such as Napier and Bermuda grasses, and high-lignin containing grasses such as switchgrass), as well as cellulose and xylan [19]. A thermophilic mixed culture [75], a co-culture of *Clostridium thermocellum* and *C. thermosaccharolyticum* [77], and *Caldicellulosiruptor saccharolyticus* [7] have also been shown to use untreated lignocellulosic biomasses. Recently *Thermoanaerobacterium thermosaccharolyticum* M18 was shown to produce H_2 with a yield of 3.23 to 3.48 mmol/g corn cob, corn stalk, or wheat straw without any physicochemical or biological pretreatment [15]. Su et al. [92] reported that the presence of thermostable cellulases and hemicellulases supported the microbes to hydrolyze plant cell wall polysaccharides into simple sugars. Table 1.4 summarizes the recent studies of H_2 production from untreated lignocellulosic biomass using thermophiles.

TABLE 1.4 H_2 Production from Untreated Lignocellulosic Materials

Feedstock	Temp (°C)	Bacterial Strain	Pretreatment	H_2 Yield	Reference
Corn cob, Corn stalk, and Wheat straw	60	*Thermoanaerobacterium thermosaccharolyticum* M18	None	3.23 to 3.48 mmol H_2/g substrate	[15]
Switchgrass (SWG) and microcrystalline cellulose (MCC)	65	*Caldicellulosiruptor saccharolyticus* DSM 8903	None	11.2 mmol H_2/g SWG and 9.4 mmol H_2/g MCC	[4]
Rice straw	55	Heat treated sludge	Physical pulverization	1.11 mmol H_2/g TS	[75]
Lignocellulosic feedstock*	30	Enriched sludge	None	0.56 mmol H_2/g Raw Sample	[134]
Potato stem peels	75	*Thermotoga neapolitana*	None	3.8 mol/mol Glucose Equivalents	[36]
Potato stem peels	72	*Caldicellulosiruptor saccharolyticus*	None	3.5 mol/mol Glucose Equivalents	[36]
Maize leaves	70	*Caldicellulosiruptor saccharolyticus*	None	0.68 mmol H_2/g Dry Biomass	[7]
Poplar, and Switchgrass	70	*Anaerocellum thermophilum* DSM 6725	None	1.6 mmol/L for Poplar and 3.8 mmol/L for Switchgrass[#]	[19]
Corn husk, Ground nut shell, and Rice husk*	37	Mixed consortia from buffalo dung compost	None	2.93 mmol H_2/g TVS	[135]

TABLE 1.4 (*Continued*)

Feedstock	Temp (°C)	Bacterial Strain	Pretreatment	H_2 Yield	Reference
Dried distillers grain (DDG), Barley hulls (BH), and Fusarium head blight contaminated barley hulls (CBH)	60	*Clostridium thermocellum* ATCC 27405	None	1.07 mmol H_2/g DDG, 1.07 mmol H_2/g BH, and 1.06 mmol H_2/g CBH	[133]

*Mesophilic study.

#Concentrations.

1.4 INDUSTRIAL OPERATION OF H_2 PRODUCTION

The majority of the laboratory studies on $BioH_2$ production under dark fermentation conditions have been performed in a batch reactor system, whereas industrial scale H_2 production may need a continuous or at least semicontinuous reactor system for enhanced and uninterrupted $BioH_2$ production [93]. CSTR is one of the preferred choices for fermentative H_2 production from various substrates [94, 95]. A biofilm-based or granule-based reactor design to retain active microbes for $BioH_2$ production has been recommended [46]. Steady state operation of CSTRs has been successfully demonstrated up to a period of 3 months producing $BioH_2$ at a rate of 56 mL H_2/L/h at a biomass concentration of 1.2 g volatile suspended solids (VSS) /L [96, 97]. Lee et al. [98] increased biomass loadings (20 and 40 g VSS/L) resulting in improved rate of H_2 production (541 and 9300 mL H_2/L/h, respectively) using CSTR with modifications. For commercial feasibility of the bioprocess of H_2 production, a waste (condensed molasses) was used as substrate in laboratory scale CSTR with *Clostridium* spp. being the dominant bacteria. In this study at an organic loading rate of 320 g COD/L with a hydraulic retention time (HRT) of 3 h, 390 mmolH_2/L was produced [99]. Kim and Lee [94] used tofu processing waste and digester sludge for H_2 production with 2.3 molH_2/mol glucose

equivalent in a batch, and also in a continuous mode using a thermophilic mixed culture.

Vatsala et al. [30] used mesophilic cocultures of *Citrobacter freundii*, *Enterobacter aerogenes* E10, and *Rhodopseudomonas palustris* P2 to produce H_2 at laboratory scale with glucose as carbon source. They also scaled up their process to 100 m^3 to evaluate the feasibility of H_2 production using distillery effluent from the sugarcane industry, and successfully produced 21.38 kg of H_2 in 40 h in a batch reactor with an average yield of 2.76 mol H_2/mol of glucose using mesophilic bacterial strains. Conversion of distillery effluents or wastewaters for H_2 production clearly well suits the overall concept of waste to energy. Use of wastewater or effluent streams for H_2 production poses dual advantages: production of energy and significant reduction of COD and BOD of wastewater.

H_2 production by dark fermentation is a strictly anaerobic process. Therefore O_2 elimination is required from the growth medium. In most of the laboratory studies, researchers use N_2 or Ar gas to remove O_2. At industrial scale, use of N_2 or Ar gas may not be feasible due to cost constraints. However, fabrication of continuous or semicontinuous reactors with recirculation of the purged gas may reduce the cost of operation. Also, a separate facility is required to recover and store BioH_2 produced during the industrial operation to shift the equilibrium towards H_2 production, otherwise increase in the partial pressure of H_2 can inhibit electron carriers (e.g., NADH and ferrodoxin). Thus, industrial scale-up of BioH_2 has multiple issues that need to be addressed adequately. These include selection and cost of the process, creating anaerobic conditions in a large reactor, purification and storage of BioH_2, and also safety parameters. Integration of the existing optimized technologies of dark and photofermentation may be a good strategy to produce BioH_2 at competitive rates.

Another challenge is overlapping features of BioH_2 production to methanogenic anaerobic digestion. By-products of BioH_2 production process such as acetate and CO_2 are quickly consumed by methanogens to form methane. To scale-up the process, H_2-consuming bacteria need to be replaced by a typical mixed culture involved in anaerobic digestion. Temperature, pH, and HRT are the most applicable methods to prevent methanogenesis in an industrial scale system of H_2 production. Extremethermophilic conditions (>70 °C) inhibit methanogens

and thermodynamically favor H_2 production as end product [100]. Short HRT (< 3 days) would favor H_2 production as methanogens need longer HRT [101]. Low pH is also an effective parameter to limit H_2 consumers thus promoting H_2 producers [102]. Heat shock and addition of 2-bromoethanesulfonic (BES) acid have been reported to inhibit methanogens. Heat shock treatment (100 °C or above) before the experiments kill methanogens, but enrich H_2 producing sporulating bacteria such as *Clostridium* sp. [103]. Inducing low pH and addition of BES may not be suitable for large-scale industrial application of H_2 production. Chen et al. [97] achieved effective removal of methanogens at 12 h HRT and effectively produced $BioH_2$ from wastewater. However, pH control alone, even at 4.5, could not inhibit methanogens at long HRT (9 days) in semi-CSTR reactors [101].

Many times laboratory results that look promising may differ significantly at industrial scale. Thus, there is a need to strengthen the focus on projects leading from laboratory to scale-up processes for $BioH_2$ production. Also, discrepancies of H_2-production have been obtained under various experimental conditions by researchers making it difficult to compare their results. Uniformity in expressing the yields of H_2 obtained will simplify the comparative analyzes. Optimized pilot-scale demonstration projects are required to explore the potential of H_2 research at industrial scale. It was estimated that H_2 produced by a 1000L bioreactor connected with "5.0 kW" proton exchange membrane fuel cell would be sufficient to meet the electricity requirement of an average residential load [13]. On site production and utilization of $BioH_2$ from renewable resources is considered to be a cost-effective and viable industrial model [104]. This will not only eliminate the transportation cost of biomass, but also produce energy that can be used to partially support the parent industrial activity that is creating the feedstock as waste material or by-product. Utilization of inexpensive substrates and appropriate bioreactors are critical for sustainable $BioH_2$ production. Combining dark and photofermentation will further help to achieve higher yields of H_2. Bridging the gap between scientists who work on $BioH_2$ production and engineers who develop H_2 fuel cell technologies is necessary for success in this field. Fuel cell engineers need to know about the rate of H_2 production by biological systems and scientists should understand the H_2 requirement in the fuel cell [105].

1.5 DECENTRALIZED INDUSTRIAL SCALE H_2 PRODUCTION

Any suitable and abundant substrate for $BioH_2$ production in one geographical location can be scarce at another location. Therefore, a decentralized system of $BioH_2$ production can be useful to materialize the scale up of this energy source [106]. Locally owned biorefineries based on regional biomass or wastes utilization may reduce treatment and handling cost with no need of arable land. In cities and towns, wastewater and kitchen waste (as a part of municipality waste) are the most appropriate substrates for $BioH_2$ production. In remote and less populated areas, however, locally available abundant feedstocks will likely be suitable substrates. In Midwestern US (Illinois, Indiana, Iowa, Minnesota, Missouri, Nebraska, North Dakota, South Dakota, and Wisconsin) corn stover, prairie cordgrass, switchgrass, and ponderosa pine are abundant feedstocks for $BioH_2$ generation. For example, approximately 750,000 tons of wood-waste from the Black Hills of South Dakota is already available as slash from previous forest thinning, and could be converted into $BioH_2$. On the other hand, Asia is rich in agricultural residues, especially rice straw, wheat straw, and sugarcane baggase, which can be used for $BioH_2$ production. Using abundantly available, inexpensive, and renewable feedstock can be the way to lower the $BioH_2$ production cost for a given region.

The U.S. Department of Energy has been promoting a decentralized system for H_2 production [107]. It circumvents the need for a costly distribution infrastructure. In a study of a decentralized system in south-west Georgia, H_2 was produced using pelletized peanut shells and pyrolysis of biomass yielded soluble and insoluble fractions of oil. Soluble bio-oil was converted to H_2 via catalytic steam reforming and shift conversion. The maximum yield achieved was 1.72 g H_2/100 g bio-oil in the overall stoichiometry whereas the insoluble fraction was used as a source of adhesive formulations [108]. After cost analysis of an efficient pyrolysis process of bio-oil (soluble fraction), the selling price of H_2 was \$6.05/GJ. This figure is promising, reflecting the abundant supply of local feedstock (peanut shells) and, coproduct value, and small-scale operation. In other research on H_2 production, Liu et al. [109] demonstrated cost-effective H_2 production through acetate in an electricity-mediated electrolysis process of an anaerobic microbial fuel cell. Acetate is a coproduct made during

H_2 production via dark fermentation. The energy generation from organic wastes such as acetate, if coupled with a dark fermentation process, has the potential to produce >4 mol H_2/mol glucose. However, in reality, existence of cost-effective scaled-up reactors with purified H_2 is scarce[104]. Integrating agricultural and industrial activities for BioH_2 production seem suitable for small-scale decentralized systems [110]. Developments in this direction will truly demonstrate the potential of H_2 energy as a major, global energy source.

1.6 SUMMARY AND CONCLUSIOINS

BioH_2 seems to be a lucrative alternate energy but it depends on how economical the BioH_2 process can be at industrial scale. To produce H_2 inexpensively a few of the prerequisites are abundant and economical biodegradable wastes—like agricultural residues, industrial effluents, or municipal waste, robust microbes, and suitable bioreactor configuration. Establishing H_2 production plants in the vicinity of a parent industry producing waste or near the site of biomass availability will surely reduce the BioH_2production cost. This decentralized H_2 production strategy will reduce the cost of transport and storage. Most of the existing laboratory scale processes of BioH_2 production from complex wastes, such as lignocellulosic feedstocks, use several steps (e.g., pretreatment, hydrolysis, removal of inhibitors, and fermentation). The inclusion of several steps reduces the overall cost-efficiency of the process. An alternative to the use of various steps in H_2 production is the development of an efficient and cost-effective single step process using thermophiles (innovative thermophilic CBP), which can degrade and ferment untreated-lignocellulose. The use of elevated temperatures offer several potential advantages such as: (i) improved hydrolysis of cellulosic substrates; (ii) higher mass transfer rates leading to better substrate solubility; and (iii) lowered risk of microbial contamination, thus improving the overall economics of the process. For these reasons, thermophilic H_2 production in a consolidated mode (e.g., CBP) can be a preferred choice at the industrial scale; and additional advantages include increased H_2 yield, favorable thermodynamic conditions, and the ability to use a wide variety of substrates. The

development of innovative thermophilic CBP will likely impact current multiple-step conversion processes of complex wastes to H_2 by providing a more efficient, sustainable, and economical process. However, there are also drawbacks of H_2 production at higher temperature, including: (a) thermophilic H_2 production under anaerobic fermentation process needs energy for heating and maintenance; and (b) low cell densities at higher temperatures reduce the H_2 yield. To overcome the first issue, energy from hot wastewater of industries such as distilleries, food and paper processing units could be recovered to maintain temperature of thermophilic bacteria. To address the second problem, cell immobilization technologies would be required to retain the cells in the reactors.

Regional industrial-academia partnership is also pertinent for successful production of H_2. A process that lends itself well to this type of cooperation is the coupling of dark fermentation and photofermentation processes of H_2 production along with localized energy production (see, for example, Fig. 1.1). Identified research groups could work in the area of substrate selection for dark fermentation, optimization of bioreactor conditions for dark fermentation or photofermentation, cost analysis, life cycle assessment studies, and issues of safety or storage of $BioH_2$, to evaluate feasibility of a sustainable industrial process. H_2 energy funding agencies, scientists, and engineers may then reliably predict the probability of successful scale-up based on thorough laboratory scale analysis of H_2 production. Finally we need to focus time and energy on building a global research group or network, working towards a common goal of industrialization of H_2 production.

1.7 ACKNOWLEDGEMENT

Aditya Bhalla, Jia Wang, David Salem, and Rajesh Sani gratefully acknowledge the financial support provided by National Science Foundation – Industry/University Cooperative Research Center. The support from the Department of Chemical and Biological Engineering at the South Dakota School of Mines and Technology is also acknowledged. Sudhir Kumar is thankful to Jaypee University of Information Technology, Solan, HP, India for granting a sabbatical leave for doing research work at the South Dakota.

KEYWORDS

- **Biohydrogen**
- **Extremophiles**
- **Hyperthermophiles**
- **Thermophiles**
- **Untreated Lignocellulosics**

REFERENCES

1. Lange, J. P. (2007). Lignocellulosic conversion: An introduction to chemistry, process and economics. *Biofuel. Bioprod. Bior*. *1*, 39–48.
2. Bhalla, A., Bansal, N., Kumar, S., Bischoff, K. M., Sani, R. K. (2013). Improved lignocellulose conversion to biofuels with thermophilic bacteria and thermostable enzymes. *Bioresour. Technol*. *128*, 751–759.
3. Lynd, L. R., van Zyl, W. H., McBride, J. E., Laser, M. (2005). Consolidated bioprocessing of cellulosic biomass: an update. *Curr. Opin. Biotechnol*. *16*, 577–583.
4. Talluri, S., Raj, S. M., Christopher, L. P. (2013). Consolidated bioprocessing of untreated switchgrass to hydrogen by the extreme thermophile *Caldicellulosiruptor saccharolyticus* DSM 8903. *Bioresour Technol*. *139*, 272–279.
5. Barnard, D., Casanueva, A., Tuffin, M., Cowan, D. (2010). Extremophiles in biofuel synthesis. *Environ. Technol*. *31*, 871–888.
6. Ntaikou, I., Antonopoulou, G., Lyberatos, G. (2010). Biohydrogen production from biomass and wastes via dark fermentation: a review. *Waste Biomass Valor. 1*, 21–39.
7. Ivanova, G., Rakhely, G., Kovacs, K. L. (2009). Thermophilic biohydrogen production from energy plants by *Caldicellulosiruptor saccharolyticus* and comparison with related studies. *Int. J. Hydrogen Energy*. *34*, 3659–3670.
8. Liu, Y., Yu, P., Song, X., Qu, Y. (2008). Hydrogen production from cellulose by co-culture of *Clostridium thermocellum* JN4 and *Thermoanaerobacterium thermosaccharolyticum* GD 17. *Int. J. Hydrogen Energy*. *33*, 2927–2933.
9. Kanai, T., Imanaka, H., Nakajima, A., Uwamori, K., Omori, Y., Fukui, T., Atomi, H., Imanaka, T. (2005). Continuous hydrogen production by the hyperthermophilic archon, *Thermococcuskodakaraensis* KOD1. *J. Biotechnol*. *116*, 271–282.
10. Saripan, A. F., Reungsang, A. (2013). Biohydrogen production by *Thermoanaerobacterium thermosaccharolyticum* KKU-ED1: culture conditions optimization using mixed xylose/arabinose as substrate. *Electronic J. Biotechnol*. *16*(*1),* DOI: 10.2225/vol16-issue1-fulltext-1.
11. Oh, Y. K., Raj, S. M., Jung, G. Y., Park, S. (2011). Current status of the metabolic engineering of microorganisms for biohydrogen production. *Bioresour. Technol*. *102*, 8357–8367.
12. Hallenbeck, P. C., Ghosh, D., Skonieczny, M. T., Yargeau, V. Microbiological and engineering aspects of biohydrogen production. *Indian J. Microbiol*. (2009). *49,* 48–59.

13. Levin, D. B., Pitt, L., Love, M. (2004). Biohydrogen production: prospects and limitations to practical application. *Int. J. Hydrogen Energy*. *29*, 173–185.
14. Willquist, K., Zeidan, A. A., van Niel, E. W. J. (2010). Physiological characteristics of the extreme thermophile *Caldicellulosiruptor saccharolyticus*: an efficient hydrogen cell factory. *Microb. Cell Fact*. *9*, 89.
15. Cao, G. L., Zhao, L., Wang, A. J., Wang, Z. Y., Ren, N. Q. (2014). Single-step bioconversion of lignocellulose to hydrogen using novel moderately thermophilic bacteria. *Biotechnol. Biofuels*. *7*, 82.
16. Raj, S. M., Talluri, S., Christopher, L. P. (2012). Thermophilic Hydrogen production from renewable resources: current status and future perspectives. *BioEnerg. Res*. *5*, 515–531.
17. Shaw, A. J., Hogsett, D. A., Lynd, L. R. Natural competence in *Thermoanaerobacter* and *Thermoanaerobacterium* species. *Appl. Environ. Microbiol*. (2010). *76,* 4713–4719.
18. Karadag, D., Mäkinen, A. E., Efimova, E., Puhakka, J. A. (2009). Thermophilic biohydrogen production by an anaerobic heat treated-hot spring culture. *Bioresour. Technol*. *100*, 5790–5795.
19. Yang, S. J., Kataeva, I., Hamilton-Brehm, S. D., Engle, N. L., Tschaplinski, T. J., Doeppke, C., Davis, M., Westpheling, J., Adams, M. W. (2009). Efficient degradation of lignocellulosic plant biomass, without pretreatment, by the thermophilic anaerobe "*Anaerocellumthermophilum*" DSM 6725. *Appl. Environ. Microbiol*. *75*, 4762–4769.
20. Levin, D. B., Sparling, R., Islam, R., Cicek, N. (2006). Hydrogen production by *Clostridium thermocellum* 27405 from cellulosic biomass substrates. *Int. J. Hydrogen Energy*. *31*, 1496–1503.
21. Saratale, G. D., Saratale, R. G., Chang, J. S. (2013). Biohydrogen from renewable resources. In: Pandey A (ed.), *Biohydrogen*. Elsevier, San Diego. 185–221.
22. Cheng, C. L., Lo, Y. C., Lee, K. S., Lee, D. J., Lin, C. Y., Chang, J. S. (2011). Biohydrogen production from lignocellulosic feedstock. *Bioresour. Technol*. *102*, 8514–8523.
23. Baghchehsaraee, B., Nakhla, G., Karamanev, D., Margaritis, A. (2010). Fermentative hydrogen production by diverse microflora. *Int. J. Hydrogen Energy*. *35*, 5021–5027.
24. Bianchi, L., Mannelli, F., Viti, C., Adessi, A., Philippis, R. D. (2010). Hydrogen-producing purple nonsulfur bacteria isolated from the trophic lake Averno (Naples, Italy). *Int. J. Hydrogen Energy*. *35*, 12216–12223.
25. de Vrije, T., Bakker, R. R., Budde, M. A., Lai, M. H., Mars, A. E., Claassen, P. A. M. (2009). Efficient hydrogen production from the lignocellulosic energy crop *Miscanthus* by the extreme thermophilic bacteria *Caldicellulosiruptor saccharolyticus* and *Thermotoganeapolitana*. *Biotechnol. Biofuels*. *2*, 12.
26. Ananyev, G., Carrieri, D., Dismukes, G. C. (2008). Optimization of metabolic capacity and flux through environmental cues to maximize hydrogen production by the cyanobacterium "*Arthrospira* (*Spirulina) maxima*". *Appl. Environ. Microbiol*. *74*, 6102–6113.
27. Gómez, X., Fernández, C., Fierro, J., Sánchez, M. E., Escapa, A., Morán, A. (2011). Hydrogen production: two stage processes for waste degradation. *Bioresour. Technol*. *102*, 8621–8627.

28. Lakshmidevi, R., Muthukumar, K. (2010). Enzymatic saccharification and fermentation of paper and pulp industry effluent for biohydrogen production. *Int. J. Hydrogen Energy*. *35*, 3389–3400.
29. Kim, J. K., Nhat, L., Chun, Y. N., Kim, S. W. (2008). Hydrogen production conditions from food waste by dark fermentation with *Clostridium beijerinckii* KCTC 1785. *Biotechnol. Bioprocess Eng*. *13*, 499–504.
30. Vatsala, T. M., Raj, S. M., Manimaran, A. (2008). A pilot-scale study of biohydrogen production from distillery effluent using defined bacterial coculture. *Int. J. Hydrogen Energy*. *33*, 5404–5415.
31. Ueno, Y., Fukui, H., Goto, M. (2007). Operation of a two-stage fermentation process producing hydrogen and methane from organic waste. *Environ. Sci. Technol*. *41*, 1413–1419.
32. Masset, J., Calusinska, M., Hamilton, C., Hiligsmann, S., Joris, B., Wilmotte, A., Thonart, P. (2012). Fermentative hydrogen production from glucose and starch using pure strains and artificial cocultures of *Clostridium* spp. *Biotechnol. Biofuels*. *5*, 35.
33. Pandu, K., Joseph, S. (2012). Comparisons and limitations of biohydrogen production processes: a review. *Int. J. Adv. Eng. Technol*. *2*, 342–356.
34. Rittmann, S., Herwig, C. (2012). A comprehensive and quantitative review of dark fermentation biohydrogen production. *Microb. Cell Fact*. *11*, 115.
35. O-Thong, S., Mamimin, C., Prasertsan, P. (2011). Effect of temperature and initial pH on biohydrogen production from palm oil mill effluents: long-term evaluation and microbial community analysis. *Electronic J. Biotechnol*. *14*(*5*), DOI: 10.2225/vol14-issue5-fulltext-9.
36. Mars, A. E., Veuskens, T., Budde, M. A. W., van Doeveren, P. F. N. M., Lips, S. J., Bakker, R. R., de Vrije, G. J., Claassen, P. A. M. (2010). Biohydrogen production from untreated and hydrolyzed potato steam peels by the extreme thermophiles *Caldicellulosiruptor saccharolyticus* and *Thermotoganeapolitana*. *Int. J. Hydrogen Energy*. *35*, 7730–7737.
37. Zeidan, A. A., Radstorm, P., van Niel, E. W. J. (2010). Stable coexistence of two *Caldicellulosiruptor* species in a de novo constructed hydrogen producing coculture. *Microb. Cell Fact*. *9*, 102.
38. Chen, S. D., Lee, K. S., Lo, Y. C., Chen, W. M., Wu, J. F., Lin, C. Y., Chang, J. S. (2008). Batch and continuous biohydrogen production from starch hydrolysate by *Clostridium* species. *Int. J. Hydrogen Energy*. *33*, 1803–1812.
39. de Vrije, T., Mars, A. E., Budde, M. A. W., Lai, M. H., Dijkeme, C., de Waard, P., Claassen, P. A. M. (2007). Glycolytic pathway and hydrogen yield studies of the extreme thermophile *Caldicellulosiruptor saccharolyticus*. *Appl. Microbiol. Biotechnol*. *74*, 1358–1367.
40. Lin, C. Y., Hung, C. H., Chen, C. H., Chung, W. T., Chen, L. H. (2006). Effects of initial pH on fermentative hydrogen production from xylose using natural mixed cultures. *Process Biochem*. *41*, 1383–1390.
41. Kádár, Z., deVrije, T., van Noorden, G. E., Budde, M. A. W., Szengyel, Z., Réczey, K., Claassen, P. A. M. (2004). Yields from glucose, xylose, and paper sludge hydrolysate during hydrogen production by the extreme thermophile *Caldicellulosiruptor saccharolyticus*. *Appl. Biochem. Biotechnol*. *114*, 497–508.

42. Lin, C. Y., Jo, C. H. (2003). Hydrogen production from sucrose using an anaerobic sequencing batch reactor process. *J. Chem. Technol. Biotechnol*. *78*, 678–684.
43. van Niel, E. W. J., Budde, M. A. W., de Haas, G. G., van der Wal, F. J., Claassen, P. A. M., Stams, A. J. M. (2002). Distinctive properties of high hydrogen producing extreme thermophiles, *Caldicellulosiruptor saccharolyticus* and *Thermotogaelffi*. *Int. J. Hydrogen Energy*. *27*, 1391–1398.
44. Vehicle Technologies Program: Fact #205: February 25, 2002. Hydrogen Cost and Worldwide Production. eere.energy.gov. Retrieved 2009–09–19.
45. Lal, R. (2004). Soil carbon sequestration impacts on global climate change and food security. *Sci*. *304*, 1623–1627.
46. Ren, N., Guo, W., Liu, B., Cao, G., Ding, J. (2011).Biological hydrogen production by dark fermentation: challenges and prospects towards scaled-up production. *Curr. Opin. Biotechnol*. *22*, 365–370.
47. Yang, H. H., Guo, L. J., Liu, F. (2010). Enhanced bio-hydrogen production from corncob by a two-step process: dark- and photo-fermentation. *Bioresour. Technol*. *101*, 2049–2052.
48. Jayalakshmi, S., Joseph, K., Sukumaran, V. (2009). Biohydrogen generation from kitchen waste in an inclined plug flow reactor. *Int. J. Hydrogen Energy*. *34*, 8854–8858.
49. Karlsson, A., Vallin, L., Ejlertsson, J. (2008). Effects of temperature, hydraulic retention time and hydrogen extraction rate on hydrogen production from the fermentation of food industry residues and manure. *Int. J. Hydrogen Energy*. *33*, 953–962.
50. Lay, J. J., Fan, K. S., Chang, J., Ku, C. H. (2003). Influence of chemical nature of organic wastes on their conversion to hydrogen by heat-shock digested sludge. *Int. J. Hydrogen Energy*. *28*, 1361–1367.
51. Wijffels, R. H., Barbosa, M. J. An outlook on microalgal biofuels. *Sci*. (2010). *329,* 796–799.
52. Williams, P. L., Laurens, L. M. L. (2010). Microalgae as biodiesel and biomass feedstock: review and analysis of the biochemistry, energetics and economics. *Energ. Environ. Sci*. *3*, 554–590.
53. Harun, R., Danquah, M. K., Forde, G. M. (2010). Microalgal biomass as a fermentation feedstock for bioethanol production. *J. Chem. Technol. Biotechnol*. *85*, 199–203.
54. Balat, H., Kirtay, E. (2010). Hydrogen from biomass – resent scenario and future prospects. *Int. J. Hydrogen Energy*. *35*, 7416–7426.
55. Demirbas, A. H. (2010). Biofuels for future transportation necessity. *Energy Educ. Sci. Technol. Part A*. 26, 13–23.
56. Singh, J., Gu, S. (2010). Commercialization potential of microalgae for biofuels production. *Renew. Sust. Energ. Rev*. *14*, 2596–2610.
57. Hallenbeck, P. C. (2011). Microbial paths to renewable hydrogen production. *Biofuels*. *2*, 285–302.
58. Sinha, P., Pandey, A. (2011). An evaluative report and challenges for fermentative biohydrogen production. *Int. J. Hydrogen Energy*. *36*, 7460–7478.
59. Abo-Hashesh, M., Wang, R., Hallenbeck, P. C. (2011). Metabolic engineering in dark fermentative hydrogen production; theory and practice. *Bioresour. Technol*. *102*, 8414–8422.

60. Hallenbeck, P. C., Ghosh, D., Abo-Hashesh, M., Wang, R. (2011). Metabolic engineering for enhanced biofuels production with emphasis on the biological production of hydrogen. *Adv. Chem. Res*. *6*, 125–154.
61. Hallenbeck, P. C., Abo-Hashesh, M., Ghosh, D. (2012). Strategies for improving biological hydrogen production. *Bioresour. Technol*. *110*, 1–9.
62. Eriksen, N. T., Riis, M. L., Holm, N. K., Iversen, N. (2011).Hydrogen synthesis from pentoses and biomass in *Thermotoga* spp. *Biotechnol. Lett*. *33*, 293–300.
63. Munro, S. A., Zinder, S. H., Walker, L. P. (2009). The fermentation stoichiometry of *Thermotoganeapolitana* and influence of temperature, oxygen, and pH on hydrogen production. *Biotechnol. Progr*. *25*, 1035–1042.
64. Chou, C. J., Shockley, K. R., Conners, S. B., Lewis, D. L., Comfort, D. A., Adams, M. W. W., Kelly, R. M. (2007). Impact of substrate glycoside linkage and elemental sulfur on bioenergetics of and hydrogen production by the hyperthermophilic archon *Pyrococcusfuriosus*. *Appl. Environ. Microbiol*. *73*, 6842–6853.
65. Verhaart, M. R. A., Bielen, A. A. M., van der Oost, J., Stams, A. J. M., Kengen, S. W. M. (2010). Hydrogen production by hyperthermophilic and extremely thermophilic bacteria and archaea: mechanisms for reductant disposal. *Environ. Technol*. *31*, 993–1003.
66. Atomi, H., Sato, T., Kanai, T. (2011).Application of hyper-thermophiles and their enzymes. *Curr.Opin. Biotechnol*. *22*, 618–626.
67. Chou, C. J., Jenney, F. E. Jr., Adams, M. W. W., Kelly, R. M. (2008). Hydrogenesis in hyperthermophilic microorganisms: implications for biofuels. *Metab. Eng. 10*, 394–404.
68. Soboh, B., Linder, D., Hedderich, R. (2004). A multisubunit membrane-bound [NiFe] hydrogenase and an NADH-dependent Fe-only hydrogenase in the fermenting bacterium *Thermoanaerobacter tengcongensis*. *Microbiol*. *15*, 2451–2463.
69. Smith, E. T., Odom, L. D., Awramko, J. A., Chiong, M., Blamey, J. (2001). Direct electrochemical characterization of hyperthermophilic *Thermococcusceler* metalloenzymes involved in hydrogen production from pyruvate. *J. Biol. Inorg. Chem*. *6*, 227–231.
70. Silva, P. J., van den Ban, E. C., Wassink, H., Haaker, H., de Castro, B., Robb, F. T., Hagen, W. R. (2000). Enzymes of hydrogen metabolism in *Pyrococcusfuriosus*. *Eur. J. Biochem*. *267*, 6541–6551.
71. Gadow, S. I., Li, Y. Y., Liu, Y. (2012). Effect of temperature on continuous hydrogen production of cellulose. *Int. J. Hydrogen Energy*. *37*, 15465–15472.
72. Kargi, F., Eren, N. S., Ozmihci, S. (2012). Bio-hydrogen production from cheese whey powder (CWP) solution: comparison of thermophilic and mesophilic dark fermentations. *Int. J. Hydrogen Energy*. *37*, 8338–8342.
73. Zuroff, T. R., Curtis, W. R. (2012). Developing symbiotic consortia for lignocellulosic biofuel production. *Appl. Microbiol. Biotechnol. 93*, 1423–1435.
74. Zeidan, A. A., van Niel, E. W. J. A quantitative analysis of hydrogen production efficiency of the extreme thermophile *Caldicellulosiruptor owensensis* OL^T. *Int. J. Hydrogen Energy*. (2010). *35*, 1128–1137.
75. Chen, C. C., Chuang, Y. S., Lin, Y. C., Lay, C. H., Sen, B. (2012). Thermophilic dark fermentation of untreated rice straw using mixed cultures for hydrogen production. *Int. J. Hydrogen Energy*. *37*, 15540–15546.

76. Nguyen, T. A. D., Kim, K. R., Kim, M. S., Sim, S. J. (2010). Thermophilic hydrogen fermentation from Korean rice straw by *Thermotoganeapolitana*. *Int. J. Hydrogen Energy*. *35*, 13392–13398.
77. Li, Q., Liu, C. Z. (2012). Co-culture of *Clostridium thermocellum* and *Clostridium thermosaccharolyticum* for enhancing hydrogen production via thermophilic fermentation of cornstalk waste. *Int. J. Hydrogen Energy*. *37*, 10648–10654.
78. Cao, G. L., Guo, W. Q., Wang, A. J., Zhao, L., Xu, C. J., Zhao, Q. L., Ren, N. Q. (2012). Enhanced cellulosic hydrogen production from lime-treated cornstalk wastes using thermophilic anaerobic microflora. *Int. J. Hydrogen Energy*. *37*, 13161–13166.
79. Kongjan, P., Angelidaki, I. (2010). Extreme thermophilic biohydrogen production from wheat straw hydrolysate using mixed culture fermentation: Effect of reactor configuration. *Bioresour. Technol*. *101*, 7789–7796.
80. Kongjan, P., O-Thong, S., Kotay, M., Min, B., Angelidaki, I. Biohydrogen production from wheat straw hydrolysate by dark fermentation using extreme thermophilic mixed culture. *Biotechnol. Bioeng*. (2010). *105,* 899–908.
81. Ren, N. Q., Cao, G. L., Guo, W. Q., Wang, A. J., Zhu, Y. H., Liu, B. F., Xu, J. F. (2010). Biological hydrogen production from corn stover by moderately thermophile *Thermoanaerobacterium thermosaccharolyticum* W16. *Int. J. Hydrogen Energy*. *35*, 2708–2712.
82. Panagiotopoulos, I. A., Bakker, R. R., de Vrije, T., Koukios, E. G., Claassen, P. A. M. (2010). Pretreatment of sweet sorghum bagasse for hydrogen production by *Caldicellulosiruptor saccharolyticus*. *Int. J. Hydrogen Energy*. *35*, 7738–7747.
83. de Vrije, T., Budde, M. A. W., Lips, S. J., Bakker, R. R., Mars, A. E., Claassen, P. A. M. (2010). Hydrogen production from carrot pulp by the extreme thermophiles *Caldicellulosiruptor saccharolyticus* and *Thermotoganeapolitana*. *Int. J. Hydrogen Energy*. *35*, 13206–13213.
84. Lee, K. Z., Li, L. S., Kuo, C. P., Chen, C. I., Tien, M. Y., Huang, Y. J., Chuang, C. P., Wong, S. C., Cheng, S. S. (2010). Thermophilic bio-energy process study on hydrogen fermentation with vegetable kitchen waste. *Int. J. Hydrogen Energy*. *35*, 13458–13466.
85. VanFossen, A. L., Ozdemir, I., Zelin, S. L., Kelly, R. M. (2011). Glycoside hydrolase inventory drives plant polysaccharide deconstruction by the extremely thermophilic bacterium *Caldicellulosiruptor saccharolyticus*. *Biotechnol. Bioeng*. *108*, 1559–1569.
86. van de Werken, H. J., Verhaart, M. R., VanFossen, A. L., Willquist, K., Lewis, D. L., Nichols, J. D., Goorissen, H. P., Mongodin, E. F., Nelson, K. E., van Niel, E. W. J., Stams, A. J., Ward, D. E., de Vos, W. M., van der Oost, J., Kelly, R. M., Kengen, S. W. (2008). Hydrogenomics of the extremely thermophilic bacterium *Caldicellulosiruptor saccharolyticus*. *Appl. Environ. Microbiol*. *74,* 6720–6729.
87. Onyenwoke, R. U., Lee, Y. J., Dabrowski, S., Ahring, B. K., Wiegel, J. (2006). Reclassification of *Thermoanaerobiumacetigenum* as *Caldicellulosiruptor acetigenus* comb. nov. and emendation of the genus description. *Int. J. Syst. Evol. Microbiol*. *56,* 1391–1395.
88. Zeidan, A. A., van Niel, E. W. J. (2009). Developing a thermophilic hydrogen-producing coculture for efficient utilization of mixed sugars. *Int. J. Hydrogen Energy*. *34*, 4524–4528.

89. Hay, J. X. W., Wu, T. Y., Juan, J. C., Jahim, J. M. (2013). Biohydrogen production through photo fermentation or dark fermentation using waste as a substrate: overview, economics, and future prospects of hydrogen usage. *Biofuel. Bioprod. Bior*. *7*, 334–352.
90. Lo, Y. C., Lu, W. C., Chen, C. Y., Chang, J. S. (2010). Dark fermentative hydrogen production from enzymatic hydrolysate of xylan and pretreated rice straw by *Clostridium butyricum* CGS5. *Bioresour. Technol*. *101*, 5885–5891.
91. Cui, M., Yuan, Z., Zhi, X., Wei, L., Shen, J. (2010). Biohydrogen production from poplar leaves pretreated by different methods using anaerobic mixed bacteria. *Int. J. Hydrogen Energy*. *35*, 4041–4047.
92. Su, X., Mackie, R. I., Cann, I. K. (2012). Biochemical and mutational analyzes of a multidomain cellulase/mannanase from *Caldicellulosiruptor bescii*. *Appl. Environ. Microbiol*. *78*, 2230–2240.
93. Brentner, L. B., Peccia, J., Zimmerman, J. B. (2010). Challenges in developing biohydrogen as a sustainable energy source: implications for a research agenda. *Environ. Sci. Technol*. *44*, 2243–2254.
94. Kim, M. S., Lee, D. Y. (2010). Fermentative hydrogen production from tofu processing waste and anaerobic digester sludge using microbial consortium. *Bioresour. Technol*. *101*, S48-S52.
95. Babu, V. L., Mohan, S. V., Sarma, P. N. (2009). Influence of reactor configuration on fermentative hydrogen production during wastewater treatment. *Int. J. Hydrogen Energy*. *34*, 3305–3312.
96. Fang, H. H., Zhang, T. (2002). Characterization of a hydrogen-producing granular sludge. *Biotechnology and Bioengineering*. *78*, 44–52.
97. Chen, C. C., Lin, C. Y., Chang, J. S. (2001). Kinetics of hydrogen production with continuous anaerobic cultures using sucrose as the limiting substrate. *Appl. Microbiol. Biotechnol*. *57*, 56–64.
98. Lee, K. S., Lo, Y. C., Lin, P. J., Chang, J. S. (2006). Improving biohydrogen production in a carrier-induced granular sludge bed by altering physical configuration and agitation pattern of the bioreactor. *Int. J. Hydrogen Energy*. *31*, 1648–1657.
99. Lay, C. H., Wu, J. H., Hsiao, C. L., Chang, J. J., Chen, C. C., Lin, C. Y. (2010). Biohydrogen production from soluble condensed molasses fermentation using anaerobic fermentation. *Int. J. Hydrogen Energy*. *24*, 13445–13451.
100. Hallenbeck, P. C. (2005). Fundamentals of the fermentative production of hydrogen. *Water Sci. Technol. 52*, 21–29.
101. Kim, I. S., Hwang, M. H., Jang, N. J., Hyun, S. H., Lee, S. T. (2004). Effect of low pH on the activity of hydrogen using methanogen in bio-hydrogen process. *Int. J. Hydrogen Energy*. *29*, 1133–1140.
102. Oh, S. E., Lyer, P., Bruns, M. A., Logan, B. E. (2004). Biological hydrogen production using a membrane bioreactor. *Biotechnol. Bioeng*. *87*, 119–127.
103. Lin, C. Y., Chang, R. C. (2004). Fermentative hydrogen production at ambient temperature. *Int. J. Hydrogen Energy*. *29*, 715–720.
104. Levin, D. B., Chahine, R. (2010). Challenges for renewable hydrogen production from biomass. *Int. J. Hydrogen Energy*. *35*, 4962–4969.
105. Levin, D. B., Carere, C. R., Cicek, N., Sparling, R. (2009). Challenges for biohydrogen production via direct lignocellulose fermentation. *Int. J. Hydrogen Energy*. *34*, 7390–7403.

106. Kumar, S., Bhalla, A., Shende, R. V., Sani, R. K. (2012). Decentralized thermophilic biohydrogen: a more efficient and cost-effective process. *BioResources*. *7*, 1–2.
107. Barreto, L., Makihira, A., Riah, K. (2003). The hydrogen economy in the twenty-first century: a sustainable development scenario. *Int. J. Hydrogen Energy*. *28*, 267–284.
108. Chornet, E., Czernik, S., Wang, D., Gregoire, C., Mann, M. (1994). Biomass to hydrogen via pyrolysis and reforming. In proceedings of the 1994 DOE/NREL Hydrogen Program Review, 407–432. Livermore, California, NREL/CP-470–6431; Conf-9404194.
109. Liu, H., Grot, S., Logan, B. E. (2005). Electrochemically assisted microbial production of hydrogen from acetate. *Environ. Sci. Technol*. *39*, 4317–4320.
110. Kotay, S. M., Das, D. (2008). Biohydrogen as a renewable energy resource-prospects and potentials. *Int. J. Hydrogen Energy*. *33*, 258–263.
111. Panagiotopoulos, I. A., Bakker, R. R., Budde, M. A. W., Vrije, D. T., Claassen, P. A. M., (2009). Koukios, for example, Fermentative hydrogen production from pretreated biomass: a comparative study. *Bioresour. Technol*. *100*, 6331–6338.
112. Sierra, R., Smith, A., Granda, C., Holtzapple, M. T. (2009). Producing fuels and chemicals from lignocellulosic biomass. *Society of Biological Engineering Special Section*, 10–18.
113. Kumari, M., Kumar, S. (2009). Biorefineries: India's future option for energy and chemical feedstock. *Asian J. Energy Environ*. *10*(*3)*, 160–164.
114. Koutrouli, E. C., Kalfas, H., Gavala, H. N., Skiadas, I. V., Stamatelatou, K., Lyberatos, G. (2009). Hydrogen and methane production through two-stage mesophilic anaerobic digestion of olive pulp. *Bioresour Technol*. *100*, 3718–3723.
115. Ntaikou, I., Kourmentza, C., Koutrouli, E. C., Stamatelatou, K., Zampraka, A., Kornaros, M., Lyberatos, G. (2009). Exploitation of olive oil mill wastewater for combined biohydrogen and biopolymers production. *Bioresour Technol*. *100*, 3724–3730.
116. Ren, Z., Ward, T. E., Logan, B. E., Regan, J. M. (2007). Characterization of the cellulolytic and hydrogen-producing activities of six mesophilic Clostridium species. *J. Appl. Microbiol*. *103*, 2258–2266.
117. Mohan, S. V., Mohanakrishna, G., Raghavulu, S. V., Sarma, P. N. (2007). Enhancing biohydrogen production from chemical wastewater treatment in anaerobic sequencing batch biofilm reactor (AnSBBR) by bioaugmenting with selectively enriched kanamycin resistant anaerobic mixed consortia. *Int. J. Hydrogen Energy*. *32*, 3284–3292.
118. Zahedi, S., Sales, D., Romero, L. I., Solera, R. (2013). Hydrogen production from the organic fraction of municipal solid waste in anaerobic thermophilic acidogenesis: influence of organic loading rate and microbial content of the solid waste. Bioresource Technology, *129*, 85–91.
119. Uduman, N., Qi, Y., Danquah, M. K., Forde, G. M., Hoadley, A. (2010). Dewatering of microalgal cultures: A major bottleneck to algae-based fuels. *J. Renew. Sustain. Ener*. *2*, 012701–15.
120. Kapdan, I. K., Kargi, F. (2006). Bio-hydrogen production from waste materials. *Enzyme Microb. Technol*. *38*, 569–582.
121. Jayasinghearachchi, H. S., Sarma, P. M., Lal, B. (2012). Biological hydrogen production by extremely thermophilic novel bacterium *Thermoanaerobacter mathranii* A3N isolated from oil producing well. *Int. J. Hydrogen Energy*. *37*, 5569–5578.

122. Ngo, T. A., Nguyen, T. H., Bui, H. T. V. (2012). Thermophilic fermentative hydrogen production by *Thermotoganeapolitana* DSM 4359. *Renew. Energ*. *37*, 174–179.
123. Zhang, K., Ren, N. Q., Cao, G. L., Wang, A. J. (2011). Biohydrogen production behavior of moderately thermophile *Thermoanaerobacterium thermosaccharolyticum* W16 under different gas-phase conditions. *Int. J. Hydrogen Energy*. *36*, 14041–14048.
124. Shaw, A. J., Hogsett, D. A., Lynd, L. R. (2009). Identification of the [FeFe]-hydrogenase responsible for hydrogen generation in *Thermoanaerobacterium saccharolyticum* and demonstration of increased ethanol yield via hydrogenase knockout. *J. Bacteriol*. *191*, 6457–6464.
125. Abreu, A. A., Karakashev, D., Angelidaki, I., Sousa, D. Z., Alves, M. M. (2012). Biohydrogen production from arabinose and glucose using extreme thermophilic anaerobic mixed cultures. *Biotechnol. Biofuels*. *5*, 6.
126. Lu, W., Fan, G., Zhao, C., Wang, H., Chi, Z. (2012). Enhancement of fermentative hydrogen production in an extreme-thermophilic (70 °C) mixed-culture environment by repeated batch cultivation. *Curr. Microbiol*. *64*, 427–432.
127. Hniman, A., O-Thong, S., Prasertsan, P. (2011). Developing a thermophilic hydrogen-producing microbial consortia from geothermal spring for efficient utilization of xylose and glucose mixed substrates and oil palm trunk hydrolysate. *Int. J. Hydrogen Energy*. *36*, 8785–8793.
128. Karadag, D., Puhakka, J. A. (2010). Enhancement of anaerobic hydrogen production by iron and nickel. *Int. J. Hydrogen Energy*. *35*, 8554–8560.
129. Zhao, C., Karakashev, D., Lu, W., Wang, H., Angelidaki, I. (2010). Xylose fermentation to biofuels (hydrogen and ethanol) by extreme thermophilic (70 °C) mixed culture. *Int. J. Hydrogen Energy*. *35*, 3415–3422.
130. Kongjan, P., Min, B., Angelidaki, I. (2009). Biohydrogen production from xylose at extreme thermophilic temperatures (70 °C) by mixed culture fermentation. *Water Res*. 43, 1414–1124.
131. Hasyim, R., Imai, T., Reungsang, A., O-Thong, S. (2011). Extreme-thermophilic biohydrogen production by an anaerobic heat treated digested sewage sludge culture. *Int. J. Hydrogen Energy*. *36*, 8727–8734.
132. Geng, A., He, Y., Qian, C., Yan, X., Zhou, Z. (2010). Effect of key factors on hydrogen production from cellulose in a coculture of *Clostridium thermocellum* and *Clostridium thermopalmarium*. *Bioresour. Technol*. *101*, 4029–4033.
133. Magnusson, L., Islam, R., Sparling, R., Levin, D., Cicek, N. (2008). Direct hydrogen production from cellulosic waste materials with a single-step dark fermentation process. *Int. J. Hydrogen Energy*. *33*, 5398–5403.
134. Ho, K. L., Lee, D. J., Su, A., Chang, J. S. (2012). Biohydrogen from lignocellulosic feedstock via one-step process. *Int. J. Hydrogen Energy*. *37*, 15569–15574.
135. Prakasham, R. S., Sathish, T., Brahmaiah, P., Rao, C. S., Rao, R. S., Hobbs, P. J. (2009). Biohydrogen production from renewable agri-waste blend: optimization using mixer design. *Int. J. Hydrogen Energy*. *34*, 6143–6148.

CHAPTER 2

BIO-HYDROGEN PRODUCTION: CURRENT TRENDS AND FUTURE PROSPECTS

VINITA MISHRA,[1,*] and ISHA SRIVASTAVA[2]

[1]Cell Biology Lab, School of Biological Sciences and Biotechnology, Indian Institute of Advanced Research, Koba Institutional Area, Gandhinagar, 382 007, Gujarat, India

[2]Department of Biotechnology, Delhi Technological University (Formerly Delhi College of Engineering), Shahbad Daulatpur, Main Bawana Road, Delhi-110 042, India

**Corresponding author's E-mail: vinita.mbif@gmail.com*

CONTENTS

2.1 Introduction 38
2.2 Bio-Hydrogen Production 39
2.2.1 Bioprocesses of Bio-Hydrogen Production 39
2.2.2 Bioreactor for Hydrogen Production 45
2.2.3 Speed Breakers in Bio-Hydrogen Production 45
2.2.4 Limitations and Challenges in Bio-Hydrogen Production 49
2.3 A Hypothetical Three Stage Hybrid System 50
2.3.1 Advantages of Three Stage Hybrid System 50
2.4 Conclusions 51
2.5 Abbreviations 53

2.6 Authors' Contributions 53
Keywords 53
References 53

ABSTRACT

Bio-hydrogen is gaining importance as a clean source of energy which can be used as fuel in future but the real problem is; bio-hydrogen production at a large scale, so that it can be commercialized. Due to this limitation bio-hydrogen production has become an important area of research and gaining attention of researchers. These issues motivated us to compile this review. This review covers the processes of bio-hydrogen production, microorganisms involved, factors that limit the bio-hydrogen production, etc. In this chapter, we have proposed a hypothetical three-stage hybrid system by keeping in view the problems associated with bio-hydrogen production. This hypothetical model can be applied in designing a bioreactor to increase the yield and efficiency of bio-hydrogen production. The findings of this review will be helpful in overcoming the problems currently associated with the bio-hydrogen production and will help researchers in designing and developing more efficient and cost effective bio-hydrogen production techniques.

2.1 INTRODUCTION

In the present global scenario, major sources of energy in the world are fossil fuels (about 80% of the present demand) and the resources of fossil energy are decreasing day by day [1]. Nowadays Hydrogen (H_2) gas is considered as a source of future energy because of the fact that it is renewable and does not contribute in creating "greenhouse effect." H_2 gas produces a large amount of energy per unit weight by combustion (143 GJ/ tons) and can be easily converted into electricity with the help of fuel cells [1]. However, hydrogen is not a primary energy source, but rather it serves as a medium through which primary energy sources such as nuclear and/or solar energy can be stored, used and transmitted for the fulfillment of our energy needs [2]. Hydrogen is ecofriendly and does not cause any harm to human beings, so it is considered as a clean source of energy [3, 4]. In recent years, due to

the requirement of hydrogen gas as a clean source of energy, development of cost-effective and efficient bio-hydrogen production technology, which can be converted into commercially viable hydrogen production technology, is gaining attention of researchers [5]. Hydrogen gas produced by biological processes due to the action of microorganisms is called bio-hydrogen, is a type of bio-fuel, like bio-ethanol, bio-diesel or bio-gas or bio-oil. Bio-fuels can be categorized into three classes on the basis of materials and technology they use; first generation (made from food crops), second generation (made from nonfood crops or wastes), third generation or advanced (made using microbe). Third generation bio-fuels are known to have several advantages over first and second generation bio-fuels for instance third generation bio-fuels are more economical in comparison to first generation bio-fuels because first generation bio-fuels have caused increase in food prices, third generation bio-fuels are more efficient in capturing sun light energy which is almost ten times higher than the second generation bio-fuels, which means that smaller areas of land will be required to produce enough fuel. Bio-hydrogen is an example of an advanced or third generation bio-fuel [3, 5]. In advanced bio-fuel technologies, microorganisms are allowed to grow in special type of bioreactors and provided with the energy and nutrients that they need for their growth including sunlight, waste organic material, CO_2 from the air or from conventional gas plants. As the microbes grow they produce bio-hydrogen [4, 5]. Demand of hydrogen gas is not limited to utilization as a source of energy. Hydrogen gas is widely used for hydrogenation of fats and oils in food industry, production of electronic devices, processing steel, desulfurization and reformulation of gasoline in refineries and is also used as feedstock for the production of chemicals [5].

2.2 BIO-HYDROGEN PRODUCTION

2.2.1 BIOPROCESSES OF BIO-HYDROGEN PRODUCTION

2.2.1.1 Biophotolysis of Water (Water Splitting) by Green Algae and Cyanobacteria

During the biophotolysis (Fig. 2.1), solar energy is converted into chemical energy (H_2 energy) by photosynthetic algae and cyanobacteria with the

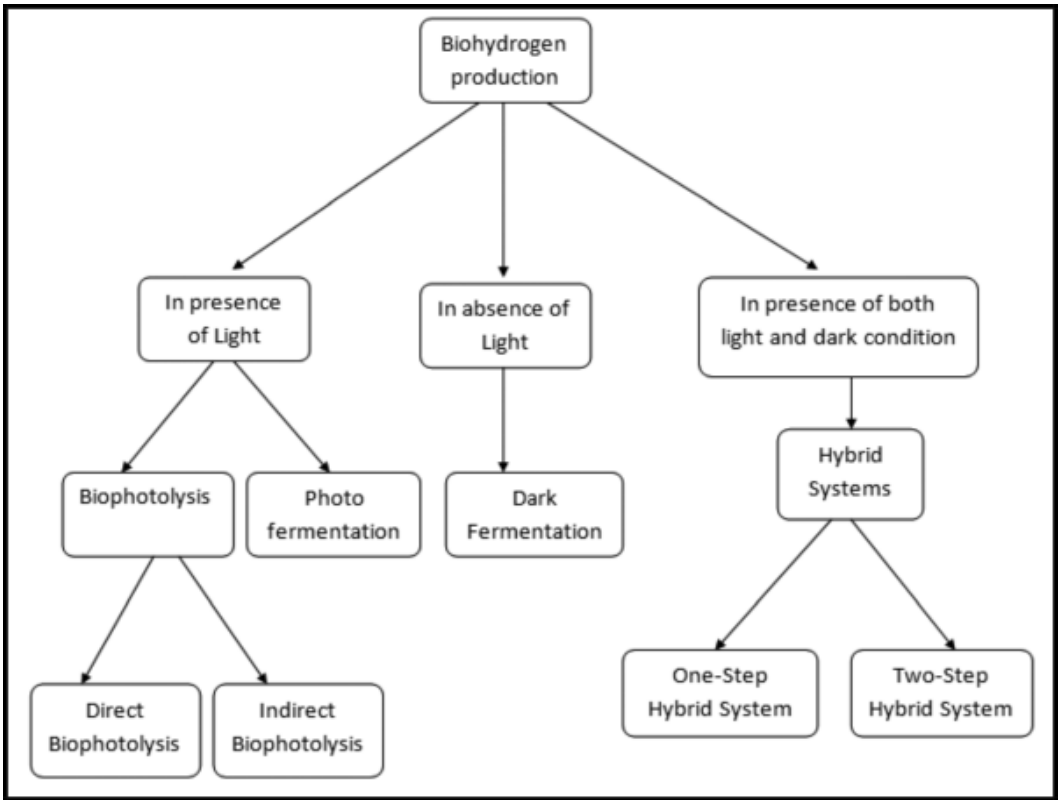

FIGURE 2.1 A diagrammatic representation of bio-hydrogen production.

help of hydrogenase and nitrogenase enzymes [2, 4] (Table 2.1). Hydrogenase and nitrogenase enzymes are highly sensitive towards presence of oxygen; therefore constant removal of oxygen must be performed for higher yield of hydrogen production via Biophotolysis [6].

Biophotolysis is possible in two ways:

1. Direct biophotolysis; and
2. Indirect biophotolysis

2.2.1.1.1 Direct Biophotolysis

Under anaerobic condition, green algae either use H_2 as electron donor in the process of CO_2 fixation or produces hydrogen (Fig. 2.1) [7]. In the process of direct biophotolysis photosystem II (PSII) absorbs the light energy, which are having wavelength lower than 680 nm as a result stream of

TABLE 2.1 Classification of Bio-Hydrogen Producing Microorganism

Process of Hydrogen Production	Class of Microorganism	Sub-Class of Microorganism	Genus of Microorganism	Hydrogen Source
Photosynthesis	Algae	Green algae	*Chlamydomonas sp.*	Water
			Scenedesmus sp.	
		Marine Green algae	*Chlorococcum sp.*	
			Playtmonas sp.	
			Chlorella sp.	
	Cyanobacteria	Marine cyanobacteria	*Anabaena sp.*	
			Oscillatoria sp.	
			Calothrix sp.	
		Marine unicellular cyanobacteria	*Cyanothece sp.*	
		Heterocystous cyanobacteria	*Anabaena sp.*	
			Nostoc sp.	
		Heterocyst filamentous cyanobacteria	*Anabaena sp.*	
		Non-nitrogen-fixing unicellular cyanobacteria	*Synechococcus sp.*	
			Microcystis sp.	
			Gloebacter sp.	
			Synechocystis sp.	
			Aphanocapsa sp.	
			Chroococcidiopsis sp.	
		Unicellular nondiazotrophic cyanobacteria	*Gloeocapsa sp.*	
		Unicellular/colony embedded in matrix	*Mycrocystis sp.*	
		Mat-building cyanobacteria	*Microcoleus sp.*	

TABLE 2.1 (*Continued*)

Process of Hydrogen Production	Class of Microorganism	Sub-Class of Microorganism	Genus of Microorganism	Hydrogen Source
Dark-Fermentation	Non-Photosynthetic Anaerobic Bacteria	Obligate	*Clostridia sp.* *Actinomyces sp.* *Porphyromonos sp.*	Carbohydrate Containing Organic Wastes
		Facultative	*Enterobacter sp.* *E. coli* *Hafnia sp.*	
	Non-Photosynthetic Aerobic Bacteria	–	*Aeromonos sp.* *Pseudomonos sp.* *Vibrio sp.*	
Photo-Fermentation	Photosynthetic anaerobic bacteria	Purple sulfur bacteria (obligate anaerobe)	*Chromatium sp.* *Thiocapsa sp.*	Sulfates
		Purple-nonsulfur (PNS) bacteria (Facultative anaerobe)	*Rhodobacter sp.* *Rhodovulum sp.* *Rhodopseudomonas sp.* *Rhodospirillum sp.*	Organic Acids

electrons, and protons are generated from water molecule. Whereas photosystem I (PSI) is induced by the light with wavelength lower than 700 nm. Cytochrome *bf,* which behaves as chain of reductors, allows the transportation of electrons from PSII to PSI. Electrons from PSI are transferred to hydrogenase enzyme via ferrodoxine, which converts the proton (H^+) into molecular hydrogen (H_2) [7], *see* Eq. (1).

$$2H_2O + \text{Light Energy} \rightarrow 2H_2 + O_2 \quad (1)$$

2.2.1.1.2 Indirect Biophotolysis

Cyanobacteria produce H_2 from water by indirect photolysis. Indirect biophotolysis can be completed in two steps (*see*, Eqs. (2)–(3)). In the first

step PSII and PSI are induced by light as it occurs in direct biophotolysis, but in this step CO_2 adsorption occurs due to presence of RuBisCO enzyme, which is fixed into glucose and oxygen, is produced as a result of photosynthesis (Fig. 2.1). In the second step decomposition of organic compound (glucose) occurs due to the presence of hydrogenase and nitrogenase enzymes in cyanobacteria [9]. Cyanobacterial species contains many enzymes, which are directly involved in H_2 metabolism and production. Out of these enzymes, nitrogenases enzyme catalyze the process of H_2 production, which is produced as by-product during the reduction of nitrogen into ammonia (NH_3) [7, 9].

$$12H_2O + 6CO_2 + \text{Light Energy} \rightarrow C_6H_{12}O_6 + 6O_2 \quad (2)$$

$$C_6H_{12}O_6 + 12H_2O + \text{Light Energy} \rightarrow 12H_2 + 6CO_2 \quad (3)$$

The algal and cyanobacterial hydrogen production could be considered as a more economical and sustainable method of bio-hydrogen production as it uses water, which is a renewable resource and consume CO_2, which is an air pollutant [5].

2.2.1.2 Dark-Fermentation by Non-Photosynthetic Bacteria

Dark fermentation occurs in the absence of light with the help of non-photosynthetic anaerobic bacteria (Fig. 2.1, Table 2.1). During the dark fermentation of carbohydrate and organic compounds rich waste; which is an acidogenic phase of anaerobic digestion, hydrogen is produced as a by-product [5] (*see*, Eq. (4)).

$$\text{Sugar} + \text{Dark (absence of light)} \rightarrow H_2 + CO_2 + \text{Organic Acids} \quad (4)$$

2.2.1.3 Photo-Fermentation by Photosynthetic Bacteria

In the presence of light and anaerobic conditions, some photo-heterotrophic bacteria such as purple nonsulfur bacteria (Fig. 2.1, Table 2.1) can

convert organic acids (acetic, lactic and butyric) into hydrogen (H_2) and carbon dioxide (CO_2) [5]. Therefore, the organic acids produced during the acidogenic phase of anaerobic digestion of organic wastes can be converted to H_2 and CO_2 with the help of these photosynthetic anaerobic bacteria [1, 5, 7] (*see*, Eq. (5)).

$$\text{Organic acids} + \text{Light Energy} \rightarrow H_2 + CO_2 + \text{Carbon Compounds} \quad (5)$$

2.2.1.4 Hybrid Systems Using Photosynthetic and Fermentative Bacteria

Hybrid systems can be created by combining both photo and dark fermentation processes (Fig. 2.1) [1]. Hybrid system uses those substrates, which are useless and difficult to operate for photo fermentation. These substrates such as saccharides can be breakdown into simpler compounds, for instance acetic or butyric acids, during the process of dark fermentation in hybrid system, which can be further, operated by PNS bacteria in photo fermentation. Two different hybrid systems have been designed so far:

1. One-step hybrid system; and
2. Two-step hybrid system

2.2.1.4.1 One-Step Hybrid System

In one-step hybrid systems both dark and photo fermentative bacteria grow in a single culture medium, that is, in a single container, as a result of which the hydrogen production from both the process almost occur simultaneously. One step hybrid system shows much higher yield and higher rate of hydrogen production in comparison to those obtained in photo or dark fermentation alone by using single culture [10, 11].

2.2.1.4.2 Two-Step Hybrid System

Two-step hybrid system can be applied for further increase in the yield and rate of hydrogen production by hybrid systems [11]. Two-step hybrid

systems allow the use of waste materials of photo-fermentation process, which are containing elements having inhibitory effect on photo-fermentation (e.g., NH_4 ions) [12] and does not affect the microorganism involved in the dark fermentation. In two-step hybrid systems both photo and dark fermentative bacteria grow in separate containers because there are greater number of parameters, which can influence hydrogen production in photo-fermentation than in dark fermentation [13]. So, both the processes must be performed in separate bioreactors.

2.2.2 BIOREACTOR FOR HYDROGEN PRODUCTION

Based on the nature of H_2 evolving reactions, Microbial bioreactors can be divided into three separate groups [1, 5, 9]:

1. Photobioreactors based on H_2 photo-production.
    a. Photobioreactors incorporating green algae (photosynthesis)
    b. Photobioreactors incorporating cyanobacteria (photosynthesis)
    c. Photobioreactors incorporating photosynthetic bacteria (photo-fermentation)
2. Bioreactors based on dark anaerobic H_2 production by bacteria.
    a. Bioreactors based on fermentation (dark-fermentation)
    b. Bioreactors based on "water-gas shift-reaction" (dark-fermentation)
3. Hybrid bioreactors based on photo and dark fermentation.

2.2.3 SPEED BREAKERS IN BIO-HYDROGEN PRODUCTION

There are several extrinsic and intrinsic factors, which behave as speed breakers on the road of bio-hydrogen production. These factors become more critical when bio-hydrogen production is aimed at industrial scale. Some of these factors are discussed in the following sub-sections.

2.2.3.1 Extrinsic Factors

These are the external factors, which are either present in the environment or produced as a byproduct during the process of bio-hydrogen production.

2.2.3.1.1 Effect of Light

Light requirement for hydrogen production varies among the different groups of microorganisms. Several hydrogen producing microorganisms such as photosynthetic green algae, cyanobacteria, and purple sulfur bacteria produce hydrogen in the presence of light whereas nonphotosynthetic anaerobic bacteria do not require light for hydrogen production.

2.2.3.1.2 Effect of Temperature

For most of the cyanobacterial species, optimum temperature for hydrogen production is in the range of 30–40 °C and varies among the cyanobacterial species. For instance, *Nostoc* showed higher hydrogen production rates when it was cultured at 22 °C than at 32 °C [14], whereas optimum hydrogen production rate by *Nostoc muscorum* SPU004 was reported at 40 °C [15]. On the other hand optimum hydrogen production by *Anabaena variabilis* SPU 003 was observed at 30 °C [16, 17]. Optimum temperature for hydrogen production by photo-fermentation with the help of photosynthetic bacteria is between 30 and 35 °C [18–25].

2.2.3.1.3 Effect of pH

Several experimental studies reported that pH can affect bio-hydrogen production in terms of yield, production rate, content of biogas and types of organic acids produced. Reported optimum pH for bio-hydrogen production is in the range of pH 5.0- 6.0 [26–30]. Whereas some investigators observed optimum pH range in between 6.8 and 8.0 [31–34]. Most of the studies on effect of pH reported that pH decreases as the process proceeds due to the production of organic acids and the final pH was found to be in between 4.0–4.8 regardless of initial pH [29, 32–37]. This gradual decrease of pH results in decreased hydrogen production as pH affects the activity of hydrogenase, which is an iron-containing enzyme [38]. It was also observed in some studies that initial pH can affect the lag phase of microbial growth during hydrogen production process, low

initial pH increases the lag period whereas high initial pH decreases lag period as a result decreased yield of hydrogen production [29, 32, 33]. So, to achieve controlled pH at the optimum level is necessary for bio-hydrogen production.

2.2.3.1.4 Effect of Salinity

It has been proved by experimental studies that salinity affects hydrogen production by microorganisms [39]. Generally fresh water cyanobacteria have shown to have lower rate of hydrogen production when the salt concentration increases. This may happen because of diversion of energy and reductants either for extrusion of Na^+ ions outside the cells or prevention of Na^+ influx [40].

2.2.3.1.5 Effect of Carbon

Carbon sources are known to influence the activity of nitrogenase enzyme as a result of which it also affects the rate of hydrogen production considerably [15]. Capabilities of electron donation by cofactor compounds to nitrogenase enzyme vary due to the presence of different carbon sources and thus influence hydrogen production [15].

2.2.3.1.6 Effect of Nitrogen

It has been reported that a number of inorganic nitrogenous compounds affect the rate of hydrogen production in different ways. It has been proved from experimental studies that nitrite, nitrate and ammonia have inhibitory effect on nitrogenase in *Anabaena variabilis* SPU003 and *Anabaena cylindrical* [15, 41]. It was observed that generally all externally added nitrogen sources have negative effect on synthesis of nitrogenase enzyme [42]. Although it was also observed in *Anabaena cylindrical* that addition of ammonium ion (0.2 mM $NH4^+$) at a given time point eventually suppresses rate of hydrogen production, but when it is periodically added in

smaller amounts (0.1 mM NH_4Cl), doesn't show inhibitory effect on production rate of hydrogen [44].

2.2.3.1.7 Effect of Molecular Nitrogen

In some studies, considerable decrease in hydrogen production has been reported due to the presence of molecular nitrogen and conclusion was made that molecular nitrogen behaves as competitive inhibitor for hydrogen production, so it becomes necessary to remove molecular nitrogen for increased hydrogen production [44].

2.2.3.1.8 Effect of Micronutrients

Several studies showed the effect of micronutrients on hydrogen production such as cobalt (Co), copper (Cu), molybdenum (Mo), zinc (Zn), and nickel (Ni) [45]. Many of these micronutrients are responsible for the activity of nitrogenase enzyme and shown to have enhancement effect on bio-hydrogen production. For instance, *Anabaena variabilis* SPU003 was found to be very sensitive to Co, Cu, Mn, Zn, Ni, Fe ions and didn't show hydrogen production at lower concentrations (below 10 mM) of these microelements [46]. The enhancement in hydrogen production was also observed in a culture of *Anabaena cylindrica*, which was grown in a medium containing 5.0 mg of Ferric ions/ liter, this enhancement was almost two times of a culture, which was grown in a medium containing 0.5 mg of Ferric ions/ liter [44].

2.2.3.1.9 Effect of Oxygen

Both hydrogenases and nitrogenases are highly sensitive to oxygen, so the process of bio-hydrogen production must be carried out in strict anaerobic conditions [47].

2.2.3.1.10 Effect of Sulfur

Sulfur deprived condition is known to have positive impact on bio-hydrogen production. It has been proved by several studies that sulfur starvation

increases the rate of hydrogen production by providing anaerobic condition and reducing the loss of activity of hydrogenases in the presence of oxygen [48, 49–52].

2.2.3.2 Intrinsic Factors

Intrinsic factors are the factors, which are present inside the microorganisms itself, and these factors such as genetic components and sensitive proteins, etc. can affect hydrogen production. Uptake Hydrogenase enzyme is one of the several intrinsic factors that limits the process of biohydrogen production [4, 6, 53]. Uptake hydrogenase enzyme, present in photo-fermentative bacteria, inhibits the hydrogen yield by using hydrogen gas produced and thus behaves as an antagonist for nitrogenase [54].

2.2.4 LIMITATIONS AND CHALLENGES IN BIO-HYDROGEN PRODUCTION

There are number of limitations and challenges in bio-hydrogen production such as low hydrogen yield, slow rate of hydrogen production, strong inhibitory effect of oxygen on hydrogenase enzyme, no waste utilization are the major limitations of hydrogen production by algae and cyanobacteria [4–6]. Whereas yield of hydrogen gas and rate of production are the limitations associated with dark fermentation and requirement of large land area is the major limitation of bio-hydrogen production via photo fermentation due to the high requirement of light [1, 5, 54]. Due to these limitations bio-hydrogen production has become the most challenging area of biotechnology. The future of bio-hydrogen production depends not only on research advancement, that is, improvement in efficiency through genetically engineering microorganisms and/or the development of bioreactors, but also on economic considerations (the cost of fossil fuels), acceptance of bio-hydrogen production at social level, and the development of hydrogen energy systems. The process requires special microorganisms, strict control of light and other environmental conditions, which can affect the yield and rate of bio-hydrogen production. Sequential or combined bioprocesses (hybrid systems) of dark and photo-fermentations seem to be

the most attractive approach resulting in high hydrogen yields for hydrogen production from carbohydrate rich wastes. Recently few hydrogen producing aerobic cultures such as *Aeromonos sp*., *Pseudomonos sp.* and *Vibrio sp.* were identified [5], but using these bacterial species in hybrid culture requires a very thorough study because many of these species are pathogenic and as we are going to improve the synthesis of hydrogen gas, which is known as a source of future energy we can't create an environment which can be a threat for the future generations so, we need to be very careful in designing any such hybrid system.

2.3 A HYPOTHETICAL THREE STAGE HYBRID SYSTEM

In this chapter, a hypothetical three-stage hybrid system has been proposed, which may overcome the limitations associated with bio-hydrogen production. This hybrid system is designed in such a way that side products produced at one stage of hybrid system will be used at later stages so that the waste materials can be used up to the maximum possible extent, which will result in higher H_2 yield and lesser side production. We had also proposed a mixture of microorganisms which can be used in this hybrid system because it has been clear from previous studies that mixture of microorganisms is more effective in H_2 production rather than using single microorganism [55]. In this mixture of microorganisms, we had proposed combination of those microorganism which are known for highest H_2 production among their class till present (Table 2.2). Diagrammatic representation of three-stage hybrid system is given in Fig. 2.2.

2.3.1 ADVANTAGES OF THREE-STAGE HYBRID SYSTEM

The proposed three-stage hybrid system is trying to overcome limitation of bio-hydrogen production in different methodologies. The advantages of hybrid systems may be as follows:

1. As we know there is no waste utilization by algae and cyanobacteria [5], we are using algae and cyanobacteria at the end of this hybrid system where only small amount of waste material will remain unused after the dark and the photo fermentation respec-

TABLE 2.2 Proposed Microorganisms for Three Stage Hybrid System

Process of H_2 Production	Class of Micro-organism	Name of Organism	H_2 Yield	Reference
DARK FERMENTATION	Anaerobic (Obligate and facultative) Bacteria	*Enterobactor cloacae IIT-BT 08*	2.2 mol/mol glucose	**[56]**
		C. pasteurium (dominant)	4.8 mol/mol sucrose	**[57]**
		Enterobactor cloacae IIT-BT 08	6 mol/mol sucrose	**[56]**
		Enterobactor aerogenes	1.09 mol/mol glucose	**[58]**
PHOTO FERMENTATION	Purple Photosynthetic Bacteria	*Rhodopseudomonas palustris*	2.8 mol/mol acetate	**[59]**
		Rhodobactor capsulatus	1.1 mol/mol acetate	**[60]**
		Rhodobactor capsulatus	2.8 mol/ mol butyrate	**[60]**
PHOTOSYNTHESIS	Green algae	*Chlamydomonas reinhardtii*		**[5]**
	Cyanobacteria	*Anabaena cylindrica*		**[5]**

tively and large amount of CO_2 and Water will remain present as a byproduct of dark and photo fermentation respectively, which is required for hydrogen production via photosynthesis and biophotolysis with the help of algae and cyanobacteria [5].

2. A mixture of microorganisms (Table 2.2) has been proposed for use at each different step of hypothetical hybrid system and these microorganisms are known to be highest H_2 yielding microorganisms so the yield will get increased by using them.

2.4 CONCLUSIONS

Hydrogen gas cannot be used as an energy source naturally because it is not present in adequate amount in earth atmosphere so we need to produce it

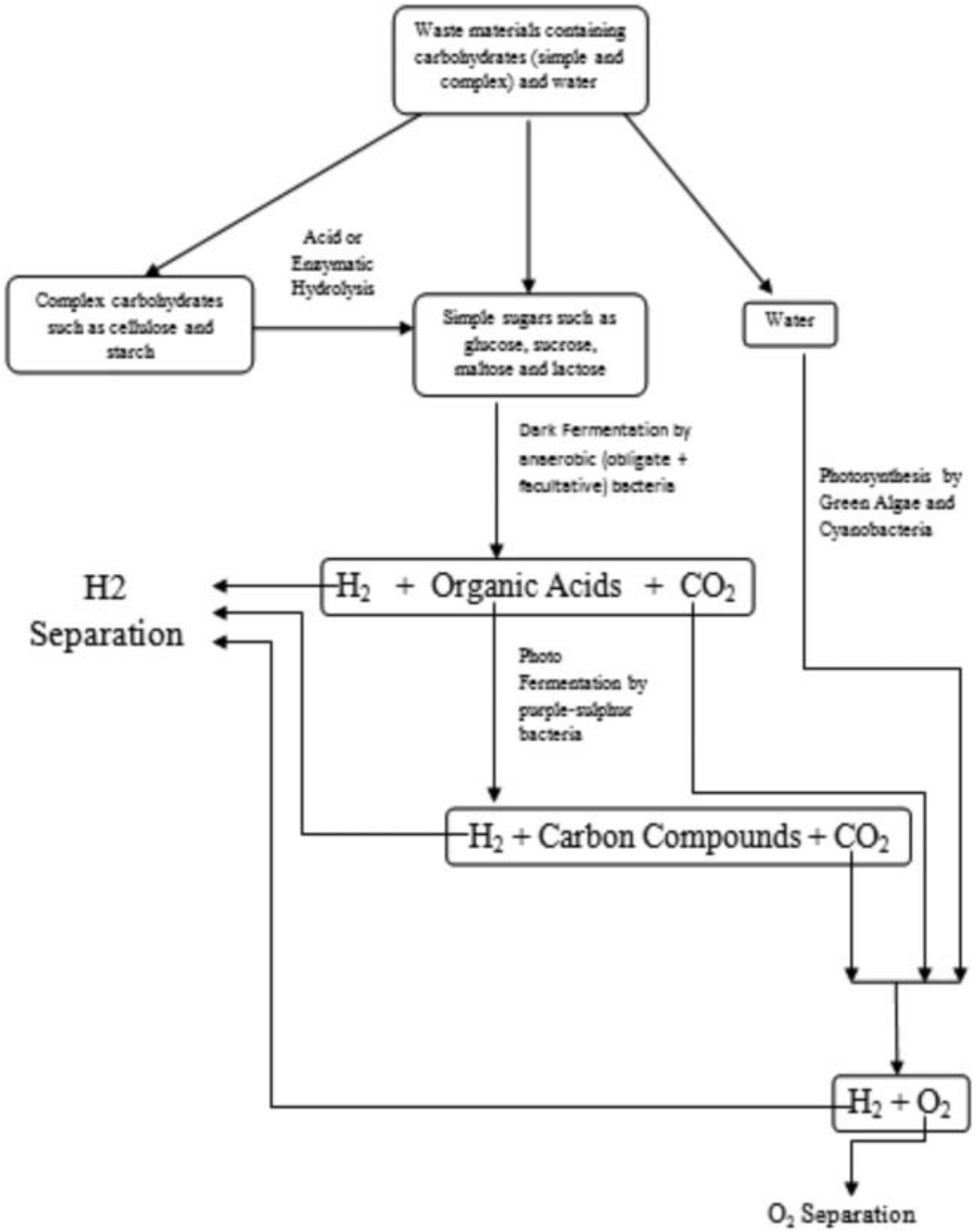

FIGURE 2.2 Proposed three-stage hybrid system.

synthetically but the major problem associated with the hydrogen production is its commercialization. There are various methods available for the hydrogen production one of which is bio-hydrogen production. Bio-hydrogen production has been proved successful in improving the rate and yield of hydrogen production but still not up to the industrial level, so we need

to come up with new methodologies which can improve the pace of bio-hydrogen production, one of the such new methodologies can be, designing a hybrid system by using existing bio-hydrogen producing processes and microorganisms, another efficient approach can be designing new microorganisms with increased bio-hydrogen production capacity through genetic engineering, in this approach *in silico* studies of genomic constitution of hydrogen producing microorganisms can speed up the process. This chapter suggests that high quality research and development activities are needed for overcoming the limitations associated with the bio-hydrogen production.

2.5 ABBREVIATIONS

H_2: Molecular hydrogen, H_2O: Water, CO_2: Carbon dioxide, NH_4: Ammonium, Ni: Nickel; Co: Cobalt, Cu: Copper, Zn: Zinc, Mn: Manganese, Na^+: Sodium ion, PNS: Purple Non Sulfur bacteria.

2.6 AUTHORS' CONTRIBUTIONS

V. Mishra and I. Srivastava contributed in literature survey and manuscript preparation. V. Mishra edited the final manuscript.

KEYWORDS

- **Bio-hydrogen production**
- **Biomass**
- **Bioreactors**
- **Hybrid systems**
- **Hydrogen yield**

REFERENCES

1. Basak, N., Das, D. (2006). The prospect of purple nonsulfur (PNS) photosynthetic bacteria for hydrogen production: the present state-of-the-art. *Springer Science+Business Media B. V.*

2. Das, D., Veziroglu, T. N. (2001). Hydrogen production by biological processes: a survey of literature. *Int. J. Hydrogen Energy. 26*, 13–28.
3. Bockris, J. O. M. (1981). The economics of Hydrogen as a fuel. *Int. J. Hydrogen Energy. 6*, 223–241.
4. Lindblad, P. (1999).Cyanobacterial H_2 Metabolism: Knowledge and Potential/Strategies for a Photobiotechnological Production of H_2. *Biotecnologia Aplicada*. *16*, 115–144.
5. Kapdan, I. K., Kargi, F. (2006). Bio-hydrogen production from waste materials, *Enzyme and Microbial Technology. 38*, 569–582.
6. Das, D., Veziroglu, T. N. (2008). Advances in biological hydrogen production processes. *Int. J. Hydrogen Energy. 33*, 6046–6057.
7. Turker, L., Gumus, S., Tapan, A. (2008). Bio-hydrogen Production: Molecular Aspects, *J. Scientific and Industrial Research. 67*, 994–1016.
8. Kars, G., Gunduz, U., Yucel, M., Rakhely, G., Kovacs, K. L., Eroglu, I. (2009). Evaluation of hydrogen production by Rhodobacter sphaeroides O. U.001 and its hupSL deficient mutant Rusing acetate and malate as carbon sources. *Int. J. Hydrogen Energy. 34*, 2184–2190.
9. Markov, S. A. (2012). Hydrogen production in bioreactors: current trends. *Energy Procedia. 29*, 394 – 400.
10. Liu, B. F., Ren, N., Tang, J., Ding, J., Liu, W. Z., Xu, J. F., Cao, G. L., Guo, W. Q., Xie, G. J. (2010). Bio-hydrogen production by mixed culture of photo-and dark-fermentation bacteria. *Int. J. Hydrogen Energy. 35*, 2858–2862.
11. Argun, H., Kargi, F., Kapdan, I. K. (2009). Hydrogen production by combined dark and light fermentation of ground wheat solution. *Int. J. Hydrogen Energy. 34*, 4305–4311.
12. Azbar, N., Tuba, F., Dokoz, C. (2010). The effect of dilution and L-malic acid addition on bio-hydrogen production with Rhodopseudomonas palustris from effluent of an acidogenic anaerobic reactor. *Int. J. Hydrogen Energy. 35*, 5028–5033.
13. Ozmihci, S., Kargi, F. (2010). Bio-hydrogen production by photo-fermentation of dark fermentation effluent with intermittent feeding and effluent removal. *Int. J. Hydrogen Energy. 35*, 6674–6680.
14. Ernst, A., Kerfin, W., Spiller, H., Boger, P. (1979). External factors influencing light-induced H2 evolution by the blue-green algae, Nostoc muscorum. *Z. Naturforsch. 34*, 820–825.
15. Madamwar, D., Garg, N., Shah, V. (2000). Cyanobacterial hydrogen production. *World J. Microbiol. Biotechnol*. *16*, 757–767.
16. Serebryakova, L. T., Sheremetieva, M. E., Lindblad, P. (2000). H2-uptake and evolution in the unicellular cyanobacterium Chroococcidiopsis thermalis CALU 758. *Plant Physiol. Biochem. 38*, 525–530.
17. Moezelaar, R., Stal, L. J. (1994). Fermentation in the unicellular cyanobacterium Microcystis PCC7806. *Arch. Microbiol. 162*, 63–69.
18. Federov, A. S., Tsygankov, A. A., Rao, K. K., Hall, D. O. (1998). Hydrogen photoproduction by Rhodobacter sphaeroides immobilized on polyurethane foam. *Biotechnol. Lett. 20*, 1007–1009.
19. Eroglu, I., Aslan, K., Gunduz, U., Yucel, M., Turker, L. (1999). Substrate consumption rate for hydrogen production by Rhodobacter sphaeroides in a column photobioreactor. *J. Biotechnol. 70*, 103–113.

20. Kim, M. S., Baek, J. S., Lee, J. K. (2006). Comparison of H2 accumulation by Rhodobacter sphaeroides KD131 and its uptake hydrogenase and PHB synthase deficient mutant. *Int. J. Hydrogen Energy. 31*, 121–127.
21. Zhu, H., Ueda, S., Asada, Y., Miyake, J. (2002). Hydrogen production as a novel process of wastewater treatment—studies on tofu wastewater with entrapped R. sphaeroides and mutagenesis. *Int. J. Hydrogen Energy. 27*, 1349–1357.
22. He, D., Bultel, Y., Magnin, J. P., Roux, C., Willison, J. C. (2005). Hydrogen photosynthesis by Rhodobacter capsulatus and its coupling to PEM fuel cell. *J. Power Sources. 141*, 19–23.
23. Oh, Y. K., Scol, E. H., Lee, E. Y., Park, S. (2002). Fermentative hydrogen production by new chemoheterotrophic bacterium Rhodopseudomonas palustris P4. *Int. J. Hydrogen Energy. 27*, 1373–1379.
24. Yokoi, H., Mori, S., Hirose, J., Hayashi, S., Takasaki, Y. (1998). H_2 production from starch by mixed culture of Clostridium butyricum and Rhodobacter sp M-19. *Biotechnol. Lett. 20*, 895–899.
25. Lee, C. M., Chen, P. C., Wang, C. C., Tung, Y. C. (2002). Photohydrogen production using purple nonsulfur bacteria with hydrogen fermentation reactor effluent. *Int. J. Hydrogen Energy. 27,* 1309–1313.
26. Fang, H. H. P., Liu, H. (2002). Effect of pH on hydrogen production from glucose by mixed culture. *Bioresour. Technol. 82,* 87–93.
27. Lay, J. J., Lee, Y. J., Noike, T. (1999). Feasibility of biological hydrogen production from organic fraction of municipal solid waste. *Water Res. 33,* 2579–2586.
28. Lay, J. J. (2000). Modeling and optimization of anaerobic digested sludge converting starch to hydrogen. *Biotechnol. Bioeng. 68,* 269–278.
29. Khanal, S. K., Chen, W. H., Li, L., Sung, S. (2004). Biological hydrogen production: effects of pH and intermediate products. *Int. J. Hydrogen Energy. 29,* 1123–1131.
30. Chen, C. C., Lin, C. Y., Chang, J. S. (2001). Kinetics of hydrogen production with continuous anaerobic cultures using sucrose as limiting substrate. *Appl. Microbiol. Biotechnol. 57,* 56–64.
31. Collet, C., Adler, N., Schwitzgu'ebel, J. P., P'eringer, P. (2004). Hydrogen production by Clostridium thermolacticum during continuous fermentation of lactose. *Int. J. Hydrogen Energy. 29,* 1479–1485.
32. Liu, G., Shen, J. (2004). Effects of culture medium and medium conditions on hydrogen production from starch using anaerobic bacteria. *J. Biosci. Bioeng. 98,* 251–256.
33. Zhang, T., Liu, H., Fang, H. H. P. (2003). Bio-hydrogen production from starch in wastewater under thermophilic conditions. *J. Environ. Manag. 69,* 149–156.
34. Lay, J. J. (2001). Bio-hydrogen generation by mesophilic anaerobic fermentation of microcrystalline cellulose. *Biotechnol. Bioeng. 74,* 281–287.
35. Yokoi, H., Saitsu, A. S., Uchida, H., Hirose, J., Hayashi, S., Takasaki, Y. (2001). Microbial hydrogen production from sweet potato starch residue. *J. Biosci. Bioeng. 91,* 58–63.
36. Liu, H., Zhang, T., Fang, H. P. P. (2003). Thermophilic H_2 production from cellulose containing waste water. *Biotechnol. Lett. 25,* 365–369.
37. Morimoto, M., Atsuko, M., Atif, A. A. Y., Ngan, M. A., Fakhru'l-Razi, A., Iyuke, S. E. et al. (2004). Biological production of hydrogen from glucose by natural anaerobic microflora. *Int. J. Hydrogen Energy. 29,* 709–713.

38. Dabrock, B., Bahl, H, Gottschalk, G. (1992). Parameters affecting solvent production by Clostridium pasteurium. *Appl. Environ. Microbiol. 58,* 1233–1239.
39. Shah, V., Garg, N., Madamwar, D. (2003). Ultrastructure of the cyanobacterium Nostoc muscorum and exploitation of the culture for hydrogen production. *Folia Microbiol.* (*Praha*). *48,* 65–70.
40. Rai, A. K., Abraham, G. (1995). Relationship of combined nitrogen sources to salt tolerance in freshwater cyanobacterium Anabena doliolum. *J. Appl. Bacteriol. 78,* 501–506.
41. Lambert, G. R., Daday, A., Smith, G. D. (1979). Hydrogen evolution from immobilized cultures of cyanobacterium Anabena cylindrica. *FEBS Lett. 101,* 125–128.
42. Rawson, D. M. (1985). The effects of exogenous aminoacids on growth and nitrogenase activity in the cyanobacterium Anabena cylindrica PCC 7122. *J. General Microbiol. 134,* 2549–2544.
43. Jeffries, T. W., Timourien, H., Ward, R. L. (1978). Hydrogen production by Anabaena cylindrica: Effect of varying ammonium and ferric ions, pH and light. *Appl. Env. Microbiol. 35,* 704–710.
44. Lambert, G. R., Smith, G. D. (1977). Hydrogen formation by marine Bluegreen algae. *FEBS Lett. 83,* 159–162.
45. Ramchandran, S., Mitsui, A. (1984). Recycling of hydrogen photoproduction system using an immobilized marine blue green algae Oscillatoria sp. Miami BG7, solar energy and seawater [abstract]. *VII Int. Biotechnology Symposium.* 183–184.
46. Moezelaar, R., Bijvank, S. M., Stal, L. J. (1996). Fermentation and sulfur reduction in the mat-building cyanobacterium Microcoleus chtonoplastes. *Appl. Environ. Microbiol*. *62,* 1752–1758.
47. Fay, P. (1992). Oxygen relations of nitrogen fixation in cyanobacteria. *Microbiol Rev. 56,* 340–373.
48. Antal, T. K., Lindblad, P. (2005). Production of H_2 by sulfur-deprived cells of the unicellular cyanobacteria Gloeocapsa alpicola and Synechocystis sp. PCC 6803 during dark incubation with methane or at various extracellular pH. *J. of Appl. Microbiol*. *98,* 114–120.
49. Guan, Y., Deng, M., Yu, X., Zang, W. (2004). Two stage photo-production of hydrogen by marine green algae Platymonas subcordiformis. *Biochem. Eng. J. 19,* 69–73.
50. Winkler, M., Hemschemeier, A., Gotor, C., Melis, A., Happer, T. (2002). [Fe]-hydrogenases in green algae: photo-fermentation and hydrogen evolution under sulfur deprivation. *Int. J. Hydrogen Energy. 27,* 1431–1439.
51. Melis, A., Zhang, L., Forestier, M., Ghirardi, M. L., Seibert, M. (2000). Sustained photohydrogen production upon reversible inactivation of oxygen evolution in the green algae Chlamydomonas reindhardtii. *Plant Physiol. 122,* 127–135.
52. Laurinavichene, T. V., Tolstygina, I. V., Galiulina, R. R., Ghirardi, M. L., Seibert, M., Tsygankov, A. A. (2002). Dilution methods to deprive Chlamydomonas reinhardtii cultures of sulfur for subsequent hydrogen photoproduction. *Int. J. Hydrogen Energy. 27,* 1245–1249.
53. Koku, H., Eroglu, I., Gunduz, U., Yucel, M., Turker, L. (2002). Aspects of metabolism of hydrogen production by Rhodobacter sphaeroides. *Int. J. Hydrogen Energy. 27,* 1315–1329.

54. Seifert, K., Thiel, M., Wicher, E., Włodarczak, M., Łaniecki, M. (2013). Microbiological Methods of Hydrogen Generation. www.intechopen.com. 223–250.
55. Chun-xiang, Q., Lu-yuan, C., Hui, R., Xiao-ming, Y. (2011). Hydrogen production by mixed culture of several facultative bacteria and anaerobic bacteria. *Progress in Natural Science*: *Materials Int. 21,* 506−511.
56. Kumar, N., Das, D. (2000). Enhancement of hydrogen production by Enterobacter cloacae IIT-BT 08. *Process. Biochem. 35,* 589–593.
57. Lin, C. Y., Chang, R. C. (2004). Fermentative hydrogen production at ambient temperature. *Int. J. Hydrogen Energy*, *29,* 715–720.
58. Fabiano, B., Perego, P. (2002). Thermodynamic study and optimization of hydrogen production by Enterobacter aerogenes. *Int. J. Hydrogen Energy*, *27,* 149–156.
59. Oh, Y. K., Scol, E. H., Kim, M. S., Park, S. (2004). Photoproduction of hydrogen from acetate by a chemoheterotrophic bacterium Rhodopseudomonas palustris P4, *Int. J. Hydrogen Energy*, *29,* 1115–1121.
60. Fang, H. H. P., Liu, H., Zhang, T. (2005). Phototrophic hydrogen production from acetate and butyrate in wastewater. *Int. J. Hydrogen Energy*, *30,* 785–793.

PART 2

MICROBIAL FUEL CELLS

CHAPTER 3

MICROBIAL FUEL CELLS: A PROMISING ALTERNATIVE ENERGY SOURCE

M. J. ANGELAA LINCY,[1] B. ASHOK KUMAR,[2] V. S. VASANTHA,[3] and P. VARALAKSHMI[1,*]

[1]*Department of Molecular Microbiology, School of Biotechnology, Madurai Kamaraj University, Madurai, Tamil Nadu*

[2]*Department of Genetic Engineering, School of Biotechnology, Madurai Kamaraj University, Madurai, Tamil Nadu*

[3]*Department of Natural Products, School of Chemistry, Madurai Kamaraj University, Madurai, Tamil Nadu*

CONTENTS

3.1 Introduction 63
3.2 Components of a Fuel Cell 66
3.2.1 Types of Fuel Cells 67
3.2.2 Types of MFC Based on the Reactor Models 74
3.2.3 Components of a Microbial Fuel Cell 75
3.2.4 Applications of Microbial Fuel Cells 76
3.2.5 Microbial Fuel Cells in Electricity Generation 76
3.2.6 Mechanism of Electricity Production 76
3.2.7 Microbial Fuel Cells in Hydrogen Production 77
3.2.8 Microbial Fuel Cells in Wastewater Treatment 78
3.2.9 Environmental Sensors 79
3.2.10 Bioremediation 79

3.2.11 Organisms Employed in Fuel Cells 79
3.3 Conclusion 80
Keywords 80
References 80

ABSTRACT

The Indian sub-continent is luxuriously bestowed with all wealth in the form of population, land and ocean. Being placed as the second highly populated nation in the world, India is under the urge to nurture the needs of its population. Its various demands such as the demand for food, employment, economy, etc., can be completely resolved if the country is adequately supplied with energy. But adequate supplying of energy to such a vast population is quiet an impossible task, which demands seek for alternative energy sources. The widely known alternative energy sources are generally, renewable energy sources such as solar cells, fuel cells and wind power. At this moment, several fuel cell types based on hydrogen and methanol work appropriately, and applications already exist for, for example, portable computers. However, the question can be raised whether this energy generation is really sustainable. Furthermore, the customer may not like to carry hydrogen gas (even captured within a metal hydride matrix) or methanol. But, Microbial fuel cells can operate on a large variety of substrates that are readily available, even in any supermarket. Substrates such as plain sugar and starch are easy to store, contain more energy than any other feed type per unit of volume, and are easy to dose. Furthermore, they have a more 'green' image than, for example, methanol. Moreover, MFCs can be developed that are environmentally friendly in terms of material composition.

When microorganisms function as biocatalysts that motivate the degradation of organic materials to produce electrons, which travel via an electric circuit, then the fuel cell is termed as a microbial fuel cell. This chapter covers an introduction to MFCs, state of art of MFCs and wide applications of MFCs technology. If the development of MFCs leads to a product that has a reasonable (read: usable) power output per unit of MFC volume, it will be a viable product. A customer will accept a larger battery,

and a larger feeding tank, provided the feeding is easy to perform and has a green and safe label.

3.1 INTRODUCTION

The Indian sub-continent is luxuriously bestowed with all wealth in the form of population, land and ocean. Being placed as the second highly populated nation in the world, India is under the urge to nurture the needs of its population. Its various demands such as the demand for food, employment, economy, etc., can be completely resolved if the country is adequately supplied with energy. But adequate supplying of energy to such a vast population is quiet an impossible task, which demands seek for alternative energy sources. The widely known alternative energy sources are generally, renewable energy sources such as solar cells, fuel cells and wind power.

Fuel cells are electrochemical devices that convert the chemical energy stored in a fuel directly into electrical power. Fuel cells have various advantages compared to conventional power sources, such as internal combustion engines or batteries. Benefits include: higher efficiency compared than diesel or gas engine, their operation is free from noise and CO_2 pollution and do not need conventional fuels such as oil or gas and can therefore reduce economic dependence on oil producing countries and the main fuel (H_2) can be produced from the natural source water, etc.

The conventional batteries have several drawbacks:

- they need to be charged for several hours in order to be used.
- they are environmentally unfriendly due to the heavy metal content.
- one needs electricity to power them up.

Therefore, different types of fuel cells are developed as follows:

- alkaline fuel cells;
- proton exchange membrane fuel cells;
- direct methanol fuel cells;
- phosphoric acid fuel cells;
- molten carbonate fuel cells;
- solid oxide fuel cells.

Alkaline fuel cell is one of the most developed fuel cell technologies. They use alkaline electrolytes such as potassium hydroxide in water and operate at 70°C. They employ cheaper, non noble metal catalysts such as nickel and silver [1, 2]. Proton exchange membrane fuel cells also known as Polymer electrolyte membrane fuel cells (PEM) are a type of fuel cell being developed for transport applications. They employ a proton conductive, water based, acidic polymer membrane as an electrolyte [3] and operate at relatively low temperatures. Direct methanol fuel cells are a sub category of Proton exchange membrane fuel cells, the fuel being methanol. It makes use of a polymer membrane as an electrolyte and operates between 60°C and 130°C [4].

Phosphoric acid fuel cells employ highly concentrated or pure liquid phosphoric acid as the electrolyte. The catalyst being finely dispersed platinum, they operate at 150°C to 220°C. Molten carbonate fuel cells represent a high temperature technology of fuel cells [5]. They employ molten carbonate salt as an electrolyte and do not require a metal catalyst. They operate at around 650°C. Solid oxide fuel cells are another type of high temperature fuel cells whose operating temperature ranges from 800°C–1000°C [5]. They use a solid ceramic such as stabilized zirconium oxide as the electrolyte and do not need a metal catalyst. They are widely used for stationary power generation.

First experimental evidence of bioelectricity was demonstrated by Luigi Galvani in the late eighteenth century by connecting the legs of a frog to a metallic conductor [6, 7]. The potential of bioelectricity was further experimented by Micheal C. Potter in 1911, who designed the first microbial fuel cell. In 1931, a potentiostat-poised half-cell was operated by Barnett Cohon and a current of 0.2 mA was obtained by applying +0.5 V [8].

In 1980s, electricity was successfully retrieved from MFCs by a British researcher, H. Peter Bennetto by employing pure cultures of bacteria to catalyze the oxidation of organics and use artificial electron mediators to facilitate electron transfer in the anode [9–11]. As on date, fuel cells can vary from tiny cells, producing few watts electricity to large power plants producing megawatts [12] and are classified into different types based on the various electrolytes employed.

Conventional microbial fuel cell is a two-chamber system, consisting of anode and cathode chambers that are separated by a solid or a liquid electrolyte that transmits electrically charged particles across them [12]. At the anode end, the fuel gets oxidized and releases electrons. At the cathode, oxygen reduction occurs. The electrolyte conducts ions from one electrode to the other, inside a fuel cell. The catalyst speeds up a chemical reaction. The reformer extracts pure hydrogen from hydrocarbons.

Microbial fuel cells have become a promising alternative for electricity generation, biomass cultivation and wastewater treatment. If the microbial fuel cells make use of solar energy to generate electricity then they are called as Photo microbial fuel cells [13]. If they use photosynthetic algae for producing electricity, then they are called as Photosynthetic algal microbial fuel cells [14].

Microbial fuel cells are believed to serve as a viable technological alternative to conventional wastewater treatment. They can harvest electricity from the energy available in organic wastewater [15]. Microorganisms like *Chlorella vulgaris* [13, 14], *Leptothrix discophora* [6], *Klebsiella pneumonia* [16], *Thiobaccillus ferrooxidance* [17], *Pseudomonas fluroscens* [18], *Rhodospirillum rubrum* [19], *G. metallireducens* [20], *D. desulfuricans* [21] and other aerobic and anaerobic bacteria have been reported to be employed in microbial fuel cells so far. Few other microorganisms like cyanobacteria and some microalgae are also believed to play remarkable roles if employed in microbial fuel cells. Improvising the functioning of these cells to give exponential yields will be the expected future of the field.

Fuel cells are electrochemical devices that convert the chemical energy stored in a fuel directly into electrical power. They are considered to be highly reliable because of their high efficiency and low or zero emission [22]. When microorganisms function as biocatalysts that motivate the degradation of organic materials to produce electrons, which travel via an electric circuit, then the fuel cell is termed as a microbial fuel cell [6].

Bacteria grow by catalyzing chemical reactions and harnessing and storing energy in the form of adenosine triphosphate (ATP). In some bacteria, reduced substrates are oxidized and electrons are transferred

to respiratory enzymes by NADH, the reduced form of nicotinamide adenine dinucleotide (NAD). These electrons flow down a respiratory chain—a series of enzymes that function to move protons across an internal membrane—creating a proton gradient. The protons flow back into the cell through the enzyme ATPase, creating 1 ATP molecule from 1 adenosine diphosphate for every 3–4 protons. The electrons are finally released to a soluble terminal electron acceptor, such as nitrate, sulfate, or oxygen. In the first type of MFC, the electrons are transferred from the bacteria to the anode without the intervention of an intermediate fermentation product [23].

First experimental evidence of bioelectricity was demonstrated by Luigi Galvani in the late eighteenth century by connecting the legs of a frog to a metallic conductor [7]. The potential of bioelectricity was further experimented by Micheal C. Potter in 1911, who designed the first microbial fuel cell. He demonstrated current flow between two electrodes emerged from a bacterial culture and in a sterile medium [24]. In 1931, a potentiostat-poised half cell was operated by Barnett Cohon and a current of 0.2 mA was obtained by applying +0.5 V [8].

In 1980s, electricity was successfully retrieved from MFCs by a British researcher, H. Peter Bennetto. He employed pure cultures of bacteria to catalyze the oxidation of organics and use artificial electron mediators to facilitate electron transfer in the anode [9–11, 91]. As on date, fuel cells can vary from tiny cells, producing few watts electricity to large power plants producing megawatts [12] and are classified into different types based on the various electrolytes employed.

3.2 COMPONENTS OF A FUEL CELL

Conventional microbial fuel cell is a two-chamber system, consisting of anode and cathode chambers that are separated by a solid or a liquid electrolyte that transmits electrically charged particles across them [12]. At the anode end, the fuel gets oxidized and releases electrons. At the cathode, oxygen reduction occurs. The electrolyte conducts ions from one electrode to the other, inside a fuel cell. The catalyst speeds up a chemical reaction. The reformer extracts pure hydrogen from hydrocarbons.

3.2.1 TYPES OF FUEL CELLS

3.2.1.1 Alkaline Fuel Cells

Alkaline fuel cell (AFC) also known as Bacon fuel cell after its British inventor, is one of the most developed fuel cell technologies. The AFC use alkaline electrolytes such as potassium hydroxide in water (Fig. 3.1). They are known to be the best performing fuel cells of the existing conventional hydrogen-oxygen fuel cells operable at temperatures below 200°C [25]. Typical operating temperatures are around 70°C. They employ cheaper, non noble metal catalysts such as nickel and silver [1, 2] and can offer high electrical efficiency.

AFC are advantageous over other fuel cells that make use of precious metal catalysts, like DMFCs, in the following ways:

1. the slow electrode kinetics problem encountered by the other cells is not found I alkaline fuel cells because it is a well established fact that the electrode kinetics of oxygen reduction is enhanced in an alkaline medium;
2. they use non precious metals as catalysts such as silver catalysts [26], nickel catalysts [27] and perovskite type oxides [28], which are less prone to methanol crossover; and

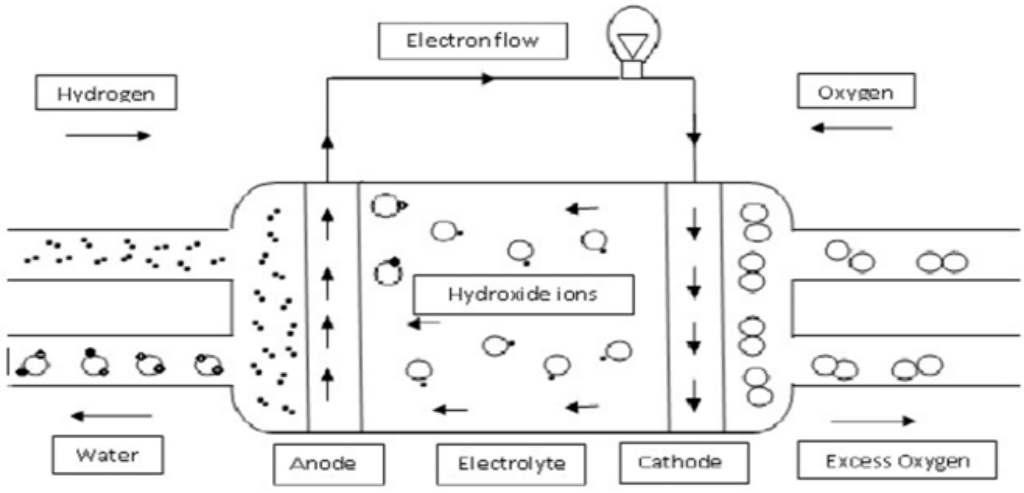

FIGURE 3.1 Schematic diagram of an Alkaline fuel cell.

3. CO poisoning of Platinum catalyst at low temperatures is another problem encountered by other fuel cells but not alkaline fuel cells.

The only problem with these fuel cells is the progressive carbonation of the alkaline solution, due to carbon dioxide release from the product of the fuel. This reduces the pH of the alkaline solution, thus decreasing the reactivity for the electro oxidation of methanol ultimately. Research is to be established in this area of alkaline fuel cells that could rectify this carbonation problem.

3.2.1.2 Proton Exchange Membrane Fuel Cells

Proton exchange membrane fuel cells also known as Polymer electrolyte membrane fuel cells, are a type of fuel cell being developed for transport applications as well as for stationery fuel cell applications. Figure 3.2 shows the schematic diagram of a Proton exchange membrane fuel cell. PEM cell uses a proton conductive, water based, acidic polymer membrane as an electrolyte [3]. The polymer membrane used is impermeable to gases but it conducts protons [29]. Among the membranes

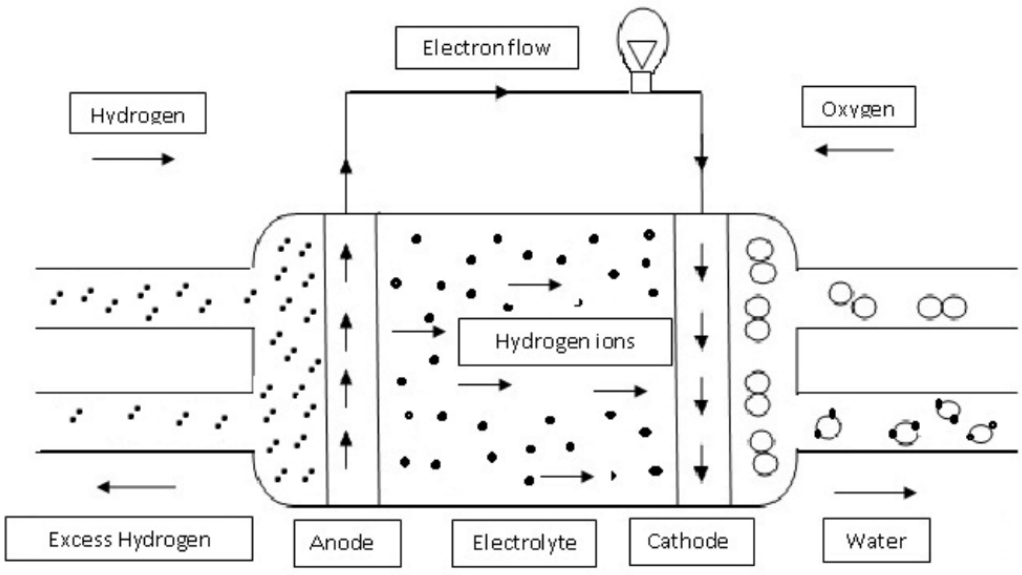

FIGURE 3.2 Schematic diagram of Proton exchange membrane fuel cell.

of hydrogen fuelled Proton exchange membrane fuel cells, perfluorosulfonic acid based membranes, mostly DuPont's Nafion [30], show complete domination upon other commercialized membranes [31].

Proton exchange membrane fuel cells operate at relatively low temperatures (below 100°C). The challenges faced while operating these cells under low temperature include fuel impurity, CO tolerance and heat rejection [30]. Their shortcomings could be surmounted at a functioning at high temperatures. High temperature may be till 200°C. But the primary problem in operating at high temperatures is that, the Relative humidity is directly proportional to the Nafion Membrane conductivity of the cells. Therefore, whenever there is a fall in the relative humidity of the cell, the conductivity of the Nafion membrane also drops down. The cells cannot yield high membrane conductivity at a range of (> 0.1 S cm^{-1}) unless an external humidification sub system is functioned with the fuel cell system [32, 33]. The electrical output is generally variable and they are ideal for vehicles. It has been reported that they show 50% higher fuel conversion efficiency than a car engine. Under favorable conditions, their efficiency can be almost 60% where a car engine has achieved only 30%.

However, there are certain factors that affect the performance of PEMFCs. They are as follows:

1. Partial pressures of reactants and pressure variations across the membrane, while the cell is functioning.
2. Hydrogen supply at the anode.
3. Oxygen starvation at the cathode.
4. Dehydrated membrane conductivity.
5. On the other hand, presence of too much water in the back plate channels also depletes the cell efficiency [34].
6. Hydrophobicity of the membrane surface [35].
7. Dehydration at the anode [36].
8. Lack of assistance to diffuse back the water produced at the cathode.

Looking upon the above-mentioned factors, the present shortcomings of these fuel cells could be surmounted and these could be argued to be the most simple and highly efficient ones [37].

3.2.1.3 Direct Methanol Fuel Cells

Direct methanol fuel cells are a sub category of Proton exchange membrane fuel cells, the fuel being methanol (Fig. 3.3). The structure of a Direct methanol fuel cell is given below. It is considered to be advantageous over the other types of cells because of the use of liquid fuel (methanol), easy refueling, low cost and ease in transport of methanol [4]. Moreover, methanol is energy dense, yet reasonably stable at all environmental conditions. However, methanol is highly volatile and toxic, which may pose severe troubles when used in portable DMFC electronic devices. Apart from this, CO poisoning of the platinum catalysts and methanol cross over are the other major issues with DMFC. Researches are being carried out upon electro – oxidation, with polyhydric alcohols in alkaline solutions using Platinum electrode and Ethylene glycol has been found to show highest reactivity among the alcohols examined in KOH and K_2CO_3 solutions. Ethylene glycol is also believed to overcome the carbonation problem, due to CO_2 release from the product of the fuel. It is much less toxic and volatile than methanol and is supposed to be safer.

DMFCs make use of a polymer membrane as an electrolyte like the PEMFC. The most effective catalysts are found to be carbon supported or unsupported platinum-ruthenium at anode and platinum at cathode [38]. They operate in temperatures between 60°C and 130°C and possess a theoretical energy density of 6094 W h/kg and a practical harvest of

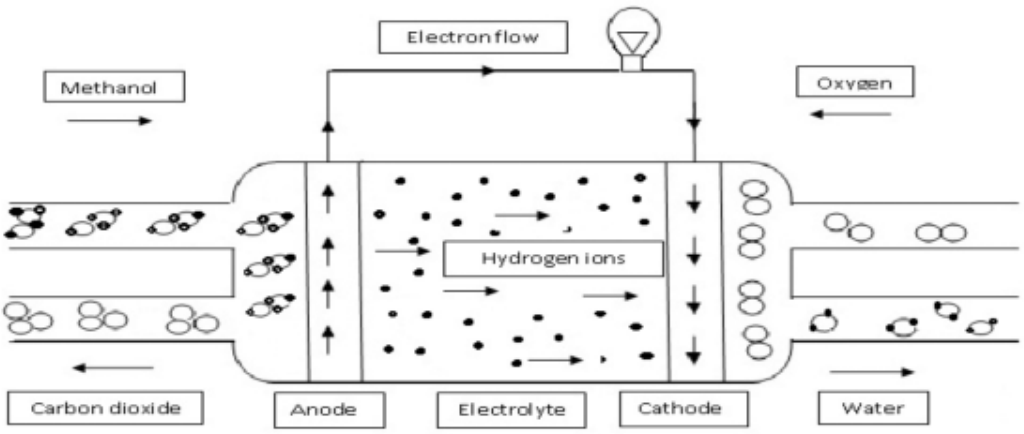

FIGURE 3.3 Schematic diagram of Direct methanol fuel cell.

1000–3000 W h/kg [39]. Their compact cell design makes them suitable for various stationary and nonstationary applications [4].

Regarding DMFCs for transportation or portable power applications, long-term stability of the anode and methanol cross over are the problems that affect the performance of the cells. Concentrating on fuel utilization, overall anode performance, conversion efficiency of the cell and platinum loading, may help improving electricity generation and stability. It has been reported that DMFC cathodes, operating on ambient air at 60°C, can deliver high performance of more than 0.85 V versus RHE at 0.100 A cm^{-2} [40]. For the cells operating at high temperature of 148°C, Nafion – Silica composite membranes doped with phosphotungstic acid has been found suitable. It shows a maximum power density of 400 mW cm^{-2} in the presence of oxygen feed and 250 mW cm^{-2} in the presence of air feed [41]. Further research is to be undertaken in this area of improving DMFCs for portable power applications.

3.2.1.4 Phosphoric Acid Fuel Cells

Phosphoric acid fuel cells developed in the mid 1960s were named after their working electrolyte, which is highly concentrated or pure liquid phosphoric acid, saturated in silicon carbide mix. They use finely dispersed platinum catalyst on carbon. Usually phosphoric acid is surrounded by a couple of porous matrix embedded in a ceramic matrix [42]. Phosphoric acid is a bad conductor and the cell needs 150°C to 220°C to work effectively [5]. Being the first commercialized fuel cells, they are extensively employed in power generators to generate 100 kW to 400 kW [43]. They have a wide range of applications in central heating plant, hospitals, dormitory, pools, office buildings, laundry and kitchen [44]. Their only disadvantage is they cannot be compatible with high temperature thermal steam applications.

There are a number of benefits in using phosphoric acid fuel cells in common use. They are as follows:

1. They are environmentally beneficial because, they emit only water, which is also very pure. They are circulated inside the fuel cell system as a coolant and liberation of a little amount of water into the environment will not be pollution causing.

2. They are highly fuel efficient with a higher heating value of 36% and a lower heating value of 40%.
3. They can be configured in such a way that they provide power back up.
4. They are low noise emitters that are too low when compared to traditional combustion technologies.
5. They are flexible enough to be sited in urban areas.

Studies have shown that addition of small amounts of fluorinated organic compounds or silicone compound, having a vapor pressure less than that of phosphoric acid, to the phosphoric acid electrolyte of a phosphoric acid fuel cell enhances oxygen solubility and diffusivity of the electrolyte. Moreover, there is a fact that decreasing polarization of the cathode increases efficiency of the cell. Using modified electrolyte increases cell efficiency by decreasing cathodic polarization [45].

3.2.1.5 Molten Carbonate Fuel Cells

Molten carbonate fuel cells represent a high temperature technology of fuel cells [5]. They use molten carbonate salts of alkali metals as electrolyte. Their anode or cathode is made of nickel oxide or cobalt oxide or rare earth element oxide [46]. Their operating temperature is as high as 650°C. That is why, rather than using a precious metal like platinum, a relatively cheap metal such as nickel is preferred as the catalyst. They can run on hydrocarbon fuels such as methane, natural gas or coal-reformed gases. Since their efficiency has been reported to be 45% which can also be raised up to 60–70% they could be considered as potential alternatives for petroleum [48].

In spite of all their advantages, a molten carbonate fuel cell using an alkali metal carbonate electrolyte encounters the following problems.

1. The presence of oxygen forms cracks on the electrode, particularly when sintered porous nickel plate is used as a cathode.
2. The particle size of the sintered porous nickel plate has decelerating effects on the output when the particle size is large.
3. Usage of a sintered porous nickel plate in the anode decreases the surface area of electrode by the sintering phenomenon of nickel and thus decreasing the cell output.

These shortcomings could be surmounted by finding an alternative electrolyte that is devoid of the above said disadvantages and is highly active, even at high operating temperatures.

3.2.1.6 Solid Oxide Fuel Cells

Solid oxide fuel cells are another type of high temperature fuel cells whose operating temperature ranges from 700°C–1000°C (Solid oxide fuel cell, spotlight). They use a solid ceramic such as stabilized zirconium oxide, oxygen ion, a proton or a mixed oxygen ion–proton conductor, which is gas impermeable and an electronic insulator [49] and do not need a metal catalyst. Their efficiency is reported to be 60%, theoretically up to 80% [5] and is widely used for stationary power generation.

Solid oxide fuel cells are highly advantageous over other fuel cells in the following aspects:

1. they are highly performative even at a temperature range of 1000°C and the electrode activity is extremely high.
2. they do not require the use of expensive catalysts such as platinum.
3. scale of equipments does not generally influence the fuel cell efficiency.
4. they have high-energy conversion capacity due to low polarization and high output voltage.

The very few disadvantages of SOFC is the ohmic resistance exhibited by the fuel electrode and air electrode, which influences power generation [50] and over voltage with Hydrogen and Carbon monoxide [51]. Studies are being carried out to rectify these discrepancies and to bring out the efficacy of the fuel cell at it's fullest.

3.2.1.7 Microbial Fuel Cells

Microbial fuel cells are devices that convert the chemical energy present in organic compounds to electrical energy through microbial catalysts [52]. They employ bacteria on the anode to carry out oxidation of organic matters and bacteria or microalgae on the cathode to undergo reduction.

3.2.2 TYPES OF MFC BASED ON THE REACTOR MODELS

MFC can be classified in to two types based on the reactor models:

In the first type of MFC, the electrons are transferred from the bacteria to the anode without the intervention of an intermediate fermentation product [23]. Since microorganisms act as a catalyst in the transfer of electrons from the substrate to the anode, the selection of a high performing microbial consortium (either pure or mixed culture) is of crucial importance in these microbial fuel cells. The electron transfer from the bacterium to the anode can proceed in a direct way from the bacterial membrane to the anode surface or indirectly by means of a mediator (Fig. 3.4).

Both transfers through bacterial contact with the electrode and through soluble shuttles can be regarded as mediated. In the first case, a bacterial redox enzyme, immobilized in the cell wall, provides the electron transfer. Examples of such bacteria are *Geobacter sulfurreducens* [53] and *Rhodoferax ferrireducens* [54]. When a soluble mediator is used, the electrons are shuttled by mediator molecules between the redox enzyme(s) of the bacteria and the electrode surface, thereby facilitating electron transport

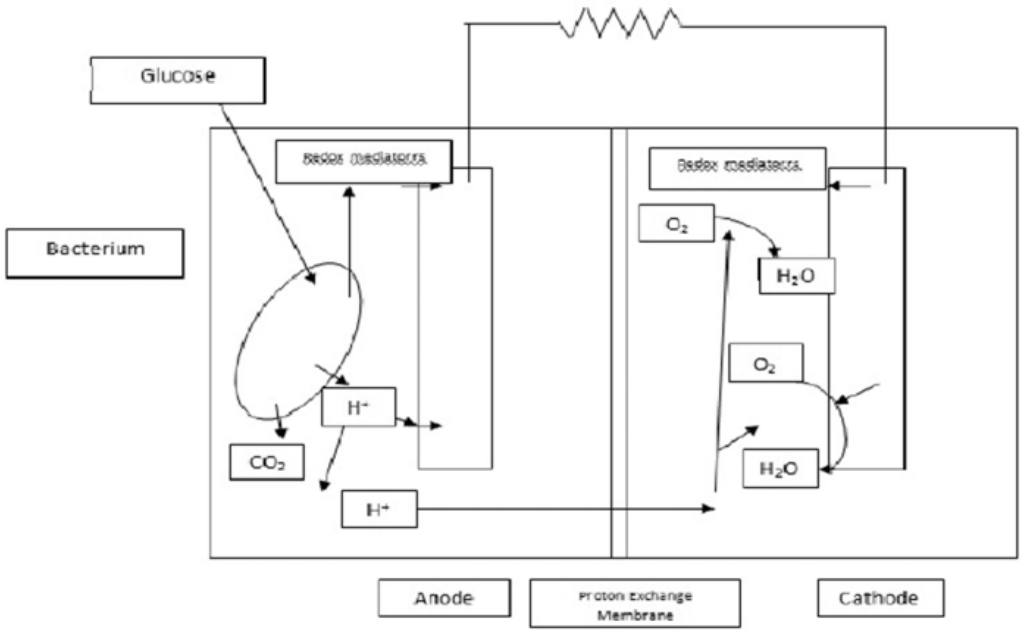

FIGURE 3.4 Schematic diagram of a microbial fuel cell.

[55]. Mediators are typically redox molecules (e.g., ubiquinones, dyes and metal complexes) that can form reversible redox couples, are stable in both oxidized and reduced form, are not biologically degraded and are not toxic towards the microbial consortium [56].

3.2.3 COMPONENTS OF A MICROBIAL FUEL CELL

Conventional microbial fuel cells contain an anode, a cathode, proton exchange membrane and a resistor through which the electrons pass to the anode. The anode is generally immobilized with a bacterial consortium [13] and the cathode compartment contains the microbial source. At times, the anode compartment is loaded with the fuel source or the organic material to be oxidized [14]. After oxidation, the protons pass through the proton exchange membrane to the cathode, where they are reduced into water.

Second type of microbial cells, which operates with a trielectrode system, is also employed in wastewater treatment and other applications. These microbial fuel cells contain three electrodes: the working electrode, the counter electrode and the reference electrode. Working electrode is the cathode that harbors the microalgae or bacteria. It may be glassy carbon electrode or platinum electrode upon which the microalgae or bacteria are immobilized. Counter electrode functions as the conductor of electricity. Reference electrode is the standard or the electrode of reference. Silver or silver in potassium chloride are the widely employed reference electrodes. The current generated is read with the help of a cyclic voltmeter.

Ideal MBFC consists of two chambers made up of glass, polycarbonate or Plexiglas with two electrodes. Very large surface areas are needed for supporting the biofilm, and the structure must be able to bear the weight of the water and biofilm. Electrode materials range from carbon cloth and carbon paper, to graphite rods, plates, granules, and RVC. Cathodes are made from the same materials, but they also contain precious metals, such as platinum, when oxygen is used as the electron acceptor. Platinum can be replaced by cobalt– and iron–organic-mixture catalysts, although the longevity of such materials is not well studied [57, 58].

3.2.4 APPLICATIONS OF MICROBIAL FUEL CELLS

Microbial fuel cells have become a promising alternative for electricity generation, biomass cultivation and wastewater treatment. If the microbial fuel cells make use of solar energy to generate electricity then they are called as Photo microbial fuel cells [13]. If they use photosynthetic algae for producing electricity, then they are called as Photosynthetic algal microbial fuel cells [14]. Therefore, Photo microbial fuel cells and Photosynthetic microbial fuel cells could be considered as the two different types of Microbial fuel cells.

3.2.5 MICROBIAL FUEL CELLS IN ELECTRICITY GENERATION

Though the launch of microbial fuel cells dates back to the late eighteenth century when Luigi Galvani first reported bioelectricity by connecting frog's legs to a metallic conductor [7], it is in the recent times that, they have been developed to harvest electricity, thus providing opportunities for practical applications [59–63].

3.2.6 MECHANISM OF ELECTRICITY PRODUCTION

The oxidation and reduction reaction that takes part in the anode and cathode chamber of a microbial fuel cell contributes to the flow of electrons, that pass through a resistance to produce current [64]. A three-chambered microbial fuel cell is built with the anode immobilized with a bacterial consortium and the cathode containing any microorganism such as the bacteria or microalgae [65–67]. Therefore, the metabolic pathways undertaken by the bacterium are solely responsible for the microbial electron and proton flow [68–70].

To understand how an MFC produces electricity, we must understand how bacteria capture and process energy. Bacteria grow by catalyzing chemical reactions and harnessing and storing energy in the form of adenosine triphosphate (ATP). In some bacteria, reduced substrates are oxidized and electrons are transferred to respiratory enzymes by NADH, the reduced form of nicotinamide adenine dinucleotide (NAD).

These electrons flow down a respiratory chain—a series of enzymes that function to move protons across an internal membrane—creating a proton gradient. The protons flow back into the cell through the enzyme ATPase, creating 1 ATP molecule from 1 adenosine diphosphate for every 3–4 protons. The electrons are finally released to a soluble terminal electron acceptor, such as nitrate, sulfate, or oxygen.

However the anode potential determines the metabolism of the bacteria [71]. When the current of the MFC increases, it eventually decreases the anode potential, thus forcing the bacteria to deliver electrons through more reduced complexes. At high anodic potentials the bacteria can use the respiratory chain in an oxidative metabolism. Normally, the current from a MFC is inhibited by the various inhibitors of the respiratory chain. At the same time, processes using oxidative phosporylation yield 65% high efficiency MF cells [61].

At low anode potentials and in the presence of an alternate electron acceptor such as sulfur, the electrons tend to be deposited onto these components and methanol production is high, indicating that, a bacterium does not use the anode [68, 72]. If no electrons acceptors like sulfur or nitrate are present, then fermentation will be the main reaction yielding a maximum of one-third of the hexose substrate electrons [73]. Thus, optimization of the anode potential can hike up the efficiency of a microbial fuel cell.

The performance of a MFC is determined by many factors like reactor configuration, pH, seed culture or substrate, electrolyte resistance and so on [52]. In spite of that they convert a wide array of electron donors with effective energy generation at low and moderate temperatures, even when the electron donor is provided at low concentrations. This makes them one of the incomparable alternative fuel sources.

3.2.7 MICROBIAL FUEL CELLS IN HYDROGEN PRODUCTION

MFCs can also be modified to produce hydrogen gas (H_2) by removing oxygen at the cathode and adding in a small voltage via the bioelectrochemically assisted microbial reactor (BEAMR) process or the biocata-

lyzed electrolysis process [43–46]. Bacteria produce an anode working potential of ~ –0.3 V. The protons and electrons that are produced at the anode can combine at the cathode to produce H_2 with only an additional total cell potential of 0.11 V [44]. In practice, however, 0.25 V or more must be put into the circuit to make H_2, because of overpotential at the cathode [74–77].

3.2.8 MICROBIAL FUEL CELLS IN WASTEWATER TREATMENT

Microbial fuel cells are believed to serve as a viable technological alternative to conventional wastewater treatment. Conventional wastewater treatments for removal of organic pollutants are energy and cost intensive because of the requirement of aeration and disposal of excess sludge generated in the process [78]. MFCs can harvest electricity from the energy available in organic wastewater [15]. They are built with cost effective systems such as activated carbon cathodes and graphite fiber brush anodes [79–81]. More specifically, PAMFCs, which are constructed with an immobilized microalga in the cathode, can generously contribute bioelectricity production, biomass production and wastewater treatment [14].

Though conventional MFCs are dual chambered, the problem with the dual chambered MFCs is the cost involved. Generally the oxygen reduction reaction is poor at the non-catalyzed cathodes. Therefore in order to improve their efficiency, costly catalysts are required which make them practically inapplicable directly on field [15]. Therefore MFCs are constructed with Separator electrode assembly (SEA) or widely Spaced electrodes (SPA). SEA has been found to reduce internal resistance when compared with SPA [81, 82]. But when it comes for Refinery wastewater (RW) treatment, SPA is found to be effective than SEA. Because, the separator electrode present in SPA reduces the overall oxygen transfer into the anode chamber, which affects overall COD removal. Whereas the SPA MFCs have higher organic removal with larger difference [82]. A report states that in the U.S, the cost of treating 33 billion gallons of wastewater is around $25 billion a year. MFCs could curb this cost by producing electricity with the organic matters dissolved in the wastewater plants [83]. Thus MFCs are not only cost effective but also productive.

3.2.9 ENVIRONMENTAL SENSORS

Data on the natural environment can be helpful in understanding and modeling ecosystem responses, but sensors distributed in the natural environment require power for operation. MFCs can possibly be used to power such devices, particularly in river and deep-water environments where it is difficult to routinely access the system to replace batteries. Sediment fuel cells are being developed to monitor environmental systems such as creeks, rivers, and the ocean [23, 84–86]. A linear correlation between the columbic of MFC and strength of organic matter in wastewater makes MFC a possible BOD sensor [87].

3.2.10 BIOREMEDIATION

The MFC is not used to produce electricity; instead, power can be put into the system to drive desired reactions to remove or degrade chemicals, such as converting soluble U (VI) to insoluble U (IV) [86]. Bacteria are not only able to donate electrons to an electrode but can also accept electrons from the cathode. By poising the electrodes at –500 mV, Gregory et al. were able to precipitate uranium directly onto a cathode because of bacterial reduction. Nitrate can also be converted to nitrite when electrodes are used as electron donors [20].

3.2.11 ORGANISMS EMPLOYED IN FUEL CELLS

MFCs have gained the attention of many researchers throughout the World in the present scenario. Different types of researches are being carried out to bring out the potency of these cells. So far, Microorganisms like *C. vulgaris* [13, 14], *L. discophora* [6], *K. pneumonia* [16], *T. ferrooxidance* [17], *P. fluroscens* [18], *R. rubrum* [19], *G. metallireducens* [20], *D. desulfuricans* [21] and other aerobic and anaerobic bacteria have been reported to be employed in microbial fuel cells. Few other microorganisms like cyanobacteria and some microalgae are also believed to play remarkable roles if employed in microbial fuel cells. Improvising the functioning of these cells to give exponential yields will be the expected future of the

field. Apart from their application in bioelectricity production, wastewater treatment and biomass production, MFCs also contribute to biohydrogen production via biohydrolysis [88], bioremediation [89], biosensors [87], in-situ power source for remote areas [90].

3.3 CONCLUSION

Though MFCs have shown remarkable increase in power outputs over the past few years, they could not be considered as energy supplying ways. Optimization and identification of sufficient sturdy materials and alternatives membranes for conventional systems are still required in order to overcome the shortcomings still present. More study in order to expand the applications of MFCs beyond power generation is our utmost need.

KEYWORDS

- **Microbial fuel cells**
- **Polymer electrolyte membrane fuel cells**
- **Substrates**
- **Wastewater treatment**

REFERENCES

1. Schulze, M., Gulzow, E. (2004). Degradation of nickel anodes in alkaline fuel cells. *J. Pow. Sources. 127,* 252–263.
2. Wagner, N., Schulze, M., Gulzow, E. (2004). Long term investigation of silver cathodes for alkaline fuel cells. *J Pow. Sourc. 127,* 264–272.
3. Barbir, F. (1997). Fuel Cell Tutorial, Presented at Future Car Challenge Workshop, Dearborn, MI, October, 25–26.
4. Hacquard, A. Thesis submitted to the faculty of Worcester Polytechnic Inst, 2005.
5. Georgi, L., Leccese, F. (2013). *The open fuel cells jour*. *6,* 1–20.
6. He, Z., Angenent, L. T. (2006). Application of bacterial biocathodes in microbial fuel cells. *Electroanalysis*. *18,* 19 – 20, 2009 – 2015.
7. Piccolino, M. (1998). Animal electricity and the birth of electrophysiology: the legacy of Luigi Galvani. *Brain. Res. Bull. 46,* 381.
8. Cohen, B. The bacterial culture as an electrical half cell. *J.Bacteriol.*1981, *21*, 18.

9. Bennetto, H., Stirling, J. L., Tanaka, K., Vaga, C. A. (1983).Anodic reactions in microbial fuel cells. *Biotechnol. Bioeng. 25*, 559- 568.
10. Bennetto, H. P., Delaney, G. M., Mason, J. P., Roller, S. D., Stirling, J. L., Thurston, C. F. (1985). Electron-transfer coupling in microbial fuel cell. *Biotechnol. Lett. 7*, 699.
11. Roller, S. D., Bennetto, H. P., Delaney, G. M., Mason, J. R., Stirling, J. L., Thurston, C. F. (1984). Electron-transfer coupling in microbial fuel cells to performance of fuel cells containing selected microorganism—mediator—substrate combinations. *J.Chem. Tech. Biotechnol*. *34* B, 3.
12. www.fuelcelltoday.com
13. Gouveia, L., Neves, C., Sebastião, D., Nobre, B. P., Matos, C. T. (2014). Effect of light on the production of bioelectricity and added value microalgae biomass in a photosynthetic alga microbial fuel cell. *Biores. Tech*. *154*, 171–177.
14. He, H., Zhou, M., Yang, J., Hu Y., Zhao, Y. (2014). Simultaneous wastewater treatment, electricity generation and biomass production by an immobilized photosynthetic algal microbial fuel cell. *Biopro. Biosyst. Eng*. *37(5)*, 873- 880.
15. Jadhav, D. A., Ghadge, A. N., Mondal, D., Ghangrekar, M. M. (2014). Comparison of oxygen and hypochlorite as cathodic electron acceptor in microbial fuel cells. *Biosourc. Technol. 154,* 330–335.
16. Rhoads, A., Beyenal, H., Lewandowski, Z. (2005). A microbial fuel cell using anaerobic respiration as an anodic reaction and biomineralized manganese as a cathodic reactant. *Environ. Sci.Technol*. *39,* 4666–4671.
17. Lovley, D. R. (1991). Dissimilatory Fe (III) and Mn (IV) reduction. *Microbiol. Rev*. *55,* 259−287.
18. Nemati, M., Harrison, S. T. L., Hansford, G. S., Webb, C. (1998). Biological oxidation of ferrous sulfate by Thiobacillus ferrooxidans: a review on the kinetic aspects. *Biochem. Eng. J. 1,* 171.
19. Berk, R. S., Canfield, J. H. (1964). Bioelectrochemical energy conversion. *Appl. Microbiol. 12,* 10.
20. Gregory, K. B., Bond, D. R., Lovley, D. R. (2004). Graphite electrodes as donors for anaerobic respiration. *Environ. Microbiol*. *6,* 596–604.
21. Goldner, B. H., Otto, L. A., Canfield, J. H. (1963). Applications of bacteriological processes to the generation of electrical power. *Dev. Ind. Microbiol. 4,* 70.
22. Liu, H., Song, C., Zhang, L., Zhang, J., Wang, H., Wilkinson, D. (2006). A review of anode catalysis in the direct methanol fuel cell. *J. Pow. Sourc*. *155,* 95–110.
23. Tender, L. M., Reimers, C. E., Stecher, H. A., Holmes, D. E., Bond, D. R., Lowy, D. A., Pilobello, K., Fertig, S. J., Lovley, D. R. (2002). Harnessing microbially generated power on the seafloor. *Nat. Biotechnol. 20*, 8, 821–825.
24. Lewis, K. (1966). Symposium on bioelectrochemistry of microorganisms. IV. Biochemical fuel cells. *Bacteriol.Rev. 30,* 101–113.
25. Kreuer, K. D. Fuel cells: Selected entries from the encyclopedia of sustainability science and technology, 2013.
26. Miao, F., Tao, B., Haochu, J. (2013). Nonenzymatic alkaline direct glucose fuel cell with a solon Microchanel plate supported electrocatalytic electrode, *J. Fuel cell Sci. Technol*. *10,* 4, 041003.

27. EG & G Services Inc. Fuel Cell Handbook, 5th ed., UD Department of Energy office of fossil energy national energy technology laboratory Inc, : Morgantown, West Virginia, USA, 2000.
28. Reimers, C. E., Girguis, P., Stecher III, H. A., Tender, L. M., Ryckelynck, N., Whaling, P. (2006). Microbial fuel cell energy from an ocean cold seep. *Geobiol. 4,* 123–136.
29. Barbir, F. PEM fuel cells: Theory and practice, Elsevier academic press, New York, 2005.
30. Yuyan, S., Yin, G., Wang, Z., Gao, Y. (2007). Proton exchange membrane fuel cell from low temperature to high temperature: Material challenges. *J. Pow. Sourc. 167,* 235- 242.
31. Neburchilov, V., Martin, J., Wang, H., Zhang, J. (2007). A review of polymer electrolyte membranes for direct methanol fuel cells. *J. Pow. Sourc. 169,* 221–238.
32. Mathias, M. F., Makharia, R., Gasteiger, H.A, ; Conley, J. J., Fuller, T. J., Gittleman, S. S., Kocha, S. S., Miller, D. P., Mittelsteadt, C. K., Xie, T., Yan, S. G., Yu, P. T. (2005). Two fuel cell cars in every garage? *Inter. 14,* 24.
33. Gasteiger, H. A., Mathias, M. F., Murthy, M., Fuller, T. F., Van, Z. (2002). Proceedings of the Third International Symposium on Proton Conducting Membrane Fuel Cells, 1.
34. Voss, H. H., Wilkinson, D. P., Pickup, P. G., Johnson, M. C., Basura, V. (1995). Low cost electrodes for proton exchange membrane fuel cells. *Electrochem. Act. 40,* 321.
35. Zawondzinski, T. A., Springer, T. A., Uribe, F., Gottesfeld, S. (1993). Characterization of polymer electrolytes for fuel cell applications. *Sol. Stat. Ton. 60,* 199–211.
36. Ge, S., Li, X., Hsing, I. (2005). Internally humidified polymer electrolyte fuel cells using water absorbing sponge. *Electrochem. Act. 50,* 1909–1916.
37. Vishnyakov, V. M. (2006). Proton exchange membrane fuel cells. *Vacc. 80,* 1053–1065.
38. Arico, A. S., Baglio, V., Antonucci, V. Electrocatalysis of Direct methanol fuel cells. Edited by Hausan Liu and Jiugisn Zhang. 2009.
39. McGrath, M. K., Prakash, S., Olah, A. G. (2004). Direct methanol fuel cells. *J. Ind. Eng. Chem. 10,* 1063–1080.
40. Thomas, C. S., Ren, Z., Gottesfeld, S., Zelenay, P. (2002). Direct methanol fuel cells: Progress in cell performance and cathode research. *Electrochem. Act. 47,* 3741–3748.
41. Staiti, P., Arico, A. S., Baglio, V., Lufrano, F., Passalacqua, E., Antonucci, V. (2001). Hybrid Nafion – silica membranes doped with heteropolyacids for application in direct methanol fuel cells. *Sol. Stat. Ion. 145 Z,* 101–107.
42. Larmine, J., Dicks, A. Fuel cell systems explained, 2nd edition; 2003.
43. Sotouchi, H., Hagiwara, A. Energy carriers and conversion systems – Vol II: Phophoric acid fuel cells – 1998.
44. Holcomb, F. H., Binder, M. J., Taylor, W. R., Torrey, J. M., Westerman, J. F. Phophoric acid fuel cells. Construction Engineers Research Laboratory Publications. 2000.
45. Bjerrum, N. J., Idhusvej, R. Z., Gang, X., Gade, S. H., Hans, A., Ijuler, I., Dronningvie., Olsen, C., Plantageve., Berg, W. R., Frenderupvej. (1992). Text book of Phosphoric acid fuel cells. 903.
46. Takeuchi, M., Katsuta., Okada, H., Tobita, H., Kitaibaraki, Okabe, S., Matsuda, S., Ibaraki., Tonami, M., Tamura, K., Nakajima, F. (1982). Molten carbonate fuel cell. 362.

47. Takizawa, N. H., Text book of fuel cells. 1998. 431.
48. Subramanian, N., Haran, B. S., Ganesan, P., White, R. E., Popov, B. N. (2003). Analysis of Molten Carbonate Fuel Cell Performance Using a Three-Phase Homogeneous Model. *J. Elec.Chem. Soc. 150,* 1, A 46–A56.
49. Zuo, C., Liu, M., Liu, M. (2012). Solid oxide fuel cells. *Sprin.* 978-1-4614-1957-0, 2.
50. Ishihara, T., Misawa, H. (1991). Solid oxide fuel cells. 671.
51. Anzai, I, ; Matsuoka, S., Uehara, J. (1995).Solid oxide fuel cell. 489.
52. Kim, S., Chae, K. J., Choi, M. J., Verstraete, W. (2008). Microbial fuel cells: recent advances, bacterial communities and application beyond electricity generation. *Environ. Eng. Res*. *13,* 2, 51–65.
53. Bond, D. R., Lovley, D. R. (2003). Electricity production by *Geobacter sulfurreducens* attached to electrodes. *Appl. Environ. Microbiol. 69,* 3, 1548–1555.
54. Chaudhuri, S. K., Lovley, D. R. (2003). Electricity generation by direct oxidation of glucose in mediatorless microbial fuel cells. *Nat. Biotechnol. 21*, 1229–1232.
55. Roller, S. D., Bennetto, H. P., Delaney, G. M., Mason, J. R., Stirling, J. L., Thurston, C. F. (1984). Electron-transfer coupling in microbial fuel-cells: Comparison of redox-mediator reduction rates and Respiratory rates of bacteria. *J. Chem. Technol. Biotechnol. B- Biotechnology. 34,* 1, 3–12.
56. Park, D. H., Zeikus, J. G. (2003). Improved fuel cell and electrode designs for producing electricity from microbial degradation. *Biotechnol. Bioeng. 81*, 3, 348–355.
57. Cheng, S., Liu, H., Logan, B. E. (2006). Power Densities Using Different Cathode Catalysts (Pt and CoTMPP) and Polymer Binders (Nafion and PTFE) in Single Chamber Microbial Fuel Cells. *Environ. Sci. Technol. 40,* 364–369.
58. Zhao, F., Hamisch, F., Schroer, U., Scholz, F., Bogdanoff, P., Hermann, I. (2006). Challenges and constraints of using oxygen cathodes in microbial fuel cells. *Environ. Sci. Technol. 40,* 5193.
59. Liu, H., Logan, B. E. (2004).Electricity generation using an air-cathode single chamber microbial fuel cell in the presence and absence of a proton exchange membrane. *Environ. Sci. technol. 38,* 4040–4046.
60. Liu, H. (2004). Production of electricity during wastewater treatment using a single chamber microbial fuel cell. *Environ. Sci. technol*. *38,* 2281–2285.
61. Rabaey, K. (2003). A microbial fuel cell capable of converting glucose to electricity at high rate and efficiency. *Biotechnol. Lett*, *25,* 1531–1535.
62. Rabaey, K. (2004). Biofuel cells select for microbial consortia that self mediate electron transfer. *Appl. Environ. Microbial*. *70,* 5373–5382.
63. Schroder, A. (2003). Generation of microbial fuel cells with current outputs boosted by more than one order of magnitude. *Angew. Chem. Int. Ed. Engl*. *42,* 2880–2883.
64. Strik, D. P. B. T. B., Hamelers, H. R. M., Snel, J. F. H., Buisman, C. J. N. (2008). Green electricity production with living plants and bacteria in a fuel cell. *Int. J. Ener. Res. 32,* 870–876.
65. Liu, H., Grot, S., Logan, B. E. (2005). Electrochemically Assisted Microbial Production of Hydrogen from Acetate. *Environ. Sci. Technol. 39,* 4317–4320.
66. Holmes, D. E., Bond, D. R., O'Neill, R. A., Reimers, C. E., Tenderad, L. R., Lovley, D. R. (2004). Microbial communities associated with electrodes harvesting electricity from a variety of aquatic sediments. *Microb.Ecol. 48*, 178–190.

67. Hasvold, O., Henribsen, H., Melvaer, E., Citi, G., Johansen, B. O., Kjonigsen, T., Galetti, R. (1997). Behavior of metal ions in microbial fuel cells. *J. Power. Sourc. 65,* 253.
68. Kim, B. H. (2004). Enrichment of microbial community generating electricity using a fuel cell type electrochemical cell. *Appl. Microbiol. Biotechnol. 63,* 672–681.
69. Lee, J. Y. (2003). Use of acetate for enrichment of electrochemically active microorganisms and their 16 s r DNA analyzes. *FEMS Microbiol. Lett. 223,* 185–191.
70. Rabaey, K., Lissens, G., Verstraete, W. Microbial fuel cells: Performances and perspectives. Text book of Microbial fuel cells.
71. Rabaey, K., Verstraete, W. (2005). Microbial fuel cells: novel biotechnology for energy generation. *Trend. In Biotechnol. 23,* 6.
72. Kim, J. R. Evaluation procedures to acclimate a microbial fuel cell for electricity production. *Appl. Microbiol. Biotechnol.* 2014.
73. Logan, B. E. (2004). Extraction of hydrogen electricity from renewable resources. *Environ. Sci. Technol.* 160A–167A.
74. Liu, H., Chang, S., Logan, B. E. Production of electricity from acetate or butyrate using a single chamber microbial fuel cell. *Environ. Sci.Technol.* (2005). *39,* 658–662.
75. Logan, B. E., Grot, S. A Bioelectrochemically Assisted Microbial Reactor (BEAMR) that Generates Hydrogen Gas.U. S. Patent Application 60/588,022, 2005.
76. Rozendal, R. A., Buisman, C. J. N. Bio-Electrochemical Process for Producing Hydrogen. International Patent WO-2005–005981, 2005.
77. Rozendal, R. A. Principle and Perspectives of Hydrogen Production through Biocatalyzed Electrolysis. *Int. J. Hydrogen Energy* (2006). in press, doi 10.1016/ hydene.2005.12.006.
78. Du, Z., Li, H., Gu, T. (2007). A state-of-the-art review on microbial fuel cells; a promizing technology for wastewater treatment and bioenergy. *Biotechnol. Adv. 25,* 5, 464–482.
79. Dong, H., Yu, H., Wang, X., Zhou, Q., Feng, J. (2012). Novel structure of scalable air cathode without Nafion and platinum by rolling activated carbon and PTFE as catalyst layer in MFCs. *Wat. Res. 46,* 17, 57777–57787.
80. Logan, B. E., Cheng, S., Watson, V., Estadt, G. (2007). Graphite fiber bush anodes for increased power production in air-cathode microbial fuel cells. *Environ. Sci. Technol. 41*, 9, 3341–3346.
81. Zhang, F., Cheng, S., Pant, D., Bogaert, G. V., Logan, C. E. (2009). Power generation using an activated carbon and metal mesh cathode in a MFC. *Electrochem. Commun. 11,* 2177–2179.
82. Zhang, F., Ahn, Y., Logan, B. E. (2014). Treating refinery wastewaters in microbial fuel cells using separator electrode assembly or spaced electrode configurations. *Biores. Technol. 152,* 46–52.
83. www.engr.psu.edu/ce/ENVE/logan.htm
84. Reimers, C. E. (2001). Harvesting Energy from the Marine Sediment–Water Interface. *Environ. Sci. Technol. 35,* 192–195.
85. Shantaram, A. (2005). Wireless Sensors Powered by Microbial Fuel Cells. *Environ. Sci. Technol. 39,* 5037–5042

86. Gregory, K. B., Lovley, D. R. (2005). Remediation and Recovery of Uranium from Contaminated Subsurface Environments with Electrodes. *Environ. Sci. Technol. 39,* 8943–8947.
87. Chang, I. S., Jang, J. K., Gil, G. C., Kim, M., Kim, H. J., Cho, B. W., Kim, B. H. (2004). Continuous determination of biochemical oxygen demand using microbial fuel cell type biosensor. *Biosens. Bioelectron. 19,* 6, 607–613.
88. Rozendal, R. A., Hamelers, H. V. M., Molenkmp, R. J., Buisman, J. N. (2007). Performance of single chamber biocatalyzed electrolysis with different types of ion exchange membranes, *Water Res. 41,* 9, 1984–1994.
89. Lovley, D. R. (2006). Microbial fuel cells: novel microbial physiologies and engineering approaches. *Curr. Opin. Biotechnol. 17,* 3, 327–332.
90. Logan, B. E., Regan, J. M. (2006). Microbial challenges and applications. *Environ. Sci. Technol. 40,* 17, 5172–5180.

CHAPTER 4

CHALLENGES TO AND OPPORTUNITIES IN MICROBIAL FUEL CELLS

J. JAYAPRIYA,[1] and V. RAMAMURTHY[2]

[1]*Department of Chemical Engineering, A.C. Tech, Anna University, Chennai – 600025, India*

[2]*Department of Biotechnology, PSG College of Technology, Coimbatore – 641004, India*

CONTENTS

4.1 Types of Microbial Fuel Cells 89
4.2 Performance of Microbial Fuel Cells 89
4.2.1 Ideal Performance 89
4.2.2 Factors That Decrease Cell Voltage 91
4.2.3 Technical Challenges 92
4.2.4 Electrodes 97
4.2.5 Anodic Material 98
4.2.6 Carbon Electrodes 98
4.2.7 Carbon Nanotubes and Conductive Polymers 100
4.2.8 Metals 101
4.2.9 Chemically Modified Carbon Electrodes (CMCEs) 103
4.2.10 Sintering and Soaking 104
4.2.11 Chemical Vapor Deposition (CVD) 105
4.2.12 Applications 111

4.3 Outlook 115
Keywords 116
References 116

ABSTRACT

A chemical fuel cell is an electrochemical device that produces electrical energy from any fuel such as hydrogen, methane, propane, methanol, etc., using oxygen or an oxidizing agent. Microbial fuel cell (MFC) is one type of fuel cell, where the conversion of the chemical energy from the fuel to electrical energy is achieved by the catalytic action of microorganisms. A typical MFC is shown schematically in Fig. 4.1. It consists of anodic and cathodic compartments separated by a proton exchange membrane (PEM). Bacteria in the anodic chamber oxidize organic matter and transfer electrons to the cathode through an external circuit producing current. Protons diffuse through the solution across the PEM to the cathode where they combine with oxygen and electrons to form water. Unlike chemical fuel cells, MFCs operate under ambient operational temperature and pressure, also at neutral pH.

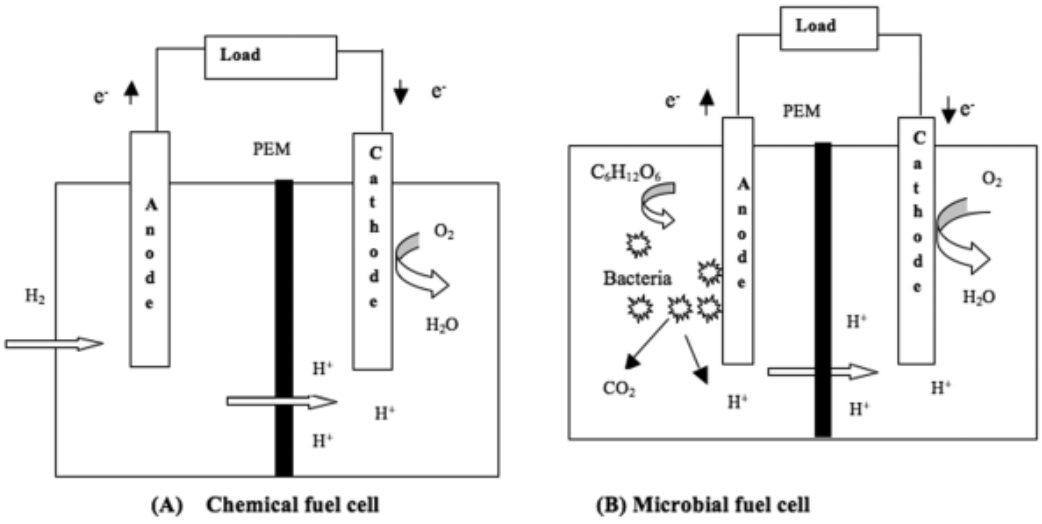

FIGURE 4.1 Schematic representations of fuel cells. (A) Chemical fuel cell (B) Microbial fuel cell.

4.1 TYPES OF MICROBIAL FUEL CELLS

MFCs can be characterized as two classes depending on how electrons are transferred from the microorganisms to the electrode (anode): mediator-employing MFCs, where electron shutters or mediators are made available in the system, and mediator-less MFCs, where no extraneous mediators are deemed necessary. Typically exogenous mediators used for enhancing the electron-transfer rate in MFC are synthetic dyes such as neutral red [1], 2-hydroxy-1,4-naphthoquinone [2], methylene blue [3], and metal organics such as Fe (III) EDTA [4].

On the other hand in mediator-less MFC, the microorganisms typically make use of electrochemically active membrane-associated cytochromes, conductive pili or secrete redox-mediating molecules that facilitate electron transfer. Many such microorganisms are capable participants in the process, some of which include metal reducing bacteria *Geobacter metallireducens* [5], *Rhodoferax ferrireducens* [6], *Shewanella putrefaciens* [7] and *Aeromonas hydrophila* [8]. Secreted soluble redox shuttles by a microbial community consisting primarily of three bacteria, *Alcaligenes fecalis, Enterococcus faecium* and *Pseudomonas aeruginosa* leads to electricity generation [9].

4.2 PERFORMANCE OF MICROBIAL FUEL CELLS

4.2.1 IDEAL PERFORMANCE

Electricity is generated in an MFC only if the overall reaction is thermodynamically favorable. The maximum amount of electrical energy (or work done) that can be delivered by an electrochemical cell depends on the change in Gibbs free energy. It can be calculated as

$$\Delta G = \Delta G^\circ + RT \ln (\gamma) \quad (1)$$

where ΔG (J) is the Gibbs free energy for the specific conditions, ΔG° (J) is the Gibbs free energy under standard conditions usually defined as 298 K, 1 bar and 1 M, R (8.314 J mol^{-1} K^{-1}) is the universal gas constant, T (K) is the absolute temperature and γ (unit less) is the reaction quotient

calculated as the activities of the products divided by those of the reactants. For MFC calculations, it is more convenient to evaluate the reaction in terms of the overall cell electromotive force (emf) cell [10–12]. E_{emf} (V), defined as the potential difference between the cathode and anode. This is related to the work, (J), produced as

$$\text{Work} = E_{emf} Q = -\Delta G \tag{2}$$

where Q=nF is the charge transferred in the reaction, expressed in Coulomb (C), which is determined by the number of electrons exchanged in the reaction, n is the number of electrons transferred per mol, and F is Faraday's constant (96,481 C mol^{-1}). Hence, the cell emf can be calculated as,

$$E_{emf} = -\Delta G/nF \tag{3}$$

Thus the overall reaction is

$$E_{emf} = E^{\circ}_{emf -} RT/nF \ln(\gamma) \tag{4}$$

where E°_{emf} (V) is the cell electromotive force at standard conditions, as defined earlier. The cell emf is a thermodynamic value that does not take into account internal losses. In practice, under open circuit conditions the measured voltage (open circuit voltage) should in principle be exactly the equilibrium voltage (E_{emf}).

4.2.1.1 Actual Performance

The actual cell potential is always lower than its ideal potential because of irreversible losses. In general, the difference between the actual (measured) cell potential and the ideal potential is referred to as overvoltage [13]

$$E_{cell} = E_{emf} - \eta_{act} - \eta_{iR} - \eta_{diff} \tag{5}$$

where η_{act} (V) is the activation overpotential due to slow electrode reactions; η_{iR} (V) is the overpotential due to ohmic resistances in the cell and

η_{diff} (V) is the overpotential due to mass diffusion limitations. In MFCs, the measured cell voltage is a linear function of the current and it can be simply described as

$$E_{cell} = OCV - R_{Int} \quad (6)$$

where R_{Int} is the sum of all internal losses of the MFC.

4.2.2 FACTORS THAT DECREASE CELL VOLTAGE

4.2.2.1 Activation Losses

Activation polarization is related to the loss of overall voltage at the expense of forcing oxidation/reduction reactions that occur during the transfer of electrons from or to a mediator reacting at the electrode surface [14]. This loss only occurs at low current densities in low temperature MFC. The extent of the activation losses can be described by the Tafel equation [15]

$$\Delta V = A \log (i/ i_0) \quad (7)$$

where ΔV is overvoltage; A (V) is the Tafel slope, i (Am^{-2}) is current density; i_0 (Am^{-2}) is exchange current density, the current density at which the overpotential is zero. Activation losses can be reduced by increasing the electrode surface area, improving electrode catalysis and enriching biofilm on the electrode (s).

4.2.2.2 Ohmic Losses

The ohmic losses (or ohmic polarization) in an MFC include both the resistance to the flow of electrons through the electrodes /interconnections and the resistance to the flow of ions through the PEM/anodic/cathodic electrolytes [14, 16]. Ohmic losses can be reduced by minimizing the electrode spacing, using a membrane with a low resistivity, increasing solution conductivity to the maximum tolerated by the bacteria.

4.2.2.3 Concentration Losses

Concentration losses occur mainly at high current densities due to depletion of reduced species near the electrode (anode). This increases the ratio between the oxidized and the reduced species at the electrode surface, which can produce an increase in the electrode potential. At the cathode side the reverse may occur, causing a drop in cathode potential due to the accumulation of product. Ultimately these effects inhibit further reaction and the cell voltage drops to zero. Mass transport limitations in the bulk fluid can limit the substrate flux to the biofilm, which is a separate type of concentration loss [13].

4.2.2.4 Fuel Crossover and Internal Currents

This type of loss is usually due to unused fuel passing through the electrolyte and stray currents due to electron conduction through the electrolyte.

4.2.2.5 Bacterial Metabolic Losses

To generate metabolic energy, bacteria transport electrons from a substrate at a low potential through the electron transport chain to the final electron acceptor (such as, oxygen or nitrate) at a higher potential. In an MFC, the anode is the final electron acceptor and its potential determines the energy gain for the bacteria [13]. The higher the difference between the redox potential of the substrate and the anode potential, the higher the possible metabolic energy gain for the bacteria, but the lower the maximum attainable MFC voltage. To maximize the MFC voltage, therefore, the potential of the anode should be kept as low (negative) as possible. However, if the anode potential becomes too low, electron transport will be inhibited and fermentation of the substrate (if possible) may provide greater energy for the microorganisms.

4.2.3 TECHNICAL CHALLENGES

MFCs are operated under a range of conditions that include differences in system configuration, substrates, microorganism, anode/cathode materials,

electrode surface area, mediators, cation exchange membrane, pH and operating conditions. Recent progress in understanding of system architecture, membranes and anode/cathode materials for MFCs has been reviewed, highlighting the characteristics, modifications, and processing of the electrode materials for MFCs. How bacteria use the soluble synthetic redox mediators and to what extent they generated the power output in MFCs has also been reviewed. It is generally accepted that MFCs show great promise as a sustainable biotechnological solution to future energy needs. However, it is yet to be commercially exploited since there are many hurdles to be overcome.

4.2.3.1 MFC Reactor Configurations

The basic MFC design comprises of anodic and cathodic compartments separated by a selective partition, such as, PEM (Fig. 4.2a). H-shaped MFC is widely used and are generally used to examine power generation with different electrode materials, membranes, type of microbial consortia with different substrates [13]. High internal resistance that reduces the power produced in this design is mainly due to the large electrode spacing and small membrane area. In order to reduce the internal resistance, cubic MFC with a larger membrane area and less electrode spacing could be used (Fig. 4.2b). So far, these designs were operated in batch mode, while

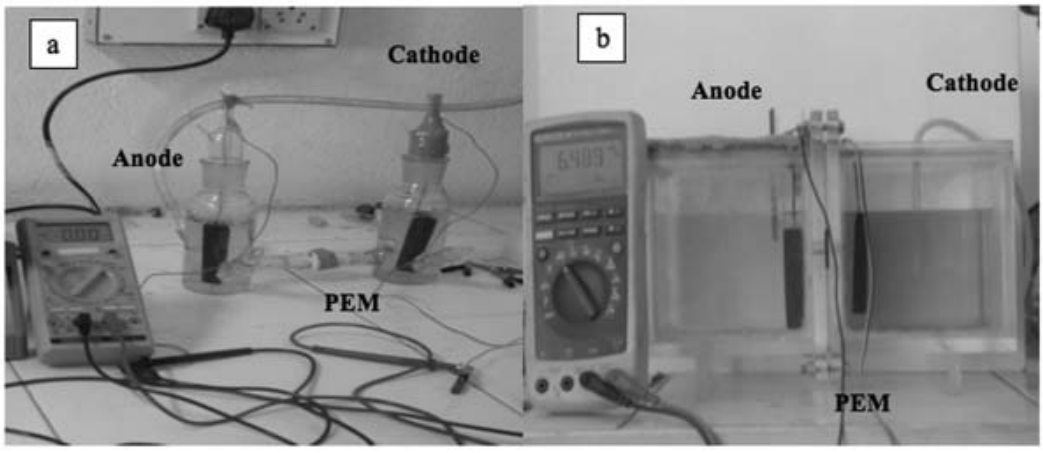

FIGURE 4.2 H shaped MFC (A) and Cube Shaped MFC (B) designed by Jayapriya and Ramamurthy [24].

the treatment of wastewater required a flow-through mode. Liu et al. [17] designed a single chamber MFC as shown in Fig.4.3a containing eight graphite electrodes (anodes) and a single air cathode which generated a maximum power density of 0.026 $W.m^{-2}$ while removing up to 80% of the COD of the wastewater. No aeration was required for cathode chamber in this system that made it cost effective when compared to H-shaped MFC. Another single chambered MFC prototype comprising a flat plate was designed by Min et al. [18] consisting of a single channel formed between two nonconductive plates that were separated into two halves by the electrode/PEM assembly, which produced a maximum power density 2.8 times higher than reported earlier.

In general, MFCs are typically designed as anode and cathode system separated by PEM. It is known that PEMs are quite expensive that limit the *applicability* of *MFC*. Liu and Logan [19] designed the MFC using carbon paper as anode and the cathode was carbon cloth bonded with PEM or rigid carbon paper without PEM (Fig. 4.3b) having a Coulombic efficiency of 28% and 20% with and without the PEM, respectively. This may be due to about 30-fold higher rate of diffusion of oxygen in MFC without PEM compared to that with PEM. However, the consequence of high oxygen flux in MFC without PEM is the loss of substrate due to the aerobic oxidation by bacteria in the anolyte. In another design up-flow mode without PEM (Fig. 4.3c) was employed by Jang et al. [20]. Despite of the relatively low Coulombic efficiencies in MFC design that lacks PEM, it could still be low a cost alternative for wastewater treatment. Using a rotating cathode **(**Fig. 4.3d**)** in river sediment MFC [21], the solubility of oxygen increased in the catholyte from 0.4 to 1.6 mg/L, leading to a higher power production (0.049 W/m^2) when compared to a non-rotating cathode (0.029 W/m^2).

So far, the voltage produced by a single MFC is not more than 0.5 V. The voltage can be enhanced by connecting the several MFC in series/parallel [22, 23]. Aelterman et al. [22] operated the stacked MFC in different modes and it was observed that MFC in parallel showed good performance. When multiple cells were stacked together, however, charge reversal could result in the reverse polarity of one or more cells and a loss of power generation [23]. The availability of low cost components needs to be increased to *make* it attractive for scale up.

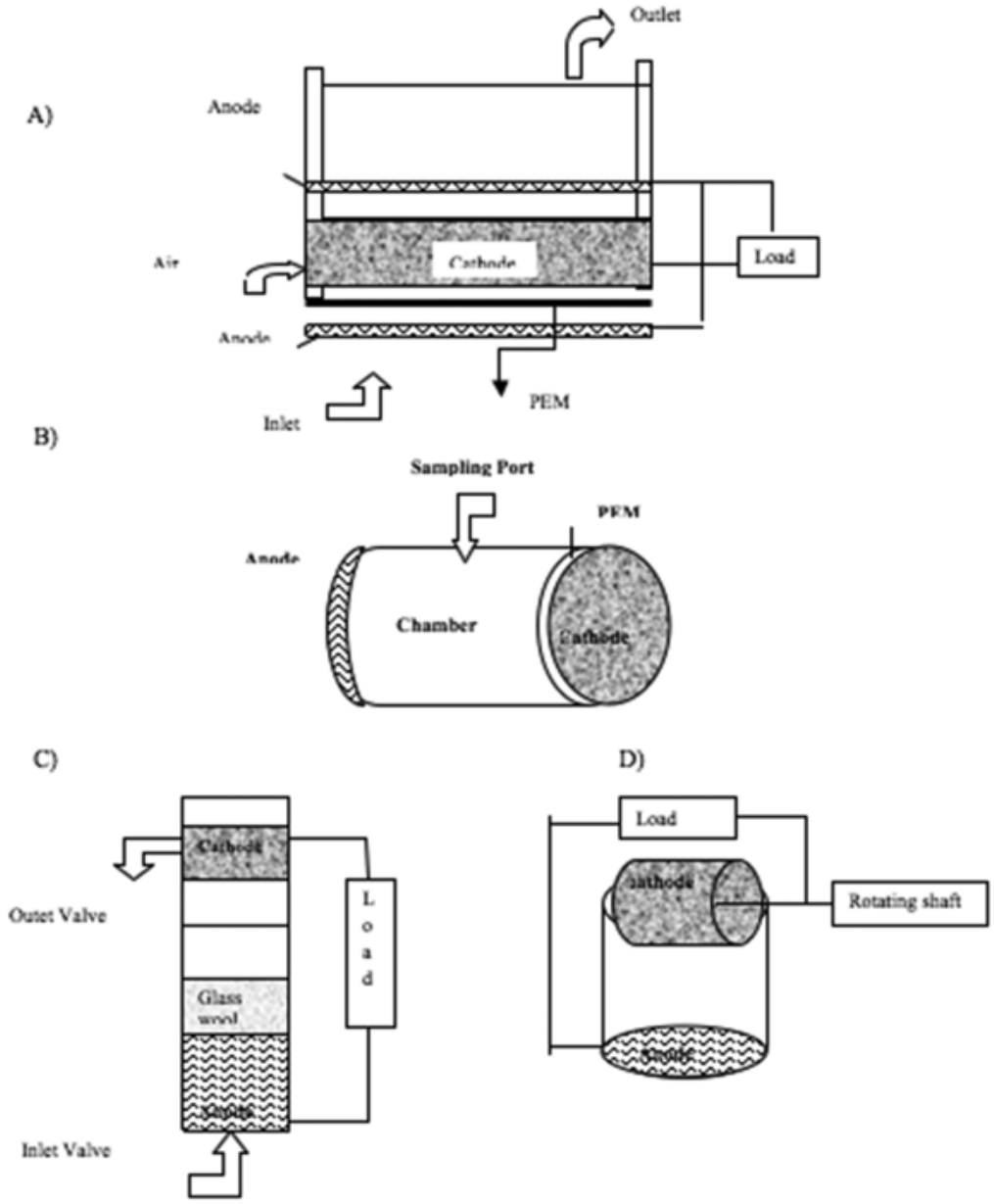

FIGURE 4.3 Schematics of different MFC designs: (a) and (b) Single chambered MFC; (c) Upflow mode MFC; (d) Rotating cathode MFC (Adapted from Liu et al. [17], Liu and Logan [19], Jang et al. [20] and He et al. [21], respectively).

4.2.3.2 Membranes

Microbial fuel cells make use of proton exchange membranes as the separating module between anode and the cathode compartments. The separator

should be able to inhibit the transfer of substrates and oxygen, but allow the protons travel efficiently. Membranes used in MFCs include fluoropolymer-containing cation exchange materials such as Nafion [5, 25, 26], polystyrene and di-vinyl benzene with sulfonic acid groups [7] and dialysis membranes: 2000–14,000 Daltons [27]. The most commonly used membrane in MFC is Nafion, a *perfluorosulfonic acid polymer* developed by DuPont because of its highly selective permeability of protons and high ionic conductivity (10^{-2} S cm^{-1}). It consists of three regions (Fig. 4.4): (i) the Teflon-like, fluorocarbon backbone, (hundreds of repeating $–CF_2–CF–CF_2–$ units in length), (ii) the side chains, $–O–CF_2–CF–O–CF_2–CF_2–$, which connect the molecular backbone to the third region, (iii) the ion clusters consisting of sulfonic acid ions, SO_3^- H^+. The negative ion, SO_3^- is permanently attached to the side chain. However, when the membrane becomes hydrated by absorbing water, the hydrogen ion becomes mobile. Ion movement occurs by protons, bonded to water molecules, hopping from one SO_3^- site to another within the membrane. Thus, solid hydrated electrolyte is an excellent conductor of hydrogen ions. In general, proton conductivity increases as the hydration level of the polymer increases, with H_2O:SO_3 ~ 15:1 being optimum [28]. However, the use of Nafion membrane may not be feasible for *large-scale* commercialization of MFC for waste water treatment due to its high cost and oxygen permeability (9.3×10^{-12} mol cm^{-1} s^{-1} [29].

Cation exchange membranes and anion exchange membranes are less expensive separators in MFC [30]. However, the transport of cation species other than protons (particularly of alkali and alkaline earth metals) through the CEM, causes a pH increase in the cathode chamber [26, 31].

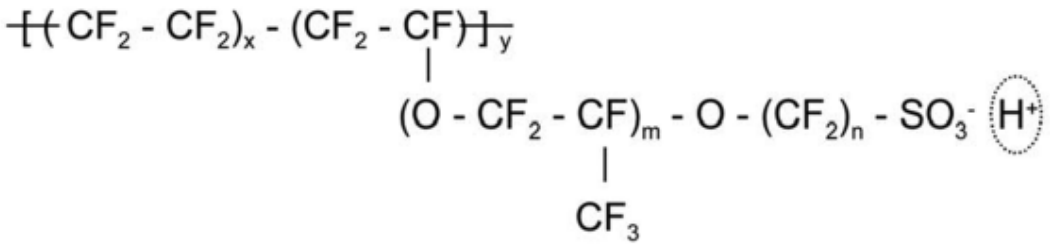

Nafion: m = 1-3, n = 2, x = 5-13, y = 1000-1200
Others: m = 0, n = 1-5, x = 1-14, y = 800-1200

FIGURE 4.4 Proton membrane structure.

This pH increase negatively affects the MFC performance. Rozendal et al. [31] observed that for every increase in 3 pH units, a potential loss of 0.18 V occurs in the cathode.

A possible solution to the pH gradient associated potential losses is the application of an anion exchange membrane (AEM) instead of a CEM. In the case of an AEM, hydrogen at the cathode is not produced from the proton reduction, but from the reduction of water that diffuses through the membrane ($2H_2O + 2e^- \rightarrow 2OH^- + H_2$). The protons in the anode chamber are consumed by these hydroxyl ions transferred from anode to cathode and thus maintain *electroneutrality in the system*. However, the pH does increase more in the cathode chamber than with Nafion. In principle, only membranes that are truly 100% proton selective can prevent pH effects in MFC performance. But these types of membranes are not available at low costs.

Ultra filtration (UF) membranes, especially those developed for wastewater applications, may be suitable for use in MFCs. In this line of thought, Kim et al. [30] tested the UF with different molecular weight cut-off in MFC and found that these membranes had high internal resistances and thus produced low power output (5 ± 1 mW/m^2) when compared with CEM/AEM (35 ± 3 mW/m^2). On the other hand, membrane fouling always occurs in MFC, as biofilm with extracellular polymers can be formed on PEM during its long-term operation [32]. This would lead to deterioration in the MFC performance [33]. Therefore*, further research is required to develop* antifouling PEM with high proton diffusion coefficients at low costs.

4.2.4 ELECTRODES

Electron transfer in microbial fuel cells depends on the conductivity of the material, its surface characteristics and compatibility of its redox potential with the microbial metabolism. Among all *MFC* components, the *electrode* materials play a crucial *role* in electricity generation since the electrode cost will be a key factor deciding the implementation of the MFC technology at a large scale. The type of anode/cathode material used, desirable properties of anode/cathode, electrode performance, modification of electrode materials and costs are discussed in this section.

4.2.5 ANODIC MATERIAL

Anodic material must be a conductive surface whose redox behavior must be suited to microbial metabolism, conducive to biofilm formation, having high porosity with enhanced active surface area and non-corrosive. Various materials ranging from noncorrosive stainless steel to versatile carbons have been explored as anodes in various forms and shapes [13]. Some of the forms of carbon evaluated are carbon paper, cloth, foams, wires, reticulated vitreous carbon (RVC), graphite plate, thick graphite rod, foams, sheets, felt, graphite granules, fibers and brushes, conductive polymers, etc.

4.2.6 CARBON ELECTRODES

Carbon electrodes have some specific advantages, including a wide potential window, low residual current, long-term stability, excellent biocompatibility, high electrical conductivity, relatively high chemical stability, high corrosion resistance, low density, low thermal expansion and low cost [34, 35]. Homogeneous forms such as glassy carbon, graphite, vitreous carbon, screen printed, fullerenes, carbon nanotubes, carbon brushes and carbon fiber, etc., or heterogeneous forms like carbon paste electrodes, carbon fiber reinforced sheets, etc., have been evaluated as electrodes [36]. The vast range of carbon materials, both natural and synthetic, that have more disordered structures have traditionally been considered as variants of one or the other of the allotropic forms, such as graphite or diamond [36]. Thus, carbon materials differ in their physicochemical properties, electrochemical behavior and structural characteristics, and by deliberate modification of the surface or bulk matrix of the material it is possible to alter its electrochemical which would be suitable for MFC applications.

Carbon cloth is a woven material consisting of extremely thin fibers composed mainly of carbon atoms with great porosity, while carbon paper is nonwoven impregnation with a binder. Cheng and Logan [37] designed a single-chamber MFC that used carbon cloth as the electrode and domestic wastewater as the anolyte that produced a maximum power

density of 1.640 Wm^{-2}. Wang et al. [38] built a single-chamber cell that produced a maximum power density of 0.483 Wm^{-2} when carbon cloth was the electrode and brewery wastewater was employed as the carbon source. The carbon cloth is currently too expensive (approximately \$1,000 m^{-2}) to be used in large scale. Carbon paper is commonly available in plain and wet-proofed versions. It has high conductivity, but lacks durability and is fragile. Min and Logan [18] designed a flat plate MFC with carbon paper as an anode, achieving a maximum power density of 0.309 Wm^{-2} when using acetate as the substrate. In the dual chamber MFC constructed using carbon paper electrodes the power density reported by Kim et al. [30] was 0.040 Wm^{-2}. Carbon mesh is a possible alternative material for an MFC anode. It has a more open structure than carbon cloth due to a more open weave, which could help to reduce the biofouling. Pretreatment of carbon mesh might be required to get adequate performance in MFC. Wang et al. [39] reported power density upto 0.922 Wm^{-2} using heated carbon mesh.

Liu et al. [17] designed a single-chamber MFC that used eight graphite rod anodes produced a maximum power of 0.026 Wm^{-2}. Reimers et al. [40] used graphite rod as an anode and reported a maximum power density of 0.034 Wm^{-2}. Mohan et al. [41] reported a maximum power yield of 0.635 W/kg COD when a graphite sheet was used. However, the utility of the graphite rods and sheets were limited due to their low porosity and low surface area for biofilm formation. Graphite sheets are not porous and thus they produced less power per geometric (projected) surface area when compared with felts or foams. Chaudhuri and Lovley [6] found that the power output was three times larger when the graphite rod was replaced by graphite felt, indicating that increasing the surface area was beneficial to the performance of the MFC. Low electrochemical activity of commercial graphite felt is still one of the major hindrances that limit its applications in MFC.

A graphite fiber brush is made of graphite fiber that is wound around one or more conductive corrosion-resistant metal wires such as titanium. This method is attractive for its high surface area and low electrode resistance. Logan et al. [42] designed a flat-type MFC with graphite brush as the anode and 1.2 mg cm^{-2} cobalt tetramethylphenylporphyrin (CoTMPP) carbon cloth as the cathode that produced a power density of

2.4 Wm^{-2}, which was four times that obtained when using carbon paper as the anode (0.6 mWm^{-2}). Ahn and Logan [43] designed a single chamber air-cathode MFC in a continuous mode that used a graphite brush as the anode, generating a maximum power density of 0.422 Wm^{-2}. One limitation of the brush architecture is that the minimum electrode spacing is constrained by the brush size, which can leads to a high ohmic resistance.

Graphite granules can be of variable size, but only granules with a diameter of 1.5 to 5 mm have been used in MFCs. The granules were conductive (0.5–1.0Ω/granule). The first use of these materials was reported by Rabaey et al. [44]. You et al. [45] built a tube-type air cathode MFC that used graphite granules as the anode, and a graphite rod was used to collect electrons, achieving a maximum power density of 50.2 Wm^{-3} when using glucose as the substrate.

RVC has a low density and thermal expansion, high corrosion resistance and high thermal and electrical conductivities. RVC is an open-pore foam material of honeycomb structure composed solely of vitreous carbon. The conductivity of the material is 200 S cm^{-1}. He et al. [46] reported obtaining a power density of 0.170 Wm^{-2} when using sucrose as substrate in upflow MFC and RVC electrodes was used. Ringeisen et al. [47] constructed a miniature MFC catalyzed by *Shewanella oneidensis* producing a maximum power density of 0.024 W m^{-2}. The main disadvantage of the material is that it is quite brittle and hence short lived.

4.2.7 CARBON NANOTUBES AND CONDUCTIVE POLYMERS

Carbon nanotubes (CNT) have become one of the materials with very high potential because of its large specific surface area, high mechanical strength and ductility, and excellent stability and conductivity. However, it has been reported that CNT have a cellular toxicity that could lead to proliferation inhibition and cell death [48, 49]. Thus, they are not suitable for MFC unless modified to reduce the cellular toxicity. Recently, conductive polymer/CNT composites have received significant interest because by incorporating CNT in conductive polymers a synergistic effect may be obtained. Qiao et al. [50] reported the feasi-

bility of an MFC using CNT/polyaniline composite as the anode material. Polyaniline as a conductive polymer, could not only protected the microorganisms but also improve their electro-catalytic activity [51]. Sahoo et al. [52] reported that polypyrrole (PPy)-coated carbon nanotubes had significantly higher electrical conductivity than that of carbon nanotubes alone. Among all the conducting polymers studied till date, PPy can be considered as one of the most attractive materials due to its excellent conductivity, stability and biocompatibility even in neutral pH. Yuan and Kim [53] modified the anode of the MFC with electropolymerized PPy and reported improvement in the power density of MFC greatly. Sharma et al. [54] developed MFC using an anode of carbon paper that was deposited with multiwalled CNT; to their great surprise, the power density was found to be approximately six times greater than that obtained with the graphite electrode. They have suggested that the carboxyl groups on the surface of multiwalled CNT could increase the chemical reactivity of metal nanoparticles.

There is no question that CNT can improve the performance of MFCs because they have very high surface areas (usually a few hundred to 1300 $m^2\ g^{-1}$), and the groove openings that are formed between CNT bundles and the outside surface area of CNT bundles are supposed to be accessible by large sorbate species such as bacteria, which makes the increased surface area effective for microscale bacteria which is significantly larger than that of traditional microporous adsorbent media [55, 56]. The high cost of CNT manufacture, which was reported to be $80–100/kg is one of the major factors that limit its applications [57].

4.2.8 METALS

Dumas et al. [58] attempted sediment MFC using stainless steel as the electrode, but the maximum power density obtained was only 0.004 Wm^{-2}. Richter et al. [59] developed a *Geobacter sulfurreducens* catalyzed MFC that produced a steady current of 0.4–0.7 mA when gold was used as an anode. However, Heijne et al. [60] have reported that titanium as the anode was found unsuitable.

4.2.8.1 Cathodic Material

The cathode materials also have an equally important impact on the power generating capacity of MFCs. They must have a high redox potential to accept the electrons. The commonly used cathode materials are graphite, carbon cloth and carbon paper. However, it is difficult to obtain high cathodic potentials unless metal catalysts are used. Moon et al. [61] designed an MFC that used graphite felt containing platinum (Pt) as the cathode, and its power density reached 150 mWm^{-2}, which was three times higher than that for the graphite cathode. Alternatives to these catalysts include nonprecious metal catalysts linked with organics, such as Cobalt tetra methyl phenyl porphyrin (CoTMPP) and iron (II) phthalo cyanine (FePc) [62, 63]. These transition metal catalysts have excellent performance (Table 4.1), although higher loading rates than those used for Pt are needed to achieve similar performance [64].

4.2.8.2 Modification of Electrode Materials

Chemical modification methods can be effective for immobilizing metals, metal oxides or other active compounds on carriers, such as carbon materials or conductive polymers, to enhance the performance of MFCs.

TABLE 4.1 Metal Catalysts of Cathode in MFCs, from Zhou et al. [65]

Type of Catalyst	Cathode Materials	Power density (mW/m^2)
CoTMPP	Carbon cloth	369
FePc	Carbon paper	634
FePc	Graphite foils	0.01
PbO_2	Ti sheeting	485
β-MnO_2	Carbon cloth	0.003
Co-OMS	Carbon cloth	180
MnO_x	Carbon cloth	161
Co/Fe/N/CNT	Carbon cloth	751
$Fe_2(SO_4)_3$	Graphite composites	1.67

The modification methods, include ammonia or acid treatment, sintering, soaking method, chemical vapor deposition, carburization, etc.

4.2.9 CHEMICALLY MODIFIED CARBON ELECTRODES (CMCES)

Ammonia has been reported to be suitable for treatment of many forms of carbon including carbon cloth and carbon paper, and it has been regarded as one of the most effective ways to improve electrode performance. Ammonia gas treatment on carbon cloth was reported by Cheng and Logan [37]. In a nitrogen environment containing 5% NH_3, carbon cloth was heated at 700° C for 60 min, which resulted in an increase in the power density by 48% compared to untreated carbon cloth. This was due to the improvement in the surface charge from 0.38 to 3.99 mequiv.m^{-2}. Other CMCEs were prepared by heating the carbon cloth at 200°C or graphite sheet at 400°C for 48 h for carbonyl generation at the surface, followed by immobilization of neutral red (NR) or methylene blue (MB) into the matrix using N, N0-dicyclohexylcarbodiimide by the formation of a peptide bond between amine group of the redox dye and carbonyl group of electrode [66]. The best performing MFC with the highest power density was the MB modified carbon cloth anode, which gave a power output of 0.194 ± 0.020 mW/m^2 when compared to plain carbon cloth 0.133 ± 0.179 mW/m^2 [67]. The performance of the MFCs using carbon cloth showed a lot of variation in replicate experiments indicating that the material was very heterogeneous and the process of preparation of the carbon cloth did not result in producing a consistent product with respect to this application. However, in dyes immobilized in carbon cloth, the performance was more consistent. An attempt to immobilize the dyes to the graphite sheet was not successful because the material was damaged and became unstable after heat treatment.

Acid treatment, a very simple procedure, has also been evaluated for electrode modifications: the electrode material was placed into an acid solution, followed by washing with deionized water and drying. Erable et al. [68] modified the graphite granules with nitric acid. This process increased the cell voltage from 660 to 1050 mV, which was due to the

formation of nitrogen containing superficial groups on the surface of graphite granules. Feng et al. [69] found that the combined process of the heat and acid treatment could result in improved power production to 1.370 Wm^{-2}, which was 34% greater than the untreated electrode.

4.2.10 SINTERING AND SOAKING

In this method the active components of catalysts were dispersed on the carriers or supports through impregnation. The steps followed included:

1. to increase the contact between the support and the active component precursor;
2. drying of the support impregnated with the active component precursor;
3. activation of the catalyst by a thermal (sintering) or reactive (soaking) process.

Park and Zeikus [25] incorporated Mn^{4+} into the anode by the soak method, and the maximum power density reported was 0.788 Wm^{-2}. Lowy et al. [70] studied the performance of MFCs using several kinds of modified electrodes by the sintering process or the soak method. They prepared the graphite electrodes modified with anthraquinone-1,6-disulfonic acid, 1,4-naphthoquinone, a graphite-ceramic composite containing Mn^{2+} and Ni^{2+} and a graphite paste containing Fe_3O_4 and Ni^{2+} and found that modified electrodes showed a power output 4–5 times that of the unmodified one.

Jayapriya et al. [66] reported the preparation of graphite/epoxy composite electrode (GECE) doped with different six types of metal ions (Zn^{2+}, Mg^{2+}, Mn^{2+}, Cu^{2+}, Co^{2+}, Fe^{3+}) enabling robustness through a wet impregnation procedure to facilitate electron transfer processes in biological applications (Fig. 4.5). It was observed that the Fe^{3+} doped GECE surfaces exhibited significantly high biofilm formation of 1.10 (± 0.18)×10^7 CFU/cm^2 as compared to other dopants. Fe^{3+} doped GECE had the highest redox potential (0.11 V) compared to all the other electrodes tested, allowed better biofilm growth either because they allowed formation of bacterial foci better or enhanced the growth of bacteria in the foci, or both. Their choice based on the closeness of their potential to the

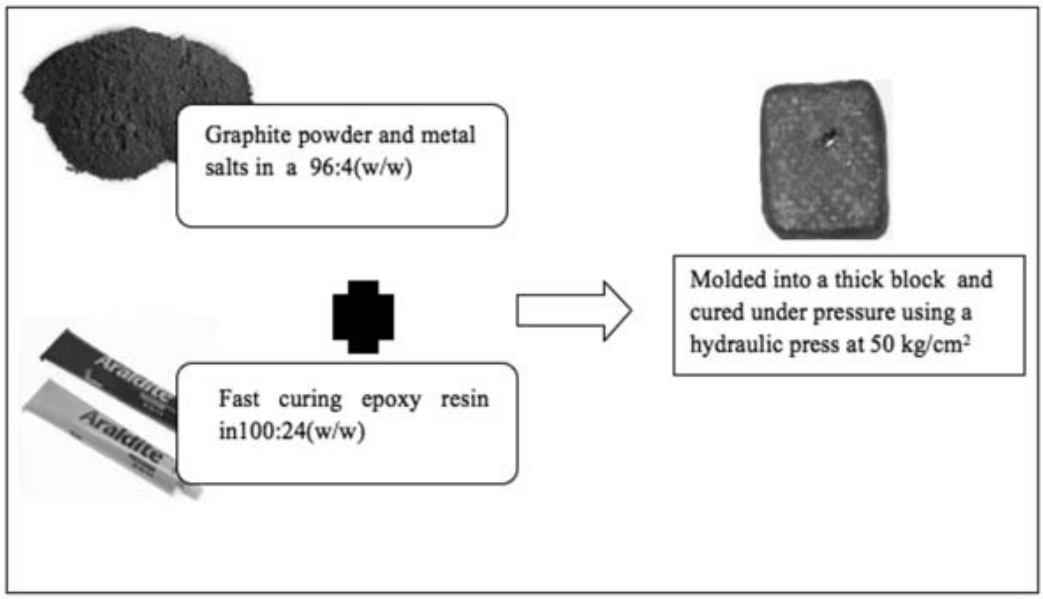

FIGURE 4.5 Preparation of Graphite epoxy composite electrodes [66].

oxidative phosphorylation chain of reactions in the bacterial membrane could have facilitated more efficient energy metabolism and thus better biofilm growth. Among the different combinations of the electrodes tested Fe^{3+} graphite cathode produced significantly higher power density (1.680 ± 0.098 mW/m^2) [67]. These studies indicate the feasibility of the improvement in electrode design on the performance of MFC for wider applications.

4.2.11 CHEMICAL VAPOR DEPOSITION (CVD)

Chemical vapor deposition is often used in the semiconductor industry to produce thin films. In a typical CVD process, the substrate is exposed to one or more volatile precursors, which react and/or decompose on the substrate surface to produce a deposit. Liu and Logan [19] coated the anode with ferric oxide by a CVD technique and observed that the power density increased noticeably from 8 to 30 mWm^{-2} because of the enrichment of metal-reducing bacteria on the anode.

4.2.11.1 Biocatalysts in Microbial Fuel Cells

A major limitation to wider application of MFCs is the relatively low electron transfer between the bacterial catalysts and the anode, leading to high internal resistance and reduced power generation. Hence, to improve MFC performance understanding the metabolic impediments, dynamics of the electrochemically active bacterial (EAB) communities in the biofilm and how the bacterial species are capable to play a part in extracellular electron transfer. Although MFCs could be operated using pure cultures[5, 6, 47, 71–74], mixed cultures are more suitable for the use of complex fuels such as wastewater [75]. MFCs that employ mixed bacterial cultures have some important advantages over MFCs driven by axenic cultures: higher resistance against process disturbances, higher substrate consumption rate, wider substrate specificity and higher power output [9]. Mostly, the electrochemically active mixed cultures are enriched either from aquatic sediments (either marine or fresh water) or activated sludge from wastewater treatment plants.

The mechanism of the electron transfer from the bacterial cell membrane or membrane organelle to anode will be addressed below.

4.2.11.2 Direct Electron Transfer

Many microorganisms possess the ability to transfer electrons derived from their metabolism to the anode without a need of redox shuttle. These microorganisms are ubiquitously present in places such as marine sediment, soil, wastewater, fresh water sediment and activated sludge [76, 77]. These microorganisms possess outer-membrane bound proteins such as multiheme proteins (c type cytochromes) or nanowires that shuttle the electron directly from the inside of the bacterial cell to solid electron acceptor.

A real breakthrough was made in MFC when some dissimilatory metal reducing bacteria (DMRB) were found to transfer the electrons directly to an anode without the need for an electron shuttle. Several isolates *Shewanella putrefaciens* [7], *Geobacter metallireducens* [5], *Rhodoferax ferrireducens* [6] have been shown to generate electricity in mediator-less

MFC systems. In terms of performance, current densities of the order of 0.2–0.6 mA and a total power density of 1–17 mWm^{-2} graphite surface have been reported for *Shewanella putrefaciens* and *Geobacter sulfurreducens* when conventional (woven) graphite electrodes was used. Chaudhuri and Lovley [6] reported a Coulombic efficiency of 83% current production from glucose by *Rhodobacter ferrireducens*. In addition to membrane bound proteins, bacterial nanowires (also known as microbial nanowires) are electrically conductive appendages produced by a number of bacteria, most notably in the genera *Geobacter* and *Shewanella*, and reported to enhance the power output in MFCs [78]. Nanowires are about 3–5 nm wide and up to tens of micrometers long that facilitate the *long-range electron transfer* across thick biofilms. Conductive nanowires have also been confirmed in the oxygenic cyanobacterium *Synechocystis* PCC6803 and a thermophilic, methanogenic coculture consisting of *Pelotomaculum thermopropionicum* and *Methanothermobacter thermoautotrophicus* [79].

Recently, Malvankar et al. [80] reported that the electrical conductivity of microbial nanowires to be around 5 $mS\ cm^{-1}$, which is comparable to those of synthetic organic metallic nanostructures that are commonly used in the electronics industry. The wires were also seen to conduct over distances of centimeters, which is thousands of times the length of a bacterium itself. These findings could influence the design of energy-capture strategies, such as conversion of biomass and wastes to methane or electricity.

4.2.11.3 Mediated Electron Transfer

More generally, for electron transfer from a microbial electron donor to an electrode to occur, an electron mediator may be required. Wilkinson [81] has summarized the attributes of effective mediators as below: (i) the oxidized mediator should easily penetrate the bacterial membrane to reach the reductive species inside the bacteria; (ii) the redox potential of the mediator should match the potential of the reductive metabolite; (iii) the reduced mediator should easily escape from the cell; (iv) both the oxidized and reduced states of the mediator should be chemically stable in the

electrolyte solution, should be easily soluble, and should not adsorb on the bacterial cells or electrode surface.

The mediators can be coupled to the MFC in two possible ways.

1. Exogenous Mediators: Many investigators [82–84] have reported that the metabolic reducing power produced by *Proteus vulgaris* or *Escherichia coli* can be converted to electricity by using electron mediators, such as thionin or 2-hydroxy-1,4-naphthoquinone (HNQ). Tanaka et al. [85] reported that light energy can be converted to electricity by *Anabaena variabilis* when HNQ was used as the electron mediator. Park et al. [86] reported that viologen dyes cross-linked with carbon polymers and absorbed on the cytoplasmic membranes of *Desulfovibro desulfuricans* mediated electron transfer from bacterial cells to electrodes or from electrodes to bacterial cells. Other organic dyes that have been tested include benzylviologen, 2,6-dichlorophenolindophenol, 2-hydroxy- 1,4-naphthoquinone, phenazines (phenazine ethosulfate, safranine), phenothiazines (alizarine brilliant blue, N,N dimethyl-disulfonated thionine, methylene blue, toluidine blue) and phenoxazines (brilliant cresyl blue, gallocyanine, resorufin) (Table 4.2). Among the dyes tested, phenoxazine, phenothiazine, phenazine, indophenol, bipyridilium derivatives, thionine and 2-hydroxy-1,4-naphthoquinone were found to be very efficient in maintaining relatively high cell voltage output when current was drawn from the biofuel cell [87]. Ferric chelate complexes (e.g., Fe (III) EDTA) were successfully used with *Lactobacillus plantarum*, *Streptococcus lactis* and *Erwinia dissolvens*, oxidizing glucose. A mixture of two mediators can be useful in optimizing the efficiency. Two mediators, namely thionine and Fe (III) EDTA were employed with *E.coli* for the oxidation of glucose. It was found that thionine was reduced over 100 times faster than Fe (III) EDTA [85].
2. Endogenous Shuttles: To facilitate the electron transfer from bacteria to the anode, addition of synthetic exogenous mediators could be helpful. However, such a solution can have some inherent disadvantage. Toxicity and instability of the added mediators can limit their applications in MFCs. One possible solution could be to use native (endogenous) electron shuttles produced

TABLE 4.2 Role of Mediators in the MFC Performance [12]

Microorganism	Substrate	Mediator	Anode	Power density ($\mu A\ cm^{-2}$)
Pseudomonas methanica	Methane	1-Naphthol-2-sulphonate indo-2,6-dichlorophenol.	Pt-black	2.8
Proteus vulgaris	Glucose	Thionine	RVC	4.3×10^{-4}
Proteus vulgaris	Glucose	HNQ	Graphite felt	0.095
Escherichia coli	Acetate	Neutral red	Graphite	1.4
Escherichia coli	Glucose	Neutral red	Graphite felt	37
Escherichia coli	Glucose	HNQ	Glassy carbon	180

by the microorganism itself. For MFC applications, the secondary metabolites which can work as redox mediators are of specific interest, as their *in situ* synthesis makes the electron transfer independent of the addition of exogenous redox shuttles. These metabolites can serve as reversible electron acceptors, carrying electrons from the bacterial cell either to an anode or into aerobic layers of biofilm, where they become reoxidized and are again available for subsequent redox processes.

Gamma proteobacteria such as *Pseudomonas aeruginosa* and *Shewanella oneidensis MR-1* have been found to produce their own electron shuttles [44, 88, 89]. The best-studied organism with respect to redox activity is *P. aeruginosa*, which is capable of producing pyocyanin and several other electron shuttling compounds [24, 90]. *Pseudomonasaeruginosa* is of interest due to its diverse metabolic activity, pathogenesis, ability to produce compounds such as siderophores and surfactants, applications in waste water treatment, etc. It is known to produce several phenazine derivatives, the regulation of which is partly determined by quorum sensing [91].

Phenazines comprise a large group of nitrogen-containing heterocyclic compounds that differ in their chemical and physical properties based on

the type and position of functional groups present. More than 100 different phenazine structural derivatives have been identified in nature (Fig. 4.6), and over 6,000 compounds that contain phenazine as a central moiety

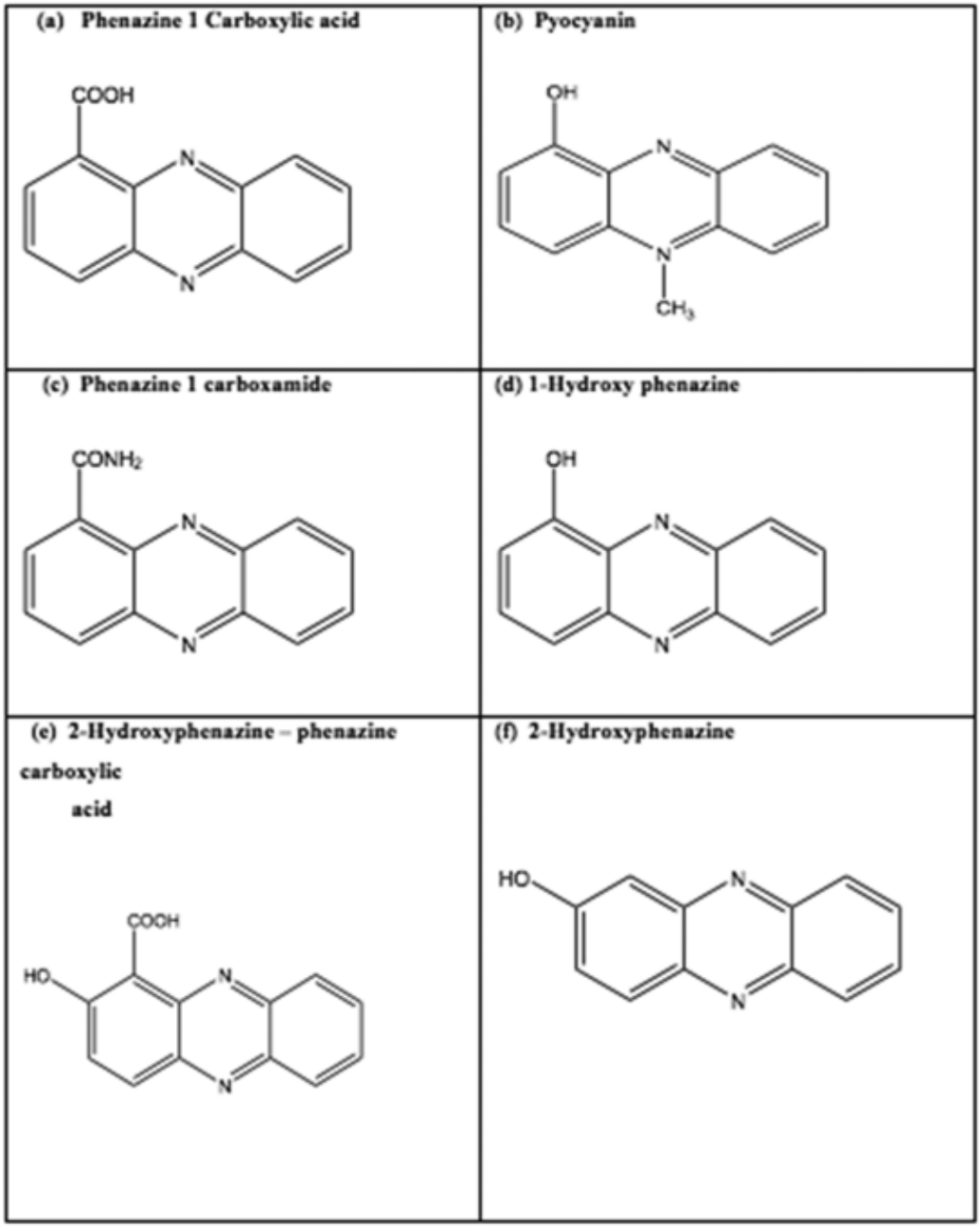

FIGURE 4.6. Some phenazine derivatives synthesized by *Pseudomonas.* (a) Phenazine 1 Carboxylic acid; (b) Pyocyanin; (c) Phenazine 1 carboxamide; (d) 1-Hydroxy phenazine; (e) 2-Hydroxyphenazine–phenazine carboxylic acid; (f) 2-Hydroxyphenazine.

have been synthesized [92]. The phenazine-based pyocyanin is of particular interest for its capability of producing reactive oxygen species [93]. It also has been reported to mediate the reoxidation of NADH under oxygen-limiting conditions, such as those found in mature biofilms [94–96]. Also several other intermediates in the pathway for pyocyanin and phenazine generation have been reported to hold electrochemical activity and could possibly exert a similar function.

P. aeruginosa catalyzed MFC has been shown to provide a unique opportunity to combine the metabolic capability of the organism and to breakdown oxidizable pollutants and salvage energy from the process [24, 90]. MFCs with P. aeruginosa MTCC 2474 using graphite block electrodes generated a maximum power density of 392 $\mu W/m^2$ and it was observed that the 23 μM pyocyanin and 4.8 μM pyorubin were generated in the anolyte [24]. External supplementation of phenazines (pyocyanin, pyorubin, tubermycin or oxychloraphin) at a concentration of 3 mM to the anolyte resulted in different levels of power generation. Addition of tubermycin and oxychloraphin, which were not normally produced by *P. aeruginosa* MTCC 2474 under aerobic condition, enhanced the power density several fold. Particularly, the addition of oxychloraphin showed about 22.9-fold higher power density when using Cu^{2+} doped GECE anode as compared to unsupplemented MFC using graphite anode. However, the addition of pyocyanin or pyorubin, which are normally produced by the *P. aeruginosa* MTCC 2474, was not very helpful in improving the performance of the MFC. Also, the addition of these phenazines inhibited the growth of bacteria as well. The native phenazines that were generated as a response to stress, when added externally inhibited the organism, while the nonnative phenazines allowed a much more efficient metabolic conversion of the substrate available [24].

4.2.12 APPLICATIONS

The concept of MFCs has been known and demonstrated from the eighteenth century, the microorganisms working as catalysts in fuel cells to produce electricity [84, 97]. However, it is only recently that the thoughts of using MFC for practical applications have been entertained with increase

in power output [68]. This was due to the paradigm shift in the discovery of microbial communities, such as dissimilatory metal reducing bacteria that directly transfer electrons without the need for exogenous mediators, development of system architecture and low cost components (electrodes, membranes, etc.) for MFCs. Some areas where MFCs offer immediate prospect of application are discussed in the following sub-sections.

4.2.12.1 Waste Water Treatment

The power consumption in the US for aerobic wastewater treatment, as estimated by Logan et al. [13] is 3% of total consumption. The cost of this process is becoming unacceptable since the immediate returns from the process are none. Domestic and industrial effluents contain a multitude of organic compounds that can fuel MFCs. Microorganisms in MFCs can discharge the dual duty of degrading the pollutants and generating power. Moreover, such a system can reduce solids generation by 50–90%, and reduce the load on their disposal [98]. Sanitary wastes, food processing wastewater, swine wastewater and corn stover are all great substrates for MFCs because their rich organic content [99–102]. About 80% of chemical oxygen demand (COD) of the domestic waste water was removed in a prototype single chambered MFC (SCMFC) reactor and generated 0.026 W/m^2 power density [19]. Using a single chamber MFC, a power density of 0.261 W/m^2, 0.205 W/m^2 and 0.672 W/m^2 had been achieved with wastewater streams of swine [101], brewery [103] and paper [104] industries. More than 80% COD removal was achieved in the combined anaerobic fluidized bed (AFB) and MFC with an electricity generation of 0.124 W/m^2 using distillery wastewater [105].

MFCs were also explored to treat the azo dyes containing textile effluent and simultaneous recovery of power [106–108]. Azo dyes form the largest class of synthetic dyes with a variety of color and structure. The color of dyes is due to azo double bond and associated chromophores. Disposal of dyes into surface water not only affects the esthetics but can also lead to toxicity to the biota present. When azo dyes were used as catholyte of MFCs under anoxic conditions they could be employed as electron donors resulting in their decoloration. The reduction reactions

in the cathode chamber are described by Goyal and Minocha [109], and Menek and Karaman [110] in which the –N=N–double bond was reduced to hydrazo (1) or amine (2) via the consumption of two or four electrons.

$$–N=N– + 2e + 2H^{+} \rightarrow –NH\text{-}NH\text{-} \quad (8)$$

$$–N=N– + 4e + 4H^{+} \rightarrow –NH_2\text{-}NH_2\text{-} \quad (9)$$

Different dyes were tested as catholytes in *Pseudomonas* catalyzed MFC by Jayapriya and Ramamurthy [67]. Compared to potassium ferricyanide and potassium permaganate, addition of methyl orange resulted in a higher power output.

Lovley [111] and Dumas et al., [58] designed MFCs using benthic organisms that oxidize the substrates in the sediment and transfer electrons to the anode either embedded in or rested on top of the sediment. The cathodes are suspended in the overlying seawater where oxygen reduction takes place. This MFC with *different industrial and domestic wastewater,* tested at *pilot scale, was found feasible, but would require higher efficiency and lower cost to be economically competitive.*

4.2.12.2 Biosensor

Another potential application of the MFC technology is to use it as a sensor for pollutant analysis and in situ process monitoring and control [112]. Although the five-day BOD test (BOD_5) is being widely used as the standard method to determine the concentration of biodegradable organics in wastewater [113], this is a time-consuming process. An MFC could be employed for real-time BOD monitoring by measuring current in an amperometric mode [114]. However, the signal from this MFC was reduced in the presence of high redox potential electron acceptors, such as nitrate and oxygen, and hence the analytes must be pretreated to remove the interfering compounds.

MFC based toxicity sensor for fast monitoring of acidic toxicity was developed by Shen et al. [115]. In principle, if a toxic event occurs, microbial activity is altered and thus the power output of the MFC is affected,

therefore an MFC could serve as an early toxicity-warning device. Recently, MFC based biosensor array was designed by Kaur et al. [116] to measure the presence of different volatile fatty acids such as acetate, propionate and butyrate concentrations with sensitivity down to 5 mg l^{-1} and up to 40 mg l^{-1}.

4.2.12.3 Hydrogen Production

Hydrogen production by electrohydrogenesis in MFC is a new method for generating hydrogen from acetate and other fermentable products [31, 117–119]. In a microbial electrolysis cell (MEC), exoelectrogens oxidize a substrate and release electrons to the anode. When acetate is used as a substrate, a voltage of >0.2 V is applied for hydrogen evolution [120, 121]. This voltage is substantially less than the 1.8–2.0 V used in practice for hydrogen production via water electrolysis under alkaline conditions [122]. In a similar way, a DC Voltage (0.8 V) was supplied to the single chambered MEC using glucose, cumulative hydrogen production for a 5-day cycle of operation was 0.16 m^3 H_2/ day [123]. But the hydrogen production in MEC was instantaneously consumed by methanogens present in the system [117, 119], which is one of the major obstacles.

4.2.12.4 Powering Gadgets

MFCs are especially suitable for powering small telemetry systems and wireless sensors that have only low power requirements to transmit signals to receivers in remote locations [3, 124]. Realistic energetically autonomous robots could be equipped with MFCs that use different fuels like sugar, fruit, dead insects, grass and weed. The robot EcoBot-II solely powers itself by MFCs to perform some behavior including motion sensing, computing and communication [125–127]. Some scientists envision that in the future a miniature MFC can be implanted in a human body to power an implantable medical device with the nutrients supplied by the human body [128]. However, only after potential health

and safety concerns related to the biocatalyst in the MFC are thoroughly understood, it could be widely deployed.

4.3 OUTLOOK

The potential of MFC has not been exploited for any specific application till date. A small but important subset of the parameters influences MFC performance: system architecture, the electrode and membrane characteristics, the roles of the microorganisms, and the need for mediators. From a practical viewpoint there have been a number of breakthroughs made in the recent years, some of which are listed below:

a. High efficiency electrodes used in conventional fuel cells such as metal coatings, carbon-polymer composites and noble-metal catalyst although are commercially available are not being used in MFCs. These electrodes were not biocompatible and are susceptible to catalyst poisoning when industrial effluents/aquatic sediments were used as a fuel. This may be overcome by the development of anodes with enhanced active surface area, conductive surface and redox behavior suited to microbial metabolism and conducive to biofilm formation [1, 51, 66].
b. EAB found in the diverse environments, understanding their metabolic impediments and physiology towards extracellular electron transfer can pave the way for significant performance improvement. The discovery of these electrochemically active bacteria/ self-mediating bacteria may overcome requirements such as the need for synthetic mediator in MFC [5–7].
c. Recent advances in MFC reactor design emphasize cost effectiveness and scalability. Some new designs are very unique such as the development of single chambered MFC without PEM (reducing the cost), stacked MFC module (gain of voltage) and rotating cathode (increasing the oxygen reduction rate) [19–22].
d. Potassium ferricyanide is widely used as the electron acceptor in MFC. However, it requires the continuous replenishment over the cycle. Instead of potassium ferricyanide, some researchers claim that azo dyes posses high redox potential so that the azo dye could

be used in the cathode with the dual objective of solving as facilitator for electron acceptor and the possibility of dye removal. These studies have suggested that the technology in the dual duty of degrading the azo dyes and simultaneous power production, by adapting the MFC for treating textile effluents could be exploited profitably. But, significant technical improvements are needed to scale up the process for addressing the industrial needs in a cost-effective way [67, 106–108].

e. The use of EAB to produce other products at cathode such as hydrogen, methane, hydrogen peroxide or ethanol by applying the voltage/ alter the design of MFC [119].
f. Some examples of commercial effort to employ MFCs are Trophos Energy (USA), Lebone (USA), IntAct Labs LLC, (USA), HySyEnce (USA), Plant-e (Netherlands) and Emefcy (Israel).

KEYWORDS

- **Anion exchange membrane**
- **Carbon nanotubes**
- **Chemical vapor deposition**
- **Chemically modified carbon electrodes**
- **Cobalt tetramethylphenylporphyrin**
- **Dissimilatory metal reducing bacteria**
- **Electrochemically active bacterial**
- **Microbial fuel cell**
- **Proton exchange membrane**
- **Reticulated vitreous carbon**
- **Ultra filtration**

REFERENCES

1. Park, D. H., Kim, S. K., Shin, I. H., Jeong, Y. J. (2000). Electricity production in biofuel cell using modified graphite electrode with Neutral Red.*Biotechnol.Lett. 22,* 1301–1304.

2. Tokuji, I., Kenji, K. (2003). Bioelectrocatalyzes-based application of quinoproteins and quinprotein- containing bacterial cells in biosensors and biofuel cells. *Biochimic. Biophys.Acta.* 1647, 121–126.
3. Ieropoulos, I. A., Greenman J., Melhuish C., Hart J. (2005). Comparative study of three types of microbial fuel cell. *Enzyme.Microb. Tech. 37,* 238–245.
4. Vega, C. A., Fernandez, I. (1987). Mediating effect of ferric chelate compounds in microbial fuel cells with *Lactobacillus plantarum, Streptococcus lactis and Erwiniadissolven*. *Bioelectrochem.Bioenerg.* 17, 217–222.
5. Bond, D. R., Lovley, D. R. (2003). Electricity production by *Geobacter sulfurreducens* attached to electrodes. *Appl. Environ. Microbiol. 69,* 1548–1555.
6. Chaudhuri, S. K., Lovley, D. R. (*2003).*Electricity generation by direct oxidation of glucose in mediatorless microbial fuel cells. *Nat. Biotechnol.* 21, *1229–1232.*
7. Kim, H. J., Park, H. S., Hyun, M. S., Chang, I. S., Kim, M., Kim, B. H. (2002). A mediator-less microbial fuel cell using a metal reducing bacterium, *Shewanella putrefacians*. *Enzyme. Microbiol. Tech. 30,* 145–152.
8. Pham, C. A., Jung, S. J., Phung, N. T., Lee J., Chang, I. S., Kim, B. H., Yi, H., Chun, J. (2003). A novel electrochemically active and Fe (III)-reducing bacterium phylogenetically related to *Aeromonas hydrophila*, isolated from a microbial fuel cell. *FEMS Microbiol.Lett. 223,* 129–134.
9. Rabaey, K., Boon, N., Siciliano, S. D., Verhaege, M., Verstraete, W. (2004).Biofuel cells select for microbial consortia that self-mediate electron transfer. *App. Environ. Microbiol.* 70, 5373–5382.
10. Bard, A. J., Parsons, R., Jordan, J. Standard Potentials in Aqueous Solutions; Marcel Dekker: New York, 1985.
11. Alberty, R. A. Thermodynamics of Biochemical Reactions; John Wiley & Sons: New York, 2003.
12. Katz, E., Shipway, A. N., Willner, I. (2003). Biofuel cells: Functional design and operation. In Handbook of Fuel Cells – Fundamental, Technology, Applications; Vielstich, W., Gastieger, H., Lamin, A., Eds., Wiley: Chichester, Vol.1; 355–381.
13. Logan, B. E., Hamelers, B., Rozendal, R., Schroder, U., Keller, J., Freguia, S., Aelterman, P., Verstraete, W., Rabaey, K. (2006). Microbial fuel cells: Methodology and technology. *Environ. Sci. Technol. 40,* 5181–5192.
14. Larminie, J., Dicks, A. Fuel cell systems explained, John Wiley & Sons, Chichester. 2000.
15. Bockris, J. O. M., Reddy, A. K. N., Gamboa, A. M. Modern Electrochemistry: Fundamentals of Electrodics. Kluwer Academic Publishers: New York, 2000.
16. Hoogers, G. Ed., Fuel Cell Technology Handbook, CRC Press: Boca Raton, FL, 2003.
17. Liu, H., Ramnarayanan, R., Logan, B. E. (2004). Production of electricity during wastewater treatment using a single chamber microbial fuel cell. *Environ. Sci. Technol. 38,* 2281–2285.
18. Min, B., Logan, B. E. (2004). Continuous Electricity Generation from Domestic Wastewater and Organic Substrates in a Flat Plate Microbial Fuel Cell. *Environ. Sci. Technol. 38*, 5809–5814.

19. Liu, H., Logan, B. E. (2004). Electricity generation using an air-cathode single chamber microbial fuel cell in the presence and absence of a proton exchange membrane. *Environ. Sci. Technol. 38,* 4040–4046.
20. Jang, J. K., Pham, T. H., Chang, I. S., Kang, K. H., Moon, H., Cho, K. S., Kim, B. H. (2004). Construction and operation of a novel mediator-and membrane-less microbial fuel cell. *Process.Biochem. 39,* 1007–1012.
21. He, Z., Shao, H., Angenent, L. T. (2007). Increased power production from a sediment microbial fuel cell with a rotating cathode. *Biosens.Bioelectron. 22,* 3252–3255.
22. Aelterman, P., Rabaey, K., Pham, H. T., Boon, N., Verstraete, W. (2006). Continuous electricity generation at high voltages and currents using stacked microbial fuel cells. *Environ. Sci Technol. 40,* 3388–3394.
23. Oh, S. E., Logan, B. E. (2007). Voltage reversal during microbial fuel cell stack operation. *J.Power. Sources. 167,* 11–17.
24. Jayapriya, J., Ramamurthy, V. (2012). Use of nonnative phenazines improve performance of *Pseudomonas aeruginosa* MTCC 2474 catalyzed fuel cells. *Bioresour. Technol. 124,* 23–28.
25. Park, D. H., Zeikus, J. G. (2003). Improved fuel cell and electrode designs for producing electricity from microbial degradation. *Biotechnol.Bioeng. 81,* 348–355.
26. Gil, G. C., Chang, I. S., Kim, B. H., Kim, M., Jang, J. K., Park, H. S., Kim, H. J. (2003). Operational parameters affecting the performance of a mediator-less microbial fuel cell. *Biosens.Bioelectron. 18,* 327–334.
27. Kim, B. H., Kim, H. J., Hyun, M. S., Park, D. H. (1999). Direct electrode reaction of Fe (III)-reducing bacterium, *Shewanella putrefaciensJ. Microbiol.Biotechnol. 9*, 127–131.
28. Okada, T., Nakamura. N., Yuasa, M., SekineI. I. (1997). Ion and water transport characteristics in membranes for polymer electrolytefuel cells containing H^+ and Ca^{2+} cations. *J. Electrochem. Soc, 144,* 2744–2750.
29. Basura, V. I., Beattie, P. D., Holdcroft, S. (1998). Solid-state electrochemical oxygen reduction at Pt/Nafions 117 and Pt/BAM3GTM 407 interfaces. *J. Electroanal. Chem*. *458*, 1–5.
30. Kim, J., Cheng, S. A., Oh, S., Logan, B. E. (2007). Power generation using different cation, anion, and ultrafiltration membranes in microbial fuel cells. *Environ. Sci. Technol. 41,* 1004–1009.
31. Rozendal, R. A., Hamelers, H. V. M., Buisman, C. J. N. (2006). Effects of membrane cation transport on pH and microbial fuel cell performance. *Environ. Sci. Technol. 40,* 5206–5211.
32. Chae, K. J., Choi, M., Ajayi, F. F., Park, W., Chang, I. S., Kim, I. S. (2008). Mass transport through a proton exchange membrane (Nafion) in microbial fuel cells. *Energy Fuels 22,* 169−176.
33. Xu, J., Sheng, G. P., Luob, H. W., Lib, W. W., Wang, L. F., Yub, H. Q. (2012). Fouling of proton exchange membrane (PEM) deteriorates the performance of microbial fuel cell, *Water Research 46,* 1817–1824.
34. Kalcher, K., Svancara, I., Metelka, R., Vytras K., Walcarius. A. (2006). Heterogeneous Carbon Electrochemical Sensors. In Encyclopedia of Sensors; Craig A. Grimes, Elizabeth C. Dickey, and Michael V. Pishko Eds., American Scientific Publishers, Stevenson Ranch, California, Vol. 4, pp. 283–430.

35. Uslu, B., Sibel, A. O. (2007). Electroanalytical application of carbon based electrodes to the Pharmaceuticals. *Anal.Lett. 40,* 817–853.
36. Greenville, W. A., Kintner, P. L. (1969). Carbon: observations on the new allotropic form. *Science 165,* 589–591.
37. Cheng, S., Logan, B. E. (2007). Ammonia treatment of carbon cloth anodes to enhance power generation of microbial fuel cells. *Electrochem.Commun. 9,* 492–496.
38. Wang, X., Feng, Y. J., Lee, H. (2008). Electricity production from beer brewery wastewater using single chamber microbial fuel cell. *Water Sci. Technol. 57,* 1117–1121.
39. Wang, X., Cheng, S., Feng, Y., Merrill, M. D., Saito, T., Logan, B. E. (2009). Use of carbon mesh anodes and the effect of different pretreatment methods on power production in microbial fuel cells. *Environ. Sci. Technol. 43,* 6870–6874.
40. Reimers, C. E., Tender, L. M., Fertig, S. J., Wang, W. (2001). Harvesting energy from the marine sediment-water interface. *Environ. Sci. Technol. 35,* 192–195.
41. Mohan, S. V., Saravanan, R., Raghavulu, S. V., Mohanakrishna, G., Sarma, P. N. (2008). Bioelectricity production from wastewater treatment in dual chambered microbial fuel cell (MFC) using selectively enriched mixed microflora: Effect of catholyte. *Bioresour Technol. 99,* 596–603.
42. Logan, B., Cheng, S., Watson, V., Estadt, G. (2007).Graphite fiber brush anodes for increased power production in air-cathode microbial fuel cells. *Environ. Sci. Technol.* 41, 3341–3346.
43. Ahn, Y., Logan, B. E. (2010). Effectiveness of domestic wastewater treatment using microbial fuel cells at ambient and mesophilic temperatures, *Bioresource. Technol. 101,* 469–475.
44. Rabaey, K., Ossieur, W., Verhaege, M., Verstraete, W. (2005). Continuous microbial fuel cells convert carbohydrates to electricity. *Water. Sci. Technol. 52,* 515–523.
45. You, S. J., Zhao, Q. L., Zhang, J. N., Jiang, J. Q., Wan, C. L., Du, M. A., Zhao, S. Q. (2007). A graphite-granule membrane-less tubular air-cathode microbial fuel cell for power generation under continuously operational conditions. *J. Power. Sources 173,* 172–177.
46. He, Z., Minteer, S. D., Angenent, L. T. (2005).Electricity generation from artificial wastewater using an upflow microbial fuel cell. *Environ. Sci. Technol.* 39, 5262–5267.
47. Ringeisen, B. R., Henderson, E., Wu, P. K., Pietron, J., Ray, R., Little, B., Biffinger, J. C., Jones-Meehan, J. M. (2006). High power density from a miniature microbial fuel cell using *Shewanella oneidensis* DSP10. *Environ Sci Technol. 40,* 2629–2634.
48. Magrez, A., Kasas, S., Salicio, V., Pasquier, N., Seo, J. W., Celio, M., Catsicas, S., Schwaller, B., Forro, L. (2006). Cellular toxicity of carbon-based nanomaterial. *Nano.Lett. 6,* 1121–1125.
49. Wu, Z., Feng, W., Feng, Y., Qiang Liu, Xu, X., Sekino, T., Fujii, A., Ozaki, M. (2007). Preparation and characterization of chitosan-grafted multiwalled carbon nanotubes and their electrochemical properties. *Carbon 45,* 1212–1218.
50. Qiao, Y., Li, C. M., Bao, S. J., Bao, Q. L. (2007). Carbon Nanotube/Polyaniline Composite as Anode Material for Microbial Fuel Cells. *J. Power. Sources 170,* 79–84.

51. Schroder, U., Niessen, J., Scholz, J. (2003). A generation of microbial fuel cells with current outputs boosted by more than one order of magnitude. *Angew. Chem. Int. Ed. 42,* 2880–2883.
52. Sahoo, N. G., Jung, Y. C., So, H. H., Cho, J. W. (2007). Polypyrrole coated carbon nanotubes: synthesis, characterization, and enhanced electrical properties. *Synthetic Metals 157,* 374–379.
53. Yuan, Y., Kim, S. (2008). Improved Performance of a Microbial Fuel Cell with Polypyrrole/Carbon Black Composite Coated Carbon Paper Anodes. *B. Kor. Chem. Soc. 29,* 1344–1348.
54. Sharma, T., Reddy, A. L. M., Chandra, T. S., Ramaprabhu, S. (2008). Devolopement of carbon nanotubes and nanofluids based microbial fuel cell. *Int. J. Hydrogen Energy 33,* 6749–6754.
55. Donaldson, K., Aitken, R., Tran, L., Stone, V., Duffin, R., Forrest, G., Alexander, A. (2006). Carbon nanotubes: A review of their properties in relation to pulmonary toxicology and workplace safety. *Toxicol. Sci. 92,* 5–22.
56. Upadhyayula, V. K. K., Gadhamshetty, V. (2010). Appreciating the role of carbon nanotubes in preventing biofouling and promoting biofilms on material surfaces in environmental engineering: review. *Biotechnol.Adv. 28,* 802–816.
57. Esawi, A. M. K., Farag, M. M. (2007). Carbon nanotube reinforced composites: Potential and current challenges. *Materials Design 28,* 2394–2401.
58. Dumas, C., Mollica, A., Féron, D., Basséguy, R., Etcheverry, L., Bergel, A. (2007). Marine microbial fuel cell: Use of stainless steel electrodes as anode and cathode materials. *Electrochim.Acta. 53,* 468–473.
59. Richter, H., McCarthy, K., Nevin, K. P., Johnson, J. P., Rotello, V. M., Lovley, D. R. (2008). Electricity generation by *Geobacter sulfurreducens* attached to gold electrodes, *Langmuir. 24,* 4376 – 4379.
60. Heijne, A. T., Hamelers, H. V. M., Saakes, M., Buisman, C. J. N. (2008). Performance of nonporous graphite and titanium-based anodes in microbial fuel cells. *Electrochim.Acta. 53,* 5697–5703.
61. Moon, H., Chang, I. S., Kim, B. H. (2006). Continuous electricity production from artificial wastewater using a mediator-less microbial fuel cell. *Bioresour. Technol. 97,* 621–627.
62. Zhao, F., Harnisch, F., Schroder, U., Scholz, F., Bogdanoff, P., Herrmann, I. (2005). Application of pyrolyzed iron (II) phthalocyanine and CoTMPP based oxygen reduction catalysts as cathode materials in microbial fuel cells, *Electrochem. Commun. 7,* 1405–1410.
63. Cheng, S., Liu, H., Logan, B. E. (2006). Power Densities Using Different Cathode Catalysts (Pt and CoTMPP) and Polymer Binders (Nafion and PTFE) in Single Chamber Microbial Fuel Cells. *Environ.Sci. Technol. 40,* 364–369.
64. Freguia, S., Rabaey, K., Yuan, Z., Keller. J. (2007). Non-catalyzed cathodic oxygen reduction at graphite granules in microbial fuel cells.*Electrochim.Acta. 53,* 598–603.
65. Zhou, M., Chi, M., Luo, J., He, H., Jin, T. (2011). An overview of electrode materials in microbial fuel cells.*J. Power Sources 196,* 4427–4435.
66. Jayapriya, J., Gopal. J., Ramamurthy, V., Kamachimudali, U., Raj, B. (2012). Preparation and characterization of biocompatible carbon electrodes. *Composites Part B-Eng. 43,* 1329–1335.

67. Jayapriya, J., Ramamurthy, V. (2014). The Role of Electrode Material in Capturing Power Generated in *Pseudomonas* catalyzed fuel Cells. *Can. J. Chem. Eng. 92*, 610–614.
68. Erable, B., Duteanu, N., Kumar, S. M. S., Feng, Y., Ghangrekar, M. M., Scott, K. (2009). Nitric acid activation of graphite granules to increase the performance of the noncatalyzed oxygen reduction reaction (ORR) for MFC applications. *Electrochem. Commun. 11,* 1547–1549.
69. Feng, Y., Yang, Q., Wang, X., Logan, B. E. (2010). Treatment of graphite fiber brush anodes for improving power generation in air-cathode microbial fuel cells. J. Power. Sources. *195,* 1841–1844.
70. Lowy, D. A., Tender, L. M., Zeikus, J. G., Park, D. H., Lovley, D. R. (2006). Harvesting energy from the marine sediment-water interface II Kinetic activity of anode materials. *Biosens.Bioelectron. 21,* 2058–2063.
71. Holmes, D. E., Bond, D. R., O'Neil, R. A., Reimers, C. E., Tender, L. R., Lovley, D. R. *(2004).Microbial communities associated with electrodes harvesting electricity from a variety of aquatic sediments.Microbial Ecol. 48,* 178*–190.*
72. Park, H. S., Kim, B. H., Kim, H. S., Kim, H. S., Kim, G. T., Kim, M., Chang, I. S., Park, Y. K., Chang, H. I. (2001). A novel electrochemically active and Fe(III)-reducing bacterium phylogenetically related to *Clostridium butyricum* isolated from a microbial fuel cell. *Anaerobe 7,* 297–306.
73. Prasad, D., Sivaram, T. K., Berchmans, S., Yegnaraman, V. (2006). Microbial fuel cell constructed with a microorganism isolated from sugar industry effluent. *J. Power. Sources 160,* 991–996.
74. Reguera, G., Nevin, K. P., Nicoll, J. S., Covalla, S. F., Woodard, T., L, Lovley, D. R. (2006). Biofilm and nanowire production leads to increased current in *Geobacter sulfurreducens* fuel cells. *Appl. Environ. Microbiol. 72,* 7345–7348.
75. Kim, J. R., Jung, S. H., Regan, J.M; Logan, B. E. (2007b). Electricity generation and microbial community analysis of alcohol powered microbial fuel cells. *Bioresour. Technol. 98*, 2568–2577.
76. Niessen, J., Harnisch, F., Rosenbaum, M., Schroder, U., Scholz, F. (2006). Heat treated soil as convenient and versatile source of bacterial communities for microbial electricity generation. *Electrochem.Commun. 8,* 869–873.
77. Zhang, E., Xu, W., Diao. G., Shuang, C. (2006). Electricity generation from acetate and glucose by sedimentary bacterium attached to electrode in microbial-anode fuel cells. *J. Power. Sources 161*, 820–825.
78. Reguera, G., McCarthy, K. D., Mehta, T., Nicoll, J. S., Tuominen. M. T., Lovley, D. R. (2005). Extracellular electron transfer via microbial nanowires. *Nature 435,* 1098–1101.
79. Gorby, Y. A., Yanina, S. McLean, J. S., Rosso, K. M., Moyles, D., Dohnalkova, A., Beveridge, T. J., Chang, I. S., Kim, B. H., Kim, K. S., Culley, D. E., Reed, S. B., Romine, M. F., Saffarini, D. A., Hill, E. A., Shi, L., Elias, D. A., Kennedy, D. W., Pinchuk, G., Watanabe, K., Ishii, S., Logan, B., Nealson, K.H; Fredrickson, J. K. (2006). Electrically conductive bacterial nanowires produced by *Shewanella oneidensis* strain MR-1 and other microorganisms. *Proc. Natl. Acad. Sci. USA 103,* 11358–11363.

80. Malvankar, N.S., Vargas, M., Nevin K. P., Franks, A. E., Leang, C., Kim, B. C., Inoue, K., Mester, T., Sean F. Covalla, S. F., Johnson, J. P., Rotello, V. M., Tuominen, M. T., Lovley, D. R. (2011). Tunable metallic-like conductivity in microbial nanowire networks. *Nature Nanotechnol. 6,* 573–579.
81. Wilkinson, S. (2000). Gastrobots – Benefits and challenges of microbial fuel cells in food powered robot applications. *Auton. Robot 9,* 99–111.
82. Dealney, G. M., Bennetto, H. P., Mason, J. R., Roller, S. D., Stirling, J. L., Thurston, C. F. (*1984).*Electron-transfer coupling in microbial fuel cells. 2. Performance of fuel cells containing selected microorganism-mediator-substrate combinations. *J. Chem. Technol. Biotechnol. 34*, 13–27.
83. Bennetto, H. P., Delaney, G. M., Mason, J. R., Roller, S. D., Stirling, J. L., Thurston, C. F. *(*1985).The sucrose fuel cell: Efficient biomass conversion using a microbial catalyst. *Biotechnol. Lett.* 7*,* 699–704.
84. Allen, R. M., Bennetto, H. P. (1993).Microbial fuel cells: Electricity production from carbohydrates. *Appl. Biochem. Biotechnol.* 39, 27–40.
85. Tanaka, K., Kashiwagi, N., Ogawa, T. *(1988).* Effects of light on the electrical output of bioelectrochemical fuel cells containing *Anabaena variabilis* M-2: mechanisms of the postillumination burst. *Chem. Technol. Biotechnol. 42,* 235–240.
86. Park, D. H., Kim, B. H., Moore, B., Hill, H. A. O., Song, M. K., Rhee, H. W. (1997). Electrode reaction of *Desulfovibrio desulfuricans* modified with organic conductive compounds. *Biotechnol.Tech. 11,* 145–148.
87. Kim, N., Choi, Y., Jung, S., Kim, S. (2000). Effect of initial carbon sources on the performance of microbial fuel cells containing *Proteus vulgaris. Biotechnol.Bioeng. 70,* 109–114.
88. Marsili, E., Baron, D, B., Shikhare, I. D., Coursolle, D., Gralnick, J. A., Bond, D. R. (2008). Shewanella secretes flavins that mediate extracellular electron transfer. *Proc. Natl. Acad. Sci. USA 105,* 3968–3973.
89. Von Canstein, H., Ogawa, J., Shimizu, S., Lloyd, J. R. (2008). Secretion of flavins by Shewanella species and their role in extracellular electron transfer. *Appl. Environ. Microbiol. 74,* 615–623.
90. Rabaey, K., Boon, N., Hofte, M., Verstraete, W. (2005a).Microbial phenazine production enhances electron transfer in biofuel cells. *Environ. Sci. Technol. 39*, 3401–3408.
91. Chin-A-W., Bloemberg, G. V., Lugtenberg, B. J. J. *(*2003). Phenazines and their role in biocontrol by *Pseudomonas* bacteria. *New.Phytol. 157*, 503–523.
92. Mavrodi, D. V., Blankenfeldt, W., Thomashow, L. S. (2006). Phenazine compounds in fluorescent *Pseudomonas* spp. Biosynthesis and regulation. *Annu. Rev. Phytopathol*. *44,* 417–445.
93. Mavrodi, D. V., Bonsall, R. F., Delaney, S. M., Soule, M. J., Phillips, G., Thomashow, L. S. (2001). Functional analysis of genes for biosynthesis of pyocyanin and phenazine-1-carboxamide from *Pseudomonas aeruginosa* PAO1. *J. Bacteriol. 183*, 6454–6465.
94. Schroder, U. Anodic electron transfer mechanisms in microbial fuel cells and their energy efficiency, *Phys. Chem. Chem. Phys.* (2007). *9,* 2619–2629.

95. Dietrich, L. E. P., Teal, T. K., Whelan A. P., Newman, D. K. (2008). Redox-active antibiotics control gene expression and community behavior in divergent bacteria. *Science 321,* 1203–1206.
96. Maddula, V. S., Pierson, E. A., Pierson, L. S. (2008). Altering the ratio of phenazines in *pseudomonas chlororaphis* (aureofaciens) strain 30–84: effects on biofilm formation and pathogen inhibition. *J. Bacteriol. 190,* 2759–2766.
97. Habermann, W. and Pommer, E. H. (1991). Biological fuel cells with sulfide storage capacity. *Appl. Microbiol. Biotechnol. 35,* 128–133.
98. Holzman, D. C. (2005).Microbe power. *Environ. Health.Persp. 113*, A754–A757.
99. Suzuki, S., Karube, I., Matsunaga, T. (1978).Application of a biochemical fuel cell to wastewater. *Biotechnol.Bioeng.Symp. 8*, 501–511.
100. Oh, S. E., Logan, B. E. (2005). Hydrogen and electricity production from a food processing wastewater using fermentation and microbial fuel cell technologies. *Water Res. 39,* 4673–4682.
101. Min, B., Kim, J. R., Oh, S. E., Regan, J. M., Logan, B. E. (2005). Electricity generation from swine wastewater using microbial fuel cells. *Water Res. 39,* 4961–4968.
102. Zuo, Y., Maness, P. C., Logan, B. E. (2006). Electricity production from steam exploded corn stover biomass. *Energy Fuels 20,* 1716–1721.
103. Feng Y., Wang X., Logan B. E., Lee, H. (2008). Brewery wastewater treatment using aircathode microbial fuel cells. *Appl. Microbiol. Biotechnol. 78,* 873–880.
104. Huang, L., Logan B. E. (2008). Electricity generation and treatment of paper recycling wastewater using a microbial fuel cell. *Appl. Microbiol. Biotechnol. 80,* 349–355.
105. Huang, J. S., Yang, P., Guo, Y., Zhang, K. (2011). Electricity generation during wastewater treatment: An approach using an AFB-MFC for alcohol distilery wastewater. *Desalination 276,* 373–378.
106. Niu, C. G., Wang, Y., Zhang, X. G., Zeng, G. M., Huang, D. W., Ruan, M., Li, X. W. (2012). Decolorization of an azo dye Orange G in microbial fuel cells using Fe (II)-EDTA catalyzed persulfate. *Bioresource Technol. 126,* 101–106.
107. Hou, B., Sun, J., Hu, Y. (2011). Simultaneous Congo red decolorization and electricity generation in air-cathode single-chamber microbial fuel cell with different microfiltration, ultrafiltration and proton exchange membranes. *Bioresource Technol. 102,* 4433–4438.
108. Liu, L., Li, F. B., Feng, C. H., Li, X. Z. (2009). Microbial fuel cell with an azo-dye-feeding cathode. *Appl. Microbiol. Biotechnol. 85,* 175–183.
109. Goyal, R. N., Minocha, A. (1985). Electrochemical behavior of the bisazo dye, direct red-81. *J. Electroanal. Chem. Interfacial.Electrochem. 193,* 231–240.
110. Menek, N., Karaman, Y. (2005). Polarographic and voltammetric investigation of 8-hydroxy-7- (4-sulfo-1-naphthylazo) -5-quinoline sulfonic acid. *Dyes Pigments 67,* 9–14.
111. Lovely, D. R. Microbial fuel cells: novel microbial physiologies and engineering approaches. Biotechnol. (2006). *17,* 327–332.
112. Chang, I. S., Moon, H., Jang, J. K., Kim, B. H. (2005). Improvement of a microbial fuel cell performance as a BOD sensor using respiratory inhibitors. *Biosens. Bioelectron. 20,* 1856–1859.

113. APHA, Standard Methods for the Examination of Water and Wastewater, American Public Health Association, Washington, DC, USA, 1995.
114. Chang, I. S., Jang, J. K., Gil, G. C., Kim, M., Kim, H.J; Cho, B. W., Kim, B. H. (2004). Continuous determination of biochemical oxygen demand using microbial fuel cell type biosensor. *Biosens. Bioelectron*. 19, 607–613.
115. Shen, Y. J., Lefebvre, O., Tan, Z., Ng, H. Y. (2012). Microbial fuel-cell-based toxicity sensor for fast monitoring of acidic toxicity. *Water Sci. Technol. 65,* 1223–1228.
116. Kaur, A., Kim, J.R, ; Michie, I, ; Dinsdale, R.M, ; Guwy, A. J., Premier, G. C. Microbial fuel cell type biosensor for specific volatile fatty acids using acclimated bacterial communities. *Biosens.Bioelectron.* (2013). *47,* 50–55.
117. Liu, H., Grot, S., Logan, B. E. (2005). Electrochemically assisted microbial production of hydrogen from acetate. *Environ. Sci. Technol. 39,* 4317–4320.
118. Rozendal, R. A. and Buisman, C. J. N. Bio-Electrochemical Process for Producing Hydrogen. Patent WO-2005–005981, 2005.
119. Call, D., Logan, B. E. (2008). Hydrogen production in a single chamber microbial electrolysis cell lacking a membrane. *Environ. Sci. Technol. 42,* 3401–3406.
120. Cheng, S., Logan, B. E. (2007). Sustainable and efficient biohydrogen production via electrohydrogenesis. *Proc. Natl. Acad. Sci. USA 104,* 18871–18873.
121. Hu, H., Fan, Y., Liu, H. (2008). Hydrogen Production Using Single-chamber Membrane-free Microbial Electrolysis Cells. *Water Res. 42,* 4172–4178.
122. Kinoshita, K. Electrochemical oxygen technology, Wiley, New York. 1992.
123. Gupta, P., Parkhey, P., Joshi, K., Mahilkar, A. (2013). Design of a microbial fuel cell and its transition to microbial electrolytic cell for hydrogen production by electrohydrogenisis. *Indian J Exp Biol. 51,* 860–865.
124. Shantaram, A., Beyenal, H., Veluchamy R. R. A., Lewandowski, Z. (2005). Wireless sensors powered by microbial fuel cells. *Environ. Sci. Technol. 39,* 5037–5042.
125. Ieropoulos, I., Melhuish, C., Greenman, J. (2005). EcoBot-II: An artificial agent with a natural metabolism. *Adv. Robot Syst. 2,* 295–300.
126. Ieropoulos, I., Melhuish, C., Greenman, J. (2004). Energetically autonomous robots. In: Intelligent autonomous systems, Groen F, et al., Eds. Amsterdam: IOS Press, Vol. 8, 128–135.
127. Melhuish, C., Ieropoulos, I., Greenman, J., Horsfield, I. (2006). Energetically autonomous robots: Food for thought. *Auton.Robot. 21,* 187–198.
128. Chiao, M. A miniaturized microbial fuel cell. In Technical digest of solid state sensors and actuators workshop.Hilton Head Island, 59–60, 2002.

CHAPTER 5

SYSTEMS BIOLOGY APPROACHES FOR MICROBIAL FUEL CELL APPLICATIONS

R. NAVANIETHA KRISHNARAJ,[1] and JONG-SUNG YU[2]

[1-]R.Navanietha Krishnaraj, National Institute of Technology Durgapur, India

[2-]Department of Advanced Materials Chemistry, Korea University, Korea

CONTENTS

5.1 Introduction 126
5.2 Systems Biology 128
5.3 Systems Biology For Understanding the Mechanism of Electron Transfer 129
5.4 Systems Biology Approach For Improving the Power Output of Microbial Fuel Cells 133
5.5 Systems Biology Approaches For Screening Microorganism 134
5.6 Future Research Directions 135
5.7 Conclusion 136
Keywords 136
References 136

ABSTRACT

Microbial fuel cells are ecofriendly electrochemical devices that help to transform the chemical energy from the organic materials into electricity with the help of the catalytic activity of the microorganisms. Numerous reports are available in the literature to improve the bioelectricity generation in Microbial fuel cells. Currently, few reports are available on the use of molecular biology and genetic engineering approaches for improving the catalytic activity and electron transfer characteristics of the microorganisms. However, most of these approaches were made based on the reductionist approach and hence they could not drastically enhance the yield of microbial fuel cells. System biology approaches seems to be a promising option for enhancing the power output of microbial fuel cells. Herein, the applications of system biology approaches for screening the electrochemically active bacteria are discussed. The chapter also discusses about the use of system biology techniques for understanding the mechanisms of electron transfer from the microorganism to the electrode. The chapter also throws light on the novel metabolic approaches for enhancing the power output of microbial fuel cells. The advantages of systems biology approaches for MFC applications and the limitations of the conventional reductionist approaches are also discussed in detail.

5.1 INTRODUCTION

Microbial fuel cells (MFCs) are devices that perform oxidative disintegration of the organic compounds with the inbuilt complex enzymatic machinery of the microorganisms thereby producing reduction equivalents for the generation of bioelectricity [1]. MFCs have several advantages over the conventional fuel cells such as its temperature of operation, pH conditions, ecofriendly nature, ease of operation and high conversion efficiency [2, 3]. Besides electricity generation, MFCs also aid in wastewater treatment, cellulose degradation, desalination, dye degradation, toxin removal and production of chemicals [4–8]. McCormick et al. [9] reported a photosynthetic MFC, which can generate electricity to run clock upon illumination with light. Efforts are also made widely with a goal of using MFCs to low

power devices, charging mobile phones and light. MFCs find its application in powering autonomous robots,which are used to monitor or perform any function where humans cannot perform such as in deep sea or space [10]. MFCs can also be used to power sensors and other electronic devices [11]. MFCs can provide electricity to wireless sensors in remote locations while requiring less maintenance and reducing overall costs [12]. Biohydrogen production can also be coupled with the production of electricity in a MFC. MFCs can also be used to produce methane, and other valuable inorganic and organic chemicals besides electricity [7]. MFCs can also perform desalination process along with bioelectricity production [13]. MFCs can be integrated with other existing wastewater treatment processes. A novel up-flow anaerobic sludge blanket reactor-microbial fuel cell-biological aerated filter system to dispose the complex molasses wastewater was reported was also reported in the literature [14].MFCs are also used to reduce toxins such as microcystins. Though the MFCs have several advantages, they suffer from low power output[15]. Research activities throughout the world are underway to improve the yield. Several attempts are made by the researchers to improve the power output of MFCs. Increasing the size of the MFCs did not greatly aid in increasing the power output because of the scaling up limitations [16, 17]. Several electrode materials such as carbon felt, graphite, carbon foam, carbon paper, nickel foam have been attempted to improve the power outputs [18, 19]. As some of these materials are toxic to microorganisms, approaches were then made to modify the electrodes with biocompatible materials [20, 21]. Electrodes modified with biopolymers such as chitosan, alginate were shown to enhance the power output ofMFCs. Nanomaterials such as nanoparticles, carbon nanotubes, graphene were also shown to improve the electron transfer properties in MFC [22–24]. Reports were also documented on the use of conducting polymers such as polyaniline, polytoluene to improve the microbial electrocatalysis.Different configurations of fuel cells were also reported to improve the yield [25]. Increasing the conductivity of the electrolyte was reported to improve the yields to a certain levels [26]. Effect of the composition of anolyte and catholyte was also explored [27]. However, most of the methods rely on the physical parameters such as configuration of MFC, electrode materials to improve the power output of the MFCs. The microorganisms (electrigens/electroactive microorganisms) are the key players

in the microbial fuel cells [28, 29]. Hence, improving the electrocatalytic activity and electron transfer characteristics of the microorganism plays a significant role in enhancing the power output of MFCs. Currently, the metabolic engineering of electroactive bacteria based on reductionist approach is attempted and they could not greatly aid in improving the power output of MFCs significantly. Systems biology approach is the ideal tool to understand the complete molecular mechanism behind the generation of bioelectricity using microorganisms and will aid to enhance the power output of the MFC.

5.2 SYSTEMS BIOLOGY

Systems biology is often hailed as the new interdisciplinary approach for studying the complex interactions in biological systems (Fig. 5.1). However, this is not always true. The classical biologists took the entire characteristics of the organisms for their experiment and made an integrative understanding of diverse biological systems. They did not consider the expression level of any particular gene or a protein or its mRNA transcript. *Gregor Johann Mendel*, the father of genetics performed his experiments by studying the complete system of *Pisum sativum*. Reductionist approaches such as proteomics, genomics or transcriptomics were not used for his investigations, instead the traits such as plant height, seed

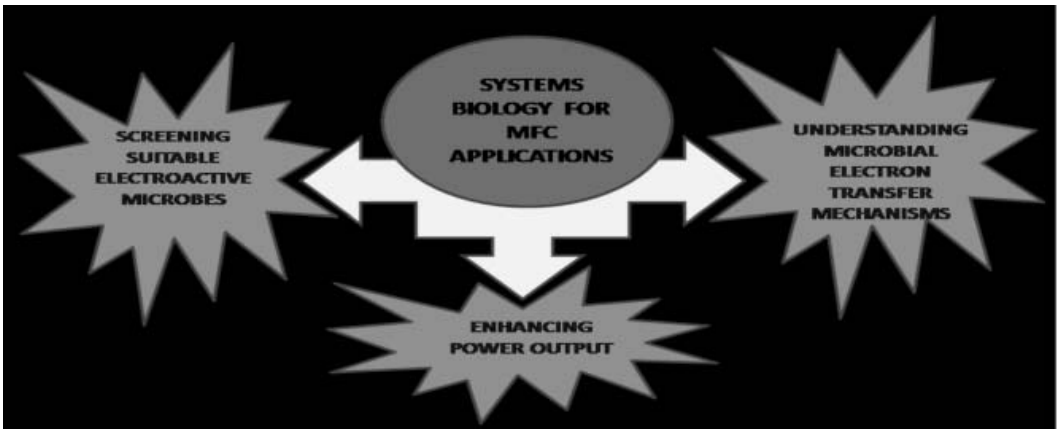

FIGURE 5.1 Systems biology for microbial fuel cell applications.

shape, pod shape, pod color, flower position, seed color and pea color was considered. Systems biology is the complete investigation on the behavior of complex biological organization and biochemical processes. It is just an opposite to that of reductionist approach. Reductionist approach studies the single/protein or a gene whereas the systems biology approach studies the expression different genes/proteins and the interactions between them. It considers the entirety of processes that happen in a biological system and helps to understand how exactly the system works. It is the detailed quantitative investigation on how the components of a biological system interact functionally with time. To understand the biology of the system, the features of the system as a whole have to be studied instead of studying the characteristics of the individual/isolated parts of the organisms. Systems biology aids in understanding the operation of the different components of the biological systems as a whole [30]. It is an emerging area and has the good potential to aid the researchers to understand the exact mechanisms of the biological systems. To enhance the yield of MFC or to identify a suitable microorganism for MFC application, one must understand the exact mechanism of oxidation/reduction of the substrate and the electron transfer characteristics of the microorganism. In the reductionist approach one take into account a single protein/gene. The biological system is very complex. Details about any one protein/gene might not give the complete picture of the electrocatalytic/electron transfer reactions. The mathematical modeling approaches and computation techniques will greatly aid in developing the models for different organisms/systems for diverse applications [31, 32]. Hence, an integrated approach such as systems biology will help to clearly understand how the microorganisms are involved in oxidizing/reducing the substrates and how the microorganisms perform electron transfer reactions [33].

5.3 SYSTEMS BIOLOGY FOR UNDERSTANDING THE MECHANISM OF ELECTRON TRANSFER

Electrocatalytic activity and electron transfer characteristics are the key features of any electrochemically active microorganisms (Fig. 5.2). Hence understanding the complete mechanism of oxidation reaction in the case

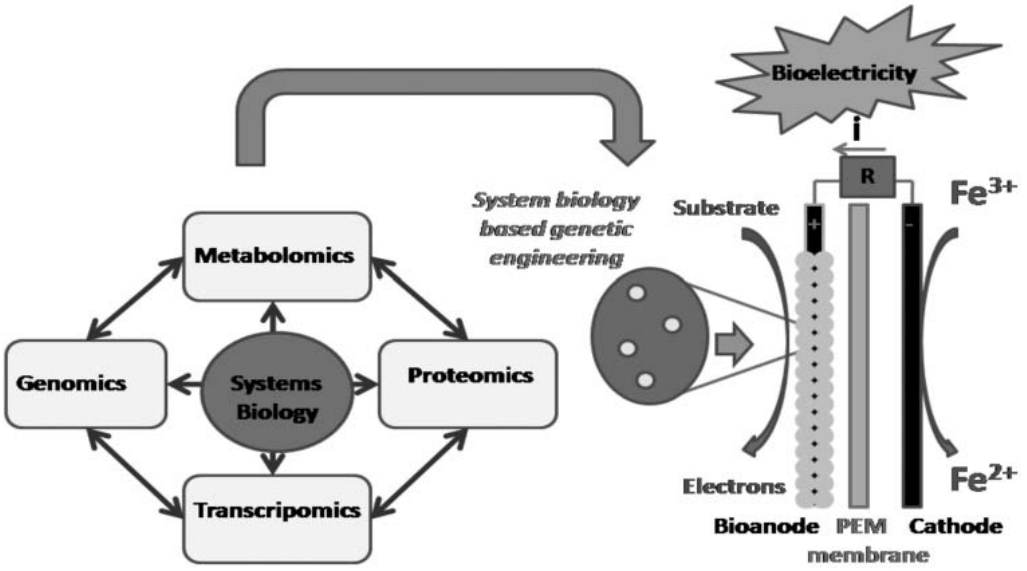

FIGURE 5.2 Developing genetic engineered microorganisms for microbial fuel cell applications.

of anodic biofilm or reduction reaction in the case of cathodic biofilm is essential. Microbial bioelectrocatalysis aids in the acceleration of the electrochemical reactions at the electrode-electrolyte interface with the aid of complex catalytic activity of the microorganisms. The electrochemical reaction aids in the transfer of electrons from the oxidation substrate to the electrode. Microorganisms differ greatly from the enzymes in their catalytic activity. Unlike enzymatic electrocatalysis that are very simple reactions, the microbial electrocatalytic reactions are very complex. The microorganisms can either perform the oxidation of substrates with a single enzyme or with the aid of a complex series of enzymes. For instance, let us look into how the microorganism catabolizes glucose. Some microorganisms are capable of producing the enzymes such as glucose oxidase or a glucose dehydrogenase. In such cases, whether the glucose oxidase or a glucose dehydrogenase enzyme are produced extracellularly or intracellularly and their catalytic rates must be investigated as these factors strongly influences the entire bioelectrochemical reactions. On the other hand, the microorganisms also have the inherent ability to perform the oxidation of glucose by the common glycolytic pathway, which involved ten different enzymes that works sequentially to finally form pyruvate.

Systems biology approaches using proteomic/genomic/transcriptomic/ metabolomic investigations might help to elucidate the mechanism of the microbial electrocatalytic reactions. There are certain enzymes such as PQQ glucose dehydrogenase that can perform both catalytic and electron transfer activities.

Investigations are also required to understand the mechanism electron transfer of the microorganisms. Microorganisms in the anodic chamber of MFCs on oxidation of the substrate transfer electrons to the anode either with the help of conductive proteins or with the help of mediators. MFCs operating with the direct electron transfer mechanism of the microorganisms are termed as mediator less MFC whereas MFCs where the shuttling of electrons happens with the aid of self-produced/externally supplemented mediators are termed as mediator based MFCs. Pham et al. [34] reported a mediatorless MFC with *Aeromonas hydrophila* for electrocatalytic activity. Karthikeyan et al. [35] reported the electrocatalytic activity of *Acetobacter aceti* and *Gluconobacter roseus*. However, in most cases, the mechanism of electron transfer from these microorganisms to the electrode is unrevealed. Microorganisms that cannot adhere to the electrode surface cannot perform direct electron transfer. To circumvent the issue, electrode modification techniques are used. However, modified electrodes did not drastically enhance the power output. Investigations on the genes involved with biofilm formation with system biology approaches will help to engineer microorganisms to perform direct electron transfer reactions. Numerous reports are available in the literature on the self produced mediators of the microorganisms used in MFC.

Freguia et al. [36] reported the use of soluble quinone excreted mediator in *Lactococcus lactis.* Fang et al. [37] documented the release of mediator such as 2,6-di-tertbutyl-p-benzoquinon (2,6-DTBBQ), as an excreted redox mediator in*K. pneumoniae strains* L17 based MFC. Mediator based MFC were reported with microorganisms such as *Erwinia dissolven, Escherichia coli, Klebsiella pneumonia, Lactobacillus plantarum* and *Proteus mirabilis* [38–40]. There are few reports in the literature on the mechanism of electron transfer mechanisms of certain well known electrochemically active microorganisms.Geobacter was reported to transfer electrons with the help of pili and cytochromes. Pili are short filamentous appendages popularly called bacterial nanowires and they

transfer the electrons with the help of pili protein. Several reports were made on the electron transfer characteristics of pili independent of c-type cytochromes. Controversial report on this was made by Liu et al. [41]. Systems biology approaches might aid in understanding the exact mechanisms. Cytochrome mediated electron transfer is reported in the case of shewanella. The microorganism might also perform direct electron transfer with the help of two different direct electron transfer mechanisms. If the microorganisms transfer the electrons to the anode by more than one electron transfer mechanism, then identifying the contribution by each mechanism will be interesting. However, such investigations are more complex and cumbersome.

The systems biology tools such as computational techniques, graph theory approaches, modeling methods will aid in developing the complete genetic/proteomic networks of the electrochemically active microorganisms of interest for investigations related electrocatalysis/electron transfer reactions. Systems biology might help to get the true and a complete picture about the electron transfer mechanisms of any microorganism of interest. System biology will enable to elucidate whether the microbe performs direct electron transfer or mediator based electron transfer or both. If the microbe is able to transfer electron directly without the help of mediators, then systems biology can be used to get the exact picture on how the direct electron transfer reaction happens in the microorganism. System biology can vividly show the role of conductive proteins of the electrochemically active bacteria such as pili or any other membrane proteins, which are involved in direct electron, transfer reactions. Systems biology approach can help to understand whether the electron transfer is possible with the help of two different types of proteins. If the electron transfer reaction can take place with the help of more than one type of protein or more than one type of mechanism, then systems biology is the perfect tool to give the details about the contribution of each type of mechanism. Another interesting point to be investigated is that how the electrocatalytic mechanisms are correlated with electron transfer reactions. Theoretically, higher electron transfer kinetics should obviously enhance the bioelectrocatalysis. Genetic maps will aid to investigate the interaction of the two different groups of genes or proteins involved in the catalysis and electron transfer reactions. But currently reductionist approaches are practiced to

understand the molecular mechanisms of electron transfer. Hence when we try to increase the one of the protein involved in electron transfer, the expression levels of the other type of electron transfer protein may go down. Hence, it is important to know complete details of the electron transfer characteristics of the microorganism. Such investigations are more essential before we can go in for a genetic engineering or a metabolic engineering of the microorganisms towards enhancing microbial electrocatalysis for microbial fuel cell applications.

5.4 SYSTEMS BIOLOGY APPROACH FOR IMPROVING THE POWER OUTPUT OF MICROBIAL FUEL CELLS

Systems biology approach can also be a suitable option for enhancing the power output of microbial fuel cells. There are a few metabolic engineering approaches for enhancing the microbial electrocatalysis for microbial fuel cell applications reported in the literature [42–44]. The use of antimycin to inhibit the ubiquinone and showed the enhancement in the power output. However, the effect of antimycin on the expression levels of different redox enzymes or conductive proteins is not explored.If such detailed investigation is made, it could really take MFC's to real time applications [43]. Hence systems biology approaches will aid to enhance either the electrocatalytic or electron transfer characteristics or both without any negative impacts on any one of the characteristics. Similarly a report was made on increasing the intracellular releasable electrons by deleting the lactate dehydrogenase gene for enhancing the power output of microbial fuel cells [45]. The increase the ratio of NADH/ NAD+ will theoretically lead to detrimental effects on the microorganisms. However, such investigations were not made/is not reported in the literature. The reductionist approaches are widely used to enhance the power output in MFC's.The molecular mechanism of bioelectricity from electroactive microorganisms is a very complex process and it involves numerous transcription and translation processes each of which are interrelated with each other in a complicated fashion as a web. Hence, current strategies based on one or few proteins cannot aid in enhancing the power output significantly.

5.5 SYSTEMS BIOLOGY APPROACHES FOR SCREENING MICROORGANISM

There are several reports in the literature on identifying the suitable microorganisms for microbial fuel cells based on their oxidation/reduction ability and their electron transfer characteristics [35] (Fig. 5.3). Currently the electrocatalytic activities of the microorganisms are analyzed widely using the electrochemical techniques such as cyclic voltammetry, amperometry, polarization studies, coulombic efficiency and impedance spectroscopy. Cyclic voltammetry (CV) is one of the most commonly used electroanalytical techniques to analyze the redox reactions of the microorganisms by applying the electrochemical potentials. The bioelectrochemical investigation of the biofilm/microorganism with the cyclic voltammetry aids to identify the reversible, quasi-reversible and irreversible electrochemical reactions. Other electrochemical techniques such as polarization and amperometric also aids in screening microorganisms based on the power output. Electrochemical impedance spectroscopy is another interesting technique helpful for the analysis of ohmic internal resistance, mass and charge transfer impedances. Unlike OMICS techniques, which are based

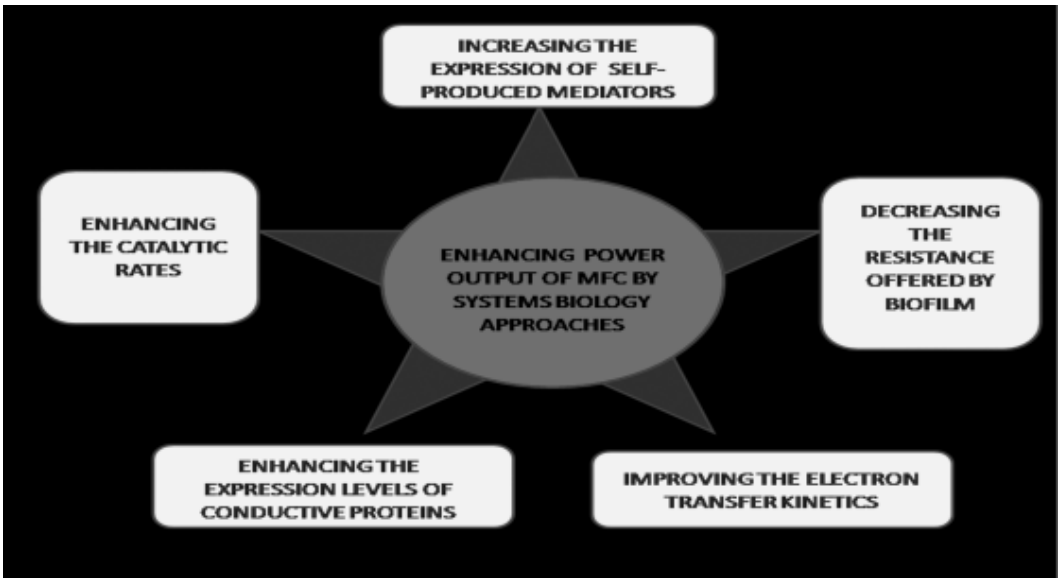

FIGURE 5.3 Routes for enhancing power output of microbial fuel cells using systems biology approaches.

on the bio-molecules such as protein, DNA, RNA or metabolites, the electrochemical techniques works based on the amount of electrons produced by the microorganisms. However, the electrochemical techniques cannot be categorized as systems biology technique or a part of it, as they do not involve molecular approaches such as genomics, proteomics, transcriptomics or metabolomics. The electrochemical techniques consider the electrocatalytic activity and electron transfer characteristics as a whole. Few genomic and proteomic investigations were also made to study the expression of certain genes/proteins from the anodic biofilm [1]. The levels of one or two proteins cannot be used as a tool for screening microorganisms because for a good electrocatalytic activity several proteins such as redox enzymes (for oxidation in the case of anodic biofilm/for reduction in the case of the reductive biofilm), conductive proteins (proteins for transferring the electron from the microorganism to the electrode such as pili, cytochromes, etc., in the case of mediator less MFC system) and the expression of mediators such as phenazine for shuttling electrons at the microbe-electrode interface. Hence systems biology approach such as a microarray by a complete investigation of several proteins/genes can be ideal tool to identify the suitable microorganism for MFC application.

5.6 FUTURE RESEARCH DIRECTIONS

Lack of proper approach for research is the key factor hindering the improvement of microbial fuel cells. Unlike other technologies, Microbial fuel cell is an interdisciplinary area where the role of physicists, materials scientists, engineers and molecular biologists is involved. But currently, more of biological approaches were not attempted. Systems biology approach is very much essential to increase the power output of MFC significantly and to improve it for commercialization. Bioinformatics techniques are now developed; however, building the models for such huge biological pathways is difficult. Hence, systems biology approaches like microarrays can be used to understand the mechanisms. Based on the data, the computational or mathematical techniques can be used to develop models for the pathways involved in electron transfer reactions.

5.7 CONCLUSION

The complete quantitative and qualitative study on the expression of all the proteins related to electrocatalytic activity and extracellular electron transfer is essential to conclude the exact electron transfer of any microorganism. Such studies can be possible only with the help of system biology approach and not by the conventional reductionist approaches. Although processing the huge volume of biological data computational techniques remains a challenging task, this can be resolved by the use of upcoming information technologies.

KEYWORDS

- **Electrode**
- **Electron transfer**
- **Microbial fuel cells**
- **Power output**

REFERENCES

1. Schröder, U. (2007). Anodic electron transfer mechanisms in microbial fuel cells and their energy efficiency. *Physical Chemistry Chemical Physics. 9,* 2619–2629.
2. Lovley, D. R. (2008). The microbe electric, conversion of organic matter to electricity. Current Opinion in Biotechnology. *19(6)*, 564–71.
3. Logan, B. E., Hamelers, B., Rozendal, R., Schröder, U., Keller, J., Freguia, S., Aelterman, P., Verstraete, W., Rabaey, K. (2006). Microbial fuel cells, methodology and technology. Environmental Science &Technology. *40*(17), 5181–5192.
4. Ahn, Y., Logan, B. E. (2013). Domestic wastewater treatment using multielectrode continuous flow MFCs with a separator electrode assembly design. *Applied Microbiology* and *Biotechnology*. *97(1),* 409–16.
5. Bhuvaneswari, A., Navanietha Krishnaraj, R., Sheela Berchmans. (2013). Metamorphosis of pathogen to electrigen at the electrode/electrolyte interface, Direct electron transfer of *Staphylococcus aureus* leading to superior electrocatalytic activity. Electrochemistry Communications. *34,* 25–28.
6. Hou, B., Sun, J., Hu, Y. (2011). Effect of enrichment procedures on performance and microbial diversity of microbial fuel cell for Congo red decolorization and electricity generation. Applied Microbiology & Biotechnology. *90(4),* 1563–72.

7. Logan, B. E., Rabaey, K. (2012). Conversion of Wastes into Bioelectricity and Chemicals by using Microbial Electrochemical Technologies. Science. 337 (6095), 686–90.
8. Yuan, Y., Chen, Q., Zhou, S., Zhuang, L., Hu, P. (2011). Bioelectricity generation and microcystins removal in a blue-green algae powered microbial fuel cell. Journal of Hazardous Materials. *187,* 591–595.
9. McCormick, A. J., Bombelli, P., Scott, A. M., Philips, A. J., Smith, A. G., Fisher, A. C., Howe, C. J. (2011). Photosynthetic biofilms in pure culture harness solar energy in a mediatorless bio-photovoltaic cell (BPV) system. Energy & Environiromental Science. *4,* 4699–4709.
10. Wilkinson, S. (2000). "Gastrobots" Benefits and challenges of microbial fuel cells in food powered robot applications. Autonomous Robots. *9,* 99–111.
11. Bond, D. R., Holmes, D. E., Tender, L. M., Lovley, D. R. Electrode-reducing micro-organisms that harvest energy from marine sediments. Science. (2002). *295,* 483–485.
12. Zhang, J., Zhang, B., Tian, C., Ye, Z., Liu, Y., Lei, Z., Huang, W., Feng, C. (2013). Simultaneous sulfide removal and electricity generation with corn stover biomass as cosubstrate in microbial fuel cells. Bioresource Technology. *138*, 198–203.
13. Luo, H., Xu, P., Roane, T. M., Jenkins, P. E., Ren, Z. (2012). Microbial desalination cells for improved performance in wastewater treatment, electricity production, and desalination. Bioresource Technology. *105,* 60–66.
14. Zhang, B. G., Zhao, H. Z., Zhou, S. G., Shi, C. H., Wang, C., Ni, J. R. (2009). A novel UASB-MFC-BAF integrated system for high strength molasses wastewater treatment and bioelectricity generation. Bioresource Technology. *100,* 5687–5693.
15. Dewan, A., Donovan, C., Heo, D., Beyenal, H. (2010). Evaluating the performance of microbial fuel cells powering electronic devices, Journal of Power Sources. *195,* 90–96.
16. Aelterman, P., Rabaey, K., Pam, H. T., Boon, N., Verstaraete, W. (2006). Continuous Electricity Generation at High Voltages and Currents Using Stacked Microbial Fuel Cells, Environmental Science &Technology. *40 (10),* 3388–3394.
17. Dewan, A., Beyenal, H., Liwandowski, Z. (2008). Scaling up Microbial Fuel Cells, Environmental Science & Technology. *42 (20),* 7643–7648.
18. Karthikeyan, R., Ganesh, V., Berchmans, S. (2012). Bio-electrocatalysis of *Aceto-bacter aceti* through direct electron transfer using a template deposited nickel anode. Catalysis Science Technology. *2(6),* 1234–1241.
19. Wei, J., Liang, P., Huang, X. (2011). Recent progress in electrodes for microbial fuel cells. Bioresource Technology. *102 (20),* 9335–9344.
20. Navanietha Krishnaraj, R., Karthikeyan, R., Berchmans, S., Saravanan Chandran, Parimal Pal. (2013). Functionalization of electrochemically deposited chitosan films with alginate and Prussian blue for enhanced performance of Microbial fuel cells. Electrochimica Acta. *112,* 465–472.
21. Liu, X. W., Sun, X. F., Huang, Y. X., Sheng, G. P., Wangand, S. G., Yu, H. Q. (2011). Carbon nanotube/chitosan nanocomposite as a biocompatible biocathode material to enhance the electricity generation of a microbial fuel cell, Environmental Science & Technology. *4,* 1422–1427.

22. Higginsa, S. R., Foerstera, D., Cheunga, A., Laua, C., Bretschgera, O., Minteera, S. D., Nealsona, K., Atanassova, P., Cooney, M. J. (2011). Fabrication of macroporous chitosan scaffolds doped with carbon nanotubes and their characterization in microbial fuel cell operation. Enzyme and Microbial Technology. *48 (6–7),* 458–65.
23. Wen, Z., Ci, S., Mao, S., Cui, S., Lu, G., Yu, K., Luo, S., He, Z., Chen, J. (2013). TiO_2 nanoparticles-decorated carbon nanotubes for significantly improved bioelectricity generation in microbial fuel cells, Journal of Power Sources. *234,* 100–106.
24. Xiao, L., Damien, J., Luo, J., Jang, H. D., Huang, J., He, Z. (2012). Crumpled graphene particles for microbial fuel cell electrodes, Journal of Power Sources. *208,* 187–192.
25. Lai, B., Tang, X., Li, H., Du, Z., Liu, X., Zhang, Q. (2011). Power production enhancement with a polyaniline modified anode in microbial fuel cells. Biosensors and Bioelectronics. *28*, 373–377.
26. Huang, L., Logan, B. E. (2008). Electricity generation and treatment of paper recycling wastewater using a microbial fuel cell. Applied Microbiology Biotechnology. *80*, 349–55.
27. Amutha, R., Josiah, J. J. M., Adriel Jebin, J., Jagannathan, P., Sheela Berchmans. (2010). Chromium hexacyanoferrate as a cathode material in microbial fuel cells, Journal of Applied Electrochemistry. *40,* 1985–1990.
28. Logan, B. E. (2009). Exoelectrogenic bacteria that power microbial fuel cells. Nature Reviews Microbiology. *7,* 375–381.
29. Liang, S., Wenzhao, J., Changjun, H., Yu, L. (2011). Microbial biosensors, A review, Biosensors and Bioelectronics. *26(5),* 1788–99.
30. Dhar, P. K., Zhu, H., Mishra, S. K. (2004). Computational approach to systems biology, from fraction to integration and beyond. IEEE Trans Nanobioscience. *3(3),* 144–52.
31. Friboulet, A., Thomas, D. (2005). Systems Biology-an interdisciplinary approach. Biosensors and Bioelectronics. *20 (12),* 2404–2407.
32. Johnson, C. G., Goldman, J. P., Gullick, W. J. (2004). Simulating complex intracellular processes using object-oriented computational modeling. Progress in *Biophysics & Molecular Biology*. *86 (3),* 379–406.
33. Kholodenko, B. N., Bruggeman, F. J, Sauro, H. M. (2005). Mechanistic and modular approaches to modeling and inference of cellular regulatory networks. Systems BiologyTopics in Current Genetics. *13,* 143–159.
34. Pham, C. A., Jung, S. J., Phung, N. T., Lee, J., Chang, I. S., Kim, B. H., Yi, H., Chun, J. (2003). A novel electrochemically active and Fe (III) -reducing bacterium phylogenetically related to *Aeromonas hydrophila*, isolated from a microbial fuel cell. FEMS Microbiology Letters. *223*, 129–134.
35. Karthikeyan, R., Sathish kumar, K., Murugesan, M., Sheela Berchmans; Yegnaraman, V. (2009). Bioelectrocatalysis of *Acetobacteraceti* and *Gluconobacter roseus*-for Current Generation, Environmental Science & Technology. *43 (22),* 8684–8689.
36. Freguia, S., Masuda, M., Tsujimura, S., Kano, K. (2009). *Lactococcus lactis* catalyzes electricity generation at microbial fuel cell anodes via excretion of a soluble quinone. Bioelectrochemistry. *76*, 14–18.

37. Fang, D. L., Bai, L. F., Gui, Z. S., Yin, H. D., Ren, N. J. (2010). A study of electron-shuttle mechanism in Klebsiella pneumoniae based-microbial fuel cells, Chinese science bulletin. *55*, 99–104.
38. Vega, C. A., Fernandez, I. (1987). Mediating effect of ferric chelate compounds in microbial fuel cells with *Lactobacillus plantarum*, *Streptococcus lactis*, and *Erwinia dissolvens*. Bioelectrochemistry & Bioenergetics. *17*, 217–222.
39. Fang, D. L., Bai, L. F., Gui, Z. S., Yin, H. D., Ren, N. J. (2010). A study of electron-shuttle mechanism in *Klebsiella pneumoniae* based-microbial fuel cells, Chinese science bulletin. *55*, 99–104.
40. Choi, Y., Jung, E., Kim, S., Jung, S. (2003). Membrane fluidity sensoring microbial fuel cell. Bioelectrochemistry. *59*, 121–127.
41. Liu. X., Tremblay. P. L., Malvankar. N. S., Nevin. K. P., Lovley. D. R., Vargas, M. (2013). *Geobacter sulfurreducens* Strain Expressing *Pseudomonas aeruginosa* Type IV Pili Localizes OmcS on Pili but is Deficient in Fe (III) Oxide Reduction and Current Production. Doi: 10. 1128/AEM. 02938-13.
42. Fishilevich, S., Amir, L., Fridman, Y., Aharoni, A., Alfonta, L. (2009). Surface Display of Redox Enzymes in Microbial Fuel Cells, Journal of American Chemical Soceity. *131*(34), 12052–12053.
43. Szczupak, A., Kol-Kalman, D., Alfonta, L. (2012). A hybrid biocathode, surface display of O_2-reducing enzymes for microbial fuel cell applications. Chemical Communications. *48,* 49.
44. Alfonta. L. (2010). Genetically Engineered Microbial Fuel Cells, Electroanalysis. *22,* 822–831.
45. Yong, Y.-C., Yu, Y.-Y., Yang, Y., Li, C. M., Jiang, R., Wang, X., Wang, J. Y., Song, H. (2012). Increasing intracellular releasable electrons dramatically enhances bioelectricity output in microbial fuel cells. Electrochemistry Communications. *49 (91),* 10754–10756.

PART 3

BIOETHANOL PRODUCTION

CHAPTER 6

POTENTIALS OF *OSCILLATORIA ANNAE* IN PRODUCING BIOETHANOL BY DEGRADATION OF SELECTED LIGNOCELLULOSICS

P. MALLIGA,* V. VISWAJITH, D. MALINI, and R. SABITHA

D. Malini, Research scholar, Dept. of Marine Biotechnology and R. Sabitha, Research scholar, Dept. of Biomedical Sciences,

**Professor, Department of Marine Biotechnology,*
Bharathidasan University, Tiruchirappalli–620024, Tamilnadu

CONTENTS

6.1 Introduction 144
6.2 Materials and Methods 146
6.2.1 Lignocellulosic Materials 146
6.2.2 Microorganism and Culture Conditions 146
6.2.3 Bioethanol Production 147
6.3 Results and Discussion 149
6.3.1 Optimization of Acid Hydrolysis and Temperature 149
6.3.2 Detoxification 158
6.3.3 Fermentation of Acid Hydrolysates 159
6.4 Conclusion 166
Keywords 167
References 167

ABSTRACT

Globally, lignocellulosic materials are considered to be the most abundant renewable source available throughout the world in large quantities for the production of ethanol. The agroeconomic perspective, the present study targeted to exploit the ability of cyanobacteria to convert lignocellulosics for ethanol production. Lignocellulosic materials, coir pith, *Prosopis juliflora* and *Lantana camara L.* were allowed to treat with fresh water cyanobacterium (*Oscillatoria annae).* Bioconversion of lignocellulosics to ethanol requires initial dilute acid hydrolysis and fermentation of yeast (*Pichia stipitis*). At 36th hour, the *O. annae* treated *L. camara* produced maximum ethanol yield of 0.41 g/g (9.36 gL^{-1}). This was succeeded by the *O. annae* treated *P. juliflora* ethanol yield of 0.42 g/g (9.022 gL^{-1}) and least amount of 0.474 g/g (4.32 gL^{-1}) was obtained with *O. annae* treated coir pith. Hence, the *O. annae* treated lignocellulosics rendered higher amount of ethanol as compared with the fermentation of yeast (*P. stipitis*) alone. Thus, the study clearly evidenced that the *O. annae* degrades lignocellulosic and making it a better source for ethanol production by yeast (*P. stipitis*) fermentation.

6.1 INTRODUCTION

Energy consumption has increased steadily over the last century as the world population has grown and more countries have become industrialized. Bioethanol can also be important in helping meet the growing demand for energy in the developing world as these countries improve the living standards of more and more people [1]. In spite of, ethanol production only uses energy from renewable sources and it plays an important role in the reduction of greenhouse gas emissions. Hence, no net carbon dioxide is added to the atmosphere, making ethanol an environmentally beneficial energy source [2, 3]. Nigam [4] scrutinized the ethanol production from wheat straw hemicellulose hydrolysate by *Pichia stipitis* and reported a maximum yield of 0.41 ± 0.01 g_p, g_s^{-1} ($g_{ethanol}$, g_{sugar}), equivalent to $80.4 \pm 0.55\%$ theoretical conversion efficiency. The route of bioethanol production from lignocellulosic material such as cereal

straw and corn stover has also been reported [5, 6]. Bioethanol production has been running for several years, improvements are required to increase process performance [7]. The choice of the best technology for lignocellulose to bioethanol conversion should be decided on the basis of overall economics (lowest cost), environmental (lowest pollutants) and energy (higher efficiencies). Deplorably, much lignocellulose waste is often disposed of by biomass burning, which is not restricted to underdeveloped countries alone, but is considered a global phenomenon [8]. In India, lignocellulosic biomass (crop residues, forestry and fruit and vegetable waste and weeds) is available in plenty. Renewable fuels particularly ethanol should get more and more attention all over the world. *Lantana camara* is an important non-edible lignocellulosic biomass, which grows widely throughout India. It contains high cellulose and no competition with the food chain makes it an ideal substrate for bioethanol production [9, 10]. *Prosopis juliflora* or mesquite is a drought resistant, grows in semiarid and arid tracts of tropical and subtropical regions of the world and is spreading fast because the leaves are unpalatable and animals do not digest its seed [11]. Aqeel [12] investigated the antidermatophytic activity of juliflorine and a benzene insoluble alkaloidal fraction obtained from *P. juliflora* against *Trichophyton mentagrophytes* infection in rabbits. The waste products of coir yarn industry are coir dust and coir pith or coco peat which is the waste obtained from the coconut (*Coccus nucifera* Linn.), which constitute about 70% of the husk. In spite of their limited use as soil conditioners, the quantity of coir dust produced is so enormous making its disposal difficult because of its lignocellulosic nature and slow degradation in the natural environment [13]. Degradation of coir pith can be effectively done with suitable species of Basidiomycetes fungus (*Pleurotus sajor caju*) and in combination with nitrogen fixing bacteria. Bacterial isolates from compost or soil, namely *Azotobacter*, *Bacillus megatarium* and *Serratia marcescens*, were capable of decolorizing or solubilizing industrial lignin [14, 15]. Ligninolytic fungi are well known, not only as decomposers of lignin but also for their ability to degrade a wide variety of organopollutants [16]. Cyanobacteria are capable of abating various kinds of pollutants and have been used in the production of energy, fertilizer [17]. Moreover, technologies for producing bioethanol

from seaweed or marine cyanobacteria have been reported, a method for producing ethanol using freshwater cyanobacteria has yet not to be reported [18]. Therefore, the intention of this study aimed to use fresh water cyanobacterium (*O. annae*) and yeast (*P. stipitis)* for the production of bioethanol by using three-lignoicellulosic materials coir pith, *L. camara* and *P. juliflora*. This study also delineates the comparative effect of bioethanol production with yeast (*P. stipitis).*

6.2 MATERIALS AND METHODS

6.2.1 LIGNOCELLULOSIC MATERIALS

Coir pith, a waste by-product of coir rope industry was collected from coir industries near Srirangam, Tiruchirappalli, Tamilnadu, India. Woody stems of *Prosopis juliflora* and *Lantana camara*, were obtained from Bharathidasan University campus, dried and ground to pass a 0.5 mm screen.

6.2.2 MICROORGANISM AND CULTURE CONDITIONS

Fresh water cyanobacterium was grown and maintained in BG11 medium [19] under white fluorescent light of 13.8 μE m^{-1} s^{-1} at 25 ±2°C with 14/10 D/L cycle. It was grown along with lignocellulosics (coir pith, *P. juliflora* and *L. camara*) separately at a dry weight ratio of 1:10 (cyanobacteria: lignocellulosics) in BG11 medium for 15 days. Large-scale cultivation of *O. annae* was carried out initially in boxes, tanks and further increased to pits dug on ground and covered with polythene sheets. Cyanobacteria with coir pith, *P. juliflora* and *L. camara* was inoculated in separate pits in urea media. After 15 days of incubation, the degraded wood materials were collected and separated from cyanobacterial mat and air-dried for further use as source for bioethanol.

Pichia stipitis NCIM 3498 was obtained from the collection of National Chemical Laboratory, Pune, India. *P. stipitis* culture was maintained in a medium containing peptone 2.0 gL^{-1}, yeast extract 2.0 gL^{-1}, $(NH)_2SO_4$ 3.0 gL^{-1}, KH_2PO_4 2.0 gL^{-1}, $MgSO_4$ 1.0 gL^{-1} and xylose 10.0 gL^{-1}.

6.2.3 BIOETHANOL PRODUCTION

6.2.3.1 Acid Hydrolysis

Dilute acid hydrolysis method by using H_2SO_4 was used for the saccharification process. Varying concentration of sulfuric acid (0.75, 1.5, 2.25, 3.0 and 3.75% v/v) was tested for the maximum release of sugars from the wood materials. Dilute acid hydrolysis was combined with heat for enhancing the release of sugars from the wood. Each concentration of dilute acid hydrolysis was combined with three different temperatures (100, 120 and 140°C) for 1 h using a special Russian autoclave.

6.2.3.2 Detoxification Methods

In order to decrease the toxicity for *P. stipitis*, considerable efforts have been focused on detoxification procedure prior to fermentation, including neutralization, overliming and overliming combined with activated charcoal.

6.2.3.3 Neutralization

Calcium hydroxide was added to the dilute acid hydrolysate to increase the pH to 5.8 and the mixture was stirred for 30 min. It was then filtered to remove any precipitate formed before using as substrate for fermentation [20].

6.2.3.4 Overlimiting

Calcium hydroxide was added to the dilute acid hydrolysate to increase the pH to 10.5 and the whole mixture was stirred for 30 min. It was then filtered and the pH was adjusted to 5.8 using 2N H_2SO_4. The sample was once again filtered and the pH was brought to 5.8 using 2N H_2SO_4 [21].

6.2.3.5 Overlimiting Combined With Activated Charcoal

Calcium hydroxide was added to the dilute acid hydrolysate to increase the pH to 10.5 and the whole mixture was stirred for 30 min. It was then filtered and 1% activated charcoal was added and stirred for 20 min. It was once again subjected to filtration [22].

6.2.3.6 Analytical Methods

Samples were withdrawn periodically to determine biomass of yeast (*P. stipitis*) cell mass, for reducing sugars and ethanol in the broth.

6.2.3.7 Reducing Sugar Estimation

According to Miller [23], 1 mL of sample (*O. annae* untreated, treated lignocellulosics), 1 mL of reagent (100 mL distilled water and 1 g Dinitrosalicylic acid (DNSA), 20 mL 2N NaOH, 30 g of Rochella (NaK tartrate)) was added. The tubes were kept in boiling water bath for 10 min. After cooling it was made up to 10 mL by adding distilled water. Absorbance was measured spectrophotometrically at 540 nm. Concentration of sugar was determined by computing optical density against the standard curve, prepared using sugar (glucose) concentration from 10–100 µg/mL.

6.2.3.8 Estimation of Total Phenolics

Two hundred and 50 µL of Folin-Ciocalteu reagent was added to 50 µL of test sample (*O. annae* untreated, treated lignocellulosics). The mixture was vortexed well and 750 µL of 20% sodium carbonate was added and the final volume of the mixture was made to 5 mL using distilled water. The mixture was incubated in dark at room temperature for 1 hr. The absorbance was read at 760 nm against blank containing distilled water instead of test sample. The standard curve was prepared using vanillin (50–500 µg/mL) [24].

6.2.3.9 Ethanol Production and Yeast Fermentations

Fermentation studies started with 3.5% (v/v) of *P. stipitis* inoculum. Ethanol fermentations by *P. stipitis* were evaluated at 30 °C in 500 mL Erlenmeyer flasks containing 100 mL appropriate media in a shaker at 150 rpm. To determine the dry weight of yeast cells, the homogenized cell suspension (1 mL) was centrifuged (10,000rpm.) in preweighed eppendorf. The cell pellets were rinsed with sterilized distilled water, recentrifuged at 10,000rpm and dried till became, constant weight at 60 °C. All the experiments were carried out in triplicates.

6.2.3.10 Ethanol Estimation

Ethanol was estimated by gas chromatography (GC) (Perkin Elmer, Clarus 500) with an elite-wax (cross bond-Poly ethylene glycol) column (30 m × 0.25 mm) at 120°C, flame ionization detector at 210°C and injector at 180°C using isopropanol as standard. The carrier gas was nitrogen (N_2). Followingly, 0.2 µL of sample was injected into the column for estimation.

6.3 RESULTS AND DISCUSSION

Lignocellulosic waste technological developments can help to move the price of bioethanol closer to or even less than that of petroleum- based fuel. The use of ethanol as an alternative motor fuel has been steadily increasing around the world for a number of reasons. Domestic production and use of ethanol for fuel can increase dependency on foreign oil, reduce trade deficits, create jobs in rural areas, and reduce global climate change and carbon dioxide buildup [25].

6.3.1 OPTIMIZATION OF ACID HYDROLYSIS AND TEMPERATURE

Several inhibitory compounds are formed during acid hydrolysis of lignocellulosic materials. Such compounds are divided into four groups:

(a) sugar degradation products including furfural and hydroxymethylfurfural; (b) lignin degradation products including several aromatic and polyaromatic compounds; (c) substances released from the hemicellulosic structure, including acetic acid, terpenes and tannins; and (d) metals released from equipment like chromium, copper, iron and nickel [26]. Optimization of acid hydrolysis for the maximal release of reducing sugars was carried out using sulfuric acid (H_2SO_4) at varying concentrations (0.75, 1.5, 2.25, 3.25 and 3.75% v/v) and at variable temperatures (100, 120 and 140°C) for 1 h. The effect of operation variables namely temperature and acid concentration were studied for the maximum sugar recovery from the lignocellulosic substrates (both untreated and *O. annae* treated coir pith, *P. juliflora* and *L. camara*). The concentration of total reducing sugars varied systematically for all the hydrolysis conditions carried out.

Acid hydrolysis leads to the higher amount of sugars in shorter time and it also commercially viable process. During acid hydrolysis of lignocellulosics, aliphatic acids (acetic, formic and levulinic acid), furan derivatives [furfural and 5-hydroxymethylfurfural (HMF)] and phenolic compounds are formed in addition to the sugars. These compounds are known to inhibit ethanol fermentation performance [27, 20]. Therefore, in order to improve the fermentability and quality of the hydrolysates, it is necessary to remove the toxic compounds prior to fermentation. Various methods of detoxification such as neutralization, overliming with calcium hydroxide ($Ca(OH)_2$) and overliming combined with activated charcoal were employed for this purpose. Irrespective of the temperature chosen all the three substrates showed an increase amount of sugar and were concentration dependent, of the three substrates subjected to pretreatments *O. annae* treated *P. juliflora* could release higher amount of sugars whereas the least was noticed with coir pith (Figs. 6.1A–6.1C).

The release of phenols with the three substrates noticed were with reference to temperature, though the phenol release was concentration dependent as far as the acid treatment is considered the maximum phenolic release observed at 140°C with *O. annae* treated coir pith (Figs. 6.2A–6.2C).

Figures 6.1–6.3 depict the phenolics released from untreated and *O. annae* treated lignocellulosics at various temperatures when treated with

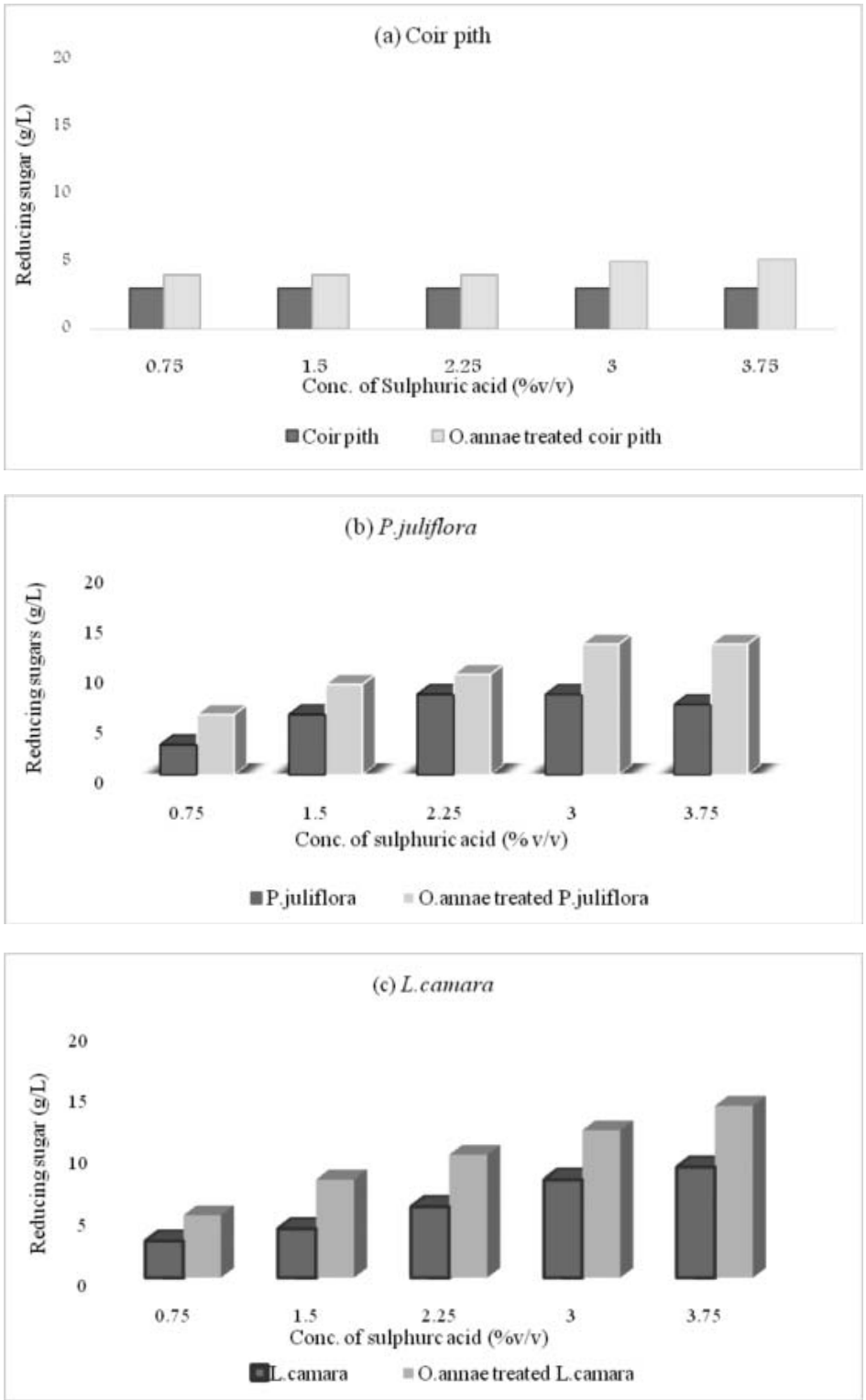

FIGURE 6.1A Effect of thermochemical pretreatment (H_2SO_4, 100°C, 1 hr) on release of reducing sugars from selected lignocellulosics.

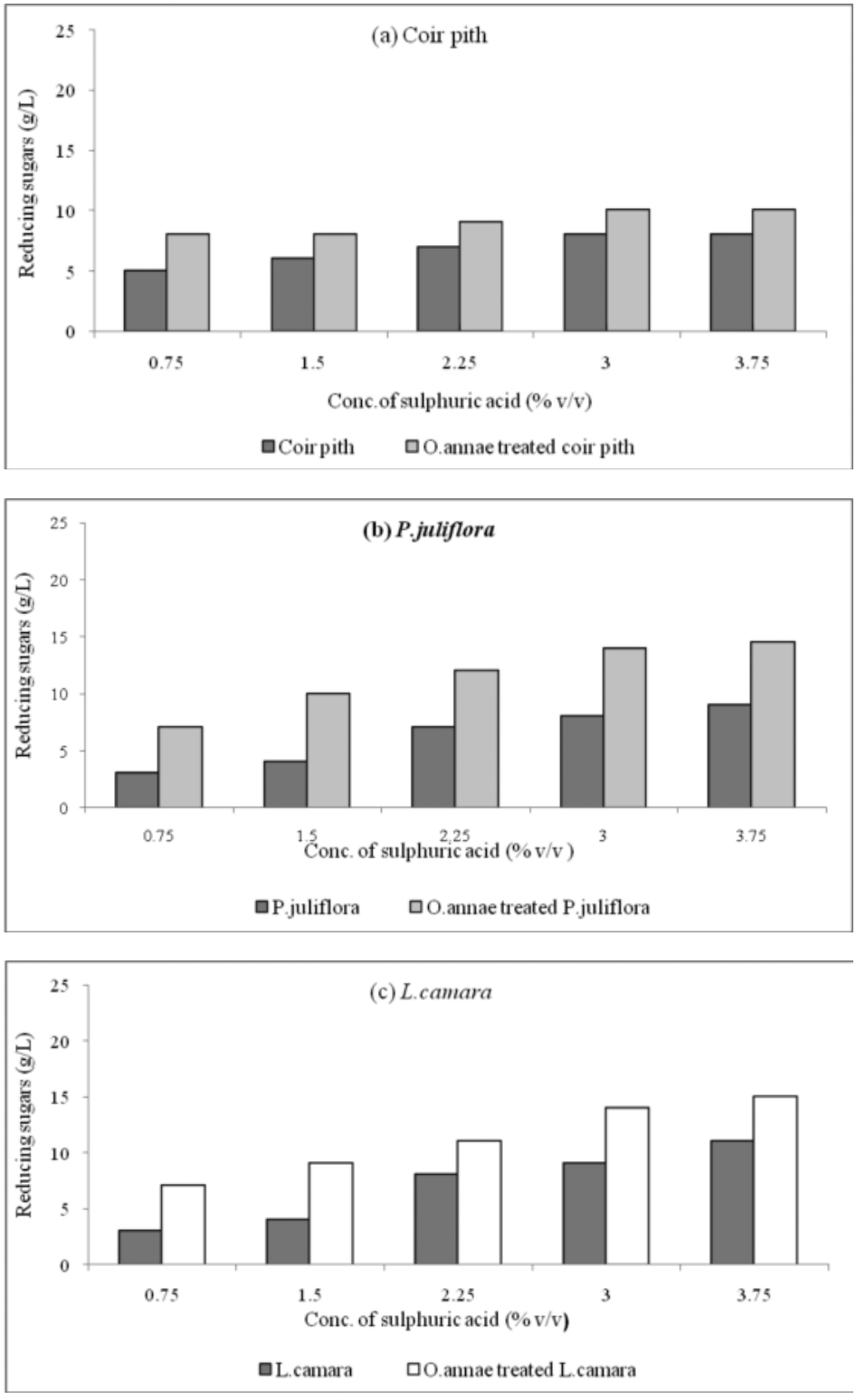

FIGURE 6.1B Effect of thermochemical pretreatment (H_2SO_4, 120°C, 1 hr) on release of reducing sugars from selected lignocellulosics.

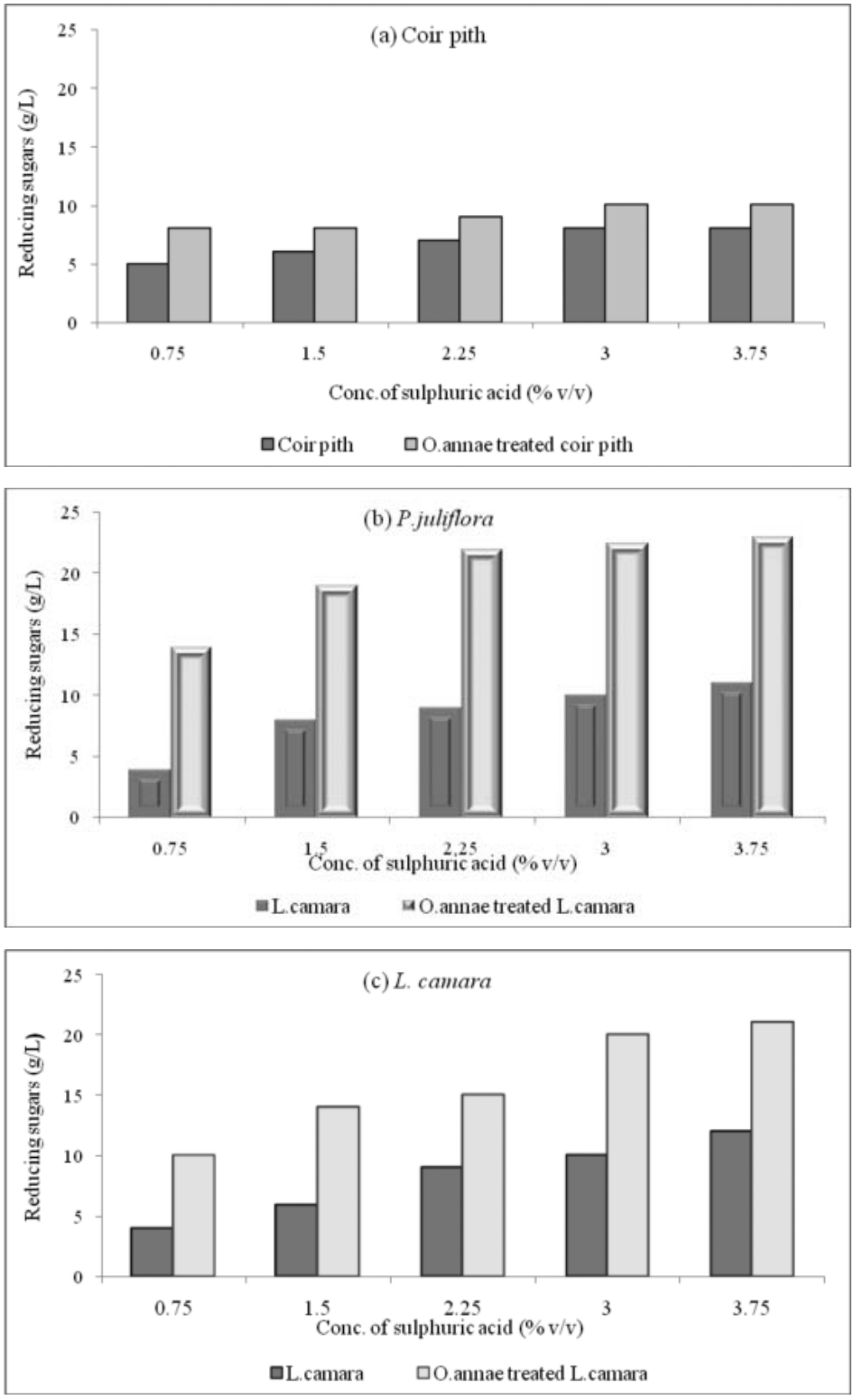

FIGURE 6.1C Effect of thermochemical pretreatment (H_2SO_4, 140°C, 1 hr) on release of reducing sugars from selected lignocellulosics.

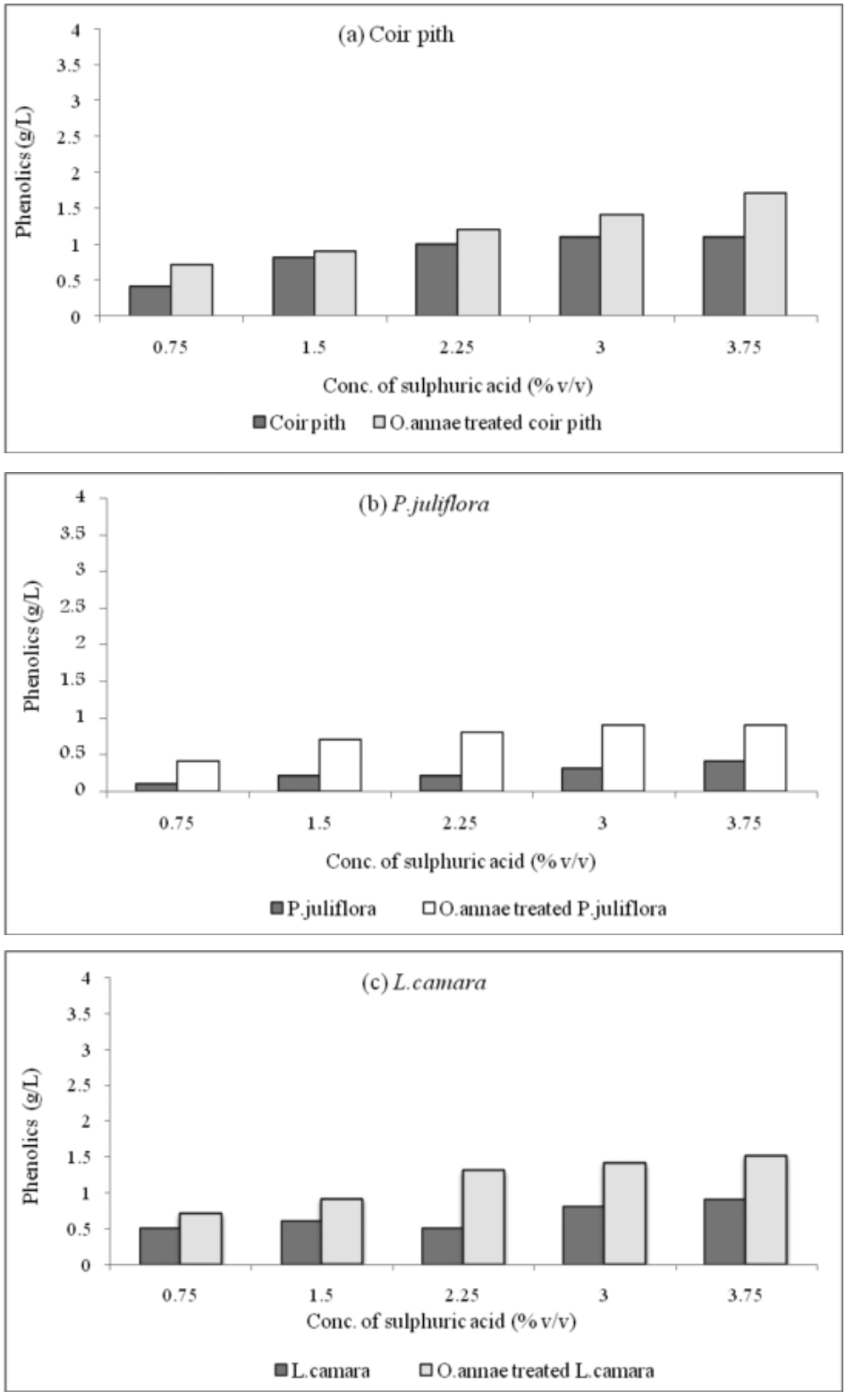

FIGURE 6.2A Effect of thermochemical pretreatment (H_2SO_4, 100°C, 1 hr) on release of phenolics from selected lignocellulosics.

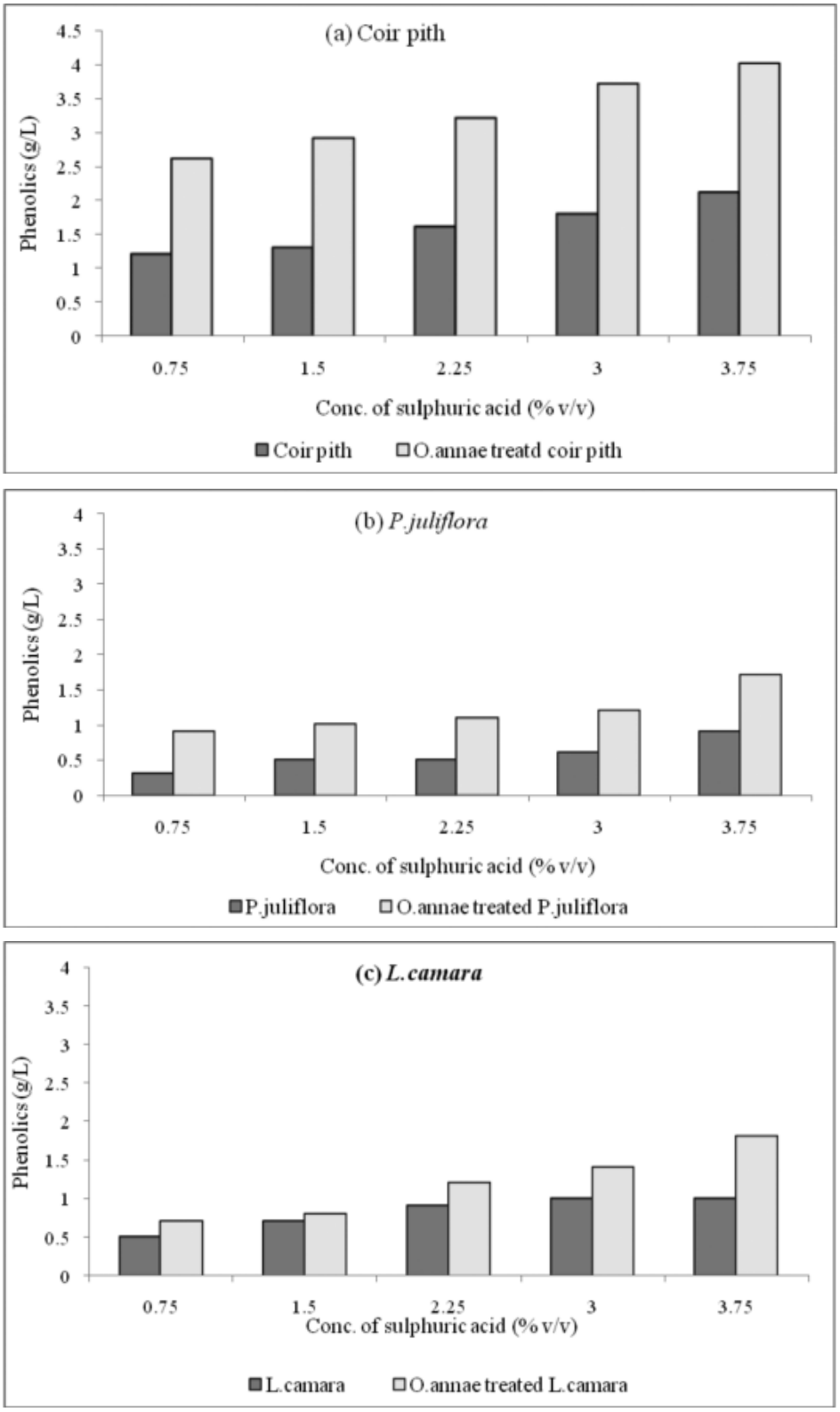

FIGURE 6.2B Effect of thermochemical pretreatment (H_2SO_4, 120°C, 1 hr) on release of phenolics from selected lignocellulosics.

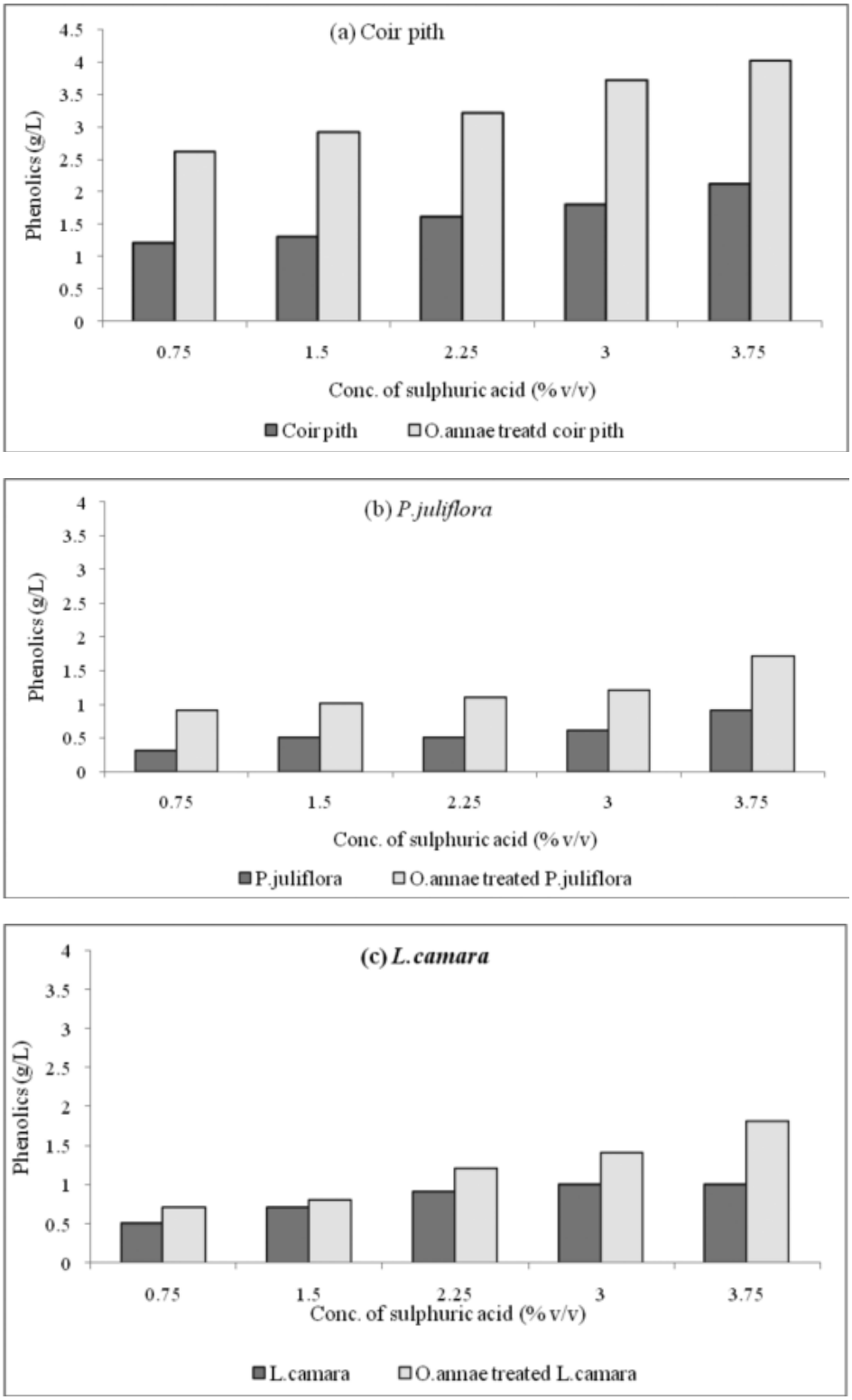

FIGURE 6.2C Effect of thermochemical pretreatment (H_2SO_4, 140°C, 1 hr) on release of phenolics from selected lignocellulosics.

varied concentrations of H_2SO_4. Primarily, all the following lignocellulosic materials were treated with O. annae. The maximum phenolics yield was obtained from *O. annae* treated coir pith 3.9 ± 0.2 gL^{-1} followed by *O. annae* treated *L. camara* 1.67 ± 0.04 g L−1 and *P. juliflora* 1.6 ± 0.08 gL^{-1} with 3.75% v/v H_2SO_4 at 140 °C for 1 hr. Among the control untreated lignocellulosics coir pith produced maximum reducing sugar of 2.1 ± 0.08 g L^{-1} followed by *L. camara* 0.97 ± 0.03 gL^{-1} and *P. juliflora* 0.84 ± 0.03 gL^{-1} with 3.75% v/v H_2SO_4 in 1 hr at 140 °C.

Though concentrated acids such as H_2SO_4 and HCl have been used to treat lignocellulosic materials dilute acid hydrolysis has been successfully developed for the hydrolysis of lignocellulosic materials. At moderate temperature, direct saccharification offered from low yields because of sugar decomposition. High temperature (300 °C) in dilute acid treatment is favorable for cellulose hydrolysis [28]. Recently developed dilute acid hydrolysis processes use less severe conditions and achieve high xylan to xylose conversion yields. Achieving high xylan to xylose conversion yields is necessary to achieve favorable overall process economics because xylan accounts for up to a third of the total carbohydrate in many lignocellulosic materials [29].

Dilute acid hydrolysis is employed for depolymerization of hemicellulosic polymer into its monomeric constituents mainly in the form of xylose. The maximum sugar yield (25.0 gL^{-1}) was achieved at 140°C, 3.5% (v/v) H_2SO_4 for 1h in the present investigation. Previous reports of recovered sugars yield from hemicellulose hydrolysis of birch and spruce [30]. Also, closely agree with those found in the present study. The acid hydrolysis using 3.75% H_2SO_4 released maximum amount of reducing sugars in both control and test samples at 140°C for 1 hr. Hence, 3.75% H_2SO_4 for 1 hr at 140°C was considered as optimum for maximum release of reducing sugars from the selected lignocellulosic materials though there have been significant differences between the release of sugars between lignocellulosic materials and the concentration of acid treatment within the lignocellulosic materials. It has been reported that the cell wall structure and components may be significantly different in plants, which may influence the biomass digestibility resulting in variation in the release of reducing sugar [31, 32].

6.3.2 DETOXIFICATION

The neutralization of acid hydrolysate by increasing the hydrolysate pH up to fermentable pH (5.8) required for yeast growth caused reduction in total phenolics (28.22%).

Overliming of acid hydrolyzates using calcium hydroxide resulted in decrease of total phenolics up to 58.13%. Increasing the pH to 10.5 by $Ca(OH)_2$ and readjustment to 6.5 with H_2SO_4 caused detoxification of lignocellulosic hydrolysate. The detoxifying effect of overliming is due to, both (a) precipitation of toxic components and (b) instability of some inhibitors at high pH. A critical issue in the conversion of dilute acid hydrolysates has been the ability to withstand inhibitors [26] and most often a detoxification step is needed to improve the fermentation efficiency. However, the introduction of a detoxification step increases the process complexity and may give precipitation problems [4].

More recently, Chandel [20] also observed similar results while detoxifying sugarcane baggase hemicellulose hydrolysate. According to Roberto [33], pH adjustment with a combination of bases and acids is a low-cost treatment that gives good results. By adjusting the pH of sugarcane bagasse hemicellulosic hydrolyzate first to 10.0 with $Ca(OH)_2$ and then to 6.5 with H_2SO_4, these authors obtained a partial removal of phenolic and other compounds and a xylitol yield of 0.48 g/g. Van Zyl [34] adjusted the pH of sugarcane bagasse hemicellulose hydrolyzate first with $Ca(OH)_2$ and then with NaOH and found that the former treatment enhanced the hydrolyzate fermentability, whereas the latter increased the precipitation of toxic compounds. Martinez [21] reported that using $Ca(OH)_2$ to adjust the pH of sugarcane bagasse hemicellulose hydrolysate (overliming treatment) to 9.0, proved to be a very efficient detoxification method. The fermentability of a corncob, acid-hydrolysates hemicellulose was considerably increased from an ethanol yield of 0.21 g/g to 0.32 g/g [35].

Among the known detoxification methods activated charcoal treatment reduces all class of fermentation inhibitors from hydrolysate because it has high capacity to adsorb toxic compounds. Thus, the combined treatment brought about reduction of 75.28% total phenolics from acid hydrolysates.

6.3.3 FERMENTATION OF ACID HYDROLYSATES

A typical fermentation profile of *P. stipitis* NCIM 3498 in batch culture using sugars from acid hydrolysate of untreated and *O. annae* treated coir pith, *P. juliflora* and *L. camara* (Figs. 6.3A–C and 6.4A–C) has been shown. The ethanol production level reached a maximum at 36th hour of incubation. The ethanol yield and productivity of control and test samples of the respective lignocellulosics were compared.

The untreated and *O. annae* pretreated (acid) hydrolysates were used for ethanol production separately in batch mode of cultivation. The fermentation of different types of hydrolysate showed distinct characteristics due to the differences in the initial concentration of sugars and the level of different fermentation inhibitors present in hydrolysates. With respect to the hydrolysate fermentation, it can be observed that the sugar consumption rate ranged from 80 to 94%, irrespective of initial concentration of sugars in medium. However, the amount of ethanol production varied significantly. The reason could be the difference in level of fermentation inhibitors present in hydrolysate even after the detoxifications. These inhibitors affect the ethanol production efficiency of yeast. Data indicates that the rate of sugar consumption, biomass production rate and ethanol production rates was much higher upon fermentation of *O. annae* pretreated and acid hydrolyzed (Table 6.1).

Variety of yeasts (*Brettanomyces, Candida, Clavispora, Kluvyveromyces, Pachysolen, Pichia* and *Schizosaccharmoyces*) has been used for ethanol production using xylose as carbon source. Among these, *Pichia stipitis* has shown promise for industrial application as it ferments xylose rapidly with a high ethanol yield (0.47 g/g) and production (22.3 g L^{-1}) [36] with insignificant amount of xylitol (0.03 gL^{-1}) [37]. Furthermore, *P. stipitis* has no absolute vitamin requirement for xylose fermentation [38, 39].

A typical fermentation profile of *P. stipitis* NCIM 3498 in batch culture is shown in Figs. 6.7 and 6.8. Bioethanol production from *O. annae* treated lignocellulosics was distinctly higher when compared to the untreated lignocellulosics. Among the lignocellulosics studied a maximum ethanol production of 9.36 gL^{-1} with 0.41 g/g ethanol yield and

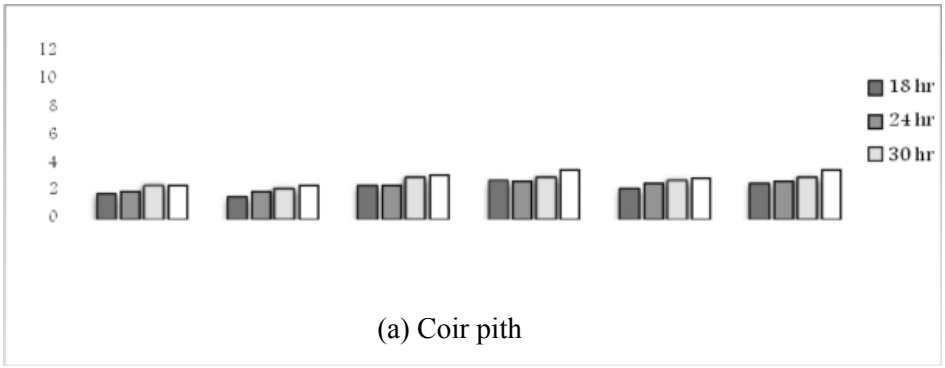

(a) Coir pith

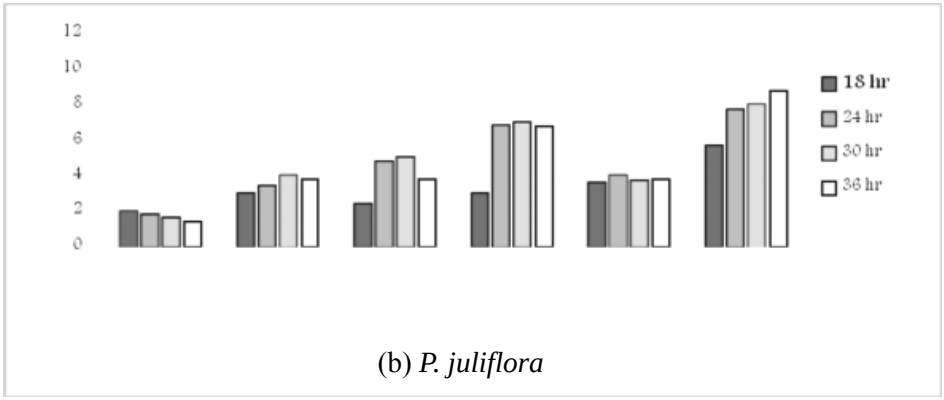

(b) *P. juliflora*

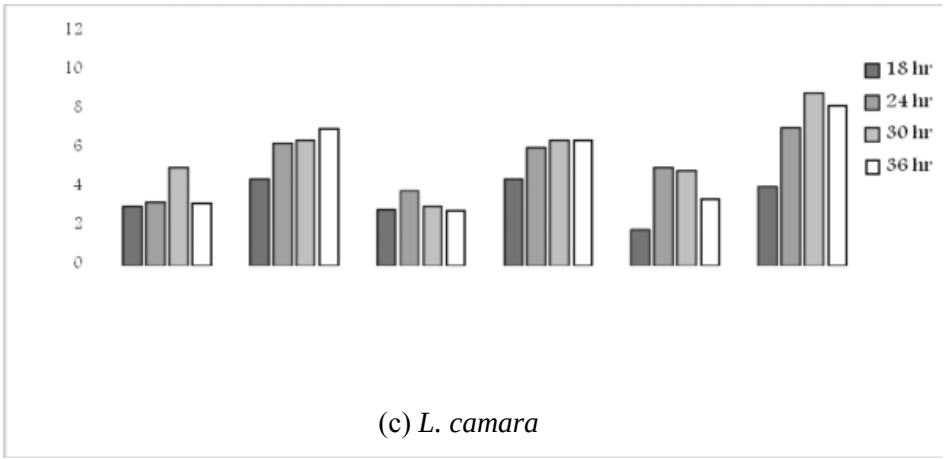

(c) *L. camara*

FIGURE 6.3 Effect of detoxification on untreated lignocellulosic hydrosylates on ethanol production by *P. stipitis* NCIM 3498.

0.26 $gL^{-1}hr^{-1}$ ethanol productivity was obtained from *O. annae* treated *L. camara* hydrolysate at 36th hour. This was followed by the *O. annae* treated *P. juliflora* bioethanol production of 9.022 gL^{-1} with 0.42 etha-

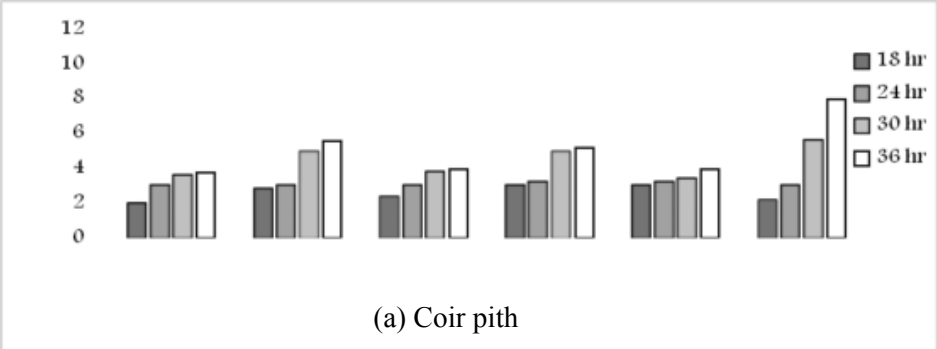

(a) Coir pith

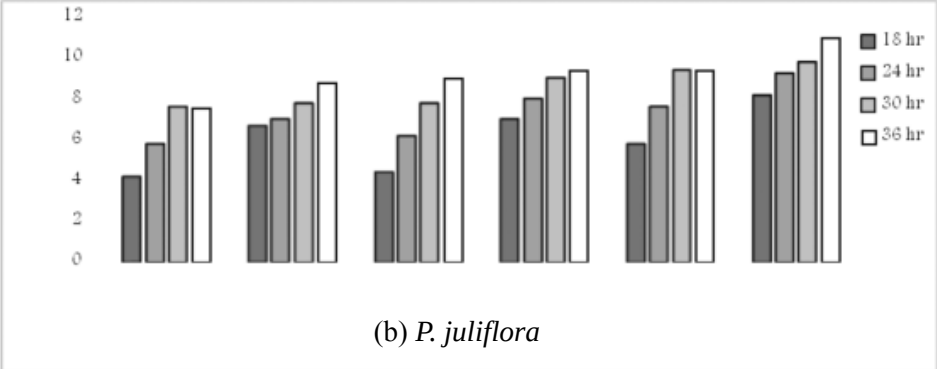

(b) *P. juliflora*

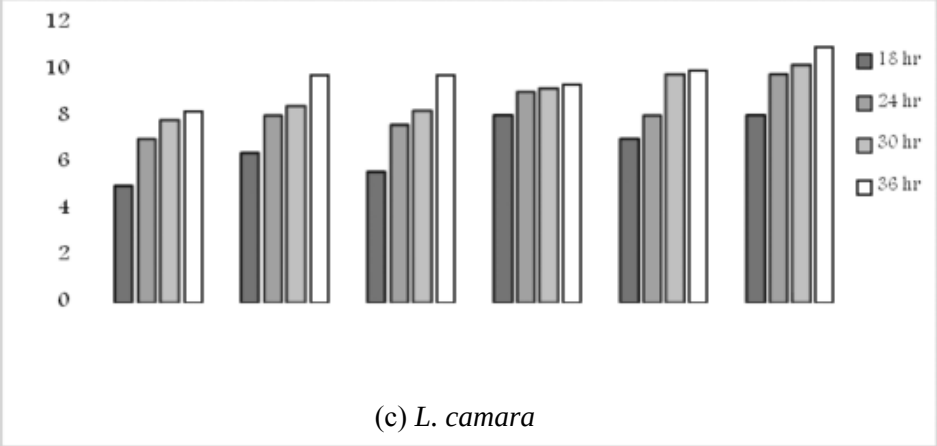

(c) *L. camara*

FIGURE 6.4 Effect of detoxification on *O.annae* treated lignocellulosic hydrolysates on ethanol production by *P. stipitis* NCIM 3498.

nol yield and ethanol productivity of 0.25 g $L^{-1}hr^{-1}$ at 36th hour. Among the test samples least amount of bioethanol production was obtained from *O. annae* treated coir pith 4.32 gL^{-1} and ethanol yield of 0.474 gL^{-1} and productivity of 0.114 $gL^{-1}hr^{-1}$. Statistical analysis showed that the etha-

TABLE 6.1 Effect of Detoxification on Untreated and *O.annae* Treated Lignocellulosic Hydrolysates for Ethanol and Biomass Yield

Samples	Method	Ethanol yield (g/g)	Biomass yield (g/g)
Untreated coir pith	Neutralization,	0.3823	0.147
	Overliming,	0.444	0.5455
	Overliming + Activated Charcoal (AC)	0.456	0.585
O.annae treated Coir pith	Neutralization,	0.416	0.591
	Overliming,	0.428	0.616
	Overliming + Activated Charcoal (AC)	0.474	0.675
Untreated *P. juliflora*	Neutralization,	0.25	0.396
	Overliming,	0.45	0.42
	Overliming + Activated Charcoal (AC)	0.39	0.512
O.annae treated *P. juliflora*	Neutralization,	0.323 0.41	0.375
	Overliming,	0.42	0.812
	Overliming + Activated Charcoal (AC)		0.875
Untreated *L. camara*	Neutralization,	0.313	0.41
	Overliming,	0.262	0.41
	Overliming + Activated Charcoal (AC)	0.37	0.48
O.annae treated *L. camara*	Neutralization,	0.35	0.71
	Overliming,	0.4	0.71
	Overliming + Activated Charcoal (AC)	0.41	0.8

nol production from test samples was statistically significant compared to respective control samples.

The higher ethanol and biomass yield and ethanol productivity of cyanobacteria pretreated lignocellulosics is due to higher release of reducing sugars and absence of fermentation inhibitors due to detoxification (Fig. 6.5 and Table 6.1).

Cp – Coir pith; Oa + Cp-*O. annae* + Coir pith;

Pj – P. juliflora; Oa +Pj-*O. annae* + *P. juliflora;*

Lc – L. camara; Oa + Lc-*O. annae* + *L. camara.*

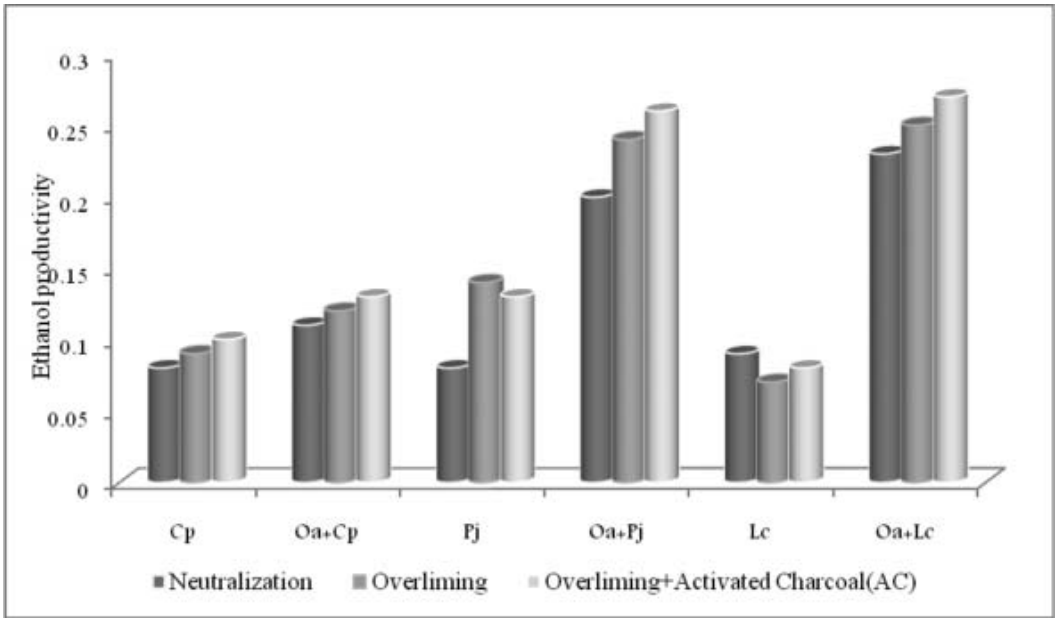

FIGURE 6.5 Effect of detoxification on untreated and *O.annae* treated lignocellulosic hydrolysates for ethanol productivity (g/l/h).

This could also be well supported by the previous studies of several authors [40–42]. Saha [43] found the better ethanol yield in acid pretreated enzymic hydrolysate fermented with recombinant *Escherichia coli* strain FBR5 giving 19 g L^{-1} ethanol with a yield of 0.24 g/g. Gupta [15] reported an ethanol production of 5.0 gL^{-1} in batch fermentation and 26.2 gL^{-1} in fed batch fermentation using *P. stipitis* NCIM-3498 from *Saccharum spontaneum*. For the detoxification three processes were undertaken namely, neutralization, overliming, overliming with activated charcoal. Both the untreated and *O. annae* treated lignocellulosic hydrolysates were able to produce ethanol with *P. stipitis.* The ethanol production was noticed to be high in combined treatment (overliming with activated charcoal). This is mainly due to the better removal of inhibitory substance [42]. The ethanol production was analyzed and estimated for 18, 24, 30, and 36 hours. Both the untreated and *O. annae* treated substrates (coir pith, *P. juliflora* and *L. camara*) showed maximum production by 36th hour. As expected when compared to neutralization process alone because of the removal of other ethanol producing inhibitory substances overliming and the combines process of overliming with activated charcoal yielded almost the double the quantity of ethanol.

Tables 6.2–6.5 depicts the ANOVA for reducing sugar released by *O. annae* with selected lignocellulosics, phenolics released by *O. annae* with

TABLE 6.2 ANOVA of Reducing Sugar Released by *O. annae* with Selected Lignocellulosics

S. no.	Parameters	99% confidence limits		Null hypothesis	Alternate hypothesis
		F	Fcrit		
1	Reducing sugar at 100°C and acid concentration of coir pith hydrolysates	28. 31301	4.45897	Rejected	Accepted
2	Reducing sugar at 120°C and acid concentration of coir pith hydrolysate	147.2966	4.45897		
3	Reducing sugar at 140°C and acid concentration of coir pith hydrolysate	861.5414	4.45897		
4	Reducing sugar at 100°C and acid concentration of *P.juliflora* hydrolysate	49.21591	4.45897		
5	Reducing sugar at 120°C and acid concentration of *P.juliflora* hydrolysate	73.43046	4.45897		
6	Reducing sugar at 140°C and acid concentration of *P.juliflora* hydrolysate	193.7169	4.45897		
7	Reducing sugar at 100°C and acid concentration of *L. camara* hydrolysate	61.82457	4.45897		
8	Reducing sugar at 120°C and acid concentration of *L. camara* hydrolysate	54.0685	4.45897		
9	Reducing sugar at 140°C and acid concentration of *L. camara* hydrolysate	66.78603	4.45897		

F = Experimental value; Fcrit = Tabulated value (significant value).

selected lignocellulosics, effect of detoxification of selected lignocellulosics hydrosylates by *O. annae* for improves bioethanol production and bioethanol yield by *O. annae* treated lignocellulosics hydrosylates. Thus, from the results it can be concluded that *O. annae* pretreatment of lignocellulosics before thermochemical treatment can be beneficially used as an effective method to enhance the release of reducing sugar from the lignocellulosic materials. Among the lignocellulosics studied *P. juliflora* and

L. camara can be considered as a better source of reducing sugar for bioethanol production due to its high sugar and low phenolics content when compared to coir pith. As far as our study concerned both *P. juliflora* and *L. camara* were adjudged to be the candidates for ethanol production after cyanobacterial growth followed by detoxification by overliming. In line with the findings of bacteria and fungi [45] fresh water cyanobacterium *O. annae*'s ability to degrade lignocellulosics and making it a better substrate for ethanol production.

TABLE 6.3 ANOVA of Phenolics Released by *O. annae* with Selected Lignocellulosics

S. no.	Parameters	99% confidence limits		Null hypothesis	Alternate hypothesis
		F	Fcrit		
1	Phenolics at 100°C and acid concentration of coir pith hydrolysates	11.30519	4.45897		
2	Phenolics at 120°C and acid concentration of coir pith hydrolysate	12.14238	4.45897		
3	Phenolics at 140°C and acid concentration of coir pith hydrolysate	19.45638	4.45897		
4	Phenolics at 100°C and acid concentration of *P.juliflora* hydrolysate	16.36974	4.45897	Rejected	Accepted
5	Phenolics at 120°C and acid concentration of *P.juliflora* hydrolysate	15.45043	4.45897		
6	Phenolics at 140°C and acid concentration of *P.juliflora* hydrolysate	14.5373	4.45897		
7	Phenolics at 100°C and acid concentration of *L. camara* hydrolysate	17.06229	4.45897		
8	Phenolics at 120°C and acid concentration of *L. camara* hydrolysate	13.67615	4.45897		
9	Phenolics at 140°C and acid concentration of *L. camara* hydrolysate	11.73684	4.45897		

F = Experimental value; Fcrit = Tabulated value (significant value).

TABLE 6.4 ANOVA on Effect of Detoxification of Selected Lignocellulosics hydrolysates by *O. annae* for Improves Bioethanol Production

S. no.	Parameters	99% confidence limits		Null hypothesis	Alternate hypothesis
		F	Fcrit		
1	Untreated coir pith	2.001896	3.885294	Rejected	Accepted
2	Treated coir pith	4.478342	3.885294		
3	Untreated *P. juliflora*	0.992912	3.159908		
4	Ttreated *P. juliflora*	6.775324	3.159908		
5	Untreated *L. camara*	3.3427673	3.159907		
6	Treated *L. camara*	6.361262	3.159908		

TABLE 6.5 ANOVA on Bioethanol Yield by *O. annae* Treated Lignocellulosics hydrolysates

S. no.	Parameters	99% confidence limits		Null hypothesis	Alternate hypothesis
		F	Fcrit		
1	Untreated coir pith	1.65313	6.94427	Rejected	Accepted
2	Treated coir pith	8.987561	2.99612		
3	Untreated *P. juliflora*	8.478342	6.944272		
4	Ttreated *P. juliflora*	8.987561	6.944272		
5	Untreated *L. camara*	4.100723	6.944272		
6	Treated *L. camara*	7.0	6.944272		

6.4 CONCLUSION

Lignocellulose (lignin, cellulose and hemicellulose) is the major structural component of woody and non woody plants make them a substrate of enormous biotechnological value. These huge amounts of residual plant biomass considered as waste can be potentially converted into various value added products namely biofuels, chemicals, and cheap energy source for fermentation. Lignocellulosic wastes such as *L.camara*, *P. juliflora* and coir pith were used in an efficient way for producing bioethanol.

Cyanobacteria are known for their ability to degrade various pollutants such as lignin, pesticides and phenol. In view of producing bioethanol, the fresh water cyanobacterium *O. annae* treated lignocellulosics (15th day) were subjected to thermochemical hydrolysis. The efficiency of bioethanol production by *Pichia stipitis* NCIM 3498 after detoxification by neutralization, overliming and overliming combined with activated charcoal were analyzed in untreated and *O. annae* treated lignocellulosics, respectively. Ethanol produced using *Pichia stipitis* NCIM 3498 were analyzed by gas chromatography and the fermentation efficacy was calculated. The above findings demonstrate that freshwater cyanobacterium *O. annae* was found to be as efficient degrader of all the three lignocellulosics namely coirpith, *P. juliflora* and *L. camara* as substrates and release fermentable sugars followed fermentation of yeast (*P. stipitis*) for bioethanol production. Hence, this is cost effective, ecofriendly, zero pollution lignocellulosic-based technology could be another lead for agroeconomy development to India.

KEYWORDS

- **Bioethanol**
- **Coir pith**
- ***Lantana camara***
- **Lignocellulosic**
- ***Oscillatoria annae***
- ***Pichia stipitis***
- ***Prosopis juliflora***

REFERENCES

1. Beck, R. J. Worldwide Petroleum Industry Outlook: 1998–2002 Projections to 2007, 14th ed., Pennwell, Tulsa, OK. 1997.
2. Bull, S. R., Riley, C. J., Tyson, K. S., Costella, R. (1992). Total fuel cycleand emission analyze of biomass to ethanol. *In:* Energy fromBiomass and wastes vol. XVI (Klass DL ed.) Institute of gas technology, Chicago, 1–14.

3. Kheshgi H. S., Prince, R. C., Marland, G. (2000). The potential of biomass fuels in the context of global climate change; Focus on transportation fuels. *Annual Rev. Energy Environ. 25,* 199–244.
4. Nigam, J. N. (2001). Ethanol production from wheat straw hemicellulose hydrolysate by *Pichia stipitis*. *J. Biotechnol. 87,* 17–27.
5. Bjerre, A. B., Olesen, A. B., Fernqvist, T. (1996). Pretreatment of wheat straw using combined wet oxidation and alkaline hydrolysis resulting in convertible cellulose and hemicellulose. *J. Biotechnol. Bioeng. 49,* 568–577.
6. Varga, E., Schmidt, A. S., Reczey, K., Thomsen, A. B. (2003). Pretreatment of corn stover using wet oxidation to enhance enzymatic digestibility. *J. Appl. Biochem. Biotechnol. 10,* 37–50.
7. Elmer, C. R., Costa, A. C., Lunelli, B. H., Maciel, M. R. W., Filho, R. M. (2007). Kinetic Modeling and Parameter Estimation in a Tower Bioreactor for Bioethanol Production. *J. Appl. Biochem. Biotechnol. 148*, 163–173.
8. Levine, J. S. (1996). Biomass burning and global change. Remote sensing and inventory development and biomass burning in Africa. *In:* Levine JS (Ed). The MIT Press, Cambridge, Massachusetts, USA. *1,* 35.
9. Hahn-Hägerdal, B., Galbe, M., Gorwa- Grauslund, M. F., Lidén, G., Zacchi, G. (2006). Bioethanol the fuel of tomorrow from the residues of today. *Trends Biotechnol. 24,* 549–56.
10. Hiremath, A. J., Bharath, S. (2005). The fire-lantana cycle hypothesis in Indian forests. *Conservat Soc*. *3,* 26–42.
11. Sawal, R. K., Ratan, R., Yadav, S. B. S. (2004). Mesquite (*Prosopis juliflora*) pods as a feed resource for livestock. *Asian Australasian J. Animal Sci. 17 (5),* 719–725.
12. Aqeel, A., Viquaruddin, A., Khalid, S. M., Ansari, F. A., Khan, K. A. (1997). Study on the antifungal efficacy of juliflorine and a benzene-insoluble alkaloid fraction of *Prosopis juliflora.Philippine J. Sci*. *126(2),* 175–182.
13. Malliga P., Uma, L., Subramanian, G. (1996). Lignolytic activity of the cyanobacterium *Anabaena azollae* ML2 and the value of coir waste as a carrier for biofertilizer. *Microbios*. *86,* 175–183.
14. Perestelo, F., Falcon, M. A., Carnicero, A., Rodriguez, A., Feunte, D. L. G. (1994). Limited degradation of industrial, synthetic and natural lignin by *Serratia marcescens*. *Biotechnol. Lett. 16,* 299–302.
15. Morii, H., Nakamiya, K., Kinnoshita, S. (1995). Isolation of lignin decolorizing bacterium. *J. Ferment. Bioeng. 80,* 296–299.
16. Bumpus, J. A., Aust, S. D. Biodegradation of DDT (1,1,1-tri-chloro-2,2-bis-(4-chlorophenyl) -ethane) by the white-rot fungus *Phanerochaete chrysosporium. Appl. Environ Microbiol.* 53, 2001–2008.
17. Hall, D. O., Markov, S. R., Watanable, Y., Rao, K. K. (1995).The potential applications of cyanobacterial photosynthesis in clean technologies. *Photosynthesis Research. 46*, 159–167.
18. Dongjin Pyo, ; Taemin Kim, ; Jisun Yoo. (2013). Efficient Extraction of Bioethanol from Freshwater Cyanobacteria Using Supercritical Fluid Pretreatment. *Bull. Korean Chem.Soc. 34,* 2, 379.

19. Rippka, R., Deruelles, J., Waterbury, J. B., Herdman, M., Stainer, R. Y. (1979). Genetic assignments, strain histories and properties of pure cultures of cyanobacteria. *J. Gen. Microbiol. 111,* 1–61.
20. Chandel, A. K., Kapoor, R. K., Singh, A., Kuhad, R. C. (2007). Detoxification of sugarcane bagasse hydrolysate improves ethanol production by *Candida shehatae* NCIM 3501. *Biores. Technol. 98, 2*, 1947–1950.
21. Martinez, A., Rodriguez, M. E., Wells, M. L., York, S. W., Preston, J. F., Ingram, L. O. (2001). Detoxification of dilute acid hydrolysates of lignocellulose with lime. *Biotechnol. Progress. 17,* 287–293.
22. Gong, C. S., Chen, C. S., Chen, L. F. (1993). Pretreatment of sugarcane bagasse hemicellulose hydrolyzate for ethanol production by yeast. *Appl. Biochem. Biotechnol. 39–40,* 83–88.
23. Miller, G. L. (1959). Use of dinitrosalicylic acid reagent for determination of reducing sugar. *Analytical Chem. 31,* 426–428.
24. Wildenradt, H. L., Singleton, V. L. (1974). The production of aldehydes as a result of oxidation of polyphenolic compounds and its relation to wine aging. *Am. J. Enol. Vitic. 25,* 119–126.
25. Badger, P. C. (2002). Ethanol from cellulose: a general review. *In:* Janick J, Whipkey A, editors. Trends in new crops and new uses. Alexandria, VA: ASHS Press; 17–21.
26. Olsson, L., Hahn-Hagerdal, B. (1996). Fermentation of lignocellulosic hydrolysates for ethanol production. *Enz. Microb. Technol. 18,* 312–331.
27. Sun, Y., Cheng, J. (2002). Hydrolysis of lignocellulosic materials for ethanol production. *Biores. Technol. 83,* 1–11.
28. McMillan, J. D. (1994). Pretreatment of lignocellulosic biomass. *In*: Conversion of Hemicellulose Hydrolyzates to Ethanol. Himmel, M. E., Baker, J. O., Overend, R. P. (editors), American Chemical Society Symposium, Washington, DC. 292–324.
29. Hinman, N. D., Schell, D. J., Riley, C. J., Bergeron, P. W., Walter, P. J. Preliminary estimate of the cost of ethanol production for SSF technology. *J. Appl. Biochem. Biotechnol.* (1992). *34–35,* 639–649.
30. Taherzadeh, M. J., Niklasson, C., Lidén, G. (1997). Acetic acid – friend or foe in anaerobic batch conversion of glucose to ethanol by *Saccharomyces cerevisiae*? *Chem. Eng. Sci. 52, 15*, 2653–2659.
31. Hartley, R. D., Jones, E. C. (1977). Phenolic components and degradability of cell walls of grass and legume species. *Phytochem. 16,* 1531–1534.
32. Hopkins, W. G. (1999). Introduction to Plant Physiology. John Wiley and Sons, Inc., New York. *12,* 1–528.
33. Roberto, C., Lacis, L. S., Barbosa, M., Mancilha, I. M. D. (1991). Utilization of sugarcane bagasse hemicellulosic hydrolysate by *Pichia stipitis* for the production of ethanol. *Process Biochem. 26,* 15–21.
34. Van Zyl, C., Prior, B. A., Preez, J. C. D. (1998). Production of ethanol from sugar cane bagasse hemicellulose hydrolysate by *Pichia stipitis*. *J. Appl. Biochem. Biotechnol. 17,* 357–369.
35. Amartey, S., Jeffries, T. (1996). An improvement in *Pichia stipitis* fermentation of acid hydrolysates hemicellulose achieved by overliming (calcium hydroxide treatment) and strain adaptation. *World J. Microbiol. Biotechnol. 12,* 281–283.

36. Kruse, B., Schugrel, K. (1996). Investigation of ethanol formation by *Pachysolen tannophilus* from xylose and glucose-xylose substrates. *Process Biochem. 31,* 389–408.
37. Dominguez, J. M., Gong, C. S., Tsao, G. T. (1996). Pretreatment of sugarcane bagasse hemicellulose hydrolyzate for xylitol production by yeast. *Appl. Biochem. Biotechnol. 57–58,* 49–56.
38. Dellweg, H., Rizzi, M., Methner, H; Debus, D. (1984). Xylose fermentation by yeasts. *Biotechnol. Lett. 6,* 354–395.
39. Du Preez, J. C., Bosch, M., Prior, B. A. (1986). The fermentation of hexose and pentose sugars by *Candida shehatae* and *Pichia stipitis*. *Appl. Microbiol. Biotechnol. 23,* 228–233.
40. Chung, I. S., Lee, Y. Y. (1985). Ethanol production of crude acid hydrolysate of cellulose using high-level yeast inocula. *Biotechnol. Bioeng. 27,* 308–315.
41. Singh, A., Das, K., Sharma, D. K. (1984). Production of xylose, furfural, fermentable sugars and ethanol from agricultural residues. *J. Chem. Technol. Biotechnol. 34,* 51–61.
42. Mussatto, S. I., Roberto, I. C. (2004). Alternatives for detoxification of diluted-acid lignocellulosic hydrolyzates for use in fermentative processes: a review. *Biores. Technol. 93,* 1–10.
43. Saha, B. C., Iten, L. B., Cotta, M. A., Wu, Y. V. Dilute acid pretreatment, enzymatic saccharification and fermentation of wheat straw to ethanol. *Process Biochem.* 2005.
44. Gupta, P. Bioethanol from *Saccharum spontaneum*. M.Sc thesis. Delhi University, New Delhi, India. 2006.
45. Zaccaro, M. C., Kato, A., Zulpa, G., Storni, M. M., Steyerthal, N., Lobasso, K., Stella, A. M. (2006). Bioactivity of *Scytonema hofmanni* (Cyanobacteria) in *Lilium alexandrae* in vitropropagation. *Electronic J. Biotechnol. 9, 3*, 210–214.

CHAPTER 7

CHALLENGES IN HARNESSING THE POTENTIAL OF LIGNOCELLULOSIC BIOFUELS AND THE PROBABLE COMBATING STRATEGIES

LAKSHMI SHRI ROY, VIJAY KUMAR GARLAPATI, and RINTU BANERJEE

Microbial Biotechnology and DSP Laboratory, Agricultural and Food Engineering Department, IIT Kharagpur, Kharagpur, West Bengal – 721302

CONTENTS

7.1 Introduction 173
7.2 Lignocellulosic Sources 175
7.2.1 Forestland Materials 175
7.2.2 Agricultural Residues 176
7.2.3 Municipal and Industrial Wastes 176
7.2.4 Marine Algae 176
7.3 Lignocellulosic Biomass Composition 177
7.3.1 Hemicellulose 177
7.3.2 Cellulose 178
7.3.3 Lignin 178
7.4 Biofuels Obtained From Lignocellulosics 179
7.4.1 Biodiesel 179

7.4.2 Other Liquid Fuels Obtained From lignocellulosics 179
7.4.3 Bioethanol 181
7.5 Biochemical Route of Bioethanol Production From Lignocellulosic Feedstocks 182
7.5.1 Pre-Treatment of Lignocellulosic Feed-Stock 184
7.5.2 Hydrolysis 184
7.6 Main Challenges During Lignocellulosic Feedstocks Bioconversion To Bioethanol 188
7.6.1 Feedstock Production 189
7.6.2 Feedstock Logistics 189
7.6.3 Challenges in Biochemical Process of Lignocellulosic Biomass Conversion 190
7.7 Recent Innovative Approaches to Combat the Bottlenecks in Lignocellulosic Bioconversion to Bioethanol 191
7.7.1 Enzyme Concoction Approach 192
7.7.2 Direct Glucose Production Using *Clostridium thermocellum* Cultures Supplemented With a Thermostable β-glucosidase 192
7.7.3 Single Step Bioethanol Production by Employing Novel Strains 193
7.7.4 Use of Super Computer in Bioethanol Production 194
7.8 Summary 195
Keywords 196
References 196

ABSTRACT

Thrust towards embarking on building a new economy based on non-fossil fuel energy has imparted impetus to research on lignocellulosic biofuel industry. Lignocellulosics form a large class of renewable feed-stocks, which include agricultural residues, municipal solid waste and food processing and industrial wastes. Although lignocellulosics are

very energy rich substrates, unlocking its potential and extending it to practical large scales has a number of bottlenecks. The challenges in instituting and exploiting these resources for biofuel production compel us to rethink current paradigm of supply and usage. Hence there is an urgent need to combat these issues to scale it up and execute at practical scales. Technological constraints do not support cost-effective and competitive production of lignocellulosic bioethanol. In order to produce lignocellulosic bioethanol economically attractive, use of cheaper substrates, inexpensive pretreatment techniques, use of overproducing and recombinant strains for maximized ethanol tolerance and yields, better recovery processes, effective bioprocess integration, exploitation of side products, and reduction of energy and waste may be encouraged. A cohesive and dedicated approach can help in realizing large-scale commercial production of lignocellulosic bioethanol. This chapter is an exhaustive overview of this aspect of lignocellulosic biofuel production. Special case studies have been included to highlight the probable strategies that may be adopted in future.

7.1 INTRODUCTION

Current focus of research is in the development of clean technologies that use a sustainably produced feedstock [1]. Contextually Biofuels, represent a significant potential for sustainability and growth of industrialized countries because they can be generated from locally available renewable material. Serious technical barriers like, ineffective biomass to fuel conversion efficiency, limited supply of key enzymes employed, use of high energy demanding process operation, limit the near-term commercial application of advanced biofuels technologies. Despite an immense future potential, large-scale expansion of advanced biofuels technologies seems unlikely unless further research and development lead to lowering these barriers. The hidden promise of biofuels is locked up in lignocellulosic biomass. Lignocellulose is a sturdy, microstructure of cellulose fibers covered by the heterogeneous hemicellulose and pectin and associated with lignin. The macromolecular structure of lignocellulose has been depicted in Fig. 7.1.

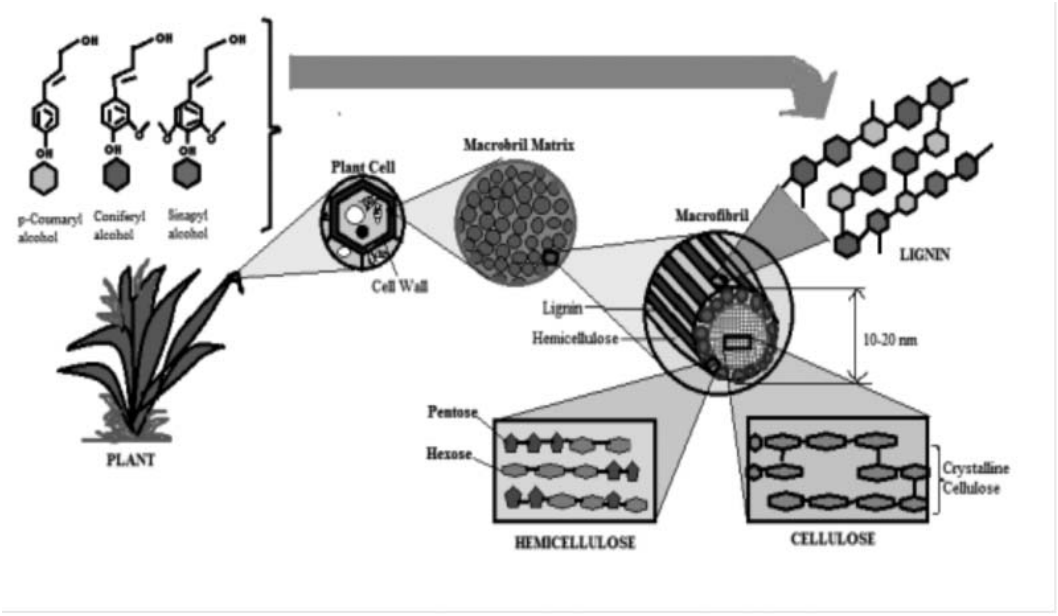

FIGURE 7.1 Molecular structure of lignocellulosic material [126].

Globally the availability of lignocellulosic raw materials is fairly consistent, unlike the fossil fuel reserves. Therefore, production of biofuels and biochemicals using nonedible lignocellulosic feedstock may prove advantageous to the society [2]. The significant benefits include production of energy from renewable and sustainable feedstock, aiding in the carbon dioxide fixation and pacifying the pertinent global warming issue, mobilizing local economic development minimizing air pollution from conventional mode of use of such feedstock by burning, decreasing the dependency on imported oils, and creating employment. Lignocellulose biomass by virtue of their high carbohydrate content holds tremendous potential for large-scale biofuel production, and need to be exploited for commercial production [3, 4]. The recalcitrance of lignocellulosic feedstock to chemicals or enzymes may be attributed to numerous natural factors. The degree of lignifications, the structural heterogeneity and complexity of cell-wall constituents, affect the conversion process. Enzymatic action is impeded while acting on an insoluble substrate. Additionally, the crystallinity and restricted solvent accessibility affect liquid penetration and/or enzyme accessibility and activity.

To realize the true potential of the lignocellulosic feedstock the various aspects of the biofuel production have to be dealt into. Low ethanol

yield at the lab scale compounded with the high production costs have till date prevented the commercial scale production of this fuel [3, 4]. However, it is anticipated that with the maturity of the technology the cost would be reduced. For biofuel production from lignocellulosic biomass, it is therefore imperative to identify the technology bottlenecks and cost-contributing factors. Critical analysis of the most recent translational research strategies can make the overall process practical and profitable at an industrial level.

7.2 LIGNOCELLULOSIC SOURCES

Several groups of lignocellulosic are available throughout the world. These groups of raw materials are differentiated by their origin, composition and structure into:

7.2.1 FORESTLAND MATERIALS

Forestland materials include mainly woody biomass. These feedstocks are classified into broad categories of either softwoods or hardwoods. Softwoods originate from conifers and gymnosperm trees [5] and possess lower densities and grow faster than the hardwoods. Gymnosperm trees include mostly evergreen species such as pine, cedar, spruce, cypress, fir, hemlock and redwood [6]. Hardwoods are angiosperm trees and are mostly deciduous [7] and include trees such as poplar, willow, oak, cottonwood and aspen [8]. Unlike agricultural biomass, woody raw materials offer flexible harvesting times, avoid long latency periods of storage [9], possess more lignin and less ash content (close to zero), high density and minimal ash content than agricultural residues. These unique characteristics of woody biomass in conjunction to lower pentose content make them very attractive to cost-effective transportation over agricultural biomass and hence more favorable for greater bioethanol conversion if recalcitrance is surmounted[9]. Forestry wastes such as sawdust from sawmill, slashes, wood chips and branches from dead trees have also been used as biofuel feedstocks [10].

7.2.2 AGRICULTURAL RESIDUES

Crop residues are mostly comprised of agricultural wastes such as corn stover, corn stalks, rice and wheat straws as well as sugarcane bagasse [11]. Pasture includes food crops and grassland that encompass primarily agricultural residues, that is, nonfood crops and switch grass and alfalfa [12]. These substrates avoid "food versus fuel" controversy and are known to possess several advantages [13, 14]. Increased growth of these plants occurs in marginal and erosive soils and with nitrogen fertilization [15]. C4 biofuel feedstock improvement is only at its inception stage [16]. These materials contain more hemicellulosic material than woody biomass (approximately 25–35%) [17]. These residues help to avoid reliance on forest woody biomass and thus reduce deforestation (nonsustainable cutting plants). Unlike trees, crop residues are characterized by a short-harvest rotation that renders them more consistently available to bioethanol production [18, 19].

7.2.3 MUNICIPAL AND INDUSTRIAL WASTES

Municipal and industrial wastes are also potential recyclable cellulosic materials that can originate either from residential or nonresidential sources such as food wastes and paper mill sludge [12, 20]. Environmental problems associated with the disposal of garbage household, processing papers, food-processing by-products, black liquors and pulps [21] are controlled by their effective utilization.

7.2.4 MARINE ALGAE

Interest in algae as a potential biofuel feedstock has received an increasing support [11] in the recent times but its development as a viable and scalable source commercial enterprise remained limited. Marine algae biomass is regaining interest as a biofuel feedstock due to the rapid biorefineries expansion, which has lead to a shortage on current energy crops. Algae would also be a feedstock for other possible applications involving bio-crude oils, bio-plastics and recovered livestock coproducts [22].

Furthermore, algae feedstock with its thin cellulose layer has a higher carbohydrate composition [23] and does not compete directly with foods. It does not require agricultural land or use of freshwater to be cultivated. It consumes a high level of CO_2 during its growth, which makes it environmentally attractive as a CO_2 sink [24].

7.3 LIGNOCELLULOSIC BIOMASS COMPOSITION

Lignocellulosic material can generally be divided into three main components: cellulose (30–50%), hemicellulose (15–35%) and lignin (10–20%) [25–28] (Fig. 7.2). Cellulose and hemicelluloses make up approximately 70% of the entire biomass and are tightly linked to the lignin component through covalent and hydrogenic bonds that make the structure highly robust and resistant to any treatment [18, 27, 29].

7.3.1 HEMICELLULOSE

Hemicellulose is an amorphous and variable structure formed of heteropolymers including hexoses (D-glucose, D-galactose and D-mannose) as well

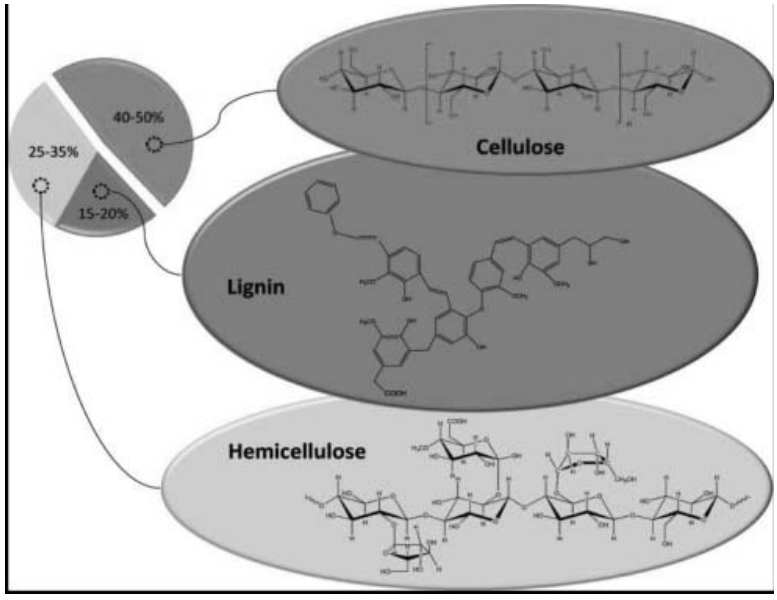

FIGURE 7.2 Lignocellulosic composition [125].

as pentose (D-xylose and L-arabinose) and may contain sugar acids (uronic acids) namely, D-glucuronic, D-galacturonic and methylgalacturonic acids [30, 31]. Its backbone chain is primarily composed of xylan b(1/4)-linkages that include D-xylose (nearly 90%) and L-arabinose (approximately 10%) [28]. Branch frequencies vary depending on the nature and the source of feedstocks. Softwood has typically glucomannans while hardwood is more frequently composed of xylans [30]. Xylan is the most abundant hemicellulose component but its composition varies in each feedstock [32]. The diversity of hemicellulose sugars, advocates the use of a wide range of enzymes for its complete hydrolysis into free monomers.

7.3.2 CELLULOSE

Cellulose is the most prevalent organic polymer and is approximately 30% of the plant composition [11]. Cotton, flax and chemical pulp represent the purest sources of cellulose while soft and hardwoods contain approximately 45% cellulose [17, 25]. Cellulose is a structural linear component of a plant's cell wall. It consists of a long-chain of glucose monomers linked b(1/4)-glycosidic bonds. The extensive hydrogen linkages among molecules lead to a crystalline and strong matrix structure [33]. Numerous Cross-linking hydroxyl groups constitute the microfibrils, which give the molecule more strength and compactness. To be converted from crystalline to amorphous texture in water, cellulose requires 320 °C as well as a pressure of 25 MPa [34].

7.3.3 LIGNIN

Lignin is an aromatic and rigid biopolymer with a molecular weight of 10,000 Da bonded via covalent bonds to xylans (hemicellulose portion) conferring rigidity and high level of compactness to the plant cell wall [27]. It is composed of three phenolic monomers of phenyl propionic alcohol namely, coumaryl, coniferyl and sinapyl alcohol. Forest woody biomass is primarily composed of cellulose and lignin polymers. Softwood barks have the highest level of lignin while grasses and agricultural residues contain the lowest level of lignin [17, 25]. Conversely, crop residues such as corn stover, rice and wheat straws are comprised mostly

of a hemicellulosic heteropolymer that includes a large number of 5-carbon pentose sugars of primarily xylose [35]. Lignin components are gaining importance because of their dilution effect on the hydrolysis process once solids are added to a fed batch hydrolytic or fermentation bioreactor in addition to their structure and concentration effects that would affect potential hydrolysis [36].

7.4 BIOFUELS OBTAINED FROM LIGNOCELLULOSICS

7.4.1 BIODIESEL

Biodiesel is the second most abundant renewable liquid fuel [37]. Its preparation is outlined schematically in Fig. 7.3 given below. First generation biodiesel [38, 39] is produced by esterification of fatty acids or transesterification of oils (triglycerides) with alcohols (normally methanol and ethanol) using a basic [40–42] or acidic catalyst [43, 44]. The fatty esters are separated from glycerol by decantation and purified for direct use as fuels. Another alternative to process oil into biofuels is hydro-treating [45] which can be carried out synergistically in the existing petroleum refinery infrastructure through mixing and coprocessing of vegetable oils with petroleum derived feedstocks [46, 47]. The main drawback of oil-based processes is the availability of inexpensive feedstocks. Challenges in biodiesel research are focused on the development of new low cost catalytic processes that allow the use of low quality or waste oils (e.g., used fryer oil). Other sources include different nonedible oils (e.g., cynara [48], Jatropha, Karanja [49]) and triglycerides derived from algae [50]. Lignocellulosic feedstocks despite their complexity are currently being used to produce biofuels from biomass.

7.4.2 OTHER LIQUID FUELS OBTAINED FROM LIGNOCELLULOSICS

Lignocellulosic biomass is converted to hydrocarbon fuels by the removal of oxygen, combined with the formation of C–C bonds to control the molecular weight of the final hydrocarbons. The various strategies adopted have been depicted in the Fig. 7.4.

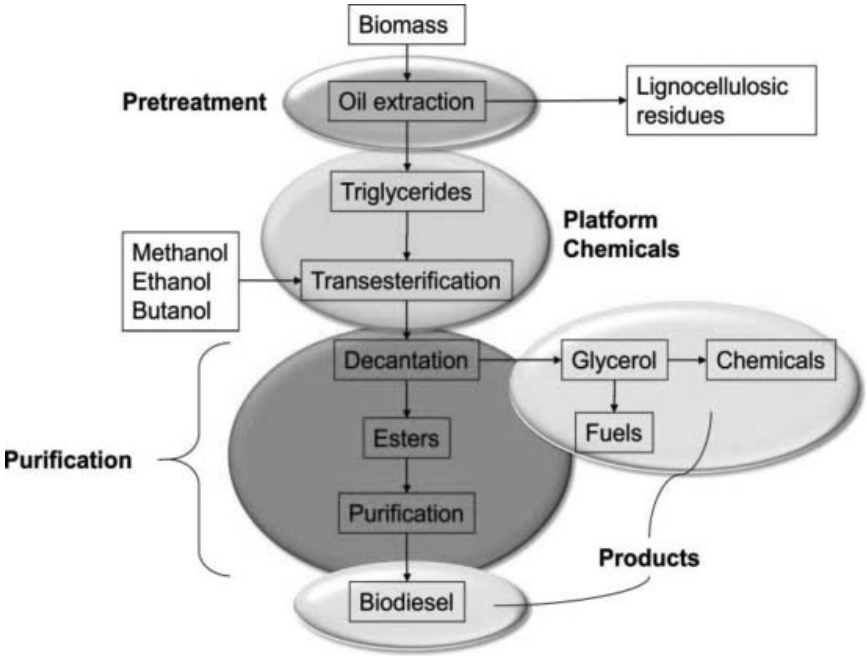

FIGURE 7.3 Process schematic: biodiesel production [125].

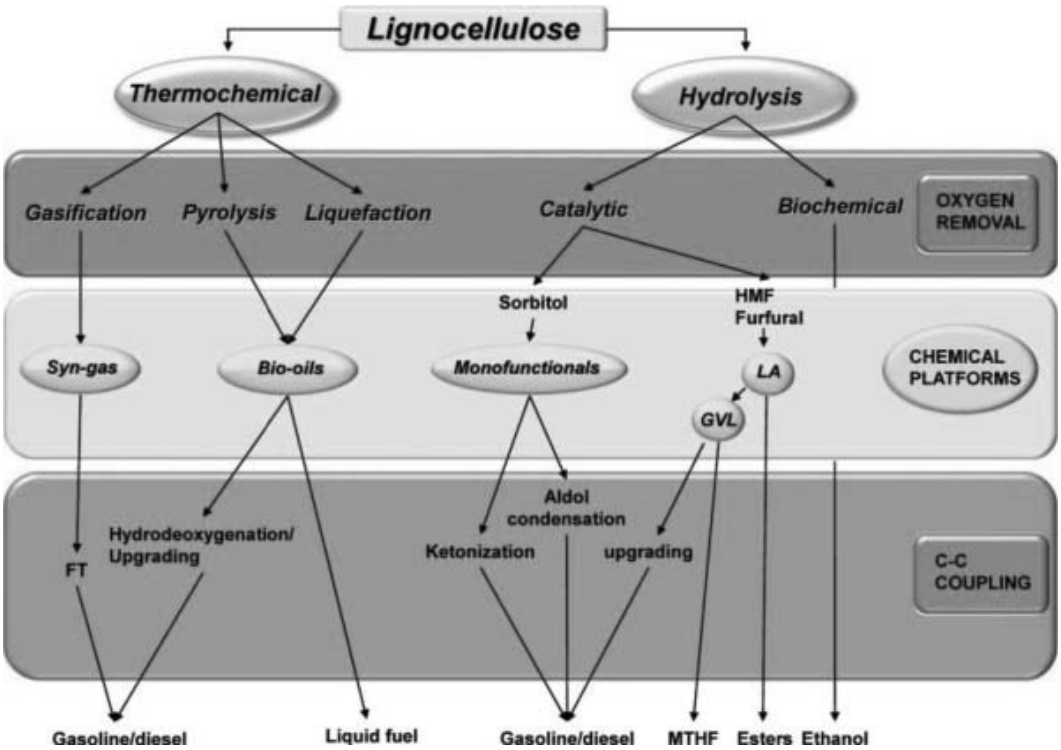

FIGURE 7.4 Strategies for conversion of lignocellulosic biomass to liquid biofuels by thermochemical and hydrolysis routes [125].

Two definite approaches include: (i) Gasification combined with Fischer–Tropsch synthesis, and (ii) Other pyrolysis and liquefaction. Other approaches include: (iii) Aqueous-phase reforming, (iv) An approach in which aqueous solutions of sugars formed by treatment of lignocellulosic biomass undergo catalytic dehydration to produce furan compounds, such as furfural and hydroxymethylfurfural (HMF). These furanic aldehydes can then be used as feedstocks for aldol-condensation reactions over basic catalysts to produce hydrocarbons suitable for Diesel fuel applications. (v) Finally, the levulinic acid platform, in which lignocellulosic biomass first undergoes treatment in acid solutions to produce levulinic acid. The aqueous solution of levulinic acid (in the presence of formic acid) then undergoes catalytic reduction to g-valerolactone (GVL), which serves as an intermediate for the production of nonane for Diesel fuel or the production of branched alkanes with molecular weights appropriate for jet fuel.

7.4.3 BIOETHANOL

Bioethanol is the most abundantly produced biofuel. It accounts for more than 94% of total biofuel production. The production of bioethanol, has been outlined in Fig. 7.5.

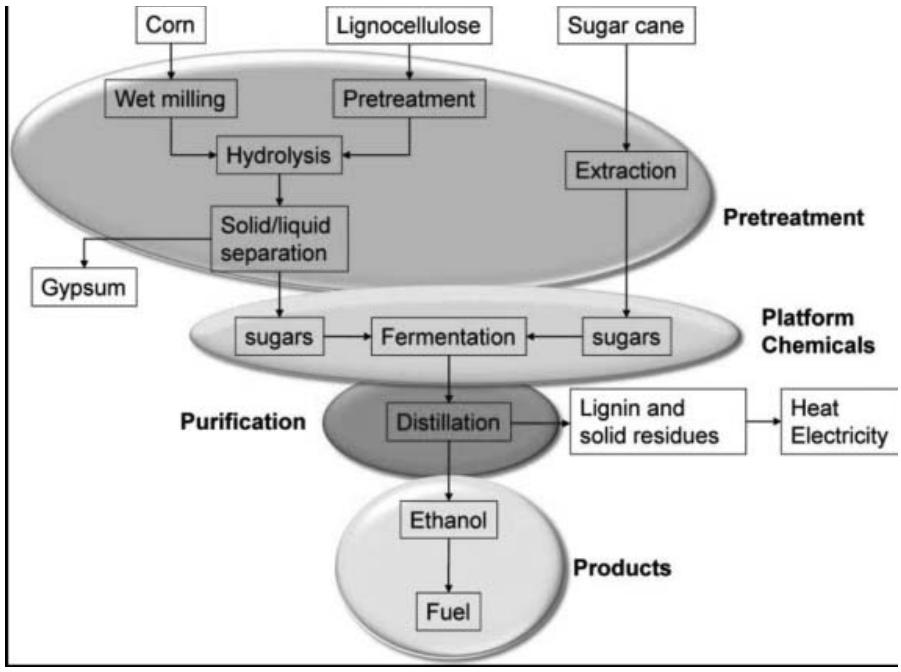

FIGURE 7.5 Process schematic: bioethanol production [125].

Lignocellulosic biomass has been considered an appropriate feedstock to produce sustainable, second generation bioethanol. An active area of research is to improve the suitability of this feedstock and the recently included algal feedstock. However, these potential alternatives are still at an early stage of development, and more research on feedstock availability and process optimization is necessary.

7.5 BIOCHEMICAL ROUTE OF BIOETHANOL PRODUCTION FROM LIGNOCELLULOSIC FEEDSTOCKS

Lignocellulosic biomass can be transformed into bioethanol via two different approaches (i.e., biochemical or thermochemical conversion) as shown in the Fig. 7.6 [51].

Both routes involve degradation of the recalcitrant cell wall structure of lignocellulose into fragments of lignin, hemicellulose and cellulose, hydrolysis of polysaccharides into sugars and finally conversion and purification of bioethanols [52, 53]. However, these conversion routes do not fundamentally follow similar techniques or pathways. Unlike the thermochemical

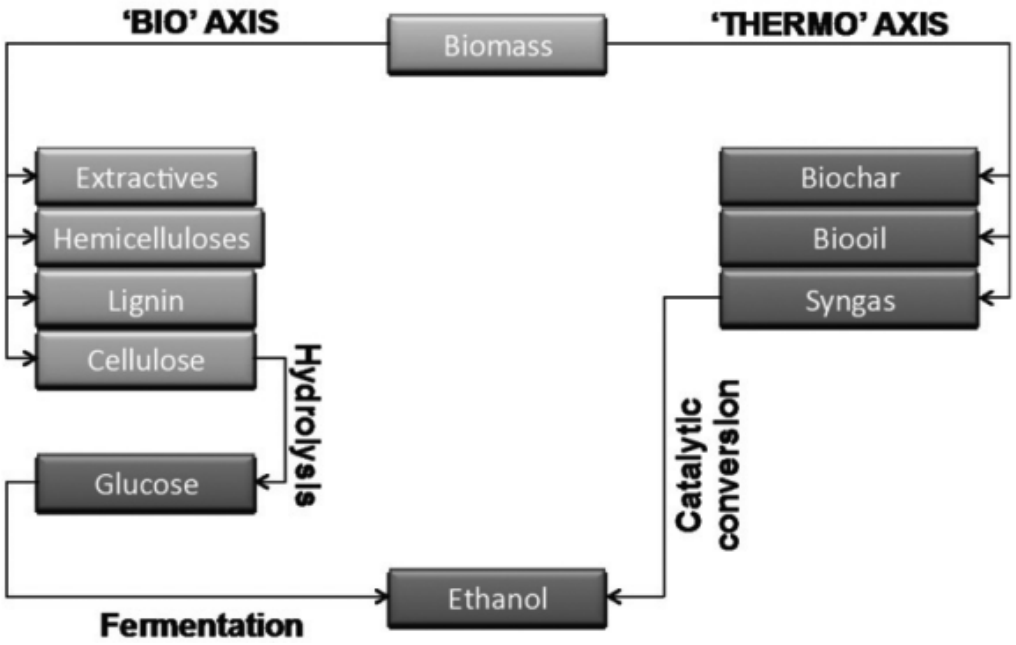

FIGURE 7.6 Two approaches for bioethanol production.

route, biochemical conversion involves physical (i.e., size reduction) or/and thermo-chemical with possible biological pretreatment [54]. Biochemical pretreatment is mainly used to overcome recalcitrant material and increase surface area to optimize cellulose accessibility to cellulases [54–56]. The upstream operation is followed by enzymatic or acidic hydrolysis of cellulosic materials (cellulolysis) and conversion of hemicellulose into monomeric free sugars (saccharification) subsequent to biological fermentation where sugars are fermented into ethanol and then purified via distillation [52, 57]. Concurrently, lignin, the most recalcitrant material of cell walls is combusted and converted into electricity and heat [53].

Overall, biochemical approaches include four unit-operations (as shown in Fig. 7.7) that can be summarized as:

i. pretreatment to degrade the recalcitrant structures of lignocelluloses to open it up for further action,
ii. enzymatic hydrolysis of the polymers into monomeric sugars, and
iii. fermentation of the sugars into alcohol,
iv. separation and recovery of bioethanol.

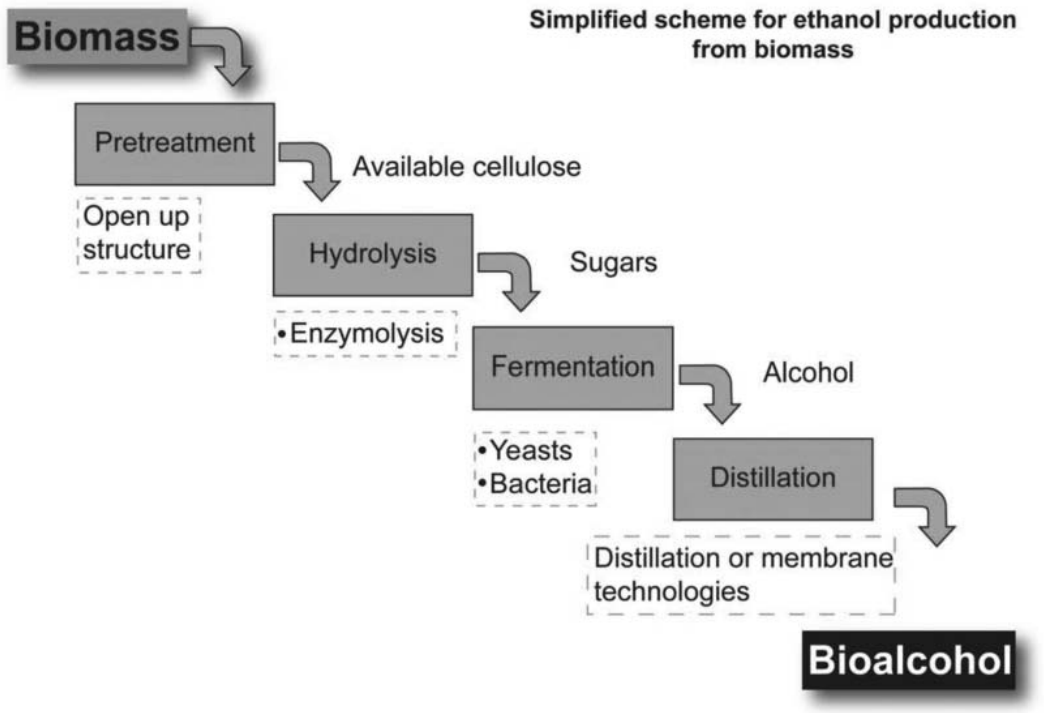

FIGURE 7.7 Simplified representation of biochemical conversion of Lignocellulosic to bioethanol.

Currently the biochemical route is the most commonly used process [58]. Following is the detailed discussion on the salient steps of the biochemical route of conversion of lignocellulosic biomass to bioethanol.

7.5.1 PRE-TREATMENT OF LIGNOCELLULOSIC FEED-STOCK

Pretreatment of recalcitrant lignocellulosic biomass is essential to degrade lignin and facilitation of cellulose and hemicelluloses digestion. Pretreatment or "prehydrolysis" is the process of exposing the cellulose component and making it more susceptible to enzymatic hydrolysis. Various pretreatment techniques involve a synergism between heat action, medium pH and duration of exposure under process conditions. All of these decrease cellulose crystallinity, and consequently, make it more susceptible to action of cellulases [59]. Prima focus of pretreatment research is on developing methods, which are mild, effective, cost-effective and environment-friendly. An effective pretreatment method should:

- degrade the crystalline matrix structure, separate the lignin and facilitate enzymatic action,
- minimize production of toxic by-products or inhibitors detrimental to the enzymes or fermentation microbes,
- reduce loss of the polymers like cellulose and hemicelluloses,
- make the process economical,
- be ecofriendly.

Several pretreatment methods include: physical, physicochemical, chemical or biological. Variation in the structural and compositional of the lignocellulosic matter of different sources, envisages the choice of different pretreatment methods or selection of more than one pretreatment method. In conclusion the selection of pretreatment method depends a lot on the source of the matter, its composition, the subsequent method of hydrolysis the pretreated matter will be subjected to, process parameters, etc.

7.5.2 HYDROLYSIS

During this reaction, the released polymer sugars, cellulose and hemicellulose are hydrolyzed into free monomer molecules readily available for

fermentation conversion to bioethanol [60]. The success of the hydrolysis step is essential to the effectiveness of a pretreatment operation [61]. There are two different types of hydrolysis processes that involve either acidic (sulfuric acid) or enzymatic reactions [62].

7.5.2.1 Acid Hydrolysis

The acidic reaction can be divided into dilute or concentrated acid hydrolysis. Concentrated acid hydrolysis, the more prevalent method, has been considered to be the most practical approach [63]. Unlike dilute acid hydrolysis, this process is not followed by high concentrations of inhibitors nor production of a high yield of free sugars (90%); however, it requires large quantities of acid as well as costly acid recycling, which makes it commercially less attractive [64].

7.5.2.2 Enzymatic Hydrolysis

While acid pretreatment results in a formation of reactive substrates when acid is used as a catalyst, acid hydrolysis causes significant chemical dehydration of the monosaccharide's formed such that aldehydes and other types of degradation products are generated [65]. This particular issue has driven development of research to improve cellulolytic-enzymes and enzymatic hydrolysis. Effective pretreatment is fundamental to a successful enzymatic hydrolysis [66]. During the pretreatment process, the lignocellulosic substrate enzymatic digestibility is improved with the increased porosity of the substrate and cellulose accessibility to cellulases. *Trichoderma reesei* is one of the most efficient and productive fungi used to produce industrial grade cellulolytic enzymes. The most common cellulase groups produced by *T. reesei* that cleave the b(1,4) glycosidic bonds are b-glucosidase, endoglucanases and exoglucanases [67]. However, cellulase enzymes exposed to lignin and phenolic-derived lignin are subjected to adverse effects [68–70] and have demonstrated that phenolic derived lignin have the most inhibitory effects on cellulases. In addition to phenolic components effect on cellulases, lignin has also an adverse effect on cellulases. As mentioned previously, the lignin adverse effect has

two aspects including nonproductive adsorption and the limitation of the accessibility of cellulose to cellulase.

Although considerable genetic modifications (GMs) have been deployed to transform lignin effects, lignin has been shown to be a potential source of self sustaining-energy and added value components. Consequently, several research studies have determined practical approaches in eliminating inhibition of cellulases without involving GM approaches. Lui et al. [71] have demonstrated that the application of metal components namely, Ca (II) and Mg (II) via lignin-metal complexation substantially enhanced enzymatic hydrolysis. Additionally, Erickson et al. [72] have reported the importance of additives namely, surfactants and bovine serum albumin (BSA) in blocking lignin interaction with cellulases. Sewalt et al. [70] have reported that the adverse effect of lignin on cellulases can be surmounted by ammonization and various N compounds. Moreover, the enzymatic treatment can be accomplished simultaneously with the engineered cofermentation microbial process known as simultaneous saccharification and fermentation (SSF) [71, 73]. This process has been of interest since the late 1970 s for its effectiveness to minimize cellulolytic product inhibition and subsequently increase alcohol production [74]. Typically, separate hydrolysis and fermentation (SHF) processes involve the inhibition of the hydrolytic enzymes (cellulases) by saccharide products such as glucose and cellobiose. Unlike SHF, the SSF process combines hydrolysis and fermentation activities simultaneously and hence keeps the concentration of saccharides too low to cause any considerable cellulase inhibition [74].

7.5.2.3 Fermentation

Pretreatment and hydrolysis processes are designed to optimize the fermentation process [61]. This natural, biological pathway depending on the conditions and raw material used requires the presence of microorganisms to ferment sugar into alcohol, lactic acid or other end products [74, 60]. Typically, during batch fermentation *S. cerevisiae* ferments hexose sugars, mainly glucose, into ethanol in a large tank via the Embdene Meyerhof pathway under anaerobic conditions and controlled temperature. In yeast

fermentation this is always accompanied by formation of CO_2 by-products and supplemented by nitrogen to enhance the reaction. This conventional strain is optimal at a temperature of approximately 30°C and resists a high osmotic pressure. It demonstrates tolerance to low pH levels of 4.0 as well as inhibitory products. *S. cerevisiae* can generate a high yield of ethanol (12.0–17.0% w/v; 90% of the theoretical) from hexose sugars.

Traditionally, separate hydrolysis and fermentation (SHF) sequential steps are used in bioethanol production. However, there is particular interest in targeting bioethanol production that can be derived from lignocellulosic biomass materials where both hexose and pentose sugars are available from the hemicellulose fraction.

Despite its broad tolerance to stressful bioethanol process conditions, *S. cerevisiae* is not able to ferment sugars other than hexose. Unfortunately, the biomass material includes a large proportion of hemicellulosic biomass that contains mainly pentose sugars such as D-xylose [78]. Moreover, an optimal fermentative microorganism should be tolerant to a high ethanol concentration and to chemical inhibitors formed during pretreatment and hydrolysis process. Inability of *S. cerevisiae* to ferment pentose sugars, has been attempted to be pacified by conducting extensive efforts to develop genetically engineered microorganisms that are capable of fermenting pentose and hexose sugars simultaneously. An optimal fermentative microorganism should be able to use both hexose and pentose simultaneously with minimal toxic end-products formation.

Different techniques including SSF and consolidated bioprocessing (CBP) have been developed to ensure the combination of hydrolysis (step 3) and fermentation (step 4) in one single reactor and thus, reduce product inhibition and operation costs. In addition to continuing downstream steps, CBP processing integrates both fermentation and cellulase formation in one fermentative/cellulolytic microorganism [79]. However, despite the extensive range of prokaryotic and eukaryotic microorganisms that have been shown to be able to produce ethanol from sugars, most of them remain limited in terms of sugars cofermentation, ethanol yield and tolerance to chemical inhibitors, high temperature and ethanol. Hydrolysis of Lignocellulosic materials not only produces fermentable sugars but also toxic compounds, such as weak acids, furan aldehydes and phenolics [80]. These substances and the presence of other stress

factors often lead to reduced capacity or complete failure of the yeast for ethanol production.

For economic production of low value bulk chemical like ethanol, suitable fermentation conditions are essential to improve the ability of yeast to utilize the lignocellulosic substrate. Rapid ethanol fermentation methods to take place even at inhibiting conditions, that is, with the presence of fermenting toxic media or lignocellulosic hydrolysates are being developed. High cell concentrations inside the reactor were achieved by two methods – yeast encapsulation and fermentation in membrane bioreactors (MBR). The limitations of rapid yeast ethanol fermentation were attempted to be overcome by using these techniques at increased stress conditions like elevated cultivation temperatures, high inhibitor levels, such as high furfural concentration, high acetic acid concentrations and high hydrolysate dilution rates.

7.5.2.4 Separation and Purification of Bioethanol

Bioethanol obtained from a fermentation conversion requires further separation and purification of ethanol from water through a distillation process. Fractional distillation is a process implemented to separate ethanol from water based on their different volatilities. This process consists simply of boiling the ethanol water mixture. Because the boiling point of water is higher than the ethanol-boiling point, ethanol gets converted to steam before water. Thus, water can be separated via a condensation procedure and ethanol distillate recaptured at a concentration of 95% [81]. Typically, most large-scale industries and biorefineries use a continuous distillation column system with multiple effects [82]. Liquid mixtures are heated and allowed to flow continuously all along the column. At the top of the column, volatiles are separated as a distillate and residue is recovered at the bottom of the column.

7.6 MAIN CHALLENGES DURING LIGNOCELLULOSIC FEEDSTOCKS BIOCONVERSION TO BIOETHANOL

To bring down the production cost, several challenges in converting lignocellulosic biomass to biofuels need to be addressed. These challenges are in the areas of:

7.6.1 FEEDSTOCK PRODUCTION

Compositional changes in plant cell wall and differences in ultrastructure greatly influence the pretreatment and the resultant pretreated biomass sugar conversion. Also, the same type of biomass harvested from the same field in different years display changes in biomass composition (due to environmental conditions). This variance poses a challenge in adjusting the processing conditions and directly influences the biofuels yield. The cost of feedstocks significantly influences the cost of biofuel production. It's a challenge to convince farmers who cultivate grains for living to switch to bioenergy feedstocks.

Also most of the lignocellulosic materials are seasonal and need to be available in large quantities to be considered as feedstocks for biofuel industries which are itself yet another challenge. Biomass harvesting is an energy intensive process that requires large machinery and demands large amounts of fuel for transportation [84, 84]. Soil contamination of biomass is considered as one of the biggest challenges in biomass harvesting. Other key challenges are the moisture content of biomass and the amount of biomass that can be harvested from the field [85].

About one-third of biofuel production cost is associated with biomass cost. The cost of biomass is directly proportional to the yield (ton per ha) [86], which is influenced by soil fertility, location, and genetics. The existing challenge is to maintain a continuous supply of the feedstocks to the industries for the production process at a reduced cost.

Solution to these challenges includes plant breeding and genetic engineering techniques that have been applied to increase the yield of several potential energy feedstocks [87, 88]. The following are gene alterations by which growth can be promoted in different energy crops: (i) photosynthetic genes, (ii) transcription factors, (iii) cell cycle machinery, (iv) hormone metabolism, (v) lignin modification [89], and (vi) microRNA. In addition to these genetic manipulations, biomass yield can be improved by manipulating pathways in both abiotic and biotic stress [90, 91].

7.6.2 FEEDSTOCK LOGISTICS

The biomass supply chain include several key processing steps, which are: (i) collection, (ii) storage, (iii) preprocessing (densification by compaction,

pelleting, and briquetting), (iv) transportation (from field to biorefinery), and (v) postprocessing at the biorefinery [92, 93]. These supply chain steps directly impact the cost of feedstock delivery. Texture variance, seasonal availability, low bulk density, and distribution over a large area are major challenges in transporting lignocellulosic biomass to biorefineries [94]. Transportation cost is also influenced by the moisture content, distance from the field to biorefinery, available infrastructure, available on-site technology, and the mode of transportation (rail or road) [95, 96].

7.6.3 CHALLENGES IN BIOCHEMICAL PROCESS OF LIGNOCELLULOSIC BIOMASS CONVERSION

Although lignocellulosic biomass is a potential feedstock for biorefineries, its recalcitrant structure and complexity remains a major economic and technical obstacle to lignocellulosic-based biofuel production [97]. The resilience of lignocellulosic materials is due to their composition and physicochemical matrix. The organization of vascular, epicuticular waxes as well as the amount of sclerenchymatous and the complexity of matrix molecules, contribute to the compactness and strength of the cellulosic material [98].

Furthermore, lignocellulosic materials as discussed previously are composed principally of three components namely, cellulose, hemicellulose and lignin. Together the polysaccharides, cellulose and hemicelluloses serve as initial substrates for subsequent saccharification and fermentation. However, these components are encapsulated via a tight covalent and hydrogen link to the lignin seal [99]. These tight bonds not only give the cell wall its compact structure but limit enzyme access to the surface area. Moreover, cellulose, a polymer of glucose molecules linked via b(1/4) -glycosidic bonds confers to cellulose a crystalline and compact structure [100].

Hemicellulose, the amorphous part of the cell wall, is composed of different hexoses and pentose sugars including xylose and arabinose bonded through xylans b(1/4)-linkages. These varieties of sugars polymers and linkages between molecules impose more complexities to the cell wall and therefore the hydrolysis process necessitates numerous cost-prohibitive enzymes to cleave polysaccharides entirely into fermentable sugar fragments.

Additionally, components including primarily xylo-oligosaccharides produced from hemicelluloses hydrolysis have been shown to be inhibitory to cellulase enzymes [101]. Although xylose causes a higher level of inhibition to cellulase enzymes than xylan, soluble xylo-oligomers are considered the inhibitoriest to cellulase and substantially influence enzymatic hydrolysis [102, 103]. Hence, the removal of these components in addition to organic acids and phenolics is desired in an attempt to achieve an efficient cellulose conversion via enzymatic hydrolysis [104]. Thus, a successful and low-cost ethanol bioconversion is closely related to the efficiency of the pretreatment step.

An effective pretreatment also requires a reduction of energy consumption with minimum toxic inhibitory products formation [105, 106]. However, in addition to these complexities and differences between components within the lignocellulosic material, lignocellulose composition from each type of biomass varies depending on the origin and geographical location. Not all types of lignocellulosic feedstocks require the same pretreatment strategy. These heterogeneities have an important impact on the choice of pretreatments and the downstream processes [107]. Currently, the SPORL treatment is of interest for its broad-spectrum ability on acting in both softwood and strong hardwood materials [108, 109]. This pretreatment degrades high lignin forest material with a limited formation of hydrolysis inhibitors [110].

Other issues include, establishment of biofuel and biochemical standards, biofuel distribution, societal acceptance, and environmental impact minimization. All of these challenging areas require expertise in agronomy, biomass logistics, biomass conversion, process engineering, chemistry, conversion technology, genetic engineering, microbial fermentation, economics, and environmental science.

7.7 RECENT INNOVATIVE APPROACHES TO COMBAT THE BOTTLENECKS IN LIGNOCELLULOSIC BIOCONVERSION TO BIOETHANOL

Several attempts have been tried to improve the quality of enzyme hydrolysis and fermentation. These include: multienzyme action, noncatalytic additives, high solids operation, multimicrobial systems, strain improvement,

simultaneous pretreatment and saccharification, and efficient design of bioreactors. Some of these are discussed in the following sub-sections.

7.7.1 ENZYME CONCOCTION APPROACH

Major costs are incurred by the enzymes, which are used to release and scarify the polysaccharides from the complex lignocellulosic structure during the bioethanol production. This is a great challenge for cost effective bioethanol production. Available cellulases suffer from inhibition due to different end products. Hence, more potent and efficient enzyme preparations are needed for the enzymatic saccharification process at reduced costs.

A large number of cellulases and other complementary enzymes will enable tailoring such cocktails. Pretreatment and the residual lignocellulosic properties is a potent determining factor in tailoring of cellulase mixtures for improvements in overall performance. Rapid screening of hydrolase and transferase functions will be required to screen for activity (e.g., endo-, exo-, betaglucosidase). With the advent of liquid handling automation, miniaturization of enzyme assays, and high throughput screening methodologies, large enzyme libraries from diverse organisms can be evaluated for their enzymic action. High throughput methods are being developed to implement protein engineering for enhancement of enzyme performance on biomass. Despite extensive research on cellulases, there are major gaps in our understanding of the actual mechanism involved in the hydrolysis of crystalline cellulose, mediated by the synergistic action of various constituents of the cellulase enzyme complex including the accessory enzymes. Approaches like enzyme engineering, reconstitution of enzyme mixtures and bioprospecting for superior enzymes are gaining importance [111]. The current scenario, however, also warrants the need for research and development of integrated biomass production and conversion systems.

7.7.2 DIRECT GLUCOSE PRODUCTION USING *CLOSTRIDIUM THERMOCELLUM* CULTURES SUPPLEMENTED WITH A THERMOSTABLE β-*GLUCOSIDASE*

Cost of Cellulases continues to be one of the major determining factors associated with the lignocellulose hydrolysis process. *Clostridium thermocellum*

is an anaerobic, thermophilic, cellulolytic bacterium that produces cellulosomes that are effective plant cell walls degraders. Designer cellulosomes [112–115] and reconstruction of recombinant cellulosomes [116, 117] have been studied for enhancing the hydrolytic action of the strain. The strains ability to grow is higher than its aerobic counterpart while its cellulose yield is lower [118]. Consolidated bioprocessing is one effective proven method capable of resolving these issues to resolve these problems. It relies on *C.thermocellum* to ferment substrate to desired products (for example, ethanol) in one step without adding externally produced enzymes. This approach is widely recognized as for the final configuration for low-cost hydrolysis and fermentation of cellulosic biomass tis method is gaining popularity. Weak tolerance to ethanol and low ethanol yield obtained with this strain limit its immediate and direct application to industrial ethanol fermentation from cellulose [119]. It has been observed that significant enhancement of its cellulolytic activity from the *C. thermocellum* S14 strain [120] could be obtained when in combination with a thermostable β-glucosidase from *Thermoanaerobacter brockii* (CglT) [121].

Moreover the end-product cellobiose, inhibits degradation for which reason the end product action has to eliminated for the successful action of this strain. In biological simultaneous enzyme production and saccharification (BSES) saccharification cultures of *C. thermocellum* cultures supplemented with thermostable β-glucosidases are employed with no additional incorporation of cellulolytic enzymes. Direct production of glucose from cellulosic materials is obtainable due to supplementation of cellulose degrading cultures with β-glucosidase. Exclusive glucose accumulation of glucose occurred when *C. thermocellum* was cultured with a thermostable β-glucosidase under a high cellulose load. This approach can successfully resolve a significant barrier to economical production of bio-based chemicals and fuels from lignocellulosic biomass.

7.7.3 SINGLE STEP BIOETHANOL PRODUCTION BY EMPLOYING NOVEL STRAINS

A process strategy that aims to encompass the critical cost-increasing item is the consolidated bioprocessing approach [122, 123]. In CBP

an organism or a mixed culture of organisms produces the requisite enzymes for hydrolysis of the polymers of lignocellulosic biomass and subsequently ferments the C5 and C6 sugars into ethanol or other valuable products without the extraneous addition of cellulolytic or hemicellulolytic enzymes. Several mesophilic and thermophilic cellulolytic as well as noncellulolytic microorganisms with engineered cellulase activity are under development for the application in CBP [122, 124]. Co-cultivation of the thermophilic cellulolytic bacterium *Clostridium thermocellum* with noncellulolytic thermophilic anaerobes at temperatures of 55–60 °C are being used in CBP. *Caldicellulosiruptor sp.* strain DIB 004C a recently discovered strain is found to be capable of producing impressive yields of ethanol from lignocellulose in fermentors. Thus the cocultures of new *Caldicellulosiruptor* strains with new Thermoanaerobacter strains establish the importance of using specific strain combinations for high ethanol yields. These thus prove effective constituents of CBP pathway for ethanol production and represent a crucial turning point for development of a highly integrated commercial ethanol production process.

7.7.4 USE OF SUPER COMPUTER IN BIOETHANOL PRODUCTION

Computer simulation analysis seem the ultimate means to make detailed structural, dynamic and functional descriptions of otherwise difficult complex biological molecular systems [125]. The simulation procedure involves entering the exhaustive information from experiment and high-level calculations (such as quantum chemistry) to generate an atomic-detail model of the system and its interactions. Subsequently high-performance computer clusters and supercomputers may be employed to follow the system evolution when it is subjected to realistic forces. The technique would aid in revealing the mechanisms of plant cell-wall deconstruction in exquisite detail. This in turn would facilitate a thorough understanding of the structures, dynamics, and degradation pathways of lignocellulosic materials. Because biomass is a multicomponent and complex multiscale material, clarifying its structure is particularly challenging. Advanced and

experimental imaging characterization techniques, such as atomic force microscopy and neutron scattering, which span a wide range of length scales (from angstroms to micrometers) may be employed to elucidate the multicomponent and multiscale structure. Differentiation of individual components from the embedded phases within the biomaterial, such as crystalline and amorphous cellulose, lignin, and hemi-cellulose may also be achieved thereby facilitating the overall bioethanol production.

7.8 SUMMARY

With the abundantly available biomass waste, the development of new technologies that will make use of biomass for biofuels and materials production represents an important opportunity to fully use our resources. Rigorous research in Ligno-cellulosic technology must be conducted to overcome significant challenges in various aspects. Development of efficient techniques to process lignocellulosic biomass into its core components will facilitate research on the production of specific biomass derived sugars, building block chemicals and ultimately value-added commodity chemicals by promoting effective utilization of all feedstock fractions. Research activities undertaken to achieve this include, improvement of the perennial biomass, manipulation of lignin structure and plant cell walls so as to achieve optimal sugar release, trials with new enzymes and improvement of the yeast strains to ferment sugars. An in-depth understanding of the mechanism of interlocking of the sugars in plant structures would further facilitate in the design and development of enzymatic digestion processes for release of sugars by enzymes. This would lead to an effective biofuel production. Currently we lack effective enzymes to digest all kinds of woody materials. Intensive research studies on the digestive process of a range of wood boring microbes, and exploitation of these microbes for extensive industrial application is advocated.

Pretreatment, the most costly step is of particular concern due to the high recalcitrance of lignocellulosic raw materials. It has been deemed imperative to design a general pretreatment combination that would be effective against a wide range of cellulosic material and hence deal with feedstock variability.

Emerging technologies including CBP represent potential improvements as they reduce operation steps as well as chemical inhibitors and can be enhanced by lignin, energy-self-sustaining coproducts. These processes are typically associated with thermophilic and cellulolytic microorganisms with some of them possessing fermentative abilities in addition to their hydrolytic properties. Genetically engineered conventional strains, *S.cerevisiae* and ethanologenic *Z. mobilis* may be preferred for their higher alcohol tolerance and yield. In conjunction to rapid molecular biology techniques, mathematical modeling including biotechnology risk assessment (BRA) can be used to ensure greater predictability for limiting antibiotic resistant microflora and GMO dissemination during operation. While technological accomplishments and multiple research coalition efforts are still progressing, an efficient combination of the most advanced systems analysis and economical techniques designed to cope with lignocellulosic feedstock versatility should emerge as the option of choice in an attempt to achieve optimal biofuel performance with minimal negative environmental, social or economic impacts needs to be adopted and enhanced.

KEYWORDS

- **Biofuels**
- **Bottlenecks**
- **Hydrolysis**
- **Lignocellulosics**
- **Pretreatment**
- **Renewable**

REFERENCES

1. Tilman, D., Socolow, R., Foley, J. A., Hill, J., Larson, E., Lynd, L., Pacala, S., Reilly, J., Searchinger, T., Somerville, C., Williams, R. (2009). Energy. Beneficial biofuels–the food, energy, and environment trilemma. *Science*, *325,* 270–271.
2. Greenwell, H. C., Loyd-Evans, M., Wenner, C. (2012). Biofuels, science and society. *Inter. Foc. 3,* 1–4.
3. Lynd, L. R., Cushman, J. H., Nichols, R. J., Wyman, C. E. (1991). Fuel ethanol from cellulosic biomass. *Science. 251,* 1318–1323.

4. Linoj Kumar, N. V., Sameer, M. Alternative feedstock for bioethanol production in India, in Biofuels: toward a greener and secure energy future, ed by Bhojvaid PP. The Energy and Resources Institute, New Delhi, 89–103 (2006).
5. Hoadley, R. B. Understanding wood: a craftsman's guide to wood technology.2nd ed. Newtown, CT: Taunton Press; 2000.
6. Boone, R. S., Kozlik, C. J., Bois, C. J. P. J., Wengert, P. P. J. E. M. Dry kiln schedules for commercial woods temperate and tropical. Gen. Tech. Rep. FPL_GTR_57.Madison, WI: U. S. Department of Agriculture, Forest Service, Forest Products Laboratory; 1988.
7. Markwardt, L. J., Wilson, T. R. C. Strength and related properties of woods grown in the United States. Tech. Bull. 479. Washington, DC: U.S. Department of Agriculture, Forest Service. U. S. Government Printing Office; 1935.
8. Kennedy, J. H. E. Cottonwood, an American wood. Washington, DC: U. S.Department of Agriculture, Forest Service; 1985.
9. Zhu, J. Y., Pan, H. J. (2010). Woody biomass treatment for cellulosic ethanol production:technology and energy consumption evaluation. *Bioresour. Technol. 101,* 4992–5002.
10. Perlack, R. D., Wright, L., Turhollow, L. A., Graham, R. L., Stokes, B., Erbach, D. C. Biomass as feedstock for a bioenergy and bioproducts industry: the technical feasibility of a billion-ton annual supply. Oak Ridge National Laboratory Report ORNL/TM-2005/66. Oak Ridge, TN: US Dept. of Energy; 2005.
11. U. S. Department of Energy Biomass Program. http://www1.eere.energy.gov/biomass/pdfs/biomass_deep_dive_pir.pdf. 2009.
12. Hu, G., Heitmann, J. A., Rojas, O. J. (2008). Feedstock pretreatments strategies for producing ethanol from wood, bark, and forest residues. *BioRes. 3,* 270–294.
13. Hill, J., Nelson, E., Tilman, D., Polasky, S., Tiffany, D. Environmental, economic, and energetic costs and benefits of biodiesel and ethanol biofuels. *Proc. Nat. Acad. Sci. USA. 103*, 11206–11210.
14. Chandel, A. K., Singh, V. (2011). Weedy lignocellulosic feedstock and microbial metabolic engineering: advancing the generation of 'Biofuel'. *App. Microbiol. Biotechnol. 89*, 1289–1303.
15. Muir, J. P., Sanderson, M. A., Ocumpaugh, W. R., Jones, R. M., Reed, R. L. (2001). Biomass production of 'Alamo' switchgrass in response to nitrogen, phosphorus, and row spacing. *Agron. J. 93,* 896–901.
16. Byrt, C. S., Grof, C. P. L., Furbank, R. T. (2011). C_4 Plants as biofuel feedstocks: optimizing biomass production and feedstock quality from a lignocellulosic perspective. *J. Integr. Plant. Biol. 53,* 120–135.
17. Demirbas, A. (2005). Bioethanol from cellulosic materials: a renewable motor fuel from biomass. *Energy. Source. 27,* 327–337.
18. Knauf, M., Moniruzzaman, M. Lignocellulosic biomass processing. *Persp. Int. Sugar. J.* (2004). *106,* 147–150.
19. Kim, S., Dale, B. E. (2005). Global potential bioethanol production from wasted crops and crops residues. *Biomass. Bioenerg. 29,* 361–375.
20. Cardona, C. A., Quintero, J. A., Paz, I. C. (2009). Production of bioethanol from sugarcane bagasse: status and perspectives. *Bioresour. Technol. 101,* 4754–4766.

21. Khanna, M. A billion tons of biomass a viable goal but at high price. *Am J Agric Econ*, http://news.illinois.edu/news/11/0216biomass_MadhuKhanna.html; 2011.
22. Emerging markets, ALGAE (2020). http://www.emerging-markets.com/algae/; 2011.
23. Rodolfi, L., Zitelli, G. C., Bassi, N., Padovani, G., Biondi, N., Bionini, G., et al. (2009). Microalgae for oil: strain selection, induction of lipid synthesis and outdoor mass cultivation in a low-cost photo-bioreactor. *Biotechnol. Bioeng. 102,* 100–112.
24. Harel, A. Noritech seaweed biotechnology Inc. Algae World Conference.Rotterdam, NL. 2009.
25. Pettersen, R. C. (1984). The chemical composition of wood. In: Rowell RM, editor. The chemistry of solid wood. Advances in chemistry series, vol. 207. Washington, DC: American Chemical Society; p. 115e6.
26. Badger, P. C. In: Jannick J, Whipsekey A, editors. (2000). Trends in new crops and new uses. Alexandria, VA: ASHS Press; p. 17e21.
27. Mielenz, J. R. (2001). Ethanol production from biomass: technology and commercialization status. *Curr. Opin. Microbiol. 4,* 324–325.
28. Girio, F. M., Fonseca, C., Carvalheiro, F., Duarte, L. C., Marques, S., Bogel-Lukasic, R. (2010). Hemicellulose. *Bioresour. Technol. 101,* 4775–4800.
29. Edye, L. A., Doherty, W. O. S. Fractionation of a lignocellulosic material. PCT Int Appl 2008; 25.
30. McMillan, J. D. (1993). Pretreatment of lignocellulosic biomass. In: Himmel ME, Baker JO, Overend RP, editors. Enzymatic conversion of biomass for fuel production. Washington, D.C: American Chemical Society; p. 292e323.
31. Saha, B. D. (2003). Hemicellulose bioconversion. *J. Ind. Microbiol. Biotechnol. 30,* 279–291.
32. Aspinall, G. O. (1980).Chemistry of cell wall polysaccharides. In: Preiss J, editor. The biochemistry of plants (a comprehensive treatise). Carbohydrates structure and function, vol. 3. NY: Academic Press; p. 473e500.
33. Ebringerova, A., Hromadkova, Z., Heinze, T. (2005). Hemicellulose. *Adv. Polym. Sci. 186,* 1–67.
34. Deguchi, S., Mukai, S. A., Tsudome, M., Horikoshi, K. (2006). Facile generation of fullerene nanoparticles by hand-grinding. *Adv. Mater. 18,* 729–732.
35. Foody, B. E., Foody, K. J. (2006). Development of an integrated system for producing ethanol from biomass. In: Klass DL, editor. Energy from biomass and waste. Chicago: Institute of Gas Technology; 1991. p. 1225e43.
36. Ladisch, M. R., Mosier, N. S., Kim, Y., Ximenes, E., Hogsett, D. (2010). Converting cellulose to biofuels. SBE special supplement biofuels. CEP *106 (3),* 56e63
37. ENERS Energy Concept. Production of biofuels in the world.Lausanne, 2009. http://www.plateforme-biocarburants.ch/en/infos/production.php?id = bioethanol.
38. Fukuda, H., Kondo, A., Noda, H. (2001). Biodiesel Fuel Production by Transesterification of Oils.*J. Biosci. Bioeng*. *92*, 405–416.
39. Ma, F. R., Hanna, M. A. (1999). Biodiesel production: a review. *Bioresour. Technol. 70,* 1–15.
40. Kim, H. J., Kang, B. S., Kim, M. J., Park, Y. M., Kim, D. K., Lee, D. S., Lee, K. Y. (2004). Transesterification of vegetable oil to biodiesel using heterogeneous base catalyst. *Catal. Today.* 93–95, 315–320.

41. Di Serio, M., Ledda, M., Cozzolino, M., Minutillo, G., Tesser, R., Santacesaria, E. (2006). Transesterification of soybean oil to biodiesel by using heterogeneous basic catalysts. *Ind. Eng. Chem. Res. 45,* 3009–3014.
42. Granados, M. L., Poves, M. D. Z., Alonso, D. M., Mariscal, R., Galisteo, F. C., Moreno-Tost, R., Santamaria, J., Fierro, J. L. G. (2007). Biodiesel from surflower oil by using activated calcium oxide. *Appl.Catal., B. 73,* 317–326.
43. Lotero, E., Liu, Y. J., Lopez, D. E., Suwannakarn, K., Bruce, D. A., Goodwin, J. G. (2005). Synthesis of biodiesel via acid catalysis. *Ind. Eng. Chem. Res. 44,* 5353–5363.
44. Melero, J. A., Iglesias, J., Morales, G. (2009). Heterogenous acid catalysts for Biodiesel production:current status and future challenges. *Green. Chem. 11*, 1285–1308
45. Huber, G. W., O'Connor, P., Corma, A. (2007). Processing biomass in conventional oil refineries: Production of high quality diesel by hydrotreating vegetable oils in heavy vacuum oil mixtures.*Appl. Catal. A. 329*, 120–129.
46. Wheals, A. E., Basso, L. C., Alves, D. M. G., Amorim, H. V. (1999). Fuel ethanol after 25 years. *Trends. Biotechnol. 17,* 482–487.
47. Li, L. X., Coppola, E., Rine, J., Miller, J. L., Walker, D. (2010). Catalytic Hydrothermal Conversion of Triglycerides. Non-ester Biofuels. *Energy. Fuel. 24,* 1305–1315.
48. Fern'andez, J., Curt, M. D., Aguado, P. L. (2006). Industrial applications of *Cynara cardunculus L*. for energy and other uses. *Ind. Crops Prod. 24*, 222–229.
49. Patil, P. D., Deng, S. (2009). Optimization of biodiesel production from edible and nonedible vegetable oils. *Fuel. 88,* 1302–1306.
50. Chisti, Y. (2007). Biodiesel from microalgae. *Biotechnol. Adv. 25,* 294–306.
51. Demirbas, A. (2007). Progress and recent trends in biofuels. *Prog. Energy. Combust. Sci. 33,* 1–18.
52. Chandel, A. K., Chan, E., Rudravaram, R., Narasu, M. L., Rao, L. V., Ravindra, P. (2007). Economics and environmental impact of bioethanol production technologies: an appraisal. *Biotechnol. Mol. Biol. Rev. 2,* 14–32.
53. Gamage, J., Howard, L., Zisheng, Z. (2010). Bioethanol production from lignocellulosic biomass. *J. Biobased. Mater. Bioenerg. 4,* 3–11.
54. Yang, B., Wyman, C. E. (2008). The key to unlocking low-cost cellulosic ethanol. Biofuels. Bioprod. Bioref. *2,* 26–40.
55. Zhu, J. Y., Pan, H. J. (2010). Woody biomass treatment for cellulosic ethanol production:technology and energy consumption evaluation. *Bioresour. Technol. 101,* 4992–5002.
56. Yang, B., Wyman, C. E. (2008). The key to unlocking low-cost cellulosic ethanol. *Biofuels. Bioprod. Bioref. 2,* 26–40.
57. Zhu, J. Y., Wang, G. S., Pan, X. J., Gleisner, R. (2009). Specific surface to evaluate the efficiencies of milling and pretreatment of wood for enzymatic saccharification. *Chem. Eng. Sci. 64,* 474–485.
58. Fehrenbacher, K. Logen suspends U. S. cellulosic ethanol plant plans [accessed October 22], http:earth2tech.com/2008/06/04/iogen-suspends-uscellulosic-ethanol-plant-plans-/; 2009.
59. Lynd, L. R., Weimer, P. J., Van Zyl, W. H., Pretorius, I. S. Microbial cellulose utilization: fundamentals and biotechnology. *Microbiol. Molecul. Biol.* Rev. (2002). *66,* 506–577.

60. Chandel, A. K., Chan, E., Rudravaram, R., Narasu, M. L., Rao, L. V., Ravindra, P. (2007). Economics and environmental impact of bioethanol production technologies: an appraisal. *Biotechnol. Mol. Biol. Rev. 2*, 14–32.
61. Gamage, J., Howard, L., Zisheng, Z. (2010). Bioethanol production from lignocellulosic biomass. *J. Biobased. Mater. Bioenerg. 4,* 3–11.
62. Nazhad, M. M., Ramos, L. P., Paszner, L., Saddler, J. N. (1995). Structural constraints affecting the initial enzymatic hydrolysis of recycled paper. *Enzyme. Microbiol. Technol. 17*, 66–74.
63. Torget, R., Walter, P., Himmel, M., Grohmann, K. (1991). Dilute acid pretreatment of short rotation woody and herbaceous crops. *Appl. Biochem. Biotechnol.* 4–25, 115–126.
64. Hamelinck, C. N., Hooijdonk, G., Faaij, A. P. C. (2005). Ethanol from lignocellulosic biomass: techno-economic performance in short-, middle- and long-term. *Biomass. Bioenerg. 28,* 384–410.
65. Sun, Y., Cheng, J. (2002). Hydrolysis of lignocellulosic materials for ethanol production: a review. *Bioresour. Technol. 83,* 1–11.
66. Hendriks, A. T. W. M., Zeeman, G. (2009). Pretreatments to enhance the digestibility of lignocellulosic biomass. *Bioresour. Technol. 100,* 10–18.
67. Eggeman, T., Elander, R. T. (2005). Process and economic analysis of pretreatments technologies. *Bioresour. Technol. 96,* 2019–2025.
68. Larsson, S., Palmqvist, E., Hahn-Hagerdal, B., Tengborg, C., Stenberg, K., Zacchi G., et al. (1999). The generation of fermentation inhibitors during dilutes acid hydrolysis of softwood. *Enzyme. Microbiol. Technol. 24,* 151–159.
69. Ximenes, E., Kim, Y., Mosier, N., Dien, B., Ladisch, M. (2010). Inhibition of cellulases by phenols. *Enzyme. Microbiol. Technol. 46,* 170–176.
70. Sewalt, V. J. H., Glasser, W. G., Beauchemin, K. A. (1997). Lignin impact on fiber degradation. 3. Reversal of inhibition of enzymatic hydrolysis by chemical modification of lignin and by additives. *J. Agric. Food. Chem. 45,* 1823–1828.
71. Cao, N. J., Krishnan, M. S., Du, J. X., Gong, C. S., Ho, N. W. Y. (1996). Ethanol production from corn cob pretreated by the ammonia steeping process using genetically engineered yeast. *Biotechnol. Lett. 118,* 1013–1018.
72. Erickson, T., Borjesson, J., Tjerneld, F. (2002). Mechanism of surfactant effect in enzymatic hydrolysis of lignocelluloses. *Enzyme. Microbiol. Technol. 31,* 353–364.
73. Bisaria, V. S., Ghose, T. K. (1981). Biodegradation of cellulosic materials: substrate, microorganisms, enzymes and products. *Enzyme. Microbiol. Technol. 3,* 90–104.
74. Kumar, S., Singh, S. P., Mishra, I. M., Adhikari, D. K. (2009). Recent advances in production of bioethanol from lignocellulosic biomass. *Chem. Eng. Technol. 32,* 517–526.
75. Hahn-Hägerdal, B., Karhumaa, H. B. K., Fonseca, C., Spencer-Martins, I., Gorwa-Grauslund, M. F. (2007). Toward industrial pentose-fermenting yeast strains. *Appl. Microbiol. Biotechnol. 74,* 937–953.
76. Bayrock, D., Ingledew, W. M. (2001). Changes in steady state on introduction of a Lactobacillus contaminant to a continuous culture ethanol fermentation. *J. Ind. Microbiol. Biotechnol. 27,* 39–45.

77. Claassen, P. A. M., Lopez, C., Sijtsma, A. M., Weusthuis, L., Van Lier, R. A., Van Niel, J.B, et al. (1999). Utilization of biomass for the supply of energy carriers. Appl. Microbiol. Biotechnol. *52,* 741–755.
78. Martin, C., Galbe Wahlbom, M., Hagerdal, B. H., Jonsson, J. L. (2002). Ethanol productionfrom enzymatic hydrolysates of sugarcane bagasses using recombinantxylose using Saccharomyces cerevisisae. *Enzyme. Microbiol. Technol. 31 (2),* 274–282.
79. Ladisch, M. R., Mosier, N. S., Kim, Y., Ximenes, E., Hogsett, D. (2010). Converting cellulose to biofuels. *SBE special supplement biofuels. CEP*, *6 (3),* 56–63.
80. Demain, A. L., Newcomb, M., Wu, J. H. D. (2005). Cellulase, clostridia and ethanol. *Microbiol. Mol. Biol. Rev. 69,* 124–154.
81. Cardona, C. A., Sanchez, O. J. (2007). Fuel ethanol production: process design trends and integration opportunities. *Bioresour. Technol. 98,* 2415–2457.
82. Kent, N. L., Evers, A. D. (1994). Malting, brewing and distiling. In: Kent's technology of cereals. 4th ed., vol. 4. Cambridge: Woodhead Publishing; p. 218–232.
83. McKendry, P. (2002). Energy production from biomass (part 1): overview of biomass. *Bioresour. Technol. 83,* 37–46.
84. Thorsell, S., Epplin, F. M., Huhnke, R. L., Taliaferro, C. M. (2004). Economics of a coordinated biorefinery feedstock harvest system: lignocellulosic biomass harvest cost. *Biomass. Bioenerg. 27,* 327–337.
85. Huggins, D. R., Karow, R. S., Collins, H. P., Ransom, J. K. (2011). Introduction: evaluating long- termimpacts of harvesting crop residues on soil quality. *Agron. J. 103,* 230–233.
86. Duffy, M. D., Nanhou, V. Y. Switchgrass Production in Iowa: Economic Analysis, Special publication for Cahriton Valley Resource Conservation District, Iowa State University Extension Publication, Iowa State University, 2002.
87. Rojas, C. A., Hemerly, A. S., Ferreira, P. C. G. (2010). Genetically modified crops for biomass increase. Genes and strategies. *GM. Crop. 1,* 137–142.
88. Dubouzet, J.G, ; Strabala, T. J., Wagner, A. (2013). Potential transgenic routes to increase tree biomass. Plant. Sci. *212,* 72–101.
89. Vanholme, R., Morreel, K., Darrah, C. et al. (2012). Metabolic engineering of novel lignin in biomass crops. *New. Phytol. 196,* 978–1000.
90. Sticklen, M. (2006). Plant genetic engineering to improve biomass characteristics for biofuels. *Curr. Opin. Biotechnol. 17,* 315–319.
91. Bhatnagar-Mathur, P., Vadez, V., Sharma, K. K. (2008). Transgenic approaches for abiotic stress tolerance in plants: retrospect and prospects. *Plant. Cell. Report. 27*, 411–424.
92. Sokhansanj, S., Hess, J. R. "Biomass supply logistics and infrastructure," in Biofuels:Methods and Protocols, J. R.Mielenz, Ed., vol. 581 of Methods in Molecular Biology, chapter 1, pp. 1–25, Springer, Berlin, Germany, 2009.
93. Sultana, A., Kumar, A., Harfield, D. (2010). Development of agripellet production cost and optimum size. *Bioresour. Technol. 101,* 5609–5621.
94. Caputo, A. C., Palumbo, M., Pelagagge, P. M., Scacchia, F. (2005). Economics of biomass energy utilization in combustion and gasification plants: effects of logistic variables. *Biomass. Bioenerg. 28,* 35–51.

95. Kumar, A., Sokhansanj, S., Flynn, P. C. (2006). Development of a multicriteria assessment model for ranking biomass feedstock collection and transportation systems. Appl. Biochem. Biotechnol. *129,* 71–87.
96. Badger, P. C. Biomass transport systems, in Encyclopedia of Agricultural, Food and Biological Engineering, vol. 1, pp. 94–98, 2003.
97. Yu, Z., Zhang, B., Yu, F., Xu, G., Song, A. (2012). A real explosion: the requirement of steam explosion pretreatment. *Bioresour. Technol. 121,* 335–341.
98. Hideno, A., Inoue, H., Tsukahara, K. et al. (2009). Wet disk milling pretreatment without sulfuric acid for enzymatic hydrolysis of rice straw. *Bioresour. Technol. 100,* 2706–2711.
99. Dadi, A. P., Schall, C. A., Varanasi, S. (2007). Mitigation of cellulose recalcitrance to enzymatic hydrolysis by ionic liquid pretreatment. *Appl. Biochem. Biotechnol.* 137–140, 407–421.
100. Kaliyan, N., Morey, R, V. (2010). Natural binders and solid bridgetype binding mechanisms in briquettes and pellets made from corn stover and switchgrass. *Bioresour. Technol. 101,* 1082–1090.
101. Zhang Y., Fu, X., Chen, H. (2012). Pretreatment based on twostep steam explosion combined with an intermediate separation of fiber cells-optimization of fermentation of corn straw hydrolysates. *Bioresour. Technol. 121,* 100–104.
102. Zheng, Y., Lin, H. M., Tsao, G. T. (1998). Pretreatment for cellulose hydrolysis by carbon dioxide explosion. *Biotechnol. Progr. 14,* 890–896.
103. S'anchez, O. J., Cardona, C. A. (2008). Trends in biotechnological production of fuel ethanol from different feedstocks. Bioresour. Technol. *99,* 5270–5295.
104. Sharma, B., Ingalls, R. G., Jones, C. L., Khanchi, A. (2013). Biomass supply chain design and analysis: basis, overview, modeling, challenges, and future. *Renew. Sust. Energy Rev. 24,* 608–627.
105. Dubouzet, J. G., Strabala, T. J., Wagner, A. (2013). Potential transgenic routes to increase tree biomass. *Plant Sci. 212,* 72–101.
106. Zhu, X., Li, X., Yao, Q., Chen, Y. (2011). Challenges and models in supporting logistics system design for dedicated-biomass-based bioenergy industry. *Bioresour. Technol. 102,* 1344–1351.
107. Balan, V., da Costa Sousa, L., Chundawat, S. P. S., Vismeh, R., Jones, A. D., Dale, B. E. (2008). Mushroom spent straw: a potential substrate for an ethanol-based biorefinery. J. Indust. Microbiol. Biotechnol. *35,* 293–301.
108. Dale, B. E., Ong, R. G. (2012). Energy, wealth, and human development: why and how biomass pretreatment research must improve. *Biotechnol. Progr. 28,* 893–898.
109. Balan, V., Bals, B., Chundawat, S. P. S., Marshall, D., Dale, B. E. Lignocellulosic biomass pretreatment using AFEX," in Biofuels: Methods and Protocols, Mielenz, J. R. Ed., vol. 581ISRN Biotechnology 27 of Methods in Molecular Biology, pp. 61–77, Humana Press, Springer Science + Business Media, LLC, 2009.
110. Chundawat, S. P. S., Bals, B., Campbell, T. et al.,"Primer on ammonia fiber expansion pretreatment," in Aqueous Pretreatment of Plant Biomass for Biological and Chemical Conversion to fuels and Chemicals, C.Wyman, Ed., Wiley Series in Renewable Resources, chapter 9, pp. 169–195, JohnWiley&Sons, NewYork, NY, USA, 1st edition, 2013.

111. Mohanram, S., Amat, D., Choudhary, J., Arora, A., Nain, L., et al. (2013). Novel perspectives for evolving enzyme cocktails for lignocellulose hydrolysis in biorefineries. *Sust. Chem. Process. 1,* 15.
112. Bayer, E., Belaich, J., Shoham, Y., Lamed, R. The cellulosomes: multienzyme machines for degradation of plant cell wall polysaccharides. *Annu. Rev. Microbiol.* (2004). *58,* 521–554.
113. Moraïs, S., Barak, Y., Caspi, J., Hadar, Y., Lamed, R., Shoham, Y., Wilson, D. B., Bayer, E. A. (2010). Cellulase-xylanase synergy in designer cellulosomes for enhanced degradation of a complex cellulosic substrate. *M. Bio.* 1.
114. Bayer, E. A., Morag, E., Lamed, R. (1994). The cellulosome–a treasure-trove for biotechnology. *Trends. Biotechnol. 12*, 379–386.
115. Doi, R. H., Kosugi, A. (2004). Cellulosomes: plant-cell-wall-degrading enzyme complexes. *Nat. Rev. Micro. 2,* 541–551.
116. Krauss, J., Zverlov, V. V., Schwarz, W. H. In vitro reconstitution of the complete Clostridium thermocellum cellulosome and synergistic activity on crystalline cellulose. *Appl. Environ. Microbiol.* (2012). *78,* 4301–4307.
117. Demain, A., Newcomb, M., Wu, J. (2005). Cellulase, clostridia, and ethanol. *Microbiol. Mol. Biol. Rev. 69,* 124–154.
118. Tachaapaikoon, C., Kosugi, A., Pason, P., Weonukul, R., Ratanakhanokchai, K., Kyu, K., Arai, T., Murata, Y., Mori, Y. (2012). Isolation and characterization of a new cellulosome-producing *Clostridium thermocellum* strain. *Biodegradation. 23,* 57–68.
119. Lynd, L., Weimer, P., Van Zyl, W., Pretorius I: Microbial cellulose utilization: fundamentals and biotechnology. *Microbiol. Mol. Biol. Rev.* (2002). *66,* 506–577.
120. Weonukul, R., Kosugi, A., Tachaapaikoon, C., Pason, P., Ratanakhanokchai, K., Prawitwong, P., Deng, L., Saito, M., Mori, Y. (2012). Efficient saccharification of ammonia soaked rice straw by combination of *Clostridium thermocellum* cellulosome and *Thermoanaerobacter brockii* β-glucosidase. *Bioresour. Technol. 107,* 352–357.
121. Svetlitchnyi, V. A., Kensch, O., Falkenhan, D. A., Korseska, S. G., Lippert, N., Prinz, M., Sassi, J., Schickor, A., Svetlitchnyi, S. C. et al. (2013). Single-step ethanol production from lignocellulose using novel extremely thermophilic bacteria. *Biotechnol. Biofuel. 6,* 31
122. Olson, D. G., McBride, J. E., Joe Shaw, A., Lynd, L. R. Recent progress in consolidated bioprocessing. *Curr. Opin. Biotechnol.* (2011). *23,* 1–10.
123. Lynd, L. R., Weimer, P. J., van Zyl, W. H. Pretorius I. S. (2002). Microbial cellulose utilization: fundamentals and biotechnology. *Microbiol. Mol. Biol. Rev. 66,* 506–577.
124. La Grange, D. C., den Haan, R., van Zyl, W. H. (2010). Engineering cellulolytic ability into bioprocessing organisms. *Appl. Microbiol. Biotechnol. 87,* 1195–1208.
125. Alonso, D. M., Bond, J. Q., Dumesic, J. A. Catalytic conversion of biomass to biofuels. *Green. Chem.* (2010). *12,* 1493–1513.
126. Roy, A., Kumar, A. (2013). Pretreatment Methods of Lignocellulosic Materials for Biofuel Production: A Review. *J. Emerg. Trend. Eng. Appl. Sci. 4,* 181–193.

PART 4

BIODESEL PRODUCTION

CHAPTER 8

BIODIESEL: PRODUCTION, OPPORTUNITIES AND CHALLENGES

DEEKSHA SACHDEVA

Department of Biochemistry, Punjab Agricultural University, Ludhiana, Punjab, India–141004; E-mail: sachdeeksha@gmail.com

CONTENTS

8.1 Introduction 208
8.2 Generations of Biofuels 209
8.2.1 First Generation Biofuels 209
8.2.2 Second Generation Biofuels 209
8.2.3 Third Generation Biofuels 209
8.2.4 Fourth Generation Biofuels 210
8.3 Sources of Biodiesel or Feedstock 210
8.3.1 Biodiesel From Waste Cooking Oil (WCO) 210
8.4 Chemical Nature of Biodiesel 212
8.5 Synthesis of Biodiesel by Trans-Esterification 213
8.6 Factors Affecting Rate of Reaction 213
8.7 Catalysis of Transesterification 214
8.7.1 Base or Acid Catalysis 214
8.7.2 Enzymatic Catalysis 214
8.8 Microbial Synthesis of Biodiesel 214
8.9 Blends 215

8.10 Benefits of Biodiesel 215
8.11 Other Uses of Biodiesel 216
8.12 Energy Balance Ratio 217
8.13 Challenges 217
8.14 Conclusion 218
Keywords 218
References 218

8.1 INTRODUCTION

Bioenergy is an energy source derived from organic matter or biomass. It can be as low-tech as burning wood on an open fire or as high-tech as developing advanced production methods for biofuels. The unifying factor with all bioenergy sources, however, is that the carbon they contain (and emit when used) comes from plants, and those plants obtain their carbon from the atmosphere. Hence, bioenergy is considered to be renewable.

In the light of the risks posed by climate change and diminishing oil reserves, energy transition from fossil fuels to low-carbon sources of energy seems imminent. Solar, wind, geothermal and biofuels all play an important role in this transition.

The main drivers for biofuels and bioenergy development are [1]:

- need to reduce greenhouse gas (GHG) emissions;
- energy security concerns;
- rising oil prices; and
- the opportunity to support the countries' rural economy.

Biodiesel, a methyl ester, is an alternative to diesel that is made from a triglyceride (like vegetable oil) and either ethanol or methanol. Biodiesel production is based on transesterification of vegetable oils and fats through the addition of alcohol and a catalyst. Feedstock includes rapeseeds, sunflower seeds, soy seeds and palm oil seeds from which the oil is extracted chemically or mechanically. Advanced processes include the replacement of methanol of fossil origin, by bioethanol to produce fatty acid ethyl ester instead of fatty acid methyl ester (the latter being the traditional bio-diesel).

8.2 GENERATIONS OF BIOFUELS

8.2.1 FIRST GENERATION BIOFUELS

First Generation Biofuels are the ones, which are produced directly from food crops by extracting the oils from them and is used for biodiesel synthesis through fermentation. Crops such as oilseed rape, sunflower seeds, etc., are used for biodiesel production. However, first generation biofuels have a number of associated problems. One major issue with first generation biofuels is "fuel v/s food". As the majority of biofuels are produced directly from food crops, the rise in demand for biofuels has led to global increase in food prices.

8.2.2 SECOND GENERATION BIOFUELS

Second Generation Biofuels have been developed to overcome the limitations of first generation biofuels. They are produced from nonfood crops such as wood, organic waste, food crop waste and specific biomass (lignocellulosic biomass) crops. Low-cost crops and forest residues, wood process wastes and the organic fraction of municipal solid wastes can be used as ligno-cellulosic feedstocks. This eliminates the main issue with the first generation biofuels.

8.2.3 THIRD GENERATION BIOFUELS

The third generation of biofuels is based on improvements in the production of biomass. It takes advantage of specially engineered energy crops such as algae as its energy source. The algae are cultured to act as a low-cost, high energy and renewable feedstock. Algae can also be grown using land and water unsuitable for food production therefore reducing the strain on already depleted water sources. Another benefit of algae based biofuels is that the fuel can be manufactured into a wide range of fuels such as diesel, petrol and jet fuel.

Production of biofuels from algae depends on the lipid content of the microorganisms. Algae species such as *Chlorella* are targeted because

of their high lipid content and high productivity [2, 3]. Algae produces 1 to 7 g/L/d of biomass in ideal growth conditions [3]. This requires large volumes of water, which is a problem for cold countries such as Canada where temperature is below 0°C during a significant part of year. High water content is again a problem while extracting lipids from the algal biomass, which needs dewatering via either centrifugation or filtration before extracting lipids. Lipids extracted from algae can be processed via transesterification [4].

8.2.4 FOURTH GENERATION BIOFUELS

Fourth Generation Biofuels involves the use of genetically modified organisms or metabolic engineering of microorganisms to as to achieve sustainable production of biofuels. Since gene expression and metabolic pathways are well understood in *E. coli* as compared to other microorganisms therefore, it is relatively easy to apply genetic engineering and metabolic engineering to improve the oil accumulation in bacteria [5]. It was reported that a metabolically engineered *E. coli* could produce biodiesel directly and the concentration of fatty acid esters obtained was 1.28 g/1 [6].

8.3 SOURCES OF BIODIESEL OR FEEDSTOCK

Biodiesel can be produced by animal fats, cooking waste and vegetable oils. Various edible and non edible vegetable oils like rice bran oil, coconut oil, *Jatrophacurcas*, castor oil, cottonseed oil, mahua, karanja which are either surplus and are nonedible type, can be used for the preparation of biodiesel [7] (Fig. 8.1, Table 8.1).

8.3.1 BIODIESEL FROM WASTE COOKING OIL (WCO)

The high cost of biodiesel is mainly due to the cost of virgin vegetable oil. Therefore, it is not surprising that the biodiesel produced from vegetable oil (e.g., pure soybean oil) costs much more than petroleum based

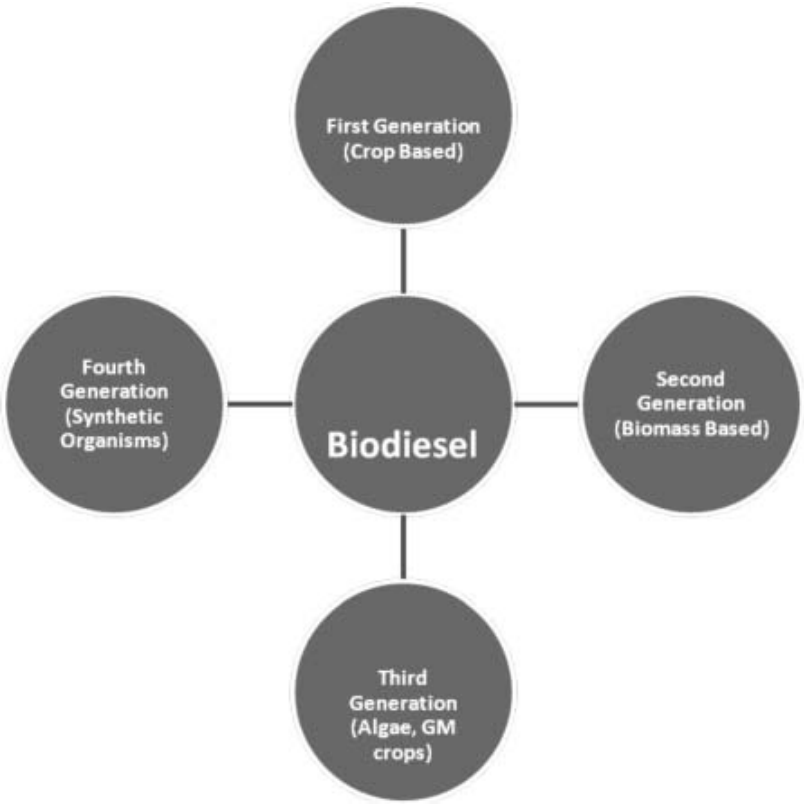

FIGURE 8.1 Sources of biodiesel.

TABLE 8.1 Sources of Biodiesel

Vegetable oils	Non-edible oils	Animal fats	Other sources
• Soybean	• Jatropha	• Fish oil	• Algae
• Sunflower	• Palm	• Poultry fat	• Microalgae
• Rapeseed	• Almond		• Cooking oil (yellow grease)
• Canola	• *Brassica napus*		• Bacteria
• Coconut	• *Brassica carinata*		• Fungi
• Cotton seed	• Camelina		

diesel. Therefore, it is necessary to explore ways to reduce production costs of biodiesel. The use of waste frying oil, instead of virgin oil, to produce biodiesel is an effective way to reduce the raw material cost because waste-frying oil is estimated to be about half the price of virgin oil [8]. Uddin et al. [9] reported the synthesis of biodiesel from waste cook oil by

a three-step method. Transesterification gives lower yield than three-step method. In the three-step method, the first step is saponification of the oil followed by acidification to produce FFA and finally esterification of FFA to produce biodiesel. The reaction yield was 79%.

8.4 CHEMICAL NATURE OF BIODIESEL

Biodiesel is produced from vegetable oils and fats by transesterification process. Fats and oils are primarily water-insoluble and hydrophobic in nature, composed of one mole of glycerol and three moles of fatty acids and commonly called as triglycerides [10]. Triglycerides have good amount of oxygen in their structure. When three fatty acids, in triglycerides, are identical it is called simple triglycerides. When they are dissimilar, they are called mixed triglycerides. Oils found in different sources have different fatty acid compositions. The fatty acids vary not only in their carbon chain length but also in the number of unsaturated bonds in the carbon chain. The fatty acids commonly found in vegetable oils are stearic, palmitic, oleic, linoleic and linolenic. The other fatty acids, which are also present in oils and fats, are myristic (tetradecanoic), palmitoleic, arachidic, linolenic and octadecatetranoic [11]. Chemically, biodiesel is mono-alkyl esters of long chain fatty acids from renewable lipid sources. In other words, biodiesel is ester based oxygenated fuel from renewable biological sources. It can be used in compression ignition engines with little or no modifications [11, 12]. On the contrary, petroleum derived diesel, called as petrodiesel, is composed of 75% saturated hyrdocarbon or 25% aromatic hydrocarbon, with average chemical formula $C_{12}H_{23}$ [13].

Depending on the fatty acid composition, the quality of fatty acid methyl esters of oil (biodiesel) was predicted. Fatty acid methyl ester of oils of 26 species including *Azadirachta indica*, *Calophyllum inophyllum*, *Jatropha curcas* and *Pongamia pinnata* were found most suitable for use as biodiesel and they meet the major specification of Biodiesel standards of USA, Germany and European Standard Organization [14]. The fatty acid methyl esters of another 11 species meet the specification of Biodiesel standard of USA only. These selected plants have great potential for biodiesel [15].

Thus, oil, ester and diesel have different number of carbon and hydrogen compound. Diesel has no oxygen atom while biodiesel is oxygenated fuel. The large size of vegetable oil molecules (typically three or more times larger than hydrocarbon fuel) and the presence of oxygen in the molecules suggests that some fuel properties of vegetable oil derived biodiesel would differ from those of hydrocarbon fuels [16].

8.5 SYNTHESIS OF BIODIESEL BY TRANSESTERIFICATION

Biodiesel is produced by a simple process called transesterification reaction. Transesterification is the process in which the methanol is reacted with triglycerides of vegetable oil to form glycerol and methyl ester. Biodiesel is chemically fatty acid esters. A catalyst is often used to improve the reaction rate and yield. The reaction is represented below:

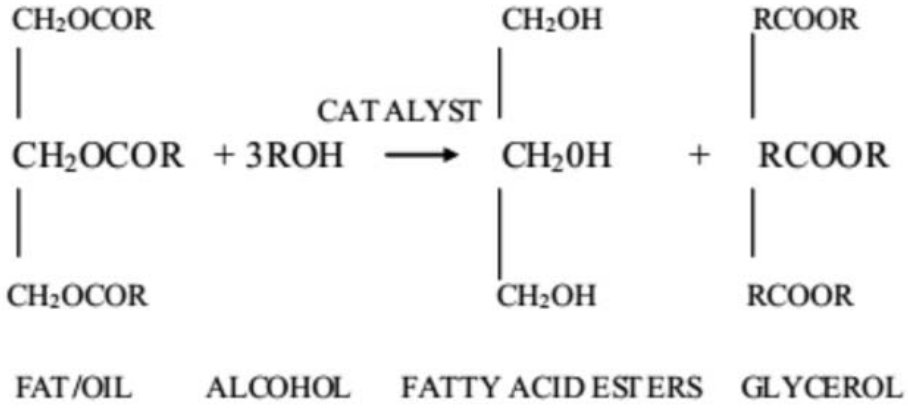

8.6 FACTORS AFFECTING RATE OF REACTION

A number of factors affect the conversion, product yield and quality [17]. Three parameters have effect on the transesterification namely [18],

- temperature (T);
- time (t); and
- ratio of oil to alcohol.

8.7 CATALYSIS OF TRANSESTERIFICATION

8.7.1 BASE OR ACID CATALYSIS

Transesterification can be catalyzed by either base or acid. In base-catalyzed transesterification, NaOH or KOH is used as catalyst, while in acid-catalyzed transesterification, acid is employed as catalyst. Most studies have focused on base-catalyzed transesterification of triglycerides. For acid-catalyzed systems, sulfuric acid has been the most investigated catalyst but other acids such as HCl, BF_3, H_3PO_4 and organic sulfonic acids have also been used [19].

8.7.2 ENZYMATIC CATALYSIS

Enzymatic synthesis of biodiesel employs lipases as catalyst. Various types of alcohols -primary, secondary and straight- or branched-chain can be employed in transesterification using lipases as catalysts. Lipases are known to act on long chain fatty alcohols better than short chain ones. Thus the efficiency of transesterification of triglycerides with methanol is likely to be very low compared to that with ethanol [20].

8.8 MICROBIAL SYNTHESIS OF BIODIESEL

There is a strong need to explore oil sources especially nonedible oils so as to achieve the rapid production of biodiesel. Microbial oils hold great potential in this regard. Microbial oils or single cell oils are produced by some oleaginous microorganisms such as yeast, fungi, bacteria and microalgae [21]. The content of fat in these oleaginous microorganisms can reach over 80% of cellular dry weight [22]. Hence these microbial oils can be used as feedstocks for biodiesel production. There are number of advantages associated with using microbial oils as compared to other vegetable oils and animal fats: short life cycle, less labor required, not dependent on season, climate and easier to scale up [23].

Autotrophic microalgae use carbon dioxide as the carbon source and sunlight as the energy for oil accumulation. Examples of autotrophic

microalgae include *Chlorella vulgaris*, *Botryococcus braunii*, *Navicula pelliculosa*, *Scenedsmus acutus, Crypthecodinium cohnii*, *Dunaliella primolecta*, *Monallanthus salina*, *Neochloris oleoabundans*, *Phaeodactylum tricornutum* and *Tetraselmis sueica* can accumulate oils [24, 25].

There are several yeast species, such as *Cryptococcus albidus*, *Lipomyces lipofera*, *Lipomyces starkeyi*, *Rhodosporidium toruloides*, *Rhodotorula glutinis*, *Trichosporon pullulan*, and *Yarrowia lipolytica*, which are also reported to accumulate oils under certain cultivation conditions [25, 26]. Cultivation conditions, such as C/N ratio, nitrogen resources, temperature, pH, oxygen and concentration of trace elements and inorganic salts, has been reported to influence the oil accumulation. The more the nitrogen compounds in medium, the lesser would be oil content in cells. Mainul et al. [27] reported that upon increasing C/N ratio from 25 to 70, oil content increased from 18% to 46%.

Bacteria belonging to the actinomycetes group such as species of *Mycobacterium*, *Rhodococcus* and *Nocardia* are able to synthesize intracellular triacylglycerides [5, 28]. Genetic engineering is also applied to improve fatty acid or biodiesel synthesis in *E.coli* by improving the acetyl-CoA biosynthetic pathway (i.e., by cloning of acetyl- CoA carboxylase genes, malonyl-CoA synthetase, a malonate transporter from *Rhizobium*, and thioesterase enzyme from plant) [6, 29].

8.9 BLENDS

Biodiesel can be blended in any ratio with petroleum diesel fuel. A blend of 20% biodiesel 80% diesel fuel is called B20. B20 is becoming a popular alternative fuel for U.S. fleets. A fleet is a group of vehicles operated from a central location such as buses or delivery trucks. B20 is appealing because it reduces emissions effectively, is reasonably priced and requires no engine modifications [30].

8.10 BENEFITS OF BIODIESEL

There are several benefits of biodiesel as a blended fuel in diesel engines [31, 32]:

- Biodiesel burns cleaner than petroleum diesel. Biodiesel' s exhaust is free of lead, sulfur dioxide, halogens and thus has reduced particulate matter, unburnt hydrocarbons, carbon monoxide and carbon dioxide [33].
- Biodiesel is biodegradable and nontoxic. Biodiesel is as biodegradable as sugar and less toxic than table salt [34].
- There are only limited or no needed modifications to current engines to be able to use biodiesel, as it allows longer engine life and produces higher cetane number. Cetane number (CN) is a measurement of the combustion quality of diesel fuel during compression ignition. It is an important factor in determining the quality of diesel fuel. The higher the cetane number, the more easily the fuel will ignite.
- Biodiesel gives almost equal engine performance and mileage as petroleum based diesel, dissipating engine heat faster, with more hours between oil changes.
- Biodiesel has a lower flash point than petroleum diesel and thus helps prevent damaging fires.

8.11 OTHER USES OF BIODIESEL

Biodiesel has number of applications other than engine fuel [30]. For example:

- Biodiesel can be used in diesel-fueled heaters, lanterns and stoves. It can be substituted for kerosene in lanterns and stoves.
- Biodiesel can be used as substitute for model aircraft fuel in model aircraft engines with glow plugs.
- Biodiesel can be used as an all-purpose machinery lubricant.
- Biodiesel can be used to clean up petroleum oil spills on land or in water [35].
- Biodiesel can be used as a solvent for nonautomotive paint, spray paint and other adhesive chemicals [36].
- Biodiesel can be used as a nontoxic crop adjuvant [36].

8.12 ENERGY BALANCE RATIO

Biodiesel has a positive energy balance ratio. An energy balance ratio is a comparison of the energy stored in a fuel to the energy required to grow, process and distribute the fuel. The energy balance ratio of biodiesel is at least 2.5 to 1 [37]. For every one unit of energy put into the fertilizer, pesticides, fuel, feedstock, extraction, refining, processing and transporting of biodiesel, there are at least 2.5 units of energy contained in the biodiesel [30].

8.13 CHALLENGES

One of the biggest challenges associated with biodiesel production is its cost and limited availability of fat and oil resources. There are two aspects of the cost of biodiesel, the costs of raw material (fats and oils) and the cost of processing. The costs of raw materials accounts for 60–75% of the total cost of biodiesel fuel [10]. The use of waste cooking oil can lower the cost significantly. However, the quality of used cooking oil can be bad [38].

Biofuel production has pushed up prices of some food crops, an expected outcome when they are also used as feedstock. To avoid the food-or-fuel dilemma, biofuels should be produced from food crops only after additional feedstocks are made available for this purpose. This can be achieved by either attaining higher yields in currently cropped areas, or expanding cultivation. Non-edible oils can also be used for making biodiesel fuel.

8.14 CONCLUSION

Biodiesel is an ecofriendly diesel fuel prepared from domestic renewable resources, for example, vegetable oils and animal fats. Biodiesel is becoming popular worldwide as an alternative energy source because it is nontoxic, biodegradable and nonflammable. Increasing population and hence increased consumption of fossil fuels is the main driving force behind developing this technology. In order to displace large quantities of petroleum with biomass oils there should be well-coordinated research projects at national and international level.

KEYWORDS

- **Biodiesel**
- **Cetane number**
- **Generations of biofuels**
- **Greenhouse gas**
- **Waste cooking oil**

REFERENCES

1. Enrique, R., Chalico, T. A. (2009). *Opportunities and Challenges For Biofuel Production in Latin America.* CIFOR Environment Briefs.
2. Liang, Y., Sarkanyet, N., Cui, Y. (2009). Biomass and lipid productivities of *Chlorella Vulgaris* under autotrophic, heterotrophic, and mixotrophic growth conditions. *Biotechnol. Lett. 31*, 1043–1049.
3. Chen, C. Y., Yeh, K. L., Aisyah, R., Lee, D. J., Chang, J. S. (2011). Cultivation, photobioreactor design, and harvesting of microalgae for biodiesel production: A critical review. *Bioresource. Technol. 102*, 71–81.
4. Tran, N., Bartlett, J., Kannangara, G., Milev, A., Volk, H., Wilson, M. (2010). Catalytic upgrading of biorefinery oil from microalgae. *Fuel. 89,* 265–274.
5. Alvarez, H. M., Steinbuchel, A. (2002). Triacylglycerols in prokaryotic microorganisms. *Appl. Microbiol. Biotechnol. 60*, 367–376.
6. Kalscheuer, R., Stolting, T., Steinbuchel, A. (2006). Microdiesel: *Escherichia coli* engineered for fuel production. *Microbiology*. *152,* 2529–2536.
7. Malhotra, R. K., Das, L. M. (1999). Biofuels as blending components for motor gasoline and diesel fuels. *J. Sci. Ind. Res. 61,* 99.
8. Zheng, S., Kates, M., Dube, M. A., Mcleon, D. D. (2006). Acid-catalyzed production of biodiesel from waste frying oil. *Biomass. Bioenergy. 30*, 267–272.
9. Uddin, M. R., Ferdous, K., Uddin, M. R., Khan, M. R., Islam, M. A. (2013). Synthesis of biodiesel from waste cooking oil. *Chem. Eng. Sci. 1,* 22–26.
10. Sonntag, N. O. V. (1979). Structure and composition of fats and oils. In: Bailey's industrial oil and fat products, Swern D., Ed., John Wiley and Sons, New York; Vol. 1, pp. 1.
11. Singh, S. P., Singh, D. (2010). Biodiesel production through the use of different sources and characterization of oils and their esters as the substitute of diesel: a review. *Renew. Sus. Energy. Rev. 14*, 200–216.
12. Demirbas, A. (2002). Diesel fuel from vegetable oil via transesterification and soap pyrolysis. *Energy. Sources*. *24*, 835–41.
13. ATSDR: *Toxicological Profile For Fuel Oils 1995*; U. S. Department of Health and Human Services, Public Health Service, Agency for Toxic Substances and Disease Registry (ATSDR): Atlanta, GA, 1995.

14. Mohibbe, A. M., Waris, A., Nahar, N. M. (2005). Prospects and potential of fatty acid methyl esters of some nontraditional seed oils for use as biodiesel in India. *Biomass. Bioenergy. 29,* 293–302.
15. Anonymous. The wealth of India: raw materials, vol. IX. Publication & Information Directorate, Council of Scientific & Industrial Research; New Delhi, 1972.
16. Goering, C. E., Schwab, A. W., Daugherty, M. J., Pryde, E. H., Heakin, A. J. (1982). Fuel properties of 11oils. *Trans. ASAE. 25,* 1472–83.
17. Divya, B., Tyagi, V. K. (2006). Biodiesel: Source, Production, Composition, Properties and Its Benefits. *J. Oleo. Sci. 55,* 487–502.
18. Kapilakarn, K., Peugtong, A. (2007). A Comparison of Costs of Biodiesel Production From Transesterication. *Int. Energy. J. 8,* 1–6.
19. Liu, K. S. (1994). Preparation of Fatty-Acid Methyl Esters for Gas- Chromatographic Analysis of Lipids inBiological-Materials. *J. Am.Oil Chem. Soc. 71,* 1179–1187.
20. Shimada, Y., Sugihara, A., Minamigawa, Y., Higasbiyama, K., Akimoto, K., Fujikawa, S., Komemushi, S., Tominaga, Y. (1998). Enzymatic enrichment of arachidonic acid from Mortierella single cell oil. *J. Am. Oil. Chem. Soc. 75,* 1213–17.
21. Ma, Y. L. (2006). Microbial oils and its research advance. *Chin. J. Bioprocess. Eng. 4,* 7–11.
22. Meng, X., Yang, J., Xu, X., Zhang, L., Nie Q., Xian, M. (2009). Biodiesel production from oleaginous microorganisms. *Renew. Energy. 34,* 1–5.
23. Li, Q., Wang, M. Y. (1997). Use food industry waste to produce microbial oil. Science and Technology of Food Industry. *6*, 65–69.
24. Chisti, Y. (2007). Biodiesel from microalgae. *Biotechnol. Adv. 25*, 294–306.
25. Liang, X. A., Dong, W.B; Miao, X. J., Dai, C. J. (2006). Production technology and influencing factors of microorganism grease. *Food. Res. Dev. 27,* 46–47.
26. Liu, S. J., Yang, W. B., Shi; A. H. (2000). Screening of the high lipid production strains and studies on its flask culture conditions. *Microbiology. 27*, 93–97.
27. Mainul, H., Philippe, J. B., Louis, M. G., Alain, P. (1996). Influence of Nitrogen and Iron Limitations on Lipid Production by Cryptococcus curvatus Grown in Batch and Fed-batch Culture. *Process. Biochem. 31*, 355–361.
28. Li, Q., Du, W., Liu, D. (2008). Perspectives of microbial oils for biodiesel production. *Appl. Microbiol. Biotechnol. 80*, 749–756.
29. Adamczak, M., Bornscheuer, U. T., Bednarski, W. (2009). The application of biotechnological methods for the synthesis of biodiesel. *Eur. J. Lipid. Sci. Technol. 111*, 808–813.
30. Tickell, J. *From the fryer to the Fuel Tank: The Complete guide to using Vegetable Oil as an alternative Fuel*. 3rd edition, Tickell Energy Consulting, Tallahassee, Florida, 2000; pp. 1–159.
31. Zhang, Y., Dub, M. A., McLean, D. D., Kates, M. (2003). Biodiesel production from waste cooking oil: Process design and technological assessment. *Elsevier. J. Bioresour. Technol. 89,* 1–16.
32. Idusuyi, N., Ajide, O. O., Abu, R. (2012). Biodiesel as an alternative energy resource in South-west Nigeria. *Int. J. Sci. Technol. 5*, 323–327.
33. Korbitz, Werner. The technical, energy and environmental properties of Biodiesel. Korbitz Consulting Vienna, Austria, 1993.

34. Walker, Kerr. (1994). Biodiesel from rapeseed. In *Journal of the Royal Agricultural Society of England*. Vol 155, 43–44.
35. Randall, V. W. *Cytosol Process: Shoreline oil spill remediation with a vegetable based biosolvent*. Presented at the fourth international marine biotechnology conference, September 1997.
36. Ahmed, I., Clements, L. D., Van Dyne, D. L. Non-fuel industrial uses of soybean oil-based esters: Final Report. Development systems/Applications International, January 31, 1997.
37. Ahmed, I., Decker, J., Morris, D. *How much energy does it take to make a gallon of soydiesel;* Institute for Local Self-Reliance, January 1994.
38. Murayama, T. (1994). Evaluating vegetable oils as a diesel fuel. *Inform. 5,* 1138–1145.

CHAPTER 9

AN OVERVIEW OF REACTOR DESIGNS FOR BIODIESEL PRODUCTION

VIJAY KUMAR GARLAPATI, LAKSHMI SHRI ROY, and RINTU BANERJEE

Microbial Biotechnology and DSP Laboratory, Agricultural and Food Engineering Department, IIT Kharagpur, Kharagpur, West Bengal – 721302

CONTENTS

9.1 Introduction 222
9.2 Biodiesel Production Methods 223
9.3 Limitations of Conventional Biodiesel Production Technology 224
9.4 Process Intensification Technologies for Biodiesel Production 226
9.4.1 Micro-Channel Reactor 227
9.4.2 Oscillatory Flow Reactor 227
9.4.3 Rotating/Spinning Tube Reactor 229
9.4.4 Cavitational Reactor 230
9.4.5 Sonochemical Reactor 231
9.4.6 Microwave Reactor 232
9.4.7 Membrane Reactor 233
9.5 Conclusions 235
Keywords 236
References 236

ABSTRACT

Nowadays, the idea of biofuels through utilization of biomass has been triggering in a exponential phase due to social, moral and environmental reasons for using hydrocarbon based crops for bioenergy. The concept of second- and third-generation biofuels from nonedible crops and wastes gains absolute social acceptance, still remains a big question. Usually, the biodiesel produced through transesterification of oils will produce in a batch mode with longer reaction times. The process economics of the biodiesel can be enhanced by implementing the continuous processes which results in a pure product (reduces down stream steps) through improved mixing with lower residence time (reduction in reactor volume). Ample scope is available for the use of process intensification techniques with an objective of making the synthesis economically viable and one such intensification approach is based on the use of different bioreactor configurations. This chapter is a comprehensive overview of current technologies and appropriate options for scale-up development, providing the basis for a proposal for the exploitation of various reactor configurations to optimize biodiesel production.

9.1 INTRODUCTION

Current energy policies emphasize cleaner, efficient and environmentally friendly technologies. Their target is to increase the supply and usage of energy [1–4]. Thus, developments in alternative renewable energy sources have become indispensable for sustainable environmental and economic growth. Among the explored alternative energy sources, considerable attention has been focused on biodiesel because it is widely available from inexhaustible feedstocks that can effectively reduce its production cost.

Biodiesel, which is also known as fatty acid methyl ester (FAME), is a mixture of monoalkyl esters of long-chain fatty acids derived from renewable lipid feedstocks, such as vegetable oil and animal fats. Because biodiesel has physical properties similar to diesel fuels it has established its commercial value in the automobile markets of Europe, US, Japan, Brazil and India [5]. Moreover, the implementation of the "directive on

the promotion of the use of biofuels" for transport in the EU (Directives 2003/30/EC) mandated the increased use of biofuels to power transportation from 2% to 5.75% between 2005 and 2010, triggering a huge demand for biodiesel [6]. Unlike conventional diesel fuel, biodiesel offers several advantages, including renewability, higher combustion efficiency [7], cleaner emission [5], higher cetane number, higher flash point, better lubrication [8] and biodegradability [9]. Depending on the climate, local soil conditions and availability, various biolipids have been used in different countries as feedstocks to produce biodiesel.

Biolipid feedstocks can be divided into four categories: virgin vegetable oils, waste vegetable oils, animal fats and nonedible oils. Virgin vegetable oil feedstock refers to rapeseed, soybean, sunflower and palm oil [10], while waste vegetable oil refers to these oils that have been used in cooking and are no longer suitable for human consumption [11, 12]. Animal fats include tallow, lard and yellow grease [13] while the nonedible oils include Jatropha [14, 15], neem oil, castor oil, tall oil [10] and microalgae [16].

9.2 BIODIESEL PRODUCTION METHODS

Four primary production methodologies for producing biodiesel have been studied extensively. The high viscosity, acid number, free fatty acid content, oxidation and polymerization problems of vegetable oils makes them unsuitable for direct usage in diesel engines. Several modification techniques, such as dilution, microemulsion, pyrolysis and transesterification have been used to reduce the viscosity of oil [17]. Of these processes, transesterification is the most widely used; this method involves the alcoholysis of vegetable oil to produce alkyl ester. Generally, the mechanism consists of three consecutive reversible reaction steps. The first step involves the conversion of triglycerides (TG) to diglycerides (DG) and later to monoglycerides (MG). Subsequently, the monoglycerides are converted to glycerol. Each reaction step produces an alkyl ester. Thus, a total of three alkyl esters are produced in the transesterification process [18]. The typical tranesterification reactions were depicted in Fig. 9.1.

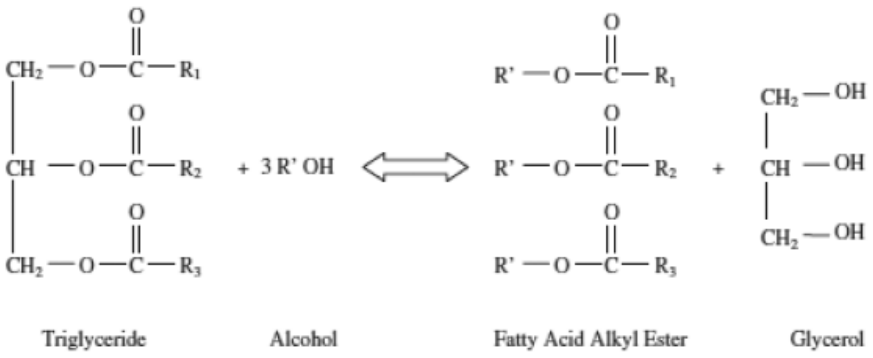

FIGURE 9.1 Typical Transesterification reaction [19].

Common transesterification reactions that are used to produce biodiesel include [20]:

- homogeneous catalyzed transesterification;
- heterogeneous catalyzed transesterification;
- enzymatic catalyzed transesterification; and
- supercritical technology.

Each of these methods has its own disadvantages that eventually limit the economic feasibility and low environmental impact of the entire biodiesel production process.

9.3 LIMITATIONS OF CONVENTIONAL BIODIESEL PRODUCTION TECHNOLOGY

In the conversion of vegetable oil by the transesterification process, the reversible reaction between the reactant and product indicates that the formation of biodiesel is highly dependent on the proportion of the reactant and the conditions of the transesterification process. According to Le Chatelier's principle, large quantities of alcohol are needed to shift the equilibrium of the reaction to the product side and increase the yield of biodiesel [21]. Unfortunately, high consumption of alcohol is associated with higher production cost. The consumption of alcohol could be reduced by using acid or alkaline catalysts, which could improve the reaction rate and biodiesel yield. However, homogeneous acid solutions that catalyze transesterification processes, such as sulfuric [22], hydrochloric [23], or

sulphonic acids [24] have been largely ignored because they increase the time consumption of the process, require a higher reaction temperature and are corrosive by nature. Although the use of homogeneous alkaline catalysts, such as sodium and potassium hydroxide could overcome these limitations, it has been reported that the alkaline catalyzed reaction is sensitive to the purity of the reactant. The presence of water and free fatty acids in the raw feedstock could induce a saponification process in which the free fatty acid produced by the hydrolysis of triglycerides reacts with the alkaline catalyst to form soap. The dissolved soap in the glycerol phase would increase the solubility of methyl ester in the glycerol and complicate the subsequent separation process [25]. Also, the removal of either the homogeneous acidic or alkaline catalyst using hot distilled water would eventually result in the need to dispose of wastewater [26].

Heterogeneous catalyst has been viewed as an alternative solution to replace the homogeneous catalyst because it is noncorrosive and environmentally benign. The heterogeneous catalytic reaction usually faces a mass transfer resistance problem due to the presence of three-phase system (triglycerides, alcohol and solid catalyst) in the reaction mixture which limits the pore diffusion process and reduces the active site availability for the catalytic reaction which in turn decreases the reaction rate [27, 28]. The lipase-mediated transesterification of oils to biodiesel is an attractive option due to usage of environment-friendly catalyst (lipase) and facilitates easier separation of products [29]. Due to requirement of longer reaction times and unfavorable product yields this process not yet commercialized compared to the alkaline catalyst. It has been reported that the enzymatic transesterification process requires 24 hr to achieve a biodiesel yield of 90% [30]. Most importantly, the major obstacle to this process is the high cost of the enzyme. The enzyme also requires very specific reaction conditions because the denaturation of the enzyme and its deactivation as a result of feed impurity could decrease its efficiency [31].

Supercritical alcohol transesterification provides a new path for the production of biodiesel without the aid of a catalyst. The supercritical condition could overcome the mass transfer limitation by enabling the mixture of triglyceride and alcohol to become a homogeneous phase [32]. However, the major drawbacks of this noncatalytic process are its large energy requirement and its infeasibility for large-scale industrial

application because of the increased production cost imposed by the high reaction temperature and pressure [33]. Moreover, the supercritical process is potentially hazardous and requires attention to personal risk and safety.

Usually the catalytic and noncatalytic transesterification downstream processes will receive unreacted reactant and catalyst along with the biodiesel and glycerol. Ineffective downstream processing of biodiesel may cause severe diesel engine problems, such as plugging of filters, coking on injectors, carbon deposits, excessive engine wear, oil ring sticking, engine knocking, and thickening and gelling of lubricant oil [34]. The downstream processing of biodiesel technology (glycerol separation, catalyst neutralization and biodiesel purification) alone constituted over 60–80% of the total cost of a transesterification process plant [35]. In addition, the multiple separation and purification stages could cause loss of the biodiesel, resulting in a decrease in the pure biodiesel yield.

9.4 PROCESS INTENSIFICATION TECHNOLOGIES FOR BIODIESEL PRODUCTION

The process intensification technologies for biodiesel production can alleviate the limitations associated with biodiesel production technology such as mass transfer, thermodynamic equilibrium, wastewater and multiple downstream processing steps [26, 27, 33, 35, 36]. These technologies involve the use of novel reactors or coupled reaction/separation processes to enhance the reaction rate and to reduce the residence time [37].

Recently, novel reactors have been developed and applied to improve the mixing and mass/heat transfer between the oil and methanol in biodiesel production [37]. Those novel reactors are:

- micro-channel reactor;
- oscillatory flow reactor;
- rotating/spinning tube reactor;
- cavitational reactor;
- sonochemical reactor;
- microwave reactor; and
- membrane reactor.

9.4.1 MICRO-CHANNEL REACTOR

The microchannel reactor can achieve a rapid reaction rate because it has a high volume/surface ratio, short diffusion distance and fast and efficient heat dissipation and mass transfer [37, 38]. The microchannel reactors used in biodiesel production include microchannel reactors with T- or Y-flow structures, zigzag microchannel reactors [38] and slit channel reactor [39]. The typical flow diagram of the microstructured reactor used for biodiesel production was depicted in Fig. 9.2. Because of the high heat transfer rate, it has been reported that the microchannel reactor consumed less energy than the conventional stirrer reactor [37]. However, the microchannel reactor suffers from the drawback of low production throughput, which is attributed to the limitations of the microfabrication technology that is used to produce the microchannel. Furthermore, the high investment cost of the microchannel reactor prohibits the addition of more reactors in parallel to amplify the production of biodiesel [39].

9.4.2 OSCILLATORY FLOW REACTOR

The oscillatory flow reactor is a type of continuous plug flow reactor (PFR) [41] in which the orifice plate baffles is equally spaced, and a piston is used to produce oscillatory flow [37]. The flow diagram of

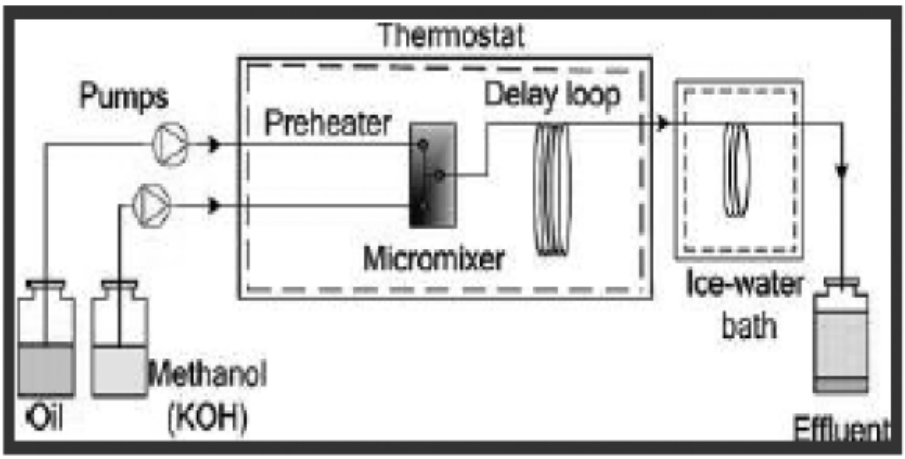

FIGURE 9.2 Flow diagram of the microstructured reactor used for the biodiesel production [40].

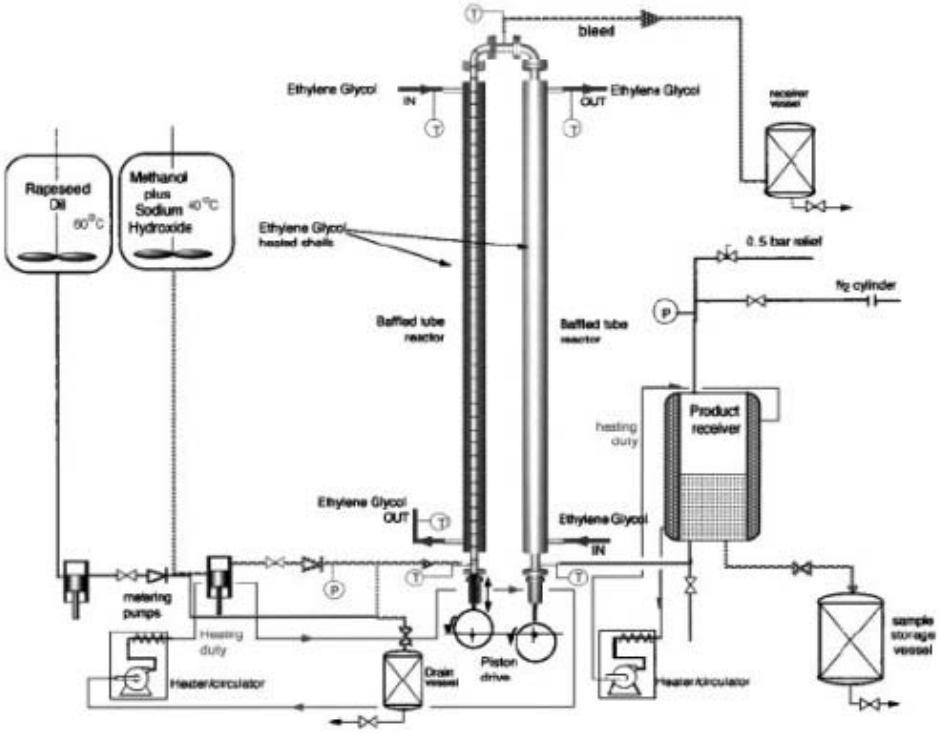

FIGURE 9.3 Flow diagram of Biodiesel production in OFR [42].

biodiesel production in oscillatory flow reactor consists of two vertically positioned jacketed QVF tubes connected at the top by an inverted QVF U-tube, which was fitted with a manual purge value. The feeds were pumped from the feed vessels using a metering pump and temperatures were maintained by Eurotherm temperature controllers. The oscillation of fluid facilitates a 'nutating cam' arrangement. OFR is well suited for laboratory use (Fig. 9.3) [42]. The combination of baffles and oscillatory motion intensifies the radial mixing by the formation of periodic vortices in the bulk fluid, causing an increase in mass and heat transfer while maintaining plug flow [37, 41]. In addition, the oscillatory flow reactor can also improve the residence time distribution (RTD) and multiphase suspension [43]. Because the oscillatory flow reactor can achieve long residence times, it can be designed with a smaller length to diameter ratio, which eventually helps to improve the economy of biodiesel production because of the smaller "footprint," lower capital, reduced pumping cost and ease of control [37].

9.4.3 ROTATING/SPINNING TUBE REACTOR

The rotating/spinning tube reactor is a shear reactor containing two tubes. The inner tube rotates rapidly within the concentric stationary outer tube. Both tubes are separated by a narrow annular gap, which produces Couette flow when the reactants are introduced (Fig. 9.4) [44]. Because of the high shear rate, the reactants are mixed and move through the gap as a coherent thin film. This thin film provides a large interfacial contact area to enhance the reaction rate between the oil and the methanol. As a result, less mixing power and reaction time are required to produce biodiesel using a rotating/spinning reactor compared to a conventional reactor. This type of reactor is suitable to handle feedstocks with high FFA because the residence time is short [37].

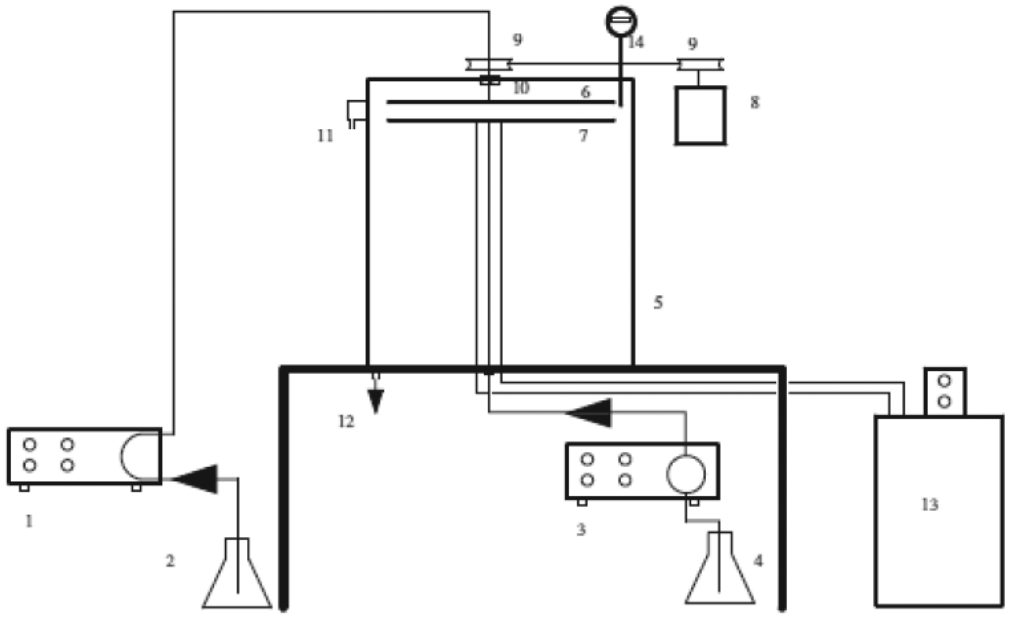

FIGURE 9.4 Experimental setup of the intensive spinning disk reactor for biodiesel synthesis. (1) Peristaltic pump; (2) canola oil vessel; (3) digital piston pump; (4) sodium methoxide vessel; (5) cylinder; (6) rotating disk; (7) stationary disk; (8) variable-speed DC motor; (9) pulley; (10) bearing; (11) sampling point; (12) products drainage; (13) heating circulator; (14) thermometer [44].

9.4.4 CAVITATIONAL REACTOR

The cavitational reactor is another type of novel reactor that has been used successfully in biodiesel production [37, 45–47]. Cavitation is defined as the generation of cavities followed by their growth and violent collapse, causing high local energy densities, temperatures and pressures [37, 45]. Cavitation enhances the mass transfer rate of the reaction by creating conditions of local intense turbulence and liquid microcirculation currents in the reactor [37, 45, 46]. Cavitational reactors can be classified into two types: hydrodynamic cavitation and acoustic cavitation [37, 46]. Hydrodynamic cavitation can be generated by using a restriction component, such as an orifice plate, a throttling valve or a venture, placed in a liquid flow [45, 46]. At the constriction area, the kinetic energy or velocity of the liquid increases, but the local pressure decreases [45]. The typical hydrodynamic cavitation reactor used for biodiesel production was depicted in Fig. 9.5 [46, 48]. It consists of a reservoir or a collecting tank, which

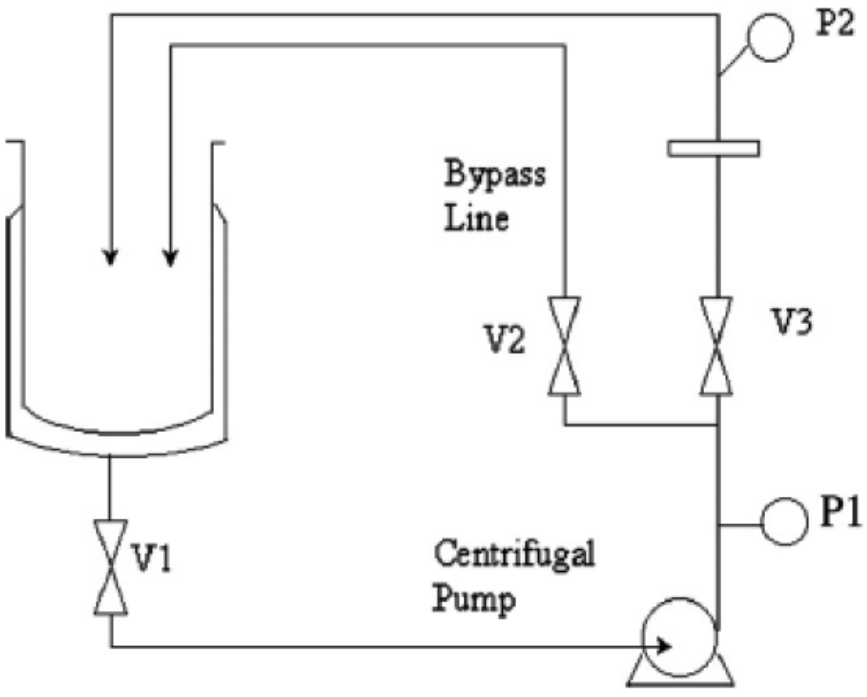

FIGURE 9.5 Schematic representation of the experimental setup for hydrodynamic cavitation reactor [46, 48].

was connected to the multistage centrifugal pump. The discharge from the pump branches into two lines which help in control of the inlet pressure and the inlet flow rate into the main line housing the orifice with the help of valves). The operating temperature of the reactor was maintained to near ambient conditions by circulating water within the jacket surrounding the tank.

A hydrodynamic cavitation reactor is more effective for mixing of immiscible liquids [47]. The mixing efficiency of a hydrodynamic cavitation reactor has been reported to be 160–400 times higher than that of the conventional mixing method [37]. Therefore, the hydrodynamic cavitation reactor consumes half of the energy required by conventional mechanical stirring [47].

9.4.5 SONOCHEMICAL REACTOR

A reactor that generates cavitation by ultrasound is known as a sonochemical reactor [45] or an acoustic cavitation reactor [37, 49]. Ultrasound causes a series of compression and rarefaction cycles by alternately compressing and stretching the molecular spacing of the medium [50]. The sonochemical reactor used for biodiesel production consists of an ultrasonic bath equipped with transducers (three) at the bottom of the tank arranged in a triangular pitch. It operates at an irradiating frequency of 20 kHz and power dissipation of 120 W and temperatures were maintained around 28°C (Fig. 9.6) [46]. Low-frequency ultrasound irradiation is useful for the emulsification of immiscible liquids, such as methanol and oil. Emulsification is a result of the induced collapse of cavitation bubbles that disrupt the phase boundary of methanol and oil [51]. Emulsions with large interfacial areas provide more reaction sites for transesterification and eventually increase the reaction rate [52]. It has been reported that the operating parameters, such as temperature, pressure, reaction time and catalyst concentration, are significantly reduced in ultrasound-assisted transesterification [53, 54]. However, sonochemical reactors suffer from erosion and particle shedding at the delivery tip surface because of the high surface energy intensity [45]. Also, the scale-up of a sonochemical reactor is relatively more difficult than it is for a

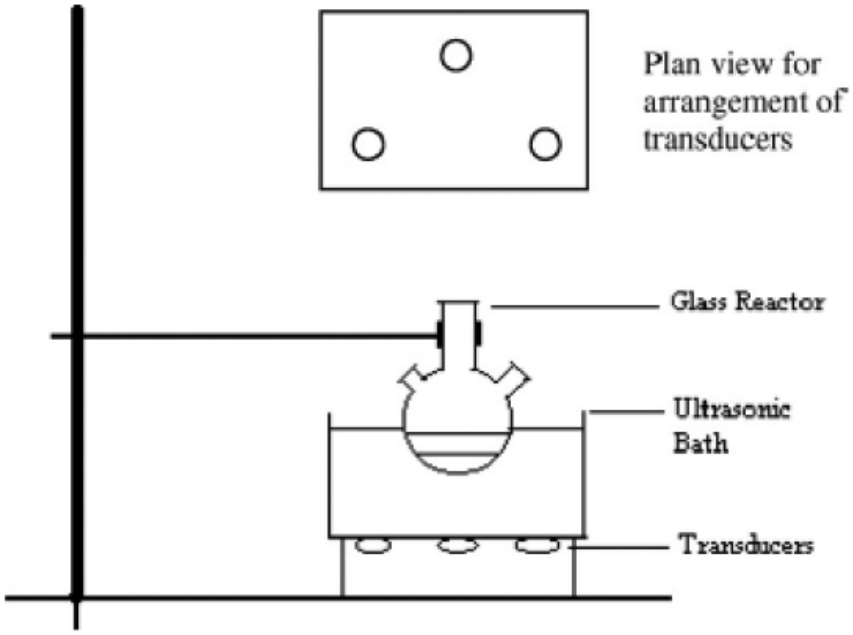

FIGURE 9.6 Schematic representation of sonochemical reactor generating acoustic cavitation [46].

hydrodynamic cavitation reactor because the former relies on a source of vibration [37].

9.4.6 MICROWAVE REACTOR

A new reactor design, to operate efficiently, is crucial. This is an area where microchem reactors particularly shine. Microchem reactors are based on the use of microwave process technology. It is a developing field of chemical processing that exploits rapid reaction rates with higher energy efficiency. This approach can result in poor control system performance for more typical conditions. The microwave reactor is another intensification technology for biodiesel production. The main function of a microwave reactor is not to improve the mixing of oil and methanol but to use its irradiation to transfer energy directly into the reactants and thus accelerate the transesterification. Because both polar and ionic components are available in the mixture of oil and methanol/alcohol, a microwave reactor plays an important role in the more efficient heating of reactants to the desired temperature because of the energy interactions at the molecular level [55].

Compared to a conventional thermal heating reactor, a microwave reactor is able to achieve similar biodiesel conversion with a shorter reaction time and in a more energy-efficient manner [37].

Modified microwave reactors from domestic microwave oven are not scalable from laboratory small-scale synthesis to industrial multi kilogram production, as they do not allow studying the process at a higher scale [56]. An efficient model for biodiesel reactor is not easy, because the microwave-assisted chemistry is poorly understood [57]. And biofuels systems are continuously subject to disturbances covering a wide range of conditions [58]. Instantaneous condition is a function of time and of the robustness of the system with respect to imminent disturbances. Transesterification reaction is highly nonlinear processes [59] and there are many effects parameters on temperature control, like heat transfer on microwave cavity, oil viscosity changes that lead to changes in flow rate, uniformity of reactant concentration, reactant temperature, power and reflected power in microwave cavity, a coolant temperature and ambient temperature. Therefore, it is a challenge to design a robust controller for nonlinear chemical process subject to model uncertainties [60]. If system modeling based on conventional mathematical tools is not well suited for dealing with ill-defined and uncertain systems, the presence of uncertainties can make a mismatch between the formulated mathematical model and the true process, which may degrade the control performance and would lead to serious stability problems consequently.

The entire above-mentioned novel reactors intensify the transesterification by either enhancing the mixing of oil and methanol or improving the heat transfer between the two liquid phases. However, none of these novel reactors, except the membrane reactor, is able to overcome the limitation caused by chemical equilibrium in transesterification. Therefore, the membrane reactor offers another interesting process intensification technology for biodiesel production

9.4.7 MEMBRANE REACTOR

A membrane reactor is also known as a membrane-based reactive separator [61]. According to IUPAC, a membrane reactor is defined as a device

that combines reaction and separation in a single unit [62]. Usually, the membrane reactors were classified based on the reactor design (extractor, distributor or contactor), the membrane used in the reaction (organic, inorganic, porous or dense membrane), whether it is an inert or catalytic membrane reactor and the reaction that occurs in membrane reactor (such as dehydrogenation [62], esterification [62, 63], water dissociation [62] or wastewater treatment [64, 65]. In addition to providing the separation, a membrane reactor also enhances the selectivity and yield of the reaction [61].The two basic configurations of membrane reactors were depicted in Fig. 9.7 [66].

Figure 9.7a shows the membrane reactor system in which the membrane reactor appears as an external process unit whereas in Fig. 7b type, the reactor combines with membrane separator as a single unit [67]. Compared with conventional biodiesel production process, the main advantage of membrane reactor system is capital and operating cost reduction, which is due to elimination of intermediate processing steps [61, 67]. Having this process advantages, the membrane reactors occupied a prominent place in biodiesel production technologies [36, 68, 69]. Undeniably, membrane reactors can be considered to be an emerging technology for biodiesel production. In order to successfully develop and commercialize membrane reactors in the biodiesel industry, knowledge is required in three major

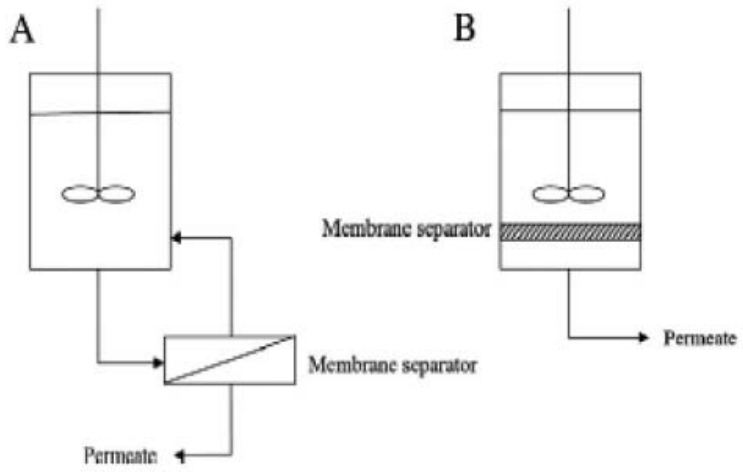

FIGURE 9.7 Membrane reactor basic layout. (a) A conventional membrane reactor system; (b) An integrated membrane reactor system [66].

fields: catalysis, membrane technology and reactor engineering. However, the desired properties, such as the mechanical properties and surface morphology of the membrane (especially in polymeric membranes), used in biodiesel production have not been fully studied. Also, most of the reported transesterification reactions via catalytic polymeric membranes have been performed in situations in which the membrane was cut into small squares and loaded together with the reactants [70−72]. Therefore, the ability of the synthesized polymeric membrane to separate glycerol from the product stream remains unstudied. Additionally, the engineering aspects of the membrane reactor have been minimally studied because most publications have only offered proofs of concepts. Biodiesel production using membrane reactors is still running under nonoptimal conditions. Therefore, it is a challenge to choose the best possible combination between catalyst and membrane. Optimization studies and modeling will be needed to advance the membrane reactor into commercial operation. Although high biodiesel yield can be obtained via catalytically inert membrane (mainly the microporous ceramic and carbon membranes), a water-washing step is still needed to purify the produced biodiesel. The purification problem can be reduced by using catalytically active membranes (constructed from polymeric membranes) in the flow configuration studied by Guerreiro et al. [24, 70]; Sarkar et al. [73] and Zhu et al. [72]. However, the polymeric membranes face the problem of low mechanical strength. It has been reported that the tested polymer membranes break before a high conversion of biodiesel could be achieved [24]. Therefore, more attention is needed to the selection of membrane and operating conditions to avoid membrane failure.

9.5 CONCLUSIONS

The obstacles faced by conventional biodiesel production processes have hindered the production of biodiesel in a way that is fully economically feasible and environmentally friendly. Very fast biodiesel production at high flow rates with low pressure drops can be achieved in microstructured reactors assembled with a micromixer and designed delay loops. With the advantages of a high throughput and a small footprint of the

microstructured reactor, this biodiesel production technique makes distributed energy production and refining on a truck quite possible. The twin-disk, spinning disk reactor demonstrated greatly increased rates of reaction for biodiesel synthesis, at a range of temperatures when compared with a stirred tank reactor. On other hand cavitational reactors appears to be very effective for intensification of chemical processing operations and harnessing the spectacular effects of cavitation, chemical as well as mechanical, for physical and chemical processing applications would lead to considerable economic savings. The future of sonochemical reactors lies in the design of multiple frequencies multiple transducer-based reactors whereas for hydrodynamic cavitation reactors, orifice plate type configuration appears to be most suitable. The emergence of membrane technology offers a solution for future biodiesel production that has the potential to be developed into large-scale commercial processes. In addition to the typical transeserification conditions (reaction temperature, methanol-to-oil ratio and catalyst concentration, etc.), the process parameters, such as reactant flow rate, transmembrane pressure, membrane thickness and pore size, are reported to have great impacts on the yield of biodiesel as well, and they cannot be ignored.

KEYWORDS

- **Biodiesel**
- **Bioreactor**
- **Cavitational**
- **Membrane**
- **Sonochemical**
- **Transesterification**

REFERENCES

1. Hammond, G. P., Kallu, S., McManus, M. C. (2008). Development of biofuels for the UK automotive market. *Appl. Energy. 85,* 506–515.
2. Hoekman, S. K. (2008). Biofuels in the U.S. Challenges and opportunities. *Renew. Energy. 34,* 14–22.

3. Monni, S., Raes, F. (2008). Multilevel climate policy: the case of the European Union, Finland and Helsinki. *Environ. Sci. Policy. 11,* 743–755.
4. Sawyer, R. F. (2009). Science based policy for addressing energy and environmental problems. *Proc. Combust. Inst. 32,* 45–56.
5. Janaun, J., Ellis, N. (2010). Perspectives on biodiesel as a sustainable fuel. *Renew. Sust. Energ. Rev. 14,* 1312–1320.
6. Mabee, W. E. (2007). Policy options to support biofuel production. *Adv. Biochem. Eng. Biotechnol. 108,* 329–357.
7. Fazal, M. A., Haseeb, A. S. M. A., Masjuki, H. H. (2011). Biodiesel feasibility study: an evaluation of material compatibility; performance; emission and engine durability. *Renew. Sust. Energ. Rev. 15,* 1314–1324.
8. Lin, L., Cunshan, Z., Vittayapadung, S., Xiangqian, S., Mingdong, D. (2011). Opportunities and challenges for biodiesel fuel. Appl. Energy. *88*, 1020–1031.
9. Wardle, D. A. (2003). Global sale of green air travel supported using biodiesel. *Renew. Sust. Energ. Rev. 7,* 1–64.
10. Demirbas, A. (2008). New liquid biofuels from vegetable oils via catalytic pyrolysis. *Energy. Educ. Sci. Technol. 21,* 1–59.
11. Conservation ADoE. (2011). How can I dispose of used cooking oils and fats?. Retrieved 13th March, from. http://www.dec.state.ak.us/eh/docs/fss/cooking.pdf.
12. Lam, M. K., Lee, K. T., Mohamed, A. R. (2010). Homogeneous, heterogeneous and enzymatic catalysis for transesterification of high free fatty acid oil (waste cooking oil) to biodiesel: a review. *Biotechnol. Adv. 28,* 500–518.
13. Atadashi, I. M., Aroua, M. K., Aziz, A. A. (2010). High quality biodiesel and its diesel engine application: a review. *Renew. Sust. Energ. Rev. 14,* 1999–2008.
14. Shuit, S. H., Lee, K. T., Kamaruddin, A. H., Yusup, S. (2010). Reactive extraction and in situ esterification of *Jatropha curcas* L. seeds for the production of biodiesel. *Fuel. 89,* 527–530.
15. Yee, K. F., Tan, K. T., Abdullah, A. Z., Lee, K. T. (2009). Life cycle assessment of palm biodiesel: revealing facts and benefits for sustainability. *Appl. Energ. 86,* S189–8196.
16. Ahmad, A. L., Yasin, N. H. M., Derek, C. J. C., Lim, J. K. (2011). Microalgae as a sustainable energy source for biodiesel production: a review. *Renew. Sust. Energ. Rev. 15,* 584–593.
17. Andrade, J. E., Pérez, A., Sebastian, P. J., Eapen, D. (2011). A review of bio-diesel production processes. *Biomass. Bioenerg. 35,* 1008–1020.
18. Sharma, Y. C., Singh, B. Development of biodiesel from karanja, a tree found in rural India. *Fuel* (2008). *67,* 1740–1742.
19. Lim, S., Teong, L. K. (2010). Recent trends, opportunities and challenges of biodiesel in Malaysia: an overview. *Renew. Sus. Energ. Rev. 14,* 938–954.
20. Marchetti, J. M., Miguel, V. U., Errazu, A. F. (2007). Possible methods for biodiesel production. *Renew. Sust. Energ. Rev. 11,* 1300–1311.
21. Othman, R., Mohammad, A. W., Ismail, M., Salimon, J. (2010). Application of polymeric solvent resistant nanofiltration membranes for biodiesel production. *J. Membr. Sci. 348,* 287–297.

22. Sahoo, P. K., Das, L. M., Babu, M. K. G., Naik, S. N. (2007). Biodiesel development from high acid value polanga seed oil and performance evaluation in a CI engine. *Fuel. 86,* 448–454.
23. Boucher, M. B., Unker, S. A., Hawley, K. R., Wilhite, B. A., Stuart, J. D., Parnas, R. S. (2008). Variables affecting homogeneous acid catalyst recoverability and reuse after esterification of concentrated omega-9 polyunsaturated fatty acids in vegetable oil triglycerides. *Green. Chem. 10,* 1331–1336.
24. Guerreiro, L., Castanheiro, J. E., Fonseca, I. M., Martin-Aranda, R. M., Ramos, A. M., Vital, J. (2006). Transesterification of soybean oil over sulfonic acid functionalised polymeric membranes. *Catal. Today. 118,* 166–171.
25. Vicente, G., Martínez, M., Aracil, J. (2004). Integrated biodiesel production: a comparison of different homogeneous catalysts systems. *Bioresour. Technol. 92,* 297–305.
26. Xie, W., Li, H. (2006). Alumina-supported potassium iodide as a heterogeneous catalyst for biodiesel production from soybean oil. *J. Mol. Catal. A: Chem. 255,* 1–9.
27. Mbaraka, I. K., Shanks, B. H. (2006). Conversion of oils and fats using advanced mesoporous heterogeneous catalysts. *J. Am. Oil. Chem. Soc. 83,* 79–91.
28. Liu, X., He, H., Wang, Y., Zhu, S., Piao, X. (2008). Transesterification of soybean oil to biodiesel using CaO as a solid base catalyst. *Fuel. 87,* 216–221.
29. Jegannathan, K. R., Abang, S., Poncelet, D., Chan, E. S., Ravindra, P. (2008). Production of biodiesel using immobilized lipase—a critical review. *Crit. Rev. Biotechnol. 28,* 253–264.
30. Oda, M., Kaieda, M., Hama, S., Yamaji, H., Kondo, A., Izumoto, E, et al. (2005). Facilitatory effect of immobilized lipase-producing *Rhizopus oryzae* cells on acyl migration in biodiesel-fuel production. *Biochem. Eng. J. 23,* 45–51.
31. Dizge, N., Aydiner, C., Imer, D. Y., Bayramoglu, M., Tanriseven, A., Keskinler, B. (2009). Biodiesel production from sunflower, soybean, and waste cooking oils by transesterification using lipase immobilized onto a novel microporous polymer. *Bioresour. Technol. 100,* 1983–1991.
32. Pinnarat, T., Savage, P. E. (2008). Assessment of noncatalytic biodiesel synthesis using supercritical reaction conditions. *Ind. Eng. Chem. Res. 47,* 6801–6808.
33. Yin, J. Z., Xiao, M., Song, J. B. (2008). Biodiesel from soybean oil in supercritical methanol with cosolvent. *Energy. Convers. Manage. 49,* 908–912.
34. Demirbas, A. (2007). Progress and recent trends in biofuels. Prog. Energy. Combust. Sci. 33:1–18.
35. Tai-Shung, N. C. (2007). Development and purification of biodiesel. *Sep. Purif. Technol. 20,* 377–381.
36. Cao, P., Dubé, M. A., Tremblay, A. Y. (2008). Methanol recycling in the production of biodiesel in a membrane reactor. *Fuel. 87,* 825–833.
37. Qiu, Z., Zhao, L., Weatherley, L. Process intensification technologies in continuous biodiesel production. *Chem. Eng. Process.* (2010). *49,* 323–330.
38. Wen, Z., Yu, X., Tu, S. T., Yan, J., Dahlquist, E. (2009). Intensification of biodiesel synthesis using zigzag microchannel reactors. *Bioresour. Technol. 100,* 3054–3060.
39. Kalu, E. E., Chen, K. S., Gedris, T. (2011). Continuous-flow biodiesel production using slit-channel reactors. *Bioresour. Technol. 102,* 4456–61

40. Sun, P., Wang, B., Yao, J., Zhang, L., Xu, N. (2010). Fast synthesis of biodiesel at high throughput in microstructured Reactors. *Ind. Eng. Chem. Res. 49,* 1259–1264.
41. Phan, A. N., Harvey, A. P., Rawcliffe, M. (2011). Continuous screening of base-catalyzed biodiesel production using new designs of mesoscale oscillatory baffled reactors. *Fuel. Process. Technol. 92,* 1560–1567.
42. Harvey, A. P., Mackley, M. R., Seliger, T. (2003). Process intensification of biodiesel production using a continuous oscillatory flow reactor. *J. Chem. Technol. Biotechnol. 78,* 338–341.
43. Zheng, M., Skelton, R. L., Mackley, M. R. (2007). Biodiesel reaction screening using oscillatory flow meso reactors. *Process. Saf. Environ. Prot. 85,* 365–371.
44. Qiu, Z., Petera, J., Weatherley, L. R. (2012). Biodiesel synthesis in an intensified spinning disk reactor. *Chem. Eng. J. 210,* 597–609.
45. Gogate, P. R., Kabadi, A. M. (2009). A review of applications of cavitation in biochemical engineering/biotechnology. *Biochem. Eng. J. 44,* 60–72.
46. Kelkar, M. A., Gogate, P. R., Pandit, A. B. (2008). Intensification of esterification of acids for synthesis of biodiesel using acoustic and hydrodynamic cavitation. *Ultrason. Sonochem. 15,* 188–194.
47. Pal, A., Verma, A., Kachhwaha, S. S., Maji, S. (2010). Biodiesel production through hydrodynamic cavitation and performance testing. *Renew. Energy. 35,* 619–624.
48. Gogate, P. R. (2008). Cavitational reactors for process intensification of chemical processing applications: A critical review. *Chem. Eng. Process. 47,* 515–527.
49. Wu, Z., Ondruschka, B., Zhang, Y., Bremner, D. H., Shen, H., Franke, M. (2009). Chemistry driven by suction. *Green. Chem. 11,* 1026–1030.
50. Colucci, J., Borrero, E., Alape, F. (2005). Biodiesel from an alkaline transesterification reaction of soybean oil using ultrasonic mixing. *J. Am. Oil. Chem. Soc. 82,* 525–530.
51. Rokhina, E. V., Lens, P., Virkutyte, J. (2009). Low-frequency ultrasound in biotechnology: state-of-the-art. *Trends. Biotechnol. 27,* 298–306.
52. Chand, P., Chintareddy, V. R., Verkade, J. G., Grewell, D. (2010). Enhancing biodiesel production from soybean oil using ultrasonics. *Energy. Fuel. 24,* 2010–2015.
53. Deshmane, V. G., Gogate, P. R., Pandit, A. B. (2008). Ultrasound-assisted synthesis of biodiesel from palm fatty acid distilate. *Ind. Eng. Chem. Res. 48,* 7923–7927.
54. Kalva, A., Sivasankar, T., Moholkar, V. S. (2008). Physical mechanism of ultrasound-assisted synthesis of biodiesel. *Ind. Eng. Chem. Res. 48,* 534–544.
55. Barnard, T. M., Leadbeater, N. E., Boucher, M. B., Stencel, L. M., Wilhite, B. A. (2007). Continuous-flow preparation of biodiesel using microwave heating. *Energy. Fuel. 21,* 1777–1781.
56. Vyas, A., Verma, J., Subrahmanyam, N. (2010). A review on fame production processes. *Fuel. 89,* 1–9.
57. Zhu J., Palchik, O., Chen, S., Gedanken, A. (2000). Microwave assisted preparation of CdSe, PbSe, and Cu_2-Xse nanoparticles. *J. Phys. Chem. 104,* 7344–7347.
58. Mu, D. T., Seager, P., Rao, J., Park, F., Zhao, A. (2011). A resilience perspective on biofuel production. *Integr. Enviro. Assess. Manage. 7,* 348–359.
59. Sohpal, V., Singh, A., Dey, A. (2011). Fuzzy modeling to evaluate the effect of temperature onbatch transesterification of *jatropha curcas* for biodiesel production, *Bull. Chem. React. Eng. Catal. 6,* 31–38.

60. Nithya, S. A., Gour, N., Sivakumaran, T. K., Radhakrishnan, T., Balasubramanian, N., Anantharaman. (2008). Design of intelligent controller for nonlinear processes. *Asian. J. Appl. Sci. 1,* 33–45.
61. Sanchez Marcano, J. G., Tsotsis, T. T. (2002). The coupling of the membrane separation process with a catalytic reaction. Catalytic Membranes and Membrane Reactor. Weinheim: Wiley-VCH; p. 5–14.
62. Caro, J. (2008). Catalysis in Micro-structured membrane reactors with nano-designed membranes. *Chin. J. Catal. 29,* 1169–1177.
63. Buonomenna, M. G., Choi, S. H., Drioli, E. (2010). Catalysis in polymeric membrane reactors: the membrane role. *Asia. Pac. J. Chem. Eng. 5,* 26–34.
64. Drioli, E., Fontananova, E., Bonchio, M., Carraro, M., Gardan, M., Scorrano, G. (2008). Catalytic membranes and membrane reactors: an integrated approach to catalytic process with a high efficiency and a low environmental impact. *Chin. J. Catal. 29,* 1152–1158.
65. Ertl, H., Knozinger, H., Schuth, F., Weitkamp, J. (2008). Catalytic membrane reactors. Handbook of heterogeneous catalysis. Weinheim: Wiley-VCH; 2198–241.
66. Lipnizki, F., Field, R. W., Ten, P. K. (1999). Pervaporation-based hybrid process: a review of process design, applications and economics. *J. Membr. Sci. 153,* 183–210.
67. Shuit, S. H., Ong, Y. T., Lee, K. T., Subhash, B., Tan, S. H. (2012). Membrane technology as a promizing alternative in biodiesel production: A review. *Biotechnol. Adv. 30,* 1364–1380.
68. Baroutian, S., Aroua, M. K., Raman, A. A. A., Sulaiman, N. M. N. (2011). A packed bed membrane reactor for production of biodiesel using activated carbon supported catalyst. *Bioresour. Technol. 102,* 1095–1102.
69. Dubé, M. A., Tremblay, A. Y., Liu, J. (2007). Biodiesel production using a membrane reactor. *Bioresour. Technol. 98,* 639–647.
70. Guerreiro, L., Pereira, P. M., Fonseca, I. M., Martin-Aranda, R. M., Ramos, A. M., Dias, J. M. L, et al. (2010). PVA embedded hydrotalcite membranes as basic catalysts for biodiesel synthesis by soybean oil methanolysis. *Catal. Today. 156,* 191–197.
71. Shi, W., He, B., Ding, J., Li, J., Yan, F., Liang, X. (2010). Preparation and characterization of the organic–inorganic hybrid membrane for biodiesel production. *Bioresour. Technol. 101,* 1501–1505.
72. Zhu, M., He, B., Shi, W., Feng, Y., Ding, J., Li. J, et al. (2010). Preparation and characterization of PSSA/PVA catalytic membrane for biodiesel production. *Fuel. 89,* 2299–2304.
73. Sarkar, B., Sridhar, S., Saravanan, K., Kale, V. (2010). Preparation of fatty acid methyl ester through temperature gradient driven pervaporation process. *Chem. Eng. J. 62,* 609–615.

CHAPTER 10

STUDIES ON THE EFFECT OF ANTIOXIDANTS ON THE LONG-TERM STORAGE STABILITY AND OXIDATION STABILITY OF *PONGAMIA PINNATA* AND *JATROPHA CURCUS* BIODIESEL

A. OBADIAH, and S. VASANTH KUMAR*

Department of Chemistry, Karunya University,
Coimbatore – 641114, Tamilnadu, India

CONTENTS

10.1 Introduction 243
10.1.1 Biodiesel Storage and Oxidation Stability Studies 244
10.2 Experimental 246
10.2.1 Biodiesel Storage Condition 246
10.2.2 Determination of Oxidative Stability 246
10.2.3 Evaluation of Storage Stability 247
10.3 Results and Discussion 247
10.3.1 Biodiesel Storage Studies 247
10.3.2 Oxidative Stability Studies of *Pongamia* and *Jatropha* Biodiesel Using Commercially Available Antioxidants 272
10.4 Conclusion 274

Keywords 275
References 275

ABSTRACT

There is increasing interest in developing alternative energy resources. An immediately applicable option is replacement of diesel fuel by biodiesel, which consists of the simple alkyl esters of fatty acids. With little modification, diesel engine vehicles can use biodiesel fuels. Biodiesel has been defined as the fatty acid methyl esters (FAME) or FA ethyl esters derived from vegetable oils or animal fats (Triglycerides, TG) by transesterification with methanol or ethanol. Its main advantages over fossil fuel are that it is renewable, biodegradable, and nontoxic. Its contribution to greenhouse gases is minimal, since the emitted CO_2 is equal to the CO_2 absorbed by the plants to create the TG. They can also be used as heating oil. Conversely, they do present other technical challenges, such as low cloud points and elevated NO_X emissions. The use of biodiesel is encouraged by governments across the world to improve energy supply security, reduce greenhouse gas emissions, and boost rural incomes and employments. One of the major drawbacks for the quality of biodiesel and its widespread commercialization is its oxidation stability. Unlike petroleum diesel fuel, the nature of biodiesel makes it more susceptible to oxidation or autoxidation during long-term storage. Storage conditions, exposure to water, and exposure to oxygen, which is naturally present in the ambient air, influence the rate of oxidation.

This study investigates the impact of various synthetic phenolic antioxidants on the oxidation stability and storage stability of Pongamia (karanja) biodiesel (PBD) and Jatropha curcus biodiesel (JBD). The results of Rancimat experiments show that the induction point (IP) increased substantially on adding certain antioxidants to the Pongamia biodiesel. The study reveals pyrogallol (PY) to be the best antioxidant, which showed the best improvement in the oxidative stability of PBD and JBD. The storage conditions employed were: (i) ordinary glass bottle with open space (OGOS), (ii) ordinary glass bottle with closed space

(OGCS), (iii) ordinary glass bottle with closed space containing nitrogen (OGCSN), (iv) amber glass bottle with open space (AGOS), (v) amber glass bottle with closed space (AGCS), and (vi) amber glass bottle with closed space containing nitrogen (AGCSN). Ambient humidity was between 41% and 72%. The samples were analyzed weekly. The storage stability studies were carried out according to the ASTM standard procedure ASTM 4625 @30 °C/50 weeks by adding different antioxidants like BHT, BHA, PY, GA and TBHQ. The induction period of PBD and JBD were determined with and without the addition of antioxidants like BHA, BHT, TBHQ, PY and GA, used at different concentrations (100, 200, 500, 1000, 2000, 3000 and 5000 ppm). Biodiesel samples stored in amber glass bottles with closed space containing nitrogen gave the best results as compared to the other five conditions tested. Pyrogallol was found to be the best commercial antioxidant for both *Pongamia* and *Jatropha* biodiesels as it increased the induction time from 0.05 hr to 4 hr, at 1000 ppm. Kinematic viscosity and acid values are good indicators of storage stability of biodiesels. BHT, TBHQ, PY, GA, and BHA, at concentrations of 1000 ppm, improved the storage stability of biodiesel.

10.1 INTRODUCTION

The word "antioxidant" has become increasingly popular in modern society as it gains publicity through mass media coverage of its health benefits. The dictionary definition of antioxidant is rather straightforward but a traditional annotation would define antioxidant as "a substance that opposes oxidation or inhibits reactions promoted by oxygen or peroxides, many of these substances (as the tocopherols) being used as preservatives in various products (as in fats, oils, food products, and soaps for retarding the development of rancidity, in gasoline and other petroleum products for retarding gum formation and other undesirable changes, and in rubber for retarding aging)." A more biologically relevant definition of antioxidants is "synthetic or natural substances added to products to prevent or delay their deterioration by action of oxygen in air [1].

Biodiesel, defined as fatty acid mono-alkyl esters made from vegetable oil or animal fat, is an alternative fuel for combustion in compression–ignition (diesel) engines. Several recent reviews have reported

on the technical characteristics of biodiesel. In short, biodiesel is made from domestically renewable feedstock, is environmentally innocuous, is relatively safe to handle (high flash points), and has an energy content, specific gravity, kinematic viscosity (KV), and cetane number (CN) comparable to petroleum middle distillate fuels (petro diesel) [2, 3].

With a production of almost 1 million tons in Europe, FAME more generally called biodiesel, has become a fast growing renewable liquid biofuel within the European Community. Just like vegetable oils or fats, fatty acid methyl esters undergo degradation over time, mainly influenced by temperature and oxygen. Degradation products of biodiesel, such as insoluble gums and sediments, or the formation of organic acids and aldehyde may cause engine and injection problems [3–5].

The bis-allylic configurations, where the central methylene group is activated by the two double bonds (i.e., -CH=CH-CH_2-CH=CH-), react with oxygen via the autoxidation mechanism, with the radical chain reaction steps of initiation, propagation, chain branching, and termination. During these reaction steps, several products can be formed, such as peroxides and hydro peroxides, low molecular weight organic acids, aldehydes and keto compounds, alcohols, as well as high molecular weight species (dimers, trimers, and cyclic acids) *via* polymerization mechanisms. The use of antioxidant additives can help slow the degradation process and improve fuel stability up to a point [6–9]. Fuel properties degrade during long-term storage as follows: (i) oxidation or autoxidation from contact with ambient air; (ii) thermal or thermal-oxidative decomposition from excess heat; (iii) hydrolysis from contact with water or moisture in tanks and fuel lines; or (iv) microbial contamination from migration of dust particles or water droplets containing bacteria or fungi into the fuel [10]. Monitoring the effects of autoxidation on biodiesel fuel quality during long-term storage presents a significant concern for biodiesel producers, suppliers, and consumers [11–13].

10.1.1 BIODIESEL STORAGE AND OXIDATION STABILITY STUDIES

The parameter of oxidation stability has been fixed at a minimum limit of a 6-hour induction period at 110°C [14, 15]. The method adopted for

determination of the oxidation stability is the so-called Rancimat method, which is commonly used in the vegetable oil sector. Especially high contents of unsaturated fatty acids, which are very sensitive to oxidative degradation, lead to very low values for the induction period. Thus, even the conditions of fuel storage directly affect the quality of the product. Several studies showed that the quality of biodiesel over a longer period of storage strongly depends on the tank material as well as on contact to air or light. Increase in viscosities and acid values and decreases in induction periods have been observed [16] during such storage. Although there are numerous publications on the effect of natural and synthetic antioxidants on the stability of oils and fats used as food and feed, little is available on the effect of antioxidants on the behavior of FAME used as biodiesel. To retard oxidative degradation and to guarantee a specific stability, it becomes necessary to find appropriate additives for biodiesel. Simkovsky [17] studied the effect of different antioxidants on the induction period of rapeseed oil methyl esters at different temperatures but did not find significant improvements. Schober [18] tested the influence of the antioxidant TBHQ on the peroxide value of soybean oil methyl esters during storage and found good improvement of stability. Canakci [19] described the effect of the antioxidants TBHQ and α-tocopherol on fuel properties of methyl soyate and found beneficial effects on retarding oxidative degradation of the sample. Das [20] described effect of commercial antioxidants used in kharanja biodiesel for storage stability. Recently Karavalakis [21] described the effect of synthetic phenolic antioxidants used for storage stability and oxidative stability. The storage stability of different biodiesel blends with automotive diesel treated with various phenolic antioxidants has also been investigated over a storage time of 10 weeks.

In the previous studies, numerous methods for assessing the oxidation status of biodiesel have been investigated, including acid value, density, and kinematic viscosity. The peroxide value may not be suitable because, after an initial increase, it decreases due to secondary oxidation reactions, although the decrease likely affects only samples oxidized beyond what may normally be expected. Thus there is the possibility of the fuel having undergone relatively extensive oxidation but displaying an acceptable peroxide value. The peroxide value is also not included

in biodiesel standards. Acid value and kinematic viscosity, however, are two facile indicators for rapid assessment of biodiesel fuel quality as they continuously increase with deteriorating fuel quality [22]. In this chapter, oxidative and storage stability of biodiesel was investigated using commercially available antioxidants.

The aim of the present study was to investigate the oxidative and storage stabilities of *Pongamia pinnata* (PBD) and *Jatropha curcus* (JBD) biodiesels with five commercially available antioxidants such as BHA, BHT, GA, TBHQ and PY. The Rancimat procedure and the ASTM procedure were employed to investigate oxidation stability and storage stability, respectively, of the biodiesels. Fuel properties such as acid value (AN) and KV of PBD and JBD were determined at regular periods of time, using the selected antioxidants at different concentrations.

10.2 EXPERIMENTAL

10.2.1 BIODIESEL STORAGE CONDITION

Normally, 200 mL of PBD and JBD biodiesel samples were stored in open Borosil glass bottles of 250 mL capacity and kept indoors, at a temperature of either 30°C or 42°C. The samples were exposed to air under daylight condition. The storage studies on PBD and JBD using commercially available antioxidants are presented in this section. Experiments were carried out at different storage conditions. The storage conditions employed were: (i) ordinary glass bottle with open space (OGOS); (ii) ordinary glass bottle with closed space (OGCS); (iii) ordinary glass bottle with closed space containing nitrogen (OGCSN); (iv) amber glass bottle with open space (AGOS); (v) amber glass bottle with closed space (AGCS); and (vi) amber glass bottle with closed space containing nitrogen (AGCSN). Ambient humidity was between 41% and 72%. The samples were analyzed weekly.

10.2.2 DETERMINATION OF OXIDATIVE STABILITY

Oxidative stability (OS) of biodiesel sample was studied with a Rancimat 873 instrument (Metrohm, Switzerland), as followed by Tang [9] Das [20]

Karavalakis [21] and Knothe [22]. The sample was heated at a constant temperature of 110°C with excess airflow which passed through a conductivity cell filled with distilled water. During this oxidation process volatile acids were formed which were carried along with the airflow resulting in a gradual increase in the conductivity of distilled water present in the conductivity cell. After a period of time, called 'induction period,' the gradual increase leads to a sudden increase in the conductivity of the distilled water. The induction period of PBD and JBD were determined with and without the addition of antioxidants like BHA, BHT, TBHQ, PY and GA, used at different concentrations (100, 200, 500, 1000, 2000, 3000 and 5000 ppm).

10.2.3 EVALUATION OF STORAGE STABILITY

To evaluate the storage stability, the ASTM procedures D-4625 – 25 weeks and D4625 – 12 weeks were employed. In the ASTM D4625 – 25 weeks procedure, the KV, PV and AN values were determined at 30°C every week over a period of 25 weeks. In the ASTM D4625 – 12 procedure, the KV, PV and AN values were monitored at 43°C every week over a period of 12 weeks. The storage container used was 250 mL bottle containing 200 mL of biodiesel and 50 mL of free space. The ambient humidity in the storage room was 41% to 72%.

10.3 RESULTS AND DISCUSSION

10.3.1 BIODIESEL STORAGE STUDIES

The study on karanja oil methyl ester was carried out by Das et al. by using three antioxidants namely butylated hydroxy anisole, butylated hydroxy toluene and propyl gallate [20]. They varied the load level of the three antioxidants from 100 to 1000 ppm and noticed decrease in peroxide values as the concentration of antioxidants increased. Peroxide value is not listed as a parameter in the biodiesel fuel specification, though viscosity and acid value were among the specifications listed within PS121 (provisional fuel standard guideline for biodiesel) and are known to be affected by the autoxidation of biodiesel. Changes in viscosity and acid value were

therefore monitored in this study, to understand the oxidative stability of *Pongamia* biodiesel. Dunn examined the effects of oxidation under controlled accelerated conditions on fuel properties of methylsoyate, where the author employed only TBHQ and α-tocopherol as antioxidants, which were found to have beneficial effects on retarding oxidative degradation of methylsoyate biodiesel [18]. Karavalakis [21] in their study evaluated the impact of biodiesel concentration in diesel fuel on the stability of the final blend. They have also discussed the effect of sulfur content in the base diesel on the oxidation stability of the blend (Fig. 10.1).

Results of storage studies of *Pongamia* and *Jatropha* biodiesel using commercially available antioxidants are presented in this chapter. The chemical structure of the selected antioxidants are given below.

Experiments were carried out at different storage conditions. The storage conditions employed were: (i) ordinary glass bottle with open space (OGOS), (ii) ordinary glass bottle with closed space (OGCS), (iii) ordinary

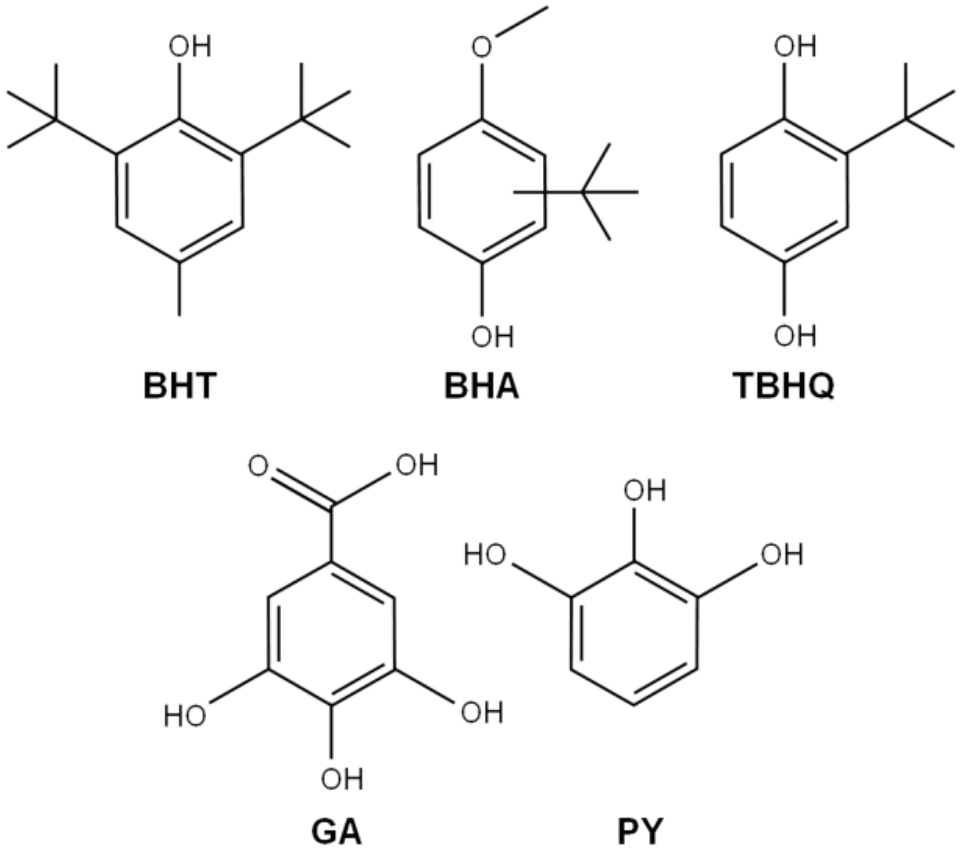

FIGURE 10.1 Chemical structure of commercially available antioxidants.

glass bottle with closed space containing nitrogen (OGCSN), (iv) amber glass bottle with open space (AGOS), (v) amber glass bottle with closed space (AGCS), and (vi) amber glass bottle with closed space containing nitrogen (AGCSN). The effect of five different antioxidants on the oxidative stability and storage stability of *Pongamia* and *Jatropha* biodiesel were evaluated using standard Rancimat procedure (EN 14214) and recommended ASTM procedure D-4625 – 25 weeks. Storage in amber glass bottle with nitrogen atmosphere was found to be the best storage condition exhibiting minimum oxidation. Figure 10.2 shows the variance of kinematic viscosity, acid value and peroxide value with respect to time in the presence of nitrogen atmosphere.

Studies using various concentrations reveal that 1000 ppm is sufficient for a storage time of 25 weeks. Figures 10.2 and 10.3 shows the variance of kinematic viscosity, acid value and peroxide value with respect to time in the presence of nitrogen atmosphere. The effects of commercial antioxidants on *Pongamia* and *Jatropha* biodiesel at different atmospheric conditions and various concentrations of antioxidants were studied and are discussed below.

10.3.1.1 *Jatropha* Biodiesel With BHA as Additive

In the absence of antioxidants (neat) JBD exhibits a KV value of 14.76 mm^2/s, PV of 9.3 mg/kg and AV of 2.47 mg KOH/g. The storage studies also reveal that in the absence of antioxidants PBD shows a KV value of 14.7 mm^2/s, PV of 6.38 mg/kg and AV of 1.68 mg KOH/g. The results presented below are from the storage studies carried out under AGCSN conditions. All other storage conditions showed higher values of KV, PV and AV)

10.3.1.2 *Pongamia* Biodiesel With BHA as Additive

Results of storage studies of *Pongamia* and *Jatropha* biodiesel using BHA as the antioxidant are shown in Figures 10.4 and 10.5. Various storage conditions such as: (i) OGOS, (ii) OGCS, (iii) OGCSN, (iv) AGOS, (v) AGCS, and (vi) AGCSN were tested. Storage in amber glass bottle with nitrogen atmosphere was found to be the best storage condition exhibiting minimum oxidation.

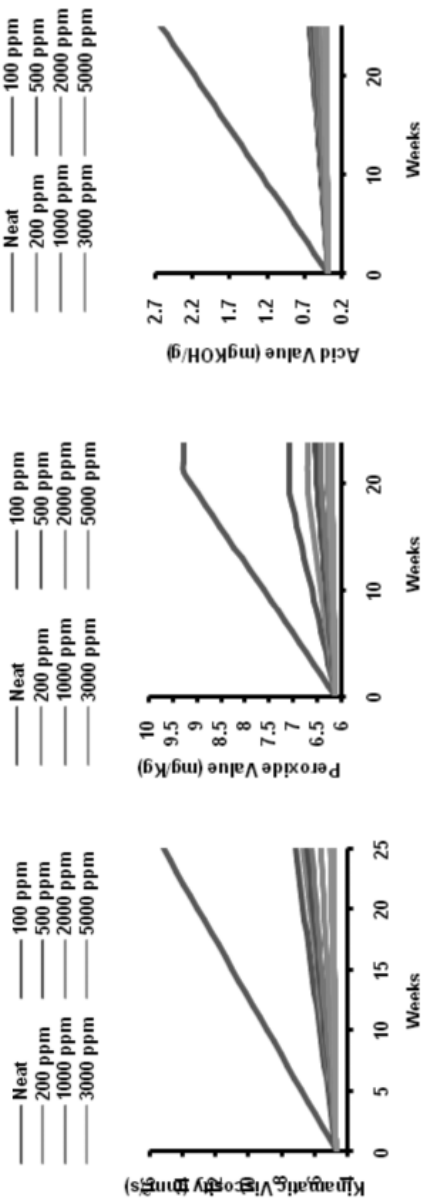

FIGURE 10.2 Storage studies using pyrogallol as additive in *Pongamia* biodiesel.

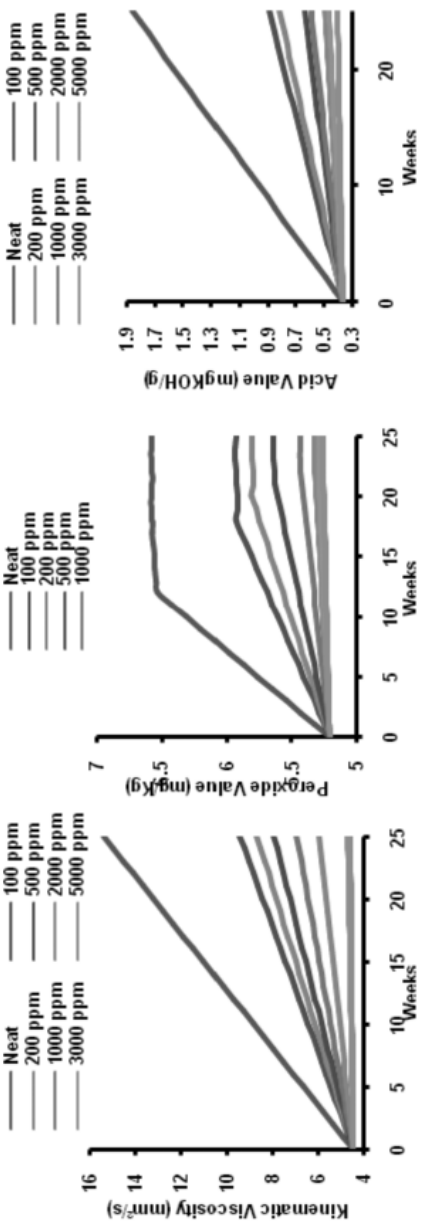

FIGURE 10.3 Storage studies using pyrogallol as additive in *Jatropha* biodiesel.

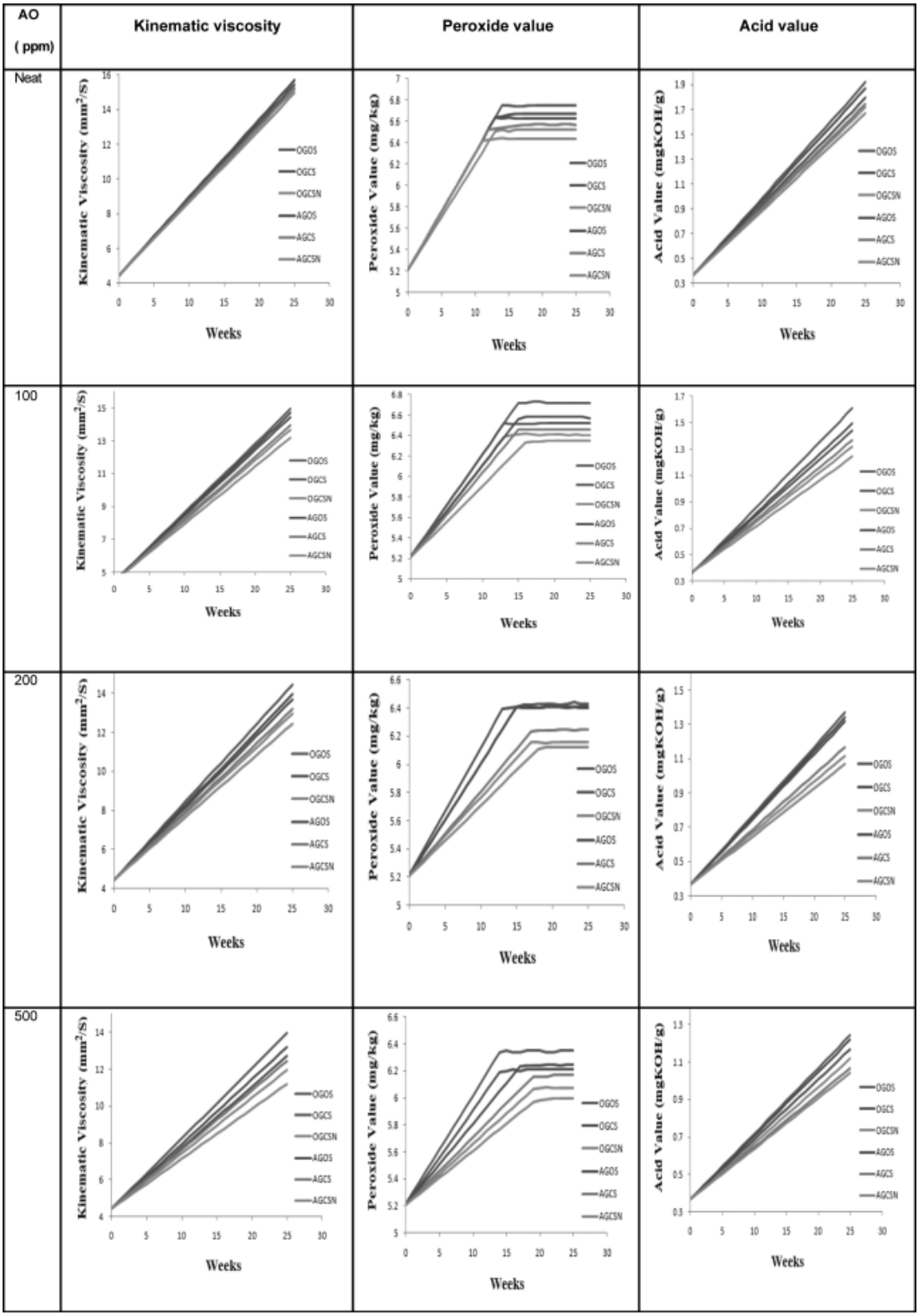

FIGURE 10.4 Storage stability of *Jatropha* biodiesel with BHA as antioxidant carried out for 25 weeks.

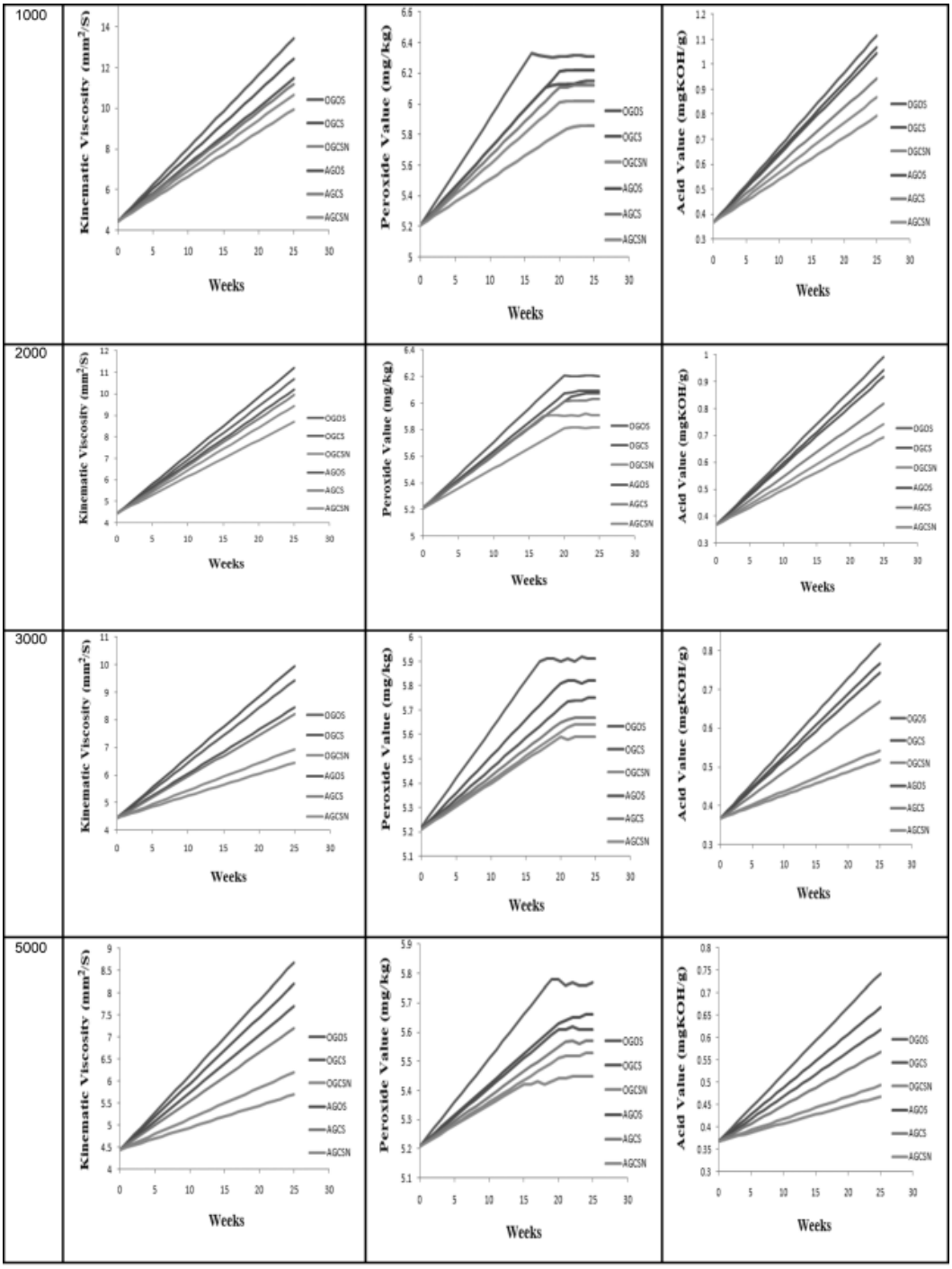

FIGURE 10.4 (*Continued*)

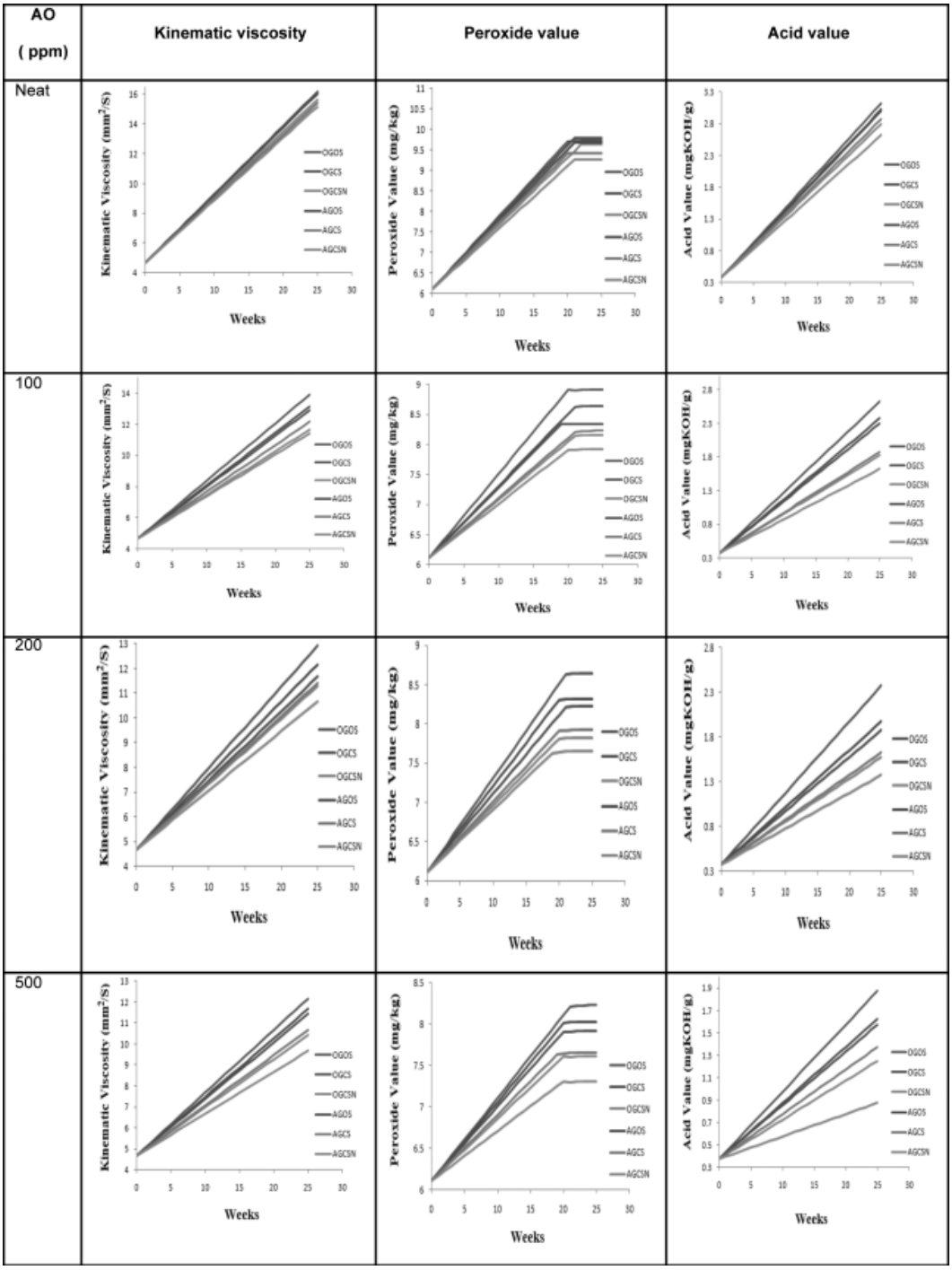

FIGURE 10.5 Storage stability of *Pongamia* biodiesel with BHA as antioxidant carried out for 25 weeks.

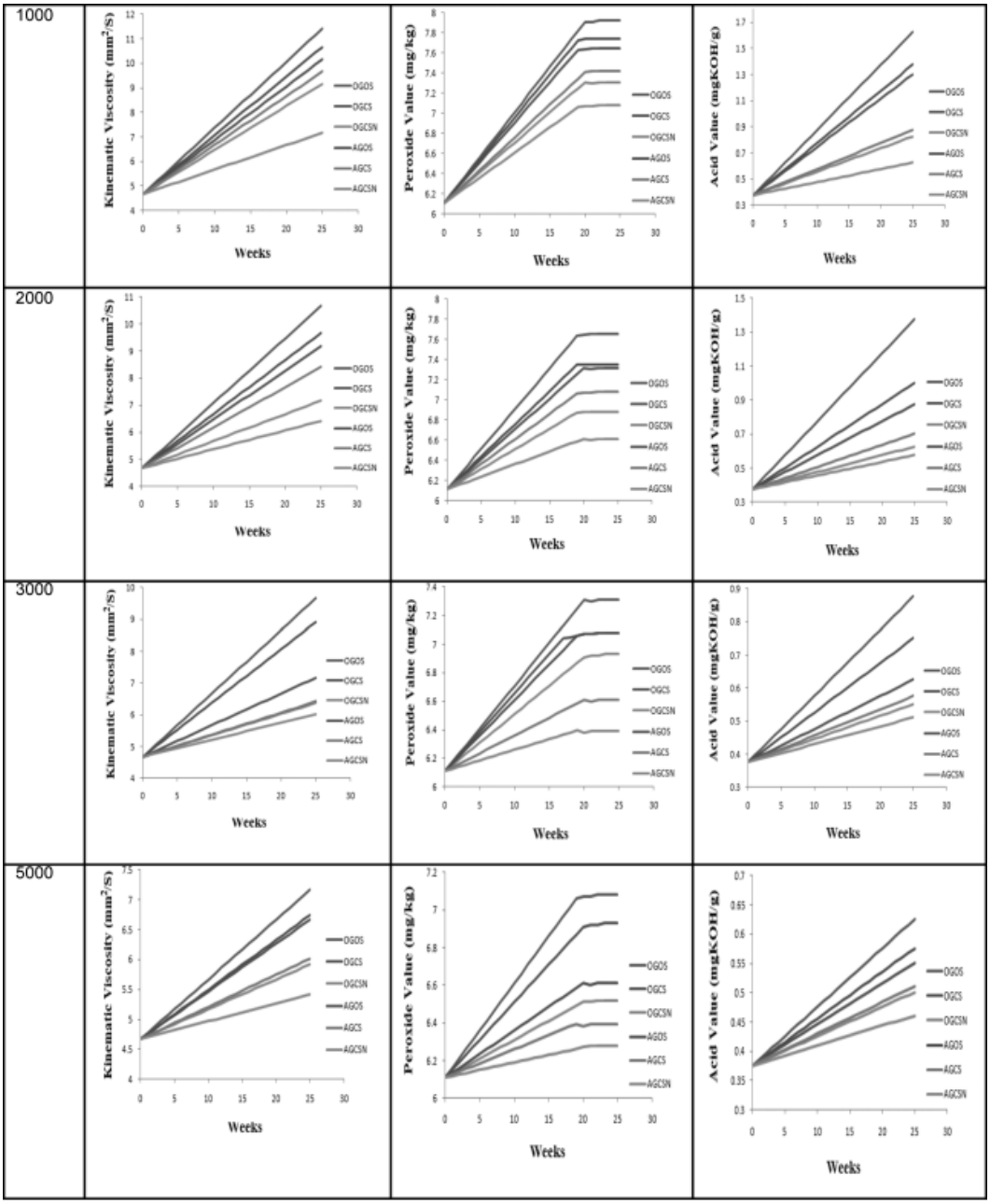

FIGURE 10.5 (*Continued*)

Results reveals that JBD with 5000 ppm BHA, under nitrogen atmosphere stored in a amber glass bottle exhibited a KV of 5.21 mm^2/s, PV of 5.42 mg/kg and AV of 0.44 mg KOH/g. The storage studies also reveal that PBD with 5000 ppm of BHA showed KV of 5.27 mm^2/s, PV of 6.2 mg/kg and AV of 0.44 mg KOH/g. The storage stability increased when the concentration of antioxidant was increased.

10.3.1.3 *Jatropha* Biodiesel With BHT as Additive

Storage stability of *Jatropha* biodiesel with BHT as antioxidant carried out for 25 weeks is shown in Fig. 10.6.

10.3.1.4 *Pongamia* Biodiesel With BHT as Additive

Results of storage studies of *Pongamia* and *Jatropha* biodiesel using BHT as the antioxidant under various storage conditions such as: (i) OGOS, (ii) OGCS, (iii) OGCSN, (iv) AGOS, (v) AGCS, and (vi) AGCSN are presented above (Figs. 10.7 and 10.8). Storage in amber glass bottle with nitrogen atmosphere was found to be the best storage condition exhibiting minimum oxidation. Figure 10.6 and 10.7 show the variance of kinematic viscosity, acid value and peroxide value with respect to time in the presence of nitrogen atmosphere.

JBD with 5000 ppm BHT under nitrogen atmosphere stored in a amber glass bottle exhibited a KV of 4.7 mm^2/s, PV of 5.28 mg/kg and AV of 0.39 mg KOH/g. The study also reveals that PBD with 5000 ppm BHT exhibits KV of 5.1 mm^2/s, PV of 6.22 mg/kg and AV of 0.41 mg KOH/g. The storage stability increased when the concentration of antioxidants was increased.

10.3.1.5 *Jatropha* Biodiesel With GA as Additive

Storage stability of *Jatropha* biodiesel with GA as antioxidant carried out for 25 weeks is shown in Fig. 10.8.

10.3.1.6 *Pongamia* Biodiesel With GA as Additive

Results of storage studies of *Pongamia* and *Jatropha* biodiesel using GA as the antioxidant under various storage conditions such as, (i) OGOS, (ii) OGCS, (iii) OGCSN, (iv) AGOS, (v) AGCS, and (vi) AGCSN are presented above. Storage in amber glass bottle with nitrogen atmosphere was found to be the best storage condition exhibiting minimum oxidation.

Figures 10.8 and 10.9 show the variance of kinematic viscosity, acid value and peroxide value with respect to time in the presence of nitrogen

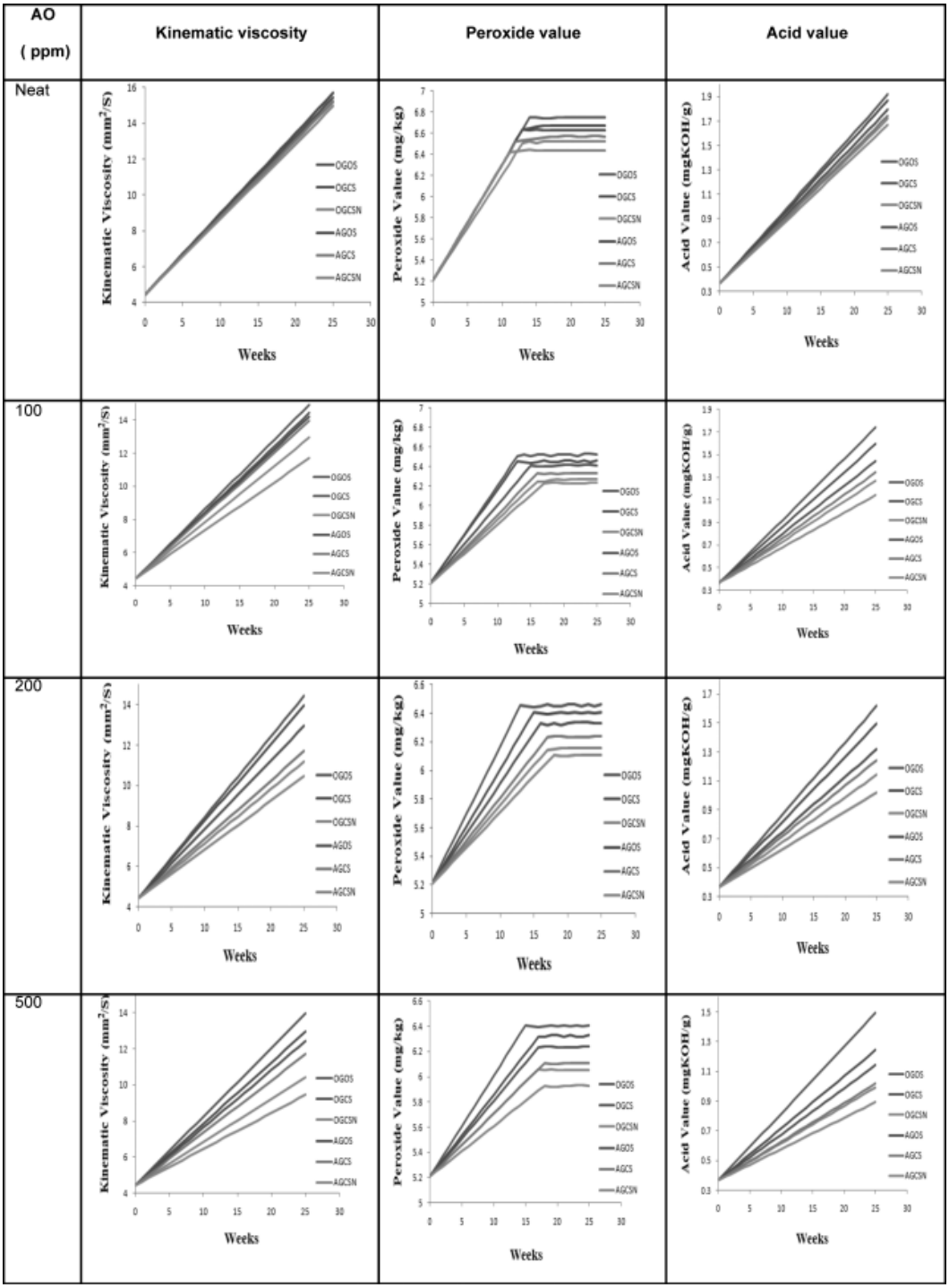

FIGURE 10.6 Storage stability of Jatropha biodiesel with BHT as antioxidant carried out for 25 weeks.

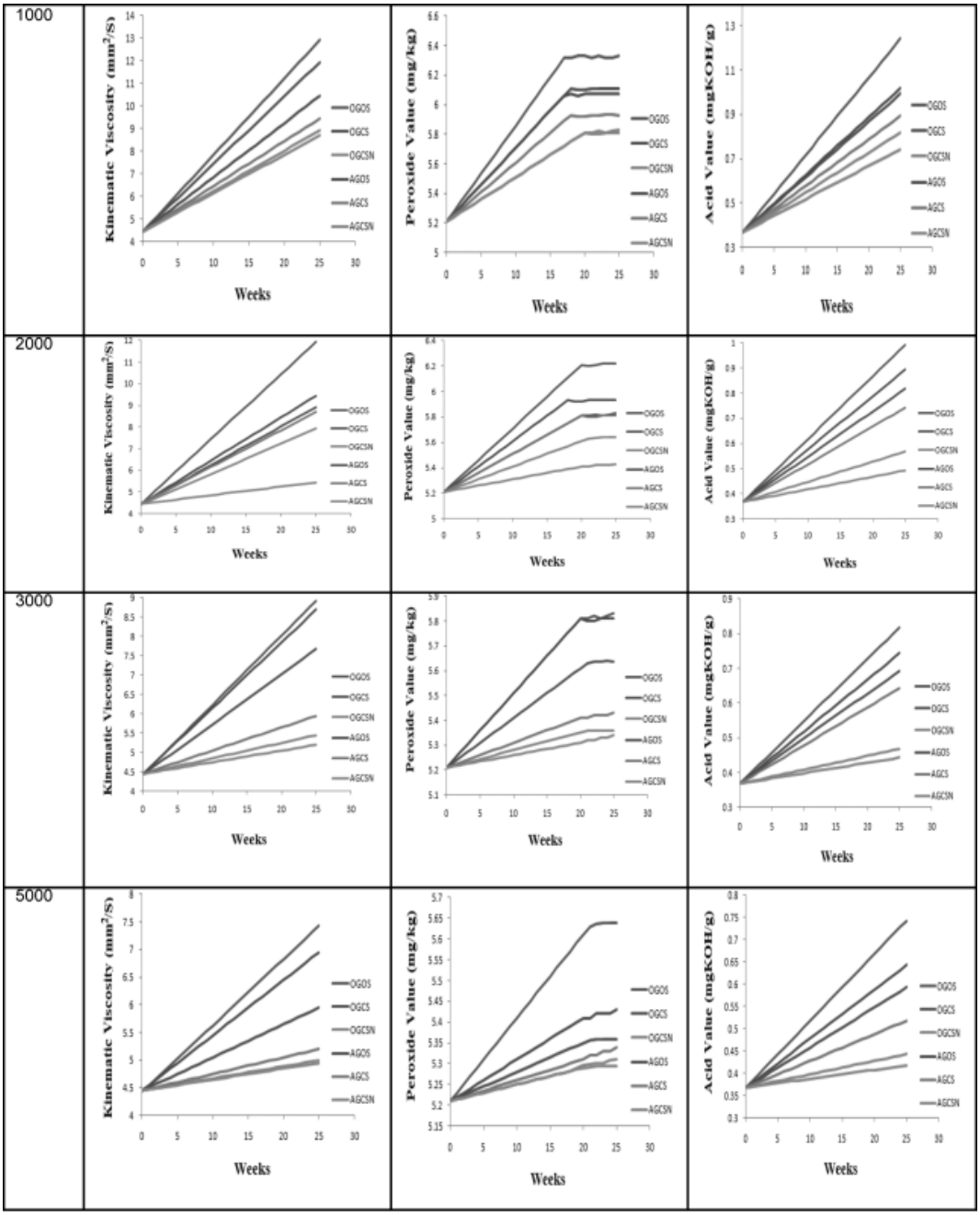

FIGURE 10.6 (*Continued*)

atmosphere. JBD with 5000 ppm GA, under nitrogen atmosphere stored in a amber glass bottle, exhibited a KV of 5.4 mm^2/s, PV of 5.33 mg/kg and AV of 0.45 mg KOH/g. The storage studies also reveals that 5000 ppm of GA in PBD shows KV of 5.1 mm^2/s, PV of 6.22 mg/kg and AV of 0.41 mg KOH/g. The storage stability increased with an increase in the concentration of GA.

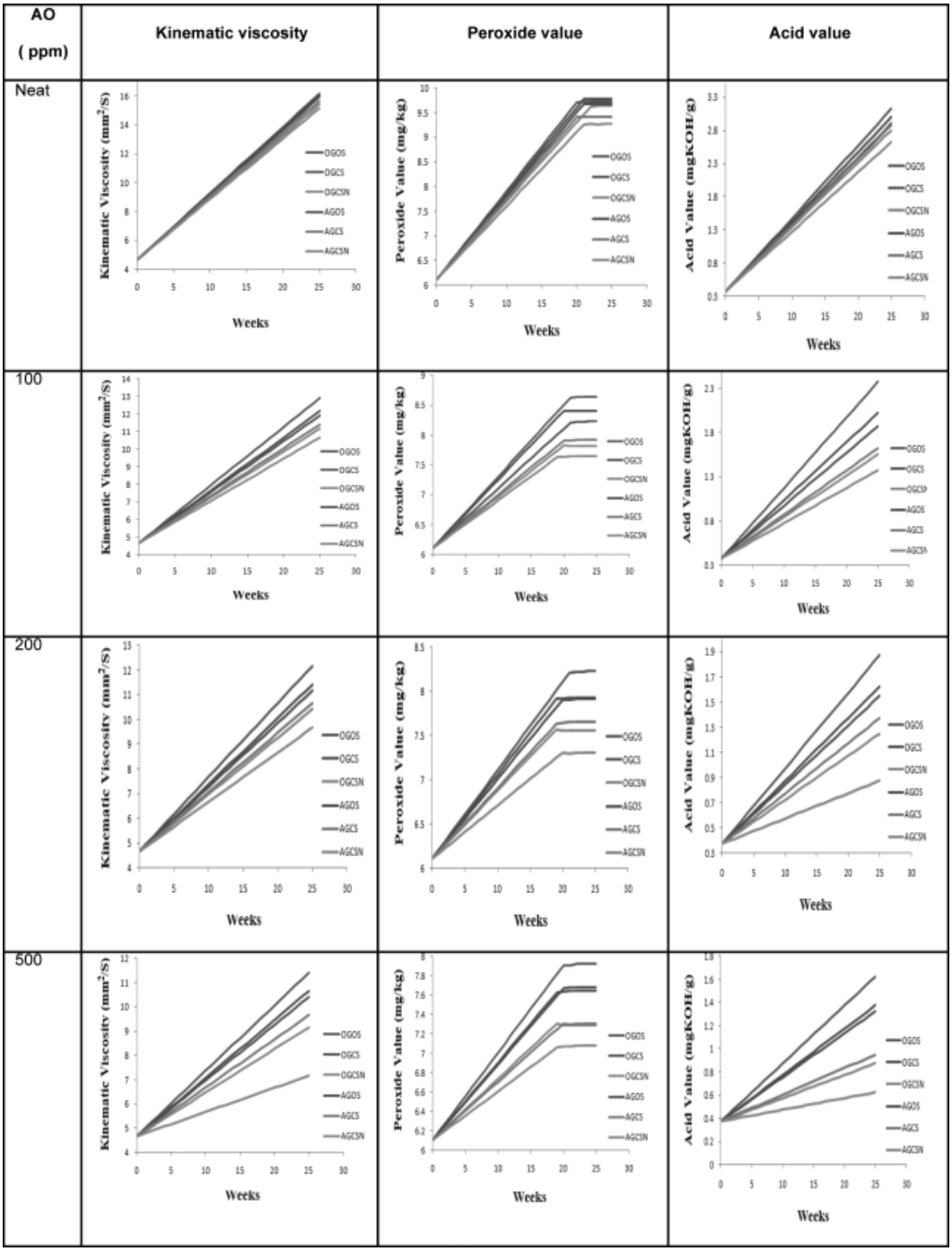

FIGURE 10.7 Storage stability of Pongamia biodiesel with BHT as antioxidant carried out for 25 weeks.

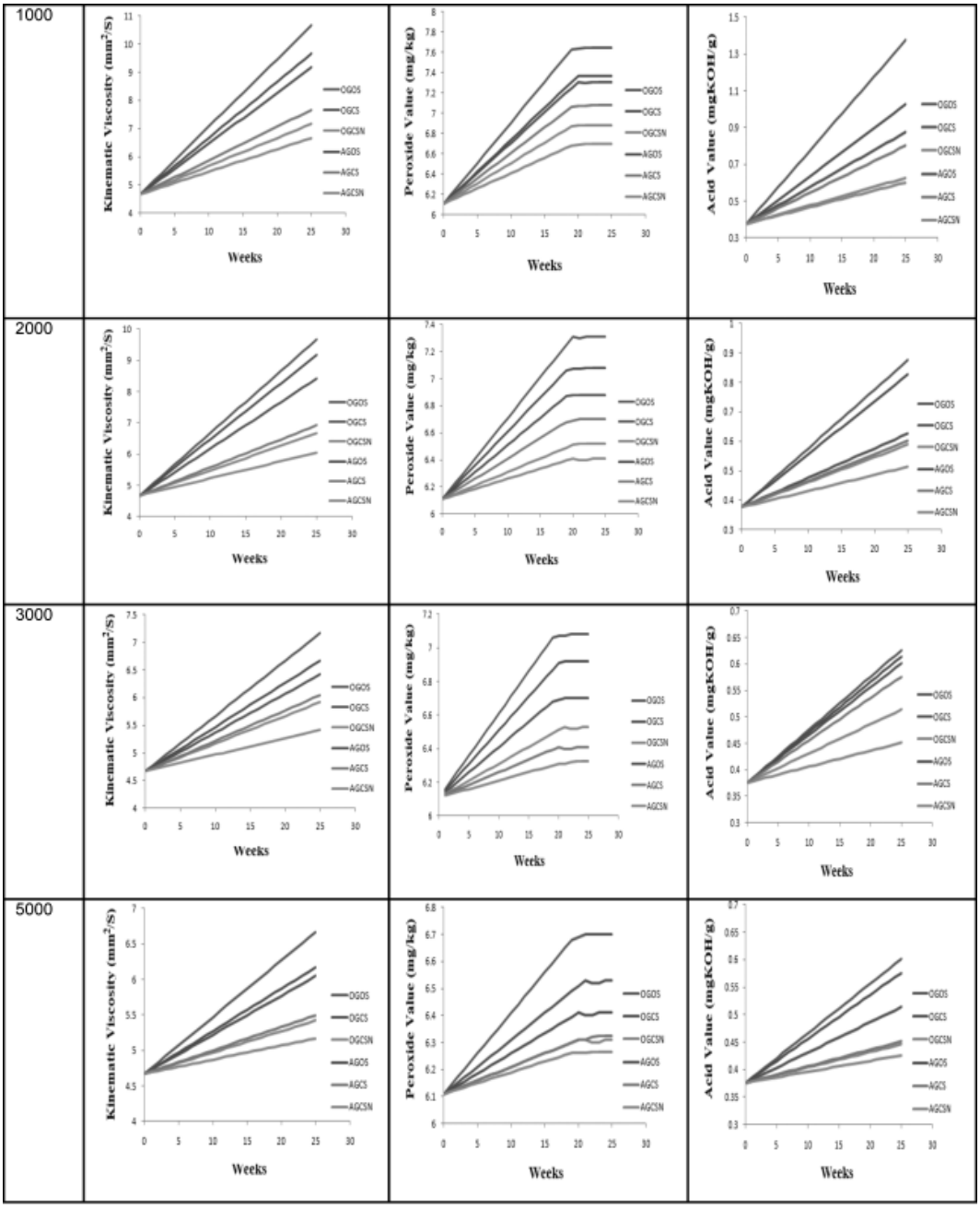

FIGURE 10.7 (*Continued*)

10.3.1.7 *Jatropha* Biodiesel With TBHQ as Additive

Storage stability of *Jatropha* biodiesel with TBHQ as antioxidant carried out for 25 weeks is shown in Fig. 10.10.

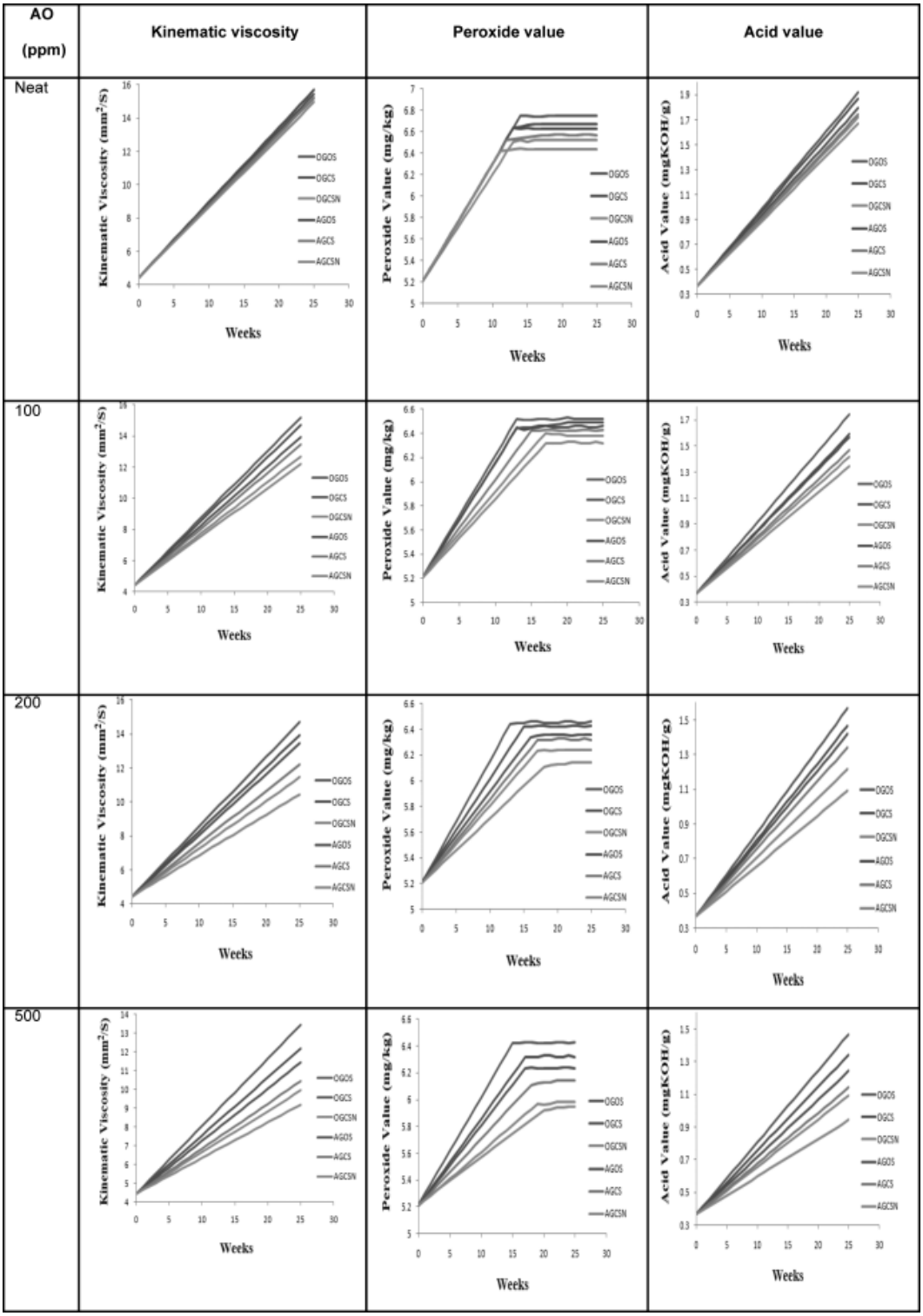

FIGURE 10.8 Storage stability of *Jatropha* biodiesel with GA as antioxidant carried out for 25 weeks.

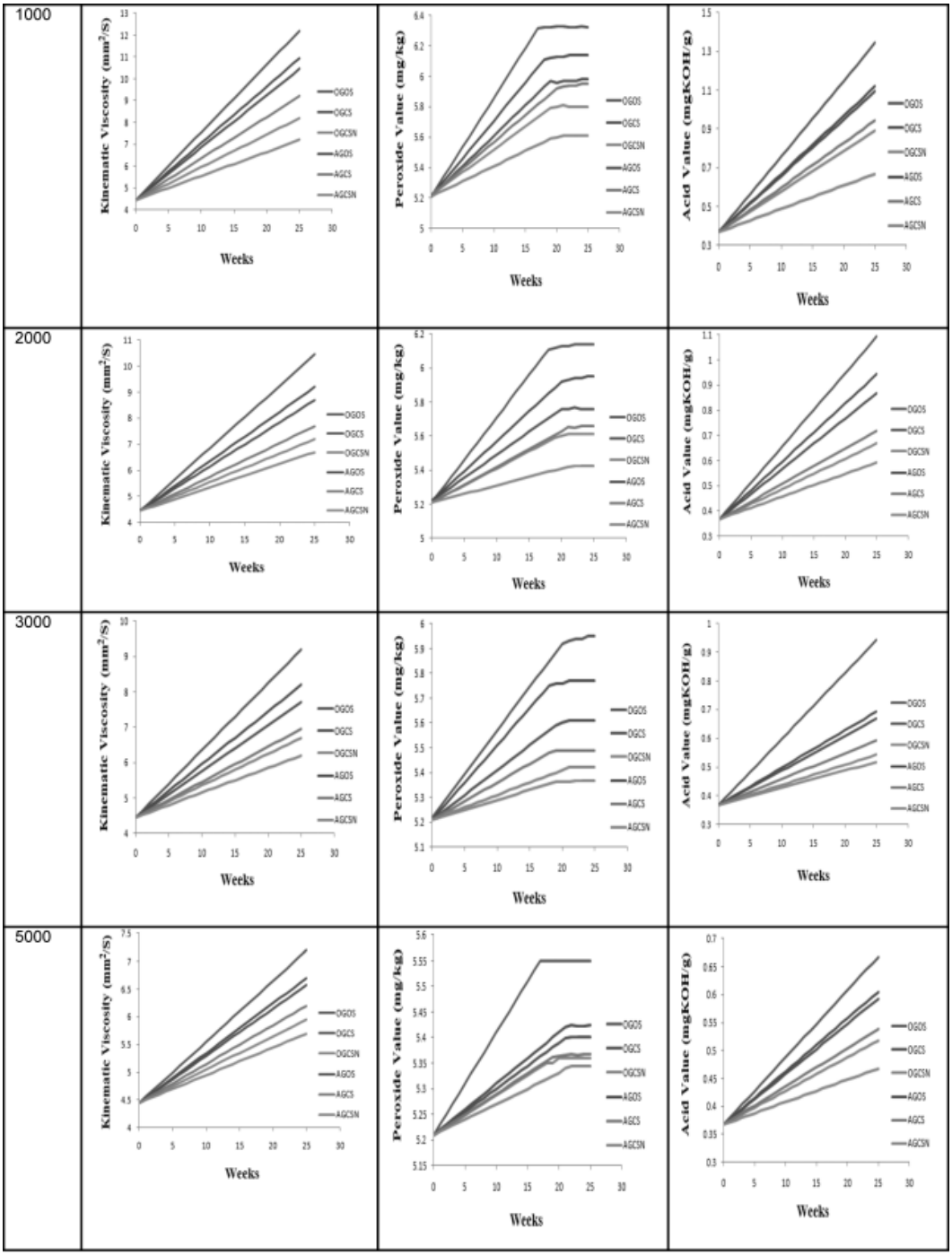

FIGURE 10.8 (*Continued*)

10.3.1.8 *Pongamia* Biodiesel With TBHQ as Additive

Results of storage studies of *Pongamia* and *Jatropha* biodiesel using TBHQ as the antioxidant were investigated under different storage condi-

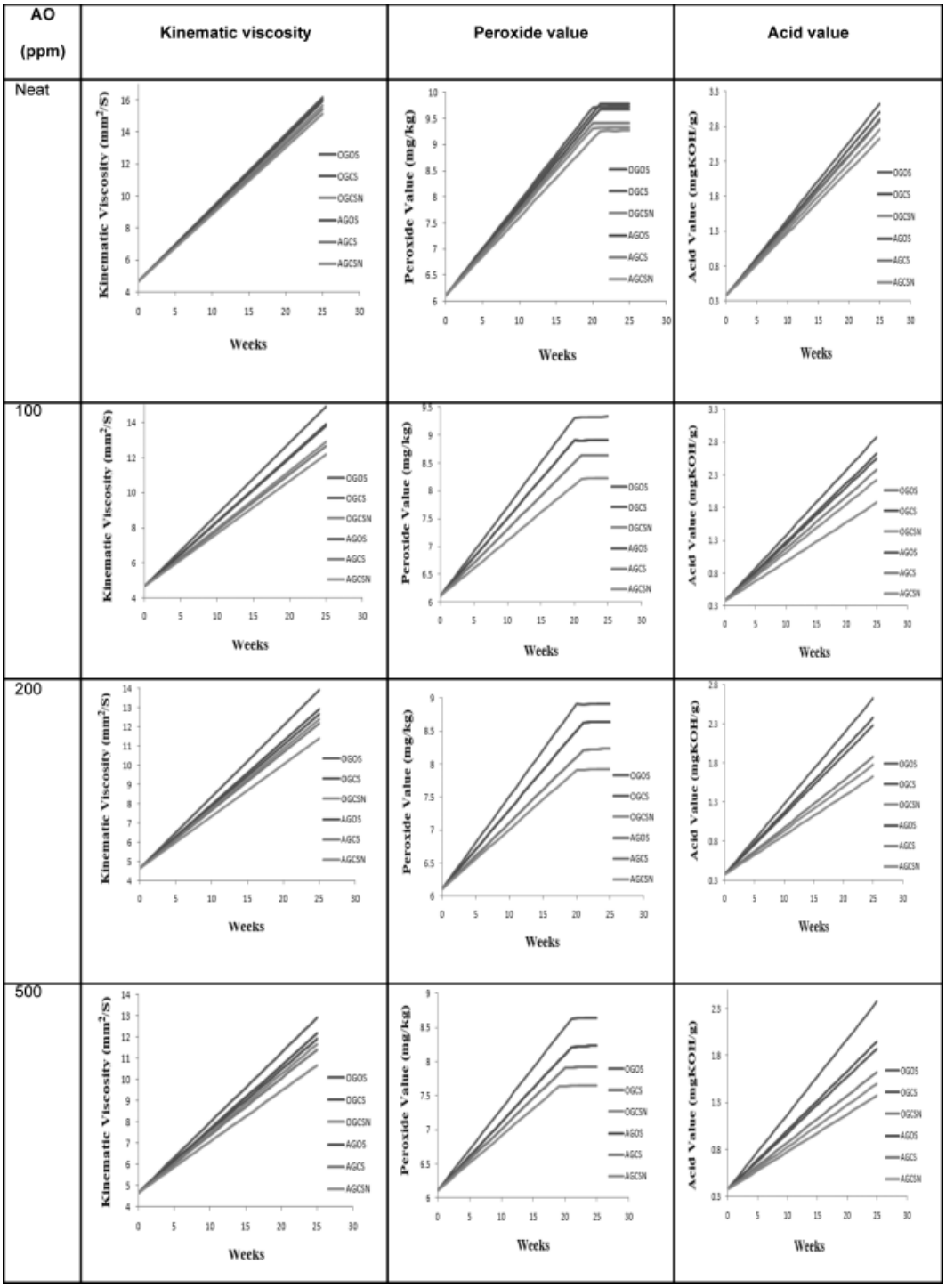

FIGURE 10.9 Storage stability of *Pongamia* biodiesel with GA as antioxidant carried out for 25 weeks.

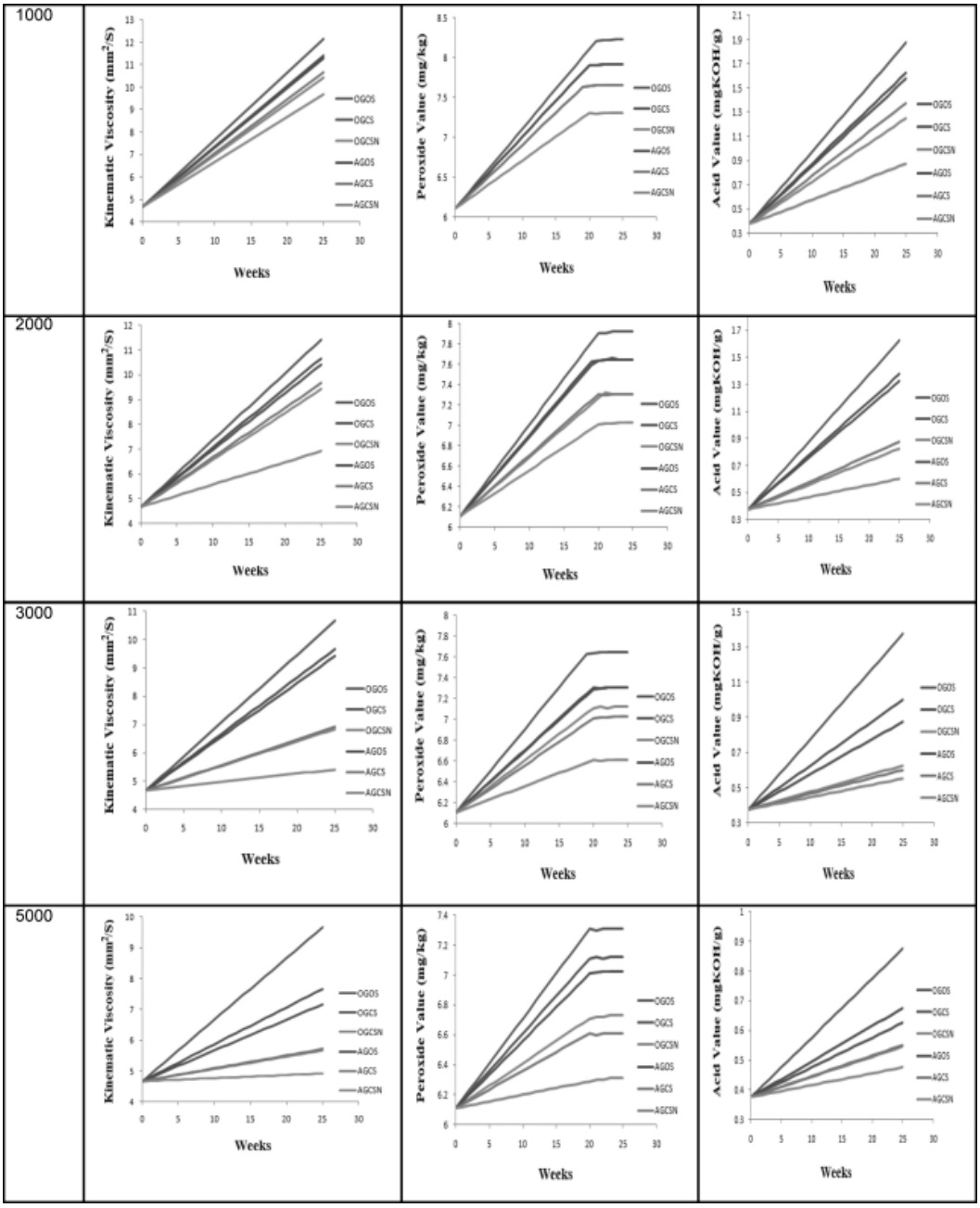

FIGURE 10.9 (*Continued*)

tions such as, (i) OGOS, (ii) OGCS, (iii) OGCSN, (iv) AGOS, (v) AGCS, and (vi) AGCSN. Storage in amber glass bottle with nitrogen atmosphere was found to be the best storage condition exhibiting minimum oxidation.

Figures 10.10 and 10.11 shows that JBD with 5000 ppm TBHQ, under nitrogen atmosphere stored in a amber glass bottle, exhibited a KV of 4.48

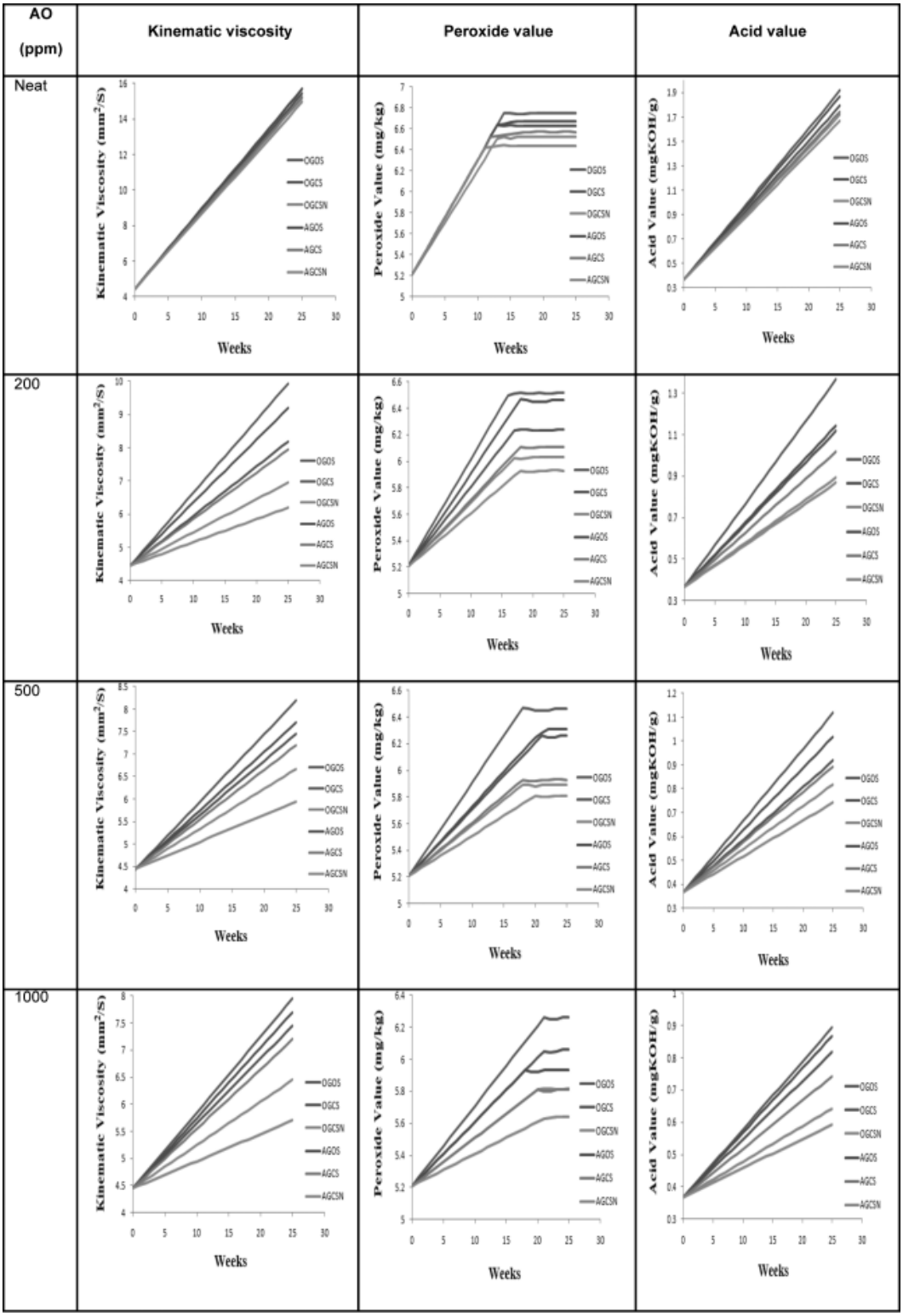

FIGURE 10.10 Storage stability of *Jatropha* biodiesel with TBHQ as antioxidant carried out for 25 weeks.

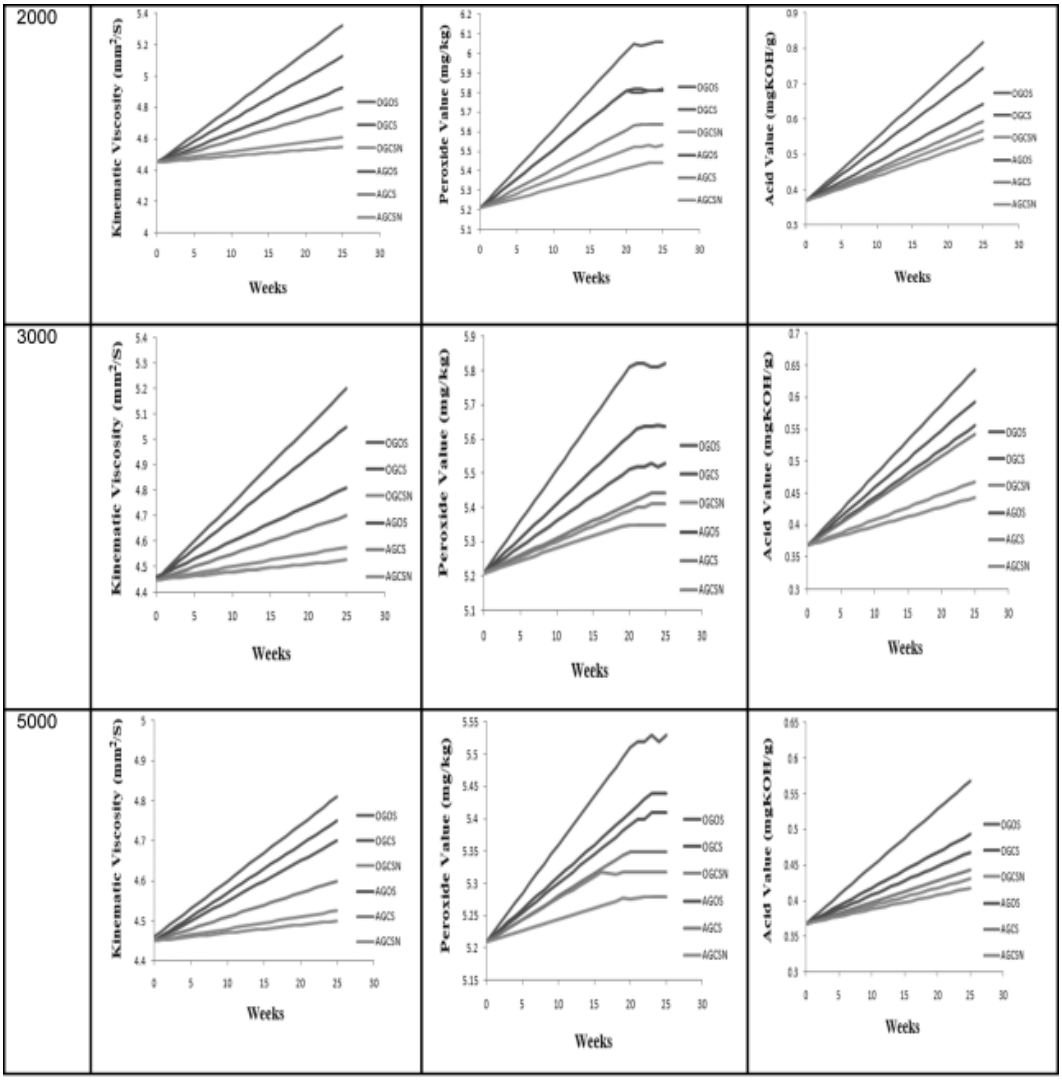

FIGURE 10.10 (*Continued*)

mm^2/s, PV of 5.28 mg/kg and AV of 0.40 mg KOH/g. PBD with 5000 ppm TBHQ under similar conditions shows KV of 4.98 mm^2/s, PV of 6.12 mg/kg and AV of 0.38 mg KOH/g. The storage stability increased when the concentration of TBHQ was increased.

10.3.1.9 *Jatropha* Biodiesel With PY as Additive

Storage stability of *Jatropha* biodiesel with PY as antioxidant carried out for 25 weeks is shown in Fig. 10.12.

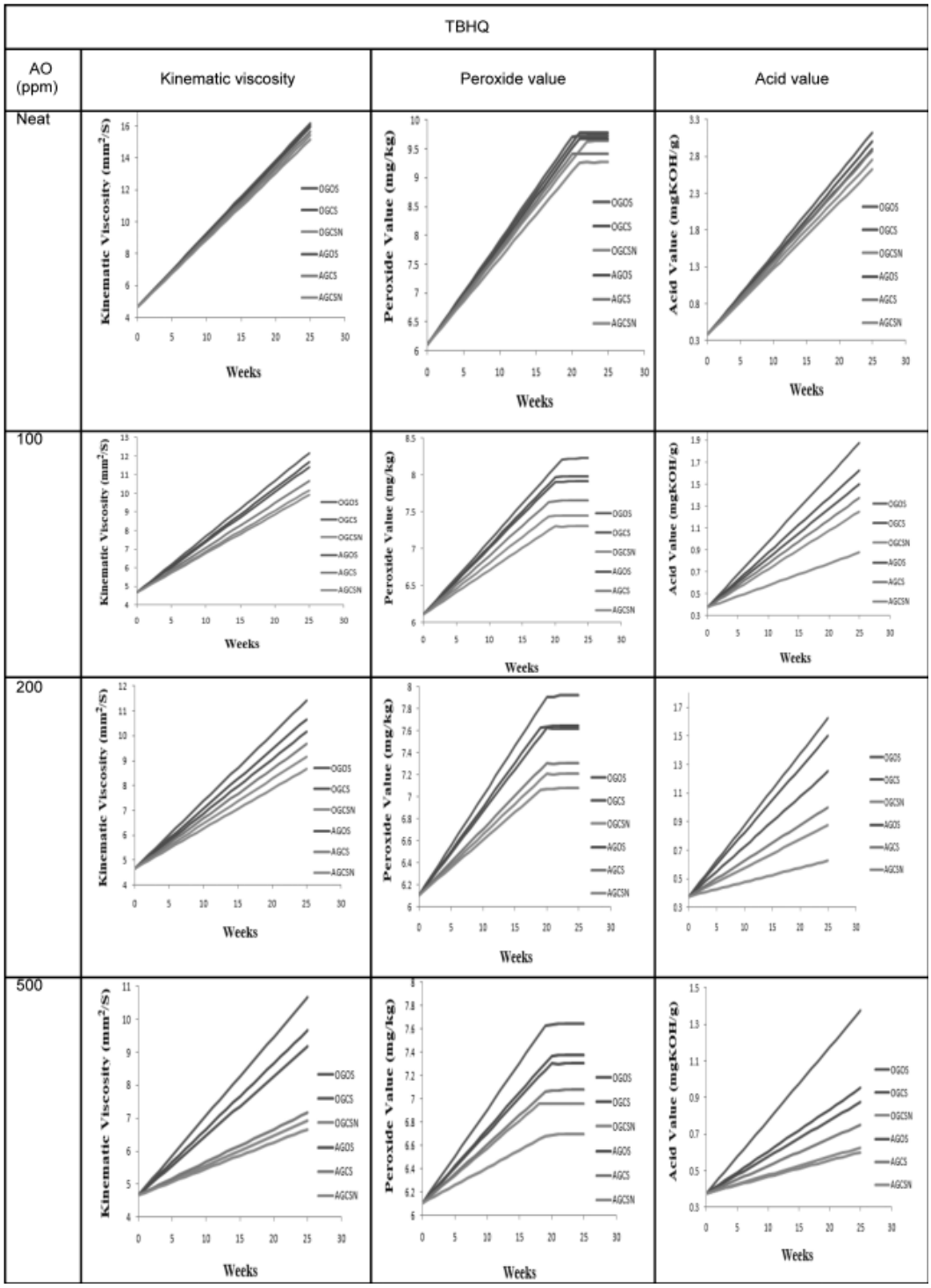

FIGURE 10.11 Storage stability of *Pongamia* biodiesel with TBHQ as antioxidant carried out for 25 weeks.

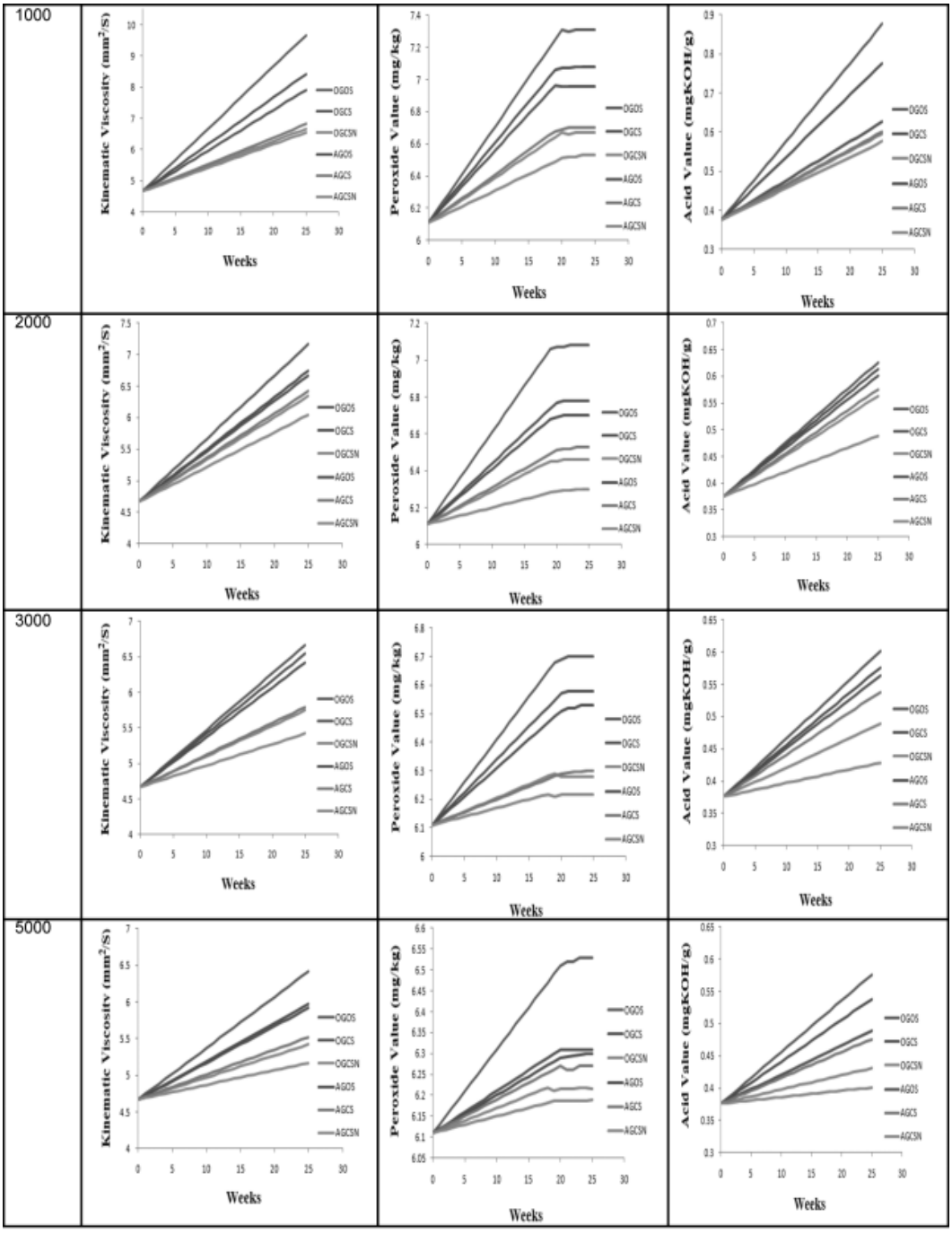

FIGURE 10.11 (*Continued*)

10.3.1.10 *Pongamia* Biodiesel With PY as Additive

Results of storage studies of *Pongamia* and *Jatropha* biodiesel using PY as the antioxidant were investigated under different storage conditions such as, (i)

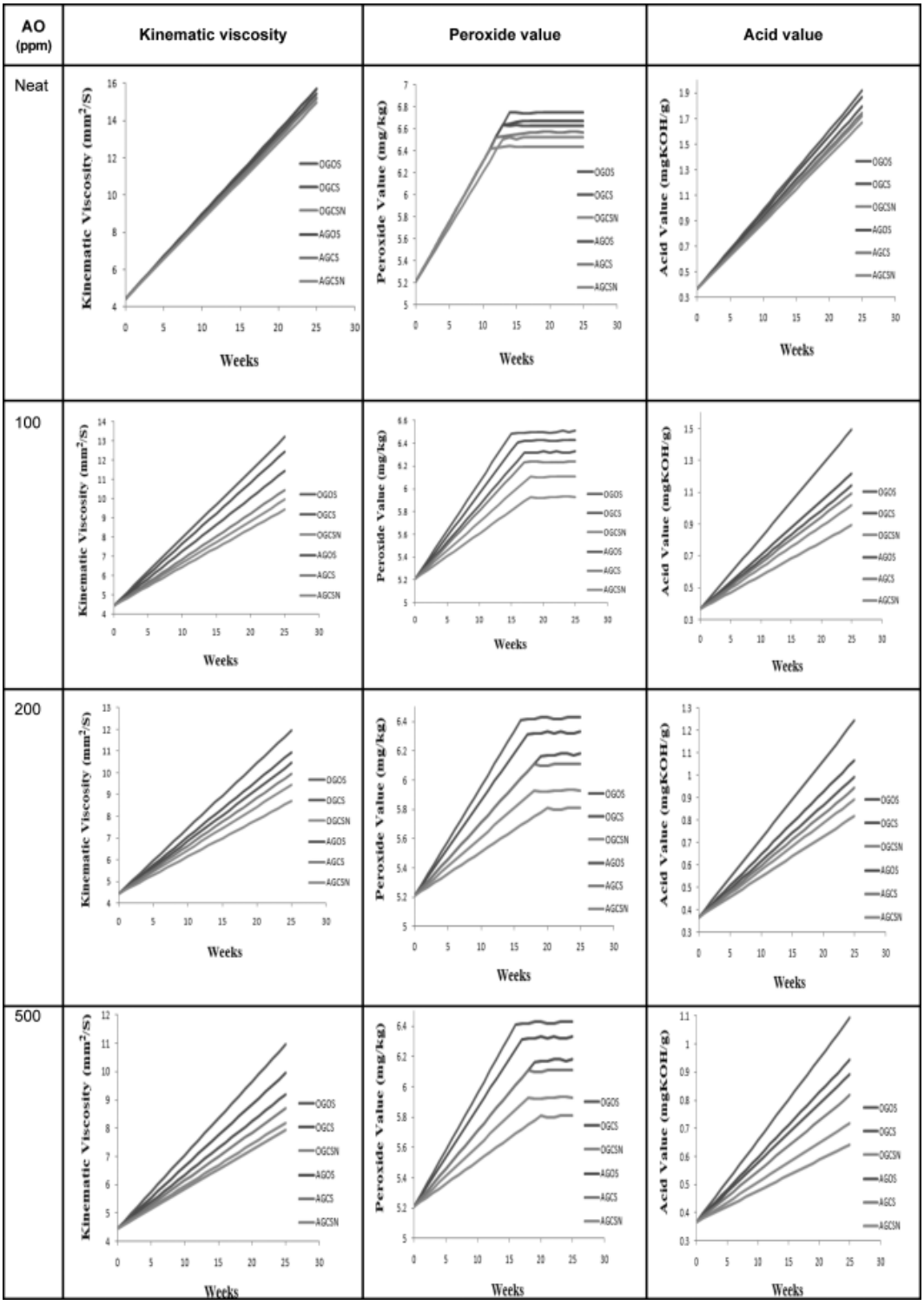

FIGURE 10.12 Storage stability of *Jatropha* biodiesel with PY as antioxidant carried out for 25 weeks.

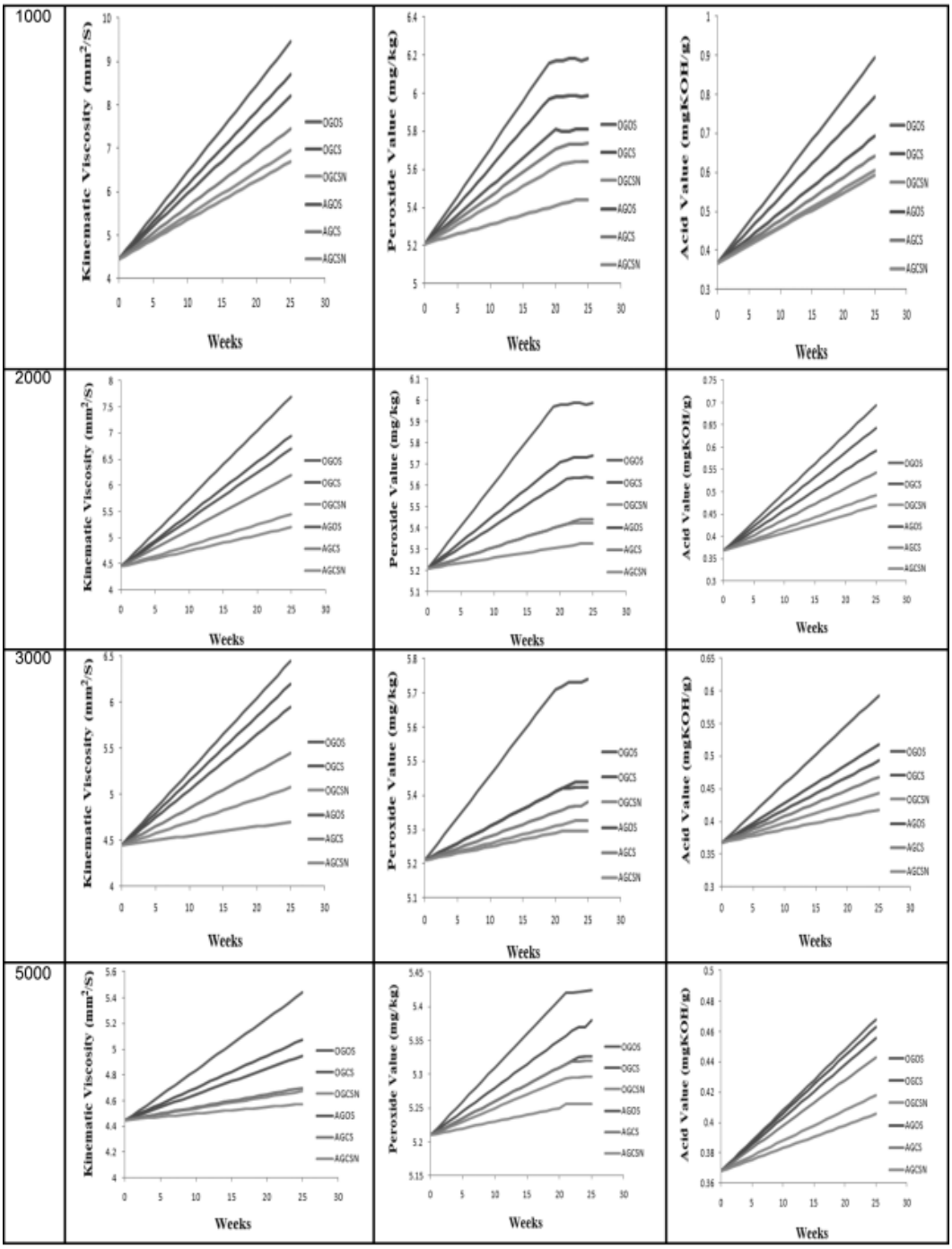

FIGURE 10.12 (*Continued*)

OGOS, (ii) OGCS, (iii) OGCSN, (iv) AGOS, (v) AGCS, and (vi) AGCSN. Storage in amber glass bottle with nitrogen atmosphere was found to be the best storage condition exhibiting minimum oxidation.

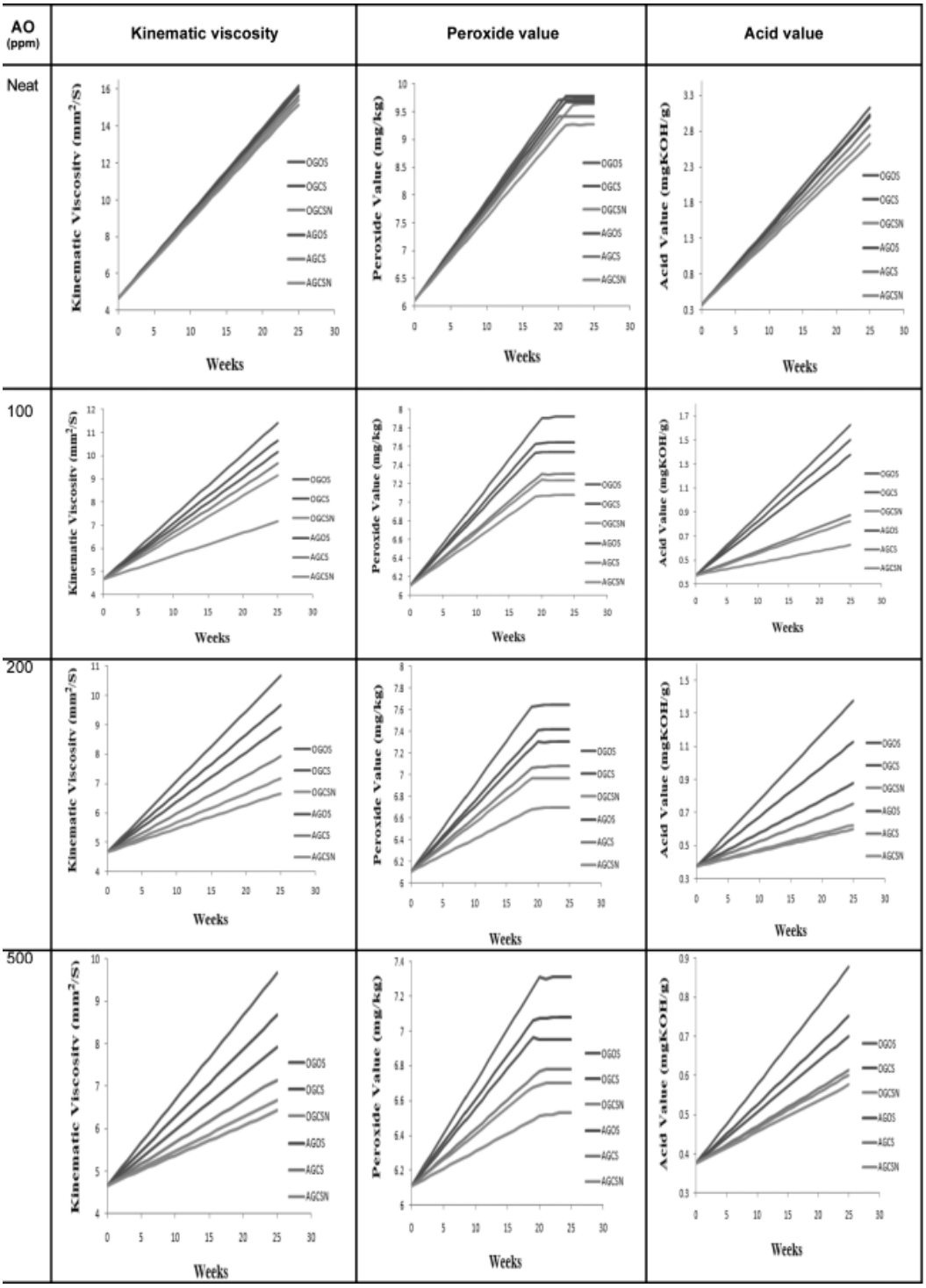

FIGURE 10.13 Storage stability of *Pongamia* biodiesel with PY as antioxidant carried out for 25 weeks.

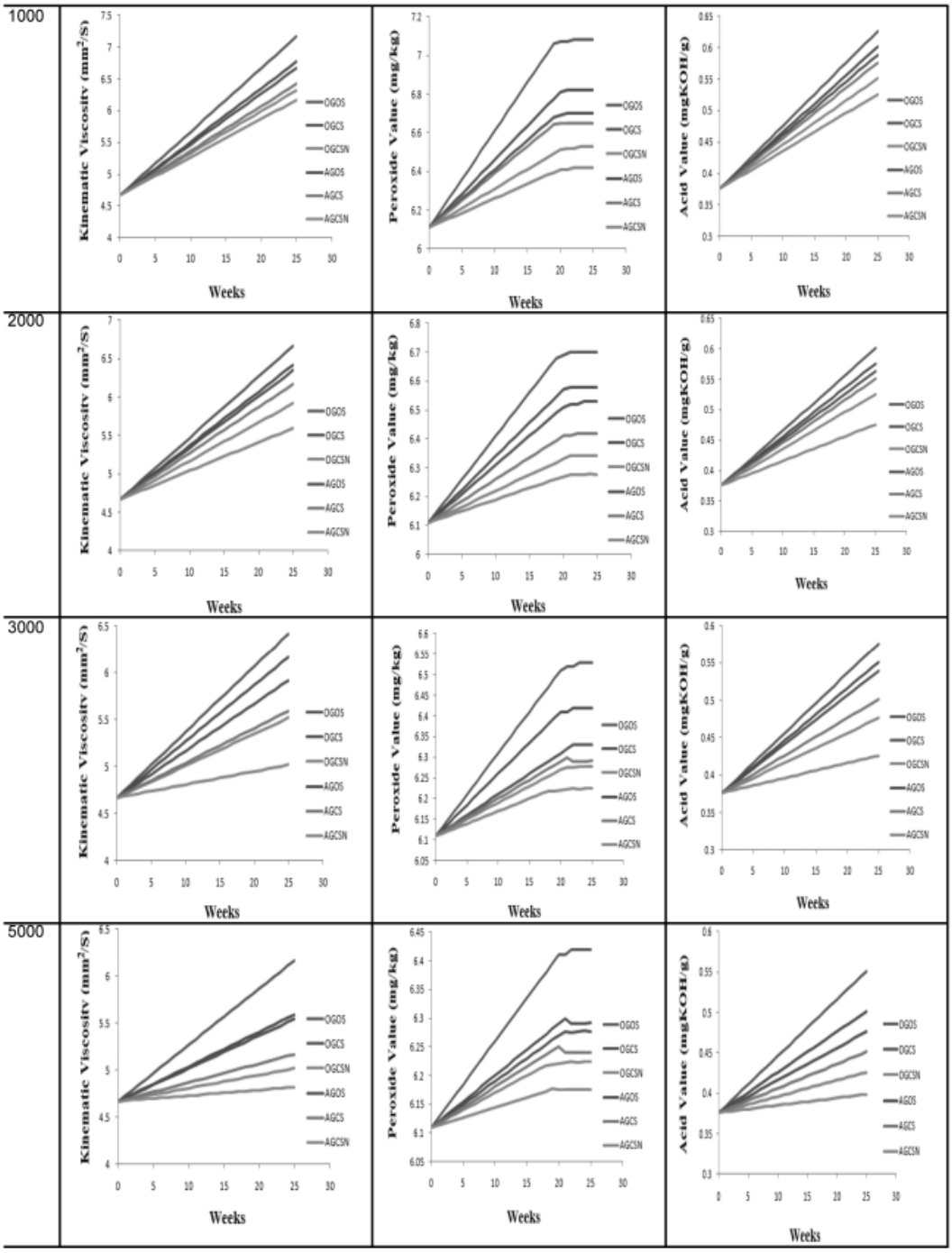

FIGURE 10.13 (*Continued*)

Figures 10.12 and 10.13 reveals that JBD with 5000 ppm PY, under nitrogen atmosphere stored in a amber glass bottle, exhibited a KV of 4.57 mm^2/s, PV of 5.23 mg/kg and AV of 0.38 mg KOH/g. The storage studies reveal that PBD with 5000 ppm PY shows KV of 4.75 mm^2/s, PV

of 5.23 mg/kg and AV of 0.38 mg KOH/g. The storage stability increased when the concentration of antioxidants was increased.

10.3.2 OXIDATIVE STABILITY STUDIES OF PONGAMIA *AND* JATROPHA *BIODIESEL USING COMMERCIALLY AVAILABLE ANTIOXIDANTS*

Rancimat method, the most commonly employed method in the vegetable oil sector, was adopted for the determination of oxidation stability. A high content of unsaturated fatty acids, which is very sensitive to oxidative degradation, leads to decreased induction times. Thus, even the conditions of fuel storage directly affect the quality of product. Several studies showed that the quality of biodiesel over a longer period of storage strongly depends on the tank material as well as on contact to air and light. Increase in viscosity and acid values leads to decrease in induction periods [11, 16]. The oxidative stability of biodiesel was studied by the Rancimat method as per EN14112 methodology using commercially available antioxidants.

All the other antioxidants like BHA, BHT, GA, and TBHQ were also used in the studies with concentrations ranging from 100 ppm to 5000 ppm under various atmospheric conditions. The different storage conditions are ordinary glass bottle with open space, ordinary glass bottle with closed space, ordinary glass bottle with nitrogen atmosphere, amber colored bottle with open space, amber colored bottle with closed space and amber colored bottle with closed space containing nitrogen atmosphere.

When investigating phenolic antioxidants, it was found that their antioxidative capabilities bear a relationship to the number of phenol groups occupying 1, 2 or 1, 4 positions in an aromatic ring, as well as to the volume and electronic characteristics of the ring substituent present. Generally, the active hydroxyl group can provide protons that inhibit the formation of free radicals or interrupt the propagation of free radical and thus delay the rate of oxidation. The effectiveness of PY, TBHQ, GA, can be explained based on their molecular structure (Fig. 10.14). These additives possess two OH groups attached to the aromatic ring, while both BHT and BHA possess one OH group attached to the aromatic ring. Thus, based on their electro-negativities, TBHQ and PY offer more sites for the formation

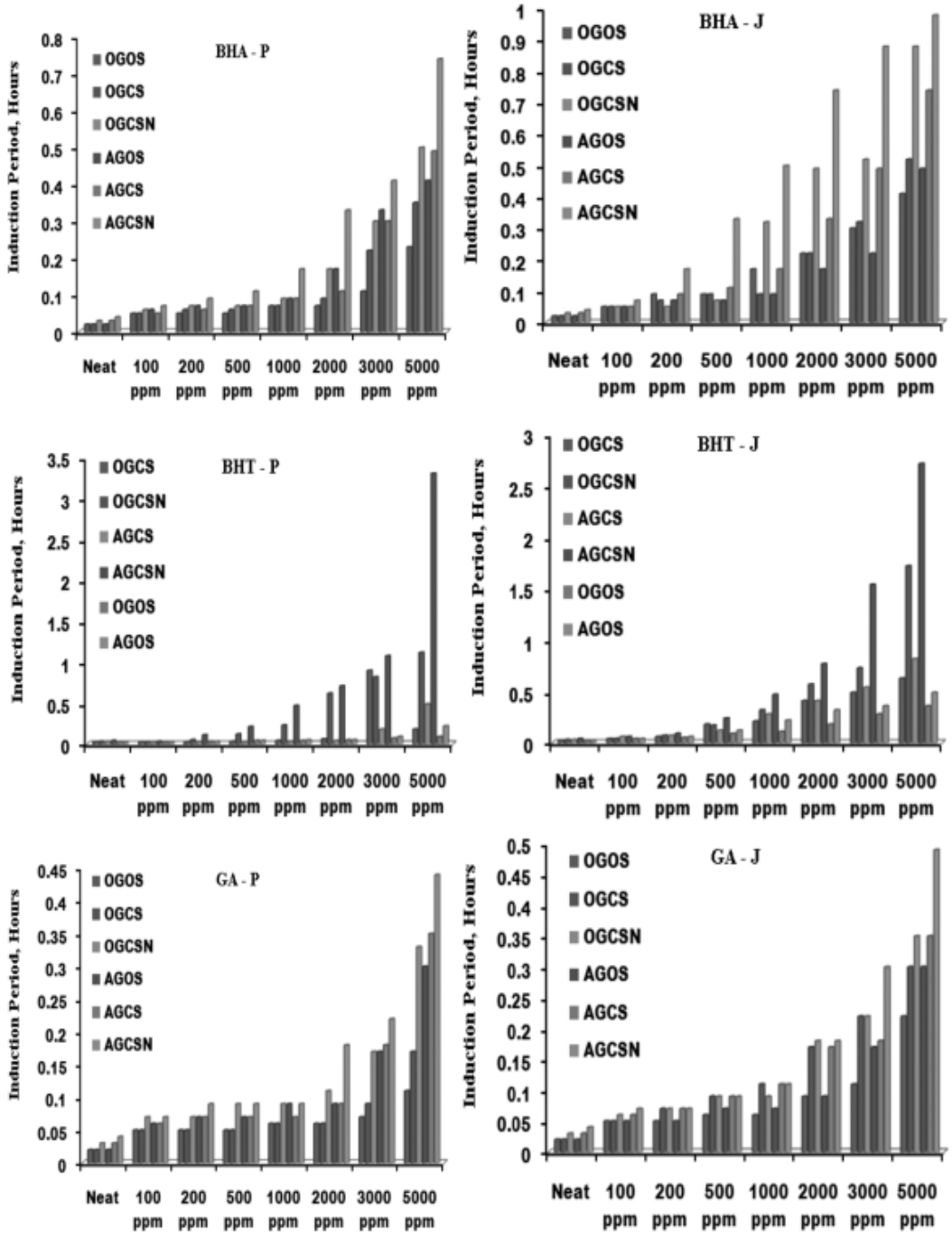

FIGURE 10.14 Oxidative stability results on *Pongamia* and *Jatropha* at different atmospheric conditions and different commercially available antioxidants.

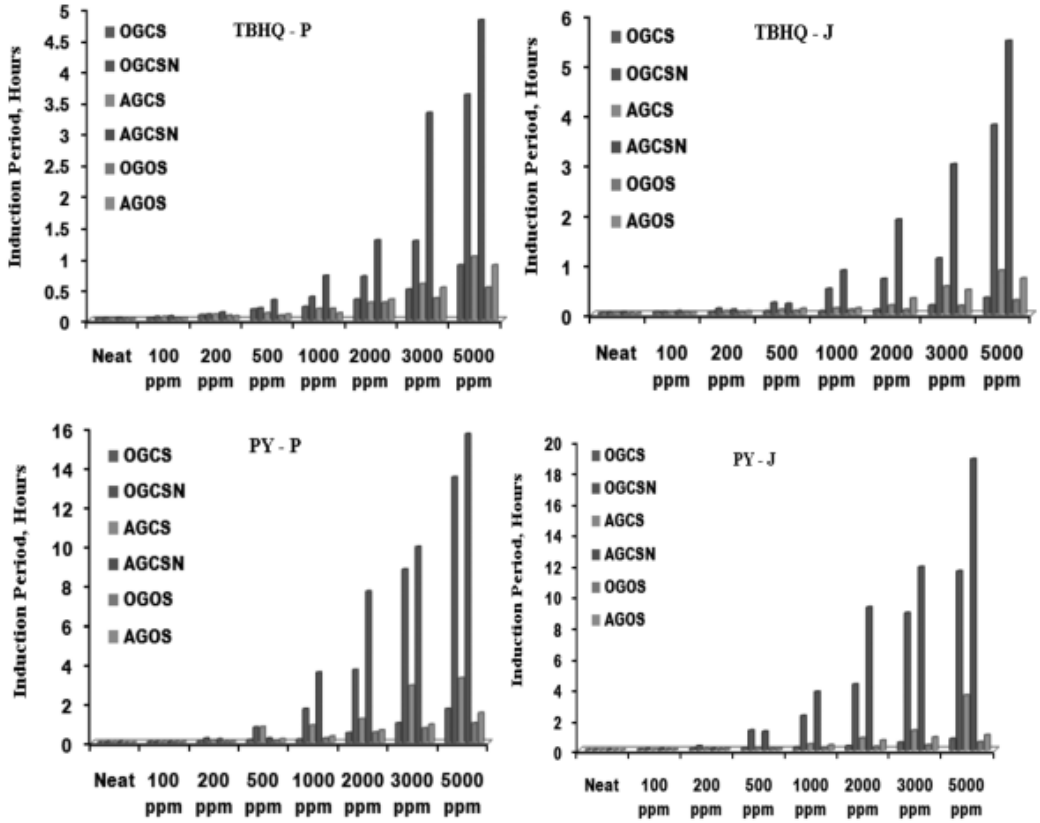

FIGURE 10.14 (*Continued*)

of a complex between free radical and antioxidant radical for the stabilization of the ester chain. Another contributing factor for the poor antioxidant performance of both BHT and BHA is their relatively low volatility, which under the operating conditions of the Rancimat method will lead to loss of additives during the early part of the test [18].

Figure 10.15 shows that the pyrogallal was found to be the best antioxidant among those commercially available, with a induction period of 3.51 h at a concentration of 1000 ppm, 15.65 h at a concentration of 5000 ppm, and 19.21 hr at concentration of 5000 ppm for both *Pongamia* and *Jatropha* biodiesel.

10.4 CONCLUSION

Biodiesel samples stored in amber glass bottles with closed space containing nitrogen gave the best results as compared to the other five conditions

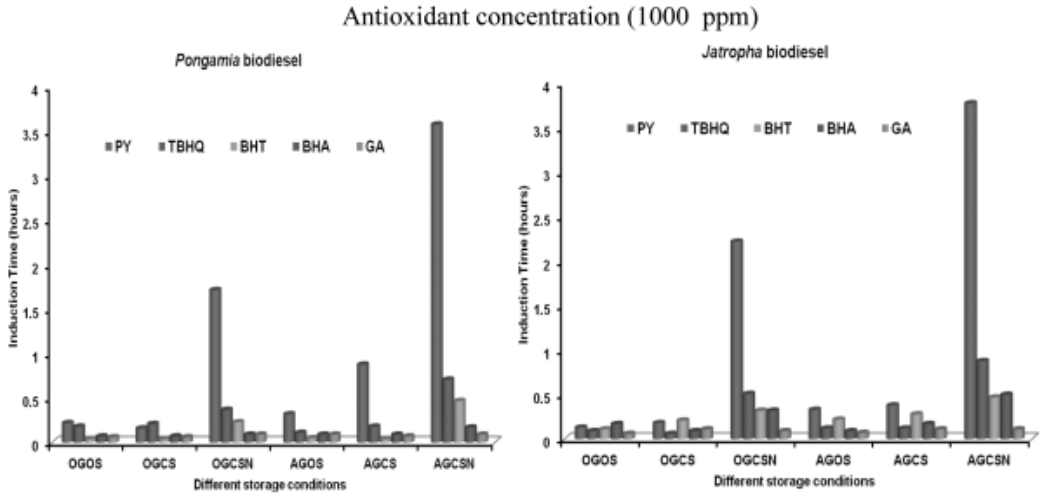

FIGURE 10.15 Oxidative stability studies on PBD and JBD at 1000 ppm commercially available antioxidants.

tested. Pyrogallol was found to be the best commercial antioxidant for both *Pongamia* and *Jatropha* biodiesels as it increased the induction time from 0.05 h to 4 hr, at 1000 ppm. Kinematic viscosity and acid values are good indicators of storage stability of biodiesels. BHT, TBHQ, PY, GA, and BHA, at concentrations of 1000 ppm, improved the storage stability of biodiesel.

KEYWORDS

- **Antioxidant**
- **Biodiesel**
- **Oxidation stability**
- **Pongamia oil**
- **Storage stability**

REFERENCES

1. Oyaizu. (2008). In vitro antioxidants estimation. *Food Res. Int. 41*, 1–15.
2. Dunn, R. O. (2005). Oxidative Stability of Soybean Oil Fatty Acid Methyl Esters by Oil Stability Index (OSI) *J. Am. Oil Chem. Soc. 82*, 381–387.

3. Lacoste, F., Lagardere, L. (2003). Quality parameters evolution during biodiesel oxidation using Rancimat test. *Eur. J. Lipid Sci. Technol. 105,* 49–55.
4. Schober, S., Mittelbach, M. (2004). The impact of antioxidants on biodiesel oxidation stability. *Eur. J. Lipid Sci. Technol. 106,* 382–389.
5. Mittelbach, M., Schober, S. (2003). Storage stability of biodiesel. *J. Am. Oil Chem. Soc. 80,* 817–823.
6. Schober, S., Mittelbach, M. (2004). The impact of antioxidants on biodiesel oxidation stability. *Eur. J. Lipid Sci. Technol. 106,* 382–389.
7. Dunn, O. (2005). Effect of antioxidants on the oxidative stability of methyl soyate (biodiesel) *Fuel Process. Technol. 86,* 1071–1085.
8. Ryu, J. H., Kim, T. J., Lee, T. Y., Lee, I. B. (2010). A study on modeling and simulation of capacitive deionization process for wastewater treatment. J. Taiwan Instit of Chem. Engg. *41 (4),* 506–511.
9. Monyem, A., Canakci, M., Gerpen, Jv. (2000). Investigation of biodiesel thermal stability under simulated in-use conditions. Appl. Eng. Agric. *16,* 373−8.
10. Bouaid, A., Martinez, M., Aracil, (2009). Production of biodiesel from bioethanol and Brassica carinata oil: oxidation stability study. J. *Biores. Technol. 100,* 2234–39.
11. McCormick, R. L., Westbrook, S. R. (2010). Storage Stability of Biodiesel and Biodiesel Blends. *Energy Fuels 24,* 690–98.
12. Evans, R. ABTS free radical scavenging modified method. 1997.
13. Cui, Y. (2005). Antioxidant effect of Inonotus obliquus *J. Ethno pharm*. *96,* 79–85.
14. Selvakumar, K., Madhan, R., Srinivasan, G., Baskar, V. (2011). Antioxidant Assays in Pharmacological Research. *As. J. Pharm. Tech.* Vol. 1: Issue 4, 99–103.
15. Mittelbach, M., Gangl, S. (2001). Long storage stability of biodiesel made from rapeseed and used frying oil. *J. Am. Oil Chem. Soc. 78,* 573–77.
16. Bondioli, P., Gasparoli, A., Lanzani, A., Fedeli, E., Veronese, S., Sala, M. J. (1995). Storage stability of biodiesel. *Am. Oil Chem. Soc. 72,* 699–02.
17. Simkovsky, N. M., Ecker, A. (1999).Effect of Antioxidants on the. Oxidative Stability of Rapeseed Oil Methyl Esters. *Erdöl Erdgas Kohle 115*, 317–318.
18. Dunn, R. O. (2002). Effect of oxidation under accelerated conditions on fuel properties of methyl soyate (biodiesel). *J. Am. Oil Chem. Soc. 79,* 915–920.
19. Canakci, M., Monyem, A., Gerpen, J. V. (1999). Accelerated oxidation process in biodiesel. *Trans. ASAE 42,* 1565–1572.
20. Das, L. M., Bora, D. K., Pradhan, S., Naik, M. K., Naik, S. N. (2009). Long-term storage stability of biodiesel produced from Karanja oil. *Fuel 88,* 2315–2318.
21. Karavalakis, G., Hilari, D., Givalou, L., Karonis, D., Stournas, S. (2011). Storage stability and aging effect of biodiesel blends treated with different antioxidants. *Energy 36,* 369−374.
22. Knothe, G. (2006). Analysis of oxidized biodiesel by ^{1}H-NMR and effect of contact area with air. *Eur. J. Lipid Sci. Technol*. *108,* 493−500.

CHAPTER 11

EFFECT OF FUNGAL BIOTIC STRESS ON PHYSIC NUT (*JATROPHA CURCAS* L.)

SEWETA SRIVASTAVA,* and ASHA SINHA

Department of Mycology and Plant Pathology,
Institute of Agricultural Sciences, Banaras Hindu University, Varanasi – 221 005, U.P., India; E-mail: shalu.bhu2008@gmail.com

CONTENTS

11.1 Introduction 278
11.2 Major Effects of Seed Mycoflora 281
11.2.1 Effect of Storage on Moisture Content and Percent Germination of Jatropha curcas Seeds 281
11.2.2 Effect of Seed Mycoflora on Biochemical Properties of Jatropha curcas Seeds 283
11.2.3 Effect of Seed Mycoflora on the Oil Quality and Quantity 285
11.2.4 Effect of Fungi on Physicochemical Properties of Jatropha curcas Oil 286
11.3 Conclusion 289
11.4 Future Prospects 289
Keywords 290
References 290

ABSTRACT

Jatropha curcas L. is a small tree that grows originally in areas near the equator. The oil plant *Jatropha curcas* L., a multipurpose drought resistant, perennial plant belonging to Euphorbiaceae family is gaining a lot of importance for the production of bio-diesel. Growth in the automotive industry, along with increases in population and gains in worldwide standards of living, has resulted in greater demand for energy sources such as biodiesel fuel. Seeds are regarded as highly effective means for transporting plant pathogens over long distances. Seed deterioration is defined as summation of all physical, physiological, biochemical changes occurring in a seed, which ultimately lead to its death. *Jatropha* seeds are constantly subjected to deterioration, which implies an irreversible degenerative change in the quality of seeds after it has reached its maximum quality of seeds after it has reached its maximum quality level. The fungi associated with seeds at the harvest stage and under storage bring about several undesirable changes and degradation of seed constituents, thus making the seed unfit for oil extraction, export purpose, consumption or sowing. These storage mycoflora affect the quality of seeds and as well as the diesel extracted by affecting their biochemical and physicochemical properties which is very essential. Biodiesel, an environmental friendly diesel fuel similar to petro-diesel in combustion properties, has received considerable attention in the recent past worldwide. There is therefore, need to explore alternative nonedible oil for use in production of biodiesel.

11.1 INTRODUCTION

Energy is the chief mover of economic growth, and plays a vital role in sustaining the modern economy and society. Utilization of waste is also way to help the nation by environmentally as well as economically. Biodiesel is the name for a variety of ester-based fuels (fatty ester) generally defined as monoalkyl ester made from renewable biological resources such as vegetable oils, recycled waste vegetable oil and animal fats. This renewable source is as efficient as petroleum diesel in powering unmodi-

fied diesel engine. Today's diesel engines require a clean burning, stable fuel operating under a variety of conditions. Using biodiesel not only helps maintaining our environment; it also helps in keeping the people around us healthy [1].

Biofuels are considered in part, a solution to such issues as sustainable development, energy security and a reduction of greenhouse gas emissions. Biodiesel, an environmental friendly diesel fuel similar to petrodiesel in combustion properties, has received considerable attention in the recent past worldwide. Our future economic growth considerably depends on the long-term accessibility of energy from the sources that are easily available, safe and affordable [2]. New sources of energy like biofuels may play a significant role in meeting the energy demands [3]. Biomass sources have turned out to be more effective in the recent days because of the insufficiency of conventional fossil fuels, their price hike and increased emissions of pollutants generated during combustion. The petroleum-based fuel reserves are concentrated in only some parts of the world and these resources are depleting day-by-day [4].

Biofuels can replace fossil fuels, such as petrol or diesel, either totally or partially in a blend. The history of biofuels goes back to the first part of last century. The inventor of the diesel engine, Rudolf Diesel, already stated in 1912 that "the diesel engine can be fed with vegetable oils and would help considerably in the development of agriculture of the countries which use it" and that "the use of vegetable oils for engine fuels may seem insignificant today; but, such oils may become in course of time as important as petroleum and the coal tar products of the present time" [5].

The seeds of physic nut are a good source of oil, which can be used as a diesel substitute [6]. Depending on the variety, the decorticated seeds contain 40–60% of oil [7–12], which is used for many purposes such as lighting, as a lubricant, for making soap [13] and most importantly as biodiesel. The seeds can be burned directly, without extracting the oil, to provide an alternative to kerosene lamps [14]. Seed yield usually ranges from 1–5 t ha^{-1} [15–17]. About 30% of the seed weight is pure plant oil [15]. Mycorrhiza (a symbiotic association between a fungus and the roots of a plant) can increase the biomass and seed production with 30% after seven months [18]. If a holistic approach is taken to use *Jatropha* fruit, it will give three times the energy of bio-diesel alone [19].

Seeds are regarded as highly effective means for transporting plant pathogens over long distances [20]. Seed-borne mycoflora have been found to effect the growth and productivity of crop plants. A seed-borne pathogen present externally or internally or associated with the seed as contaminant, may cause abortion, seed rot, seed necrosis, reduction or elimination of germination capacity as well as seedling damage. This results in development of diseases at later stages of plant growth by systemic or local infection [21, 22].

Seed deterioration is defined by Delouche [23] as summation of all physical, physiological, biochemical changes occurring in a seed, which ultimately lead to its death. He also characterized seed deterioration as inexorable, irreversible, inevitable and minimal at the time of physiological maturity and variable among the seed kinds, varieties and seed lots of same variety and among individual seeds. Many researchers have opinion that seed deterioration is a progressive deleterious process, which has far reaching consequences [24, 25].

Jatropha seeds are constantly subjected to deterioration, which implies an irreversible degenerative change in the quality of seeds after it has reached its maximum quality of seeds after it has reached its maximum quality level [26, 27]. The fungi associated with seeds at the harvest stage and under storage bring about several undesirable changes and degradation of seed constituents, thus making the seed unfit for oil extraction, export purpose, consumption or sowing. Chelkowski [28] reported that in many cases, fungi infecting seeds are seed-borne pathogens. They play an important role in the transmission of numerous pathogenic fungal species to seedlings as well as to the soil.

Storage fungi are those that grow on stored products. Most of them are able to grow without free water, and on media with a high osmotic pressure. Most of the storage floras are the species of *Aspergillus* and *Penicillium,* which are active at relative humidities ranging from 70 to 90%. It has been established that storage fungi usually do not invade before harvest [29, 30] but they may be found on the seed in very low percentages often below 1 percent, nevertheless providing for the presence of inoculum of storage fungi [31–33]. They may be present not only as contamination but as dormant mycelium within the tissues of pericarp or seed coat [34].

Improper storage makes the oilseeds vulnerable to storage fungi, which deteriorates the stored oilseeds both qualitatively and quantitatively. They bring about the variety of biochemical changes in suitable conditions. It was found that *Alternaria dianthicola, Curvularia lunata, Fusarium oxysporum, Fusarium equiseti, Macrophomina phaseolina* and *Rhizopus stolonifer* causes decrease in reducing sugars of oilseeds. *Alternaria dianthicola, Curvularia pellescens, Macrophomina phaseolina, Penicillium digitatum* and *Penicillium chrysogenum* hampered the fat content of oilseeds. *Curvularia lunata, Curvularia pellescens, Fusarium oxysporum, Macrophomina phaseolina, Rhizopus stolonifer* and *Penicillium digitatum* increased the fiber content in oilseeds [35]. Therefore, keeping in the view of above facts, the present investigation aims to achieve the following objective, that is, Effect of seed-borne fungi on the deterioration of the seeds and extracted oil quality.

11.2 MAJOR EFFECTS OF SEED MYCOFLORA

11.2.1 EFFECT OF STORAGE ON MOISTURE CONTENT AND PERCENT GERMINATION OF JATROPHA CURCAS *SEEDS*

Parreno-de Guzman and Aquino were reported [36] that the storage behavior of *Jatropha curcas* seed is one of the main constraints. The slight moisture content increase against long-term storage period might be due to the hydrolysis or breakdown of lipid, carbohydrate and proteins and release of water molecules. The release of free fatty acids from lipid degradation by fungi is well known and hydrolysis of starch and proteins for utilization by the microorganisms also, has been studied from the earlier findings [29]. Storage under high relative humidity and temperature (85% and 30 °C) was observed to promote *Aspergillus* spp. growth that resulted in the loss of germination in seed within six months [37].

Seed storage behavior of Euphorbiaceae is generally orthodox [38]. Orthodox seed storage behavior means “Mature whole seeds not only survive considerable desiccation (to at least 5% moisture content) but their longevity in air-dry storage is increased in a predictable way by reduction inseed storage moisture content and temperature (e.g., to those values employed in long-term seed stores)” [39]. Physic nut also has orthodox

seeds. Two- or six-month-old seeds received for the provenance trials described above, were stored in unsealed plastic bags at ambient temperatures (approximately 20 °C) for 5 months and germinated on average by 62% (ranging from 19 to 79%) after having been seeded in soil. When stored for 7 years in plastic bags (not sealed) at a temperature of approximately16 °C, the seeds still showed an average germinating capacity of 47% (ranging from 0 to 82%) when tested with the "between paper" method [40, 41]. When the seeds were analyzed for their chemical composition after 3 years of storage, they had moisture content of 6.2% (average of all provenances).

The fungi *Aspergillus flavus, Aspergillus niger, Pencillium* spp. *Fusarium* spp., and *Rhizopus* spp. were commonly found fungi causing considerable reduction in viability of stored seeds [42]. The safe moisture content for storing physic nut seeds was 7–9% [43]. The moisture contents increased after one month of storage, and became relatively constant up to 6 months of storage. The range of moisture contents (7.9–8.4%) was safe for storage of physic nut seeds. Lipid contents, viabilities and vigors decreased with the increase of storage duration, while free fatty acids and lipase activities increased. Under uncontrolled conditions, physic nut seeds packed in plastic material can be stored up to one month for seeds to be planted, while it can be stored up to five months for producing oil [26].

Seed germination percentage declined slowly with the longer storage periods when dry seeds stored under room temperature. The results indicated the slow deterioration of seeds with time [44]. However, Pasabutr and Suthiponpaiboon found that [45] physic nut seed stored under room temperature for 8 months gave germination up to 80% but decreased to 42% after 9 months storage. Therefore, it may be of high advantage to store seeds in a low temperature as low as 20 °C where high respiration rate could be reduced, thus it may be possible to prevent the rapid deterioration of seeds since oil seeds obviously loss its vigor more rapidly with time when store in a high environmental temperature. The germination of 80–90% has been obtained for seeds collected during October to December. The seed had been dried in shade, and stored dry indoors. The seeds retained germinating ability for >2 years. *Jatropha* planting material is mainly raised through seedlings currently [46].

11.2.2 EFFECT OF SEED MYCOFLORA ON BIOCHEMICAL PROPERTIES OF JATROPHA CURCAS *SEEDS*

Fungi association brings certain biochemical changes in seeds during storage by decreasing reducing sugars and oil content [47].

11.2.2.1 Effect on Protein Contents

Gradual loss of protein content was found in the deteriorated seeds [48]. Significant decrease in protein, oil content and total sugars and increase in free fatty acids and reducing sugars in deteriorated seeds [49] and carbohydrates increased with decrease in protein content in deteriorated seeds [50]. There was also reported that 1.5- to 3-fold decrease in protein level was observed in moderately infected and highly infected seeds compared to healthy seeds [51].

11.2.2.2 Effect on Amino Acid Contents

Concentrations of the isolated free amino acid fractions significantly decreased with seed size except for phenylalanine, which significantly increased, with seed size [52]. Significant changes also occurred in the free amino acid fractions across storage periods up to nine months in duration. These results are the first to document a change in amino acids during the storage of peanuts. Deswal and Sheoran reported that [53] permeability of membrane increases with increase in storage period and leads to loss of electrolytes, sugars, amino acids and phenols. Further decline in seeds and seedling vigor parameters was also related to decrease in both quantity and quality of food reserves like sugars, amino acids, oil content, protein, etc. in different crops [54, 55] but the total free amino acids increased with aging of seeds [56].

11.2.2.3 Effect on Carbohydrate Contents

Carbohydrates increase the severity of the infection and that they may serve as easily metabolized carbon substrates for the pathogen [57–59].

The gradual loss of carbohydrate content of seeds due to *A. flavus* and *A. niger* during storage [48]. The sharp decline in the levels of soluble carbohydrates during the desiccation of seeds [60]. Sucrose and raffinose level declined in stored seeds of maize although the monosacharides, glucose fructose and galactose diminished faster [61]. There was 1.5 to 3 fold decreases in protein, carbohydrate and phenol levels and 2–3 fold increase in reducing sugar were observed in moderately infected and highly infected seeds compared to healthy seeds [51] therefore indicate the degradation of protein and carbohydrates and accumulation of reducing sugar due to degradation of carbohydrates, by the pathogen.

11.2.2.4 Effect on Phenol Contents

The antimicrobial property of phenolic compounds and especially those of the flavonol group is well documented [62, 63]. The first stage of defense mechanism involves a rapid accumulation of phenols at the infection site, which restricts or slows the growth of the pathogens [64]. The changes in the level of total phenolic compounds in chickpea as influence by *Aspergillus flavus, A. niger, Fusarium maniliforme* and *Pencillium oxalicum* infection [65]. The four days after treatment, infected pods always contained the highest amount of phenolics followed by the wounded, and finally by intact pod [66]. The results showed that the increase in phenolic content could be correlated to the aging, the wounding and the infection of the pods. This could account for a higher synthesis of disease-related molecules like phenols and hydroxyproline-rich glycoproteins, which generally accumulate in fungus infected plants [67]. The increase amount of phenol might be responsible for resistance response in plant [68].

11.2.2.5 Effect on Lipid Contents

Storage duration gave very significant differences on lipid contents of physic nut seeds. The lipid contents decreased with the increase of storage duration [26]. The fatty acid contents of physic nut seeds were dominated by unsaturated fatty acids, that is, oleic acid followed by linoleic acid will cause hydrolyzes process [27]. This process caused the decrease of lipid

and increased free fatty acid contents, either in the seeds or in the oil itself. Sukesh and Chandrashekar reported that [56] lipid peroxidation (refers to the oxidative degradation of lipids) is considered to be the primary cause for seed deterioration. The occurrence of fungi will accelerate the degradation of lipid during storage. The decrease of lipid content was probably due to the activity of lipolytic fungi, which grew dominantly and can live for long period. This condition caused the production of free fatty acid and rancidity. Lipid of seeds can be degraded by lipase into free fatty acid and glycerol, especially if the moisture content of seeds was high. Free fatty acid was an index of deteriorated seeds containing lipid during storage. *Aspergillus, Cladosporium* and *Penicillium* were capable to degrade lipid compound and have high lipolytic activity [69]. These fungal species were often isolated from seeds containing high lipid. There has been the possibility of lipid breakdown and release of free fatty acids (FFA) may occur during the growth of fungi in stored Jatropha seeds and other oil seeds [70, 71].

11.2.3 EFFECT OF SEED MYCOFLORA ON THE OIL QUALITY AND QUANTITY

Freshly harvested seeds are more likely to be free from fungal infection and will express maximum seed oil [37]. Similar results were observed by Gupta and Rao [72] that on keeping the *Jatropha* seeds for long time, oil content of the seeds declines. Cost of bio-diesel is sensitive to storage time of seeds as well as raw oil. This also supports to Oladimeji and Kolapo who observed decrease in oil content of sunflower after a period of storage. The preheating the seeds for 4 min by microwave before the extraction improved the oil recovery up to 2% [73]. Ultrasonication and microwave did not affect the oil quality in terms of free fatty acid content [74].

Basha and Pancholy reported a decrease in oil, iodine value, soluble carbohydrates and protein contents in seed infested with *Aspergillus* spp. [75]. Reduction in seed oil content at the end of the storage period may be attributed to the effect of the storage conditions, the seed moisture content and the fungi associated with the seed [37, 76]. Decrease in oil content was

positively correlated with increase in lipase activity on account of fungal infection [77–79].

11.2.4 EFFECT OF FUNGI ON PHYSICOCHEMICAL PROPERTIES OF JATROPHA CURCAS *OIL*

11.2.4.1 Effect on Acid Value

Acid value increases during storage [80]. Higher acid value and free fatty acids (%) were reported in *J. curcas* [81]. Free fatty acid was an index of deteriorated seeds containing lipid during storage [69]. Free fatty acid contents increased with the increase of storage duration [27]. The free fatty acid content of the biodiesel should be less than 1 percent. It was observed that lesser the free fatty acid in oil, better is the bio diesel recovery. Higher free fatty acid oil can also be used but the bio diesel recovery will depend upon oil type and the amount of NaOH used [82]. FFA content of raw *Jatropha* oil increases with time. Higher FFA results in loss of more oil as precipitate while neutralizing. It is therefore recommended that raw oil should not be stored for a long time [72]. Drying at 80 °C gave the highest oil yield of 47.06% but also the highest acid value. The high acid value indicated high free fatty acid, which caused high abrasion on metal. Drying at 40 °C gave less oil yield at 36.83% but the lowest acid value, which indicated a better usage quality [83]. According to Sauer, the decrease of seed quality was followed by the increase of free fatty acid value. The level of free fatty acid value gave an indication concerning the decrease of seed quality. The level of free fatty acid depends on fungal species infecting the seeds [84].

11.2.4.2 Effect on Iodine Value

The iodine value should be less than 115 as per biodiesel standards [82]. Seed sources with higher iodine value may not be suitable for the production of bio-diesel [85]. *Jatropha* fatty acid methyl ester, with higher cetane number is preferred for use as biodiesel. The specifications of bio-diesel are such that it can be mixed with any diesel. Cetane number of the bio-diesel

is in the range of 48–60 [82]. The acid value, peroxide value and viscosity, increased while the iodine value decreased with increasing storage time of the *brassica carinata* biodiesel [86]. Iodine values decreased as extraction temperature increased [87]. Gulla and Waghray reported that iodine value decreased gradually during storage in the oil blends studied [88]. The iodine value of the biodiesel decreased during storage period. It indicates that the oxidation of the biodiesel which results in reduction in double bonds [89]. The iodine value of *Jatropha* oil is higher than other oil reported. High iodine value of *Jatropha* is caused by high content of unsaturation fatty acid such as oleic acid and linoleic acid. The high iodine value and oxidative stability shows that the seed oil upholds the good qualities of semidrying oil purposes [75]. A decrease in oil, iodine value, soluble carbohydrates and protein contents in seed infested with *Aspergillus* spp. [75].

11.2.4.3 Effect on Saponification Value

Saponification value is an index of the average size of fatty acid present, which depends upon the molecular weight and percent concentration of fatty acids components in the oil. Saponification value will be higher if the oil contains more of saturated fatty acids (C14:0, C16:0, C18:0) as it determines the length of carbon chain and increase cloud point, Cetane number and improve stability of bio-diesel [82]. Similar results were earlier documented in *J. curcas* by several workers [81, 90]. Oil infested from *Fusarium* spp. shows increased saponification value but decreased iodine value [91]. The acid value, iodine value and saponification value increase during storage. The reasons for these increases may be attributed to the absorption of moisture from the surroundings, oxidation, heat, light and metal. When these occur there is the likelihood of microorganisms affecting the oils, which in turn may lead to spoilage. The low free fatty acid values suggest that the samples are good edible oils. High acid values are usually indicative of damage or high moisture, which enables the enzyme lipase to convert the triglycerides to free fatty acids. The higher levels obtained there after indicated deterioration. The iodine value is often the most useful figure for identifying oil or placing it into a particular group. It is an index of unsaturation which shows the

molecular weight for their fatty acids in the two investigated oils to be mainly nondrying [92].

11.2.4.4 Effect on Cetane Value

Cetane number determines the ignition performance of transport fuel [93]. Conventional diesel must have a Cetane number of at least 40. This accords biodiesel better cold start properties, minimized formation of white smoke (emissions), less engine noise hence engine durability and reduced fuel consumption [94]. Cetane values of biodiesel are slightly higher than synthetic diesel, which is favorable for combustion [95]. The Cetane Number of the biodiesel was considerably increased and well within the ASTM specified limit, which indicates the better combustion quality of the fuel. The higher Cetane index of biodiesel compared to petrodiesel was indicated that it will be the high potential for engine performance [96].

11.2.4.5 Effect on Viscosity

The viscosity of the pure plant oil is more or less constant for a given kind of oil, but may increase with aging of the pure plant oil. The viscosity is dependent on the temperature of the oil. For pure plant oil from *Jatropha*, the viscosity at room temperature is much higher than for rapeseed [97]. *Jatropha* oil has higher viscosity than conventional diesel fuel and biodiesel. High viscosity leads to poorer atomization of the fuel spray and less accurate operation of the fuel injectors [96]. Similarly, Sundar Raj and Sahayaraj reported that the viscosity of *Jatropha* oil is higher than palm, coconut and sunflower oil [98]. High viscosity of the seed oil is not suitable if it is used directly as engine fuel, often results in operational problems, such as, carbon deposits, oil ring sticking, and thickening and gelling of lubricating oil as a result of contamination by the oils. Different methods such as preheating, blending, ultrasonically assisted methanol transesterification and supercritical methanol transesterification can reduce the viscosity and make them suitable for engine applications [99].

11.2.4.6 Effect on Refractive Index

The standard refractive index of *J. curcas* seed oil was 1.465 [99] and also reported the refractive index of the transesterified *Jatropha* oil was found to be 1.45 [100]. Fungal infested oil emitted moldy odor and the refractive index increased [91].

11.3 CONCLUSION

Deteriorated *Jatropha* seeds show decrement in their protein content, amino-acid content, carbohydrate content and lipid content. Phenol content of deteriorated *Jatropha* seeds were increased which might be responsible for resistance response against pathogen. These isolated seed mycoflora also affect the quality of *Jatropha* oil by effecting its physicochemical properties *viz.,* color, acid-value, iodine-value, saponification-value, cetane value, refractive index and viscosity. Oil content of *Jatropha curcas* L. was declined due to infestation of seed mycoflora and it is also the main cause of deterioration of seeds during storage.

Improper storage makes the oilseeds vulnerable to storage fungi, which deteriorate the stored oilseeds both qualitatively and quantitatively. They bring about the variety of biochemical changes in the suitable conditions. *Jatropha* seeds are constantly subjected to deterioration, which implies an irreversible degenerative change in the quality of seeds after it has reached its maximum quality level. The fungi associated with seeds at the harvest stage and under storage bring about several undesirable changes and degradation of seed constituents, thus making the seed unfit for oil extraction, export purpose, consumption or sowing. In many cases, fungi infecting seeds are seed-borne pathogens. They play an important role in the transmission of numerous pathogenic fungal species to seedlings as well as to the soil.

11.4 FUTURE PROSPECTS

Current global trends in energy supply and consumption are patently unsustainable: environmentally, economically and socially. That indicates a global need to secure the supply of reliable and affordable energy and to effect a rapid

transformation to a low-carbon efficient and environmentally benign system of energy supply. It is also clear that current energy fossil fuel consumption trend will have severe consequences on natural ecosystems and social communities. Switching to renewable energy will therefore reduce global warming and curb actual trends [101]. These are the reasons why a search for alternatives to fossil fuels, such as renewable energy from solar, wind, water, biomass and nuclear, has been provoked. Biofuels are considered in part; a solution to such issues in sustainable development, energy security and a reduction of green house gas emission. Biodiesel, an environmental friendly diesel fuel similar to petro-diesel in combustion properties, has received considerable attention in the recent past worldwide. There is therefore, need to explore alter nonedible oil for use in production of biodiesel.

KEYWORDS

- **Biodiesel**
- **Ester-based fuels**
- ***Jatropha curcas* L.**
- **Petro-diesel combustion properties**

REFERENCES

1. Muche, A., Sahu, O. (2014). *Jatropha curcas* Oil for the Production of Biodiesel. *Internat. J. Biosci. Bioinform. 1 (1),* 001–007.
2. Liaquat, A. M., Kalam, M. A., Masjuki, H. H., Jayed, M. H. (2010). Potential emission reduction in road transport sector using biofuels in developing countries. *Atmos. Environ*. *44,* 3869–3877.
3. Boey, P. L., Ganesan, S., Maniam, G. P., Khairuddean, M., Lim, S. L. (2012). A new catalyst system in transesterification of palm olein: Tolerance of water and free fatty acids. *Energy Convers. Manag*. *56,* 46–52.
4. Anitescu, G., Bruno, T. J. (2011). Fluid properties needed in supercritical transesterification of triglyceride feedstocks to biodiesel fuels for efficient and clean combustion—A review. J. Supercrit. *Fluids*, *63*,133–149.
5. Wood, J. (2008). 'An amazingly timely quote by Rudolph diesel.' http://dieselnews.wordpress.com/2008/05/15/an-amazingly-timely-quote-by-rudolph-diesel-the-inventor-of-the-diesel-engine/.
6. Kumar, A., Sharma, S. (2008). An evaluation of multipurpose oil seed crop for industrial uses (*Jatropha curcas* L.): a review. *Ind. Crops Prod*. *28,* 1–10.

7. Liberalino, A. A., Bambirra, E. A., Moraes-Santos, T., Vieira, E. C. (1988). *Jatropha curcas* L. seeds: chemical analysis and toxicity. *Arq. Biol. Technol*. *31,* 539–550.
8. Gandhi, V. M., Cherian, K. M., Mulky, M. J. (1995). Toxicological studies on ratanjyot oil. *Food Chem. Toxicol*. *33,* 39–42.
9. Sharma, G. D., Gupta, S. N., Khabiruddin, M. (1997). Cultivation of *J. curcas* as a future source of hydrocarbons and other industrial products. In Biofuels and industrial products from *Jatropha curcas*; Gubitz, G. M., Mittelbach, M., Trabi, M., Ed., pp. 19–21.
10. Wink, M., Koschmieder, C., Sauerwein, M., Sporer, F. (1997). Phorbol esters of *J. curcas* – biological activities and potential applications. In Biofuels and industrial products from *Jatropha curcas*; Gubitz, G. M., Mittelbach, M., Trabi, M., Ed., pp. 160–166.
11. Makkar, H. P. S., Becker, K., Sporer, F., Wink, M. (1997). Studies on nutritive potential and toxic constituents of different provenanaces of *Jatropha curcas*. *J. Agric. Food Chem*. *45*, 3152–3157.
12. Openshaw, K. (2000). A review of Jatropha curcas: an oil plant of unfulfilled promise. *Biom. Bioener*. *19,* 1–15.
13. Rivera-Lorca, J. A., Ku-Vera, J. C. (1997). Chemical composition of three different varieties of *J. curcas* from Mexico. In Biofuels and industrial products from *Jatropha curcas*; Gubitz, G. M., Mittelbach, M., Trabi, M., (Ed.), pp. 47–52.
14. Slavin, T. 2008. When oil grows on trees: India's new oil bonanza could revitalize its wastelands – or starve its poor. *Green Futures: The Sustainable Solutions Magazine*. http://www.forumforthefuture.org/greenfutures/articles/whenoilgrowsontrees.
15. Jongschaap, R., Corré, W., Bindraban, P., Brandenburg, W. (2007). 'Claims and facts on *Jatropha curcas* L.' Report 158, Plant Research International, Droevendaalsesteeg 1, PO Box 16, 6700AA Wageningen, The Netherlands.
16. Abou Kheira, A., Atta, N. (2008). 'Response of *Jatropha curcas* L. to water deficit: Yield, water uses efficiency and oilseed characteristics.' Biom. Bioener. 1–8.
17. Heller, J. Physic Nut. Jatropha curcas L. Promoting the Conservation and Use of Underused and Neglected Crops. Institute of Plant Genetics and Crop Plant Research, Gatersleben/International Plant Genetic Resources Institute, Rome, 1996.
18. Achten, W., Verchot, L., Franken, Y., Mathijs, E., Singh, V., Aerts, R., Muys, B. (2008). 'Jatropha bio-diesel production and use.' *Biom. Bioener*. *32,* 1063–1084.
19. Singh, R. N., Vyas, D. K., Srivastava, N. S. L., Narra, M. (2008). SPRERI experience on holistic approach to use all parts of Jatropha curcas fruit for energy. *Renew. Ener*. 33, 1868–1873.
20. Agarwal, V. K., Sinclair, J. B. (1996). *Principles of Pathology*. 2nd Edn., CRC Press, Inc., Boca Raton, Fl. pp: 539.
21. Bateman, G. L., Kwasna, H. (1999). Effects of number of winter wheat crops grown successively on fungal communities on wheat roots. *Appl. Soil Ecol*. *13,* 271–282.
22. Khanzada, K. A., Rajput, M. A., Shah, G. S., Lodhi, A. M., Mehboob, F. (2002). Effect of seed dressing fungicides for the control of seed borne mycoflora of Wheat. *Asian J. Pl. Sci*. *1 (4),* 441–444.
23. Delouche, J. C. (1973).Precepts of seed storage (Revised). *South Canada Proceedings*, Mississippi State University, pp. 97–122.

24. Ellis, R. H., Roberts, E. H. (1981). The quantification of aging and survival in orthodox seeds. *Seed Sci. Technol*. *9,* 373–409.
25. Ghosh, B., Adhikari, J., Banerjee, N. C. (1981). Changes in some metabolites in rice seeds during aging. *Seed Sci. Technol*. *9,* 469–473.
26. Worang, R. L., Dharmaputra, O. S., Syarief, R., Miftahudin, (2008). The quality of physic nut (*Jatropha curcas*) seeds packed in plastic material during storage. *Biotropia*. *15 (1),* 25–36.
27. Dharmaputra, O. S., Worang, R. L., Syarief, R., Miftahudin, (2009). The quality of physic nut (*Jatropha curcas*) seeds Effected by water activity and duration of storage. *Microbiol*. *3 (3),* 139–145.
28. Chelkowski, J. (1991). Fungal Pathogens Influencing Cereal seed Quality at Harvest. In: Cereal Grains; Mycotoxins, Fungi and Quality in Drying and Storage, Chelkowski, J. (Ed.). Elsevier Publisher, Amsterdam, pp. 53–66.
29. Christensen, C. M., Kaufman, H. H. (1969). Influence of moisture content, temperature and time of storage upon invasion of rough rice by storage fungi. *Phytopathl*. *59,* 145–148.
30. Christensen, C. M. (1971). Evaluating conditions and storability of sunflower seeds. *J. Stored Prod. Res*. *7,* 163–169.
31. Tuite, J. (1959). Low incidence of storage molds in freshly harvested seed of soft red winter wheat. *Pl. Dis. Reptr*. *43*, 470.
32. Tuite, J. (1960). The natural occurrence of tobacco ring spot virus. *Phytopathol*. *50,* 296–298.
33. Qasem, S. A., Christensen, C. M. (1958). Influence of moisture content, temperature and time on the deterioration of stored corn by fungi. *Phytopathol*. *48*, 544–549.
34. Warnock, D. W., Preece, T. F. (1971). Location and extent of fungal mycelium in grains of barley. *Trans. Br. Mycol. Soc*. *56,* 267–273.
35. Kakde, R. B., Chavan, A. M. (2011). Deteriorative changes in oilseeds due to storage fungi and efficacy of botanicals. *Curr. Botany*. *2 (1),* 17–22.
36. Parreño-de Guzman, L. E., Aquino, A. L. (2009). Seed characteristics and storage behavior of physic nut (*Jatropha curcas* L.). *Philippine J. Crop Sci*. *34 (1),* 13–21.
37. Neergaard, P. (1977). Seed Pathology, Vol. I, The Macmillan Press Ltd London and Basingstoke, UK. pp. 285–288. *61*, 53, 294.
38. Ellis, R. H., Hong, T. D., Roberts, E. H. Handbooks for Genebanks No. 3. Handbook of Seed Technology for Genebanks. Vol. II. Compendium of Specific Germination Information and Test Recommendations. International Board for Plant Genetic Resources, Rome, 1985.
39. Hong, T. D., Linington, S., Ellis, R. H. Seed Storage Behaviour: a Compendium. IPGRI, Rome, 1996.
40. Heller, J. Investigation of the genetic potential and improvement of cultivation and propagation practices of physic nut (*Jatropha curcas* L.). Final report submitted to Deutsche Gesellschaft für Technische Zusammenarbeit (GTZ) GmbH (German Agency for Technical Cooperation), Eschborn, 1991.
41. Heller, J. Untersuchungen über genotypische Eigenschaften und Vermehrungsund Anbauverfahren bei der Purgiernuß (*Jatropha curcas* L.) [Studies on genotypic characteristics and propagation and cultivation methods for physic nuts (*Jatrophacurcas* L.)]. Dr. Kovac, Hamburg, 1992.

42. Narayanaswamy, S., Shambulingappa, K. G. (1994). Diversity in seed borne fungal pathogens in groundnut. *J. Oilseed Res. 11 (2)*, 294–299.
43. [Dirjenbun] Direktorat Jenderal Perkebunan. Pedoman Mutu Benih Jarak Pagar Sistem dan Prosedur Pembangunan Sumber Benih dan Peredaran Benih Jarak Pagar. Jakarta: Dirjenbun, 2006.
44. Ratree, S. (2004). A preliminary study on physic nut (*Jatropha curcas* L.) in Thailand. *Pak. J. Biologic. Sci. 7 (9),* 1620–1623.
45. Pasabutr, R., Suthiponpaiboon, S. (2001). Outstanding features of Physic nut oil on diesel engines. Kaset *Kaona J. 14,* 60–66.
46. Deng, Z. J., Cheng, H. Y., Song, S. Q. (2005). Studies on *Jatropha curcas* seed. *Acta Botanica Yunnanica. 27 (6),* 605–612.
47. Mathur, S. K., Sinha, S. (1978). Certain biochemical changes in bajra (*Pennisetum typhoides*) seeds during storage. *Seed Res. 6 (2),* 172–180.
48. Saxena, N., Karan, D. (1991). Effect of seed borne – fungi on protein and carbohydrate contents of sesame and sunflower seeds. *Indian Phytopathol. 44,* 134–136.
49. Arulnandhy, V., Senanayake, D. A. (1991). Changes in viability, vigor and chemical composition of soybean seeds stored under humid tropical conditions. *Legume Res. 14 (3),* 135–144.
50. Verma, S. S., Tomer, R. P. S., Verma, U. (2003). Loss of viability and vigor in Indian mustard seeds stored under Ambient conditions. *Seed Res. 31 (1),* 98–101.
51. Begum, M., Lokesh, S., Ravishankar, R. V., Shailaja, M. D., Kumar, T. V., Shetty, H. S. Evaluation of certain storage conditions for okra (*Abelmoschus esculentus* (L.) Moench) seeds against potential fungal pathogens. *Internat. J. Agri. Biol. 7 (4),* 550–554.
52. Pattee, H. E., Young, C. T., Giesbrecht, F. G. (1981). Free Amino Acids in Peanuts as Effected by Seed Size and Storage Time. *Peanut Sci. 8 (2),* 113–116.
53. Deswal, D. P., Sheoran, I. S. (1993). A simple method of seed leakage measurement applicable to single seed of any size. *Seed Sci. Technol. 21,* 179–185.
54. Agrawal, P. K. (1980). Relative storability of seeds of ten species under ambient conditions. *Seed Res. 8,* 94–99.
55. Gupta, A., Aneja, K. R. (2004). Seed deterioration in soybean varieties during storage: Physiological Attributes. *Seed Res. 32 (1),* 26–32.
56. Sukesh; Chandrashekar, K. R. (2011). Biochemical Changes During the Storage of Seeds of *Hopea ponga* (Dennst.) Mabberly: An Endemic Species of Western Ghats. *Res. J. Seed Sci. 4,* 106–116.
57. Hwang, B. K. (1983). Contents of sugars, fruit acids, amino acids and phenolic compounds of apple fruits in relation to their susceptibility to *Botryosphaeria ribis*. *Phytopathologische Zeitschrift. 108*, 1–11.
58. Patil, S. H., Hedge, R. K., Anahosur, K. H. (1985). Role of sugars and phenols in charcoal rot resistance of sorghum. *PhytopathologischeZeitschrift. 113*, 30–35.
59. Jeun, Y. C., Hwang, B. K. (1991). Carbohydrate, amino acid, phenolic and mineral nutrient contents of pepper plants in relation to agerelated resistance to *Phytophthora capsici*. *J. Phytopathol. 131,* 40–52.
60. Saha, P. K., Bhattacharya, A., Ganguly, S. N. (1992). Problems with regard to the loss of seed viability of *Shorea robusta* Gaertn. *F. Indian For. 118,* 70–76.
61. Bernal-Lugu, I., Leopold, A. C. (1992). Changes in soluble carbohydrates during seed storage. *Pl. Physiol. 30,* 195–236.

62. Smith, D. A., Banks, S. W. (1986). Molecular communication in interactions between plants and microbial pathogens. *Ann. Rev. Pl. Physiol*. *41*, 339–367.
63. Hahlbrock, K., Scheel, D. (1989). Physiology and molecular biology of phenylpropanoid metabolism. *Ann. Rev. Pl. Physiol. Mol. Biol*. *40*, 347–369.
64. Martern, U., Kneusel, R. E. (1988). Phenolic compounds in plant disease resistance. *Phytoparasitica*. *16,* 153–170.
65. Dwivedi, S. N. (1990). Changes in the concentration of total phenolic compounds in gram seeds as influenced by fungal invasion during storage. *Indian Phytopathol*. *43,* 96–98.
66. Ndoumou, D. O., Ndzomo, G. T., Djocgoue, P. F. (1996). Changes in carbohydrate, amino acid and phenol contents in cocoa pods from three clones after infection with *Phytophthora megakarya* Bra and Grif. *Ann. Bot*. *77,* 153–158.
67. Esquerre-Tucaye, M. T., Lamport, D. T. A. (1979). Cell-surfaces in plant-microorganisminteractions. I- A structural investigation of cell-wallhydroxyproline-rich glycoproteins which accumulate infungus infected plants. *Pl. Physiol*. *64*, 314–319.
68. Mishra, V. K., Biswas, S. K., Rajik, M. (2011). Biochemical Mechanism of Resistance to *Alternaria* Blight by Different Varieties of Wheat. *Internat. J. Pl. Pathol*. *2,* 72–80.
69. Pomeranz, Y. (1992). Biological, Functional, and Nutritive Changes of Cereal Grains and Their Product. St. Paul: American of Cereal Chemist Inc. pp. 55–141.
70. Hanny, J. B. (2008). "Biodiesel production from crude *Jatropha curcas* L. seed oil with high content of free fatty acids." *Bioresour. Technol*. 1716–1721.
71. Bothast, R. J. Fungal deterioration and related phenomena in cereals, legumes and oilseeds. Northern Regional Research Center Agricultural Research Service U. S. Department of Agriculture Peoria, IL 61604, 2009.
72. Gupta, R. C., Rao, D. G. (2008). Effect of storage time on yield and free fatty acid (FFA) content of raw *Jatropha* oil. XXXII National Systems Conference, NSC, pp. 440–443.
73. Oladimeji, G. R., Kolapo, A. L. (2008). Evaluation of proximate Changes and Microbiology of stored defatted residues of some selected Nigerian oil seeds. *African J. Agricultural Res*. *3 (2),* 126 – 129.
74. Sayyar, S., Abidin, Z. Z., Yunus, R., Muhammad, A. (2011). Solid liquid extraction of *Jatropha* seeds by microwave pretreatment and ultrasound assisted methods. *J. Appl. Sci*. *11 (13),* 2444–2447.
75. Basha, S. M., Pancholy, S. K. (1986). Qualitative and quantitative changes in the protein composition of peanut (*Arachis hypogaea* L.) seed following infestation with *Aspergillus* spp. differing in aflatoxin production. *J. Agri. Food Chemistry* (*USA*). *34,* 638–643.
76. Simic, B., Popovic, R., Sudaric, A., Rozman, V., Kalinovic, I., Cosic J. (2007). Influence of storage condition on seed oil content of maize, soybean and sunflower. *CCS Agriculturae Conspectus Scienticus*. *72 (3),* 211–213.
77. Saraswat, R. P., Mathur, S. K. (1985). Lipase production by seed borne fungi of linseed. *Seed Res*. *13 (2),* 123–124.
78. Saxena, N., Karan, D., (1998). Mohana, Enzymatic studies of seed borne fungi of safflower seeds and their role in seed deterioration during storage. *Seed Tech News*. *28,* 25–26.

79. Taung, U., McDonald, M. B. (1995). Changes in esterase activity associated with peanut (*Arachis hypogaea* L.) seed deterioration. *Seed Sci. Technol*. *23,* 101–111.
80. Sadasivam, S., Manickam, A. Biochemicals Methods. (3rd ed.) New Age International (P) Limited, New Delhi, 2008.
81. Bhasabutra, R., Sutiponpeibun, S. (1982). *Jatropha curcas* oil as a substitute for diesel engine oil. *Renewable Energy Rev. J*. *4 (2),* 56–67.
82. Anonymous. Report of the Committee on Development of Biofuel, Planning Commission. Government of India, New Delhi, 2003.
83. Sirisomboona, P., Kitchaiya, P. (2009). Physical properties of *Jatropha curcas* L. kernels after heat treatments. *Biosyst. Engin*. *102,* 244–250.
84. Sauer, D. B. (1988). Effects of fungal deterioration on grain: nutritional value, toxicity, germination. *Int. J. Food Microbiol*. *7,* 267–275.
85. Parthiban, K. T., Selvan, P., Paramathma, M., Umesh Kanna, S., Kumar, P., Subbulakshmi, V., Vennila, S. (2011). Physicochemical characterization of seed oil from *Jatropha curcas* L. genetic resources. *J. Ecol. and the Natural Environment*, *3 (5)*, 163–167.
86. Abderrahim, B., Mercedes M., Jose, A. (2009). Production of biodiesel from bioethanol and *Brassica carinata* oil: Oxidation stability study. *Biores. Technol*. *100 (7)*, 2234–2239.
87. Asoiro, F. U., Akubuo, C. O. (2011). Effect of Temperature on Oil Extraction of *Jatropha curcas* L. Kernel. *The Pacific J. Sci. Technol*. *12 (2)*, 456–463.
88. Gulla, S., Waghray, K. (2011). Effect of Storage on Physicochemical Characteristics and Fatty Acid Composition of Selected Oil Blends. *J. L. S. 3 (1),* 35–46.
89. Kapilan, N., Sekar, C. B. (2011). Production and evaluation of storage stability of Honge biodiesel. *Annals of Faculty Engineering Hunedoara – Internat. J. Engin*. IX (3), 267–269.
90. Bringi, N. V. Non-traditional oilseeds and oils of India. New Delhi: Oxford and IBH Publishing Co. Pvt. Ltd. 1987.
91. Ashraf, S. S., Basu Chaudhary, K. C. (1986). Effect of Seed-Borne *Fusarium* Species on the PhysicoChemical Properties of Rapeseed Oil. *J. Phytopathol*. *117 (2),* 107–112.
92. Abulude, F. O., Ogunkoya, M. O., Ogunleye, R. F. (2007). Storage properties of oils of two Nigerian oil seeds *Jatropha curcas* (Physic Nut) and *Helianthus annus* (Sunflower). *Am. J. Food Technol*. *2,* 207–211.
93. Foidl, N., Foidl, G., Sanchez, M., Mittelbach, M., Hackel, S. (1996). *Jatropha curcas* L. as a source for the production of biofuel in Nicaragua. *Biores. Technol*. *58,* 77–82.
94. Russell, T. (1989). *Additives Influencing Diesel Fuel Performance*, John Wiley and Sons: Chichoster; pp. 65–104.
95. Singh, R. K., Padhi, S. K. (2009). Characterization of *Jatropha* oil for the preparation of biodiesel. *Nature Product Radiance*. *8 (2)*, 127–132.
96. Kyne, T. T., Oo, M. M. (2009). Production of Biodiesel from Jatropha Oil (*Jatropha curcas*) in Pilot Plant. *Proceedings of World Acad. Sci. Engin. Technol*. *38*, 481–487.
97. Arrakis, J. de J., Ingenia, T. A. (2007). *Jatropha* oil quality related to use in diesel engines and refining methods. *Technical Note*. pp. 1–11.
98. Sundar Raj, F. R. M., Sahayaraj, J. W. (2010). A comparative study over alternative fuel (biodiesel) for environmental friendly emission. *IEEE*, pp. 80–86.

99. Akintayo, E. T. (2004). Characteristics and composition of *Parkia biglobbossa* and *Jatropha curcas* oils and cakes. *Biores. Technol*. *92*, 307–310.
100. Payawan Jr., L. M., Damasco, J. A., Sy Piecco, K. W. E. (2010). Transesterification of Oil Extract from Locally Cultivated *Jatropha curcas* using a Heterogeneous Base Catalyst and Determination of its Properties as a Viable Biodiesel. *Philippine J. Sci*. *139 (1),* 105–116.
101. International Energy Agency. *World Energy Outlook*, IEA, Paris, 2006.

PART 5

CATALYSIS FOR BIOFUELS

CHAPTER 12

A CHEMIST'S PERSPECTIVE ON BIOENERGY—OPPORTUNITIES AND CHALLENGES

SANNAPANENI JANARDAN,[1] B. B. PAVANKUMAR,[1] SHIVENDU RANJAN,[2] NANDITA DASGUPTA,[2] MELVIN SAMUEL,[2] CHIDAMBARAM RAMALINGAM,[2] AKELLA SIVARAMAKRISHNA,[1]* and KARI VIJAYAKRISHNA[1]*

[1]*Department of Chemistry, School of Advanced Sciences, VIT University, Vellore*

[2]*School of Bio Sciences and Technology, VIT University, Vellore, Tamil Nadu, India*

CONTENTS

12.1 Introduction 300
12.2 Methods 302
12.2.1 Thermochemical Approaches 302
12.2.2 Microwave Approach For Biofuel Production 308
12.2.3 Photo-Electrochemical Reactions 310
12.2.4 Bio-Approaches 312
12.2.5 Catalytic Methods 325
12.3 Conclusions and Future Prospects 336
12.4 Acknowledgements 338
Keywords 338
References 338

12.1 INTRODUCTION

Since the crude oil resources are finite, there is however an increasing demand for ecofriendly, renewable and sustainable fuels, particularly for the transport purpose. At present, the entire world is looking for alternative, efficient and sustainable energy sources such as solar, wind, hydro, biomass and geothermal energy. The main drawback of these energy sources is that they need to be converted to energy carriers such as electricity, hydrogen or biofuels primarily before considering them to the transport purposes. Among all the energy sources, hydrogen is the ideal fuel for an energy efficient fuel cell with water as a by-product. However, there are several problems associated with conversion and storage of hydrogen gas although the efficiency of catalytic conversion of biomass to hydrogen was substantially improved recently [1, 2]. All these aspects are driving the scientists for the production of liquid biofuels from the biomass.

The main components in biomass are cellulose, a polymer of glucose, lignin (a highly cross-linked polymer built up of syringyl and sinapyl units) and hemi-cellulose (an oligomer of both C_6-glucose and C_5-xylose sugars), which are formed from CO_2 and H_2O using sunlight as energy source. It is significant to note that the energy content per mass unit increases with decreasing oxygen content of the building blocks. An overview of the components typically present in biomass is given in Fig. 12.1 [3]. Biofuels are already on the market in the form of ethanol for gasoline engines and fatty acid methyl esters (FAMEs) for diesel engines. Biomass can also be converted into various types of fuels such as hydrogen, synthetic natural gas (SNG), dimethyl ethanol (DME), and Fischer–Tropsch (FT) diesel [4, 5].

Higher oxygen content in biomass (carbohydrates) is the major difference between biomass and other fossil fuels like gasoline or diesel, which can bring the changes in the parameters as shown in Table 12.1. In view of this, the present techniques are focused on the elimination of oxygen from biomass (Fig. 12.2).

Elimination of molecular oxygen from cellulosic biomass to form hydrocarbons is exactly opposite to highly endothermic combustion of hydrocarbons. The removal of oxygen in the form of CO_2 or H_2O must

have a combustion enthalpy equal to zero. The formation of carbon dioxide as the oxygen carrying molecule from a C6– hydrocarbon would result in [C_3H_{12}], a hypothetical molecule which can split into either three methane (CH_4) units or propane with two hydrogen molecules ($C_3H_8 + 2H_2$) (Fig. 12.2). It is very important to convert the biomass in to higher alkanes as methane, charcoal or synthesis gas cannot be blended with liquid transport fuels. Otherwise the coupling of methane (biogas) to form higher alkanes in the presence of a suitable catalyst would be a key discovery [6].

Elimination of all oxygen from carbohydrates in biomass thus automatically leads to a conversion route with synthesis gas as intermediate from which higher alkanes for diesel can be derived by the Fischer Tropsch reaction [7].

$$nCH_4 + ½\ O_2 \rightarrow [–CH_2–]_n + nH_2O \quad (1)$$

This chapter mainly focuses on possible routes from biomass to bioenergy systems as seen from a chemist's perspective.

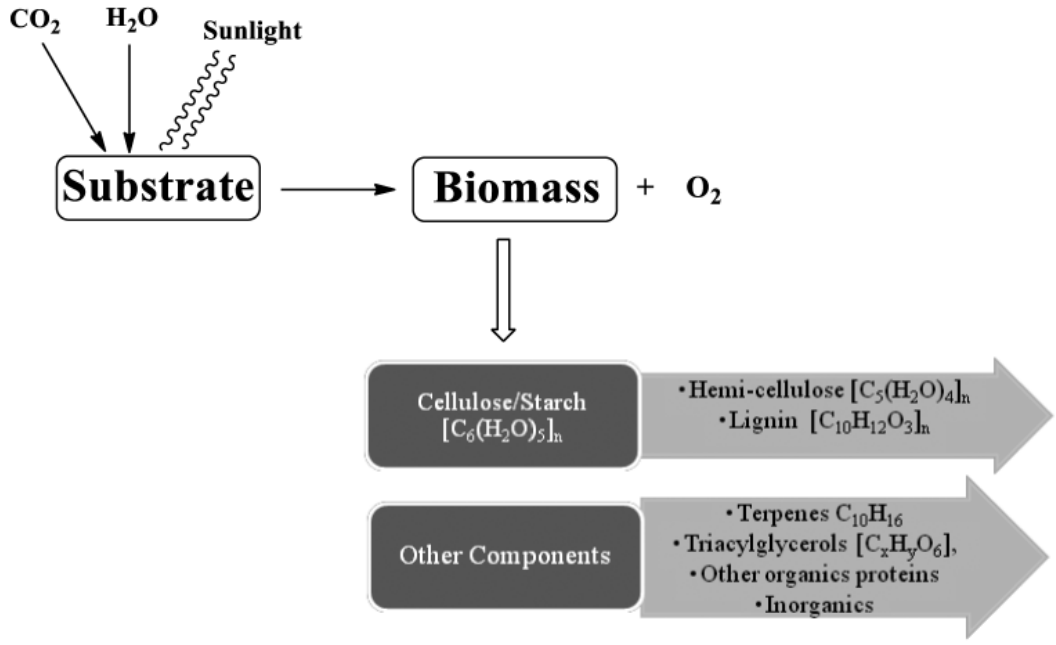

FIGURE 12.1 Components of Biomass.

TABLE 12.1 Difference Between Carbohydrate, Gasoline and Diesel

	Carbohydrate	Gasoline	Gasoil/Diesel
Chain length	[5–6]n	5–10	12–20
O/C molar ratio	1	0	0
H/C molar ratio	2	1–2	~2
Phase behavior	Solid	Liquid	Liquid
Polarity	Polar	Non polar	Non polar

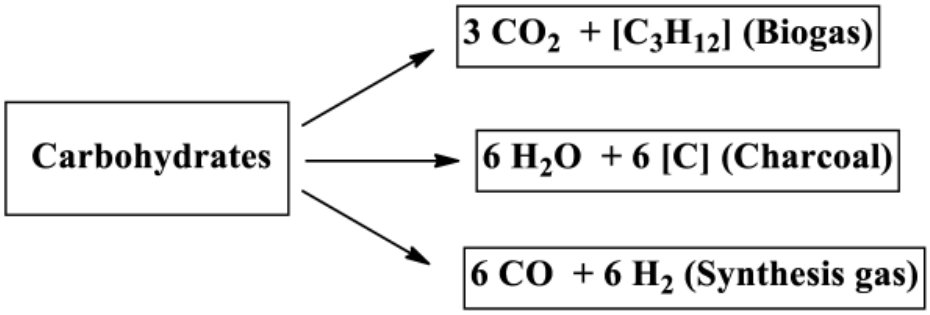

FIGURE 12.2 Elimination of oxygen species from carbohydrates.

12.2 METHODS

12.2.1 THERMOCHEMICAL APPROACHES

In general, the thermo-chemical conversion processes have two basic approaches. The first is the gasification of biomass and its conversion to hydrocarbons. The second approach is to liquefy biomass directly by high-temperature pyrolysis, high-pressure liquefaction, ultrapyrolysis, or super-critical extraction. These processes convert the waste biomass into energy rich useful products. Choice of conversion process depends upon the type and quantity of biomass feedstock, the desired form of the energy. Different thermo-chemical conversion processes include combustion, gasification, liquefaction, hydrogenation and pyrolysis. Pyrolysis has received special attention as it can convert biomass directly into solid, liquid and gaseous products by thermal decomposition of biomass in the absence of oxygen. Pyrolysis offers efficient utilization of particular importance for agriculture countries with vastly available biomass by-products. The efficiency of thermochemical methods strongly depends on temperature,

holding time, rate of heating and nature of catalysts. Various available conventional processes have been discussed in brief (Fig. 12.3).

12.2.1.1 Combustion

The biomass is directly burnt with air to convert chemical energy stored in biomass into heat, mechanical power, or electricity, etc., for stoves, furnaces, boilers, steam turbines, turbo-generators. Though it is possible to burn any type of biomass but it is necessary that biomass should not have the moisture content for combustion. One of the major drawbacks of combustion process is that it requires some pretreatment like drying, chopping, grinding, etc., which in turn is associated with financial costs and energy expenditure [8, 9]. Combustion of biomass produces hot gases at temperatures around 800–1000°C. Net bio-energy conversion efficiencies for biomass combustion power plants range from 20% to 40%. [10].

12.2.1.2 Gasification

This process involves conversion of biomass into a syngas by the partial oxidation of biomass at high temperatures as summarized in Fig. 12.4. At high temperature solid biomass is converted into combustible gas mixtures (known as synthesis gas or syngas) through simultaneous occurrence of exothermic oxidation and endothermic pyrolysis under limited oxygen supply [10].

The advantage of gasification is that it is not constrained to a particular plant-based feedstock, and thus any lignocellulosic biomass can be considered appropriate. However, the amount of water in the biomass and impurities in the gases produced can be problematic in downstream processes, where a clean gas feed is required. Gasification is normally carried out at temperatures above 1000 K, but recently is has been demonstrated that H_2 and CO can be produced through the aqueous phase reforming of glycerol at lower temperatures (<620 K). The ratio of CO/H_2 can be modified by the water gas shift reaction ($CO+H_2O \rightarrow CO_2+H_2$) [11].

Fixed bed and fluidized bed gasification are more common. Different gasification agents can be applied, as air, oxygen or steam. The use of

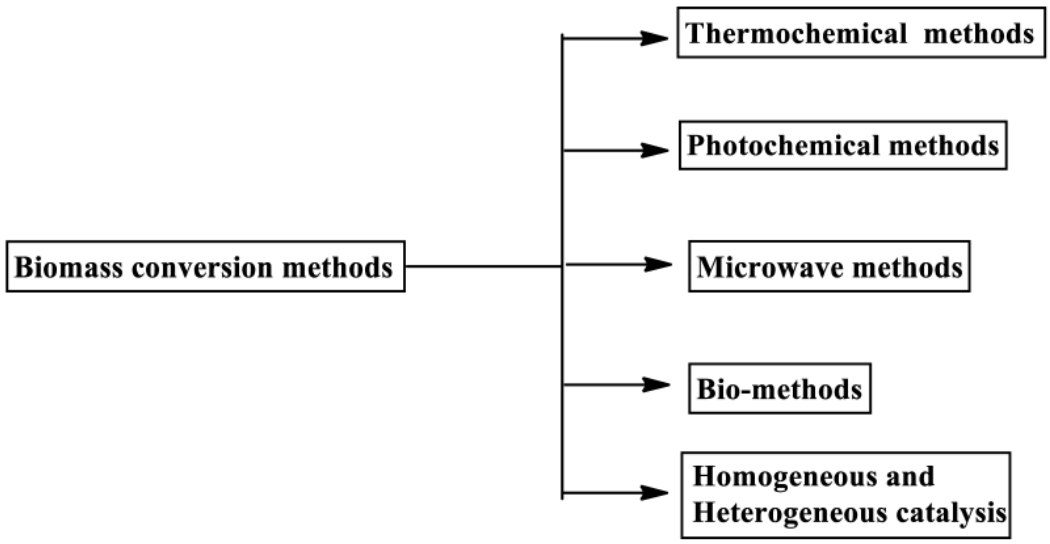

FIGURE 12.3 Broad classification of biomass treatment methods.

air as a gasifying agent is most common in industry but yields low heating value gas [12]. A high H_2/CO ratio is required for producing liquid fuels through Fischer–Tropsch synthesis and also benefits the production of H_2 for use in fuel cells. However, high capital costs and complex system design have hindered the applications of steam and oxygen gasification at a large industrial scale [13]. Earlier Fischer–Tropsch (FT) synthesis from atmospheric biomass gasification with a shift reactor was reported. In 2013, Nadia et al. highlighted the improved thermal process energy efficiencies by 10.7% without the shift process; although the liquid fuel energy production is 5% less [14].

In another approach by Kwangsu et al., to long-term operation of the biomass-to-liquid (BTL) process was conducted with a focus on the production of bio-syngas that satisfies the purity standards for the Fischer–Tropsch process. The integrated BTL system consists of a bubbling fluidized bed (BFB) gasifier, gas cleaning unit, syngas compression unit, acid gas removing unit, and an FT reactor. Since the raw syngas from the gasifier contains different types of contaminants, such as particulates, condensable tars, and acid gases, which can cause various mechanical problems or deactivate the FT catalyst, the syngas was purified by passing through cyclones, a gravitational dust collector, a two-stage wet scrubber (packing-type), and a methanol absorption

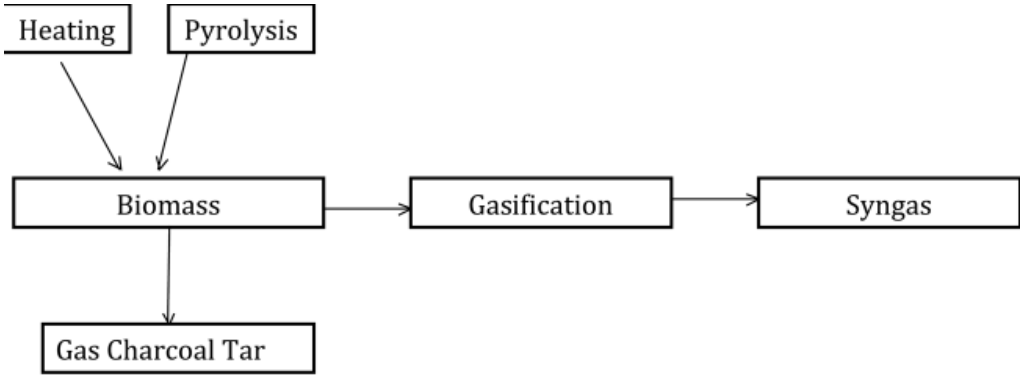

FIGURE 12.4 Schematic diagram for biomass gasification.

tower. The integrated system was operated for 500 h over several runs, and stable operating conditions for each component were achieved. The cleaned syngas contained no sulfur compounds and satisfied the requirements for the FT process [15].

In 2014, Berrueco et al. [16] researched on the pressurized gasification of torrefied woody biomass in a lab scale fluidized bed. This work reported experimental results concerning the influence of torrefaction level and pressure on product yields and composition during fluidized bed O_2/steam gasification of two different raw biomasses. The results show an increase in gas yield with pressure and torrefaction level for both types of biomass considered [16]. Danica et al., have evaluated costs for biofuel production in four biofuel polygeneration plants and the plants were integrated with district heating production. The revenues from by-produced electricity and heat were included as negative costs. The production costs depend on energy market and district heating conditions [17].

12.2.1.3 Liquefaction

Liquefaction consists of the catalytic thermal decomposition of large molecules to unstable shorter species that polymerize again into a bio-oil. Biomass is mixed with water and basic catalysts like sodium carbonate, and the process is carried out at lower temperatures than pyrolysis (525–725 K) but higher pressures (5–20 atm.) and longer residence times. These factors combine to make liquefaction a more expensive process; however,

the liquid product obtained contains less oxygen (12–14%) than the bio oil produced by pyrolysis and typically requires less extensive processing [18, 19].

Recently liquefaction of many microorganisms and use of hydrothermal liquefaction have been attempted to increase the efficiency also many byproducts/coproducts have been collected. α-glucan has been isolated as a coproduct of biofuel by hydrothermal liquefaction of *Chlorella sorokiniana* biomass, which will be beneficial for industries [20]. The comparative analysis has been done on land, water, and nutrient consumption between algae to biofuel conversion pathways. The study was based on spatial model of algae growth and resource availability for coterminous United States. Also, hydrothermal liquefaction compared to lipid extraction, with nutrient recycling technologies. And they have concluded with that for a given production target, hydrothermal liquefaction consumes far less land, water and phosphorous than lipid extraction. Also, nitrogen consumption is significantly increased over lipid extraction, but further recovery is still possible [21]. Also, Bahar et al., has givena cost effective approach for biofuel production, which is an alternative for synthetic fuels carried out by liquefaction of kenaf (*Hibiscus cannabinus* L.) biomass [22].

12.2.1.4 Pyrolysis

Pyrolysis, like gasification, is an advanced thermal treatment that converts a material into a syngas but at lower temperatures and in the absence of oxygen. Despite the calorific value of a gas derived from pyrolysis being higher than that of gasification, the volume of gas produced is usually much lower due to the lack of the oxygen carrier [23, 24].

Pyrolysis is the thermal decomposition of materials in the absence of oxygen or when significantly less oxygen is present than required for complete combustion. Pyrolysis also can be described as the direct thermal decomposition of the organic matrix that could obtain solid, liquid and gas products. Temperature is the most important factor for the product distribution of pyrolysis, most interesting range for the production of the pyrolysis products is between 625 and 775 K [25].

Pyrolysis process is an attractive, low cost strategy for the production of upgradeable liquid feedstocks (bio-oils) from lignocellulose. It does not require biomass pretreatment and fractionation, and offer potential for lignin utilization. However, bio oils require extensive hydrodeoxygenation before use in internal combustion engines or selective upgrading to larger hydrocarbons [26].

Recently microwave assisted pyrolysis is the emerging field to increase the efficiency of the biofuel production. Yinhas given a brief on 2nd-generation biofuels from biomass residues and waste feedstock. He presented a state-of-the-art review of microwave-assisted pyrolysis of biomass. First, conventional fast pyrolysis and microwave dielectric heating is briefly introduced. Then microwave-assisted pyrolysis process is thoroughly discussed stepwise from biomass pretreatment to bio-oil collection. The existing efforts are summarized in a table, providing a handy overview of the activities (e.g., feedstock and pretreatment, reactor/pyrolysis conditions) and findings (e.g., pyrolysis products) of various investigations [27]. Shoujie et al. first studied of integrated microwave torrefaction and pyrolysis of corn stover. They concluded that microwave torrefied pyrolysis favored phenols and hydrocarbons production. Organic acids were significantly reduced in bio-oils also up to 26.7 area % hydrocarbons in the bio-oil were produced [28].

In slow pyrolysis process, the biomass is pyrolyzed at slow heating rates (5–7 K/min) to lead to less liquid and gaseous product distribution and more of char production. Slow pyrolysis of sugarcane bagasse gives 23–28% yield of charcoal and fixed bed pyrolysis of Euphorbia rigida, sunflower presses bagasse and hazelnut shell were carried out [29–31]. These studies indicate that the efficiency increases with a rise in temperature in the presence of N_2 atmosphere.

As the slow pyrolysis produces more char, the higher yield of desirable liquid product can be obtained by fast pyrolysis with rapid heating of biomass (300°C/min). Fluidized bed reactors as it offers high heating rates, rapid de-volatilization, easy control, easy product collection, etc., can be used to carry out the fast pyrolysis [32]. The next option is flash pyrolysis process with special reactor configuration in which the reaction of small size samples (105–250 mm) completes in few seconds at very

high temperature. Flash hydro-pyrolysis was also done in hydrogen atmosphere to get the saturated products [33, 34].

Other wet processes that produce bio-oils are hydrothermal gasification and hydrothermal liquefaction. The conversion of biomass in a wet environment at high pressure yields partly oxygenated hydrocarbons. Since the development of efficient wet processes is currently a growing area, the interest in liquefaction is low because the reactors and fuel-feeding systems are more complex and more expensive than pyrolysis processes.

12.2.2 MICROWAVE APPROACH FOR BIOFUEL PRODUCTION

Bio-diesel, an ideal alternative to fossil fuels, is very imperative for the sustainable development of mankind. Although the calorific value of the oils obtained from biological sources is as good as diesel fuel, the main drawback of these oils to use as fuel source is of low volatility and high viscosity, prohibits its direct application as fuel for diesel engines. To overcome these problems the oils obtained from natural sources (plant, bacteria, fungi, and oleaginous algae) undergo transesterification in which the triglycerides (vegetable oils) react with alcohol in presence of catalyst to produce bio-diesel and glycerin [35]. Promising options are there for converting the vegetable oils into prospective precursors for the preparation of activated carbon, and biodiesel. Among the reported techniques, microwave heating has been reported to be more energy efficient than other conventional methods for the transesterification reaction [36]. Figure 12.5 shows the biodiesel production process [37].

The influence of microwave on chemical reactions could be due to the molecular attrition caused by increase in the medium temperature and reaction rates. In the biodiesel production process, a satisfactory conversion can be achieved in shorter time duration under microwave irradiation, when compared with that obtained under conventional heating [38, 39]. The reaction for the transesterification process can undergo either by acid or base catalyzed. The mechanism for base catalyzed trans-esterification is shown in Scheme 12.1. The microwave efficiency is increased by the high polarity and high dielectric loss of methanol. Indeed, the dielectric

constant of methanol at 25°C and 2.45 GHz is 32.7 compared with that of water at 78.5, which is high, and that of oil is only between 3 and 4. In general, conversions are high at very short reaction times in comparison with conventionally heated systems for homogenous base-catalyzed transesterification reactions under microwave irradiation in batch conditions.

The first pretreatment step required is to reduce the acidity of the oil obtained from waste cooking oils and from other biological sources. Both physical (i.e., drying, filtration, or distillation) and chemical pretreatment were used. Chemical treatment is carried out with an acid-catalyzed esterification reaction. The fatty acids in the oil react with methanol producing methyl esters and water. This is an immiscible liquid–liquid reaction, which is mass-transfer limited. The esterification reaction the tri, di and mono glycerides remains in the oil layer and the remaining waste was left in water layer. Following the esterification reaction and after a water removal step, the pretreated oil is then transformed using a base-catalyzed transesterification. Like the esterification reaction, the transesterification reaction is mass-transfer limited at the beginning due to the immiscibility of triglycerides and methanol, as well as at the end of the reaction because most of the catalyst is in the glycerol phase.

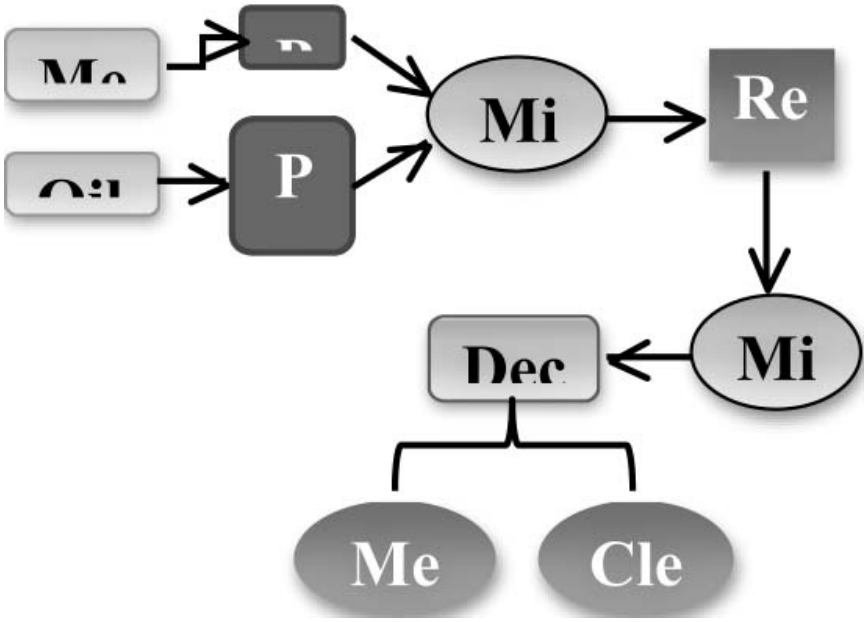

FIGURE 12.5 Biodiesel Production block diagram.

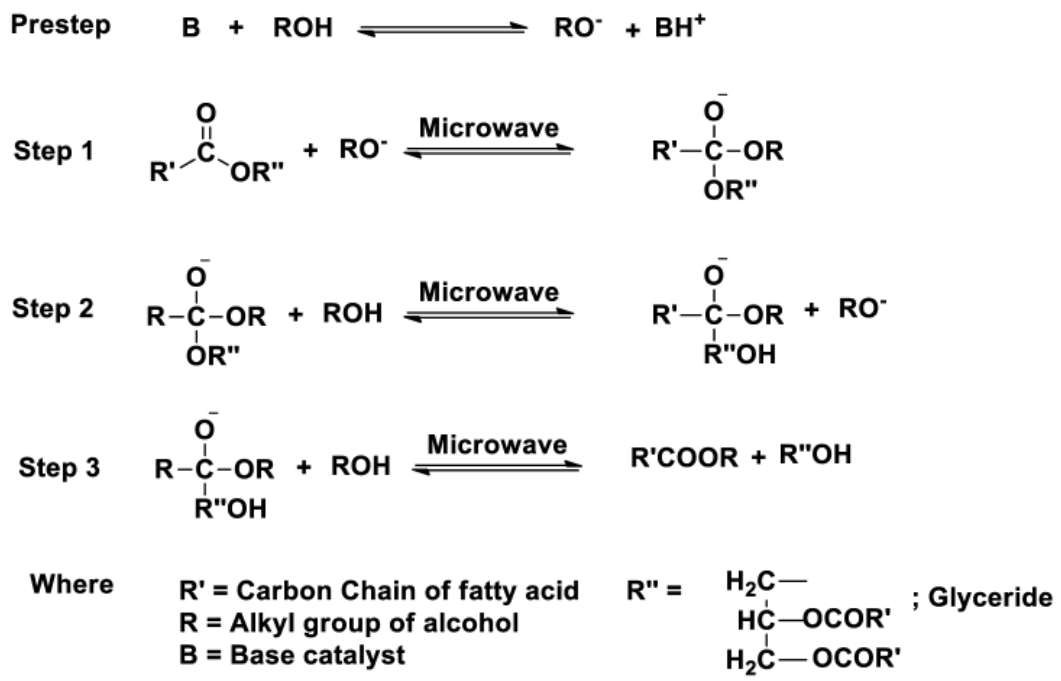

SCHEME 12.1 Step wise base catalyzed transesterification under microwave condition.

12.2.3 PHOTO-ELECTROCHEMICAL REACTIONS

In this method, photoelectrochemical (PEC) cell is used to degrade the organic waste by photocatalysis reaction to produce the biofuels under ambient conditions. However, not all organic substances result in the same energy outputs in terms of either electricity or molecular hydrogen production. In addition, water can be split in a PEC cell to produce fuel. A good amount of study is devoted on methanol, ethanol or glycerol as a model fuel due to their formation as bio-related compounds and their presence in biomass (Table 12.3). Generally the reaction is carried out in absence of oxygen and water. The reaction can be summarized as follows:

$$C_xH_yO_z + (2x - z)\,H_2O \rightarrow xCO_2 + (2x - z + (y/z))\,H_2 \qquad (2)$$

In another study, a wide variety of biological wastes is used in a PEC to liberate hydrogen that can be used as an energy source, which have been very well reviewed [60].

TABLE 12.2 Parameters Required For High Yields Conversion of Oils From Various Biological Sources to Biodiesel

S. No.	Source	Solvent/Catalyst	Watts/ temp	Time	Conversion, %	Ref.
1.	Cryptococcus curvatus (yeast strain)	Methanol/KOH	900 W	5 min	63.88	[40]
2.	Soy oil	Ionic liquid 4-allyl-4-methylmorpholin-4-ium bromine/ KOH	70°C	6 min	99.4	[36]
3.	Nannochloropsis sp., CCMP1776	KOH	800W	9 min	71.5	[37]
4.	Pongamia pinnata	NaOH: KOH (6:1)	60°C	10 min	96	[35]
5.	Oil palm empty fruit bunch (EFBAC)	KOH	600W	7 min	73.78	[41]
6.	Waste cooking oil	Cation ion exchange Resin particles (CERP)/ PES catalytic membrane	360W	90 min	97.4	[41]
7.	Chlorella pyrenoidosa (algae)	Chloroforl:methanol: sulfuric acid (1:1:0.1)	60°C	30 min	94	[42]
8.	Jatropha curcas L. seed	5 N KOH in ethanol	100 W	35 min	97.29	[43]
9.	Palm oil	Eggshells by simple calcination in air as catalyst	900 W	4 min	96.7	[44]
10.	Dry microalgae powder (Far East Bio-Tec Co., Taiwan)	Methanol/Li4SiO4	68°C	4 h	76.2	[45]
11.	Jatropha curcas	Methanol/NaOH	80 W	24 h	96.5	[46]
12.	Jatropha oil	KOH impregnated CaO	120 W	60 min	96.5	[47]
13.	Waste cooking oil	Sodium methoxide	750 W	3 m	97.7	[48]

TABLE 12.2 (*Continued*)

S. No.	Source	Solvent/Catalyst	Watts/ temp	Time	Conversion, %	Ref.
14.	Waste cooking oil	Aminophosphonic acid resin D418	81°C	420 min	90	[49]
15.	Waste frying Palm oil	Methanol/NaOH	800W	0.5 min	97	[50]
16.	Rapeseed oil	NaOH: MeOH:Oil (0.03: 1.27: 2.3)	60°C	1 min	97	[51]
17.	Soya bean oil	Nanopowder calcium oxide	65°C	60 min	96.6	[52]
18.	Sunflower oil	Carborundum	400 W	9 min	-	[53]
19.	Amazon flint kaolin	0.2 M KOH	400W	15 min	96.5	[54]
20.	Waste frying oil	$NaOCH_3$:Oil:Methanol (1.5:1:6)	60°C	9 min	97.74	[55]
21.	Palm oil	CH3ONa:Oil:Methanol (0.75:1:6)	750 W	6 min	99.5	[56]
22.	Pongamia pinnata	Methanol–oil ratio 33.4 (w/w) % KOH catalyst concentration 1.33 (w/w) %	180 W	2 min	89.9	[57]
23.	Carthamus tinctorius L	Methanol:Oil:NaOH (10:1:1)	60°C	6 min	98.4	[58]
24.	Nagchampa oil	KOH	88°C	210 min	-	[59]

12.2.4 BIO-APPROACHES

12.2.4.1 Enzyme Based Catalysis

Biofuels/bioethanol can be prepared by enzymatic conversion of bio-waste products. It has been observed that enzymes such as cellulase, hemicellulases, xylulase, amylase, lignicellulase, etc., can be used to act on different substrate and undergo chemical reaction to yield biofuel. Hereby we describe two of the commonly used enzymes – amylolytic enzymes and

TABLE 12.3 Performance of Various Cells (Photovoltaic, PEC and Gratzel) For Biomass Conversion

Type of Cell	Efficiency, %
Crystalline silicon	24
Multicrystalline silicon	18
Amorphous silicon	7
$CuInSe_2$	19
Dye-sensitized nanomaterial	10–11
Bipolar AlGaAs/Si	19–20
Organic solar cells	2–3

cellulosic enzymes that have been commercialized for biofuel production [61, 62].

12.2.4.1.1 Amylolytic Enzyme

Amylases have received a great deal of attention because of their significance especially in biotechnology. Amylases belong to a class of enzymes that has been extensively studied and is commercialized for different purposes. It can be obtained from different sources including plants, animals and microorganisms [63]. Amylases are starch hydrolyzing enzymes. They are mainly being employed in the starch processing industries for the hydrolysis of starch into simple sugar constituents [64–66]. Amylases are being commercially used in different industrial sectors. Amylase constitutes a class of industrial enzymes having approximately 25% of the enzyme market world-wide [67]. The main use of enzymes includes hydrolysis of starch to yield glucose syrup, amylase-rich flour and in the formation of dextrin during baking in food industries. Furthermore, in the textile industry, amylases are used for removal of starch sizing and as additives in detergents. In biotech industries, amylases are of the most important enzymes used [68]. Currently two types of amylases, glucoamylase and alpha-glucosidase are important for starch hydrolysis. Glucoamylase attacks – 1,4-bonds releasing D-glucose molecules [69]. This enzyme also attacks 1,6 bonds at branching points in the amylopectin molecule but much more slowly than 1,4 linkage [70]. Alpha-glucosidase catalyzes

the splitting of alpha-D-glucozyl residues from the nonreducing end of substrates to release alpha-glucose [71]. Though, amylases are applicable for different sectors the production cost hinder its full utilization. The cost of procurement by developing countries can be even higher as a result of importation.

Thus, research has been focused to find alternate methods of amylase production. Microbial sources provide a great source for cheap and easy production of amylase. Many Bacillus species and thermostable Actinomycetes like *Actinomycetes thermomonospora* and *Actinomycetes thermoactinomyces* are versatile producers of amylase [72]. It has been observed that Bacillus species can produce a large range of extracellular enzymes such as amylases and proteases are of industrial importance [73, 74]. Cheap and readily available agricultural waste such as Potato peels, which presently constitutes a menace to solid waste management, may be a rich source of amylolytic bacteria [75].

Amylases have also been commercialized for enzymatic conversion of starch into bioethanol. For this process, starch has to be solubilized and then submitted to two enzymatic steps in order to obtain fermentable sugars [76, 77]. Since ethanol is the most used biofuel and starch provides a cheap and readily available raw material, amylases comprise some of the most reported groups of enzymes for the production of biofuels. Generally, these enzymes are of microbial origin: fungal and bacterial origins. Such enzymes have been used at industrial scale for decades, using conventional processes (dry grinding and wet milling) for the production of bioethanol, and recently nonconventional process is developed named cold starch hydrolysis (or granular starch hydrolysis) [78].

In the conventional process, starch is converted into ethanol by microorganisms that produce amylases extracellularly or externally adding enzymes such as glucoamylase and α-amylase, followed by fermentation. This process is known as saccharification wherein sugar is converted into ethanol using an ethanol-fermenting microorganism such as yeast *Saccharomyces cerevisiae* [79]. In order to obtain a new yeast strain that can directly produce ethanol from starch without the need for a separate saccharifying process, protoplast fusion was performed between the amylolytic yeast *Saccharomyces fibuligera* and *S. cerevisiae* [80]. Among bacteria, α-amylase obtained from thermoresistant bacteria like *Bacillus*

licheniformis or from engineered strains of *Escherichia coli* or *Bacillus subtilis* is used during the first step of hydrolysis of starch suspensions [81]. In recent years, the many research projects have been performed for designing of microbial strains with more ethanol production capacity and enhancement of process ethanol efficiency. In addition, *Saccharomyces cerevisiae* has more specific characters biotechnologically, genetically, and physiologically than other microorganisms and considers the best microbial strain for bioethanol production. One of the best methods for bioethanol efficiency increment is the isolation of yeast mutant cells that resistant to high concentration of ethanol and capable to produce more bioethanol. Based on recent reports, the suitable yeast mutant strains have been isolated for more bioethanol productivity [82]. These mutant strains could produce 7% (W/V) bioethanol and tolerate up to 12% (V/V) exogenous ethanol but could not grow in the presence of other alcoholic compounds such as 2-propanol and 1-butanol. In addition, *Saccharomyces cerevisiae* is a safe microorganism and classify to GRAS (Generally Recognized As Safe) group. There are accepted biosafety rules in developed countries such as Japan about integration of other safe yeast genes to *Saccharomyces cerevisiae* genome and designing of recombinant *Saccharomyces* spp. by auxotrophic markers [83]. Details about the use of microbes for agro-industrials application is given in Table 12.4.

12.2.4.1.2 Cellulosic/Lignocellulosic Enzyme

Biofuels can also be generated using wood, grasses, or the inedible parts of plants. Cellulosic and lignocellulosic enzymes can act on these substrates to yield cellulosic ethanol. Lignocellulose is a structural material that comprises much of the mass of plants. Lignocellulose is composed mainly of cellulose, hemicellulose and lignin. Lignocelluloses can act on a variety of cheap and readily available substrates such as corn stover, *Panicum virgatum* (switch grass), *Miscanthus* grass species, wood chips and the by-products of lawn and tree maintenance which can be enzymatically converted for ethanol production. Lignocellulose usage has the advantage that abundant and diverse raw materials can be used compared to sources such as corn and cane sugars, but requires a greater amount of processing

TABLE 12.4 A Brief Summary on Biofuel Formation by Various Microorganisms

S. No.	Microorganism	Feedstock	Fermentative Process	Optimum temperature (°C)	Enzyme	Process time	Ref.
1.	*Aspergillus awamori* MTCC 7383	Soluble starch	Submerged fermentation	31	α-amylase or glucoamylase	96 h	[84]
2.	*Aspergillus awamori* NRRL 3112	Wheat flour		30	Glucoamylase	120 h	[85]
3.	*Aspergillus kawachii* IFO 4308	Wheat bran		30	α-amylase	48 h	[86]
4.	*Aspergillus flavus* A 1.1	Soluble starch		45	Glucoamylase	96 h	[87]
5.	*Aspergillus oryzae PTCC5164*	Soluble starch		35	α-amylase	48 h	[88]
6.	*Bacillus circulans GRS 313*	Soybean meal and wheat bran		40	α-amylase	48 h	[89]
7.	*Rhizobium sp.*	Peach palm flour		28	α-amylase	96 h	[90]
8.	*Rhizopus microsporus var. Rhizopodiformis*	Soluble starch and cassava flour		45	α-amylase	72 h	[91]
9.	*Aspergillus niger* 198	Soluble starch and potato starch		30	α-amylase	48 h	[92]
10.	*Citrobacter sp.*	Sorghum flour and soybean meal		28	α-amylase	60 h	[93]

11.	*Aspergillus niger* CCT 3312	Rice straw and bran	Solid-state	30	Glucoamylase	72 h	[94]
12.	*Aspergillus oryzae*	Wheat bran	fermentation	30	Glucoamylase	120 h	[95]
13.	*Aspergillus sp. HA-2*	Wheat bran		28	Glucoamylase	96 h	[96]
14.	*Penicillium janthinellum NCIM 4960*	Wheat bran		35	α-amylase	96 h	[97]
15.	*Penicillium sp. X-1*	Wheat bran		30	Glucoamylase	36 h	[98]
16.	*Thermomucor indicae-seudaticae*	Wheat bran		40	Glucoamylase	96 h	[99]
17.	*Thermomyces lanuginosus ATCC 58160*	Wheat bean		50	α-amylase	120 h	[100]
18.	*Aplysia kurodai*	Sea lettuce		37	α-Amylase; α-Glucosidase	28 h	[101]

to make the sugar monomers available to the microorganisms typically used to produce ethanol by fermentation [102].

There are mainly two ways for cellulosic ethanol production, which includes cellulolysis and gasification. In cellulolysis processes, lignocellulosic materials are hydrolyzed and pretreated with enzymes to break complex cellulose into simple sugars such as glucose followed by fermentation and distillation. While in gasification process, the lignocellulosic raw materials are first converted to gaseous carbon monoxide and hydrogen and then converted to ethanol by fermentation or chemical catalysis. The ethanol obtained is further purified by distillation process [61, 103]. Thus, ethanol production by cellulosic enzyme can be summarized into four steps, pretreatment, cellulolysis, microbial fermentation and gasification.

The first step to ethanol production by cellulose is the "pretreatment" phase. In this step, lignocellulosic material such as wood or straw is made amenable to hydrolysis. However, most of the pretreatment processes are ineffective when the substrates used have with high lignin content, such as forest biomass or feedstocks. For this purpose, organosolv and SPORL (sulfite pretreatment to overcome recalcitrance of lignocellulose) are the only two processes that can achieve over 90% cellulose conversion for forest biomass, especially those of softwood species. SPORL is a better treatment process in terms of energy efficiency (sugar production per unit energy consumption in pretreatment) and robustness for pretreatment of forest biomass since very low fermentation inhibitors are produced. Organosolv pulping is particularly effective for hardwoods and offers easy recovery of a hydrophobic lignin product by dilution and precipitation [104].

The next step is the cellulose hydrolysis or "cellulolysis" which involves the breakdown of the molecules into sugars. Since, the cellulose molecules are composed of long chains of sugar molecules; it needs to be hydrolyzed to free sugars before it is fermented for alcohol production. Cellulolysis can be done either by chemical reaction using acids, or by enzymatic reaction. Chemical reaction using acids: In this process, acid is used for hydrolysis. Dilute acid may be used under high heat and high pressure, or more concentrated acid can be used at lower temperatures and atmospheric pressure. A significant obstacle to the dilute acid process is

that the hydrolysis is so harsh that toxic degradation products are produced that can interfere with fermentation. The pretreated decrystalized cellulosic mixture of acid and sugars reacts in the presence of water to complete individual sugar molecules (hydrolysis). The product thus obtained, is then neutralized and yeast is added for fermentation.

Enzymatic hydrolysis: This process is similar to the reaction occurring in the stomachs of ruminants such as cattle and sheep, where the enzymes are produced by microbes. The reaction occurs at body temperature and usually involves a mixture of enzymes produced by different microbes. In this process, cellulose chains are broken into glucose molecules by cellulase enzymes. Similarly, such enzyme mixture can be used for lignocellulosic materials for effective cellulose breakdown without the formation of byproducts that would otherwise inhibit enzyme activity. The enzymatic hydrolysis requires relatively mild condition (50 °C and pH 5). All major pretreatment methods, including dilute acid, require an enzymatic hydrolysis step to achieve high sugar yield for ethanol fermentation. It should be noted that lignin and other sugars has to be separated before going for the microbial fermentation.

The sugar solution is then allowed to ferment by microbes for conversion of cellulose for ethanol production. Generally, baker's yeast (*Saccharomyces cerevisiae*), has long been used in the brewery industry to produce ethanol from hexoses (six-carbon sugars). Due to the complex nature of the carbohydrates present in lignocellulosic biomass, a significant amount of xylose and arabinose (five-carbon sugars derived from the hemicellulose portion of the lignocellulose) is also present in the hydrolysate. For example, in the hydrolysate of corn stover, approximately 30% of the total fermentable sugars is xylose. As a result, the ability of the fermenting microorganisms to use the whole range of sugars available from the hydrolysate is vital to increase the economic competitiveness of cellulosic ethanol and potentially biobased proteins. In recent years, metabolic engineering for microorganisms used in fuel ethanol production has shown significant progress. Besides *Saccharomyces cerevisiae*, microorganisms such as *Zymomonas mobilis* and *Escherichia coli* have been targeted through metabolic engineering for cellulosic ethanol production [105]. Recently, engineered yeasts have

been described efficiently fermenting xylose [105, 106], arabinose [107] and even both together [108]. Yeast cells are especially attractive for cellulosic ethanol processes because they have been used in biotechnology for hundreds of years, are tolerant to high ethanol and inhibitor concentrations and can grow at low pH values to reduce bacterial contamination.

The "gasification" process does not rely on chemical decomposition of the cellulose chain (cellulolysis). Instead of breaking the cellulose into sugar molecules, the carbon in the raw material is converted into synthesis gas, using what amounts to partial combustion. The carbon monoxide, carbon dioxide and hydrogen may then be fed into a special kind of fermenter. Instead of sugar fermentation with yeast, this process uses *Clostridium ljungdahlii* bacteria. A recent study has found a novel Clostridium bacterium that seems to be twice as efficient in making ethanol from carbon monoxide as the one mentioned above [109].

12.2.4.2 Microbial Approaches

Energy is most critical for life and industry development. It is the major global economy as far as concerned. Fossil fuels include about 88% of the total global energy consumption, in which natural gas, oils and coals are the major economy fuels. The other energies *viz.* nuclear energy and hydroelectricity contribute only 5–6%. So, there is an urgent need to look for an alternative energy source apart from fossil fuels, as these fossils are getting depleted or unsustainable due to limited resources [110–113]. The first generation of biofuels is the greenhouse gases that contribute to global warming in large scale and also creates greater impact on the environment and human life. In recent years, potential threat has occurred to the marine environment due to the fossil fuels-associated CO_2 emission, which is directed into the oceans, where about 20 billion tons were dumped resulting in pH shift towards more acidic, affecting the marine ecosystem [114, 115]. The second generation of biofuels is from the plant tissue that includes energy crops, agricultural residues, harvesting residues from forest and waste of wood. The above-mentioned problems are needed to be exploited and global strategies for energy security should be

addressed. In this chapter we have discussed about the biological methods for bioenergy production and its applications.

12.2.4.2.1 Biological Method For Bioenergy Production

The biological method for production of bioenergy is being explored nowadays. The recent exploration of microalgae, which could generate biofuels that are more effective than petroleum, and also the usage of land and water is minimal. Several eukaryotic microalgae have ability to store TAG (tri-acylglycerol) and starch, the energy rich compounds, which could be used for production of biofuels such as biodiesel and ethanol [116]. Microalgae or cyanobacteria is being used for the conversion of CO_2 into alcohols and also estimated that the recombinant of microalgae can yield up to 5.5 g/L biofuel. These cultures are now being used in few startup companies in order to commercialize algal fuels. Nevertheless these practices are still under trial and not being implemented for large scale productions [117–120]. There are few bacteria reported for production of biofuels is given in Table 12.5.

12.2.4.2.2 Microalgal Bacterial Consortia

In this consortia model, microalgae provide oxygen and organic molecules. The combined use of algae and bacteria as a consortium model has developed an interest in the field of biotechnology. This consortia model is being used as an alternative method for the enhancement of bioenergy and also reduces the algal biomass consumption in bioenergy production. This process is integrated with CO_2 and pollutant removal [128, 129]. *A. brasilense* stimulation of *Chlorella sp*. growth, lipids and starch accumulation indicates a significant potential in biotechnological application of microbial–bacterial consortium model to bioenergy. *Pseudomonas sp* is known for its bioremediation potential and for biodegradation of toxic metals such nitrophenol, etc. Similarly, the *Pseudomonas* GM41 strain along with *Synechocystissp* PCC6803 increased the productivity of bioenergy, hereby helping to degrade toxic compounds commonly found in polluted water [130]. Another application

TABLE 12.5 Consolidated Bioprocessing Microbes and Their Production of Biofuels

Strains	Substrate	Pretreatment condition	Final product	Ref.
Yeast	Cellulose with yeast extract	Phosphoric acid	Ethanol	[121]
E. coli	Brich wood xylan	Acid hydolysis	Ethanol	[122]
Marine microbes	Sugarcane bagasse with chicken manure	Lime	Carboxylic acid	[123]
C. cellulolyticum	Saccharified sugar and beet pulp	NA	Isobutanol	[124]
Bacillus subtilis	Avicel	Phosphoric Acid	Lactate	[125]
Thermobifidiafusca	Switchgrass	NA	n-propanol	[126]
Caldicellulosiruptor saccharolyticus DSM 8903	Switchgrass	NA	Hydrogen gas	[127]

of microalgal–bacterial consortia is the development of microbial solar cells that comprises photoautotrophic microorganisms to harvest solar energy and release organic compounds that are used by electrochemically active microorganisms to generate electricity [131]. Genetic engineering technique is employed in microalgae to enhance their valuable compounds. Most of genetic engineering techniques are involved in the improvement of microalgae and identifying the metabolic pathway for biofuel production. Especially genetic engineering tools are applicable for finding out the complete genome sequence of microalgae species that reveals several pathways involved in their metabolic processes. The application of genetic engineering tool in microalgae is mainly for the improvement of biofuel production in microalgae.

12.2.4.2.3 Microbial Fuel Cell

Microbial fuel cell (MFC) is a recent technique considered for the treatment of organic wastes and it can be used for the recovery of bioenergy from wastes such as waste from the food industries, sludge from

sewerage, etc. MFC mainly works on the microbial catabolic activities to generate bioenergy (electricity) from the organic waste material. Researches in this area have found that MFC is a better technique than the anaerobic biogas technology for bioenergy production. Earlier, the conversion of biogas to electricity results in a significant energy loss. MFC are applied to wastewater that contains mainly volatile fatty acids and high amount of CO_2, nitrogen, and sulfur [132, 133]. This technique is currently under discussion and not been implanted in the practical waste material treatment. This is mainly because of the insufficient technical support and the efficiency of bioenergy production is also less when compared to the methanogenic anaerobic digesters. So based on the above-mentioned challenges it has been considered difficult to construct in large scale. When it comes to the improvement of the MFC performance, the values of the organic-treatment and electricity-generation comes in to play. While considering MFC process as an alternative to wastewater-treatment, the organic-treatment and electricity-generation treatment has limitations and the quality of the treated water becomes more important than energy efficiency [134, 135]. This MFC requires less energy compared to other conventional process.

12.2.4.2.4 MFC Fundamentals

In the early 1990s it was reported that in some bacterial species self-mediated extracellular electron transfer occur at substantial rates. The bacteria *Shewanellaputrefaciens* and *Shewanellaoneidensis* are able to use electrodes for conserving the electrochemical energy called as electrode respiration. Reports reveal that a ferric iron-reducing bacterium *Shewanellaputrefaciens* grew on lactate by using an electrode as the sole electron acceptor without the addition of an artificial mediator required for their growth. Many bacterial species such as *Shewanellaoneidensis* [136], *Geobactersulfurreducens* [137, 138], *Pseudomonas aeruginosa* [139] and *Clostridium butyricum* [140] have been reported for its ability to perform electrode respiration. Among these few bacteria are able to self-produce mediator compounds. While other makes use of cell surface cytochromes. Species like *Shewanellaoneidensis* can

use both mechanisms for extracellular electron transfer. These findings have facilitated the construction of better MFC's that do not require any additional artificial mediators.

12.2.4.2.5 Microbial Nanowires For Bioenergy Application

Nanowires or nanowire mimetic is the recent finding in bioenergy application the scientist and the researchers in the field believe that this method will improve the bioenergy strategies, which relies upon the extracellular electron exchange, such as microbial electrosynthesis. As far as reports are concerned, there are only two microorganisms, *Shewanellaoneidensis* and *Geobactersulfurreducens* studied for microbial nanowires formation. Microbial nanowires have been implicated in extracellular electron transfer in many organisms. The nanowires formed by *G. sulfurreducens*, a type IV pili, is reported to possess metal conducting property. Microbial nanowires plays a vital role in contributing to bioenergy. Anaerobic digestion is one of the well-known methods for obtaining/extracting energy from organic wastes in the form of methane [141]. The *Geobacter* sp. and its closely related microorganisms are used in anaerobic digesters. These microorganisms are likely to function as anaerobic fermentation/methanogenesis or syntrophs. *G. metallireducens* microorganisms growth/capacity in the presence of anaerobic fermentation is studied. *G. metallireducens* is similar to *G. sulfurreducen,* which requires a pili for long range extracellular electron transfer [142, 143]

The advantages are:

- Microalgae or cyanobacteria used in biofuel production consumes less energy.
- These bacteria have exponential/growth phase which could actually double the biomass production.
- The time taken for biomass production in exponential phase is very less, that is, 3.5 hr.
- It is being estimated that the Oleaginous microalgae, produces oil more productively *viz.* exceeding ten-fold more than that of the best oilseed crops.

- They require only less water than the terrestrial crops used for bioenergy production.
- These microorganisms can uptake nutrients such as CO_2, nitrogen and phosphorous from the industrial or municipal waste, thereby helping in waste disposal.
- They do not require additional nutrients, herbicides or pesticides for growth.
- They produce proteins and oils as by-products where few strains produce biohydrogen.

The disadvantages do arise with the biological method in the production of bioenergy due to technical barriers such as slow growth rate, less the amount of biomass production, less lipid content and ability to survive under extreme pH and temperature [111, 112]. So, in order, to overcome all these drawbacks conventional microalgae breeding technique is being adopted for efficient and economical bioenergy production.

12.2.5 CATALYTIC METHODS

12.2.5.1 Ionic Liquids in Bio-fuel Production

The biofuel can be considered as a potential alternative for the nonrenewable fossil fuel. From renewable feedstock biodiesel can be produced by simple and well-known transesterification. But this process needs lots of organic or inorganic solvents, which have environmental, constrains. To overcome these problems ionic liquids (ILs) has been widely applied as an alternative green solvent because of their unique properties. ILs which are organic salts with melting point below 100 °C are currently receiving significant global attention due to their unique physiochemical properties such as high thermal stability, chemical stability, high ionic conductivity, controllable hydrophobicity and low vapor pressure. Owing to their intrinsic properties like nonflammability, nonvolatility and fire resistance; ILs are often being known as "green solvents" replacing traditional organic solvents in different reactions [144]. Also, ILs acquired a wide range of applications in different research areas. The biodiesel is said to be carbon neutral due to the net CO_2 emission is zero. This means whatever the CO_2

emitted from the biodiesel vehicles will be used by plants for photosynthesis [145] as shown in Fig. 12.6.

Based on the type, the applied ILs in biofuel generation will have multiple roles such as solvent, lipid extractant, catalyst support and catalyst. These ILs can be recycled and reused that supports the economical prospective. IL mediated biodiesel synthesis is considered as homogeneous catalysis. The advantages of ILs mediated biodiesel process include higher catalyst activity, easy separation of the final product, recyclability of ILs, high stability, environmentally benign. These advantages make ILs as superior catalysts than conventional catalysts (liquid and solid) [146]. Bronsted acid ILs are more commonly used catalysts in biodiesel production [147] and they are preferred over basic ILs (Table 12.6). This is because the formation of soap in based ILs catalyzed reactions won't occur when Bronsted acid ILs as it involves in the transesterification of feedstock having high content of free fatty acids and prevent the problem related to the formation of soap. In general, elevated temperatures are required for the high biodiesel production [148].

TABLE 12.6 Ionic Liquid Used as Catalyst in Biodiesel Synthesis

Catalyst	Feedstock	Time (h)	Reaction Temp. (°C)	Alcohol oil molar ratio	Biodiesel yield (%)	Ref.
[BMIM][CH_3SO_3]-$FeCl_3$	Jatropha oil	5	120	2:1	99.7	[149]
[NMP][CH_3SO_3]	Oleic acid	5	70	2:1	96.5	[150]
[C_3SO_3HMIM][HSO_4]	Tung oil	6	150	17:1	97.7	[151]
IMC_2OH	Cotton-seed oil	5	60	12:1	98.6	[152]
[BMIM][OH]	Glycerol triolate	8	120	9:1	87.2	[153]
ChCl.$ZnCl_5$.H_2SO_4	Palm oil	4	65	15:1	92.0	[154]
[Et_3NH][Cl]-$AlCl_3$	Soybean oil	9	70	12:1	98.5	[155]

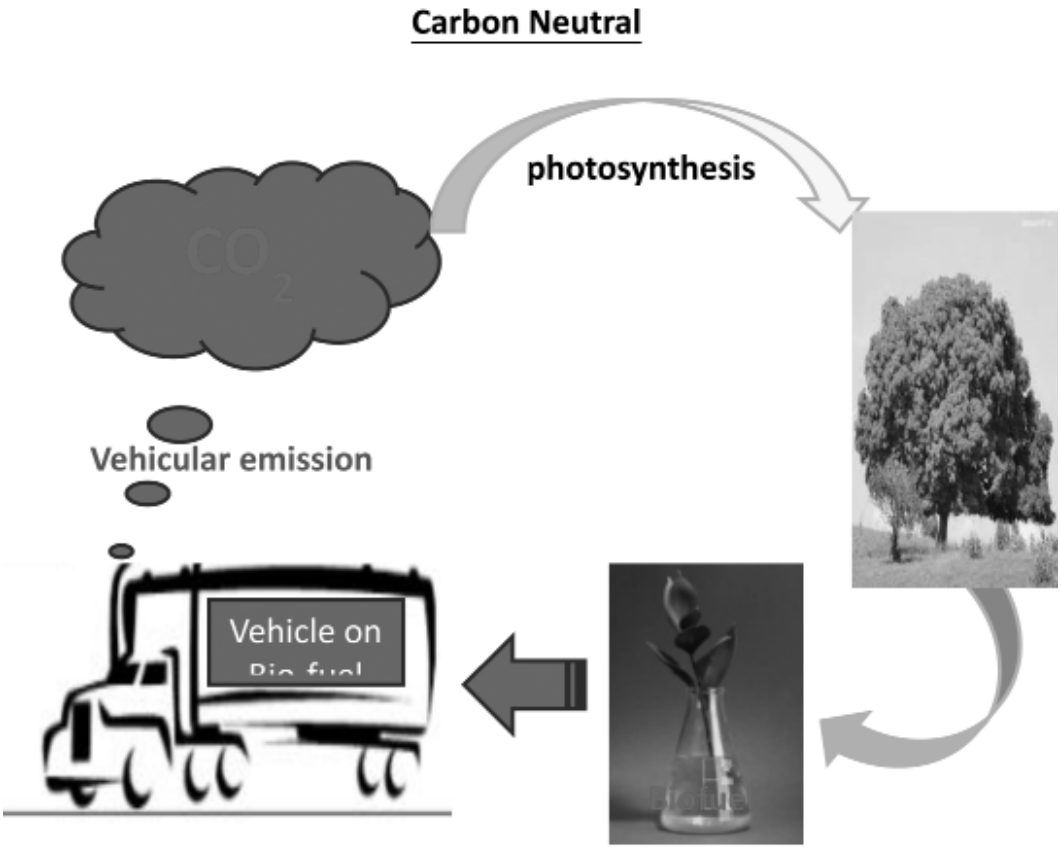

FIGURE 12.6. Carbon neutral cycle.

12.2.5.1.1 Ionic Liquids For Cellulose Dissolution and Pretreatment

Generally the raw material used for the production of biofuel is feedstocks, which are abundantly enriched with cellulose. So for the production of biofuel one can dissolve the cellulose into sugars and these sugars are subjected to dehydration process results HMF a key intermediate in biofuel production. For this pretreatment of cellulose in feed stocks generally conventional solvents are used but these solvents having the solubility problems. In order to overcoming this solubility problem, recent day's ILs are attaining greater attention as an ideal solvent for the dissolution of cellulose and pretreatment of biomass [156].

12.2.5.1.2 Acid Catalyzed Hydrolysis of Biomass in ILs

ILs in combination with acid catalyst is an efficient system for dissolution of lignocellulosic materials under mild conditions that produce wonderful conversions of key intermediates in biofuels and total reducing sugars like some of monosaccharides (e.g., glucose, fructose, glyceraldehyde and galactose) and also disaccharides (maltose and lactose). For instance 1-butyl-3-methyl imidazolium chloride with catalytic amount of HCl hydrolyzes biomasses like pine wood bagasse, rice straw, corn stalk at 100 °C for 60 min that results in 81% of TRS [157]. The same catalyst showed 100% conversion at mild temperatures in the case of carbohydrates [158]. In the same way 1-ethyl-3-imidazolium chloride with catalytic amount of HCl gives 90% of conversion of cellulose to monosaccharide at 105 °C with continuous addition of water. However, water also plays a key role in ILs mediated biomass dissolution. In some cases it will increase the rate of reaction, and with some ILs it will decrease the rate of reaction by aggregating the cellulose moieties. For Instance 1-butyl-3 methylimidazolium chloride, needs high water, but 1,3-dimethyl imidazolium dimethyl phosphate works if it is anhydrous [159].

12.2.5.1.3 Metal Catalyzed Hydrolysis of Biomass in ILs

Transition metals also used as catalysts for biomass production [160–162]. Various metal chlorides ($CrCl_2$, $FeCl_2$, CuCl, $RuCl_3$, etc.) with ILs are efficient systems for dehydration of monosaccharides to HMF with good yields. N-heterocyclic carbenes can selectively hydrolyze the monosaccharide and the conversion will depend up on the catalyst loading and substrate used for the reaction [163]. Metal mediated microwave method in combination with ILs emerging as a cost effective and energy efficient system for HMF production [164–166]. In some of the metal catalyzed hydrolysis of biomass in ILs the HMF formation depends up on the hydrophobic nature of the imidazolium ring. Yetterbium based metal salts are preferred over chromium salts due its toxic nature towards nature [167].

12.2.5.1.4 Functional Ionic Liquids Used in Biofuel Synthesis

There are different types of ILs that played an important role in biofuel production (Fig. 12.7). In IL mediated biofuel synthesis it is observed that functionalized ionic liquids showing better results than normal ILs. These functionalized ILs can be used as alternative for the mineral acids like sulfuric acid and hydrochloric acid [168]. Based on the functionalities these ILs can be classified as (i) bifunctional ionic liquids (BILs), (ii) functional polymeric reusable ionic liquis (FPILs), (iii) dicationic acidic ILs (DAILs), and (iv) dicataionic basic ILs (DIBILs) [169–171]. Cr^{3+} and SO_4^{2-} ions derived from BFIL weaken the glycosidic bonds through binding with a glycosidic oxygen atom of cellulose that eases the dissolution to monosaccharide. Polymeric ionic liquids (FPILs) functionalized with SO_3H and different anionic counterparts show good catalytic activity that

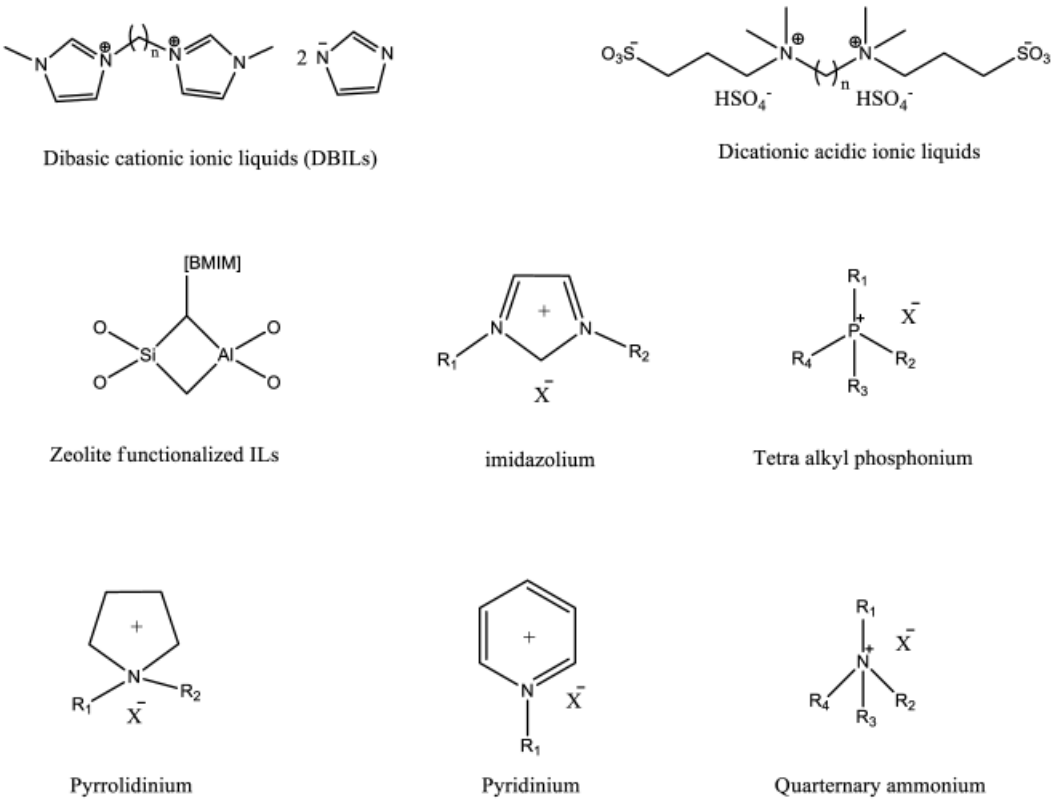

FIGURE 12.7 Ionic liquids used in biofuel synthesis.

involved in dissolution of cellulose to monosaccarides on further isomerization followed by dehydration to give HMF in good yields (96%).

12.2.5.2 Homogenous and Heterogeneous Catalysis For Transesterification

Among different existing methods for the conversion of biomass to biofuel, transesterification is the one of the best processes that produces biodiesel in pure quality [172]. In general, the triglycerides of biomass are treated with alcohol (methanol) and the applied catalyst catalyzes the transesterification to produce glycerol and the biodiesel as shown in Scheme 12.2. The quality of biodiesel strongly depends on various factors including temperature, reaction period, type of feedstock, amount of catalyst to alcohol ratio, etc. [173].

Both homogenous and heterogeneous catalysts were well studied in the transesterification process for production of biofuel. Homogenous catalysts require neutralization, separation, washing and recovery including salt waste disposal operations with serious economic and environmental penalties. There are different types of homogeneous catalysts used in the biofuel conversion and they can be classified as shown in Fig. 12.8. The homogeneous catalysts have some significant disadvantages about their reusability, neutralization, requirement of huge amount of water to leach out the homogenous catalyst, production of undesired by-products and a low-grade glycerol [174].

The general reaction mechanism of transesterification of triglycerides with acid and base catalysts is shown in Schemes 12.3 and 12.4, respectively. Although there are several types of homogenous base catalysts

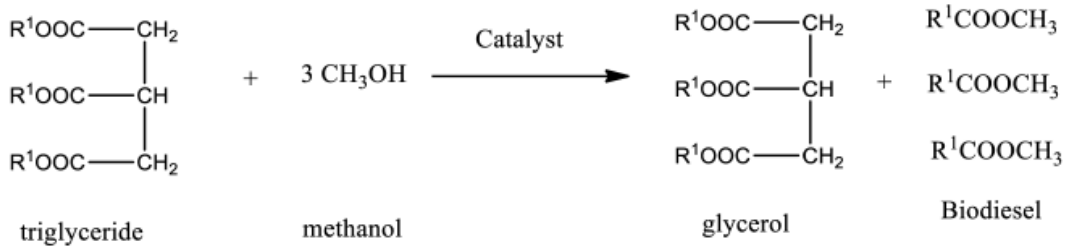

SCHEME 12.2 General reaction involved in transesterification of triglycerides with alcohol.

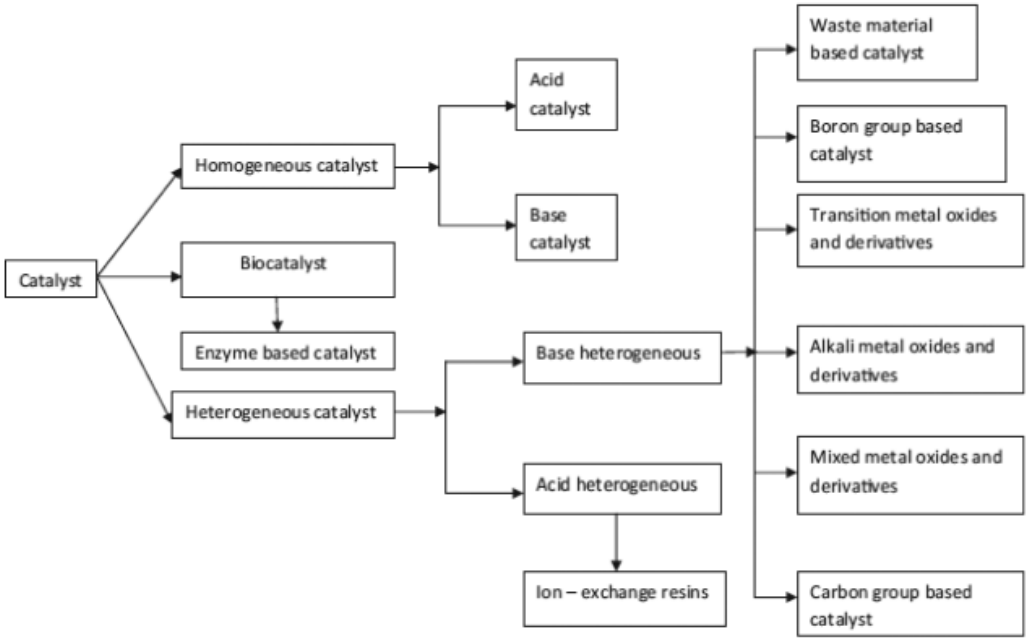

FIGURE 12.8 Classification of catalyst used for transesterification [175].

used in the biofuel production, the commonly used catalysts are NaOH, NaOMe KOH and KOMe. Among bases like NaOH, KOH, NaOMe, and KOMe, 1% NaOMe (w/v) with methanol/oil molar ratio 6 showed better conversion efficiency (98%) at 60 °C [176]. The best optimized conditions for transesterification reactions are found to be temperature between 55 to 70°C at 1–2 hr. Sodium methoxide is more effective than sodium hydroxide because of ionization of sodium methoxide to CH_3O^- and Na^+ and the ionization of sodium hydroxide leads to the formation of water that affects the rate of reaction. Even though sodium and potassium alkoxides show better conversions, NaOH and KOH are generally preferred because of their low cost [175]. Among these bases, NaOH is more favored because of ease of emulsification, ease of separation and economically more viable [177, 178].

It is significant to note that acid catalysts (homogenous and heterogeneous) more preferred over base catalysts for biofuel production. This is because all the feedstock used for biofuel production having water and free fatty acids, which decrease the activity of base catalyst.

Some of the benefits of heterogeneous catalysis over homogenous catalysis are separation of the products; recycling and reusability of the

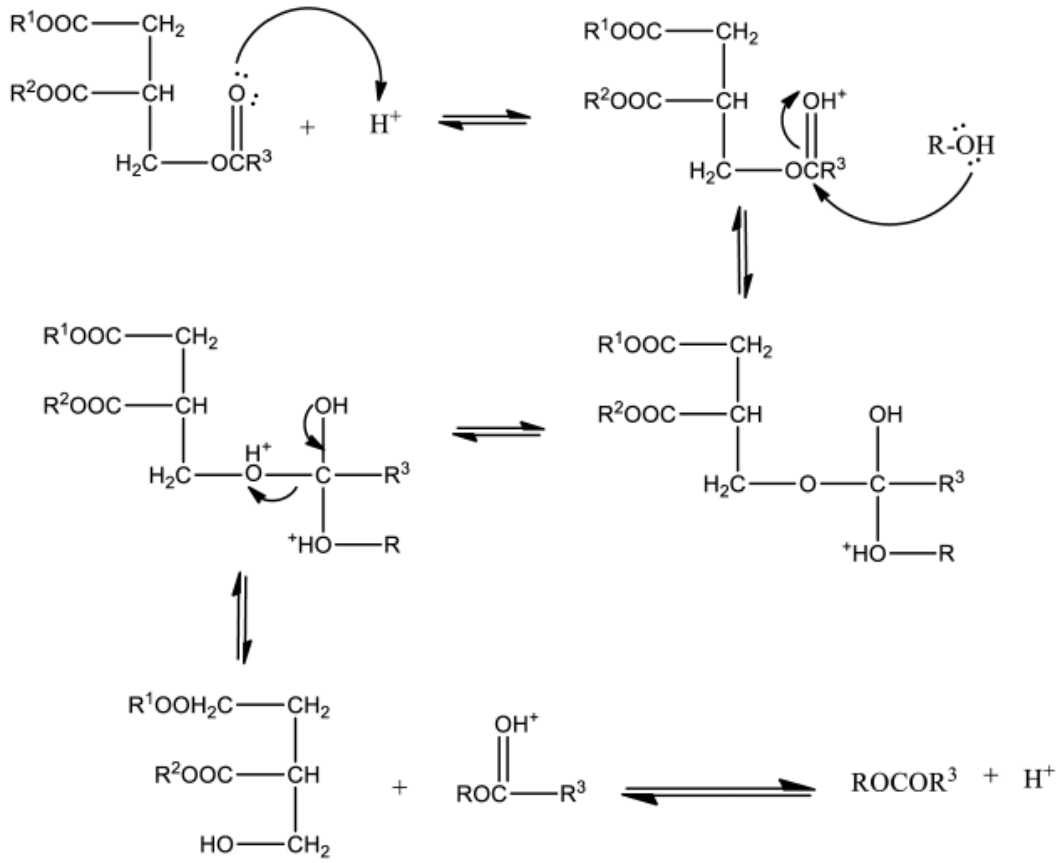

SCHEME 12.3 General reaction mechanism for acid catalyzed transesterification of triglycerides [174].

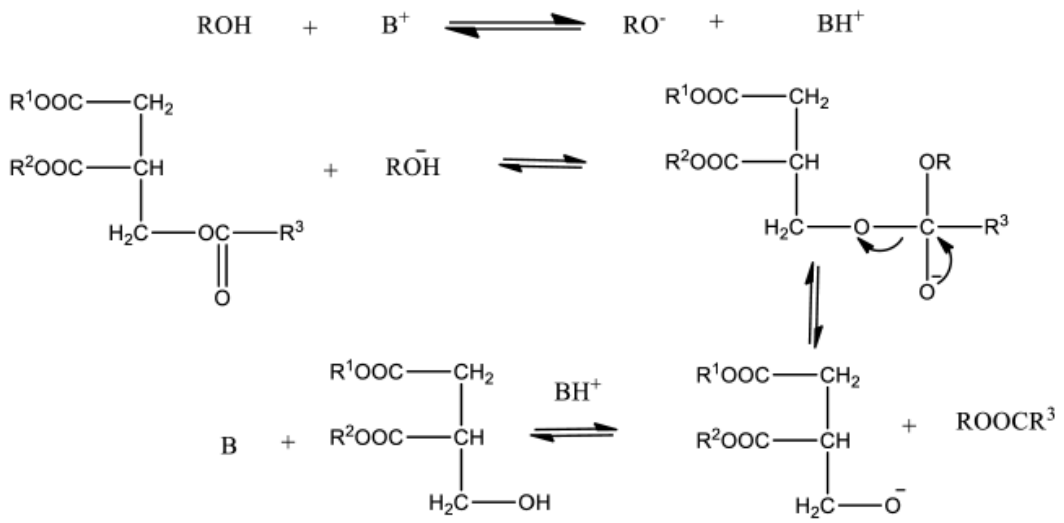

SCHEME 12.4 General reaction mechanism for base catalyzed transesterification of triglycerides [174].

catalyst; ultimately the product is free from any major catalytic impurities. Commonly used solid base catalysts are alkaline earth metal oxides, zeolite, KNO_3 loaded on Al_2O_3, KNO_3/Al_2O_3, BaO, SrO, CaO, MgO, etc. Among the solid base catalysts BaO takes minimum time while MgO takes the maximum time to complete the reaction.

12.2.5.2.1 Different Heterogeneous Catalysts For Biodiesel Production

The development of stable and cost-effective heterogeneous catalysts has been studied using different transesterification conversion technologies for biodiesel synthesis based on ultrasonication and microwave- assisted treatment, super critical fluid extraction, solvent engineering and synergetics of different mixed metal oxides. As a bulk commodity with low revenue, biodiesel production is strongly affected by the prices of oil feedstock. Hence, value-added derivatives are highly significant [179]. In esterification and transesterification processes, the triglycerides are converted to FAMEs and glycerol as a by-product. Additionally, the high yield production of biodiesel is influenced by the purity of the feedstock, amount of catalyst, temperature and oil to methanol ratio. In general, it is required to give a pretreatment to the feedstock to remove the FFAs and water. In fact, many researchers have reported the potential advantages of the use of mixed metal oxide catalyst over homogeneous catalysis. The heterogeneous requires 4–20% refining cost, which is comparatively less compared to homogeneous catalyst. However, many additional and challenging issues remain to be resolved before efficient solid catalyst can be developed, and many investigations are underway. The transesterification with the mixed metal oxides can be catalyzed either by either acid or base catalyzed but base catalyzed manifest much higher catalytic than acid catalysts, but are suitable for deriving biodiesel from the refined oils having low content of free fatty acids (FFA) less than 0.5% [180]**.** Xu et al. synthesized KF/Zn(Al)O catalyst and its activity was compares with that of Zn-Al hydrotalcite-like compounds Zn(Al)O, KF, KF/γ-Al_2O_3 and KF/Zn, they observed that the KF/Zn(Al) O catalyst shows highest activity among other mixed oxides. For the effective results of catalyst in transesterification reaction is optimized with the

oil to methanol ratio 6:1, 3wt.% KF/Zn(Al)O and temperature 65°C for 3 hr yielding more than 95%, so the optimization is the key aspect for the effective catalytic activity. Materials to show enhanced catalytic activity they should have higher basicity, specific surface area, pore volume and size [181]. However, the optimization conditions like temperature, oil to methanol/ethanol ratio and catalyst in mole percentage are the prerequisites to obtain bio diesel in high yields. Among the current transesterification processes, the heterogeneous catalysis, that is, mixed metal oxides shows promising conversions than others.

12.2.5.2.2 Design of An Ideal Heterogeneous Catalyst

It is necessary for the researchers to find an ideal catalyst and also to know what are the factors affecting the stability, productivity, inactivity of a catalyst in transesterification process. This can lead to the designing of a catalyst in such a manner that it is showing highly stable and highly productive under different reaction conditions. There are some chemical and physical properties that can affect the stability and productivity of a heterogeneous catalyst. The chemical properties include: (i) acidic and basic properties of a catalyst, (ii) hydrophobic/hydrophilic character, (iii) calcination temperature, and (iv) leaching/reusability and physical properties include size, shape, pore structure, surface area and mechanical strength [182–184]. The basic catalysts, for example, KI, KF and KNO_3 doped with Al_2O_3 show good catalytic activity due to their basic sites involved in the formation of active species like K_2O and Aluminum alkoxides at low temperatures [66–68]. Active basic sites originated by the ionization of the Na and K from catalysts like Na/NaOH/γ-Al_2O_3 and K/KOH/γ-AI_2O_3 [185, 186] but the leachablity of these ions makes the process least stable towards the reaction conditions. Among the catalysts $Ca(NO_3)_2/Al_2O_3$, $LiNO_3/Al_2O_3$, $NaNO_3/Al_2O_3$ and $Mg(NO_3)_2/Al_2O_3$, calcium nitrate/aluminate is showing better catalytic activity and also stable towards transesterification than any other because of the formation of inactive forms like Na and Mg aluminum phases and leaching of Li ions form lithium nitrate aluminates [187]. Metal oxides are widely (CaO, SrO, BaO) used in the biofuel production, but they required high calcination temperatures (500–1050°C) and CaO undergo

calcination process by nucelophic reaction and increases the basic properties of catalyst [188]. This could be due to the reaction of CaO with alcohol to form an protonated catalyst and alkoxide (RO^-) ion which undergoes a nucleophilic attack on carbonyl group of the triglycerides then generates a tetrahedral intermediate [189] and then the ester is generated. It is imperative that in all metallic catalysts should be designed in such a way that the catalyst is having the property of making the carbonyl group is more electophilic during catalyst- substrate interaction and it is susceptible to the nucleohilic attack [190–192]. In the case of CaOMe the ionized methoxide ion is a stronger base and increases the rate of reaction. In case of SrO, the calcination temperature needed is 1200 °C for high yields of biofuel [193]. In the case of hydrotalcites (MgO/Al_2O_3) the temperatures required is above 180 °C for achieving 90% yields [194]. Further, the doping of small amount of Al^{3+} to pure MgO makes it more basic than in its pure form because of generation of Lewis acid-strong base sites [195] this clearly shows the dependence of catalytic activity on surface area and basic sites [196]. The catalytic activity of zeolites depends up on the ion exchange capacity, which is directly related to its basicity and size and porosity of the zeolite. So the bigger size zeolite like CsX is having least conversion efficiency than KX. Even water, FFA present in feedstock affects the rate of reaction. The presence of 1.0% to 4.0% of water decreases the yield of methyl ester drastically from 95.39% to 86.72% [197]. However, the catalytic activity can be increased by introducing hydrophobic nature to the catalyst.

(a) Influence of Hydrophobic Character of the Catalyst

The hydrophilic and hydrophobic characters of a catalyst exhibit important role in the catalyst design. The hydrophobic character of a catalyst requires the following properties: (i) it is necessary to absorb the oil on to its surface, (ii) the adsorption is not to deactivate the catalyst sites [198]. When it is strongly adsorbed and the by-products like glycerol and water are produced which are going to be involved in saponification process leading to low yields. Hydrophobicity of acidic and basic zeolites zeolite is controlled by the use of Si/Al ratio [199, 200]. Similarly hydrophobic nature is also achieved by sulfonation of incompletely carbonized starch [201].

(b) Influence of Pore Size of the Material

Porosity of a material plays an important role in activity of the catalyst and the pore size starts from 2 to 50 nm [202]. Even though mesoporous materials are thermally least stable and showing least reactivity than zeolite materials [203], but a combination of these mesoporous materials with different catalysts exhibit wonderful results. Sulfonated mesoporous carbon having strong acidic sites gives more stability and catalytic activity to the catalyst [204]. It is necessary to make the pore size more than 1.2 nm which allows the fatty acid molecule to undergo transesterification otherwise it blocks the pore and activity of the catalyst decreases [205]. For example, MCM-41 catalyst gives lower yields than polystyrene [206]. Mesoporous calcium methoxide (H_3PO_4/Al_2O_3) catalysts having a bigger pore size (100 and 1400 nm) on its surface area make the material more catalytic and high conversion rates when compared with the lower pore size materials. This is because of an accumulation of water and methanol at hydrophilic sites and hinders the activity of the catalyst.

(c) Influence of Surface Area

Generally an increase in the surface area leads to better catalytic activity [207, 208] and this property depends upon the calcination temperatures. The surface area of tungstated zirconia is decreased to 20% (58-m^2/g) from the actual (325-m^2/g) during the calcination temperature changed from 800 to 900°C [209]. Among catalysts like TiO_2, ZrO_2, TiO_2-SO_4^{2-} and ZrO_2-SO_4^{2-} surface area of TiO_2 and ZrO_2 increases by introducing sulfate, efficiency of the catalyst also increases [210]. For instance mixed metal carbonate precursor (CaO/ZnO) are showing better activity than the calcinated metal oxides, this is because of lose in the active sites in surface area at calcinated temperatures [211, 212].

12.3 CONCLUSIONS AND FUTURE PROSPECTS

There are many issues remain still unclear and require further research for the efficient bioenergy systems. The most studied examples were carried out with small-scale experiments using small batch mini-autoclaves. The product separation from thermochemical conversion of biomass is

also a critical issue as it may affect the conversions of biocrude oil. The high heating rate may also influence the recovery of either catalysts or microorganisms, and there are not much details available on this topic. Experiments should be designed in such a way that they represent the real conditions as close as possible.

Conversion of biomass materials to energy is an environmentally friendly approach to meet the energy demands and this can address waste issues. Biomass, an alternative feedstock, can be converted into liquid and gaseous biofuels through thermochemical, photochemical, catalytic and bio-methods. The photocatalytic treatment of biomass using nanocrystalline titania photocatalysts has recently become more attractive. Also, hydrogen production through the photocatalysis of water as the cathodic reaction of an optically illuminate photochemical is effective in an aqueous electrolyte containing a biomass product (carbohydrates) thus producing liquid fuels and useful chemicals. Therefore, fuel cell system provides a novel way of energy conversion for the future research. The two main technologies presently used to convert biomass into energy are thermochemical and biochemical approaches. The selection of a conversion technology for biomass depends on the form in which the energy is required. Among them, pyrolysis and transesterification produce liquid fuels suitable for use as transportation fuels. Gasification/pyrolysis and anaerobic digestion is currently a cost-effective fuel.

For this purpose a defined set of technology breakthroughs will be required to develop the optimum utilization of algal biomass for the commercial production of biofuel. If these technological breakthroughs occur, biofuels based on algal biomass will play a role in the future energy systems. At the current stage of development, it is still too early to comments on any preferred routes of biofuels production from algal biomass. Finally, comprehensive life cycle assessment of algal biofuels illustrating environmental benefits and impacts can and should be a tool for guiding technology development as well as for policy decisions. Hydrothermal liquefaction of microalgae appears to be a very promising technology for biofuel production, but still in a very early stage of development. Nowadays, the development of bioenergy industries has gained importance for its sustainable energy production and deliverance all over the world. Even though fossil fuels, nuclear energy and hydroelectricity contribute to the

bioenergy production, the availability of bioenergy is still in scarce level. There are various techniques being adopted for the production of bioenergy in sustainable environment considering the pollution as a major factor. Due to the limitations from the conventional technology, MFC is an attractive application in terms of bioenergy production as well wastewater treatment.

12.4 ACKNOWLEDGEMENTS

The authors are grateful to VIT University for providing the facilities and constant encouragement.

KEYWORDS

- **Cellulose**
- **Crude oil resources**
- **Dimethyl ethanol**
- **Fatty acid methyl esters**
- **Fischer–tropsch diesel**
- **Hemi-cellulose**
- **Hydrogen**
- **Lignin**
- **Polymer of glucose**
- **Synthetic natural gas**

REFERENCES

1. Freni, S., Cavallaro, S. (2003). Production of hydrogen for MC fuel cell by steam reforming of ethanol over MgO supported Ni and Co catalysts, Catal. Commun., *6,* 259–268; (1a) Frusteri, F., Freni, S., Spadaro, L., Chiodo, V., Bonura, G., Donato, S; Cavallaro, S. (2004). H2 production for MC fuel cell by steam reforming of ethanol over MgO supported Pd, Rh, Ni and Co catalysts, Catal. Commun., *5,* 611–615.
2. Huber, G. W., Shabaker, J. W., Dumesic, J. A. (2003). Raney Ni–Sn catalyst for H2 production from biomass-derived hydrocarbons, Science, *300,* 2075–2077.

3. Ragauskas, A. J., Williams, C. K., Davison, B. H., Britovsek, G., Cairney, J., Eckert, C. A., Frederick, W. J., Hallett, J. P., Leak, D. J., Liotta, C. L., Mielenz, J. R., Murphy, R., Templer, R., Tschaplinski, T. (2006). The path forward for biofuels and biomaterials, Science, *311,* 484–489.
4. Moon, J. H., Lee, J. W., Lee, U. D. (2011). Economic analysis of biomass power generation schemes under renewable energy initiative with Renewable Portfolio Standards (RPS) in Korea. Bioresour. Technol. *102,* 9550–9557.
5. Tijmensen, M. J. A., Faaij, A. P. C., Hamelinck, C. N., van Hardeveld, M. R. M. (2002). Exploration of the possibilities for production of Fischer Tropsch liquids and power via biomass gasification. Biomass Bioenergy. *23,* 129–152.
6. Liu, S., Tan, X., Li, K., Hughes, R. (2001). Methane coupling using catalytic membrane reactors, Catal. Rev. Sci. Eng. *43,* 147–198.
7. Petrus, L., Minke, A. (2006). Noordermeer. Biomass to biofuels, a chemical perspective, Green Chem. *8,* 861–867.
8. McKendry P. Energy production from biomass (Part 2): overview of biomass. Bioresour. Technol. (2002). *83,* 37–46.
9. Bridgwater, A. V., Peacocke, G. V. C. (2000). Fast pyrolysis process for biomass. Renew Sustain Energy Rev. *4,* 1–73.
10. Goyal, H. B., Seal, D., Saxena, R. C. (2008). Bio-fuels from thermochemical conversion of renewable resources: a review. Renew Sustain Energy Rev. *12,* 504–517.
11. Simonetti, D. A., Hansen, R. J., Kunkes, E. L., Soares, R. R., Dumesic, J. A. (2007). Coupling of glycerol processing with Fischer-Tropsch synthesis for production of liquid fuels. Green Chem. *9,* 1073–1083.
12. Kalinci, Y., Hepbasli, A., Dincer, I. (2012). Exergoeconomic analysis and performance assessment of hydrogen and power production using different gasification systems. Fuel. *102,* 187–198.
13. Swanson, R., Platon, A., Satrio. J., Brown, R. C. (2010). Techno-economic analysis of biomass-to-liquids production based on gasification. Fuel. *89,* 11–19.
14. Nadia, H. L., Akinwale, O. A., Johannes, H. K., Johann, F. G. (2013). Process efficiency of biofuel production via gasification and Fischer–Tropsch synthesis. Fuel. *109,* 484–492.
15. Kwangsu, K., Youngdoo, K., Changwon, Y., Jihong, M., Beomjong, K., Jeongwoo, L., Uendo, L., Seehoon, L., Jaeho, K., Wonhyun, E., Sangbong, L., Myungjin, K., Yunje, L. (2013). Long-term operation of biomass-to-liquid systems coupled to gasification and Fischer–Tropsch processes for biofuel production. Biores Technol. *127,* 391–399.
16. Berrueco, C., Recari, J., Matas, G. B., Del, A. G. (2014). Pressurized gasification of torrefied woody biomass in a lab scale fluidized bed. Energy. *70,* 68–78.
17. Danica, D. I., Erik, D., Louise, T., Göran, B. (2014). Integration of biofuel production into district heating- part I: an evaluation of biofuel production costs using four types of biofuel production plants as case studies. J. Cleaner Prod. *69,* 176–187.
18. Elliott, D. C. (2007). Historical Developments in Hydroprocessing Bio-oils. Energy Fuels *21,* 1792–1815.
19. Diego, L. B., Wolter, P., Frederik, R., Wim, B. (2013). Hydrothermal liquefaction (HTL) of microalgae for biofuel production: State-of-the-art review and future prospects. Biomass Bioenergy. *53,* 113–127.

20. Moumita, C., Armando, G. M., Caleb. N., Shulin, C. (2013). An α-glucan isolated as a coproduct of biofuel by hydrothermal liquefaction of *Chlorella sorokiniana* biomass. Algal Res. *2,* 230–236.
21. Erik, R. V., Richard, L. S., Mark, S. W., Andre, M. C. (2014). A national-scale comparison of resource and nutrient demands for algae-based biofuel production by lipid extraction and hydrothermal liquefaction. Biomass Bioenergy. *64,* 276–290.
22. Bahar, M., Arif, H., Sibel, I., Oktay, E. (2014). Biofuel production by liquefaction of kenaf (*Hibiscus cannabinus* L.). Biores Technol. *151*, 278–283.
23. Lupa C. J., Wylie, S. R., Shaw, A., Al-Shamma'a. A., Sweetman, A. J., Herbert, B. M. J. (2012). Experimental analysis of biomass pyrolysis using microwave-induced plasma. Fuel Process Technology. *97,* 79–84.
24. Carlos, J. D. N., Eduardo, B. S., Ricardo, A., Dolivar, C. N., Carlos, R. S. (2014). Production of biofuels from algal biomass by fast pyrolysis. Biofuels from Algae. *1,* 143–153.
25. Mohan, D., Pittman, C. U., Steele, P. H. (2006). Pyrolysis of wood/biomass for bio-oil: a critical review. Energy Fuels. *20,* 848–889.
26. David, M. A., Jesse, Q. B., James, A. D. (2010). Catalytic conversion of biomass to biofuels. Green Chem. *12,* 1493–1513.
27. Yin, C. (2012). Microwave-assisted pyrolysis of biomass for liquid biofuels production. Biores Technol. *120,* 273–284.
28. Shoujie, R., Hanwu, L., Lu, W., Gayatri, Y., Yupeng, L., James, J. The integrated process of microwave torrefaction and pyrolysis of corn stover for biofuel production. J. Anal. Appl. Pyrolysis. 2014; DOI: 10.1016/j.jaap.2014.04.008.
29. Putun, A. E., Ozcan, A., Gercel, H. F., Putun, E. (2001). Production of biocrudes from biomass in a fixed bed tubular reactor. Fuel. *80,* 1371–1378.
30. Ozbay, N., Putun, A. E., Uzun, B. V., Putun, E. (2001). Biocrude from biomass: pyrolysis of cotton seed cake. Renew Energy. *24,* 615–25.
31. Onay, O., Kockar, O. M. (2004). Fixed bed pyrolysis of rapeseed (Brassica napus L.). Biomass Bioenergy. *26,* 289–99.
32. Luo, Z., Wang, S., Liao, Y., Zhou, J., Gu, Y., Cen, K. (2004). Research on biomass fast pyrolysis for liquid fuel. Biomass Bioenergy. *26,* 455–62.
33. Gercel, H. F. (2002). Production and characterization of pyrolysis liquids from sunflower pressed bagasse. Bioresource Technol. *85,* 113–7.
34. Lede, J., Bouton, O. Flash pyrolysis of biomass submitted to a concentrated radiation. Application to the study of the primary steps of cellulose thermal decomposition. In: Division of fuel chemistry; reprints of symposia, vol. 44 (2), 217th ACS meeting, 21–25 March, Anaheim, USA, 1999.
35. Kumar, R., Kumar, R. G. (2011). Microwave assisted alkali-catalyzed transesterification of Pongamia pinnata seed oil for biodiesel production. Bioresour. Technol. *102,* 6617–662.
36. Lin, Y. C., Yang, P. M. (2013). Biodiesel production assisted by 4-allyl-4-methylmorpholin-4-ium bromine ionic liquid and a microwave heating system. Appl. Therm. Eng. *61,* 570–576.
37. Wali, W. A., Hassan, K. H. (2013). Real time monitoring and intelligent control for novel advanced microwave biodiesel reactor. Measurement, *46,* 823–839.

38. Yan, Y., Xiang Li, X. (2014). Biotechnological preparation of biodiesel and its high-valued derivatives: A review. Appl. Energy, *113,* 1614–1631.
39. Patil, P. D., Gnaneswar, V. G. (2011). Optimization of microwave-assisted transesterification of dry algal biomass using response surface methodology. Bioresour. Technol. *102,* 1399–1405.
40. Cui, Y., Liang, Y. (2014). Direct transesterification of wet Cryptococcus curvatus cells to biodiesel through use of microwave irradiation. Appl. Energy. *119,* 438–444.
41. Foo, K. Y., Hameed, B. H. Microwave-assisted preparation and adsorption performance of activated carbon from biodiesel industry solid reside: Influence of operational parameters. Bioresour. Technol.2012, 103, 398–404.
42. Cheng, J., Tao Yu, T. (2013). Using wet microalgae for direct biodiesel production via microwave irradiation. Bioresour. Technol. *131,* 531–535.
43. Jaliliannosrati. H; Amin, N. A. S. (2013). Microwave assisted biodiesel production from Jatropha curcas L. seed by two-step insitu process: Optimization using response surface methodology. Bioresour. Technol. *136,* 565–573.
44. Khemthong, P., Luadthong, C. (2012). Industrial eggshell wastes as the heterogeneous catalysts for microwave-assisted biodiesel production. Catal. Today. *190,* 112–116.
45. Dai, Y. M; Chen, K. T. (2014). Study of the microwave lipid extraction from microalgae for biodiesel production. Chem. Eng. J. *250,* 267–273.
46. Liaob, C. C., Chung, T. W. (2011). Analysis of parameters and interaction between parameters of the microwave-assisted continuous transesterification process of Jatropha oil using response surface methodology. Chem. Eng. Res. Des. *89,* 2575–2581.
47. Liao, C. C., Chung. T. W. (2013). Optimization of process conditions using response surfacemethodology for the microwave-assisted transesterificationof Jatropha oil with KOH impregnated CaO as catalyst. Chem. Eng. Res. Des. *91*, 2457–2464.
48. Chen K. S., Lin, Y. C. (2012). Improving biodiesel yields from waste cooking oil by using sodium methoxide and a microwave heating system. Energy. *38,* 151–156.
49. Liu, W., Yin, P. (2013).Microwave assisted esterification of free fatty acid over a heterogeneous catalyst for biodiesel production. Energy Convers. Manage. *76*, 1009–1014.
50. Lertsathapornsuka, V., Pairintra, R. (2008). Microwave assisted in continuous biodiesel production from waste frying palm oil and its performance in a 100 kW diesel generator. Fuel Process. Technol. *89,* 1330–1336.
51. Hernando, J; Leton. P. (2007). Biodiesel and FAME synthesis assisted by microwaves: Homogeneous batch and flow processes. Fuel. *86,* 1641–16.
52. Hsiao, M. C., Lin, C. C. (2011). Microwave irradiation-assisted transesterification of soybean oil to biodiesel catalyzed by nanopowder calcium oxide. Fuel *90,* 1963–1967.
53. Manco, I., Giordani, L. (2012). Microwave technology for the biodiesel production: Analytical assessments. Fuel *95,* 108–112.
54. Alex de Nazaré de Oliveira. (2013). Microwave-assisted preparation of a new esterification catalyst from wasted flint kaolin. Fuel. *103,* 626–631.
55. Azcan, N; Yilmaz, O. (2013). Microwave assisted transesterification of waste frying oil and concentrate methyl ester content of biodiesel by molecular distilation. Fuel. *104,* 614–619.

56. Lin, Y. C., Hsu, K. H. (2014). Rapid palm-biodiesel production assisted by a microwave system and sodium methoxide catalyst. Fuel. *115,* 306–311.
57. Kamath, V. H., Regupathi, I. (2011).Optimization of two step karanja biodiesel synthesis under microwave irradiation. Fuel Process. Technol. *92*, 100–105.
58. Duz, Z. M., Saydut, A. (2011).Alkali catalyzed transesterification of safflower seed oil assisted by microwave irradiation. Fuel Process. Technol. *92*, 308–313.
59. Gole, V. L., Gogate, P. R. (2013). Intensification of synthesis of biodiesel from nonedible oil using sequential combination of microwave and ultrasound. Fuel Process. Technol. *106,* 62–69.
60. Ibrahim, N., Kamarudin, S. K., Minggu, L. J. (2014). Biofuel from biomass via photo-electrochemical reactions: An overview. J. Power Sour. *259,* 33–42.
61. Trent, C. Y., Jyothi, K., Samuel, A., Miranda, M., Xiangling, L., Fan, L., Wensheng Q. (2014). Chapter 5: Biofuels and Bioproducts Produced through Microbial Conversion of Biomass. Bioenergy Research: Advances Applications. *1,* 71–93.
62. Nicolas, L. F., Antoine, M., Senta, B., Jean-Guy, B. (2014). Chapter 17—Use of Cellulases from Trichoderma reesei in the Twenty-First Century—Part I: Current Industrial Uses and Future Applications in the Production of Second Ethanol Generation. Biotechnology Biology of Trichoderma. *1,* 245–261.
63. Horikoshi, K. (1996). Alkaliphiles from an industrial point of view. FEMS Microbiol Rev. *18,* 259–270.
64. Mitchell, D. A., Lousane, B. K., In general principles of solid state fermentation, Monogram, Ed. By Doelle H. W., Ro13c. Publication of Oxford Univ., London. 1990.
65. Akpon, A. A., Adebiyi, A. B., Akinyanju, J. A. (1996). Partial purification and characterization of Alpha amylase from *Bacillus cereus* BC 19. J Agric Sci Technol. *2,* 152–157.
66. El-Saadany, R. M. A., Salem, F. A., El-Manawaty, H. K. (2006). A high yield of amylase from *Aspergillus niger*by effect of gamma irradiation. Starch. *36,* 64–66.
67. Sindhu, M. K., Singh, B. K., Prased, T. (1997). Changes in starch content of anhar seed due to fungal attack. In. Phytopathol. *34,* 269–271.
68. Aneja, K. R. (2003). Experiments in Microbiology Plant Pathology and Biotechnology, New Age International (P) Ltd., Publishers, New Delhi, Fourth Edition.
69. Guzman-Maldonato, H., Paredes-Lopes. O. (1995). Amylolytic enzymes and products derived from starch: a review. Crit Rev Food Sci Nut. *35,* 373–403.
70. James, J. A., Lee, B. H. (1997). Glucoamylases: Microbial sources, industrial application and molecular biology-A review. J Food Biochem. *21,* 1–52.
71. Pandey, A., Nigam, P., Soccol, C. R., Soccol, V. T., Singh. D., Mohan, R. (2002). Advances in microbiological amylases. Biotechnol Appl Biochem. *31,* 136–152.
72. Buzzini, P., Martini, A. (2002). Extracellular enzymatic activity profiles in yeast and yeast-like strains isolated from tropical environments. J. Applied Microbiol. *93,* 1020–1050.
73. Bajpai, P., Bajpai, P. K. (1999). High-temperature alkaline alpha-amylase from *Bacillus licheniformis* TCRDC-B13. J. Biotechnol. *33,* 72–78.
74. Demiorijan, D., Moris-Varas, F., Cassidy, C. (2001). Enzymes from extremophiles. J. Microbiol, *57,* 144–151.

75. Burhan, A., Nisa, U., Gokhan, C., Colak, Ö., Ashabil, A., Osmair, G. (2003). Enzymatic properties of a novel thermostable, thermophilic, alkaline and chelator resistant amylase from an alkaliphilic Bacillus sp. isolate ANT-6. Process Biochem. *38,* 1397–1403.
76. Sanchez, O. J., Cardona, C. A. (2008). Trends in biotechnological production of fuel ethanol from different feedstocks. Biores Technol. *99,* 5270–5295.
77. Moraes, L. M. P., Filho, S. A., Ulhoa, C. J. (1999). Purification and some properties of an α-amylase glucoamylase fusion protein from *Saccharomyces cerevisiae*. World J Microbiol Biotechnol. *15,* 561–564.
78. Aline, M. C., Leda, R. C., Denise, M. G. F. (2011). An overview on advances of amylases productionand their use in the production of bioethanol by conventional and nonconventional processes. Biomass Conv Bioref. *1,* 245–255.
79. Toksoy, O. E. (2006). Optimization of ethanol production from starch by an amylolytic nuclear petite *Saccharomyces cerevisiae* strain. Yeast. *23,* 849–856.
80. Chi, Z., Chi, Z., Liu, G., Wang, F., Ju, L., Zhang, T. (2009). *Saccharomycopsis fibuligera* and its applications in biotechnology. Biotechnol Adv. *27,* 423–43.
81. Saxena, R. K., Dutt, K., Agarwal, L., Nayyar, P. A. (2007). A highly thermostable and alkaline amylase from a *Bacillus sp*. PN5. Biores Technol. *98,* 260–265.
82. Mobini-Dehkordi, M; Nahvi. I., Zarkesh-Esfahani, H., Ghaedi, K., Tavassoli, M., Akada, R. (2008). Isolation of a novel mutant strain of Saccharomyces cerevisiae by ethyl methyl sulfonate mutagenesis approach as a high producer of bioethanol. J Biosci Bioengin. *105,* 403–408.
83. Mobini-Dehkordi, M., Nahvi, I., Zarkesh, H., Ghaedi, K., Akada, R. (2011). Characterization of an interesting novel mutant strain of commercial *Saccharomyces cerevisiae*. Iranian J. Biotechnol. *9,* 109–114.
84. Prakasham, R. S., Rao, C. S., Rao, R. S., Sarma, P. N. Enhancement of acid amylase production by an isolated *Aspergillus awamori*. J Appl Microbiol 2007; 102, 204–211.
85. Al-Turki, A. I., Khattab, A. A., Ihab, A. M. (2008). Improvement of glucoamylase production by *Aspergillus awamori* using microbial biotechnology techniques. Biotechnol. *7,* 456–462.
86. Nagamine, K., Murashima, K., Kato, T., Shimoi, H. (2003). Mode of α-amylase production by the shochu koji mold *Aspergillus kawachii*. Biosci Biotechnol Biochem. *67,* 2194–2202.
87. Gomes, E., Souza, S. R., Grandi, R. P., Silva, R. (2005). Production of thermostable glucoamylase by newly isolated *Aspergillus flavus* A 1.1 and *Thermomyces lanuginosus* A 13.37. Braz J Microbiol. *36,* 75–82.
88. Esfahanibolandbalaie, Z., Rostami, K., Mirdamadi, S. S. (2008). Some studies of α-amylase production using Aspergillus oryzae. Pak J Biol Sci. *11,* 2553–2559.
89. Gargi, D., Abhijit, M., Rintu, B., Maiti, B. R. (2001). Enhanced production of amylase by optimization of nutritional constituents using response surface methodology. Biochem. Eng. J. *7,* 227–231.
90. Oliveira, A. N., Oliveira, L. A., Andrade, J. S., Chagas Junior, A. F. (2007). Rhizobia amylase production using various starchy substances as carbon substrates. Braz J Microbiol. *38,* 208–216.

91. Peixoto, S. C., Jorge, J. A., Terenzi, H. F., Polizeli, M. L. T. M. (2003). Rhizopus microsporus var. rhizopodiformis: a thermotolerant fungus with potential for production of thermostable amylases. Int Microbiol. *6,* 269–273.
92. Shafique, S., Bajwa, R., Shafique, S. (2009). Screening of *Aspergillus niger* and *A. flavus* strains for extra cellular alpha-amylase activity. Pak J Bot. *41,* 897–905.
93. Orji, J. C., Nweke, C. O., Nwabueze, R. N., Nwanyanwu, C. E., Alisi, C. S., Etim-Osowo, E. N. (2008). Production and properties of α-amylase from Citrobacterspecies. Ambiente e Água Interdiscip. J Appl Sci. *4,* 45–57.
94. Costa, J. A. V., Eliane, C., Glênio, M., Lucielen, O. D. S., Mauricio, V., Telma, E. B. (2007). Simultaneous Amyloglucosidase and Exo-polygalacturonase Production by *Aspergillus niger* using Solid-state Fermentation. Brazilian Archives of Biology And Technology. *50,* 759–766.
95. Zambare, V. (2010). Solid state fermentation of *Aspergillus oryzae* for glucoamylase production on agro residues. Int J Life Sci. *4,* 16–25.
96. Anto, H., Trivedi, U. B., Patel, K. C. (2006). Glucoamylase production by solid-state fermentation using rice flake manufacturing waste products as substrate. Biores Technol. *97,* 1161–1166.
97. Sindhu, R., Suprabha, G. N., Shashidhar, S. (2009). Optimization of process parameters for the production of α-amylase from *Penicillium janthinellum* (NCIM 4960) under solid state fermentation. Afr J Microbiol Res. *3,* 498–503.
98. Haiyan, S., Xiangyang, G., Weiguo, Z. (2007). Production of novel raw-starch-digesting glucoamylase by *Penicillium* sp. X-1 under solid state fermentation and its use in direct hydrolysis of raw starch. World J Microbiol Biotechnol. *23,* 603–613.
99. Kumar, S., Satyanarayana, T. Statistical optimization of a thermostable and neutral glucoamylase production by a thermophilic mold *Thermomucor indicae-seudaticae* in solid-state fermentation. World J Microbiol Biotechnol. (2004). *20,* 895–902.
100. Kunamneni. A., Permaul. K., Singh, S. (2005). Amylase production in solid state fermentation by the thermophilic fungus *Thermomyces lanuginosus*. J Biosci Bioeng. *100,* 168–171.
101. Akihiko, T., Nami, N., Miki, O., Saori. M., Shuji. K., Masataka. S., Keizo. Y., Comprehensive enzymatic analysis of the amylolytic system in the digestive fluid of the sea hare, Aplysia kurodai: Unique properties of two α-amylases and two α-glucosidases. FEBS Open Bio 2014; DOI: 10.1016/j.fob.2014.06.002.
102. Edem, C. B., Moses. M. Chemical Pretreatment Methods for the Production of Cellulosic Ethanol: Technologies and Innovations. Int J Chem Eng 2013; DOI: 10.1155/2013/719607.
103. Zhu, J. Y., Pan, X. J., Wang, G. S., Gleisner, R. (2009). Sulfite pretreatment (SPORL) for Robust enzymatic saccharification of spruce and red pine. Biores Technology. *100,* 2411–2418.
104. Macfarlane, A. L., Farid, M. M. Chen JJJ. Organosolv delignification of willow Lambert Academic Press, 2010; ISBN 978-3-8383-9155-7.
105. Jeffries, T. W., Jin, Y. S. (2004). Metabolic engineering for improved fermentation of pentoses by yeasts. Appl Microbiol Biotechnol. *63,* 495–509.
106. Ohgren, K., Bengtsson, O., Gorwa-Grauslund, M. F., Galbe, M., Hahn-Hagerdal, B., Zacchi, G. (2006). Simultaneous saccharification and cofermentation of glucose

and xylose in steam-pretreated corn stover at high fiber content with Saccharomyces cerevisiae TMB3400. J Biotechnol. *126,* 488–498.
107. Becker, J., Boles, E. A modified *Saccharomyces cerevisiae* strain that consumes L-Arabinose and produces ethanol. Appl Environ Microbiol. (2003). *69,* 4144–4150.
108. Karhumaa, K., Wiedemann, B., Hahn-Hagerdal, B., Boles, E., Gorwa-Grauslund, M. F. (2006). Co-utilization of L-arabinose and D-xylose by laboratory and industrial *Saccharomyces cerevisiae* strains. Microb Cell Fact. DOI: 10.1186/1475-2859-5-18.
109. Srini, R., Rohit, P. D., Randy, S. L. (2002). Formation of ethanol from carbon monoxide via a new microbial catalyst. Biomass and Bioenergy. 23. 487–493.
110. British Petroleum, BP Statistical Review of World Energy; 2009.
111. Brennan, L., Wende, P. O. (2010). Biofuels from microalgae—a review of technologies for production, processing, and extractions of biofuels and coproducts. Renew. Sust. Energ. Rev. *14,* 557–577.
112. Khan, S. A., Rashm, R., Hussain, Z., Prasad, S., Banerjee, U. C. (2009). Prospects of biodiesel production from microalgae in India. Renew.Sust. Energ. Rev. *13,* 2361–2372.
113. Ugarte, D. G., Walsh, M. E., Shapouri, H., Slinsky, P. (2003). The economic impacts of bioenergy crop production in US agriculture, USDA Agricultural Economic Report. *41,* 816.
114. Banerjee, A., Sharma, R., Chisti, Y., Banerjee, U. C. (2002). Botryococcusbrauni: a renewable source of hydrocarbons and other chemicals. Crit. Rev.Biotechnol. *22,* 245–279.
115. Ormerod, W. G., Freund, P., Smith, A., Davison, J. (2002). Ocean storage of CO. IEAgreenhouse gas R&D program. UK, IE.
116. Radakovits, R., Jinkerson, R. E., Darzins, A., Posewitz, M. C. (2010). Genetic engineering of algae for enhanced biofuel production. Eukaryot. Cell. *9,* 486–501.
117. Wijffels, R. H., Barbosa, M. J. (2010). An outlook on microalgal biofuels. Science. *329,* 796–799.
118. Rasala, B. A. (2013). Genetic engineering to improve algal biofuels production. In Algae for Biofuels and Energy (Borowitzka, M.A and Moheimani, N. R., eds), 99–113.
119. Chisti, Y., Yan, J. (2011). Energy from algae: current status and future trends: algal biofuels: a status report. Appl. Energy. *88,* 3277–3279.
120. Petkov, G. (2012). A critical look at the microalgae biodiesel. Eur. J. Lipid Sci. Technol. *114,* 103–111.
121. Den Haan, R., Rose, S. H., Lynd, L. R., van Zyl, W. H. (2007). Hydrolysis and fermentation of amorphous cellulose by recombinant Saccharomyces cerevisiae. Metab. Eng. *9,* 87–94.
122. Shin, H. D., McClendon, S., Vo, T., Chen, R. R. (2010). Escherichia colibinary culture engineered for direct fermentation of hemicellulose to a biofuel. Appl. Environ. Microbiol. *76,* 8150–8159.
123. Fu, Z., Holtzapple, M. T. (2010). Consolidated bioprocessing of sugarcane bagasse and chicken manure to ammonium carboxylates by a mixed culture of marine microorganisms. Bioresour. Technol. *101*, 2825–2836.

124. Higashide, W., Li, Y., Yang, Y., Liao, J. C. (2011). Metabolic engineering ofClostridiumcellulolyticum for isobutanol production from cellulose. Appl. Environ. Microbiol. *77,* 2727–2733.
125. Zhang, X. Z., Sathitsuksanoh, N., Zhu, Z., Percival Zhang, Y. H. (2011). One-step production of lactate from cellulose as the sole carbon source without any other organic nutrient by recombinant cellulolyticBacillussubtilis. Metab. Eng. *13*, 364–372.
126. Deng, Y., Fong, S. S. (2011). Metabolic engineering of Thermobifidafuscafor direct aerobic bioconversion of untreated lignocellulosic biomass to 1-propanol. Metab. Eng. *13,* 570–577.
127. Talluri, S., Raj, S. M., Christopher, L. P. (2013).Consolidated bioprocessing of untreated switchgrass to hydrogen by the extreme thermophile Caldicellulosiruptorsaccharolyticus DSM 8903. Bioresour. Technol. *139*, 272–279.
128. Choix, F. J. (2012). Enhanced accumulation of starch and total carbohydrates in alginate-immobilized Chlorella spp. induced by Azospirillumbrasilense: II. Heterotrophic conditions. Enzyme. Microb. Technol. *51,* 300–330.
129. de-Bashan, L. E. (2002). Removal of ammonium and phosphorus ions from synthetic wastewater by the microalgae Chlorella vulgaris co immobilized in alginate beads with the microalgae growthpromoting bacterium Azospirillumbrasilense. Water. Res. *36,* 2941–2948.
130. Abed, R. M. M. (2010). Interaction between cyanobacteria and aerobic heterotrophic bacteria in the degradation of hydrocarbons. Int. Biodeterior. Biodegrad. *64,* 58–64.
131. Strik, D. P. B. T. B. (2011). Microbial solar cells: applying photosynthetic and electrochemically active organisms. Trends Biotechnol. *29,* 41–49.
132. Rittmann, B. E. (2008). Opportunities for renewable bioenergy using microorganisms. Biotechnol. Bioeng. *100,* 203–212.
133. Kaspar, H. F., Wuhrmann, K. (1978). Product inhibition in sludge digestion. Microb. Ecol. *4*, 241–248.
134. Lettinga, G. (1995). Anaerobic digestion and wastewater treatment systems. Antonie Van Leeuwenhoek, *67*, 3–28.
135. McCarty, P. L., Smith, D. P. (1986). Anaerobic wastewater treatment. Environ. Sci. Technol. *20,* 200–1206.
136. Logan, B. E., Regan, J. M. (2006). Electricity-producing bacterial communities in microbial fuel cells. Trends Microbiol. *14,* 512–518.
137. Lovley, R. D. (2006). Microbial fuel cells: novel microbial physiologies and engineering approaches. Curr. Opin. Biotechnol. *17,* 327–332.
138. Bond, D. R., Lovley, D. R. (2003). Electricity production by Geobactersulfurreducens attached to electrodes. Appl. Environ.Microbiol. *69,* 1548–1555.
139. Rabaey, K., Boon, N., Hofte, M., Verstraete, W. (2005). Microbial phenazine production enhances electron transfer in biofuel cells. Environ. Sci. Technol. *39,* 3401–3408.
140. Park, H. S., Kim, B. H., Kim, H. S., Kim, H. J., Kim, G. T., Kim, M., Chang, I. S., Park, Y. K., Chang, H. I. (2001). A novel electrochemically active and Fe (III)-reducing bacterium phylogenetically related to Clostridium butyricumisolated from a microbial fuel cell. Anaerobe. *7,* 297–306.
141. McCarty, P. L., Bae, J., Kim, J. (2011). Domestic wastewater treatment as a net energy producer – can this be achieved. Environ. Sci. Technol. *45,* 7100–7106.

142. Lovley, D. R. (2011). Live wires: direct extracellular electron exchange for bioenergy and the bioremediation of energy-related contamination. Energy. Environ. Sci. *4,* 4896–4906.
143. Smith, J. A., Lovley, D. R., Tremblay, P. L. (2013). Outer cell surface components essential for Fe (III) oxide reduction by Geobactermetallireducens. Appl. Environ. Microbiol. *79,* 901–907.
144. Mallakpour, S., Dinari, M. (2012). Ionic Liquids as Green Solvents: Progress and Prospects. In *Green Solvents II*, Mohammad, A., Inamuddin, D., Eds. Springer Netherlands, 1–32.
145. Atadashi, I. M., Aroua, M. K., Aziz, A. (2010). A High quality biodiesel and its diesel engine application: a review. Renew Sust Energ Rev. *14,* 1999–2008.
146. Wu, Q., Chen, H., Han, M., Wang, D., Wang, J. (2007). Transesterification of cottonseed oil catalyzed by Brønsted acidic ionic liquids. Industrial and Engineering Chemistry Research *46*, 7955–7960.
147. Zhang. L., Xian, M., He, Y., Li, L., Yang, J., Yu, S et al. (2009). A Bronsted acidic ionic liquid as an efficient and environmentally benign catalyst for biodiesel synthesis from free fatty acids and alcohols. Bioresour. Technol. *100,* 4368–4373.
148. Wang, C., CuiG., LuoX., XuY., LiH., Dai S. Highly efficient and reversible SO_2 capture by tunableazole-based ionic liquids through multiple-site chemical absorption. J. Am. Chem. Soc. *133,* 11916–11919.
149. Zhang. L., Xian, M., He, Y., Li, L., Yang, J., Yu S, et al. (2011). A Bronsted acidic ionic liquid as an efficient and environmentally benign catalyst for biodiesel synthesis from free fatty acids and alcohols. Bioresour. Technol. (2009). *100,* 4368–73.
150. Zhou, J., Lu, Y., Huang, B., Huo, Y., Zhang, K. (2011). Preparation of biodiesel from tung oil catalyzed by sulfonic-functional Bronested acidic ionic liquids. Adv. Mater. Res. 314–316, 1459–1462.
151. Liang, J. H., Ren, X. Q., Wang, J. T., Jinag, M., Li, Z. J. (2010). Preparation of biodiesel by transesterification from cottonseed oil using the basic dication ionic liquids as catalysts. Journal of Fuel Chemistry and Technology, *38,* 275–280.
152. Zhou, S., Liu, L., Wang, B., Xu, F., Sun, R. C. (2012). Biodiesel preparation from transester- ification of glycerol trioleate catalyzed by basic ionic liquids. Chin. Chem. Lett. *23,* 379–82.
153. Isahak, W. N. R. W., Ismail, M., Mohd Jahim, J., Salimon, J., Yarmo, M. A. (2011). Transester- ification of palm oil by using ionic liquids as a new potential catalyst. Trends Appl. Sci. Res. *6*, 1055–62.
154. Liang, X., Gong, G., Wu, H., Yang, J. (2009). Highly efficient procedure for the synthesis of biodiesel from soybean oil using chloroaluminate ionic liquid as catalyst. Fuel. *88,* 613–616.
155. Advances on biomass pretreatment using ionic liquids: An overview Haregewine Tadesse and Rafael Luque Energy Environ. Sci., (2011). *4,* 3913.
156. Charles, G., Cellulose Solution, US Patent 1 943 175, 1934.
157. Marzialetti, T., Olarte, M. B. V., Sievers, C., Hoskins, T. J. C., Agrawal, P. K., Jones, C. W. (2008). Dilute Acid Hydrolysis of Loblolly Pine: A Comprehensive Approach. Ind. Eng. Chem. Res. *47,* 7131–7140.
158. Mazza, M., Catana, D. A., Vaca-Garcia, C., Cecutti, C. (2009). Influence of water on the dissolution of cellulose in selected ionic liquids. Cellulose. *16,* 207–215.

159. Binder, J. B., Raines, R. T. (2009). Simple Chemical Transformation of Lignocellulosic Biomass into Furans for Fuels and Chemicals. J. Am. Chem. Soc. *131,* 1979–1985.
160. Stahlberg, T., Sorensen, M. G., Riisager, A. (2010). Direct conversion of glucose to 5-(hydroxymethyl) furfural in ionic liquids with lanthanide catalysts. Green Chem. *12,* 321–325.
161. Chun, J. A., Lee, J. W., Yi, Y. B., Hong, S. S., Chung, C. H. (2010). Catalytic production of hydroxymethylfurfural from sucrose using 1-methyl-3-octylimidazolium chloride ionic liquid. Korean J. Chem. Eng. *27,* 930–935.
162. Yong, G., Zhang, Y. G., Ying, J. Y. (2008). Efficient Catalytic System for the Selective Production of 5-Hydroxymethylfurfural from Glucose and Fructose. Angew. Chem., Int. Ed. *47,* 9345–9348.
163. Li, C. Z., Zhang, Z. H., Zhao, Z. B. K. Direct conversion of glucose and cellulose to 5-hydroxymethylfurfural in ionic liquid under microwave irradiation Tetrahedron Lett. (2009). *50,* 5403–5405.
164. Zhang, Z. H., Zhao, Z. B. K. (2010). Microwave-assisted conversion of lignocellulosic biomass into furans in ionic liquid Bioresour. Technol. *101,* 1111–1114.
165. Hu, S. Q., Zhang, Z. F., Song, J. L., Zhou, Y. X., Han, B. X. (2009). Efficient conversion of glucose into 5-hydroxymethylfurfural catalyzed by a common Lewis acid $SnCl_4$ in an ionic liquid. Green Chem. *11,* 1746–1749.
166. Stahlberg, T., Sorensen. M. G., Riisager, A. (2010). Direct conversion of glucose to 5-(hydroxymethyl) furfural in ionic liquids with lanthanide catalysts. Green Chem. *12,* 321–325.
167. Zhao, H. B., Holladay, J. E., Brown, H., Zhang, Z. C. (2007). Metal Chlorides in Ionic Liquid Solvents Convert Sugars to 5-Hydroxymethylfurfural.Science. *316,* 1597–1600.
168. Fan, M., Yang, J., Jiang, P., Zhang, P., Li, S. (2013). Synthesis of novel dicationic basic ionic liquids and its catalytic activities for biodiesel production. RSC Adv. *3,* 752.
169. Fang, D., Yang, J., Jiao, C. (2011). Dicationic Ionic Liquids as Environmentally Benign Catalysts for Biodiesel Synthesis. ACS Catal. *1,* 42–47.
170. Hu, L., Wua, Z., Xu, J., Sun, Y., Linc, L., Liu, S. (2014). Zeolite-promoted transformation of glucose into 5-hydroxymethylfurfural in ionic liquid. Chem. Eng. J. *244,* 137–144.
171. Guo, F., Fang, Z., Tian, X. F., Long, Y. D., Jiang, L. Q. (2011). One-step production of biodiesel from Jatropha oil with high-acid value in ionic liquids. Bioresour. Technol. *102,* 6469–6472.
172. Sinha, S., Agarwal, A., K, Garg S. (2008). Biodiesel development from rice bran oil: transesterification process optimization and fuel characterization. Energy Conver Manage, *49,* 1248–57.
173. Ejaz, M., Shahid, E., M., Jamal, Y. (2011). Production of biodiesel: A technical review Renewable and Sustainable Energy Reviews, *15,* 4732– 4745.
174. Sivasamy, A., Cheah, K., Y., Fornasiero, P., Kemausuor, F., Zinoviev, S., Miertus S. (2009). Catalytic Applications in the Production of Biodiesel from Vegetable Oils. Chem. Sus. Chem. *2,* 278–300.

175. Singh, S. P., Singh, D. (2010). Biodiesel production through the use of different sources and characterization of oils and their esters as the substitute of diesel: a review. Renew Sustain Energy Rev, *14,* 200–216.
176. Rashid, U., Anwar, F., Moser, B., R., Ashraf, S. (2008). Production of sunflower oil methyl esters by optimized alkali-catalyzed methanolysis. Biomass Bioenergy, *32,* 1202–5.
177. Math, M., C., Irfan G. (2007). Optimization of resturant waste oil methyl ester yield. J Sci Ind Res, *66,* 772–226.
178. Saifuddin, N., Chua, K. H. (2004).Production of ethyl ester (biodiesel) from used frying oil: optimization of transesterification process using microwave irradiation. Malaysian J Chem, *6,* 77–82.
179. Yan, Y., Li, X. (2014).Biotechnological preparation of biodiesel and its high-valued derivatives: A review. Appl. Energy, *113,* 1614–1631.
180. Lee, J. S., Saka, S. (2010). Biodiesel production by heterogeneous catalysts and supercritical technologies. Bioresour. Technol, *101,* 7191–7200.
181. Xu, C., Sun, J. (2010). On the study of KF/Zn(Al)O catalyst for biodiesel production from vegetable oil. Appl. Catal., B, *99,* 111–117.
182. Xie, W., Huang, X. (2006). Synthesis of biodiesel from soybean oil using heterogeneous KF/ZnO catalyst. Cat. Lett. *107,* 53–59.
183. Xie, W., Li, H. (2006). Alumina-supported potassium iodide as a heterogeneous catalyst for biodiesel production from soybean oil. J. Mol. Catal. A: Chem. *255,* 1–9.
184. Vyas, A. P., Subrahmanyam, N., Patal, P. A. (2009). Production of biodiesel through transesterification of Jatropha oil using KNO_3/Al_2O_3 solid catalyst. Fuel *88,* 625–628.
185. Ma, H., Li, S., Wang, B., Wang, R., Tian, S. (2008). Transesterification of rapeseed oil for synthesizing biodiesel by K/KOH/-Al_2O_3 as heterogeneous base catalyst. J. Am. Oil Chem. Soc. *85,* 263–270.
186. Kim, H. J., Kang, B. S., Kim, M. J., Park, Y. M., Kim, D. K., Lee, J. S., Lee, K. Y. (2004). Transesterification of vegetable oil to biodiesel using heterogeneous base catalyst. Catal. Today 93–95, 315–320.
187. Benjapornkulaphong, S., Ngamcharussrivichai, C., Bunyakiat, K. (2009). Al_2O_3-supported alkali and alkali earth metal oxides for transesterification of palm kernel oil and coconut oil. Chem. Eng. J. *145,* 468–474.
188. Kouzu, M., Kasuno, T., Tajik, M., Sugimoto, Y., Yamanaka, S., Hidaka, J. (2008). Calcium oxide as a solid base catalyst for transesterification of soybean oil and its application to biodiesel production. Fuel *87,* 2798–2806.
189. Lotero, E., Goodwin, J. G., Bruce, D. A., Suwannakarn, K., Liu, Y., Lopez, D. E. (2006). The catalysis of biodiesel synthesis. J. Catal. *19,* 41–84.
190. Tateno, T., Sasaki, T. Process for producing fatty acid fuels comprizing fatty acids esters. US Patent 6818026, 2004.
191. Antunes, W. M., Veloso, C. D. O., Assumpc, C., Henriques, O. (2008). Transesterification of soybean oil with methanol catalyzed by basic solids. Catal. Today, 133–135, 548–554.
192. Leclercq, E., Finiels, A., Moreau, C. (2001). Transesterification of rapeseed oil in the presence of basic zeolites and related solid catalysts. J. Am. Oil Chem. Soc. *78,* 1161–1165.

193. Liu, X., He, H., Wang, Y., Zhu, S. (2007). Transesterification of soybean oil to biodiesel using SrO as a solid base catalyst. Catal. Commun. *8,* 1107–1111.
194. Serio, M. D., Ledda, M., Cozzolino, M., Minutillo, G., Tesser, R., Santacesaria, E. (2006). Transesterification of soybean oil to biodiesel by using heterogeneous basic catalysts. Ind. Eng. Chem. Res. *45,* 3009–3014.
195. Cosimo, J. I. D., Dıez, V. K., Xu, M., Iglesi, E., Apesteguı, C. R. (1998). Structure and surface and catalytic properties of Mg–Al basic oxides. J. Catal. *178,* 499–510.
196. Albuquerque, M. C. G., Santamaria-Gonzalez, J., Merida-Robles, J. M., Moreno-Tost, R., Rodriguez-Castellon, E., Jimenez-Lopez, A., Azevedo, D. C. S., Cavalcante Jr., C. L., Maireles-Torres, P. (2008). MgM (M = Al and Ca) oxides as basic catalysts in transesterification processes. Appl. Catal. A *347,* 162–168.
197. Liu, X., Xiong, X., Liu, C., Liu, D., Wu, A., Hu, Q., Liu, C. (2010). Preparation of biodiesel by transesterification of rapeseed oil with methanol using solid base catalyst calcined K_2CO_3/-Al_2O_3. J. Am. Oil Chem. Soc, *87,* 817–823.
198. Melero, J. A., Grieken, R. V., Morales, G. (2006). Advances in thesynthesis and catalytic applications of organosulfonic-functionalized mesostructured materials. Chem. Rev. *106,* 3790–3812.
199. Kiss, A. A., Omota, F., Dimian, A. C., Rothenberg, G. (2006). The heterogeneous advantage: biodiesel by catalytic reactive distilation. Top. Catal. *40,* 141–150.
200. Canakci, M., Gerpen, J. V. (1999). Biodiesel production via acid catalysis. Trans. ASAE, *42,* 1203–1210.
201. Lou, W. Y., Zong, M. H., Duan, Z. Q. (2008). Efficient production of biodiesel from high free fatty acid-containing waste oils using various carbohydrate-derived solid acid catalysts. Bioresour. Technol, *99,* 8752–8758.
202. Islama, A., Taufiq-Yapb, Y. H., Chua, C., M., Chanc, E., S., Ravindraa P. (2013). Studies on design of heterogeneous catalysts for biodiesel production. Process Safety and Environ. Prot. *91,* 131–144.
203. Beck, J. S., Vartuli, J. C., Roth, W. J., Leonowicz, M. E., Kresge, C. T., Schmitt, K. D., Chu, C. T. W., Olson, D. H., Sheppard, E. W., McCullen, S. B. (1992). A new family of mesoporous molecular sieves prepared with liquid crystal templates. J. Am. Chem. Soc, *114,* 10834–10843.
204. Xiao, F. S. (2004). Hydrothermally stable and catalytically active ordered mesoporous materials assembled from preformed zeolites nanoclusters. Catal. Surv. Asia, *35,* 151–159.
205. Liu, X., Piao, X., Wang, Y., Zhu, S. (2008). Calcium ethoxide as a solid base catalyst for the transesterification of soybean oil to biodiesel. Energy Fuel, *22,* 1313–7.
206. Mbaraka, I. K., Shanks, B. H. (2006). Conversion of oils and fats using advanced mesoporous heterogeneous catalysts. J. Am. Oil Chem. Soc, *83*, 79–91.
207. Sercheli, R., Vargas, R. M., Schuchardt, U. Alkyguanidine-catalyzed heterogeneous transesterification of soybean oil. J. Am. Oil Chem. Soc, (1999). *76,* 1207–1210.
208. Buchmeiser, M. R. (2001). New synthetic ways for the preparation of high-performance liquid chromatography supports. J. Chromatogr. A, *918,* 233–266.
209. Kirkland, J. J., Truszkowski, F. A., Dilks Jr., C. H., Engel, G. S. (2000). High pH mobile phase effects on silica-based reversed-phase high-performance liquid chromatographic columns. J. Chromatogr. A, *890,* 3–19.

210. Lopez, D. E., Suwannakarn, K., Bruce, D. A., Goodwin Jr., J. G. (2007). Esterification and transesterification on tungstated zirconia: effect of calcination temperature. J. Catal, *247,* 43–50.
211. He, C., Baoxiang, P., Dezheng, W., Jinfu, W. (2007). Biodiesel production by the transesterification of cottonseed oil by solid acid catalysts. Front. Chem. Eng. Chin, 1, 11–15.
212. Ngamcharussrivichai, C., Totarat, P., Bunyakiat, K. (2008). Ca and Zn mixed oxide as a heterogeneous base catalyst for transesterification of palm kernel oil. Appl. Catal, A, *341,* 77–85.

INDEX

A

Acetate, 12–17, 24, 109
Acetobacter aceti, 131
Acid catalyzed hydrolysis of biomass in ILs, 328
Acid hydrolysis, 144, 147, 149, 150, 157, 185
Acid treatment, 103
Acid value, 245–247, 249, 255, 286, 287
Activated charcoal, 147, 148, 150, 158, 163, 167
Activation losses, 91
Activation polarization, 91
Adenosine triphosphate, 65, 76
Aeromonas hydrophila, 89, 131
Aeromonos sp., 42, 50
Agricultural residues, 19, 24, 25, 172, 175, 176, 178, 320
Alcaligenes fecalis, 89
Algal biomass, 9, 10, 210, 321, 337
Alkaline fuel cells, 63, 64, 67, 68
Alternaria dianthicola, 281
Amber glass bottle with closed space, 243, 246, 249
Amber glass bottle with closed space containing nitrogen, 243, 246, 249
Amber glass bottle with open space, 243, 246, 249
Amperometry, 134
Amylolytic enzyme, 313
Anabaena cylindrica, 48, 51
Anabaena cylindrical, 47
Anabaena variabilis SPU 003, 46, 47, 48, 108
Anaerobic fluidized bed, 112
Anaerobic microbial fuel cell, 24
Angiosperm trees, 175
Anion exchange membrane, 97
Anodic material, 98
ANOVA of phenolics, 165
ANOVA on bioethanol yield, 166
ANOVA on effect of detoxification of selected lignocellulosics hydrosylates, 166
Antagonist for nitrogenase, 49
Antioxidant, 242–245, 249, 251, 253–256, 258–268, 270, 274, 275
Aphanocapsa sp., 41
Applications of microbial fuel cells, 76
Arabinose, 14, 178, 190, 319, 320
Azadirachta indica, 212
Azotobacter, 145

B

Bacillus coagulans, 13
Bacillus megatarium, 145
Bacon fuel cell, 67
Bacterial metabolic losses, 92
Baker's yeast, 319
  Saccharomyces cerevisiae, 319
Base or acid catalysis, 214
Basideomycetes fungus, 145
Benefits of biodiesel, 215, 216
Bifunctional ionic liquids, 329
Bio-hydrogen production, 49, 52
Biochemical route of bioethanol production from lignocellulosic feedstocks, 182
Biodiesel production, 180, 209, 214, 222, 224, 226–228, 230–236, 308, 326, 333
  biodegradable, 217
  compression-ignition (diesel) engines, 243
  ecofriendly diesel fuel, 217
  fatty acid mono-alkyl esters, 243
  nonflammable, 217
  nontoxic, 217

Biodiesel purification, 226
Bioelectricity generation, 126
Bioelectrochemically assisted microbial reactor, 77
Bioethanol, 143–145, 147, 149, 157, 159, 163, 165–167, 172, 181, 188
Biofuels obtained from lignocellulosics, 179
  Biodiesel, 179
  Bioethanol, 181
  diesel fuel, 181
  jet fuel, 181
Biohydrogen (BioH) production, 4
Biological method for bioenergy production, 321
Biological simultaneous enzyme production and saccharification, 193
Biomass-to-liquid (BTL) process, 304
Biophotolysis methods, 40
  direct biophotolysis, 40–42
  indirect biophotolysis, 40, 42, 43
Bioreactor design, 6
Bioreactor for hydrogen production, 45
Bioremediation, 79, 80, 321
Biosensor, 113
Biotechnology risk assessment, 196
Black Hills of South Dakotais, 24
Blended fuel, 215
Botryococcus braunii, 215
Bottlenecks, 173, 175, 196
Brettanomyces, 159
Bromoethanesulfonic acid, 23
Bubbling fluidized bed (BFB) gasifier, 304

C

Calcium hydroxide, 147, 148
Caldicellulosiruptor kristjanssonii, 13
Caldicellulosiruptor saccharolyticus, 5, 13–17, 19, 20
Caldicellulosiruptor sp. strain, 194
Calophyllum inophyllum, 212
Candida, 159
Carbohydrate rich wastes, 50
Carbon electrodes, 98
Carbon mesh, 99
Carbon nanotubes, 100, 116
Carbon paper, 99, 102
Carrot pulp hydrolysate, 14
Catalysis of transesterification, 214
  base or acid catalysis, 214
  enzymatic catalysis, 214
Catalyst neutralization, 226
Catalytic methods, 325
  homogenous and heterogeneous catalysis for transesterification, 330
  ionic liquids in bio-fuel production, 325–229
Cathode materials, 92, 93, 102
Cavitational reactor, 226, 230
Cell cycle machinery, 189
Cellobiose, 12, 14, 186, 193
Cellulolysis, 183, 318, 320
Cellulose, 15–17, 171, 177, 178, 322, 338
Cellulosic/lignocellulosic enzyme, 315
Central moiety, 110
Ceramic matrix, 71
Cetane number, 216, 218, 223, 244, 286–288
Challenges of biodiesel production, 217
Chemical fuel cell, 88
Chemical nature of biodiesel, 212
Chemical oxygen demand, 112
Chemical vapor deposition, 105, 116
Chemically modified carbon electrodes, 103, 116
  acid treatment, 103
  graphite granules, 103
  methylene blue, 103
  neutral red, 103
  nitric acid, 103
Chlorella sorokiniana biomass, 306
Chlorella vulgaris, 65, 215
Chroococcidiopsis sp., 41
Citrobacter freundii, 22
Cladicellulosiruptor saccharolyticus, 12
Clavispora, 159
Clostridia sp., 42
Clostridium pasteurianum, 15
Clostridium stercorarium, 15

Clostridium thermocellum, 5, 15, 16, 17, 19, 172, 192, 194
Cobalt tetramethylphenylporphyrin, 99, 102, 116
Coir pith, 144–146, 150, 157, 159–167
  coir rope industry , 146
  lignocellulosic materials, 146
  woody stems, 146
Coir rope industry, 146
Combustion of biomass, 303
Combustion, 303
Complex solid wastes, 7
  kitchen food, 7, 8
  mixed wastes, 7, 8
  municipal, 7, 8
Components of a microbial fuel cell, 75
Compression-ignition (diesel) engines, 243
Concentration losses, 92
Conifers, 175
Consolidated bioprocessing, 187, 193
Contaminated barley hulls, 21
Continuous stirred tank reactor, 11
Conventional microbial fuel cell, 65, 66
  two-chamber system, 66
Corn stover, 7, 14, 24, 112, 145, 176, 178, 307, 315, 319
Cornstalk waste, 14, 15
Coulomb, 90
Coulombic efficiency, 94, 107, 134
Crude oil resources, 300, 338
Crypthecodinium cohnii, 215
Curvularia lunata, 281
Cyanobacteria, 10, 39, 41–43, 45, 46, 49–51, 65, 79, 144–146, 162, 167, 321, 324
Cyanobacterial species, 43
Cyclic voltammetry, 134

D

Dark fermentation process, 4, 5, 6, 10, 11, 18, 22, 25, 26, 42–45, 49
Decentralized industrial scale H_2 production, 24
  anaerobic microbial fuel cell, 24
  Black Hills of South Dakotais, 24
  rice straw, 24
  sugarcane baggase, 24
  U.S. Department of Energy, 24
  wheat straw, 24
Designer cellulosomes, 193
Desulfovibro desulfuricans, 108
Deteriorated seeds, 283, 285, 286
Detoxification methods, 147, 158
2,6-di-tertbutyl-p-benzoquinon, 131
Dicataionic basic ILs, 329
Dicationic acidic ILs, 329
Diesel engine problems, 226
  carbon deposits, 226
  coking on injectors, 226
  engine knocking, 226
  excessive engine wear, 226
  oil ring sticking, 226
  plugging of filters, 226
  thickening and gelling of lubricant oil, 226
Diesel fuel, 181
Diglycerides, 223
Dilute acid hydrolysis method, 147
Dimethyl ethanol, 300, 338
Dinitrosalicylic acid, 148
Direct and indirect biophotolysis, 6
Direct biophotolysis photosystem II, 40
Direct electron transfer, 106, 131, 132
  dissimilatory metal reducing bacteria, 106
  long-range electron transfer, 107
Direct glucose production using *Clostridium Thermocellum* cultures, 192
Direct methanol fuel cells, 63, 64, 70
Dissimilatory metal reducing bacteria, 106, 112, 116
Domestic and industrial effluents, 112
Downstream processes, 191, 226, 303
Downstream processing of biodiesel technology, 226
  biodiesel purification, 226
  catalyst neutralization, 226
  glycerol separation, 226
Dried distillers grain, 21

Dry grinding and wet milling processes, 314
Dunaliella primolecta, 215
DuPont's Nafion membrane, 69

E

Economical process, 5, 26
Effect of,
fungi on physicochemical properties, 286
seed mycoflora on biochemical properties, 283
amino acid contents, 283
carbohydrate contents, 283
lipid contents, 284
phenol contents, 284
protein contents, 283
seed mycoflora on the oil quality and quantity, 285
Effect on,
acid value, 286
amino acid contents, 283
carbohydrate contents, 283
cetane value, 288
iodine value, 286
lipid contents, 284
phenol contents, 284
protein contents, 283
refractive index, 289
saponification value, 287
viscosity, 288
Electricity, 23, 24, 38, 63–66, 71, 75, 76, 78, 79, 89, 97, 106–108, 111, 112, 126, 127, 183, 300, 303, 305, 310, 322, 323
Electrocatalytic/electron transfer reactions, 129
Electrochemical devices, 63, 65, 126
Electrochemical techniques, 134, 135
amperometry, 134
coulombic efficiency, 134
cyclic voltammetry, 134
impedance spectroscopy, 134
polarization studies, 134
Electrochemically active bacterial, 106, 116
Electrode-electrolyte interface, 130
Electrolysis of H_2O, 6
Electromotive force, 90
Electroneutrality in the system, 97
Energy balance ratio, 217
Energy consumption, 144
Energy crops, 7
corn, 7
lignocellulosic residues, 7
sorghum, 7
sugar beet, 7
sugarcane, 7
wheat, 7
Energy efficient system for HMF production, 328
Enterobacter aerogenes E10, 22
Enterobacter sp., 42
Enterococcus faecium, 89
Environmental sensors, 79
Enzymatic catalysis, 214
Enzymatic hydrolysis, 18, 19, 183–186, 191, 319
Trichoderma reesei, 185
Enzymatic saccharification, 10, 192
Enzyme based catalysis, 312
Enzyme concoction approach, 192
Epicuticular waxes, 190
Erwinia dissolven, 131
Erwinia dissolvens, 108
Escherichia coli, 11, 108, 109, 131, 163, 315, 319
Ester-based fuels, 278, 290
Estimation of total phenolics, 148
Ethanol, 12–17, 149, 162, 167, 322
estimation, 149
gas chromatography , 149
production, 144, 149, 159, 160, 161, 163, 165, 188, 194, 315, 318, 319
Euphorbia rigida, 307
Euphorbiaceae family, 278

F

Factors affecting rate of reaction, 213

ratio of oil to alcohol, 213
temperature, 213
time, 213
Factors decrease cell voltage, 91
activation losses, 91
bacterial metabolic losses, 92
concentration losses, 92
fuel crossover and internal currents, 92
ohmic losses, 91
Fatty acid methyl ester, 208, 212, 222, 242, 244, 286, 300, 338
Fatty acid mono-alkyl esters, 243
Feedstock logistics, 189
collection 189
postprocessing at the biorefinery, 190
preprocessing 189
storage 189
transportation 190
Feedstock production, 189
Feedstocks for H_2 production, 6
dark fermentation, 6
direct and indirect biophotolysis, 6
electrolysis of H2O, 6
photofermentation, 6
solar thermochemical gasification, 6
supercritical conversion, 6
thermocatalytic reformation, 6
Feedstocks types for BioH production, 7, 8
also see, microalgae
complex solid wastes, 7, 8
energy crops lignocellulosic residues, 7, 8
wastewater, 7, 8
Fermentable substrates, 6, 7
Ferric chelate complexes, 108
First generation biofuels, 209
Fischer-Tropsch (FT) diesel, 300
Fischer-Tropsch (FT) synthesis, 304
Fischer-Tropsch diesel, 338
Fluoropolymer containing cation exchange materials, 96
Nafion, 96
polystyrene and di-vinyl benzene with sulfonic acid groups, 96
Folin-Ciocalteu reagent, 148
Forestland materials, 175
conifers, 175
gymnosperm trees, 175
hardwoods, 175
softwoods, 175
woody biomass, 175
Forestry wastes, 175
sawdust from sawmill, 175
slashes, wood chips and branches from dead trees, 175
Fossil fuels, 4, 5, 38, 49, 174, 208, 217, 242, 279, 290, 300, 308, 320, 325, 337
Fourth generation biofuels, 210
Free fatty acids, 225, 281–283, 285–287, 326, 331, 333
Fresh water cyanobacteria, 47
Fuel cells, 63, 65
electrochemical devices, 63
Fuel crossover and internal currents, 92
Functionalized polymeric ionic liquids, 329
reusable ionic liquids, 329
Fusarium equiseti, 281
Fusarium oxysporum, 281

G

Gas chromatography, 149, 167
Gasification of biomass, 303
Gasification, 302–306, 308, 318, 320
Generations of biofuels, 209, 210
first generation biofuels, 209
fourth generation biofuels, 210
second generation biofuels, 209
third generation biofuels, 209
Genetic modifications, 186
Geobacter metallireducens, 89, 106
Geobacter sulfurreducens, 74, 101, 107, 323, 324
Gloebacter sp., 41
Gloeocapsa sp., 41
Glucoamylase, 313, 314, 316
Gluconobacter roseus, 131
Glucose, 4–7, 11–22, 25, 43, 51, 100, 107–109, 114, 130, 131, 148, 172,

177, 178, 186, 190, 193, 284, 300, 313, 314, 318, 319, 328
dehydrogenase, 130
oxidase, 130
Glycerol separation, 226
Graphite granules, 98, 100, 103, 104
Graphite sheets, 99
Graphite/epoxy composite electrode, 104
Green solvents, 325
Greenhouse gas emissions, 4, 144, 208, 242, 279
Gregor Johann Mendel, 128
Gymnosperm trees, 175

H

Hardwoods, 175
angiosperm trees, 175
aspen, 175
cottonwood, 175
oak, 175
poplar, 175
willow, 175
Hemi-cellulose, 171, 177, 190, 195, 300, 338
Heterogeneities, 191
Heterogeneous catalyst, 225
Hibiscus cannabinus L., 306
High cost of photobioreactors, 10
Homogeneous catalysis, 326, 333
Homogenous and heterogeneous catalysis for transesterification, 330
design of an ideal heterogeneous catalyst, 334
different heterogeneous catalysts for biodiesel production, 333
Hormone metabolism, 189
Hybrid systems using photosynthetic and fermentative bacteria, 44
One-step hybrid system, 44
Two-step hybrid system, 44, 45
Hybrid systems, 44, 45, 49, 50, 52
Hydraulic retention time, 21
Hydrogen gas, 38, 39, 51
clean source of energy, 38, 39
source of future energy, 38
Hydrogen production, 114
Hydrogen yield, 52
Hydrogenase enzyme, 10, 11, 42, 49
Hydrogenation of fats and oils in food industry, 39
Hydrolysis inhibitors, 191
2-hydroxy-1,4-naphthoquinone, 89, 108
Hydroxymethylfurfural, 19, 150, 181
2-Hydroxyphenazine, 110
2-Hydroxyphenazine–phenazinecarboxylic acid, 110
Hyperthermophiles, 11, 12, 14
Hyperthermophilic microorganisms, 4, 5, 11
Pyrococcus furiosus DSM 3638, 11
Thermotoga neapolitana DSM 4359, 11
Hypothetical three-stage hybrid system, 38, 50

I

Impedance spectroscopy, 134
Indian sub-continent, 62, 63
Induction point, 242
Industrial effluents, 4, 9, 25, 115
Ionic liquids in bio-fuel production, 325–229
acid catalyzed hydrolysis of biomass in ILs, 327
functional ionic liquids used in biofuel synthesis, 329
ionic liquids for cellulose dissolution and pretreatment, 327
metal catalyzed hydrolysis of biomass in ILs, 328

J

Jatropha biodiesel with,
BHA as additive, 249
BHT as additive, 255
GA as additive, 255
PY as additive, 265
TBHQ as additive, 259

Jatropha curcas L., 212, 242, 246, 278, 281, 289, 290, 311
Jatropha fruit, 279
Jatropha seeds, 278, 280, 285, 289
Jet fuel, 181, 209

K

Kenaf, 306
  Hibiscus cannabinus L., 306
Kinematic viscosity, 244–246, 249, 255
Klebsiella pneumonia, 65, 131
Kluvyveromyces, 159

L

L-arabinose, 178
Laboratory scale, 4, 6, 21, 22, 26
Lactate, 12–17, 322
  dehydrogenase gene, 5, 133
Lactobacillus plantarum, 108, 131
Lactococcus lactis, 131
Lantana camara L., 144–146, 167
Le Chatelier's principle, 224
Leptothrix discophora, 65
Lignin modification, 189
Lignin, 171, 178, 179, 338
Ligno-cellulosic technology, 195
Lignocellulosic biomass, 4–6, 9, 19, 145, 173, 175, 180, 181, 184, 187–190, 193–195, 303, 319
Lignocellulose composition, 166, 177, 178
  cellulose, 166, 178
  hemicellulose, 166, 177
  lignin, 166, 178
Lignocellulosic materials, 14, 144, 146, 149, 157, 164, 189, 190, 194, 318, 319, 328
Lignocellulosic residues, 7
  corn stover, 7
  rice, 7
  sugarcane and sweet sorghum bagasse, 7
  tree and shrub residues, 7
  wheat straw and bran, 7
  wood fibers, 7
  wood waste, 7
Lignocellulosic wastes, 166
  coir pith, 166
  L.camara, 166
  P. juliflora, 166
  technological developments, 149
Liquefaction, 305
Low efficiency of light conversion, 10

M

Macrophomina phaseolina, 281
Maize leaves and sugarcane baggase, 14
Marine algae biomass, 176
Mechanism of electricity production, 76
  adenosine triphosphate, 76
  nicotinamide adenine dinucleotide, 76
  see, microbial fuel cell
Mediated electron transfer, 107, 108, 132
  endogenous shuttles, 108
  exogenous mediators, 108
Membrane bioreactors, 188
Membrane reactor, 226, 233–235
Mesophilic process, 5, 10, 11, 22, 194
Methanol-to-oil ratio, 236
Methanothermobacter thermoautotrophicus, 107
Methylene blue, 89, 103, 108
MFC fundamentals, 323
MFC reactor configurations, 93
Micro-channel reactor, 226, 227
Microalgae, 7, 10, 65, 73–76, 79, 214, 215, 223, 311, 321–325, 337
Microalgal bacterial consortia, 321
Microbial electrolysis cell, 114
Microbial fuel cells, 62, 64, 65, 66, 73, 74, 76–78, 80, 88, 95, 116, 126, 127, 128, 130, 133, 136, 322
  in electricity generation, 76
  in hydrogen production, 77
  in wastewater treatment, 78
    refinery wastewater treatment, 78
    separator electrode assembly, 78
    widely spaced electrodes, 78
Microbial nanowires for bioenergy application, 324

Microcoleus sp., 41
Microcrystalline cellulose, 18, 20
Microcystis sp., 41
Microorganism and culture conditions, 146
MicroRNA, 189
Microwave approach for biofuel production, 308
Microwave reactor, 226, 232, 233
Microwave-assisted pyrolysis process, 307
Molten carbonate fuel cells, 63, 64, 72
Monallanthus salina, 215
Monoalkyl esters, 222
Monoglycerides, 223
Monosaccharides, 14, 328
Municipal and industrial wastes, 176
Municipal solid wastes, 9, 209
Mycrocystis sp., 41

N

Navicula pelliculosa, 215
Neochloris oleoabundans, 215
Neutral red, 89, 103
Neutralization, 147, 150, 158, 163, 167, 330
Nicotinamide adenine dinucleotide, 66, 76
Nitric acid, 103
Nitrogenase enzyme, 10, 47, 48
Nostoc muscorum SPU004, 46
Novel reactors, 226–235
  cavitational reactor, 226, 230, 232
  membrane reactor, 226, 233–235
  micro-channel reactor, 226, 227
  microwave reactor, 226, 232
  oscillatory flow reactor, 226–228
  rotating/spinning tube reactor, 226, 229
  sonochemical reactor, 226, 231, 232

O

Ohmic losses, 91
Ohmic resistance, 73, 100
Optimized pilot-scale demonstration, 23
Ordinary glass bottle with closed space containing nitrogen, 243, 246
Ordinary glass bottle with closed space, 242, 246, 248, 272
Ordinary glass bottle with open space, 242, 246, 248, 272
Organic acids, 18, 44, 46, 191, 244
  acetate, 18
  butyrate, 18
  formate, 18
  lactate, 18
  propionate, 18
Organic load, 8, 9
Organisms employed in fuel cells, 79
Oscillatoria annae, 144, 167
Oscillatory flow reactor, 226, 227, 228
Overlimiting, 147
Oxidation stability, 275
Oxidative phosphorylation chain of reactions, 105
Oxidative stability, 246, 273, 275
Oxygen sensitivity of hydrogenase enzyme, 10

P

Pachysolen, 159
Peanut shells, 24
Pelotomaculum thermopropionicum, 107
Penicillium digitatum, 281
Perfluorosulfonic acid polymer, 96
Petro-diesel combustion properties, 290
Phaeodactylum tricornutum, 215
Phenazine, 108–111, 135
  central moiety, 110
Phenazine 1 carboxamide, 110
Phenazine 1 carboxylic acid, 110
Phosphoric acid fuel cells, 63, 64, 71
  ceramic matrix, 71
  pure liquid phosphoric acid, 71
Photo-electrochemical reactions, 310
Photo-fermentation process, 42, 43, 45
Photocatalysis reaction, 310
Photofermentation, 6, 10, 18, 23, 26, 45

Photosynthetic algal microbial fuel cells, 65
Photosynthetic genes, 189
Photosynthetic green algae, 46
Photosystem I, 42
Photosystem II, 40
Pichia stipitis NCIM 3498, 146, 167
Pichia, 144, 146, 159, 167
Pisum sativum, 128
Pleurotus sajor caju, 145
Polarization studies, 134
Polyaniline, 101
Polymer electrolyte membrane fuel cells, 64
Polymer of glucose, 338
Polypyrrole, 101
Pongamia (karanja) biodiesel, 242
Pongamia biodiesel with,
  BHA as additive, 249
  BHT as additive, 255
  GA as additive, 255
  PY as additive, 267
  TBHQ as additive, 261
Pongamia pinnata, 212, 246, 311
Portable computers, 62
Potato stem peels, 16, 20
Powering gadgets, 114
Prairie cordgrass, 24
Pre-treatment of lignocellulosic feedstock, 184
Pretreatment cost of lignocellulosic feedstocks, 9
Process intensification technologies for biodiesel production, 226
Prosopis juliflora, 144–146, 167
Proteus mirabilis, 131
Proteus vulgaris, 108, 109
Proton exchange membrane fuel cells, 63, 64, 68
  polymer electrolyte membrane fuel cells, 64, 68
Proton exchange membrane, 23, 63, 64, 75, 88, 116
Pseudomonas aeruginosa, 89, 109, 323
Pseudomonas fluroscens, 65
Pseudomonos sp., 42, 50
Purple sulfur bacteria, 46
Pyocyanin, 110
Pyrococcus furiosus DSM 3638, 11, 12
Pyrogallol, 242, 250
Pyrolysis process, 307, 308
Pyrolysis, 302, 306
Pyruvate, 5, 130

Q

Quorum sensing, 109

R

Rancimat method, 245, 272, 274
Reducing sugar estimation, 148
Reduction of ferrodoxin, 10
Refinery wastewater treatment, 78
Regional industrial-academia partnership, 26
Reticulated vitreous carbon, 98, 116
Rhizopus stolonifer, 281
Rhodobacter ferrireducens, 107
Rhodobacter sp., 42
Rhodoferax ferrireducens, 74, 89, 106
Rhodopseudomonas palustris P2, 22
Rhodopseudomonas sp., 42
Rhodospirillum rubrum, 65
Rhodospirillum sp., 42
Rhodovulum sp., 42
Rice straw, 14–16, 20, 24, 317, 328
Robot EcoBotII, 114
Rotating/spinning tube reactor, 226, 229
Russian autoclave, 147

S

Saccharomyces cerevisiae yeast, 314
Saccharum spontaneum, 163
Salinity, 9, 47
Sanitary wastes, 112
Saponification process, 225, 335
Saponification value, 287
Scenedsmus acutus, 215
Schizosaccharmoyces, 159
Second generation biofuels, 209
Seed germination percentage, 282

Separate hydrolysis and fermentation, 186, 187
Separation and purification of bioethanol, 188
Separator electrode assembly, 78
Sequential dark-photo fermentations (SDPF), 18
Serratia marcescens, 145
Shewanella case, 132
Shewanella oneidensis, 100, 109
Shewanella putrefaciens, 89, 106, 107
Shredded paper waste, 14, 17
Simultaneous saccharification and fermentation, 186
Single chambered MFC, 94, 112, 115
Single step bioethanol production by employing novel strains, 193
Sintering and soaking, 104
Softwoods, 175
  conifers, 175
  gymnosperm trees, 175
Solar thermochemical gasification, 6
Solid oxide fuel cells, 63
Sonochemical reactor, 226, 231, 232
Source of future energy, 38, 50
Sources of lignocellulosic, 175
  agricultural residues, 176
  forestland materials, 175
  marine algae, 176
  municipal and industrial wastes, 176
South Dakota School of Mines and Technology, 3, 26
Speed breakers in bio-hydrogen production, 45
  effect of, extrinsic factors, 45, 46
    carbon, 47
    light, 46
    micronutrients, 48
    molecular nitrogen, 48
    nitrogen, 47
    oxygen, 48
    pH, 46
    salinity, 47
    sulfur, 48
    temperature, 46
  intrinsic factors 49
SPORL treatment, 191
Stabilized zirconium oxide, 64, 73
Starch, 6, 8, 15, 62, 281, 313–316, 321, 335
Sterility, 9
Storage conditions, 242, 246, 248
  amber glass bottle with closed space containing nitrogen, 243, 246, 249
  amber glass bottle with closed space, 243, 246, 249
  amber glass bottle with open space, 243, 246, 249
  ordinary glass bottle with closed space containing nitrogen, 243, 246, 248
  ordinary glass bottle with closed space, 242, 246, 248
  ordinary glass bottle with open space, 242, 246, 248
Storage stability, 251, 253, 255, 256, 258–260, 262, 264–266, 268, 270, 275
Streptococcus lactis, 108
Sucrose, 6, 51, 100
Sugarcane bagasse, 14, 158, 176, 307
Sugarcane baggase, 158
Sulfite pretreatment to overcome lignocellulose recalcitrance, 318
Supercritical alcohol transesterification, 225
Supercritical conversion, 6
Sweet sorghum, 7, 14
Swine wastewater, 112
Switchgrass, 5, 19, 20, 24, 322
Synechococcus sp., 41
Synechocystis sp., 41
Synthesis of biodiesel by transesterification, 213
Synthetic natural gas, 300, 338
Systems biology, 128, 129, 131–133, 135

T

Tafel slope, 91
Tetraselmis sueica, 215

Thermo-chemical conversion processes, 302
Thermoanaerobacter brockii, 193
Thermoanaerobacter mathranii A3N, 12
Thermoanaerobacterium sp., 12–17
Thermoanaerobacterium aotearoense, 14
Thermoanaerobacterium saccharolyticum, 12, 15
Thermoanaerobacterium thermosaccharolyticum GD17, 12, 16–18
Thermocatalytic reformation, 6
Thermococcus kodakaraensis, 5, 13
Thermophiles, 4–6, 11, 12, 14, 19, 25
Thermophilic biohydrogen production, 3–6
  bioreactor design, 6
  dark fermentation process, 4
  economical process, 5
  fossil fuel, 5
  hyperthermophilic microorganisms, 4
  laboratory scale, 4
  lactate dehydrogenase gene, 5
  mesophilic processes, 5
  see, lignocellulosic biomass
  thermophiles, 6
  thermophilic microorganisms, 4
  waste to energy, 4
Thermophilic microbial dark fermentation, 11
Thermophilic microorganisms, 4, 5
  Caldicellulosiruptor saccharolyticus, 5
  Clostridium thermocellum, 5
  Thermococcus kodakaraensis, 5
Thermotoga elfii DSM 9442, 13
Thermotoga neapolitana, 11, 12, 16, 20
Thiobaccillus ferrooxidance, 65
Thiocapsa sp., 42
Third generation bio-fuels, 39
Third generation biofuels, 209
Tocopherols, 243
Transcription factors, 189
Transeserification conditions, 236
  reaction temperature, 236
  methanol-to-oil ratio, 236
  catalyst concentration, 236
Transesterification process, 212, 223–226, 308, 330, 334
Transition metals, 328
Trichoderma reesei, 185
Trichophyton mentagrophytes infection, 145
Trielectrode system, 75
Triglyceride (like vegetable oil), 208
Triglycerides, 179, 212–214, 223, 225, 242, 287, 308, 309, 330, 332, 333, 335
Types of bio-fuels, 39
  first generation (made from food crops), 39
  second generation (made from non-food crops or wastes), 39
  third generation (made using microbe), 39
Types of fuel cells, 63
  alkaline fuel cells, 63
  direct methanol fuel cells, 63
  molten carbonate fuel cells, 63
  phosphoric acid fuel cells, 63
  proton exchange membrane fuel cells, 63
  solid oxide fuel cells, 63
Types of MFC based on the reactor models, 74
Types of microbial fuel cells, 89

U

U.S. Department of Energy, 24
Ultra filtration (UF) membranes, 97, 116
Untreated Lignocellulosics, 27
Use of super computer in bioethanol production, 194
Uses of biodiesel, 216

V

Variety of alternative fuels, 4
  biobutanol, 4
  biodiesel, 4
  bioethanol, 4
  biogas, 4
  biohydrogen (BioH), 4
Vegetable kitchen waste, 14

Vibrio sp., 42, 50
Viscosity of oil, 223

W

Waste cooking oil, 210, 217
Waste to energy, 4, 22
Wastewater treatment, 7, 8, 65, 75, 76, 78, 80, 94, 106, 112, 126, 127, 234, 338
  cattle, 8
  cheese whey, 8
  dairy, 8
  distillery and molasses based, 8
  food industry waste water, 8
  olive mill, 8
  paper mill, 8
  starch hydrolysate, 8
Wheat straw, 7, 14, 16, 19, 20, 24, 144
Widely spaced electrodes, 78
Woody stems, 146

X

Xylanolytic enzymes, 14
Xylose, 6, 14, 17, 146, 157, 159, 178, 179, 187, 190, 191, 300, 319, 320

Y

Yeast fermentations, 149
Yeast varieties, 159
  Brettanomyces, 159
  Candida, 159
  Clavispora, 159
  Kluvyveromyces, 159
  Pachysolen, 159
  Pichia, 159
  Schizosaccharmoyces, 159
Yetterbium based metal salts, 328

Webology, Volume 12, Number 1, June, 2015

Characterizing relatedness of web and requirements engineering

Akshi Kumar
Dept. of Computer Science & Engineering, Delhi Technological University, Delhi, India.
E-mail: akshi.kumar@gmail.com

M.P.S. Bhatia
Division of Computer Engineering, Netaji Subhas Institute of Technology, Delhi, India.
E-mail: mps.bhatia@nsit.ac.in

Rohit Beniwal
Division of Computer Engineering, Netaji Subhas Institute of Technology, Delhi, India.
E-mail: rohitbeniwal@yahoo.co.in

Received October 15, 2014; Accepted June 15, 2015

Abstract

Web and Requirements Engineering have been well- recognized as two individual active areas of research in the past. Convergence between these two notable areas has been a point-of-discussion in recent years and offers new avenues of research. This paper explores this alliance from two perspectives; firstly, where Requirement Engineering can be viewed as a process for Web application development as it primarily concerns with adapting the Requirement Engineering process to the Web applications which are special in characteristics as compared to traditional software applications and secondly, where Web can be viewed as a supporting technology for improving the requirements engineering process and enabling new capabilities. The basics of this two-way relationship are examined along with state-of-art and potential opportunities to equip a better understanding.

Keywords

Web application; Requirements engineering; Web 2.0; Web 3.0

Introduction

Requirements Engineering is an intricate, multifaceted and time-consuming process. Its objective is to essentially assure the quality of resulting software. More recently, as our dependence and reliance on Web has increased; there has been a rising interest in the development of methodologies including processes, models and techniques to build web applications. An expected alliance of the two notable and active areas of research, requirements engineering and Web has been much advocated.

We characterize that the relation between Web and Requirements Engineering (RE) can be interpreted in two ways. Firstly, RE can be viewed as a process for Web application development where it primarily looks into adapting of RE process to the Web applications which are special in characteristics as compared to traditional software applications. Secondly, Web can be viewed as a supporting technology for improving the requirements engineering process and enabling new capabilities. Thus, this relation can be examined from two different perspectives, each opening new avenues of research.

The intensive use of Web Applications has produced, among others, a rising interest in the development of methodological approaches providing a suitable support for the construction of Web applications (Escalona & Koch, 2004). Web Applications (Web Apps) necessitate a more extensive and efficient Requirements Engineering (RE) process as they are typical as possibility compared to conventional software. Key discerning characteristics which compel distinctive and special management are the heterogeneity of stakeholders involved, the diversity of the requirements, dynamic technology and environment (user needs), lack of communication with end-users and the high likelihood of risk.

Knowledge management in requirements engineering has persistently been a concern for better software development and maintenance. There is always some gap in understanding about what the business partners and stakeholders want, how software designers and managers design the modules and how software developers implement the design (Guha, 2011). With time, this gap is broadened due to the heterogeneous involvement of parties and constantly varying requirements of the software. Thus, the problem of requirement management manifolds with vague, inconsistent, incomplete, ambiguous and dynamic nature of requirements, and the much anticipated trend of Web is a savior. The web technologies serve as supporting technology that has found many valuable applications in the field of requirements engineering. Especially the advent of Web 2.0 and Web 3.0, the Social and the Semantic Web (Aghaei et al., 2012) respectively, has assisted in surmounting few challenges and limitations of requirements management.

Requirements Engineering

A *requirement* is a necessary, quantifiable, and verifiable capability, function, property, characteristic, or behavior that a product must exhibit to solve a real-world problem, or a constraint that it must satisfy or be satisfied during the development of a product (Ferreira & Loucopoulos, 2001). Requirements describe what the system will do without describing how it will do. Once these business needs also known as requirements are gathered, they are analyzed for their validity and studied for feasibility. *Requirements Engineering (RE)* is defined as the principles, methods, and tools for eliciting, describing, validating, and managing project goals and needs. It is an iterative and co-operative process with the objective to analyze the problem, to document the results in a variety of formats and evaluate the precision of the results produced (Ferreira & Loucopoulos, 2001). The iterative process of requirements engineering consists of three main activities, namely, requirements elicitation; requirements specification; requirements validation (Lowe, 1999). Some classic techniques to elicit, specify and validate requirements have been listed in Table 1 below.

Table 1. Description of techniques of RE phases

Requirements Elicitation	Requirements Specification	Requirements Validation
○ Interviewing ○ Joint Application Development (JAD). ○ Brainstorming ○ Concept Mapping ○ Sketching and Story Boarding ○ Use Case Modeling ○ Questionnaire and Checklist	○ Natural language ○ Glossary and ontology ○ Templates ○ Scenarios ○ Use case Modeling ○ Formal Description ○ Prototypes	○ Reviews or Walkthrough ○ Audit ○ Traceability metrics ○ Prototype for validation

RE is imperative for an accomplished proposal in terms of projection of the system, improved product quality and significant reduction in probability of project failure. Prolifically published studies have demonstrated consequences of not applying RE properly. Primary concerns are inadequate software architecture, unexpected problems like budget overrun, delay in production and "that's not what I asked for" and low user acceptance. The vital role of "requirement" in successful completion of project can be substantiated through much prolifically published work. (Field, 1997) tells that "projects fail too often because the project scope was not fully appreciated and/or user needs not fully understood." Likewise, (O'Brochta, 2002) says "the big problem with assessing project success is that it is not precise".

According to the 1995 *The Standish Group Report* (1995), the reasons for failed or challenged projects which deal to requirement engineering are incomplete requirement; lack of user involvement; lack of resources and unclear objectives. IBM systems magazine, on an article in 2012 on project pitfalls (Gulla, 2012) has defined 7 major reasons of failure of the project,

namely, poor project planning and direction; insufficient communication; ineffective management; failure to align with stakeholders and constituents; ineffective involvement of executive management; lack of soft skills or the ability to adopt; poor or missing methodology and tools. As we can observe, that there is an endless list of authors as well as so many survey reports (range of past two decades, including recent) which consider that RE is a critical initial stage, but often poorly executed and handled with less relevance (Kumar & Sharma, 2015). It is worth noting that challenged projects are those which were completed, but were over cost, over time, and/or lacking all of the features and functions that were originally specified.

The Emergence of Web

The World Wide Web is a huge, widely distributed, global source for information services, hyper-link information, access and usage information and web site content and organization (Bhatia & Khalid, 2008). During the last decade, the World Wide Web has evolved as an information space. The authors in (Aghaei et al., 2012) provide an overview of the evolution of the Web. It is summarized in the following Table 2.

Table 2. Evolution of Web

Evolution of Web	Characteristics
Web 1.0 (1991-2003)	○ It is a heteronym that refers to the state of the World Wide Web, and any website design style used before the advent of the Web 2.0 phenomenon. ○ Information-oriented Web. ○ It is Read only Web. ○ Connects real people to the World Wide Web ○ A Web of cognition.
Web 2.0 (2004-till date)	○ The term Web 2.0 is primarily linked with Web Apps that assist interactive information sharing, collaboration, user-centered design, and interoperability on the World Wide Web. ○ Social Web: connects real people who use the World Wide Web. ○ It is a Read/Write Web. ○ A Web 2.0 site gives its users the free choice to interact or collaborate with each other in the dynamic environment of social media in contrast to websites where users are limited to the passive viewing of content. ○ A Web of communication.
Web 3.0 (2006-Till date)	○ It refers to the latest version of the Web. ○ There are two different perspectives for defining Web 3.0. It can either be viewed as the **Semantic Web (or the meaning of data)** or as **intelligent web**, where software agents will collate and integrate information to give "intelligent" responses to human operators. ○ A Web of co-operation.

Requirement Engineering for Web

In the development of conventional (pre-Web) applications both practitioners and process experts regard requirements engineering as an imperative phase in the development process since the most common and time-consuming errors as well as the most expensive ones to repair, are errors that result from the inadequate engineering of requirements (Kumar & Sharma, 2015). The promising area of *Web Requirements Engineering* (WRE) which has been a point-of-discussion in numerous latest research projects and papers, entails addressing the technological challenges of requirements engineering activities for web applications. A Web Application is customization software developed for a network, based on technologies and standards of the World Wide Web Consortium (W3C) that offers an explicit purpose and functionality. These are programs which are written for the internet and to be hosted via a browser (Acunetix, n.d.). Fundamentally, till date, the Web-applications have been divided into nine categories (Deshpande & Hansen, 2001) with the development timeline depicting more sophistication and high complexity of new Web Apps. The Web evolution effectively fits in all the categories of web applications that exist till date. The following Table 3 depicts the same relation.

Table 3. Web Application Categories

Application	Characteristics	Web Evolution
Document Centric	○ precursor to Web applications ○ stored on a Web server as ready-made, that is static, HTML documents and sent to the Web client in response to a request ○ contents are frequently represented redundantly on several Web pages ○ simplicity and stability ○ short response time	Web 1.0
Interactive Web Applications	○ web pages and links to other pages are generated dynamically according to user input ○ uses CGI, ASP, PHP and HTML form ○ for example, virtual exhibitions, news sites, or timetable information	Web 2.0
Transactional	○ provide more interactivity ○ performing updates on the underlying content ○ efficient and consistent handling of the increasing amount of content ○ offer the possibility of structured queries ○ for example, online banking, online shopping, and booking systems	Web 2.0
Workflow	○ handling of workflows between different companies, public authorities, and private users ○ availability of appropriate Web services to guarantee interoperability ○ for example, Business-to-Business solutions (B2B solutions) in e-commerce, e-government applications.	Web 2.0
Collaborative	○ especially for cooperation purposes in unstructured operations (groupware) ○ communication between the cooperating users ○ support shared information and workspaces ○ for example, wiki, Weblogs, scheduling systems, e-learning platforms	Web 2.0

Social	○ anonymity traditionally characterized World Wide Web ○ Moving towards *communities of interest* ○ *Examples:* Blogs, collaborative filtering systems, social bookmarking (for example, del.icio.us) ○ Integration with other forms of web applications (e.g., NetFlix)	Web 2.0
Portal oriented	○ provide a single point of access to separate, potentially heterogeneous sources of information and services ○ for example, online shopping malls, community portals	Web 2.0
Ubiquitous	○ provides customized services anytime anywhere and for any device ○ facilitating ubiquitous access ○ either personalization or location-aware services or multi-platform delivery	Web 2.0
Semantic Web	○ present information on the Web ○ not merely for humans, ○ but also in a machine readable form ○ facilitate knowledge management on the Web ○ linking and reuse of knowledge (content syndication) ○ locating new relevant knowledge ○ interoperation on the semantic level and the possibility of automating tasks (via software agents)	Web 3.0

Classical requirement engineering methods are applicable for traditional system applications but developing web applications is distinctive. The key characteristics what make RE for Web "special" are multidisciplinary teams, unavailability of stakeholders, rapidly changing requirements and constraints, unpredictable operational environment, no manual for the user interface, content management (Ginige & Murugesan, 2001; Escalona & Koch, 2004). Thus, there is a strong need of some special, typical requirement engineering techniques which could handle these issues efficiently. Adapting RE methods to Web application development needs to address and focus on some important issues, viz., types of requirements vital for the Web application mainly identifying critical requirements; the level of documentation and description of these requirements; tools suited for the particular project needs. As a step to provide an insight to the RE adaptation to Web Apps, the authors in (Kumar & Sharma, 2015) present SWOT Analysis of Web Requirement Engineering that necessitates a holistic and proactive approach to Web Requirement Engineering to bring the current chaos in web application development under control, minimize risk, and enhance its maintainability and quality. The work done by authors in (Escalona & Koch, 2004) cites the state of the art of requirements engineering in methodologies used for the development of Web applications.

Web for Requirements Engineering

Requirements Engineering has a prominent effect on the success or failure of a software project. Inaccurate, inadequate, or misunderstood requirements are the most common causes of poor quality, cost overruns and late delivery of software systems (El Emam & Madhavji, 1995). Fundamental problems of requirement engineering have been widely acknowledged across

numerous published studies. Some examples of fairly common problems with the RE process are as follows (El Emam & Madhavji, 1995; Siddiqi & Shekaran, 1996; Sommerville & Kotonya, 1998; Nikula et al., 2000; Nuseibeh & Easterbrook, 2000; Hall et al., 2002):

- Vague requirements,
- Undefined requirements process,
- Inadequate requirements traceability,
- Lack of stakeholder involvement,
- Business needs are not considered,
- Lack of requirements management,
- The requirements do not reflect the real needs of the customers,
- Requirements are ambiguous (more possible interpretations), inconsistent (contains contradictions), and/or in complete (forgotten features),
- It is expensive to make changes to requirements after they have been agreed,
- There are misunderstandings between customers and software engineers,
- Requirements growth, and
- Stakeholders communication problems.

Specifically, the operative challenges motivating researchers in the area of Requirements Engineering can be categorized as either related to the stakeholders involved or to the requirements management, apart from some miscellaneous problems. The inception of Web, especially with the advent of Web 2.0 and Web 3.0, many momentous applications in the field of requirements engineering have been realized that assist in surmounting few challenges and limitations of requirements management and stakeholder communication issues. In this paper, we have tried to depict how Web has been utilized as a supporting technology to overcome some if not all issues related to requirements engineering phase. The following Table 4 portrays this relation of Web and requirement engineering where specifically the role of Web 2.0 and Web 3.0 is examined to improve requirements engineering process.

Table 4. Web as supporting technology for RE process

	Problem	Solution	Weakness
Stakeholders	**Lack of stakeholder involvement** **Stakeholders communication problems** o Participants are geographically distributed o Face-to-face contact is limited.	**Web 2.0** o Web-based, community-centered applications (Hippner, 2006) o Social Software Engineering (Lohmann et al., 2009) o Many existing commercial tools that support collaborative development of requirements. For example Rational RequisitePro (Rational Software Corporation, 2003), Borland Caliber RM (Whitehead, 2007), and Telelogic DOORS (Telelogic, 2004), RavenFlow (Ravenflow, 2007), Gatherspace (Gatherspace.com, 2007) and eRequirements (eRequirements, 2007).	o Security and privacy breaches in social applications. o Lack of Trust among participants o Collaboration among stakeholders happens independent of RE tools (Lohmann et al., 2009).
Requirements Management	**Vague Requirements** o Absence of key requirements. o Work based on incorrect supposition.	**Integration of ontologies (Web 3.0) and models** o Use of models such as petri nets to represent requirement, removing vagueness to some extent (Brockmans, 2006). o Petri nets require semantic annotation for formal analysis, ontologies have been used to provide semantic annotation to petri nets (Baek Jorgensen & Bossen, 2004; Gašević et al., 2009).	**Relying on Models such as Petri nets** o Require models to represent requirements in the form of use cases.
	Inadequate requirements traceability o High human effort for requirements categorization, conflict analysis and tracing, especially with a large number of requirements (Farfeleder et al., 2011).	**Semantic links (Web 3.0)** o Helps in establishing traceability. o Concepts in ontology can be associated with requirement specification items (Gašević et al., 2009; Zhao et al., 2009).	

	Requirements are ambiguous, inconsistent and/or incomplete ○ Diverse stakeholders, who produce different interpretations of the same requirement. Moreover, one stakeholder can interpret the same requirement in diverse ways. ○ Contains Contradictions ○ Incompleteness (Farfeleder et al., 2011) of requirements categorization and conflict identification, in particular, when performed manually.	**Ontology Reasoning (Web 3.0)** ○ Ontology reasoning with closed world assumption has been used to remove inconsistency and incompleteness among requirements (Siegemund et al., 2012).	**Relying on closed world assumption** ○ As requirements are dynamic and changing, relying on closed world assumption never seems to be a solution
	Dynamic and Changing Requirements ○ Constant requirements revision in order to help to understand new client's needs and to identify how they can be satisfied.	**Ontology (Web 3.0) driven requirement engineering (Siegemund et al., 2011)** ○ Requires ontology evolution (ontology maintenance) in order to adapt new changes (Flouris & Plexousakis, 2005) ○ Includes task such as ontology alignment, mapping, merging, articulation, versioning, et cetera.	○ Complicated and multifaceted task (Flouris & Plexousakis, 2005) ○ Human intervention required ○ Cost incurred
Miscellaneous	○ Business needs are not considered. ○ The requirements do not reflect the real needs of the customers. ○ There are misunderstandings between customers and software engineers.	**Web 3.0: Ontology based Computing (Lee & Gandhi, 2005)** ○ Use ontologies to enable communication (or mappings) among multiple disciplines (for example, to the engineering team members, to marketing, to management and to customers), ○ Employ semantic descriptions of application domains, ○ Designed to capture natural language descriptions of domains of interest, ○ Provide more consistent representations of such domains, ○ Reduce ambiguity inherent in communication, ○ Reduce error via the structuring of knowledge, and ○ Provide ways to extend and specialize captured domain knowledge.	

Thus, as a supporting technology, social web technology (Web 2.0) explores collaborative development of requirements and overcomes stakeholder problems to some extent. At the same time, Semantic web (Web 3.0) can be used in capturing, modeling, developing, checking, and validating of requirements specifications. It can play a vital role in all phases of requirement engineering such as in requirement elicitation (Al Balushi et al., 2006), requirement analysis (Caralt & Kim, 2007), requirement documentation (Bhatia et al., 2015) and requirement review (Kaiya & Saeki, 2005; Zhu & Jin, 2005a; 2005b).

Conclusion

We characterized that the relation between the Web and Requirements Engineering (RE) can be interpreted in two ways. As a process for Web application development, a need for more extensive and detailed requirements engineering is identified to bring the current chaos in web application development under control, minimize risk, and enhance its maintainability and quality. At the same time, the Web can impact requirement engineering processes to develop quality software by assisting in surmounting few challenges and limitations of requirements management. As a supporting technology, the Web especially the current generations, Web 2.0 and Web 3.0, enables new capabilities and has opened up new avenues of research.

References

Acunetix. (n.d.). Web applications: What are they? What of them? Retrieved March 10, 2015, from http://www.acunetix.com/websitesecurity/web-applications/

Aghaei, S., Nematbakhsh, M. A., &Farsani, H. K. (2012). Evolution of the World Wide Web: From WEB 1.0 tO WEB 4.0. *International Journal of Web & Semantic Technology*, 3(1), 1-10.

Al Balushi, T.H., Sampaio, P. R. F., Dabhi, D., & Loucopoulos, P. (2006, July). Performing requirements elicitation activities supported by quality ontologies. In *SEKE* (pp. 343-348).

Baek Jorgensen, J., & Bossen, C. (2004). Executable use cases: Requirements for a pervasive health care system. *Software, IEEE*, 21(2), 34-41.

Bhatia, M. P. S., & Kumar, A. (2008). Information retrieval and machine learning: Supporting technologies for web mining research and practice. *Webology*, *5*(2), article 55. Retrieved March 10, 2015, from http://www.webology.org/2008/v5n2/a55.html

Bhatia, M., Kumar, A., & Beniwal, R. (2015, March). Ontology based Framework for automatic software's documentation. In *Computing for Sustainable Global Development, 2015 2nd International Conference on* (pp. 725-728). IEEE.

Brockmans, S., Ehrig, M., Koschmider, A., Oberweis, A., & Studer, R. (2006, May). Semantic alignment of business processes. In *ICEIS* (3) (pp. 191-196).

Caralt, J. C. C., & Kim, J. W. (2007, January). Ontology driven requirements query. In *40th Annual Hawaii International Conference on System Sciences, HICSS 2007*, 3-6 Jan. 2007, pp. 197c.

Deshpande, Y., & Hansen, S. (2001). Web engineering: Creating a discipline among disciplines. *Multimedia, IEEE*, 8(2), 82-87.

El Emam, K., & Madhavji, N. H. (1995, March). A field study of requirements engineering practices in information systems development. In *Requirements Engineering, 1995, Proceedings of the Second IEEE International Symposium on* (pp. 68-80).

eRequirements. (2007). eRequirements product tour. Retrieved March 10, 2015, from http://www.erequirements.com/app?service=page/ProductTour

Escalona, M. J., & Koch, N. (2004). Requirements engineering for web applications-a comparative study. *Journal of Web Engineering*, 2(3), 193-212.

Farfeleder, S., Moser, T., Krall, A., Stalhane, T., Omoronyia, I., & Zojer, H. (2011). Ontology-driven guidance for requirements elicitation. In *The Semantic Web: Research and Applications* (pp. 212-226). Springer, Berlin.

Ferreira, M. J., &Loucopoulos, P. (2001). Organization of analysis patterns for effective reuse. In *ICEIS (2)* (pp. 766-773).

Field, T. (1997). When bad things happen to good projects: The warning signs of failure are detectable long before a project falls apart. *CIO-FRAMINGHAM MA*, 11, 54-56.

Flouris, G., & Plexousakis, D. (2005). Handling ontology change: Survey and proposal for a future research direction. *Institute of Computer Science, Forth. Greece, Technical Report TR-362 FORTH-ICS*. Retrieved March 10, 2015, from http://www.ics.forth.gr/isl/publications/paperlink/fgeo_TR362.pdf

Gašević, D., Kaviani, N., & Milanović, M. (2009).Ontologies and software engineering. In *Handbook on Ontologies* (pp. 593-615). Berlin: Springer.

GATHERSPACE.COM. (2007). Gatherspace: Requirements management and use case software. Retrieved March 10, 2015, from http://www.gatherspace.com/static/product2.html

Ginige, A., & Murugesan, S. (2001). Guest editors' introduction: The essence of web engineering-managing the diversity and complexity of web application development. *IEEE Multimedia*, *8*(2), 22-25.

Guha, R. (2011). Software engineering on semantic web and cloud computing platform. Retrieved March 10, 2015, from http://people.cs.pitt.edu/~chang/231/y11/papers/cloudSE.pdf

Gulla, J. (February, 2012). Seven reasons IT projects fail. Retrieved March 10, 2015, from http://www.ibmsystemsmag.com/power/Systems-Management/Workload-Management/project_pitfalls/

Hall, T., Beecham, S., & Rainer, A. (2002). Requirements problems in twelve software companies: an empirical analysis. *IEE Proceedings-Software*, 149(5), 153-160.

Hippner, H. (2006). Bedeutung, anwendungen und einsatzpotenziale von social software. *HMD–Praxis der Wirtschaftsinformatik*, 43(252 S 6).

Kaiya, H., & Saeki, M. (2005, September). Ontology based requirements analysis: Lightweight semantic processing approach. In *Quality Software, 2005. (QSIC 2005). Fifth International Conference on* (pp. 223-230). IEEE.

Kumar, A., & Sharma, A. (2015, April). Swot analysis of requirements engineering for web applications. *International Journal of Advance Research in Science and Engineering (IJARSE)*, 4(4), 34-43.

Lee, S. W., & Gandhi, R. A. (2005, December). Ontology-based active requirements engineering framework. In *Software Engineering Conference, 2005. APSEC'05. 12th Asia-Pacific* (pp. 8).

Lohmann, S., Dietzold, S., Heim, P., & Heino, N. (2009). A web platform for social requirements engineering. In *Software Engineering (Workshops)* (Vol. 150, pp. 309-315).

Lowe, D. (1999). Hypermedia and the Web: An engineering approach. John Wiley & Sons, Inc.

Nikula, U., Sajaniemi, J., & Kälviäinen, H. (2000). Management view on current requirements engineering practices in small and medium enterprises. *Queensland University of Technology*. Retrieved March 10, 2015, from http://citeseerx.ist.psu.edu/viewdoc/summary?doi=10.1.1.2.6132

Nuseibeh, B., & Easterbrook, S. (2000, May). Requirements engineering: a roadmap. In *Proceedings of the Conference on the Future of Software Engineering* (pp. 35-46).

O'Brochta, M. (2002, October). Project success - What are the criteria and whose opinion counts. In *PMI Annual Seminars & Symposium*.

Rational Software Corporation. (2003, June). Rational Requisite ProUser's Guide. Retrieved March 10, 2015, from ftp://ftp.software.ibm.com/software/rational/docs/v2003/win_solutions/rational_requisitepro/reqpro_user.pdf

Ravenflow. (2007). RAVEN: Requirements Authoring and Validation Environment. Retrieved March 10, 2015, from http://www.ravenflow.com/products/index.php

The Standish Group. (1994). *The Standish Group Report: CHAOS*. Retrieved March 10, 2015, from http://www.projectsmart.co.uk/docs/chaos-report.pdf

Siddiqi, J., & Shekaran, M. C. (1996). Requirements engineering: The emerging wisdom. *IEEE Software*, *13*(2), 15-19.

Siegemund, K., Thomas, E. J., Zhao, Y., Pan, J., & Assmann, U. (2011, October). Towards ontology-driven requirements engineering. In *Workshop Semantic Web Enabled Software Engineering at 10th International Semantic Web Conference (ISWC)*, Bonn.

Siegemund, K., Zhao, Y., Pan, J. Z., & Assmann, U. (2012). Measure software requirement specifications by ontology reasoning. In *8th International Workshop on Semantic Web Enabled Software Engineering (SWESE'2012)* Nara, Japan.

Sommerville, I., & Kotonya, G. (1998). *Requirements engineering: processes and techniques*. John Wiley & Sons, Inc.

Telelogic. (2004, February). *Getting Started with DOORS (DOORS 7.1)*. Retrieved March 10, 2015, from http://endymion.ugent.be/~stijn/doors/doors_getting_started.pdf

Whitehead, J. (2007). Collaboration in software engineering: A roadmap. *Proceedings of FOSE 07: Future of Software Engineering*, 2007, 214-225.

Zhao, Y., Dong, J., & Peng, T. (2009). Ontology classification for semantic-web-based software engineering. *IEEE Transactions on Services Computing*, 2(4), 303-317.

Zhu, X., & Jin, Z. (2005). Ontology-based inconsistency management of software requirements specifications. In *SOFSEM 2005: Theory and Practice of Computer Science* (pp. 340-349). Springer Berlin Heidelberg.

Zhu, X., & Jin, Z. (2005, June). Inconsistency measurement of software requirements specifications: An ontology-based approach. In *Engineering of Complex Computer Systems, 2005. ICECCS 2005. Proceedings. 10th IEEE International Conference on* (pp. 402-410). IEEE.

Bibliographic information of this paper for citing:

Kumar, Akshi, Bhatia, M.P.S., & Beniwal, Rohit (2015). "Characterizing relatedness of web and requirements engineering." *Webology*, 12(1), Article 136. Available at: http://www.webology.org/2015/v12n1/a136.pdf

Copyright © 2015, Akshi Kumar, MPS Bhatia and Rohit Beniwal.

ISSN (Online) 2321 – 2004
ISSN (Print) 2321 – 5526

INTERNATIONAL JOURNAL OF INNOVATIVE RESEARCH IN ELECTRICAL, ELECTRONICS, INSTRUMENTATION AND CONTROL ENGINEERING
Vol. 3, Issue 8, August 2015

Digital Watermarking of Video using DWT, PCA and Arnold Scrambling Technique applied on a Binary Watermark

Temshichang Jongko[1], Jeebananda Panda[2], Asok Bhattacharyya [3]

Department of E&C Engineering, Delhi Technological University, New Delhi, India[1]

Associate Professor, Department of E&C Engineering, Delhi Technological University, New Delhi, India[2]

Professor, Department of E&C Engineering, Delhi Technological University, New Delhi, India[3]

Abstract: In this paper analysis have been performed for a good trade-off between the perceptual quality of the video after watermarking and the robustness of the video against various attacks by embedding the binary watermark into the video frame. The embedding and the extraction of watermark is done in the high frequency domain of Discrete Wavelet Transform since small modifications done in this domain are not perceived by human eye. Arnold Cat Map Scrambling technique is used in the algorithm, which is applied on the binary watermark before embedding to provide some level of security. In the paper four watermarking algorithms are presented to do a comparative study. The normalized correlation and bit error is used to compute the measure of the extracted watermark. The experimental results shows high imperceptibility and high robustness against several attacks especially noisy attacks and filtering attacks in all the cases. The comparison has been shown in the result section.

Keywords: Digital Video Watermarking, Discrete Wavelet Transform, Principal Component Analysis, Arnold Cat Map.

I. INTRODUCTION

In recent years, the advancement in the digital multimedia technologies has brought many facilities in reproduction, transmission and data manipulation. However this advancement has also brought the problem such as copyright issues. For copyright protection of digital multimedia, watermarking [1] has been proposed. A signal (watermark) is embedded into the data which will indicate whether the content is copyrighted or not. Most of digital video watermarking schemes are based on the techniques of image watermarking. Video watermarking [2] requires specific approaches as it is characterized by temporal and inter frame characteristics. There are two categories for embedding the watermark [3] in a video frame based on the domain which is used for hiding the watermark bits namely the spatial domain and the transform domain. The first one is the spatial domain watermarking where embedding and detection is performed by directly manipulating the pixel intensity value of the video frame. Least significant bit (LSB) is the simplest technique in the spatial domain techniques [4] which directly modifies the intensities of some selected pixels. The second category is the transform domain watermarking, in which the watermark is embedded by changing the frequency components of the video frame. The transformation adopted may be Discrete Cosine transform (DCT), Discrete Fourier Transform (DFT) and Discrete Wavelet transform (DWT) etc. After Applying transformation, the watermark is embedded in the transformed coefficients such that watermark is not visible. The transform domain watermarking scheme are relatively more robust than the spatial domain watermarking particularly in lossy compression, noise addition, pixel removal, cropping, rescaling and rotation.

Discrete wavelet transform (DWT) is computationally more efficient than other transforms like DFT and DCT because of its excellent time-frequency localization properties, DWT is very suitable to identify areas in the host video frames where watermark can be embedded imperceptibility. It is known that there exists some amount of correlation between wavelet coefficients even after the decomposition of the video frame.

Wang et al. [5] adopt a key dependent wavelet transform. To take advantage of the localisation and multi resolution property of the wavelet transform. Tao et al. [6] put forward a discrete wavelet based multiple watermarking algorithm, where to improve the robustness the watermark is embedded on the LL and HH sub bands. Wang and Lin [7] proposed a tree based watermarking algorithm. Lou et al. [8] introduce an integer wavelet to protect the copyright of digital data by utilizing encryption technique to enhance the security.

Yung et al. [9] proposed a multiple logo watermarking scheme by on integer wavelet. Where the watermark is permuted using the Arnold transform and is embedded by modifying the coefficients of the HH and LL sub bands. Lin et al.[10] proposed a DWT based blind watermarking scheme by scrambling the watermark using the chaos sequence. Jeebananda Panda et al.[11] proposed a hybrid watermarking scheme based on integer wavelet and Singular value decomposition, where watermark is embedded after performing a chaotic scrambling.

ISSN (Online) 2321 – 2004
ISSN (Print) 2321 – 5526
INTERNATIONAL JOURNAL OF INNOVATIVE RESEARCH IN ELECTRICAL, ELECTRONICS, INSTRUMENTATION AND CONTROL ENGINEERING
Vol. 3, Issue 8, August 2015

Principal component analysis (PCA) has the property of removing the correlation among the data and is used to hybridize the algorithm i.e. wavelet coefficients, which helps in distributing the watermark bits over the sub-bands used for embedding thus resulting in robust watermarking scheme which is robust to almost all attacks. The PCA can be used in different ways in image and video watermarking methods. Here we have presented a new approach that incorporates wavelet transformation, principal component analysis and Arnold cat map scrambling technique. It was found that the proposed technique is robust to a wide range of attacks.

Section II presents the proposed watermarking method and Section III shows experimental results of the proposed method. Conclusion is presented in Section IV.

II. RELATED BACKGROUND

This section briefly describes the techniques and methods that have been used by the watermarking schemes in the paper, namely. The discrete wavelet transform, Principal component analysis and the Arnold transform.

A. Discrete Wavelet Transform

The DWT is commonly used in signal processing applications. 2D Discrete Wavelet Transform (DWT) decomposes a video frames into sub images, 3 details and 1 approximation. The approximation sub images is lower resolution approximation image (LL) however the details sub images are horizontal (HL), vertical (LH) and diagonal (HH) detail components. The main advantage of wavelet transform is its compatibility with the model aspect of the Human Visual System (HVS) as compared to FFT or DCT. In general most of the image energy is concentrated at the lower frequency coefficient sets LL and therefore embedding watermarks in these coefficient sets may degrade the image significantly. Embedding in the low frequency coefficient sets, however, could increase robustness significantly. On the other hand, the high frequency coefficient sets HH include the edges and textures of the image and the human eye is not generally sensitive to changes in such coefficient sets. This allows the watermark to be embedded without being perceived by the human eye. For a one level decomposition, the two dimensional discrete wavelet transform of the image function f(x,y) can be written as

$$LL = [(f(x,y) * \phi(-x)\phi(-y))(2n, 2m)]_{(n,m)\in Z^2} \quad (1)$$

$$LH = [(f(x,y) * \phi(-x)\psi(-y))(2n, 2m)]_{(n,m)\in Z^2} \quad (2)$$

$$HL = [(f(x,y) * \psi(-x)\phi(-y))(2n, 2m)]_{(n,m)\in Z^2} \quad (3)$$

$$HH = [(f(x,y) * \phi(-x)\phi(-y))(2n, 2m)]_{(n,m)\in Z^2} \quad (4)$$

B. Principal Component Analysis

Principal component analysis (PCA) is a mathematical procedure that is concerned with data reduction and interpretation by explaining the variance-covariance structure of the data with the help of linear combination of the original variables. Moreover, principal component analysis can also be thought as a mathematical tool that transform a number of correlated variables into uncorrelated variables called the principal components.To obtain the Principal components of matrix I, firstly calculate the covariance matrix

$$C_I = E\{(I - m) \times (I - m)^T\} \quad (5)$$

Where E, m and T denote expectation operation, mean of matrix X and matrix transpose, respectively. The principal components of X are the eigenvectors of C_I which is obtain as

$$C_I\Phi=\lambda\Phi \quad (6)$$

Where Φ and λ are the matrices of the eigenvectors and the eigen values defined as $\Phi=(e_1,e_2,e_3,...,e_n)$ and $\lambda=(\lambda_1, \lambda_2, \lambda_3, \dots, \lambda_n)$. The matrix Φ is an orthogonal matrix called basis function of PCA. Principal component analysis transforms the correlated image into uncorrelated coefficients by taking the inner product of the image with basis function denoted by Φ

$$Y = \Phi^T I \quad (7)$$

Where Y is the PC matrix which represents the principle component of matrix I.

C. Arnold Cat Map

Two dimensional Arnold cat map shuffles the pixels positions of the original image without changing the pixels gray level intensities. The 2D Arnold cat map can be obtained by

$$X' = [X + pY] mod(n) \quad (8)$$

$$Y' = [qX + (pq + 1)Y] mod(n) \quad (9)$$

Here, (X', Y') represents the new position of (X, Y) after Arnold's cat transform and n is the dimension of the image. p and q are the initial values in which the sensitivity of cat map depends. Therefore p and q can be used as keys.

The main aim for using the Arnold transform is to provide security to the watermarking scheme, by scrambling the watermark before embedding.

D. Binary watermark

The advantages of binary watermark over the colour watermark are that there is a lot of complexity in embedding a value for each intensity value for a colour watermark or a gray scale watermark. At the same time in the extraction process it is difficult to get a true colour value.

III.THE ALGORITHMS USED

In this section different algorithms are presented which were performed in order to do a comparative study to bring out the proposed method.

A. Scrambled watermark embedded on the principal components of the wavelet coefficients

In this algorithm the host video frame is decomposed to wavelet coefficients using 3 level DWT from there the principal component is calculated and the scrambled watermark which is scrambled watermark using Arnold

ISSN (Online) 2321 – 2004
ISSN (Print) 2321 – 5526
INTERNATIONAL JOURNAL OF INNOVATIVE RESEARCH IN ELECTRICAL, ELECTRONICS, INSTRUMENTATION AND CONTROL ENGINEERING
Vol. 3, Issue 8, August 2015

transformism embedded on the principal component. The detailed algorithm for embedding and extraction watermark is discussed in the following

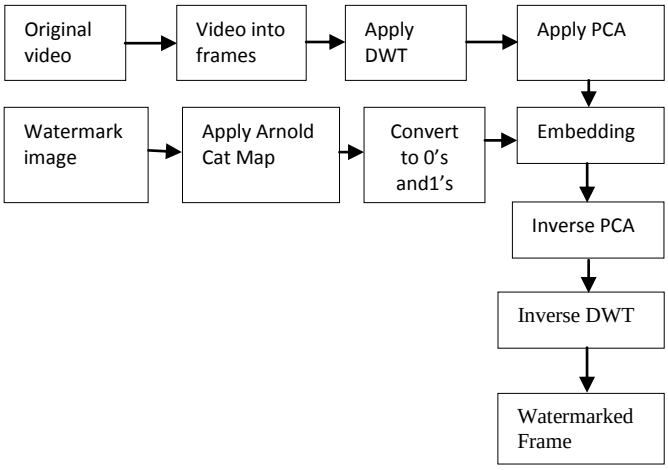

Fig.1. Watermark embedding algorithm for watermarking scheme where scrambled watermark is applied on Principal components of the Wavelet coefficients.

Watermark Embedding

Step1. The Host video is read and is divided into video frames.
Step2. From each frame the RGB components is separated and from there the red component is selected for embedding the watermark.
Step3. A 3 level DWT is performed on the red color component of the video frame. The diagonal (HH_{34}) detailed component of the wavelet transform is selected to embedding the watermark.
Step4. The diagonal (HH_{34}) detailed component is divided into non-overlapping blocks and PCA is applied to obtain the Principal components for embedding the watermark.
Step5. The binary watermark image BW is read and Arnold Cat Map is performing on the watermark image. The initial value and the number of iterations is hold as the security for the proposed watermarking algorithm.
Step6. Convert the scrambled binary watermark into a vector of BW' $=\{bw_1', bw_2', \ldots, bw_{m,n'}\}$ of '0's and'1's.**Step7.** The watermark is embedded into the Principal components PCB of each non-overlapping block using the following Equation.

$$PCB'(m,n) = PCB(m,n) + k.w(m,n) \quad (10)$$

Where, k is the embedding strength. The PCB' and PCB are the modified principal components and the original principal components.
Step8. Apply inverse PCA on the modified Principal components of the HH_{34} band to obtain the modified wavelet coefficients.
Step9. Apply inverse DWT to obtain the Red component of the frame. Then reconstruct the watermarked frame X_w.

Watermark Extraction

Step1. Read the watermarked video and divide it into video frames.
Step2. From each watermarked frame the RGB colour component is separated and from there component is selected for extracting the watermark.
Step3. Apply 3 levels DWT on the red component of the watermarked video frame. The multi-level DWT is applied to obtain HH_{34} detailed component as same as in the embedding procedure.
Step4. Divide the sub band HH_{34} into non overlapping block.
Step5. Block based PCA is applied on each non overlapping block of HH_{34}subband to obtain the watermarked Principal components PCB'.
Step6. The watermark is extracted from each non-overlapping block using the following equation

$$BW' = (PCB'-PCB)/k. \quad (11)$$

Where PCB' and PCB are the principal components of watermarked and original video frame and k is the embedding strength.
Step7. Apply Arnold Cat map on the extracted watermark and apply thresholding to obtain the embedded watermark image.

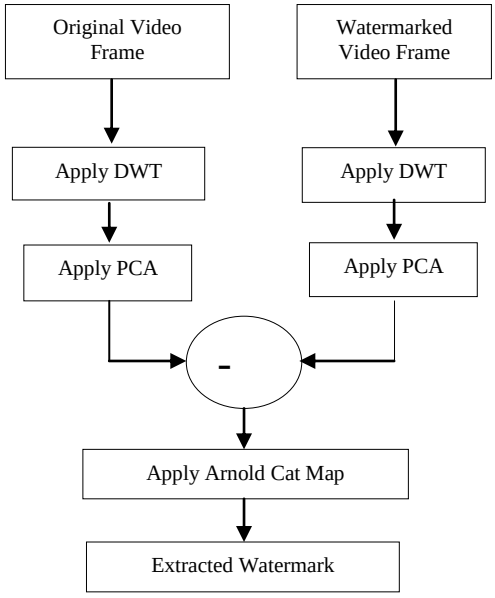

Fig.2. Watermark Extraction Algorithm for watermarking scheme where scrambled watermark is applied on Principal components of the Wavelet coefficients.

B. Scrambled watermark embedded on the wavelet coefficient

In this the host video frame is decomposed using three 3 level DWT and the scramble watermark obtain from Arnold transform is embedded on the wavelet coefficients. The algorithm for embedding and the extraction watermark is discussed in the following.

Embedding

Step1. Read the video frames and select the red component for embedding the watermark.
Step2. Apply 3 levels DWT on the Red component and select HH_{34} sub band and divide it into non-overlapping blocks.

ISSN (Online) 2321 – 2004
ISSN (Print) 2321 – 5526
INTERNATIONAL JOURNAL OF INNOVATIVE RESEARCH IN ELECTRICAL, ELECTRONICS, INSTRUMENTATION AND CONTROL ENGINEERING
Vol. 3, Issue 8, August 2015

Step3. Read the binary watermark image.
Step4. Apply Arnold Cat Map on the binary image and convert the scrambled image into vectors of 0's and 1's.
Step5. The watermark bits is inserted on each non-overlapping blocks of the wavelet coefficients as.

$$cH' = cH + k.W \quad (12)$$

Where cH is the wavelet coefficient obtained after apply 3 level DWT, k is the embedding strength and W is the watermark bit obtained after scrambling. cH' is the modified wavelet coefficient.
Step6. Apply inverse 3 levels DWT
Step7. Merge colour component to obtain the watermarked frame.

Extraction

Step1. Read the watermarked Frame and select the Red colour component for extraction.
Step2. Apply 3 level DWT on the Red colour Component and select HH_{34} sub band and divide it into non-overlapping blocks.
Step3. The watermark bits is extracted from each non-overlapping blocks by as

$$W' = (cH_w - cH)/k. \quad (13)$$

Where cH_w is the discrete wavelet coefficient obtained after applying 3 levels DWT. And cH is the Discrete Wavelet coefficient of the Host video frame.
Step4. Convert back to binary image and apply Arnold Cat map to the extracted watermark bits to obtain the watermark image.

C. Principal components of the scrambled watermark embedded on the wavelet coefficients

In this, the host video frame is decomposed using 3 level DWT and the principal components of the scrambled watermark is embedded on the obtained wavelet coefficients. The detailed embedding and extraction algorithm is discussed in the following

Embedding

Step1. Read the video frame and select Red colour component for embedding.
Step2. Apply 3 levels DWT to the Red component, select HH_{34} sub band and divide it into non-overlapping blocks.
Step3. Read the binary Watermark.
Step4. Apply Arnold Cat map to watermark image and convert it into 0's and 1's.
Step5. Apply PCA on the scrambled watermark bits.
Step6. The watermark bits is embedded into each non-overlapping blocks of the wavelet coefficients as

$$cH' = cH + \alpha k.W_{pca} \quad (14)$$

where cH is the wavelet coefficient after 3 level DWT, W_{pca} is the principal components after applying PCA in scrambled watermark bits and αk is the embedding strength.
Step7. Apply inverse 3 levels DWT
Step8. Merge colour to obtain the watermarked frame.

Extraction

Step1. Read the watermarked frame and select the red colour component for watermark extraction.
Step2. Apply 3 levels DWT on the red colour component, select the HH_{34} sub band and divide it into non-overlapping blocks.
Step3. The watermark bits is extracted from each non-overlapping blocks using the equation as

$$W'_{Pca} = (cH_w - cH)/k. \quad (15)$$

Where cH_w is the coefficient obtains after DWT on the watermarked frame and cH is the coefficient obtain after DWT on the original video frame.
Step4. Apply inverse PCA.
Step5. Convert the extracted watermark into binary image.
Step6. Apply Arnold cat map to obtain the watermark image.

D. The principal components of the scrambled watermark is embedded on the principal components of the wavelet coefficients

In this, the host video frame is decomposed using 3 levels DWT and the principal components of the wavelet coefficients is calculated. The principal components of the scrambled watermark are embedded on the principal components of the wavelet coefficients. The detail embedding and the extraction algorithm is discussed in the following.

Embedding

Step1. Read the Video Frames and select red colour component for watermark insertion.
Step2. Apply 3 levels DWT on the Red component and select HH_{34} sub-band and divide it into non-overlapping blocks.
Step3. Apply based PCA on the non-overlapping blocks.
Step4. Read the binary watermark.
Step5. Apply Arnold Cat Map on the watermark image and convert it to vectors of 0's and 1's.
Step6. Apply PCA on the scrambled watermark image.
Step7. The watermark bits are inserted on each non-overlapping block using the equation

$$PCA' = PCA + k.W_{pca} \quad (16)$$

Where PCA' is the modified Principal components and PCA is the principal components obtain after applying PCA on the HH_{34} sub-band. k is the embedding strength.
Step8. Apply inverse PCA on the modified Principal components.
Step9. Apply inverse DWT on the obtained.
Step10. Merge the colour component to obtain the watermarked frame.

Extraction

Step1. Read the watermarked video frame and select the red colour component for watermark extraction.
Step2. Apply 3 levels DWT on the red colour component and select the HH_{34} sub band and divide it into non-overlapping blocks.
Step3. Apply PCA on the non-overlapping blocks to obtain the principal component PCAw.

ISSN (Online) 2321 – 2004
ISSN (Print) 2321 – 5526
INTERNATIONAL JOURNAL OF INNOVATIVE RESEARCH IN ELECTRICAL, ELECTRONICS, INSTRUMENTATION AND CONTROL ENGINEERING
Vol. 3, Issue 8, August 2015

Step4. The watermark bit are extracted from each non-overlapping using the equation

$$W'_{Pca}W'_{Pca} = (PCA_w - PCA)/k \quad (17)$$

Where PCA_w is the Principal component obtained after applying PCA on the watermarked frame. And PCA is the Principal components of the original Video frame.

Step5. Apply inverse PCA on the extracted watermark bits.

Step6. Convert the bits into binary image and apply Arnold Cat map to obtain the watermark image to obtain the extracted watermark.

IV.EXPERIMENTAL RESULTS

For the experimental analysis sample video of sequence 'Xylophone.avi' of dimension 512×512 and binary watermark logo 'apple.gif' of size 32×32 is used for all the algorithms. For all the algorithms both the p and q value for Arnold cat map scrambling function is chosen to be 1. The embedding strength for the entire algorithm is set to 22. Fig3. and Fig4. Shows the original video frame and the watermark in the experiment.

Fig.3. Original Frame

Fig.4. Original watermark

For evaluating the perceptual quality of the watermarking schemes, Peak Signal to Noise Ratio (PSNR) is used which is given by

$$PSNR = 10\log\frac{256^2}{MSE} \quad (18)$$

$$MSE = \sum_{i=1}^{M}\sum_{j=1}^{N}[I(i,j) - I'(i,j)]^2 \quad (19)$$

Where M,N are the size of the frame. I, I' are the original and watermarked video frame.

Also the Bit error is used to measure the robustness the algorithm

$$BER = \frac{\sum_{i=1}^{M}\sum_{j=1}^{N} W(i,j) \oplus W'(i,j)}{M.N} \quad (20)$$

Where W and W' is the original and extracted watermark.

Normalised cross-correlation method is also used to measure similarity between the watermark and the extracted watermark

$$NC = \frac{\sum_i \sum_j W(i,j)W'(i,j)}{\sqrt{\sum_i \sum_j W(i,j) \sum_i \sum_j W(i,j)}} \quad (21)$$

Where W and W' are the original and watermark image.

To measure the robustness of the watermarking scheme some attacks are applied to the watermarked frame.

The attack analysis of the watermarking schemes is as shown below.

Algorithm A→ Scrambled watermark embedded on the principal components of the wavelet coefficients.

Algorithm B→ Scrambled watermark embedded on the wavelet coefficient.

Algorithm C→ Principal Components of the scrambled watermark embedded on the wavelet coefficients.

Algorithm D→ the principal components of the scrambled watermark is embedded on the principal components of the wavelet coefficients

Attacks	Bit error			
	Algorithm A	Algorithm B	Algorithm C	Algorithm D
Salt&pepper noise(0.001)	0.0079	0.0107	0.0225	0.0098
Salt&pepper noise (0.01)	0.0615	0.1250	0.2063	0.1025
Poisson noise	0.0225	0.2432	0.2280	0.0586
Speckle noise(0.001)	0.0137	0.7627	0.0371	0.0291
Speckle Noise (0.01)	0.0332	0.2539	0.2329	0.0732
Gaussian noise(0.001)	0.0049	0.2510	0.1672	0.0273
Gaussian noise(0.01)	0.1877	0.3145	0.3936	0.2471
Gaussian Filter[2 2]	0.0303	0.1094	0.1028	0.0488

Attacks	Bit error			
	Algorithm A	Algorithm B	Algorithm C	Algorithm D
Gaussian Filter[3 3]	0.0078	0.0527	0.0090	0.0081
Gaussian Filter[5 5]	0.0079	0.0547	0.0100	0.0090
Median Filter[2 2]	0.0771	0.1063	0.1040	0.1387
Median Filter[3 3]	0.1309	0.3398	0.1484	0.1357
Median Filter[5 5]	0.2964	0.4287	0.3457	0.3032
Mean Filter[2 2]	0.0303	0.1094	0.1028	0.0488
Mean Filter[3 3]	0.4075	0.4600	0.4292	0.4277
Mean Filter[5 5]	0.4575	0.5706	0.4707	0.4756
Histo-equal	0.0527	0.2285	0.0420	0.0031
Gamma-correction	0.0020	0.2070	0.0052	0.0003
Cropping (10%)	0.0020	0.1709	0.2161	0.0031
Cropping (20%)	0.0743	0.1094	0.0859	0.8083
Cropping (30%)	0.1495	0.3359	0.3291	0.9801

ISSN (Online) 2321 – 2004
ISSN (Print) 2321 – 5526
INTERNATIONAL JOURNAL OF INNOVATIVE RESEARCH IN ELECTRICAL, ELECTRONICS, INSTRUMENTATION AND CONTROL ENGINEERING
Vol. 3, Issue 8, August 2015

Table.1. Comparison between algorithms in terms of bit error

Attacks	Normalised Correlation			
	Algorithm A	Algorithm B	Algorithm C	Algorithm D
Salt & pepper noise(0.001)	0.9927	0.9893	0.9783	0.9901
Salt & pepper noise(0.01)	0.9440	0.7345	0.8192	0.8900
Poisson noise	0.9754	0.8915	0.8011	0.9494
Gaussian noise(0.001)	0.9898	0.8021	0.8373	0.9711
Gaussian noise(0.01)	0.8373	0.6855	0.5895	0.7251
Speckle noise(0.001)	0.9934	0.7627	0.9602	0.9168
Gaussian Filter[2 2]	0.9788	0.9500	0.9024	0.9450

Attacks	Normalised correlation			
	Algorithm A	Algorithm B	Algorithm C	Algorithm D
Gaussian Filter[3 3]	0.9927	0.9473	0.9901	0.9921
Gaussian Filter[5 5]	0.9934	0.9453	0.9845	0.9910
Mean Filter[2 2]	0.9788	0.7890	0.9024	0.9458
Mean Filter[3 3]	0.6136	0.5908	0.5696	0.5823
Mean Filter[5 5]	0.5600	0.4600	0.4919	0.5823
Median Filter [2 2]	0.9125	0.7634	0.8499	0.8300
Median Filter [3 3]	0.7621	0.6602	0.7089	0.7589
Median Filter [5 5]	0.3964	0.5713	0.6438	0.6949
Histo-equal	0.9024	0.7715	0.9446	0.9538
Gamma-correction	0.9982	0.7930	0.9821	0.9993
Cropping (10%)	0.9643	0.8402	0.8205	0.9403
Cropping (20%)	0.9287	0.8906	0.8879	0.9012
Cropping (30%)	0.8503	0.6641	0.6420	0.8083

Table.2. Comparison between Algorithms using Normalised Correlation

From the table it is observed that the Algorithm A i.e. the algorithm where the host video frame is decomposed using 3 level DWT and the scrambled watermark is embedded on the principal component of the wavelet coefficients obtained after decomposing the host video frame gives a better result under attack as compared to the other three algorithm, except for gamma-correction and histogram equalisation attack where the Algorithm 4 i.e. the algorithm where the principal component of the scrambled watermark is embedded on the principal component of the wavelet coefficient obtained after decomposing the host video frame , gives a better result.

For the proposed Algorithm-A, the PSNR value between watermarked and the original video frame without attack is found to be 44.3278 and the Bit error rate of the extracted watermarked is found to be 0.0068, normalised correlation .9892.

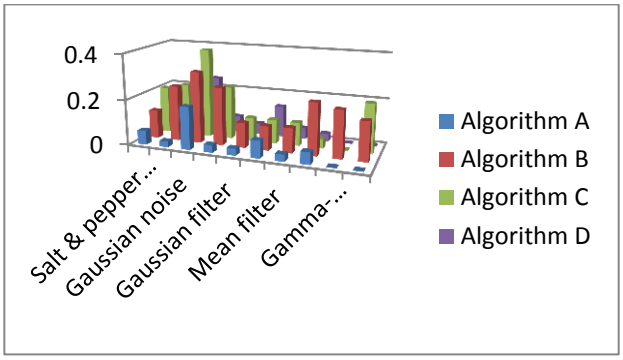

Fig.5. Bar chart for bit error

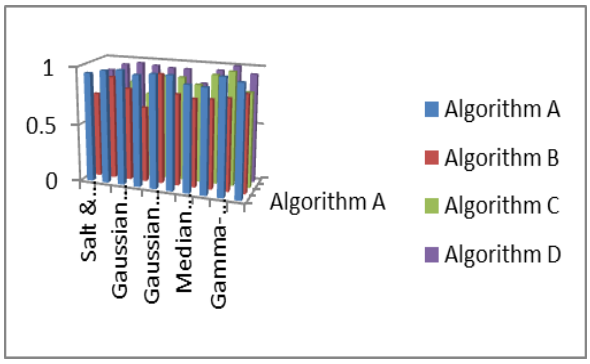

Fig.6. Bar chart for Normalised correlation

Figure below shows some of the watermarked image after attacks and their corresponding extracted watermark.

Watermarked Frame after attack	Extracted Watermark

Fig.7. after Gaussian Noise attack

Watermarked Frame after attack	Extracted watermark
	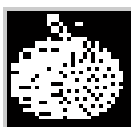

Fig.8. after cropping attack

Copyright to IJIREEICE
DOI 10.17148/IJIREEICE.2015.3825

ISSN (Online) 2321 – 2004
ISSN (Print) 2321 – 5526
INTERNATIONAL JOURNAL OF INNOVATIVE RESEARCH IN ELECTRICAL, ELECTRONICS, INSTRUMENTATION AND CONTROL ENGINEERING
Vol. 3, Issue 8, August 2015

Watermarked Frame after attack	Extracted watermark

Fig.9. after Gamma Correction attack

Watermaked Frame after attack	Extracted Watermark
	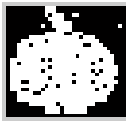

Fig.10. After histogram correction attack

V. CONCLUSION

After analysing the performance of all the algorithms after attacks it was found that the proposed watermarking Algorithm-A gives a better performance than the other algorithms. The proposed watermarking method is robust against a wide variety of attacks such as the Gaussian noise, salt and pepper noise attack, speckle noise, Poisson attack, cropping, Gaussian filtering Median filtering, Histogram-equalization and Gamma correction. It is observed all the algorithms could not withstand rotation attack which can be dealt in the future. The proposed watermarking algorithm gives a great level of imperceptibility, which is major requirement for a watermarking technique.

REFERENCES

[1] H. H. Yu, D. Kundur, and C.-Y. Li. Spies, thieves, and lies: The battle for multimedia in the digital era
[2] J. Dittmann, M. Steinebach, P. Wohlmacher, and R. Ackermann. Digital watermarks enablingE-commerce strategies: conditional and user specific access to services and resources. EURASIP Journal on Applied Signal Processing, 2002(2):174–184, Feb. 2002.
[3] Van Schyndel, R.G., Tirkel, A.Z, and Osborne, C.F, "A digital Watermark." Proc. of the IEEE Int. Conference on Image Processing. Vol. 2, (1994): pp. 86-90.
[4] Parthasarathy A.k, Kak S. "An Improved Method of Content Based Image Watermarking". IEEE Transaction on broadcasting, Vol.53, no.2, pp.468-479, June 2007.
[5] Wang Y., Doherty J.F, Dyck V.R.E. "A wavelet-based watermarking algorithm for ownership verification of digital images". IEEE Trans. Image process, 11, pp.77-88, 2002.
[6] Tao P., Eskicioglu A.M... "A robust multiple watermarking scheme in the discrete wavelet transform domain". Proceeding of the SPIE, Vol.5601, pp.133-144, 2004.
[7] Wang S.H., Lin Y.P. "Wavelet Tree quantization for copyright protection for watermarking", IEEE Trans. Image Process, pp.154-165, 2002.
[8] Lou Y et al. "Study of digital elevation mode data watermark via integer wavelets." Journal software, 16(6), pp.1096-1103,2005
[9] Yang Y, Huang D, Liu D, "An integer wavelet based multiple logo-watermarking schemes". In IEEE, vol.2. pp.175-179,2006
[10] Lin.Q, LiuZ. Feng G. "DWT based on watermarking algorithm and its implementing with DSP", IEEE Explore, pp.131-134, 2009.
[11] J Panda et.al. Digital watermarking in integer wavelet domain using hybrid technique in Advance in Computer Engineering (ACE), 2010 International Conference on 2010.IEEE

Geotech Geol Eng
DOI 10.1007/s10706-015-9915-3

COMMENTS/DISCUSSIONS AND REPLIES

Discussion on Principle of Super Position of Rate of Settlement in 2D and 3D Consolidations, Geotech Geol Eng. Doi 10.1007/s10706-015-9903-7 by Anjeshnu Trivedi and Ashutosh Trivedi

Ashutosh Trivedi · Anjeshnu Trivedi

Received: 3 August 2015 / Accepted: 10 August 2015
© Springer International Publishing Switzerland 2015

List of symbols

C_z, C_x, C_y	Coefficient of consolidation in z, x, y directions
e	Void ratio
e_0	Initial void ratio
E	Deformation modulus
$2H$	A descriptor of thickness of sample
L_z, L_x, L_y	Drainage path along x-direction and y-direction respectively
k_z, k_x, k_y	Coefficient of permeability in z, x, y directions
r	Ratio of coefficient of consolidation
r_z, r_x, r_y	Ratio of coefficient of consolidation in the z, x, y directions
T_0	Non-dimensional time factor
u	Pore water pressure at time 't'
u_i	Initial excess pore water pressure
U_{av}	Average degree of consolidation
U_{1D}, U_{2D}, U_{3D}	Average degree of consolidation in 1D, 2D and 3D consolidation
U_z, U_x, U_y	Degree of consolidation at distance of z, x, y
γ	Bulk unit weight
γ_w	Unit weight of water

The concept of fluid flow under consolidation pressure amid micro porous media generated keen interest among several early investigators conceiving effective stresses as early as Terzaghi (1925) and reported by De Boer (2005). The Biot's (1941) brought significant development to the understanding of 3D consolidation. Along with the progresses in anisotropic consolidation (Kubik 1979; Kubik and Sawczuk 1983), the author offers an impressive set of observations on the rate of consolidation of granular materials. The trends revealed by the paper are, overall, coherent with numerical data on initially isotropic consolidation process bifurcating from 1-D drainage characteristics and tend to adopt 2-D or 3-D drainage. However, owing to depositional and sedimentation dependent anisotropy (Trivedi et al. 2015a) the consolidation process may be anisotropic and resultant deformations can be estimated by a numerically consistent formulation. This discussion focuses on one admittedly minor but nevertheless intriguing result that is the

A. Trivedi (✉)
Department of Civil Engineering, Delhi Technological University, Delhi, India
e-mail: prof.trivedi@yahoo.com

A. Trivedi
Department of Civil Engineering, IIT BHU, Varanasi, India

Published online: 19 August 2015

observed differences between 2D and 3D solutions offered by the author and the discusser with few innate similarities and minor differences.

The observed consolidation in 1D, 2D and 3D drainage conditions respectively is evaluated numerically using following differential equation as considered by the author and the discussers as,

$$C_z \frac{\partial^2 u}{\partial z^2} = \frac{\partial u}{\partial t} \tag{1a}$$

$$C_z \frac{\partial^2 u}{\partial z^2} + C_x \frac{\partial^2 u}{\partial x^2} = \frac{\partial u}{\partial t} \tag{1b}$$

$$C_z \frac{\partial^2 u}{\partial x^2} + C_x \frac{\partial^2 u}{\partial y^2} + C_y \frac{\partial^2 u}{\partial z^2} = \frac{\partial u}{\partial t} \tag{1c}$$

where, C_x, C_y, C_z are directional coefficients for the distribution of pore water pressure in the reference time, t, within 1D, 2D, 3D vector space, respectively as, $z \in R$; $z, x \in R^2$ and $z, x, y \in R^3$ with average degree of consolidation U_z, U_x, U_y, represented in the orthogonal directions z, x, y respectively.

The Fourier analysis of the partial differential equation given by Eq. (1a) provides the following solution for the case of 1-D consolidation with 1-D drainage:

$$u = \sum_{n=1}^{n\to\infty} \left(\frac{1}{H} \int_0^{2H} u_i \sin \frac{n\pi z}{2H} \mathrm{d}z \right) \sin \frac{n\pi z}{2H} \exp\left(\frac{-n^2\pi^2 T_0}{4} \right) \tag{2a}$$

The degree of consolidation at a given distance and time is a quantity defined as

$$U_z = \frac{u_i(z) - u_t(z)}{u_i(z)}, U_x = \frac{u_i(x) - u_t(x)}{u_i(x)}, U_y = \frac{u_i(y) - u_t(y)}{u_i(y)} \tag{2b}$$

In Eq. (2a), H represents the thickness of the longest drainage path in the sample (a two-way vertical drainage condition has been assumed; thus $2H$ is the thickness of the sample), and, $u_t(z), u_t(x), u_t(y)$ is the pore water pressure at z, x, y distance at a given time, t, and $u_i(z), u_i(x), u_i(y)$ are the initial pore water pressure at the distance respectively of z, x, y. T_0 is the non-dimensional time factor, such that $T_0 = c't/H^2$, where c' is coefficient of consolidation of the sample, and $c' = \mathrm{kE}/\gamma_w$ as k is the permeability, E is the deformation modulus and γ_w is the unit weight of the sample.

The average degree of consolidation in 1D, 2D and 3D can be obtained in generalised form as,In 1D case,

$$U_{1D} = 1 - \frac{\frac{1}{2\cdot Lz}\int_0^{2Lz} u\, dz}{\frac{1}{2\cdot Lz}\int_0^{2Lz} u_i\, dz} \tag{2c}$$

To compute the value of U_{1D}, initial pore pressure is integrated over the z directions as,

$$\int_0^{2Lz} u_i\, dz = 2u_0\, Lz \tag{2d}$$

where u_0 is the initial pore pressure which is constant throughout the porous mass. In 2D case,

$$U_{2D} = 1 - \frac{\frac{1}{4Lz\cdot Lx}\int_0^{2Lz}\int_0^{2Lx} u\, dx\, dz}{\frac{1}{4Lz\cdot Lx}\int_0^{2Lz}\int_0^{2Lx} u_i\, dx\, dz} \tag{2e}$$

To compute the value of U_{2D}, initial pore pressure is integrated over the z and x-directions as,

$$\int_0^{2Lz}\int_0^{2Lx} u_i\, dz\, dx = 4u_0\, Lz \cdot Lx \tag{2f}$$

In 3D case,

$$U_{3D} = 1 - \frac{\frac{1}{8Lz\cdot Lx\cdot Ly}\int_0^{2Lz}\int_0^{2Lx}\int_0^{2Ly} u\, dz\, dx\, dy}{\frac{1}{8Lz\cdot Lx\cdot Ly}\int_0^{2Lz}\int_0^{2Lx}\int_0^{2Ly} u_i\, dz\, dx\, dy} \tag{2g}$$

To compute the value of U_{3D}, initial pore pressure is integrated over the z, x, y directions as,

$$\int_0^{2Lz}\int_0^{2Lx}\int_0^{2Ly} u_i\, dz\, dx\, dy = 8u_0\, Lz \cdot Lx \cdot Ly \tag{2h}$$

1 Uniqueness of 1D, 2D and 3D Consolidation Case and Rate of Consolidation

As per Trivedi et al. (2015b), the solution of the differential equation in Eqs. (1a–1c) is presented as following expressions presuming process of consolidation is 1D, 2D or 3D respectively as,

$$U_{1D} = 1 - \sum_{k=0}^{\infty} \frac{8}{m^2\pi^2} \exp\left[-T_0 r_z \frac{m^2\pi^2}{4} \right] \tag{3a}$$

$$U_{2D} = 1 - \sum_{k=0}^{\infty}\sum_{l=0}^{\infty} \frac{64}{m^2 n^2 (\pi^2)^2} \times \exp\left[-T_0\left(r_z \frac{m^2\pi^2}{4} + r_x \frac{n^2\pi^2}{4}\right)\right] \quad (3b)$$

$$U_{3D} = 1 - \sum_{k=0}^{\infty}\sum_{l=0}^{\infty}\sum_{j=0}^{\infty} \frac{512}{m^2 n^2 p^2 (\pi^2)^3} \times \exp\left[-T_0\left(r_z \frac{m^2\pi^2}{4} + r_x \frac{n^2\pi^2}{4} + r_y \frac{p^2\pi^2}{4}\right)\right] \quad (3c)$$

The Eq. (3a) is as per Terzaghi (1925) and Eqs. (3b–3c) is as per Trivedi et al. (2015a, b).

Where, $m = 2\,k + 1$, $n = 2\,l + 1$, $p = 2j + 1$, while $k, l, j \in N$

$r_x = \frac{C_x}{C'} \cdot \frac{(2H)^2}{(2Lx)^2}, r_y = \frac{C_y}{C'} \cdot \frac{(2H)^2}{(2Ly)^2}, r_z = \frac{C_z}{C'} \cdot \frac{(2H)^2}{(2Lz)^2}; T_0 = \frac{C'}{(H)^2} t$ where, T_0 is dimensionless time factor, t is the real time in the applied frame of reference; and, $\frac{(H)^2}{C'} = t'$ is reference time evolving from sample's frame of reference and has a unit of time. C' is intrinsic viscosity parameter (having unit of $m^2\ s^{-1}$) and $2H$ is the observed size of the sample in double drainage case (thickness of the sample in the double draining 1D consolidation cell). For vertical drain case, $r_x = r_y = r$, is substituted in Eq. (3b) to get a simple solution.

The observed consolidation in 1D, 2D and 3D drainage conditions respectively is evaluated numerically using a very simple relationship as considered by Newman (1931), Carillo (1942), and Scott (1963), as,

$$U_{1D} = 1 - (1 - U_z) \quad (4a)$$

$$U_{2D} = 1 - (1 - U_x)(1 - U_z) \quad (4b)$$

$$U_{3D} = 1 - (1 - U_x)(1 - U_y)(1 - U_z) \quad (4c)$$

The algebraic substitution of Eq. (3a) in (4a) and so obtained U_z is substituted in Eqs. (4b–4c) such that $U_x = U_z$ for 2D and $U_x = U_y = U_z$ for 3D isotropic consolidation respectively. Differentiating Eqs. (3a–3c) with respect to the time the rate of consolidation is obtained.

The average degree of consolidation and rate of consolidation using Fourier transformation is shown in Figs. 1 and 2. Figure 3 shows convergence rate of consolidation using Eqs. (3a) and (3b) at higher values of time factor ($T_0 = 0.2$).There appear minor differences in the numerical solutions if the range of time factor is considered at varied rates as shown in Fig. 2. However, using Fourier transform such inconsistencies largely disappear as shown in Fig. 4.

2 Bifurcation and Trifurcation from Initially 1D to 2D and 1D to 3D Consolidation Case

It implies that, the 1D, 2D and 3D consolidation can be uniquely represented by Eqs. (3a–3c). However, if the consolidation process is initially 1D then bifurcates to 2D or trifurcates or 3D case then the numerical representation as implied by the author may be presented alternatively as,

$$U_{1D} = 1 - \sum_{k=0}^{\infty} \frac{8}{m^2\pi^2} \exp r_z \left[-T_0 \frac{m^2\pi^2}{4}\right] \quad (5a)$$

$$U_{1D\ to\ 2D} = 1 - \sum_{k=0}^{\infty} \frac{8}{m^2\pi^2} \exp r_z \left[-T_0 (1 + r_x/r_z) \frac{m^2\pi^2}{4}\right] \quad (5b)$$

$$U_{1D\ to\ 3D} = 1 - \sum_{k=0}^{\infty} \frac{8}{m^2\pi^2} \exp r_z \times \left[-T_0 \left(1 + r_x/r_z + r_y/r_z\right) \frac{m^2\pi^2}{4}\right] \quad (5c)$$

3 Convergence of Initially 2D to 1D and 3D to 1D Consolidation Case

Initially 2D and 3D consolidation cases can be represented by Eqs. (3b) and (3c). Consideration of $r_x = 0$ in Eq. (3b) and $r_x = r_y = 0$ in Eq. (3c) brings convergence of initially 2D to 1D and 3D to 1D consolidation. The resultant expression may be represented as,

$$U_{2D\ to\ 1D} = 1 - \sum_{k=0}^{\infty}\sum_{l=0}^{\infty} \frac{64}{m^2 n^2 (\pi^2)^2} \times \exp r_z \left[-T_0 \left(\frac{m^2\pi^2}{4}\right)\right] \quad (6a)$$

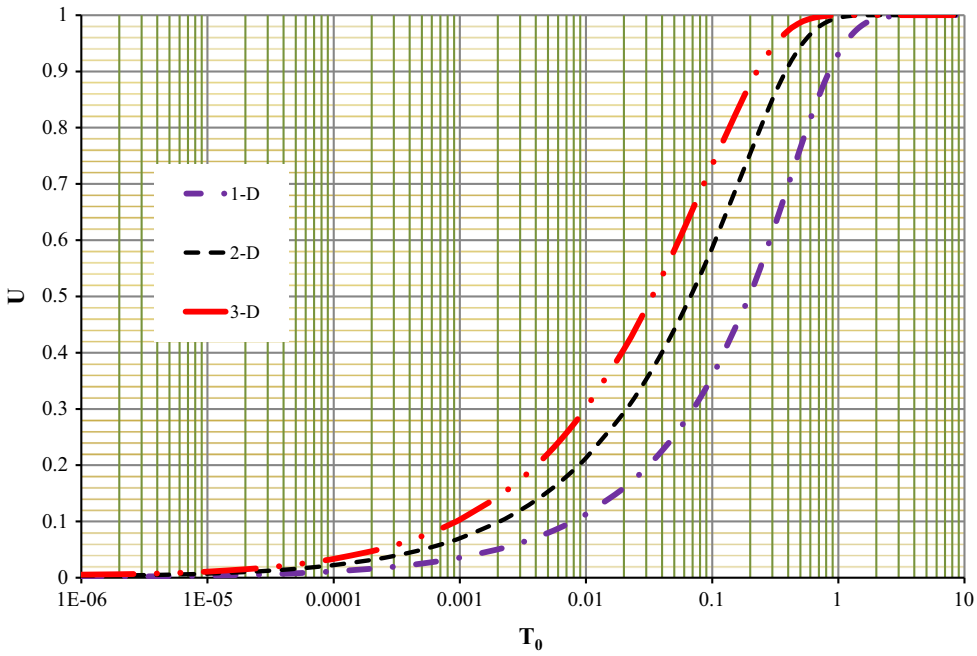

Fig. 1 Degree of consolidation in 1D, 2D and 3D versus time factor using Fourier transform

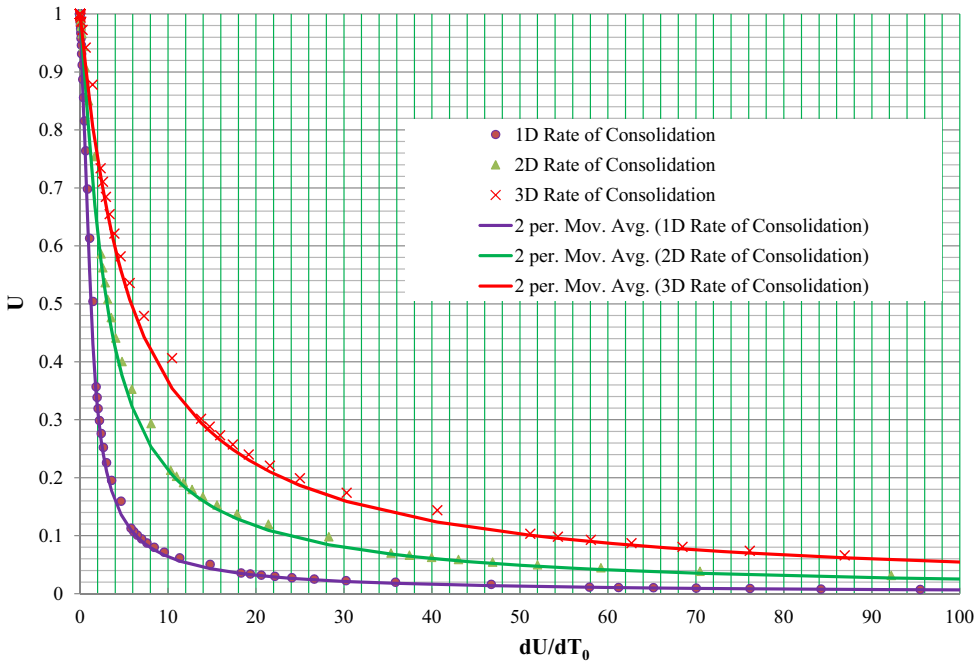

Fig. 2 Degree of consolidation versus rate of consolidation on linear scale for 1D, 2D, 3D using approximation on a range of time factor

$$U_{\text{3D to 1D}} = 1 - \sum_{k=0}^{\infty}\sum_{l=0}^{\infty}\sum_{j=0}^{\infty}\frac{512}{m^2n^2p^2(\pi^2)^3} \times \exp r_z\left[-T_0\left(\frac{m^2\pi^2}{4}\right)\right] \quad (6b)$$

4 Convergence of Initially 3D to 2D Consolidation Case

Initially 2D and 3D consolidation cases can be represented by Eqs. (3b) and (3c). Consideration of

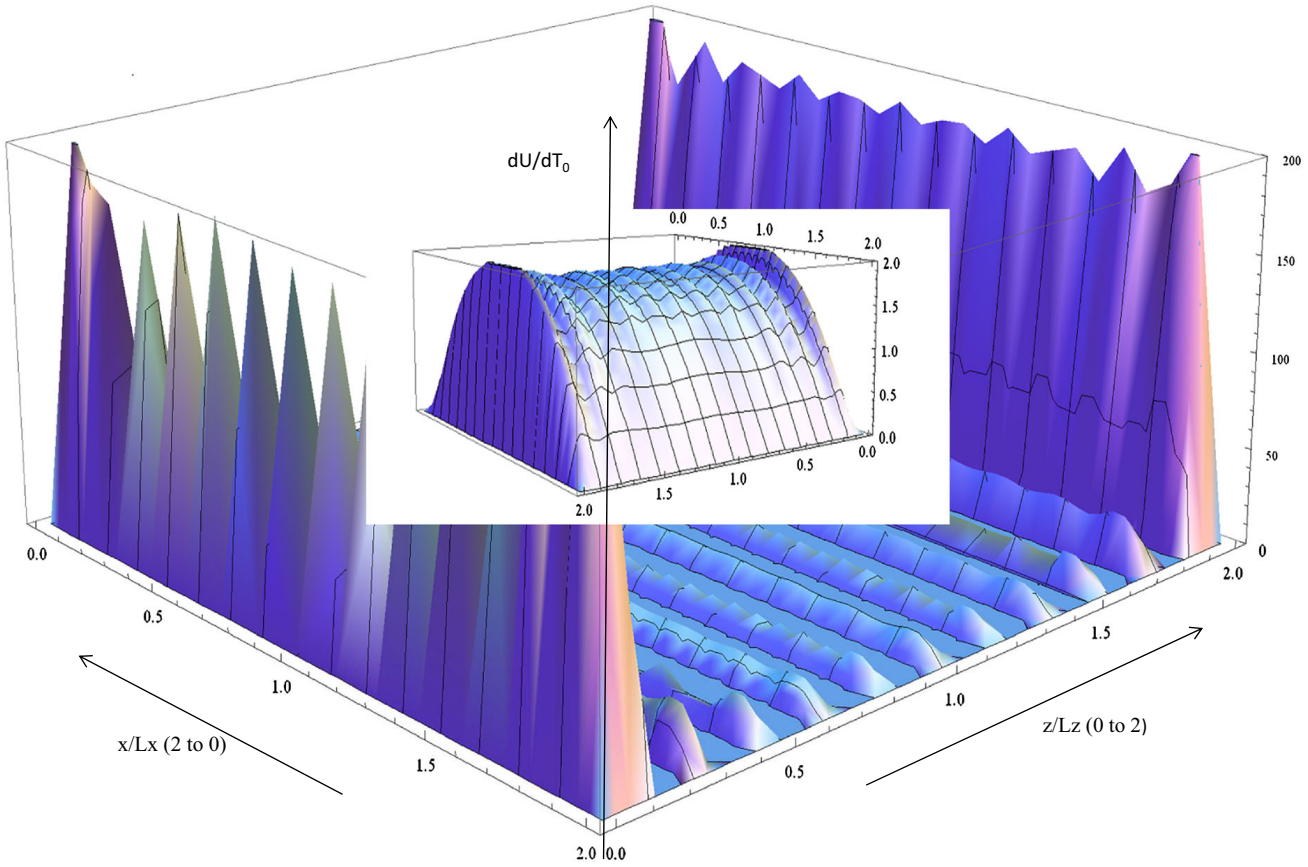

Fig. 3 An example of rate of consolidation (dU/dT_0) on vertical axis at time factor = 0.001 for outer frame; and time factor = 0.2 for inner frame, two orthogonal axis are along z and x at rx = 0 using Eq. (3b). For outer frame dU/dT_0 ranges among 0 to 200 while for inner frame it is among 0 to 2 only

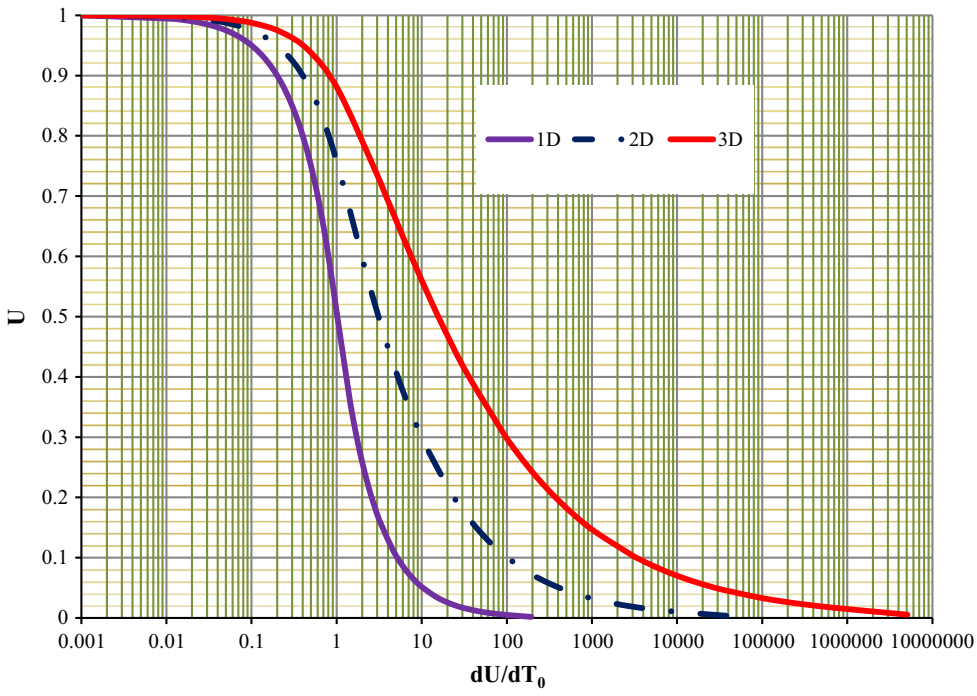

Fig. 4 Degree of consolidation in 1D, 2D and 3D cases using Fourier transform

$r_y = 0$ in Eq. (3c) brings convergence of initially 3D to 2D consolidation. The resultant expression may be represented as,

$$U_{3D\text{ to }2D} = 1 - \sum_{k=0}^{\infty}\sum_{l=0}^{\infty}\sum_{j=0}^{\infty}\frac{512}{m^2n^2p^2(\pi^2)^3} \times \exp r_z\left[-T_0\left(\frac{m^2\pi^2}{4} + (r_x/r_z)\frac{n^2\pi^2}{4}\right)\right] \quad (7)$$

Nevertheless, the author has brought a very useful insight to the 1D, 2D and 3D rate of consolidation through a set of arguments, observations, and published work and set forth the advancement of the concepts.

References

Biot M (1941) General theory of three-dimensional consolidation. J Appl Phys 12(2):155–164

Carillo N (1942) Simple two and three dimension cases in the theory of consolidation of soils. J Math Phys 21(1):11–18

De Boer R (2005) The engineer and the scandal. Springer, Berlin

Kubik J (1979) Permeability tensor and porosity of materials with rectilinear channels. Bull Acad Pol Sci Ser Tech 27:445–453

Kubik IJ, Sawczuk IA (1983) A theory of anisotropic consolidation. Ingenieur-Archiv 53(2):133–143

Newman AB (1931) the drying of porous solids: diffusion calculations. Trans. AICE, 310

Scott RF (1963) Principles of soil mechanics. Addison-Wesley, London

Terzaghi K (1925) Erdbaumechanik auf Bodenphysikalischer Grundlage. F. Deuticke, Vienna

Trivedi A et al (2015a) Consolidation of clayey gouge amid permeating rock masses. Environ Geotech 2(3):137–154. http://www.icevirtuallibrary.com/content/article/10.1680/envgeo.13.00043

Trivedi A et al (2015b) Discussion: Consolidation of clayey gouge amid permeating rock masses. Environ Geotech 2:237–248. http://www.icevirtuallibrary.com/content/article/10.1680/envgeo.14.00038

ResearchGate

See discussions, stats, and author profiles for this publication at: http://www.researchgate.net/publication/280609061

Effect Of Welding Variables On Tensile Strength Of Cu-Steel Weldments Through Design Of Experiments And Regression Mode

ARTICLE · APRIL 2015

DOWNLOADS
5

VIEWS
5

6 AUTHORS, INCLUDING:

Ramakant Rana
Maharaja Agarsain Institute of Technology
9 PUBLICATIONS **3** CITATIONS

SEE PROFILE

Available from: Ramakant Rana
Retrieved on: 18 August 2015

International Journal of Advance Research In Science And Engineering http://www.ijarse.com
IJARSE, Vol. No.4, Issue 04, April 2015 ISSN-2319-8354(E)

EFFECT OF WELDING VARIABLES ON TENSILE STRENGTH OF CU-STEEL WELDMENTS THROUGH DESIGN OF EXPERIMENTS AND REGRESSION MODEL

Surabhi Lata[1], Ramakant Rana[2], Alok Shankaran3,

Vinay Sharma4, Amit Saraswat5, Roop Lal[6]

[1,2]Assistant Professor, [3,4,5] Student, Mechanical and Automation Engineering,

Maharaja Agrasen Institute of Technology, Delhi(India)

[6] Assistant Professor, Mechanical Engineering, Delhi Technological University, Delhi, (India)

ABSTRACT

In this paper, Response Surface Methodology (RSM) is used to investigate the effect of twoprocess variables viz. Welding Speed and Current forTensile Strength of the weld of Copper and Steel. A Central Composite Design (CCD) is used to study the proposed model for Tensile Strength and to estimate the model coefficients of the two factors, which are supposed to influence the Tensile Strengthof the weld.Experiments were conducted on Copper and Steel. The RSM technique is used to model the response on experimental data. The significant coefficients are obtained by performing Analysis of Variance (ANOVA) at 5% level of significance.

Keywords: Tensile Strength, RSM, Welding, Dissimilar Metals, Modelling

I. INTRODUCTION AND LITERATURE REVIEW

Out of the various types of welding methods available in the weld industry Gas metal arc welding (GMAW) is one of the most important one, due to its flexibility, possibility of welding in different thicknesses, possibility of automatic implementation and high production capability [Moore et al. (2003), Tzafestas et al. (2000)].Industries have an increasing demand of dissimilar metal joints for various applications, viz. reduction in weight, concern regarding environment, high performance, cost saving and energy saving [Dong et al. (2012), Uzun et al. (2005)]. The transportation industry widely uses aluminium alloys for the purpose of reduction in weight [Chen et al. (2013), Zhang et al. (2007)]. [Korenyuk (1975)] tried to weld Aluminium to Titanium, this combination was not accomplished successfully by conventional arc welding processes. [Gorin (1964), Lv et al. (2012)] welded Titanium to nickel, an attempt to weld Ti and Ni using TIG was not successful. However, they used copper alloy as an insert which, led to a joint without harmful intermetallic compounds. [Mikhailov et al. (1965)] successfully welded Titanium to Copper, their produced joints were with the highest tensile strength and ductility with Ti-30Cb and Ti-

3Al-6.5Mo-11Cr. [O'Brien (2011)] welded Copper alloys to Nickel, and found that, the Copper and nickel are mutually soluble in each other. [Shao et al. (2015)] welded Aluminium and Galvanized Steel. Their thermodynamic calculations predicted that the Fe_2Al_5 intermetallic compound layer was formed first in the steel side, when temperature gradually reduced. The joining of steel and copperhas become an essential research and application focus [Chen (2015)]. It is nevertheless difficult to join them together due to the differences in physical characteristics such as the melting temperature, the poor metallurgical compatibility and thermal expansion, of these two metals.In this paper, gas metal arc welding (GMAW) method was used to join steel and copper.

II. EXPERIMENTAL SET-UP

The experiments were conducted to study the effects of various parameters of welding onjoining Copper and Steel with GMAW. These studies were undertaken to investigate the effects of Welding Speed and CurrentforTensile Strength. The workpiece material selected for the research work was Copper (100%) and steel (composition shown in Table 1). Due to its emergent range of applications in the field of manufacturing tools in mould industries, we selected Steel. Workpiece materials used were steel square plates of dimensions 100×80 mm and of thickness 6 mm. the welding process is shown in Figure 2 (b) and the Tensile Strength Specimens are shown in figure 2 (a).The test conditions are depicted in Table II.

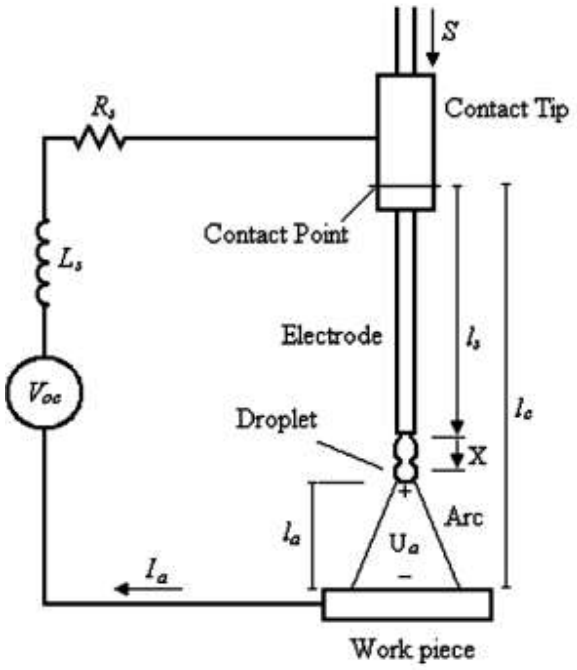

Figure 1: **Model of GMAW Process [Shao et al. (2015)]**

Table I: Composition of Steel Welded with copper

Carbon	Silicon	Manganese	Phosphorus	Sulphur	Chromium	Molybdenum	Nickel	Copper	Titanium	Cobalt	Vanadium
.352	.178	.61	.035	.037	.243	.033	.080	.089	.007	.003	.003

(a)

(b)

Figure 2: Welded Process being conducted

III. RESPONSE SURFACE METHODOLOGY

The collection of statistical and mathematical techniques named Response Surface Methodology (RSM) is useful for modelling and analysis of the problems in several input variables influences the responses. RSM objective is to find the correlation between the variables investigated and the response [Rana et al. (2014), Montgomery (2001)]. Design of Experiments (DOE) was used to estimate an unknown function for which only a few values were computed. Least square error fitting was used to model the generated relations of the response surface.A Central Composite Design (CCD) gives a comparatively accurate prediction of all response variable averages related to quantities measured during experimentation, hence it was used [Mason et al. (2003)]. Central Composite Design (CCD) offers the advantage that certain level adjustments are acceptable and can be applied in the two-step chronological RSM. In these methods, there is a possibility that the experiments will stop with few runs and decide that the prediction model is satisfactory.

Table I: DIFFERENT VARIABLES USED IN THE EXPERIMENT AND THEIR LEVEL

Variable	CODE	LEVELS	
		1	2
Current (A)	A	200	240
Welding Speed (mm/s)	B	1.11	1.44

The Current, and Welding Speedwere the variables selected for this investigation. The different levels taken for this study are shown in Table I. Three replications of Tensile Strength were taken, and the average value of Tensile Strengthused in the design matrix, is shown in Table II.

Table II: PLANNING MATRIX OF THE EXPERIMENTS WITH THE OPTIMAL MODEL DATA.

Current(A)	Welding speed(mm/s)	Tensile Strength(N/mm^2)
240	1.11	133
240	1.44	86
200	1.44	114
200	1.11	108

The experimental values were analysed and then a mathematical model was developed which, illustrated the relationship between the process response and the variables. The model in equation 1 explains the behaviour of the system.

$$y = \beta_0 + \beta_1 x_1 + \beta_2 x_2 + \in \quad \ldots 1$$

Where y = Hardness, x_1 = Current (A), x_2 = Welding speed (mm/s) and β_1, β_2= Partial Regressors.

IV. RESULT AND DISCUSSION

Based on the experimental data gathered, statistical regression analysis enabled to study the correlation of process parameters with the Tensile Strength. In this study, a polynomial regression was modelled for two variables under consideration. For simplicity, a quadratic model of Tensile Strengthwas proposed.

The coefficients of regression model was estimated from the experimental results. The effects of these variables and the interaction between them were included in this analyses and the developed model is expressed as interaction equation:

Tensile Strength (N/mm^2) = 198 - 0.037 Current (A) - 62.1 Welding speed (mm/s) …2

TABLE III: ANOVA TABLE FOR TENSILE STRENGTH

Term	**Coef SE**	**Coef**	**T-Value**	**P-Value**
Constant	198	179	1.11	0.468
Current (A)	-0.037	0.663	-0.06	0.964
Welding Speed (mm/s)	-62.1	80.3	-0.77	0.581

The unknown coefficients were determined from the experimental data as presented in Table III. The standard errors on estimation of the coefficients were tabulated in the column 'SE coef'.

It was important to check the adequateness of the model, because under-specified or an incorrect model could have lead us to misleading conclusion. The model adequateness checking included the test for significance of the model coefficients, lack of fit and regression model, which were carried out subsequently using ANOVA on the curtailed model (Table. IV).

Table IV: ANALYSIS OF VARIANCE TABLE FOR THE FITTED MODELS:

Source	DOF	Adj. SS	Adj. MS	F-Value	P-Value
Regression	2	422.50	211.250	0.30	0.790
Current(A)	1	2.25	2.250	0.0	0.964
Welding speed(mm/s)	1	420.25	420.250	0.60	0.581
Error	1	702.25	702.250	*	*
Total	3	1124.75	*	*	*

Current decreases the Tensile Strength with the increase in its value, as that is depicted in the figure 3. From figure 3 it is also vindicated that lower value of Welding Speed produces welds of high Tensile Strength. The figure 4 depicts that, the optimum value of Tensile Strength can be achieved with both the Current and Welding Speed. The surface plot of the Tensile Strength vs Welding Speed (mm/s) and Current (A) is plotted in figure 5.

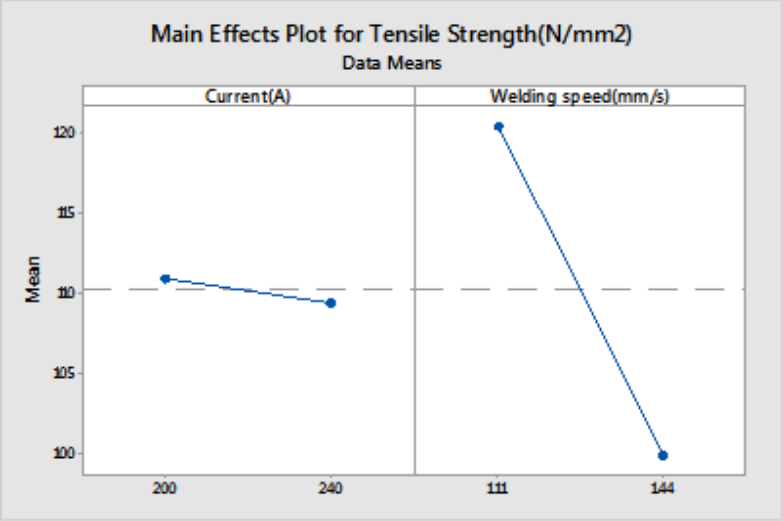

Figure 3: Effect of Current and Welding Speed on Tensile Strength

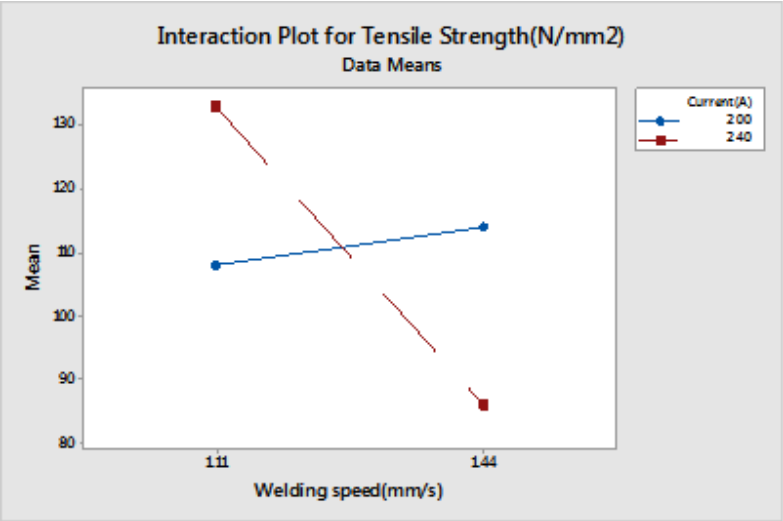

Figure 4: interaction plot of Current vs Welding Speed

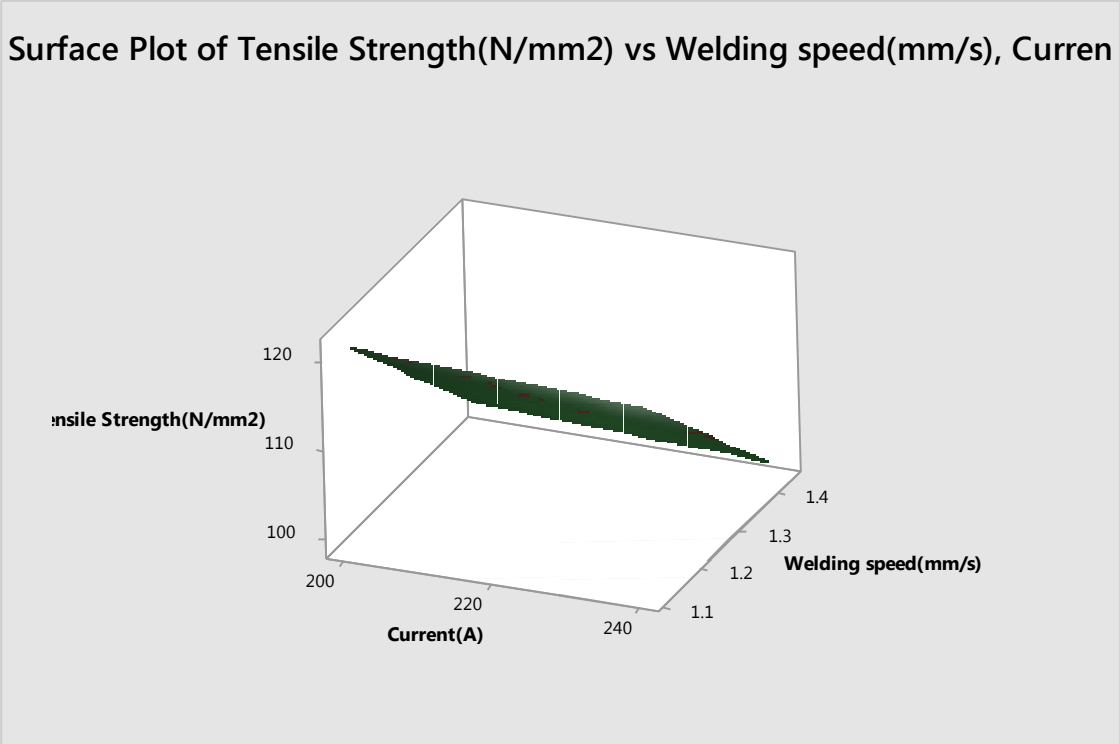

Figure 5: Surface plot of the Tensile Strength vs Welding Speed (mm/s) and Current (A)

V CONCLUSION

In thispaper, the process parameters with significant influence on Tensile Strengthwas determined by using RSM. A response model of these parameters were developed and it was found that the Current, Welding Speed, and interaction term of Current with Welding Speed significantly affect the Tensile Strength. Tensile Strength is inversely proportional to the linear effect of Welding Speed and Current. The higher value of Tensile Strength is achieved with I = 200 A, and Welding Speed = 1.11 mm/s within the experimental domain. The research findings of the present study is based on RSM models, and can be used effectively in joining of Steel with Copper, in order to obtain best possible strength of weld. This research can also help researches and industries for developing a reliable and robust knowledge base along with early prediction of Tensile Strength without experimenting with joining of materials.

REFERENCES

1. Chen Shuhai, Huang Jihua, Xia Jun, Zhao Xingke, Lin Sanbao, “Influence of processing parameters on the characteristics of stainlesssteel/copper laser welding”, Journal of Materials Processing Technology, Vol. 222, 2015, pp. 43–51
2. Chen Y, Weyland M, Hutchinson CR. The effect of interrupted aging on the yield strength and uniform elongation of precipitation-hardened Al alloys. Acta Mater 2013, 61 pp. 5877–5894.

3. Cook, LA, &Stavish, MF. (1956). Welding aluminium to copper using the inert gas metal arc process. Welding Journal, 35(5), 348–355.
4. Dong HG, Liao CQ, Chen GQ, Dong C. Butt jointing of aluminum to steel by arc brazing process. Mater Manuf Process 2012, 27:1392–6.
5. Gorin, LG. (1964). Welding titanium alloys to nickel-base alloys. Welding Products, 11(12), 46–53.
6. Korenyuk, YM. (1975). Interaction of liquid aluminium and solid titanium in fusion welding [J]. Welding Production, 22(6), 3–5.
7. Lezovskaya, AV, &Rabkin, DM. (1966). Fusion welding aluminum to copper. Automatic Welding, 19(7), 65–66.
8. Lv, SX, Jing, XJ, Huang, YX, Xu, YQ, Zheng, CQ, & Yang, SQ. (2012). Investigation on TIG arc welding–brazing of Ti/Al dissimilar alloys with Al based fillers. Science and Technology of Welding and Joining, 17(7), 519–524.
9. Mason R. L., Gunst , R. F., Texas D. and Hess J. L., "Statistical Design and Analysis of Experiments With Applications to Engineering and Science", 2nd Edition, A John Wiley & sons publication, 2003.
10. Mikhailov, AS, Slonimaky, EV, Senic, AM, &Sukhorukov, AP. (1965). Welding titanium to copper and its alloys. Weld Product, 12(8), 1–6.
11. Minitab14, Minitab User Manual Release 14 MINITAB Inc, State College, PA, USA,, 2003.
12. Montgomery D. C., "Design and analysis of experiments," John wiley and Sons Inc., 2001.
13. Murray, JL. (1982). The magnesium-aluminum phase diagram. Bulletin Alloy Diagrams, 3, 60–74.
14. O'Brien, A. (2011). Welding handbook, volume 4 - material and application. Part 1, 9th edn. Doral: American Welding Society (AWS).
15. Rana Ramakant, Rajput Kunal, Saini Rohit, LalRoop, "Opimization of Tool Wear: A Review", International Journal of Modern Engineering Research, Nov, 2014, vol. 4, Issue 11.
16. Shao L., Shi Y., Huang J.K., Wua S.J., "Effect of joining parameters on microstructure of dissimilar metal joints between aluminum and galvanized steel", Materials and Design, Vol. 66,2015, pp. 453–458.
17. Uzun H, Donne CD, Argagnotto A, Ghidini T, Gambaro C. Friction stir welding of dissimilar Al of 6013-T4 to X5CrNi18-10 stainless steel. Mater Des 2005, 26:41–6.
18. Zhang HT, Feng JC, He P, Hackl H. Interfacial microstructure and mechanical properties of aluminum–zinc-coated steel joints made by a modified metal inert gas welding–brazing process. Mater Charact, 2007, 58, pp. 588–92.
19. Moore K.L., Naidu D.S., Ozcelik S., Modeling, Sensing and Control of Gas Metal Arc Welding, Elsevier, 2003.
20. Tzafestas S.G., Kyriannakis E.J., Regulation of GMA welding thermal characteristics via a hierarchical MIMO predictive control scheme assuring stability, IEEE Transactions on Industrial Electronics 47 (3), 2000,pp. 668–678.

Employment at High-end IT Enabled Services in India

Dr Seema Singh
Faculty in Economics, Delhi College of Engineering
Delhi- 110 042, INDIA

Abstract
Emergence of information and communication technology (ICT) has made possible to digitally shift part of the business process to a place where it will have competitive advantage. Consequently, developed countries are shifting its labour intensive business process, even to other countries where it can be performed at a fraction of cost without compromising on its quality. India is one of the preferred destination for such work due to robust communication infrastructure, large pool of English speaking young knowledge workers, stable democracy. Growth of IT enabled services (ITES) has remained phenomenal both in terms of revenue and employment generation. However, most of the ITES which is being done at present in India are at the lowest rung of the value-chain which fetches lower profit and there is stiff competition in this segment as other countries with even cheaper labour are in the fray. ITES will have to move up in the value chain to become sustainable. Though, there is large potential for high-end ITES and recent trend have shown signs of moving towards high-end ITES but even now it constitute very small segment. In this background, an attempt has been made to discuss that India has huge technical education infrastructure both physical as laboratory, workshops etc. and human as faculty members, students etc. It may be utilized to harnesses in basic applied research and development (R&D) activities for upward movement of ITES. All the stake holders of higher and technical education will have to work together to utilize existing educational infrastructure to its maximum as well as to create new world class facilities. In this context, ICT may play crucial role. National Research and Development Information System (NR&DMIS) may be developed for establishing lateral as well as forward-backward linkage among all the stake holders as technical institutes, research laboratories and funding agencies as well as those companies which are outsourcing activity to facilitate R&D activity in cost effective way.

I. Introduction

Emergence of information and communication technology (ICT) has made possible to digitally shift part of the business process even to another countries[1] where it has advantage. Consequently, developed countries are shifting its labour intensive business processes to developing countries[1] where it can be performed at a fraction of cost without compromising on its quality. Beside, cost advantage, some of the other equally important factors are

superior competency, utilization improvement, economy of scale and business risk mitigation for adoption of business process outsourcing. As corporations merge and consolidate operations, this trend towards outsourcing non-core business processes has become a new business model for international cooperation between developed countries like USA, UK and developing countries like India, Singapore, Hong Kong, China, Philippines, Mexico, Ireland etc.

Among developing countries, India is one of the preferred destinations and has experienced phenomenal growth as IT enabled services (ITES) destination in recent years[2] and pace of outsourcing is going to increases even further. Mainly low end outsourcing[3] activities are performed by Indian providers (D'Costa, 2003). However, due to intense competition prices for some of the low end outsourced services have fallen so dramatically that many ITES companies are already struggling to survive. Also, it is very likely that other developing nations with even cheaper labour will compete with India in the near future. Moving up the value chain for Indian service providers is very important to sustain. There is large potential for outsourcing in High-end ITES segment as well as recent trend have shown signs of moving towards high-end ITES, though it constitute very small segment. In this background an effort has been made in this paper to discuss that India's huge technical educational infrastructure both physical as well as human which need to be harnessed for upward movement of ITES. The paper is divided in six sections. The second section discusses trend of high-end ITES. Third and fourth section deals with technical manpower resource and state of technical education in India. Framework for effective utilization of existing infrastructure for India so that it works as hub of engineering and managerial service outsourcing has been discussed in fifth section. Last section concludes the discussion.

II. Trend in High End ITES in India

Though shifting of some of the business process to a place where it can be performed in more efficient way started with low-end processes, companies of the west are continuously outsourcing non core-activities so that they can concentrate on their core area. A 2005 survey by Booz Allen and Duke University Centres for International Business Education & Research (GIBER) found that 36 percent of the companies surveyed sent some of their engineering offshore, 31 percent some R&D, 16 percent shipped out of the portion of their product design and 9% innovation services (NASSCOM, 2006.a).

Deregulation of the telecom sector has enhanced long distance national/ international connectivity which ultimately has facilitated growth of ITES in India. It is young and nascent sector and has been in existence for almost six years. Despite its recent arrival on the Indian scene, the industry has grown phenomenally and has now become a very important part of the export-oriented IT software and service environment. Since beginning, ITES has continuously been able to achieve double digit growth. According to NASSCOM estimate, export revenue earned in terms of US$ was 0.6 billion in 1999-2000 which rose to 5.2 billion in 2004-05 and likely to become more than a trillion industry by 2020. Not only that number of workers in ITES sector has increased rapidly from 41 thousand in 1999-2000 to almost 4 lakh in 2004-05. Along with increased presence of Indian IT companies across the globe, new service lines/ segment are also emerging and the Industry has reached the next level of services offered. However, in spite of the growth seen so far both in terms of quantity as well as quality, it is estimated that less than 10 percent of the addressable market for globally sourced IT-ITES has been captured till date which it shares with Canada, China, Mexico and

Eastern Europe indicating significant headroom for growth (NASSCOM, 2006.b). Thus, there is huge potential for high-end ITES.

At the moment, even the Indian talent supply looks sufficient even for high end outsourcing. The Indian service providers are technically proficient and have a zealous eye for detail ensuring that service levels remain as good or far superior to those in countries like the US. However, in the long run China is a formidable competitor for India While India has advantage in terms of fluency in English language skill, cultural compatibility with the west, a robust political and legal system and relatively strong protection of intellectual property (IP). China has a much stronger infrastructure and well developed manufacturing base (NASSCOM, 2006. a pp7).

III. Technical Manpower Resource in India

ITES is highly labour intensive sector. The employee base in this sector has grown at a compound annual growth rate of 52.6 % and is employing more than 4 lakh in 2005-06. And will require at least, 80, 000 more each year in the foreseeable future (with some 35,000 leaving the industry each year). Initially, low end services were outsourced to India. Workers were mainly employed in voice based outsourcing services or labour intensive applications of IT like data entry and other back office services. To grab this young set one model which was used was fun at the work place. Employees are expected to respond to some queries. Office environment is good. However, there is neither intellectual stimulation nor many lines opening up after 3-4 years. Career upward movement is clear from manager to senior manager, and then it gets fuzzy. Consequently, people perception about employment in ITES is of job and not of career. They join ITES just as a platform to get proper job or to fill the

gap between two educational degrees. As a result, this sector is working under pressure due to huge attrition rate and a consequent spiraling of retraining cost (Singh, 2005.a). At present, there is not paucity of workers with skill set to perform low end job. But as India is creating newer opportunities from different process or segment and has become sought after destination, though at a small scale for R&D outsourcing[4], patent document or equity research at a fraction of cost in the developed countries with no compromise on the quality of work. Nearly 100 MNCs have R&D facilities in India. She has great strengths in bio-technology and pharmaceuticals and huge reservoir of creativity exists in traditional knowledge and local entrepreneurship (Dohlman and Ulz, 2005, p.10). However, as the industry tries to move up the value chain to knowledge process outsourcing (KPO), the demand for fresh graduate is being replaced by demand for more qualified MBAs, MCAs, engineers along with Ph.D. in Physics, chemistry, economics, accountancy etc. At the moment situation looks quite comfortable. More than 350 universities and engineering colleges and 2,300 recognized private training institutes contributes to second largest pool of English-speaking technically trained manpower resource pool of India which is only after the US. However, looking at the potential and nature of ITES, there is need to take up skill formation and skill up gradation more aggressively (Singh, 2005.a). China which is likely to be a formidable competitor for India has been giving a great thrust on higher education that number of graduates and post graduates with soft skills and proficiency in English is growing phenomenally.

ITES sector is quite competitive and it does not have time to mature. Till three years back, Ire land was considered as BPO capital of the world but now its position has slipped down. If India has to maintain its competitiveness and move up in the value chain as

destination R&D, it has to prepare itself to face challenges of skill gap and quality problem in the long run. Many efforts are being made at firm level. Training is becoming part and parcel of the hiring policy as industry learns to cope with quality problems. Business Process Outsourcing (BPO) firms are adopting various 'routes' and methods to enable their employees to develop relevant expertise and competencies and enhance their knowledge base. In line with known HR practices of manufacturing, infrastructure and financial services corporation, BPO sector is developing people on-the-job and off-the-job. On-the-job training, self-learning interactive web-based training session, short-term workshops, regular refresher course and hand-on projects on clients sites in foreign locations are being taken up depending on the requirement for voice and accent improvement, personality development and up gradation of technical skills for each level of management depending on specific needs. Some of the captive BPO firms are also sponsoring part-time MBA and domain specific programs of talented employees with high end outsourcing services like automotive engineering and design software products, R&D, financial data modeling and analysis. It is imperative for them to ensure that employees are cued into the best-of-breed technologies and latest techniques and methodologies. Relevant domain knowledge can be enhanced by introducing fast-track course in engineering and technical discipline. Critical fundamentals can also be brushed up from time to time. These can be supplemented through practical training on projects and assignments and mentoring can play a key role in enhancing the learning experience. Clearly, with HR back on the agenda as a competitive determinant, BPOs are hoping to develop best practices in various functional disciplines. In whatever way the benefits are parleyed, employees hope that such HR measures and initiative are entwined with core organizational visions and are not some passing attrition controlling gimmicks and

shot run motivational inducements. A large Mumbai-based international BPO is ensuring that their employees are at the cutting edge of training and skill sets development. Employees access a US-base enterprise e-learning provider's site either through the Internet or through the company Internet with the help of unique log-ins (which can also be accessed from home). They can choose from a string of courses on technology skills, business skills. Exhaustive yet 'easy-step' courses like MS office, MS power point and MS Excel are among the more popular ones. Employees are eagerly availing of these courses and programmes with flexi learning sessions and hours enabling them to chart out their work schedules accordingly. Some IT companies have also worked in this direction. TCS, for example, has put in place a comprehensive academic interface programme (AIP) process framework and proper infrastructure. Under this programme, professors from academia are also sent on sabbatical to TCS. Zenzer Technologies has partnered with Symbiosis International Educational Centre to offer placement guarantees to successful graduates of the institutes management course in information technology. Admission to this course are on the basis of a national entrance examination. The batch of 90 students in the course includes engineering students from premier institutions as well as non-engineering graduates from relevant streams. Parametric Technology Corporation (PTC) is another company that has made available its specified CAD/CAM software Pro-Engineering Programme to colleges across the world and is providing training on its platform. The company has entered into a partnership with ITC Infotech to promote technological literacy among secondary school students throughout India and has provided over 200 engineering colleges including the IITs, BITs and RECs with Pro/ Engineer Software for their class room (Majumdar, 2005).

However, looking at the potential and nature of ITES, there is need to take skill formation and skill upgradation more aggresively.

IV State of Technical Education in India

India has made huge strides in the area of technical education which churns out lakhs of engineers, MBA and MCA every year. In 2004-05, there were 1436 degree and 1244 diploma level institution with intake capacity of 450000 and 265000 respectively (Table 1) while only 65000 in US. There are lakhs of faculty member, Ph.D. and post graduate students. These human as well as physical as laboratory, workshop etc. at technical institutes may be used for carrying out outsourcing work for basic and applied scientific research (Singh, 2004). However, research culture is not well developed in most of the technical institute or even if it is there, some time, there is no enthusiasm on the part of student to pursue Ph. D. programs in technical discipline. Added to it, quality is another problem area. Even there are problems of duplication and replication also in research work. To enhance R&D culture in technical institutions, it may be made an integral part of technical education and examination system and on line of compulsory industrial training in BE course, technology development may be incorporated at graduation and post-graduation level. A well developed technology incubator may be made mandatory for all technical institutions where young students may be encouraged to visit very frequently. Senior students under guidance of faculty member may undertake outsourced R&D work which has demand in the market. To assess the demand, institution may be encouraged to establish partnership with industry, organizations, government bodies and academia. Concept of 'earn while you learn' may be

introduced under which even student can undertake outsourcing work. The institute can take nominal share of consultancy work done by student for infrastructural help.

One of the main reasons for MNCs are coming to India with enormous business opportunity is its large pool of very efficient technical manpower. If they will not be able to get, they will fly to other countries (Singh, 2005.b). There is large number of institutions in India but all the institutions are not of the same quality. Technical Institutions may be ranked on the basis of index which may be made on the basis of number, size and quality of laboratory, placement performance, frequency of syllabus revision, patent applied for, paper written by faculty members and students by All India Council of Technical Education (AICTE). It will give institutions motivation to improve themselves as well as the companies to know about the specific area of work and their national ranking.

To continuously improve and upgrade standard of teaching, yllabus may be revised periodically in consultation with companies. Along with strong foundation in technological fundamental, students must be trained in soft skills, customer friendliness and rapid response to customer problems to make them more employable for outsourced work. They must be made acquainted with related engineering software tools such as AutoCAD, Catia, Pro/E, I-deas or Ansys. To achieve excellence, institution may be encouraged to establish partnership with industry, organization, government and academia. Most importantly, rules and regulation of universities may be made more flexible to accommodate outsourced R&D activities.

V. Framework for R&D work in Technical Institutes

Outsourcing activity is highly volatile. It can move within and between countries depending on comparative advantage. As technical institutes have advantage for outsourced activities in R&D, thus outsourced work on basic and applied research from the corporate houses may be taken by technical Institutes. They may under take engineering design and detailing, structural steel detailing, modeling and simulation. However, scientific and technological knowledge yields its greatest benefit when it is used within a complex system of institutions and integrated through web (Bhushan, 2005). Hence, concerted effort will have to be made together by all the stake holders of higher and technical education to utilize existing educational infrastructure as well as to create new world class facilities. In this context, ICT may play crucial role. National Research and Development Management Information System (N R&D M I S) may be developed to establish lateral as well as forward-backward linkages among research laboratories and funding agencies to facilitate outsourced R&D activities with technical institutions at helm of affairs (Fig 1). NR&DMIS may play as an interface between companies which outsource work and institute of technical education and research. Whenever companies decide to outsource some work they may approach NR&DMIS. As it will have all the information about capabilities and skill available to technical institutions, relevant information may be shared with company. The company will save time and effort and approach directly to the right institute. Governments though various department and other organizations such as All India Council for Technical Education (AICTE), Council for Scientific and Industrial Research (CSIR), Department of Science and Technology (DST) finance research projects. If there is proper coordination between all the stakeholders, all of them will know about type of outsourced work as it comes to institute. Funding agencies may partially finance the outsourced work to technical institutions under various scheme, it will

further decrease the cost of R&D which will ultimately make the institutions more competitive. Those outsourced work which can not be done by single institutions can be shared by two or more institutions.

VI. Conclusion

ITES has potential for phenomenal growth both in terms of revenue as well as employment. However, low-end outsourced work is not sustainable in the long run. To make it sustainable, ITES will have to move up in the value chain. At the same time, technical education has experienced large scale expansion in recent years. Infrastructure, both in terms of human as faculty members, student and physical as laboratory, workshop etc. available at technical institutes may be used for high-end ITES. As all technical institutes are not same in terms of quality. Technical Institutions may be ranked on the basis of an index which may be developed on the basis of number, size and quality of laboratory, placement performance, frequency of syllabus revision, patent applied for, paper written by faculty members and students by All India Council of Technical Education (AICTE). It will give institutions motivation to improve themselves as well as inform the companies which is going to outsource its work about their status as well as its specific area of work. To continuously improve the quality of education, syllabus may be revised periodically in consultation with companies. Along with strong foundation in technological fundamental, students must be trained in soft skills, customer friendliness and rapid response to customer problems. National R&D Management Information System (N R&D M I S) may be developed to establish lateral as well as forward-backward linkages among research laboratories and funding agencies to facilitate outsourced R&D activities with technical institutions at helm of

affairs. NR&DMIS may play as an interface between companies which outsource work and institute of technical education and research. Whenever companies decide to outsource some work they may approach to NR&DMIS. As information system will have all the information about capabilities and skill available to technical institutions, it can share information with company. The company will save time and effort and approach directly to the right institute. Governments though various department and other organizations such as AICTE, CSIR, DST finance research projects. If there is proper coordination between all the stakeholders, all of them will know about type of outsourced work as it comes to institute. Funding agencies may partially finance the outsourced work to technical institutions under various scheme, it will further decrease the cost of R&D which will ultimately make the institution more competitive. Those outsourced work which can not be done by single institutions can be shared by two or more institutions.

Notes:

1. Such transactions are called as Mode 1 trade in service in WTO terminology.
2. Robust communication infrastructure, large pool of English speaking manpower and stable democracy are some of the advantage for India. Countries like Nigeria can prove cheaper solution than India. But unstable polity hanpers investment in Africa.
3. Mainly five type of works are being done by BPO sector i.e. voice based, back office services, IT or web based, management based services and engineering based sevices. Voice based outsourcing include electronic and voice help desk/ event tracking software, inbound and outbound communications. Wide range of activities comes under back office services. Some of them are data entry, word processing, pay roll, health claims administration etc. Voice based and back office outsourcing together can be termed as low-end outsourcing. Under IT or web based outsourcing, specialized IT services comes as web design, PC hardware and services etc. IT based outsourcing along with management services outsourcing and engineering services outsourcing makes high end outsourcing services. Enterprise management, supply chain management, human resource management is example of management services outsourcing. A range of engineering services such as domain registration, R&D activities, automotive, industrial machinery and tools design, electronic circuitry design comes under engineering service outsourcing activity.
4. P&G for example has had a mandate that 50% of its R&D that will be commercialized will be developed from outside and that's where bases like Brazil, Russia, China and India Become important (Round table VII, Business World)

Reference

AICTE (2004-05), "Annual Report" All India Council for Technical Education, New Delhi.

Bhushan Shudhansu (2005), "Knowledge Economy and Higher Education" The Indian Journal of Labour Economics, Volume. 48, Number 4, October-December, pp. 869- 880.

Dahlman, Carl and Ulz, Anjula (2005), "India and the knowledge Economy Leveraging Strengths and Oppertunities", World Bank Finance and Private Sector Development Unit South Asia Region and World Bank Institute.

D'Costa, Anthony (2003), "Uneven and Combined Development: Understanding India's Software Exports", World development, Vol. 31, No. 1, pp. 211-226.

Majumdar Shyamal (2005), "How to stop BPO attrition" Business Standard, June 17, pp 08.

NASSCOM (2006.a). Indian IT sector to top US $ 36 Billiob in 2006, http:// www.nasscom.in/upload/49042/Executive520Summary.pdf downloaded on 12.8.2006.

NASSCOM (2006.b). Indian IT sector to top US $ 36 Billiob in 2006, http:// www.ibef.org/artdisplay.aspx?tdy=1&Cat_id=60&art_id=9754 downloaded on 12.8.2006.

Singh Seema (2004), Role of Engineering Institute in Maki8ng Micro and Small Manufacturing Enterprises Sustainable, University News, 42(46) pp 124-127.

Singh Seema (2005.a), "Skills and Career of Knowledge Workers in the BPO Sector" paper presented in 47th ISLE Conference at JNU, New Delhi between December 15-17, 2005.

Singh Seema (2005.b), "MNCs Effect on Employment of Engineers" The Indian Journal of Technical education, 28 (2), pp 38-44.

The BW Round Table VII in Association with NASSCOM, "Indian IT and ITES Industry, Turning Point", Business World, 22 (42), pp. 44-46.

Table1: Institutions providing Technical Education in 2004-05

	Number of Institution	Intake Capacity
Engineering		
Degree	1436	4,50,000
Diploma	1244	2,65,000
Management		
MBA	1007	75,000
MCA	1051	57,000
Pharmacy		
Degree	445	25,000
Diploma	415	24,000

Source: AICTE, 2004-05.

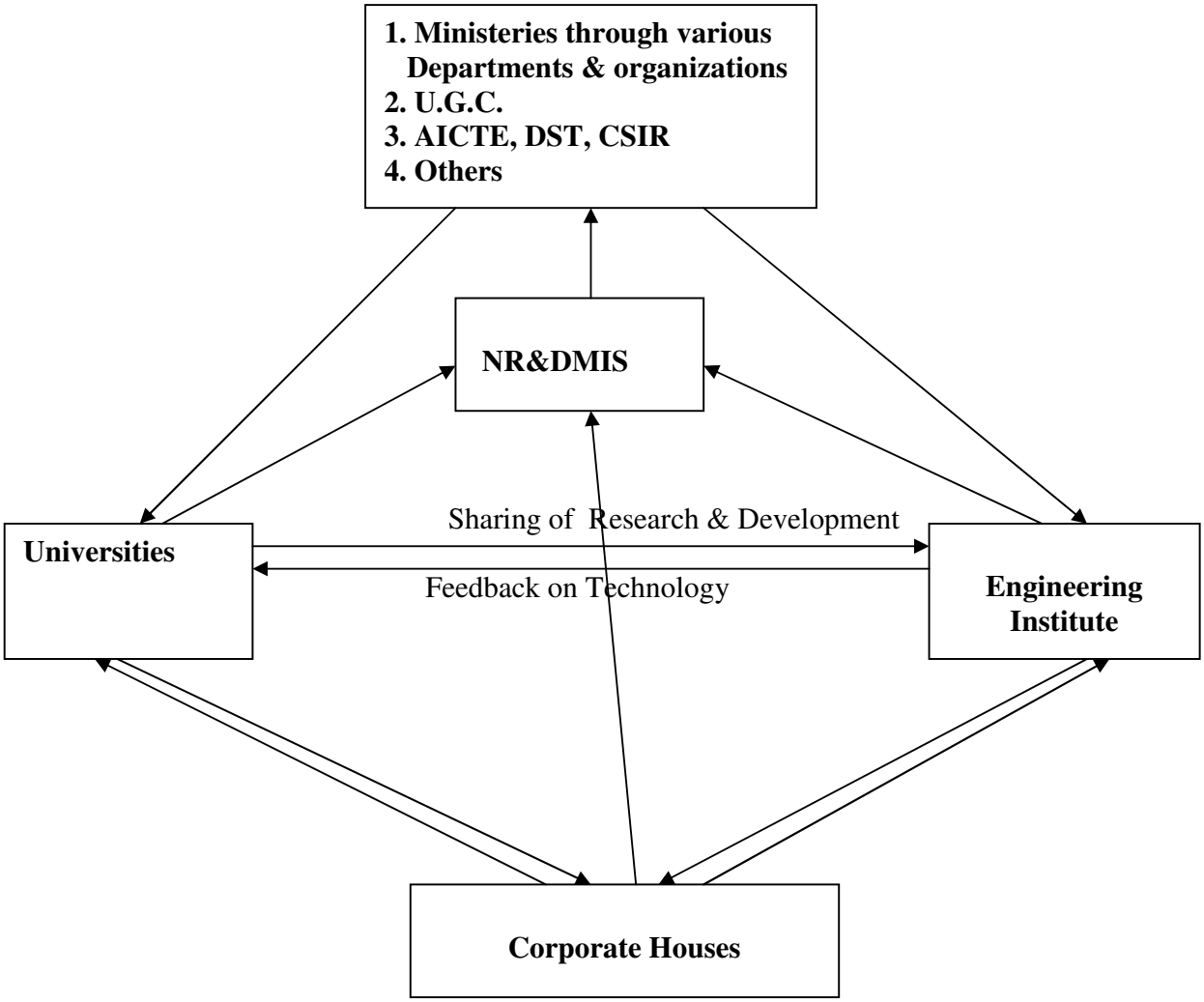

Fig 1- Framework for Outsourcing Work in R&D in Higher Educational Institutes

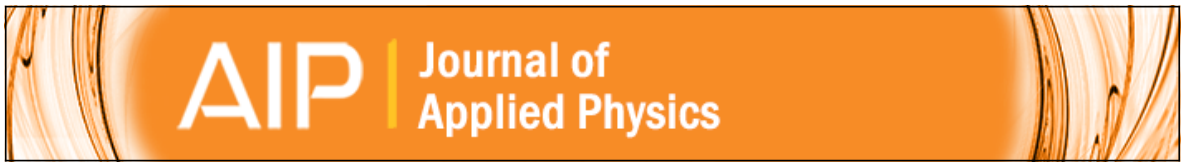

Enhanced ferroelectric photovoltaic response of BiFeO3/BaTiO3 multilayered structure

Savita Sharma, Monika Tomar, Ashok Kumar, Nitin K. Puri, and Vinay Gupta

Citation: Journal of Applied Physics **118**, 074103 (2015); doi: 10.1063/1.4928964
View online: http://dx.doi.org/10.1063/1.4928964
View Table of Contents: http://scitation.aip.org/content/aip/journal/jap/118/7?ver=pdfcov
Published by the AIP Publishing

Articles you may be interested in

Enhanced ferroelectricity, piezoelectricity, and ferromagnetism in Nd-modified BiFeO3-BaTiO3 lead-free ceramics
J. Appl. Phys. **116**, 184101 (2014); 10.1063/1.4901198

Studies of the switchable photovoltaic effect in co-substituted BiFeO3 thin films
Appl. Phys. Lett. **105**, 172904 (2014); 10.1063/1.4900755

Switchable photovoltaic response from polarization modulated interfaces in BiFeO3 thin films
Appl. Phys. Lett. **104**, 142903 (2014); 10.1063/1.4870972

High quality multiferroic BiFeO3 films prepared by pulsed laser deposition on glass substrates at reduced temperatures
J. Appl. Phys. **113**, 17D917 (2013); 10.1063/1.4796194

Enhanced photovoltaic properties in graphene/polycrystalline BiFeO3/Pt heterojunction structure
Appl. Phys. Lett. **99**, 132904 (2011); 10.1063/1.3644134

[This article is copyrighted as indicated in the article. Reuse of AIP content is subject to the terms at: http://scitation.aip.org/termsconditions. Downloaded to] IP: 14.139.251.107 On: Tue, 25 Aug 2015 06:26:21

JOURNAL OF APPLIED PHYSICS **118**, 074103 (2015)

Enhanced ferroelectric photovoltaic response of $BiFeO_3/BaTiO_3$ multilayered structure

Savita Sharma,[1,2] Monika Tomar,[3] Ashok Kumar,[4] Nitin K. Puri,[2] and Vinay Gupta[1,a)]
[1]*Department of Physics and Astrophysics, University of Delhi, Delhi 110007, India*
[2]*Department of Applied Physics, Delhi Technological University, Delhi 110042, India*
[3]*Physics Department, Miranda House, University of Delhi, Delhi 110007, India*
[4]*CSIR-National Physical Laboratory, Dr. K. S. Krishnan Marg, Delhi 110012, India*

(Received 31 March 2015; accepted 8 August 2015; published online 21 August 2015)

The present work is based on the photovoltaic properties of multilayered structure of Bismuth ferrite (BFO) and Barium titanate (BTO) thin films prepared by pulsed laser deposition technique on platinum coated silicon substrate. The multilayered structure possesses enhanced ferroelectric properties and shows a remarkable increase in photocurrent (from 1.56×10^{-7} A to 6.96×10^{-5} A) upon illumination with laser light of wavelength 405 nm at an intensity of 160 mW/cm^2. The values of short circuit photocurrent and open circuit voltage were found to be 0.3184 mA/cm^2 and −1.25 V, respectively, with a light-to-electricity conversion efficiency of 0.067%. A relatively high efficiency calculated at 405 nm for the developed multilayered BFO/BTO structure highlights its practical application in ferroelectric photovoltaics. © *2015 AIP Publishing LLC*.
[http://dx.doi.org/10.1063/1.4928964]

I. INTRODUCTION

Over several decades, researchers have been striving to open different corridors for the production of renewable energy to curb the evolving demands for inexhaustible energy and clean fuel sources.[1–5] The exceptional advantages of ferroelectric photovoltaic effect (FE-PV) over the conventional p-n junction based photovoltaic (PV) devices, such as high output voltage and polarization controlled PV response, appear promising for the realization of efficient functional devices.[1,6–8] FE-PV effect is observed in several perovskite oxide systems, such as $Pb(Zr,Ti)O_3$ (PZT), $BaTiO_3$ (BTO), etc.,[3,7–10] but disappointingly, the photovoltaic efficiency in such materials undergoes quenching due to their small current density (of the order of 10^{-9} A/m^2) and large optical band gap (typically ∼3.5 eV). Therefore, it becomes imperative to tailor the physiochemical properties of these ferroelectric materials for possible device applications.

Most notable of the available ferroelectric materials, Bismuth ferrite (BFO) with its small optical band gap and good chemical stability, has fueled interest of the research community in past several years. Moreover, the lead free nature of BFO does not constrict its potential applications as compared to its non-environment friendly counterpart, lead zirconium Titanate (PZT).[6] BFO is a room temperature multiferroic material having high ferroelectric Curie temperature (∼1120 K) and antiferromagnetic Neel temperature (∼643 K).[11–13] However, the inherent high leakage current reduces its ferroelectric polarization and hence is a major concern for onward applications.[2]

Several reports are available on A-site and B-site doping for improving the ferroelectric properties of BFO thin films[13,14] as well as on the study of tip enhanced photovoltaic properties of BFO.[15] Gupta *et al*. discussed the effect of doping at "A" and "B" sites in BFO and reported a remarkable enhancement in photovoltaic properties but the efficiency was still compromised.[16] Doping may induce unwanted parasitic phase formation which restricts any enhancement of FE-PV effect. Hence, it is important to come up with strategic ideologies to fully exploit the potential material traits for obtaining an enhanced response in BFO.

On the other hand, BTO is an equally attractive perovskite ferroelectric material employed in various devices, including capacitors, ferroelectric memories, etc., due to its unique dielectric, piezoelectric, and ferroelectric properties.[5,9,17] However, BTO, being a wide band gap (∼3.3 eV) semiconductor, cannot be employed for FE-PV applications, especially in the visible spectral region. Reportedly, multilayered structures possess superior ferroelectric properties compared to individual parent materials in terms of high polarization, high dielectric constant, and relatively lower losses.[14] Thus, in order to improve the ferroelectric properties of BFO while simultaneously reducing the band gap of BTO, fabrication of the multilayered structure of BFO and BTO could be beneficial.

There are several reports where band gap engineering has been demonstrated by fabricating layered thin film structure.[18,19] Some research groups have also studied BFO/BTO multilayered structures, but their photovoltaic properties are scarcely reported.[20,21] Toupet *et al*.[22] and Yang *et al*.[23] examined the multiferroic property of the BFO/BTO multilayered structure and conclusively reported an improvement in the magnetic property of the system. There exists a correlation between the phenomena of ferroelectricity and photoconductivity observed in certain materials. Ferroelectric polarization acts as a driving force for the separation of photo-generated charge carriers within a photovoltaic cell. When light with a wavelength corresponding to the energy

a)Electronic addresses: vgupta@physics.du.ac.in and drguptavinay@gmail.com

 © 2015 AIP Publishing LLC

[This article is copyrighted as indicated in the article. Reuse of AIP content is subject to the terms at: http://scitation.aip.org/termsconditions. Downloaded to] IP: 14.139.251.107 On: Tue, 25 Aug 2015 06:26:21

band gap of the ferroelectric thin film is made incident on it, photon energy is utilized for the generation of charge carriers—electrons and holes. The photo-generated electrons and holes are driven by the polarization-induced internal electric field in opposite directions and thus, contribute to the photovoltaic output. A BFO-BTO integrated system might result in a composite with effectively lower band gap and high ferroelectric polarization (i.e., low leakage current) which could then be utilized for the realization of an efficient FE-PV device. In the present study, a BFO/BTO multilayered structure has been prepared on Pt(111)/Ti/SiO_2/Si(100) substrate using pulsed laser deposition (PLD) technique and its structural, optical, ferroelectric, and PV properties have been studied in detail.

II. EXPERIMENTAL

A BFO/BTO multilayered (five layered) structure was prepared by PLD technique. Single phase 1 in. diameter ceramic targets of BFO and BTO were prepared via conventional solid state reaction method using Bi_2O_3, Fe_2O_3, $BaCO_3$, and TiO_2 (99.9% pure) as precursor materials. 20% excess Bi was used in the BFO target to avoid the Bi loss during high temperature processing due to its volatile nature. The powders for BFO and BTO were separately ball-milled, dried, and pressed into discs followed by sintering at 850 °C and 1250 °C, respectively. The targets were then polished and mounted on target holders for the deposition of thin films.

The targets were ablated sequentially using the 4th harmonic of Nd:YAG pulsed laser ($\lambda = 266$ nm) and a multilayered structure of BFO/BTO was prepared on Pt/Ti/SiO_2/Si substrate. A 70 nm thin layer of Pt metal was deposited over the passivated Si (SiO_2/Si) substrate by E-beam evaporation technique. A buffer layer of Ti (20 nm) was deposited *in-situ* over SiO_2/Si substrate prior to Pt deposition to improve the adhesion of Pt. Typical deposition parameters used for deposition of BFO and BTO thin films are summarized in Table I.

Total thickness of the multilayered structures was kept fixed at 350 nm, while thickness of individual layers of BFO and BTO was about 70 nm. The multilayered structure was prepared at a substrate temperature of 750 °C. Thickness of individual layers and multilayered structure was measured using surface profiler (Dektak 150). The number of layers in the multilayered structure was kept fixed to be five, keeping BTO as the bottom layer. The ferroelectric measurements were made in metal-ferroelectric-metal (MFM) configuration where Pt layer deposited on SiO_2/Si substrate was considered as the bottom electrode. The top circular electrodes (600 μm diameter, 40 nm thickness) of Au were deposited by thermal evaporation technique through a shadow mask on the surface of multilayered BFO/BTO structure. The schematic of MFM capacitor configuration (Au/BTO/BFO/…/BTO/Pt/SiO_2/Si) is shown in Fig. 1. For comparison, thin films of both BFO and BTO of same thickness (350 nm) were also grown under similar deposition conditions on Pt/SiO_2/Si substrate. For studying the optical properties, thin films were deposited on fused quartz substrate.

TABLE I. PLD processing conditions for the growth of BFO/BTO multilayered structure.

Parameters	Deposited conditions
Ceramic targets	20% Bi-excess BFO, BTO (1 in. diameter)
Substrate	Pt/Ti/SiO_2/Si
Substrate temperature	750 °C
Deposition pressure	200 mT
T-S distance	4.5 cm
Laser type	Nd:YAG (266 nm)
Fluence	120 mJ
Thickness of BTO and BFO	70 nm

Structural characterization of prepared samples was carried out using X-ray diffraction (XRD) analysis (Bruker D8). The lattice parameters of BFO and BTO thin films in the multilayered thin film structure were calculated by Le-Bail fitting using Bruker Topas 3 software. Optical properties were studied using UV-Visible spectrophotometer (Perkin Elmer Lambda 35). A radiant technology precision ferroelectric workstation was used to measure the room temperature ferroelectric polarization (PE hysteresis) of the prepared samples at a frequency of 1 kHz and at an applied bias of 10 V. For the photovoltaic measurements, the BFO/BTO multilayered sample was illuminated with violet laser light ($\lambda = 405$ nm) and the current-voltage (I-V) characteristics of prepared samples were monitored using Keithley (4200) semiconductor characterization system.

III. RESULTS AND DISCUSSIONS

Figure 2 shows the XRD pattern of the prepared five layered BTO/BFO structure. For comparison, XRD patterns of the single layer BFO and BTO thin films (350 nm thin) fabricated under identical conditions on Si substrates have also been included. It may be seen that all prepared samples are polycrystalline in nature depicting rhombohedral distorted structure for BFO and tetragonal structure for BTO. XRD pattern of the BFO/BTO multilayered structure (Fig. 2) reveals that all the observed peaks correspond to either BFO or BTO phases only. Absence of any extra XRD peak in all

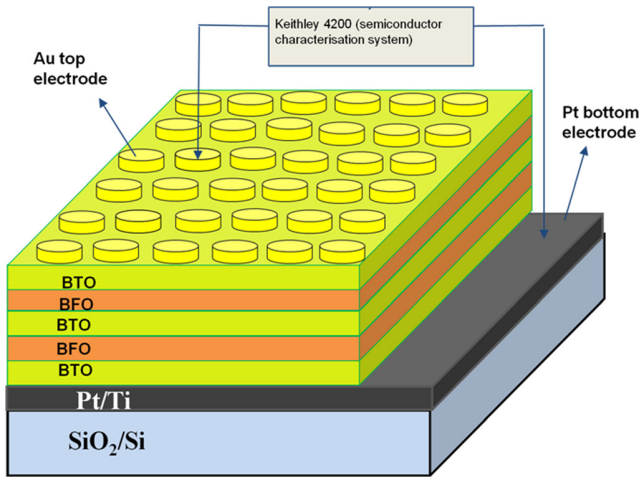

FIG. 1. Schematic of the MFM capacitor configuration of the BFO/BTO multilayer structure.

[This article is copyrighted as indicated in the article. Reuse of AIP content is subject to the terms at: http://scitation.aip.org/termsconditions. Downloaded to] IP: 14.139.251.107 On: Tue, 25 Aug 2015 06:26:21

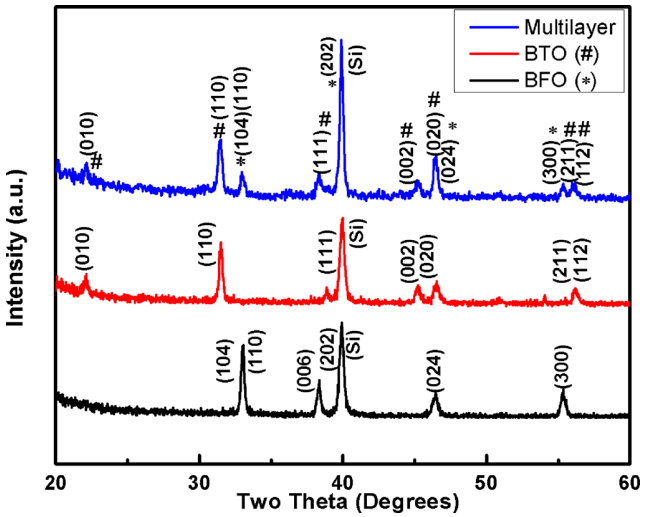

FIG. 2. XRD pattern of BFO/BTO multilayered structure. XRD pattern of bare BFO and BTO thin films is also included for comparison.

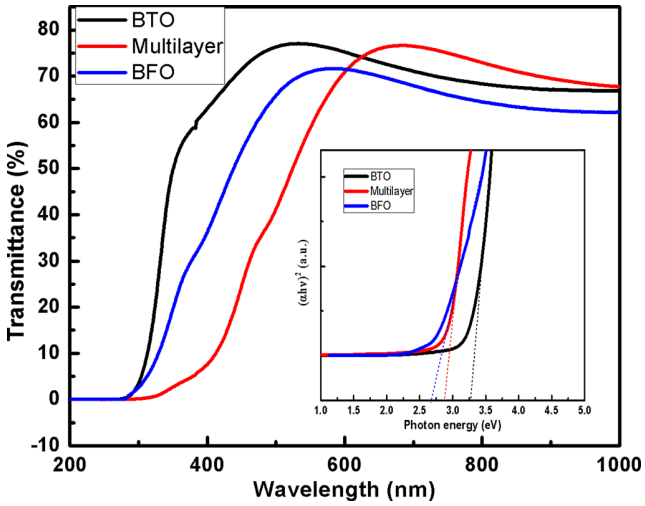

FIG. 3. UV-Visible transmission spectra of bare BTO film, bare BFO film, and BFO/BTO multilayered structure. Inset shows the Tauc plot of all the three prepared samples.

prepared samples clearly rules out the possibility of formation of any impure secondary phase. Furthermore, two XRD peaks around $2\theta = 45°$ corresponding to BTO can be easily observed for the multilayered structure (Fig. 2), indicating that BTO possesses a tetragonal structure. Lattice parameters ("a" and "c"), unit cell volume "V," and stress modulus for both BTO and BFO in the multilayered structure were determined using LeBail Intensity Extraction method with the help of Bruker TOPAS 3 Software and are summarized in Table II. For comparison, the corresponding bulk values for BTO and BFO are also included in Table II [JCPDS card No. 01-072-0138 and 01-072-2035]. The estimated values of lattice parameters a and c are 4.38 Å and 4.07 Å, respectively, for BTO film and 5.53 Å and 13.54 Å, respectively, for BFO film. These values are slightly lower than the corresponding reported values for bulk BFO but greater than that of bulk BTO (Table II), indicating the introduction of tensile and compressive stress, respectively, in BTO and BFO thin films in the multilayered structure. The stress modulus in both layers is calculated using the equation, stress $= |(c_o - c)|/c_o$ in %, where "c" is the lattice constant of BFO or BTO thin film in multilayered structure and "c_o" is the corresponding bulk value. The value of stress modulus (%) for BTO and BFO was found to be about 1.11% and 2.04%, respectively. A large value of stress modulus present in the BFO thin film indicates a large lattice distortion which may lead to improved ferroelectric property.

Figure 3 shows the optical transmission spectra of multilayered BFO/BTO structure deposited on quartz substrate over a wavelength range of 190–1100 nm. The transmission spectra of bare BFO and BTO thin films are also included in Fig. 3 for comparison. It can be seen from Fig. 3 that the bare BFO and BTO thin films were highly transparent (~80%) in the visible region demonstrating the growth of thin films with good optical quality and low absorption losses. However, transmittance in the case of multilayered structure drops to 70% (Fig. 3) and may be due to refraction of light at the multiple interfaces. The Tauc plot of $(\alpha h\nu)^2$ versus photon energy ($h\nu$) (where α is absorption coefficient, h is Planck's constant, and ν is frequency of the incident radiation) of the multilayered structure and bare thin films is shown in the inset of Fig. 3. The estimated values of bandgap for all the prepared samples are also summarized in Table III. Optical bandgap of the multilayered structure as calculated from the extrapolation of linear region in Tauc plot is about 2.87 eV which is much less than that of pure BTO (3.27 eV) thin film and close to that of BFO thin film (2.66 eV). It can be easily seen from Table III that the integration of BFO with BTO has indeed helped in reducing the band gap of the overall multilayered structure and is suitable for ferroelectric photovoltaic applications.

Figure 4 shows the typical ferroelectric P-E hysteresis loop of the mutilayered BFO/BTO structure at an applied bias of 10 V and 1 kHz frequency. For comparison, hysteresis loops of bare BTO and BFO thin films grown under similar conditions have also been included in Fig. 4. It may be seen from Fig. 4 that the ferroelectric properties of the multilayered BFO/BTO structure are better in comparison to that of

TABLE II. Lattice parameters "a" and "c," cell volume "V" and stress modulus for BFO and BTO thin films in BFO/BTO multilayer (five layer) structure.

	BTO thin film					BFO thin film				
	Lattice parameter		Volume	Stress modulus	c/a distortion	Lattice parameter		Volume	Stress modulus	c/a distortion
	a (Å)	c (Å)	V (Å)^3	(%)	ratio	a (Å)	c (Å)	V (Å)^3	(%)	ratio
Bulk value	3.999	4.033	64.36	—	1.0085	5.876	13.867	374.94	—	2.3599
multilayer	4.381	4.078	77.661	1.11	0.9308	5.5301	13.584	358.82	2.04	2.4563

[This article is copyrighted as indicated in the article. Reuse of AIP content is subject to the terms at: http://scitation.aip.org/termsconditions. Downloaded to] IP: 14.139.251.107 On: Tue, 25 Aug 2015 06:26:21

TABLE III. Ferroelectric parameters and band gap of multilayered BFO/BTO sample. The corresponding values for bare BFO and BTO thin films are also included for comparison.

	P_r ($\mu C/cm^2$)	P_s ($\mu C/cm^2$)	$2E_c$ (kV/cm)	E_g (eV)
BTO	43.28	74.82	4.85	3.27
BFO	12.23	20.61	5.35	2.66
Multilayer	45.71	64.69	11.27	2.87

bare BFO thin film and comparable to the bare BTO thin film. The obtained values of remnant polarization (P_r), saturation polarization (P_s), and coercive field (E_c) for all the structures are summarized in Table III. The multilayered system exhibits a saturation polarization (P_s) of around 64.69 $\mu C/cm^2$, which is much greater than that obtained for bare BFO thin film (20.61 $\mu C/cm^2$). The value of $P_s = 64.69\ \mu C/cm^2$ and $P_r = 45.71\ \mu C/cm^2$ obtained for multilayered BFO/BTO structure in the present work is relatively higher in comparison to the corresponding values reported by various workers for multilayered structure of BFO with other materials or doped BFO thin film.[2,6,13,14,24] The improved ferroelectric property of the multilayered structure may be related to the stress induced at the interfaces. Furthermore, the observed slight asymmetry in the hysteresis loops (Fig. 4) is attributed to the presence of different top and bottom metal (Pt and Au) electrodes in MFM structure. It may be noted that the presence of BFO and BTO films in the multilayered structure results in a lower bandgap and higher ferroelectric polarization, making the fabricated multilayered structure suitable for ferroelectric photovoltaic applications.

Figure 5 shows the current density–voltage (J–V) curve obtained for multilayered BFO/BTO sample under both dark condition and light illumination ($\lambda = 405$ nm). The J–V curve under light illumination (Fig. 5) shows a typical ferroelectric photovoltaic effect. The photovoltaic open-circuit voltage (V_{oc}) and short-circuit current density (J_{sc}) are found to be about -1.25 V and 0.3184 mA/cm^2, respectively, as

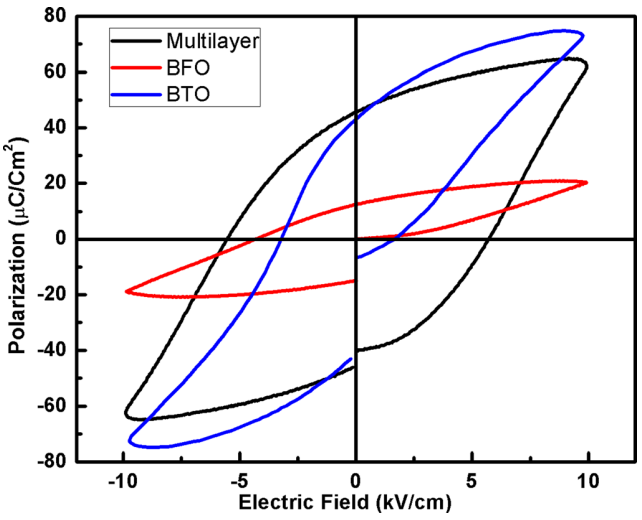

FIG. 4. Room temperature ferroelectric (P-E) hysteresis curves of bare BFO and BTO thin films and multilayered BFO/BTO structure.

determined from the intercept on the horizontal and the vertical axes (Fig. 5). The photovoltage obtained is considerably larger than that reported by other researchers for individual ferroelectric thin films.[9,16,24–26] It is well known that the value of J_{SC} and V_{OC} for ferroelectric thin films under illumination depends on the internally generated electric field. The internal electric field in ferroelectric thin films is given as $E = E_{bi} + E_p$, where E_{bi} is the built-in field and E_p is the depolarization field. The built in field E_{bi} in ferroelectric thin films is driven by various factors.[27–29] The depolarization field E_p is directly proportional to the strength of polarization: $E_p = \frac{-P}{\varepsilon_o \varepsilon_F}\left(\frac{2\varepsilon_F/d}{2\varepsilon_F/d+\varepsilon_e/\lambda}\right)$, where ε_F *is* the relative dielectric constant of the ferroelectric thin film, ε_e is the relative dielectric constant of the electrode layer, λ is the screening length, P is the polarization value, and d is the thickness of ferroelectric thin film.[4] Therefore, high photovoltaic output obtained for BFO/BTO multilayered structure can be attributed to its higher internal field caused by the larger remnant polarization (Fig. 4). The large depolarization field could effectively separate the photogenerated electrons and holes and hence, resulting in enhanced photovoltaic output for BFO/BTO multilayered structure. Inset of Fig. 5 shows the transient response characteristics of photocurrent density measured at zero bias for multilayered BFO/BTO structure under continuous on and off conditions of laser light ($\lambda = 405$ nm) at a regular interval of 20 s. The photoresponse of multilayered BFO/BTO structure shows a rapid increase in the photocurrent with illumination on its surface, and subsequently saturates at a constant value (inset of Fig. 5). When the incident light is turned off, the photocurrent decreases rapidly and reaches its original value. Now to compare the photovoltaic response of BFO/BTO multilayered structure with that of BFO single layer, photovoltaic measurement on BFO single layer was performed and is shown in Figure 5(b). A very small open circuit voltage and short circuit current ($V_{oc} = -0.33$ V and $J_{sc} = 1.30 \times 10^{-4}$ A/cm^2) are generated in the case of single layer BFO thin film. On the other hand, BTO with its wide band-gap energy (3.27 eV as calculated) which is larger than the energy corresponding to 405 nm wavelength exhibits no absorption of the incident energy. Hence, BTO thin film failed to exhibit photovoltaic effect at this wavelength of 405 nm and thus photovoltaic response is not included for BTO single layer. In the case of multilayered structure, the presence of BFO is crucial due to its band gap compatibility in correspondence with the wavelength of incident light ($\lambda = 405$ nm), whereas BTO induces an internal field in response to the large polarization, thereby accelerating the separation of photogenerated charge carriers. Collectively BFO/BTO multilayered system exhibits an enhanced photovoltaic response at 405 nm as compared to single layered BFO or BTO.

The photocurrent responsivity, i.e., ratio of the short circuit photocurrent density (Acm^{-2}) to the input optical power density (mWcm^{-2}) is also calculated for the multilayered BFO/BTO structure from the J-V curve and is estimated to be about 1.99 mAW^{-1} at an input power of 160 mWcm^{-2}. Light-to-power conversion efficiency, η, can be determined

[This article is copyrighted as indicated in the article. Reuse of AIP content is subject to the terms at: http://scitation.aip.org/termsconditions. Downloaded to] IP: 14.139.251.107 On: Tue, 25 Aug 2015 06:26:21

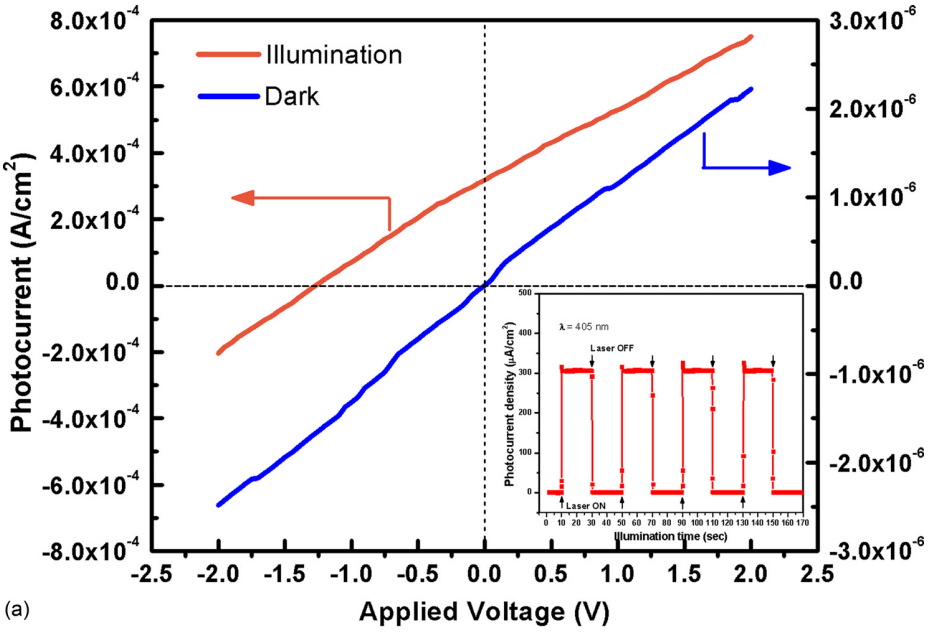

(a)

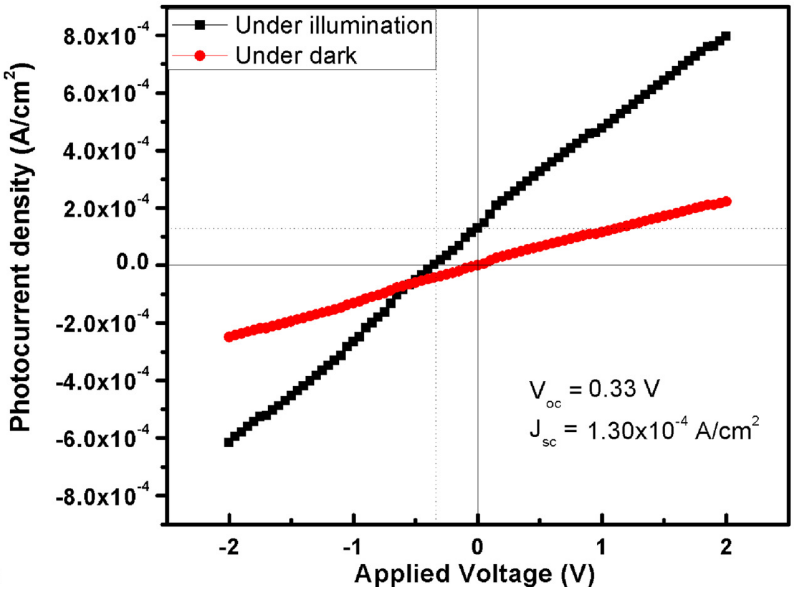

(b)

FIG. 5. (a) J-V curves for multilayered BFO/BTO structure under both dark condition and illumination of light. Inset shows transient response of short circuit photocurrent density of multilayered BFO/BTO structure when laser beam is switched on and off at regular intervals of 20 s. (b) J-V curve for BFO single layer thin film under both dark condition and illumination of light to compare the photovoltaic response with BFO/BTO multilayer structure.

from the J-V curve obtained under photo illumination. We calculated the power conversion efficiency of the investigated structure at 405 nm. The power conversion efficiency η is the ratio of the output electrical power density (P_{out}) to the input optical power density (P_{in}). The input power density, P_{in} (mWcm^{-2}) is the intensity of light incident on the surface of the sample and the output power density, P_{out} (mWcm^{-2}) at a certain point (J,V) of the J-V curve is the area enclosed by the point (J,V) and two axes (i.e., $P_{out} = JV$ mW/cm^2). The power conversion efficiency η at the point (J,V) can be calculated as[16] $\eta = \frac{Pout}{Pin} = \frac{JV}{Pin}$.

The voltage dependence of power conversion efficiency of the multilayered BFO/BTO structure is presented in Fig. 6. It can be observed from Fig. 6 that the maximum power conversion efficiency (0.067%) occurs at half the value of open circuit photovoltage. The power conversion efficiency is associated with the separation and subsequent

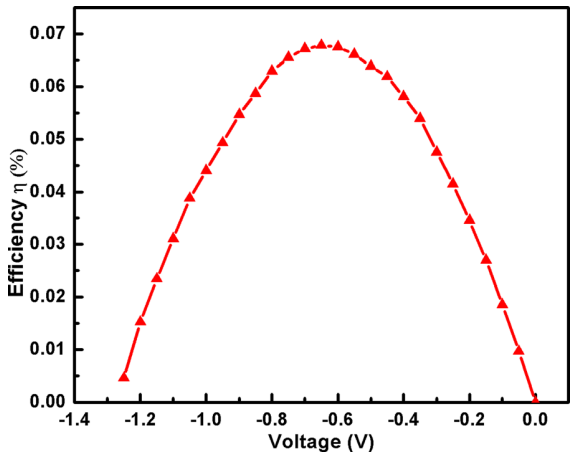

FIG. 6. The variation of power conversion efficiency calculated at 405 nm as a function of applied voltage for BFO/BTO multilayer structure.

[This article is copyrighted as indicated in the article. Reuse of AIP content is subject to the terms at: http://scitation.aip.org/termsconditions. Downloaded to] IP: 14.139.251.107 On: Tue, 25 Aug 2015 06:26:21

movement of polarization led photogenerated charge carriers. The higher value of remnant polarization of the multilayered BFO/BTO structure provides a large internal electric field (depolarization field) which acts as a driving force that separates the photogenerated electron-hole carriers resulting in higher power conversion efficiency.[4] The power conversion efficiency calculated at 405 nm in the case of developed BFO/BTO multilayered structure is higher compared to the photovoltaic efficiency reported recently for BFO.[16,26,30] However, there are few reports where higher power conversion efficiency compared to that observed in the present work has also been reported.[4] It was identified that when ITO was used as a top electrode, more absorption of incident photons in the visible region occurred. The open circuit voltage and short circuit current for multilayered BFO/BTO structure are -1.25 V and 3.184×10^{-4} A/cm^2, respectively.

It may be inferred that the prepared multilayered BFO/BTO structure exhibits a large remnant polarization ($45.71\ \mu$C/cm^2) and hence high photovoltaic output that makes it attractive for photovoltaic applications.

IV. CONCLUSION

Multilayered structure having five alternating layers of single phase BFO and BTO thin films was deposited using PLD technique. Multilayered BFO/BTO structure exhibits a good ferroelectric hysteresis loop with high saturation polarization, $P_s = 64.69\ \mu$C/Cm^2 and remnant polarization, $P_r = 45.71\ \mu$C/Cm^2. The low optical band gap coupled with the high ferroelectric polarization results in good ferroelectric photovoltaic response of BFO/BTO multilayered structure. The short circuit photocurrent density and open circuit voltage are about $9.96\ \mu$A/cm^2 and -1.25 V, respectively. The light-to-electricity power conversion efficiency calculated at 405 nm is relatively high (0.067%). The enhanced photovoltaic response observed in present work is attributed to the presence of strong depolarization field due to higher remnant polarization and lower band gap of the multilayered BFO/BTO structure. The obtained results show that the prepared BFO/BTO multilayered system could be used efficiently for energy harvesting and other photovoltaic applications.

ACKNOWLEDGMENTS

Authors are thankful to Department of Science and Technology (DST) and University of Delhi for the financial support. One of the authors (S.S.) is thankful to the Delhi Technological University (DTU) for the teaching assistantship.

[1]S. Y. Yang, J. Seidel, S. J. Byrnes, P. Shafer, C.-H. Yang, M. D. Rossell, P. Yu, Y.-H. Chu, J. F. Scott, J. W. Ager III, L. W. Martin, and R. Ramesh, Nat. Nanotechnol. **5**, 143 (2010).
[2]S. Y. Yang, L. W. Martin, S. J. Byrnes, T. E. Conry, S. R. Basu, D. Paran, L. Reichertz, J. Ihlefeld, C. Adamo, A. Melville, Y.-H. Chu, C.-H. Yang, J. L. Musfeldt, D. G. Schlom, J. W. Ager III, and R. Ramesh, Appl. Phys. Lett. **95**, 062909 (2009).
[3]J. Zhang, X. Su, M. Shen, Z. Dai, L. Zhang, X. He, W. Cheng, M. Cao, and G. Zou, Nat. Sci. Rep. **3**, 2109 (2013).
[4]B. Chen, M. Li, Y. Liu, Z. Zuo, F. Zhuge, Q. F. Zhan, and R. W. Li, Nanotechnology **22**, 195201 (2011).
[5]W. Cai, C. Fu, J. Gao, Q. Guo, X. Deng, and C. Zhang, Physica B **406**, 3583 (2011).
[6]Z. Lin, W. Cai, W. Jiang, C. Fu, C. Li, and Y. Song, Ceram. Int. **39**, 8729 (2013).
[7]K. Yao, B. K. Gan, M. Chen, and S. Shannigrahi, Appl. Phys. Lett. **87**, 212906 (2005).
[8]M. Qin, K. Yao, and Y. C. Liang, Appl. Phys. Lett. **93**, 122904 (2008).
[9]W. Jiang, W. Cai, Z. Lin, and C. Fu, Mater. Res. Bull. **48**, 3092 (2013).
[10]L. Chen, B. C. Luo, N. Y. Chan, J. Y. Dai, M. Hoffman, S. Li, and D. Y. Wang, J. Alloys Compd. **587**, 339 (2014).
[11]J. F. Ihlefeld, N. J. Podraza, Z. K. Liu, R. C. Rai, X. Xu, T. Heeg, Y. B. Chen, J. Li, R. W. Collins, J. L. Musfeldt, X. Q. Pan, J. Schubert, R. Ramesh, and D. G. Schlom, Appl. Phys. Lett. **92**, 142908 (2008).
[12]S. Gupta, M. Tomar, and V. Gupta, J. Exp. Nanosci. **8**(3), 261 (2013).
[13]H. W. Chang, F. T. Yuan, Y. C. Yu, P. C. Chen, C. R. Wang, C. S. Tu, and S. U. Jen, J. Alloys Compd. **574**, 402 (2013).
[14]N. M. Murari, A. Kumar, R. Thomas, and R. S. Katiyar, Appl. Phys. Lett. **92**, 132904 (2008).
[15]M. Alexe and D. Hesse, "Tip-enhanced photovoltaic effects in bismuth ferrite," Nat. Commun. **2**(256), 1–4 (2011).
[16]S. Gupta, M. Tomar, and V. Gupta, J. Appl. Phys. **115**, 014102 (2014).
[17]Y. H. Chen, W. H. Tuan, and J. Shieh, J. Eur. Ceram. Soc. **30**, 2577 (2010).
[18]H. K. Yadav, K. Sreenivas, and V. Gupta, Appl. Phys. Lett. **96**, 223507 (2010).
[19]H. K. Yadav, K. Sreenivas, and V. Gupta, Appl. Phys. Lett. **90**, 172113 (2007).
[20]S. Sharma, M. Tomar, A. Kumar, N. K. Puri, and V. Gupta, Physica B **448**, 125 (2014).
[21]M. Lorenz, V. Lazenka, P. Schwinkendorf, F. Bern, M. Ziese, H. Modarresi, A. Volodin, M. J. V. Bael, K. Temst, A. Vantomme, and M. Grundmann, J. Phys. D: Appl. Phys. **47**, 135303 (2014).
[22]H. Toupet, V. V. Shvartsman, F. Lemarrec, P. Borisov, W. Kleemann, and M. Karkut, Integr. Ferroelectr. **100**, 165 (2008).
[23]P. Yang, K. M. Kim, J. Y. Lee, J. Zhu, and H. Y. Lee, Integr. Ferroelectr. **113**, 26 (2010).
[24]R. S. Katiyar, P. Misra, S. Sahoo, G. Morell, and R. S. Katiyar, J. Alloys Compd. **609**, 168 (2014).
[25]W. Dong, Y. Guo, B. Guo, H. Liu, H. Li, and H. Liu, Mater. Lett. **91**, 359 (2013).
[26]W. Dong, Y. Guo, B. Guo, H. Liu, H. Li, and H. Liu, Mater. Lett. **88**, 140 (2012).
[27]K. Abe, N. Yanase, T. Yasumoto, and T. Kawakubo, J. Appl. Phys. **91**(1), 323 (2002).
[28]D. J. Kim, J. Y. Jo, Y. S. Kim, Y. J. Chang, J. S. Lee, J. G. Yoon, T. K. Song, and T. W. Noh, Phys. Rev. Lett. **95**, 237602 (2005).
[29]A. Gruverman, A. Kholkin, A. Kingon, and H. Tokumoto, Appl. Phys. Lett. **78**, 2751 (2001).
[30]S. Gupta, M. Tomar, A. Kumar, and V. Gupta, Adv. Sci. Lett. **20**, 971–976(6) (2014).

[This article is copyrighted as indicated in the article. Reuse of AIP content is subject to the terms at: http://scitation.aip.org/termsconditions. Downloaded to] IP: 14.139.251.107 On: Tue, 25 Aug 2015 06:26:21

ResearchGate

See discussions, stats, and author profiles for this publication at: http://www.researchgate.net/publication/279192226

Evaluating Water Quality of River Yamuna in Delhi by Regression Analysis

ARTICLE · JULY 2015

DOWNLOADS
38

VIEWS
12

Available from: S. K. Singh
Retrieved on: 06 August 2015

www.ijemr.net ISSN (ONLINE): 2250-0758, ISSN (PRINT): 2394-6962

Volume-5, Issue-3, June-2015

International Journal of Engineering and Management Research

Page Number: 218-221

Evaluating Water Quality of River Yamuna in Delhi by Regression Analysis

Shashank Shekhar Singh[1], Dr. S. K. Singh[2]

[1]Research Scholar, Environmental Engineering Department, Delhi Technological University (DTU), Delhi , INDIA

[2]Professor, HOD, Environmental Engineering Department, Delhi Technological University (DTU), Delhi , INDIA

ABSTRACT

The present study deals with the variation of water quality characteristics over an urban stretch of the Yamuna River covering areas upstream, downstream and the entire length of the Delhi city. The study has been conducted over a period of six months. Water samples collected systematically from nine sites during October to February and examined for water quality evaluation through application of Regression analysis models. A regional perspective is provided with river water quality being interpreted in relation to catchment geography and to the observed point and non-point source inputs to the catchment. Point source inputs are important for phosphate, nitrate and micro-organic pollutants. Diffuse agricultural sources are particularly important in upstream arable areas, e.g. for nitrate, phosphate and micro-organics. In addition, widespread background geological sources contribute to loads of sulfate and phosphate. Sewage effluent is the most widespread and most significant point source of many pollutant chemicals in the study area. Low biochemical oxygen demand, nitrate, chloride and phosphate result from domestic effluent and commercial inputs, e.g. from sectors such as public places and fishery. Fish farms cause depletion in dissolved oxygen but on the whole, these changes were not observed to cause problems on a wider scale as of now. From the findings, a subset was selected for the water quality indices (WQI) analysis. Water quality of the Yamuna River at different points assessed by the WQI was compared. According to the quality indices during the study period, water quality in the study area of the river was average to good. To support and strengthen the findings, an analyses of the data based on multiple regression was done to examine whether seasonal or spatial variation in different parameters can be explained and predicted based upon their interrelationships in terms of source and mobility.

***Keywords*-----** WQI, Regression analysis, Mobility

I. INTRODUCTION

Yamuna, the main river in the Northern part in India, arises in the Himalayas (56.12°S, 12.34°E, altitude 5300m), flows east wards followed by west wards with a total length of 2900 km. Its main source is in a great glacier-mass of the northernmost chain of the Himalayas, called Kubigangri, about 82°N and it receives various tributaries including one formerly regarded as the true source from the pass of Mariam La (15,500 ft.), which separates its basin from the eastern affluent of the Mansarowar lakes, at least 100 m. south-east of those of the Indus. The Yamuna River water is often used for irrigation and as the main drinking water source. A systematic studyon the river water quality is of great necessity and significance. This report presents the results of studies on some major chemical parameters of the Yamuna water system for a six months study period.

In order to monitor the trends of river pollution, hydrobiological investigations of nine selected parameters were carried out from September 2013 to February 2014 and the multiplicative weighted index applied. The water quality index (WQI) is represented by a number between 0 and 100. Rivers with WQI values between 0-25, 26-50 and 51-70 are grouped as very bad, bad and medium, respectively, while waters of good and excellent quality have WQI values of 71-90 and 91-100, respectively. Besides trend analysis and WQI studies, statistical studies like regression analyses were applied to the dataset for an enhanced understanding through diverse interpretation tools.

II. OBJECTIVES & APPROACH

The objective envisaged for this study is evaluation of present status of water quality of river

Copyright © 2011-15. Vandana Publications. All Rights Reserved.

Yamuna in Delhi Stretch. For this purpose , the required information has been collected and analyzed as below.

1. To characterize water quality of the study area (most human impacted part of the river) and identify changes or trends in water quality over time.
2. To identify specific existing or emerging water quality problems based on analysis of the data using WQI and multiple regression analysis .
3. To examine whether compliance with pollution regulations or implementation of effective pollution control actions are being met.
4. To suggest specific water quality alleviation and/or pollution prevention/ remediation strategies by synthesizing the findings of the study.
5. To characterize water quality of the study area (most human impacted part of the river) and identify changes or trends in water quality over time.
6. To identify specific existing or emerging water quality problems based on analysis of the data using WQI and multiple regression analysis with the help of able GIS tools (kriging).
7. To examine whether compliance with pollution regulations or implementation of effective pollution control actions are being met.
8. To suggest specific water quality alleviation and/or pollution prevention/ remediation strategies by synthesizing the findings of the study.

III. MATERIALS AND METHODS

3.1 Study Area

The region of sampling covers a wide range of catchments and surface water types river, tributaries, ditches etc.). The main pollutant loads include domestic wastewaters, agricultural runoff, animal husbandry, industrial effluents and fishery. Yamuna is the longest river in India with a total length of nearly 2900 km and the average annual discharge 51.0450 million cubic meters (CPCB, 2000). The area of Yamuna basin is 580000 Km^2. During the rains the Yamuna floods hundreds of square miles of country, reaching a height of 30 to 40 ft. above its usual level.

3.2 Materials and Methodology

The total work was divided into three phases. In the first phase, samples were collected in one litre bottles Then those samples were preserved in the refrigerator for further analyses, after measurement of pH, conductivity, dissolved oxygen, BOD5, and COD.In the second phase, samples were taken out and left for some times to achieve the room temperature.In the third phase, interpretations of all the analyses results obtained in the second phase were performed using Regression Analysis.

3.2.1 Regression Analysis

Regression analysis is used for explaining or modeling the relationship between a single variable *y*, called the response, an output or dependent variable, and one or more predictor, input, independent or explanatory variables, *x1*, ……, *xp*. When $p = 1$, it is called simple regression, but when $p > 1$ it is called multiple regression or sometimes multivariate regression. When there is more than one *y*, then it is called multivariate multiple regression. Regression analyses have several possible objectives including (Faraway 2002):

1. Prediction of future observations.
2. Assessment of the effect of, or relationship between, explanatory variables on the response.
3. A general description of data structure.

It can be linear as well as non-linear. The simplest multiple linear regression equation becomes:

$\Sigma = a + \varepsilon_i + \sum_{i=1}^{i=n} b_i x_i$

0where, quantities *b1, b2, …,bn*are termed partial regression coefficient.

IV. RESULTS & DISCUSSIONS

Twelve parameters were analyzed for three batches of aqueous samples from nine sites over a five months time span (October 2013- February 2014). For a better understanding, each of the months has been denoted

Copyright © 2011-15. Vandana Publications. All Rights Reserved.

by a legend based on the prevailing climatic conditions. The legends and corresponding months are given in Table

Table : Legends for the sampling months with corresponding seasons

S.No	Month	Legend
1	October	Receding Monsoon
2	December	Winter Season
3	February	Receding Winter Season

4.1 Analysis of the Observed Data, Based on Multiple Regressions

A range of water quality data were generated and examined in the present work for a comprehensive water quality evaluation. However as required, only a subset was selected for the WQI analysis. Now, to support and strengthen the findings so far, an analysis of the data, based on multiple regression, was attempted. This was done to examine whether seasonal or spatial variation in different parameters can be explained and predicted based upon their interrelationship in terms of source and mobility.From analysis point of view, twelve parameters were selected to set up the regression model. The dependent variable was Electrical Conductivity (EC) and the independent variables were TDS, Na^{+}, K^{+}, Ca^{+2}, NO_3 -, HCO_{3-}, $SO4^{-2}$, pH, $PO4^{-3}$, DO, and Hardness. The modeling has been done based on three different approaches:

4.1.1 Model: October

In this model the approach was to consider all the twelve parameters and all the sampling data for the entire study period. Based on that approach, the multiple linear regressions as well as the multiple non-linear regression analysis has been done. The final empirical equations observed from this model are given below:

EC = (253.8 + (0 x pH) - (0.2 x TDS) + (0.6 x Hardness) - (14 x DO) + (0 x BOD_5) - (3.5 x HCO_3 -) + (0.49 x Alkalinity) + (8.9 x Turbidity) + (0 x PO_4^{3-}) + (6.6 x Ca^{2+}) + (0 x Mg^{2+}))

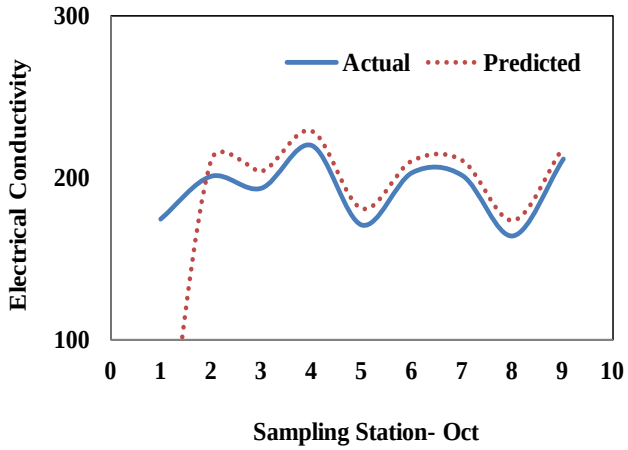

Figure : Comparison of actual and predicted data of electrical conductivity for October season

4.1.2 Model : November

In this model the approach was to consider all the twelve parameters and all the sampling data for the entire study period. Based on that approach, the multiple linear regression as well as the multiple non-linear regression analysis has been done. The final empirical equations observed from this model are given below:

EC = (326.5 + (49 x pH)-(0.26 x TDS)+(1.01 x Hardness)+(0 x DO)+(0 x BOD_5)+(0.7 x HCO_3 -)-(1.1 x Alkalinity)-(2.3 x Turbidity)+(0 x PO_4^{3-})-(27 x Ca^{2+})+ (0 x Mg^{2+}))

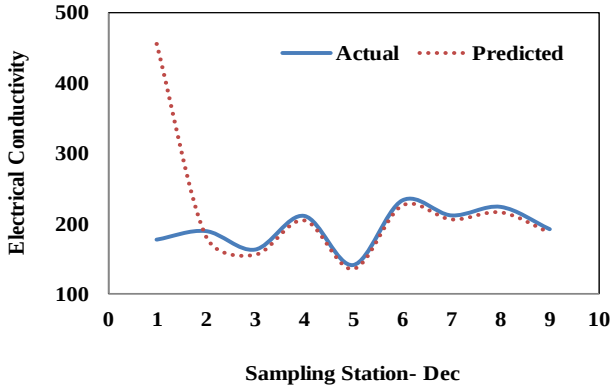

Figure : Comparison of actual and predicted data of electrical conductivity for December season

4.1.3 Model : February

In this model the approach was to consider all the twelve parameters and all the sampling data for the entire study period. Based on that approach, the multiple linear regression as well as the multiple non-linear regression analysis has been done. The final empirical equations observed from this model are given below:

Copyright © 2011-15. Vandana Publications. All Rights Reserved.

EC=(506.3+(0 x pH)-(0.96 x TDS)+(1.16 x Hardness)-(19.9 x DO)+(0 x BOD_5)-(2.1 x HCO_3^-)+(0.17 x Alkalinity)+(3.96 x Turbidity)+(0 x PO_4^{3-})-(3.05 x Ca^{2+})+(0 x Mg^2))

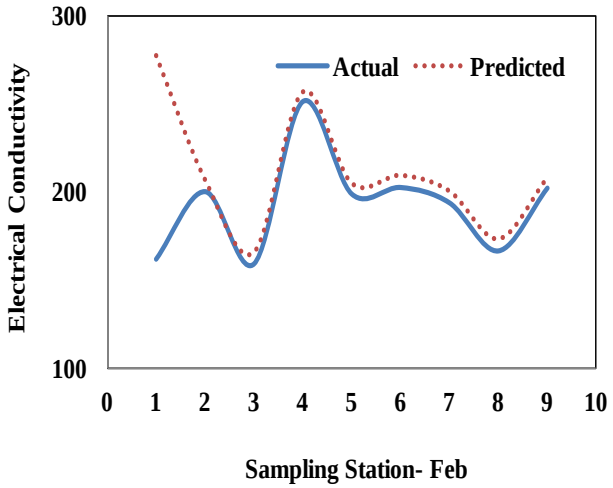

Figure: Comparison of actual and predicted data of electrical conductivity for February season

V. CONCLUSIONS

Based on the findings, following conclusions can be drawn:

[1] The Yamuna River water adjoining the Delhi city is alkaline in nature with pH level reaching the value of 8.5 during the dry season.

[2] Electrical Conductivity changes with season indicating seasonal variation in dissolved ion chemistry. Cl^-, HCO_3^- and SO_4^{-2} make up the major anions and Ca^{+2}, Mg^{+2}, Na^+ and K^+ the major cations.

[3] Impact of waste water inflow from city drainage is indicated but found to be minimum during the monsoon peak flow, due to dilution by high volume of surface water, accompanied by other natural attenuation processes, whereas the effect were more pronounced in the winter season.

[4] The application of a water quality indices approach to the study area allows a water quality classification both spatially and temporally that is reproducible within the watershed by means of uniform, objective criteria.

[5] From the regression analysis it has been observed that, there are three significant variables (Na^+, K^+ and hardness) which are all strongly correlated with the EC values of the Yamuna River.

[6] The variation of different parameters has occurred mainly due to four causes: seasonal variations in flow conditions, upstream contribution of algae and other constituents, the geometry of the study area and the effluent from Delhi city.

REFERENCES

[1] Evaluation of Drinking Water Pollution and Health Effects in Baghdad, Iraq Journal of Environmental Protection Vol.3 No.6, June 21, 2012 ,Allaa M. Aenab, S. K. Singh

[2] AGARWAL, C.S. (1998) Study of drainage pattern through aerialdata in Nahagarh area of Varansi district, U.P. Jour. Indian Soc.Remote Sensing v.26(4), pp.169-175.

[3] DAS, A.K. and MUKHRJEE, S. (2005) Drainage morphometry usingsatellite data and GIS in Raigad district, Maharashtra. Jour.Geol. Soc. India, v.65, pp.577-586.

[4] ANGALAKUNTA, P., et al. (2004) Drainage morphometry and itsinfluence on landform characteristics in a basaltic terrain, CentralIndia – a remote sensing and GIS approach. Inter. Jour. Appld.Earth and Geoinformation v.6, pp.1-16.

[5] Evaluating Water Quality of Ganga River Within Uttar Pradesh State by Water Quality Index Analysis Using C++ Program Allaa M. Aenab, S. K. Singh

[6] GOTTSCHALK, L.C. (1964) Reservoir Sedimentation. *In:* V.T. Chow(Ed.), Handbook of Applied Hydrology. McGraw Hill BookCompany, New York, Section 7-I.

[7] HERON, A.M. (1922) The Gwalior and Vindhyan systems in southeasternRajputana. Mem. Geol. Surv. India, v.45, pp.129-189.

[8] HORTON, R.E. (1932) Drainage basin characteristics. Trans. Amer.Geophys. Union v.13, pp.350-360.

[9] HORTON, R.E. (1945) Erosional development of stream and theirdrainage basin. Hydrogeological approach to quantitativemorphology. Bull. Geol. Soc. Amer., v.56, pp.275-370.

[10] JAIN, S and SINHA, R. (2005) Response of active tectonic in alluvialBaghmati River, Himalayan foreland basin, eastern India. Jour.Geomorph., v.70, pp.339-356.

[11] JACKSON, J and LEEDER, M. (1994) Drainage development of normalfaults, and example from pleasant valley, Nevada. Jour. Struc.Geol. Geophys., v.41, pp.377-385.

[12] LANGBEIN, W.B. (1947) Topographic characteristic of DrainageBasin. USGS Water-Supply Paper, v.986 (C) pp.157-159.

[13] MELTON, M.A. (1958a) A derivation of Strahler's Channel-orderingsystem. Jour. Geol., v.67, pp.345-346.

[14] STRAHLER, A.N. (1957) Quantitative analysis of watershedgeomorphology. Trans. Amer. Geophys. Union, v.38, pp.913-920.

Copyright © 2011-15. Vandana Publications. All Rights Reserved.

EventBuilder: Real-time Multimedia Event Summarization by Visualizing Social Media

Rajiv Ratn Shah
School of Computing, National University of Singapore, Singapore
rajiv@comp.nus.edu.sg

Anwar Dilawar Shaikh
Department of Computer Engineering, Delhi Technological University, India
anwardshaikh@gmail.com

Yi Yu
Digital Content and Media Sciences Research, National Institute of Informatics, Japan
yiyu@nii.ac.jp

Wenjing Geng
Department of Computer Science & Technology, Nanjing University, China
wjgeng@smail.nju.edu.cn

Roger Zimmermann
School of Computing, National University of Singapore, Singapore
rogerz@comp.nus.edu.sg

Gangshan Wu
Department of Computer Science & Technology, Nanjing University, China
gswu@nju.edu.cn

ABSTRACT

Due to the ubiquitous availability of smartphones and digital cameras, the number of photos/videos online has increased rapidly. Therefore, it is challenging to efficiently browse multimedia content and obtain a summary of an event from a large collection of photos/videos aggregated in social media sharing platforms such as Flickr and Instagram. To this end, this paper presents the EventBuilder system that enables people to automatically generate a summary for a given event in real-time by visualizing different social media such as Wikipedia and Flickr. EventBuilder has two novel characteristics: (i) leveraging Wikipedia as event background knowledge to obtain more contextual information about an input event, and (ii) visualizing an interesting event in real-time with a diverse set of social media activities. According to our initial experiments on the YFCC100M dataset from Flickr, the proposed algorithm efficiently summarizes knowledge structures based on the metadata of photos/videos and Wikipedia articles.

Categories and Subject Descriptors

H.3.1 [**Information Storage and Retrieval**]: Content Analysis and Indexing; H.5.1 [**Information Interfaces and Presentation**]: Multimedia Information Systems

Keywords

Event detection; event summarization; event visualization

1. MOTIVATION AND BACKGROUND

The EventBuilder system presented in this study is our solution to the ACM Multimedia 2015 Grand Challenge on automatic event summarization from a large collection of photos/videos. EventBuilder[1] is a real-time multimedia event summarization system which produces an event summary by visualizing social media such as Flickr. The number of photos/videos on social media sites has increased rapidly due to the advancement in smartphone and digital camera technologies and affordable network connectivity. However, obtaining an overview of an event from a large collection of photos/videos, such as the YFCC100M dataset (Ð), is still a very challenging task due to the following reasons: (i) the existence of much noise in Flickr metadata, (ii) the big size of such datasets, and (iii) the difficulty in capturing the semantics of photos/videos. EventBuilder leverages metadata such as user tags, descriptions, spatial information, *etc.*, of all photos/videos in Ð, and content of Wikipedia articles, using a feature-pivot approach to build the indices of event-datasets in Ð. Moreover, EventBuilder introduces a summarization system which considers aspects such as quality, diversity, coverage, and redundancy, during the building process. The summarization system consists of three steps: (i) the identification of important *concepts* which should be described in the event summary, (ii) the composition of a text digest which covers the maximal number of important *concepts* by selecting the minimal number of sentences from available texts, within the desired summary length, and (iii) the geo-graphical visualization of the event on Google Maps.

For efficient and fast processing, we compute scores of all multimedia contents in Ð for the given events and build indices for event datasets ($\mathcal{F}$) during pre-processing. We include only those photos/videos in $\mathcal{F}$ whose scores are above a threshold δ. Next, we formulate the problem and introduce a solution to produce text summaries of events by employing a sentence selection algorithm inspired by the greedy algorithm [3]. In the summarization process we consider a representative set of $\mathcal{M}$ photos/videos ($\mathcal{R}$) from $\mathcal{F}$ with the highest scores. In this way, the proposed EventBuilder system provides an overview of events through text summaries and improves the visualization of events by displaying only multimedia contents and their descriptions from $\mathcal{R}$.

[1]URL: eventbuilder.geovid.org

Permission to make digital or hard copies of part or all of this work for personal or classroom use is granted without fee provided that copies are not made or distributed for profit or commercial advantage and that copies bear this notice and the full citation on the first page. Copyrights for third-party components of this work must be honored. For all other uses, contact the Owner/Author. Copyright is held by the owner/author(s).
MM '15, October 26–30, 2015, Brisbane, Australia.
Copyright 2015 ACM 978-1-4503-3459-4/15/10.
http://dx.doi.org/10.1145/2733373.2809932.

Since EventBuilder detects events from photos/videos offline rather than at search time, our system is time-efficient and scales well to large repositories. Since we use Wikipedia as background knowledge for more contextual information about the event to be summarized, our system can work well for new events by constructing feature vectors for those events by leveraging information from Wikipedia. An event summarization system can schedule event detection algorithms for newly uploaded photos/videos at regular time intervals to update event datasets.

2. RELATED WORK

There exists significant prior work in the area of event modeling, detection, and understanding from multimedia [5, 7, 10, 11]. Earlier methods [4, 9, 15] leveraged metadata such as user tags, spatial and temporal information to detect events automatically from a large collection of photos/videos such as Flickr. Rattenbury *et al.* [9] extracted place and event semantics for tags using Flickr metadata. Raad *et al.* [8] presented a clustering algorithm for automatically detecting personal events from photos shared online on the social network of a specific user by defining an event model that captures event triggers and relationships that can exist between events. They also detected multi-site, multi-day, and multi-person events using the appropriate time-space granularities. Fabro *et al.* [2] presented an algorithm for the summarization of real-life events based on community-contributed multimedia content using photos from Flickr and videos from YouTube. They evaluated the coverage of the produced summaries by comparing them with Wikipedia articles that report on the corresponding events. Atrey *et al.* [1] presented the detection of surveillance events such as human movements and objects being abandoned, by exploiting visual and aural information. Shah *et al.* [12] presented the ATLAS system which detects events such as slide transitions in a lecture video by exploiting its visual content and audio transcription. Low level visual features are often used for event detections or the selection of representative images from a collection of images/videos [7]. Recently, Papagiannopoulou and Mezaris [6] presented a clustering approach to produce an event-related image collection summarization using trained visual concept detectors based on image features such as SIFT, RGB-SIFT and OpponentSIFT. Wang *et al.* [14] summarized events based on the minimum description length principle, which is achieved through learning an HMM from the event data. Filatova and Hatzivassiloglou [3] proposed a set of event-based features which not only offers an improvement in summary quality over words as features (based on *tf-idf* scores), but also avoids redundancies in event summaries.

3. SYSTEM OVERVIEW

Figure 1 shows the system framework of EventBuilder. First, it performs event-wise classification and indexing of all photos/videos in social media datasets such as YFCC100M (Ð). Next, it solves the problem formulation of event summarization based on a greedy algorithm using event-based features which represent *concepts* (*i.e.*, important event-related information), as described by Filatova and Hatzivassiloglou [3]. *Concepts* associate the actions described in texts extracted from user descriptions and Wikipedia articles through verbs or action nouns labeling the event itself. Hence, an event summarization can be formulated as a maximum coverage problem. However, this problem is NP-hard, as it can be reduced to the well-known set cover problem. Thus, event summarization can be solved only in polynomial time by approximation algorithms.

Notations. Let N_e, T_e, S_e, and K_e be the feature vectors for event name, temporal information, spatial information, and keywords of an event e, respectively. The keywords of e are selected from the noun phrases used in the Wikipedia article of e. Let D be the list of 1080 camera models from Flickr, which are ranked based on their sensor sizes. Let N_i, T_i, S_i, K_i, and D_i be the feature vectors of photo/video i in Ð for event name, temporal information, spatial information, keywords, and camera model, respectively, and let $\xi(N_i, N_e)$, $\lambda(T_i, T_e)$, $\gamma(S_i, S_e)$, $\mu(K_i, K_e)$, and $\rho(D_i, D)$ be their corresponding similarity scores with e. Let $\mathcal{R}$ be the representative set for e, consisting of the top $\mathcal{M}$ photos/videos with the highest scores in an event dataset $\mathcal{F}$. Let $\mathcal{T}$ be the set of all sentences which are extracted from the description of photos/videos in $\mathcal{R}$ and contents of the Wikipedia article of e, and are used to produce a text summary $\mathcal{S}$. Let $|\mathcal{S}|$ and $\bar{\mathcal{L}}$ be the current word count and the word limit for $\mathcal{S}$, respectively. Let $\mathcal{K}$ and $\mathcal{Y}$ be the set of all *concepts* (c_k) of e and the set of corresponding weights (y_k), respectively. Let $v(s)$ be the score for a sentence s, which is the sum of the weights of all concepts it covers. Let $t(i)$ be the upload time of i. Let $\omega_{(s)}$ be a binary indicator variable which indicates if s is selected in the summary or not. Let $d(i)$ be a binary indicator variable which specifies if i has a description or not. Let $p(c, s)$ and $\beta(s, i)$ be 1 if $c \in s$ and $s \in i$, respectively, or otherwise 0.

Event Dataset and Experimental Settings. The score $u(i, e)$ of i for e is computed by a linear combination of similarity scores as follows: $u(i, e) = (w_1\ \xi(N_i, N_e) + w_2\ \lambda(T_i, T_e) + w_3\ \gamma(S_i, S_e) + w_4\ \mu(K_i, K_e) + w_5\ \rho(D_i, D))$, where $w_{i\prime}{}_{i\prime=1}^{5}$ are weights for different similarity scores such that $\sum_{i\prime=1}^{5} w_{i\prime} = 1$. We construct the event dataset $\mathcal{F}$ by indexing only those photos/videos of Ð whose scores $u(i, e)$ are above threshold δ. We set the weights as follows: $w_1 = 0.40$, $w_2 = 0.20$, $w_3 = 0.15$, $w_4 = 0.20$, and $w_5 = 0.05$, after initial experiments on the development set for event detection. We allocate only 5% of the total score for the camera model based on the heuristic that a good camera leads to a better quality photo/video which results in a better visualization of the event. All similarity scores, thresholds, and other scores are normalized to values [0, 1]. Let $\bar{\mathcal{L}}$ and $\mathcal{M}$ be system parameters to limit the summary length (number of words) and the number of photos/videos to be considered in the event summarization, respectively.

Problem Formulation for Text Summary. An event summary $\mathcal{S}$ is produced by extracting some sentences from $\mathcal{T}$, which cover important *concepts*. With the above notations and functions, we write the problem formulation for the event summarization as follows:

$$\min \sum_{(s\in\mathcal{T})\wedge(i\in\mathcal{R})} \omega(s)\beta(s,i) \tag{1a}$$

$$s.t. \sum_{s\in\mathcal{T}} \omega(s)\ p(c,s) \geq 1,\ \forall\ c \in \mathcal{K} \tag{1b}$$

$$v(s) \geq \eta,\ \ \forall\ s \in \mathcal{T} \tag{1c}$$

$$|\mathcal{S}| \leq \bar{\mathcal{L}}, \tag{1d}$$

$$d(i) = 1,\ \forall\ i \in \mathcal{R} \tag{1e}$$

$$t(i) \leq \tau,\ \forall\ i \in \mathcal{R} \tag{1f}$$

$$\omega(s) \in \{0, 1\},\ \forall\ s \in \mathcal{T} \tag{1g}$$

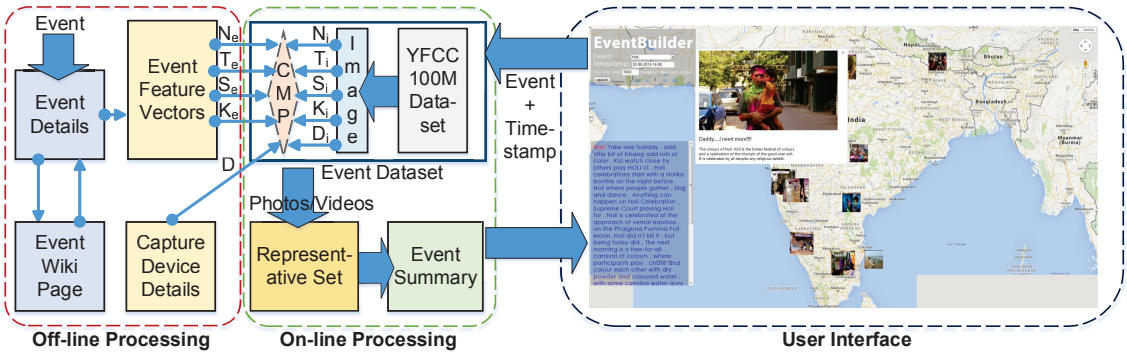

Figure 1: System framework of EventBuilder.

	c_1	c_2	c_3	c_4	...	$c_{\|\mathcal{K}\|}$
s_1	1	1	0	1	...	1
s_2	0	1	1	0	...	0
...	...	...	...	...	...	...
$s_{\|\mathcal{T}\|}$	1	0	0	1	...	1

Table 1: Matrix model for event summarization.

$$p(c,s) \in \{0,1\}, \forall\ s \in \mathcal{T}, \forall\ c \in \mathcal{K} \quad \text{(1h)}$$
$$\beta(s,i) \in \{0,1\}, \forall\ s \in \mathcal{T}, \forall\ i \in \mathcal{R} \quad \text{(1i)}$$

The objective function in Eq. (1a) solves the problem of event summarization and selects the minimal number of sentences which cover the maximal number of important concepts within the desired length of a summary. Eqs. (1b) and (1c) ensure that each concept is covered by at least one sentence with a score above threshold η. Eq. (1d) assures that the length constraint of the summarization is met. Eqs. (1e) and (1f) ensure that i has a description and is uploaded before the given timestamp τ. Eqs. (1g), (1h), and (1i) ensure that a concept, sentence, and photo is either present or absent in the sentence selected for the summarization.

Algorithm 1 Event summarization algorithm.

procedure EventSummarization
  INPUT: An event e and a time stamp τ
  OUTPUT: A text summary $\mathcal{SV}$
  $\bar{\mathcal{K}} = []$, $|\mathcal{S}| = 0$, $\bar{\mathcal{S}} = 200$ ▷ initialization.
  $(\mathcal{K}, \mathcal{Y})$ = getEventConceptsAndWeights(e) ▷ see [3].
  $\mathcal{F}$ = getEventDataset(e) ▷ pre-processed event dataset.
  $\mathcal{R}$ = getRepresentativeSet(e, $\mathcal{F}$) ▷ representative photos.
  $\mathcal{T}$ = getSentences(e, $\mathcal{R}$) ▷ user description, Wiki texts.
  while $((|\mathcal{S}| \leq \bar{\mathcal{L}}) \wedge (\mathcal{K} \neq \bar{\mathcal{K}}))$ **do** ▷ $\bar{\mathcal{K}}$ is covered concepts.
    c = getUncoveredConcept($\mathcal{K}$, $\bar{\mathcal{K}}$) ▷ important c first.
    s = getSentence(c, $\mathcal{Y}$, $\bar{\mathcal{K}}$, $\mathcal{T}$) ▷ $c \in s \wedge v(s)$ is max.
    updateCoveredConceptList(s, $\bar{\mathcal{K}}$) ▷ add all $c \in s$ to $\bar{\mathcal{K}}$.
    addToEventTextSummary(s, $\mathcal{S}$) ▷ add s to summary.
    for each sentence $s \in \mathcal{T}$ **do** ▷ say, $s \in$ photo/video i.
      updScr(s, $\mathcal{Y}$, $\bar{\mathcal{K}}$) ▷ v(s)= u(i,e) $\times \sum_{c \in s, c \notin \bar{\mathcal{K}}} y$.

Solution. A greedy algorithm is reportedly the best possible polynomial approximation algorithm to solve NP-hard problems such as the set cover problem (*i.e.*, an event summarization problem in our case). We introduce a greedy algorithm which iteratively adds sentences to the event summary $\mathcal{S}$, until it either achieves the desired length $\bar{\mathcal{L}}$ or covers all *concepts*. Hence, the maximal number of important *concepts* are covered in the summary. Every time, when a new sentence is added to the summary, we check whether it contains enough new important *concepts* to avoid redundancy. We have formulated the problem of event summarization in terms of a matrix model, as shown in Table 1. Sentences and important concepts are mapped onto a $|\mathcal{T}| \times |\mathcal{K}|$ matrix. An entry of this matrix is 1 if the concept (column) is present in the sentence (row), otherwise it is 0. We take advantage of this model matrix to avoid redundancy by globally selecting the sentences that cover the most important concepts (*i.e.*, information) present in user descriptions and Wikipedia articles. Using the above matrix, it is possible to formulate the event summarization problem as equivalent to extracting the minimal number of sentences which cover all the important concepts. In our approximation algorithm, we constrain the total length of the summary with respect to the total weight of covered concepts, in order to handle the cost of long summaries. Our adaptive greedy algorithm for the event summarization is motivated by the summarization algorithm presented by Filatova and Hatzivassiloglou [3].

Algorithm 1 presents our summarization algorithm. First, we determine all event-related important concepts and their weights, as described by Filatova and Hatzivassiloglou [3]. Next, we extract all sentences from the user description of photos/videos in the representative set and texts in the Wikipedia article of an event e. We compute the score of a sentence by multiplying the sum of weights of all concepts it covers and the score of the photo/video which this sentence belongs to. Since each concept has different importance, we cover important concepts first. We consider only those sentences that contain the concept with the highest weight that has not yet been covered. Among these sentences, we choose the sentence with the highest total score and add it to the final event summary. Then we add the concepts which are covered by this sentence to the list of covered concepts $\bar{\mathcal{K}}$ in the final summary. Before adding further sentences to the event summary, we recalculate the scores of all sentences by not considering the weight of all the concepts that are already covered in the event summary. We continue adding sentences to $\mathcal{S}$ until we obtain a summary of the desired length $\bar{\mathcal{L}}$ or a summary covering all concepts.

4. EVALUATION

Dataset. The YFCC100M [13] (Yahoo! Flickr Creative Commons 100M) dataset, consisting of a total of 100 million photos/videos (approximately 99 million photos and 1 million videos) from Flickr, were provided with several metadata annotations such as user tags, spatial and temporal information, *etc.*, for the Yahoo-Flickr Event Summarization Challenge. To evaluate the proposed automatic summarization systems, the organizers have provided several events and timestamps, as listed in Table 2.

Event Name	Timestamp @ 12:00am UTC	Informative	Experience	Acceptance	Event Name	Timestamp @ 12:00am UTC	Informative	Experience	Acceptance
Holi	8 March 2009	3.93	4.13	4.00	Olympic Games	25 June 2012	3.00	2.60	2.80
	1 April 2009	3.80	3.80	3.66		1 Oct 2012	3.33	2.93	3.06
	1 April 2011	3.93	4.00	3.93		1 Jan 2015	3.27	3.13	3.13
	Avg. Rating	3.87	3.98	3.86		**Avg. Rating**	3.20	2.87	3.00
Eyjafjallajökull Eruption	1 April 2010	3.93	3.73	3.80	Batkid	15 Nov 2013	3.93	4.00	3.80
	18 April 2010	3.73	3.73	3.73		16 Nov 2013	3.80	4.00	3.73
	1 Jan 2014	4.06	4.13	4.0		1 Jan 2014	3.73	3.80	3.67
	Avg. Rating	3.91	3.86	3.86		**Avg. Rating**	3.61	3.93	3.76
Occupy Movement	19 Sep 2011	2.46	2.53	2.20	Byron Bay Bluesfest	1 June 2011	3.53	3.53	3.40
	1 Nov 2011	3.60	3.53	2.93		1 Jan 2015	3.53	3.60	3.60
	19 Sep 2012	3.67	3.67	3.67		-	-	-	-
	Avg. Rating	2.40	3.24	2.93		**Avg. Rating**	3.53	3.57	3.50
Hanami	1 Feb 2013	3.60	3.60	3.80	**All Events**	**Avg. Rating**	**3.46**	**3.61**	**3.54**
	1 June 2013	3.80	4.00	3.93					
	Avg. Rating	3.70	3.80	3.87					

Table 2: Evaluation results for the Yahoo-Flickr Event Summarization Challenge (YFCC100M dataset).

Results. The same algorithm was used for all summaries. No event-specific tuning was performed. All event summaries in our evaluation cover the maximal number of important concepts and their summary length is within the desired word limit. Since the summary evaluation is subjective in nature, we evaluated the performance through a user study. We asked fifteen evaluators to assess EventBuilder and provide scores from 1 to 5, with a higher score indicating better satisfaction. We defined three perspectives that evaluators should consider: (i) informativeness, which indicates to what degree a user feels that the summary captures the essence of the event, (ii) experience, which indicates if the user thinks the summary is helpful for understanding the event, and (iii) acceptance, which indicates if a user would be willing to use this event summarization function if Flickr were to incorporate it into their system. The default event summary length $\bar{\mathcal{L}}$ was set to 200 words during evaluation. Experimental results (see Table 2) indicate that users generally think that the summaries are informative and can help them to obtain a quick overview of an event.

5. CONCLUSIONS

The proposed EventBuilder system is a real-time automatic event detection and summarization system. First, it computes event-wise scores for each photo/video in social media datasets such as YFCC100M for the given events and builds event-wise indices. Next, it produces event summaries based on the given events and timestamps in real-time and facilitates efficient access to a large collection of photos/videos. In our future work we plan to extend the approach by exploiting visual contents, in addition to the available texts, using machine learning methods.

ACKNOWLEDGMENTS

This research has been supported by the Singapore National Research Foundation under its International Research Centre @ Singapore Funding Initiative and administered by the IDM Programme Office through the Centre of Social Media Innovations for Communities (COSMIC).

6. REFERENCES

[1] P. K. Atrey, A. El Saddik, and M. S. Kankanhalli. Effective Multimedia Surveillance using a Human-centric Approach. *Springer Multimedia Tools and Applications*, 51(2):697–721, 2011.

[2] M. Del Fabro, A. Sobe, and L. Böszörmenyi. Summarization of real-life events based on community-contributed content. In *MMEDIA*, 2012.

[3] E. Filatova and V. Hatzivassiloglou. Event-based Extractive Summarization. In *ACL Workshop on Summarization*, pages 104–111, 2004.

[4] C. S. Firan, M. Georgescu, W. Nejdl, and R. Paiu. Bringing Order to Your Photos: Event-driven Classification of Flickr Images based on Social Knowledge. In *ACM CIKM*, pages 189–198, 2010.

[5] V. Mezaris, A. Scherp, R. Jain, and M. S. Kankanhalli. Real-life Events in Multimedia: Detection, Representation, Retrieval, and Applications. *Springer Multimedia Tools and Applications*, 70(1):1–6, 2014.

[6] C. Papagiannopoulou and V. Mezaris. Concept-based Image Clustering and Summarization of Event-related Image Collections. In *Workshop on HuEvent at ACM Multimedia*, pages 23–28, 2014.

[7] G. Petkos, S. Papadopoulos, V. Mezaris, R. Troncy, P. Cimiano, T. Reuter, and Y. Kompatsiaris. Social Event Detection at MediaEval: a Three-Year Retrospect of Tasks and Results. In *Workshop on SEWM at ACM ICMR*, 2014.

[8] E. J. Raad and R. Chbeir. Foto2Events: From Photos to Event Discovery and Linking in Online Social Networks. In *IEEE BdCloud*, pages 508–515, 2014.

[9] T. Rattenbury, N. Good, and M. Naaman. Towards Automatic Extraction of Event and Place Semantics from Flickr Tags. In *ACM SIGIR*, pages 103–110, 2007.

[10] A. Scherp and V. Mezaris. Survey on Modeling and Indexing Events in Multimedia. *Springer Multimedia Tools and Applications*, 70(1):7–23, 2014.

[11] A. Scherp, V. Mezaris, B. Ionescu, and F. De Natale. HuEvent '14: Workshop on Human-Centered Event Understanding from Multimedia. In *ACM Multimedia*, pages 1253–1254, 2014.

[12] R. R. Shah, Y. Yu, A. D. Shaikh, S. Tang, and R. Zimmermann. ATLAS: Automatic Temporal Segmentation and Annotation of Lecture Videos Based on Modelling Transition Time. In *ACM Multimedia*, pages 209–212, 2014.

[13] B. Thomee, D. A. Shamma, G. Friedland, B. Elizalde, K. Ni, D. Poland, D. Borth, and L.-J. Li. The New Data and New Challenges in Multimedia Research. *arXiv preprint arXiv:1503.01817*, 2015.

[14] P. Wang, H. Wang, M. Liu, and W. Wang. An Algorithmic Approach to Event Summarization. In *ACM SIGMOD*, pages 183–194, 2010.

[15] M. Zaharieva, M. Zeppelzauer, and C. Breiteneder. Automated Social Event Detection in Large Photo Collections. In *ACM ICMR*, pages 167–174, 2013.

ResearchGate

See discussions, stats, and author profiles for this publication at: http://www.researchgate.net/publication/280610841

Fixed Bed Column Study and Adsorption Modelling on the Adsorption of Malachite Green dye from wastewater using Acid Activated Sawdust

ARTICLE *in* INTERNATIONAL JOURNAL OF ADVANCED RESEARCH · JULY 2015

Impact Factor: 4.59

4 AUTHORS, INCLUDING:

S. K. Singh

Delhi Technological University

73 PUBLICATIONS **72** CITATIONS

SEE PROFILE

Available from: S. K. Singh

Retrieved on: 03 September 2015

ISSN NO. 2320-5407

Journal homepage: http://www.journalijar.com

INTERNATIONAL JOURNAL OF ADVANCED RESEARCH

RESEARCH ARTICLE

Fixed Bed Column Study and Adsorption Modelling on the Adsorption of Malachite Green dye from wastewater using Acid Activated Sawdust

S.K. Singh[1] , Dhruv Katoria[2], Dhruv Mehta[2], Dhruv Sehgal[2]

1. Professor, Department of Environmental Engineering, Delhi Technological University, New Delhi-42, India

2.Graduate Student, Department of Environmental Engineering, Delhi Technological University, New Delhi-42, India

Manuscript Info

Manuscript History:

Received: 15 May 2015
Final Accepted: 22 June 2015
Published Online: July 2015

Key words:

Adsorption, Acid Activated Sawdust, Breakthrough Curve, Fixed Bed Column, Malachite Green

Corresponding Author

S.K. Singh

Abstract

The sorption capability of Acid Activated Sawdust for removing Malachite Green from wastewater was evaluated in a fixed bed column. The column experiment was conducted by varying the bed height, initial dye concentration and solution flow rate. An increase in bed depth extended the life of the column while an increase in flow rate and initial concentration exhausted the column earlier. Several column adsorption models were applied to the experimental data. The adsorption capacity using the Thomas model was found to be 10.06 mg/g. Among the various models applied the Bohart-Adam model fitted the experimental data well with an r^2>0.9. The Yoon–Nelson model also estimated the 50% breakthrough curve and provided the estimate break-through time for the column systems. The results indicated that Acid Activated Sawdust could be used for adsorption of Malachite Green containing waste water.

Copy Right, IJAR, 2015,. All rights reserved

INTRODUCTION

Dyes are chemical substances which are used during the manufacturing process to impart value to the final product. Industries such as tanneries, food, paper and pulp use dyes and pigments to colour their products. Colour is an observable pollutant whose presence in even a very minute amount of colouring substance makes it undesirable due to its appearance [1]. Besides this the dye effluent from industries has high Biochemical Oxygen Demand (BOD) and Chemical Oxygen Demand (COD) values. Also, the reduction in light penetration leads to the instability of the biotic component of the receiving body [2]. They may also be a complication if their partial deterioration takes place under anaerobic conditions by the bacteria leading to creation of toxic amine [3]. Therefore the threats posed by dyes have not gone unnoticed and over the past several years many different techniques have been researched for the effective removal of dye from the industrial effluent.

The conventional methods adopted by industries for the removal of colour were froth flotation, coagulation and flocculation [4]. However these techniques were inefficient and thus the attention shifted on innovating new techniques which were not only highly efficient but were also less capital extensive. Recently researchers have shifted their focus on the use of adsorption technique for the removal of dye pollutants from industrial effluent. A survey of the available literature reveals a large number of waste products which have been successfully used for the adsorption of various pollutants [5-11].

The present paper attempts to investigate the usability of acid treated sawdust of Tectona Grandis for the removal of Malachite Green (MG), a tri-phenyl methane dye from the industrial effluent. MG has long been used as colouring agent for leather products, cotton and wool [12]. In addition, as an external applicant, its use as an antiseptic and antifungal has been clearly established in literature [13-14]. However the presence of nitrogen makes it toxic, hazardous and carcinogenic if consumed orally [15]. Sawdust is a waste material produced during manufacture of

woodwork. It is an undesirable material which is collected and dumped in landfills. Even though considerable research has been done on the use of acid activated sawdust (AAS) for the removal of various dyes and metals, none has established a relationship between the removal capabilities of MG by AAS.
Furthermore, batch adsorption processes may not be convenient during the industrial operations with high flow rates. Fixed bed columns can be used continuously at higher flow rates for effective adsorption. In this study column study has been performed to understand the adsorption capability of MG by AAS.

2. Materials and Methods

2.1 Adsorbent Preparation

Sawdust of Tectona Grandis was collected from a local wood market based in Keshav Puram, New Delhi and washed under tap water to remove any dust and impurities on the sawdust surface. The sawdust was then sun dried for 2 days to remove the moisture content after which the dried sawdust was ground in a crushed to obtain finer aggregates prior to transportation to the laboratory. In the laboratory, the dried sawdust was mixed with 1.2 N conc. H_2SO_4 (35 % w/v) and the mixture was allowed to react for a period of 24 hours at room temperature. The reacted mixture was extracted and washed with 0.1N $NaHCO_3$ solution to neutralize the solution pH. The sawdust was then washed with distilled water and finally dried in an oven at 105° C till dry. The dried sawdust was subsequently passed through a sieve to obtain an average grain size of 500 µm.

2.2 Preparation of dye solution

Analytical grade chemicals and reagents were used throughout the course of the experiment. The stock solution of MG was obtained by dissolving predetermined amounts of MG in distilled water to obtain a concentration of 1000 mg/L. Different concentration solutions of MG were obtained by dilution the stock solution with distilled water.

2.3 Column Experiments

For the column experiments, a PVC column with an inner diameter of 3.85 cm and a length 22.5 cm was used. The bottom of the column was sealed off with a plastic cap to prevent the loss of adsorbent during the infiltration process. The design of the column experiment is illustrated in fig 1. AAS of known quantity was filled in the column and wetted with distilled water in the downward direction in order to remove any air trapped between the particles. The dye working solution was continuously fed in the downward direction using a peristaltic pump. At different pre-defined intervals samples were collected in a test tube and measured for residual dye concentration in a spectrophotometer at 618nm wavelength.

2.3.1 Effect of Initial Dye Concentration

Working solutions of 200 and 500 mg/L were used as an influent to study the ability of sawdust to remove the MG dye of different concentrations. The flow rate during the experiments was controlled at 100 cc/hr while the bed depth remained at 7.5 cm. The effluent was collected at pre-defined intervals to measure the residual dye concentration.

2.3.2 Effect of Flow Rate

The contact period between the dye and the sawdust surface is directly influenced by the rate of flow of the influent. During this study, the flow rate of influent dye was varied from 100 to 200 cc/hr. The initial dye concentration remained at 500 mg/L. The effluent was collected at pre-defined intervals to measure the residual dye concentration.

2.3.3 Effect of Bed Height

To evaluate the effect of bed height, different amounts of sawdust is filled in 3 separate columns up to a height of 7.5, 15 and 22.5 cm respectively. The working MG dye solution of 500 mg/L was fed into the columns separately with a flow rate of 100 cc/hr. At different pre-defined intervals the effluent was collected for analysis.

3. Results and Discussion

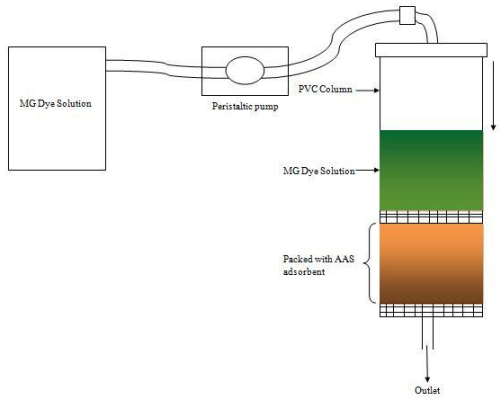

Fig 1. Continuous column bed Diagram

3.1 Effect of bed Study

3.1.1 Effect of initial dye concentration

In order to establish optimum conditions for the adsorption of MG dye in a column by AAS, the initial dye concentration is varied to 200 and 500 mg/L. Fig. 2 illustrates the breakthrough curve between C_t/C_o (Concentration at time t/ initial concentration) and time t. With an increase in initial concentration from 200 to 500 mg/L, the value of C_t/C_o increases from 0.3 to 0.45. This represents a steeper slope in case of 500 mg/L dye concentration. The breakthrough time decreases from 120 min to 70 min with an increase in initial dye concentration which is due to a larger mass transfer coefficient. The presence of more dye ions provided an increased competition for the lesser available biding sites on the adsorbent [16]. Therefore it is concluded that the adsorption process is concentration dependent. Similar results were obtained for biosorption of reactive black by bamboo waste based activated carbon [17].

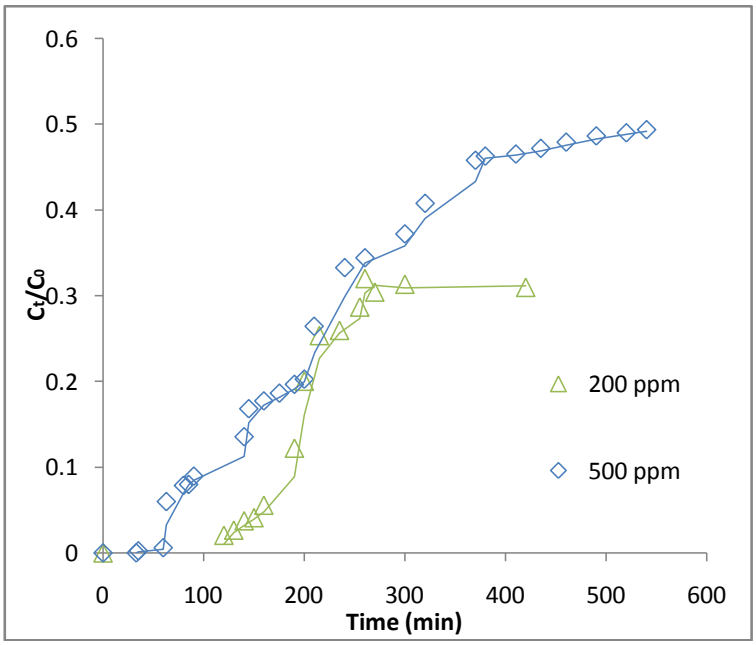

Fig 2. Breakthrough curve for adsorption of MG by AAS at different initial MG concentrations.

3.1.2 Effect of the solution flow rate

The influent flow rate as seen from Fig 3. has a significant effect on malachite green adsorption in the fixed bed column. The flow rates were varied from 100 to 200 cc/hr with a constant bed height and initial concentration of 500 mg/L. The breakthrough is achieved faster at a higher influent flow rate which is visible from the fact that the breakthrough time decreases from 75 min to approximately 25 min as flow rate increases from 100 to 200 cc/hr. The

inadequate time experienced by the adsorbent strips the dye solution the privilege of diffusing into the adsorbent pores which consequently decreases the adsorbent's adsorption capacity. The high flow rates didn't allow for sufficient time to achieve equilibrium conditions before the exit of dye from the column leading to a faster breakthrough at higher flow rate.

3.1.3 Effect of bed height

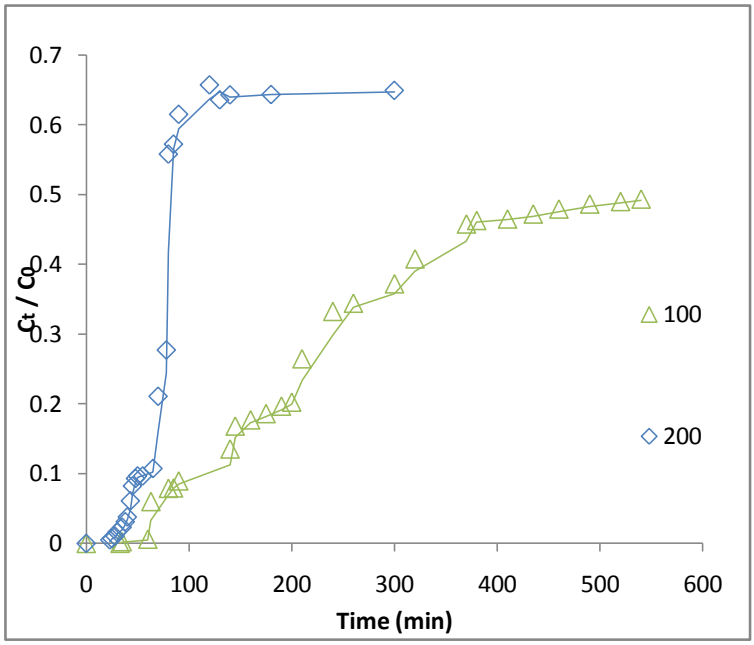

Fig 3. Breakthrough curve for adsorption of MG by AAS at different solution flow rates.

To determine the breakthrough of MG dye, various bed heights i.e. 7.5, 15, 22.5 cm were applied and the results are represented in Fig 4. It is observed from the breakthrough curve that with an increase in bed depth, slope of breakthrough curve decreases [18]. An increase in breakthrough time from 50 min at 7.5 cm to 210 min at 15cm depth and subsequently to 570 min at 22.5 cm is observed from the graph. The variation may be due to an increase in bed height which offers more of the surface area to MG ions resulting in more contact time with AAS which in turn results into lower concentration of dye in the effluent. Higher surface area of AAS generates more active sites for adsorption to take place and it also broadens the mass transfer zone length [17-19].

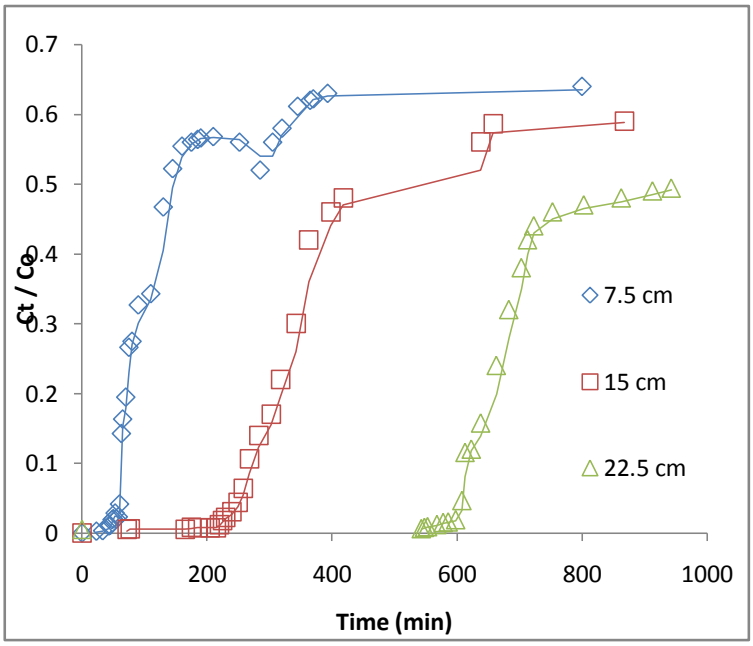

Fig 4. Breakthrough curve for adsorption of MG by AAS at different

3.2 Analysis of Fixed Bed Models

3.2.1 Bohart- Adams Model

Bohart Adams Model is assumed to follow "step isotherm" in which the rate of adsorption is found to be proportional to the fractional adsorption capacity available at the surface of an adsorbent [17] . This concept also follows the basic principle of surface reaction theory [20-21]. The linear expression of the model provides characteristic parameters such as kinetic constant (k) and adsorption capacity (N_o). The following is the expression:

$$t_b = \frac{N_o Z}{C_o v} - \frac{\ln(\frac{C_o}{C_b}-1)}{k_{AB}\, C_o} \quad (1)$$

Where, k_{AB} is the Bohart Adams rate constant (L/mg-min), C_o and C_b are the initial and breakthrough concentration in mg/L respectively, N_o is the adsorption capacity of adsorbent (mg/l), v and t_b are linear velocity and breakthrough time respectively (min), Z is the bed depth in cm. The above equation can be generalised in a simpler form as

$$t_b = aZ + b \quad (2)$$

$$a = \frac{N_o}{C_o v} \quad (3)$$

$$b = \ln[\left(\frac{C_o}{C_b}\right) - 1] * \frac{1}{C_o k_{AB}} \quad (4)$$

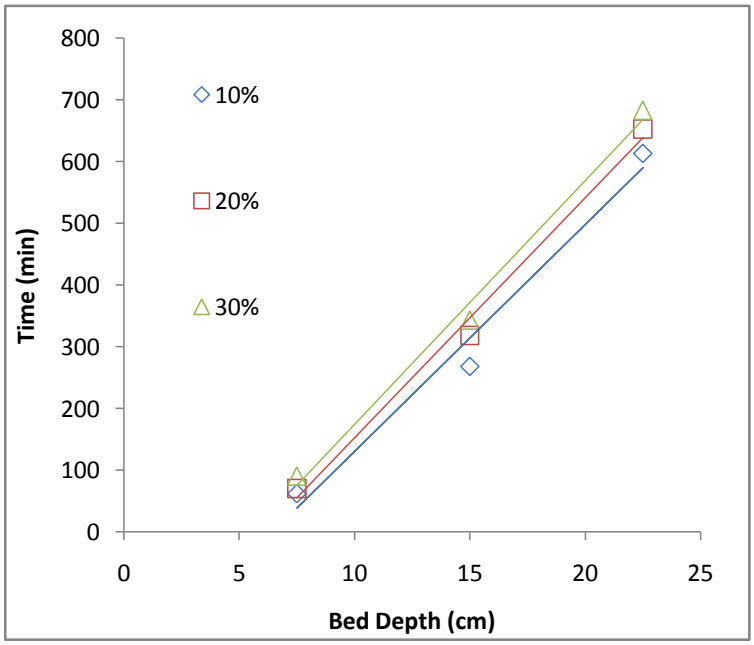

Fig 5. Bohart Adams Linearized Model

A linear plot between time and bed depth representing iso-removal points of different bed depths at constant flow rate and initial malachite green concentration is shown in Fig 5. Values of slope and intercept are further used to calculate the rate constant and adsorption capacity as depicted in Table 1.

Adsorption capacity (N_o) lies in the range of 671.88 -721 mg/L for iso- removal lines (10%, 20% and 30%). A slight decrease in the value of kinetic constant from $1.86*10^{-5}$ to $0.77*10^{-5}$ is observed with increase in removal percentage. Further, it is clear from the high value of Regression constant that Bohart – Adams model explains the sorption process in a better way.

Table 1. Bohart-Adams model constants for the adsorption of MG on AAS in a fixed bed column

Iso –Removal Percentage	A_i (min/cm)	B_i (min)	N_o (mg/L)	K_{ab} (L/min.mg)	R^2
10	36.73	-236.6	671.88	$1.86*10^{-5}$	0.979

20	38.86	-236	710.5	$1.17*10^{-5}$	0.992
30	39.53	-221	722.72	$0.77*10^{-5}$	0.992

3.2.2 Clark model

This model is based on Freundlich isotherm model where Freundlich constant n=2.06 is used for the calculation of Clark model parameters A and r (min^{-1}) [17] [22-23] .The linearized form of the model is represented as:

$$\ln[(\frac{C_o}{C_t})^{n-1} - 1] = -rt + \ln A \quad (5)$$

The predicted Clark model parameters calculated are depicted in Table 2. It is observed from Table 2, that the value of rate constant decreases and the value of A increased with an increase in bed height.

Intial Concentration (mg/L)	Bed Height (cm)	Flow Rate (cm^3/hr)	Rate constant (L/min)	A	R^2

Table 2. Clark model constants for the adsorption of MG on AAS in a fixed bed column

500	7.5	100	0.065	1396.8	0.811
500	15	100	0.024	2881.3	0.937
500	22.5	100	0.019	1745	0.808
500	7.5	200	0.006	17.3	0.903
200	7.5	100	0.02	476.27	0.903

3.2.3 Thomas model:

Thomas model which follows the Langmuir kinetics of adsorption and desorption [24] is widely used to calculate the performance of a column and predict its breakthrough curves [18]. It is based on the assumption of negligible axial dispersion. Its main limitation is that the model is based on second order kinetics and hence doesn't restrict the sorption by a chemical reaction and is controlled by mass transfer at the surface [25]. The model is represented by the following formula:

$$\ln\left[\frac{C_O}{C_t} - 1\right] = \frac{k_{th} q_0 m}{Q} - k_{th} C_o t \quad (6)$$

Where K_{th} is the Thomas rate constant (mL min^{-1} mg^{-1}), Q_o is the equilibrium Malachite green uptake per g of the adsorbent (mg/ g). X is the amount of adsorbent in the column (g), C_o is the influent malachite green concentration (mg/L), C_t is the concentration of effluent at time t (mg/L), v is flow rate (ml/min). C_t/C_o is the ratio of effluent and influent malachite green concentrations. Thomas constant Q_o and K_{th} can be obtained through graph plotted between ln $[(C_o/C_t)-1]$ against t [26].

Table 3. Thomas model constants for the adsorption of MG on AAS in a fixed bed column

Bed Height (cm)	Flow Rate (ml/min)	Initial dye Conc. (mg/L)	Q_o (mg/g)	K_{th} (L/mg min)	R^2
7.5	100	500	4.5	9.2*10-5	0.8
15	100	500	10.06	5*10-5	0.947
22.5	100	500	7.4	4.6*10-5	0.88

The predicted Thomas parameters are given in Table 3. Here, the value of K_{th} decreases with an increase in bed depth. Value of K_{th} decreases from 9.2 x 10^{-5} to 4.6 x 10^{-5} as the bed depth increases from 7.5 to 22.5 cm.. Adsorption capacity is found to be in range of 4.5-10.06 mg/g which is much better than the various adsorbents used till now for malachite green.

3.2.4 Yoon-Nelson:

This model is applied to a range of concentrations of the effluent between the breakthrough and saturation time of the column and is based on the assumption that the rate of decrease in the probability of adsorption for each

adsorbate molecule is proportional to the probability of adsorbate adsorption and probability of adsorbate breakthrough on the adsorbent [25].The equation of Yoon-Nelson model can be given as:

$$\ln\left[\frac{C_t}{C_o - C_t}\right] = k_{YN}t - \mathcal{I}k_{YN} \quad (7)$$

Where K_{YN} is the rate constant (per minute) and τ is the time required for 50% adsorbate breakthrough (min). The approach involves a plot of $C_t/(C_o-C_t)$ versus sampling time (t)[24].The parameters of k_{YN} and $\mathcal{I}$ can be obtained using the non-linear regressive method[26].

Table 4. Yoon-Nelson model constants for the adsorption of MG on AAS in a fixed bed column

Concentration (mg/L)	Bed Height (cm)	Flow Rate (cm^3/hr)	$k_{YN}(Lmin^{-1})$	t(min)	R^2
500	7.5	100	0.062	110.7	0.813
500	15	100	0.025	313	0.947
500	22.5	100	0.018	271	0.81
500	7.5	200	0.006	459..5	0.919
200	7.5	100	0.023	284.8	0.941

It is observed from Table 4 that value of rate constant increases from 0.006 $Lmin^{-1}$ to 0.023 $Lmin^{-1}$ with a subsequent decrease in concentration of dye from 500 mg/L to 200 mg/L. A proportional relationship was seen between rate constant and Bed Height. The results obtained were similar to the results of Dutta et al [17].

4. Conclusion

The chemically treated sawdust prepared from sawdust of Tectona Grandis is found to be effective in removal of Malachite green from aqueous solution. The removal efficiency of dye was found to be strongly dependent on flow rate, initial concentration and bed depth. It was established that exhaustion of column increased with increase in flow rate and initial concentration and decreased with increase in bed depth. The models studied gave good approximations of experimental data amongst various models applied to analyze the data obtained. The adsorption capacity got by Thomas Model was found to be up to 10.06 mg/g which is comparatively good amongst various adsorbents available for removal of Malachite green dye. The bed sorption capacity (N_o) obtained from Bohart Adams Model is in the range of 671.88 – 722 mg/L. The Yoon–Nelson model also estimated the 50% breakthrough curve and provided the estimate break-through time for the column systems. The Clark model is found suitable to describe column adsorption obeying the Freundlich isotherm. Therefore information obtained from the fixed bed column study suggested that the treated sawdust could be used as an efficient and economical adsorbent for treatment of malachite green dye from waste water.

References

1. Hamdaoui, O., Saoudi, F., Chiha, M., & Naffrechoux, E. (2008). Sorption of malachite green by a novel sorbent, dead leaves of plane tree: Equilibrium and kinetic modeling. *Chemical Engineering Journal* , 73-84.

2. Hameed, B., & Ahmad, A. (2009). Batch adsorption of methylene blue from aqueous solution by garlic peel, an agricultural waste biomass. *Journal of Hazardous Materials* , 870-875.

3. Weber, E., & Wolfe, N. (1987). Kinetics studies of reduction of aromatic azo compounds in anerobic sediment/water systems. *Environmental Toxicology and Chemistry* , 911-920.

4. Gupya, V. K., Mittal, A., & Gajbe, V. (2004). Adsorption kinetics and column operations for the removal and recovery of malachite green from wastewater using bottom ash. *Separation and Purification Technology* , 87-96.

5. Kalavathy, M. H., & Miranda, L. R. (2010). Comparison of copper adsorption from aqueous solution using modified and unmodified Hevea brasiliensis saw dust. *Desalination* , 165-174.

6. Hossain, M. A., Ngo, H. H., Guo, W. S., & Setiadi, T. (2012). Adsorption and desorption of copper(II) ions onto garden grass. *Bioresource Technology* , 386-395.

7. Wang, L.-H., Lin, C.-I., & Wu, F.-C. (2010). Kinetic study of adsorption of copper (II) ion from aqueous solution using rice hull ash. *Journal of the Taiwan Institute of Chemical Engineers*, 599-605.

8. El-Ashtoukhy, E., Amin, N., & Abdelwahab, O. (2008). Removal of lead (II) and copper (II) from aqueous solution using pomegranate peel as a new adsorbent. *Desalination* , 162-173.

9. Mahony, T. O., Guibal, E., & Tobin, J. (2002). Reactive dye biosorption by Rhizopus arrhizus biomass. *Enzyme and Microbial Technology* , 456-463.

10. Waranusantigul, P., Pokethitiyook, P., Kruatrachue, M., & Upatham, E. (2003). Kinetics of basic dye (methylene blue) biosorption by giant duckweed (Spirodela polyrrhiza). *Environmental Pollution*, 385-392.

11. Fiorentin, L. D., Trigueros, D. E., Módenes, A. N., Espinoza-Quiñones, F. R., Pereira, N. C., Barros, S. T., et al. (2010). Biosorption of reactive blue 5G dye onto drying orange bagasse in batch system: Kinetic and equilibrium modeling. *Chemical Engineering Journal* , 68-77.

12. Khattri, S.D., & Singh, M.K. (1999). Colour removal from dye wastewater using sugar cane dust as an adsorbent. *Adsorption Science & Technology*, 269-282.

13. Alderman, D.J. (1985). Malachite Green- A Review. *Journal of Fish Diseases*, 289-298.

14. Sawa, Y., & Hoten, M. (2001). Antibacterial activity of basic dyes on the dyed acrylic fibers. *Sen'I Gakkaishi*, 153-158.

15. Mckay, G., & Otterburn, M.S. (1985). Fullers earth and fired clay as adsorbent for dye stuffs, equilibrium and rate constants. *Water, Air & Soil Pollution*, 307-322.

[16] Sivakumar, P. and Palanisamy, P N. (2009) Packed bed column studies for the removal of Acid blue 92 and Basic red 29 using non-conventional adsorbent. *Indian J. of Chemical Technology*, Vol. 16, 301-307.

[17] Dutta, M., Basu, J K., Faraz, H., Gautam, N. and Kumar, A. (2012) Fixed-bed Column Study of Textile Dye Direct Blue 86 by using A Composite Adsorbent. *Scholars Research Library*, 4 (2):882-891

[18] Manase Auta (2012) Fixed bed adsorption studies of Rhoda mine B dye using oil palm empty fruits bunch activated carbon. *Journal of Engineering Research and Studies*, Vol. 3.

[19] Noreen, S., Bhatti, H N., Nausheen, S., Sadaf, S. and Ashfaq M. (2013) Batch and fixed bed adsorption study for the removal of DrimarineBlack CL-B dye from aqueous solution using a lignocellulosic waste:A cost affective adsorbent. *Industrial Crops and Products*, 568– 579

[20] Ansari, R., Seyghali, B., Mohammad-khah, A., and Zanjanchi, M. A., (2012) Highly efficient adsorption of anionic dyes from aqueous solutions using sawdust modified by cationic surfactant of cetyltrimethylammonium bromide. *Journal of Surfactants and Detergents* 15(5): 557-565

[21] C.P. Thurgood (2007) Estimation of Parametersfor the Bohart-Adams Model Electrochemical Power Sources Group *Royal Military College of Canada*

[22] Hanen, N., and Abdelmottaleb, O. (2013). Modeling of the Dynamics Adsorption of Phenol from an Aqueous Solution on Activated Carbon Produced from Olive Stones. *J. Chemical Engineering & Process Technology*

[23] Zhe XU, Jian-guo CAI and Bing-cai PAN (2013) Mathematically modeling fixed-bed adsorption in aqueous systems. *Journal of Zhejiang University-SCIENCE A (Applied Physics & Engineering)*

[24] R. Rajeshkannan, M. Rajasimman and N. Raja Mohan (2013) Packed Bed column studies for the removal of dye using novel sorbent. *Chemical Industry and Chemical Engineering Quarterly*, 19(4) 461-470.

[25] Kandaswamy, S. B. and SriKrishna, P T R. (2013) Fixed-bed column studies on bio sorption of crystal violet from aqueous solution by Citrullus lanatus rind and Cyperusrotundus. *Applied Water Science,* 3: 673-687.

[26] Han, R., Ding, D., Xu, Y., Zou, W., Wang, Y., Li, Y., Zou, L. (2007) Use of rice husk for the adsorption of congo red from aqueous solution in column mode. *Bioresource Technology,* 99(8): 2938-46.

[27] Neetu Sharma, D.P. Tiwari, S.K. Singh, (2014), "The Efficiency Appraisal for Removal of Malachite Green by Potato Peel and Neem Bark: Isotherm and Kinetic Studies", *International Journal of Chemical and Environmental Engineering*, 5(2): 83-88

[28] Singh,S.K. and Kute, Sunil, (1993), " Removal of colour from dye waste water by activated carbon", *Jour. of IPHE*,vol.1993, No.3.

[29] D.P.Tiwari, S.K.Singh, Neetu Sharma (2014), "Sorption of Methylene Blue on Treated Agricultural Adsorbents: Equilibrium and Kinetic Studies", Journal of Applied water Science, 4 (1)

[30] Abhas Jain, S.K. Singh (2014), "Defluoridation of Water Using Alum Impregnated Brick Powder And Its Comparison with Brick Powder", International Journal of Engineering Science and Innovative Technology , 3(2)

[31] Neetu Sharma, D.P.Tiwari, S.K.Singh, (2014), " efficiency of chemically treated potato peel and neem bark for Sorption of direct Red Dye-81 from aquous solution", Rasayan , 7 (4): 399-407

[32]Alla M. Aenab and S.K. Singh (2012), "Evaluation of Drinking Water Pollution and Health Effects in Baghdad", Iraq Journal of Environment Protection, 2012 (3), 533-537.

[33] Neetu Sharma, DP Tiwari and S.K. Singh (2012), "Decolorisation of synthetic dyes by Agricultural Waste a Review"., international Journal at Scientific & Engineering Research, 3 (2), 1-10.

[34] SK Singh, Lokesh Kumar (2014), " Removal of chloride by bio adsorption". International Journal of advanced research 2(4) :140-145

[35] SK Singh, Lokesh Kumar (2014), "Characterization of rural drinking water sources in Bhiwani District, Haryana: A Case Study". International Journal of Interdisciplinary Research and Innovations 2(4) : 27-37

[36] Dhruv Mehta, Siddharth Mazumdar, **S.K. Singh** (2015). Magnetic adsorbents for the treatment of water/wastewater - A review . Water Process Enginnering- Elsevier 7 (9):244-265

ResearchGate

See discussions, stats, and author profiles for this publication at: http://www.researchgate.net/publication/279726153

Flow Visualization around Perforated Circular Finned Tubes by CFD

ARTICLE · JANUARY 2014

DOWNLOADS
2

VIEWS
8

3 AUTHORS, INCLUDING:

M. Zunaid
Delhi Technological University
6 PUBLICATIONS **4** CITATIONS

SEE PROFILE

Available from: M. Zunaid
Retrieved on: 04 August 2015

ISSN: 2319-8753

International Journal of Innovative Research in Science, Engineering and Technology

(An ISO 3297: 2007 Certified Organization)

Vol. 3, Issue 6, June 2014

Flow Visualization around Perforated Circular Finned Tubes by CFD.

Yogesh Pal[1], Naushad Ahmad Ansari[2], M. Zunaid[3]

U.G Student, Department of Mechanical Engineering, Delhi Technological University, Delhi, India[1]

Assistant Professor, Department of Mechanical Engineering, Delhi Technological University, Delhi, India[2]

Assistant Professor, Department of Mechanical Engineering, Delhi Technological University, Delhi, India[3]

ABSTRACT: Rate of heat transfer increases by several folds with the increase in the surface area of heat exchangers, in practice this is often achieved by having fins at the surface of heat exchangers. The objective of the present study was to visualize the air flow around perforated circular finned tube (PCFT) through computational fluid dynamics (CFD). The air-side flow was visualized through simulation in fluent. Visualization of flow of air around the tube and fin for various cases were studied. These cases include the different positions of perforations on fins with respect to stagnation point. The different positions selected for perforations with respect to stagnation point are no holes and holes at an angle of 90 degree, 100 degree, 110 degree, 115 degree, 120 degree, 140 degree, 145 degree, 150 degree, 160 degree, and 170 degree. Gambit was used for construction of geometry and k-epsilon model was used for flow visualization. The perforation at an angle of 120 degree with respect to stagnation point was found to be the best location because recirculation of flow at this location found to be least. However perforations at the angles greater than 90 degree but less than 170 degree were effective in reducing the recirculation.

KEYWORDS: CFD; Flow visualization,Perforated circular fins, Recirculation, Stagnation point.

I. INTRODUCTION

Finned surfaces are commonly used in practice to enhance heat transfer, and they often increase the rate of heat transfer from a surface several fold. There are a variety of innovative fin designs available in the market, and they seem to be limited only by imagination. The closely packed thin metal sheets attached to hot water tubes increase the surface area of convection and thus rate of convection heat transfer from the tubes to the air many times [1]. Heat transfer characteristics at the air side have been studied with various fin geometries with both experimental and analytical methods to improve the performance of the finned-tube heat exchanger [2]. In many applications circular finned tubes are being used due to their low manufacturing cost and in addition to it circular finned tube heat exchangers are also known with their high efficiency [2,3].Many researchers have investigated various techniques to enhance the convective heat transfer performance of circular finned-tubes heat exchangers. Perforated circular finned tube (PCFT) can reduce the air-side recirculation region behind the finned tube and thus enhance the convective heat transfer performance. The separation and detachment of air flow were delayed by introducing the perforations at the flow-separation locations on the finned tube, and the recirculation region was thus decreased thereafter [4]. Number of perforations on a circular finned tube affected both the convective heat transfer coefficient and pressure drop at the air side. The increase in the convective heat transfer coefficient at the air side by the introduction of the perforations was considered to be mostly related to the reduction of a recirculation region [5,6]. CFD is a science that can be helpful for studying fluid flow, heat transfer, chemical reactions etc. by solving mathematical equations with the help of numerical analysis [7]. CFD employs a very simple principle of resolving the entire system in small cells or grids and applying governing equations on these discrete elements to find numerical solutions regarding pressure distribution, temperature gradients and other flow parameters in a shorter time at a lower cost because of reduced required experimental work [8,9]. The air-side flow was visualized through simulation in fluent 6.3.26. In order to compute complex airflows through a fin-and-tube heat exchanger, CFD assumes greater importance [10].Chan HyeokJeong et al. developed a new shape of plate fin heat exchanger by applying ceases and holes on the plate fin has observed thatthe more the crease

ISSN: 2319-8753

International Journal of Innovative Research in Science, Engineering and Technology

(An ISO 3297: 2007 Certified Organization)

Vol. 3, Issue 6, June 2014

angle (q) increases, the more the crease cycle (l) decreases, and the more the number of holes (N) increases, the more the pressure loss and heat transfer performance increase together [11].
The objective of the present study was to visualize the air flow around perforated circular finned tube (PCFT) through computational fluid dynamics (CFD) only for 2-holes case because Lee et al. [4] investigated that in the case of the 4-hole PCFT there is a greater pressure drop which might be due to excessive flow disturbances produced by multiple perforations.

II. FLOW VISUALIZATION PROCEDURE

Visualization of air flow around the tube and fin for various positions of perforations on fins with respect to stagnation point are studied. The positions selected for perforations are no holes and holes at an angle of 90 degree, 100 degree, 110 degree, 115 degree, 120 degree, 140 degree, 145 degree, 150 degree, 160 degree, and 170 degree with respect to stagnation point. Visualization of flow was carried out in following steps.

1. Physical model- the construction of geometry was done on gambit 2.4.6. The geometry consisted of a tube of length (along z-axis) 8 centimetres and radius 5 centimetres on which six circular fins were attached of radius 10 centimetres and thickness 0.2 centimetres. Spacing between the fins were taken at 0.5 centimetres. The whole apparatus was then enclosed in a brick of dimensions 22×22×10 centimetres. Due to uniform air flow parallel to fins, flow visualization was done for only for symmetry face as shown in figure below:

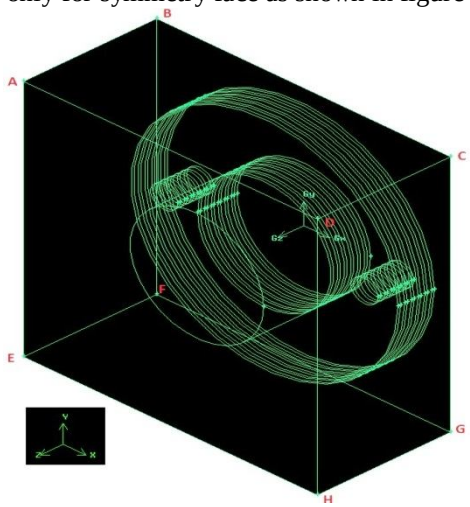

Fig. 1 Tube and fin geometry enclosed in a brick (flow volume)

2. Boundary conditions-to simulate the air flow boundary conditions have been given to the required faces. In figure 1, face EFGH represents the velocity inlet, face ABCD represents pressure outlet, face BCGF represents symmetry and rest faces i.e. CDHG, ADHE, AEFB, and faces of tube and fins are set as wall. After generating the required volume, meshing was generated as shown in figure 2.

ISSN: 2319-8753

International Journal of Innovative Research in Science, Engineering and Technology

(An ISO 3297: 2007 Certified Organization)

Vol. 3, Issue 6, June 2014

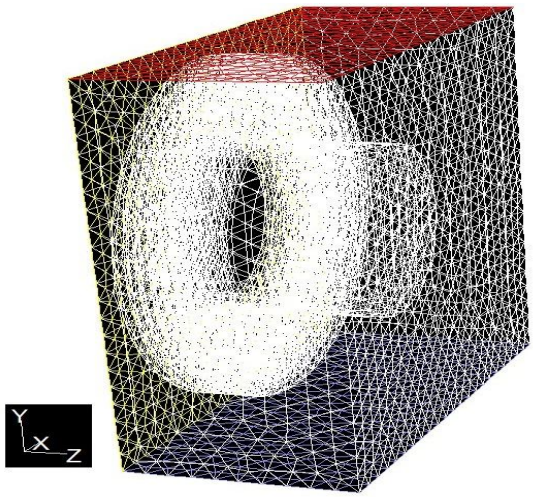

Fig. 2Meshed volume

3. Simulation- after exporting a mesh file from gambit by selecting solver as fluent 5/6. The mesh file was read on fluent 6.3.26. Scale factor was applied to have length of grids in centimetres. After that k-epsilon model was selected. Thetransport Equations for the Standard k-epsilon Model are as follows:

$$\frac{\partial}{\partial t}(\rho k) + \frac{\partial}{\partial x_i}(\rho k u_i) = \frac{\partial}{\partial x_j}\left[\left(\mu + \frac{\mu_t}{\sigma_k}\right)\frac{\partial k}{\partial x_j}\right] + G_k + G_b - \rho\epsilon - Y_M + S_k \quad (1)$$

and

$$\frac{\partial}{\partial t}(\rho \epsilon) + \frac{\partial}{\partial x_i}(\rho \epsilon u_i) = \frac{\partial}{\partial x_j}\left[\left(\mu + \frac{\mu_t}{\sigma_\epsilon}\right)\frac{\partial \epsilon}{\partial x_j}\right] + C_{1\epsilon}\frac{\epsilon}{k}(G_k + C_{3\epsilon}G_b) - C_{2\epsilon}\rho\frac{\epsilon^2}{k} + S_\epsilon \quad (2)$$

The turbulence kinetic energy, k, and its rate of dissipation, ε, are obtained from these equations. In these equations, G_k represents the generation of turbulence kinetic energy due to the mean velocity gradients, G_b is the generation of turbulence kinetic energy due to buoyancy, Y_M represents the contribution of the fuctuating dilatation in compressible turbulence to the overall dissipation rate, $C_{1\varepsilon}$, $C_{2\varepsilon}$, and $C_{3\varepsilon}$ are constants.$\mathbf{S_k}$ and $\mathbf{S_e}$are the turbulent Prandtl numbers for k and ε, respectively. $S_k$and S_ε are user-defined source terms.

Fluid selected as air whose density= 1.225 kg/m3 and viscosity= 1.7894e-05 kg/m-s. Operating conditions were set as pressure= 101325 Pascal and temperature = 300 K. Velocity of air at inlet= 10 m/s which is normal to face (along positive y-direction), turbulent kinetic energy as 1 m2/s2, and turbulent dissipation rate as 1 m2/s3. Zero gauge pressure was set at the face ABCD. Flow was initialized with the velocity inlet face then iterations were performed until convergence was formed.

ISSN: 2319-8753

International Journal of Innovative Research in Science, Engineering and Technology

(An ISO 3297: 2007 Certified Organization)

Vol. 3, Issue 6, June 2014

III. EXPERIMENTAL RESULTS

After displaying velocity path lines, flow of air around the tubes and fins could be visualized. Some important figures are shown below:

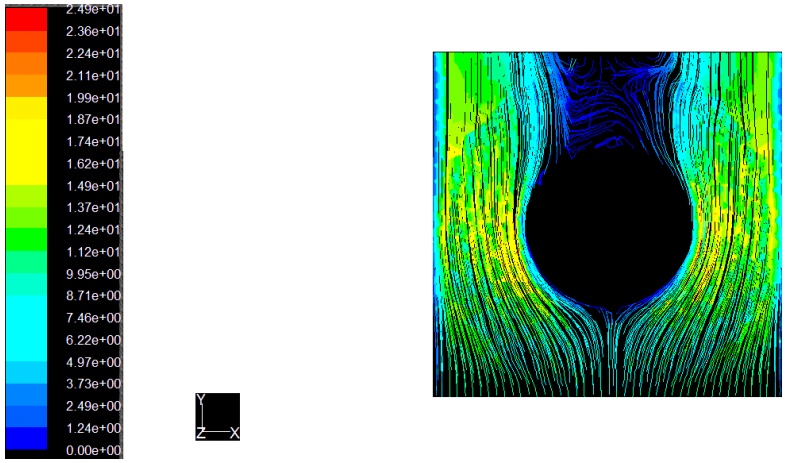

Fig. 3 Airflow around tube with circular fins having no holes

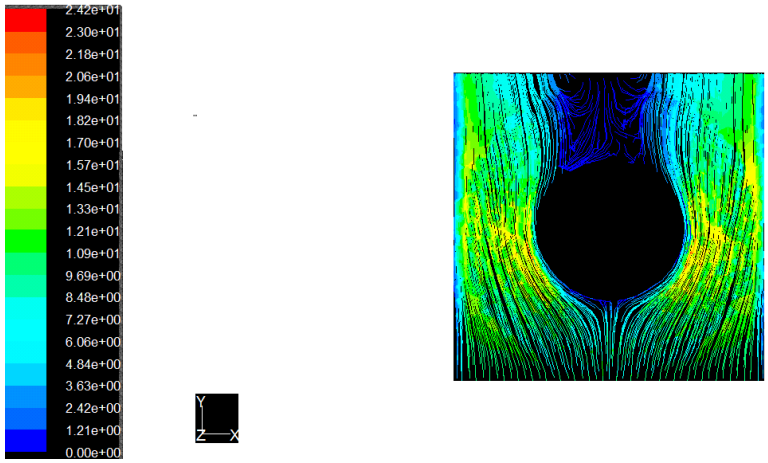

Fig. 4 Airflow around tube with circular fins having holes at an angle of 90 degree

ISSN: 2319-8753

International Journal of Innovative Research in Science, Engineering and Technology

(An ISO 3297: 2007 Certified Organization)

Vol. 3, Issue 6, June 2014

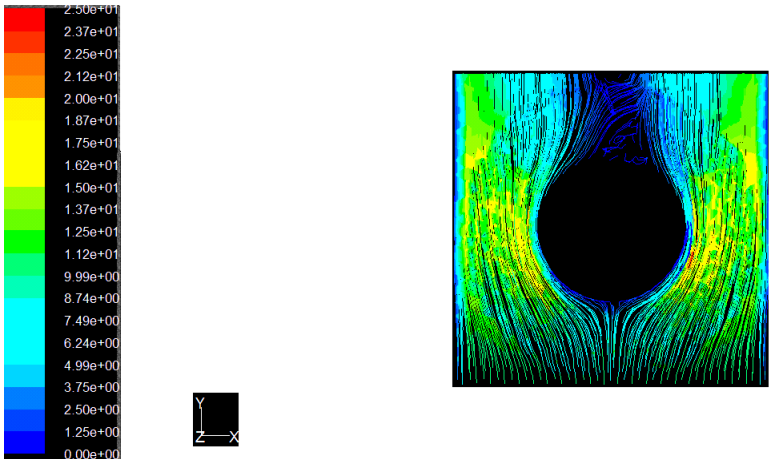

Fig. 5 Airflow around tube with circular fins having holes at 120 degree

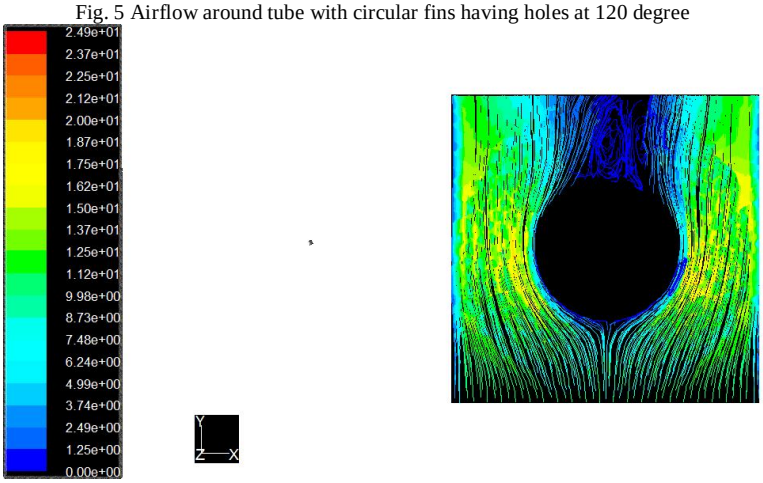

Fig. 6 Airflow around tube with circular fins having holes at 150 degree

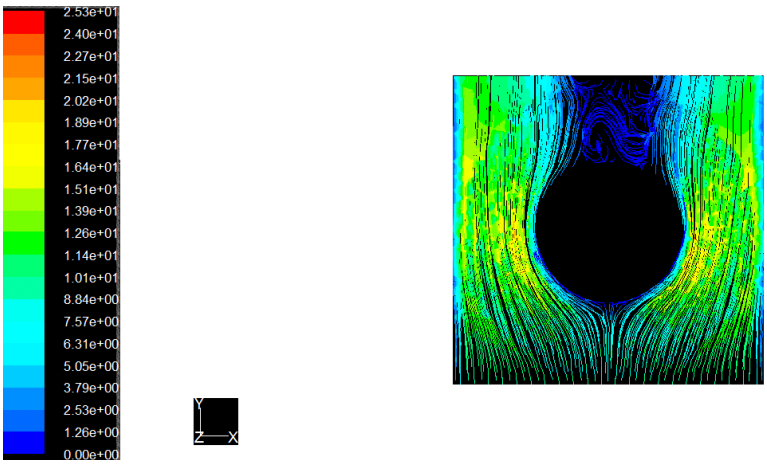

Fig. 7 Airflow around tube with circular fins having holes at 170 degree

ISSN: 2319-8753

International Journal of Innovative Research in Science, Engineering and Technology

(An ISO 3297: 2007 Certified Organization)

Vol. 3, Issue 6, June 2014

From figure 3 which was the case of plane fins, it can be seen that there is separation and detachment of air flow from the tube at an angle of approximately 120 degree with respect to stagnation point. In the case of two holes at an angle of 90 degree i.e. figure 4, it can be seen there is more recirculation of air flow around fins as compared to the case of fins without holes. As the angle increases beyond 90 degree, recirculation is decreasing that can be observed in figure 5 i.e. the case of holes at 120 degree in which recirculation is disappeared to a greater extent. As the angle further increases which is closed to 170 degree, recirculation is found to be more than the case of plane fins, this can be observed in figure 7.According to Lee et al. [4] the separation and detachment of air flow were delayed by introducing the perforations at the flow-separation locations on the finned tube, and the recirculation region was thus decreased thereafter. As we see in figure 3 that flow separation is taking place at an angle of approximately 120 degree with respect to stagnation point in the case of plane fins. Therefore, perforations at 120 degree on fins are most effective in reducing the separation and detachment of air flow. Hence, the above result could be validated.

IV. CONCLUSION

From above discussion it can be concluded that the perforations at an angle of 120 degree with respect to stagnation point is the best location because recirculation of air flow is vanishing up to a greater extent in this case. Hence there could be more convective heat transfer obtained between fluid flowing inside the tube and air flowing over the tube. This result might be helpful in reducing size of heat exchangers because with perforations on the fins, a higher value of convective heat transfer coefficient could be obtained as compared to the plane fins. Also, further investigations are recommended to study the effect of size of hole on recirculation region.

REFERENCES

[1] Yunus A.Cengel,"Text book of heat transfer a practical approach", Tata McGraw-Hill second edition, 2002.
[2] M. Lee, T. Kang, Y. Kim,"Air-side heat transfer characteristics of spiral-type circular fin-tube heat exchangers", International Journal of Refrigeration vol. 33, no. 2, pp. 313–320, 2010.
[3] M. Lee, T. Kang, Y. Joo, Y. Kim,"Heat transfer characteristics of spirally-coiled circular fin-tube heat exchangers operating under frosting conditions. International Journal of Refrigeration",vol. 34, no. 1, pp. 328–336, 2011.
[4] Dong H. Lee, Jin M. Jung, Jong H. Ha, Young I. Cho,"Improvement of heat transfer with perforated circular holes in finned tubes of air-cooled heat exchanger", International Communications in Heat and Mass Transfer,vol. 39, pp. 161–166, 2012.
[5] A. Nuntaphan, T. Kiatsiriroat, C. Wang,"Air side performance at low Reynolds number of cross-flow heat exchanger using crimped spiral fins", International Communications in Heat and Mass Transfer, vol. 32, no. 1–2, pp. 151–165, 2005.
[6] C.C.Wang, J. Lo, Y.T. Lin, C.S.Wei,"Flow visualization of annular and delta win let vortex generators in fin-and-tube heat exchanger application", International Journal of Heat and Mass Transfer, vol. 45, no. 18, pp. 3803–3815, 2002.
[7] Muhammad Mahmood AslamBhutta, Nasir Hayat, Muhammad Hassan Bashir, AhmerRais Khan, KanwarNaveed Ahmad, Sarfaraz Khan,"CFD applications in various heat exchangers design: A review", Applied Thermal Engineering,vol. 32, pp. 1-12, 2012.
[8] A.G. Kanaris, A.A. Mouza, S.V. Paras,"Flow and heat transfer prediction in a corrugated plate heat exchanger using a CFD code", Chem. Eng. Technol, vol. 8, pp. 923-930, 2006.
[9] Y. Wang, Q. Dong, M. Liu,"Characteristics of fluid flow and heat transfer in shell side of heat exchangers with longitudinal flow of shell side fluid with different supporting structures", International Conference on Power Engineering, Hangzhou, China, pp.23-27,2007.
[10] Varun Singh, Omar Abdelaziz, Vikrant Aute, ReinhardRadermacher,"Simulation of air-to refrigerant fin-and-tube heat exchanger with CFD-based air propagation", International journal of refrigeration, vol. 34, pp. 1883-1897, 2011.
[11] Chan HyeokJeong, HyungRak Kim, Man Yeong Ha, Sung Wan Son, Jae Seok Lee, Pan Yeong Kim,"Numerical investigation of thermal enhancement of plate fin type heat exchanger with creases and holes in construction machinery",Applied Thermal Engineering,vol. 62, pp. 529-544, 2014.

BIOGRAPHY

Yogesh pal

He is a final year student at Delhi Technological University pursuing B.tech in mechanical engineering. This paper is his first publication in the field of research and technology. Currently, he is working on 'heat transfer modeling of heat exchangers by cfd'.

Naushad Ahmad Ansari

Pursuing PhD from Delhi Technological University, Delhi (India), M. Tech (Thermal Sciences) from Aligarh Muslim University, Aligarh (India) in 2000, Bachelor of Engineering (Mechanical) from Aligarh Muslim University (India)

ISSN: 2319-8753

International Journal of Innovative Research in Science, Engineering and Technology

(An ISO 3297: 2007 Certified Organization)

Vol. 3, Issue 6, June 2014

in1995. Major field of study is Refrigeration and Air-Conditioning, Fluid Mechanics & CFD, Heat and mass transfer and I.C. Engine. published research papers are "Theoretical Exergy Analysis of HFO-1234yf and HFO-1234ze as an Alternative Replacement of HFC-134a in Simple Vapour Compression Refrigeration System''. International journal of Scientific and Engineering Research, vol.4, Issue8, 137-144, 2013,"Exhaust Gas Analysis and Parametric Study of Ethanol Blended Gasoline Fuel in Spark Ignition Engine''. American journal of Engineering Research, vol.2, Issue7, 49-61, 2013, and "Emission Characteristics of a Diesel Engine Using Soyabean Oil and Diesel Blends''. International journal of Research in Engineering and Technology, vol.2, Issue5, 793-798, 2013. Mr. Naushad is a life time member of Indian Society of Technical Education (ISTE) and Solar Energy Society of India (SESI).

M. Zunaid

Pursuing PhD in from Delhi Technological University, Delhi (India), M. Tech (Thermal Sciences) from Aligarh Muslim University, Aligarh (India) in 2005, Bachelor of Engineering (Mechanical) from Aligarh Muslim University, Aligarh (India) in 2003, Diploma in Engineering (Mechanical) from Aligarh Muslim University, Aligarh in 1999. Major field of study is CFD, Heat and mass transfer and RAC. He has published one research paper on "Numerical Simulation of Liquid Metals in Differentially Heated Enclosure Undergoing Orthogonal Rotation" in International Journal of Heat and Mass Transfer, Volume 49, Issues 19-20, September 2006, Pages 3500-3513, and other research paper on "Effect of External Body Force on Natural Convection in Square Enclosure" in Journal of Enhance Heat Transfer, Volume 13, Issues 4, (2006), pages 333-353. Mr. Zunaid is a life time member of Indian Society of Heat and Mass Transfer (ISHMT), Indian Society of Technical Education (ISTE) and Solar Energy Society of India (SESI).

Int J Theor Phys
DOI 10.1007/s10773-015-2767-z

Friedmann Cosmology with Matter Creation in Modified $f(R, T)$ Gravity

Vijay Singh[1] · **C. P. Singh**[1]

Received: 10 March 2015 / Accepted: 10 August 2015
© Springer Science+Business Media New York 2015

Abstract The theoretical and observational consequences of thermodynamics of open systems which allow matter creation, are investigated in modified $f(R, T)$ (R is the Ricci scalar and T is the trace of energy-momentum tensor) theory of gravity within the framework of a flat Friedmann-Robertson-Walker line element. The simplest model $f(R, T) = R + 2f(T)$ with "gamma-law" equation of state $p = (\gamma - 1)\rho$ is assumed to obtain the exact solution. A power-law expansion model is proposed by considering the natural phenomenological particle creation rate $\psi = 3\beta nH$, where β is a pure number of the order of unity, n the particle number density and H is the Hubble parameter. A Big Rip singularity is observed for $\gamma < 0$ describing phantom cosmology. The accelerated expansion of the Universe is driven by the particle creation. The density parameter shows the negative curvature of the Universe due to particle creation. The entropy increases with the evolution of the Universe. Some kinematics tests such as lookback time, luminosity distance, proper distance, angular diameter *versus* redshift are discussed in detail to observe the role of particle creation in early and late time evolution of the Universe.

Keywords Cosmology · Modified gravity theory · Matter creation

1 Introduction

Many theoretical and observational studies of the Universe, such as Type Ia supernovae [1, 2], Planck collaboration [3], cosmic microwave background (CMB) anisotropy [4], large

✉ C. P. Singh
cpsphd@rediffmail.com

Vijay Singh
gtrcosmo@gmail.com

[1] Department of Applied Mathematics, Delhi Technological University
(Formerly Delhi College of Engineering), Bawana Road, Delhi-110 042, India

Published online: 25 August 2015

scale structures (LSS) [5] etc., have shown that a pure Friedmann-Lamaitre-Robertson-Walker (FLRW) cosmology with matter and radiation does not explain all the large scale properties of our Universe. The late time cosmic acceleration is usually assumed to be driven by a cosmic fluid/field generically known as dark energy (DE) [6–8], which can be observed only by its gravitational effects [9–11]. Since the time of the discovery of accelerating Universe in 1998, a large number of probable candidates of DE have been proposed. The simplest DE model is the standard ΛCDM model [12] where Λ is known as cosmological constant assumed possibly to be the quantum vacuum energy. In the context of early Universe, the standard ΛCDM model presents several theoretical and observational difficulties, such as the singularity problem [13], flatness and horizon problem, reheating during the inflationary epoch [14], confliction between the age of the Universe and the age of the oldest stars in globular clusters (age problem) [15], the entropy problem [16] etc.

The flatness and horizon problems together with the entropy problem have been resolved (up to a certain extent) by the inflationary model proposed by Guth [17]. The age confliction [18] is not an isolated complication, it comes with another serious trouble that is structure formation through gravitational amplification of small primeval density perturbation. These issues opened the door of investigations of different alternative theories of gravity not only alleviate the issues related to early Universe [19–21] but the mystery of unpredicted late time cosmic acceleration as well. Among the ways to resolve the problems of early Universe, Dirac's large number hypothesis [22] inspired a class of new cosmology named particle creation [23]. The steady state model introduced by Bondi and Gold [24] on the foundation of perfect cosmological principle (PCP) also asserts the continuous generation of matter in the Universe. Hoyle [25] and Narlikar [26] independently proposed a creation field theory and studied the matter creation during the evolution of the Universe. Tryon [27] and Fomin [28] in their individual work proposed a theoretical concept of the creation of the Universe as a vacuum fluctuation. Brout et al. [29–31] proposed a strong foundation of simultaneous creation of matter and curvature from a quantum fluctuation of the Minkowskian space-time vacuum.

Fulling and collaborator [32] investigated the evolution of the Universe where the material content of the Universe may have had its origin in the continuous creation of radiation and matter from the gravitational field of the expanding cosmos acting on the quantum vacuum. Later on, Gunzig et al. [33] and Prigogine et al. [34] established the theoretical scenario of matter creation in the framework of cosmology. They showed that the second law of thermodynamics might be modified to accommodate the flow of energy from gravitational field to the matter field, resulting in the creation of particles and consequently entropy. The work might suggest that at the expense of the gravitational field, particle creation takes place as an irreversible process constrained by the usual requirements of the non-equilibrium thermodynamics, however, the reverse process (matter destruction) thermodynamically forbidden. Calv*á*o et al. [35] extended this new theoretical concept of matter creation under adiabatic conditions. The further results were generalized by Lima and Germano [36] through a contravariant formulation allowing specific entropy variation as usually expected for non-equilibrium process in fluids. Lima and Alcaniz [37], and Alcaniz and Lima [38] investigated observational consequences of FRW models driven by adiabatic matter creation through some kinematical tests.

After the discovery of accelerating Universe, the matter creation theory was reconsidered to explain it and obtained unexpected results. The studies of matter creation rapidly recognize to explain dark energy. The negative pressure due to particle creation, might play the role of exotic matter component. Zimdahl et al. [39], Qiang et al. [40], Lima et al.

[41] and Steigman et al. [42] have presented a model with matter creation where a transition from decelerated to accelerated phase exists which are consistent with SNe Ia data. Cárdenas [43] studied a model which offers a possible way to understand the current accelerated expansion. Singh and Beesham [44, 45], and Singh [46, 47] studied early Universe in FRW cosmology with particle creation through some kinematical tests. Lima et al. [48] proposed a creation cold dark matter cosmology with one free parameter that is equivalent to the ΛCDM evolution. Recently, many authors [49–51] have paid attention on the cosmologies driven by gravitational "adiabatic " particle production where matter and entropy are generated but the specific entropy remains constant. Even a complete cosmology where the space-time matter evolves between an early and a late time de Sitter phase driven by particle production has been proposed and its predictions has beeen compared with the available astronomical data.

On the other hand, a number of pioneer concepts of modifying the general relativity (GR) have been proposed to reconcile the problems plagued in cosmology [52]. The simplest modification is replacing the Ricci scalar curvature R with the general function of R called $f(R)$ theories of gravity, describe transition from decelerated to accelerated expansion of the Universe [53]. Bertolami et al. [54] have generalized $f(R)$ theories by introducing an explicit coupling between arbitrary function of the Ricci scalar R and the matter Lagrangian density. Harko [55] has extended this new concept to the arbitrary coupling between matter and geometry. Harko et al. [56] have considered another extension of GR, where the gravitational Lagrangian is given by an arbitrary function of the Ricci scalar R and of the trace T of the stress-energy tensor, so called $f(R, T)$ theory of gravity. The authors have argued that due to the coupling between matter and geometry the theory depends on a source term, representing the variation of the matter-stress-energy tensor with respect to the metric. Consequently, the cosmic acceleration in $f(R, T)$ gravity results not only from geometrical effect but also from the matter contribution. These interesting features of $f(R, T)$ gravity motivate many authors to study it for resolving several issues of current interest in cosmology and astrophysics [57–65]. This newly proposed concept of modified gravity motivates us to study the particle creation phenomena and its effects on early and late time evolution of the Universe in $f(R, T)$ gravity.

In this paper, we investigate the theoretical and observational implication of particle creation in modified $f(R, T)$ gravity theory in a flat Friedmann-Robertson-Walker model. Exact solutions of the field equations are obtained by assuming the suitable form of $f(R, T) = R + 2f(T)$, equation of state, and particle creation rate. We study some kinematical tests to explain the physical significance of particle creation during early and late time evolution of the Universe.

The paper is organized as follows. The thermodynamics of particle creation is presented in the Section 2. A brief review of modified $f(R, T)$ gravity theory and its field equations are given in Section 3. In Section 4, the model and field equations are presented with particle creation. The exact solutions of the field equations with suitable assumptions are obtained in Section 5. Section 6 and its subsections are devoted to study some kinematical tests of the model. Finally, the outcomes are summarized in concluding Section 7.

2 Theory of Particle Creation

If we regard the whole Universe as a closed thermodynamical system in which the number of the particles in a given volume is constant, then the laws of thermodynamics have the

form [14]

$$d(\rho_m V) = dQ - p_m dV, \tag{1}$$

and

$$TdS = d(\rho_m V) + p_m dV, \tag{2}$$

where ρ_m, V, p_m, T and S are the energy density, volume, thermodynamical pressure, temperature, and entropy, respectively. Here, dQ is the heat received by the system during time dt. It is observed from (1) and (2) that the entropy production is given by

$$TdS = dQ. \tag{3}$$

Equation (3) shows that the entropy remains stationary, *i.e.*, $dS = 0$ for a closed adiabatic system for which $dQ = 0$. However, if we treat the Universe as an open thermodynamic system allowing irreversible matter creation from the energy of the gravitational field, we can account for entropy production right from the beginning, and the second law of thermodynamics is also incorporated into the evolutionary equations in a more meaningful way. Thus, the creation of matter acts as a source of internal energy. In such situation the number of particles N in a given volume V is not to be a constant but is time -dependent. Therefore, (1) modifies as

$$d(\rho_m V) = dQ - p_m dV + (h/n)\, d(nV), \tag{4}$$

where $N = nV$, n is the particle number density, and $h = (\rho_m + p_m)$ is the enthalpy per unit volume of the system. In case of adiabatic system where $dQ = 0$, (4) for an open system reduces to

$$d(\rho_m V) + p_m dV = (h/n)\, d(nV). \tag{5}$$

We see that in such a system the thermal energy is received due to the change of the number of particles. In cosmology, this change may be considered as a transformation of energy from gravitational field to the matter.

In the context of an open system, (5) can be rewritten as

$$d(\rho_m V) = -(p_m + p_c)dV, \tag{6}$$

where

$$p_c = -(h/n)(dN/dV). \tag{7}$$

Equation (6) suggests that the creation of matter in an open thermodynamic system corresponds to a supplementary pressure p_c, which must be considered as a part of the cosmological pressure entering into the Einstein field equations (decaying of matter leads to a positive decay pressure) and is equivalent to adding the term p_c given by (7) to the thermodynamic pressure p_m. It is to be noted that p_c is negative or zero depending on the presence or absence of particle creation.

Since the increment in entropy for an adiabatic system is only caused by creation of matter, the entropy is an extensive property of the system. In present scenario, S is proportional to the number of particles included in the system. Therefore, the entropy change dS for open systems from (2) and (5) becomes

$$TdS = (h/n)\, d(nV) - \mu\, d(nV) = (TS/N)dN \Rightarrow \frac{dS}{S} = \frac{dN}{N}, \tag{8}$$

where μ is the chemical potential given by $\mu = (h - Ts)/n$, $s = S/V$. Since the second law of thermodynamics is a fundamental law in physics, the presence or absence of particle creation can not affect it. This law basically requires $dS \geq 0$, consequently, (8) gives

$$dN \geq 0. \tag{9}$$

The above inequality implies that the space-time can produce matter, whereas the reverse process is thermodynamically not admissible.

The basic idea of this entire formulation is to modify the usual energy momentum conservation law in an open thermodynamical system, which leads to the explicit use of a balance equation for the number density of the particles created, in addition to Einstein's field equations.

The particle flux vector is given by

$$N^{\alpha} = nu^{\alpha}, \tag{10}$$

and N^{α} is assumed to satisfy the balance equation [34, 66]

$$N^{\alpha}{}_{;\alpha} = \psi, \tag{11}$$

where the function ψ denotes a source term of particle creation which is positive or negative depending on whether there is production or annihilation of particles. In standard cosmology ψ is usually assumed to be zero.

In the presence of a gravitational particle source, the balance equation (11) for the particle flux becomes

$$\dot{n} + 3nH = \psi, \tag{12}$$

where n and $V = a^3$ are the particle number density and volume, respectively.

Thus, the pressure creation p_c depends on the particle creation rate, and for adiabatic matter creation, (7) takes the following form [36]

$$p_c = -\frac{(\rho_m + p_m)}{3nH}\,\psi. \tag{13}$$

Therefore, (13) shows that p_c is negative for $\psi > 0$, which can help to drive the era of accelerated cosmic expansion.

3 A Brief Review of Modified $f(R, T)$ Gravity Theory

The $f(R, T)$ theory is a modified theory of gravity, in which the Einstein-Hilbert Lagrangian is modified by replacing Ricci scalar curvature R by an arbitrary function of R and trace T of energy-momentum tensor, *i.e.*, $f(R, T)$. So the gravitational action for $f(R, T)$ modified theory of gravity [56] in the units $G = 1 = c$ takes the following form.

$$S = \frac{1}{8\pi}\int d^4x\sqrt{-g}\left[\frac{f(R,T)}{2} + \mathcal{L}_m\right], \tag{14}$$

where g is the determinant of the metric tensor $g_{\mu\nu}$ and $\mathcal{L}_m$ corresponds to matter Lagrangian. The energy-momentum tensor $T_{\mu\nu}$, defined by fluid Lagrangian density is given by

$$T_{\mu\nu} = -\frac{2}{\sqrt{-g}}\frac{\delta(\sqrt{-g}\,\mathcal{L}_m)}{\delta g^{\mu\nu}}, \tag{15}$$

and its trace, $T = g^{\mu\nu}T_{\mu\nu}$. By assuming that the matter Lagrangian density $\mathcal{L}_m$ depends only on the metric tensor components $g_{\mu\nu}$, not on its derivatives, we obtain

$$T_{\mu\nu} = g_{\mu\nu}\mathcal{L}_m - 2\frac{\partial\mathcal{L}_m}{\partial g^{\mu\nu}}. \tag{16}$$

The equations of motion by varying the action (14) with respect to metric tensor become

$$f_R(R,T)R_{\mu\nu} - \frac{1}{2}f(R,T)g_{\mu\nu} + (g_{\mu\nu}\Box - \nabla_\mu\nabla_\nu)f_R(R,T) = 8\pi T_{\mu\nu} - f_T(R,T)T_{\mu\nu} - f_T(R,T)\ominus_{\mu\nu}, \quad (17)$$

where f_R and f_T denote the derivatives of $f(R,T)$ with respect to R and T, respectively. Here, ∇_μ is covariant derivative and $\Box \equiv \nabla_\mu\nabla^\mu$ is the d'Alembert operator and $\ominus_{\mu\nu}$ is defined by

$$\ominus_{\mu\nu} \equiv g^{\alpha\beta}\frac{\delta T_{\alpha\beta}}{\delta g^{\mu\nu}}. \quad (18)$$

Using (16) into (18), we get

$$\ominus_{\mu\nu} = -2T_{\mu\nu} + g_{\mu\nu}\mathcal{L}_m - 2g^{\alpha\beta}\frac{\partial^2\mathcal{L}_m}{\partial g^{\mu\nu}\partial g^{\alpha\beta}}. \quad (19)$$

As the field equations of $f(R,T)$ gravity depend on $\ominus_{\mu\nu}$, *i.e.*, on the physical nature of the matter. A number of models corresponding to different form of $f(R,T)$, e.g., $f(R,T) = R + 2f(T)$, $f(R,T) = \mu f_1(R) + \nu f_2(T)$, where $f_1(R)$ and $f_2(T)$ are arbitrary functions of R and T, and μ and ν are real constants, respectively [56–58], and $f(R,T) = R\ f(T)$ [60], etc., may be assumed depending on the nature of the matter source to solve the field equations. In this paper we assume the following simplest form [56]:

$$f(R,T) = R + 2f(T), \quad (20)$$

where R is a function of cosmic time t and $f(T)$ is an arbitrary function of the trace of energy-momentum tensor of matter. Equation (20) shows that the action is given by the same Einstein-Hilbert of General Relativity plus a function of T. The term $2f(T)$ in the gravitational action modifies the gravitational interaction between matter and curvature.

Using (20), one can re-write the gravitational field equations defined in (17) as

$$R_{\mu\nu} - \frac{1}{2}Rg_{\mu\nu} = 8\pi T_{\mu\nu} - 2(T_{\mu\nu} + \ominus_{\mu\nu})f'(T) + f(T)g_{\mu\nu}. \quad (21)$$

Here, a prime stands for derivative of $f(T)$ with respect to T.

The main issue now arises on the matter contents of the Universe through the energy momentum tensor and consequently on the matter Lagrangian $\mathcal{L}_m$ and the trace of the energy momentum tensor. We assume the universe is filled with a perfect fluid which is incorporated in the next section.

4 Model and Field Equations

We consider a homogenous and isotropic universe with spatially flat geometry described by flat Friedmann-Robertson-Walker (FRW) metric

$$ds^2 = dt^2 - a^2(t)(dx^2 + dy^2 + dz^2), \quad (22)$$

where $a(t)$ is the scale factor, which is a function of cosmic time t only.

In the formalism of particle creation, the second law of thermodynamics leads naturally to a modification of the energy momentum tensor with an additional creation pressure depends on the rate of creation of particles. In the presence of particle creation, the energy momentum tensor of perfect fluid is given by

$$T_{\mu\nu} = (\rho_m + p_m + p_c)u_\mu u_\nu - (p_m + p_c)g_{\mu\nu}, \quad (23)$$

where u_μ is the four velocity of the fluid such that $u_\mu u^\nu = 1$, and in comoving coordinates $u^\mu = \delta^\mu_0$.

The trace of energy momentum tensor (23), gives

$$T = \rho_m - 3(p_m + p_c). \tag{24}$$

We treat the scalar invariant $\mathcal{L}_m$ as the effective pressure of the perfect fluid matter and pressure originated by creation of particles. Therefore, the matter Lagrangian may be assumed as $\mathcal{L}_m = -(p_m + p_c)$, therefore, (19) becomes

$$\ominus_{\mu\nu} = -2T_{\mu\nu} - (p_m + p_c)g_{\mu\nu}. \tag{25}$$

In view of (25), the field (21) can be rewritten as

$$R_{\mu\nu} - \frac{1}{2}g_{\mu\nu}R = 8\pi T_{\mu\nu} + 2\left[T_{\mu\nu} + g_{\mu\nu}(p_m + p_c)\right] f'(T) + g_{\mu\nu} f(T). \tag{26}$$

The field equations (26) for a fluid endowed with matter creation (23) in the background of metric (22), yield

$$3H^2 = 8\pi\rho_m + 2(\rho_m + p_m + p_c) f'(T) + f(T), \tag{27}$$

$$2\dot{H} + 3H^2 = -8\pi(p_m + p_c) + f(T), \tag{28}$$

where $H(t) = \dot{a}/a$ is the Hubble parameter. A dot denotes derivative with respect to cosmic time t.

5 Solution of Field Equations

We have two field equations (27)–(28) and five unknowns variables, namely, H, ρ_m, p_m, p_c and $f(T)$. Therefore, one needs three more relations in order to construct a definite cosmological scenario.

In first choice, we consider a particular function given by [56]

$$f(T) = \lambda T, \quad (\lambda \quad \text{is a constant}). \tag{29}$$

Using (29) and (24), the field (27) and (28) yield

$$3H^2 = (8\pi + 3\lambda)\rho_m - \lambda(p_m + p_c), \tag{30}$$

$$2\dot{H} + 3H^2 = -(8\pi + 3\lambda)(p_m + p_c) + \lambda\rho_m. \tag{31}$$

In order to obtain the exact solution of the field equations, we assume two more additional relations: the equation of state and the matter creation rate. In the cosmological domain, the former is usually given by the "gamma-law" form

$$p_m = (\gamma - 1)\rho_m, \tag{32}$$

where γ is a constant lies in the interval [0, 2] and known as the EoS parameter of the perfect fluid.

Using (32) into (30) and (31), and simplifying, we get a single evolution equation for H:

$$2\dot{H} + (8\pi + 2\lambda)(\gamma\rho_m + p_c) = 0. \tag{33}$$

We confine our attention to the simple phenomenological expression for the matter creation rate [16]

$$\psi(t) = 3\beta n H, \tag{34}$$

where the parameter β lies in the interval [0, 1] and is assumed to be a constant.

Using (32) and (34) into (13), we have

$$p_c = -\beta\gamma\rho_m, \tag{35}$$

Substituting (32) and (35) into (30), we obtain

$$\rho_m = \frac{3H^2}{8\pi + 4\lambda - \gamma\lambda(1-\beta)}. \tag{36}$$

Using (35) and (36) into (33), we get

$$\dot{H} + \frac{3}{2}\frac{\gamma(8\pi + 2\lambda)(1-\beta)}{[8\pi + 4\lambda - \gamma\lambda(1-\beta)]}\, H^2 = 0. \tag{37}$$

The solution of (37) for $\gamma \neq 0$ and for all values of λ and β is given by

$$H(t) = \left(C + \frac{3}{2}\frac{\gamma(8\pi + 2\lambda)(1-\beta)}{[8\pi + 4\lambda - (1-\beta)\gamma\lambda]}\, t\right)^{-1}, \tag{38}$$

where C is an integration constant. For $\gamma = 0$, the well known de-Sitter scale factor $a(t) = a_0\, e^{H_0 t}$ is obtained.

From (38) we find the following expression for the scale factor

$$a(t) = D\left(C + \frac{3}{2}A\gamma\, t\right)^{\frac{2}{3A\gamma}}, \tag{39}$$

where D is a new integration constant and $A = (8\pi + 2\lambda)(1-\beta)/8\pi + 4\lambda - \gamma\lambda(1-\beta)$.

The above scale factor may be rewritten as

$$a(t) = a_0\left(1 + \frac{3}{2}A\gamma H_0(t - t_0)\right)^{\frac{2}{3A\gamma}}, \tag{40}$$

where $H = H_0 > 0$ at $t = t_0$. The subscript '0' refers to the present values of parameters. Since $0 \leq \gamma \leq 2$, we must have $A > 0$ for expansion of the Universe. Also, $A > 0$ implies $\lambda > 0$ as $0 \leq \beta < 1$.

If $\gamma < 0$, we have a Big -Rip singularity at a finite value of cosmic time $t_{br} = t - t_0 = -2/3H_0A\gamma$. Thus, we have a phantom cosmology for $\gamma < 0$. If one choose $t_0 = 2H_0^{-1}/3A\gamma$, Eq. (40) takes the familiar form of power-law expansion of the Universe, *i.e.*,

$$a(t) = a_0\left(\frac{3}{2}A\gamma H_0\, t\right)^{\frac{2}{3A\gamma}}. \tag{41}$$

If $\lambda = 0 = \beta$, (39) and (41) reduce to the well-known expressions of power-law expansion of scale factor for a flat FRW model in GR.

By use of (40) one may express the energy density of matter, particle creation pressure and the particle number density as functions of the scale factor a. These parameters respectively have the following forms

$$\rho_m = \rho_0\left(\frac{a_0}{a}\right)^{3A\gamma}, \tag{42}$$

$$p_c = -\beta\gamma\rho_0\left(\frac{a_0}{a}\right)^{3A\gamma}, \tag{43}$$

$$n = n_0\left(\frac{a_0}{a}\right)^{3(1-\beta)}, \tag{44}$$

where $\rho_0 = 3H_0^2/[8\pi + 4\lambda - \gamma\lambda(1-\beta)]$ is the present value of energy density. Here, n_0 is the present value of particle number density for any values of β. The above results show that

the transition from one phase to other phase, in the course of expansion, happens exactly as in the standard cosmological model.

The number of particles N in a given volume V is given by

$$N = N_0 \left(\frac{a}{a_0}\right)^{3\beta}, \tag{45}$$

which shows that N increases with time. If $\beta = 0$, N would remain constant throughout the evolution of the Universe and we would recover the standard FRW model of the Universe in $f(R, T)$ theory. Again, from (8) $S = S_0(N/N_0)$, the entropy in terms of scale factor is given by

$$S = S_0 \left(\frac{a}{a_0}\right)^{3\beta}. \tag{46}$$

The deceleration parameter defined as $q = -a\ddot{a}/\dot{a}^2$, gives

$$q = -1 + \frac{3\gamma A}{2} = \left[\frac{3\gamma}{2}\frac{(8\pi + 2\lambda)(1-\beta)}{[8\pi + 4\lambda - (1-\beta)\gamma\lambda]} - 1\right]. \tag{47}$$

which shows that q is independent of cosmic time t. Therefore, there is no transition from one phase to other. The decelerated or accelerated phase is described according the sign of q. Here, q may be positive or negative for a given set of values of β and λ. We know that the model accelerates for $q < 0$, therefore, the value of A must be $0 < A < 2/3\gamma$ for an accelerated universe.

As expected, the above solutions reduce to the standard FRW model of GR for $\beta = 0$ and $\lambda = 0$ and for all values of γ. In what follows, we study the role of $f(R, T)$ gravity and particle creation in early and late time evolution of the Universe.

Case 1 $\gamma = \frac{2}{3}$

Figure 1 plots the scale factor as a function of time for $\gamma = 2/3$ and some selected values of λ and β. We observe that if $\beta = 0$, $q < 0$ for all $\lambda > 0$, therefore, we find that the Universe accelerates in $f(R, T)$ gravity without particle creation. Similarly, if $\lambda = 0$, *i.e.*, in the absence of $f(T)$, $q = -\beta < 0$ for any values of $\beta > 0$. Thus, the acceleration occurs due to particle creation. The rate of expansion increases more rapidly for non-zero values of β and λ. It is to be noted that if $\lambda = 0 = \beta$ then the the marginal inflationary phase of GR is recovered, *i.e.*, $a \sim t$ and $q = 0$.

Case 2 $\gamma = \frac{4}{3}$

In this case, if $\beta = 0$ and $\lambda > 0$, we have $q > 0$. This shows that the Universe decelerates in the absence of particle creation. If $\lambda = 0$ then $q \geq 0$ for $0 < \beta \leq 1/2$, and $q < 0$ for $1/2 < \beta < 1$. Therefore, the Universe decelerates or accelerates depending on the rate of particle creation. However, if $\lambda \neq 0$ and $\beta \neq 0$, the deceleration or acceleration of the Universe depend on the following constrains, respectively:

$$0 < \beta \leq \frac{1}{4},\ \lambda > 0 \ \ or \ \ \frac{1}{4} < \beta < \frac{1}{2},\ 0 < \lambda < \frac{6\pi - 12\pi\beta}{-1 + 4\beta}, \tag{48}$$

$$\frac{1}{4} < \beta \leq \frac{1}{2},\ \lambda > \frac{6\pi - 12\pi\beta}{-1 + 4\beta} \ \ or \ \ \frac{1}{2} < \beta < 1,\ \lambda > 0. \tag{49}$$

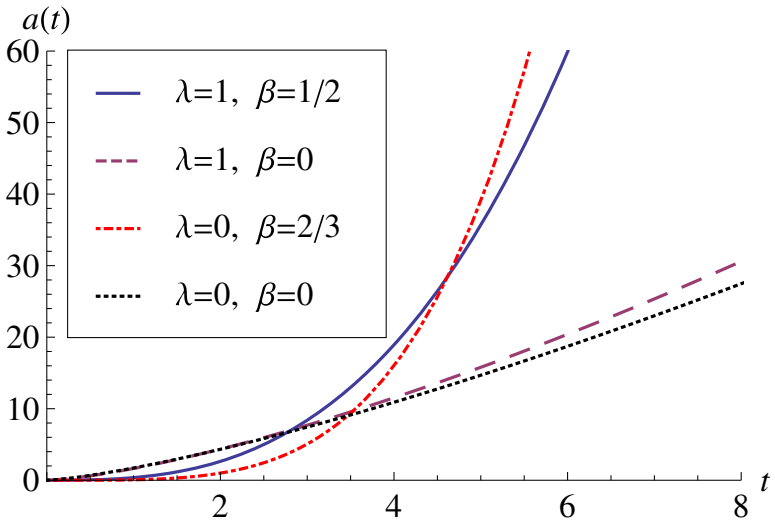

Fig. 1 Scale factor as a function of time for $\gamma = \frac{2}{3}$ and some selected values of λ and β

The behavior of scale factor *versus* time is shown in Fig. 2 for some selected values of λ and β. The figure shows that the Universe accelerates fast due to higher particle creation rate. For $\lambda = 0 = \beta$, $a \sim t^{1/2}$ and $q = 1$, which is the radiation phase in GR.

Case 3 $\gamma = 1$

In this case, the Universe expands with decelerated rate as $q > 0$ for $\beta = 0$ and $\lambda > 0$. Figure 3 plots graph between scale factor *versus* time for some selected values of λ and β. For $\lambda = 0$, we have $q > 0$ for $0 < \beta < 1/3$, and $q < 0$ for $1/3 < \beta < 1$. The critical case ($\beta = 1/3$, $q = 0$), describes a coasting cosmology. For $\lambda \neq 0$ and $\beta \neq 0$, the model decelerates or accelerates under the following constraints:

$$0 < \beta < \frac{1}{3}, \ 0 < \lambda < \frac{\pi - 3\pi\beta}{\beta}, \tag{50}$$

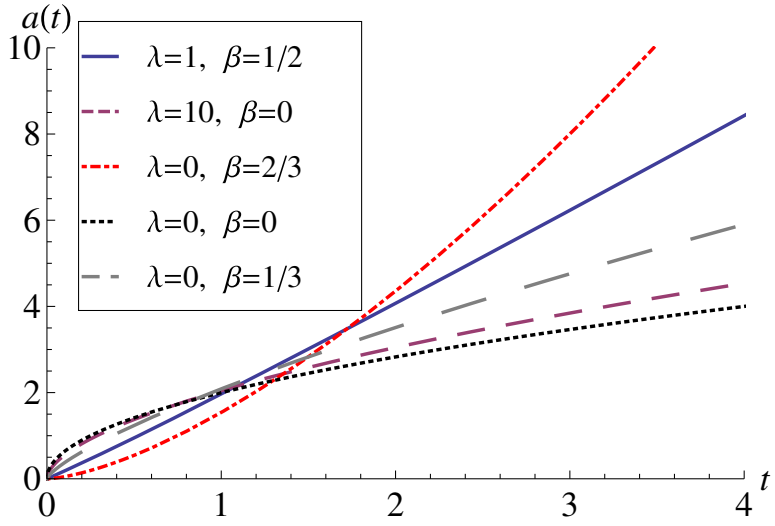

Fig. 2 Scale factor as a function of time for $\gamma = \frac{4}{3}$ and some selected values of λ and β

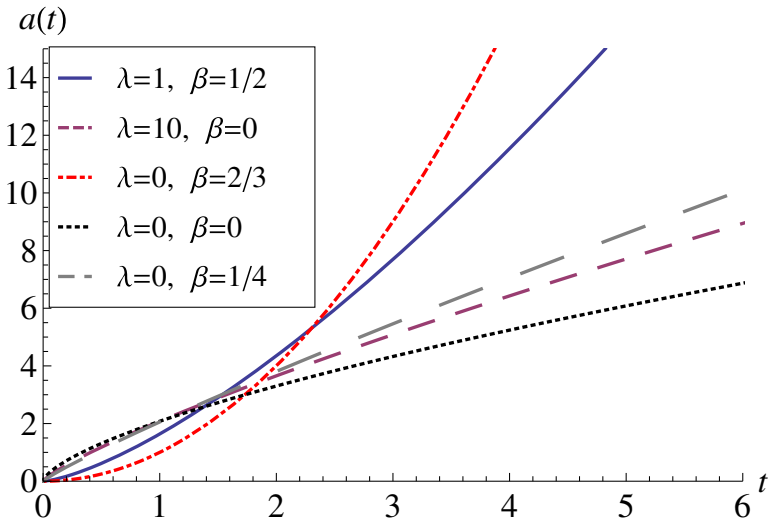

Fig. 3 Scale factor as a function of time for $\gamma = 1$ and some selected values of λ and β

$$0 < \beta \leq \frac{1}{3},\ \lambda > \frac{\pi - 3\pi\beta}{\beta} \quad or \quad \frac{1}{3} < \beta < 1,\ \lambda > 0, \tag{51}$$

respectively. As expected, for $\lambda = 0 = \beta$, we have $a \sim t^{2/3}$ and $q = 1/2$, *i.e.*, the model reduces to standard matter-dominated era of GR.

Case 4 $\gamma = \frac{1}{2}$

In this case, if $\lambda = 0 = \beta$, $a \sim t^{4/3}$ and $q = -1/4$, which corresponds to the present accelerated phase of the Universe of the standard FRW universe in GR. Since the Universe accelerates even in absence of both $f(T)$ and particle creation, therefore, the contribution of $f(R, T)$ gravity or particle creation just enhance the rate of acceleration of the Universe. Figure 4 plots the dynamics of scale factor *versus* t, which is similar to case I.

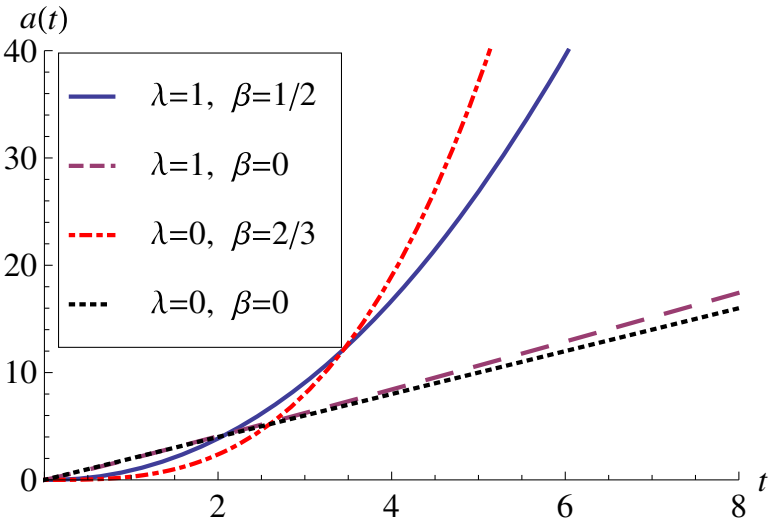

Fig. 4 Scale factor as a function of time for $\gamma = \frac{1}{2}$ and some selected values of λ and β

6 Kinematic Tests

Now, we derive some kinematical relations of the model as proposed in the preceding sections.

6.1 The Density Parameter

The density parameter, defined as $\Omega_m = \rho_m/\rho_c$, where $\rho_c = 3H^2/8\pi$, is given by

$$\Omega_m = \frac{8\pi}{8\pi + 4\lambda - (1-\beta)\gamma\lambda}. \tag{52}$$

Therefore, it is clear that $\Omega_m < 1$ for all values of $0 \leq \gamma \leq 2$, $0 < \beta < 1$ and $\lambda > 0$. Hence the Universe is negatively curved. In absence of both λ and β, we have $\Omega_m = 1$ for all γ, *i.e.*, the flat model of GR is recovered.

6.2 Lookback Time-Redshift

The lookback time $\Delta t = t_0 - t(z)$, is the difference between the age of the Universe at the present time $z = 0$ and the age of the Universe when a particular right ray at redshift z was emitted.

For a given redshift z, the scale factor $a(t_z)$ is related to a_0 by

$$a(t_z) = a_0(1+z)^{-1}. \tag{53}$$

From (41) and (53), the cosmic time in terms of redshift is given by

$$t(z) = \frac{2H_0^{-1}}{3\gamma A}(1+z)^{-\frac{3\gamma A}{2}}, \tag{54}$$

where H_0 is expressed in the usual practical observational units of $km\ s^{-1}\ Mpc^{-1}$ and its value is believing to be somewhere between 50-80 $km\ s^{-1}\ Mpc^{-1}$. However, H_0 is dimensionally similar to the reciprocal of time. The reciprocal of Hubble constant is called the Hubble time t_H : $t_H = H_0^{-1}$, where t_H is expressed in s and H_0 in s^{-1}. If H_0 is expressed in $km\ s^{-1}\ Mpc^{-1}$ and t_H in $gigayears$ ($1\ gr = 1\ milion\ years = 10^9\ years$) then $t_H = 977.8/H_0$.

Therefore, from (54) we have

$$t_0 - t(z) = \frac{2H_0^{-1}}{3\gamma A}\left[1 - (1+z)^{-\frac{3\gamma A}{2}}\right]. \tag{55}$$

Figure 5 plots lookback time *versus* redshift for $\gamma = 1$ and some selected values of λ and β. All models coincide for lower redshift since they follow the same behavior. The graph shows that the lookback time increases for higher values of β. Thus, the Universes with larger matter creation rate are older.

For small values of redshift, (55) becomes

$$H_0\,(t_0 - t(z)) = z - \left(1 + \frac{3\gamma A}{2}\right)z^2 + \cdots. \tag{56}$$

Taking lim $z \to \infty$ in (55), the present age of the universe is

$$t_0 = \frac{2H_0^{-1}}{3\gamma A} = \frac{H_0^{-1}}{1+q}. \tag{57}$$

Thus, the age of the Universe depends on both parameters β and λ.

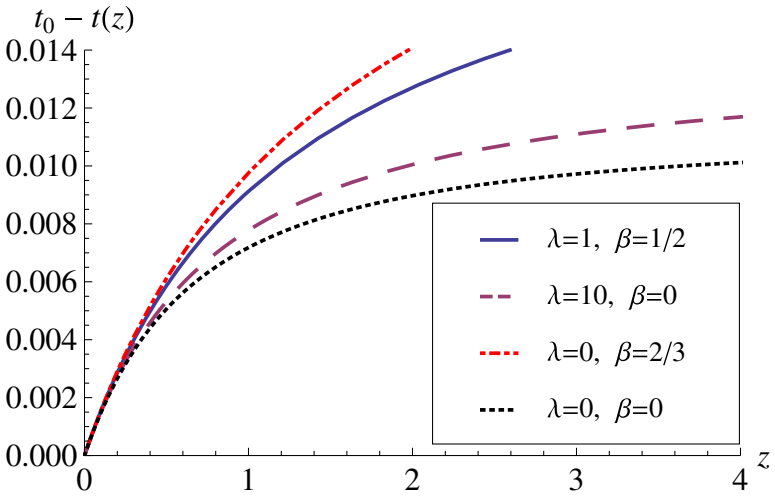

Fig. 5 Lookback time versus redshift for $\gamma = 1$, $H_0 = 60$ and some selected values of λ and β

6.3 Proper Distance-Redshift

The proper distance between the source and observer is defined as $d(z) = a_0 r(z)$, where $r(z)$ is the radial distance of the object at light emission in term of redshift given by

$$r(z) = \int_t^{t_0} \frac{dt}{a(t)} = \frac{H_0^{-1}}{a_0\left(\frac{3\gamma A}{2} - 1\right)}\left[1 - (1+z)^{-\left(\frac{3\gamma A}{2}-1\right)}\right]. \tag{58}$$

Consequently, the proper distance becomes

$$d(z) = \frac{H_0^{-1}}{\left(\frac{3\gamma A}{2} - 1\right)}\left[1 - (1+z)^{-\left(\frac{3\gamma A}{2}-1\right)}\right]. \tag{59}$$

The proper distance as a function of redshift for some selected values of β and λ are displayed in Fig. 6. We observe that the $f(T)$ contribution in $f(R, T)$ and particle creation gives rise to proper distance.

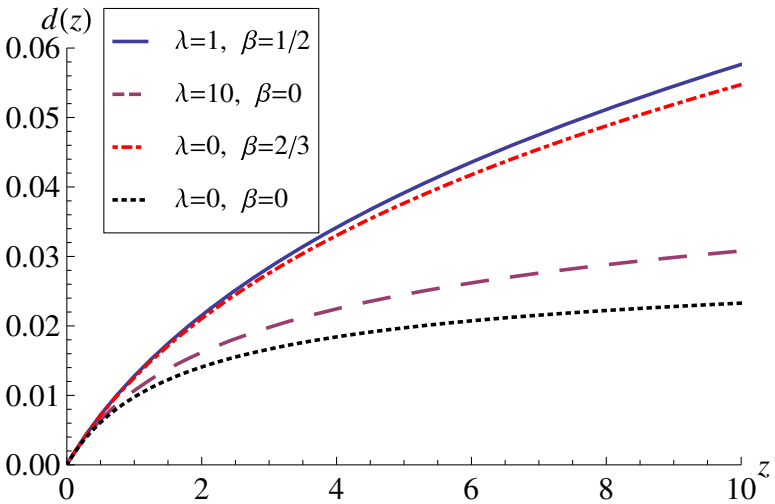

Fig. 6 Proper distance versus redshift for $\gamma = 1$, $H_0 = 60$ and some selected values of λ and β

Equation (59) can be rewritten as

$$H_0 d(z) = z - \frac{3\gamma A}{4} z^2 + \cdots . \tag{60}$$

From (59), it is observed that the distance dz is maximum at $z \to \infty$. Hence,

$$H_0 d(z \to \infty) = \frac{1}{\frac{3\gamma A}{2} - 1} = \frac{1}{q}. \tag{61}$$

6.4 Luminosity Distance-Redshift

The best-known way to trace the evolution of the Universe observationally is to look into the redshift-luminosity distance relation. The luminosity distance d_l is defined by the relation $d_l^2 = \frac{l}{4\pi L}$, where l is the luminosity of the object and L is the measured flux from the object. In standard FRW cosmology it is defined in terms of redshift as

$$d_l = a_0(1+z)r(z) = (1+z)d(z). \tag{62}$$

From (59) and (62), we get

$$d_l H_0 = \frac{1}{\left(\frac{3\gamma A}{2} - 1\right)} \left[(1+z) - (1+z)^{-\left(\frac{3\gamma A}{2} - 2\right)} \right]. \tag{63}$$

The graph between Luminosity distance and redshift for some selected values of β and λ is plotted in Fig. 7. One may observe that the luminosity distance corresponding to any specific value of redshift rises due to $f(R, T)$ gravity and particle creation.

Expanding (63) for small z, we find

$$H_0 d_l = z - \frac{1}{2}\left(\frac{3\gamma A}{2} - 2\right) z^2 + \cdots . \tag{64}$$

As expected, we find the same behavior for different models at $z \ll 1$ and the possible difference in behaviors for different models come at large redshift ($z \gg 1$). In Fig. 7 we observe that all curves start off with the linear Hubble law ($z = d_l H_0$) for small z, but then, only the curve for $q = 1$, *i.e.*, $\beta = 0 = \lambda$ stays linear all the way. We also note that for the small redshift the luminosity distance is larger for lower values of q.

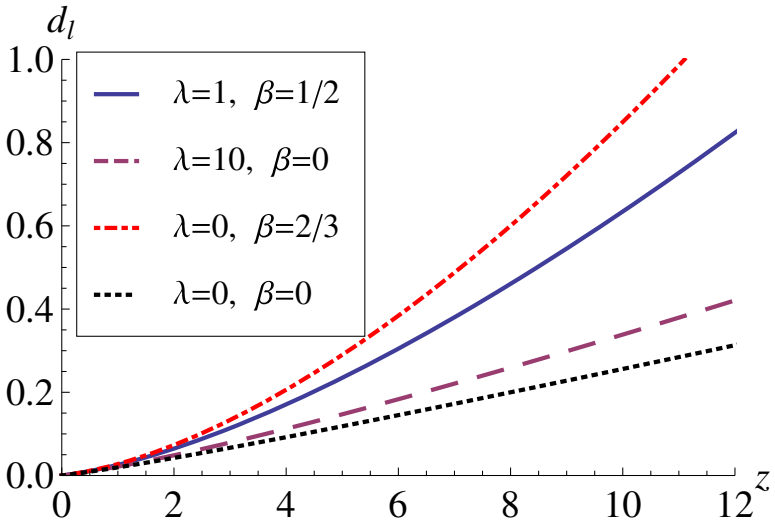

Fig. 7 Luminosity distance versus redshift for $\gamma = 1$, $H_0 = 60$ and some selected values of λ and β

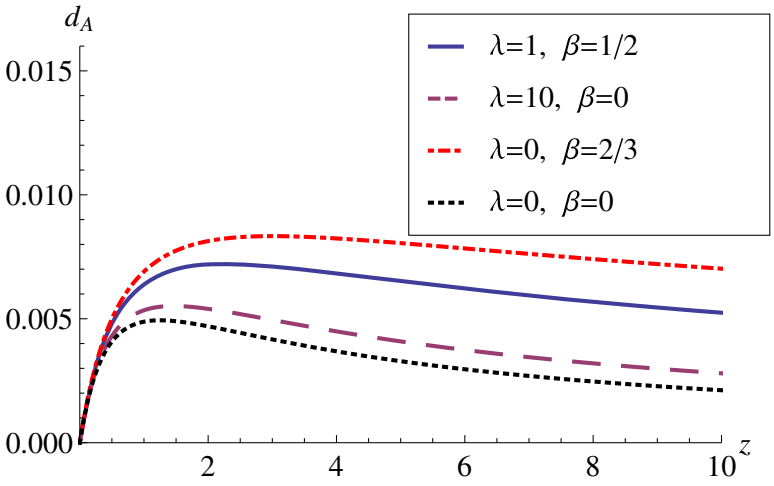

Fig. 8 Angular diameter distance versus redshift for $\gamma = 1$, $H_0 = 60$ and some selected values of λ and β

6.5 Angular Diameter Distance-Redshift

The angular diameter distance d_A is the ratio of physical transverse size of an object to its angular size (in radians). In terms of z, it is given by

$$d_A = \frac{d(z)}{1+z} = \frac{d_l}{(1+z)^2}. \tag{65}$$

Using (59), we have

$$H_0 d_A = \frac{1}{\left(\frac{3\gamma A}{2} - 1\right)} \left[(1+z)^{-1} - (1+z)^{-\frac{3\gamma A}{2}}\right]. \tag{66}$$

In Fig. 8 we plot the angular diameter distance *versus* redshift for some selected values of β and λ. The graph shows that the $f(R,T)$ and particle creation enhance the angular distance. The angular diameter distance initially increases with increasing z and eventually begins to decrease.

On expanding (66), we get

$$H_0 d_A = z + \left[1 - \frac{\left(\frac{3\gamma A}{2} + 1\right)\left(\frac{3\gamma A}{2} + 2\right)}{2\left(\frac{3\gamma A}{2} - 1\right)}\right] z^2 + \cdots. \tag{67}$$

Thus, the angular diameter shows linear behavior up to first approximation whereas it has quadratic up to second approximation.

7 Conclusion

In this paper, we have studied a flat FRW cosmological model described by an open thermodynamic system including particle creation at the expense of gravitational field in $f(R,T)$ theory of gravity. We have obtained exact solutions for the scale factor and various physical quantities by assuming a suitable form of $f(R,T) = R + 2f(T)$ and "gamma-law" equation of state. The model exhibits non-singular power-law expansion of the Universe for $0 \leq \gamma \leq 2$. The model shows Big Rip singularity for $\gamma < 0$. The dynamics of the scale

factor and other physical quantities have been examined through some graphical representations in various phases of evolution of the Universe with some selected values of λ and β. The expressions of the energy densities and particle number density as function of scale factor have been established.

It has been observed that the scale factor always increases with decelerated and accelerated rate depending upon the contribution of particle creation and the parameter λ. It has been noticed that the Universe expands with slow rate in early time but fast during late time. The energy density and effective pressure always decrease with time and both tend to zero in late time for $0 \leq \gamma \leq 2$. The number of particles increase with time in all phases. The number of particles in the absence of particle production remain constant throughout the evolution of the Universe, which is quit obvious. The deceleration parameter has been found as a constant, which exhibits both decelerated and accelerated Universe under some constraints on different parameters. The density parameter shows that the model becomes open in the presence of particle creation in $f(R, T)$ theory.

We have also discussed some observational consequences of the model through some kinematics tests such as lookback time, proper distance, luminosity distance and angular diameter distance with respect to redshift. The results for the cosmological tests are found to be compatible with the recent observations. These tests are found to be depend on λ and β. The Universe with particle creation is always older than the usual FRW model in absence of particle creation. The model of Lima et al. [16] may be recovered for $\lambda = 0$.

In summary, we have studied a cosmological model with particle creation in $f(R, T)$ gravity theory to understand the current acceleration expansion of the Universe. We have found that the negative pressure due to the matter creation may play the role of dark energy and derive the accelerating expansion of the universe in $f(R, T)$ theory. We may expect that the process of particle creation is also an ingredient which accounts this unexpected observational results. The changes introduced by the particle creation process, which is quantified by the parameter β, provide reasonable observational results. The new fact justifying the present work is that we have considered the thermodynamics approach for which particle creation is at the expense of the gravitational field. One may find that the particle creation changes the predictions of standard cosmology, thereby alleviating the problem of reconciling observations with the inflationary scenario. In future work, one may plan to constraint cosmological model with matter creation using complimentary astronomical observations.

Acknowledgments The authors are very thankful to the referees for their constructive comments to improve the quality of the manuscript. The authors would like to thank Prof. T. Harko for helpful discussions.

References

1. Riess, A.G., et al.: Astrophys. J. **116**, 1009 (1998)
2. Perlmutter, S., et al.: Astrophys. J. **517**, 565 (1999)
3. Suzuki, N., et al.: Astrophys. J. **746**, 85 (2012). arXiv:1105.3470 [astro-ph.CO]
4. Netterfield, C.B., et al.: Astrophys. J. **571**, 604 (2002)
5. Spergel, D.N., et al.: Astrophys. J. Suppl. **148**, 175 (2003). [astro-ph/0302209]
6. Sahni, V.: Lec. Notes Phys. **653**, 141 (2004). [astro-ph/0403324]
7. Frieman, J., et al.: Ann. Rev. Astron. Astrophys. **46**, 385 (2008). [astro-ph/0803.0982]
8. Caldwell, R.R., Kamionkowski, M.: Ann. Rev. Nucl. Part. Sci. **59**, 397 (2008). [astro-ph/0903.0866]
9. Krauss, L.M., Turner, M.: Gen. Rel. Grav. **27**, 1137 (1995)
10. Turner, M.S., White, M.: Phys. Rev. D **56**, R4439 (1997)
11. Chiba, T., Sugiyama, N., Nakamura, T.: Mon. Not. Roy. Astron. Soc. **289**, L5 (1997)
12. Padmanabhan, T.: Phys. Rep. **380**, 235 (2003). [hep-th/0212290]

13. Abramo, L.R.W., Lima, J.A.S.: Class. Quant. Grav. **13**, 2953 (1996)
14. Zimdhal, W., Pavón, P.: Mon. Not. Roy. Astron. Soc. **266**, 872 (1994)
15. Lima, J.A.S., Abramo, L.R.W.: Phys. Lett. A **257**, 123 (1999)
16. Lima, J.A.S., Germano, A.S., Abramo, L.R.W.: Phys. Rev. D **53**, 4287 (1996)
17. Guth, A.H.: Phys. Rev. D **23**, 347 (1981)
18. Freedman, W.L., Olinto, A., Friemaan, J., Schramm, D.: Proceedings of the 18th Texas Symposium on Relativistic Astrophys. World Scietific (1998)
19. Brans, C., Dicke, R.H.: Phys. Rev. D **124**, 925 (1961)
20. Nortvedt, K.: Astrophys. J. **161**, 1059 (1970)
21. Wagoner, R.V.: Phys. Rev. D **1**, 3209 (1970)
22. Dirac, P.A.M.: Nature **139**, 323 (1937)
23. Canuto, V., Adoms, P.J., Hsieh, S.H., Tsiang, E.: Phys. Rev. D **16**, 1643 (1977)
24. Bondi, H., Gold, T.: Mon. Not. Roy. Astron. Soc. **108**, 252 (1948)
25. Hoyle, F.: Mon. Not. Roy. Astron. Soc. **109**, 365 (1949)
26. Narlikar, J.V.: Nonstandard cosmologies. In: Novello, M. (ed.) Vth Brazilian school of cosmology and Gravitation, p. 152. World Scientific, Singapore (1987)
27. Tryon, E.P.: Nature **246**, 396 (1973)
28. Fomin, P.I.: Dokl. Akad. Nank SSSR A **9**, 831 (1975)
29. Brout, R., Englert, F., Gunzig, E.: Ann. Phys. (NY) **115**, 78 (1978)
30. Brout, R., Englert, F., Spindel, P.: Phys. Rev. Lett. **43**, 417 (1979)
31. Brout, R., Englert, F., Frére, F., Gunzig, J.M., Nardone, P., Spindel, P., Tuffin, C., Gunzig, E.: Nucl. Phys. B **170**, 228 (1980)
32. Fulling, S.A., Parker, L., Hu, B.L. Phys. Rev. D **10**, 3905 (1974)
33. Gunzig, E., Gehenian, J., Prigogine, I.: Nature **330**, 621 (1983)
34. Prigogine, I., Gohenian, J., Gunzig, E., Nardone, P.: Proc. Natl. Acad. Sci. USA **85**, 7428 (1988)
35. Calvão, M.O., Lima, J.A.S., Waga, I.: Phys. Lett. A **162**, 223 (1992)
36. Lima, J.A.S., Germano, A.S.: Phys. Lett. A **170**, 373 (1992)
37. Lima, J.A.S., Alcaniz, J.S.: Astron. Astrophys. **348**, 1 (1999)
38. Alcaniz, J.S., Lima, J.A.S.: Astron. Astrophys. **349**, 72 (1999)
39. Zimdahl, W., et al.: Phys. Rev. D **64**, 063501 (2001)
40. Qiang, Y., Jiezhang, T., Ze-Long, Y.: Astrophys. Space Sci. **311**, 407 (2007). arXiv:astro-ph/0503123
41. Lima, J.A.S., Silva, F.E., Santos, R.C.: Class. Quantum Grav. **25**, 205006 (2008)
42. Steigman, G., Santos, R.C., Lima, J.A.S.: J. cosmol. Astropart. Phys. **0906**, 033 (2009)
43. Cárdenas, V.H.: Eur. Phys. J. C **72**, 2149 (2012)
44. Singh, C.P., Beesham, A.: Astrophys. Space Sci. **336**, 469 (2011)
45. Singh, C.P., Beesham, A.: Int. J. Theor. Phys. **51**, 3951 (2012)
46. Singh, C.P.: Astrophys. Space Sci. **338**, 411 (2012)
47. Singh, C.P.: Mod. Phys. Lett. A **27**, 1250070 (2012)
48. Lima, J.A.S., Basilakos, S.: Phys. Rev. D **82**, 023504 (2010)
49. Lima, J.A.S., Baranov, I.: Phys. Rev. D **90**, 043515 (2014)
50. Quintin, J., Cai, Y.i.-Fu., Brandenberger, R.H.: Phys. Rev. D **90**, 63507 (2014)
51. Nunes, R.C., Paón, D.: Phys. Rev. D **91**, 063526 (2015)
52. Clifton, T., Ferreira, P.G., Padilla, A., Skordis, C.: Phys. Rep. **513**, 1 (2012). arXiv:astro-ph/1106.2476
53. Nojiri, S., Odintsov, S.D.: Phys. Rev. D **74**, 086005 (2006)
54. Bertolami, O., Bochmer, C.G., Harko, T., Lobo, F.S.N.: Phys. Rev. D **75**, 104016 (2007)
55. Harko, T.: Phys. Lett. B **669**, 376 (2008)
56. Harko, T., Lobo, F.S.N., Nojiri, S., Odintsov, S.D.: Phys. Rev. D **84**, 024020 (2011). arXiv:gr-qc/1104.2669
57. Jamil, M., Momeni, D., Raza, M., Myrzakulov, R.: Eur. Phys. J. C **72**, 1999 (2012)
58. Houndjo, M.J.S., Batista, C.E.M., Campos, J.P., Piattella, O.F.: Canadian J. Phys. **91**, 548 (2013). arXiv:gr-qc/1203.6084
59. Sharif, M., Rani, S., Myrzakulov, R.: Eur. Phys. J. Plus **128**, 123 (2013). arXiv:gr-qc/1210.2714
60. Chakraborty, S.: Gen. Rel. Grav. **45**, 2039 (2013). arXiv:gen-ph/1212.3050
61. Alvarenga, F.G., de la Cruz-Dombriz, A., Houndjo, M.J.S., Rodrigues, M.E., Sáez-Gómez, D.: Phys. Rev. D **87**, 103526 (2013). arXiv:gr-qc/1302.1866
62. Pasqua, A., Chattopadhyay, S., Khomenkoc, I.: Canadian J. Phys. **91**, 632 (2013)
63. Shabani, H., Farhoudi, M.: Phys. Rev. D **88**, 044048 (2013)
64. Sharif, M., Zubair, M.: J. Phys. Soc. Jpn. **82**, 064001 (2013). arXiv:gr-qc/1310.1067
65. Singh, C.P., Singh, V.: Gen. Rel. Grav. **46**, 1696 (2014)
66. Prigogine, I., Gohenian, J., Gunzig, E., Nardone, P.: Gen. Rel. Grav. **21**, 767 (1989)

Holographic dark energy with statefinder diagnostic in modified $f(R,T)$ gravity

C. P. Singh [1] and Pankaj Kumar [2]

[1,2] *Department of Applied Mathematics, Delhi Technological University*
Bawana Road, Delhi-110 042, India.
[1] cpsphd@rediffmail.com
[2] pankaj.11dtu@gmail.com

arXiv:1507.07314v1 [gr-qc] 27 Jul 2015

Abstract In this paper we study the holographic dark energy in the formalism of modified $f(R,T)$ gravity within the framework of a homogeneous and isotropic flat Friedmann-Robertson-Walker Universe. We show that the Hubble horizon as an IR cut-off in this modified theory is suitable to explain the recent accelerated expansion of the Universe. We also discuss the statefinder parameters and obtain the fixed point value of statefinder pair $\{r,s\}=\{1,0\}$ as in the case of ΛCDM model under suitable constraints. As we know that the phase transition is an integral part of the cosmic history, but we do not get phase transition as the deceleration parameter comes out to be a constant in this case. Therefore, we extend our analysis to viscous holographic dark energy with same IR cut-off which gives the recent phase transition of the Universe. In this case, we find that the value of statefinder pair matches with ΛCDM model and shows the kinessence like behavior for the suitable value of parameters.

[1] Corresponding author

1 Introduction

It is now well known that our Universe is undergoing an accelerated expansion, confirmed by the recent observations like supernovae Ia [1], cosmic microwave background radiation [2], baryon acoustic oscillation [3] and Planck data [4]. Within the framework of general relativity (GR), the cause of the acceleration can be attributed to the existence of a mysterious component of the Universe dubbed as "dark energy" (DE), which makes up $\sim 70\%$ of the total cosmic energy in the Universe. The ΛCDM model presents the simplest and most successful description of the recent accelerated expansion scenario and accommodates the observations very well. Despite of many attractive features, it has some theoretical problems like fine-tuning and cosmic coincidence problems [5]. To overcome these problems, a number of dynamical dark energy models such as scalar field (quintessence, phantom, k-essence, etc.) models [6], chaplygin gas models [7], holographic dark energy (HDE) models [8], etc. have been explored in the literature .

In the recent years, the HDE models have been emerged as a viable candidate to explain the problems of modern cosmology. The HDE models explain the recent accelerated expansion as well as the coincidence problem of the Universe [9, 10]. The concept of HDE is based on holographic principle proposed by 't Hooft [11] and found it's roots in the quantum field theory. Cohan et al. [12] have shown that in the quantum field theory, the formation of black hole set a limit which relates UV cut-off Λ to IR cut-off L. According to the authors, the quantum zero-point energy $\rho_h = \Lambda^4$ of a system of size L should not exceed the mass of a black hole of the same size, i.e., $L^3\rho_h \leq LM_p^2$, where $M_p = (8\pi G)^{-1/2}$ is the reduced Planck mass. In a paper [9], Li has taken the largest allowed L to saturate this inequality and thus obtained dark energy density of the Universe $\rho_h = 3c^2M_p^2L^{-2}$, known as HDE density. In the formalism of HDE, the Hubble horizon is a most natural choice for IR cut-off, but it leads to a wrong equation of state (EoS) of dark energy [13]. However, Pavón and Zimdhal [10], and Banerjee and Pavón [14] have shown that the viable EoS of dark energy could be achieved by taking the interaction between HDE and dark matter (DM).

On the other hand, the modified theories of gravity such as $f(R)$ gravity [15], $f(G)$ gravity [16], $f(R,G)$ gravity [17], etc. have also been proposed to explain the recent accelerated expansion of the Universe. The $f(R)$ gravity is one of the simplest and successful modified theory of GR, which fits with the observation very well. Recently, Harko et al. [18] have proposed a new modified gravity theory known as $f(R,T)$ gravity, where R as usual stands for the Ricci scalar and T denotes the trace of the energy-momentum tensor, which presents a maximal coupling between geometry and matter. A number of authors [19] have discussed the modified $f(R,T)$ gravity in different context to explain the early and late time acceleration of the Universe. In a recent paper [20], the authors have discussed the viscous cosmology in this theory which shows the recent phase transition under certain constraints.

In this paper, we are interested to discuss HDE with Hubble horizon as an IR cut-off in the framework of $f(R,T)$ gravity. It has been shown in GR and Brans-Dicke theory that the Hubble horizon as an IR cut-off is a suitable candidate to explain the recent accelerated expansion if we consider interaction between HDE and DM [10, 14]. As is known, the $f(R,T)$ gravity has inbuilt interaction between geometry and matter, therefore, it will be interesting to discuss HDE with Hubble horizon as an IR cut-off in this modified theory. It is assumed that only HDE component of the total matter (HDE +DM) interacts with the geometry of the Universe. Therefore, we consider T of $f(R,T)$ as the trace of the energy-momentum tensor of HDE only. We show that the Hubble horizon as an IR cut-off is suitable to explain the recent accelerated expansion in this modified gravity theory.

The Hubble parameter H and the deceleration parameter q are well known cosmological parameters which explain the evolution of the Universe. However, these two parameters can not discriminate among various DE models. In this context, Sahni et al. [22] have introduced a new geometrical diagnostic pair $\{r,s\}$, known as statefinder parameter, which is constructed from the scale factor and its derivatives up to the third order. The statefinder pair $\{r,s\}$ is geometrical in nature as it is con-

structed from the space-time metric directly. Therefore, statefinder pair is more universal parameter to study the DE models than any other physical parameters. In a flat ΛCDM model, the statefinder pair has a fixed point value $\{r, s\} = \{1, 0\}$. One can plot the trajectories in $r - s$ and $r - q$ planes to discriminate the various DE models. We discuss the statefinder diagnostic and obtain the fixed point value of statefinder pair $\{r, s\} = \{1, 1\}$ and $\{r, s\} = \{1, 0\}$ as in the case of SCDM and ΛCDM models, respectively, under suitable constraints.

To be more realistic, the prefect fluid universe is just an approximation of viscous Universe. It has been shown that inflation and recent acceleration can be explained using the viscous behavior of the Universe. It also plays an important role in the phase transition of the Universe [21]. Any model may not be considered a good model without explaining the phase transition of the universe. The non-viscous HDE model does not show phase transition. Therefore, we extend our analysis to viscous HDE with same IR cut-off which gives the recent phase transition of the Universe. However, the energy momentum tensor of DM is assumed to be a perfect fluid. We obtain the statefinder parameters for viscous HDE which achieve the value of ΛCDM model and show similarity with kinessence model for suitable value of parameters.

The paper is outlined as follows. In the next section we discuss the HDE with Hubble horizon as an IR cut-off in the framework of $f(R, T)$ gravity. We find the scale factor, deceleration parameter and statefinder parameters as function of the cosmic time t and discuss their behaviors. The viscous HDE cosmology is the subject of section 3. In this section, we also obtain the values of the parameters as in section 2 and discuss their behaviors. Section 4 presents the summary of our findings.

2 Holographic dark energy in $f(R, T)$ gravity

The general form of Einstein-Hilbert action for $f(R, T)$ gravity in the unit $8\pi G = 1$ is as follows [18, 20]:

$$S = \frac{1}{2}\int d^4x\sqrt{-g}\,[f(R, T) + 2\mathcal{L}_m], \tag{1}$$

where g stands for the determinant of the metric tensor $g_{\mu\nu}$ and $\mathcal{L}_m$ denotes the matter Lagrangian density. In the above action (1), the speed of light is taken to be unity.
Varying the action (1) w.r.t. the metric tensor $g_{\mu\nu}$ and assuming a simple form [18, 20]

$$f(R, T) = R + f(T), \tag{2}$$

we get the following field equations

$$R_{\mu\nu} - \frac{1}{2}Rg_{\mu\nu} = T_{\mu\nu} - (T_{\mu\nu} + \ominus_{\mu\nu})f'(T) + \frac{1}{2}f(T)g_{\mu\nu}, \tag{3}$$

where prime denotes the derivative with respect to the argument. The second term $f(T)$ in right hand side of (2) modifies the general relativity and represents a coupling with geometry of the Universe. The tensor $\ominus_{\mu\nu}$ in (3) is given by

$$\ominus_{\mu\nu} = -2T_{\mu\nu} + g_{\mu\nu}\mathcal{L}_m - 2g^{\alpha\beta}\frac{\partial^2\mathcal{L}_m}{\partial g^{\mu\nu}\partial g^{\alpha\beta}}. \tag{4}$$

The matter Lagrangian $\mathcal{L}_m$ may be chosen as $\mathcal{L}_m = -p$ [18], where p is the thermodynamical pressure of matter content of the Universe. Now, Eq. (4) gives $\ominus_{\mu\nu} = -2T_{\mu\nu} - pg_{\mu\nu}$. Using this result, the field equations (3) reduce to

$$R_{\mu\nu} - \frac{1}{2}Rg_{\mu\nu} = T_{\mu\nu} + (T_{\mu\nu} + p\,g_{\mu\nu})f'(T) + \frac{1}{2}f(T)g_{\mu\nu}. \tag{5}$$

We consider the HDE in the framework of $f(R,T)$ gravity and assume that the Universe is filled with HDE and pressureless DM (excluding baryonic matter). The total energy-momentum tensor of matter content (HDE+DM) is given by

$$T_{\mu\nu} = T^h_{\mu\nu} + T^m_{\mu\nu}, \tag{6}$$

where $T^h_{\mu\nu}$ and $T^m_{\mu\nu}$ represent the energy-momentum tensors of HDE and DM, respectively. As earlier explained in introduction, it is assumed that only HDE component of total matter (HDE +DM) interacts with the geometry of the Universe. Therefore, we consider $T = g^{\mu\nu}T^h_{\mu\nu}$ as the trace of energy-momentum tensor of HDE.

The observations suggest that the Universe is almost homogeneous, isotropic and flat at present. Therefore, we consider a homogeneous and isotropic flat Friedmann-Robertson-Walker (FRW) metric

$$ds^2 = dt^2 - a^2(t)(dx^2 + dy^2 + dz^2), \tag{7}$$

where $a(t)$ stands for the cosmic scale factor. Using (6) and (7) into (5), we obtain

$$3H^2 = \rho_m + \rho_h + (\rho_m + \rho_h + p_h)f'(T) + \frac{1}{2}f(T), \tag{8}$$

$$2\dot{H} + 3H^2 = -p_h + \frac{1}{2}f(T), \tag{9}$$

where ρ_m, ρ_h and p_h denote the energy density of DM, the energy density of HDE and the pressure of HDE, respectively. An overdot denotes the derivative with respect to cosmic time t. As the field equations (8) and (9) are highly non -linear, therefore, we consider $f(T) = \alpha\, T$ [see, ref. 18], where α is a coupling parameter. Now, the field equations (8) and (9) reduce as

$$3H^2 = \rho_m + \rho_h + \alpha(\rho_m + \rho_h + p_h) + \frac{1}{2}\,\alpha\, T, \tag{10}$$

$$2\dot{H} + 3H^2 = -p_h + \frac{1}{2}\,\alpha\, T. \tag{11}$$

The equation of state (EoS) and the trace of energy-momentum tensor of HDE are given by $p_h = w_h\rho_h$ and $T = \rho_h - 3p_h$, respectively. Now, from (10) and (11), a combined evolution equation for H can be written as

$$2\dot{H} + (1+\alpha)[(1+w_h)\rho_m + \rho_h] = 0. \tag{12}$$

In the literature, various forms of HDE (the general form is $\rho_h = 3c^2M_p^2L^{-2}$, where c^2 is a dimensionless constant, M_p stands for the reduced Planck mass and L denotes the IR cut-off radius) have been discussed depending on the choices of IR cut-off such as Hubble horizon, future event horizon, apparent horizon, Granda-Oliveros cut-off, etc. Many authors have shown that HDE with Hubble horizon as an IR cut-off describes the recent accelerated expansion when HDE and DM interact. The $f(R,T)$ gravity has inbuilt coupling between geometry and matter. Therefore, we consider interaction of HDE with Hubble horizon as an IR cut-off with the geometry of $f(R,T)$ gravity to discuss the accelerated expansion. Taking the Hubble horizon ($L = H^{-1}$) as an IR cut-off, the energy density ρ_h of HDE is given by

$$\rho_h = 3\,c^2H^2. \tag{13}$$

Form (10) and (13), the energy density of DM can be written as

$$\rho_m = \frac{3(\alpha c^2 w_h - 3\alpha c^2 - 2c^2 + 2)}{2(1+\alpha)}\,H^2. \tag{14}$$

Using (13) and (14) into (12), we finally get

$$\dot{H} + \frac{3}{4}(3\alpha c^2 w_h + 2c^2 w_h - \alpha c^2 + 2)\, H^2 = 0, \tag{15}$$

which, on solving it gives

$$H = \frac{1}{c_0 + \frac{3}{4}(3\alpha c^2 w_h + 2c^2 w_h - \alpha c^2 + 2)t}, \tag{16}$$

where c_0 is a positive constant of integration. Eq. (16) can be rewritten as

$$H = \frac{H_0}{1 + \frac{3H_0}{4}(3\alpha c^2 w_h + 2c^2 w_h - \alpha c^2 + 2)(t - t_0)}, \tag{17}$$

where H_0 is the present value of the Hubble parameter at the cosmic time $t = t_0$, the time where the HDE starts to dominate. Using the relation $H = \frac{\dot{a}}{a}$, the cosmic scale factor a is given by

$$a = c_1 \left[1 + \frac{3}{4}H_0(3\alpha c^2 w_h + 2c^2 w_h - \alpha c^2 + 2)(t - t_0)\right]^{\frac{4}{3(3\alpha c^2 w_h + 2c^2 w_h - \alpha c^2 + 2)}}, \tag{18}$$

where c_1 is an another positive constant of integration. One can rewrite a as follows

$$a = a_0 \left[1 + \frac{3}{4}H_0(3\alpha c^2 w_h + 2c^2 w_h - \alpha c^2 + 2)(t - t_0)\right]^{\frac{4}{3(3\alpha c^2 w_h + 2c^2 w_h - \alpha c^2 + 2)}}, \tag{19}$$

where a_0 is the present value of the scale factor at the cosmic time $t = t_0$. We obtain the power-law of evolution of the Universe which avoids the big-bang singularity.

The deceleration parameter q, which is defined as $q = -a\ddot{a}/\dot{a}^2$, is a geometric parameter which describes the acceleration or deceleration of the Universe depending on the negative or positive value. In this case, the deceleration parameter is given by

$$q = \frac{1}{2} + \frac{3}{4}c^2(3\alpha w_h + 2w_h - \alpha). \tag{20}$$

Here, we obtain a constant deceleration parameter as expected due to power-law of the evolution. As we observe that for a given value of w_h, one can obtain an accelerated expansion for coupling parameter α satisfying the constraint $\alpha > \frac{6c^2 w_h + 2}{3c^2(1 - 3w_h)}$. For example, one can take $\alpha > -\frac{1}{3}$ for $c^2 = 1$ and $w_h = -1$ to observe the accelerated expansion. Thus, the accelerated expansion in the framework of HDE with Hubble horizon as an IR cut-off can be successfully explained in $f(R, T)$ gravity without assuming the interaction between HDE and DM in contrast to the works done in [10, 29]. It is to be noted that this model does not show the phase transition as a constant deceleration parameter is obtained.

In order to do robust analysis of HDE, we consider the statefinder parameters as defined in [22]. The statefinder pair $\{r, s\}$ is a new geometrical diagnostic pair which provides a very comprehensive description of the dynamics of the Universe and consequently the nature of the DE. It is defined as

$$r = \frac{\dddot{a}}{aH^3}, \qquad s = \frac{r - 1}{3(q - 1/2)}. \tag{21}$$

In this model, we obtain the statefinder parameters r and s as

$$r = \frac{9}{8}\, c^4(3\alpha w_h + 2w_h - \alpha)^2 + \frac{9}{4}\, c^2(3\alpha w_h + 2w_h - \alpha) + 1, \tag{22}$$

$$s = \frac{c^2}{2}\left(3\alpha w_h + 2w_h - \alpha\right) + 1. \tag{23}$$

We observe that the statefinder parameters $\{r, s\}$ are constant and the values of these parameters depend on the coupling parameter α, constant c and EoS parameter w_h of HDE. In the paper [22], it has been observed that SCDM model and ΛCDM model have fixed point value of statefinder pair $\{r, s\} = \{1, 1\}$ and $\{r, s\} = \{1, 0\}$, respectively. In our work, it is observed that SCDM model can be achieved for $\alpha = \frac{2w_h}{1-3w_h}$ for any values of c. Thus, for a suitable value of w_h which may be obtained by observations, we can find the coupling parameter α for which $\{r, s\} = \{1, 1\}$ and viceversa.

In a paper, Li et al. [23] have studied the Planck constraints on HDE and obtained the tightest and self-consistent value of constant c from Planck+WP+BAO+HST+lensing as $c = 0.495 \pm 0.039$. Therefore, let us consider here and thereafter $c = 0.5$ for further discussion which is lying in this observed range. Now, assuming any values of w_h, we can get the value of coupling parameter α, e.g., $c = 0.5$ and $w_h = -1$, we have $\alpha = 1.5$, which achieves the fixed point of ΛCDM model $\{r, s\} = \{1, 0\}$. Observations show that EoS of HDE is not exactly the same of cosmological constant ($w_h = -1$), in fact it may lie in quintessence region ($-1 < w_h < -1/3$) or phantom region $w_h < -1$. The coupling parameter α provides us the flexibility to obtain the ΛCDM model for any values of w_h lying in the quintessence/phantom region. At the boundary of quintessence region i.e. $w_h = -1/3$ and $c = 0.5$, we have $\alpha = 11/3$ for which $\{r, s\} = \{1, 0\}$. Here, we observe that as we increase the value of w_h from -1/3 to -1, the value of α decreases from 11/3 to 3/2 to obtain $\{r, s\} = \{1, 0\}$. Similarly, one can get $\{r, s\} = \{1, 0\}$ in phantom region for suitable value of α.

3 Viscous holographic dark energy in $f(R, T)$ gravity

In an isotropic and homogeneous FRW model, the dissipative process may be treated via the relativistic theory of bulk viscosity proposed by Eckart [24] and later on pursued by Landau and Lifshitz [25]. It was found that the bulk viscous fluid can produce acceleration in the expansion of the Universe even without dark energy matter due to the presence of an effective negative pressure. In an accelerating Universe, it may be natural to assume that the expansion process is actually a collection of state out of thermal equilibrium in a small fraction of time due to the existence of bulk viscosity. Recently, the present authors [20, 21] have studied the effect of viscous fluid in $f(R, T)$ gravity and discussed the recent accelerated expansion of the Universe. In section 2, we have presented a non-viscous HDE model in modified $f(R, T)$ gravity which explains the recent acceleration of the Universe. As we know that the phase transition is an integral part of the cosmic history, but we do not get phase transition as the deceleration parameter and statefinder parameters come out to be a constant in non-viscous HDE model. Therefore, in this section we extend our analysis to viscous holographic dark energy with same IR cut-off to discuss the recent phase transition of the Universe.

Let us assume that the effective pressure of HDE due to bulk viscosity is given by

$$P_{eff} = p_h + \Pi, \tag{24}$$

where $\Pi = -3\zeta H$ [25] is the viscous pressure. Here, ζ is the coefficient of the bulk viscosity which is assumed to be positive. Now, for matter lagrangian $\mathcal{L}_m = -P_{eff}$ for which Eq. (4) gives $\ominus_{\mu\nu} = -2T_{\mu\nu} - P_{eff}g_{\mu\nu}$. Using this result and $f(T) = \alpha T$ into (3), we obtain the field equations of viscous HDE in the framework of $f(R, T)$ gravity as

$$3H^2 = \rho_m + \rho_h + \alpha(\rho_m + \rho_h + p_h - 3\zeta H) + \frac{1}{2}\alpha T, \tag{25}$$

$$2\dot{H} + 3H^2 = -p_h + 3\zeta H + \frac{1}{2}\alpha T. \tag{26}$$

Using $T = \rho_h - 3(p_h - 3\zeta H)$ into (25) and (26), a single evolution equation of H is given by

$$2\dot{H} + (\alpha+1)(\rho_m + \rho_h + p_h) - 3(\alpha+1)\zeta H = 0. \tag{27}$$

Also, Eq.(25) gives

$$\rho_m = \frac{3}{2(\alpha+1)}\, H\, [(\alpha c^2 w_h - 3\alpha c^2 - 2c^2 + 2)H - \alpha\zeta]. \tag{28}$$

Now, Using (13) and (28) into (27), we get

$$\dot{H} + \frac{3}{4}(3\alpha c^2 w_h + 2c^2 w_h - \alpha c^2 + 2)H^2 - \frac{3}{4}(3\alpha+2)\zeta H = 0. \tag{29}$$

Eq. (29) is solvable for H if the coefficient of bulk viscosity ζ is known. Many authors have studied the cosmological models by assuming the various form of bulk viscous coefficient (for review, see [26]). Here, we assume the bulk viscous coefficient to be a constant, i.e., $\zeta = \zeta_0$, which is the simplest form of $\zeta = \zeta_0 + \zeta_1 H$ [20, 27] by taking $\zeta_1 = 0$. Now, Eq. (29) reduces to

$$\dot{H} + \frac{3}{4}(3\ \alpha\ c^2 w_h + 2\ c^2 w_h - \alpha\ c^2 + 2)H^2 - \frac{3}{4}(3\ \alpha + 2)\zeta_0 H = 0. \tag{30}$$

The solution of (30) is given by

$$H = \frac{e^{\frac{3}{4}(3\alpha+2)\zeta_0 t}}{c_2 + \frac{(3\ \alpha\ c^2 w_h + 2\ c^2 w_h - \alpha\ c^2 + 2)}{(3\alpha+2)\zeta_0} e^{\frac{3}{4}(3\alpha+2)\zeta_0 t}}, \tag{31}$$

where c_2 is a constant of integration. The scale factor a in the terms of cosmic time t is

$$a = c_3 \left[c_2 + \frac{(3\alpha c^2 w_h + 2c^2 w_h - \alpha c^2 + 2)}{(3\alpha+2)\zeta_0} e^{\frac{3}{4}(3\alpha+2)\zeta_0 t}\right]^{\frac{4}{3(3\alpha c^2 w_h + 2c^2 w_h - \alpha c^2 + 2)}}, \tag{32}$$

where $c_3 > 0$ is another constant of integration. Eq. (32) can be rewritten as

$$a = a_0 \left[1 + \frac{(3\alpha c^2 w_h + 2c^2 w_h - \alpha c^2 + 2)}{(3\alpha+2)\zeta_0} H_0 (e^{\frac{3}{4}(3\alpha+2)\zeta_0 (t-t_0)} - 1)\right]^{\frac{4}{3(3\alpha c^2 w_h + 2c^2 w_h - \alpha c^2 + 2)}}. \tag{33}$$

One can observe that the model avoids the big-bang singularity.

The phase transition of the Universe can be explained using deceleration parameter q. In this case, the deceleration parameter is given by

$$q = \frac{\frac{3}{4H_0}[(3\alpha c^2 w_h + 2c^2 w_w - \alpha c^2 + 2)H_0 - (3\alpha+2)\zeta_0]}{e^{\frac{3}{4}(3\alpha+2)\zeta_0 (t-t_0)}} - 1. \tag{34}$$

It is observed that the value of q is time-dependent which comes due to the introduction of bulk viscous term in HDE. It may be noticed that a constant q has been observed in non-viscous HDE as discuss in section 2. The deceleration parameter q must change sign from positive to negative to explain the recent phase transition (deceleration to acceleration) of the Universe. In fact, q must change the sign at the time $t = t_0$ because we have assumed t_0 is the time where HDE begins to dominate. In other words, the Universe must decelerate for $t < t_0$ (matter dominated epoch) and accelerate for $t > t_0$ (HDE dominated epoch). We observe that the Universe shows the transition from decelerated to accelerated phase for $\alpha = -\frac{2}{3}(1 + \frac{5H_0}{3w_h H_0 - 12\zeta_0 - H_0})$ at cosmic time t_0. Therefore, the value of coupling parameter α can be obtained for a given value of w_h, which may be obtained from observations, or vice-versa to get the transition. Thus, we have shown that the bulk viscous HDE with Hubble horizon

as an IR cut-off can explain the recent phase transition of the Universe in the framework of $f(R,T)$ gravity.

Next, we discuss the another geometrical parameter, i.e., statefinder parameters. In this case, the statefinder parameter r is obtained as

$$r = \frac{9}{16H_0}[(3\alpha c^2 w_h + 2c^2 w_h - \alpha c^2 + 2)H_0 - (3\alpha+2)\zeta_0] \tag{35}$$
$$\times \left[\frac{(3\alpha c^2 w_h + 2c^2 w_h - \alpha c^2 + 2)H_0 - (3\alpha+2)\zeta_0}{H_0 e^{\frac{3}{2}(3\alpha+2)\zeta_0(t-t_0)}} + \frac{(3\alpha c^2 w_h + 2c^2 w_h - \alpha c^2 - 2)H_0}{e^{\frac{3}{4}(3\alpha+2)\zeta_0(t-t_0)}}\right] + 1.$$

The second statefinder parameter s is not given here due to complexity but one can find it by using the values of q and r from (34) and (35) in $s = \frac{r-1}{3(q-1/2)}$. Our model reproduces the fixed point value $\{r,s\} = \{1,0\}$ of ΛCDM model when the parameter α satisfies the condition $\alpha = -\frac{2}{3}(1 + \frac{13H_0}{3w_h H_0 - 12\zeta_0 - H_0})$. For this value of α, the statefinder pair is independent of time and remains fixed throughout the evolution as in ΛCDM model. Indeed, we have obtained time-dependent statefinder pair which means that a general study of the behaviour of this pair is needed. We plot the trajectories in $r-s$ and $r-q$ planes for some particular values of parameters α and w_h to discriminate our model with existing models of DE.

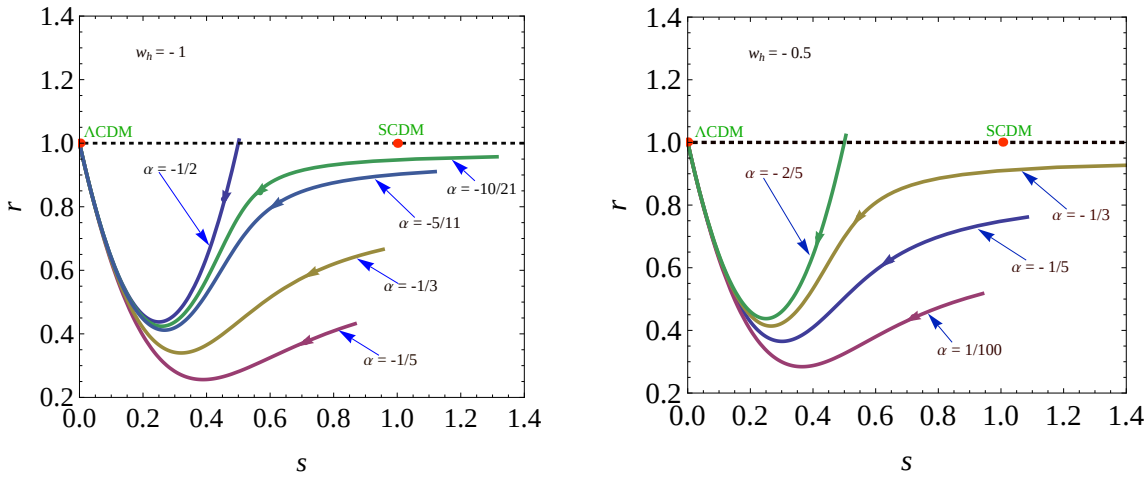

(a) **(b)**

Figure 1. The trajectories in $r-s$ plane are plotted for $w_h = -1$ in left panel (a) and for $w_h = -0.5$ in right panel (b) for different values of α. Here, we have taken $c = 0.5$, $H_0 = 1$ and $\zeta = 0.05$.

In Figs. 1a, b, it is noticed that the fixed points $\{r,s\} = \{1,1\}$ and $\{r,s\} = \{1,0\}$ have been shown as SCDM model and ΛCDM model, respectively. It is obvious from both figures that for any values of α and w_h, the viscous HDE model always approaches to the ΛCDM model, i.e., $\{r,s\} = \{1,0\}$ in late time evolution. However, in early time of evolution our model can approach in the vicinity of SCDM model for some values of α as can be seen in Figs. 1a, b. It is possible for some negative values of α for which viscous HDE model starts from ΛCDM in early time and approaches to same ΛCDM model during late time of evolution.

In quiessence model with constant EoS (Q-model) [22] and Ricci dark energy (RDE) [28], it has been shown that the trajectories in $r-s$ plane are vertically straight lines. In both models, s is constant throughout the evolution of the Universe, while r increases in RDE model and decreases in

Q-model starting from initial point $r = 1$. It has also been shown in [22] that the trajectories for the Kinessence scalar field model ($K-$model) where the scalar potential $V(\phi)$ varies as $V(\phi) \propto \phi^{-\beta}, \beta \geq 1$ approaches asymptotically to the ΛCDM model in late time. Comparing this viscous HDE model with $Q-$model and RDE model, we find that our viscous HDE model produces the curved trajectories which approaches to ΛCDM model in late time. Further, we observe that our model almost shows the similar trajectories like $K-$model for some values of α and w_h in $r-s$ plane, e.g., for $\alpha = -0.5$, $w_h = -1$ and $\alpha = -0.4$, $w_h = -0.5$ as shown in Figs. 1a, b, respectively, show the similar trajectories as $K-$model for $\beta = 2$ [22].

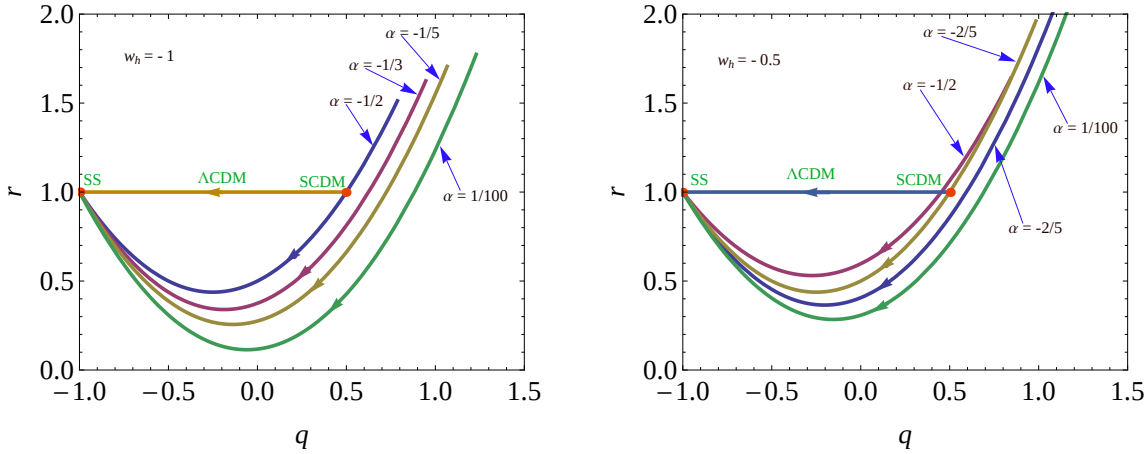

Figure 2. The trajectories in $r - q$ are plotted for $w_h = -1$ in left panel (a) and for $w_h = -0.5$ in right panel (b) for different values of α. Here, we have taken $c = 0.5$, $H_0 = 1$ and $\zeta = 0.05$.

Figs. 2a, b plot the trajectories in $r-q$ plane. The fixed points $\{r, q\} = \{1, 0.5\}$ and $\{r, q\} = \{1, -1\}$ have been shown as SCDM model and SS model (steady-state cosmology), respectively. The horizontal line in Figs. 2a, b represent the evolution of trajectory corresponding to ΛCDM model starting from the fixed point $\{r, q\} = \{1, 0.5\}$ of SCDM model and end at the fixed point $\{r, q\} = \{1, -1\}$ of SS model. It can be observed from both the figures that for any values of α and w_h, the viscous HDE model always approaches asymptotically to the SS model, i.e., $\{r, q\} = \{1, -1\}$ as ΛCDM model in late time evolution. However, in early time of evolution the model passes through SCDM model for some values of α as shown in Figs. 2a, b. The trajectories corresponding to our model starts from the higher values of the pair $\{r, q\}$ but after a certain time span it shows the K-model like behaviour. Again, comparing our viscous HDE model with Q-model, RDE model and $K-$model, we find that viscous HDE model is compatible with $K-$model.

4 Conclusion

In this work, we have studied non-viscous and viscous HDE models with Hubble horizon as an IR cut-off in the frame work of modified $f(R, T)$ gravity. In GR and Brans-Dicke theory, some authors [13, 29] have found that the Hubble horizon is not a viable candidate to explain the accelerated expansion of the Universe. However, Pavón and Zimdahl [10], and Banerjee and Pavón [14] have shown that the interaction between HDE and DM can describe the accelerated expansion. Therefore, it is clear that one can observe accelerated expansion if the interaction between the different matter contents is considered. Since the $f(R, T)$ gravity theory has inbuilt interaction between matter and

geometry, therefore, we have explored the consequences of the coupling of matter with the geometry of the Universe instead of taking the interaction between HDE and DM as many authors have studied. However, we have assumed that only HDE of total matter (HDE+DM) couple with geometry. We have investigated the possibility whether the Hubble horizon as an IR cut-off may achieve an accelerated expansion in $f(R,T)$ gravity by assuming the interaction between HDE and geometry. We have shown that the non-viscous and viscous HDE models with Hubble horizon as an IR cut-off can explain accelerated expansion in the frame work of this modified theory for suitable values of parameters. Further, we have investigated statefinder pair $\{r,s\}$ to descriminate our non-viscous and viscous HDE models with other existing DE models.

In non-viscous HDE model, we have found an accelerated expansion under the constraint of parameters. In this case, we have obtained constant deceleration and statefinder parameters. Due to constant q it is not possible to analyze the phase transition of the Universe. We have found the fixed points $\{r,s\}=\{1,1\}$ and $\{r,s\}=\{1,0\}$ of SCDM and ΛCDM model, respectively, for suitable choice of the parameters.

In viscous HDE model, we have obtained the recent phase transition of the Universe as the deceleration parameter comes out to be time-dependent. In this model, the statefinder parameters are the function of cosmic time t. These time-dependent parameters are possible due to the inclusion of bulk viscous fluid in HDE model which could explain the recent phase transition in a better way. It is interesting to note that the viscous HDE model gives the ΛCDM model fixed point $\{r,s\}=\{1,0\}$ and remains fixed in ΛCDM model throughout the evolution for a specific value of α as discussed in section 3. The statefinder diagnostic have been discussed through the trajectories of $r-s$ and $r-q$ planes as shown in Figs. 1 and 2 to discriminate our model with the existing DE models. In Figs. 1a, b, it has been observed that some of the trajectories pass through the vicinity of SCDM during early time but ultimately all approach to ΛCDM model in late time. In Figs 2a, b, it can be seen that one of the trajectories passes through SCDM model for a suitable value of α in early time but all the trajectories approach to SS model in late time of evolution. It has been noticed that for some values of α the trajectories of the viscous HDE model are similar to the trajectories of $K-$model[22]. Therefore, the viscous HDE in the framework of $f(R,T)$ gravity gives more general results in comparison to ΛCDM and $K-$model at least at the level of statefinder diagnostic as we are able to achieve the behavior of both the models.

Acknowledgements

One of the author PK expresses his sincere thank to University Grant Commission(UGC), India for providing grant of Senior Research Fellowship (SRF).

References

[1] A.G. Riess, et al., Astrophys. J. **659**, 98 (2007);
N. Suzuki, et al., Astrophys. J. **746**, 85 (2012)
[2] C.L. Bennett, et al., Astrophys. J. **148**, 1 (2003);
E. Komatsu, et al., Astrophys. J. Suppl. **192**, 18 (2011).
[3] W.J. Percival, et al., Mon. Not. R. Astro. Soc. **401**, 2148 (2010).
[4] P.A.R. Ade, et al., Astron. Astrophys. **571**, A16 (2014).
[5] S.M. Carroll, Living Rev. Rel. **4**, 1 (2001);
P.J.E. Peebles, B. Ratra, Rev. Mod. Phys. **75**, 559 (2003);
T. Padmanabhan, Phys. Rept. **380**, 235 (2003).
[6] T. Chiba, T. Okaba, M. Yamaguchi, Phys. Rev. D **62**, 023511 (2000);
R.R. Caldwell, Phys. Lett. B **545**, 23 (2002);
T. Padmanabhan, Phys. Rev. D **66**, 021301 (2002);

E.J. Copeland, M. Sami, S. Tsujikawa, Int. J. Mod. Phys. D **15**, 1753 (2006).
[7] M.C. bento, O. Bertolami, A.A. Sen, Phys. Rev. D **66**, 043507 (2002).
[8] M.R. Setare, Phys. Lett. B **644**, 99 (2007);
L. Xu, J. Cosmol. Astropart. Phys. **09**, 016 (2009);
A. Sheykhi, M. Jamil, Phys. Lett. B **694**, 284 (2011).
[9] M. Li, Phys. Lett. B **603**, 1 (2004).
[10] D. Pavón, W. Zimdahl, Phys. Lett. B **628**, 206 (2005).
[11] G. 't Hooft, arXiv:gr-qc/9310026.
[12] A.G. Cohen, D.B. Kaplan, A.E. Nelson, Phys. Rev. Lett. **82**, 4971 (1999).
[13] S.D.H. Hsu, Phys. Lett. B **594**, 13 (2004).
[14] N. Banerjee, D. Pavón, Phys. Lett. B **647**, 477 (2007).
[15] K. Bamba, S. Nojiri, S.D. Odintsov, J. Cosmol. Astropart. Phys. **0180**, 045 (2008);
S. Nojiri, S.D. Odintsov, Phys. Rep. **505**, 59 (2011).
[16] S. Nojiri, S.D. Odintsov, Phys. Lett. B **631**, 1 (2005);
A. De Felice, S. Tsujikawa, Phys. Rev. D **80**, 063516 (2009).
[17] K. Bamba, et al., Eur. Phys. J. C **67**, 295 (2010);
E. Elizalde, et al., Class. Quantum Grav. **27**, 095007 (2010).
[18] T. Harko, et al., Phys. Rev. D **8**, 024020 (2011).
[19] M. Sharif, M. Zubair, J. Cosmol. Astropart. Phys. **03**, 28 (2012);
S. Chakraborty, Gen. Relativ. Gravit. **45**, 2039 (2013);
T. Harko, Phys. Rev. D **90**, 044067 (2014);
C.P. Singh, V. Singh, Gen. Relativ. Gravit. **46**, 1696 (2014);
E.H. Baffou, et al., Astrophys. Space Sci. **356**, 173 (2015).
[20] C.P. Singh, P. Kumar, Eur. Phys. J. C **74**, 3070 (2014).
[21] G.L. Murphy, Phys. Rev. D **8**, 4231 (1973);
I. Brevik, O. Gorbunova, Gen. Relativ. Gravit. **37**, 2039 (2005);
M.-G. Hu, X.-H. Meng, Phys. Lett. B **635**, 186 (2006);
C.P. Singh, S. Kumar, A. Pradhan, Class. Quantum Grav. **24**, 455 (2007);
P. Kumar, C.P. Singh, Astrophys. Space Sci. **357**, 120 (2015).
[22] V. Sahni, et al., JETP Lett. **77**, 201 (2003);
U. Alam, et al., Mon. Not. R. Astron. Soc. **344**, 1057 (2003).
[23] M. li, et al., J. Cosmol. Astropart. Phys. **09**, 021 (2013).
[24] C. Eckart, Phys. Rev. **58**, 919 (1940).
[25] L.D. Landau and E.M. Lifshitz, Fluid Machanics (Butterworth Heineman, 1987).
[26] R. Maarten, Class. Quantum Gravit. **12**, 1455 (1995).
[27] A. Avelino, U. Nucamendi, J. Cosmol. Astropart. Phys. **08**, 009 (2010).
[28] C.J. Feng, Phys. Lett. B **670**, 231 (2008).
[29] L. Xu, W. Li, J. Lu, Eur. Phys. J. C **60**, 135 (2009).

ResearchGate

See discussions, stats, and author profiles for this publication at: http://www.researchgate.net/publication/279198703

Identification and Comparison of Flaws in Conventional Treatment Techniques of Fluoride

ARTICLE · JULY 2015

DOWNLOADS
27

VIEWS
7

2 AUTHORS, INCLUDING:

S. K. Singh
Delhi Technological University
72 PUBLICATIONS **69** CITATIONS

SEE PROFILE

Available from: S. K. Singh
Retrieved on: 06 August 2015

www.ijemr.net ISSN (ONLINE): 2250-0758, ISSN (PRINT): 2394-6962

Volume-5, Issue-3, June-2015

International Journal of Engineering and Management Research

Page Number: 215-217

Identification and Comparison of Flaws in Conventional Treatment Techniques of Fluoride

Shashank Shekhar Singh[1], Dr. S. K. Singh[2]

[1]Research Scholar, Environmental Engineering Department, Delhi Technological University (DTU), Delhi , INDIA

[2]Professor, HOD, Environmental Engineering Department, Delhi Technological University (DTU), Delhi , INDIA

ABSTRACT

Fluoride, a normal constituent of natural waters has dual significance. At optimum concentration it has a protective effect on teeth. At concentrations exceeding a certain limit, it acts as a cumulative toxin, adversely affecting every tissue and organ in the body. Since water is one of the major sources of fluoride for man, defluoridation of drinking water is one of the most important remedial measures to solve high fluoride problem. Over the years several defluoridation techniques have been developed and put to test, some at the laboratory level and others at the community level. This thesis attempts to review the procedure, pros and cons of conventional water defluoridation techniques done in India. A comparison of conventional defluoridation techniques is done in a tabular form depending upon several technical parameters.

Keywords----- **D**efluoridation, Nalgonda technique, Fluoride Removal Techniques

I. INTRODUCTION

1. Fluoride in Drinking Water

Fluorine is the lightest member of the halogen group and is one of the most reactive of all chemical elements. It is not, therefore, found as fluorine in the environment. It is the most electronegative of all the elements which means that it has a strong tendency to acquire a negative charge, and insolution forms F^- ions. Other oxidation states are not found in natural systems,although uncharged complexes may be. Fluoride ions have the same chargeand nearly the same radius as hydroxide ions and may replace each other inmineral structure. Fluoride thus forms mineral complexes with anumber of cations and some fairly common mineral species of low solubilitycontain fluoride.

Fluorine in the environment is therefore found as fluorides which togetherrepresent about 0.06–0.09 per cent of the earth's crust. The average crustal abundanceis 300 mg kg^{-1}. Fluorides are found at significant levels in awide variety of minerals, including fluorspar, rock phosphate, cryolite, apatite,mica, hornblende and others . Fluorite (CaF2) is a common fluoridemineral of low solubility occurring in both igneous and sedimentary rocks.Fluoride is commonly associated with volcanic activity and fumarolicgases.Thermal waters, especially those of high pH, are also rich in minerals of commercial importance include cryolite androck phosphates. The fluoride salt cryolite is used for the production ofaluminium and as a pesticide. Rock phosphatesare converted into phosphate fertilizers by the removal of up to 4.2 per cent fluoride; the removed and purified Fluoride (as fluorosilicates) is asource of fluoride that in some countries is added to drinking-water in order toprotect against dental caries.

1.1 Guidelines

- (WHO) has set the upper limit of fluoride concentration in drinking water at 1.5 mg/l
- The BIS , has therefore, laid down Indian standards as 1.0 mg/l as maximum Permissible limit of fluoride

Copyright © 2011-15. Vandana Publications. All Rights Reserved.

Maximum Mean Temperature of Region (°C)	Maximum Recommended Concentration of Fluoride (mg F/l)
0	2.1
10	1.3
20	0.9
30	0.7
40	0.6
50	0.5
60	0.4

II. HUMAN HEALTH EFFECTS

Fluoride has beneficial effects on teeth at low concentrations in drinking-water,but excessive exposure to fluoride in drinking-water, or in combination withexposure to fluoride from other sources, can give rise to a number of adverse effects. These range from mild dental fluorosis to crippling skeletal fluorosis as the level and period of exposure increases. Crippling skeletal fluorosis is a significant cause of morbidity in a number of regions of the world.Both national and international groups havecomprehensively reviewed available data on the metabolism and health effectsof fluoride in both laboratory animals and humans.

III. MEASURING FLUORIDE

Because the presence of fluoride in water is tasteless, odorless, and color less, there is no way to identify the concentration of fluoride in a body of water without the use of instrumentation. The use of a fluoride selective electrode is often considered the most reliable way of testing water for fluoride, though this method is difficult to do outside of a lab setting. The electrode consists of a lanthanum fluoride crystal (LaF_6) that experiences a electro-potential when in the presence of fluoride ions. Several methods have been developed for testing fluoride concentrations in the field. Most of these are colorimetric tests that result in fluoride interacting with chemicals and dyes such as the SPADNS method. Though less accurate than an electrode, these methods can be used to evaluate if a body of water is safe to consume.

IV. FLUORIDE REMOVAL TECHNIQUES

Occurrence of fluoride at excessive levels in drinking-water in developing countries is a serious problem. Its detection demands analytical grade chemicals and laboratory equipment and skills. Similarly, the prevention of fluorosis through management of drinking-water is a difficult task, which requires favorable conditions combining knowledge, motivation, prioritization, discipline and technical and organizational support. Many filter media and several water treatment methods are known to remove fluoride from water. However, many initiatives on defluoridation of water have resulted in frustration and failure(COWI, 1998). Therefore, in any attempt to mitigate fluoride contamination for an affected community, the provision of safe, low fluoride water from alternativesources, either as an alternative source or for blending, should be investigated asthe first option.In cases where alternative sources are not available, defluoridation of water is the only measure remaining to prevent fluorosis . However, there areseveral different defluoridation methods. What may work in one community may not work in another. What may be appropriate at a certain time and stage of urbanization, may not be at another. It is therefore most important to select an appropriate defluoridation method carefully if a sustainable solution to afluorosis problem is to be achieved.

This paper introduces the basic characterization of the removal methods, followed by discussion of the most promising defluoridation methods; bone charcoal, contact precipitation, Nalgonda, activated alumina and clay. Finally the methods discussed are compared using indicators, which may be appropriatein developing countries.

V. TECHNIQUES OF DEFLUORIDATION

Defluoridation was the conventional and widely tested method for supplying safe water to the fluorosis affected communities. Defluoridation is defined as, “The downward adjustment of level of fluoride in drinking water to the optimal level. Various techniques and materials were tried throughout the world for defluoridation of water. Defluoridation techniques can be broadly classified in to four categories;

1. Adsorption technique
2. Ion-exchange technique
3. Precipitation technique
4. Other techniques, which include electro chemical defluoridation and Reverse Osmosis.

5.1 Conventional techniques

5.1.1 Nalgonda technique

After extensive testing of many materials and processes including activated alumina since 1961, National Environmental Engineering Research Institute (NEERI), Nagpur has evolved an economical and simple method for removal of fluoride which is referred to as „NalgondaTechnique.Nalgonda Technique involves addition of Aluminium salts, lime and bleaching powder followed by rapid mixing, flocculation, sedimentation, filtration and disinfection. Aluminium salt may be added as aluminiumsulphate (alum) or aluminium chloride or

Copyright © 2011-15. Vandana Publications. All Rights Reserved.

combination of these two. It is responsible for removal of fluoride from water. The dose of aluminium salt increases with increase in the fluoride and alkalinity levels of the raw water. The selection of either aluminiumsulphate or aluminium chloride depends on sulphate and chloride contents of the raw water to avoid them exceeding their permissible limits. Lime facilitates forming dense flocks for rapid settling of insoluble fluoride salts. The dose of lime is empirically 1/20th of that of the dose of aluminium salt. Bleaching powder is added to the raw water at the rate of 3 mg/l for disinfection. Approximate doses of alum required to obtain water with acceptable limit of fluoride (<1.0 mg/l) at various fluoride and alkalinity levels in raw water are given below (Table 2).Bulusu et al. stated in 1979 that Nalgonda Technique was preferable at all levels because of the low price and ease of handling . The technique is highly versatile and has the applications like; for large communities, fill and draw technique for small communities, fill-and-Draw defluoridation plant for rural water supply, for domestic defluoridation, etc.

5.1.1.1 Merits of Nalgonda technique

- Regeneration of media is not required.
- No handling of caustic acids and alkalies.
- The chemicals required are readily available and are used in conventional municipal water treatment.
- Adaptable to domestic use.
- Economical
- Can be used to treat water in large quantities for community usage.
- Applicable in batch as well as in continuous operation to suit needs.
- Simplicity of design, construction, operation and maintenance.
- Local semi-skilled workers can be readily employed.
- Highly efficient removal of fluorides from high levels to desirable levels.
- Simultaneous removal of color, odor, turbidity, bacteria and organic contaminants.
- Normally, associated alkalinity ensures fluoride removal efficiency.
- Sludge generated is convertible to alum for use elsewhere.

5.1.1.2 Demerits of Nalgonda technique

- Desalination may be necessary when the total dissolved solids exceed 1500 mg/l.
- Hardness of the raw water in the range of 200 mg/l to 600 mg/l requires precipitation softening and beyond 600 mg/l becomes a cause for rejection or adoption of desalination.
- Generation of higher quantity of sludge compared to electrochemical defluoridation [14].
- The large amount of alum needed to remove fluoride.
- Careful pH control of treated water is required.
- High residual aluminium is reported in treated water by some authors.
- The daily operations require a trained and conscientious operator

An Overall Comparison of Fluoride Removal Techniques

	Activated Alumina	Bone Char	Nalgonda
No daily dosage of chemicals (i.e. no daily working load)	+	+	-
Dosage designed for Fluoride Conc. independent of unit or plant	-	-	+
No risk of false treatment due to breakpoint	-	-	+
Removal capacity of medium is independent of Fluoride conc.	-	-	-
No regeneration or renewal of medium is required	-	-	+
High removal efficiency can be ensured	+	+	-
Easy to construct, even by users	+	+	++
Construction materials are cheap and widely available	+	+	++
Can be sized for one or several families or e.g. a school	+	+	+
No risk of medium/chemicals unacceptability	+	-	+
No risk of deterioration of original water quality	-/+	-/+	-/+

REFERENCES

[1] Fluoride in water: An overview, Unicef. (Accessed on 29-09-2007). Available from: URL:http://www.unicef.org/programme/wes/info/fluor.htm.

[2] S. Kumar and K. Gopal.A Review on Fluorosis and its Preventive Strategies. Indian J. Environmental Protection. June 2000;20(6):430-6.

[3] Siddiqui, A. H.: Fluorosis in Nalgonda District, Hyderabad - Deccan. Brit. Med. J. 1955;2:1408-13

[4] Gupta M. Indian Journal of Environmental Health, 1994, 36 (1), 43-46.

[5] R. Mehrotra, B. S. Kapoor and B. Narayan, Defluoridation of Drinking Water Using Low Cost Adsorbent, *Indian J.Environmental Health*, 41(1), 53-58 (1999)

[6] Fluoride in Drinking-water edited by K. Bailey, J. Chilton, E. Dahi, M. Lennon, P. Jackson and J. Fawell. (2006)

[7] The International Journal Of Engineering And Science (Ijes)

[8] Thompson J, McGarvey FX. Ion-Exchange Treatment of Water Supplies. Journal American Water Works Association 1953; 45: 145-152.

Copyright © 2011-15. Vandana Publications. All Rights Reserved.

Available Online at www.ijcsmc.com

International Journal of Computer Science and Mobile Computing

A Monthly Journal of Computer Science and Information Technology

ISSN 2320–088X

IJCSMC, Vol. 4, Issue. 8, August 2015, pg.177 – 187

RESEARCH ARTICLE

Improved Energy Efficient AODV Routing using K-means Algorithm for Cluster Head Selection

Arthur Ndlovu[1]

[1]Computer Science and Engineering, Delhi Technological University, India

[1] arthurndlovu08@gmail.com

Abstract— A Mobile adhoc network is a collection of wireless mobile nodes which can provide scalability and independence for mobile topologies. These wireless mobile nodes are battery powered hence the need for energy conservation in order to allow an increase in network lifetime. Energy conservation is very important in applications such as Military operations and Emergency Rescue operations where network infrastructure is not readily available. In this research we developed an improved energy efficient algorithm which uses K-means algorithm as the Clusterhead head selection method that is aimed at improving the network performance of AODV (adhoc on-demand distance vector) routing protocol. The improved energy idea uses the concept of drain count in sensor nodes which works as follows:

Each node is set with an initial energy value which basically determines how long it's going to last in a network and to make sure our network has the highest lifetime possible we set up a threshold energy value. If a particular path has a single node with its energy lesser than that of the set threshold, then the drain count of that particular path is incremented by a factor of one (1). The drain count will serve as the parameter on which we can choose the path that is most likely to prolong the network lifetime. The path with the least drain count will be the one that is chosen because it has few nodes with energy below the energy threshold. We then introduce K-means algorithm in the energy efficient system for the formation of clusters in our system and again this will help in shortening the transmission path. The proposed strategy is compared with the traditional AODV routing protocol and performance evaluations are done with respect to network lifetime, throughput, end-to-end delay, packet delivery ratio using Ns2 simulator.

Keywords— Network lifetime, energy efficiency, Drain count, Ns2

I. INTRODUCTION

Wireless networking is an existing technology that allows users to communicate and access information and services electronically regardless of their geographical position. Wireless communication is now popular in every communication network environment and it owes it success to an outburst of research and performance advancements which in turn has enabled wireless networks to transmit higher data rates at reasonably lower prices. We currently have two main approaches for enabling Wireless communications between hosts namely Fixed Network Infrastructure and Adhoc-Network Infrastructure.

© 2015, IJCSMC All Rights Reserved

a) Fixed Network Infrastructure- This is also known as the Cellular network, mobile hosts communicate with each other through a fixed and wired gateway (access point) within the network. In this infrastructure Handoff is the main problem because it is difficult to transfer a connection from one base station to another without compromising the packets or without a risk of disconnection. It is depended on the existence of the infrastructure.

b) Adhoc-Network Infrastructure/Infrastructureless- These types of networks have no fixed routers like the case of fixed infrastructure networks. All nodes are capable of movement and can be connected dynamically in arbitrary manner. The responsibilities for organizing and controlling the network are distributed among the terminals themselves. The entire network is mobile and the individual terminals are allowed to move at will relative to each other. In this type of network some pairs of terminals may not be able to communicate directly to each other due to some transmission distance restrictions of individual terminals and relaying of some messages is required so that they are delivered to their destinations. The nodes of these networks also function as routers which discover and maintain routes to other nodes in the networks. Our proposed system looks at wireless sensor networks which fall in this category. Energy conservation in MANET has always been a critical issue because the desire is to have a network that can last as long as possible in terms of lifetime. Sensor nodes are tiny devices and hence they have small battery power and this calls for innovative ways of communication in order to utilise the energy of these network devices effectively.

II. RELATED WORK

Several researches have been carried out particularly on the performance evaluation of the AODV routing protocol against other traditional protocols like DSDV and DSR routing protocols [2], [4] and [6]. However none of these researches have attempted to borrow algorithms from other fields to improve network operations of AODV routing protocols. Some research has been done however to optimize the network using multipath routing [7], [8], [9]. The proposed work is aimed at developing energy efficient AODV routing protocol that uses K-means algorithm to create clusters in the network. This section documents some of the many energy efficient schemes based on AODV developed by researchers in the field. In [7], Jin-Man Kim and Jong-Wook Jang proposed an enhanced AODV routing protocol which is a modified version of AODV which uses an algorithm called Energy mean value algorithm to improve the network lifetime by considering energy aware in node selection for route discovery. Increase in the number of applications which use Ad hoc network has led to an increase in the development of algorithms which consider energy efficiency as the cost metric.

In [8], Yumei Liu, Lili Guo, Huizhu Ma and Tao Jiang propose a multipath routing protocol for mobile ad hoc networks, called MMRE-AOMDV, which extends the Ad Hoc On-demand Multipath Distance Vector (AOMDV) routing protocol. The key idea of the protocol is to find the minimal nodal residual energy of each route in the process of selecting path and sort multi-route by descending nodal residual energy. Once a new route with greater nodal residual energy is emerging, it is reselected to forward rest of the data packets. It can balance individual node's battery power utilization and hence prolong the entire network's lifetime. In [9], Zhang Zhaoxiao, Pei Tingrui and Zeng Wenli propose a new mechanism of energy-aware routing named EAODV which aims to improve the classical AODV protocol. EAODV adopted the backup routing strategy in case the chosen route fails.

III. METHODOLOGY

A. *Traditional Routing Protocols for MANETs*

MANETs mainly use three types of routing protocols. The reactive protocols such as Dynamic Source Routing (DSR), Ad hoc On-demand Distance Vector (AODV) and Temporally Ordered Routing Algorithm (TORA) dynamically determine the routing path as and when there is a demand to transmit some data. The proactive protocols such as Destination Sequenced Distance Vector (DSDV), Optimized Link State Routing (OLSR) and Fisheye State Routing (FSR) dictates that routing tables be maintained at each node. Hybrid routing protocols such as Zone Routing Protocol (ZRP) are also used, which integrates the characteristics of proactive and reactive protocols, but also has demerits i.e. cannot be evaluated for unidirectional links and it can be applied only for very large networks [6]. AODV protocol favors the least congested route instead of the shortest route and it also supports both unicast and multicast packet transmissions even for nodes in constant movement. It also responds very quickly to the topological changes that affect the active routes. AODV does not put any additional overhead on data packets as it does not make use of source routing. Whereas, DSR protocol is not scalable to large networks and even requires significantly more processing resources [3] [4]. Basically, in order to obtain the routing information, each node must spend lot of time to process any control packet it receives, even if it is not the intended recipient. Even DSDV introduces large amounts of overhead to the network due to the requirement of the periodic update messages [4]**.**

© 2015, IJCSMC All Rights Reserved

B. ***AODV Routing Protocol***

AODV is a packet routing protocol designed for use in mobile ad hoc networks (MANET).

The route discovery mechanism is invoked only if a route to a destination is not known. UDP is the transport layer protocol and Source, destination and next hop are addressed using IP addressing. Each node maintains a routing table that contains information about reaching destination nodes. Each entry is keyed to a destination node. AODV allows nodes to respond to link breakages and changes in network topology in a timely manner.

The operation of AODV is loop free, and by avoiding the Bellman-ford "counting to infinity" problem it offers quick convergence when the topology changes. When links breaks, AODV causes the affected set of nodes to be notified so that they are able to invalidate the routes using the lost link.

Its distinguishing feature is its use of a destination sequence number for each route entry. This number is created by the destination node and is included along with any route information it sends to the requesting node. Using this number ensures loop freedom, the node with the greatest sequence number is selected at all times.

Sequence numbers for both destination and source are used. Managing the sequence number is the key to efficient routing and route maintenance.

1. Sequence numbers are used to indicate the relative freshness of routing information.
2. Updated by an originating node, e.g., at initiation of route discovery or a route reply.
3. Observed by other nodes to determine freshness.

The basic message set consists of:

1. RREQ – Route request
2. RREP – Route reply
3. RERR – Route error
4. HELLO – For link status monitoring

C. ***Energy efficiency in AODV Routing Protocol***

Every node in the initial stages is given an energy value which is basically the battery status at the start of the network. As activity happens in the network the nodes will spent their energy in transmitting and reception of control and data packets. Depending with path selection some nodes will have more energy than the others within the network because not every node is used in transmitting or reception. Therefore for total energy consideration there are basically four modes of energy consumption that must be considered and these include:

1. **Transmission mode**- this is the energy spent in transmitting the packet and is actually dependent on packet size.

$$T_x = \frac{(330 * Plength)}{2 * 10^6} \qquad P_T = \frac{T_x}{T_t}$$

Where T_x is the transmission energy.

P_T – This is the transmission power.

T_t – This is the time taken to transmit data packet

$Plength$-this is the length of the data packet in bits.

2. **Reception mode –** this is the energy that is spent in receiving a packet.

$$R_x = \frac{(230 * Plength)}{2 * 10^6} \qquad P_R = \frac{R_x}{T_x}$$

Where R_x is the reception energy.

P_R – This is the reception power.

T_x – This is the time taken to receive data packet

$Plength$-this is the length of the data packet in bits.

3. **Idle mode-** this is a mode where the node is either neither transmitting nor is it receiving but some considerable energy will be used in hearing. Nodes have to listen to the network activity in case there is incoming packets directed to it. In that case it is imperative that the particular node moves from being in idle state to reception mode. The power consumed in this mode is as follows:

$$P_i = P_R$$

© 2015, IJCSMC All Rights Reserved

Where P_i is the actual power that is consumed while the node is in idle mode and P_R is the power that is consumed in reception mode.

4. **Overhearing mode-** sometimes nodes may receive packets that do not belong to them and that is called overhearing. Some energy is actually lost because of that.

$$P = P_R$$

Where P is the power consumed in overhearing mode and P_R is the power that is consumed in reception mode.

The above four modes are key to an efficient energy aware system as they cover all node energy usage areas.

IV. PROPOSED SYSTEM

The work is divided into two parts, with the first part being the **K-means clustering algorithm** and the second part being the **Improved Energy efficient AODV routing protocol (IEE_AODV)**. The **K-means clustering algorithm** approach will create clusters and enable the selection of cluster heads in the network.

Why K-means Clustering

1. K-means is simple to use
2. If variables (nodes) are huge, then K-Means is computationally faster than hierarchical clustering, if we keep k smalls.
3. K-Means produce tighter clusters than hierarchical clustering, especially if the clusters are globular

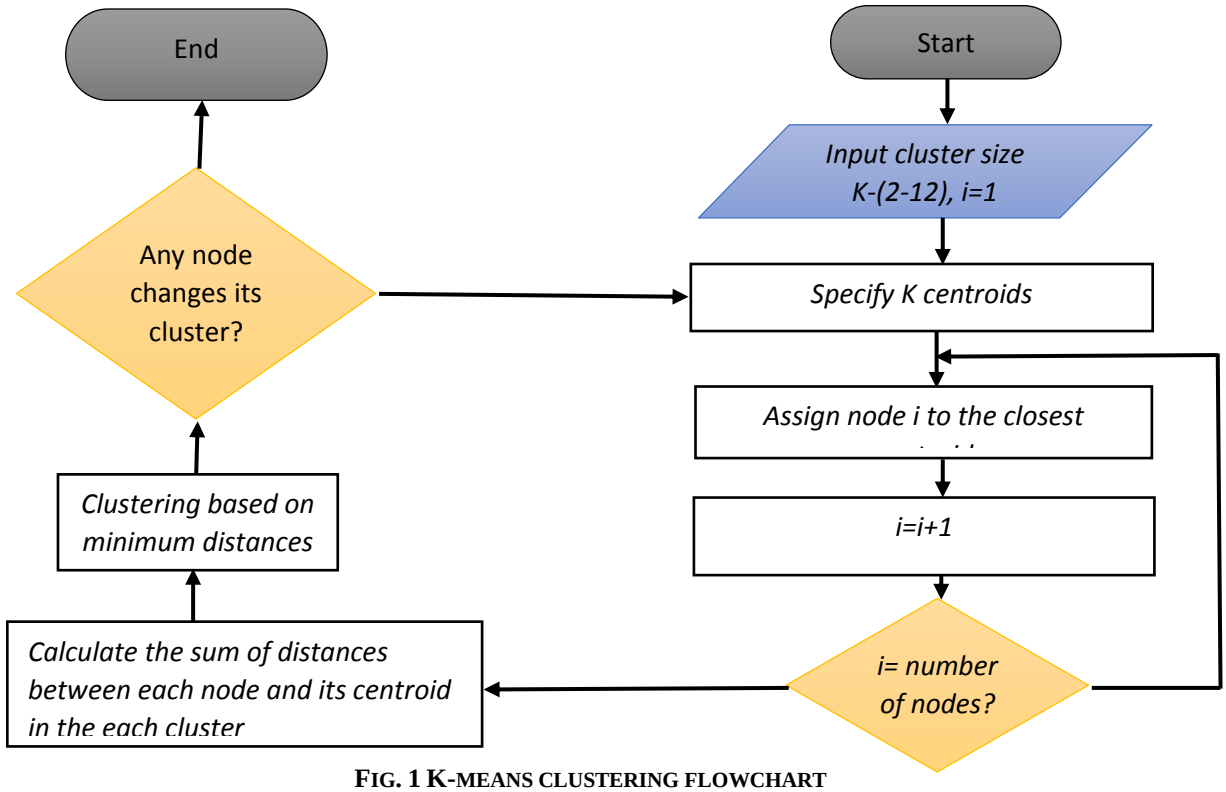

FIG. 1 K-MEANS CLUSTERING FLOWCHART

IMPROVED ENERGY EFFICIENT ROUTING PROTOCOL AODV (IEE_AODV)

The main purpose of introducing the IEE_AODV was to improve the network lifetime as wireless sensor nodes have a constraint in power due to their limited battery power. The lifetime of the network in this proposed system will be determined by the drain **count energy metric**.

Drain rate is the consumption rate of energy by each node within a wireless sensor network. The key to a successful realization of maximum network lifetime is to choose the path with the least drain rate.

© 2015, IJCSMC All Rights Reserved

Proposed Algorithm

1. **Calculate the residual energy of each node**
   a. Let E_t be the amount of energy consumed in transmitting one packet, therefore
   $E_t = P_T * T_t$
   P_T - This is the transmission power.
   T_t – This is the time taken to transmit data packet
   Therefore the **remaining energy** of a node will be calculated as:
   $E_{new} = E_{curr} - E_t$
   b. Let E_r be the amount of energy consumed in receiving one packet, therefore
   $E_r = P_R * T_r$
   Therefore the **remaining energy** of a node will be calculated as:

   $E_{new} = E_{curr} - E_r$

2. **Use the residual energy calculated in step 1 to get the energy status of each node as follows:**

   If (**residual node battery < 20% of the node's initial energy**) then

   Set $E_{res} = 1$

   Else if (**20% of the node's initial energy < residual node battery < 60% of the node's initial energy**) then

   Set $E_{res} = 2$

   Else (**residual node battery > 60% of the node's initial energy**) then

   Set $E_{res} = 3$

3. **Then calculate drain count as follows:**
   If ($E_{res} = 1$) Then

   $N_{drain} = N_{drain} + 1$ (Node energy below energy threshold value)

4. **Choose the path with the least drain count:**
   If N_{drain}(path1) > N_{drain}(path2) then

   Path 2 is the better path

5. Finish

Modified AODV route request packet header

Type	Reserved	Hop Count
RREQ ID		
Destination IP address		
Destination Sequence Number		
Originator IP Address		
Lifetime		
Timestamp		

© 2015, IJCSMC All Rights Reserved

Remaining Energy
Drain Count
Record

Figure 2: Modified AODV route request packet header

The **record** field tracks the path that is traversed by the control packets and helps in updating the routing table along a chosen path. The remaining energy is determined at every node and is compared to the set threshold value. The implementation methodology that is being used to simulate this protocol on MANETs is NS2 and is simulated for networks of different sizes from 10 to 50 nodes.

V. TESTING AND RESULTS

The proposed system was simulated together with the conventional AODV routing protocols in similar simulation environment. In order to cover a number of scenarios node density is going to be varied from 10,20, 30,40 and 50 nodes with node density 10 and 20 representing low node density network and 40 and 50 nodes representing high node densities. It is however important to note that in this research we varied node densities to monitor if our main research modifications can handle scalability and at the same time improve the network lifetime on the network.

Network Scenario for simulation

The network scenario for the proposed system is outlined in the following table:

SIMULATOR	**Network Simulator 2**
NUMBER OF NODES	**10,20,30,40,50 nodes**
INTERFACE TYPE	**Phy/WirelessPhy**
CHANNEL	**Wireless Channel**
MAC TYPE	**Mac/802_11**
QUEUE TYPE	**Queue/DropTail/PriQueue**
QUEUE LENGTH	**201 Packets**
ANTENNA TYPE	**Omni Antenna**
PROPAGATION TYPE	**TwoRay Ground**
SIZE OF PACKET (BYTES)	**Five hundred and twelve (512)**
PROTOCOL	**IEE_AODV**
TRAFFIC	**TCP**
Initial Energy	**10.0 joules**
TxPower	**0.075**
RxPower	**0.075**
Idle Power	**0.005**
PERFORMANCEEVALUATION METRICS	**Average end-to-end delay, throughput, network lifetime, packet delivery ratio**

Table 1: network scenario for Ns2 simulation topology

© 2015, IJCSMC All Rights Reserved

Simulation Screenshot

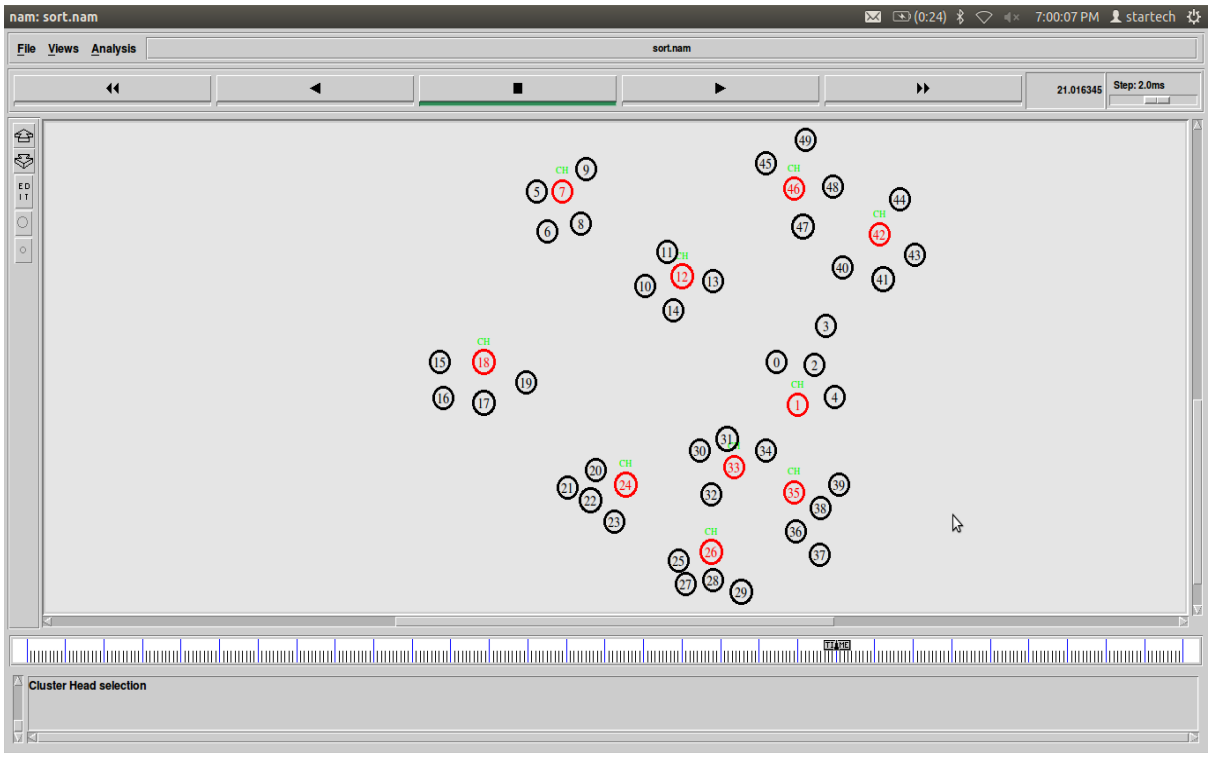

Figure 3: Cluster head selection using K-means clustering algorithm

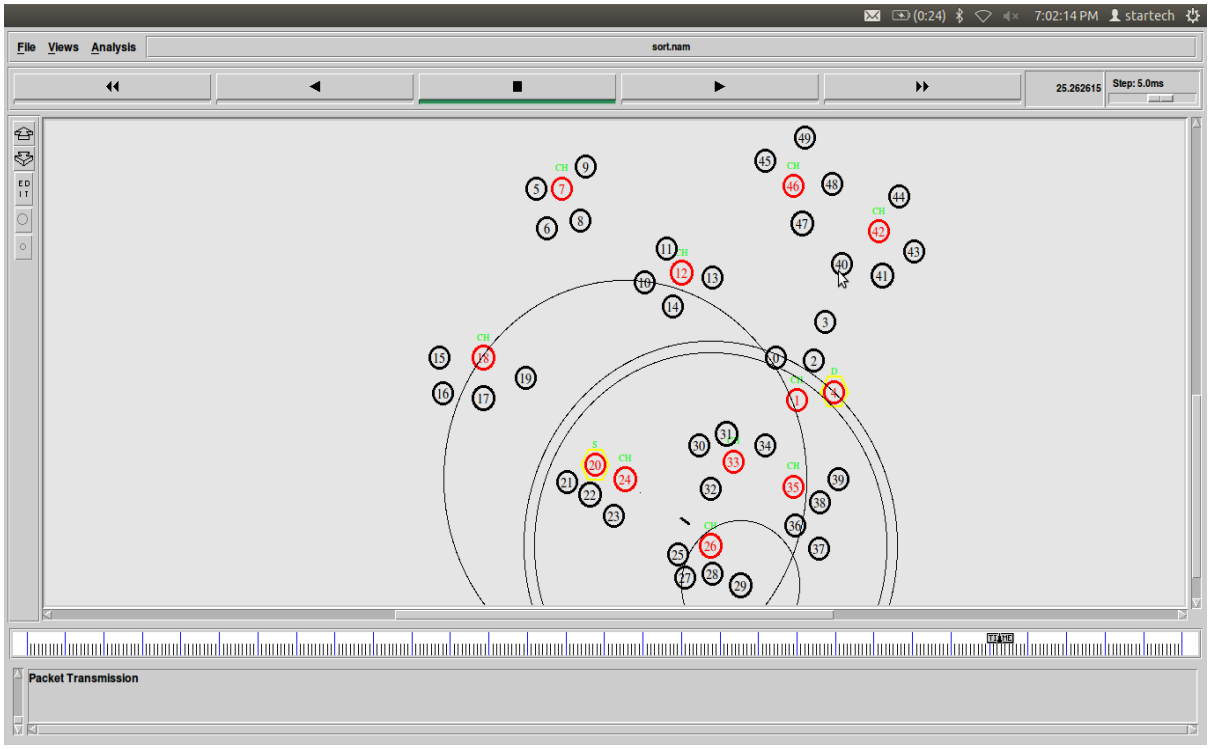

FIGURE 4: PACKET TRANSMISSION

© 2015, IJCSMC All Rights Reserved

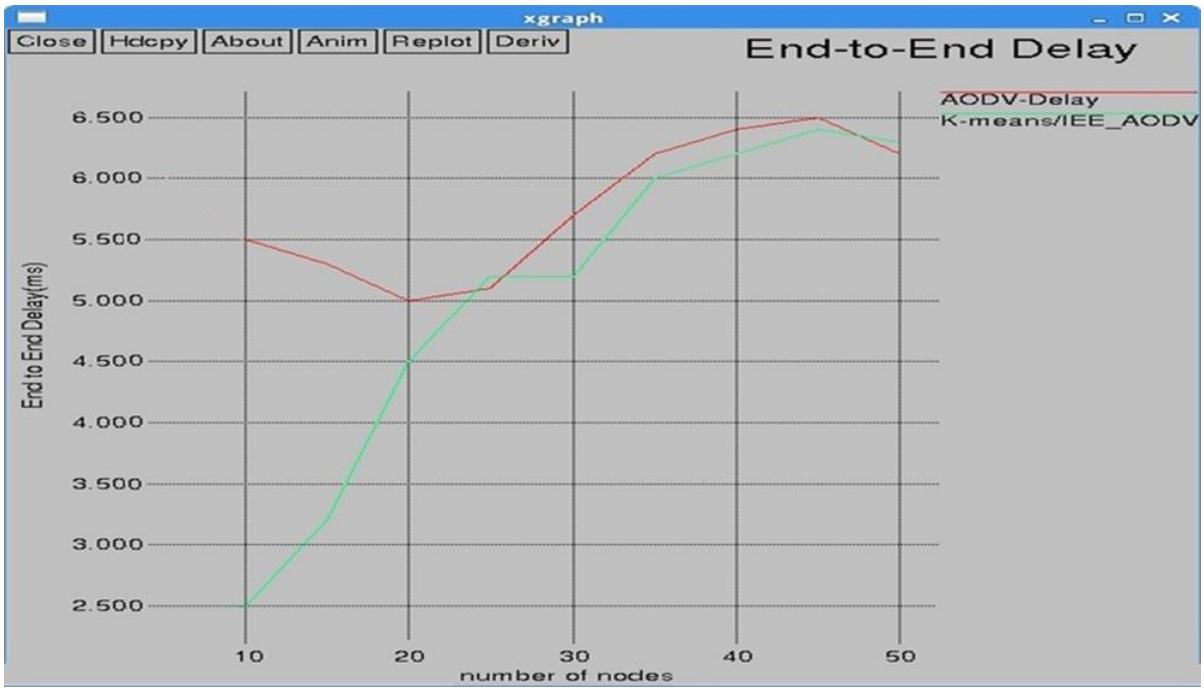

Figure 5: results of delay vs. no. of nodes

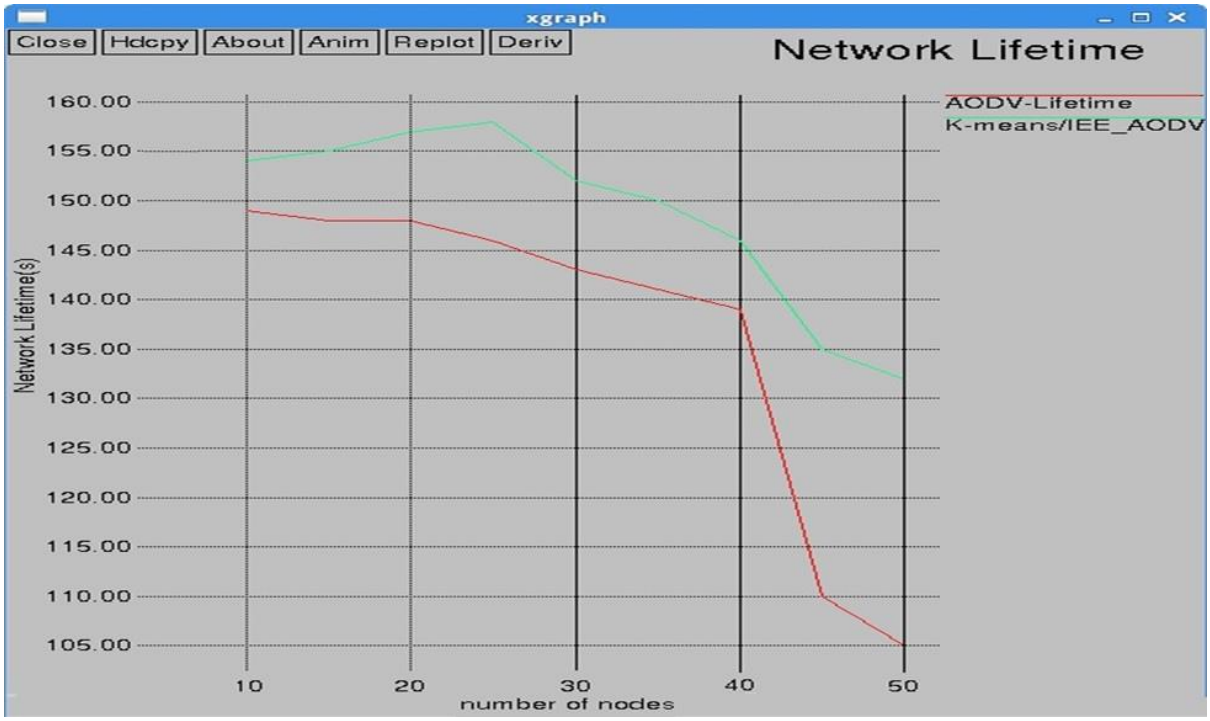

Figure 6: results of network lifetime vs. no. of nodes

© 2015, IJCSMC All Rights Reserved

Figure 7: results of pdr vs. no. of nodes

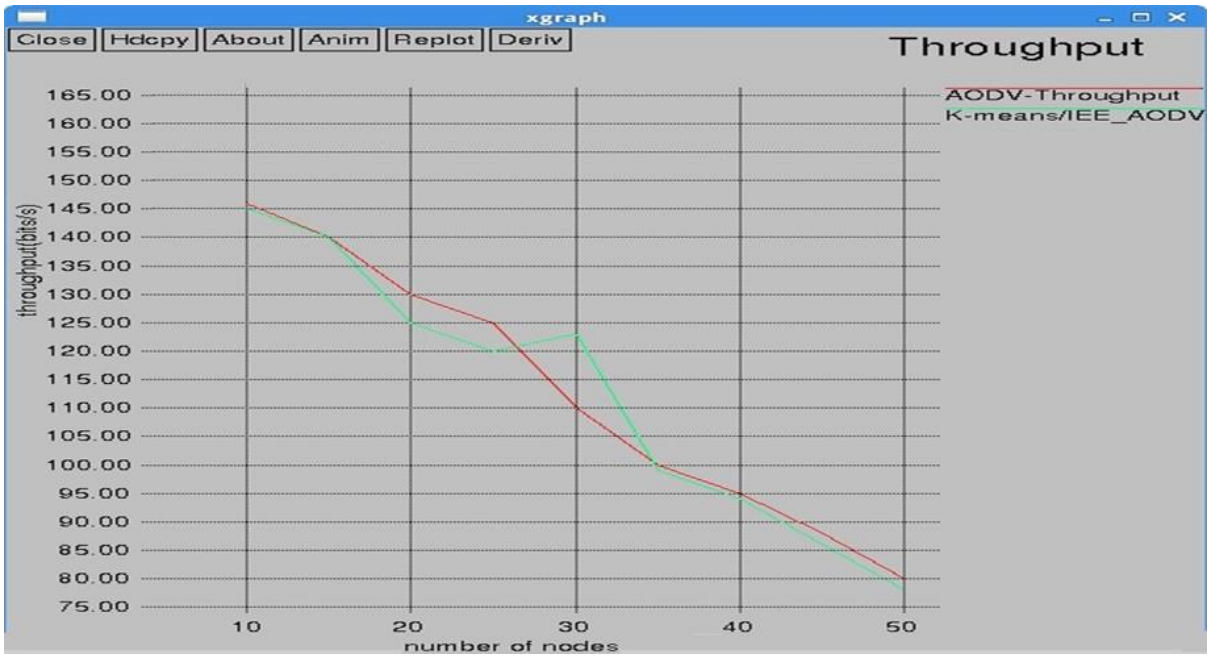

Figure 8: results of throughput vs. no. of nodes

From the graph shown in figure 5 it can be noted that average end-to-end delivery has drastically dropped in our proposed system compared to that of the AODV routing protocol. When node density is low the delay in our proposed system is really low because of the quick convergence that happens with our system as there are few nodes. As the proposed system uses K-means algorithm to optimize its routes if the number of nodes are few then the faster the convergence in the algorithm that is why we have less delay when node density is low. However the delay for AODV routing protocol is high as the route discovery process takes time to find routes to the destination but once the routes are established we see the delay slightly improving but overall as the node density increases (number of nodes) both systems delay increases too. This is generally the case in almost all

© 2015, IJCSMC All Rights Reserved

systems because an increase in node density would imply more connections to be made and hence this extra addition will introduce some delays compared to lesser node density network. Also to note is that the reduction in delay for our proposed system has also been caused the creation of a strong virtual backbone in our proposed system.

From the graph shown in figure 6 it can be noted that when there is low node density in the network the lifetime of the network is high for both the K-means/IEE_AODV and the AODV routing protocols. This is attributed to the fact that there are fewer connections for both networks when the network size is low and hence fewer energy usage is realized. There is less traffic running around the network therefore nodes will be saving power. Energy is consumed when nodes transmit or receive packets during packet transmission. It is observed the **K-means/IEE_AODV** strategy has the best network lifetime for the most part of the network life compared to AODV routing protocol for all node densities and this is so because our proposed approach select the most energy efficient path to transmit packets from the source node to the destination node. AODV's energy consumption depreciates drastically as the node increases in the network mainly because there are more connections and hence more energy is going to be spent in making sure that packets are received by the intended destination node.

The graph in figure 7 clearly shows that the proposed system has a better edge than the AODV routing protocol. In fewer number of nodes the PDR is really high for both approaches because there are less connections in these networks therefore packet delivery is almost guaranteed. As the nodes increase it can be noted that the packet delivery ratio will decrease as well because more connections means that there will be an increase in the likelihood of packet failing to reach to their destinations. Packets are likely to drop if the multihop network size is increased. However the K-means/IEE_AODV strategy has optimized routes cutesy of the K-means algorithm and therefore its packet delivery ratio is greater than that of AODV routing protocol for the most part of the network life.

In figure 8 it can be noted that the throughput of AODV routing protocol is higher than that of the proposed system in most situations. AODV routing has consistently better values of throughput and this is caused by the fact that K-means/IEE_AODV has a lot of control packets exchange before the actual transmission of data packets. Furthermore K-means/IEE_AODV computations of drain count occurs on each and every node in the network. The calculations to determine the amount of energy each node has (residual energy) and the incrementing of drain count has to be performed on each and every node and this introduces extra overheads that will affect the network's throughput in our proposed network. Overall it can be noted that in less dense networks the network throughput is high in all system but will drop as the number of nodes increase due to an increase in network connections. AODV has slightly higher throughput because of the extra control packets that K-means/IEE_AODV has but the difference is negligible.

VI. CONCLUSION

In this research we have implemented an improved energy efficient AODV routing (IEE_AODV) protocol with **K-means** as a network optimization technique, these two techniques where chosen to address critical aspects of mobile adhoc networks. IEE_AODV routing protocol was chosen in order to have a network which is energy efficient that is a network which is mostly likely to have a longer network lifetime by using the route that has nodes with the highest energy levels. K-means on the other hand was used to create clusters in the network and optimize them in such a way that the nodes within a cluster have shortest path to their cluster head. This optimization will ensure that the path or route chosen will achieve packet delivery in the shortest time.

It is observed from the results that the battery life of our nodes in the K-means/IEE_AODV techniques will be fully utilized because the system chooses the path with the maximum energy. Therefore it's been proved that the amount of remaining energy of each node will be important in probabilistically determining the efficient path. This system will avoid link failures due to power issues in the network because routes chosen will have maximum energy.

We also evaluated our system using other performance metrics like packet delivery ratio, throughput, average end-to-end delay and results show that our proposed system has improved in all this regard and of particular importance is the packet delivery ratio. Some recent researches have shown that AODV routing protocol has better PDR than IEE_AODV because not all the energy efficient paths are reliable, some routes might even be longer and hence packet loss will be prone in that regard. It is however clear that the problem has been addressed in this research by the introduction of K-means algorithm. This algorithm will optimize the nodes in the network so that a minimum number of nodes are traversed if data packets are to be transmitted for the source node to the destination node.

Future work

The concept on energy efficiency using the drained nodes can be implemented further using Bio-inspired computing techniques like Ant colony optimization and it can be used on hybrid routing protocols to save energy usage.

© 2015, IJCSMC All Rights Reserved

ACKNOWLEDGEMENT

The author thanks Mr Vinod Kumar for his constant guidance, encouragement and support. His valuable guidance has provided the author with a deep insight into the topic.

REFERENCES

[1] Patil, Annapurna P., et al. "An improved energy efficient AODV routing protocol for MANETs." *Wireless and Optical Communications Networks (WOCN), 2014 Eleventh International Conference on*. IEEE, 2014.
[2] Lijuan Cao, Teresa Dahlberg and Yu Wang, "Performance Evaluation of Energy Efficient Ad Hoc Routing Protocols", IEEE 2007.S. Zhang, C. Zhu, J. K. O. Sin, and P. K. T. Mok, "A novel ultrathin elevated channel low-temperature poly-Si TFT," *IEEE Electron Device Lett.*, vol. 20, pp. 569–571, Nov. 1999.
[3] C. Siva Ram Murthy, B. S. Manoj, "Ad Hoc Wireless Networks Architecture and Protocols", 2nd ed, Pearson Education, 2005.
[4] Ioanis Nikolaidis, Michel Barbeau, Evangelos Kranakis, "Ad-Hoc, Mobile, and Wireless Networks", Third International Conference, ADHOC_NOW 2004.
[5] M. Pushpalatha, Revathi Venkataraman, and T. Ramarao, "Trust Based Energy Aware Reliable Reactive Protocol in Mobile Ad Hoc Networks", World Academy of Science, Engineering and Technology 2009.
[6] G.Vijaya Kumar, Y.Vasudeva Reddyr and Dr.M.Nagendra, "Current Research Work on Routing Protocols for MANET: A Literature Survey", (IJCSE) International Journal on Computer Science and Engineering 2010.
[7] Jin-Man Kim, Jong-Wook Jang, "AODV based Energy Efficient Routing Protocol for Maximum Lifetime in MANET", IEEE 2006.
[8] Liu, Lili Guo,Huizhu Ma,Tao Jiang, "Energy Efficient on–demand Multipath Routing Protocol for Multi-hop Ad Hoc Networks", IEEE 2008.
[9] Zhang Zhaoxiao, Pei Tingrui, Zeng Wenli, "Modified Energy-Aware AODV Routing for Ad hoc Networks",IEEE 2009.
[10] S. Yin, X. Lin, "Multipath minimum energy routing in adhoc network", Proc. Int. Conf.Communications (ICC), IEEE, 2005, pp. 3182-3186.

© 2015, IJCSMC All Rights Reserved

Progress In Electromagnetics Research Letters, Vol. 54, 123–128, 2015

Instability of Ion Beam Driven Electrostatic Ion-Cyclotron Waves in Collisional Magnetized Two-Ion Component Plasma

Jyotsna Sharma[1], Suresh C. Sharma[2, *], and Daljeet Kaur[3]

Abstract—We have studied the instability of electrostatic ion-cyclotron waves in collisional magnetized two-ion component plasma (light positive K^+ ions and heavy positive Cs^+ ions). An ion beam propagating through collisional magnetized plasma containing electrons and two positive ion components drives electrostatic ion cyclotron (EIC) waves to instability via Cerenkov interaction. Analytical expressions & numerical calculations have been carried out for the frequency and growth rate of ion cyclotron waves for two EIC wave modes for existing experimental parameters, and it is found that the unstable mode frequency does not depend on electron collision frequency, while the growth rate is increased linearly with the electron collision frequency. Moreover, as the light ion concentration is increased, the frequency of the heavy ion mode moves closer to its gyrofrequency. Similarly, the frequency of the light ion mode approaches the light ion cyclotron frequency as the heavy ion concentration is increased. It is also found that the normalized unstable mode frequencies remains unchanged with electron collision frequencies, while the growth rate is increased linearly with the electron collision frequencies. In addition, the unstable mode frequencies are found to be dependent on the magnetic field strengths.

1. INTRODUCTION

The electrostatic ion cyclotron instability (EIC) is a low frequency field-aligned current driven instability [1] which is of quite interest because it has one of the lowest threshold drift velocities [2] among current driven instabilities. Several subsequent measurements of EIC oscillations and related phenomenon were made under almost the same configuration, and the results were discussed on the basis of current-driven instability [3–8].

EIC waves in multi-component plasmas have attracted great deal of interest to physicists for the last three decades [9–23]. The excitation of electrostatic ion-cyclotron oscillations by a transverse current were observed by Ivanov and Murav'ev [12]. Song et al. [13] have studied the EIC waves in a plasma with negative ions in a Q machine, and the results indicate that the frequencies of two EIC wave modes increase with the relative density of negative ions, while the critical electron drift velocities for the excitation of either mode decrease with increasing relative ion density.

Chow and Rosenberg [14] have used kinetic theory to show that the critical electron drift velocity for the excitation of both the positive ion and negative ion modes decreased as the relative density of the negative ions increased. In this case, it was found that the frequencies and growth rate of both the unstable modes in presence of negative and positive ions increase, with the relative density of negative ions. Experimental and theoretical investigations of EIC wave excitation in plasma containing negatively charged dust particles were performed by Barkan et al. [17], and Chow and Rosenberg [18]. Sharma and Sharma [21] have studied the excitation of EIC waves by an ion beam in a two-component plasma without collisional effect. As far as the authors' knowledge, nobody has developed a theoretical model on collisional EIC waves in a magnetized plasma containing two positive ion species. Sharma and

Received 27 April 2015, Accepted 29 July 2015, Scheduled 5 August 2015
* Corresponding author: Suresh C. Sharma (suresh321sharma@gmail.com).
[1] School of Basic & Applied Sciences, K. R. Mangalam University, Gurgaon 122103, India. [2] Department of Applied Physics, Delhi Technological University, Delhi 110042, India. [3] Department of Physics, Guru Teg Bahadur Institute of Technology, Rajouri Garden, New Delhi, India.

Sharma [22] have also developed a model of higher harmonics of excitation of ion-cyclotron waves in a plasma cylinder with heavy negative ions.

In this paper, we study the instability of electrostatic ion-cyclotron (EIC) waves by an ion beam in a collisional magnetized plasma containing two positive ion species (K^+ light positive ions and Cs^+ heavy positive ions). In Section 2, we obtain the expression for unstable mode frequencies and the growth rate of two modes (K^+ and Cs^+) using first order perturbation technique. Finally, results and discussion part is given in Section 3.

2. INSTABILITY ANALYSIS

We have developed a theoretical model, where a cylindrical collisional magnetized plasma column of radius a contains electrons, light positive ions K^+ and heavy positive ions Cs^+ with equilibrium electrons, light positive and heavy positive ion densities as $n_{0e} = n_{0p}$, $n_{0l+} = \alpha_{l0} n_{0p}$ and $n_{0h+} = \alpha_{h0} n_{0p}$ immersed in a static magnetic field $B_s \parallel \hat{z}$ along z-axis, where α_{l0} is the concentration of light positive ions and α_{h0} $(= 1 - \alpha_{l0})$ the concentration of heavy positive ions. The electrons have a drift velocity v_{de0} along the magnetic field direction, i.e., along z-axis. The charge, mass and temperature of three species are $(-e, m_e, T_e)$, (e, m_l, T_l) and (e, m_h, T_h), respectively, where $T_e = T_l = T_h$. The plasma is collisional with electron collisional frequency v_{e0}. An ion beam with velocity $v_{0b}\hat{z}$, mass m_b, density n_{0b} and radius $r_0 (\cong a)$ propagates through the plasma along the magnetic field. The beam plasma system prior to the perturbation is quasineutral, such that $en_{0e} - en_{0l+} - en_{0h+} - en_{0b} \approx 0$, since we have taken $n_{0p} \gg n_{0b}$. There is no electric field present in the equilibrium, and plasma is partially uniform. The equilibrium is perturbed by an electrostatic perturbation to potential

$$\phi_1 = \phi_0(r) \exp\left[-i(\omega t - k_z z)\right]. \tag{1}$$

All the three species (electrons, light positive ions and heavy positive ions) are treated as fluids, described by the equations of motion and continuity, which on linearization (equation of motion and continuity) yields the density perturbations as given below:

$$n_{1e} = n_{0e} \frac{e\phi_1}{T_e \left[1 - \frac{i v_{e0}(\omega - k_z v_{de0})}{k_z^2 (T_e/m_e)}\right]}, \tag{2}$$

$$n_{1l+} = -\frac{n_{0p}\alpha_{l0} e c_{l0}^2}{T_e} \left(\frac{\nabla_\perp^2 \phi_1}{\omega^2 - \omega_{l+}^2} - \frac{k_z^2 \phi_1}{\omega^2} \right), \tag{3}$$

$$n_{1h+} = -\frac{n_{0p}\alpha_{h0} e c_{h0}^2}{T_e} \left(\frac{\nabla_\perp^2 \phi_1}{\omega^2 - \omega_{h+}^2} - \frac{k_z^2 \phi_1}{\omega^2} \right), \tag{4}$$

$$n_{1b} = \frac{n_{0b} e k_z^2 \phi_1}{m_b \left(\omega - k_z v_{0b}\right)^2}. \tag{5}$$

Here, v_{e0} is electron collisional frequency, and v_{de0} the drift velocity of the electrons. c_{l0} $[= (T_l/m_l)^{1/2}]$ and c_{h0} $[= (T_h/m_h)^{1/2}]$ are the thermal velocities of light positive & heavy positive ions, and ω_{l+} $(= eB_s/m_l c)$ and ω_{h+} $(= eB_s/m_h c)$ are the cyclotron frequencies of light positive ions & heavy positive ions, respectively.

Using Equations (2), (3), (4) and (5) in the Poisson equation,

$$\nabla^2 \phi_1 = 4\pi e \left(n_{1e} - n_{1l+} - n_{1h+} - n_{1b}\right), \tag{6}$$

we obtain

$$1 + \frac{\omega_{pe}^2}{k_\perp^2 v_{te}^2} + \frac{\omega_{pe}^2 i v_{e0}(\omega - k_z v_{de})}{k_\perp^2 v_{te}^4 k_z^2} - \frac{\omega_{pl}^2 \alpha_{l0}}{\left(\omega^2 - \omega_{l+}^2\right)} - \frac{\omega_{pl}^2 \alpha_{l0} k_z^2}{\omega^2 k_\perp^2} - \frac{\omega_{ph}^2 k_z^2 \alpha_{h0}}{\omega^2 k_\perp^2} - \frac{\omega_{ph}^2 \alpha_{h0}}{\left(\omega^2 - \omega_{h+}^2\right)} - \frac{\omega_{pb}^2 k_z^2}{(\omega - k_z v_{0b})^2 k_\perp^2} = 0, \tag{7}$$

where $\omega_{pl}^2 = \frac{4\pi n_{op}\alpha_{l0} e^2}{m_l}$, $\omega_2 = (\omega - k_z v_{0b})$, $v_{te}^2 = \frac{T_e}{m_e}$, $\omega_{ph}^2 = \frac{4\pi n_{0p}\alpha_h e^2}{m_h}$, $\omega_{pe}^2 = \frac{4\pi n_{0e} e^2}{m_e}$.

Equation (7) can be rewritten as

$$\varepsilon_r(\omega, k) + i\varepsilon_i(\omega, k) = 0, \tag{8}$$

where

$$\varepsilon_r(\omega,k)=1+\frac{\omega_{pe}^2}{k_\perp^2 v_{te}^2}-\frac{\omega_{pl}^2\alpha_{l0}}{\left(\omega^2-\omega_{l+}^2\right)}-\frac{\omega_{pl}^2\alpha_{l0}k_z^2}{\omega^2k_\perp^2}-\frac{\omega_{ph}^2\alpha_{h0}}{\left(\omega^2-\omega_{h+}^2\right)}-\frac{\omega_{ph}^2\alpha_{h0}k_z^2}{\omega^2k_\perp^2}-\frac{\omega_{pb}^2k_z^2}{\omega_2^2k_\perp^2},$$

and

$$\varepsilon_i(\omega,k)=\frac{v_{e0}(\omega-k_zv_{de0})\omega_{pe}^2}{k_\perp^2k_z^2v_{te}^4}. \tag{9}$$

Let us write $\omega=\omega_r+i\Gamma$ and assume that the wave is either weakly damped or growing, i.e., ($|\Gamma|\ll\omega_r$) then we may set

$$\varepsilon_r(\omega=\omega_r,k)=0. \tag{10}$$

Equations (9) and (10) yield

$$\frac{\partial\varepsilon_r(\omega,k)}{\partial\omega_r}=\frac{2\omega_r\omega_{pl}^2\alpha_{l0}}{\left(\omega^2-\omega_{l+}^2\right)^2}+\frac{2\omega_{pl}^2\alpha_{l0}k_z^2}{\omega_r^3k_\perp^2}+\frac{2\omega_r\omega_{ph}^2\alpha_{h0}}{\left(\omega_r^2-\omega_{h+}^2\right)^2}+\frac{2\omega_{ph}^2\alpha_{h0}k_z^2}{\omega_r^3k_\perp^2}-\frac{2\omega_{pb}^2k_z^2}{(\omega_r-k_zv_{0b})^3k_\perp^2}, \tag{11}$$

and $\varepsilon_i(\omega_r,k)=\frac{(\omega_r-k_zv_{de0})v_{e0}\omega_{pe}^2}{k_z^2k_\perp^2v_{te}^4}$. Here $v_{de0}>(\omega_r/k_z)$.

The growth rate is given as $\Gamma=-\frac{\varepsilon_i(\omega_r,k)}{\partial\varepsilon_r(\omega_r,k)/\partial\omega_r}$ or

$$\Gamma=-\frac{v_{e0}\ [1-v_{de0}/(\omega_r/k_z)]\omega_{pe}^2}{2k_z^2k_\perp^2v_{te}^4\left[\frac{\omega_{pl}^2\alpha_{l0}}{\left(\omega_r^2-\omega_{l+}^2\right)^2}+\frac{\omega_{pl}^2\alpha_{l0}k_z^2}{\omega_r^4k_\perp^2}+\frac{\omega_{ph}^2\alpha_{h0}}{\left(\omega_r^2-\omega_{h+}^2\right)^2}+\frac{\omega_{ph}^2\alpha_{h0}k_z^2}{\omega_r^4k_\perp^2}-\frac{\omega_{pb}^2k_z^2}{\omega_r(\omega_r-k_zv_{0b})^3k_\perp^2}\right]}. \tag{12}$$

2.1. Case (a): Light Ion EIC Mode (K^+) in the Absence of Ion Beam

In the absence of heavy positive ions and ion beam, we put $\varepsilon_r(\omega,k)$=0. The Equation (7) can be rewritten as

$$1+\frac{\omega_{pe}^2}{k_\perp^2v_{te}^2}-\frac{\omega_{pl}^2\alpha_{l0}}{\left(\omega_r^2-\omega_{l+}^2\right)}-\frac{\omega_{pl}^2\alpha_{l0}k_z^2}{\omega_r^2k_\perp^2}=0\quad\text{and}\quad1-\frac{\omega_{pl}^2\alpha_{l0}}{\left(\omega_r^2-\omega_{l+}^2\right)\alpha_e}-\frac{\omega_{pl}^2\alpha_{l0}k_z^2}{\omega_r^2k_\perp^2\alpha_e}=0, \tag{13}$$

where $\alpha_e=1+\frac{\omega_{pe}^2}{k_\perp^2v_{te}^2}$ and $k_\perp^2=k_z^2+p_n^2$; $p_n=x_n/a$, x_n are the zeros of Bessel function $J_0(x)$ and a is the plasma column radius. Multiplying Equation (13) by $\omega_r^2/(\omega_r^2-\omega_{l+}^2)$ and solving the equation, we get two solutions

$$\omega_r^2=F_1^2=\omega_{l+}^2+R_0\alpha_{l0}c_{h0}^2k_\perp^2, \tag{14}$$

and

$$\omega_r^2=F_2^2=\frac{\omega_{l+}^2R_0\alpha_{l0}c_{h0}^2k_z^2}{\omega_{l+}^2+R_0\alpha_{l0}c_{h0}^2(k_\perp^2+k_z^2)}, \tag{15}$$

where $R_0=m_h/m_l$ and Equation (14) gives the dispersion relation of the unstable light positive ion mode.

2.2. Case (b): Heavy Ion EIC Mode (C_S^+) in the Absence of Ion Beam

In the absence of light positive ions and ion beam, we put $\varepsilon_r(\omega,k)=0$. Equation (7) can be rewritten as

$$1-\frac{\omega_{ph}^2\alpha_{h0}}{\left(\omega_r^2-\omega_{h+}^2\right)\alpha_e}-\frac{\omega_{ph}^2\alpha_{h0}k_z^2}{\omega_r^2k_\perp^2\alpha_e}=0. \tag{16}$$

Following the same procedure as done earlier, we get the dispersion relation as:

$$\omega_r^2=G_1^2=\omega_{h+}^2+\alpha_{h0}c_{h0}^2k_\perp^2, \tag{17}$$

and the other solution is

$$\omega_r^2=G_2^2=\frac{\omega_{h+}^2\alpha_{h0}c_{l0}^2k_z^2}{R_0\omega_{h+}^2+\alpha_{h0}c_{l0}^2(k_\perp^2+k_z^2)}. \tag{18}$$

2.3. Case (c): Light Ion EIC Mode in the Presence of Ion Beam

In the absence of heavy positive ions and the presence of an ion beam, the real and imaginary parts of Equation (7) can be solved to obtain the growth rate for light positive ions as

$$\Gamma = -\frac{v_{e0}\ [1 - v_{de0}/(\omega_r/k_z)]\omega_{pe}^2}{2k_z^2 k_\perp^2 v_{te}^4 \left[\frac{\omega_{pl}^2 \alpha_{l0}}{\left(\omega_r^2 - \omega_{l+}^2\right)^2} + \frac{\omega_{pl}^2 \alpha_{l0} k_z^2}{\omega_r^4 k_\perp^2} + \frac{\omega_{pb}^2 k_z^2}{\omega_r(\omega_r - k_z v_{0b})^3 k_\perp^2}\right]}. \tag{19}$$

The dispersion relation for light positive ions can be obtained by putting $\varepsilon_r(\omega_r, k) = 0$, which is given as

$$\omega_r^2 = J_1^2 = \frac{\omega_{l+}^2 + \omega_{pl}^2 \left(\alpha_{l0}/\alpha_e\right)\left(k^2/k_\perp^2\right) - \omega_{pb}^2 \left(\omega_{l+}^2/\alpha_e k_\perp^2 v_{0b}^2\right)}{1 - \left(\omega_{pb}^2/\alpha_e k_\perp^2 v_{0b}^2\right)}. \tag{20}$$

2.4. Case (d): Heavy Ion EIC Mode (C_s^+) in the Presence of an Ion Beam

In the absence of light positive ions (in the presence of an ion beam) and following the same procedure as done in case (c), we get the growth rate expression as:

$$\Gamma = -\frac{v_{e0}\ [1 - v_{de0}/(\omega_r/k_z)]\omega_{pe}^2}{2k_z^2 k_\perp^2 v_{te}^4 \left[\frac{\omega_{ph}^2 \alpha_{l0}}{\left(\omega_r^2 - \omega_{h+}^2\right)^2} + \frac{\omega_{ph}^2 \alpha_{h0} k_z^2}{\omega_r^4 k_\perp^2} + \frac{\omega_{pb}^2 k_z^2}{\omega_r(\omega_r - k_z v_{0b})^3 k_\perp^2}\right]}. \tag{21}$$

The dispersion relation for unstable heavy ion mode in the presence of beam is

$$\omega_r^2 = J_2^2 = \frac{\omega_{h+}^2 + \omega_{ph}^2 \left(\alpha_{h0}/\alpha_e\right)\left(k^2/k_\perp^2\right) - \omega_{pb}^2 \left(\omega_{h+}^2/\alpha_e k_\perp^2 v_{b0}^2\right)}{1 - \left(\omega_{pb}^2/\alpha_e k_\perp^2 v_{b0}^2\right)}. \tag{22}$$

3. RESULTS AND DISCUSSIONS

In the numerical calculations we have used typical experimental parameters. Using Equations (20) & (22) we have plotted, in Figure 1, the dispersion curves of ion cyclotron waves with light positive and heavy positive ions and beam mode for potassium ion beam having energy $E_b = 10\,\text{eV}$ or ion beam velocity $v_{0b}[= (20\,\text{eV}/m_i)^{1/2}] = 7 \times 10^5\,\text{cm/sec}$ and density $n_{0b} = 2.5 \times 10^7\,\text{cm}^{-3}$, respectively, for the following parameters: plasma density $n_{0p} = 10^9\,\text{cm}^{-3}$, $T_e = 0.2\,\text{eV}$, magnetic field $B_s = 2.5 \times 10^3\,\text{G}$, plasma radius $a = 2\,\text{cm}$, $R_0 = m_h/m_l = 3.4$. The frequencies and corresponding wave numbers of the unstable modes are obtained by the point of intersections between the beam mode and the two unstable modes. From Figure 1, it is clear that the frequency of heavy ion mode shifts towards the heavy ion cyclotron frequency as the light ion concentration is increased. Likewise, the frequency of the light positive mode approaches the light ion cyclotron frequency as the heavy ion concentration is increased. The critical drift velocity for the excitation of each EIC mode depends on the relative ion concentrations. Using Equations (19) & (21), the growth rates of the light positive and heavy positive unstable modes are plotted in Figures 2 & 3 as a function of their relative ion concentrations for different values of electron collision frequencies.

The growth rates of both the unstable modes increases with the relative ion concentrations. However, the growth rate of light positive ion mode increases by an average factor ∼2.4 when α_{l0} changes from 0.05 to 0.50 and by an average factor ∼1.4 when α_{l0} changes from 0.50 to 0.95. Similarly, the growth rate of heavy positive ion mode increases by an average factor ∼1.4 when α_{h0} changes from 0.05 to 0.50 and by an average factor ∼1.2 when α_{h0} changes from 0.50 to 0.95. It is well known that the electron collisions can lead to a destabilization of the current driven EIC waves as shown by Chaturvedi and Kaw [24], Milic [25], Satyanarayana et al. [26].

Suszcynsky et al. [16] have observed that the critical drift velocity for heavy positive ions decreases with relative ion concentration [cf. Figure 10 of [16]], and hence the growth rate increases with the relative ion concentrations. So, we can say that our theoretical growth rate results are in line with the experimental observations of Suszcynsky et al. [16].

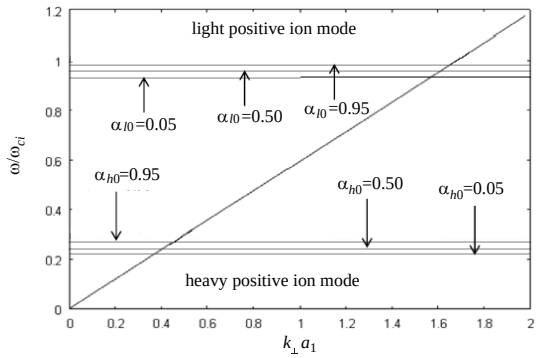

Figure 1. Dispersion curves of ion cyclotron waves of both the unstable modes and a beam mode.

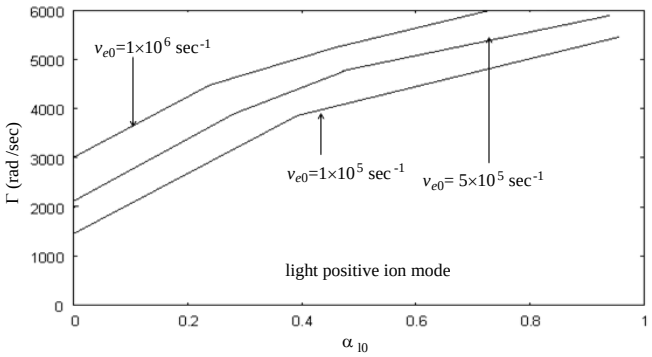

Figure 2. Growth rate of light positive ion mode as a function of α_{l0} for different values of electron collisional frequency.

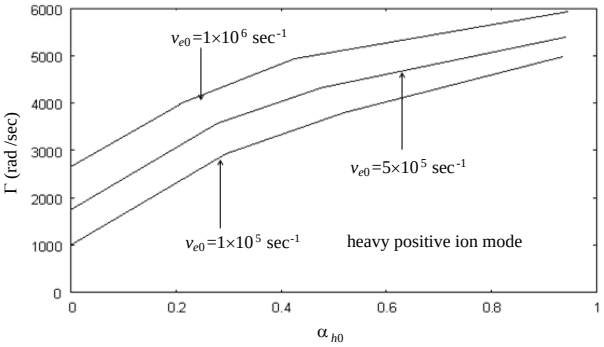

Figure 3. Growth rate of the heavy positive ion mode as a function of its relative ion concentration for different values of electron collisional frequency.

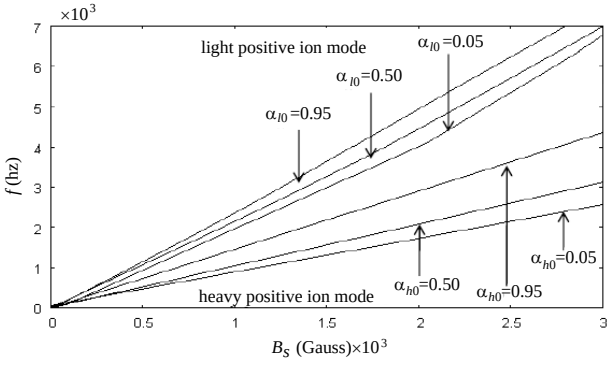

Figure 4. Frequency f ($= \omega_r/2\pi$ in Hz) of both the unstable modes as a function of the magnetic field for different values of their relative ion concentrations and for electron collision frequency $\nu_{e0} = 5 \times 10^5\,\mathrm{sec}^{-1}$.

From Figure 4, it can be seen that the frequency of both the unstable modes increases with increasing magnetic fields and this increase in frequency is linear, i.e., both the unstable modes have frequencies proportional to the magnetic field strength. Moreover, the growth rates of both the unstable modes in presence of K^+ and C_S^+ ions increase with the beam density [cf. Equations (19) & (21)]. If we compare Figure 4 of our paper with Figure 4 of [16], we can say that the trend of our plots is in line with the experimental observations.

In conclusion, we may say that the EIC waves are driven to instability in a collisional magnetized plasma cylinder with two positive (light positive and heavy positive) ions by an ion beam via Cerenkov interaction. The unstable wave frequencies of both the modes increase with the relative density of positive ions. The frequencies of the unstable modes also increase with the magnetic fields. The unstable mode frequencies remains unchanged with electron collision frequencies (ν_{e0}), while the growth rate is increased linearly with the electron collision frequencies. Our work may find some applications in plasma aided nanostructures [27] (where multispecies ions with concentration varying are present).

REFERENCES

1. D'Angelo, N. and R. W. Motley, "Electrostatic oscillations near the ion cyclotron frequency," *Phys. Fluids*, Vol. 5, 633, 1962.
2. Motley, R. W. and N. D'Angelo, "Excitation of electrostatic plasma oscillations near the ion-cyclotron frequency," *Phys. Fluids*, Vol. 6, 296, 1963.

3. Chen, F. F., *Plasma Physics and Controlled Fusion*, Vol. 1, Plasma Physics, Plenum, New York, 1984.
4. Benford, G., N. Rynn, J. J. Thomson, and W. S. Williamson, "Turbulent dispersion of ion cyclotron waves: Theory and experiment," *Phys. Fluids*, Vol. 17, 1001, 1974.
5. Correl, D. L., N. Rynn, and H. Bohmer, "Onset, growth, and saturation of the current-driven ion cyclotron instability," *Phys. Fluids*, Vol. 18, 1800, 1975.
6. Hendel, H. W. and M. Yamada, "Identification of ion-cyclotron instability with discrete and continuous spectra," *Phys. Rev. Lett.*, Vol. 33, 1076, 1974.
7. Schrittwieser, R., R. Rynn, R. Koslover, and R. Karim, "Electrostatic ion-cyclotron instability driven by a slow electron drift," *Plasma Phys. Controlled Fusion*, Vol. 26, 1597, 1984.
8. Van Niekerk, E. G., P. H. Krumm, and M. J. Alport, "Electrostatic ion cyclotron waves driven by a radial electric field," *Plasma Phys. Controlled Fusion*, Vol. 33, 375, 1991.
9. Sharma, S. C. and J. Sharma, "Excitation of ion cyclotron waves by a spiraling ion beam in a magnetized dusty plasma cylinder," *Phys. Plasmas*, Vol. 17, 043704, 2010.
10. D'Angelo, N. and R. L. Merlino, "EIC waves in a plasma with negative ions," *IEEE Trans. Plasma Sci.*, Vol. 14, 285, 1986.
11. Shukla P. K. and A. A. Mamun, *Introduction to Dusty Plasma Physics*, IOP, Bristol, 2002.
12. Ivanov, A. A. and V. F. Murav'ev, "Excitation of electrostatic ion-cyclotron oscillations by a transverse current," *Soy. Phys. — Doklady*, Vol. 16, 971, 1972.
13. Song, B., D. Suszcynsky, N. D'Angelo, and R. L. Merlino, "Electrostatic ion-cyclotron waves in a plasma with negative ions," *Phys. Fluids B*, Vol. 1, 2316, 1989.
14. Chow, V. W. and M. Rosenberg, "Electrostatic ion-cyclotron instabilities in negative ion plasmas," *Phys. Plasmas*, Vol. 3, 1202, 1996.
15. D'Angelo, N., "Low-frequency electrostatic waves in dusty plasmas," *Planet. Space Sci.*, Vol. 38, 1143, 1990.
16. Suszcynsky, D. M., N. D'Angelo, and R. L. Merlino, "An experimental study of electrostatic ion-cyclotron waves in a two-ion component plasma," *J. Geophys. Res.*, Vol. 94, 8966, 1989.
17. Barkan, A., N. D'Angelo, and R. L. Merlino, "Laboratory study of EIC waves in a dusty plasma," *Planet. Space Sci.*, Vol. 43, 905, 1995.
18. Chow, V. W. and M. Rosenberg, "Electrostatic ion-cyclotron instability in dusty plasmas," *Planet. Space Sci.*, Vol. 43, 613, 1995.
19. Sharma, S. C. and M. Sugawa, "The effect of dust charge fluctuations on ion cyclotron wave instability in the presence of an ion beam in a plasma cylinder," *Phys. Plasmas*, Vol. 6, 444, 1999.
20. Sharma, J., S. C. Sharma, V. K. Jain, and A. Gahlot, "Excitation of lower hybrid waves by a gyrating ion beam in a negative ion plasma," *Phys. Plasmas*, Vol. 20, 3, 2013.
21. Sharma, J. and S. C. Sharma, "Excitation of electrostatic ion-cyclotron waves by an ion beam in a two-ion component plasma," *Phys. Plasmas*, Vol. 17, 123701, 2010.
22. Sharma, J., S. C. Sharma, V. K. Jain, and A. Gahlot, "Higher harmonic generation by spiraling ion beam magnetized heavy negative ion plasma," *J. Plasma Phys.*, Vol. 79, 05, 2013.
23. Sharma, S. C. and V. K. Tripathi, "Excitation of ion-cyclotron waves by a spiralling ion beam in a plasma cylinder," *J. Plasma Phys.*, Vol. 50, 331, 1993.
24. Chaturvedi, P. K. and P. K. Kaw, "Current driven ion cyclotron waves in collisional plasma," *Plasma Phys. Contr. Fusion*, Vol. 17, 447, 1975.
25. Milic, B., "Spontaneous excitation of the long-wave ion-cyclotron and ion-acoustic oscillations in fully ionized plasmas," *Phys. Fluids*, Vol. 15, 1630, 1972.
26. Satyanarayana, P., P. K. Chaturvedi, M. J. Keskinen, J. D. Huba, and S. L. Ossakow, "Theory of the current-driven ion cyclotron instability in the bottomside ionosphere," *J. Geophys. Res.*, Vol. 90, 12209, 1985.
27. Ostrikov, K. and S. Xu, *Plasma Aided Nanofabrication from Plasma Sources to Nanoassembly*, Wiley, New York, 2007.

International Journal of Advancement in Engineering Technology, Management & Applied Science
Volume 2, Issue 7 July 2015 ISSN No: 2349-3224

Isolation of a Novel Laccase-producing Fungus from Litter in Upper Soil Horizon

Faria Fatima[1], Ira Chaudhary [1], Smita Rastogi [2], Neelam Pathak [1*]
[1]Department of Biosciences, Integral University, Lucknow, India
[2]Department of Biotechnology, Delhi Technological University, Delhi-110042,India

Abstract

Fungal cultures were screened by laccase plate assay method and observed in LMM medium at pH 6.0, the highest laccase activity was showed by *Verticillum* sp. (18.1 U/ml), followed by *Helminthosporium* sp. amounting to 14.7 U/ml. It was conclude that the *Verticillum* sp. and *Helminthosporium* sp. were the most promising candidates for lignin degradation.
Keywords: *Helminthosporium* sp.; Laccase; Lignin; *Verticillum* sp.

Abbreviations**:** U – Unit; L- Litre ; Δ – Delta; Abs – Absorbance; **ε** - The molar extinction coefficient; R - Supernatant volume in ml; T - Reaction time in minutes.

Lignin is a complex racemic aromatic heteropolymer containing hydrophobic network phenylpropanoid units by oxidative polymerization of three types of hydroxycinnamyl alcohol precursors (monolignols) (8, 22, and 18). Moreover, lignin provides protection for plants against the microorganisms. Fungal degradation is considered the main mechanism of biological cycling of lignin, causing oxidation of propyl chains, demethylation of 3- and 5-methoxyl groups and aromatic ring cleavage. White-rot basidiomycete fungi and actinomycetes have ability to degrade lignin (11) during the secondary metabolism or in the absence of nitrogen, carbon or sulphur.

The ligninolytic microbes exhibit a unique strategy for lignin degradation, which is based on unspecific one-electron oxidation of the benzenic rings catalyzed by synergistic action of extracellular hemeperoxidases and peroxide-generating oxidases. Laccase (EC 1.10.3.2) [benzenediol: oxygen oxidoreductase; *p*-diphenol oxidase], belongs to a family of blue multicopper oxidases, which also include ascorbate oxidase, ceruloplasmin and bilirubin oxidase (9). It catalyzes the oxidation of various aromatic compounds, predominantly phenols, with the reduction of oxygen to water (21, 12). Four copper atoms

in laccase play important role in its catalytic mechanism.

Laccases act as substrate-specific enzymes and act on diphenols, polyphenols, different substituted phenols, diamines, aromatic amines, benzenethiols and even some inorganic compounds such as iodine (23).

Laccases from fungi have role in delignification, pigmentation, fruiting body formation as well as in pathogenesis and in protection from toxic phenolic monomers of polyphenols. Laccases are used in industries, paper and dye industries (1), prevention of wine discoloration, and detoxification of environmental pollutants and production of chemicals from lignin (7). In view of its importance in large-scale application, the present work aims on screening and isolation of highly-efficient laccase-producing fungi.

Sample collection, screening and identification

Litter samples from various locations were subjected to serial dilution in saline water and 100 µl each of 10^{-6} to 10^{-9} dilutions were plated for screening of lignin-degrading fungi. Screening was done on a medium comprising peptone 0.3%; glucose 1.0%; KH_2PO_4 0.03%; $ZnSO_4$ 0.0001%; K_2HPO_4 0.004%; $FeSO_4$ 0.00005%; $MnSO_4$ 0.0005%; $MgSO_4$ 0.0005%, agar 2.0% and 0.02% guaiacol (indicator), pH6.0. The plates were incubated for 6-12 days at 30°C. Positive cultures were screened by observing brown coloration Olga et al. (15). The positive fungal isolates were grown on Sabouraud media [10 g/L peptone; 40 g/L dextrose; 15 g/L agar; pH 6.0] for their identification on basis of morphology.

Cultivation of fungal cultures and biomass studies

The isolated fungi were cultivated in LMM media (per liter: glucose 10 g; sodium tartrate 2.0 g; KH_2PO_4 1.0 g; $MgSO_4.7H_2O$ 0.5 g; KCl 0.5 g; yeast extract 1.0 g; $CuSO_4$ 150 µM; Na_2EDTA 0.5 g; $FeSO_4$ 0.2 g; $ZnSO_4.7H_2O$ 0.01 g; $MnCl_2.4H_2O$ 0.003 g; H_3BO_4 0.03 g; $CoCl_2.6H_2O$ 0.02 g; $CuCl_2.2H_2O$ 0.001 g; $Na_2MoO_4.2H_2O$ 0.003 g] Dhouib et al. (4) at 120 rpm for 5-10 days at 30^0C. The cultures were aseptically filtered through preweighed Whatman No 1 filter paper and mycelial mat was separated from the culture filtrate. The biomass of the fungal mat was determined after drying the filter paper along with mycelial mat was dried at 70°C until constant weight and subtracting the weight of filter paper from that of filter paper bearing mycelial mat. The experiment was

performed in triplicate. Fungal growth was expressed in terms of g/flask.The maximal fungal biomass accumulation was evaluated by varying media pH (4-8) and allowing growth up to 10 days.

Laccase enzyme activity

Fungal colonies tested positive on laccase plate assay were inoculated in LMM medium Dhouib et al. (4) and incubated at 30°C, 120 rpm for 6-14 days. 10 ml of the fungal culture was taken and filtered through Whatman no. 1 filter paper.

The filtrate was analyzed spectrophotometrically for presence of laccase activity according to the protocol described by Li et al. (13). The reaction mixture for laccase activity analysis comprised of 50 mM sodium tartrate buffer (pH 4.5), 0.5 mM 2,2'-azino-bis-(3-ethylbenzothiazoline)-6-sulphonic acid (ABTS), 1.0 ml filtrate sample and distilled water (final volume 3.0 ml). The contents were mixed well and the increase in absorbance was observed for 1 min at 420 nm (extinction coefficient 36 x 10^{-4}/mM cm) against reagent blank. Each assay was performed in triplicate. The protein concentration was determined Lowry et al. (14) using Bovine Serum Albumin (BSA) as standard. Enzyme activities were expressed in U/ml that means µmol of substrate oxidized per minute of reaction, according to the followed equation: Enzymatic activity (U/ml) = $(\Delta Abs x 10^6)$ $(\varepsilon RT)^{-1}$

Where, ΔAbs is the difference between final and initial absorbances, ε is the molar extinction coefficient of each enzyme (ε_{420} = 36 x 10^{-4}/mM cm), R is the volume of supernatant in ml and T is the reaction time in min.

Results and Discussion

The screening of laccase-producing fungi from upper horizons of litter showed that out of twenty eight positive species two formed fast and large reddish brown zones in medium due to oxidative polymerization of guaiacol (Fig. 1 (a) & (b). On the basis of microscopic structure, the selected laccase- positive fungi were identified to be *Verticillum* sp. and *Helminthosporium* sp. (Fig. 1 (c) & (d).

The Comparative analysis of biomass accumulation at various pH in culture broth showed maximum growth at pH 6.0 in both the selected fungi Studies on incubation time periods showed a maximum biomass production on the 10th day of incubation in both fungi, with 2.112 g accumulation in *Verticillum* sp. and a net 1.124 g in *Helminthosporium* sp.. At the 10th day of incubation, 900 µg/ml of extracellular protein secreted by *Verticillum* sp. into the culture broth and 750 µg/ml by *Helminthosporium* sp. as assayed by Lowry's

method.

Maximum laccase production by both fungi was also observed at the 10th day of incubation. The extinction coefficient values for laccase, as estimated by the standard protocol (Li et al. 2008) were found to be 18.1 U/ml and 14.7 U/ml for *Verticillum* sp. and *Helminthosporium* sp., respectively (Fig 2). In this study, *Verticillum* sp. represented a stronger potential for ABTS (substrate) reduction as compared to *Helminthosporium* sp. The study also clearly indicated that the laccase from *Verticillum* sp. possesses a higher catalyzing potential for the oxidation of *p*-diphenol with respect to *Helminthosporium* sp.

Verticillum sp. and *Helminthosporium sp*. produced an appreciable amount of laccase at levels compared to those reported for various white and brown rot fungi. (20, 3, 6, 16)The ease of their availability in litter or soil samples as well as efficient biomass production under culture conditions adds to their potential for development as laccase -producing strains. The laccase-producing fungi are currently the focus of much attention on submerged liquid culture (17) and this places a high value on the importance of fungi in soil ecology (2). It has been also reported that few plant pathogenic fungi like brown-rot fungi generate cathecol derivatives as result of demethylation which leads to lignin degradation (5). These fungal strains, therefore, offer promise for use in several bioprocesses involving laccase applications, such as biopulping, biobleaching, bioremediation, food technology and treatment of industrial waste water (10) and (19).

It has been concluded that, from a high number of fungal strains isolated from litter samples, the fungal isolates *Verticillum* sp. and *Helminthosporium* sp. were chosen because they exhibited a conspicuous oxidation of guaiacol on agar plates.

The cultivation studies on fungal strains showed high biomass accumulation as well high protein in LMM broth at pH 6.0 for 10th days. *Verticillum* sp. showed a laccase activity i.e., 18.1 U/ml whereas, 14.7 U/ml laccase activity was detected in culture supernatant of *Helminthosporium* sp. Therefore, the plant pathogenic fungal isolates, *Verticillum* sp. *and Helminthosporium* sp. were the most promising candidates for laccase enzyme production.

Acknowledgement: Financial support in the form of research project from CST (UP), India is greatly acknowledged.

References

1. Abadulla, E.; Tzanov, T.; Costa, S.; Robra, K.H.; Cavaco, Paula, A.; Gübitz, G.M. (2000). Decolorization and detoxification of textile dyes with a Laccase from *Trametes hirsuta*. *Appl. Environ. Microbiol.* 66, 3357-3362.
2. Bucher, V.V.C.; Hyde, K.D.; Pointing, S.B.; Reddy, C.A. (2004). Production of wood decay enzymes, mass loss and lignin solubilization in wood by marine ascomycetes and their anamorphs. *Fungal. Diversity*. 15, 1-14.
3. Coll, P. M., Tabernero, C., Santamarı´a, R., Pe´rez, P. (1993). Characterization and structural analysis of the laccase I gene from the newly isolated ligninolytic basidiomycete PM1 (CECT 2971). *Appl. Environ. Microbiol*. 59, 4129–4135.
4. Dhouib, A.; Hamza, M.; Zouari, H.; Mechichi, T.; H'midi, R.; Labat, M.; Martínez, M.J.; Sayadi, S. (2005). Autochthonous fungal strains with high ligninolytic activities from Tunisian biotopes. *Afr. J. Biotechnol.* 4, 431-436.
5. Filley, T.R., Hatcher, P.G., Shortle, W.C. and Praseuth, R.T. (2000), The application of 13C-labeled teramethylammonium hydroxide (13C-TMAH) thermochemolysis to the study of fungal degradation of wood. *Organic Geochem.*, 31, 181-198.
6. Fukushima, Y., Kirk, T. K. (1995). Laccase component of the Ceriporiopsis subvermispora lignin-degrading system. *Appl. Environ. Microbiol*. 61, 872–876.
7. Gianfreda, L.; Xu, F.; Bollag, J.M. (1999). Laccases: a useful group of oxidoreductive enzymes. *Bioremed. J.* 3, 1-25.
8. Higuchi, T. (1990). Lignin biochemistry: biosynthesis and biodegradation.

IJAETMAS

9. Hoegger, P.J.; Kilaru, S.; James, T.Y.; Thacker, J.R.; Kuees, U. (2006). Phylogenetic comparison and classification of Laccase and related multicopper oxidase protein sequences. *FEBS. J.* 273, 2308-2326.

10. Hublik, G.; Schinner, F. (2000). Characterization and immobilization of the laccase from *Pleurotus ostreatus* and its use for the continuous limitation of phenolic pollutant. *Enzyme. Microb. Technol.* 27, 330-336.

11. Kajikawa, H., Kudo, H., Kondo, T., Jodai, K., Honda, Y., Kuwahara, M. and Watanabe, T. (2000), Degradation of benzyl ether bonds of lignin by ruminal microbes. *FEMS Microbiol. Lett.*, 187, 15- 20.

12. Karam, J.; Nicell, J.A. (1997). Potential applications of enzymes in waste treatment. *J. Chemical. Technol. Biotechnol.* 69, 141-153.

13. Li, A.; Zhu, Y.; Xu, L.; Zhu, W.; Tian, X. (2008). Comparative study on the determination of assay for Laccase of *Trametes sp*. *Afr. J. Biochem. Res*. 2, 181-183

14. Lowry, O.M.; Rosebrough, N.J.; Farr, A.L.; Randall, R.J. (1951). Protein measurement with Folin Phenol reagent. *J. Biol. Chem*. 193, 265-275.

15. Olga, V.K.S.; Elena, V.S.; Valeria, P.G.; Olga, V.M.; Natalia, V.L.; Aida, N.D.; Alexander, I.J.; Alexander, M. (1998). Purification and characterization of the constitutive form of Laccase from basidiomycete Coriolus hirsutus and effect of inducers on Laccase synthesis. *Biotechnol. Appl. Biochem*. 28, 47-54.

16. Pela´ez, F., Martı´nez, M. J., Martı´nez, A. T. (1995). Screening of 68 species of basidiomycetes involved in lignin degradation. Mycol. Res. 99, 37–42.

17. Pointing, S.B.; Jones, E.B.G.; Vrijmoed, L.L.P. (2000). Optimization of laccase production by *Pycnoporus sanguineus* in submerged liquid culture.

IJAETMAS

18. Rastogi, S.; Dwivedi, U.N. (2008). Manipulation of lignin in plants with special reference to O-methyltransferase. *Plant. Sci.* 174, 264-277.
19. Robinson, T.; Chandran, B.; Nigam, P. (2001). Studies on the production of enzymes by white-rot fungi for the decolourisation of textile dyes. *Enzyme. Microb. Technol.* 29, 575-579.
20. Silva,.I.S; Menezes, C.R.; Franciscon, E.; Santos, E.C.; Durrant, L.R. (2010). Degradation of Lignosulfonic and Tannic Acids by Ligninolytic Soil Fungi Cultivated under Icroaerobic Conditions. *Braz. Arch. Biol. Technol.* 53, n. 3, 693-699.
21. Thurston, C. (1994). The structure and function of fungal Laccases. *Microbiology.* 140, 19-26.
22. Vinardell, M.; Ugartondo, V.; Mitjans, M. (2008). Potential applications of antioxidant lignins from different sources. *Indus. Crops. Products.* 27, 220-223.
23. Xu, F.; Shin, W.; Brown, S.H.; Wahleithner, J.A.; Sundaram, U.M.; Solomon, E.I.A. (1996). Study of a series of recombinant fungal Laccases and bilirubin oxidase that exhibit significant difference in redox potential, substrate specificity, and stability. *Biochim. Biophys. Acta.* 1292, 303- 311.

IJAETMAS

International Journal of Advancement in Engineering Technology, Management & Applied Science
Volume 2, Issue 7 July 2015 ISSN No: 2349-3224

List of Figures

Fig. 1

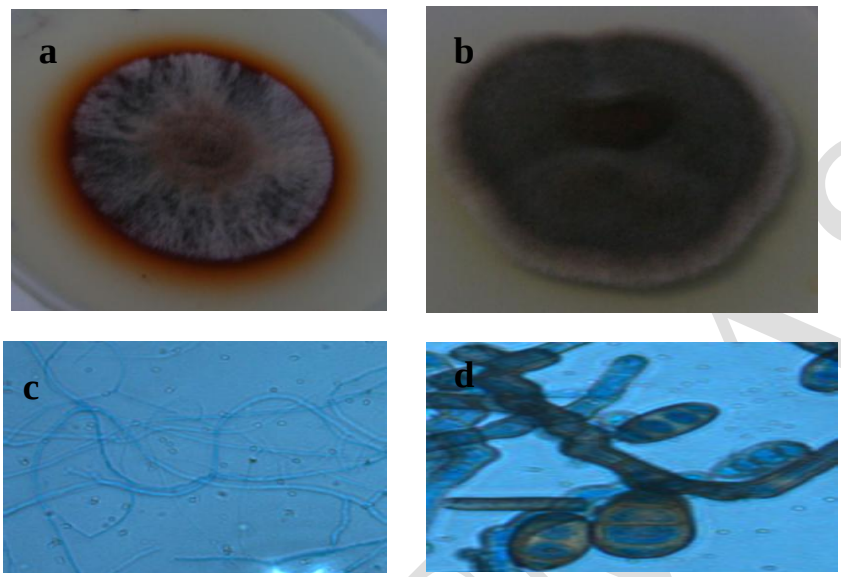

Fig. 2

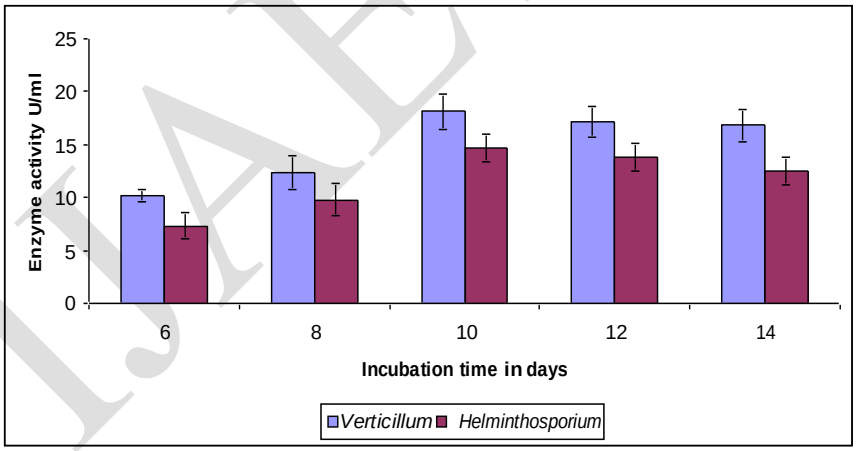

IJAETMAS

LEVERAGING INDIAN LABOUR FOR AUGMENTING FOREIGN DIRECT INVESTMENT

Dr. Archana Singh*

*Assistant Professor (Finance)

Delhi School of Management, Delhi Technological University, Delhi

(Formerly known as Delhi College of Engineering)

Ms. Priya Gupta Corresponding Author**

**Research Scholar

Delhi School of Management, Delhi Technological University, Delhi

(Formerly known as Delhi College of Engineering)

And

Assistant Professor (Finance) , Apeejay School of Management, Dwarka, New Delhi

Abstract

The aim of this study is to determine the extent of causality between labour force availability and Foreign Direct Investment (FDI) inflows in India, one of the emerging countries of the world, for the period 1990- 2013. Johansen Cointegration Technique followed by Vector Error Correction Model (VECM) and Coefficient Diagnostics (Wald Test Statistics) are employed to investigate this causality (whether long run or short run or both). The Johansen Cointegration result establishes a single cointegrating vector (long run relationship) between labour force availability and FDI inflows for India. After proving a cointegration, VECM and Wald Test Statistics revealed that there exists both long- run and short run causality running from labour force availability to FDI inflows. In other words, the demographic advantage is bringing more FDI inflows in India both in short and long run. With these findings, the study suggests that more labour reforms for the wages, social security, safety, welfare and working conditions should be brought out by the Indian Government to encourage more number of people to be able to contribute their skills and expertise to various industries. This in turn would enhance the output and capital formation of the country leading to more FDI inflows and competitiveness. This would also enable the domestic companies to increase their efforts to frame better sustainable strategies to remain in the market of globalized era.

Keywords: Foreign Direct Investment, Labour, Johansen Cointegration, Vector Error Correction Model, India

COPY RIGHT © 2015 Institute of Interdisciplinary Business Research

1. Introduction

Foreign Direct Investment (FDI) is a category of investment that reflects the objective of establishing a lasting interest by a resident enterprise in one economy (direct investor) in an enterprise (direct investment enterprise) that is resident in an economy other than that of the direct investor. The lasting interest implies the existence of a long-term relationship between the direct investor and the direct investment enterprise and a significant degree of influence (not necessarily control) on the management of the enterprise. The direct or indirect ownership of 10% or more of the voting power of an enterprise resident in one economy by an investor resident in another economy is the statistical evidence of such a relationship.

One of the noticeable tendencies in the world economy over the past two decades has been its increasing global economic integration. The world economy has seen an increasing internationalization with rising volumes of international trade and increasing levels of foreign investment flows, particularly that of direct investment. The latter primarily initiated by the Multinational Corporations (MNCs) and often seen as vehicles of international transfers of technology and finance.

However, the impact of globalization has been uneven across regions, countries and sectors. Some countries and regions have been able to get more integrated with the world economy with growing magnitudes of inward and outward Foreign Direct Investment (FDI) flows and other types of cross-border transactions, while others have been left relatively untouched. In this process new sources of FDI and technology have played an important role. Policy decisions concerning how to deal with large capital flows require an understanding about the factors driving such flows. The most pervasive idea among researchers and policy makers is that FDI enhances growth through diverse ways. It raises the capital base and employment opportunities; brings technological development for local firms, which in turn improves the productivity of host countries and stimulate economic growth. There are various existing theories related to contribution of FDI inflows to economic growth of the recipient countries, the findings of which are explained as under:

Endogenous Growth Models propounded by Romer (1986, 1987); Lucas (1988, 1990); Mankiw (1992); Balasubramanyam et. al. (1996) found that FDI leads to significant contribution towards Human Capital which includes both the managerial skills and Research & Development that ultimately enables the economies to grow in the long run. The other school of thought was given by the Dependency School Theory, supported by Stoneman (1975); Bornschier (1980); O' hearn (1990), which showed that FDI inflows lead to a negative impact on any economy in the long run because the first world nations become wealthy by extracting labour and other resources from Third World Nations and the Developing countries are insufficiently compensated for their natural resources which lead to continuing poverty. These theorists reached to this conclusion because they found that capitalism is a reason for global division of labour which leads to distortion which inturn hinders growth and increases income inequality and therefore there is negative impact on long term economic growth. Another coveted theory that explained the mid-

COPY RIGHT © 2015 Institute of Interdisciplinary Business Research

way between the above two theories is the Neo- Classical Growth Models advocated by Solow (1956); Ramirez (2000); Ram and Zhang (2002) who established that there exists negligible long-run growth effects of FDI flows. This phenomenon happens because the returns to physical capital keep on diminishing steadily and there is huge outflow of funds in the form of remittances of profits and dividends. Because of these contrasting opinions provided by eminent economists, this study attempts to understand whether labour force availability actually affects the FDI inflows in a country like India where there is a huge demographic advantage next to China.

Therefore, the rest of this paper is structured as follows: Section 2 provides a literature review on the potential determinants of FDI. Section 3 highlights the need of the study. Section 4 presents the Data, Methodological Framework and Modelling. This is followed by Section 5, Empirical Results while the final section 6 concludes with a summary and the policy implications of the study.

2. Literature Review

Several studies have analyzed the determinants of FDI for individual countries or groups of countries that are part of developing or developed markets. Marcelo Braga Nonnemberg and Mario Jorge Cardoso de Mendonca (2004) concluded that FDI is correlated to level of schooling, economy's degree of openness, inflation, risk and average rate of economic growth in developing countries. Khondoker Abdul Mottaleb and Kaliappa Kalirajan (2010) also demonstrated that developing countries with larger GDPs, higher GDP growth rates, higher proportion of international trade and a more business-friendly environment are more successful in attracting FDI. Harinder Singh and Kwang W. Jun (1995) found export orientation as the strongest variable for explaining why a developing country attracts FDI.

Various studies pertaining to specific developing countries include studies by Boopen Seetanah and Sawkut Rojid, (2011) who emphasized on trade openness, wages and the quality of labor as the most instrumental factors for attracting FDI in Mauritius. Andreia Alexandra Faria Severiano (2011) showed the importance of GDP per capita, degree of openness to trade, exchange rate, minimum wage, corporate tax rate and labor market flexibility while analyzing the determining factors for FDI in primary, secondary and tertiary sectors of Portugal. Another study which confirmed the results of the previous studies was by Gilmore et.al. (2003) who concluded that FDI is a preference to other forms of foreign market entry, size and growth of the host market, government emphasis on FDI and financial incentives, economic policy, cultural closeness, costs of transport, materials and labor, resources, technology, political stability and infrastructure are important determinants of FDI for Northern Ireland and Bahrain. Another study by Nguyen Ngoc Anh and Nguyen Thang (2007) in the Vietnam context gave importance to market, labor and infrastructure in attracting FDI. Elizabeth Asiedu (2001) suggested that *g*ood infrastructure, liberalized trade regimes and better government policies can help Africa to get more FDI flows. The main result is that natural resources and large markets promote FDI (Elizabeth Asiedu (2006)). Openness to trade, the size of the domestic market, stock of human

COPY RIGHT © 2015 Institute of Interdisciplinary Business Research

capital played a positive role while political instability and labor cost a negative role in attracting FDI in the African markets as explored by Sawkut et. al.(2009). Yuko Kinoshita and Nauro F. Campos (2003) explored institutions, agglomeration and trade openness as main determinants for FDI inflows in transition economies.

A study in China by Owen C. H. Ho (2004) indicated that market size, wage rate, degree of economic reform and innovation activities are important determinants of sectoral FDI in China. Chien-Hsun Chen (1996), Lv Na and W.S. Lightfoot (2006) determined that market expansion potential, labor cost, allocative efficiency, transportation linkages, and technological filtering are able to attract more FDI in the mainland China. Junjie Hong (2008) also emphasized the labor cost as an essential determinant for attracting FDI flows in China. Angelo et. al. (2010) concluded the importance of the consumer market and strength of consumer sales as the most important factor in explaining capital movements into Brazil. Bergsman et. al. (1999) suggested that Russia should switch to a more modern policy approach to FDI by eliminating the relatively extensive non-tariff protection given to the domestic market, phasing out existing tax preferences for foreign investors, and reducing significantly restrictions on FDI to a limited number of activities. Priya Gupta and Archana Singh (2013, 2014) also concluded in a very recent study on BRIC Nations that the most important factors for attracting FDI inflows are inflation rate, international liquidity, debt service as a percentage of export of goods and services of the country, current account as percentage of GDP, current account as percentage of export of goods and services, budget balance as a percentage of GDP and percentage unemployment in the country.

There are various studies pertaining to determinants influencing the FDI inflows in India specifically or as a part of some group like Vijayakumar et. al. (2010) concluded that Market size, Labor cost, Infrastructure, Currency value and Gross Capital formation are the potential determinants of FDI inflows of BRICS countries (which is an acronym commonly used to refer to Brazil, Russia, India, China and South Africa). Muhammad Azam and Ling Lukman (2010) also revealed that market size, external debt, domestic investment, trade openness, and physical infrastructure are the important economic determinants of FDI in Pakistan, India and Indonesia. Balasundram Maniam and Amitava Chatterjee (1998) conferred the importance of exchange rate for attracting US FDI in a developing country like India. Monica Singhania and Akshay Gupta (2011) revealed that GDP, inflation rate, scientific research, and FDI Policy changes have had a significant impact on FDI inflows into India. The financial strength of the state, development level of the state, size of the market and level of infrastructure were some other determining factors for FDI in India as studied by Neerja Dhingra and H.S. Sidhu (2011).

Thus, it can be seen from the above literature that there may be various studies regarding the causality (both short-run and long-run) between FDI and other economic determinants but there is hardly any study which captures the relationship between labour availability and FDI inflows in the context of India. This study also agrees that these relationships may vary from one country to another, one set of time period to another and is also influenced by numerous institutional

COPY RIGHT © 2015 Institute of Interdisciplinary Business Research

factors which must be considered before making any strategic changes in the policies affecting FDI inflows.

3. Need and objective of the study

This study is significant because there are various researchers who have contributed to the literature of FDI and economic determinants relationship but there is hardly any study which documents specifically whether labour availability in India induces the FDI inflows. The objective of this study is, thus, to determine whether there is any long run or short run relationship between these two variables using the VECM and Wald (1945) test statistics.

4. Data, Methodological Framework and Modelling

To study the inter-relationship between FDI and labour force availability, FDI net inflows (US bn. $) and Labour Force Availability (bn.) series are used. The sample country is India only. The period of analysis is from 1990-2013. Both the data series are compiled from World Development Indicators published by World Bank.

Johansen's (1988) Cointegration Test, Vector Error Correction Model (VECM) and Wald Test Statistics have been applied. Before implementing these techniques, econometric methodology needs to verify the stationarity of each individual time series since most macro economic data tend to be non- stationary. Thus, the Augmented Dickey Fuller (ADF) test is employed to examine stationary property of the selected data series.

5. Empirical Results and Discussions

The unit root property of the data series is crucial for the cointegration and causality analyses. Table 1 depicts the results of ADF test for the FDI and Labour Force series for India. The unit root test results revealed that the null hypothesis of unit root for the selected variables was not rejected at levels. But, when the series are first differenced, the FDI series is found to be stationary but there was no stationarity in Labour Series even after first difference. To conduct a test of cointegration both the variables should be integrated of the same order. So, after second differencing, it was found that both the series become stationary and are therefore integrated at the order of two, I*(2)*.

[Insert Table 1 here]

Proven that both the series are integrated of the same order I(*2*), the Johansen Cointegration test is performed to examine the presence of long run association between FDI and Labour Force for India and the results are presented in Table 2. In the table, the Johansen's Trace Statistics and Maximum Eigen Statistics indicates that the null hypothesis of no cointegrating vector (r=0) can be rejected at five percent significance level and the alternative hypothesis of at most one cointegrating vector ($r \geq 1$) can be accepted. Therefore, the results support the hypothesis of

COPY RIGHT © 2015 Institute of Interdisciplinary Business Research

cointegration between FDI and Labour Force, implying that there is stable long-run relationship between the two variables in case of India.

[Insert Table 2 here]

After confirming the existence of single cointegrating vector among FDI and Labour Force, a proper VECM is to be developed to determine the direction of long run causation. By using the definition of cointegration, the Granger Representation Theorem (Engle and Granger (1987)) states that if a set of variables are cointegrated, then there exists valid error correction representations of the data. For the purpose, the VECM is estimated and its results are presented in Table 3. Besides, the VECM is sensitive to the selection of optimal lag length. Thus, the necessary lag length of FDI and Labour Force series is determined by Schwarz Information Criteria (SC) and it reveals the optimal lag length of five in this case.

[Insert Table 3 here]

The value of coefficient of C(1), i.e. the Error Correction term is -2.838520 (it must be negative as this shows the speed of adjustment towards equilibrium). It is in this case 283% which is statistically significant at 5% level as its value is less than 0.05 (i.e. 0.0011). The value of C(2) to C(11) represent the coefficients of the independent variable, i.e. past lags of Labour Force which are also known as short run coefficients. C(2), C(3), C(4), C(6), C(7) and C(8) are statistically significant at 5% level of significance (p-value is less than 0.05) and thus impacting the FDI inflows of India. C(10) is also impacting the FDI inflows significantly at 10% level of significance (p- value is less than 0.1). R- square of the model is 92% which is also more than 60%. Thus, it is a model of good fit. F-statistic of the model is 6.764529 and its probability is 0.014354 which is less than 0.05, i.e. all the independent variables jointly are significantly impacting/ influencing the value of dependent variable, i.e. FDI inflows.

Once the long run causality among the variables is tested, short run causal relation can also be tested among the dependent and past values of independent variable jointly. It can be tested with the help of Wald Statistics. Null Hypothesis for testing the short run causality is that the past lags of independent variable, i.e. FDI can not jointly influence the value of dependent variable, i.e. Labour Force. If the probability value of Chi- square in the Wald Statistics is less than 0.05, the Null Hypothesis is rejected or vice versa. The results of the short run causality are summarized in the following table:

[Insert Table 4 here]

The above table related to Coefficient Diagnostics (i.e. Wald Statistics) reveals that there is also a short run causality running from labour force availability to FDI inflows as the Chi-square Statistics is statistically significant at one percent level. This means that even in a short period of time, labour force can make a difference in the FDI inflows coming to India as this is one of the most important determinants for attracting FDI inflows as proven in the above models.

COPY RIGHT © 2015 Institute of Interdisciplinary Business Research

6. Conclusion and Policy Implications

The Johansen Cointegration result establishes a single cointegrating vector (long run relationship) between labour force availability and FDI inflows for India. After proving a cointegration, VECM and Wald Test Statistics revealed that there exists both long- run and short run causality running from labour force availability to FDI inflows. In other words, the demographic advantage is bringing more FDI inflows in India both in short and long run. With these findings, the study suggests that more labour reforms for the wages, social security, safety, welfare and working conditions should be brought out by the Indian Government to encourage more number of people to be able to contribute their skills and expertise to various industries. This in turn would enhance the output and capital formation of the country leading to more FDI inflows and competitiveness. This would also enable the domestic companies to increase their efforts to frame better sustainable strategies to remain in the market of globalized era. More specifically, this study emphasizes that labour market conditions in a country have a significant impact in determining the extent of FDI inflows.

COPY RIGHT © 2015 Institute of Interdisciplinary Business Research

References

Alexandra, A. F. S (2011), The Determinants of FDI in Portugal – A Sectoral Approach, Dissertation submitted in partial fulfillment of requirements for the degree of Master of Science in Economics, at the Universidade Católica Portuguesa from www.clsbe.lisboa.ucp.pt/resources/.../Andreia%20Severiano.pdf.

Angelo et.al. (2010), Determinants of FDI in Emerging Markets: Evidence from Brazil, *International Journal of Commerce and Management*, 20(3), 203 – 216.

Asiedu, E (2001), On the Determinants of Foreign Direct Investment to Developing Countries: Is Africa Different?, Available at SSRN: http://ssrn.com/abstract=280062 or http://dx.doi.org/10.2139/ssrn.280062.

Asiedu, E (2006), Foreign Direct Investment in Africa: The Role of Natural Resources, Market Size, Government Policy, Institutions and Political Instability, *The World Economy*, 29(1), 63-77, Available at SSRN: http://ssrn.com/abstract=875105 or http://dx.doi.org/10.1111/j.1467-9701.2006.00758.x.

Azam, M and Lukman, L (2010), Determinants of Foreign Direct Investment in India, Indonesia and Pakistan: A Quantitative Approach, *Journal of Managerial Sciences*, IV(1), 31-44.

Balasubramanyam, V. N., Salisu, M. A. and Sapsford, D. (1996), Foreign Direct Investment and Growth in EP and IS countries, *Economics Journal*, 106, 92-105.

Bergsman et. al. (1999), Improving Russia's Foreign Direct Investment Policy Regime, Available at SSRN: http://ssrn.com/abstract=288774 or http://dx.doi.org/10.2139/ssrn.288774.

Bornschier, V. (1980), Multinational Corporations and Economic Growth: A Cross National Test of the Decapitalisation, Thesis, *Journal of Development Economics*, 7(2), 115-135.

Campos, N. F. and Kinoshita, Y. (2002), Foreign Direct Investment as Technology Transferred: Some Panel Evidence from the Transition Economies, *CPER Discussion Paper* no. 3417, centre for Economic Policy Research, London, United Kingdom.

Chen, C-H (1996), Regional Determinants of Foreign Direct Investment in Mainland China, *Journal of Economic Studies*, 23(2), 18 – 30.

Dhingra, N and Sidhu, H.S. (2011), Determinants of Foreign Direct Investment Inflows to India, *European Journal of Social Sciences*, 25(1), 21-31.

Engle, R. F. and Granger, C. W. J. (1987), Co-integration and Error Correction Representation, Estimation and Testing, *Econometrica*, 55(5), 286-301.

Gilmore et.al. (2003), Factors influencing Foreign Direct Investment and International Joint Ventures: A Comparative Study of Northern Ireland and Bahrain, *International Marketing Review*, 20(2), 195 – 215.

Gupta, P and Singh, A (2013), Determinants of FDI In BRIC Nations: A Review of Existing Literature In Kama, K. et.al. (Eds.), *Innovative Financial Practices and Development:*

COPY RIGHT © 2015 Institute of Interdisciplinary Business Research

Emerging Financial Paradigms. Paper presented at Apeejay School of Management, India, 20 December, 103- 117.

Gupta, P and Singh, A (2014), Macro Economic Determinants of Foreign Direct Investment in BRIC Nations, *South Asian Journal of Marketing & Management Research (SAJMMR)*, 4(2), 1-12.

Ho. H. C. O (2004), Determinants of Foreign Direct Investment in China: A Sectoral Analysis, 4(18) of Discussion paper, the University of Western Australia, Business School, Economics, 1-29.

Hong, J (2008), WTO Accession and Foreign Direct Investment in China, *Journal of Chinese Economic and Foreign Trade Studies*, 1(2), 136 – 147.

Johansen, S. (1988), Statistical Analysis and Cointegrating Vectors, *Journal of Economic Dynamics and Control*, 12(2-3), 231-254.

Kinoshita, Y. and Campos, N. F. (2003), Why does FDI Go Where it Goes? New Evidence from the Transition Economies, *William Davidson Institute Working Paper* No. 573. Available at SSRN: http://ssrn.com/abstract=414540 or http://dx.doi.org/10.2139/ssrn.414540.

Lucas, L. (1990), Why doesn't Capital Flow from Rich to Poor Countries, *AEA papers and Proceedings*, 80(2), 92-96.

Lucas, R. (1988), On the Mechanics of Economic Development, *Journal of Monetary Economics*, 22(1), 3-42.

Maniam, B and Chatterjee, A (1998), The Determinants of US Foreign Investment in India: Implications and Policy Issues, *Managerial Finance*, 24(7), 53 – 62.

Mankiw, N., Romer, D., and Weil, D. (1992), A Contribution to the Empirics of Economic Growth, *The Quarterly Journal of Economics*, 107(2), 408-437.

Mottaleb, K. A. and Kalirajan, K (2010), Determinants of Foreign Direct Investment in Developing Countries: A Comparative Analysis, Margin— *The Journal of Applied Economic Research*, 4(4), 369–404.

Na, L and Lightfoot, W.S. (2006), Determinants of Foreign Direct Investment at the Regional Level in China, *Journal of Technology Management in China*, 1(3), 262 – 278.

Nguyen, A. N. and Nguyen, T (2007), Foreign Direct Investment in Vietnam: An Overview and Analysis the Determinants of Spatial Distribution across Provinces, Available at SSRN: http://ssrn.com/abstract=999550 or http://dx.doi.org/10.2139/ssrn.999550.

Nonnemberg, M. B. and Mendonca, M. J. C. (2004), www.anpec.org.br/encontro2004/artigos/A04A061.pdf.

O'Hearn, D. (1990), TNCs, Intervening Mechanisms and Economic Growth in Ireland: A Longitudinal Test and Extension of Bornschier Model, *World Development*, 18(1), 417- 429.

COPY RIGHT © 2015 Institute of Interdisciplinary Business Research

Osterwald- Lenum, M. (1992), A Note with Quantiles of the Asymptotic Distribution of the Maximum Likelihood Cointegration Rank Test Statistic, *Oxford Bulletin of Economics and Statistics*, 54(3), 461-472.

Ram, R. and Zhang, K. H. (2002), Foreign Direct Investment and Economic Growth: Evidence from Cross- Country Data for the 1990s, *Economic Development and Cultural Change*, 51(1), 205-215.

Ramirez, M. D. (2000), Foreign Direct Investment in Mexico: A Cointegration Analysis, *The Journal of Development Studies*, 37(1), 138-162.

Romer, M. (1986), Increasing Returns and Long- Run Growth, *Journal of Political Economy*, 94(5), 1002-1037.

Romer, M. (1987), Growth Based on Increasing Returns due to Specialization, *American Economic Review*, 77(1), 56-62.

Sawkut et. al. (2009), Determinants of FDI: Lessons from the African Economies, *Journal of Applied Business and Economics*, 9(1), 1-16.

Seetanah, B and Rojid, S (2011), The Determinants of FDI in Mauritius: A Dynamic Time Series Investigation, *African Journal of Economic and Management Studies,* 2(1), 24 – 41.

Singh, H and Jun, K. W. (1995), Some New Evidence on Determinants of Foreign Direct Investment in Developing Countries, *World Bank Policy Research* Working Paper No. 1531. Available at SSRN: http://ssrn.com/abstract=623885.

Singhania, M and Gupta, A (2011), Determinants of Foreign Direct Investment in India, *Journal of International Trade Law and Policy,* 10(1), 64 – 82.

Solow, R. M. (1956), A Contribution to the Theory of Economic Growth, *Quarterly Journal of Economics*, 70(1), 65-94.

Stoneman, C. (1975), Foreign Capital and Economic Growth, *World Development*, 3(1), 11-26.

Vijayakumar et.al. (2010), Determinants of FDI in BRICS Countries: A panel analysis**,** *International Journal of Business Science and Applied Management,* 5(3), 1-13.

Wald, A. (1945), Sequential Tests of Statistical Hypotheses, *The Annals of Mathematical Statistics*, 16(2), 117-186.

COPY RIGHT © 2015 Institute of Interdisciplinary Business Research

Table 1: Results of ADF Unit Root Test (At Levels, First Difference and Second Difference)

Variables	At Levels		
	Intercept	**With Intercept and Trend**	**Without Intercept and Trend**
FDI	-0.924114	-2.203794	-0.117994
Labour Force	-1.028078	-3.073236	1.384076
	At First Difference		
	Intercept	**With Intercept and Trend**	**Without Intercept and Trend**
FDI	-5.391866*	-5.264502*	-5.278753*
Labour Force	-1.848493	-1.836990	-0.896317
	At Second Difference		
	Intercept	**With Intercept and Trend**	**Without Intercept and Trend**
FDI	-8.956067*	-8.730990*	-9.195318*
Labour Force	-4.449411*	-4.307621**	-4.585308*

Note: ** and ** indicates significance at one and five percent level respectively. Optimal Lag Length is determined by the Schwarz Information Criteria (SC) for the ADF Test.*

Table 2: Results of Johansen's Cointegration Test

Vector (s)	Trace Statistics	Max-Eigen Statistics	5 percent Critical Value for Trace Statistics	5 percent Critical Value for Max- Eigen Statistics	Remarks
H_0: r=0	24.90707*	17.49400**	15.49471	14.26460	***Cointegration***
H_1: r≥1	7.413070*	7.413070*	3.841466	3.841466	

Notes: ** and ** indicates significance at one and five percent level respectively. The significance of the statistics is based on one and five percent critical values obtained from Osterwald- Lenum (1992), r is the number of cointegrating vectors. H_0 represents the null hypothesis of presence of no cointegrating vector and H_1 represents the alternative hypothesis of presence of cointegrating vector.*

COPY RIGHT © 2015 Institute of Interdisciplinary Business Research

Table 3: Results of VECM pertaining to Causal Nexus between FDI and Labour Force (LONG RUN CAUSALITY)

	Coefficient	Std. Error	t-Statistic	Prob.
C(1)	-2.838520	0.483643	-5.869043	0.0011
C(2)	1.513819	0.339518	4.458729	0.0043
C(3)	0.973302	0.229024	4.249779	0.0054
C(4)	0.519531	0.202700	2.563062	0.0427
C(5)	-0.078811	0.123379	-0.638771	0.5466
C(6)	0.286024	0.098113	2.915260	0.0268
C(7)	-41.82364	8.894563	-4.702158	0.0033
C(8)	-55.10815	12.87923	-4.278839	0.0052
C(9)	-18.03549	12.33633	-1.461982	0.1941
C(10)	-29.21630	13.99030	-2.088325	0.0818
C(11)	0.631882	8.702313	0.072611	0.9445
C(12)	1.731847	0.330530	5.239608	0.0019
R-squared	0.925382	Mean dependent var		0.143064
Adjusted R-squared	0.788583	S.D. dependent var		0.370542
S.E. of regression	0.170376	Akaike info criterion		0.466900
Sum squared resid	0.174167	Schwarz criterion		0.126682
Log likelihood	16.20210	Hannan-Quinn criter.		0.385053
F-statistic	6.764529**	Durbin-Watson stat		2.945667
Prob(F-statistic)	0.014354			

Note: *** indicates significance at five percent level.*

Table 4: Results of Coefficient Diagnostics (i.e. Wald Statistics) pertaining to Causal Nexus between FDI and Labour Force (SHORT RUN CAUSALITY)

Chi- square Statistics	Probability	Inference (Short Run Causality running from)
43.36550*	0.0000	**Labour Force → FDI inflows**

Note: *Optimal Lag Length is determined by the Schwarz Information Criterion (SC). * denotes the significance at one percent level.*

COPY RIGHT © 2015 Institute of Interdisciplinary Business Research

APPENDIX

Foreign Direct Investment Net Inflows (Us Bn. $) and Labour Force Availability (Bn.)

Year	FDI net inflows (US bn. $)	Labour (bn.)
1990	0.23669	0.33072
1991	0.073538	0.338668
1992	0.276512	0.346803
1993	0.55037	0.355116
1994	0.973271	0.363
1995	2.143628	0.369789
1996	2.426057	0.377266
1997	3.57733	0.384187
1998	2.634652	0.391155
1999	2.168591	0.398161
2000	3.584217	0.40519
2001	5.471947	0.417145
2002	5.62604	0.428602
2003	4.322748	0.440213
2004	5.771297	0.451935
2005	7.269407	0.464498
2006	20.02912	0.465456
2007	25.22774	0.466033
2008	43.40628	0.466234
2009	35.58137	0.466896
2010	27.39689	0.466391
2011	36.49865	0.469805
2012	23.99569	0.472126
2013	28.15303	0.481236

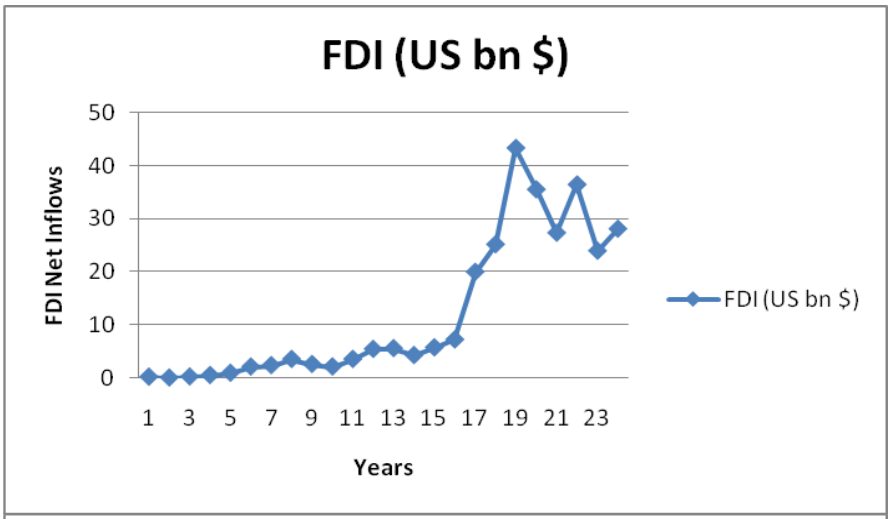

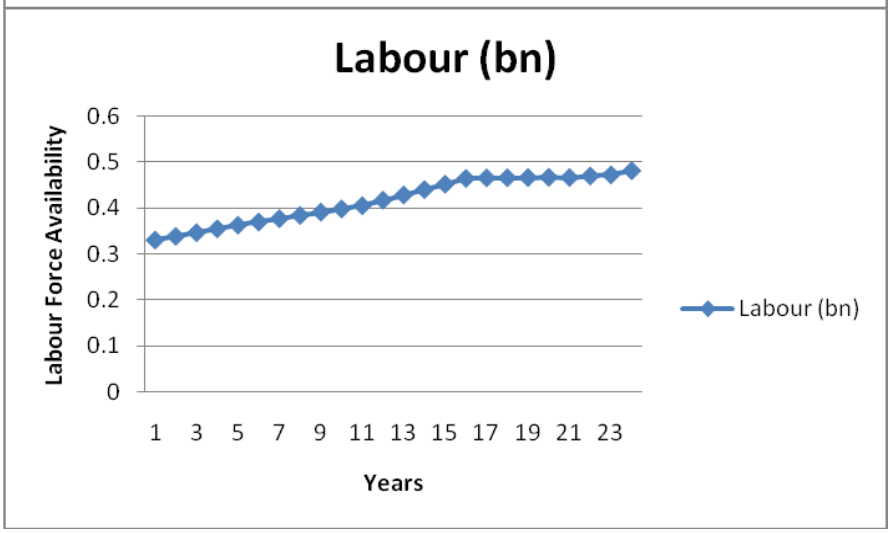

Source: *World Development Indicators, Published by World Bank (Accessed on 21.4.2015). Table and figures are author's own compilation.*

COPY RIGHT © 2015 Institute of Interdisciplinary Business Research

Accepted Manuscript

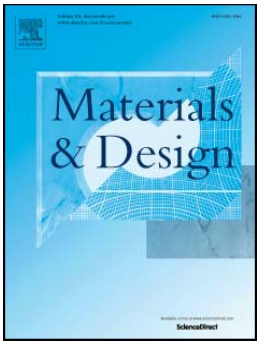

Mechanical properties and microstructure of spark plasma sintered nanostructured p-type SiGe thermoelectric alloys

Sivaiah Bathula, M. Jayasimhadri, Ajay Dhar

PII: S0264-1275(15)30267-7
DOI: doi: 10.1016/j.matdes.2015.08.017
Reference: JMADE 425

To appear in:

Received date: 8 June 2015
Revised date: 9 July 2015
Accepted date: 3 August 2015

Please cite this article as: Sivaiah Bathula, M. Jayasimhadri, Ajay Dhar, Mechanical properties and microstructure of spark plasma sintered nanostructured p-type SiGe thermoelectric alloys, (2015), doi: 10.1016/j.matdes.2015.08.017

This is a PDF file of an unedited manuscript that has been accepted for publication. As a service to our customers we are providing this early version of the manuscript. The manuscript will undergo copyediting, typesetting, and review of the resulting proof before it is published in its final form. Please note that during the production process errors may be discovered which could affect the content, and all legal disclaimers that apply to the journal pertain.

ACCEPTED MANUSCRIPT

Mechanical properties and microstructure of spark plasma sintered nanostructured p-type SiGe thermoelectric alloys

Sivaiah Bathula[1,2], M. Jayasimhadri[2] and Ajay Dhar[1,*]

[1]*CSIR-Network of Institutes for Solar Energy, CSIR-National Physical Laboratory, Dr. K. S. Krishnan Marg, New Delhi -110012, India*
[2]*Department of Applied Physics, Delhi Technological University, Delhi, India*

Abstract

SiGe based thermoelectric (TE) materials have been employed for the past four decades for power generation in Radio-isotope thermoelectric generators (RTG). Recently "nanostructuring" has resulted in significantly increasing the figure-of-merit (ZT) of both n and p-type of SiGe and thus nanostructured $Si_{80}Ge_{20}$ alloys are evolving as a potential replacement for their conventional bulk counterparts in designing efficient RTGs. However, apart from ZT, their mechanical properties are equally important for the long term reliability of their TE modules. Thus, we report the mechanical properties of p-type nanostructured $Si_{80}Ge_{20}$ alloys, which were synthesized employing spark plasma sintering of mechanically alloyed nanopowders of its constituent elements with 1.2% boron doping. Nanostructured p-type $Si_{80}Ge_{20}$ alloys exhibited a hardness of ~9 ± 0.1 GPa, an elastic modulus of ~135 ± 1.9 GPa, a compressive strength of 108 ± 0.2 MPa, fracture toughness of ~1.66 ± 0.04 MPa√m with a thermal shock resistance value of 391 ± 21 Wm^{-1}. This combination of good mechanical properties coupled with higher reported ZT of nanostructured p-type $Si_{80}Ge_{20}$ alloys are render it to be a potential material for power generation applications, compared to its bulk counterpart.

Keywords: Nanostructured p-type $Si_{80}Ge_{20}$ alloy, Thermal Shock Resistance, Fracture Toughness, Spark Plasma Sintering, Compressive Strength, Hardness, Elastic Modulus.

* Corresponding author: adhar@nplindia.org
Tel.: +91 11 4560 9456; Fax: +91 11 4560 9310

ACCEPTED MANUSCRIPT

1. Introduction

The direct conversion of heat into electricity based on Seebeck effect is an eco-friendly alternative for power generation owing to the energy crisis due to the fast depleting fossil fuels, expensive oil and gas[1] coupled with growing concerns for environmental pollution[2]. With the advent of efficient thermoelectric materials (TE) the thermoelectric power generation technology is gradually evolving as a suitable alternative to the other existing renewable sources of energy.[1] Currently, there are a host of TE materials that are available[3, 4] with relatively high figure-of-merit (ZT) in the low & intermediate temperature range which includes chalcogenide based materials[1], half-Heusler based[5], oxide based[6] and other complex alloys[7-10]. However, among the high temperature TE materials SiGe alloys represent a unique class of materials which possess reasonably high thermoelectric performance, are chemically stable and can be synthesized both as n & p-type materials[11]. Due to their unique properties these alloys have been extensively used as a power source in radioisotope TE generators (RTGs), in spacecrafts for remote terrestrial and extraterrestrial deep space missions[11, 12]. Due to its ideal thermoelectric and other related properties SiGe-based alloys are also being explored for their application in conventional thermoelectric devices for energy generation by replacing the expensive Ge with some cheaper dopants without compromising the ZT[13-15].

Despite being extensively used in RTG application, bulk SiGe suffers from an impediment in terms of their limited TE conversion efficiency of their devices ~ 5 - 6%, which is primarily due to the low ZT values of both, their n-type (ZT = 0.93)[11, 16] and p-type (ZT = 0.5)[11, 17]. However, in the recent past, “nanostructuring” has led to a significant increase in their ZT values for both, n and p-type nanostructured $Si_{80}Ge_{20}$ alloys[18-20], which are significantly higher than their bulk counterparts[11], currently used for RTG applications. Owing to their enhanced TE performance, these nanostructured SiGe alloys are being seriously considered for the application

ACCEPTED MANUSCRIPT

in RTGs, replacing their conventional bulk counterparts [15, 19, 21]. Most of the research done thus far on SiGe has been primarily directed towards enhancing their ZT for increasing their thermoelectric conversion efficiency[17, 22] by optimizing their thermal and electrical transport properties,[23] employing various approaches[9, 24]. However, in order to ensure the performance and long term reliability of SiGe-based TE modules the knowledge of their mechanical properties is equally important[25, 26]. In TE devices for power generation, the individual TE elements are subjected to significant stresses under actual service conditions, due to thermal cycling as well as thermal expansion mismatch. This more true for TE devices operating at high temperature, such as, SiGe-based devices, as thermal recycling at these high temperatures (~ 900°C) can generate significant amount stress at the SiGe interfaces. Also, in order to ensure the structural reliability of TE modules, it is imperative that their device elements must withstand numerous mechanical vibrations and thermal stresses while in-operation[27]. Thus, apart from ZT, the mechanical properties of SiGe alloys are equally vital in order to avoid catastrophic failure of their TE modules. Despite this there is no comprehensive reported data in the existing literature on a complete set of mechanical properties of nanostructured p-type $Si_{80}Ge_{20}$ alloy[28], although these properties have been recently reported for its n-type nanostructured $Si_{80}Ge_{20}$ counterpart by the authors[29, 30].

In the present study, we report the detailed mechanical properties of nanostructured p-type $Si_{80}Ge_{20}$ alloys at room temperature, synthesized employing the Spark Plasma Sintering (SPS) of mechanically alloyed nanostructured powders. The results suggest that these nanostructured alloys exhibit superior mechanical properties compared to most of the existing state-of-the-art TE materials in terms of hardness and fracture toughness. However, these properties of the p-type nanostructured $Si_{80}Ge_{20}$ alloy, synthesized in the present study, are lower to those reported earlier for n-type nanostructured $Si_{80}Ge_{20}$ counterpart[31-34], but the fracture toughness was

ACCEPTED MANUSCRIPT

found to be comparable[35]. The thermal shock resistance of the p-type nanostructured $Si_{80}Ge_{20}$ alloys, which is the main parameter for designing TE devices, exhibited a value which is superior to other existing TE materials[29, 36]. Although, it would have been more meaningful to report the mechanical properties of nanostructured SiGe alloys at actual device operating temperatures (~ 900°C), however, such tests at these high temperatures are rather challenging and are presently in progress and would be reported in due course of time.

2. Experimental procedure

Si (99.99%), Ge (99.99%) and 1.2% of B (99.99%) powders all from *M/s. Alfa Aesar, USA* were taken in chemical stoichiometric proportion and mechanically milled in a high-energy ball-mill *(Fritsch, Model: Pulverisette-4)* in an argon atmosphere with a speed of 400 rpm for an optimized time period of ~90 hours. The vial of the ball-mill and the milling media were made of stainless steel and the ball-to-powder weight ratio was optimized at 20:1. About 2 wt.% of stearic acid was added as a process control agent, to promote fracturing of the powder particles. Prior to sintering, ball milled alloy powders were processed in a glove box *(Mbraun, MB20)* to avoid oxidation and other atmospheric contamination. Phase identification and crystallite size determination were carried out employing x-ray powder diffraction *(XRD, Rigaku Inc., Japan)*. The ball-milled nanostructured alloy powders were subsequently consolidated and sintered under vacuum (~4 Pa) using spark plasma sintering *(SPS Syntex, SPS 725)* under a pressure of 60 MPa an optimized at temperature of 1150°C with a soaking time of 3 minutes. SPS heating rate of 400°C/minute was maintained in all sintering conditions where graphite die and punches were used to form a circular disk of size 12.7 mm diameter. Transmission electron microscopy (HRTEM) experiments were performed by using a HRTEM *(FEI, Tecnai G2 F30 STWIN)* operated at the electron accelerating voltage of 300 kV using field emission gun as an electron

ACCEPTED MANUSCRIPT

source. Specimens for electron microscopy were prepared by employing mechanical polishing followed by subsequent ion milling. Mechanical polishing was carried out on the specimen of 3 mm diameter disc to 100 μm and further thickness was reduced to 20 to 30 μm by utilizing a dimple grinder *(South Bay Technology, 515 CE,)*. Subsequently ion beam milling was carried out using an ion milling system *(South Bay Technology, Baltec RES 101)* at 7 kV and low angle milling to have an ultimate perforation to make the specimen transparent to the electron beam. Field Emission Scanning Electron Microscope *(FESEM, Zeiss, Supra 40VP)* was used to study the morphology and indentation-crack length determination. The density was measured using the conventional Archimedes principle and all the nanostructured samples were exhibited a density of ~ 98.3%. Fracture toughness measurements were carried out employing the indentation-crack technique using Vickers micro-hardness tester *(Future Tech. Corp., FM-e7)* with a load of 19.6 N for 10 s of indentation time. Elastic modulus and hardness were determined using nano-indentation technique *(Fischer-Cripps)* at a load of 10 mN and mechanical properties were derived from the measured load-penetration depth curves under loading/unloading through standard data analysis software. Compression tests (Instron, 4204) were performed at room temperature as per ASTM standard (ASTM: E9-09) with an aspect ratio of ~2.5 under uniaxial compressive loading with a strain rate of 2×10^{-5} s^{-1}. All the mechanical property parameters were measured on 8 samples and their average values have been reported.

3. Results and Discussion

3.1 Microstructural characterization

Fig.1 shows the XRD patterns of un-milled starting powders of Si and Ge Fig. 1(a), their mechanically alloyed nanostructured powders (Fig. 1(b)) and spark plasma sintered nanostructured $Si_{80}Ge_{20}$ alloy (Fig. 1(c)). It is apparent from Fig. 1(a &b) that after 90 hours of

ACCEPTED MANUSCRIPT

high energy ball-milling, Ge completely dissolves in the Si matrix and the peaks exhibit a significant broadening. This peak broadening is attributed to nanostructuring as well as a considerable amount of strain in the nanopowders due to the impact and shear forces of milling media during milling which usually leads to the sub-grain formation along with high angle grain boundaries in the nanostructured powders[37, 38]. The average crystallite size of $Si_{80}Ge_{20}$ nanopowders after 90 hours of high energy ball-milling (Fig. 1b), calculated using Williamson-Hall method[39] was found to be ~13 nm. Fig. 1 (c) further suggests that after SPS of $Si_{80}Ge_{20}$ nanopowders at 1150°C, the XRD patterns indicate a single-phase SiGe and its crystallite size was estimated to be ~ 20 nm. It is well known that $Si_{80}Ge_{20}$ alloy is an isomorphous binary phase system where Ge has a complete solid solubility in Si[40]. It was observed from the analysis of the XRD data that nanostructured $Si_{80}Ge_{20}$ alloy exhibited a diamond-like cubic structure, space group of $Fd\bar{3}m$, with a lattice parameter 5.47Å, which was in perfect agreement with that calculated using modified Vegard's law[15]. The HRTEM image of ball-milled $Si_{80}Ge_{20}$ nanopowders, as shown in Fig. 2 (a), suggests agglomerated particles in the size range of ~ 50 - 200 nm. However, the atomic/lattice scale images of these nanopowders, as shown in Fig. 2 (b), revealed randomly oriented individual crystallites in the size range ~ 9 - 14 nm, with an average crystallite size of ~12 nm, which is in reasonable agreement with that estimated from the XRD data ((Fig.1(b)). A detailed microstructural characterization of spark plasma sintered nanostructured $Si_{80}Ge_{20}$ alloy employing HRTEM elucidated several interesting microstructural features on a lattice scale. Fig. 3(a) typically elucidates two well-oriented nanocrystallites (marked as A & B) with an inter-planar spacing of 0.32 nm corresponding Si: hkl-indices of 111 and their grain boundary is marked by a white dotted line. It can also be noted from this figure that the angular separation between these two variants of 111 plane was about 75°, which was further confirmed by measuring the angle between these two planes in reciprocal space by

ACCEPTED MANUSCRIPT

recording their corresponding fast fourier transform (FFT) (inset in Fig. 3a). Fig. 3(b), which shows an atomic scale image of nanostructured $Si_{80}Ge_{20}$ alloy, clearly shows crystallites of SiGe matrix of different dimension, randomly oriented with respect to each other. These post-sintering nano-scale features were attributed to the rapid heating rates achieved by DC pulsated current employed during SPS, which considerably inhibited the grain growth[41, 42]. SPS is known to result in sintered products with near-theoretical density while retaining the nano-scale features introduced during ball milling[43]. The Raman spectrum for un-milled, high-energy ball-milled and the sintered nanostructured $Si_{80}Ge_{20}$ alloys is shown in Fig. 4. The shift of the peak position (Si-Si) to the lower wave-numbers was attributed to the deformation of the lattice[44] due to nanostructuring and lattice scale defects[45] introduced during high-energy ball-milling and similar kind of behavior has also been reported by earlier in strained Si-Ge alloys[46].

3.2 Mechanical properties

3.2.1 Nanoindentation

Hardness and elastic modulus of nanostructured $Si_{80}Ge_{20}$ alloy has been measured employing nanoindentation technique[47, 48] using a Berkovich indenter with a load of 10 mN in the submicron depth range with nanometer resolution. A typical load-displacement curve for nanostructured $Si_{80}Ge_{20}$ alloy is shown in Fig. 5, which includes both the elastic and plastic deformation. The elastic modulus was determined from the slope of the unloading curve (dP/dh) and the depth of the contact circle (h_c) at maximum load (P_{max}). Further, the hardness values were derived from the indentation load and projected contact area [48-51]. The measured hardness and elastic modulus values estimated from this technique were found to be ~9 ± 0.1 GPa and ~135 ± 1.9 GPa, respectively. Although these values are considerably higher than those

ACCEPTED MANUSCRIPT

reported for other state-of-the-art TE materials[29, 30, 32, 34, 35, 52], but are lower than those reported by the authors for n-type $Si_{80}Ge_{20}$ nanostructured alloys[29, 30].

3.2.2 Fracture Toughness

Accurately measuring the fracture toughness of brittle materials can often be challenging. Creating sharp pre-cracks can be difficult without catastrophically failing the specimen, while fracture toughness data using notched specimens can give erroneously values. Owing to these reasons, estimating fracture toughness by making direct measurements of cracks created using a sharp diamond indenter, such as Vickers, Knoop, or Berkovich, can appear to be an attractive alternative to more specialized fracture toughness testing techniques[53], as they are relatively quick and easy to perform, require little specialized equipment. Although, some doubts have been raised on the accuracy of this technique[35], nevertheless, it is still widely used for determining the fracture toughness of brittle materials, although with a limited accuracy[30, 53]. The fracture toughness (K_{IC}) was calculated using the palmqvist crack model,[53-55] employing the Vicker's indentation-crack technique that was initially proposed by Nihara et al.,[56] which has been found to be reasonably accurate in determining the fracture toughness for a range of brittle materials including, heavily doped semiconductors. The fracture toughness is given as,

$$K_{IC} = 0.0089\left(\frac{E}{H}\right)^{2/5} \times \frac{P}{al^{1/2}} \qquad 2.5 \geq {}^{l}\!/_{a} \geq 0.25 \tag{1}$$

Where, P is the load (Newtons), l the crack length (meters) resulting from the indent on the material surface after indenter removal, a is the half-diagonal of Vicker's indentation (meters), E is the Young's modulus (GPa) and H is the Vickers hardness (GPa).

ACCEPTED MANUSCRIPT

The polished nanostructured $Si_{80}Ge_{20}$ alloy samples were indented using a Vicker's diamond shaped indenter at a load of 19.6 N with a dwell time of 10 sec to produce cracks on the nanostructured $Si_{80}Ge_{20}$ sample surface. Subsequently, the indent and crack lengths were measured using FESEM for a better accuracy. The crack length (l) on the material surface after indenter removal and the half-diagonal of Vickers indentation mark (a) were typically measured to be 63.8 μm and 23.3 μm, respectively, as shown in Fig. 6. Based on the l/a ratio=1.67, equation (1) was used for the calculation of fracture toughness, which was evaluated to be 1.66 ±0.04 MPa√m and this value significantly higher than those reported in literature for other state-of-the-art TE materials[30], as shown in Fig. 7(a). The high fracture toughness for p-type nanostructured alloys was mainly attributed to the nano-scale grain size of $Si_{80}Ge_{20}$ alloys, which aids in minimizing the dislocation pile-up stresses which in turn results in the improvement of fracture toughness[57]. Additionally, the fine nanocrystallites in the matrix of SiGe alloy are also expected to enhance the fracture toughness as during the steady-state of crack initiation[57, 58], the work done by the applied stress is considered to be dissipated as heat by specific rotational deformation, grain boundary sliding and diffusion[59-61]. In the present study, the low average crystallite size of ~ 20 nm of nanostructured p-type $Si_{80}Ge_{20}$ matrix is expected to assist in the localized fracture processes, which generally occur during crack extension as reported for other nanostructured materials[58]. Fig. 7 (a&b), which shows a comparison of the fracture toughness and hardness values of p-type nanostructured $Si_{80}Ge_{20}$ alloys with other state-of-the-art TE materials from the literature, suggests that the mechanical properties of p-type nanostructured $Si_{80}Ge_{20}$ alloys are far superior to other contemporary TE materials.

3.2.3 Compressive strength

The compressive strength of nanostructured $Si_{80}Ge_{20}$ alloy was evaluated at room temperature under uni-axial compressive loading and a typical stress-strain curve is shown in Fig. 8. The

ACCEPTED MANUSCRIPT

nature of the stress - strain curve is typical of a brittle fracture with a compressive strength of 108 ± 0.2 MPa and a percentage strain of 11 % prior to fracture. This high magnitude of the observed strength in our nanostructured $Si_{80}Ge_{20}$ alloy can be associated with the "grain refinement strengthening" due to its nano-sized crystallite size (~20 nm) in accordance with the Hall-Petch equation[62]. Further, "solid solution strengthening"[63] is also expected to play a dominant role in enhancing the strength due to a considerable difference in the atomic radii of Si and Ge. FESEM image of the as-fractured surface of the nanostructured $Si_{80}Ge_{20}$ alloy is shown as an inset in Fig. 8. This figure suggests that the fracture morphology has been observed to be more or like a cleavage-type (brittle fracture) and this may be attributed to the fact that in brittle materials the strain energy[64, 65] release rate during the crack initiation was more than the energy required to grow the crack[58, 66].

3.2.4 Thermal shock resistance analysis

The thermal shock resistance in TE materials is one of the most important property for designing their TE devices as these materials[67] are subjected to large temperature gradients and repeated thermal cycling under compressive stress, due to thermal expansion mismatch and mechanical vibration during their in-service operation[68]. This property is more important for TE devices operating at high temperatures, such as, SiGe-based devices, as thermal recycling at these high temperatures (~ 900°C) can generate significant amount stress at the SiGe interfaces. Hence, the thermal shock resistance value of the SiGe nanoalloys, especially for high operating temperature thermoelectric materials, is as important as their TE performance. The thermal shock resistance value for nanostructured p-type $Si_{80}Ge_{20}$ alloys has been calculated using[36],

ACCEPTED MANUSCRIPT

$$R_T = \frac{\sigma(1-\nu)\kappa}{\alpha E} \quad (2)$$

where, R_T is thermal shock resistance parameter, σ the fracture strength, ν the Poisson's ratio, κ the thermal conductivity, α the coefficient of thermal expansion and E is the elastic modulus. The thermal shock resistance of p-type nanostructured $Si_{80}Ge_{20}$ alloy samples was calculated employing equation (2) and using the experimentally determined values of σ=0.043 GPa, E=135 GPa, κ=2.04 W/mK[69] and α[70], ν[71] values were taken from the literature of similar alloy composition. The value of thermal shock resistance parameter was found to be ~ 391 ± 21 Wm^{-1} and this value is comparable or better than those reported for other state-of-the-art TE materials [20, 29, 36] as shown in Fig. 9.

It has generally been observed that materials (especially nanostructured materials) sintered employing SPS result in better mechanical properties than those sintered using other conventional techniques[72, 73]. SPS is a pressure-assisted sintering process in which high amperage pulsed direct current is employed to sinter the samples under pressure. This sintering process lowers both the sintering temperature as well the sintering time because the particles are heated rapid by a spark plasma, which has a surface activating and cleaning effect on the particles being sintered. The main advantage of SPS over its rival sintering techniques is that it leads to near-theoretical density in the SPS product while retaining the nano-scale features of the starting nanopowders post-sintering, both of which result in better mechanical properties of the sintered material[72, 74]. However, this is very difficult in conventional sintering processes, because densification during sintering is always accompanied by microstructural coarsening due to extensive boundary and volume diffusion at longer duration of sintering cycles.

ACCEPTED MANUSCRIPT

Figs. 7 (a&b) and 9, suggest that although the mechanical properties of p-type nanostructured alloys are better than most of the existing state-of-the-art TE materials. However, except the fracture toughness, other mechanical properties such as hardness and thermal shock resistance are lower than those reported for their nanostructured n-type counterpart[29], despite their similar matrix composition ($Si_{80}Ge_{20}$). One apparent reason for this difference could be the different nano-crystallite size of SiGe matrix, obtained in n and p-type SiGe alloys. Additionally this discrepancy in reported mechanical properties of nanostructured n-type SiGe with those obtained for its p-type counterpart in the current study could be attributed to the different dopants (boron and phosphorus for n and p-type SiGe, respectively), employed for their synthesis, which govern the kinetics of the precipitation processes and the solid solubility of boron and phosphorous in SiGe alloys. It has been reported that the precipitation of boron is much slower and takes place at much higher temperatures[75, 76] compared to that of phosphorus[76] owing to their vastly different diffusion rates in SiGe alloys. Further to note that, in the case of p-type nanostructured SiGe alloys, the nature of precipitation is reversible with excess boron diffusing into the grain boundaries[77] as opposed to n-type nanostructured SiGe alloy wherein the excess phosphorus forms fine nano-scale precipitates of SiP[29], which are preferentially decorated at the grain boundaries. Further, as boron has far less solid solubility in Si and Ge as compared to phosphorus[29], the precipitation kinetics and the solid solubility are expected to play an important role in strengthening and fracture mechanisms, which determine the mechanical properties.

ACCEPTED MANUSCRIPT

4. Conclusions

In summary, the nanostructured p-type $Si_{80}Ge_{20}$ alloys were synthesized using high-energy ball-milling followed by consolidation of the resulting nanostructured powders using spark plasma sintering technique. This nanostructured alloy exhibited a hardness of ~ 9 ± 0.1 GPa, an elastic modulus of ~135 ± 1.9 GPa with a compressive strength of ~ 108 ± 0.2 MPa. The fracture toughness and the thermal shock resistance values were estimated to be ~1.66 ± 0.04 MPa√m and 391 ± 21 Wm^{-1}, respectively and these values are comparable to best reported values for other state-of-the-art thermoelectric materials. However, the mechanical properties of p-type nanostructured $Si_{80}Ge_{20}$ alloys were found to be lower than its n-type counterpart, which has been attributed to the kinetics of the precipitation processes and the solid solubility of boron and phosphorous in SiGe alloys. The combination of good mechanical properties coupled with their high thermoelectric figure-of-merit suggests that nanostructured p-type $Si_{80}Ge_{20}$ alloys could be the better choice for thermoelectric power generation in RTG applications.

Acknowledgements

This work was supported by CSIR-TAPSUN (CSIR-NWP-54) program entitled *"Novel approaches for solar energy conversion under technologies and products for solar energy utilization through networking"*. The authors are grateful to Dr. Bhasker Gahtori, Mr. Radhey Shyam, Mr. N. K. Upadhyay, Mr. Niraj Kumar Singh, Ms. Kriti Tyagi and Mr. S. K. Tripathy for their technical and experimental support.

ACCEPTED MANUSCRIPT

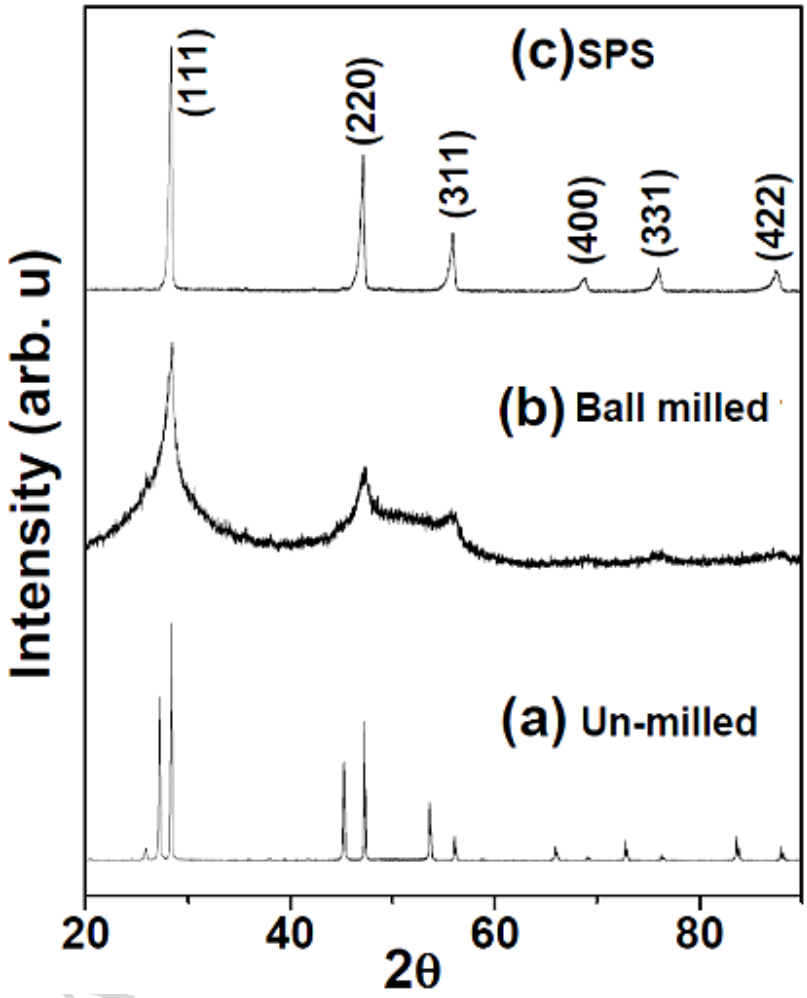

FIG. 1: X-ray powder diffraction pattern of p-type $Si_{80}Ge_{20}$ alloy for (a) un-milled, (b) ball-milled for 90 hours in argon atmosphere and (c) spark plasma sintered at 1150°C.

ACCEPTED MANUSCRIPT

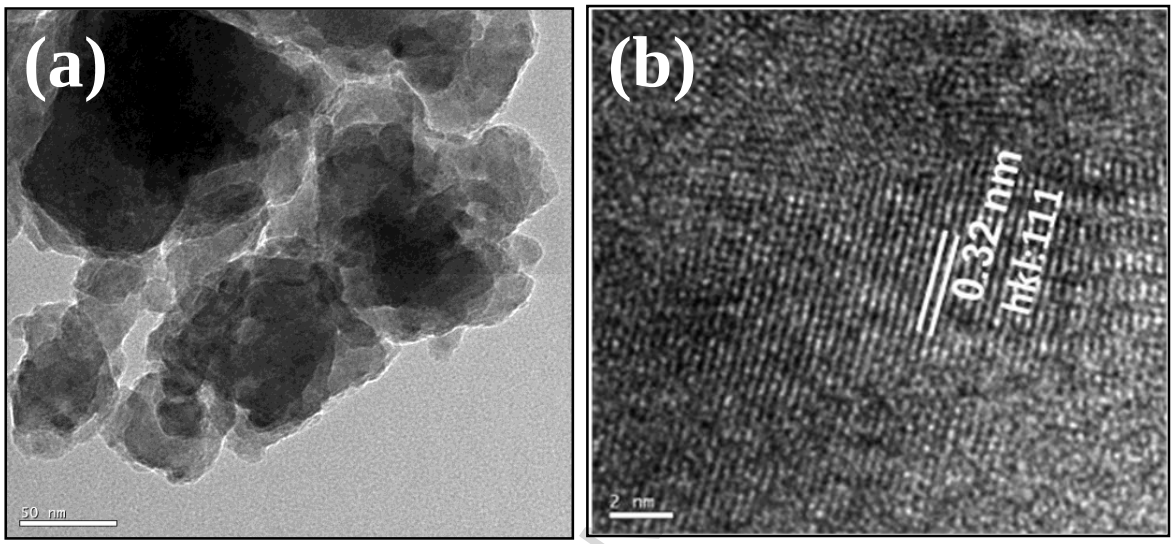

FIG. 2: HRTEM images of $Si_{80}Ge_{20}$ nanostructured powder ball-milled for 90 hours in argon atmosphere, showing (a) agglomerated nanocrystalline particles and (b) individual nanocrystallites having an inter-planar spacing of 0.32 nm for Si.

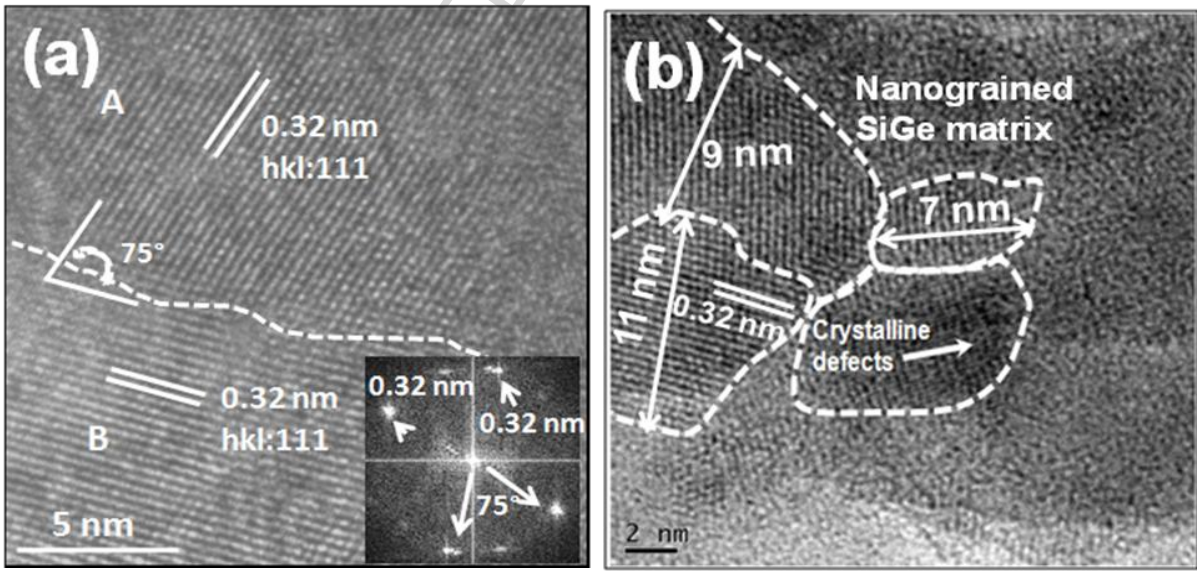

FIG. 3: HRTEM images of spark plasma sintered p-type $Si_{80}Ge_{20}$ nanostructured alloy, showing (a) two variants of 111 planes of a cubic crystal at atomic scale, (b) distribution of different sized, randomly oriented nano-crystallites with boundaries marked with white dotted lines. Inset in (a) FFT revealing two variants of 111 planes.

ACCEPTED MANUSCRIPT

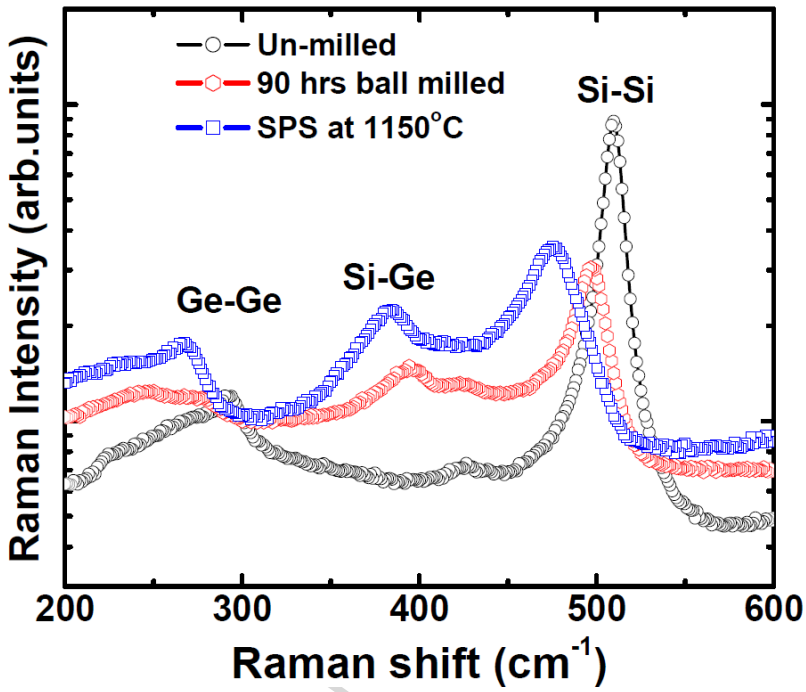

FIG. 4 *(Color online)* Raman spectra of p-type $Si_{80}Ge_{20}$ alloy for samples un-milled, ball-milled for 90 hours and spark plasma sintered.

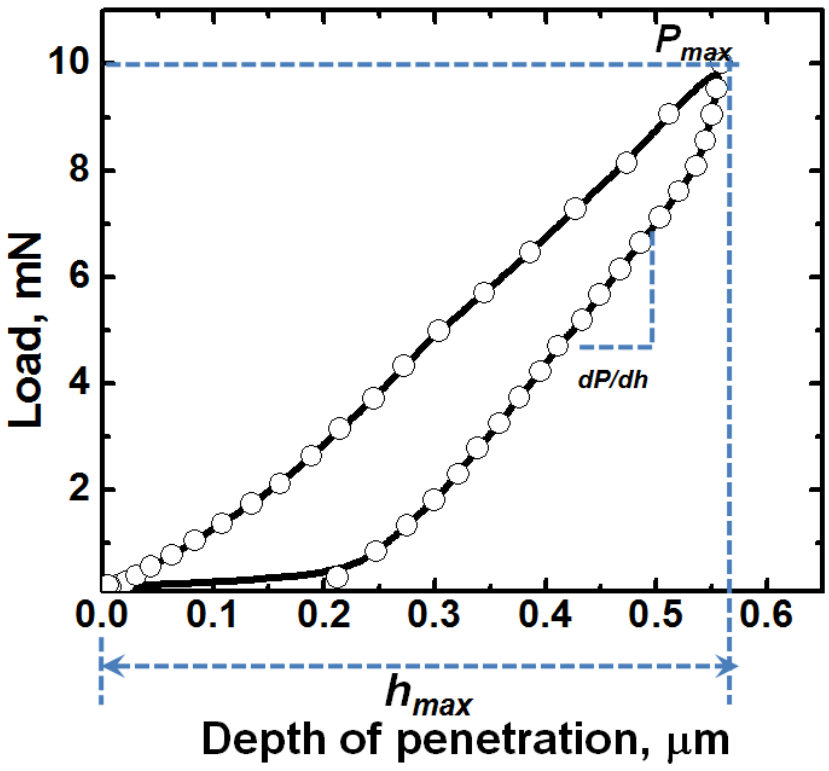

FIG. 5 Typical Nanoindentation curve of p-type nanostructured $Si_{80}Ge_{20}$ alloy during loading and un-loading.

ACCEPTED MANUSCRIPT

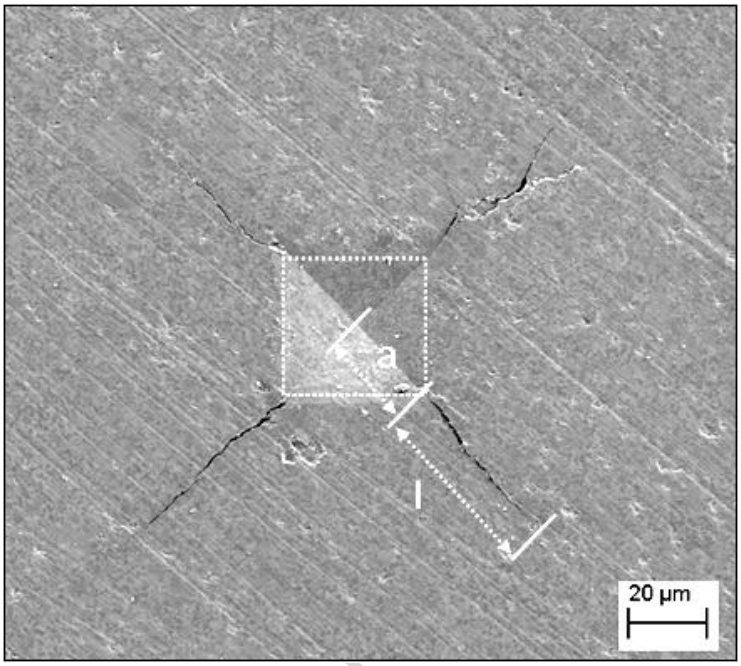

FIG. 6 FESEM of indentation mark for p-type nanostructured $Si_{80}Ge_{20}$ alloy developed at a load of 19.6 N, indentation crack length (*l*) and the half-diagonal of Vickers indentation mark (*a*), are marked.

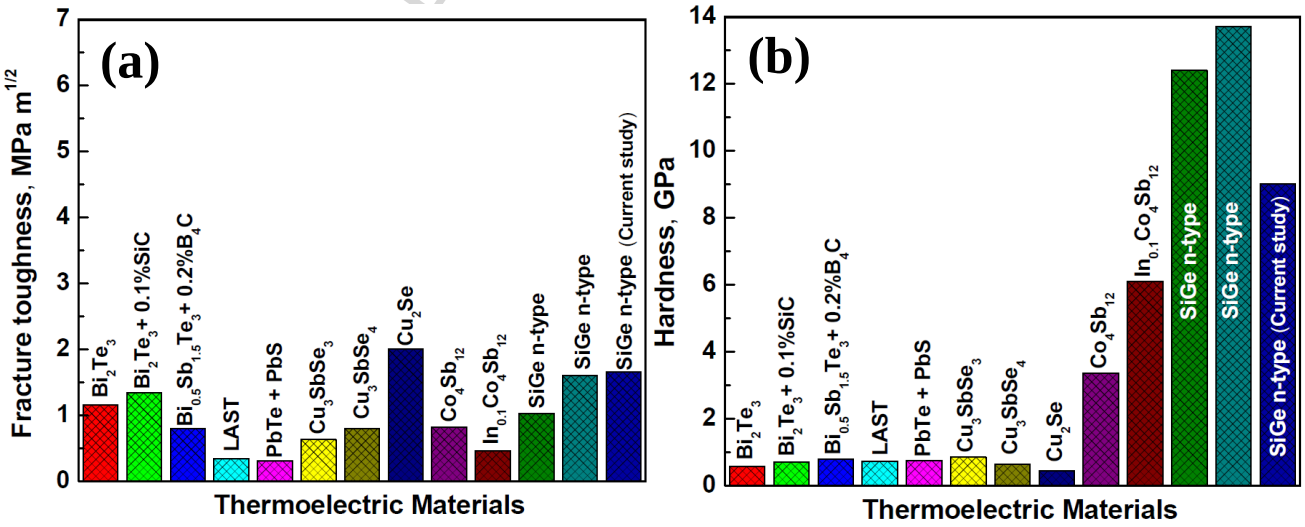

FIG. 7 (a) *(Color online)*Fracture toughness and (b) hardness of p-type nanostructured $Si_{80}Ge_{20}$ alloy compared with other state-of-the-art thermoelectric materials, such as Bi_2Te_3,[33] Bi_2Te_3+0.1Vol.%SiC[33],LAST[78], $Bi_{0.5}Sb_{1.5}Te_3$+0.2Vol.%B_4C[79], PbTe+PbS[80], Cu_3SbSe_3 and Cu_3SbSe_4[34], Cu_2Se[52], Co_4Sb_{12}[35], $In_{0.1}Co_4Sb_{12}$[35], n-type nanostructured $Si_{80}Ge_{20}$ alloys[29, 30].

ACCEPTED MANUSCRIPT

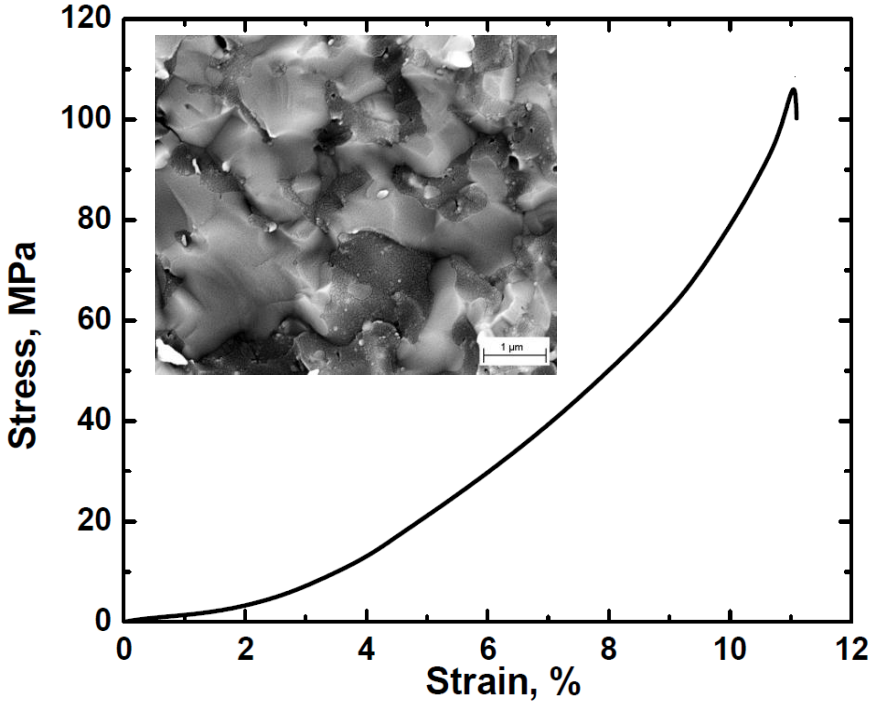

FIG. 8 Stress-Strain curve of nanostructured p-type $Si_{80}Ge_{20}$ alloy under uni-axial compression, inset shows the FESEM image of the fractured surface.

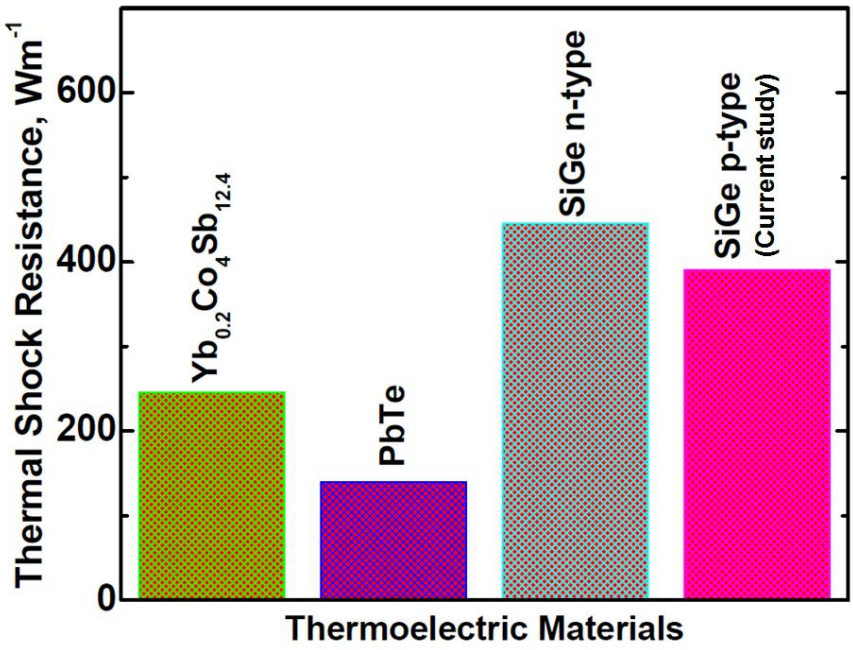

FIG. 9 *(Color online)*Thermal shock resistance of p-type nanostructured $Si_{80}Ge_{20}$ alloy compared with other state-of-the-art thermoelectric materials, such as $Yb_{0.2}Co_4Sb_{12.4}$[36], PbTe[36] and n-type nanostructured $Si_{80}Ge_{20}$ alloy[29].

ACCEPTED MANUSCRIPT

References

[1] Snyder GJ, Toberer ES. Complex thermoelectric materials. Nature materials. 2008;7:105-14.
[2] Poudel B, Hao Q, Ma Y, Lan Y, Minnich A, Yu B, et al. High-thermoelectric performance of nanostructured bismuth antimony telluride bulk alloys. Science. 2008;320:634-8.
[3] Hsu KF, Loo S, Guo F, Chen W, Dyck JS, Uher C, et al. Cubic AgPbmSbTe2+ m: bulk thermoelectric materials with high figure of merit. Science. 2004;303:818-21.
[4] Biswas K, He J, Blum ID, Wu C-I, Hogan TP, Seidman DN, et al. High-performance bulk thermoelectrics with all-scale hierarchical architectures. Nature. 2012;489:414-8.
[5] Liu W, Yan X, Chen G, Ren Z. Recent advances in thermoelectric nanocomposites. Nano Energy. 2012;1:42-56.
[6] Lan JL, Liu YC, Zhan B, Lin YH, Zhang B, Yuan X, et al. Enhanced Thermoelectric Properties of Pb-doped BiCuSeO Ceramics. Advanced Materials. 2013;25:5086-90.
[7] He J, Kanatzidis MG, Dravid VP. High performance bulk thermoelectrics via a panoscopic approach. Materials Today. 2013;16:166-76.
[8] Lan Y, Minnich AJ, Chen G, Ren Z. Enhancement of Thermoelectric Figure-of-Merit by a Bulk Nanostructuring Approach. Advanced Functional Materials. 2010;20:357-76.
[9] Chen Z-G, Han G, Yang L, Cheng L, Zou J. Nanostructured thermoelectric materials: Current research and future challenge. Progress in Natural Science: Materials International. 2012;22:535-49.
[10] Brown SR, Kauzlarich SM, Gascoin F, Snyder GJ. Yb14MnSb11: New high efficiency thermoelectric material for power generation. Chemistry of Materials. 2006;18:1873-7.
[11] Rowe DM. CRC handbook of thermoelectrics: CRC press; 1995.
[12] Dismukes J, Ekstrom L, Steigmeier E, Kudman I, Beers D. Thermal and Electrical Properties of Heavily Doped Ge-Si Alloys up to 1300° K. Journal of applied physics. 2004;35:2899-907.
[13] Yu B, Liu W, Chen S, Wang H, Wang H, Chen G, et al. Thermoelectric properties of copper selenide with ordered selenium layer and disordered copper layer. Nano Energy. 2012;1:472-8.
[14] Rowe DM. Thermoelectrics handbook: macro to nano: CRC press; 2005.
[15] Harame DL. SiGe and Ge: Materials, Processing, and Devices. The Electrochemical Society; 2006.
[16] Vining CB. A model for the high-temperature transport properties of heavily doped n-type silicon-germanium alloys. Journal of applied physics. 1991;69:331-41.
[17] Vining CB, Laskow W, Hanson JO, Van der Beck RR, Gorsuch PD. Thermoelectric properties of pressure-sintered Si0. 8Ge0. 2 thermoelectric alloys. Journal of applied physics. 1991;69:4333-40.
[18] Bathula S, Jayasimhadri M, Singh N, Srivastava A, Pulikkotil J, Dhar A, et al. Enhanced thermoelectric figure-of-merit in spark plasma sintered nanostructured n-type SiGe alloys. Applied Physics Letters. 2012;101:213902.
[19] Joshi G, Lee H, Lan Y, Wang X, Zhu G, Wang D, et al. Enhanced thermoelectric figure-of-merit in nanostructured p-type silicon germanium bulk alloys. Nano letters. 2008;8:4670-4.
[20] Basu R, Bhattacharya S, Bhatt R, Roy M, Ahmad S, Singh A, et al. Improved thermoelectric performance of hot pressed nanostructured n-type SiGe bulk alloys. Journal of Materials Chemistry A. 2014;2:6922-30.

ACCEPTED MANUSCRIPT

[21] Wang X, Lee H, Lan Y, Zhu G, Joshi G, Wang D, et al. Enhanced thermoelectric figure of merit in nanostructured n-type silicon germanium bulk alloy. Applied Physics Letters. 2008;93:193121.
[22] Lee H, Vashaee D, Wang D, Dresselhaus MS, Ren Z, Chen G. Effects of nanoscale porosity on thermoelectric properties of SiGe. Journal of applied physics. 2010;107:094308.
[23] Cook B, Harringa J, Han S, Vining C. Si80Ge20 thermoelectric alloys prepared with GaP additions. Journal of applied physics. 1995;78:5474-80.
[24] Harman T, Walsh M, Turner G. Nanostructured thermoelectric materials. Journal of electronic materials. 2005;34:L19-L22.
[25] Snyder GJ, Ursell TS. Thermoelectric efficiency and compatibility. Physical review letters. 2003;91:148301.
[26] Snyder GJ. Application of the compatibility factor to the design of segmented and cascaded thermoelectric generators. Applied Physics Letters. 2004;84:2436-8.
[27] Ngan PH, Christensen DV, Snyder GJ, Hung LT, Linderoth S, Nong NV, et al. Towards high efficiency segmented thermoelectric unicouples. physica status solidi (a). 2014;211:9-17.
[28] Gladden J, Li G, Adebisi R, Firdosy S, Caillat T, Ravi V. High-temperature elastic moduli of bulk nanostructured n-and p-type silicon germanium. Physical Review B. 2010;82:045209.
[29] Bathula S, Gahtori B, Jayasimhadri M, Tripathy S, Tyagi K, Srivastava A, et al. Microstructure and mechanical properties of thermoelectric nanostructured n-type silicon-germanium alloys synthesized employing spark plasma sintering. Applied Physics Letters. 2014;105:061902.
[30] Kallel A, Roux G, Martin C. Thermoelectric and mechanical properties of a hot pressed nanostructured n-type Si 80 Ge 20 alloy. Materials Science and Engineering: A. 2013;564:65-70.
[31] Ma JM, Firdosy SA, Kaner RB, Fleurial J-P, Ravi VA. Hardness and fracture toughness of thermoelectric La3− x Te4. Journal of Materials Science. 2014;49:1150-6.
[32] Ren F, Case E, Timm E, Schock H. Hardness as a function of composition for n-type LAST thermoelectric material. Journal of Alloys and Compounds. 2008;455:340-5.
[33] Zhao L-D, Zhang B-P, Li J-F, Zhou M, Liu W-S, Liu J. Thermoelectric and mechanical properties of nano-SiC-dispersed Bi 2 Te 3 fabricated by mechanical alloying and spark plasma sintering. Journal of Alloys and Compounds. 2008;455:259-64.
[34] Tyagi K, Gahtori B, Bathula S, Toutam V, Sharma S, Singh NK, et al. Thermoelectric and mechanical properties of spark plasma sintered Cu3SbSe3 and Cu3SbSe4: Promising thermoelectric materials. Applied Physics Letters. 2014;105:261902.
[35] Eilertsen J, Subramanian M, Kruzic J. Fracture toughness of Co 4 Sb 12 and In 0.1 Co 4 Sb 12 thermoelectric skutterudites evaluated by three methods. Journal of Alloys and Compounds. 2013;552:492-8.
[36] Salvador J, Yang J, Shi X, Wang H, Wereszczak A, Kong H, et al. Transport and mechanical properties of Yb-filled skutterudites. Philosophical Magazine. 2009;89:1517-34.
[37] Bathula S, Anandani R, Dhar A, Srivastava A. Microstructural features and mechanical properties of Al 5083/SiC< sub> p</sub> metal matrix nanocomposites produced by high energy ball milling and spark plasma sintering. Materials Science and Engineering: A. 2012;545:97-102.

ACCEPTED MANUSCRIPT

[38] Davis RM, Koch C. Mechanical alloying of brittle components: silicon and germanium. Scripta metallurgica. 1987;21:305-10.
[39] Ungár T, RRévész Á, Borbély A. Dislocations and grain size in electrodeposited nanocrystalline Ni determined by the modified Williamson–Hall and Warren–Averbach procedures. Journal of applied crystallography. 1998;31:554-8.
[40] Olesinski RW, Abbaschian GJ. The Ge−Si (Germanium-Silicon) system. Bulletin of Alloy Phase Diagrams. 1984;5:180-3.
[41] Zamanipour Z, Salahinejad E, Norouzzadeh P, Krasinski JS, Tayebi L, Vashaee D. The effect of phase heterogeneity on thermoelectric properties of nanostructured silicon germanium alloy. Journal of applied physics. 2013;114:023705.
[42] Zamanipour Z, Shi X, Dehkordi AM, Krasinski JS, Vashaee D. The effect of synthesis parameters on transport properties of nanostructured bulk thermoelectric p-type silicon germanium alloy. physica status solidi (a). 2012;209:2049-58.
[43] Tokita M. Mechanism of spark plasma sintering. Proceeding of NEDO International Symposium on Functionally Graded Materials: Japan; 1999. p. 22.
[44] Nakashima S, Mitani T, Ninomiya M, Matsumoto K. Raman investigation of strain in Si/ SiGe heterostructures: Precise determination of the strain-shift coefficient of Si bands. Journal of Applied Physics. 2006;99:053512.
[45] Alonso MI, Winer K. Raman spectra of c-Si 1-x Ge x alloys. Physical Review B. 1989;39:10056.
[46] Venkatasubramanian R, Siivola E, Colpitts T, O'quinn B. Thin-film thermoelectric devices with high room-temperature figures of merit. Nature. 2001;413:597-602.
[47] Gong J, Miao H, Peng Z. Analysis of the nanoindentation data measured with a Berkovich indenter for brittle materials: effect of the residual contact stress. Acta Materialia. 2004;52:785-93.
[48] Larsson P-L, Giannakopoulos A, Söderlund E, Rowcliffe D, Vestergaard R. Analysis of Berkovich indentation. International Journal of Solids and Structures. 1996;33:221-48.
[49] Pharr G. Measurement of mechanical properties by ultra-low load indentation. Materials Science and Engineering: A. 1998;253:151-9.
[50] Leitao C, Costa M, Khanijomdi K, Rodrigues D. Assessing strength and local plastic behaviour of welds by shear testing. Materials & Design. 2013;51:968-74.
[51] Dey T, Dey A, Ghosh PC, Bose M, Mukhopadhyay AK, Basu RN. Influence of microstructure on nano-mechanical properties of single planar solid oxide fuel cell in pre- and post-reduced conditions. Materials & Design. 2014;53:182-91.
[52] Tyagi K, Gahtori B, Bathula S, Jayasimhadri M, Sharma S, Singh NK, et al. Crystal structure and mechanical properties of spark plasma sintered Cu 2 Se: An efficient photovoltaic and thermoelectric material. Solid State Communications. 2015;207:21-5.
[53] Rios C, Contieri R, Souza S, Cremasco A, Hayama A, Caram R. Fracture toughness of a directionally solidified Al–Nb–Ni ternary eutectic. Materials & Design. 2012;33:563-8.
[54] Palmqvist S. Method of determining the toughness of brittle materials, particularly sintered carbides. Jernkontorets Ann. 1957;141:300-7.
[55] Li Z, Ghosh A, Kobayashi AS, Bradt RC. Indentation fracture toughness of sintered silicon carbide in the Palmqvist crack regime. Journal of the American Ceramic Society. 1989;72:904-11.
[56] Niihara K, Morena R, Hasselman D. Evaluation ofK Ic of brittle solids by the indentation method with low crack-to-indent ratios. Journal of Materials Science Letters. 1982;1:13-6.

ACCEPTED MANUSCRIPT

[57] Padmanabhan K. Mechanical properties of nanostructured materials. Materials Science and Engineering: A. 2001;304:200-5.
[58] Zhou J, Hu L, Liu H, Hu M. An energy approach to account for crack initiation in nanocrystalline materials. Materials & Design. 2013;52:30-5.
[59] Turner C, Kolednik O. Application of energy dissipation rate arguments to stable crack growth. Fatigue & Fracture of Engineering Materials & Structures. 1994;17:1109-27.
[60] Deng J, Lin Y, Li S-S, Chen J, Ding Y. Hot tensile deformation and fracture behaviors of AZ31 magnesium alloy. Materials & Design. 2013;49:209-19.
[61] Jiang B, Zhang C, Wang T, Qu Z, Wu R, Zhang M. Creep behaviors of Mg–5Li–3Al–(0, 1) Ca alloys. Materials & Design. 2012;34:863-6.
[62] Blum W, Li Y, Chen J, Zeng X, Lu K. On the Hall–Petch relation between flow stress and grain size: Dedicated to Professor Eckard Macherauch on the occasion of the 80th anniversary of his birth. Zeitschrift für Metallkunde. 2006;97:1661-6.
[63] Guo X, Wu R, Zhang J, Liu B, Zhang M. Influences of solid solution parameters on the microstrucuture and hardness of Mg–9Li–6Al and Mg–9Li–6Al–2Y. Materials & Design. 2014;53:528-33.
[64] Yoffe E. Elastic stress fields caused by indenting brittle materials. Philosophical Magazine A. 1982;46:617-28.
[65] Torabi A, Campagnolo A, Berto F. Local strain energy density to predict mode II brittle fracture in Brazilian disk specimens weakened by V-notches with end holes. Materials & Design. 2015;69:22-9.
[66] Sih GC. Strain-energy-density factor applied to mixed mode crack problems. International Journal of fracture. 1974;10:305-21.
[67] Hatzikraniotis E, Zorbas K, Samaras I, Kyratsi T, Paraskevopoulos K. Efficiency study of a commercial thermoelectric power generator (TEG) under thermal cycling. Journal of electronic materials. 2010;39:2112-6.
[68] Salvador JR, Yang J, Wereszczak AA, Wang H, Cho JY. Temperature Dependent Tensile Fracture Stress of n-and p-Type Filled-Skutterudite Materials. Science of Advanced Materials. 2011;3:577-86.
[69] Bathula S, Mula J, Bhasker B, Singh NK, Tyagi K, Srivastava AK, et al. Role of nanoscale defect features in enhancing the thermoelectric performance of p-type nanostructured SiGe alloys. Nanoscale. 2015.
[70] Schaffler F. Properties of Advanced Semiconductor Materials GaN, AlN, InN, BN, SiC, SiGe. Eds Levinshtein ME, Rumyantsev SL, Shur MS, John Wiley & Sons, Inc, New York. 2001:149-88.
[71] Wortman J, Evans R. Young's modulus, shear modulus, and Poisson's ratio in silicon and germanium. Journal of applied physics. 1965;36:153-6.
[72] Průša F, Vojtěch D, Bláhová M, Michalcová A, Kubatík TF, Čížek J. Structure and mechanical properties of Al–Si–Fe alloys prepared by short-term mechanical alloying and spark plasma sintering. Materials & Design. 2015;75:65-75.
[73] Rumman MR, Xie Z, Hong S-J, Ghomashchi R. Effect of spark plasma sintering pressure on mechanical properties of WC–7.5 wt% Nano Co. Materials & Design. 2015;68:221-7.
[74] Liu Z-F, Zhang Z-H, Lu J-F, Korznikov AV, Korznikova E, Wang F-C. Effect of sintering temperature on microstructures and mechanical properties of spark plasma sintered nanocrystalline aluminum. Materials & Design. 2014;64:625-30.
[75] Landi E, Guimaraes S, Solmi S. Influence of nucleation on the kinetics of boron precipitation in silicon. Applied Physics A. 1987;44:135-41.

ACCEPTED MANUSCRIPT

[76] Armigliato A. D. Nobili, P. Ostoja, M. Servidori and S. Solmi. Semiconductor Silicon. 1977:638.
[77] Zamanipour Z, Krasinski JS, Vashaee D. Comparison of boron precipitation in p-type bulk nanostructured and polycrystalline silicon germanium alloy. Journal of Applied Physics. 2013;113:143715.
[78] Ren F, Hall BD, Ni JE, Case ED, Sootsman J, Kanatzidis MG, et al. Mechanical characterization of PbTe-based thermoelectric materials. MRS Proceedings: Cambridge Univ Press; 2007. p. 1044-U04-04.
[79] Williams HR, Ambrosi RM, Chen K, Friedman U, Ning H, Reece M, et al. Spark plasma sintered bismuth telluride-based thermoelectric materials incorporating dispersed boron carbide. Journal of Alloys and Compounds. 2015;626:368-74.
[80] Ni JE, Case ED, Khabir KN, Stewart RC, Wu C-I, Hogan TP, et al. Room temperature Young's modulus, shear modulus, Poisson's ratio and hardness of PbTe–PbS thermoelectric materials. Materials Science and Engineering: B. 2010;170:58-66.

ACCEPTED MANUSCRIPT

ACCEPTED MANUSCRIPT

Graphical abstract

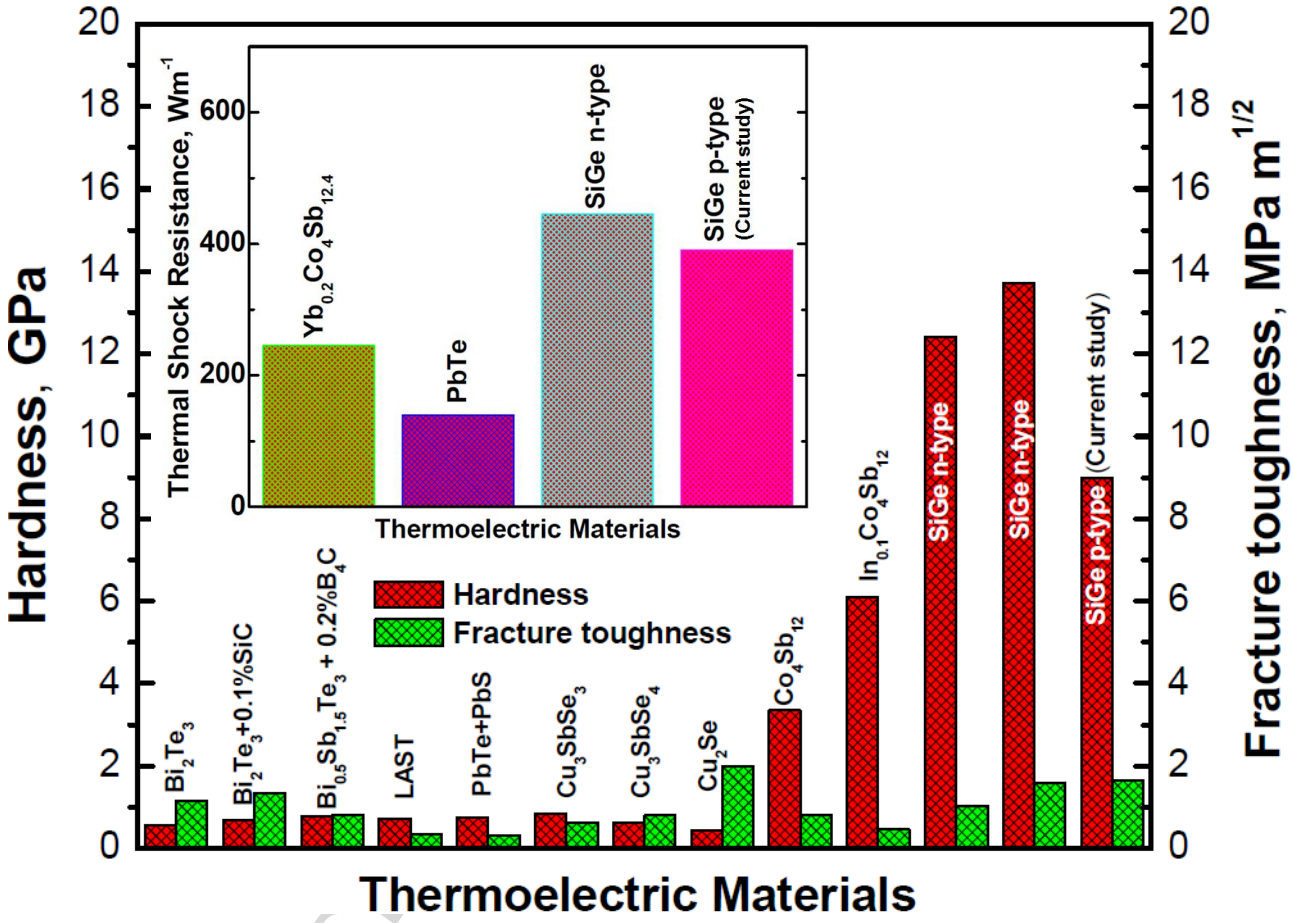

ACCEPTED MANUSCRIPT

Highlights of the current work

(i) First report on mechanical properties of thermoelectric p-type $Si_{80}Ge_{20}$ nanostructured alloys.

(ii) Nanostructuring of p-type SiGe alloys leads to improved thermal shock resistance.

(iii) Post sintering nano-scale features result in enhanced mechanical properties.

ACCEPTED MANUSCRIPT

Reviewed Paper | Volume 2 | Issue 11 | July 2015

International Journal of Informative & Futuristic Research | ISSN (Online): 2347-1697

Scope & Comparison Of Student Housing Industry In India

Paper ID	IJIFR/ V2/ E11/ 055	Page No.	4263-4271	Research Area	Housing Industry
Key Words	Student Housing Industry, Student Accommodation, Higher Education Institutes, Rental, Real Estate Industry, Upcoming Market, Hostel Industry				
Received On	18-07-2015	Accepted On	27-07-2015	Published On	29-07-2015

Sagar Agarwal [1]	Students, Department of Mechanical Engineering Delhi Technological University, Delhi
Kounal Gupta [2]	Students, Department of Mechanical Engineering Delhi Technological University, Delhi
Mayank Garg [3]	Students, Department of Mechanical Engineering Delhi Technological University, Delhi

Abstract

This paper offers a unique and one of a kind market research for student housing industry in India wherein the top prospective cities are identified which offers most favorable business opportunity in this sector. Next, the best three cities among these have been shortlisted through qualitative approaches like brainstorming with the SME's and trend analysis of associated KPI's. Now, in order to build up the growth momentum for a potential private player who is optimistic for this industry, a good start is necessary in order to transform a potential industry into existence. Therefore, using analytical techniques we have selected that one city which offers highest returns in the shortest period not only in tangible forms but also intangible forms like publicity at a mass level which not only attracts potential business partners but also venture capitalists.

1. Introduction

The improvements in the education levels and increasing enrolments of students in Higher Education Institutes has made the student accommodation as the important sector of commercial

Copyright © IJIFR 2015

ISSN (Online): 2347-1697
International Journal of Informative & Futuristic Research (IJIFR)
Volume - 2, Issue - 11, July 2015
23rd Edition, Page No: 4263-4271

property and is attracting the interest of many investors. Previously the student accommodation was only provided by the universities but due to increased enrolments in the educational institutes there is strong need of alternate form of accommodation as these universities are not able to cater the increasing demand. The global tertiary enrolments in 2000 were 98 million which grew to 165 million by 2009 and it is expected to grow to 263 million by 2025. The rise in the supply has not been fast to accommodate this steep rise in the housing demand thus resulting in the unbalanced student housing market. In US, 29% of students get accommodation on campus, 62% of students get accommodation in off campus private rentals which are often overpriced and poorly maintained and only 9 % of students get accommodation in private purpose built housing [1].

The need for student housing providers is to focus on improving service quality in order to remain competitive in the market. The different types of student housing quality dimensions are as discussed below:

- Enabling Facility Quality: This dimension includes factors such as security, rule and regulations, interpersonal relationship, behavior of landlord/lady, availability of transport, reading room facility, and overall quality of a housing facility.
- Core Facility Quality: This dimension includes bedroom facility, bathroom facility, and toilet facility.
- Supporting Facility: This dimension includes desirable value added services such as garage facility, junior common room, and entertainment facilities.
- Financial Cost: This dimension includes searching cost, housing rent, or fees per period. [2]

The student housing industry is emerging as a good investment sector and is attracting the interest of many investors. The business has low risk option and it characterizes secure and steady rental growth. It has high occupancy rate due to greater demand than the supply. The sector has well performed even during the times of downturn due to increase in student enrolments even during the recession periods. The sector has minor default risks due to parental financial guarantee and minimum commitment from universities. There is high investment opportunity with the global market being currently valued at US$ 200 billion. Privatization of student hostels is a good alternative financing solution for universities which can provide ability to meet the increased demand of student housing along with a new revenue stream to support financial operations of university. Thus it can provide relief to capital capacity constraints for university. Private housing not only provide financial alternative to university but also innovative housing plans according to student needs. [3]

Student housing sector is gaining popularity in India and is one of the most vibrant real estate markets in near future. Unlike other conventional real estate markets it offers relatively more stable income and resilient performance in downturns. Dense student populations that exist around prominent colleges positively affect the demand for residential spaces as well as restaurants and small retail spaces. The Indian higher education system has exhibited impressive growth over the last decade to become one of the world's largest systems of higher education. Higher education enrollment has grown at a healthy pace, with 3.6 million students being added over the last four years. India's higher education system is the world's third largest with respect to student enrollment, next only to China and the USA. The role of private investors in student housing in India assumes greater significance because of high potential of higher education and also has largest target market in the world. The expenditure made by the government is insufficient to create capacity for increasing demand. The demand and supply is widening due to infrastructure and

ISSN (Online): 2347-1697
International Journal of Informative & Futuristic Research (IJIFR)
Volume - 2, Issue - 11, July 2015
23rd Edition, Page No: 4263-4271

investment deficit thus it is growth opportunity for private sector players. India is to meet its 30% GER (Gross Enrolment Ratio) target by 2020 and about 40 million students would be enrolled in the higher education by 2020. Currently, 14.6 million students are enrolled in the higher education sector. Therefore, an additional capacity of about 25 million seats would be required over the next decade to cater to the increased demand [4].

2. Literature Review

Student accommodation industry has been traditionally dominated by unorganized players. Twenty first century has brought about a paradigm shift in this tradition. Organized and big real estate firms have identified huge potential and void this industry has to offer. According to the report by Dawn Wotapka [5] Lennar Corp., a large real estate builder, identified huge potential in the student accommodation business from the students of University of Texas and established its first off-campus apartment community near University of Texas in Austin. Similarly, Toll Brothers Inc. known for its dominance in traditional real estate business of suburban homes purchased a land near the University of Maryland in College Park and Penn State University in State College on which it plans to build student housing. These moves were taken by the real state developers to diversify their portfolio in areas that are considered less sensitive to downturns during an economic recession. Even during real estate crash, prices of single family homes declines and apartment landlord reduced rents but student housing landlords continued to raise rents without any objection from the students.

There is huge gap in the student housing industry. In the MIT faculty newsletter, Brian Spatocco regarded lack of graduate student housing as a serious problem and stated that if this issue is left unchecked it will not only have a profound effect on the quality of life of many off-campus MIT community members but it may also markedly impact the ability to attract the talent as well as maintain the level of productivity which fuel their academic pursuits [6]. The emphasis was also given on living close to the place of work that is a walking distance from the campus as it is important to the safety, well-being and quality of life of the graduate. Thus, penetration of big firms in this industry can prove to be highly rewarding in the long run and may also give first mover advantage.

The student accommodation is a captive niche market to investors and the investment feasibility of student housing is enumerated in the study made by Mathew E. Pace [7], where he says that the student population is rising twice as fast as the total U.S. population and University owned supply has failed to keep pace with demand growth as well as the private sector is slow to fill the void. The per unit rents or student housing generally exceed those for conventional apartments, as units have more tenants paying rent. Despite a growing institutional presence, the student housing market is still highly fragmented and dominated by small, undercapitalized owners, whose market share would be vulnerable to capture by larger, more professional institutional developers, managers, investors, and owners.

Various business models can be executed in this industry. The private development of student housing by partnership with the institution provide interactive and enriching student living experience possible for the least cost. These partnerships allow the institution to benefit from the efficiencies of private development according to a report by John Martin and Mark Allen. It further stated two projects which were developed through successful partnerships, College Row at Franklin

ISSN (Online): 2347-1697
International Journal of Informative & Futuristic Research (IJIFR)
Volume - 2, Issue - 11, July 2015
23rd Edition, Page No: 4263-4271

& Marshall College and South Campus Gateway at Ohio State University [8]. A generation of students has become accustomed to colleges and universities competing for their enrollment with improved housing options thus housing to student expectations for a comfortable and engaging environment is an established trend in residential life.

The academic performance of the student is directly influenced by the quality and quantity of their residential accommodation. Observing this, the Federal Government of Nigeria directed Heads of Tertiary Educational Institutions in the country to hand over hostels in campuses to private managers and also encouraged private investors to build hostels for students [10]. In the study made by Bassey Ubong, few benefits of the hostel accommodation were highlighted. These benefits include students staying in hostels enhances desire to read with fewer distractions, moreover, activities of studious students can force less serious ones to read. Students in hostels enjoy greater opportunities of participating in co-curricular activities. Students go under moral training such as proper code of conduct and individual behavior in group situations during their stay in hostels.

Though investment in student housing industry does not generate a high ROI but it certainly reaps stable and guaranteed success if backed by a proper market research and effective execution of its suggestions. According to the report by JLL (Jones Lang LaSalle), the student housing industry is emerging as mainstream investment category. This is all due to rise in student numbers worldwide and increase in international student mobility [1]. In 2000-2011 global tertiary enrollments rapidly rose from 98 million to 165 million in 2011 and it is expected to reach 263 million by 2065. The special attributes of this sector are the stable rental income with solid annual growth, resilient performance in downturns and high occupancy rates as student enrollments are rising at a higher rate than supply.

Although this industry offers great opportunity, aspiring players should not be over ambitious. A study conducted on student housing in the city of Pretoria, South Africa revealed that the university can only accommodate less than 34% of the to total enrolled students [11]. Thus the private student housing clearly plays a critical role in bridging the existing gap and a partnership between the private housing providers and the university may help optimize entrepreneurship ability and potential. Government entrepreneurship financing agencies like Independent Development Corporation (IDC) and National Youth Development Commission (NYDC) could benefit both the student community and the general public if engaged in joint housing provision venture.

3. Scope of Student Housing in India

India is witnessing growing number of educational hubs throughout the country due to increased student mobility from all the states. The growing influx of students in these educational hubs has created growing demand of student accommodation which the educational institutes are not able to cater. The educational hubs in India are Delhi-NCR, Pune, Chennai, Mumbai, Kota, Jaipur, Nagpur, Kolkata, and Hyderabad.

Pune, Delhi-NCR and Chennai have witnessed a strong growth in number of student enrollments in recent years and also increase in number of private higher education institutes. They have relatively more number of outstation students studying compared to other Indian cities. Mumbai has fallen to lower positions in catering education demands of the students firstly due to a high living cost in the city for the students secondly due to shortage of land and which has thus increased real estate prices. Kota is a popular coaching destination for competitive exam preparation for engineering and medical colleges. The scope of student housing industry is limited as the major outstation students

ISSN (Online): 2347-1697
International Journal of Informative & Futuristic Research (IJIFR)
Volume - 2, Issue - 11, July 2015
23rd Edition, Page No: 4263-4271

are in the city for coaching facility which lies under supplementary education thus there is uncertainty in continuity of the coaching tenure due to high dropout rate.

Jaipur, Nagpur, Kolkata and Hyderabad are cities with low per capita income and relatively the local governments also generates lower revenue per capita (Less than Rs.50,000/- in 2013). Moreover, these cities are facing growing rate of poverty crisis ***(y%)*** and persistently acute state of law and order along with corruption resulting in lower investments in education infrastructure ***(x%)*** as per xyz report. This has resulted in low attraction of the outstation students to migrate to these cities for pursuing higher education. Thus, the state of infrastructure remains an issue along with shortage of land allocation for setting up educational institute and residential accommodation for the same. This factor cumulatively makes scope of student housing industry in these cities dim.

3.1 Scope Student Housing Industry in Pune

Pune, also referred to as "the Oxford of the East", is an important education hub that attracts students from all over the country (470 institutions with over 3, 40,000 enrolments). The city has several premier engineering, management and polytechnic institutes including College of Engineering, Pune (CoEP), Symbiosis University, MIT, Fergusson College, etc. There are about 2, 00,000 outstation students studying in Pune. Close to 54% of the total students enrolled are from all different parts of the country while 5% are international students mainly from Afro-Asian countries. Pune has students from 74 different countries. Pune has also seen a growth in private investment to set up colleges and universities.

3.1.1. Hostel Overview: College hostels are the most cost effective option for students, however quality of facilities is poor and infrastructure is limited. It has been observed, that several college hostels have poor canteen facilities, inadequate water supply, no hot water and no Wi-Fi facilities. Also college hostels generally provide accommodation to first year students and after that, these students have to explore other alternate modes. Student feedback suggests that higher rental rates of the college hostels did not necessarily provide students with better facilities and environment. Thus the facilities provided in most of the college hostels are inadequate and do not even provide basic amenities to the students.

3.1.2. Private Hostel Overview: The city currently has only 40 registered private hostels. The majority of private hostels are unorganized and it is estimated that there are between 500 – 600 unorganized hostels, which have a capacity of between 2 – 10 rooms. The facilities provided in these hostels are also not adequate. Hence only 10% of the outstation students prefer this mode of accommodation. The private hostels in Pune are very limited thus they are not able to accommodate the increasing number of students with a need for affordable college accommodation.

3.1.3. Paying Guest Overview: Paying Guest accommodation is the most popular choice for outstation candidates in Pune. As there are large number of small colleges in the city and the profile of the Paying Guest varies greatly with different areas. Most of the families living adjacent to the colleges have started renting out a part of their flat to outstation students. Paying Guest accommodation in Pune is generally on a sharing basis and due to the diverse profile of the students the preference is to share their accommodation with friends or acquaintances. Approximately 60% of the outstation students in Pune are non-Maharashtrian and are keen to stay in a family based environment that is offered by paying guest.

3.1.4. Rented Flats Overview: Most of the colleges in Pune provide college hostel facility only to first year students. After which students generally prefer to opt for rented flats. However, renting

ISSN (Online): 2347-1697
International Journal of Informative & Futuristic Research (IJIFR)
Volume - 2, Issue - 11, July 2015
23rd Edition, Page No: 4263-4271

flats is a costly option for students in Pune as the rentals are higher than the alternate modes of accommodation. This escalation in rentals has been caused by high demand for housing from IT professionals. The rising rates have forced many students to move to the outskirts of the city. Though students save on rental but they have a longer commuting time and eventually end up paying higher transportation costs.

3.2 Scope of Student Housing Industry in Delhi-NCR

The region is one of the leading education centers in India that attracts students from all parts of the country as well as international students (656 institutes with over 9, 30,000 enrolments). The region has some of the prominent undergraduate degree colleges' medical institutes, engineering, and management institutes. Approximately 41% of the students come from other parts of India while about 4% are international students. In the recent decade, several private players have set up private educational institutes in Noida and Gurgaon. Besides several private as well as government universities and colleges, the region is also a hub for UPSC examination coaching institutes.

3.2.1 College Hostel Overview: Delhi NCR is one of the preferred location in India for outstation students, with nearly 45% of students enrolling across Delhi colleges from other cities. Priority for securing a college hostel seats is mostly on merit. The fees for College hostels in Delhi NCR area have witnessed an increase by 20 to 30% between 2011 and 2013. This has been due to the rising cost of all amenities as well as increase in maintenance cost charged for the upkeep of the hostel. Generally most of the college hostels in Delhi NCR do not have the supporting infrastructure to accommodate a large number of students and thus only 12% of the outstation students manage to get accommodation in these hostels.

3.2.2 Private Hostel Overview: The colleges in Delhi and NCR have a limited number of hostel seats for undergraduate students and thus a large number of students especially women opt for private hostel facilities. Private hostels are located in residential clusters close to key college campuses. Increased demand for private hostel facilities has resulted in higher rental charges for the facilities. As such the rentals of private hostels are generally higher than PG facility in some cases.

3.2.3 Paying Guest Overview: Paying Guest (PG) accommodation is a popular choice for students and also caters to young professionals working in the region. Home style food, hygienic and spacious rooms; with Wi-Fi connectivity make PG a preferred option for students in the city. With rising costs of paying guest accommodation, students on are being evaluating areas away from their college including Gurgaon, Noida, and Indirapuram.

3.2.4 Rented Flats Overview: Shared rental flats are an attractive alternative for students and single professionals, offering independent living arrangements. This option is more popular among male students. As safety is a key concern for female students in Delhi, renting shared flats is not a preferred option for female students due to low security. With increased security and safety concerns, landlords are becoming particular on renting flats to students. This has resulted in a shift to rented rooms being let out in unauthorized and irregular colonies.

3.3. Scope of Student Housing Chennai

Chennai is home to several education and research institutes that are ranked among the top institutes in India. These include three central universities, deemed universities, reputed engineering and medical colleges as well as several Arts and Sciences colleges (348 institutes with an enrollment of over 4,16,000). Chennai attracts a large number of outstation students including

ISSN (Online): 2347-1697
International Journal of Informative & Futuristic Research (IJIFR)
Volume - 2, Issue - 11, July 2015
23rd Edition, Page No: 4263-4271

foreign students as well and approximately 68% students come from outside Chennai and the other 2% are international students.

3.3.1. **College Hostel Overview:** Hostel rooms are allocated on a first-come-first-serve basis and those students unable to secure a college hostel seat must look for private accommodation. Amenities at college hostels are poor and inadequate as facilities have not been expanded and upgraded to balance the increase in student intake. College hostels in Chennai have been criticized for poor infrastructure, sanitation and quality of food. Some college hostels lack basic facilities such as adequate water supply and provision for drinking water.

3.3.2. **Private Hostel Overview:** The lack of safety, poor quality of food and hygiene are common problems faced by students in private hostels. There is no regularization or licensing as far as private hostels in Chennai are concerned. Hostels are not covered by the Chennai Corporation and are treated as residences.

3.3.3. **Paying Guest Overview:** Chennai attracts a stream of students and young professionals who demand temporary, cost effective housing that paying guest accommodation provides. However, demand for paying guest facilities in Chennai is driven by non Tamil speaking working population.

3.3.4. **Rented Flats Overview:** A number of foreign students pool resources and share a common apartment flat. Students however face difficulties when finding rental accommodation as flat owners are unwilling to rent their flats to bachelors and international students. Also, owners are continuously revising the rentals due to high demand. Besides, students have to pay 2 months advance rental along with 1 month's security deposit.

4. Comparison Between Pune, Delhi-NCR, Chennai

Among Pune, Delhi-NCR, Chennai to reason out the best city in India to set up the student housing industry we have used an analytical method. We have picked up seven dominating factors in student housing industry and have assigned weight to each factor. This is done by pair-wise comparison method in which each factor is compared with every other and is given 1 point if it carries more importance than the other. As shown in the Table 1.

Table 4.1: Pairwise Comparison

Factor	No. of Students	No. of Outstation students	No of students who don't get hostel accommodation	Living Cost	Buying Power	Competition	(students/ km)	Score
No. of Students	-		1	1	1			3
No. of Outstation students		-		1	1			2
No of students who don't get hostel accommodation		1	-	1	1	1	1	5
Living Cost				-	1			1
Buying Power					-		1	1
Competition	1	1		1	1	-	1	5
Average	1			1			-	2

ISSN (Online): 2347-1697
International Journal of Informative & Futuristic Research (IJIFR)
Volume - 2, Issue - 11, July 2015
23rd Edition, Page No: 4263-4271

Density of students in the city (students/ km)								

On the basis of the total score obtained by the each factor in Table 1, we have calculated weightage by dividing the factor score with total score. Weightage of each factor is shown in the Table 2.

Table 4.2: Weightage Calculation

Factor	Score	Weightage (Score/19)
No. of Students	3	0.157895
No. of Outstation students	2	0.105263
No of students who don't get hostel accommodation	5	0.263158
Living Cost	1	0.052632
Buying Power	1	0.052632
Competition	5	0.263158
Average Density of students in the city (students/ km)	2	0.105263

Finally with weightage of each factor obtained we have multiplied the weightage with factor value corresponding to each city. Factor value is 3 if the factor is best suited to a city and 1 if it is least suited to the city. Then a cumulative score of each city has been calculated as shown in the Table 3.

Table 4.3: Cumulative score of each city

Factor	Weightage	Delhi	Pune	Chennai
No. of Students	0.157895	930,000 (3)	340,000 (1)	416,000 (2)
No. of Outstation students	0.105263	421,626 (3)	200,000 (1)	291,328 (2)
No of students who don't get hostel accommodation	0.263158	372,780 (3)	164,000 (1)	244,715 (2)
Living Cost	0.052632	5,550 (3)	4,500 (2)	4200 (1)
Buying Power	0.052632	6800 (3)	4500 (1)	6000 (2)
Competition	0.263158	3 (2)	3 (2)	2 (1)
Average Density of students in the city (students/ km)	0.105263	251 (3)	234 (2)	209 (1)
SCORE	-	2.21	1.42	1.57

ISSN (Online): 2347-1697
International Journal of Informative & Futuristic Research (IJIFR)
Volume - 2, Issue - 11, July 2015
23rd Edition, Page No: 4263-4271

5. Conclusion

The student housing industry is emerging as the good investment sector which has a huge scope in India. This is due to the impressive growth rates in education facilities in the country. The increase in number of student enrollments in higher education institutes has created a increase in demand of student accommodation which these institutes are incapable of catering. Thus infrastructure needs to be created not for education facilities but for providing student housing.

Among the nine cities (Delhi-NCR, Pune, Chennai, Mumbai, Kota, Indore, Nagpur, Kolkata, Hyderabad) initially considered to set up the student housing industry in India we came down to best three cities (Delhi-NCR, Pune, Chennai). Finally by using a analytical technique from top three cities we came down to one city i.e. Delhi-NCR which is most favorable city to set up student housing industry in India.

References

[1] Jones Lang Lasalle, "Student Housing: a new global asset class".

[2] F. K. Bondinuba, S. G. Nimako, N. K. Karley, "Developing Student Housing Quality Scale in Higher Institutions of Learning: A Factor Analysis Approach", Urban Studies Research, 2013.

[3] K. K.-Griswold, "Privatizing of Student Housing, A Financing Alternative", 2013.

[4] Ernst and Young, "Private Sector Participation in Indian Higher education".

[5] D. Wotapka, "Real Estate Firms going to School", The Wall Street Journal, 2013.

[6] B. Spatocco, MIT Faculty Newsletter, vol. 25, 2013.

[7] M. E. Pace, "Green Luxury Student Housing: A Real Estate Feasibility Study", 2007.

[8] J. Martin, M Allen, "Students in my Backyard Housing at the Campus Edge and other Emerging Trends in Residential Developments".

[9] F. Khozaei, N. Ayub, A. S. Hassan, Z. Khozaei, "The factors predicting students satisfaction with university hostels Case Study, Universiti Sains Malaysia", Asian Culture and History, vol. 2, pp. 148-158, 2010.

[10] B. Ubong, "Hostel Accommodation in Tertiary Educational Institutions in Nigeria: To Be or Not To Be", 2007.

[11] Tswai, F. Netswera, "Student Housing in South Africa- a Conflated Housing Mandate Between the State and Higher Education", Presented at GBATA Fifteenth Annual International Conference in Helsinki, Finland, 2013.

Available online at www.sciencedirect.com

ScienceDirect

Procedia Computer Science 57 (2015) 988 – 995

Procedia Computer Science

3rd International Conference on Recent Trends in Computing 2015 (ICRTC-2015)

Sensor Node Deployment based on OTLBO in WSN

Anand Prakash*, R. K. Yadav, Dr. Daya Gupta

Department of Computer Engineering, Delhi Technological University, Delhi 110042, India

Abstract

A Wireless Sensor Network (WSN) can be defined as a collection of spatially distributed sensor nodes with a common goal to obtain global information from locally collected data. The nodes communicate wirelessly, operate autonomously and perform cooperative actions. In order to make good use of the locally collected data, the nodes have to collaborate with each other and should form a network to perform any common application. WSNs may be deployed in large numbers in various environments, including remote and hostile regions. In this paper, we have addressed one of the fundamental issues in WSN, namely coverage which reflects how well a sensor network is monitored or tracked by sensors. If the sensors are considered as mobile nodes then the effectiveness of the Wireless Sensor Network will depend on the coverage of the sensor node deployment scheme. This paper considers sensors that move in the monitoring field according to OTLBO (Orthogonal Teaching Learning Based Optimization) in order to improve network coverage. OTLBO is an improvement over TLBO (Teaching Learning Based Optimization) that makes TLBO fast to converge and more robust. OTLBO is a recent approach in the optimization field.

© 2015 Published by Elsevier B.V. This is an open access article under the CC BY-NC-ND license (http://creativecommons.org/licenses/by-nc-nd/4.0/).
Peer-review under responsibility of organizing committee of the 3rd International Conference on Recent Trends in Computing 2015 (ICRTC-2015)

Keywords: WSN; Node Coverage; OTLBO; TLBO.

1. Introduction

Teaching Learning Based Optimization is a recent nature inspired global optimization method which is originally developed by Rao et al. (Rao et al. 2011a; Rao et al. 2012; Rao & Savsani 2012a). TLBO is a Population-based iterative learning method that uses a population of initial solutions to obtain the global solution. The technique is based on a simple fact that a teacher in a class can influence the performance of learners. TLBO works in two phases, the

* Corresponding author. Tel.: +91 9711475592
E-mail address: adprakash2006@gmail.com; fax: +011-27871023

1877-0509 © 2015 Published by Elsevier B.V. This is an open access article under the CC BY-NC-ND license (http://creativecommons.org/licenses/by-nc-nd/4.0/).
Peer-review under responsibility of organizing committee of the 3rd International Conference on Recent Trends in Computing 2015 (ICRTC-2015)
doi:10.1016/j.procs.2015.07.500

first phase is called “Teacher Phase” which means learning from the teacher and the second phase is called “Learner Phase” which means learning through the interaction between learners.

As teacher is considered most knowledgeable person in the society, so in each evolutionary step the best learner is considered as a teacher. The teacher tries to disseminate knowledge among learners, which will in turn increase the knowledge level of the whole class and help learners to get good marks or grades i.e. the presence of a teacher may increase the performance of all learners in the class. The teacher increases the mean of the performance of the class according to his or her capability i.e. the teacher T1 will try to move mean M1 towards her own level according to her capability, thereby increasing the learners’ level to a new mean M2.

Learners can increase their knowledge by two different approaches: First, with the help of input from the teacher and Second, with the help of interaction between themselves. A learner interacts randomly with other learners with the help of group discussions, presentations, formal communications, etc. A learner adds something new to her knowledge if the other learner has more knowledge than her. Orthogonal Teaching Learning Based Optimization (OTLBO) is an improvement over TLBO which is based on orthogonal design concept that can be efficiently applied on multi-factor and multi-level problems. OTLBO makes TLBO faster and robust. It is known empirically that OTLBO has high performance in solving some benchmark functions comprising many parameters, as compared with some existing Evolutionary Algorithms. Here “Teaching Learning Based Optimization (TLBO)” is used as a function optimization technique and the “Orthogonal design (OD)” represents some properties of the orthogonal design method.

In this paper OTLBO is used to deploy mobile nodes in order to maximize the coverage of the sensor nodes keeping in mind no two sensors can collect redundant information and thus utilizing the node’s energy in efficient manner. Furthermore, these deployed nodes can be scheduled to track a target in the WSN in an energy efficient manner.

The rest of the paper is organized as follows: in section 2, we review the related works. In section 3, we describe the TLBO and OTLBO and then we describe how these algorithms can be utilized to get optimal node deployment in WSN and finally we conclude our paper

2. Related Work

Wireless sensor networks (WSNs) have been successfully applied in many strategic applications such as target tracking, surveillance and classification. Coverage and target detection probability are the two most significant factors for the performance of WSNs.

To obtain optimized coverage in the monitoring field, sensor nodes have to be deployed according to an effective scheme, thus sensor nodes deployment has heavy impact on the performance of WSN.

Node deployment is mainly classified in two categories: static and dynamic deployment. The static node deployment chooses the best location according to some optimization strategy, and the location of the sensor nodes will not change in the lifetime of the WSN.

At present, the static deployment includes the deterministic deployment and the randomly deployment. In the study of the deterministic sensor node deployment based on the target coverage, the paper [1] proposes a deployment approach of sensor nodes by using the maximum multi-overlapping domains of target points and the genetic algorithm, which reduces the network deployment cost and realizes the optimal allocation of spaces resources in wireless sensor networks. The paper [2] proposes a method with target coverage based on grid scan. Moreover, the deployment of wireless sensor network in deterministic space with obstacles is researched in paper [3].

The dynamic deployment may be backed to the deployment of the robot. In order to make the sensor networks get the maximum performance, sensor nodes need automatically move to proper location, then start to work. Random deployment, namely randomly throw nodes firstly, and then using a variety of optimization algorithm for deployment optimization. Such as virtual force algorithm [4], virtual force oriented particles algorithm [5], simulated annealing algorithm [6], particle swarm optimization algorithm [7] and simulated annealing genetic algorithm [8] more details can be found in paper [9].

Recently, mobile sensor networks have been under investigation and it has been shown that mobility, while complicating the design of higher layer algorithms, can also improve the network, for instance, in terms of capacity, coverage, life time, etc. Most of PSO applications in communications have been focused on clustering in ad-hoc networks aiming to minimize energy consumption. PSO has been used for distance based clustering of WSN.

PSO algorithms have been classified according to: task to accomplish, optimization criterion, scheme used (i.e. centralized or distributed) and type of work (i.e. simulation or real deployment). Three works [10], [11], [12] are cited

as algorithms proposed for supporting the deployment of mobile nodes in order to maximize the coverage of the sensor network. Specifically in [10], PSO is used to deploy the sensors in the field, while the evaluation of the coverage is done by using the Voronoi Tessellation. In order to evaluate the fitness function, they considered not only the vertex of the various polygons, but also those of n points randomly selected along the edges of polygons. Authors of [11] consider the maximization of the coverage as an optimization criterion by implementing a centralized technique as their technique is based on a modified PSO strategy they called their techniques Particle Swarm Genetic Optimization (PSGO).

In [12], authors propose a dynamic deployment algorithm named Virtual force directed co-evolutionary PSO (VFCPSO) where they combine the co-evolutionary PSO (CPSO) with the Virtual Force algorithm, exploiting the advantages of both the techniques. The CPSO algorithm requires global information in order to make nodes update their velocities. Three more algorithms have been proposed that are not cited in [23]: two of them are based on PSO through the usage of Voronoi Tessellation [13], [26] and third proposes a deployment strategy based on global information that exploits parallel PSO (PPSO) to reach an effective coverage [30].

All the cited PSO algorithms for coverage have in common the usage of a centralized scheme and/or the need of global information to solve the problem by using PSO. Under this respect, it is important to observe that in WSNs distributed approaches are preferred in respect of centralized solutions even though a distributed strategy is more difficult to be designed. The technique proposed in this work is of distributed type; thus, in what follows, we focus our attention on the scientific contributions that consider distributed approaches. Important results in this sense have been given in [22], [19], where the localization of wireless sensor nodes is handled. Applications for sensor networks based on consensus include load balancing [16], multi-vehicle control and navigation [25], flocking [27]. Much of the existing work is focused on average- consensus problems. There is one recent approach in [31] "Particle Swarm Optimization Schemes Based on Consensus for Wireless Sensor Networks" that effectively handles this problem while the author of this algorithm has not considered when the problem is multi-factor, multi-level search space. The study of the recent literature allows us to conclude that the formulation of WSNs issues as multidimensional optimization problems and through nature-inspired technique is a research field in full swing. The issue faced by the proposed technique is the deployment of wireless sensor nodes through a distributed approach to obtain a better coverage of regions of interest .To the best of our knowledge there is no a similar technique in literature that works for the same task and directly comparable to our solution strategy.

3. Proposed Scheme

In this section, first we give some relevant details about TLBO and OTLBO and then we introduce how this particular scheme can be utilized for our purpose, more details about TLBO and OTLBO can be found in [32].

3.1. Teaching Learning Based Optimization (TLBO)

The scheme TLBO is divided into two phases. The first part consists of the "Teacher Phase" and the second part consists of the "Learner Phase".

3.1.1. Teacher Phase

As teacher is considered most knowledgeable person in the society, the best learner in the class is treated as a teacher. The teacher tries to disseminate knowledge among learners, which will in turn increase the knowledge level of the whole class and help learners to get good marks or grades. So a teacher increases the mean of the class according to her capability i.e. the teacher T_i will try to move mean M_i towards her own level according to her capability, thereby increasing the learners' level to a new mean M_j. Teacher T_i will put maximum effort into teaching her students, but students will gain knowledge according to the quality of teaching delivered by a teacher and the quality of students present in the class. The quality of the students is judged from the mean value of the population. Teacher T_i puts effort in so as to increase the quality of the students from M_i to M_j, at which stage the students require a new teacher, of superior quality than themselves, i.e. in this case the new teacher is T_j.

Let M_k be the mean and T_k be the teacher at any iteration k. T_k will try to move mean M_k towards its own level, so now the new mean will be M_{new}. The solution is updated according to the difference between the existing and the

new mean given by

$$X_{new,k} = X_{old,k} + r_k(M_{new} - T_F M_k) \quad (1)$$

Where T_F is a teaching factor that decides the value of mean to be changed, $X_{new,k}$ and $X_{old,k}$ are new and existing solution. In this equation T_F can be calculated as follows:

$$T_F = round[1 + rand(0,1) \times (2-1)] \quad (2)$$

3.1.2. Learner Phase

A learner learns something new if the other learner has more knowledge than her. Learner modification is expressed as follows:

for $i = 1$ ***to*** P_n ***do***
  $Randomly\ Select\ two\ learners\ X_i\ and\ X_j, where\ i \neq j$
  if $f(X_i) < f(X_j)$
    $X_{new,i} = X_{old,i} + r_i(X_i - X_j)$
  else
    $X_{new,i} = X_{old,i} + r_i(X_j - X_i)$
end
Accept X_{new} if it gives a better function value.

3.2. Orthogonal Design

Consider a problem that involves some factors, each of which has several possible values called levels. Suppose that there are P factors and each factor has Q levels, then total no of combination is Q^P, we can see here that for large P and Q it is not practical to evaluate all combinations.

Orthogonal design has been developed as a mathematical tool to study multi-factor, multi-level problems. It aims to extract an orthogonal array L of M rows, where each row represents a combination to be evaluated. The array has three key properties:

- During the experiment, the array represents a subset of M combinations, from all possible Q^P combinations. Computation is reduced considerably because M << QP.
- Each column represents a factor. If some columns are deleted from the array, it means a smaller number of factors are considered.
- The columns of the array are orthogonal to each other. The selected subset is scattered uniformly over the search space to ensure its diversity.

A simple but efficient method is proposed in the work (Wing-Leung & Yuping 2001) to generate an orthogonal array L where, $M = Q \times Q\ and\ P = Q + 1$. The steps of this method are shown in the algorithm described as follows:

Algorithm-1: Procedure for generating an Orthogonal array L.

input: $The\ number\ of\ levels\ Q$
output: $An\ orthogonal\ array\ L$
$Calculate\ M = Q \times Q\ and\ P = Q + 1$
$Initialize\ a\ zero\ matrix\ L\ with\ M\ rows\ and\ P\ columns.$
for $i = 1$ ***to*** M ***do***
  $L_{i,1} = mod(\lfloor (i-1)/q \rfloor, q)$
  $L_{i,2} = mod(i-1, q)$
  for $j = 1$ ***to*** $P - 2$ ***do***
    $L_{i,2+j} = mod(L_{i,1} \times j + L_{i,2}, q)$

end
end

3.2.1. Optimizer (OTLBO)

In this approach each learner in the class of learners can be divided into several partial vectors where each of them acts as a factor in the orthogonal design. Orthogonal design is then employed to search the best scales among all the various combinations.

3.2.2. OD-based operator and updating strategy

The standard TLBO algorithm updates the current learner by comparing with best learner (i.e. teacher) in teacher phase and with a randomly select learner in learner phase. It lacks the interaction between neighboring learners and it may easily trapped into local minima. One technique to address this problem is to employ the multi-parent crossover during evolution and this technique has been shown to improve the convergence rate when applied to GAs.

Algoritm-2: OD-based operator for m learners.

input: $m\ particles\ X_{i,j},\ \ i \epsilon [1,m]\ and\ j \epsilon [1,N]$
output: $A\ new\ set\ of\ m\ learners\ \ p_{i,j}$
$Construct\ the\ orthogonal\ array\ L_{m\times m}\ (m^m + 1)$ using Algorithm1
$Delete\ the\ last\ (m + 1 - n)\ columns\ of\ L_{m\times m}(m^m + 1)$ to get
$A = L_{m\times m}(m^n)$
$Generate\ m\ new\ learners$:
for $i = 1$ **to** m **do**
  for $j = 1$ **to** N **do**
    $index = A_{i,j}$
    $p_{i,j} = X_{index,j}$
  end
end

3.2.3. Steps of OD-based TLBO

To obtain a more precise solution compared to the standard TLBO, the OD-based operator is employed. The elitism preservation strategy for upgrading the current population is proposed, in which the learner is updated only if its fitness is improved.

The procedure for the OD-based TLBO is shown in Algorithm 3. A convergence criterion or the maximum run can be used as the termination condition.

Algorithm-3: OD-based TLBO

input: $Population\ Size\ S, Maximum\ iterations\ K$
output: $Best\ Learner$
$Construct\ a\ random\ initial\ population\ of\ learners\ X_i,\ \ i \epsilon [1,s]$

for $t = 1$ **to** K **do**
  for $i = 1$ **to** S **do**
    $Update\ learners\ through\ teacher\ phase\ as\ inoriginal\ TLBO\ applying\ elitism\ preservation\ strategy$:
      $Select\ m\ particles\ randomly\ andexecute\ algorithm\ 2.$

$Set\ p_i = X_i^{t+1}\ if\ f(X_i^{t+1}) < f(p_i)$
$Set\ g = arg\ min\ f(p_i)$
end
Check the termination condition
end

4. System Model

For the analysis of OTLBO algorithm on the given problem, we consider the monitoring field as a square sensor field (Z), where a certain number of mobile sensors (N) is deployed randomly or uniformly. Events happen in the limited and measurable space according to a probability density function F(z), where z is the surface unit over Z. The idea is to distribute the sensors present in the sensor field according to the events probability function. The fraction of nodes n that should cover a region R of Z can be computed by the following ratio of surface integrals:

$$n = \frac{\int_R \mathrm{F(z)\,dz}}{\int_Z \mathrm{F}(z)\,\mathrm{dz}} \tag{3}$$

The objective function consider the position of the node in respect of the events that occurred in the whole sensor field. Hence, the objective function needs global information.

To evaluate the scheme, we consider the difference between the ideal numbers of sensors in each area ($n_i.N$) and the number of sensors located in the same area as the performance parameter at the time of convergence. The Energy for the movement has been set to a proportional cost model that depends on traveled distance d, as follows:

$$E_m(d) = kd \tag{4}$$

Where the constant k can take value between 0.1 and $1\frac{J}{m}$. This system model has been defined in detail in [31] where the author considers two objective functions Global and Local Objective Functions calculated at each iteration by each node. GOF takes into consideration the position of the node in respect of the events that occurred in the whole sensor field. Hence, this version needs global information. LOF takes into consideration only the events that occurred within the node's sensing area. In this case, each node can calculate the objective function depending only on local information and it is called Local Objective Function.

The design variables in equation (3) and (4) can be optimized by considering equation (1) and (2), then OTLBO described in section-3 can be applied to get faster convergence rate on the optimization scheme TLBO.

5. Conclusion

We can conclude by saying that OTLBO is a very powerful approach of optimizing different types of problems which are separable, non-separable, unimodal and multimodal in providing quality optimum results in faster convergence time compared to very popular evolutionary techniques like PSO, DE , GA and its variants. As a further research it remains to be seen how this adapts to multi-objective optimization problems and also some engineering applications from mechanical, chemical or data mining may be investigated.

When we apply this technique on the sensor nodes deployment in WSN we can get better result, the convergence rate is faster because we are using orthogonal design on TLBO to obtain OTLBO which is an improvement over TLBO.

References

[1] X. He, X. L. Gui, and J. An, "A Deterministic Deployment Approach of Nodes in Wireless Sensor Networks for Target Coverage", Journal of XiAn Jiaotong University Vol. 44, No.6, 2010, pp.6-10.

[2] X. M. Guo, C. J. Zhao, X. T. Yang et al, "A Deterministic Sensor Node Deployment Method with Target Coverage Based on Grid Scan", Chinese Journal of Sensors and Actuators, Vol.25, No.1, 2012, pp.104-109

[3] Y. Z. Zhang, C. D. Wu, L. Cheng et al, "Research of node deployment strategy for wireless sensor in

deterministic space", Control and Decision, Vol. 25, No. 11, 2010, pp. 1625-1629
[4] Q. Luo, and Z. M. PAN, "An Algorithm of Deployment in Small-Scale Underwater Wireless Sensor Networks", Chinese Journal of Sensors and Actuators, Vo. 24, No. 7, 2011, pp. 1043-1047
[5] X. Wang, S. Wang, and J. J. MA, "Dynamic Sensor Deployment Strategy Based on Virtuai Force-Directed Particle Swarm Optimization in Wireless Sensor Networks", Acta Electronica Sinica, Vol. 35, No. 11, 2007, pp. 2038-2042
[6] F. Y. S. Lin, and P. L. Chiu, "A Near-optimal Sensor Placement Algorithm to Achieve Complete Coverage Discrimination in Sensor Network," IEEE Communications Letters, Vol. 9, No. 1, 2005, pp43-45
[7] Y. Liu, "Wireless Sensor Network Deployment Based on Genetic Algorithm and Simulated Annealing Algorithm", Computer Simulation, Vol. 28, No.5, 2011, pp. 171-174
[8] W. H. Liao, Y. C. Kao, and Y. S. Li, "A Sensor Deployment Approach Using Glowworm Swarm Optimization Algorithm in Wireless Sensor Networks", Expert Systems with Applications, Vol. 38, No. 2011, pp. 12180–12188.
[9] A Review on Node Deployment of Wireless Sensor Network Haitao Zhang and Cuiping Liu IJCSI International Journal of Computer Science Issues, Vol. 9, Issue 6, No 3, November 2012 ISSN (Online): 1694-0814
[10] N. A. B. A. Aziz and A. W. Mohemmed and B. S. Daya Sagar, "Particle Swarm Optimization and Voronoi Diagram for Wireless Sensor Networks Coverage Optimization", in international Conference on Intelligent and Advanced System, ICIAS, pp. 961-965, November 2007.
[11] J. Li, K. Li, and W. Zhu, "Improving Sensing coverage of wireless sensor networks by employing mobile robots", in Proc. Int. Conf. Robot. Biomimetics, pp. 899-903, 2007.
[12] X. Wang, S. Wang, and J. J. Ma, "An improved co-evolutionary particle swarm optimization for wireless sensor networks with dynamic deployment", in Sensors, vol. 7, pp. 354-370, 2007.
[13] N. A. B. A. Aziz and A. W. Mohemmed and M. Y. Alias, "A Wireless Sensor Network Coverage Optimization algorithm based on particle swarm optimization and Voronoi diagram", in International Conference on Networking Sensing and Control, ICNSC, pp. 602-607, March 2009.
[14] T. Blackwell and J. Branke and X. Li, "Particle Swarms for Dynamic Optimization Problems" in Swarm Intelligence, pp. 193-217, 2008.
[15] F. Bullo and J. Cortes and S. Martinez, "Distributed Control of Robotic Networks" Princeton University Press, Applied Mathematics Series, ISBN 978-0-691-14195-4, 2009.
[16] G. Cybenko, "Dynamic load balancing for distributed memory multiprocessors" in Journal of Parallel and Distributed Computing, pp. 279-301, N.2, Vol. 7, October 1989.
[17] M. Grossglauser and D. Tse, "Mobility Increases the Capacity of Ad-hoc Wireless Networks" in IEEE/ACM Transactions on Networking, Vol. 10 pp. 477-486, 2001.
[18] F.Guesrriero, A. Violi, E. Natalizio, V. Loscri, C. Costanzo, "Modeling and Solving Optimal Placement problems in Wireless Sensor Network" in Applied Mathematical Modeling" Volume 35 Issue 1, pp. 230-241, 2011.
[19] H. Guo, K.-S. Low, and H.-A. Nguyen, "Optimizing the localization of a wireless sensor network in real time based on a low cost microcontroller," IEEE Transactions on Industrial Electronics, Vol. 58, No. 3, pp. 741-749, March 2011.
[20] S.M. Guru and S.K. Halgamuge and S. Fernando, "Particle Swarm Optimisers for Cluster formation in Wireless Sensor Networks," in Proc. International conference on intelligent sensors, sensor networks and information processing, pp. 219-224, 2005.
[21] A. Howard and M. J. Mataric and G. S. Sukhatme, "An Incremental Self-Deployment Algorithm for Mobile Sensor Networks," in Autonomous Robots, Special Issue on Intelligent Embedded Systems, pp. 113-126, Vol. 13, 2001.
[22] A. Howard and M. J. Mataric and G. S. Sukhatme, "Mobile Sensor Network Deployment using Potential Fields: A Distributed, Scalable Solution to the Area Coverage Problem," in Proceedings of the 6th International Symposium on Distributed Autonomous Robotics Systems DARS, pp. 299-308, 2002.
[23] Raghavendra V. Kulkarnu and Ganesh Kumar Venayagamoorthy, "Particle Swarm Optimization in Wireless-Sensor Networks: A brief Survey," in IEEE Transactions on Systems, Man and Cybernetics, Part C: Applications and Reviews, March 2011, Vol. 41, Issue: 2, pp. 262-267.
[24] K. S. Low, H. A. Nguyen, and H. Guo, "A particle swarm optimization approach for the localization of a wireless sensor network," in Proceedings of the IEEE International Symposium on Industrial Electronics (ISIE), 2008, pp. 1820-1825.
[25] R. Olfati-saber and J. A. Fax and R. M. Murray, "Consensus and cooperation in networked multi-agent systems," in Proceedings of the IEEE, pp. 215-233, Vol. 95, issue 1, January 2007.
[26] M. Richards and D. Ventura, "Choosing a starting configuration for particle swarm optimization," in Proceedings IEEE International Joint Conference on Neural Networks, pp. 2309-2312, Vol. 3, July 2004.
[27] H. Tanner and A. Jadbabaie and G. J. Pappas, "Flocking in fixed and switching networks," in IEEE Transactions on

Automatic Control, pp. 863, 868, Vol. 52, issue 5, October 2007.
[28] P. A. Tipler, "Physics for Scientists and Engineers," in Worth Publishers, 1991.
[29] T. Vicsek and A. and Czir´ok and E. Ben-Jacob and I. Cohen and O. Shochet, "Novel Type of Phase Transition in a System of Self-Driven Particles," in Phys. Rev.Lett., pp. 1226-1229, Vol 75, issue 6, August 1995.
[30] X. Wang and S. Wang and J. Ma, "Dynamic Deploy- ment Optimization in Wireless Sensor Networks," in Lecture Notes in Control and Information Sciences, pp. 182-187, Vol. 344, October 2006.
[31] Valeria Loscrí, Enrico Natalizio and Francesca Guerriero, "Particle Swarm Optimization Schemes Based on Consensus for Wireless Sensor Networks".
[32] Chandra Satapathy, Anima Naik, and K. Parvathi, "A teaching learning based optimization based on orthogonal design for solving global Optimization problems Suresh" in SpringerPlus 2013.

International Journal of Scientific Engineering and Technology Research

ISSN 2319-8885
Vol.04,Issue.23,
July-2015,
Pages:4444-4447

www.ijsetr.com

Single Feed Dual Band Circularly Polarized Patch Antenna with F and T Shaped Slots

GARIMA RAJPUT[1], PROF. DR. P. K. CHOPRA[2]

[1]PG Scholar, Dept of ECE, Ajay Kumar Garg Engineering College, Ghaziabad, India.
[2]HOD, Dept of ECE, Ajay Kumar Garg Engineering College, Ghaziabad, India.

Abstract: In this paper, a dual frequency resonance antenna is designed by introducing rotated T and F shaped slots on the square patch. The designed antenna is applicable for GPS and WLAN application and operational frequencies are 1.575 and 2.4 GHz with 25 and 60 MHz bandwidth. Opposite corners of the square patch are truncated in order to make the antenna circularly polarized. The axial ratio is measured less than 3 dB at the resonance frequencies, demonstrating a circularly polarized operation and makes it applicable for wireless communication, and also VSWR<2, gain, directivity of antenna and shape of radiation pattern are simulated and presented in this paper by using commercial Ansoft HFSS software.

Keywords: Circular Polarization, Dual-Band, Patch Antenna.

I. INTRODUCTION

GPS is a space based satellite navigation system, that tells the position and time information of the object in all weather conditions. It comprises of 3 segments i.e Space, Control and User segment. User segment is divided into two categories. Civilian user, accuracy provided to civilian user is approx. 10 to 30 m, and the band allotted is L1 band with carrier frequency of 1.575 GHz. Military User, accuracy provided to military user is approx. 1 m, and the bands allotted are L1 and L2 band with carrier frequency of 1.174 GHz, 1.227 GHz. The main aim of next generation wireless communication system is high speed networking service for multimedia communication. Microstrip antennas attracts many microwave and wireless communication systems due to their various advantages like light weight, gain efficiency, easy fabrication, low cost. Microstrip patch antenna can be fed by single or multiple feeding and can operate in single, dual and multiband. The design in [1-2] shows that the antenna is operating in single band, and [3-4] shows antenna operating in dual band, [5-6] shows antenna operating in multiband. Multiple and dual band antennas are used in wireless communication in order to reduce the number and volume of antenna used. In [7] folded patches sharing a common shorting strip is used in order to reduce its size. Stacking of patches is done in [8] to make antenna operable in multiband and also two coaxial feeding techniques is used at 0° and 90° hybrid to achieve good Right Hand Circular Polarization. Proximity probe feed is used in [9] to enhance impedance bandwidth and matching condition. To enhance gain in [10] the antenna is fed by two orthogonal H shaped aperture with 3dB hybrid and in [11] a substrate of low dielectric constant is used. Stacking is used in [12] to make antenna operable in dual band and corner of patch are truncated to make it circularly polarized. In this paper, a novel design for dual frequency antenna is proposed. Dual band is achieved by cutting two slots on square patch, opposite side of patch are truncated to make it circularly polarized. Antenna is fed by coaxial probe into the substrate, with an input impedance of 50Ω. Details designed antenna is discussed.

II. ANTENNA DESIGN

Fig. 1 shows the geometry of the proposed antenna. The dimension of ground is 76 x 76 mm^2, substrate used is FR4 with a width of 4.8 mm and relative permittivity of 4.4. a small size square patch of dimension 30 x 30 mm^2 is designed on the substrate with two cut slots, one is F slot rotated at 90° in clock-wise direction and other is T shaped slot rotated 90° in anti Clock-wise direction, opposite sides of square patch are truncated with a dimension of 2.5 mm and 3.5 mm. The location of feed is (5, 4.5). The dimension of F and T sots are taken to be appropriate which helps in operating antenna in WLAN and L1 band. Single probe coaxial feed of 50Ω input impedance is connected to the ground plane with a radius of 1.75mm.

TABLE I: Dimension of Proposed Antenna

Parameter	a	b	c	d
Value(mm)	15	6	14.6	16.6
Parameter	e	f, g	h	i
Value(mm)	2	0.5	0.75	0.61
Parameter	j	k	l	m
Value(mm)	0.77	13.9	13	2

III. RESULTS

Fig. 2 shows return loss of proposed antenna. At both the resonating frequencies value of VSWR are less than 2.

Copyright @ 2015 IJSETR. All rights reserved.

VSWR determines the amount of power reflected back from antenna. It is required to be less than 2, so that antenna may scatter all the waves' incident on it.

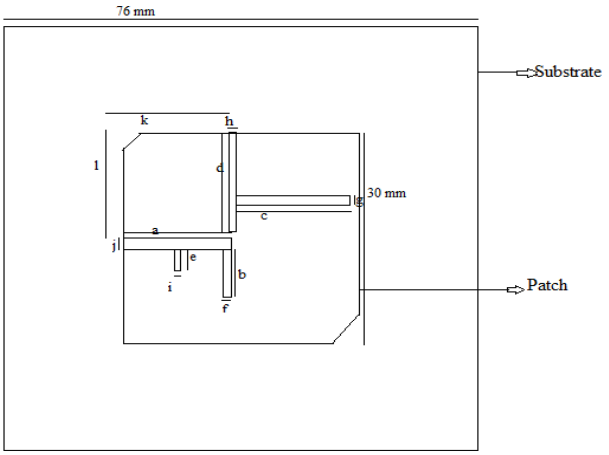

Fig.1. Top view of proposed antenna model.

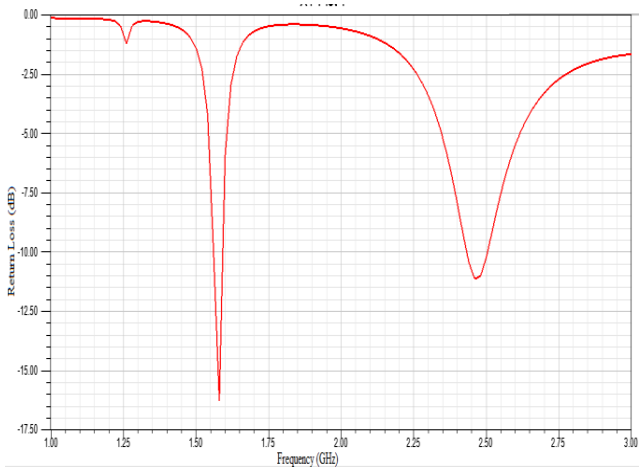

Fig. 2. Return Loss of proposed antenna.

Generally, antenna of high gain is preferred, so a thick substrate is used in this to achieve high gain. Gain of proposed antenna is shown in Fig. 3. Gain defines how much power is radiated in given direction.

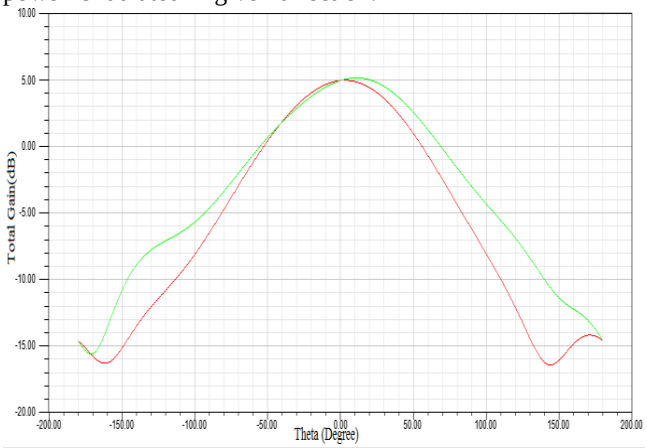

Fig. 3. Gain of proposed antenna.

The radiation pattern is shown in Fig.4. The designed antenna shows directional radiation pattern.

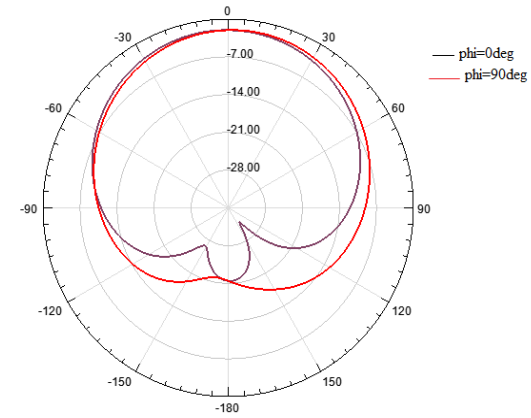

(a)

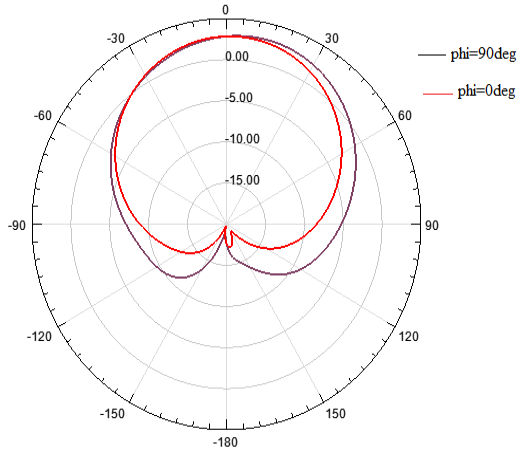

(b)

Fig.4. Radiation patterns of proposed antenna at different frequencies: (a) 1575 MHz (b) 2440 MHz.

Directivity of the proposed antenna is shown in Fig. 5, since the antenna have directional radiation pattern, so it have a directivity of 4.9 and 6.8 dB at 1575 and 2440 GHz. Axial Ratio is the ratio of orthogonal E-field component of equal amplitudes. Axial ratio of proposed antenna is shown in Fig. 6.

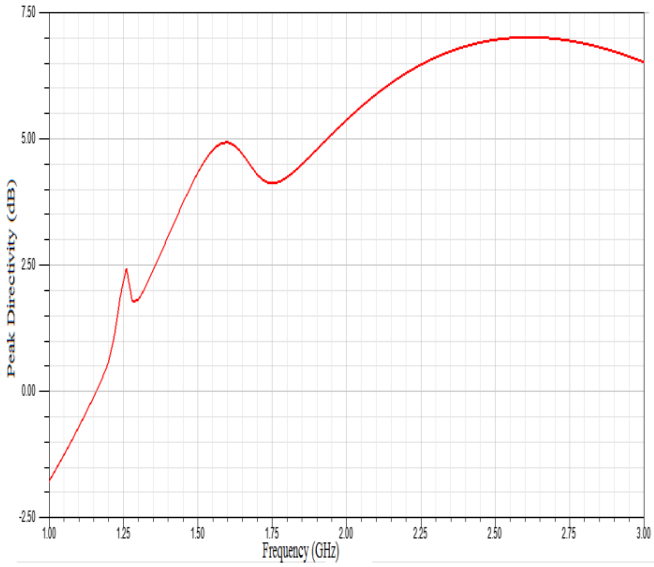

Fig. 5. Directivity of proposed antenna.

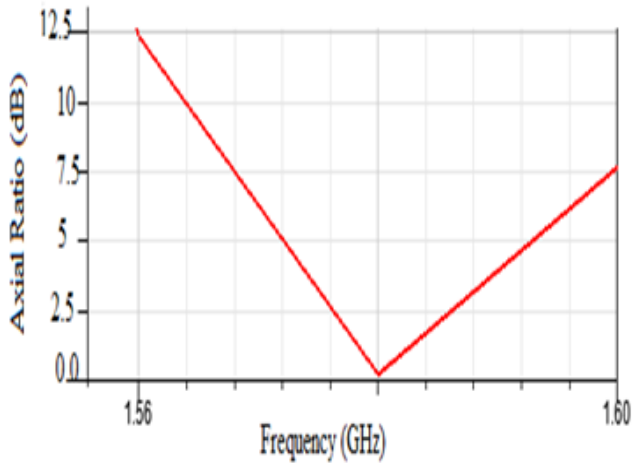

(a)

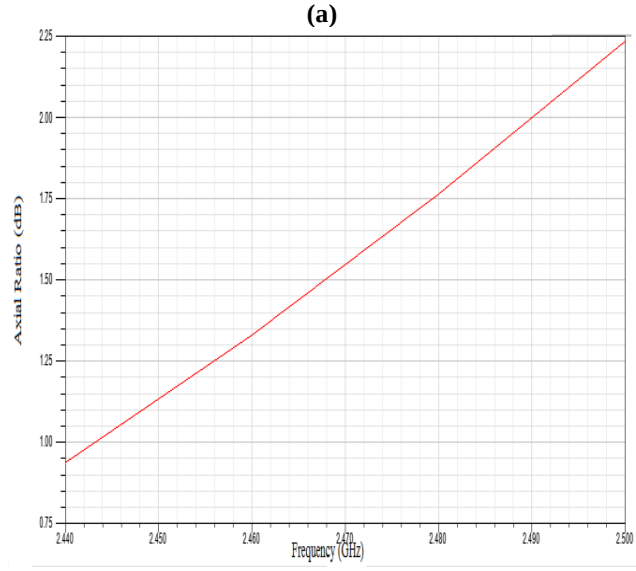

(b)

Fig. 6 Axial Ratio at different frequencies: (a) 1575 MHz (b) 2440 MHz.

IV. CONCLUSION

In this, we have presented a design of an antenna that is capable for operating in WLAN and GPS L1 band. The antenna is made by using a square patch of small size with rotated F and T slots and corners of patch are truncated to make it circularly polarized. Low cost FR4 substrate is used as it is easily available. Simulation is done by using HFSS. The achieved results states that designed antenna fulfill the requirements of antenna used for wireless communication.

Future Scope: A dual band antenna is proposed here for WLAN and GPS L1 band. But with the growing technology better results may be achieved than this proposed work. GPS tracking will continue to grow in both the business and commercial sectors. Due to heavy investment and demand, the cost of GPS tracking will decrease over the new few years, making an even more affordable proposition for businesses.

V. ACKNOWLEDGEMENT

I sincerely thanks ECE department of Ajay Kumar Garg Engineering College, Ghaziabad for providing the opportunity and guidance for research work.

VI. REFERENCES

[1] X. L. Bao, G. Ruvio, M. J. Ammann, and M. John, (2006), A Novel GPS Patch Antenna on a Fractal Hi-Impedance Surface Substrate, IEEE Antennas and Wireless Propagation Letters, Vol. 5, pp. 323-326.

[2] Filiberto Bilotti, Senior Member, IEEE, and Claudio Vegni, (2010), Design of High-Performing Microstrip Receiving GPS Antennas With Multiple Feeds, IEEE Transactions on Antennas and Propagation, No. 9, pp. 248-251.

[3] Peter Callaghan and John C. Batchelor, 2008, Dual-Band Pin-Patch Antenna for Wi-Fi Applications, IEEE Antennas and Wireless Propagation Letters, Vol. 7, pp. 757-760.

[4]Zhongbao Wang, Shaojun Fang, Shiqiang Fu, and Shanwei Lü, (2009), Dual-Band Probe-Fed Stacked Patch Antenna for GNSS Applications, IEEE Transactions on Antennas and Propagation, Vol. 8, pp. 100-103.

[5]Y.-Y. Cui, Y.-Q. Sun, H.-C. Yang, C.-L. Ruan, 2008, a new triple-band cpw-fed monopole antenna for wlan and wimax applications, Progress In Electromagnetics Research M, Vol. 2, pp. 141-151.

[6] Wen-Chung Liu, Chao Ming Wu, and Yang Dai, 2011, Design of Triple-Frequency Microstrip-Fed Monopole Antenna using Defected Ground Plane, IEEE Transactions on Antennas and Propogation, Vol 59, No. 7, pp. 2457-2462.

[7]Yong-Xin Guo, Irene Ang, and M. Y. W. Chia,2003, Compact Internal Multiband Antennas for Mobile Handsets, IEEE Antennas and Wireless Propagation Letters, Vol. 2, pp. 143-146.

[8] Yijun Zhou, Chi-Chih Chen, and John L. Volakis (2007), Dual Band Proximity-Fed Stacked Patch Antenna for Tri-Band GPS Applications, IEEE Transactions on Antennas and Propagation, Vol. 55, No. 1, pp. 220-223.

[9]Zhongbao Wang, Shaojun Fang, Shiqiang Fu, and Shanwei Lü, (2009), Dual-Band Probe-Fed Stacked Patch Antenna for GNSS Applications, IEEE Transactions on Antennas and Propagation, Vol. 8, pp. 100-103.

[10]Xiaoye Sun, Zhijun Zhang, and Zhenghe Feng, (2011), Dual-Band Circularly Polarized Stacked Annular-Ring Patch Antenna for GPS Application, IEEE Transactions on Antennas and Propagation, No. 10, pp. 49-52.

[11]V.Anitha, S.Sri Jaya Lakshmi, M.L.S.N.S. Lakshmi, K. Ashok Kumar, Ch. Ravi Teja, T.Rajashekar Reddy (2012), A circulary polarized stacked patch antenna using Ployflon Substrate for Wireless Applications, IJERA, Vol. 2, Issue 3, pp. 903-905.

[12]Shun-Lai Ma and Jeen-Sheen Row (2011), Design of Single-Feed Dual-Frequency Patch Antenna for GPS and WLAN Applications, IEEE Transactions on Antennas and Propagation, Vol. 59, No. 9, pp. 3433-3436.

Author's Profile:

GARIMA RAJPUT received the B.Tech degree in Electronics and Communication Engineering from BBDIT, GBTU, in 2013. She is persuing M.Tech in Electronics and Communication Engineering from Ajay Kumar Garg Engineering College, UPTU, from 2013. She completed Engineering with Honors and her area of interest is Microstrip

patch antenna for wireless communication.
She qualified Gate exam in 2013. Currently she is working on project, microstrip patch antenna for wireless communication.

GP. CAPT. PRADEEP KUMAR CHOPRA (R), VSM entered the field of education in the year 2004 after 24 years of exemplary service in the technical branch of Indian Air Force. He earned his bachelor degree in Engineering (Electronics) from Delhi College of Engineering in the Year 1979 and masters in Technology from IIT Delhi in the year 1985. He also graduated from the prestigious Defence Services Staff College, Wellington and earned Master's degree in Defence studies in the year 1993 from Madras University. While he was in Indian Air Force he was part of, and headed, a number of important technical projects. For his exemplary services he was awarded "Vishist Seva Medal" by the president of India for engineering skills of highest order in the year 1993. He took voluntary retirement from the IAF in the year 2004 and entered the field of education. He has done his Ph.D in the field of 'Electronics and Communication Engineering' from the prestigious G.G.S.I.P University, New Delhi. Presently he is the Dean and Head of Department of Electronics and Communication Engineering and Electronics and Instrumentation Engineering. His area of specialization is Radar and Satellite Communication. He is fellow of Electronics & Telecommunication Engineers, New Delhi.

ResearchGate

See discussions, stats, and author profiles for this publication at: http://www.researchgate.net/publication/280614463

TCAD Analysis of Silicon-Germanium (SiGe) based Back-Contact Back-Junction (BC-BJ) solar cell as an alternative for silicon based cells

CONFERENCE PAPER · JUNE 2015

DOI: 10.13140/RG.2.1.1008.6246

DOWNLOADS
8

VIEWS
3

2 AUTHORS:

Rahul Pandey
Delhi Technological University
2 PUBLICATIONS **0** CITATIONS
SEE PROFILE

Rishu Chaujar
Delhi Technological University
70 PUBLICATIONS **102** CITATIONS
SEE PROFILE

Available from: Rahul Pandey
Retrieved on: 12 August 2015

TCAD Analysis of Silicon-Germanium (SiGe) based Back-Contact Back-Junction (BC-BJ) solar cell as an alternative for silicon based cells

R. Pandey* and R. Chaujar**

Microelectronics Research Lab, Department of Engineering Physics,
Delhi Technological University, Bawana Road, Delhi-110042, India
*Rahulpandey@dtu.ac.in
**Rishu.phy@dce.edu

ABSTRACT

In this work, an ultra-thin, Back-Contact Back-Junction (BC-BJ) Silicon-Germanium (SiGe) solar cell device structure called BC-BJ SiGe solar cell has been proposed, which shows enhanced photovoltaic properties, External Quantum Efficiency (EQE) > 76% in the spectrum range of 400-700 nm wavelength have been achieved. Results further, reveal that proposed device is less affected by carrier recombination, resulting in 13.5 % power conversion efficiency (PCE). Also we obtained the impact of material thickness on device parameters and we found that the 5µm thick SiGe cell is as efficient as 10µm thick silicon cell. The PCE of 5µm thick SiGe cell and 10µm thick silicon cell was 11.3% and 11.8%, respectively. It indicates that the proposed device significantly save the material cost over the silicon cell. All the simulations have been done using DEVEDIT and ATLAS device simulator.

Keywords: Efficiency, Recombination, Silicon-Germanim, Solar cell

1 INTRODUCTION

Crystalline silicon is the largest component of the solar photovoltaic (PV) cells. Over 80% installed solar PV in 2011 used silicon as their largest material. Silicon is widely used material for PV due to its reliability, abundance, and mature fabrication process. In Silicon PV technology, absorption coefficient of Silicon is small, to absorb enough of the solar cell spectrum. The thickness of conventional silicon cell is typically more than 100µm, in order to absorb the solar spectrum. Now since, thickness is large, in order to collect light generated carrier, minority carrier lifetime must be high enough and the recombination coefficient should be low. This requirement of large volume and high quality silicon significantly increases the module cost. In order to make photovoltaic system feasible at large scale, it should be cost effective, with module cost to be < $0.5/W [1]. In this paper, we proposed SiGe as an alternative to silicon solar cell, due to its higher minority carrier lifetime and lower recombination coefficient. Reducing the thickness of PV materials used in solar cell production is a major goal of solar cell industry, due to its fruitful contribution to the overall cost of a PV system. However, thin silicon cells are not effective, due to severe Auger recombination and increased surface to volume ratio [2].

One promising high-efficiency solar cell concept is the back-contact back- junction solar cell [3, 4] having both, junction and the electrodes at back side of the device. Now, since the junction and contacts are at the back side, Front surface can be designed for optimum optical performance [5].

Here, we proposed novel 10µm thick crystalline SiGe back-contact back-junction solar cell, which overcomes the critical problems of thin devices: Auger and surface recombination etc. Further, we have obtained the impact of material thickness on photovoltaic parameters. In SiGe technology the electrical properties of silicon are modified with germanium. SiGe processing is simple because the physical and electrical properties of silicon and germanium are similar [6]. Also SiGe possesses higher mechanical strength, and suppresses the high intensity degradation of solar cell under illumination [7]. Optical absorption of SiGe can further be modified by varying Ge content [8, 9].

2 DEVICE STRUCTURE AND PHYSICAL MODELS

Silvaco ATLAS used to simulate the device optoelectronic characteristics. ATLAS is a device simulator capable of modeling the electrical, thermal, and optical characteristics of semiconductor devices.

In the simulation, we assume a two dimensional structure, BC-BJ solar cell as shown in Fig. 1. The $Si_{0.9}Ge_{0.1}$ was used during the simulation, very small fraction of germanium is used. Because, if we increase the germanium content the bandgap of SiGe decreases [10] The substrate was N-type, with doping density of $3x10^{15}$ cm^{-3}, whereas N+/P+ region has the doping density of $4x10^{20}$ cm^{-3}. The depth of P+ and N+ region was 3µm and 2.5µm, respectively, whereas the width was 40µm and 30µm, respectively. The Nitride (Si_3N_4) is used as anti-reflecting front surface passivation, and modeled as an optical layer with the thickness of 70 nm. The Oxide (SiO_2) is used as back surface passivation with thickness of 50nm.

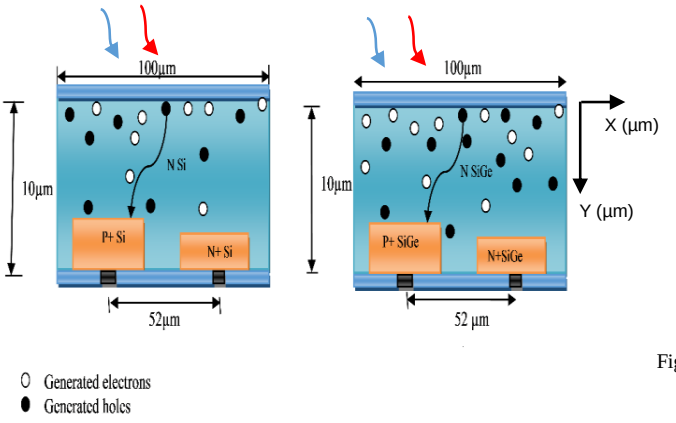

Fig.1. Simulated device: - 10µm thick BC-BJ solar cell: (a) Silicon (b) SiGe

To obtain the J-V curve under illumination, we used the standard AM1.5 solar spectrum, divided into 400 points. The models used in the simulation assume a concentration dependent mobility using default software values for electron and holes [11]. Shockley – Read-Hall and Auger recombination mechanisms were taking into account. Auger recombination was modeled with the default software values of Auger coefficient $2.8x10^{-32}$ cm^6s^{-1} for electrons and $9.9x10^{-32}$ cm^6s^{-1} for holes, in case of silicon, whereas $9.9x10^{-31}$ cm^6s^{-1} for electrons and $1.8x10^{-31}$ cm^6s^{-1} for holes were used, in case of SiGe. The minority carrier lifetime of 10^{-6}s and 10^{-5}s has been used for silicon and SiGe, respectively. The Poisson equation together with the continuity equation for electrons and holes are solved simultaneously by the software to obtain the J-V characteristics.

3 SIMULATION RESULTS

Figure 2 shows the contour plot of recombination rate. The magnitude of recombination rate in silicon cell is in the order of (10^{20} /cm^3s), whereas in proposed device it is (10^{18} /cm^3s).

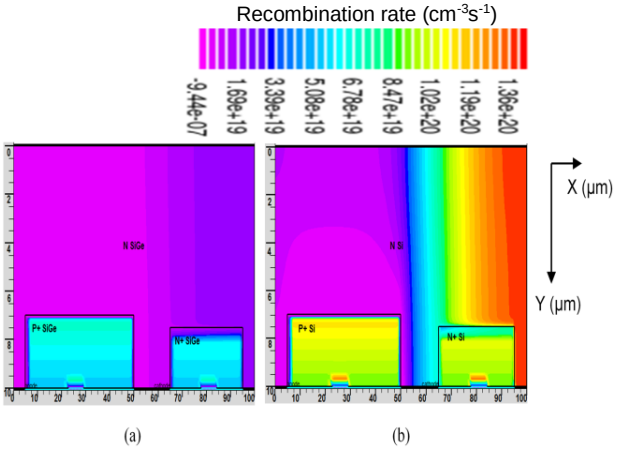

Fig. 2. Recombination rate contour (logarithmic plot): (a) 10µm thick BC-BJ SiGe solar cell (b) 10µm thick BC-BJ Si solar cell.

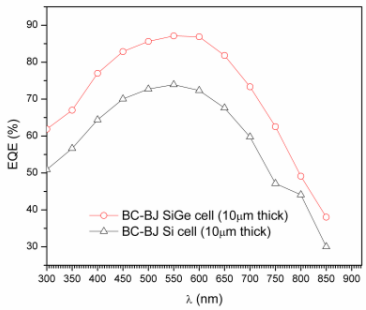

Fig. 3. Comparison of External Quantum Efficiency (EQE)

At the interface, recombination rate is higher in right side of the devices because collection probabilty of minority carriers (hole) is decreases. The lower recombination is observed in novel device because minority carrier lifetime is higher compared to silicon cell. In back contact design, most of the carriers are generated near the front surface, while the junction is far at the back surface. Lower recombination ensure higher carrier collection efficiency.

Also, the EQE of the proposed device is higher than silicon cell as shown in Fig 3. The proposed device shows EQE>76% in the spectrum range of 400-700 nm wavelength whereas in silicon cell, EQE>60% was obtained. The proposed device shows 26% higher EQE compared to silicon cell, due to the presence of Ge. Since, the no. of free electrons in the germanium is higher than the silicon at given temperature, which results in higher conductivity of Ge.

Further, we have obtained the impact of device thickness on photovoltaic parameters. We have decreased the device dimension to half the initial dimensions, discussed earlier, keeping the aspect ratio (Width/Depth) of P+ and N+ region fixed 1/15 and 1/12, respectively. The length of the pitch becomes 26µm. The electrical parameters of 10µm thick devices and 5µm thick devices are plotted in Fig 4. Fig. 4(a&d), shows the current density-volatge (J-V) curve and PCE bar for different devices, when thickness of silicon cell decreased from 10µm to 5µm, change in short circuit current density J_{SC} and PCE was 26.6% and 26.2%, respectively, whereas for SiGe it was 17.7% and 16.3%, respectively. It shows that proposed device is less affected by the thickness variation compared to the conventional silicon cell. Also Fig. 4(b&d) shows that the maximum output power density (P_M) of 10µm thick silicon cell and 5µm thick SiGe cell was approximately same, 11.8mW/cm^2 in 10µm thick silicon cell and 11.3mW/cm^2 in 5µm thick SiGe cell, respectively. Also, open circuit volatge (V_{OC}) can be obtained by taking the intercept to x- axis form the sharp minima, shown in Fig. 4c. Proposed device shows superior photovoltaic properties comparing to conventional silicon cell due to lower recombination [12]. Detailed comparisons of electrical parameters are shown in Table 1. Table 1, shows that the performance of 5µm thick SiGe was approximately equal to the 10µm thick silicon cell, indicating that the proposed device significantly saves the material cost over silicon cell.

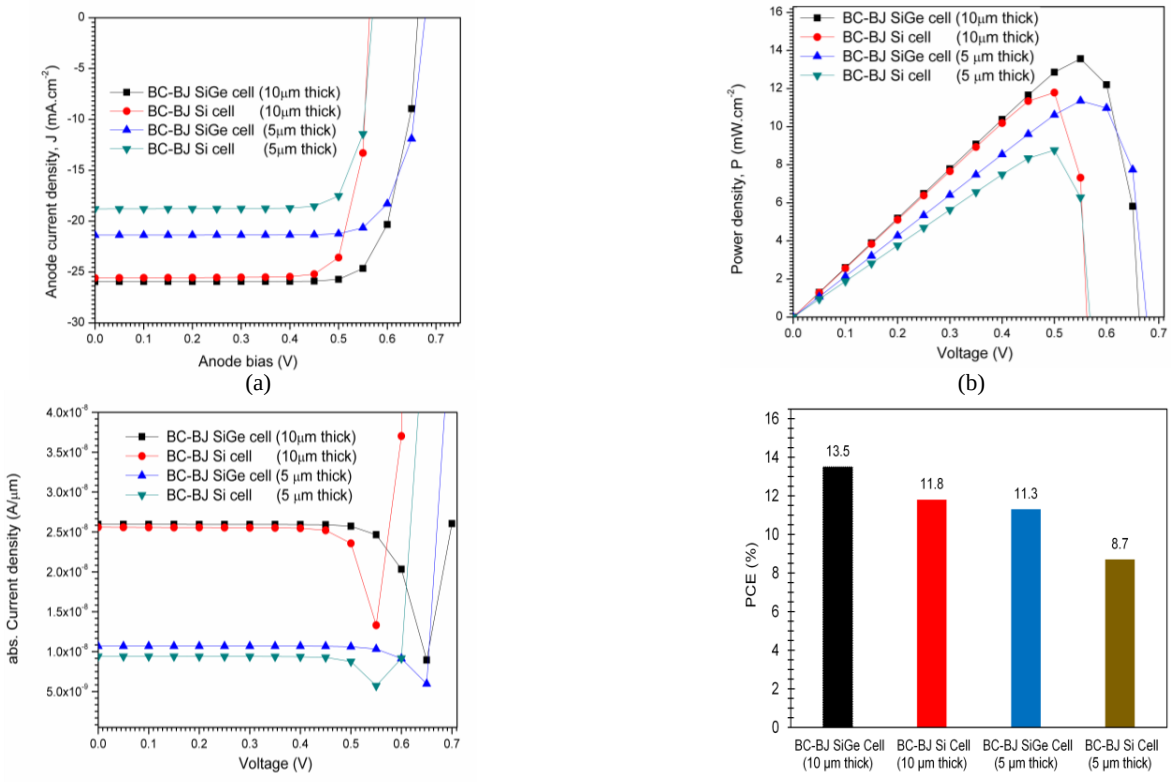

Fig.4. Comparisons of electrical characteristics of different devices: (a) J-V, (b) Power density-voltage, (c) Abs.current density-voltage (d) PCE.

Table1. Detailed comparisons of electrical parameters

Device	Voc (V)	Jsc ($mAcm^{-2}$)	FF (%)	PCE (%)
Silicon cell (10μm thick)	0.563	25.6	81.8	11.8
SiGe cell (10μm thick)	0.663	25.9	78.8	13.5
Silicon cell (5μm thick)	0.569	18.8	81.9	8.7
SiGe cell (5μm thick)	0.677	21.3	78.4	11.3
FF-fill factor, PCE- power conversion Efficiency.				

4 CONCLUSION

In this work, we proposed a novel 10μm thick BC-BJ SiGe Solar cell design, as a cost-effective solution for energy efficient applications. The work analyse and compares the optical and electrical characteristics of proposed design using Silvaco Atlas device simulator.

Proposed device shows superior photovoltaic parameters compared to silicon cell. Also results reveal that when the thickness of proposed device is reduced to 5μm, its PCE, 11.3% was approximately equal to PCE, 11.8% of 10μm thick silicon cell. It indicates that the proposed device significantly saves the material cost over silicon cell. Proposed device shows improved photovoltaic parameters: EQE> 76% in the spectrum range of 400-700 nm wavelength, Jsc 25.9$mAcm^{-2}$, Voc 663mV, fill factor (FF) 78.8% and PCE of 13.5%. Simulation result shows SiGe semiconductor as an alternative to expensive materials for thin BC-BJ solar cell design.

ACKNOWLEDGMENT

The authors would like to thank Microelectronics Research Lab, Department of Engineering Physics, Delhi Technological University to carry out this work. Rahul Pandey (JRF) acknowledges UGC, Govt. of India for providing fellowship.

REFERENCES

[1] S. Jeong, M. D. McGehee and Y. Cui , "All-back-contact ultra-thin silicon nanocone solar cells with 13.7% power conversion efficiency" Nature Communications 4, Article number: 2950: 1-7, 2013.

[2] R. R. King, R. A. Sinton, and R. M. Swanson, Studies of diffused phosphorus emitters: saturation current, surface recombination velocity, and quantum efficiency. IEEE Trans. Electron Dev. 37, 365–371, 1990.

[3] R. J. Schwartz and M. D. Lammert. Silicon solar cells for high concentration applications. In IEEE International Electron Devices Meeting, pages 350–352, 1975.

[4] E. V. Kerschaver and G. Beaucarne. Back-contact solar cells: A review Progress in Photovoltaics, 14(2):107–123, 2006.

[5] D.diouf, J.P. Kleider, T.desrues, P.-J. Ribeyron" Study of interdigitated back contact silicon heterojunction solar cells by two-dimensional numerical simulations", Material Science and Engineering B 159-160:291-294. 2009

[6] J.Ouellete,"Silicon-Germanium Gives Semiconductor the Edge" American institute of physics, 2002:22-25.

[7] D.Yang, X.Yu, X. Li, P.Wang, L. Wang, "Germanium-doped crystal silicon for solar cells," Solid-State and Integrated Circuit Technology (ICSICT), 2010 10th IEEE International Conference on, vol., no.,1994,1994, 1-4 Nov. 2010.

[8] C.C.Wang, D.S.Wuu, S.Y. Lien, Y.S. Lin, C.Y. Liu, C.H. Hsu, and C.F. Chen , "Characterization of Nanocrystalline SiGe Thin Film Solar Cell with Double Graded-Dead Absorption Layer " International Journal of Photoenergy Volume 2012, 6 pages

[9] H. Povolny, P. Agarwal, S. Han, and X. Deng, "Comparison Study of a-SiGe Solar Cells and Materials Deposited Using Different Hydrogen Dilution " Mat. Res. Soc. Symp. Proc. Vol. 609, 2000.

[10] G.G. Pethuraja et al., Materials Sciences and Applications, 3, pp.67-71, 2012.

[11] ATLAS User's Manual DEVICE SIMULATION SOFTWARE. May 17, 2012.324.

[12] S.M.Sze," Physics of Semiconductor Devices 2nd Edition": 811-813

International Journal of Industrial Engineering and Technology.
ISSN 0974-3146 Volume 7, Number 1 (2015), pp. 31-38
© International Research Publication House
http://www.irphouse.com

The Evaluation and Implementation of Various Techniques in Lean Manufacturing

Ankit Agarwal[1], Himanshu[2], Anup Kumar[3], Dr.A.K.Madan[4]

[1,2,3,4] Department of Production and Industrial Engineering
Delhi Technological University (formerly Delhi College of Engineering),
New Delhi, India.

Abstract

The idea of lean manufacturing was originated for maximizing the resource utilization by minimizing the waste. Due to fast changes in business environment the industries are compelled to face challenges and complications. Any institution either manufacturing or service related to survive may eventually depends on its ability to systematically respond to these changes for increasing the product value. Therefore adding value to the process is important to attain this perfection; hence implementing a lean manufacturing system is becoming important for any type of institution to sustain. In this paper, we aimed to develop a lean route map for the institutions to carry out the lean manufacturing system.

Keywords— Cellular manufacturing, Pull system

1. Introduction

Lean Manufacturing is considered to be a waste reduction technique, but in practice lean manufacturing increases the value of the product through reduction of waste. Lean principles provides value to product/service as required by the customer and then making the flow in-line with the customer for perfection through continuous improvement in elimination of waste by sorting out Value Added activity(VA) and Non-Value Added activity(NVA). The sources for the NVA activity wastes are Transportation, Inventory, Motion Waiting, Overproduction, Over processing and Defects. The NVA activity waste is vital hurdle for VA activity. Elimination of these wastes is achieved through the successful implementation of lean elements. Various Survey demonstrate that most of the researcher focus on one or two elements for

finding out the existence of wastes and suggest their views on implementing these elements.

2. Overview of Lean Elements

The major elements considered by the earlier researchers for the implementation of the lean manufacturing system are Cellular Manufacturing defines the facility grouping in order to produce the product with minimum process time, waiting time, and transportation by smoothen the process flow. Further fluctuating line flow is improved by U-line concept and line balancing concept, Kanban is Material Flow Control mechanism (MFC) which delivers the right quantity of parts at right time. Stages of this Kanban implementation are production stage and withdrawal stage. Production Levelling enhances production volume as well as production mix and production efficiency by means of reducing waste, unevenness, and overburden of people or equipment. Levelling of parts leads to successful implementation of lean manufacturing.

3. Review of Lean Implementation

The perfect strive of the manufacturing system can be achieved through successful implementation of lean elements. Most of the survey on lean elements focuses on only one or two element or combination of two or three elements. For successful implementation of lean, practically need incorporation of all lean elements and sequencing of implementation task. This literature review explains the incorporation and sequencing of lean elements during implementation period along with implementation issues.

3.1 Scheduling

Scheduling includes deciding the preference order for different jobs and decides the starting and finishing time of every job. It also involves scheduling of machine tools, equipments, inspection and raw material etc. By defining a clear production plan any organization can start initializing the manufacturing system implementation.

3.2 Group Technology

Group Technology is a methodology in which similar parts are identified and grouped together to take advantage of their similarities in design and production. It reduces the work in process inventory and reduces lead time. Shunk et al. suggested that the complete utilization of flexible manufacturing system needs grouping of parts using similarity among the design and manufacturing attribute which make the production plan and manufacturing process flexible. After grouping of parts by similarity in process, dissimilar machines are grouped together to form a cell. Formation of Cell entirely depends upon the nature of the process which changes from institution to institution.

3.3 Cellular manufacturing (CM)

Cellular Manufacturing includes processing a collection of similar parts on a dedicated batch of machines or manufacturing process. Parts are identified such that they will be ideally processed within a machine cell. Wemmerlov et al. suggest those dissimilar machines are clustered in sequential manner in order to meet process need of a family of product. Metternich et al. suggested that the effective and efficient clustering of machine or cell is improved by moving employees, Workstations, or both into a U-shaped line which improve the employees' interaction. CM reduces the manufacturing lead time by decreasing the setup, work part handling, waiting time and batch size. CM improves the quality by allowing each cell to specialize in producing smaller number of different parts which in turn will reduce process variability. The success of Cellular Manufacturing system depends on the successful utilization of U-Line manufacturing system, Line balancing, and Flow manufacturing.

3.4 U-line manufacturing system

In U-line Manufacturing System entry and exit is located at the same position. A narrow U-shape line is generally formed because both ends of the line are located narrowly together. It reduces number of work station, improve line balancing, visibility, communication, quality, flexibility, material handling. Guerriero et al. clearly define the line flexibility for stochastic U line system and suggested that when demand uncertainty occurs, U-line layout provides greater flexibility to increase or decrease the necessary number of workers.

The performance of U-Line was evaluated by minimum number of workstations, minimum work relatedness, and minimum workload smoothness. Generally U-line flexibility is disturbed by line imbalance in mixed product production line. To remove this imbalance analysis of both balancing and sequencing task is to be carry out together.

3.5 Line balancing

Line Balancing means assigning operations to workstations along an assembly line in such a way that the assignment be optimal. Line balancing tries to achieve a best combination between facility, labour and resources to provide a given volume of production. Monden et al. suggested that the consideration of task time variability is due to human factors or various disruptions which leads to line balancing problem. The variability in task time is mainly due to the instability in the work rate of humans and failure sensitivity of complex processes. Becker et al. and Chiang et al. suggested task itself a sources of variability and explains the worker performing the task, and the environment where the task is performed. These sources of variability are controlled by minimizing the moving cost of men and machine. The operator walking time and fluctuation of man and machine cycle time leads to line imbalance. Also the change over time creates imbalance in the line for mixed model line which is necessary for lean. Based on demand, the number of worker and machine within the workstation are increased or decreased in order to overcome the line imbalance. Man-machine flexibility is achieved through free flow of material and information in the manufacturing process.

3.6 Flow Manufacturing

The principle of flow manufacturing is producing an item at a time at a rate equal to the cycle time, the successful implementation of flow manufacturing needs U-line layout, multi-skill operator, standardized cycle time, designing operator work as standing and walking manner and the equipment/machine should be standard and less expensive user friendly. Miltenburg et al. Suggested that the break-through or tedious process flow can be balanced by introducing the customized machine in the workstation in order to balance the machine with the workstation cycle time. The mixed model flow is smoothened by designing the workstation with Quick changeover and Small lot size.

3.7 Small Lot size/Small Batch

A batch is a group of parts of the same part family. While part families are supposed to be given prior, lot sizing is a part of the decision making process. Conventional manufacturing systems are run based on buffer production system. The built-in inventory system was involved to overcome the material flow disturbance in case of machine break down, absenteeism which lead to high quality problem and lead time. In order to keep the material flow smooth and to overcome the problem of quality and lead time, inventory quantity should be optimized. In practice, Lean is associated with zero inventories to increase the visibility of product flows and optimize the utilization of capacity.

3.8 Inventory

Inventory may be defined as any resource that serves has a buffer or safety against ill planning and continuous production, when the demand for the item will arise. Studies from various research shows that 60% of wastes in production system are due to inventory. These Inventories are in the form of Raw material (RM), Work-in-process (WIP) (semi finished goods), Finished goods (FG). Increase in inventory of RM, WIP or FG leads to less inventory turnover. Inventory plays a vital role in firm's turnover. Present trend is to go for Minimum inventory level because large inventory is a sign of inefficiency. Sakakibara et al. suggested that the large RM is due to poor implementation of product plan, availability of raw material, defective parts, waiting for processing leads to more WIP, and unnecessary transportation between working stations or plants increases WIP inventory, overproduction of parts beyond the plan leads to FG inventories which wait long time in the warehouse or might never be sold. Inventories are reduced by improving the quality levels, rejection rates, delivery rate, lead time and customer satisfaction. Demete et al. suggested that WIP is controlled by implementing cellular manufacturing/dedicated line Assemble or manufacture the parts against the customer order reduces FG which means FG goes to customer without unusual delay. Imperfection due to lack of process control in the manufacturing system creates the WIP requirement in workstation. In order to reduce the impact adjacent process, the decoupling buffers is placed between processes to overcome the imperfection. The inventory allow each of the teams to make decisions regarding stopping the line to fix problems. Inventory contradicts the lean system but in real condition safety buffer is important in case of system variations.

3.9 Kanban

Kanban is to increase system efficiency or productivity and to secure operator involvement and participation to accomplish high productivity by making a highly visible means to monitor the product flow through the production system and the build-up levels of inventory within the system. Sipper et al. Classify the Kanban system into the two cards Kanban system for signalling production and withdrawal. During demand uncertainty the inventory is important for smoothening of production flow and reconfigures the Kanban System in order to lower the inventory. Therefore Kanban system gives mixed model production along with optimum inventory levels which results in reduction of lead time in the delivery of product and active use of resources like man, tools, machines etc.

3.10 Production Levelling

Present business environment are volatile which leads to variations in customer demand, these variations leads to variability in the production. In order to overcome this variation initially levelling of customer demand is required, without levelling, these variations leads to un-utilized resources such as man and machine idle times or quality problems, breakdowns, and defects. Bohnen et al. suggested that the levelling low volume and high mix production based on the principles of Group Technology is necessary for fluctuating demand of customer. Bohnen et al. develop the cluster technique for part family formation and family oriented levelling pattern for implementing low volume, and high mix production system. The concept of product levelling is to control the variability of the job arrival sequence to allow higher capacity utilization, also it removes ups and downs in the production schedule.

3.11 Continuous Improvement (CI)

Continuous Improvement (CI) is defines as "Improvement initiatives that increase successes and reduce failures" Continuous Improvement is the tool to determine the reason for any inefficiencies and to take effective measures to control those inefficiencies. Research shows that CI can take place at three different levels within the organization: at the management, group, and individual levels. At the management level, the implications of CI are on the organization's strategy. Group level CI involves problem-solving tasks at a broad level, while individual level CI deals with improvement on a micro scale, i.e. on low level, day-to-day tasks. In order to get maximum benefits from a CI program, managers must implement CI at each of these levels.

In the present ambitious environment CI is very important to sustain in the market, but the benefits of the Continuous improvement rely on employee attitude, acceptance of variations, team work, leader commitment, interest, initiative, and training. CI training includes process problem solving, tools and technique, development of idea management and development of reward and recognition system.

3.12 Standardized Work

Standardized work is one of the most important tools of lean manufacturing. As the standards are improved, the new standards become the baseline for further

improvements, and so on. Improving standardized work is a never-ending process. It helps in reduction in variability, easier training of new operators, reductions in injuries and strain. Berger at al. suggested that the Standard Work is the basic tool for continuous improvement. Standard Work refers to the safest and most effective method to carry out a job in the shortest repeatable time as a result the utilization of resources such as people, machines, and material is effective.

Standardization of work is defined as a set of Standard Operating Procedures (SOPs). SOP contain operator work process like process steps, work sequences, cycle time, work-in-process, process control etc., SOPs represent the best method to do a particular job within the target time.

4. Summary

Implementation and sequencing of lean elements with dependent elements are the vital factor for the successful implementation of lean manufacturing system as suggested by most of the research. In this paper, a lean road map is recommended for the implementation of lean elements along with other interdependent elements. Steps in implementing the Lean elements are as follows first step is implementation of Group Technology; here parts are grouped into part family and machines are grouped based on these part family. The Second step is implementation of Cellular Manufacturing. Cell formation depends on group technology and part family. Further U-line system is streamline through Line Balancing and material/information flow is streamline through Flow manufacturing. The successful implementation of Flow Manufacturing depends on Lot size reduction which stream line RM, FG and WIP. The Third step is implementation of Kanban system for triggering the production. The Fourth step is Production Levelling; implementation of this element depends on successful implementation of all the above said elements. The Fifth step is simultaneous Standardization and Continuous Improvement. In order to sustain in the competitive market five steps should be repeated.

5. Conclusion

Conclusion of this paper concludes that for implementation of Lean Manufacturing system requires assimilation and simultaneous implementation of Lean elements in a given order. The Paper also gives the thorough Road Map which gives a different theory for Lean Manufacturing System implementation. Therefore the given implementation reduces the duration and production system divergence. As a result it is recommended that the Lean Manufacturing System is important tool to sustain in this competitive business environment.

6. References

[1] Graves, R., Konopka, J.M., Milne, R.J., 1995. Literature review of material flow control mechanisms. Production Planning and Control 6 (5), 395-403

[2] S.G. Li, Y.L. Rong, The reliable design of one-piece flow production system using fuzzy ant colony optimization, Computers & Operations Research 36 (2009) 1656-1663.

[3] Shingo, A Revolution in Manufacturing: The SMED System, Productivity Press, Portland, 1985.

[4] David Losonci, Krisztina, Demeter,Istvan Jenei, Factors influencing employee perceptions in lean transformations, Int. J. Production Economics 131 (2011) 30-43.

[5] Fawaz A. Abdulmalek, Jayant Rajgopal, Analyzing the benefits of lean manufacturing and value stream mapping via simulation: A process sector case study, Int. J. Production Economics 107 (2007) 223-236.

[6] McDonald T, Van Aken E.M, Rentes A.F, Utilizing simulation to enhance value stream mapping: a manufacturing, case application. International Journal of Logistics, Research and Applications 5 (2) 2002 213-232.

[7] K. Das, R.S. Lashkari,_, S. Sengupta, Reliability consideration in the design and analysis of cellular manufacturing systems, Int. J. Production Economics 105 (2007) 243-262.

[8] Joachim Metternich, Sven Bechtloff, Stefan Seifermann, Efficiency and Economic Evaluation of Cellular Manufacturing to enable Lean Machining, Procedia CIRP 7 (2013) 592-597.

[9] Guerriero F, Miltenburg J,The stochastic U-line balancing problem, Naval Research Logistics 50 (1) (2003) 31-57.

[10] Monden Y, Toyota Production System. Industrial Engineering and Management Press, Norcross, GA 1983

[11] Christian Becker, Armin Scholl, A survey on problems and methods in generalized assembly line balancing, European Journal of Operational Research 168 (2006) 694-715

[12] Wen-Chyuan Chiang, Timothy L. Urban,The stochastic U-line balancing problem:A heuristic procedure, European Journal of Operational Research 175 (2006) 1767-1781.

[13] John Miltenburg, U-shaped production lines: A review of theory and practice Int. J. Production Economics 70 (2001) 201-204.

[14] Ali Allahverdi a C.T. Ng b, T.C.E. Cheng b, Mikhail Y. Kovalyov, A survey of scheduling problems with setup times or costs, European Journal of Operational Research 187 (2008) 985-1032.

[15] Krisztina Demete, Zsolt Matyusz, The impact of lean practices on inventory turnover, International Journal of Production Economics 133(1) (2011) 154-163.

[16] Sakakibara, S., Flynn, B.B., Schroeder, R.G., Morris, W.T., 1997. The impact of just-in-time manufacturing and its infrastructure on manufacturing performance. Management Science 43 (9), 1246-1257

[17] Krisztina Demete, Zsolt Matyusz, The impact of lean practices on inventory turnover, International Journal of Production Economics 133(1) (2011) 154-163.

[18] Halvor Holtskog,Continuous Improvement beyond the Lean understanding, Procedia CIRP 00 (2013) 000-000.

[19] Anders Berger, Continuous improvement and kaizen: standardization and organizational designs, Integrated Manufacturing Systems, 89 (2) (1997) 110-117.

[20] John Bessant, David Francis, Developing strategic continuous improvement capability, International Journal of Operations & Production Management, 9(11) (1999) 1106-1119

[21] S.G. Li, Y.L. Rong, The reliable design of one-piece flow production system using fuzzy ant colony Optimization, Computers & Operations Research 36 (2009) 1656-1663

[22] Miltenburg J, One-piece flow manufacturing on U-shaped production lines: a tutorial source. IIE Transactions 33 (2001) 303--21. 2001

[23] Fabian Bohnen, Thomas Maschek, Jochen Deuse, Leveling of low volume and high mix production based on a Group Technology approach, CIRP Journal of Manufacturing Science and Technology 4 (2011) 247-25. R. Sundar et al. / Procedia Engineering 97 (2014) 1875

[24] Andreas Huttmeir, SuzannedeTreville, AnnvanAckere, Leonard Monnier, Johann Prenninger, Trading off between heijunka and just-in-sequence, Int. J. Production Economics 118 (2009) 501-507.

[25] Muris LageJunior, MoacirGodinhoFilho, Variations ofthekanbansystem:Literaturereviewandclassification, Int. J. Production Economics 125 (2010) 13-21

[26] Sipper, D, Bulfin Jr, R.L. Production: Planning, Control, and Integration, Mcgraw-Hill, New York, 1997

ResearchGate

See discussions, stats, and author profiles for this publication at: http://www.researchgate.net/publication/280614357

Threshold voltage model of a Hetero Gate Dielectric Dual Material Gate GAA Tunnel FET

CONFERENCE PAPER · JUNE 2014

DOI: 10.13140/RG.2.1.3081.2003

DOWNLOADS
11

VIEWS
6

3 AUTHORS, INCLUDING:

Jaya Madan
Delhi Technological University
3 PUBLICATIONS **0** CITATIONS
SEE PROFILE

Rishu Chaujar
Delhi Technological University
70 PUBLICATIONS **102** CITATIONS
SEE PROFILE

Available from: Jaya Madan
Retrieved on: 12 August 2015

Threshold voltage model of a Hetero Gate Dielectric Dual Material Gate GAA Tunnel FET

J. Madan[*], R.S. Gupta[**] and R. Chaujar[*]

[*]Delhi Technological University, Bawana Road
Delhi-110042, India, jayamadan.2012@gmail.com, rishu.phy@dce.edu
[**]Maharaja Agrasen Institute of Technology, Rohini, Delhi, India, rsgupta1943@gmail.com

ABSTRACT

In this paper, a hetero gate dielectric, dual material gate, gate all around tunnel field effect transistor (HD-DMG-GAA-TFET) has been proposed. An analytical model for the same has been developed to examine the band to band tunneling, surface potential and the device behavior. The parabolic approximation is used to solve the 2-D Poisson equation with appropriate boundary conditions to evaluate analytical expressions for surface potential and electric field. The analytical results obtained from the proposed model shows excellent agreement with the simulated results obtained with the 3D-ATLAS device simulator.

Keywords: band to band tunneling (BTBT), barrier width, dual material gate (DMG), hetero gate dielectric (HD), tunnel field effect transistor(TFET).

1 INTRODUCTION

During the last decades, MOSFET devices have been continuously scaled down so that they reached the nanoscale domain. But as the technological nodes tend towards the tens of nano meters, the major problems with the normal MOSFET arises. Out of which, one is the fundamental physical limit of (KT/q) ln10 on the subthreshold swing (SS~60mV/decade) at normal room temperature which resist the further scaling of its power supply voltage. Hence, the new devices which use a new carrier transport mechanism other than diffusion over a thermal barrier came into existence. Among these devices, tunnel field effect transistor (TFET) which uses a band to band tunneling (BTBT) mechanism to overcome this fundamental limit of SS, acts as a promising candidate for further extending the Moore's law [1].

Along with steeper SS, TFET also have very low I_{OFF} which leads to higher I_{ON} /I_{OFF} and hence, improves the device performance. Therefore, TFET has been regarded as the most promising candidate for low standby power applications. But the major roadblock with TFET is low ON-current because of its small amount of BTBT at the source channel junction. So the major engineering challenge with TFET is to boost the lower I_{ON} without degrading the I_{OFF}. Many architectures have been reported to enhance the I_{ON} such as delta layer of SiGe at the edge of the source [2], double gate architecture [3], a high- K gate dielectric [4] dual material gate [5], and a low-K spacer [6].

Another major problem with TFET is the ambipolar conduction [7] means conduction in two directions, both for positive and negative gate voltages. In order to overcome ambipolarity, many methods are reported such as: the hetero Gate (HG) dielectric TFET proposed by Choi *et.al* [8], asymmetric source/drain doping [9], and gate drain underlap or short gate TFET [10], and hetero-junction TFET [11].

Moreover Tunneling rate can be increased by using a high-K dielectric which basically improves the electrical coupling between the gate and the tunneling junction (the source channel junction) due to increase in gate capacitance [12]. As high-K dielectric near source side leads to reduction in the minima of conduction band and hence the tunneling barrier width, it leads to higher I_{ON} due to higher tunneling rate caused by lower tunneling barrier. Thus the use of high-K at the source side will increase the I_{ON} and with low-K dielectric such as SiO_2 ambipolar current will be reduced. So the advantage of high-K is to improve the ON-state characteristics of the device and the low-K dielectric at the drain side improves the OFF-state characteristics by reducing the ambipolarity [13]. Hence, we have chosen hetero gate dielectric architecture.

With the help of dual material gate, the lower work function metal near the source side increases the band overlap in the ON state. This increased band overlap results into decrease in the tunneling barrier width, which further results into increase in the tunneling probability of electrons from valence band of the source to conduction band of the channel. These electrons after tunneling from source to channel move towards drain side by drift diffusion. Simultaneously the higher metal work function near the drain side increases the tunneling barrier width in the OFF state and hence reduction of tunneling probability which eventually decreases the OFF current [14].

2 DEVICE STRUCTURE: PARAMETERS AND SIMULATION MODELS

The Gate All Around geometry is considered with 50nm channel length which is basically equal to the sum of L_1 (20nm) and L_2 (30nm), radius of 10nm and gate oxide thickness (t_{ox}) of 3nm. The source is p+ type doped ($10^{20}cm^{-3}$) and drain is n+ doped (5×10^{18} cm^{-3}) and body is lightly p type doped ($10^{16}cm^{-3}$). To reduce ambipolarity

effect source and drain are doped asymmetrically. The region 1 consists of dielectric constant ε_1=21 and metal work function Φ_{M1}=4.1eV (near the source) and region 2 consists of ε_2=3.9 and Φ_{M2}=4.4eV (near the drain). The source and drain junctions are abruptly doped for an effective band to band tunneling and the interface of high-k and SiO_2 is abrupt.

The simulation device structure i.e. HD-DMG-GAA-TFET consisting of Dual material gate and heterogate dielectric is shown in Fig 1. All simulations have been performed using the ATLAS 3D device simulator. The models activated during simulation are as follows: concentration and field dependent mobility model, Shockley-Read-Hall for carrier recombination, non-local band to band tunneling, band gap narrowing and Fermi Dirac statistics [15].

3 MODEL FORMULATION FOR HD-DMG-GAA-TFET

Assuming the influence of the charge carrier and fixed carriers are uniform in the channel and hence it can be neglected. The Poisson's equation can be written as

$$\frac{1}{r}\frac{d}{dr}\left(r\frac{d\psi_s(r,z)}{\partial r}\right)+\frac{\partial^2\psi_s(r,z)}{\partial z^2}=\frac{qN_{ch}}{\varepsilon_{si}} \quad (1)$$

Where, $\psi_s(r,z)$ denotes the surface potential, N_{ch} is the channel doping, ε_{Si} is the permittivity of silicon.

Assuming parabolic potential profile along the radial direction.

$$\psi_s(r,z)=p_0+p_1r+p_2r^2 \quad (2)$$

The following boundary conditions are applied to evaluate the coefficients p_0, p_1 and p_2.

1). The surface potential is only z dependent

$$\psi_s(R,z)=\psi_s(z) \quad (3)$$

2).The Electric field at the center of the channel is zero

$$\left.\frac{d\psi_s(r,z)}{dr}\right|_{r=0}=0 \quad (4)$$

3). Electric field at Si/SiO_2 interface is continuous

$$\left.\frac{d\psi_s(r,z)}{dr}\right|_{r=R}=\frac{C_{fi}}{\varepsilon_{si}}\left[V_{GS}-\psi_s(z)-V_{FBi}\right] \quad (5)$$

Where $V_{FBi}=\phi_{mi}-\phi_s$ is the flatband voltage.

i=1and 2 for region 1 and 2 respectively, and Φ_s is the semiconductor work function.

$$\phi_s=\chi_{si}+E_g/2q+\phi_F \quad (6)$$

Where χ_{si} is the electron affinity, E_g is the silicon bandgap, and $\phi_F=KT/q(\ln(N_{Ch}/n_i))$ is the fermi potential.

C_{f1} and C_{f2} are the capacitances per unit area of the gate dielectric for region 1 and 2 respectively, and are given by

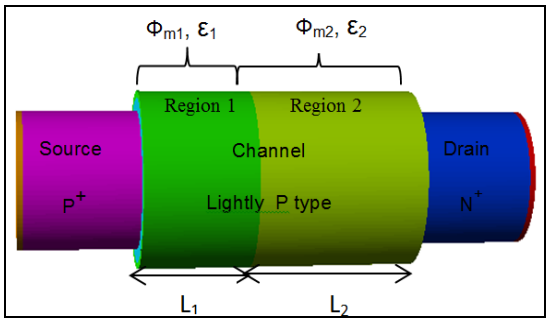

Fig.1: Hetero Gate Dielectric Dual Material Gate GAA n-TFET architecture

$$C_{f1}=\frac{\varepsilon_1}{R\ln\left(1+\frac{t_1}{R}\right)} \text{ and } C_{f2}=\frac{\varepsilon_2}{R\ln\left(1+\frac{t_2}{R}\right)} \quad (7)$$

Where $t_1=t_2=t_{ox}$, is the gate oxide thickness.

Solving equations (1)-(7) we can obtain

$$\frac{\partial^2\psi_s(z)}{\partial z^2}-k^2\psi_s(z)=\eta \quad (8)$$

The general solution of (8) is

$$\psi_s(z)=A_x\exp(kz)+A_y\exp(-kz)-\frac{\eta}{k^2} \quad (9)$$

The solution for region 1 ($0\le z\le L_1$) from (9) is

$$\psi_{s1}(z)=A_1\exp(k_1z)+A_2\exp(-k_1z)-\frac{\eta_1}{k_1^2} \quad (10)$$

The solution for region 2 ($L_1\le z\le L_2$) from (9) is

$$\psi_{s2}(z)=A_3\exp(k_2z)+A_4\exp(-k_2z)-\frac{\eta_2}{k_2^2} \quad (11)$$

Where $\eta_1=\frac{qN_{ch}}{\varepsilon_{Si}}-k_1^2\left[V_{GS}-V_{FB1}\right]$

$V_{FB1}=\phi_{M1}-\phi_{Si}$

$k_1^2=2C_{f1}/(\varepsilon_{Si}R)$ (12a)

and $\eta_2=\frac{qN_{ch}}{\varepsilon_{Si}}-k_2^2\left[V_{GS}-V_{FB2}\right]$

$V_{FB2}=\phi_{M2}-\phi_{Si}$

$k_2^2=2C_{f2}/(\varepsilon_{Si}R)$ (12b)

Now using the following boundary conditions at the interface of each region, coefficients A_1, A_2, A_3 and A_4 can be determined.

At the source end

$$\psi_s(0)=-\frac{KT}{q}\ln\left(\frac{N_{source}}{n_i}\right)=V_{bi1} \quad (13a)$$

and at the drain end

$$\psi_s(L_g) = \frac{KT}{q}\ln\left(\frac{N_{Drain}}{n_i}\right) + V_{DS} = V_{bi2} + V_{DS} \qquad (13b)$$

At the interface of region 1 and region 2,

$$\psi_{s1}(L_1) = \psi_{s2}(L_1) \qquad (13c)$$

$$\left.\frac{d\psi_{S1}}{dz}\right|_{z=L_1} = \left.\frac{d\psi_{S2}}{dz}\right|_{z=L_1} \qquad (13d)$$

The electric field is given by

$$E(z) = \frac{d\psi_s(z)}{dz} \qquad (14)$$

4 RESULTS VERIFICATION AND DICUSSION

The analytical model proposed in this work has been verified though the results obtained from the ATLAS 3-D device simulation. Figure 2 shows the variation of the surface potential along the channel from source end to the drain end. The variation of surface potential shows an increase in potential from source to drain from V_{bi1} to (V_{bi2}+V_{DS}) in accordance with the applied boundary conditions which govern the physics of the device. The enhancement of surface potential with gate voltage leads to lowering in barrier width, due to which band to band tunneling rate of electrons increases. It can be clearly seen that the simulated potential is in well agreement with the modeled results.

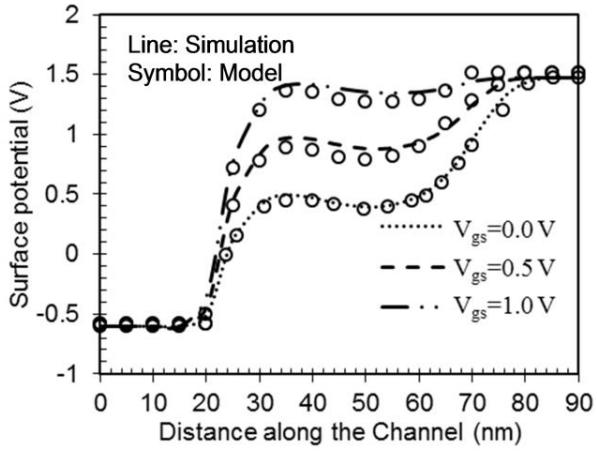

Fig.2: Surface Potential along the length from source to drain, for V_{gs}=0.0 V, 0.5 V and 1.0 V at V_{ds}=1V.

Figure 3 shows the variation of the conduction and valence band energy along the channel from source end to the drain end. The lowering of barrier width is clearly shown with enhanced gate voltage. At the tunneling junction i.e. the source and channel junction, the barrier width is very small for higher gate voltages such that the band to band tunneling of electrons from valence band of source to conduction band of the channel can take place easily leading to an increased ON current. Again it can be clearly seen that the simulated energy bands are in well agreement with the modeled energy bands.

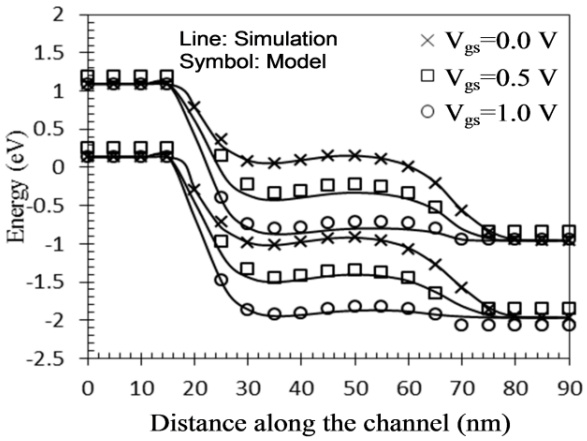

Fig.3: Energy Band Profile along the length from source to drain, for V_{gs}=0.0 V, 0.5 V and 1.0 V at V_{ds}=1V.

Figure 4 shows the electric field at the source and drain end for different gate voltages. It can be clearly seen from the bar graph that the electric field at source is manifold greater than the electric field at drain end. Which results in the increase in tunneling rate at the tunneling junction (source-channel junction) and hence will improve the device performance by increasing the ON current, I_{ON}/I_{OFF} ratio, device gain and simultaneously the lower value of electric field near drain side will reduce the hot carrier effects intensely.

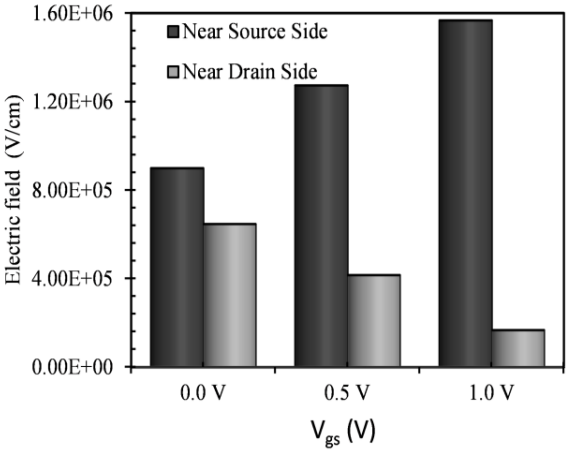

Fig.4: Electric field at source and drain end, for V_{gs}=0.0 V, 0.5 V and 1.0 V at V_{ds}=1V.

Figure 5 shows the effect of gate voltage on Nonlocal band to band tunneling rate. It is clear from the figure that the BBT tunneling rate increases by an order of 1000 with an increase in gate voltage. This increase in tunneling rate will finally lead to increase in tunneling current.

Figure 6 shows the effect of gate voltage on tunneling barrier width. It is clear from the figure that the tunneling barrier width decreases with an increase in gate voltage.

This saturation of decrease in barrier width gives the threshold voltage of the device.

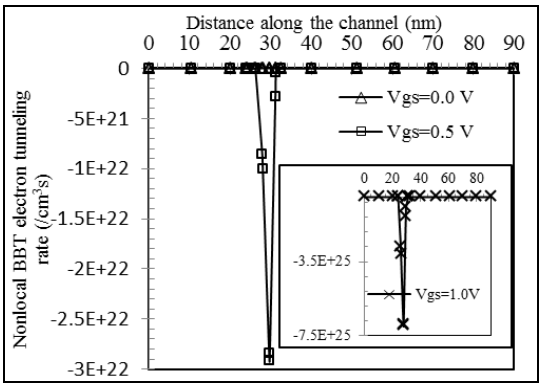

Fig.5: Nonlocal BBT electron tunneling rate along the channel length for the applied gate voltage V_{gs}=0.0 V, 0.5 V and 1.0 V at drain voltage V_{ds}=1V.

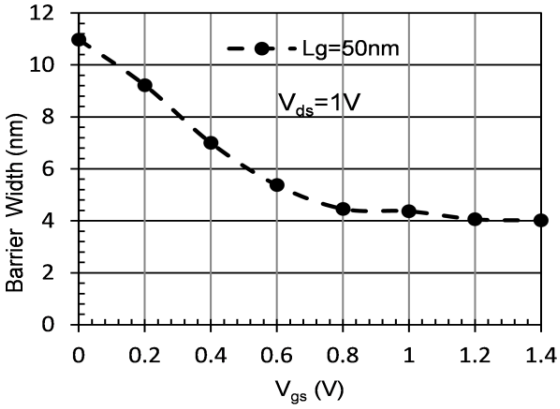

Fig. 6: Impact of Gate voltage on Tunneling Barrier width.

5 CONCLUSION

In conclusion a 2D surface potential model for HD-DMG-GAA-TFET has been developed. It is evident from the results that simulated and analytical model are in well agreement, which also indicates a lower barrier width with increased gate voltage. The electric field is lowered at the drain side which is appropriate for sub nanometer devices.

ACKNOWLEDGMENT

Authors would like to thank to Microelectronics Research Lab, Department of Engineering Physics Delhi Technological University to carry out this work. One of the authors (Jaya Madan) would like to thank University Grants Commission, Govt. of India, for providing the necessary financial assistance during the course of this research work.

REFERENCES

[1] W.Y.Choi, B.G. Park, J. D. Lee, and T.J.K. Liu, "Tunneling field-effect transistors (TFETs) with subthreshold swing (SS) less than 60 mV/dec," IEEE Electron Device Lett., 28(8), 743–745, 2007.

[2] K. K. Bhuwalka, J. Schulze, and I. Eisele, "Performance enhancement of vertical tunnel field-effect transistor with SiGe in the δp+layer," Jpn. J. Appl. Phys., 43(7A), 4073–4078, 2004.

[3] E.H. Toh, G. H. Wang, L. Chan, D. Sylvester, C.H. Heng, G. S. Samudra, and Y.C. Lee, "Device design and scalability of a double-gate tunneling field-effect transistor with silicon– germanium source," Jpn. J. Appl. Phys., 47(4), 2593–2597, 2008.

[4] K. Boucart and A. M. Ionescu, "Double-gate tunnel FET with high-k gate dielectric," IEEE Trans. Electron Devices, 54(7), 1725–1733, 2007.

[5] T.S.A. Samuel, N.B. Balamurugan, "An analytical modeling and simulation of dual material double gate TFET for low power applications," J Electr Eng Technology, 9(1), 247-253, 2014.

[6] M. Schlosser, K. K. Bhuwalka, M. Sauter, T. Zilbauer, T. Sulima, and I. Eisele, "Fringing-induced drain current improvement in the tunnel field effect transistor with high-k gate dielectrics," IEEE Trans. Electron Devices, 56(1), 100–108, 2009.

[7] P F. Wang et.al." Complementary tunneling transistor for low power application". Solid-State Electronics, 48(12), 2281–2286, 2004.

[8] W. Y. Choi and W. Lee, "Hetero-Gate-Dielectric Tunneling Field-Effect Transistors", IEEE Trans. Electron Devices, 57(9), 2317-2319, 2010.

[9] W. M. Reddick and G.A.J. Amaratunga, "Silicon Surface tunnel transistor". Applied physics letters, 67, 494–496, 1995.

[10] A.S.Verhulst, W.G.Vandenberghe, K.Maex, and G.Groeseneken, "Tunnel field-effect transistor without gate-drain overlap," Appl. Phys. Lett., 91, 053102, 2007.

[11] S.J. Cho, et.al., "Design Optimization of a Type-I Heterojunction Tunneling Field-Effect Transistor (I-HTFET) for High Performance Logic Technology," J. Semiconductor Technology and Science, 11(3), 182-189, 2011.

[12] J.S. Lee, W.Y. Choi, I.M. Kang, " Characteristics of Gate All Around hetero gate dielectric tunneling field effect transistor" Jpn. J. Appl. Phys, 51, 06FE03, 2012.

[13] B. Bhowmick, S. Baishya, "Influence of Hetero material gate dielectric of double gate Tunnel FET on electrical characteristics", International Journal of Wisdom Based Computing, 1 (3), 28-31, 2011.

[14] S. Saurabh and M. J. Kumar, "Novel Attributes of a Dual Material Gate Nanoscale Tunnel Field-Effect Transistor," IEEE Trans. Electron Devices, 58(2), 404-410, 2011.

[15] ATLAS User's guide, SILVACO International, Version 5.14.0.R, 2010.

HCTL Open International Journal of Technology Innovations and Research (IJTIR)
http://ijtir.hctl.org
Volume 16, July 2015
e-ISSN: 2321-1814, ISBN (Print): 978-1-943730-43-8

Traffic Noise Estimation using Genetic Algorithm (GA) Approach

Paras Kumar

paraskum007@rediffmail.com

Abstract

In the present work, vehicular traffic noise prediction models have been developed for Patiala city (Punjab) using GA and regression approach. The various terminologies related to GA and acoustics analysis are discussed. The models predict equivalent continuous sound level (L_{eq}) as the function of vehicle volume (Log Q) and percentage of heavy vehicles (P %). A large number of data have recorded at different dates/timings to account variability. Three commonly used GA selection operators (uniform, roulette wheel, and tournament) are used to analyze the accuracy of GA models. The GA model performs better as compared to regression model. The average mean square error (MSE) using GA model is 0.59 as compared to 0.76 for regression model. Among all GA selection operators, tournament selection shows better result.

Keywords

Regression, Genetic Algorithm, Modelling, traffic noise, vehicle volume, percentage of heavy vehicles.

Introduction

In India, the growing number of vehicles creates a serious threat to the environment. The noise pollution level increases with increases in number of vehicles. Traffic noise problem is contributed by various kinds of vehicles including heavy, medium trucks/buses, automobiles and two wheelers. Researchers have developed various noise prediction model in India and abroad using traditional [1-9] and advanced [10, 11] techniques. Campbell [8] has critically reviewed the most commonly used traffic noise prediction models like CORTN, FHWA and ASJ etc. Kumar P. [9] developed two mathematical models to predict, equivalent continuous sound level (L_{eq}) and 10 percentile exceeded sound level (L_{10}), traffic noise descriptors Rahmani et al. [10] have modelled road traffic noise using genetic algorithm. Kumar et al. [11] developed a multilayer feed forward back propagation (BP) neural network (ANN) for predicting highway traffic noise.

[1]Assistant Professor, Mechanical Engineering Department, Delhi Technological University, Delhi-110042, India.

The ANN has been trained using Levenberg–Marquardt (L–M) algorithm. The developed ANN model predicts 10 Percentile exceeded sound level (L_{10}) and Equivalent continuous sound level (L_{eq}) in dB (A).

Different researchers have adopted different methodology and traffic noise parameters to predict different traffic noise descriptors. Very few researchers have advanced with newer techniques like artificial neural network [11] and GA [10]. In the present work, two different noise prediction models have been developed and compared using GA and regression analysis. Models predict equivalent continuous sound level (L_{eq}) as the function of vehicle volume (Log Q) and percentage of heavy vehicles (P %). Different GA crossover operators have also been explored to predict the accuracy of developed GA models. A large number of data sets have measured and recorded at different dates/timings to account variability.

Measuring Instrument and procedure

A smooth flowing straight road patch is selected at 4 km away from Patiala (Punjab, India) toward Sirhind road. Sound pressure level is obtained using a Sound level meter (SLM) (CESVA SC-310). SLM is placed at a height of 1.2 m and at distance of 8.5 m from centre of the inner and outer lanes to measure equivalent continuous sound level (L_{eq}) in dB (A) (Fig.1). The SLM is first calibrated before any measurement. Number of Vehicle of each category are also measured in inner and outer lanes and then the total vehicle volume (Q) and percentage of heavy vehicles (P %) are computed. The measurements are made at different date and timing to account variability in measured data.

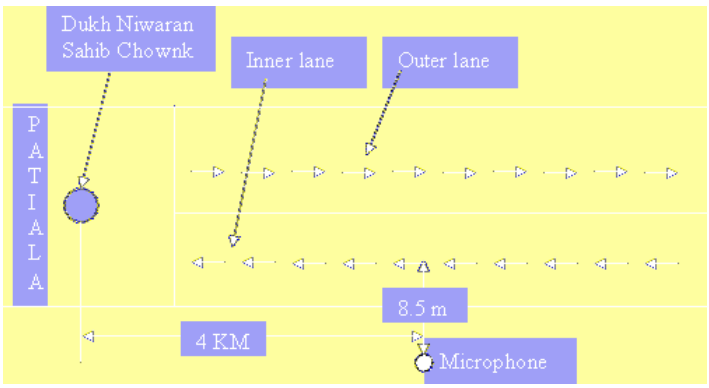

Figure 1: Data collection points (same location as right on left side) [9]

Genetic Algorithm (GA)

GA was invented by John Holland in the year 1975 and is based on the principle of survival of fittest. It is popularly used optimizing technique in frontier area of research. The important steps include population initialization, fitness function evaluation, crossover, mutation, elitism and next generation population etc. Various step involved in GA implementation are:

1. Generate random population of given size and calculate fitness function at each population.

2. Ranked according to the fitness value.
3. Produce next offspring from parent using crossover and mutation operator.
4. Repeat step 1-3 until the stopping criterion (maximum generation reached, elapse time, no change in fitness function, stall time limit) meets or the desired goal achieves.

Table-1 Measured input and output parameters

Sample No	Log(Q)	P (%)	L_{eq} dB (A)
1	3.14	10.2	75.3
2	3.06	9.4	74.1
3	3.03	7.4	73.7
4	3.01	12.9	74.5
5	3.09	10.7	74.4
6	3.2	9.1	75.9
7	3.24	7.1	75.0
8	3.23	8.1	75.0
9	3.11	10.3	72.9
10	3.23	10.4	76.1
11	3.18	9.2	75.7
12	3.17	9.4	75.4
13	3.16	8.1	75.5
14	3.1	9.9	74.5
15	3.14	9.6	75.4
16	3.21	8.9	77.4
17	3.14	11.0	75.4
18	3.11	9.3	75.0
19	3.07	12.1	74.2
20	3.19	10.2	76.8
21	3.20	8.8	75.8
22	3.24	6.3	75.2
23	3.22	7.2	75.9
24	3.08	9.7	74.4
25	3.23	6.1	74.1

The main objective of the present study is to minimizing the sum of squared error between experimental and predicted output and find the various multiplication factors of different input variables to fit into linear model. The objective function is defined as

$$E=min \sum [(L_{eq})_{exp} - (L_{eq})_{prd}]^2 \quad (1)$$

The linear model to predict equivalent continuous sound level (L_{eq}) is expressed as

$$L_{eq}[dB(A)] = a(1)+a(2)*Log\ Q +a(3)*P \quad (2)$$

The model written by Eq.-2 inputs total vehicle volume (Q) and percentage of heavy vehicles (P %) and predicts equivalent continuous sound level in dB (A).

Results and discussion

The measured input and output parameters are shown in Table-1. After measuring total vehicle volume (Q), percentage of heavy vehicles (P %) and equivalent continuous sound level (L_{eq}), a regression models is fitted as shown in Eq.-3.

$$L_{eq}\,[dB\,(A)] = 57.56+5.357^{*}\,Log\,Q\,+0.0325^{*}\,P \qquad (3)$$

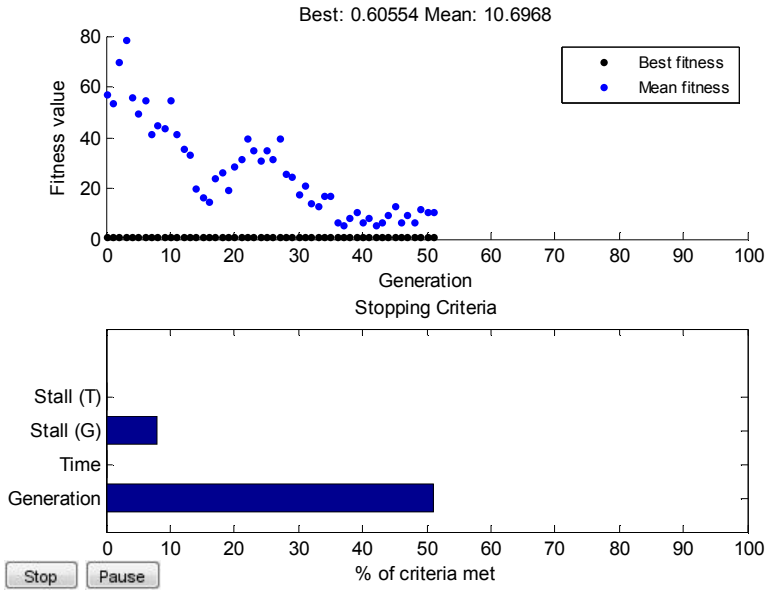

Figure 2(a): Convergence and stopping criterion (Uniform crossover operator)

As far as GA is concern, an initial population of size 30 is selected uniformly. The other parameters settings are default except crossover function (=two point). The minimum and maximum range for three constant a(1), a(2) and a(3) are LB=[50 5 0.2] and UB=[60 10 0.08] . Three different crossover operator namely uniform, roulette wheel, and tournament selection are also used to predict the accuracy of noise descriptors.

Figures-2(a) and 2(b) show the convergence and comparision of various results for unform crossover operator. At each chromosome , fitness function value are calculated and converges as shown in Fig.2(a). In each iteration two values are plotted, one is best fitness and other mean fitness value. At 50th interation the algorithm terminates since it fulfil the stopping criterion of stall gneration and no further improvement in the fitness value has observed.

On the other hand, Fig.-2(b) compares the experimental, regression and GA results. The GA shows better results as compared with regression by showing less mean square error of 0.6055.

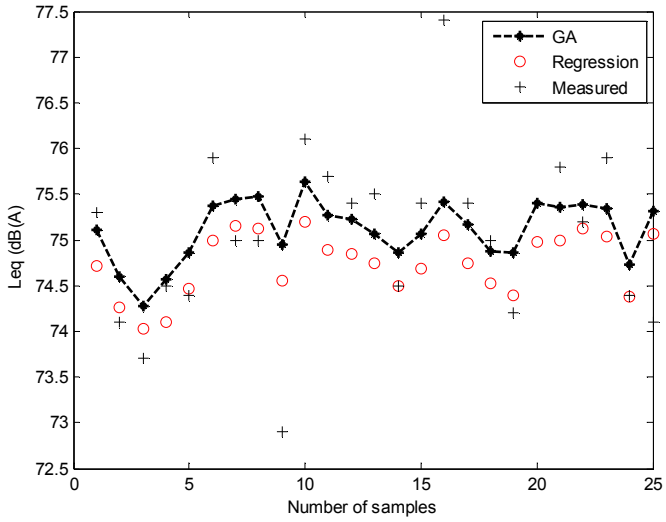

Figure 2(b): Comparison of experimental, regression and GA results (Uniform crossover operator)

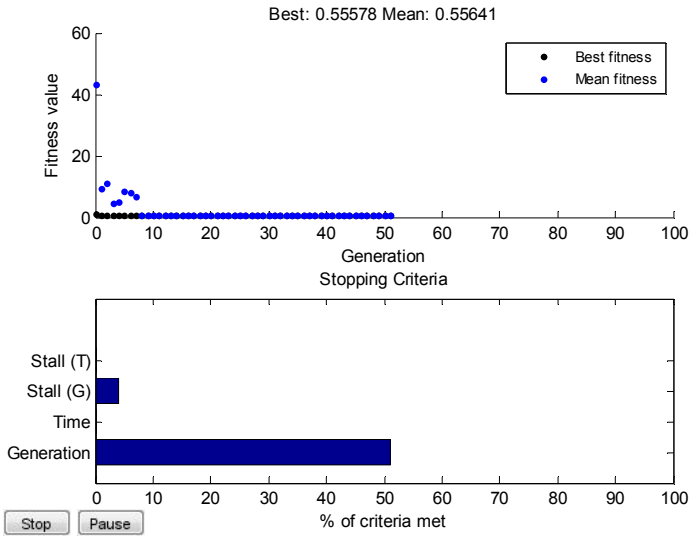

Figure 3(a): Convergence and stopping criterion (Tournament selection)

Figures 3(a) and 3(b) show the convergence and comparison results for Tournament selection. Fig.3 (a) shows faster convergence as compared with uniform crossover.

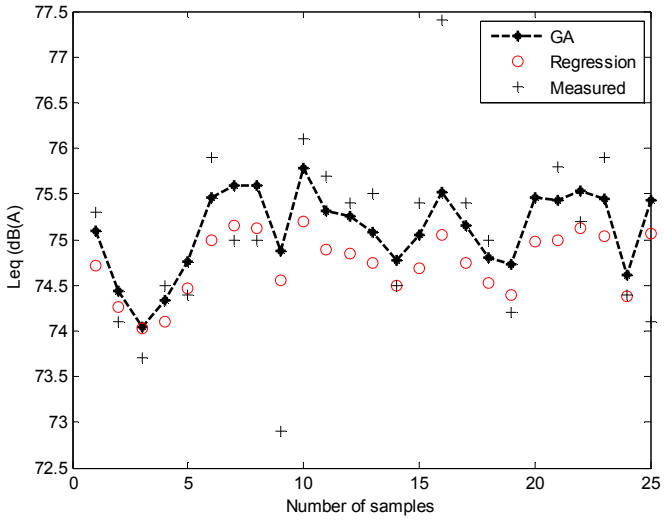

Figure 3(b): Comparison of experimental, regression and GA results (Tournament selection)

The compared results, as shown in Fig.3 (b), shows better performance as compared with uniform crossover. The mean square error (MSE) in GA is 0.5558 as compared with 0.7575 in regression.

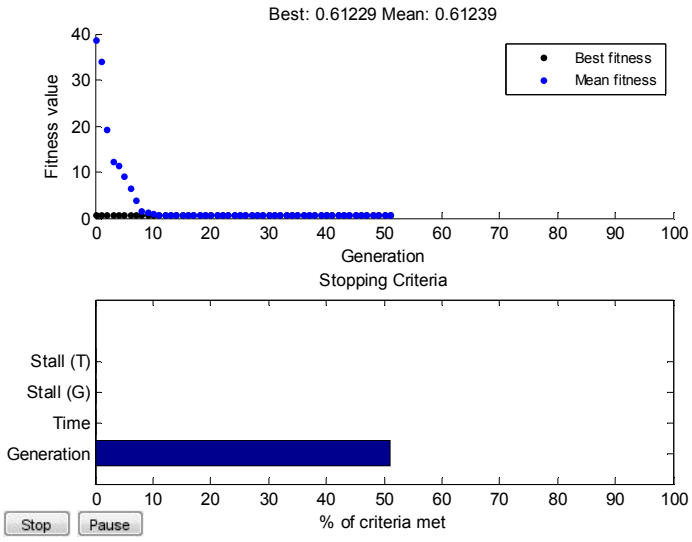

Figure 4(a): Convergence and stopping criterion (Roulette wheel selection)

Figures 4(a) and 4(b) compare results using Roulette wheel selection. The convergnce is better than unform but slower as compred to Tournament selection.

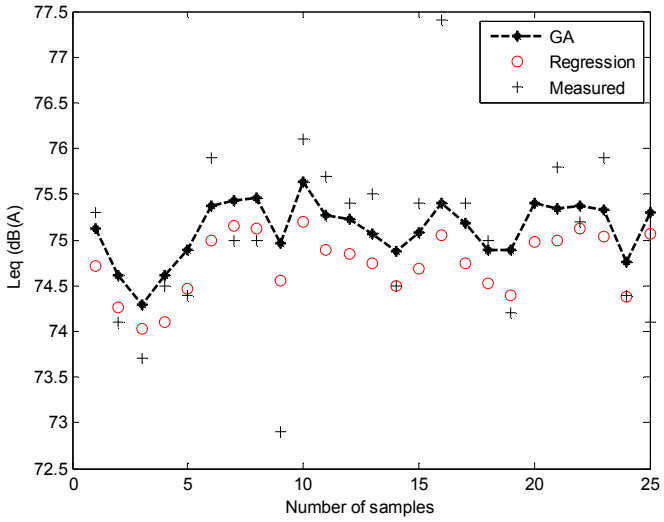

Figure 4(b): Comparison of experimental, regression and GA results (Roulette wheel selection)

Figure 4(b) shows better performance in GA by showing lesser mean square error as compared with regression. Some time the experimental data shows higher fluctuation due to honking or more traffic density during that time duration.

Table-2 optimum parameters setting for different crossover operator

GA Crossover operator	Optimum parameters setting			Fitness function	MSE between	
	a(1)	a(2)	a(3)		Experimental and GA	Experimental and regression
Uniform	56.4303	5.7064	0.0750	0.6055	0.6055	0.7595
Tournament selection	**50.8439**	**7.4631**	**0.0799**	**0.5558**	**0.5558**	**0.7575**
Roulette wheel	57.0111	5.5136	0.0782	0.6123	0.6123	0.7623

Table-2 compares the performance of GA with regression analysis. Out of the 30 population after 50th iteration, the parameters values [a(1), a(2) a(3)] in the table show the best parameters setting to minimize the objective function. The mean square value for GA shows better performance as compared to regression in all the cases. Among GA performance, the Tournament selection shows best result by registering least value of MSE as 0.5558.

Conclusions

The present work compares the performance of GA with regression. The regression and GA models have developed from experimentally measured observation. The models input total vehicle volume (Q), percentage of heavy vehicles (P %) and predicts equivalent continuous sound level (L_{eq}) in dB (A). The following conclusions are drawn from the analysis:

1. The mean square error (MSE) for GA models is in range of 0.5558-0.6123, while the regression model shows error range from 0.7575-0.7623.
2. The GA models perform better as compared with regression model.
3. Among all the GA models, the model using Tournament selection shows best output.
4. The experimental data at some instances shows higher values due to honking noise more traffic in that time duration.

References

[1] D.R. Johnson and E.G Saunders, The evaluation of Noise from freely flowing road traffic, Journal of Sound and vibration 287-309, (1968).

[2] D.M. Harman and M.A Burgess., Traffic Noise in an urban situation, Applied Acoustics 269-276, (1973).

[3] A.D. Clayden, R.W.D. Culley and P.S. Marsh, Modeling traffic Noise mathematically, Applied Acoustic 1-12, (1975).

[4] M. E. Delany, D. G. Harland, R.A. Hood and W.E. Scholes, The prediction of Noise levels L_{10} due to road traffic, Journal of Sound and Vibration 305-325, (1976).

[5] R.N.S. Hammad and M.K. Abdelazeez, Measurements and analysis of the traffic Noise in amman, jordan and its effects, Applied Acoustics, 309-320, (1987).

[6] P. Ramalingeswara Rao and M.G. Seshagiri Rao, Prediction of $LA_{10}T$ traffic Noise levels in the city of Visakhapatnam, India, Applied Acoustics, 101-110, (1991).

[7] K. Kumar and V.K. Jain, A study of Noise in various modes of transport in Delhi, Applied Acoustics 57-65, (1994).

[8] S. Campbell, A critical review of some traffic Noise prediction models, Applied Acoustics 271-287, (2001).

[9] P. Kumar, Traffic noise measurement and prediction in Patiala city, Punjab (India), International Journal of Advance Research In Science And Engineering, 78-83, (2015).

[10] S. Rahmani, S.M. Mousavi and M.J. Kamali, Modeling of road traffic noise with the use of genetic algorithm, applied soft computing 1008-1013, (2011).

[11] P. Kumar, S.P. Nigam, and N. Kumar, Vehicular traffic noise modelling using artificial neural approach, Transportation research part-C: Emerging technologies, 111-122, (2014).

This article is an open access article distributed under the terms and conditions of the Creative Commons Attribution 4.0 International License (https://creativecommons.org/licenses/by/4.0/).

© 2015 by the Authors. Licensed by HCTL Open, India.

Knowledge-Based Systems xxx (2015) xxx–xxx

Contents lists available at ScienceDirect

Knowledge-Based Systems

journal homepage: www.elsevier.com/locate/knosys

Two-phase anticipatory system design based on extended species abundance model of biogeography for intelligent battlefield preparation

Lavika Goel [a,*], Daya Gupta [b], V.K. Panchal [c]

[a] Dept. of Computer Science & Information Systems Engineering, BITS Pilani, Pilani Campus, Vidya Vihar, Rajasthan 333031, India
[b] Department of Computer Science & Engineering, Delhi Technological University (DTU), Delhi, India
[c] SBIT, Sonipat & (Retd.) Defense Terrain & Research Lab, Defense & Research Development Organization, Metcalfe House, Delhi, India

ARTICLE INFO

Article history:
Received 14 April 2014
Received in revised form 18 July 2015
Accepted 20 July 2015
Available online xxxx

Keywords:
Anticipatory system
Enemy base station
Biogeography based optimization
Ant colony optimization
Particle swarm optimization
Troop deployment strategies

ABSTRACT

This paper presents an extended model of biogeography based optimization (BBO) as opposed to the classical BBO wherein the HSI value of a habitat is not solely dependent upon the emigration and immigration rates of species but the HSI value is a function of different combinations of SIVs depending upon the characteristics of the habitat under consideration. The extended model also introduces a new concept of efforts required in migration from a low HSI solution to a high HSI solution for optimization in BBO. Hence, the proposed extended model of BBO presents an advanced optimization technique that was originally proposed by Dan Simon as BBO in December, 2008. Based on the concepts introduced in our extended model of BBO and its mathematics, we design a two – phase anticipatory system architecture for intelligent preparation of the battlefield which is the targeted optimization problem in our case. The proposed anticipatory system serves a dual purpose by predicting the deployment strategies of enemy troops in the battlefield and also finding the shortest and the best feasible path for attack on the enemy base station. Hence, the proposed anticipatory system can be used to improve the traditional approaches, since they lack the ability to predict the destination and can only find a suitable path to the given destination, leading to coordination problems and target misidentification which can lead to severe casualties. The designed system can be of major use for the commanders in the battlefield who have been using traditional decision making techniques of limited accuracy for predicting the destination. Using the above natural computation technique can help in enabling the commanders in the battlefield for intelligent preparation of the battlefield by automating the process of assessing the likely base stations of the enemy and the ways in which these can be attacked, given the environment and the terrain considerations. The results on two natural terrain scenarios that of plain/desert region of Alwar and hilly region of Mussourie are taken to demonstrate the performance of the technique where the proposed technique clearly outperforms the traditional methods and the other EAs like ACO, PSO, SGA, SOFM, FI, GA, etc. that have been used till date for path planning applications on satellite images with the smallest pixel count of 351 and 310 respectively. For location prediction application, the highest prediction efficiencies of the traditional method on Alwar and Mussourie was only 13% and 8% respectively as compared to the proposed method.

© 2015 Elsevier B.V. All rights reserved.

1. Introduction

In this modern warfare era, it has become necessary to have the ability to anticipate the likely actions of the enemy's maneuver and the troop mobilization strategies. The ability to accurately predict the deployment strategy of the enemy troops –to identify the most likely location for the enemy to position their forces and finding a feasible route is of critical importance to the commanders in the battlefield [38]. To understand and simulate the best available routes for attacking the enemy forces and to predict the ability of the enemy to position forces and mount attack, this paper has put forward natural computation algorithm. Natural computing refers to computational processes observed in nature and human designed computing inspired by nature.

ACO, PSO, BBO, Swarm intelligence, and artificial neural networks are some of the techniques under natural computation. For our military application, we have used the combination of three natural computation techniques of ACO, PSO and BBO, which

* Corresponding author at: S-E-142A, Shastri Nagar, Ghaziabad, Uttar Pradesh 201002, India. Mobile: +91 9899973105, +91 9811052141.
E-mail address: goel.lavika@gmail.com (L. Goel).

http://dx.doi.org/10.1016/j.knosys.2015.07.023
0950-7051/© 2015 Elsevier B.V. All rights reserved.

Please cite this article in press as: L. Goel et al., Two-phase anticipatory system design based on extended species abundance model of biogeography for intelligent battlefield preparation, Knowl. Based Syst. (2015), http://dx.doi.org/10.1016/j.knosys.2015.07.023

UNCORRECTED PROOF

Abbreviations

SIVs	Suitability Index Variables	SOFM	Self Organizing Feature Maps
HSI	Habitat Suitability Index (Similarity Threshold)	FI	Fuzzy Inference Mechanism
PSO	Particle Swarm Optimization	P_{ij}	Probability of choosing 'j' as the next city when at city 'i'
ACO	Ant Colony Optimization	E	Maximum Emigration Rate
BBO	Biogeography Based Optimization	I	Maximum Immigration Rate
T_{ij}	Pheromone value	S_{max}	Maximum No. of species = Maximum No. of SIVs in the feature habitat
N_{ij}	$1/d_{ij}$	SGA	Stud Genetic Algorithms
D_{ij}	Distance between city 'i' and city 'j'	GA	Genetic Algorithms
F_{ki}	Feasible neighborhood of the ant 'k' when being at 'i'		
ES	Evolutionary Strategy		

are all a part of population based optimization. The reason for the selection of these techniques is the versatile and distributive nature of the soft computing techniques of swarm intelligence. The main aim of the work done in this paper is to enhance the decision capability which will enable the commanders in the battlefield to make better strategies to combat the actions of enemy.

ACO is a class of Swarm Intelligence Technique which means it is the study of the collective behavior of decentralized, self-organized systems. It is in the nature of ant colonies to discover and travel upon the shortest from their nest to the food source. This search for the shortest path is based on a heuristic function and update of pheromone values upon each iteration [6]. PSO is a stochastic, population-based computer algorithm for problem solving. It is a kind of swarm intelligence that is based on social-psychological principles and provides insights into social behavior, as well as contributing to engineering applications. The particle swarm optimization algorithm was first described in 1995 by James Kennedy and Russell C. Eberhart [20]. The particle swarm simulates social influence and social learning. A problem is given, and some way to evaluate a proposed solution to it exists in the form of a fitness function. The swarm is typically modeled by particles in multidimensional space that have a position and a velocity. These particles fly through hyperspace and have two essential reasoning capabilities: their memory of their own best position and knowledge of the global or their neighborhood's best. So a particle has the information to make a suitable change in its position and velocity. BBO, first introduced by Dan Simon in December 2008 [36,37] is a class of biology based optimization technique and is an optimization technique based on the geographical distribution of the biological species. Geographical areas that are well suited for biological species are said to have a high habitat suitability index (HSI). The variables that characterize the habitability are called the Suitability Index Variables (SIVs). SIVs are the independent variables and HSI the dependent variable. The migration of SIVs from bad to good solutions raises the quality of those solutions which is the main mechanism of optimization in the said technique. BBO has been used in a variety of applications one of them being biogeography based land cover feature extraction [31].

In our application, the base stations (habitats, according to the algorithm) that best suit the military purpose of the enemy troops for positioning their forces (depending upon certain influential parameters called the Suitability Index Variables) are assigned high HSI values than the other less suitable stations. Each of the suitable base stations can be considered as a candidate solution to the problem of finding the best suitable base station. High HSI solutions resist change more than low HSI solutions. High HSI solutions tend to share their features (SIVs) with low HSI solutions. Poor solutions accept a lot of new features (SIVs) from good solutions. With probability P_{mod}, we modify each solution based on other solutions. If a given solution is selected to be modified, then we use its immigration rate to probabilistically decide whether or not to modify each suitability index variable (SIV) in that solution. If a given SIV in a given solution S_i is selected to be modified, then we use the emigration rates of the other solutions to probabilistically decide which of the solutions should migrate a randomly selected SIV to solution S_i. This addition of new features to low HSI solutions may raise the quality of those solutions hence in turn leading to the best solution. This approach to problem solving is basically what is called the biogeography-based optimization that will eventually lead to the best solution which represents the best base station for the enemy troops, in our military application.

Hence, we find the best suitable base station for the enemy (with a very high probability since we have found the most probable solution) to position its forces and mount attack. Having found the destination, now we proceed to find the shortest and the safest path to this base station using a hybrid of the extended BBO technique with the ACO Technique [6] and the PSO [20] techniques. PSO path extraction and ACO path planning algorithm is used for the purpose [9,19]. To make a path more smooth morphological operations are implemented to minimize the effects of shadows, trees and inconvenient areas so that an optimized path can be more quickly planned even in a complex environment by effectively extracting the obstacles and finding the shortest and safest path. Thus, the proposed anticipatory system integrates the process of finding the shortest and the best feasible path to a destination after fixing the most feasible destination. Deciding efficient routes has so far been an intuitive and a cognitive process for the troop commanders. Automated simulation of the terrain (of the war area) and of the available routes, will allow the commanders to understand the implications of the terrain for effective maneuver. When simulated on the enemy's terrain coupled with the provision for the automated prediction of the enemy base station, the system will help to predict the intents of the enemy's troop deployment and the ways of attack.

Section 2 presents the related work section. Section 3 basics of biogeography based optimization technique. Section 4 presents the proposed problem solving framework based on extended form of biogeography based optimization. Section 5 discusses the proposed two-phase anticipatory system architecture design based on the proposed model of biogeography based optimization. Section 6 presents the design and implementation of the proposed two-phase anticipatory system on synthetic scenarios. Section 7 presents the performance comparison results of the two-phase anticipatory system with the traditional decision making techniques as well as the other recent optimization techniques. Section 8 presents the conclusion and future scope of the work.

UNCORRECTED PROOF

Please cite this article in press as: L. Goel et al., Two-phase anticipatory system design based on extended species abundance model of biogeography for intelligent battlefield preparation, Knowl. Based Syst. (2015), http://dx.doi.org/10.1016/j.knosys.2015.07.023

2. Related work

In 1995, Gilson introduced the concept of anticipatory computing in warfield was identified during World War I where 'the importance of gaining an awareness of the enemy before the enemy gained a similar awareness, and devised methods for accomplishing this' was realized [8]. This idea of separation between the human operators understanding of system status and actual system status is the basis of the definition of anticipatory computing. One explanation for the considerable time lag between initial identification of the phenomena and maturity of the concept is the degree to which a real problem was perceived [40]. In 1997, the initial push for research and development came from the aviation industry, where there is considerable pressure for pilots and air traffic controllers to develop better situational awareness [18]. This call has arisen with the increased realization that system design is no longer optimized for human operation and, under some conditions, has 'overstepped the human's capability to keep track.' It is perhaps no surprise that the coming of age of the research into situational awareness is closely coupled with the increase in the degree of automation in defense control systems. There are a few works available in this field of anticipatory computing for situation awareness [2], which we modify to suit our purpose of intelligent battlefield planning. Some of which are disaster situation awareness [17], terrorist camps detection [35] and electronic situation awareness [16]. But as such no computing method is available for the prediction of enemy base station directly. The known available methods for the prediction of the enemy base camps are still the conventional methods employed by military which involve manual study of geography of the area and various other factors. Nature inspired techniques have been extensively used in varying applications in related areas like UCAV path planning, supply chain management, bilevel programming with multiple objectives, etc. [42,44,46].

3. Biogeography based optimization

BBO [36,37] is an evolutionary algorithm motivated by the migration mechanisms of ecosystems. In BBO each candidate solution is called as a habitat and is characterized by a habitat suitability index (HSI) which is determined by factors called as the suitability index variables (SIV). Habitats with a high HSI are characterized by greater number of species, lower immigration rate, higher emigration rate and a dynamic species distribution and vice versa for habitats with a low HSI value [25–27]. A good solution is treated as an island with a high HSI and a poor solution indicates an island with a low HSI. High HSI solutions resist change more than low HSI solutions but tend to share their features with low HSI solutions. Poor solutions accept a lot of new features from good solutions. This addition of new features to low HSI solutions may raise the quality of those solutions. This approach to problem solving is called biogeography-based optimization [36,37]. The theory of biogeography is summarized below [36,37]:

[1] Suppose that we have a problem and some candidate solutions characterized by an index which we call as the HSI and is analogous to "fitness" in other population-based optimization algorithms. HSI is determined by factors which we call as the SIVs.
[2] High HSI solutions represent habitats with many species, and low HSI solutions represent habitats with few species however, it is assumed that each solution (habitat) has an identical species curve (with $\mu_{max} = \lambda_{max}$), but the value represented by the solution depends on its HSI.
[3] The immigration rate λ_1 for a low HSI solution S_1 will, therefore, be higher than the immigration rate λ_2 for high HSI solution S_2 and the emigration rate μ_1 for S_1 will be lower than the emigration rate μ_2 for S_2.
[4] The emigration and immigration rates of each solution are used to share information between habitats. If a given solution is selected to be modified, then its immigration rate λ is used to decide whether or not to modify each SIV in that solution. If a given SIV in a given solution S_i is selected to be modified, then the emigration rates μ of the other solutions is used to decide which of the solutions should migrate a randomly selected SIV to solution S_i.

The concept of SIV mutation is also included in BBO to incorporate the changes in the species count from equilibrium condition and the species count probabilities are used to determine mutation rates. The mutation approach makes low HSI solutions likely to mutate, which gives them a chance of improving. The algorithm for biogeography based optimization is given in Fig. 1. The immigration and the emigration rates are functions of the species count of the habitat and are calculated as given in Eq. (1).

$$\lambda_i = \lambda_{max}\left(1 - \frac{k(i)}{n}\right), \quad \mu_i = \mu_{max}\left(\frac{k(i)}{n}\right) \tag{1}$$

where I is the maximum possible immigration rate; E is the maximum possible emigration rate; $k(i)$ is the fitness rank of the ith individual (1 is worst and n is best); and n is the number of candidate solutions in the population. The mutation probability is as was given by the original BBO algorithm inversely proportional to the solution probability [36,37] and is defined by Eq. (2).

$$m_i = m_{max}\left(1 - \frac{P_i}{P_{max}}\right) \tag{2}$$

where m_{max} is the user defined maximum mutation probability, $P_{max} = argmax P_i$, $i = 1, \ldots, n$ (n is population size), and P_i is the solution probability. For more details refer [36,37].

BBO has demonstrated good optimization performance on various benchmark functions as demonstrated in the work by Simon [36,37]. In the original BBO paper [36], it was illustrated that BBO is competitive with other EAs [33]. It could become a popular EA if it continues to improve with additional extensions and modifications (for example, oppositional BBO [7] and blended BBO [25–27]), and if it is applied to additional practical engineering problems (for example, ECG diagnosis [30], power system optimization [34], economic load dispatch [4], satellite image classification [11,31] and ground water exploration [32]).

4. Extended BBO model

This section presents the extended form of BBO based on the extended species abundance model of biogeography that we proposed in our papers [10,12] by considering the fact that the characteristics of each habitat vary greatly and hence, comparing all the habitats using the same set of SIVs may be misleading and also may not lead to an optimum solution. This is equivalent to the coefficient of that particular SIV in the solution vector becoming zero. Hence, the HSI value of a habitat is not solely dependent upon the emigration and immigration rates of species but it is a function of different combinations of SIVs depending upon the characteristics of the habitat under consideration as detailed and discussed in our papers [10,12].

Let the problem dimension be t. Now, t is constant for all solutions. The number of decision variables is equal to t for all solution vectors which is analogous to SIVs. We define HSI as the function of SIVs i.e.

UNCORRECTED PROOF

Please cite this article in press as: L. Goel et al., Two-phase anticipatory system design based on extended species abundance model of biogeography for intelligent battlefield preparation, Knowl. Based Syst. (2015), http://dx.doi.org/10.1016/j.knosys.2015.07.023

Initialize the BBO parameters. /* This means mapping problem solutions to SIVs and habitats which is problem dependent. */
Initialize the maximum species count S_{max}, the maximum emigration rate μ_{max}, the maximum immigration rate λ_{max}, the maximum mutation rate m_{max}, elitism parameter.
Initialize a random set of habitats H_i.
/* Each H_i corresponds to a potential solution to the problem. */
For each H_i
Map the HSI to the number of species S, the immigration rate λ, and the emigration rate μ.
Probabilistically use λ and μ to modify each non-elite habitat H_l.
Update the probability of its species count. Then mutate each H_l based on its probability and re-compute each HSI.
End For
End.

Fig. 1. Algorithm for biogeography based optimization.

$$HSI_i = f_i(SIVs) \tag{3}$$

where i signifies the ith habitat ranging from 1 to n.

Let the set of SIVs range from $x_1, x_2, \ldots, x_t$.

Since, we consider each solution vector to be characterized by a different set of SIVs, the HSI of a given habitat i will be calculated as given by equation below.

$$HSI_i = \alpha_1 x_1^{\theta_1} + \alpha_2 x_2^{\theta_2} + \alpha_3 x_3^{\theta_3} + \cdots + \alpha_t x_t^{\theta_t} = \sum_{j=1}^{t} \alpha_j x_j^{\theta_j} \tag{4}$$

The SIVs which are not applicable for the given habitat is removed during the calculation of HSI by making the coefficient of those SIVs in the solution vector as zero. For the purpose, we calculate the factor of relevance of a particular SIV in the HSI calculation on different habitats and eliminate the SIVs for which the relevance factor value is below 50%. This will be useful when we consider the problem of finding the best suited destination enemy base station on different terrain types such as plain or a desert region and mountainous region since some SIVs may be more relevant on a plain/desert terrain and may not be applicable for a hilly terrain and vice versa.

Also, the contributions of each SIV for the HSI calculation may be different for different habitats (representing different terrain types in our case) and hence the HSI function may change dynamically depending upon the type of terrain under consideration and its characteristics. This is well modeled through the factor α that is added in the HSI calculation for a given habitat. The factor α is also called the weight assigned to each SIV in the HSI calculation for a given habitat.

In the initial stage of the algorithm, number of species = number of candidate solutions to the problem and each of these solutions are put in the universal habitat. We also consider an isolated habitat with zero SIVs. This habitat represents the state of no solution in the initial stage of the algorithm. We also construct a standard habitat which is analogous to an ideal solution with ideal characteristics. This habitat is called the feature habitat and consists of the collection of standard SIVs (or ideal SIVs). The feature habitat is used for comparison with the candidate solutions in the universal habitat. Next, we calculate the HSI of the feature habitat based on its SIVs and hence calculate the ideal HSI value (SIV_{ideal}) and the threshold HSI value ($SIV_{threshold}$).

Now calculate the HSI for the candidate solution based on its SIVs based on the corresponding HSI formula and compare the HSI of the habitat (base station) with the threshold HSI. The threshold HSI denotes that the candidate solutions of the Universal habitat can only be made feature habitat after migration if their HSI falls within this range (i.e. it is greater than the threshold HSI). If the HSI is greater than the threshold HSI value, then find out the SIVs to be migrated and the effort required for migration using the weights assigned to those SIVs (on a scale of 1–5). Probabilistically use immigration and emigration to modify the non elite solution by immigrating the ideal SIVs of the feature habitat that match with the SIVs of the candidate input solution of the universal habitat to the universal habitat & emigrating the SIVs of the candidate input solution that do not match with the ideal SIVs of the feature habitat from the universal habitat to the isolated habitat. This is the effort required in migrating the SIV's during the computation for the selection of the best solution and is measured by the difference in ideal and actual SIV values for each SIV multiplied by its weight to calculate the effort required in making a particular solution to become an ideal solution. If the amount of effort required is infinite or very large, then this solution will never be able to become an ideal solution as it does not satisfy the threshold condition for HSI. We calculate the effort required for each candidate solution by using Eq. (5).

$$Effort = \sum_i (SIV_{ideal} - SIV_i) \times \alpha_i \tag{5}$$

where SIV_{ideal} is the ideal value of the ith SIV and SIV_i is the actual value of the ith SIV and i ranges from 1 *to n*. (depending upon the No. of factors (SIVs) considered). α_i is the weight assigned to ith SIV. If the HSI is less than the threshold, transfer the SIVs of this candidate solution to isolated habitat. This input solution will not be considered further and is removed from the Universal habitat. Repeat the steps for each of the candidate solutions in the Universal Habitat. Next, calculate the selectivity factor for the remaining solutions in the Universal Habitat. We define the term selectivity factor which is the factor which determines the selectivity of the candidate solution to be chosen as the best solution. The solution which has the highest selectivity factor is most likely to be the best solution and hence at the end of the processing by our algorithm, this candidate solution will be the one which will be anticipated by the system to be considered as the best solution. To calculate the selectivity factor, we subtract the threshold HSI value from the candidate base station's calculated HSI value and then divide it by the effort as below

$$Selectivity\ Factor = \frac{(HSI_i - HSI_{Threshold})}{Effort} \tag{6}$$

where 'i' ranges from 1 to n.

Hence, the proposed algorithm incorporates the changes in the definition of HSI function during the optimization process. The proposed extended form of the biogeography based optimization is presented in Fig. 2.

5. Two-phase anticipatory system architecture based on extended model of BBO

This section presents our proposed two-phase anticipatory system design. The section is further divided into four subsections wherein the first section gives some important relevant definitions for the first and the second phase of the anticipatory system, the second section presents the two-phase anticipatory system architecture. The third section presents the functional architecture of the two-phase anticipatory system and the algorithms for both

UNCORRECTED PROOF

Begin
/* *BBO ecosystem initialization* */
Create a Universal habitat consisting of all the candidate solutions to be considered also called as the species (population) $H_1, H_2, \ldots, H_n$ which comprises H_u;
Create a Feature habitat H_f consisting of the ideal solution and an isolated habitat H_i with zero species;
/*Compute the corresponding HSI values */
While $(i \leq n)$
Compute the HSI for each species H_i in H_u based on the corresponding function $f_i(HSI) = f_i(SIVs)$

$$HSI_i = \sum_{k=1}^{t} \alpha_k x_k^{\theta_k}$$

Where $\alpha_j = 0$ for the j for which the factor of relevance f_i is zero.
Also, calculate the HSI for each of the feature habitats H_j.
End while
/* *End of BBO parameter initialization* */
For each species H_i in the Universal habitat H_u
Select a species from H_u
For each of the feature habitat H_j.
Migrate the specie H_i to H_j.
If $HSI_i > HSI_{Threshold}$
Find out the SIVs to be migrated and the effort required for migration using the weights assigned to those SIVs.

$$Effort = \sum_i \sum_k \alpha_k . (x_{ideal\,(k)} - x_k)$$

Else
Transfer the SIVs of this solution to the isolated habitat H_i /* remove this solution from the universal habitat */
End If
End For
End For

Calculate the selectivity factor for each of the remaining solutions in the Universal Habitat.

$$Selectivity\ Factor = \frac{(HSI_i - HSI_{Threshold})}{Effort}$$

The candidate solution with the highest selectivity factor is the best solution.

Fig. 2. Extended biogeography based optimization based on HSI function modeling.

the phases. The fourth section gives the mathematical formulation of the anticipatory system which takes as input the candidate base stations and gives as output the best feasible destination base station and the most suitable path of attack.

5.1. Definitions

We now identify some important relevant definitions of the parameters originally proposed by Dan Simon [36,37] which have been modified to suit our purpose of enemy base station prediction and thereafter finding the most feasible path of attack [9,13,36,37]. These parameters define the preprocessing steps of the two-phase anticipatory system design. Following are some important relevant definitions of the parameters and the details of the other concepts used in the design of the proposed anticipatory system [13].

Definition 1. *Suitability Index Variables (SIVs):* To predict the best suited destination for the enemy to position its forces, the following SIVs [9,36] are defined.

a. Features that correlate with HSI for our prediction include factors [9,36] which are called the Suitability Index Variables (SIVs). A Suitability Index Variable SIV $\bar{C}$ C is an integer that is allowed in a habitat. In accordance with the problem statement and the expert knowledge of the military domain, the following SIV's are taken into consideration for deciding the HSI for the Base Stations. Each of these factors are weighted on a scale of 1–5 where 1–5 are decoded as below depending upon their values in the ideal and the actual scenario.

[1] Insignificant/very low
[2] Low
[3] Average
[4] High
[5] Very high

Also, we assign each of these factors (SIVs) a weight according to their relative importance in deciding the most probable base station for the enemy to position its forces. The factors are:

a. *Transportation network availability (N).* The more the accessible the area is with respect to transport facilities, the greater are the chances of it being selected as the probable base station for the enemy to position their forces since the transportation of logistics and mobile forces would be easier. In case of a mountainous region, the ease of deployment of air traffic is a major factor in the consideration of the most likely base station of the enemy since the areas which are nearby to an airfield network are more suitable for Air lifting of forces such as para-commandos and launching of aircrafts and are also favorable for the replenishment of arms and ammunition. Hence, the transportation network availability should be high in order for a base station to be selected and hence, HSI is directly proportional to N ($HSI \propto N$).
b. *Concentration of signal traffic (S).* Signal traffic is undesirable since it can lead to congestion and jamming situations and hence, HSI is inversely proportional to S ($HSI \propto 1/S$).
c. *Safety and fast deployment (D).* Areas where the enemy can safely deploy their troops Deployment of enemy troops with minimum amount of effort invested in terms of time are more likely to become the destination base station for the enemy to position its forces. Hence, HSI is directly proportional to D i.e. ($HSI \propto D$).

UNCORRECTED

d. *Enemy and firepower range constraints (F)*. Firepower range is a constraint since an enemy's base station has an arc of influence within which the arms and ammunition are effective on the war theater. The enemy's base station which has more firepower range is more probable for being selected by the enemy as their base station. Hence, HSI is directly proportional to the enemy's firepower range constraints ($HSI \propto F$).

e. *Concentration of enemy stores & logistics (L)*. Concentration of logistics like ammunition & communication equipments, tanks, missiles, boffer guns & other strategic assets play an important role in the selection of the destination base station. The more the concentration of logistics in a particular area, the more is that candidate base station likely to be the enemy's base station for positioning their troops. Hence, HSI is directly proportional to L ($HSI \propto L$).

f. *Ease of setting up forward base stations and maintaining all-time, all-weather connectivity with the headquarters (C)*. Better connectivity with the neighboring areas is a desirable factor in the selection of a base station as the destination base station. Hence, HSI is directly proportional to the connectivity factor ($HSI \propto C$).

g. *Mobility factor or the difficulty factor (MF)* (depends upon the terrain)- HSI is directly proportional to M_F i.e. ($HSI \propto MF$). M_F can be measured by analyzing the evenness of the area. This can be determined by considering the neighboring area of the small area taken into consideration at a time. If the neighboring area was of similar height than the area was considered even. The levels were decided by considering the percentage of area (around the area under consideration) that is even. Table 1 gives the scale from 1 to 5.

h. *Enemy's ability to influence the friendly base stations (I)*. Enemy's ability to influence the friendly base station is also an important factor while considering the location suited for the enemy to position its forces. The areas that are geographically located in areas where the enemy can get an indepth access into the territory of the friendly forces is more suitable to be chosen. Hence, $HSI \propto I$.

i. *Aspect (direction/angle) (H)*. Aspect can be measured in terms of alignment of the area under consideration. The area which is more vertically aligned towards the enemy is more suitable for becoming the likely base station for the enemy troops deployment since it can act as a natural shield for them. The aspect can be categorized in the range of 0–360 degrees at an interval of 45 degrees as 0–45, 45–90, 90–135, 135–180, 180–225, 225–270, 270–315, 315–360 degrees. Based on these categories the scales for I can be classified as under ($HSI \propto H$). Table 2 gives the scales for Aspect.

j. *Enemy,s ability to counter maneuver and counter deployment of troops (A)*. The enemy's ability to counter-maneuver can be measured by the area covered under slope. More is the area covered under slope the greater is the probability of locating a base station there since the visual access improves on such regions. In mountainous regions, this area under slope plays a major role since more is the area under slope, more is the dominating height ground and hence more suitable for setting up of a base station. The area covered under slope can be classified into subcategories as: less than 5%, 6–10%, 11–16% and greater than 16% are covered under slope. Hence, $HSI \propto A$. Table 3 gives the scales.

k. *Areas of Strategic importance (G)*. The areas which are strategically important for the enemy troops are more likely to be selected. An area can be of strategic importance for the enemy to select it as the base station if it gives in depth access into the friendly base station's territory. These are also the areas where the enemy can retrieve strategically important statistics through geo-stationary satellite observations and such strategically important areas are more suitable for the setting up of a base station. The strategic importance of an area is measured in terms of the elevation of the area which can be calculated through the Digital Elevation Model (DEM) values by fixing ranges on a scale of 1–5. However, since a region with lower elevation is more desirable, hence, $HSI \propto 1/G$. These ranges are categorized as in Table 4.

l. *Ease of Terrain Activities (T)*. Terrain where activities like mine clearance, bridging, track improvement, vehicle movement, etc. can be performed with ease and hence, HSI $\propto$ T where T depends upon the terrain (terrain can be urban (U), rocky (R), vegetation (V), water (W) or barren land (B)) and can be measured on a scale of $1-5$ for each of the type of terrain as below. Table 5 gives the ranges.

m. *Perception of enemy strengths, weaknesses and intent (P)*. Ability to perceive the enemy's intents is a measure of the cognition of the commanders in the battlefield. This factor is an important factor which indicates the enemy's ability to anticipate the manoeuver and locate their most probable location and accordingly position themselves at alternate positions. In other words, the perception ability of the enemy is an important factor in the choice of the destination base station. Hence, the base station which provides relatively lower perception of enemy strengths and weaknesses is more likely to be selected by the enemy and hence, $HSI \propto 1/P$.

Table 1
Scales for mobility factor.

1	Very low	Less than equal to 11%
2	Low	12% to 23%
3	Medium	24% to 44%
4	High	45% to 67%
5	Very high	Greater than equal to 68%

Table 2
Scales for aspect.

1	Least desired	Category 6, 7, 8
2	Less desired	Category 5
3	Moderately desired	Category 4
4	Highly desired	Category 1, 3
5	Extremely desired	Category 2

Table 3
Scales for area under slope.

1	Very low	< 5%
2	Low	6–10%
3	Medium	11–15%
4	High	$\geqslant$ 16%

Table 4
Ranges for areas of strategic importance.

1	Very low	247–256
2	Low	257–278
3	Medium	279–325
4	High	326–419
5	Very high	420–593

Each SIV is assigned a weight value according to its priority place in deciding the best location for the enemy to position themselves. SIV's are assigned equal weights if they have the same role and equal priority in deciding the location. The weights assigned to each of these factors are as given in Table 6 below (based on military inputs).

UNCORRECTED PROOF

Please cite this article in press as: L. Goel et al., Two-phase anticipatory system design based on extended species abundance model of biogeography for intelligent battlefield preparation, Knowl. Based Syst. (2015), http://dx.doi.org/10.1016/j.knosys.2015.07.023

Table 5
Ranges for ease of terrain activities.

1	Very low	$\leqslant 11\%$
2	Low	12–23%
3	Average	23–44%
4	High	45–67%
5	Very high	$\geqslant 68\%$

Table 6
SIV's and their assigned weights.

S. no.	SIVs	Assigned weight (α_k)
1	Transportation network availability (N)	5
2	Concentration of signal traffic (S)	4
3	Safety and fast deployment (D)	4
4	Firepower range constraints (F)	4
5	Concentration of logistics (L)	3
6	Ease of setting up forward base stations and maintaining all-time, all-weather connectivity with the headquarters (C)	4
7	Mobility/difficulty factor (M_F)	3
8	Enemy's ability to influence the friendly base stations (I)	4
9	Aspect(direction/angle) (H)	3
10	Ability to counter–maneuver or counter-deployment of troops (A)	3
11	Areas of strategic importance (G)	5
12	Ease of terrain activities (T) (V, R, U, B, W)	5
13	Perception of Enemy's strengths, weaknesses and intents (P)	5

Definition 2. *Habitat Suitability Index:* A habitat $H \in (SIV^m)$ is a vector of m integers that represent a feasible base station for the enemy. A *Habitat Suitability Index* HSI: $H \rightarrow R$ is a measure of the goodness of the solution that is represented by the habitat. In our algorithm, we first calculate the HSI of the ideal base station and then for the other candidate base stations using the formulation derived in (7) which has been derived from the interpretation of military data and by analyzing the results of a statistical survey of the military camping areas.

$$HSI = \begin{cases} \dfrac{\left((F*L)+\left(N+D+\frac{M_F}{G}+T+C\right)+\left(\frac{I}{5}\right)+\left(\frac{H*A}{10}\right)\right)}{P} & (H > 3)\ (\mathrm{I}) \\ \dfrac{\left((F*L)+\left(N+D+\frac{M_F}{G}+T+C\right)+\left(\frac{I}{5}\right)-\left(\frac{H*A}{10}\right)\right)}{P} & (H \leqslant 3)\ (\mathrm{II}) \end{cases} \quad (7)$$

where, $T = (V + mod((6 - R), 4) - U - B - (W - 2))$

It is to be noted that in Eq. (7), the weights α and the power θ of each SIV x is taken as unity. However, depending upon the factor of relevance of each SIV to a given terrain, the value of α may be fixed as 1 or 0 to include or exclude the SIV from HSI calculation.

Definition 3. *Required effort*: We also define a variable called Effort which calculates the amount of effort required in migrating the SIV's during the computation for the selection of the most probable base station which enemy is likely to choose and in our case, this is the destination base station which the second phase of the algorithm takes as input. We calculate the effort for each base station using Eq. (5).

Definition 4. *Ideal base station:* We define the term ideal base station which is the base station which is the collection of ideal values of each SIV under consideration. The ideal SIV values are determined by a statistical data analysis and through the expert knowledge in the military domain. These values are then normalized so that they range on a scale of 1–5. The HSI calculated for this base station is also ideal and used for comparison in the algorithm.

Definition 5. *Threshold HSI:* is defined as the minimum HSI value which makes the input/candidate base station an eligible candidate for the further consideration in the algorithm for the choice of the destination base station. If the HSI value for the input base station is less than the threshold HSI, then the base station is rejected without proceeding further in the algorithm because this base station cannot be an enemy base station.

Definition 6. *Selectivity factor*: We define the term Selectivity Factor which is the factor which determines the selectivity of the candidate base station to be chosen by the enemy as their base station. The base station which has the highest selectivity factor is most likely to be chosen by the enemy and hence at the end of the processing by our algorithm, this candidate base station will be the one which will be anticipated by the system to be considered by the friendly troops as the enemy base station and the destination base station for the next phase of the algorithm to begin with. To calculate the selectivity factor, we subtract the threshold HSI value from the candidate base station's calculated HSI value and then divide it by the effort as in Eq. (6).

Definition 7. *Ecosystem:* An *ecosystem* H^n is a group of n habitats. The size 'n' of an ecosystem is constant. Here 'n' is the No. of candidate base stations of the enemy which are put in the universal habitat plus one standard habitat with ideal SIVs for matching in order to find the best solution; which is called the feature habitat, since it contains all the features which are required in the destination base station.

Definition 8. *Migration rates: Immigration rate* λ (HSI): $R \rightarrow R$ is a monotonically non-increasing function of HSI and is proportional to the likelihood that SIVs from neighboring habitats will migrate into habitat H_i. *Emigration rate* μ (HSI): $R \rightarrow R$ is a monotonically non-decreasing function of HSI and is proportional to the likelihood that SIVs from the habitat H_i will migrate to the neighboring habitats.

Definition 9. *Habitat modification* Ω (λ, μ): $H^n \rightarrow H$ is a probabilistic operator that adjusts habitat H based on the ecosystem H^n. The probability (between [0,1]) that H is modified is proportional to its immigration rate λ_j, and the probability that the source of the modification comes from H_j is proportional to the emigration rate μ_j. An *ecosystem transition function* Ψ = (m, n, λ, μ, Ω, M).

$$\Psi = \lambda^n \circ \mu^n \circ \Omega^n \circ HSI^n \circ M^n \circ HSI^n \quad (8)$$

which begins by calculating the immigration and the emigration rates followed by habitat modification (Ω) and HSI calculation in turn followed by mutation (M) and finally HSI recalculation.

Definition 10. *Pheromone value.* T_{ij} – Pheromone value

Definition 11. *Heuristic function.* $N_{ij} = 1/dij$, where d_{ij} represents the heuristic information.

D_{ij} – distance between city i and city j

F_{ki} – Feasible neighborhood of the ant k when being at city i.

Definition 12. P_{ij}-Probability of choosing j as the next city when at city i.'a' and 'b' are the parameters that determine the relative influence of the pheromone trail and the heuristic information.

UNCORRECTED PROOF

(i) If $a = 0$, the closest nodes are more likely to be selected.
(ii) If $b = 0$, then only pheromone is used to select the next node without using the heuristics.

Hence, P_{ij} is given by the following Eq. (9).

$$P_{ij}^{k} = \frac{[T_{ij}]^{a}[N_{ij}]^{b}}{\sum_{l \in N_{ij}}[T_{il}]^{a}[N_{il}]^{b}} \text{ if } j \in n. \quad (9)$$

where 'n' is the feasible neighborhood of ant 'k' when at city 'i'.

Definition 13

$$\tau_{if}(t+1) = (1-\rho)\tau_{if}(t) + \Delta\tau_{if} \quad (10)$$

5.2. System architecture

In our research, we demonstrate the performance of our proposed extended BBO model for designing an anticipatory system which anticipates the most suitable destination base station for the enemy troops to position their forces and also finds the shortest and the best feasible path of attack on it. We have proposed the implementation of the two-phase anticipatory system wherein the first phase is the automated prediction of the deployment strategies followed by the enemy troops in warfare coupled with the prediction of the shortest and the safest route for attack on the enemy which forms the second phase of our anticipatory system. In the second phase of the anticipatory system design, we integrate the proposed model with the Particle Swarm Optimization technique and the Ant Colony Optimization technique for the computation of global thresholds and the detection of the shortest path respectively. The system architecture of the two-phase anticipatory system based on the extended BBO model is shown in Fig. 3.

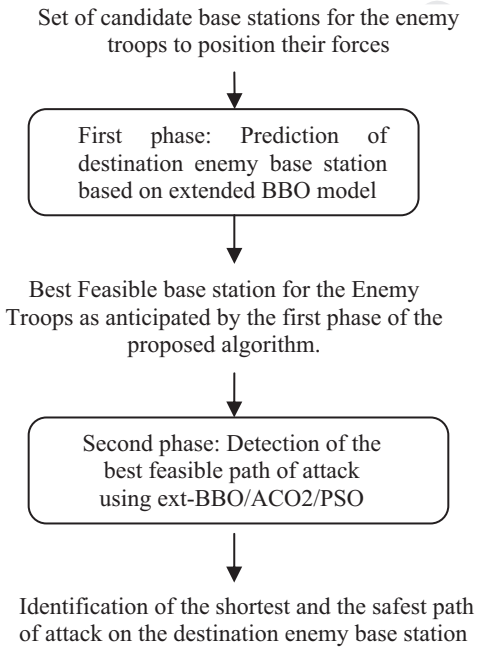

Fig. 3. Two-phase anticipatory system architecture based on the extended BBO model.

5.3. Functional architecture

In the original BBO, the HSI of a habitat is determined by the immigration and emigration rates solely. The habitats with a high HSI value are characterized by a high immigration rate and habitats with a low HSI are characterized by a high emigration rate. However, the above HSI calculation does not take into account the population evolution and extinction rates which play a significant role in the determination of the species count on a habitat at a given time instant as proposed in our papers [10,12] and as explained in the previous section.

We have implemented the extended BBO model combined with the ACO2/PSO technique for the purpose of two-phase anticipatory system design. The generic functional architecture of our Two-phase Anticipatory System is given below in Fig. 4 and is explained layer by layer next. The procedures in each of the layers are necessary as each one performs a specific functionality to add sophistication to the proposed model of our anticipatory system. The first phase of the anticipatory system begins by taking as input the set of candidate base stations feasible and initializes the universal habitat, feature habitat and the isolated habitat which contain the set of candidate base stations, ideal base station and rejected base stations respectively in the *Universal Habitat Initializer Layer*. *Habitat Suitability Index Function Calculation Layer* is then used for dynamic HSI function modeling based on terrain characteristic analysis and using the relevance factor for HSI definition and then calculating the HSI values for each candidate base station based on the chosen HSI function definition. This layer also calculates the ideal and threshold HSI values. Next, *Threshold HSI based Selective Base Station Elimination Layer* is used to eliminate the base stations which have their HSI values lower than the threshold value and migration efforts are calculated for the remaining base stations in the Universal habitat. *Selectivity Factor Analyzer Layer* is then used to compare the selectivity factor of these remaining base stations in order to choose the one with the highest value which is the output of the first phase in the *Destination Base Station Assignment Layer*. The second phase takes as input the friendly base station and the destination enemy base station as output by the second phase. The *Ecosystem Initialization Layer* initializes a new ecosystem consisting of universal, local and global feature habitats corresponding to local and global best positions in the current iteration of the path planning algorithm. *Path Extractor Layer* is used to initialize random positions and HSI calculation based on which local and global feature habitats are updated and universal habitat's position and velocity values are updated. Next, based on the histogram analysis of the agents' pixel DN values, the *Global Threshold HSI Computation Layer* calculates the local and global best values. The value of global best position is called as the threshold HSI which is then used by the *Obstacle Detection Layer* to categorize the obstacles. Next, a binary image is obtained where the obstacles and the accessible pixels are clearly distinguished and further morphological operations are applied in the *Path Refinement Layer* for smoothening of the image. Next, a shortest path is planned using the ACO technique and effort and selectivity factor values are calculated in the *Path Planning Layer*. The path with the highest value of selectivity factor is chosen as the safest and shortest path which is then output as the best feasible path of attack. The detailed architecture is explained layer by layer below:

(i) First phase of the Anticipatory System

The first phase of the anticipatory system is used to predict the deployment strategies of enemy troops by predicting the location of the enemy base station for positioning their forces [9]. The input to the phase is the set of suitable base stations for the enemy to position its forces and the output is the most probable enemy base station detection. The functional architecture for the first phase of

Please cite this article in press as: L. Goel et al., Two-phase anticipatory system design based on extended species abundance model of biogeography for intelligent battlefield preparation, Knowl. Based Syst. (2015), http://dx.doi.org/10.1016/j.knosys.2015.07.023

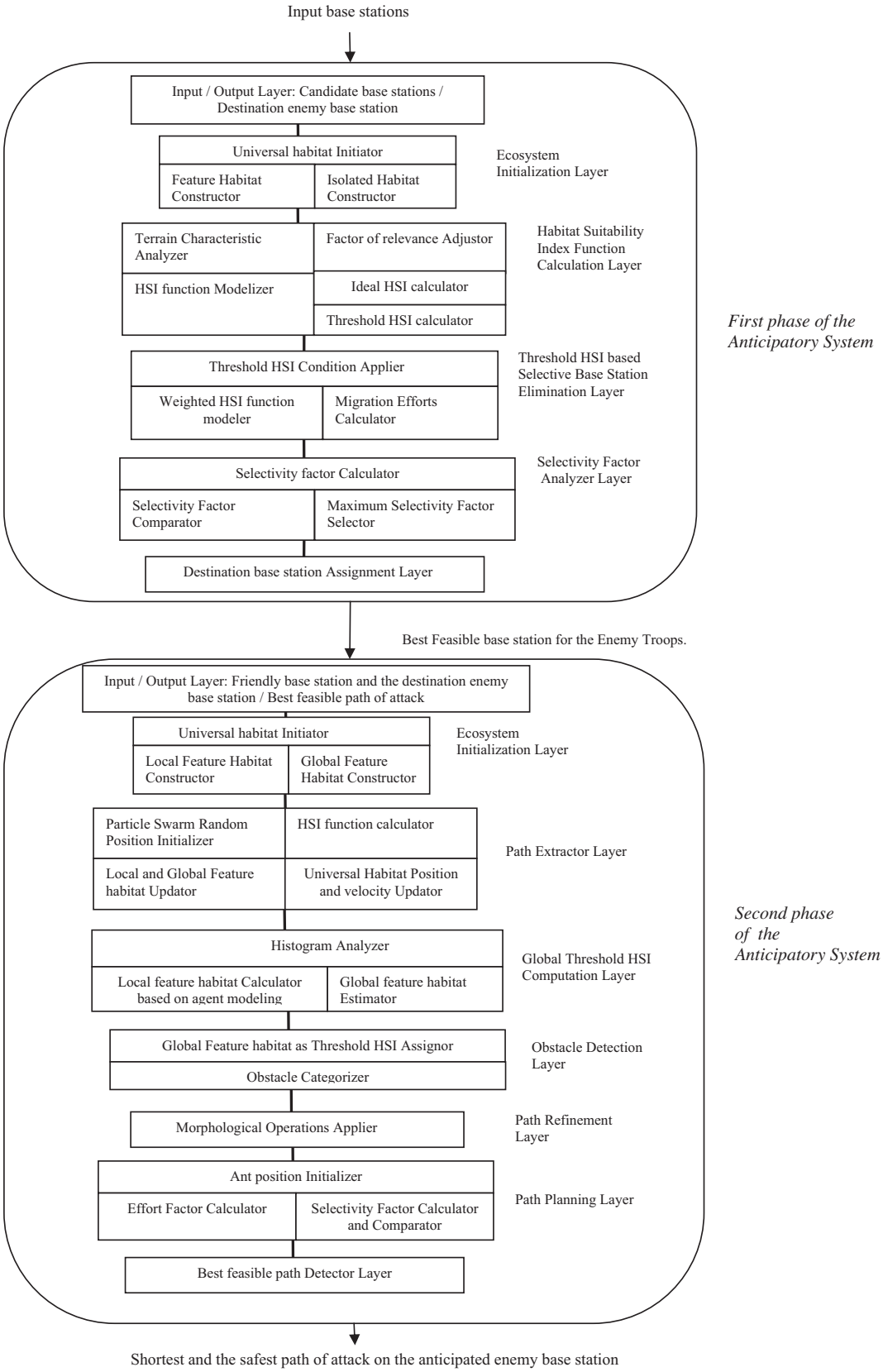

Fig. 4. Functional architecture of the two-phase anticipatory system.

Please cite this article in press as: L. Goel et al., Two-phase anticipatory system design based on extended species abundance model of biogeography for intelligent battlefield preparation, Knowl. Based Syst. (2015), http://dx.doi.org/10.1016/j.knosys.2015.07.023

our model based on extended BBO for enemy base station prediction is detailed next.

Assumptions:

[1] Initially it is considered that there exists a Universal habitat consisting of all the candidate base stations.
[2] It has been assumed that the SIVs migrate between the Universal habitat, Feature habitat and the isolated habitat.
[3] All the candidate base stations are considered exactly once.
[4] At the completion of the algorithm we get a base station that is best suited as the destination base station.

Input/output layer. This layer is used to input the set of candidate base stations suitable for the enemy to position its forces and mount attack and output the best feasible base station for the enemy troops to mount attack.

Ecosystem initialization layer.This layer is responsible for the initialization of the ecosystem comprising of the Universal habitat, feature habitat and the isolated habitat.

(a) *Universal habitat initiator*. This layer is responsible for initializing the set of species which correspond to the set of candidate solutions to the problem in the Universal habitat. The No. of species in the Universal habitat is equal to the No. of candidate solutions to the problem. In our system design, the universal habitat is initialized with the set of suitable base stations for the enemy to position its forces. Hence, we put the set of the above base stations in the Universal Habitat.
(b) *Isolated habitat constructor*. This layer is responsible for isolated habitat construction and initialization. The isolated habitat represents the state of no solution in the initial stage of the algorithm. Hence, in our system design, we initialize the isolated habitat with zero SIVs.
(c) *Feature habitat constructor*. The feature habitat represents a standard habitat is constructed which is analogous to the ideal solution. The feature Habitat is used for comparison with the candidate solutions in the Universal Habitat.
In our case, it consists of the collection of Standard SIVs (or ideal SIVs) on the basis of historic and intelligence data obtained through a statistical survey of the area, the parameters (SIVs) of which were defined in sections before. The feature Habitat is used for comparison with the candidate base stations in the Universal Habitat.

Habitat suitability index function calculation layer. This layer is responsible for calculation of the HSI function value for each of the habitats using the appropriate HSI function applicable depending upon the habitat characteristics. Also, the ideal and the threshold HSI are calculated in this layer. The subunits that are categorized under this layer are described in detail next.

(a) *Terrain characteristic analyzer*. The HSI function used depends upon the characteristics of the habitat under consideration. In other words, the HSI function for each of the base stations in H_u will depend upon the type of terrain under consideration since the SIVs which are applicable on a particular terrain may not be relevant for the other types of terrain. Hence, this layer analyzes the terrain under consideration for the decision about the applicable HSI function. In our case, we have taken up two case studies one, is that of a plain or a desert region (Alwar region in Rajasthan) which have similar characteristics from the viewpoint of base station location prediction, and the other, is of mountainous/hilly region (Mussourie region in Himachal Pradesh).
(b) *Factor of relevance adjustor*. Based upon the terrain characteristics, we define the HSI for each of the base stations in the universal habitat. This layer models this phenomenon through the factor of relevance adjustor by calculating the factor of relevance of a particular SIV in the HSI function calculation. The SIVs which are less relevant are eliminated from the HSI function of Eq. (3). In our case, the SIVs which have their factor of relevance value, $f_r < 0.5$, are eliminated. The value 0.5 is a logical value chosen based upon the quality of solution required, the factors which have less than 50% relevance to the particular terrain are those which can be removed from consideration without affecting the search for the best base station (fixed based on military inputs). Hence, depending upon the habitat characteristics, the HSI function gets modified since some SIVs get eliminated.
(c) *HSI function modeler*. Since, the HSI function is not a fixed function of SIVs and changes dynamically, the function chosen for HSI calculation may vary for each base station in H_u and hence this layer models the HSI function. To model this phenomenon for our system design, we define two HSI functions depending upon the value of H, where H is the enemy's ability to counter-maneuver or counter deployment of troops which in turn depends upon the Aspect (Direction/Angle) of the area under consideration. If the value of H is less than 3, we use the first function else the second. The value of 3 is the threshold for the angle which is defined as $\cos(\pi/2 \times \mathrm{H})$ and will be negative in the second case and thus the two equations are formulated as given in Eq. (7).
(d) *Ideal HSI calculator*. This layer is responsible for calculating the HSI of the feature habitat based on its SIVs and hence calculating the Ideal HSI value ($\mathrm{SIV}_{\mathrm{ideal}}$) using a similar procedure as above.
(e) *Threshold HSI calculator*. This layer is responsible for calculating the threshold HSI value. We calculate the threshold HSI value in our system design by taking one-third of the ideal HSI value (based on military inputs). The threshold in our case has been fixed to this value for simplification and the best result with highest selectivity factor value has been taken as output in the first iteration only however, the threshold may be varied to allow the algorithm to proceed iteratively until it converges to the best solution indicated by an acceptable selectivity factor value out of the obtained ones as is done in the standard BBO algorithm. This will be the iterative procedure incorporating all the features of standard BBO however, the one discussed in the paper is a close representation of the original BBO and incorporates all essential features which are needed to demonstrate the effectiveness of the proposed anticipatory system.

Threshold HSI based selective base station elimination layer. This layer is responsible for elimination of the candidate base stations which do not satisfy the threshold HSI condition. The subunits under this layer are:

(a) *Threshold HSI condition applier*. This layer compares the HSI of the habitat (in our system design, candidate base station) with the threshold HSI. The threshold HSI denotes that the candidate base stations of the Universal habitat can only be made feature habitat after migration if their HSI falls within this range i.e. it is greater than the threshold HSI.
(b) *Weighted HSI function modeler*. If the HSI value of the base station under consideration is greater than the threshold HSI value, then this layer finds out the find out the SIVs to be migrated and the effort required for migration using the

UNCORRECTED PROOF

Please cite this article in press as: L. Goel et al., Two-phase anticipatory system design based on extended species abundance model of biogeography for intelligent battlefield preparation, Knowl. Based Syst. (2015), http://dx.doi.org/10.1016/j.knosys.2015.07.023

*weights*assigned to those SIVs (on a scale of 1 to 5). This is how this layer models the concept proposed in our extended BBO that the contributions of each SIV for the HSI calculation may be different and hence the HSI function should reflect this phenomenon. This is well modeled through the factor α that is added in the HSI calculation for a given habitat in Eq. (4). The factor $\alpha$is also called the weight assigned to each SIV in the HSI calculation for a given habitat.

(c) *Migration efforts calculator*. This layer models the factor α in the migration efforts calculation for the choice of the best suited enemy base station amongst the remaining base stations in H_u. We probabilistically use immigration and emigration to modify the non elite base station by immigrating the ideal SIVs of the feature habitat that match with the SIVs of the input base station of the universal habitat to the universal habitat & emigrating the SIVs of the input base station that do not match with the ideal SIVs of the feature habitat from the universal habitat to the isolated habitat. This is the effort required in the migration of SIVs to and from the universal habitat which can be calculated from the formula in Eq. (5). If the HSI is less than the threshold, transfer the SIVs of this base station to isolated habitat. This base station will not be considered further and is removed from the Universal habitat. We repeat the steps above for each of the candidate base stations in the Universal Habitat. This step forms the main mechanism of the proposed system since a base station which might appear as a near-ideal combination of SIVs may require a very large effort value to make it an ideal solution and hence its feasibility of selection will be zero. This may reflect upon the advantage of the proposed algorithm over the straightforward Euclidean distance calculation using traditional method.

Selectivity factor analyzer layer: This layer calculates and analyzes the selectivity factor for the remaining candidate solutions in our case, base stations, in the Universal Habitat.

(a) *SelectivityFactorCalculator*: This layer calculates the selectivity factor for the remaining base stations in H_u using the formula given in Eq. (6). In our case, these are the set of left over base stations, one among which will be the most likely enemy base station and the output of the first phase of the 2-phase anticipatory system algorithm.

(b) *SelectivityFactorComparator*: This layer is responsible for comparing the selectivity factor of all the base stations so that the base stations with high selectivity factors can be sidelined.

(c) *MaximumSelectivityFactorSelector*: This layer selects the base station with the highest selectivity factor.

Destination base station assignment layer: The base station with the highest selectivity factor is the most suitable base station for the enemy troops for their deployment and this layer assigns this base station as the destination base station for the friendly troops to mount attack on.

(ii) Second phase of the anticipatory system

The algorithm for finding the shortest as well as an obstacle free i.e. best feasible path of attack from the friendly to the destination enemy base station is the second phase of the anticipatory system. The algorithm begins by the obstacle detection and path extraction of image procedures by automatically categorizing all pixels in the image into roads, forest, barren land, water bodies and settlements [19,39]. Next, we extract the paths from image using PSO algorithm. To do this, appropriate threshold values have to be computed and then segmentation is performed [19]. Now, obstacles have to be avoided and we need to reach the goal through the shortest path for which we use the ACO technique [6,19,39]. The algorithm in this phase is a hybrid of ACO, PSO and bases itself on extended BBO concepts. The reason for the selection of ACO and PSO for the purpose of path finding and obstacle detection is that the performance of ACO on this application far outperforms BBO which may be well suited for classification applications but is less competent over path planning application as ACO demonstrates a faster convergence speed than BBO [1,15,19]. PSO is used for the purpose of obstacle avoidance by calculating global threshold values and applying morphological operations thereafter. However, BBO remains to be the basic framework of design for these algorithms in our proposed system. The steps followed in the algorithm are explained in detail layer by layer below.

Input/output layer: This layer is used to input the friendly base station and the best suited enemy base station obtained as the output of the first phase and output the shortest and the safest path for attacking the enemy base station.

Ecosystem initialization layer: This layer is responsible for the initialization of the ecosystem comprising of the Universal habitat and the feature habitat.

(a) *Universal habitat initiator*: This layer is responsible for initializing the set of species which correspond to the set of candidate solutions to the problem in the Universal habitat. The No. of species in the Universal habitat is equal to the No. of candidate solutions to the problem. In our system design, this layer initializes a Universal habitat consisting of a set of random positions from the source to the destination base station also called as the species (population) $H_1, H_2, \ldots, H_n$ which comprises H_u.

(b) *Local and global feature habitat constructor*: The feature habitat represents a standard habitat is constructed which is analogous to the ideal solution. The feature habitat is used for comparison with the candidate solutions in the Universal Habitat. Hence, this layer initializes a feature habitat H_g representing the global best position and $H_l$representing the local best position.

Path extractor layer: This layer is responsible for extracting the probable paths for reaching the destination enemy base station by means of detection of inaccessible area and an analysis of the histogram of satellite image for which it applies the modified Particle Swarm Optimization Algorithm.

(a) *Particle swarm random position initializer*: In this layer, the particles are initialized, which scan their respective regions to find the global best (threshold value). Particle$_i$ ($i = 1, 2, 3 \ldots, n$) is randomly selected where n is the total number of particles.

(b) *HSI function calculator*: This layer is responsible for the HSI function calculation in order to determine the next best position of each particle. Consider $X_i(n)$ and $v_i(n)$ as the current position and velocity of particle i. Let f(i) be the HSI function also called as the fitness function in PSO terminology to calculate the next best position of each particle. If T_x and T_y are the x, y coordinates of the target(accessible area) and S_x and S_y are the x, y coordinates of the source (current position of particle) then HSI function is given by Eq. (11).

$$HSI_i = \frac{1}{\sqrt{(S_x - T_x)^2 + (S_y - T_y)^2}} \tag{11}$$

For each candidate position H_i in H_u , this layer computes the *HSI* at a random position H_i based on the corresponding function $f_i(HSI) = f_i(SIVs)$.

UNCORRECTED PROOF

Please cite this article in press as: L. Goel et al., Two-phase anticipatory system design based on extended species abundance model of biogeography for intelligent battlefield preparation, Knowl. Based Syst. (2015), http://dx.doi.org/10.1016/j.knosys.2015.07.023

```
Create a Feature habitat Hf representing the nearest position to Hi.
For each species Hi in the Universal habitat Hu
    Select a species from Hu
    For each of the feature habitat Hf.
        Migrate the specie Hi to Hf.
            If (HSIi > HSI Threshold )
                Hi is a obstacle
            Else
                Hi is an accessible area.
    End For
End For
```

Fig. 5. Pseudo-code for obstacle detector.

(c) *Local and global feature habitat updator*: After calculating HSI function from equation above, this layer searches for the next best position. Let $H_l(i)$ represents the local best position of the particle (feature habitat) which has been found so far and it is updated as in Eq. (12).

If $(HSI_i < HSI_{i-1})$

/*Update the H_l value */

$$H_l(i+1) = \begin{pmatrix} H_l(i) & f(X_j(i+1)) > f(H_l(i)) \\ X_j(i+1) & f(X_j(i+1)) < f(H_l(i)) \end{pmatrix}$$

End For

/*Find global best position */

$H_g(i)$ represents the global best position of the swarm and is to be updated as:

$$H_g(i+1) = arg\ min\ f(H_l(i+1)) \tag{12}$$

(d) *Universal habitat position and velocity updator*: This layer updates the position and velocity of each H_i in H_u. After getting local best and global best position from equations above, we use Eq. (13) for updating the position and velocity of each particle:

$$v_j(i+1) = \left[v_j(i) + c_1.r_1\left(H_l(i) - X_j(i)\right) + c_2.r_2\left(H_g(i) - X_j(i)\right)\right] \tag{13}$$

$$X_j(i+1) = X_j(i) + v_j(i+1)$$

where c_1 and c_2 are positive constants; r_1 and r_2 are random variables.

Global threshold HSI function computation layer: This layer assigns the value of H_g as the threshold HSI value, $HSI_{threshold}$ to be used as input for the obstacle detection layer. For calculation of the global threshold (average), this layer uses the PSO algorithm.

(a) *Histogram analyzer*: To obtain the desired results, this layer plots the histograms of several of the scenes in the database containing Objects, for analysis. Based on the observations, the histogram is divided in five main regions. Region I starts from the lowest intensity values to half of the midway of average intensity. For most of the cases, the intensity values on this region cover water bodies. Region II covers intensities that go from approximately half of the midway of the average intensity to midway of average intensity, and typically covers trees.
Region III goes from midway of average intensity, to average intensity and covers bright gray objects such as highways. Region IV goes approximately from average intensity to midway of highest intensity and generally covers bright objects like buildings, road dividers, etc. Region V goes approximately from midway of highest intensity to highest intensity and generally covers barren land [19,39].

(b) *Local feature habitat calculator based on agent modeling*: In this layer, a numerical simulation model based on agent modeling is devised for calculation of the local feature habitat value. To evaluate the threshold values, we create ten agents which scan their respective regions assigned to them from the image. Every agent scans the image row wise to find local best values for each row.

(c) *Global feature habitat estimator*: This layer is responsible for estimating the global best value. For the purpose, every agent scans the image row wise to find local best values for each row and eventually evaluates the global best for the assigned region. Among these regional global bests the agents select the most suitable candidate solution by communicating with each other. This is known as the Threshold value or the Global best (global feature habitat value).

Obstacle detection layer: This layer is responsible for calculating the threshold value (global best) which is used in the image to extract the paths as accessible area (barren area) and obstacles (like vegetation, water, rocky area etc.). This corresponds to converting the satellite image into a binary image in which 0 (black = 0) predicts inaccessible area and 1 (white = 1) predicts the paths. For the purpose, we proceed as detailed next.

(a) *Global feature habitat as threshold HSI assignor*: This layer assigns the value of H_g as the threshold HSI value, $HSI_{threshold}$ for the obstacle detection step.

(b) *Obstacle categorizer*: This layer is responsible for categorizing the paths as obstacle free or an inaccessible area by using the global threshold HSI value which is the output of the previous layer. The pseudo-code for the obstacle detector is detailed next in Fig. 5.

Path refinement layer: This layer is responsible for refining of the paths obtained as output of the previous layers using morphological operations.

(a) *Morphological operations applier*: This layer refines the extracted paths using morphological operations. After the extraction of the paths from the output of the previous layer, it is observed that there are some isolated white pixels that correspond to trees, shadows etc. and therefore for further refinement of the paths, we use the morphological operations [19]. Four morphological operations are applied in our system design as given in Fig. 6.

Path planning layer: This layer is responsible for path planning using ACO. After the operations in the previous layers, many possible paths are extracted amidst the cross-country. In this layer, ants are created and randomly initialized from the starting point. They randomly chose different ways of getting to the target. While moving to the target they deposit pheromone, after reaching to the target they retrace their respective paths. The path of the ant which reaches the starting point earliest is considered the shortest. Now the shortest path is obtained. While finding the way to next node they check for the obstacle, if obstacle occurs they choose the next node. Hence, the ants avoid obstacles coming in their way. On the whole, we have the safest and shortest path. The numerical simulation model for this phase is explained next.

(a) *Ant position initializer*: This layer is responsible for initializing the ants at the starting point wherein they chose random paths fro getting to the target. Ant_i (i = 1, 2, 3, . . ., m) denotes an ant in the ant colony where i ranges from 1 to m and m is

UNCORRECTED PROOF

Please cite this article in press as: L. Goel et al., Two-phase anticipatory system design based on extended species abundance model of biogeography for intelligent battlefield preparation, Knowl. Based Syst. (2015), http://dx.doi.org/10.1016/j.knosys.2015.07.023

Clean: Remove isolated pixels (0's surrounded by 1's).
Majority: Set a pixel to 0 if five or more pixels in its 3-by-3 neighborhood are 0's.
Fill: Fill isolated interior pixels (1's surrounded by 0's).
Holes: Fill the holes in the binary image.

Fig. 6. Morphological operations.

the total number of ants. τ_{if} denotes the pheromone between g_i and g_f (g_i, $g_f \in$ RS and $g_i \neq g_f$). RS is research space.

(b) *Effort factor calculator*: This layer is responsible for effort factor calculation for the next nearest node. In our system design, we proceed as detailed next. Given g_i is the current position of the ant and g_f is the neighborhood of g_i, or the intervisible area of the ants at g_i. d_{if} is the distance between g_i and g_f. Suppose at time t_i, ant_k is at g_i. The probability of this ant choosing g_f as its next point is modeled by the effort factor in the extended BBO algorithm we proposed. The pseudo-code for the above procedure is presented below in Fig. 7.
where α and β are the tuning parameters for balancing the effects of pheromone τ and heuristics η.

(c) *Selectivity factor calculator and comparator*: The distance between the current position and the neighborhood is the selectivity factor since here this distance plays the role of the deciding factor in determining the choice of the best path (shortest and the best feasible path) [22,24]. From equation above, the effort factor is calculated for the next nearest node. Then the pheromone is deposited on length (L) covered and the distance covered so far is calculated also called as the selectivity factor i.e. the total distance covered by each ant was obtained according to equation in the pseudo-code above.

Best feasible path detector layer: This layer selects the path with the highest selectivity factor which corresponds to the shortest distance among the given paths. The obtained path is the shortest and the safest path.

5.4. Mathematical framework for the two-phase anticipatory system based on extended BBO

The functional architecture of the proposed two – phase anticipatory system can be represented mathematically the form of the following equation. The equation presented in Fig. 8 is the combined representation of the output of the first and the second phases of the anticipatory system. In the first part of the mathematical equation, the set of candidate base stations suitable for the enemy to position its forces is taken as input and the best feasible base station for the enemy troops to mount attack is the output base station and the corresponding output of the first phase of the anticipatory system. The output of the first part of the equation is Max(c) which is the base station with the maximum value of selectivity factor and also the output of the first part of the equation. The value of Max(c) is expressed in Eq. (14).

$$Max(c) = \underset{c=1}{\overset{z}{Max}} \left(\frac{(HSI_c - HSI_{Threshold})}{Effort} \right) \tag{14}$$

where 'z' is the subset of the initial candidate base stations in H_u since it contains the stations for which

$$HSI_c > HSI_{Threshold}$$

where

$$HSI_c = f_c^{(1,2)} \left(\sum_{k=1}^{t} k \right)$$

In the second part of the mathematical equation, the set of friendly base station and the destination enemy base station for the enemy to position its forces is taken as input and the shortest and the safest path of attack for the enemy troops to mount attack is the output path and the corresponding output of the second phase of the anticipatory system. The output of the second part of the equation is Max(i) which is the best feasible path of attack with the maximum value of selectivity factor and also the output of the second part of the equation. The value of Max(i) is expressed by Eq. (15).

$$Max(i) = \underset{i=1}{\overset{d}{Max}} \left(\tau_{if}(t+1) = (1-\rho)\tau_{if}(t) + \sum_{k=1}^{m} \Delta\tau_{if} \right) \tag{15}$$

where 'd' is the subset of the initial candidate paths in H_u since it contains the paths for which

$$HSI_i > HSI_{Threshold}$$

$$where\ HSI_i = \frac{1}{\sqrt{(S_x - T_x)^2 + (S_y - T_y)^2}}$$

/* *Ant Colony Optimization* */
For each species H_i in the Universal habitat H_u
Select a species from H_u
For each of the feature habitat H_f.
If ($HSI_i > HSI_{Threshold}$)
Migrate the specie H_i to H_f.

$$Effort = P_{if} = \frac{(\tau_{if})^{\alpha}(\eta_{if})^{\beta}}{\sum (\tau_{if})^{\alpha}(\eta_{if})^{\beta}}$$

$$Selectivity\ Factor = \tau_{if}(t+1) = (1-\rho)\tau_{if}(t) + \sum_{k=1}^{m} \Delta\tau_{if}$$

End If
End For
End For

Fig. 7. Pseudo-code for effort calculator.

6. Two-phase anticipatory system on varied natural terrain scenarios

Now we evaluate the truth value of the proposed framework on different natural terrain scenarios. For the purpose, we consider two scenarios mainly, plain/desert region and the mountainous region. The reason for choosing the above two scenarios is that the SIVs (factors) under consideration for the choice of the most likely enemy base station for the plain as well as the desert region are the same (concluded from military inputs). Also the weights assigned to each of these SIVs is also equal for both the regions and hence the plain and the desert regions are both considered on equal grounds while proving the proposed framework for our two-phase anticipatory system. The mountainous region is a different scenario since it will have different factors for consideration in

CORRECTED PROOF

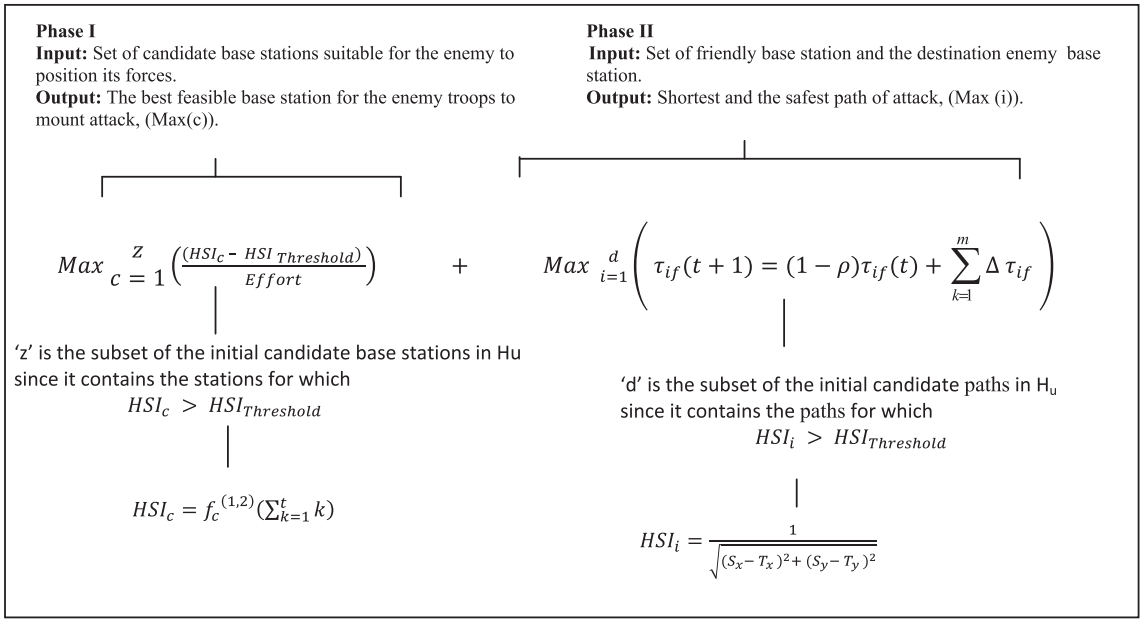

Fig. 8. Mathematical framework for the two-phase anticipatory system based on extended BBO.

making a particular base station more suitable than the other candidate base stations in the hilly region. We also define the SIVs applicable to a base station in each of the scenarios. Thus, we demonstrate the implementation of the newly introduced concepts of migration efforts calculation and dynamically modeling the HSI function in our extended BBO by presenting the implementation results of the two-phase anticipatory system for military application of battlefield preparation on two different terrains that of Alwar area in Rajasthan(Plain/Desert) and that of Mussourie region in Himachal Pradesh(Mountainous/hilly) [22]. The datasets chosen are satellite images taken through LISS-III sensor obtained courtesy of DRDO with candidate stations marked based on military inputs.

6.1. Plain/desert region

For the demonstration of the implementation of our extended BBO based two-phase anticipatory system, we choose the Alwar area in Rajasthan, India (Desert Scenario) of size 472 × 576 with the ground resolution of 23.5 meters taken through LISS-III sensor (courtesy of DTRL, DRDO) as shown in Fig. 9 [22].

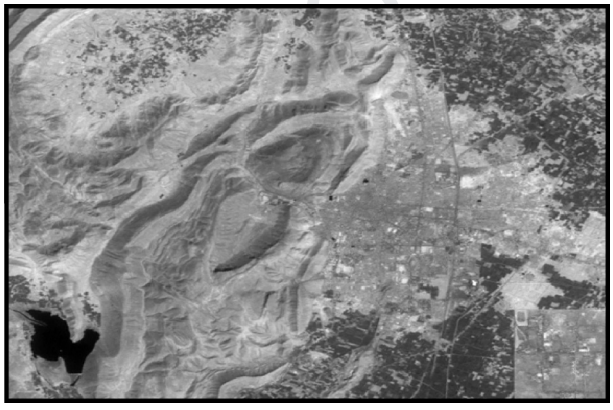

Fig. 9. 7-band FCC satellite image of size 472 × 546 of Alwar area in Rajasthan.

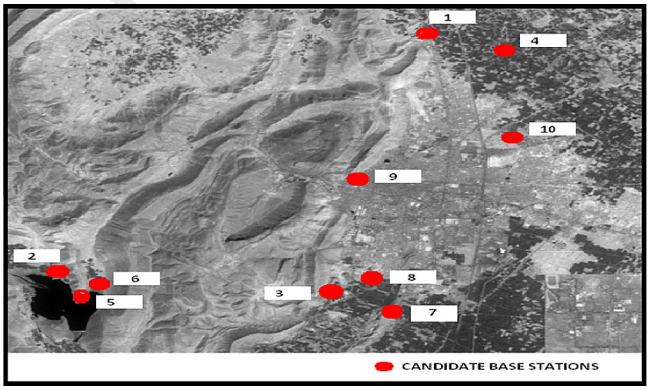

Fig. 10. 7-band Alwar Image with the areas suited as candidate base stations marked in red. (For interpretation of the references to colour in this figure legend, the reader is referred to the web version of this article.)

(i) First phase of the anticipatory system

This section describes the implementation of the proposed system on the dataset of Alwar where the HSI values for each station is calculated and hence the effort and selectivity factor values based on the proposed extended-BBO model are evaluated. The selectivity factor values are normalized based upon which the decision regarding the best feasible station is taken.

Input/output layer: We input the set of candidate base stations suitable for the enemy to position its forces and mount attack [22] on the Alwar image (shown in red in Fig. 9).

Ecosystem initialization layer: In this layer, the ecosystem consisting of the universal habitat, feature habitat and the isolated habitat is initialized.

(a) Universal habitat initializer: The ecosystem is initialized with the Universal habitat consisting of the set of suitable base stations for the enemy to position its forces. In our case, the H_u consists of 'n' base stations, where $n = 10$, and we input all the SIV values for each of the base stations as shown in Fig. 10 (based on military inputs).

Please cite this article in press as: L. Goel et al., Two-phase anticipatory system design based on extended species abundance model of biogeography for intelligent battlefield preparation, Knowl. Based Syst. (2015), http://dx.doi.org/10.1016/j.knosys.2015.07.023

Table 7
Applicable SIVs and their ideal values.

1	Transportation network constraints (N)	3
2	Concentration of signal traffic (S)	1
3	Safety and fast deployment (D)	3
4	Firepower range constraints (F)	3
5	Concentration of enemy stores & logistics (L)	3
6	Ease of setting up forward base stations and maintaining all-time, all-weather connectivity with the headquarters (C)	3
7	Ability to influence the friendly base stations (I)	3
8	Ease of Terrain Activities (T)	5
	(a) Degree of forest (V)	
	(b) Degree of rocky region (R)	3
	(b) Degree of urbanity (U)	1
	(c) Degree of barren land (B)	1
	(d) Degree of water (W)	2
9	Perception of enemy strengths, weaknesses and intents (P)	1

(b) Isolated habitat constructor: The Isolated habitat is initialized with zero SIVs.

(c) Feature habitat constructor: The feature habitat which represents a standard habitat is constructed which is analogous to the ideal solution. Table 7 fixes the SIVs and the corresponding ideal values on a scale of 1–5 for an Ideal Base station in a Plain/Desert region.

Habitat suitability index function calculation layer: This layer is responsible for calculation of the HSI function value for each of the habitats using the appropriate HSI function applicable.

Terrain characteristic analyzer: Since Alwar region is a desert region, some SIVs may not be relevant for the HSI calculation on this type of terrain and hence, the applicable HSI function may be different. We begin with the terrain characteristic analysis wherein we observe that in a plain/desert region, the aspect factor is of less importance since it is the hilly regions in which the choice of the base station location is more aspect-driven, we have not considered the Aspect factor. Also, in a planar region, M_F and G are not applicable. Same is the case with A i.e. the area under the slope which is also applicable in case of a mountainous region [22,39].

(a) Factor of relevance adjustor: Hence, the above 4 factors have their factor of relevance values $f_r < 0.5$ and therefore in the factor of relevance adjustor layer, these SIVs are omitted from the HSI function calculation.

(b) HSI function modeler: In our case, the factor H was eliminated in the factor of relevance adjustor layer and hence, the HSI function becomes fixed since, the parameter governing the dynamic modeling of the HSI function is no longer relevant in a desert scenario. Hence, the HSI function remains the same as in the previous layer and is given by:

$$HSI = [[(F * L) + (N + D + T + C) + (I/S)]/P]$$

where,

$$T = (V + mod((6 - R), 4) - U - B - (W - 2))$$

(c) Ideal HSI calculator:

$$\begin{aligned} Ideal\ HSI\ value &= [[(3*3) + (3+3+(5+3-1-1-0)+3) + (3/1)]/1] \\ &= 27 \end{aligned}$$

(d) Threshold HSI calculator:

$$\begin{aligned} Threshold\ HSI &= 1/3 * HSI\ ideal \\ &= 1/3 * 27 = 9 \end{aligned}$$

Threshold HSI based selective base station elimination layer:

(a) Threshold HSI condition applier: This layer compares the HSI of each of the 10 candidate base stations with the threshold HSI value of 9. From the Table 7, we observe that the HSI values for the candidate base stations 3, 5, 6 and 9 being 6.33, 7.56, 8.5 and 5.58 respectively is less than the threshold value of 9 and hence these base stations are preliminarily rejected.

(b) Weighted HSI function modeler: Since the HSI value of the base stations 1,2,4,7,8 and 10 is greater than the threshold HSI value, the effort required for migration will be calculated for these base stations using the weights assigned to the SIVs (on a scale of 1 to 5). Adding weights to the applicable SIVs, the mathematical formula for calculating the effort can be formulated and modified.

(c) Migration efforts calculator: For each of the 6 remaining base stations, the migration efforts is calculated as shown in Table 8 which depicts the HSI, effort and selectivity factor calculations for each of the candidate base stations.

Selectivity Factor analyzer layer: This layer calculates and analyzes the selectivity factor for the remaining candidate base stations in H_u. It is this factor which demarcates between good and bad stations based on the amount of effort required for migration and the difference in HSI values of ideal and input base station (Eqs. (5) and (6)). Thus, the selectivity factor values are a reflection of the station fitness and is normalized between 0 and 1 generally.

(a) Selectivity factor calculator: This layer calculates the selectivity factor values for the set of left over base stations, one among which will be the most likely enemy base station and the output of the first phase of the 2-phase anticipatory system algorithm. The selectivity factor calculations are shown in Table 8.

(b) Selectivity factor comparator: This layer is responsible for comparing the selectivity factor of all the base stations by means of normalization of our results by considering the normalized value of the selectivity factor for the base station with the highest selectivity factor as 1. After obtaining the selectivity factors for each of the remaining base stations, the remaining base stations normalized selectivity factor's values are then calculated by calculating their value as a percentage of the highest selectivity factor value. This is done so that the base stations can be categorized into different probability classes and the base stations with high selectivity factors can be sidelined.
We categorize our findings based on the Normalized selectivity factor values into the following ranges as given in Table 10.
(1) Since base station 4 is the base station with the Normalized selectivity factor value as 1, the destination base station is $n = 4$ and this is the 'n' which is also the output to the next phase of the algorithm to begin.
(2) Since $0.5 < N_{SF\ (n=1,\ 2)} < 1.0$, base stations 1 & 2 are most likely to be the Destination enemy base stations.
(3) Since $0.3 < N_{SF\ (n=10)} < 0.5$, base station 10 is a likely destination enemy base station.
(4) Since $0 < N_{SF\ (n=7,\ 8)} < 0.3$, base stations 7 & 8 are the least likely base stations for the enemy troops to position their forces.
(5) Since $N_{SF} = 0$ for base stations 3, 5, 6 & 9, these are not considered as candidate base stations.
Table 9 is the table of categorized output wherein each of the candidate base stations is classified into a category based on the outputs of Table 7 and is represented through color coding as in Fig. 11.

(c) Maximum selectivity factor selector: This layer selects the base station with the highest selectivity factor.

UNCORRECTED PROOF

Table 8
HSI, effort and selectivity factor calculation for each of the candidate base stations.

S. no. (n)	F	L	N	D	T					C	I	S	P	HSI	Effort	Selectivity factor	Normalized selectivity factor
					V	R	U	B	W								
1	3	3	2	3	5	3	1	1	1	2	3	2	1	24.500	18	0.86	0.54
2	4	4	2	2	3	2	1	1	4	2	5	2	2	13.750	62	0.077	0.05
3	4	2	2	1	3	2	1	1	2	1	2	1	3	6.333	∞	0	0
4	3	3	2	3	5	3	2	1	2	3	3	1	1	25.000	10	1.6	1.000
5	4	2	3	2	4	2	1	1	4	4	2	3	3	7.567	∞	0	0
6	2	2	1	1	5	4	1	1	1	1	4	1	2	8.500	∞	0	0
7	3	2	3	2	3	4	1	2	3	2	4	3	1	17.333	48	0.174	0.11
8	5	4	2	1	3	3	2	1	3	2	3	2	2	14.250	57	0.09	0.06
9	5	4	2	1	1	5	1	5	1	1	4	3	4	5.583	∞	0	0
10	4	2	3	3	4	3	1	2	2	2	3	2	1	21.500	25	0.5	0.31

Table 9
Categorization of the base stations based on the normalized selectivity factor values.

Normalized Selectivity Factor Range (N_{SF})	Category
$N_{SF} = 1$	Destination Enemy Base Station (Output to the second phase)
$0.5 < N_{SF} < 1.0$	Most likely Destination Enemy base stations
$0.3 < N_{SF} < 0.5$	Likely Destination Enemy base stations
$0 < N_{SF} < 0.3$	Least likely Destination Enemy base stations
$N_{SF} = 0$	Not a base station

Table 10
Table of categorized output.

Base stations (n)	Category
4	Destination Enemy Base Station (Output to the second phase)
1	Most likely Destination Enemy base stations
10	Likely Destination Enemy base stations
2, 7, 8	Least likely Destination Enemy base stations
3, 5, 6, 9	Not a base station

Destination Base station assignment layer: The base station with the highest selectivity factor is the most suitable base station for the enemy troops for their deployment and this layer assigns this base station as the destination base station for the friendly troops to mount attack on.

(ii) Second phase of the anticipatory system

The next phase is prediction of feasible path to this predicted base station for which a combination of ext-BBO/ACO2/PSO has been used and the corresponding path has been traced in the form of a table. The results of the second phase of the anticipatory system on the Alwar image are described in this section.

Input/output layer: This layer is used to input the friendly base station with coordinates (250,7) and the best suited enemy base station obtained which has coordinates (26, 164) as the output of the first phase. Fig. 12 below represents a portion of the Alwar image with the source (friendly) base station and the destination enemy base station marked in red. The destination enemy base station is obtained as the output of the first phase of the two-phase anticipatory system where we obtained the base station numbered as 4 ($n = 4$) as the destination enemy base station. The source base station is chosen to demonstrate the second phase of the anticipatory system.

Ecosystem initialization layer: This layer is responsible for the initialization of the Universal habitat and the feature habitat.

(a) Universal habitat initiator: In our system design, this layer initializes a Universal habitat consisting of a set of random positions from the source to the destination base station also called as the species (population) $H_1, H_2, \ldots, H_n$ which comprises H_u.

(b) Local and global feature habitat constructor: This layer initializes a feature habitat H_g representing the global best position and H_l representing the local best position.

Path extractor layer: This layer analyzes the histogram of satellite image for which it applies the modified PSO.

(a) Particle swarm random position initializer: In this layer, ten agents are created and particles are initialized, which scan their respective regions to find the global best (threshold value). $\text{Particle}_i\,(i = 1, 2, 3, \ldots, n)$ is randomly selected where n is the total number of particles.
(b) HSI function calculator: This layer is responsible for the HSI function calculation in order to determine the next best position of each particle using Eq. (11).
(c) Local and global feature habitat updator: After calculating HSI function from Eq. (11), this layer searches for the next best position.
(d) Universal habitat position and velocity updator: This layer updates the position and velocity of each H_i in H_u .

Global Threshold HSI function computation layer: This layer assigns the value of H_g as the threshold HSI value, $\text{HSI}_{\text{threshold}}$ to be used as input for the obstacle detection layer.

(a) Histogram analyzer: Based on the observations, the histogram is divided in five main regions as described in the functional architecture in the section before.

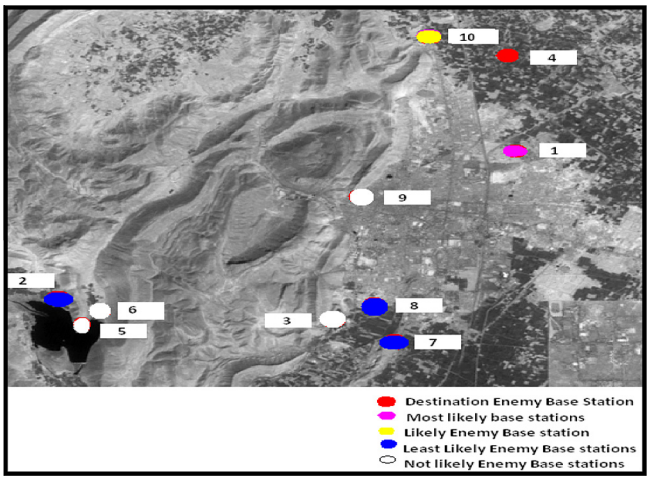

Fig. 11. 7-band Alwar image with the candidate base stations categorized into respective classes.

UNCORRECTED PROOF

Please cite this article in press as: L. Goel et al., Two-phase anticipatory system design based on extended species abundance model of biogeography for intelligent battlefield preparation, Knowl. Based Syst. (2015), http://dx.doi.org/10.1016/j.knosys.2015.07.023

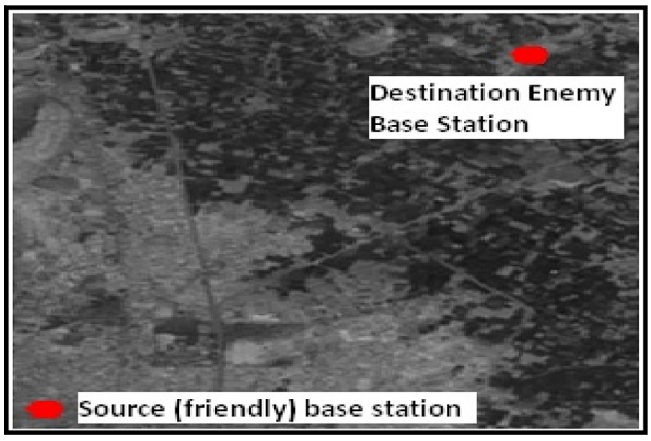

Fig. 12. Portion of the Alwar image with the source and the target marked in red. (For interpretation of the references to colour in this figure legend, the reader is referred to the web version of this article.)

(b) Local feature habitat calculator based on agent modeling: To evaluate the threshold values, the agents scan their respective regions assigned to them from the image. Every agent scans the image row wise to find local best values for each row. The local feature habitat calculations for each of the ten agents are represented in Table 11.
(c) Global feature habitat estimator: Every agent scans the image row wise to find local best values for each row and eventually evaluates the global best for the assigned region. The global feature habitat calculations for each of the ten agents are represented in Table 11.

Obstacle detection layer: This layer is responsible for calculating the threshold value (global best) which is used in the image to extract the paths as accessible area (barren area) and obstacles (like vegetation, water, rocky area etc.).

(a) Global feature habitat as threshold HSI assignor: This layer assigns the value of H_g as the threshold HSI value, $HSI_{threshold}$ for the obstacle detection step.
(b) Obstacle categorizer: This layer is responsible for categorizing the paths as obstacle free or an inaccessible area by using the global threshold HSI value which is the output of the previous layer.

The paths extracted after applying PSO is shown in Fig. 13, where black area depicts inaccessible area and white depicts the accessible path.

Path refinement layer: This layer is responsible for refining of the paths obtained as output of the previous layers using morphological operations. The image obtained with the paths refined after applying morphological operations is shown in Fig. 14 below.

Path planning layer: This layer is responsible for path planning using ACO.

(a) Ant position initializer: This layer is responsible for initializing the ants at the starting point wherein they chose random paths from getting to the target.
(b) Effort factor calculator: This layer is responsible for effort factor calculation for the next nearest node. In our system design, we model the effort factor by calculating the HSI function as a function of the shortest distance from the current position to the destination base station which is based on the observation that the destination coordinates is reached when the HSI function or the fitness value of the solution at that step becomes infinity or the shortest distance between the current position and the target becomes zero.
(c) Selectivity factor calculator and comparator: The distance between the current position and the neighborhood is the selectivity factor since here this distance plays the role of the deciding factor in determining the choice of the best path (shortest and the best feasible path). At each step, the neighborhood position with the highest value of selectivity factor is chosen as the next best position. Table 12 presents the table of highest selectivity factor values chosen at each step as the next best position.

Best feasible path detector layer: This layer is the formation of the path with the highest selectivity factor values which corresponds to the safest and the shortest path between the source friendly base station (250, 7) and the destination base station (26, 164) on the Alwar image as shown in Fig. 15.

6.2. Mountainous/hilly region

The second case study for the demonstration of the concepts of our extended BBO for the development of the anticipatory system is the Mussourie area in Himachal Pradesh, India (Mountainous scenario) of size 472 × 576 with the ground resolution of 23.5 m taken through LISS-III sensor (courtesy of DTRL, DRDO) as shown in Fig. 16 [22]:

(i) First phase of the anticipatory system

Input/output layer: We input the set of candidate base stations suitable for the enemy to position its forces and mount attack [22] on the Mussourie image (shown in red in Fig. 17).

Ecosystem initialization layer: In this layer, the ecosystem consisting of the universal habitat, feature habitat and the isolated habitat is initialized.

(a) Universal habitat initializer: We consider our Universal habitat as consisting of $4n/5$ base stations in a mountainous region (since the ratio of No. of base stations in a mountainous region to a plain/desert region is 4: 5 derived from military inputs) as shown in Fig. 17 and input all the SIV values for each of the base stations (based on military inputs) as given by Table 13. Hence, $n = 8$.
(b) Isolated habitat constructor: The Isolated habitat is initialized with zero SIVs.
(c) Feature habitat constructor: The feature habitat which represents a standard habitat is constructed which is analogous to the ideal solution. Fixing the SIV's and the corresponding ideal values on a scale of 1–5 for an ideal base station in a Mountainous/hilly region. (For our study, we chose the Mussourie region in Himachal Pradesh).

Habitat suitability index function calculation layer: This layer is responsible for calculation of the HSI function value for each of the habitats using the appropriate HSI function applicable.

(a) Terrain characteristic analyzer: Since Mussourie region is a mountainous region, some SIVs may not be relevant for the HSI calculation on this type of terrain and hence, the applicable HSI function may be different. We begin with the terrain characteristic analysis wherein we observe that in a hilly region, the aspect factor is very important since it is the hilly regions in which the choice of the base station location is more aspect-driven. Also, in a hilly region, M_F is also applicable. In a hilly region, a base station is chosen depending upon its strategic importance which is decided on the basis of measuring the elevation of the area under

UNCORRECTED PROOF

Table 11
Local and global feature habitat update in the global threshold HSI computation layer.

Candidate position 'n'	Global best position for 'n' (H_f)	Local best position (H_l)									
1	88.20	91.08	105.56	90.04	89.72	99.56	99.56	106.88	98.84	101.92	99.24
		94.32	86.60	73.88	73.76	66.48	56.20	61.20	79.20	94.88	95.12
2	54.50	48	60	80	44	84	39	23	27	23	35
		46	27	52	64	109	82	89	85	25	48
3	60.20	29	74	82	39	41	33	27	37	76	68
		78	72	113	52	33	31	37	101	125	56
4	47.30	29	27	25	27	50	89	105	56	50	17
		39	37	85	48	29	33	29	25	37	109
5	49.25	31	35	31	39	39	25	25	35	42	37
		29	33	29	23	27	85	91	97	123	109
6	80.85	27	44	41	29	62	125	119	117	109	105
		123	103	136	95	80	119	80	35	29	39
7	33.95	64	23	35	54	62	31	50	109	44	21
		21	19	19	17	25	11	13	19	19	23
8	85.40	127	89	76	93	103	91	64	54	82	132
		121	127	107	76	37	39	41	72	115	62
9	61.10	50	95	58	89	87	87	93	111	33	29
		25	21	99	87	19	27	42	48	52	70
10	44.35	29	23	29	31	64	109	76	23	23	66
		54	21	33	44	31	91	60	33	37	52

Fig. 13. Paths extracted after applying PSO.

consideration. Ability to counter-maneuver and counter deployment of troops depends upon the area covered under slope which is also applicable in case of mountainous/hilly regions and hence, we consider A as an SIV in case of hilly region.

(b) Factor of relevance adjustor: Hence, the above 4 factors have their factor of relevance values $f_r > 0.5$ and therefore in the factor of relevance adjustor layer, these SIVs are included in the HSI function calculation.

(c) HSI function modeler: In this case, the factor H is included in the factor of relevance adjustor layer and hence, the HSI function becomes dynamic since, the parameter governing the HSI function modeling becomes relevant in a mountainous scenario. To model this phenomenon for our system design, we define two HSI functions depending upon the value of H. If the value of H is less than 3, we use the first function else the second.

Hence,

if $(H > 3)$

$$HSI = [[(F * L) + (N + D + (MF/G) + T + C) + (I/S) + ((H * A)/10)]/P]$$

else

$$HSI = [[(F * L) + (N + D + (MF/G) + T + C) + (I/S) - ((H * A)/10)]/P]$$

where,

$$T = (V + mod((6 - R), 4) - U - B - (W - 2))$$

Threshold HSI condition applier: This layer compares the HSI of each of the 8 candidate base stations with the threshold HSI value of 9.33. From the Table 14, we observe that the HSI values for the candidate base stations 4 and 7 being 9.1 and 6.433 respectively is less than the threshold value of 9.33 and hence these base stations are preliminarily rejected.

(a) Weighted HSI function modeler: Adding weights to the applicable SIVs, the mathematical formula for calculating the HSI value can be derived in the form of the equation above for HSI in a mountainous/hilly region.

(b) Migration efforts calculator: For each of the 6 remaining base stations, the migration efforts is calculated as shown in Table 14 which depicts the HSI, effort and selectivity factor calculations for each of the candidate base stations.

Selectivity Factor analyzer layer: This layer calculates and analyzes the selectivity factor for the remaining candidate base stations in H_u.

(a) Selectivity factor calculator: This layer calculates the selectivity factor values for the set of left over base stations, one among which will be the most likely enemy base station and the output of the first phase of the 2-phase anticipatory system algorithm. Hence, we derive the values as calculated in the following table (Table 14). The table also shows which

Fig. 14. Refined paths after morphological operations.

Please cite this article in press as: L. Goel et al., Two-phase anticipatory system design based on extended species abundance model of biogeography for intelligent battlefield preparation, Knowl. Based Syst. (2015), http://dx.doi.org/10.1016/j.knosys.2015.07.023

Table 12
HSI computation and path planning by ACO. Table presents the HSI determination factor, the Euclidean distance calculations from the friendly base station to the destination enemy base station.

Initial position (Source friendly base station) = (250,7) $[g_i]$									
123.15	122.59	122.04	121.76	121.20	120.65	120.37	119.82	119.27	118.98
118.43	117.89	117.60	117.05	116.50	116.21	115.66	115.12	114.83	114.28
113.74	113.44	112.90	112.36	112.06	111.52	110.98	110.68	110.14	109.60
109.29	108.76	108.23	107.91	107.38	106.85	106.53	106.00	105.48	105.15
104.62	104.10	103.77	103.25	102.73	102.40	101.87	101.36	101.02	100.50
99.99	99.64	99.13	98.62	98.27	97.75	97.25	96.90	96.38	95.88
95.52	95.02	94.51	94.15	93.65	93.15	92.78	92.28	91.79	91.42
90.92	90.43	90.05	89.55	89.07	88.68	88.19	87.71	87.32	86.83
86.35	85.96	85.48	85.00	84.60	84.12	83.65	83.24	82.76	82.30
81.88	81.41	80.95	80.53	80.06	79.61	79.18	78.71	78.26	77.83
77.37	76.92	76.48	76.03	75.58	75.13	74.69	74.25	73.79	73.35
72.92	72.45	72.01	71.59	71.11	70.68	70.26	69.78	69.35	68.94
68.45	68.03	67.62	67.12	66.71	66.31	65.80	65.39	65.00	64.47
64.08	63.69	63.98	63.56	63.16	63.51	63.07	62.65	63.06	62.61
62.17	62.18	61.72	61.27	61.29	60.83	60.37	60.42	59.94	59.48
59.54	59.06	58.59	58.67	58.18	57.71	57.80	57.31	56.82	57.45
56.94	56.44	56.60	56.08	55.57	55.23	54.71	54.20	53.85	53.34
52.84	52.48	51.97	51.48	51.11	50.61	50.12	49.74	49.24	48.76
48.37	47.89	47.41	47.01	46.53	46.07	45.65	45.18	44.72	44.29
43.83	43.38	42.94	42.49	42.05	41.59	41.15	40.72	40.25	39.81
39.40	38.91	38.48	38.08	37.58	37.16	36.77	37.16	36.77	36.40
36.77	36.40	36.06	35.47	35.11	34.79	34.18	33.84	33.53	32.89
32.57	32.28	31.62	31.32	31.05	30.36	30.08	29.83	29.73	29.41
29.12	29.15	28.79	28.46	28.23	27.86	27.51	27.31	26.93	26.57
26.40	26.00	25.63	25.50	25.08	24.70	25.06	24.60	24.17	24.19
23.71	23.26	23.32	22.83	22.36	22.47	21.95	21.47	21.10	20.59
20.12	19.72	19.24	18.79	18.36	17.89	17.46	17.00	16.55	16.16
15.65	15.23	14.87	14.32	13.93	13.60	13.00	12.65	12.37	11.70
11.40	11.18	10.44	10.20	10.05	9.22	9.06	9.00	8.06	8.00
7.28	7.07	7.00	6.71	6.32	6.08	5.83	5.39	5.10	4.47
4.12	4.00	3.16	3.00	2.24	2.00	1.41	1.00	1.00	0.00
Final position (Destination Enemy Base Station) = (26, 164)									

Decreasing Euclidean distance values from the destination station (g_{if}) and correspondingly increasing HSI values and hence, increasing inverse selectivity factor values.

Note: The destination base station coordinates are reached when the distance

$$\sqrt{(S_x - T_x)^2 + (S_y - T_y)^2} = 0$$

Fig. 15. Alwar image with the safest and the shortest path from the source base station to the target enemy base station.

of the two formulae of HSI is applicable on each of the candidate base stations by representing this information in brackets along with the HSI calculation in Table 14.

(b) Selectivity factor comparator: This layer is responsible for comparing the selectivity factor of all the base stations by means of normalization of our results by considering the normalized value of the selectivity factor for the base station with the highest selectivity factor as 1 as described earlier.

We categorize our findings based on the Normalized selectivity factor values into the following ranges as was given in Table 9.

(1) Since base station 3 is the base station with the Normalized selectivity factor value as 1, the Destination base station is $n = 3$ and this is the 'n' which is also the output to the next phase of the algorithm to begin.
(2) Since $0.5 < N_{SF\ (n=1,\ 2)} < 1.0$, base station 1 are most likely to be the Destination enemy base stations,
(3) Since $0.3 < N_{SF\ (n=10)} < 0.5$, base station 8 is a likely destination enemy base station.
(4) Since $0 < N_{SF\ (n=7,\ 8)} < 0.3$, base stations 2, 5 & 6 are the least likely base stations for the enemy troops to position their forces.
(5) Since $N_{SF} = 0$ for base stations 4 and 7, these are not considered as candidate base stations.

Fig. 16. Google Earth Image of size 472 × 576 of Mussourie region in Himachal Pradesh.

Fig. 17. Mussourie image with the areas suited as candidate base stations marked in red. (For interpretation of the references to colour in this figure legend, the reader is referred to the web version of this article.)

Table 15 is the table of categorized output wherein each of the candidate base stations is classified into a category based on the outputs of Table 14 and is represented through color coding as in Fig. 18.

(c) Maximum selectivity factor selector: This layer selects the base station with the highest selectivity factor.
Destination base station assignment layer: The base station with the highest selectivity factor is the most suitable base station for the enemy troops for their deployment and this layer assigns this base station as the destination base station for the friendly troops to mount attack on.

(ii) Second phase of the anticipatory system

The results of the second phase of the anticipatory system on the Mussourie image are described in this section.

Input/output layer: This layer is used to input the friendly base station with coordinates (250, 7) and the best suited enemy base station obtained which has coordinates (16, 190) as the output of the first phase. Fig. 19 below represents a portion of the Mussourie image with the source (friendly) base station and the destination enemy base station marked in red. The destination enemy base station is obtained as the output of the first phase of the two-phase anticipatory system where we obtained the base station numbered as 3 ($n = 3$) as the destination enemy base station. The source base station is chosen to demonstrate the second phase of the anticipatory system.

Table 13
Applicable SIVs and their ideal values.

1	Transportation network availability (N)	3
2	Concentration of signal traffic (S)	1
3	Safety and fast deployment (D)	3
4	Firepower range constraints (F)	3
5	Concentration of logistics (L)	3
6	Ease of setting up forward base stations and maintaining all-time, all-weather connectivity with the headquarters (C)	3
7	Mobility/difficulty factor (M_F)	3
8	Enemy's ability to influence the friendly base stations (I)	3
9	Aspect(direction/angle) (H)	5
10	Ability to counter–maneuver or counter-deployment of troops (A)	4
11	Areas of strategic importance (G)	1
12	Ease of terrain activities (T)	
	(a) Degree of forest (V)	5
	(b) Degree of rocky region (R)	3
	(c) Degree of urbanity (U)	1
	(d) Degree of barren land (B)	1
	(e) Degree of water (W)	2
13	Perception of enemy strengths, weaknesses and intents (P)	1

Ecosystem initialization layer: This layer is responsible for the initialization of the Universal habitat and the feature habitat.

(a) Universal habitat initiator: In our system design, this layer initializes a Universal habitat consisting of a set of random positions from the source to the destination base station also called as the species (population) $H_1, H_2, \ldots, H_n$ which comprises H_u.
(b) Local and global feature habitat constructor: This layer initializes a feature habitat H_g representing the global best position and H_l representing the local best position.

Path extractor layer: This layer analyzes the histogram of satellite image for which it applies the modified Particle Swarm Optimization Algorithm.

(a) Particle swarm random position initializer: In this layer, ten agents are created and particles are initialized, which scan their respective regions to find the global best (threshold value). Particle$_i$ ($i = 1, 2, 3, \ldots, n$) is randomly selected where n is the total number of particles.
(b) HSI function calculator: This layer is responsible for the HSI function calculation in order to determine the next best position of each particle using Eq. (11).
(c) Local and global feature habitat updator: After calculating HSI function from Eq. (11), this layer searches for the next best position.
(d) Universal habitat position and velocity updator: This layer updates the position and velocity of each H_i in H_u .

Global threshold HSI function computation layer: This layer assigns the value of H_g as the threshold HSI value, $HSI_{threshold}$ to be used as input for the obstacle detection layer.

(a) Histogram analyzer: Based on the observations, the histogram is divided in five main regions as described in the functional architecture in sections before.
(b) Local feature habitat calculator based on agent modeling: To evaluate the threshold values, the agents scan their respective regions assigned to them from the image. Every agent

Please cite this article in press as: L. Goel et al., Two-phase anticipatory system design based on extended species abundance model of biogeography for intelligent battlefield preparation, Knowl. Based Syst. (2015), http://dx.doi.org/10.1016/j.knosys.2015.07.023

Table 14
HSI, effort and selectivity factor calculation for each of the candidate base stations.

S. no. (n)	F	L	N	D	M_F	G	T					C	I	S	H	A	P	HSI	Effort	Selectivity Factor	N_{SF}
							V	R	U	B	W										
1	3	3	2	3	3	1	5	3	1	1	1	2	3	2	4	4	1	25.90 (ii)	21	0.81	0.50
2	4	4	2	2	3	3	3	2	1	1	4	2	5	2	3	4	2	15.95 (i)	78	0.089	0.05
3	3	3	2	3	3	1	5	3	2	1	2	3	3	1	5	4	1	26.00 (ii)	10	1.7	1.00
4	2	2	1	1	1	3	5	4	1	1	1	1	4	1	3	2	2	9.10 (i)	∞	0	0
5	3	2	3	2	2	2	3	4	1	2	3	2	4	3	3	4	1	19.53 (i)	62	0.169	0.10
6	5	4	2	1	2	4	3	3	2	1	3	2	3	2	4	2	2	13.95 (ii)	92	0.054	0.03
7	5	4	2	1	1	4	1	5	1	5	1	1	4	3	3	2	4	6.43 (i)	∞	0	0
8	4	2	3	3	4	1	4	3	1	2	2	2	3	2	4	5	1	23.50 (ii)	34	0.43	0.25

Table 15
Table of categorized output.

Base stations (n)	Category
3	Destination Enemy Base Station (Output to the second phase)
1	Most likely Destination Enemy base station
8	Likely Destination Enemy base station
2, 5, 6	Least likely Destination Enemy base stations
4, 7	Not a base station

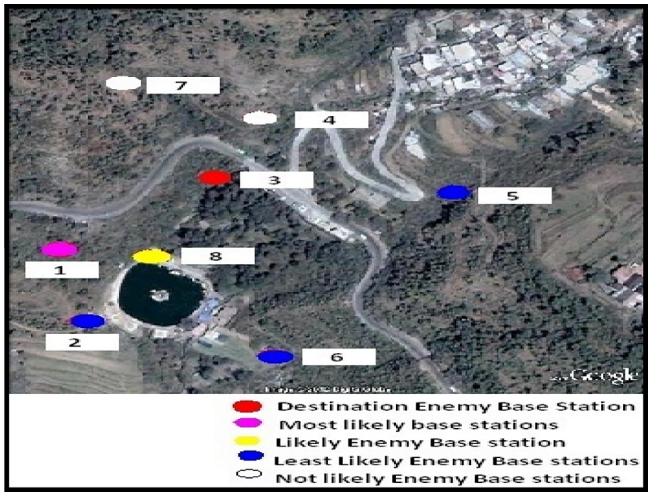

Fig. 18. Mussourie image with the candidate base stations categorized into respective classes.

scans the image row wise to find local best values for each row. The local feature habitat calculations for each of the ten agents are represented in Table 16.

(c) Global feature habitat estimator: Every agent scans the image row wise to find local best values for each row and eventually evaluates the global best for the assigned region. The global feature habitat calculations for each of the ten agents are represented in Table 16.

Obstacle detection layer: This layer is responsible for calculating the threshold value (global best) which is used in the image to extract the paths as accessible area (barren area) and obstacles (like vegetation, water, rocky area etc.).

(a) Global feature habitat as threshold HSI assignor: This layer assigns the value of H_g as the threshold HSI value, $HSI_{threshold}$ for the obstacle detection step.

Fig. 19. Portion of Mussourie image with source and destination base stations marked in red. (For interpretation of the references to colour in this figure legend, the reader is referred to the web version of this article.)

(b) Obstacle categorizer: This layer is responsible for categorizing the paths as obstacle free or an inaccessible area by using the global threshold HSI value which is the output of the previous layer. The paths extracted after applying PSO is shown in Fig. 20, where black area depicts inaccessible area and white depicts the accessible path.

Path refinement layer: This layer is responsible for refining of the paths obtained as output of the previous layers using morphological operations. The image obtained with the paths refined after applying morphological operations is shown in Fig. 21 below.

Path planning layer: This layer is responsible for path planning using ACO.

(a) Ant position initializer: This layer is responsible for initializing the ants at the starting point wherein they chose random paths from getting to the target.

(b) Effort factor calculator: This layer is responsible for effort factor calculation for the next nearest node. In our system design, we model the effort factor by calculating the HSI function as a function of the shortest distance from the current position to the destination base station which is based on the observation that the destination coordinates is reached when the HSI function or the fitness value of the solution at that step becomes infinity or the shortest distance between the current position and the target becomes zero.

Please cite this article in press as: L. Goel et al., Two-phase anticipatory system design based on extended species abundance model of biogeography for intelligent battlefield preparation, Knowl. Based Syst. (2015), http://dx.doi.org/10.1016/j.knosys.2015.07.023

Table 16
Local and global feature habitat update in the global threshold HSI computation layer.

Candidate position 'n'	Global best position for 'n' (H_f)	Local best position (H_l)									
1	85.83	86.60	87.20	86.56	82.16	76.32	75.12	81.52	89.24	90.52	86.84
		84.56	86.04	88.16	87.52	85.24	83.60	85.32	89.40	92.12	92.56
2	95.55	116	133	122	101	62	72	103	122	139	136
		91	50	60	71	74	90	97	92	86	94
3	136.85	105	124	136	130	120	120	123	118	119	119
		129	139	140	140	150	165	167	165	168	160
4	128.95	189	108	78	107	140	152	144	132	146	148
		140	138	130	124	123	122	124	121	111	102
5	96.90	103	86	90	116	101	92	96	91	92	91
		99	106	88	79	89	106	111	110	99	93
6	96.05	93	88	79	65	70	82	94	105	114	113
		107	94	100	98	95	91	99	113	111	110
7	49.35	161	150	78	37	46	37	35	40	27	33
		38	41	42	42	35	27	28	28	31	31
8	30.00	29	29	29	28	28	29	30	31	30	29
		30	29	30	28	29	32	33	34	24	39
9	33.80	30	31	40	46	56	37	36	31	28	35
		37	32	29	31	33	32	28	29	28	27
10	89.44	29	36	40	38	33	29	38	31	28	33
		39	45	59	157	200	185	175	168	126	97

Fig. 20. Paths extracted after applying PSO.

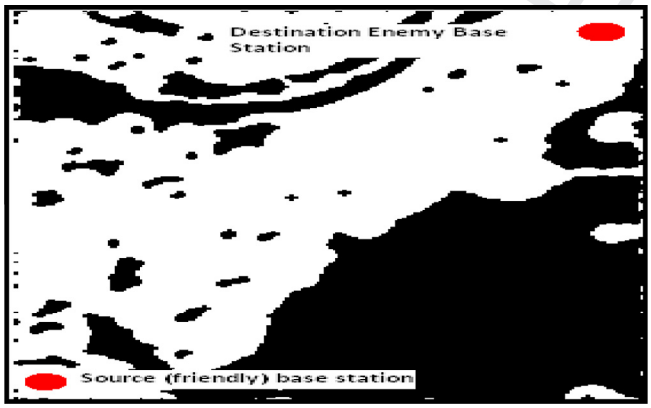

Fig. 21. Refined paths after morphological operations.

(c) Selectivity factor calculator and comparator: The distance between the current position and the neighborhood is the selectivity factor since here this distance plays the role of the deciding factor in determining the choice of the best path (shortest and the best feasible path). At each step, the neighborhood position with the highest value of selectivity factor is chosen as the next best position. Table 17 presents the table of highest selectivity factor values chosen at each step as the next best position.

Best feasible path detector layer: This layer is the formation of the path with the highest selectivity factor values which corresponds to the safest and the shortest path between the source friendly base station (250, 7) and the destination base station (16, 190) on the Alwar image as shown in Fig. 22.

7. Performance analysis of the two-phase anticipatory system

This section presents the performance analysis of both the phases of the proposed two-phase anticipatory system. In order to demonstrate the efficiency of the proposed system accurately which integrates three techniques that of extended BBO based on HSI function modeling, the PSO and the ACO2 techniques, we present the performance comparison results of each of the two phases of the anticipatory system separately.

7.1. First phase of the anticipatory system

The first phase of the anticipatory system which is used to predict the deployment strategies of enemy troops by predicting the location of the enemy base station for positioning their forces is based on the extended model of BBO [9]. Hence, we compare the performance of the extended BBO with the traditional decision making techniques that have been used till date for anticipating the probable enemy base stations but have shown limited accuracy. Table 19 presents the results of the performance analysis of the Extended-BBO technique (first phase) on the datasets of the Alwar and Mussourie regions. From expert knowledge and military inputs, the destined enemy base stations are known to be station 4 and station 3 for Alwar and Mussourie regions respectively. From the results in Table 10 and 15, we know that the proposed extended BBO model for predicting the enemy base station resulted in the 4th and the 3rd base stations as the destination enemy base stations for the Alwar and the Mussourie images respectively which is correct. Traditional decision making involves a simple sum of the factors affecting the fitness function and picking up the one with the near-ideal fitness value. Thus, if the traditional decision making would have been applied, the SIV values should have been added up linearly for each of the candidate base stations and the value that is nearest to the ideal value will be chosen as the output base station. Using the above traditional decision making, the HSI values for each of the candidate base stations for

UNCORRECTED PROOF

Please cite this article in press as: L. Goel et al., Two-phase anticipatory system design based on extended species abundance model of biogeography for intelligent battlefield preparation, Knowl. Based Syst. (2015), http://dx.doi.org/10.1016/j.knosys.2015.07.023

Table 17
HSI Computation and path planning by ACO. Table presents the HSI determination factor, the Euclidean distance calculations from the friendly base station to the destination enemy base station.

Initial position (Source friendly base station) = (250,7)									
123.15	122.59	122.04	121.76	121.20	120.65	120.37	119.82	119.27	118.98
118.43	117.89	117.60	117.05	116.50	116.21	115.66	115.12	114.83	114.28
113.74	113.44	112.90	112.36	112.06	111.52	110.98	110.68	110.14	109.60
109.29	108.76	108.23	107.91	107.38	106.85	107.38	106.85	106.33	106.85
106.33	105.82	105.48	104.96	104.45	104.10	103.59	103.08	102.73	102.22
101.71	101.36	100.85	100.34	99.99	99.48	98.98	98.62	98.11	97.62
97.25	96.75	96.25	95.88	95.38	94.89	94.51	94.02	93.54	94.89
94.41	93.94	95.29	94.83	94.37	95.71	95.26	94.81	96.18	95.71
95.26	95.77	95.29	94.83	95.38	94.89	94.41	95.02	94.51	94.02
94.67	94.15	93.65	95.19	94.67	94.15	95.52	95.02	94.51	96.04
95.52	95.02	95.72	95.19	94.67	96.25	95.72	95.19	95.96	95.41
94.87	95.69	95.13	94.58	95.44	94.87	94.30	94.63	94.05	93.48
93.23	92.66	92.09	92.42	91.84	91.26	91.61	91.02	90.44	90.80
90.21	89.63	89.40	88.81	88.23	88.60	88.01	87.42	87.80	87.20
86.61	87.01	86.40	85.80	86.21	85.60	85.00	84.81	84.20	83.60
84.02	83.41	82.80	83.24	82.62	82.01	82.46	81.84	81.22	82.33
81.69	81.06	81.57	80.92	80.28	81.47	80.81	80.16	80.72	80.06
79.40	79.98	79.31	78.64	79.25	78.57	77.90	78.52	77.83	77.16
77.79	77.10	76.42	77.78	77.08	76.38	77.08	76.37	75.66	75.66
74.95	74.25	74.25	73.54	72.84	72.84	72.12	71.42	71.42	70.71
70.01	70.01	69.30	68.59	68.59	67.88	67.18	67.18	66.47	65.76
65.76	65.05	64.35	64.35	63.64	62.94	62.94	62.23	61.52	61.52
60.81	60.11	60.11	59.40	58.69	58.69	57.98	57.28	57.28	56.57
55.87	55.87	55.15	54.45	54.45	53.74	53.04	53.04	52.33	51.62
51.62	50.91	50.21	50.91	50.21	49.52	49.50	48.80	48.10	48.08
47.38	46.69	46.67	45.97	45.28	45.25	44.55	43.86	43.84	43.14
42.45	42.43	41.73	41.04	41.01	40.31	39.62	39.60	38.90	38.21
38.18	37.48	36.80	36.77	36.07	35.38	35.36	34.66	33.97	33.94
33.24	32.56	32.53	31.83	31.14	31.11	30.41	29.73	29.70	29.00
28.32	28.28	27.59	26.91	26.87	26.17	25.50	25.46	24.76	24.08
24.04	23.35	22.67	22.63	21.93	21.26	21.21	20.52	19.85	19.80
19.11	18.44	18.38	17.69	17.03	16.97	16.28	15.62	15.56	14.87
14.21	14.14	13.45	12.81	12.73	12.04	11.40	11.31	10.63	10.00
9.90	9.22	8.60	8.49	7.81	7.21	7.07	6.40	5.83	5.66
5.00	4.47	4.24	3.61	3.16	2.83	2.24	2.00	1.41	1.00
1.00	0.00								
Final position (Destination Enemy base station) = (16, 190)									

Decreasing Euclidean distance values from the destination station (g_{if}) and correspondingly increasing HSI values and hence, increasing inverse selectivity factor values.

Note: The destination base station coordinates are reached when the distance

$$\sqrt{(S_x - T_x)^2 + (S_y - T_y} = 0$$

UNCORRECTED PROOF

the Alwar and the Mussourie regions is calculated as given by Table 18.

From the above table, the base stations which are closest to the ideal HSI values are 2, 4 and 10 for Alwar and 3 and 6 for the Mussourie region. This means that the traditional decision making technique could not produce refined results since it resulted in more than one (3 for Alwar and 2 for Mussourie) base stations as output. Thus, traditional decision making fails to produce a unique output which is where lies the weakness of this technique. Also, if we model the probability of the selection of the 4th and the 3rd base stations through traditional decision making technique, then the probability of their selection is 1/3rd and 1/2 respectively. In other words, the efficiency of the destination enemy base station prediction of the traditional technique can be written as 33% and 50% for Alwar and Mussourie regions respectively. Also, for the Alwar image, the base stations 2 and 10 which have been outputted as the destination base stations are categorized as 'Least Likely' and 'Likely' base stations by our proposed system selection

Please cite this article in press as: L. Goel et al., Two-phase anticipatory system design based on extended species abundance model of biogeography for intelligent battlefield preparation, Knowl. Based Syst. (2015), http://dx.doi.org/10.1016/j.knosys.2015.07.023

Table 18
HSI calculations using traditional decision making.

Base station/dataset	Alwar ($HSI_{ideal} = 32) HSI = \sum_{i=1}^{10} SIV_i$	Mussourie ($HSI_{ideal} = 45) HSI = \sum_{i=1}^{8} SIV_i$
1	30	42
2	32	47
3	25	45
4	32	35
5	35	44
6	26	45
7	33	47
8	33	46
9	37	–
10	32	–

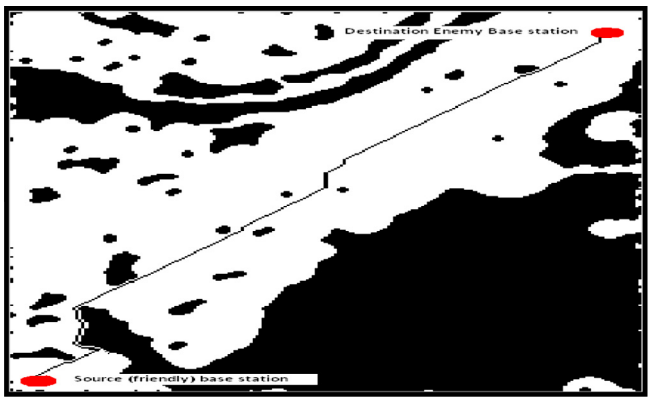

Fig. 22. Mussourie image with the safest and the shortest path from the source (friendly) base station to the target destination enemy base station.

with the N_{SF} values as '0–0.3' and '0.3–0.5' respectively. This also is in contradiction to the predictions made by the traditional method and its classification accuracy derived as a percentage of that predicted by the proposed model is only $1/3 \times ((0 + 0.3)/2) \times 100$ and $1/3 \times ((0.3 + 0.5)/2) \times 100$ i.e. 5% and 13% respectively. For the Mussourie image, the base station 6 which has been outputted as the destination base stations is categorized as 'Least Likely' base stations by our proposed system selection with the N_{SF} value as '0–0.3' and the classification accuracy as $1/2 \times ((0 + 0.3)/2) \times 100$ i.e. 8%. Also, the secondary outputted base stations 5 and 8 which can be considered as the next closest categorized as 'Least Likely' and 'Likely' base stations by our proposed system selection with the N_{SF} values as'0–0.3' and'0.3–0.5' and the classification accuracy as $1/2 \times ((0 + 0.3)/2) \times 100$ and $1/2 \times ((0.3 + 0.5)/2) \times 100$ i.e. 8% and 20% respectively. From the above discussion, it is reflected that the results of the traditional decision making techniques are imprecise and do not reflect a true suitability index which is reflected by the lower values of normalized selectivity factor range of the base stations outputted by this technique as destination base stations. Moreover, the technique is imprecise as it does not produce a single output and produces multiple base stations as output of the first phase.

7.2. Second phase of the anticipatory system

The second phase of the anticipatory system which is used to find the best feasible path of attack (the safest (obstacle-free) and shortest) on the enemy base station is based on an integration of extended BBO with the PSO and ACO techniques of path extraction and path planning respectively [6,20]. Hence, we compare the performance of the hybrid technique that we employed with the results obtained by the use of other optimization techniques [15] such as Ant Colony Optimization (ACO) [6], Particle Swarm Optimization (PSO) [20,43] (For details on how PSO is used for path planning application, the reader is referred to the paper [43]), hybrid ACO2/PSO [19], fuzzy inference mechanism [23], genetic algorithms [5,29], etc. that have been used extensively for path planning applications which form the second phase of our anticipatory system. Table 20 presents the results of path planning implementation for the Alwar as well as the Mussourie images using the optimization techniques of Ant Colony Optimization [6], Particle Swarm Optimization [20,43], Hybrid ACO2/PSO [19], Stud Genetic Algorithm (SGA) [1,21], Evolutionary Strategy (ES) [3,41], Self-Organizing Feature Maps (SOFM) [1], Fuzzy Inference mechanism (FI) [1] and Genetic Algorithms (GA) [14,28]. The figures in the table are the pixel count of the path planned from the source to the destination base station. In other words, it is the distance of the path planned from the friendly to the destination enemy base station by using each of the said optimization techniques on Alwar as well as the Mussourie region. From the table, it can be seen that the proposed extended BBO based hybrid ACO2/PSO technique employed in the second phase produces the lowest pixel count of 351 for Alwar and 310 for Mussourie region when compared to the other techniques of ACO, PSO, hybrid ACO2/PSO, SGA, ES, SOFM, FI and GA that were implemented for the path planning application which produce a pixel count of

Table 19
Prediction efficiency of traditional decision making v/s the proposed extended BBO model.

Technique used/dataset	Traditional decision making						Extended BBO model	Ideal results (expert knowledge based)
Alwar	Output base station [2,4,11]	Base station 2 10	Probability of selection 1/3 1/3	Prediction efficiency 33% 33%	N_{SF} Range 0–0.3 0.3–0.5	%Efficiency 5% 13%	Output base station = 4	Output base station = 4
Mussourie [3,6]	Output Base stations = [3,6]	6	1/2	50%	0–0.3	8%	Output base station = 3	Output base stations = 3

Table 20
Results of path planning on the given datasets by various optimization techniques.

Optimization technique used/dataset	Ext-BBO/ACO2/PSO based anticipatory system	ACO	PSO	Hybrid ACO2/PSO	Stud genetic algorithm	Evolutionary strategy	Self-organizing feature maps	Fuzzy inference	Genetic algorithm
Alwar	351	355	354	353	352	358	363	361	358
Mussourie	310	314	313	312	311	316	321	319	316

Please cite this article in press as: L. Goel et al., Two-phase anticipatory system design based on extended species abundance model of biogeography for intelligent battlefield preparation, Knowl. Based Syst. (2015), http://dx.doi.org/10.1016/j.knosys.2015.07.023

UNCORRECTED PROOF

352, 358, 363, 361 and 358 for Alwar and 311, 316, 321, 319 and 316 for Mussourie region. This means that the path planned by the proposed technique is the shortest and the safest path of attack on the enemy base station for both the datasets used.

8. Conclusion and future scope

Based on the results of the proposed two-phase anticipatory system, the commanders in the war theater will have an increased battlefield awareness since they can now anticipate the destined enemy base station and can also select the shortest path to attack the enemy base station hence anticipating enemy's future actions. This will be of prime importance since in the modern warfare strategies, the ability of an army to position it's troops at an effective geographical location (having predicted the location of the enemy base station), in the shortest possible time, will significantly gain a tactical advantage over the enemy and prove to be the deciding factor for winning. Thus the proposed system is very well suited for anticipating the next action of the enemy – to anticipate the enemy's deployment strategies and can replace the currently employed traditional decision making techniques.

The proposed hybrid algorithm can be of major use to the military and the commanders in the battlefield as demonstrated in the paper. However, the algorithm can be generalized to fit in commercial applications also, such as in predicting the most suitable location for establishing a manufacturing plant for some industry and thereafter finding the shortest and the safest path for transportation of finished goods and raw materials to and from the manufacturing plant. The algorithm can also be used to predict the best location for exploration of ground water possibilities by taking the ideal features required in it as the feature habitat consisting of the set of ideal SIVs. The set of attributes that comprise of the SIVs are obtained by considering factors such as geology, land form, soil, land use, slope, and linearment, etc. In fact, the algorithm can be generalized in such a way so that it can be used in any application wherein the best suited location and the shortest path for reaching there has to be found out. Thus, the algorithm can be of major use in both military and scientific applications and commercial applications as well.

The proposed work can be further refined by modifying the existing SIVs and the addition of some more SIVs. Addition of new SIVs such as climate/weather conditions; state-liquid (water/petrol), solid (land/mountain), vapor (clouds), gaseous extracts (fog/smog); distance from roads (highways); water transportation modes; air strips supporting landing and flying of aircrafts (various sizes); railway network, land mine prone areas etc.; can help in building of a more versatile anticipatory system. Refinement of present SIVs by the inclusion of factors such as dimension (Height/Length/Breadth), habitat, animals (Friendly/Dangerous), vegetation (Edible/Poisonous/Allergic), surprise Factor, etc. can further refine the anticipatory system to make it more efficient and robust. Couple of factors such as weapon capability and skills of the enemy are certain things which require human interpretation as these cannot be judged by the machine. Also the surprise factor contributes negatively to the comfort factor in other words we can say these are inversely proportional to each other. This would further help in determining additional information aiding in building a very refined anticipatory system that can be of great help in designing of the war/battlefield strategies. Also we can sample the above SIVs round the year to generate very precise and accurate results. Also, in future, the proposed path planning algorithm in the second phase of the two-phase anticipatory system can be compared with new and more sophisticated algorithms like Artificial Bee Colony Optimization [45] to prove its effectiveness over advanced algorithms too.

References

[1] Hifza Afaq, Sanjay Saini, On the solutions to the travelling salesman problem using nature inspired computing techniques, IJCSI Int. J. Comput. Sci. Issues 8 (4) (2011) 326–334.
[2] Ethem Alpaydin, Introduction to Machine Learning, MIT Press, 2004.
[3] T. Back, Evolutionary Algorithms in Theory and Practice, Oxford Univ. Press., Oxford, U.K., 1996.
[4] A. Bhattacharya, P. Chattopadhyay, Solving complex economic load dispatch problems using biogeography-based optimization, Expert Syst. Appl. 37 (5) (2010) 3605–3615.
[5] Hagen Burchardt, Ralf Salomon, Implementation of path planning using genetic algorithms on mobile robots, IEEE Congr. Evol. Comput. (2006) 1831–1836.
[6] Macro Dorigo, Thomas Stutzle, Ant Colony Optimization, 2004.
[7] M. Ergezer, D. Simon, D.W. Du, Oppositional biogeography-based optimization, in: Proceeding of IEEE the Conference on Systems, Man, and Cybernetics, San Antonio, TX, 2009, pp. 1035–1040.
[8] R.D. Gilson, Situation awareness, Spec. Issue Preface: Hum. Fact. 37 (1) (1995) 3–4.
[9] Lavika Goel, V.K. Panchal, Daya Gupta, Rajiv Bhola, Hybrid ACO-BBO approach for predicting the deployment strategies of enemy troops in a military terrain application, IISN, 2010.
[10] Lavika Goel, Daya Gupta, V.K. Panchal, Dynamic model of blended biogeography based optimization for land cover feature extraction, in: International Conference on Contemporary Computing (IC3), Springer Communications in Computer & Information Sciences (CCIS-LNCS), vol. 306, 2012, pp. 8–19.
[11] Lavika Goel, V.K. Panchal, Daya Gupta, Hybrid bio-inspired techniques for land cover feature extraction: a remote sensing perspective, Appl. Soft Comput. J. 12 (2012) 832–849.
[12] Lavika Goel, Daya Gupta, V.K. Panchal, Extended species abundance models of biogeography based optimization, in: IEEE conference on Computational Intelligence, Modelling and Simulation (CIMSim), IEEE Xplore and CSDL, Kuantan, Malaysia, 2012, pp. 7–12.
[13] Lavika Goel, Daya Gupta, V.K. Panchal, Biogeography based anticipatory computing framework for intelligent battlefield planning, in: International Conference on Hybrid Intelligent Systems (HIS), Pune, 2012, pp. 41–46.
[14] D. Goldberg, Genetic Algorithms in Search, Optimization, and Machine Learning, Addison-Wesley, Reading, MA, 1989.
[15] Zhifeng Hao, Han Huang, Ruichu Cai, Bio-inspired algorithms for TSP and generalized TSP, Book: Travelling Salesman Problem, 2008, pp. 202, ISBN: 978-953-7619-10-7.
[16] Patrick Chisan Hew, The Generation of Situational Awareness Within Autonomous Systems – A Near to Mid Term Study. Issues by Defence Systems Analysis Division Information Sciences Laboratory DSTO-GD-0467, DSTO Information Sciences Laboratory, 2006.
[17] Rajeev Kumar Jaiswal, Saumitra Mukherjee, Kumaran D. Raju, Rajesh Saxena, Forest fire risk zone mapping from satellite imagery and GIS, Int. J. Appl. Earth Obs. Geoinform. 4 (2002) 1–10.
[18] R.S. Jensen, "The Boundaries of Aviation Psychology, Human Factors" aeronautical decision making, situation awareness, and crew resource management, Int. J. Aviat. Psychol. 7 (4) (1997) 259–267.
[19] Preetinder Kaur, Simerjeet Kaur, Gurvinder Singh Aulakh, V.K. Panchal, Hybrid approach using PSO and ACO for cross-country path planning, IISN, 2010.
[20] James Kennedy, Russell C. Eberhart, Swarm Intelligence, Academic Press, USA, 2001.
[21] W. Khatib, P. Fleming, The stud GA: a mini revolution?, in: A. Eiben, T. Back, M. Schoenauer, H. Schwefel (Eds.), Parallel Problem Solving from Nature, Springer, New York, 1998.
[22] Ralph W. Kiefer, Thomes M. Lillesand, Principles of Remote Sensing, 2006.
[23] B.N. Kimt, Kwont, K.H. Kimtt, E.H. Leet, S.H. Hongttt, A Study On Path Planning for Mobile Robot Based on Fuzzy Logic Controller, IEEE TENCON, 1999.
[24] Ying Li, Bo Cheng, An Improved k-Nearest Neighbor Algorithm and Its Application to High Resolution Remote Sensing Image Classification, in: 17th International Conference on Geoinformatics, 2009.
[25] Haiping Ma, Suhong Ni, Man Sun, Equilibrium species counts and migration model tradeoffs for biogeography based optimization, in: IEEE Conference on Decision and Control, 2009, pp. 3306–3310.
[26] H.P. Ma, D. Simon, Biogeography-based optimization with blended migration for constrained optimization problems, in: Proceedings of GECCO-2010, Portland, Oregon, 2010.
[27] H. Ma, An analysis of the equilibrium of migration models for biogeography-based optimization, in: Proceedings of Inf. Sci., 2010, pp. 3444–3464.
[28] Z. Michalewicz, Genetic Algorithms + Data Structures = Evolution Programs, Springer, New York, 1992.
[29] H. Muhlenbein, D. Schlierkamp-Voosen, Predictive models for the breeder genetic algorithm, I. Continuous parameter optimization, Evol. Comput. 1 (1993) 25–49.
[30] M. Ovreiu, D. Simon, Biogeography-based optimization of neuro-fuzzy system parameters for diagnosis of cardiac disease, in: Proceedings of GECCO-2010, 2010.
[31] V.K. Panchal, Samiksha Goel, Mitul Bhatnagar, 2009. Biogeography Based Land Cover Feature Extraction. World Congress on Nature and Biologically Inspired Computing, (NaBIC'09), pp. 1588–1591.

UNCORRECTED PROOF

Please cite this article in press as: L. Goel et al., Two-phase anticipatory system design based on extended species abundance model of biogeography for intelligent battlefield preparation, Knowl. Based Syst. (2015), http://dx.doi.org/10.1016/j.knosys.2015.07.023

[32] V.K. Panchal, Harish Kundra, Amanpreet Kaur, 2009. Biogeography based Groundwater Exploration, CISIM.
[33] I. Parmee, Evolutionary and Adaptive Computing in Engineering Design, Springer, New York, 2001.
[34] R. Rarick, D. Simon, F.E. Villaseca, B. Vyakaranam, 2009. Biogeography-based optimization and the solution of the power flow problem. In: Proceedings of the IEEE on Systems, Man, and Cybernetics, San Antonio, Texas, pp. 1029–1034.
[35] Yasar Guneri Sahin, Tuncay Ercan, Detection of hidden hostile/terrorist groups in harsh territories by using animals as mobile biological sensors, Sensors 8 (2008) 4365–4383, http://dx.doi.org/10.3390/s8074365.
[36] D. Simon, Biogeography-based optimization, IEEE Trans. Evol. Comput., vol. 12, IEEE Computer Society Press, 2008, pp. 702–713 (6).
[37] D. Simon, D. Du, M. Ergezer, 2009. Biogeography – based optimization combined with evolutionary strategy and immigration refusal. In: proceedings of IEEE International Conference on System, Man and Cybernetics, San Antonio, U.S.A.
[38] Sun Tzu, "The Art of War, A Chinese Military Treatise", Chapter 3, 6th Century BC.
[39] Zhou,Wei, 2008. Survey and Analysis of Land Satellite Remote Sensing Applied in Highway Transportations Infrastructure and System Engineering, IGARSS.
[40] D.D. Woods, Coping with complexity: the psychology of human behaviour in complex systems, in: L.P. Goodstein, H.B. Andersen, S.E. Olsen (Eds.), Tasks, Errors and Mental Models, Taylor & Francis, London, 1988.
[41] X. Yao, Y. Liu, G. Lin, Evolutionary programming made faster, IEEE Trans. Evol. Comput. 3 (1999) 82–102.
[42] G. Zhang, J. Lu, Fuzzy bilevel programming with multiple objectives and cooperative multiple followers, Int. J. Glob. Opt. 47 (3) (2008) 403–419.
[43] G. Zhang, Y. Gao, J. Lu, H.M. Wee, Particle swarm optimization for bi-level pricing problems in supply chains, Int. J. Glob. Opt. 51 (3) (2011) 245–254.
[44] G. Zhang, G. Zhang, Y. Gao, J. Lu, Competitive strategic bidding optimization in electricity markets using bilevel programming and swarm technique, IEEE Trans. Ind. Electr. 58 (6) (2001) 2138–2146.
[45] Y. Zhang, L. Wu, S. Wang, UCAV path planning based on FSCABC, Inform. – Int. Interdiscipl. J. 14 (3) (2011) 687–692.
[46] Y. Zhang, L. Wu, S. Wang, UCAV path planning by fitness-scaling adaptive chaotic particle swarm optimization, Int. J. Math. Prob. Eng. 2013 (2013) 1–9 (Article ID 705238, 9 pages).

UNCORRECTED PROOF

Please cite this article in press as: L. Goel et al., Two-phase anticipatory system design based on extended species abundance model of biogeography for intelligent battlefield preparation, Knowl. Based Syst. (2015), http://dx.doi.org/10.1016/j.knosys.2015.07.023